United States
Environmental Protection
Agency

Office of Research and
Development
Washington DC 20460

EPA/600/R-99/030
March 1999

EPA

Science Algorithms of the EPA Models-3 Community Multiscale Air Quality (CMAQ) Modeling System

United States Environmental Protection Agency

Office of Research and Development
Washington, DC 20460

EPA/600/R-99/030
March 1999

SCIENCE ALGORITHMS OF THE EPA MODELS-3 COMMUNITY MULTISCALE AIR QUALITY (CMAQ) MODELING SYSTEM

Edited by:

D. W. BYUN* and J. K. S. CHING*
Atmospheric Modeling Division
National Exposure Research Laboratory
U.S. Environmental Protection Agency
Research Triangle Park, NC 27711

*On assignment from the National Oceanic and Atmospheric Administration, U.S. Department of Commerce

Printed on Recycled Paper

DISCLAIMER

The information in this document has been funded wholly or in part by the United States Environmental Protection Agency. It has been subjected to the Agency's peer and administrative review, and has been approved for publication as an EPA document. Mention of trade names or commercial products does not constitute endorsement nor recommendation for use.

FOREWORD

The Models-3 Community Multiscale Air Quality (CMAQ) modeling system has been developed under the leadership of the Atmospheric Modeling Division of the EPA National Exposure Research Laboratory in Research Triangle Park, NC. This new generation of modeling software was under development for seven years and was made available in June 1998 without charge for use by air quality regulators, policy makers, industry, and scientists to address multiscale, multi-pollutant air quality concerns.

Models-3/CMAQ has a unique framework and science design that enables scientists and regulators to build their own modeling system to suit their needs. Users can access pre-installed modeling systems provided by the EPA or can incorporate their own modeling systems to work within the existing framework software.

This direct user involvement is key to the concept of a community modeling and analysis system. This approach to model development, application, and analysis leverages the community's complementary talents and resources to set new standards for rapid incorporation of better science into air quality model applications. The resulting comprehensive system forms the foundation upon which the community, including governments, industry, academia, and other stakeholders, can collaborate in the examination of issues and the subsequent development of strategies that meet society challenges of environmental protection.

The release of Models-3/CMAQ is one of the many steps which we hope will unite the community under the common goal of advancing our knowledge and abilities to tackle critical problems of the future in far more effective ways than have been attempted in the past. Scientifically sound modeling systems, developed and supported by the community, are one method of achieving this goal.

The June 1998 release of the Models-3/CMAQ computer code was accompanied by a User Manual [EPA-600/R-98/069(b)] to serve as a reference on how to use the software system. This Science Document is the counterpart to the User Manual in that it presents the peer reviewed scientific bases for the Models-3/CMAQ modeling systems. This document also includes components such as interface processors, process analysis routines, and the present and planned evaluation program.

F. A. Schiermeier
March 1999

CONTENTS

FOREWORD v

ACRONYMS xvii

ACKNOWLEDGMENTS xxi

EXECUTIVE SUMMARY ES-1

1. INTRODUCTION TO THE MODELS-3 FRAMEWORK AND THE COMMUNITY MULTISCALE AIR QUALITY MODEL (CMAQ)
(J. Ching and D. Byun)
Abstract 1-1
1.0 Introduction to the Models-3 Framework and the Community Multiscale Air Quality Model (CMAQ) 1-2
1.1 The Models-3 Emissions, Meteorology, and the CMAQ Modeling Systems .. 1-4
1.2 CMAQ Interface Processors 1-6
1.3 The CMAQ Chemical Transport Model (CCTM) 1-8
1.4 Analysis of CMAQ Output 1-10
1.4.1 Process Analysis (Chapter 16) 1-10
1.4.2 Aggregation (Chapter 17) 1-11
1.5 Management of CMAQ Science Information Objects and Codes in Models-3 1-11
1.5.1 Program Control Processors (Chapter 15) 1-11
1.5.2 CMAQ Code Integration (Chapter 18) 1-12
1.6 Post Release Studies and Near-Future Plans 1-12
1.6.1 CMAQ Evaluation Study 1-12
1.6.2 Testing Operational Configurations 1-12
1.6.3 Extensions and Science Additions 1-13
1.7 Opportunities and Encouragement for Long Term Extensions and Science Community Involvement 1-13
1.8 References 1-15

2. MODELS-3 ARCHITECTURE: A UNIFYING FRAMEWORK FOR ENVIRONMENTAL MODELING AND ASSESSMENT
(J. Novak and S. Leduc)
Abstract 2-1
2.0 Models-3 Architecture: A Unifying Framework for Environmental Modeling and Assessment 2-2
2.1 Introduction 2-2
2.2 Overview of the Models-3 Framework 2-2

2.2.1 Dataset Manager 2-2
2.2.2 Program Manager 2-3
2.2.3 Study Planner 2-3
2.2.4 Strategy Manager 2-4
2.2.5 Tool Manager 2-4
2.2.6 Science Manager 2-6
2.2.7 Model Builder 2-6
2.2.8 Source Code Manager 2-7
2.2.9 Framework Administrator 2-7
2.3 Models-3 System Architecture 2-7
2.4. Schedule and Future Plans 2-10
2.5 References 2-10

3. DEVELOPING METEOROLOGICAL FIELDS
(T. Otte)
Abstract 3-1
3.0 Developing Meteorological Fields 3-2
3.1 Credits and Disclaimers for Use of MM5 3-2
3.2 Meteorology Model Pre-Processing 3-2
3.2.1 Defining the Simulation Domain (*TERRAIN*) 3-2
3.2.2 Processing the Meteorological Background Fields (*DATAGRID*) 3-3
3.2.3 Objective Analysis (*RAWINS*) 3-3
3.2.4 Setting the Initial and Boundary Conditions (*INTERP*) 3-4
3.3 The Meteorology Model (MM5) 3-4
3.3.1 Brief History 3-4
3.3.2 Horizontal and Vertical Grid 3-5
3.3.3 Prognostic Equations 3-5
3.3.4 Model Physics 3-6
3.3.5 Nesting 3-10
3.3.6 Four-Dimensional Data Assimilation 3-10
3.4 Meteorology Model Post-Processing 3-11
3.5 Changes to the MM5 System's Software for Models-3 3-11
3.6 References 3-12

4. EMISSION SUBSYSTEM
(B. Benjey, J. Godowitch, and G. Gipson)
Abstract 4-1
4.0 Emission Subsystem 4-2
4.1 Emission Inventory Processors 4-2
4.1.1 Discussion 4-2
4.1.2 General MEPPS Structure 4-11
4.2 The MEPPS Emission Processing System 4-12
4.2.1 The Inventory Data Analyzer (IDA) 4-14

4.2.2 The MEPPS Input Processor (INPRO) 4-16
4.2.3 Processing Procedure 4-17
4.2.4 Modeled Emission Data 4-33
4.2.5 Chemical Speciation of Emission Data 4-78
4.2.6 Output Processor (OUTPRO) 4-90
4.3 Models-3 Emission Projection Processor (MEPRO) 4-91
4.4 Emission Processing Interface 4-94
4.4.1 Overview of Key Features of ECIP 4-94
4.4.2 Plume Rise of Point Source Emissions 4-96
4.4.3 Method for the Treatment of Initial Vertical Plume Spread 4-99
4.4.4 Vertical Allocation of Plume Emissions 4-100
4.4.5 Generation of 3-D Emissions 4-100
4.5 Data Requirements 4-100
4.6 Plans for Improvement 4-102
4.7 References 4-103

5. FUNDAMENTALS OF ONE-ATMOSPHERE DYNAMICS FOR MULTISCALE AIR QUALITY MODELING
(D. Byun)
Abstract 5-1
5.0 Fundamentals of One-Atmosphere Dynamics for Multiscale Air Quality Modeling 5-2
5.1 Governing Equations and Approximations for the Atmosphere 5-2
5.1.1 Governing Equations in a Generalized Curvilinear Coordinate System 5-3
5.1.2 Assumptions of Atmospheric Dynamics 5-6
5.2 Choice of Vertical Coordinate System for Air Quality Modeling 5-11
5.3 Coupling of Meteorology and Air Quality 5-18
5.3.1 Meteorological Data for Air Quality Modeling 5-18
5.3.2 Off-line and On-line Modeling Paradigms 5-18
5.4 Mass Conservation 5-22
5.4.1 Mass Consistency in Meteorological Data 5-22
5.4.2 Techniques for Mass Conservation in Air Quality Models 5-23
5.4.3 Temporal Interpolation of Meteorological Data 5-25
5.5 Conclusion 5-26
5.6 References 5-27
Appendix 5A. Tensor Primer and Derivation of the Continuity Equation in a Generalized Curvilinear Coordinate System 5-30

6. **GOVERNING EQUATIONS AND COMPUTATIONAL STRUCTURE OF THE COMMUNITY MULTISCALE AIR QUALITY (CMAQ) CHEMICAL TRANSPORT MODEL**
(D. Byun, J. Young, and M.T. Odman)
Abstract 6-1
6.0 Governing Equations And Computational Structure of The Community Multiscale Air Quality (CMAQ) Chemical Transport Model 6-2
6.1 Derivation of the Atmospheric Diffusion Equation 6-3
6.2 Representation of Science Processes in CMAQ Modeling System 6-9
6.2.1 Supporting Models and Interface Processors 6-9
6.2.2 Modularity Concept of CMAQ 6-10
6.2.3 Description of Science Processes 6-15
6.3 Equivalent Model Formulations for Different Vertical Coordinates 6-26
6.4 Nesting Techniques 6-28
6.5 Summary 6-31
6.6 References 6-31
Appendix 6A. Concentration Units Used for Air Quality Studies 6-34

7. **NUMERICAL TRANSPORT ALGORITHMS FOR THE COMMUNITY MULTISCALE AIR QUALITY (CMAQ) CHEMICAL TRANSPORT MODEL IN GENERALIZED COORDINATES**
(D. Byun, J. Young, J. Pleim, M.T. Odman, and K. Alapaty)
Abstract 7-1
7.0 Numerical Transport Algorithms for the Community Multiscale Air Quality (CMAQ) Chemical Transport Model in Generalized Coordinates 7-2
7.1 Numerical Advection Algorithms 7-3
7.1.1 Conservation Form Equation for Advection 7-4
7.1.2 Classification of Advection Schemes 7-6
7.1.3 Description of Advection Schemes in CCTM 7-6
7.1.4 Treatment of Boundary Conditions 7-11
7.1.5 Test of Algorithms with Idealized Linear Horizontal Flow Fields 7-12
7.1.6 Vertical Advection 7-15
7.1.7 Adjustment of Mass Conservation Error 7-16
7.2 Vertical Mixing Algorithms 7-18
7.2.1 Closure Problem 7-19
7.2.2 Computing Vertical Mixing with the Eddy Diffusion Formulation: K-Theory 7-21
7.2.3 Flux Form Representation of Vertical Mixing 7-31
7.3 Horizontal Mixing Algorithms 7-43
7.4 Conclusions 7-45
7.5 References 7-46
Appendix 7A Numerical Solvers for Diffusion Equations 7-51

8. GAS-PHASE CHEMISTRY

(G. Gipson and J. Young)

Abstract 8-1
8.0 Gas-Phase Chemistry 8-2
8.1 Background 8-3
8.2 Chemical Mechanisms in the CMAQ System 8-4
8.2.1 CB4 Mechanism 8-5
8.2.2 RADM2 Mechanism 8-6
8.2.3 SAPRC-97 Mechanism 8-7
8.2.4 Extended Mechanisms 8-8
8.2.5 Changing or Adding Mechanisms in CMAQ 8-11
8.3 Reaction Kinetics 8-12
8.3.1 Reaction Rates 8-12
8.3.2 Rate Constant Expressions 8-13
8.4 Mathematical Modeling 8-15
8.4.1 Governing Equations 8-16
8.4.2 SMVGEAR 8-18
8.4.3 QSSA Solver 8-22
8.4.4 Summary 8-25
8.5 References 8-25
Appendix 8A Chemical Mechanisms Included in the CMAQ System 8-29

9. PLUME-IN-GRID TREATMENT OF MAJOR POINT SOURCE EMISSIONS

(N. Gillani and J. Godowitch)

Abstract 9-1
9.0 Plume-in-Grid Treatment of Major Point Source Emissions 9-2
9.1 Introduction 9-2
9.2 Overview of the Conceptual Framework of the Plume-in-Grid Treatment .. 9-4
9.3 Formulation of the Plume-in-Grid Modeling Components 9-5
9.3.1 Description of the Plume Dynamics Model 9-5
9.3.2 Formulation of the Plume-in-Grid Module 9-12
9.4 Summary 9-28
9.5 References 9-28

10. AEROSOLS IN MODELS-3 CMAQ
(F. Binkowski)
Abstract 10-1
10.0 Aerosols in Models-3 CMAQ 10-2
10.1 Aerosol Dynamics 10-4
10.1.1 Modal Definitions 10-4
10.1.2 New Particle Production by Nucleation 10-5
10.1.3 Primary Emissions 10-6
10.1.4 Numerical Solvers 10-7
10.1.5 Mode Merging by Renaming 10-10
10.2 Aerosol Dry Deposition 10-11
10.3 Cloud Processing of Aerosols 10-11
10.4 Aerosol Chemistry 10-14
10.5 Visibility 10-15
10.6 Summary 10-17
10.7 References 10-17

11. CLOUD DYNAMICS AND CHEMISTRY
(S. Roselle and F. Binkowski)
Abstract 11-1
11.0 Cloud Dynamics and Chemistry 11-2
11.1 Background 11-2
11.2 Model Description 11-2
11.2.1 Subgrid Convective Cloud Scheme 11-3
11.2.2 Resolved Cloud Scheme 11-7
11.3 Conclusions 11-8
11.4 References 11-9

12. METEOROLOGY-CHEMISTRY INTERFACE PROCESSOR (MCIP) FOR MODELS-3 COMMUNITY MULTISCALE AIR QUALITY (CMAQ) MODELING SYSTEM
(D. Byun, J. Pleim, R. Tang, and A. Bourgeois)
Abstract 12-1
12.0 Meteorology-Chemistry Interface Processor (MCIP) For Models-3 Community Multiscale Air Quality (CMAQ) Modeling System 12-2
12.1 Introduction 12-2
12.1.1 MCIP Functions 12-4
12.1.2 MCIP's Data Dependency 12-6
12.1.3 Computational Structure 12-8
12.2 Data Types, Coordinates, and Grids 12-10
12.2.1 Meteorological Data Types 12-10
12.2.2 Coordinates 12-14
12.2.3 Modification of Grid Structure 12-18

12.3 Estimation of Physical Parameters 12-23
12.3.1 PBL Parameters 12-23
12.3.2 Dry Deposition Velocities 12-37
12.3.3 Cloud Parameters and Solar Radiation 12-49
12.4 Meteorological Data for CCTM with Generalized Coordinate System 12-52
12.4.1 Thermodynamic Variables: Pressure, Density and Entropy 12-52
12.4.2 Vertical Jacobian and Layer Height 12-54
12.4.3 Contravariant Velocity Components 12-57
12.4.4 Mass Consistent Temporal Interpolation of Meteorological Parameters 12-60
12.4.5 Optional Conversion of Nonhydrostatic Data to Hydrostatic Meteorological Data for MM5 12-61
12.5 Operation of MCIP 12-63
12.5.1 MCIP Modules 12-63
12.5.2 Building MCIP 12-63
12.5.3 Executing MCIP 12-65
12.5.4 Defining Grid and Domain for MCIP 12-68
12.5.5 Extension of MCIP for Other Meteorological Models 12-72
12.6 Concluding Remarks 12-73
12.7 References 12-74
Appendix 12A MCIP Output Data 12-80
Appendix 12B Examples of Nest Domain Definitions for CMAQ system 12-83
Appendix 12C Sample MCIP Configuration File 12-85
Appendix 12D Sample MCIP Run Script 12-87

13. THE INITIAL CONCENTRATION AND BOUNDARY CONDITION PROCESSORS
(G. Gipson)
Abstract 13-1
13.0 The Initial Concentration and Boundary Condition Processors 13-2
13.1 Introduction 13-2
13.2 Overview of the ICON and BCON Processors 13-2
13.3 Input Sources 13-3
13.3.1 Time Invariant Concentration Profiles 13-3
13.3.2 CCTM Concentration files 13-5
13.3.3 Tracer Species 13-5
13.4 Spatial Interpolation 13-7
13.4.1 Horizontal Interpolation 13-7
13.4.2 Vertical Interpolation 13-8
13.5 ICON/BCON Species Processing 13-9
13.6 Mechanism Conversions 13-11
13.7 ICON/BCON Applications 13-12
13.8 References 13-13

14. PHOTOLYSIS RATES FOR CMAQ
(S. Roselle, K. Schere, J. Pleim, A. Hanna)
Abstract 14-1
14.0 Photolysis Rates for CMAQ 14-2
14.1 Background 14-2
14.2 Preprocessor JPROC: Calculate Clear-sky Photolysis Rate Table 14-3
14.3 Subroutine PHOT: Table Interpolation and Cloud Attenuation 14-4
14.4 Conclusions 14-5
14.5 References 14-6

15. PROGRAM CONTROL PROCESSING IN MODELS-3
(J. Young)
Abstract 15-1
15.0 Program Control Processing in Models-3 15-2
15.1 Domain Configuration 15-3
15.2 Input/Output Applications Programming Interface 15-4
15.3 Other CCTM Configuration Control 15-4
15.3.1 CCTM Process Analysis 15-4
15.3.2 CCTM Fixed Data 15-5
15.4 Generalized Chemistry 15-6
15.4.1 Design 15-6
15.4.2 Operation 15-7
15.4.3 Supported Reaction Types 15-9
15.4.4 Mechanism Parsing Rules 15-10
15.4.5 Chemical Species Include Files 15-10
15.6 Conclusion 15-16
15.7 References 15-16

16. PROCESS ANALYSIS
(G. Gipson)
Abstract 16-1
16.0 Process Analysis 16-2
16.1 Integrated Process Rate Analysis 16-3
16.1.1 Computation of Integrated Process Rates 16-3
16.1.2 Example IPR Analyses 16-5
16.1.3 Implementation of IPR Analysis in the CMAQ System 16-6
16.1.4 Use of the PACP to set up an IPR Analysis 16-7
16.2 Integrated Reaction Rate Analysis 16-9
16.2.1 Computation of Integrated Reaction Rates 16-10
16.2.2 Example IRR Analyses 16-11
16.2.3 Implementation of IRR Analysis the CMAQ system 16-13
16.2.4 Use of the PACP to set up an IRR Analysis 16-14

16.3 Conclusion 16-19
16.4 References 16-20

17. AN AGGREGATION AND EPISODE SELECTION SCHEME DESIGNED TO SUPPORT MODELS-3 CMAQ
(R. Cohn, B. Eder, and S. Leduc)
Abstract 17-1
17.0 An Aggregation and Episode Selection Scheme Designed to Support Models-3 CMAQ 17-2
17.1 Introduction 17-2
17.1.1 Background 17-2
17.1.2 Objectives 17-3
17.2 Summary of the Approach 17-4
17.2.1 Basic Elements of the Methodology 17-4
17.2.2 Rationale, Scope, and Limitations 17-5
17.2.3 Strategy 17-6
17.3 Cluster Analysis of Wind Fields 17-8
17.3.1 Description of Wind Data 17-8
17.3.2 Basic Cluster Analysis Technique 17-8
17.3.3 Illustration of Cluster Analysis Results 17-9
17.4 Evaluation of Alternative Aggregation Approaches 17-11
17.4.1 Description of Alternative Approaches 17-11
17.4.2 Description of Meteorological Data 17-12
17.4.3 Analysis Methods 17-12
17.4.4 Results 17-13
17.5 Refinement of the Sampling Approach 17-21
17.5.1 Determination of Appropriate Numbers of Strata and Events 17-22
17.5.2 Selection of Stratified Sample of Events 17-27
17.6 Application and Evaluation 17-29
17.6.1 Application of the Aggregation Procedure 17-29
17.6.2 Evaluation 17-31
17.7 Summary and Discussion 17-32
17.8 References 17-33

18. INTEGRATION OF SCIENCE CODES INTO MODELS-3
(J. Young)
Abstract 18-1
18.0 Integration of Science Codes into Models-3 18-2
18.1 Introduction 18-2
18.2 Classes and Modules 18-4
18.2.1 Operational Design 18-4
18.2.2 CGRID 18-5
18.2.3 Class Driver 18-6

18.2.4 Synchronization Time Step 18-7
18.3 Input/Output Applications Programming Interface 18-8
18.4 Code Configuration Management 18-10
18.4.1 The Need 18-10
18.4.2 The Tool 18-11
18.4.3 The Repository 18-12
18.5 How a Model is Constructed 18-14
18.5.1 Object Oriented Concepts 18-14
18.5.2 Global Name Table Data 18-14
18.5.3 Build Template 18-15
18.6 How a Model is Executed 18-18
18.7 Using the Models-3 Framework 18-18
18.8 Conformant Code 18-19
18.8.1 Thin Interface 18-19
18.8.2 Coding Rules 18-20
18.8.3 Science Process Code Template 18-21
18.8.4 Robustness and Computational Efficiency 18-24
18.9 Conclusion 18-25
18.10 References 18-25

ACRONYMS

ADEOS	Advanced Earth Observing Satellite
ADOM	Acid Deposition and Oxidant Model
AQM	Air Quality Model
ASD	Accurate Space Derivative advection scheme
AVS	Advanced Visualization System
BCs	Boundary Conditions
BCON	Boundary Conditions processor
BDF	Backward Differentiation Formulae
BEIS	Biogenic Emissions Inventory System
BEIS2	Biogenic Emissions Inventory System - version 2
BELD	Biogenic Emissions Landuse Database
BOT	Bott Scheme for advection
CAAA-90	Clean Air Act Amendments of 1990
CB-IV (or CB-4)	Carbon Bond-IV chemical mechanism
CBWQM	Chesapeake Bay Water Quality Model
CCM2	Community Climate Model Version 2
CCTM	CMAQ Chemical Transport Model processor
CEM	Continuous Emission Monitor
CFL	Courant-Friedrich-Levy condition
CG	Coarser Grid
CMAQ	Community Multiscale Air Quality model
CORBA	Common Object Request Broker Architecture
CPU	Central Processing Unit of a computer
CTM	Chemical Transport Model
CVS	Concurrent Versions System
ECIP	Emissions-Chemistry Interface Processor
EMPRO	Emissions Processor
EPA	Environmental Protection Agency
FAST	Flow Analysis Software Toolkit
FDDA	Four-Dimensional Data-Assimilation
FG	Finer Grid
FIPS	Federal Identification Protocol System
FSL	Forecast Systems Laboratory
GCIP	GEWAX Continental Scale International Project
GEMAP	Geocoded Emission Modeling and Projection
HSPF	Hydrologic Simulation Program FORTRAN
I/O API	Input/Output Applications Programming Interface
ICs	Initial Concentration
ICON	Initial Conditions processor
IDA	Inventory Data Analyzer
IEEE	Institute of Electrical and Electronics Engineers, Inc.

INPRO	MEPPS Input Processor
IPR	Integrated Process Rates
IRR	Integrated Reaction Rates
JPROC	Photolysis Rate Processor
LRPM	LaGrangian Reaction Plume Module
LUPROC	Landuse processor for MCIP
MAPS/RUC	Mesoscale Analysis and Prediction System/Rapid Update Cycle
MCIP	Meteorology-Chemistry Interface processor
MEPPS	Models-3 Emissions Processing and Projection System
MEPRO	Models-3 Emissions Projection Processor
MEPSE	Major Elevated Point Source Emitter
MEPSEs	Major Elevated Point Source Emitters
MM5	Fifth Generation Mesoscale Model
MPS	Multiple Projection System
MRF	Medium Range Forecast
NAAQS	National Ambient Air Quality Standards
NARSTO-NE	North American Research Strategy for Tropospheric Ozone - Northeast
NASA	National Aeronautics and Space Administration
NCAR	National Center for Atmospheric Research
NCEP	National Centers for Environmental Prediction
NOAA	National Oceanic and Atmospheric Administration
NO_x	Oxides of Nitrogen
NQS	Network Queuing Service
NSSDC	National Satellite Service Data Center
O_3	Ozone
ODE	Ordinary Differential Equations
OODBMS	Object Oriented Data Base Management System
OUTPRO	MEPPS Output Processor
PACP	Process Anaylsis Control Program
PAN	Peroxy Acetyl Nitrate
PART5	Mobile Source Particulate Model 5
PAVE	Package for Analysis and Visualization of Environmental Data
PBL	Planetary Boundary Layer
PCP	Program Control Processor
PDM	Plume Dynamics Model
PinG	Plume-in-Grid
PM	Particulate Matter
PM10	Particulate Matter less than 10 μm in diameter
PM2.5	Particulate Matter less than 2.5 μm in diameter
PPM	Piecewise-Parabolic Method advective scheme
PSU	Pennsylvania State University
QSSA	Quasi-Steady State Approximation method
RADM	Regional Acid Deposition Model

RADM2	Regional Acid Deposition Model Version 2
RCS	Revision Control System
RELMAP	Regional Lagrangian Modeling of Air Pollution
RMSE	Root Mean Square Error
ROG	Reactive Organic Gases
ROM	Regional Oxidant Model
RPM	Regional Particulate Model
SAPRC	State Air Pollution Research Center chemical mechanisms
SAQM	SARMAP Air Quality Model
SAS	Statistical Analysis System
SCC	Source Classification Code
SCCS	Source Code Control System
SIP	State Implementation Plan
SMO	Smolarkiewicz advection scheme
SMOKE	Sparse Matrix Operator Kernel Emissions system
SMVGEAR	Sparse Matrix Vectorized Gear algorithm
TOG	Total Organic Gases
SO_x	Oxides of Sulfur
STEM	Sulfur Transport and Emissions Model
SVOC	Semi-Volatile Organic Compounds
TKE	Turbulent Kinetic Energy
TOMS	Total Ozone Mapping Spectrometer
UAM	Urban Airshed Model
UCAR	University Corporation for Atmospheric Research
UTC	Universal Time Coordinate
VMT	Vehicle Miles Traveled
VOC	Volatile Organic Compound
WRF	Weather Research and Forecasting
XDR	eXternal Data Representation
YAM	Yamartino-Blackman Cubic Scheme for advection

ACKNOWLEDGMENTS

The development of the science components of the Models-3 Community Multiscale Air Quality (CMAQ) system represents a major undertaking by a large team of dedicated atmospheric scientists and a relatively long term effort beginning in the early 1990s, and covers a wide area of subject material as embodied in each of the contributing chapters. Most of the EPA Models-3 CMAQ Science Team are from the Atmospheric Modeling Division (AMD) in the EPA Office of Research And Development's National Exposure Research Laboratory (NERL). With several exceptions the contributing authors from this Division are on detail from the Air Resources Laboratory of the National Oceanic and Atmospheric Administration (NOAA). The NOAA-AMD effort is supported through Interagency Agreement (DW13937252) with the EPA. The authors of each of the chapters of this document would like to collectively express their gratitude to the other members of the NOAA Division. In particular we acknowledge the encouragement and support of the Director of the Atmospheric Modeling Division, Francis Schiermeier. We are indebted to Dr. Robin Dennis for his vision and role in ensuring the implementation of holistic-one-atmosphere approach into CMAQ. We also recognize the technical help from our colleagues Tom Pierce, Steven Howard, Alfreida Torian, and Gary Walter.

We also want to recognize the contributions, helpful discussions, and assistance of many members of the science community, either through formal agreements or through peer interest. For example, the work was supported by several cooperative agreements including:

- Atmospheric Modeling Research-Scientific and Computational (CR-822066: MCNC), Principal Investigator (PI): Kenneth Galluppi Ed Bilicki, Steve Fine, Alison Eyth, and Rohit Mathur;
- Research on Computational Framework in Generic Grids, Adaptive Grids, and Subgrid Treatment of Air Quality Simulation (CR-822053: MCNC), PI: Talat Odman; with R.K. Srivastava and D.S. McRae, North Carolina State University);
- Transport Algorithms for Air Quality Simulation Models (CR-822059, MCNC), PI: Talat Odman;
- Emissions Modeling Research with High-Performance Computing (CR-822074: MCNC), PI: Carlie Coats;
- Advanced Modeling of Meteorology in Support of Air Quality Models (CR-822628: (MCNC), PI: Aijun Xiu, Kiran Alapaty, John N. McHenry, and Adel F. Hanna; with Nelson L. Seaman and Aijun Deng, Pennsylvania State University; and John S. Kain, National Severe Storms Laboratory);
- A Flexible and Efficient Methodology for Modeling Aerosol for Air Quality Models (CR-823634: MCNC), PI: Uma Shankar, Mark Read and Atanas Trayanov; with Anthony Wexler, University of Delaware; and John H. Seinfeld, California Institute of Technology;
- Develop Methods for Technology Transfer of Advanced Regional/Urban Air Quality Models (CR-822080: NCSU), PI: Alan Schula; and
- Plume-in-Grid development for a Multiscale Air Quality Modeling System (IAG DW64937190, Tennessee Valley Authority (TVA)), PI's: Robert E. Imhoff; with Noor Gillani, Arastoo Biazar (now at Monash University, Australia), and Yu-Ling Lu,

University of Alabama, Huntsville).
The following scientists also contributed under the formal contracts listed: Ruen Tang, Chris Maxwell, and Hao Jin of the Technical Support Group, Dyntel Corp. (General Services Administration IAG DW47937823); Tod Plessel, and Yan Ching Zhang of the Visualization Laboratory, Lockheed Martin (EPA Contract 68-W7-0055); and Nick Moghari, Joe Susick, and Dave Tivel of Science Applications International Corporation (SAIC) (EPA Contract 68-W1-0055).

Significant contributions were made by: visiting scientists, including Sang-Mi Lee of the Seoul National University, Korea, Chong Bum Lee of the KangWeon University, Korea, and Seiji Sugata of the National Institute for Environmental Studies, Japan; UCAR's post doctoral fellows Yonghong Li, Qingyuan Song and Shoba Kondragunta; and Dr. Ingmar Akermann of Ford Research in Aachen, Germany.

It is also a pleasure to thank the colleagues who engaged us in many seminal technical discussions on various aspects of the CMAQ system. We recognize Professors Harvey Jeffries, University of North Carolina at Chapel Hill; Ted Russell, Georgia Institute of Technology; Nelson Seaman and Jack Kain, Pennsylvania State University; Dick McNider, University of Alabama, Sonia Kreidenweis, Colorado State University, Panos Georgeopolus of Rutgers University, and Itsushi Uno of Kyushu University, Japan. Many of our EPA colleagues provided stimulating discussion or reviews of our effort including Gail Tonnesen, Deborah Luecken, Carey Jang, John S. Irwin (NOAA) and Ed Edney.

We are indebted to the following peer reviewers, who gave unselfishly of their time and whose comments and suggestions were extremely valuable in improving the scientific aspects of the report. Listed in alphabetical order, the reviewers are followed by the chapter(s) they reviewed: Jeff Brook, Atmospheric Environment Service, Canada (Ch. 17); David Chock, Ford Research Laboratory (Ch. 2 and 7); Henry Hogo, Southern California Air Quality Modeling Division (Ch. 8 and 16); Sasha Madronich, National Center for Atmospheric Research (Ch. 14); Paulette Middleton, RAND Environmental Science & Policy Center (Ch. 10); Ted Russell, Georgia Institute of Technology (Ch. 18); Nelson Seaman, Pennsylvania State University (Ch. 3); Christian Seigneur, Atmospheric and Environmental Research, Inc. (Ch. 10 and 11); Trevor Sholtz, ORTECH Corporation (Ch. 4); Saffet Tanrikulu, California Environmental Protection Agency (Ch. 9 and 12); Robert Yarmartino, Earth Tech (Ch. 5 and 6); and Zion Wang (Ch. 13, 15, and 16).

Finally, the editors note with great appreciation, the efforts of Brian Eder, who facilitated many of the activities and tasks involved in the preparation and completion of this document. We thank the Raleigh, North Carolina, staff of SAIC, especially Alice Gilliland (now with NOAA-AMD) and Andrea Verykoukis for their critical contributions in the area of technical editing, assuring a high level of consistency and quality in all the chapters of this manuscript. We are also grateful to Alice Gilliland for her invaluable work on the Executive Summary.

EXECUTIVE SUMMARY

THIS SCIENCE DOCUMENT PRESENTS THE PROCESSORS AND ALGORITHMS THAT EMBODY THE INITIAL RELEASE OF THE MODELS-3 COMMUNITY MULTISCALE AIR QUALITY (CMAQ) MODELING SYSTEM. CMAQ IS A MULTIPLE POLLUTANT MODEL THAT CONTAINS NEW SCIENTIFIC APPROACHES TO AIR QUALITY MODELING, WHICH REPRESENT THE CURRENT STATE OF SCIENCE. This CMAQ Science Document is a living document that will be updated as the state of the science progresses. The CMAQ Science Document provides a basis and point of reference for the state of the science captured in the June1998 initial release of Models-3. Current and future efforts to improve the Models-3 modeling system(s) will depart from the scientific reference points presented in this document.

Models-3 is a flexible software system that provides a user-interface framework for CMAQ air quality modeling applications and tools for analysis, management of model input/output, and visualization of data. The Models-3 framework relies on two modeling systems to provide the meteorological and emissions data needed for air quality modeling. With this data, the Models-3 CMAQ modeling system can be used for urban and regional scale air quality simulation of tropospheric ozone, acid deposition, visibility, and particulate matter ($PM_{2.5}$ and PM_{10}). The meteorological and emissions modeling systems that are provided with the current release of Models-3 will be described in this document. However, CMAQ is designed as an open system where alternative models can be used to generate the data.

This CMAQ Science Document contains chapters that address specific scientific and technical issues involved in the development and application of the Models-3 CMAQ modeling system. The principal researchers for each model component or function authored the coinciding chapter in this document. They serve as the points of contact for scientific questions regarding their CMAQ air quality model components. For instructions on using the Models-3 framework and using the MM5, MEPPS, and CMAQ modeling systems, refer to the Models-3 *User Manual* (EPA/600/R-98/069b, National Exposure Research Laboratory, Research Triangle Park, NC) and *Tutorial* (EPA/600/R-98/069c, National Exposure Research Laboratory, Research Triangle Park, NC).

An overview of the MEPPS emissions, MM5 meteorology, and CMAQ air quality modeling systems is provided in Chapter 1. Chapter 2 then introduces the Models-3 framework and structure and explains how the framework's user-interface is used with the MEPPS and CMAQ modeling systems. More detailed discussions on the modeling systems are then discussed separately in the following chapters. The amount of detail and the length of these discussions vary depending on whether this information has already been provided elsewhere. Some chapters provide a synopsis of the scientific components and refer to previously published material on the subject, while other chapters provide extensive detail on new scientific techniques that are not currently described in other publications.

MM5 Meteorological data are essential for many processes simulated in the CMAQ chemical transport model including transport, chemistry, and cloud processes. The Fifth-Generation Penn State/NCAR Mesoscale Model (MM5) is the only meteorology model compatible with the initial release of Models-3. MM5 is a complex, state-of-the-science community model, and it is maintained by NCAR. MM5 is well documented by its primary developers in technical notes and refereed journal articles. Chapter 3 briefly describes the scientific aspects of MM5, including grid definitions, model physics, nesting, and four dimensional data assimilation. These descriptions generally direct the user to more complete documentation about particular aspects of MM5. To promote the flexibility of CMAQ, additional meteorology models will be compatible with Models-3 future releases.

MEPPS Chapter 4 provides a description of the Models-3 Emission Processing and Projection System (MEPPS) structure, its scientific approach, and the assumptions used in modeling and processing emission data in the Models-3 framework. The chapter also discusses data flow and quality control used with emission inventory and meteorological input data for MEPPS. The description of the main Emission Processor addresses the basis of spatial and temporal allocation procedures, and the methods and assumptions used in modeling mobile and biogenic emissions and in the "lumping" of individual chemical species are also presented. This chapter also explains the procedures used by the Models-3 Emission Projection Processor to estimate emission data for use in modeling future air quality scenarios.

THE CMAQ CHEMICAL TRANSPORT MODEL (CCTM)

Fundamentals of One-Atmosphere Dynamics for Multiscale Air Quality Modeling Chapter 5 provides information essential to the proper use of meteorological data in air quality modeling systems. The chapter introduces a robust and fully compressible set of governing equations for the atmosphere, which provides an integral view of atmospheric modeling. The limitations of several simplifying assumptions on atmospheric dynamics are presented, as are concepts of on-line and off-line coupling of meteorological and air quality models. In addition, this chapter describes a procedure for conserving the mixing ratio of trace species even in the case of meteorological data that are not mass consistent. In summary, Chapter 5 attempts to bridge the information gap between dynamic meteorologists and air quality modelers by highlighting the implication of using different meteorological coordinates and dynamic assumptions for air quality simulations.

Governing Equations and Computational Structure In Chapter 6, the governing diffusion equation is derived in a generalized coordinate system, which is suitable for multiscale atmospheric applications. CMAQ's use of generalized coordinates for its governing equations provides the flexibility to span multiple scales and to incorporate meteorological data on different coordinates. The CMAQ system's modularity concepts and fractional time-step formulation, and CCTM's key science processes are described. Chapter 6 also presents the dynamic formulations of several popular Eulerian air quality

models as emulated by the governing diffusion equations in the generalized coordinate system.

Numerical Transport Algorithms The transport processes in the atmosphere primarily consist of advection and diffusion. In Chapter 7, CMAQ's numerical algorithms for advection and vertical and horizontal diffusion are discussed. To provide the CMAQ system with multiscale capability, the transport processes, both advection and diffusion, are formulated in conservation (i.e., flux) forms for the generalized coordinate system. Therefore, CMAQ's numerical transport algorithms will function under a wide variety of dynamical situations and concentration distribution characteristics. Users are encouraged to experiment with their own algorithms to test different numerical schemes for air quality simulations.

Gas Phase Chemistry Chapter 8 examines the way gas-phase chemistry is treated in CMAQ. The CMAQ system currently includes two base chemical mechanisms, RADM2 and CB4, while the incorporation of a third, the SAPRC97 mechanism, is planned for the future. Chapter 8 describes each of these chemical mechanisms as well as the manner in which the first two are linked to the aqueous chemistry and aerosol formation processes. The chapter also discusses procedures for entering new chemical mechanisms in the CMAQ system, the representation of reaction kinetics, the numerical modeling of gas-phase chemistry, and the two numerical solvers included in CMAQ, SMVGEAR and a variant of the QSSA method.

Plume-in-Grid Chapter 9 introduces the plume-in-grid (PinG) technique developed for CMAQ. PinG is designed to treat more realistically the dynamic and chemical processes impacting selected major point source pollutant plumes in CMAQ. The Plume Dynamics Model (PDM) simulates plume rise, horizontal and vertical plume growth, and transport of each plume section during the subgrid scale phase. The PinG module simulates the relevant physical and chemical processes during a subgrid scale phase. This technique is in contrast to the traditional Eulerian grid modeling method of instantly mixing the point source emissions into an entire grid cell volume. Chapter 9 describes the technical approach and model formulation of the relevant processes, and discusses the capabilities and limitations of the initial version of the PinG approach.

The Aerosol Module One of CMAQ's key strengths is that it is a multi-pollutant model that fully addresses the criteria pollutants PM and ozone. Chapter 10 discusses the aerosol module of CMAQ, which is designed to be an efficient and economical depiction of aerosol dynamics in the atmosphere. This chapter discusses the techniques for distributing particulates in three modes: coagulation, particle growth by the addition of new mass, and particle formation. The aerosol module considers both $PM_{2.5}$ and PM_{10} and includes estimates of the primary emissions of elemental and organic carbon, dust, and other species not further specified. Secondary species considered are sulfate, nitrate, ammonium, water and organic from precursors of anthropogenic and biogenic origin.

Cloud Chemistry and Dynamics Chapter 11 discusses the role and functions of clouds in CMAQ. Clouds are involved in aqueous chemical reactions, vertical mixing of pollutants, and removal of aerosols by wet deposition, all of which affect the concentration of air pollutants. CMAQ's cloud module performs several functions related to cloud physics and chemistry, and it models three types of clouds: sub-grid convective precipitating clouds, sub-grid non-precipitating clouds, and grid-resolved clouds. The cloud module vertically redistributes pollutants for the sub-grid clouds, calculates in-cloud and precipitation scavenging, performs aqueous chemistry, and accumulates wet deposition amounts.

CMAQ INTERFACE PROCESSORS PREPARE INPUT DATA FROM SOURCES INCLUDING THE EMISSION AND METEOROLOGICAL MODELING SYSTEMS FOR USE IN THE CMAQ CTM. EACH OF THESE PROCESSORS, EACH OF WHICH HAVE SPECIFIC FUNCTIONS, ARE DESCRIBED IN THE CHAPTERS MENTIONED BELOW. The interface processors that handle input data from the emissions and meteorological models are essential because CMAQ is an open system in which meteorological and emissions data are calculated separately (i.e., "off-line"), rather than during the chemical transport model simulation. These interface processors also add extra quality control, so that inconsistencies between input data and the CCTM are minimized.

ECIP In addition to describing the Models-3 MEPPS emission modeling system, Chapter 4 discusses the Emission-Chemistry Interface Processor (ECIP). ECIP serves as the key link between the MEPPS system and CCTM. ECIP's primary function is to generate hourly 3-D emission data files for CCTM from the individual emission file types produced by the MEPPS. The key inputs for ECIP are the area emissions file, the stack parameter and emission files for the point sources generated in MEPPS, and a set of meteorological data files generated by the Meteorology-Chemistry Interface Processor (MCIP) for the CCTM domain. All major point sources are subject to plume-rise and initial vertical dispersion processes before being allocated to a particular vertical model layer.

MCIP Chapter 12 describes MCIP, which links meteorological models, such as MM5, with the CCTM system to provide the complete set of meteorological data needed for air quality simulation. To support CCTM's multiscale generalized coordinate implementation, MCIP provides appropriate dynamic meteorological parameters to allow mass-consistent air quality computations. MCIP deals with issues related to data format translation, conversion of parameter units, diagnostic estimations of parameters not provided, extraction of data for appropriate window domains, and reconstruction of meteorological data on different grid and layer structures. MCIP also relies on the **Landuse Processor** (LUPROC) to provide landuse and vegetation information to define surface characteristics to compute dry deposition and other PBL parameters. LUPROC extracts information about landuse in the CMAQ domain from a landuse database and converts it into the fractional landuse data used in MCIP.

Initial and Boundary Conditions Initial conditions provide a simulation's starting point, while boundary conditions define influences from outside the domain. Chapter 13 describes the two interface processors that generate the concentration fields for the initial and boundary conditions for CCTM. The chapter describes how the initial condition (ICON) and boundary condition (BCON) processors can be used to generate the concentration fields from either predefined default vertical profiles or from other CMAQ simulation results when model nesting is being performed. This chapter also discusses generating initial and boundary concentrations for special tracer species and procedures for horizontal and vertical interpolation and conversions between chemical mechanisms.

Photolysis Rate Processor Many chemical reactions in the atmosphere are initiated by the photodissociation of numerous trace gases, including NO_2, O_3, and HCHO. Chapter 14 describes the photolysis rate processor (JPROC) that produces the photolysis rates used in the CMAQ chemical transport simulation. JPROC predicts photolysis rates for various altitudes, latitudes, and zenith angles. Currently, the radiative transfer algorithm assumes clear-sky conditions (i.e., no clouds present), and CCTM then attenuates for cloudiness.

As described above, each of the CMAQ interface processors incorporate raw data for CMAQ and perform functions such as calculating parameters and interpolating or converting data. The functions of the interface processors also include capabilities to handle raw data with various resolutions or measurement units. Raw input data is currently specified in the source code for JPROC, LUPROC, ICON, and BCON; however, the interface processors in future releases of CMAQ will be modified to handle a more generalized set of input data.

PROGRAM CONTROL PROCESSORS, A SET OF PROGRAMS EMBEDDED IN THE MODELS-3 FRAMEWORK, HANDLE SCIENCE INFORMATION OBJECTS SUCH AS GRID AND LAYER SPECIFICATIONS, CHEMICAL MECHANISMS, AND MODEL CONFIGURATIONS FOR REPEATED USE ACROSS SEVERAL PROCESS COMPONENTS OF CMAQ.

Program Control Processing (PCP) Chapter 15 explains how PCP is used within Models-3 to set up internal arrays, map species names, define global parameters, and establish linkages among processors in the Models-3 CMAQ system. Specifications needed for the CCTM simulation (e.g., grid and coordinate conditions and chemical species names) are entered into the Models-3 system once by the graphical user interfaces, and an object-oriented database accessible by all model components is established. PCP utilizes this information in the object database and automatically generates the required global FORTRAN include files. As a part of PCP, Models-3 CMAQ system employs a generalized chemistry mechanism processor (MP), also called the "mechanism reader." It greatly simplifies the task of implementing or altering gas-phase chemistry mechanisms

and provides the capability of easily and safely using different mechanisms in the CMAQ system.

Integration of Science Codes into Models-3 One of the major objectives of the Models-3 project was to develop a flexible, comprehensive air quality modeling system with a modular coding structure that allows easy replacement of science process components. Chapter 18 describes the modularity concepts, code management method, and integration schemes of CMAQ science code with the Models-3 framework. The CMAQ FORTRAN code was integrated into the Models-3 framework with the following set of design, coding, and implementation standards: (1) modularity to allow easy exchange of science process solvers, (2) a standard subroutine interface at the module level, (3) restriction of coding practices, (4) the Models-3 I/O API (http://www.iceis.mcnc.org/EDSS/ioapi/index.html/), which contains standardized file I/O functions and a modeler-friendly interface built on top of self-describing netCDF (http://www.unidata.ucar.edu/packages/netcdf/) files that are portable across most Unix platforms.

MODELS-3 ALSO PROVIDES ANALYSIS ROUTINES FOR USE WITH CMAQ OUTPUT, WHICH CAN BE USED TO PROVIDE PROCESS ANALYSIS RESULTS AND STATISTICAL AGGREGATION TECHNIQUES.

Process Analysis Chapter 16 describes the implementation of process analysis techniques in the CMAQ modeling system. These techniques can be used in CMAQ to provide insights into how model predictions are obtained, which is particularly useful when modeling nonlinear systems like atmospheric photochemistry. Two techniques are available in the CMAQ system, integrated process rate (IPR) analysis and integrated reaction rate (IRR) analysis. IPR analysis can be used to determine the relative contributions of individual physical and chemical processes, and IRR analysis can help elucidate important chemical pathways and identify key chemical characteristics.

Aggregation Chapter 17 discusses a statistical procedure called aggregation that is applied to CMAQ's outputs in order to derive the seasonal and annual estimates required by assessment studies. Assessment studies require CMAQ-based distributional estimates of ozone, acidic deposition, and $PM_{2.5}$, as well as visibility, on seasonal and annual time frames. Unfortunately, it is not financially feasible to execute CMAQ over such extended time periods. Therefore, in practice CMAQ must be executed for a finite number of episodes or "events," which are selected to represent a variety of meteorological classes. The aggregation technique is used to incorporate these episode simulations into annual and seasonal estimates.

THE MODEL-3 CMAQ MODELING SYSTEM IS BEING FORMALLY EVALUATED TO ASSESS THE PERFORMANCE OF CMAQ'S NEW DEVELOPMENTS IN AIR QUALITY

MODELING. THE EVALUATION WILL PROVIDE THE BASIS FOR UNDERSTANDING THE STRENGTHS OR WEAKNESSES OF THE CURRENT STATE-OF-SCIENCE IN CMAQ. With an evaluation of CMAQ simulations of 36, 12, and 4 km grid resolution, CMAQ's performance can be evaluated on both the regional and urban scales. This evaluation will include an initial comparison of relative performance against the RADM model and diagnostic evaluation against databases from regional studies such as the 1995 Southern Oxidant Study conducted in the vicinity of Nashville, TN and the 1995 NARSTO-NE study.

CMAQ can be configured for a wide range of applications, from scientific studies to regulatory applications. While the scientific community can take advantage of CMAQ's ability to create alternative applications for research and development purposes, regulatory applications depend upon a standardized, evaluated form of CMAQ for regulatory applications. The CMAQ evaluation program will provide the scientific benchmark needed for this.

FUTURE EXTENSIONS OF CMAQ INCLUDE NEAR-TERM EFFORTS TO PROVIDE A NEW CHEMICAL MECHANISM AND EMISSION MODELING SYSTEM.

> **The SAPRC-97 gas phase mechanism** will soon be incorporated into CMAQ, in addition to the current CB-IV and RADM2 mechanisms available. The SAPRC mechanism will be incorporated with a fixed subset of the approximately 100 organic species contained in the semi-explicit version of the SAPRC mechanism.
>
> **The Sparse Matrix Operator Kernel Emissions modeling system (SMOKE)** (http://envpro.ncsc.org/products/) will also be incorporated into CMAQ in the near-term. The SMOKE model formulates emissions modeling in terms of sparse matrix operations which require considerably less time to perform than current systems.

WE ENCOURAGE THE FULL PARTICIPATION AND INVOLVEMENT OF THE SCIENTIFIC AND MODELING COMMUNITIES IN THE GROWTH AND USE OF MODELS-3 CMAQ. THERE ARE MANY IDEAS AND PLANS FOR FUTURE DEVELOPMENTS OF CMAQ, INCLUDING TOXIC POLLUTANT MODELING AND LINKAGES TO OTHER MODELS.

> **Modeling atmospheric toxic pollutants** A key opportunity for CMAQ is developing the capability to model toxic pollutants. Models of airborne toxic pollutants are essential for human exposure and risk assessments. They can also be used to assess the exchange of toxic compounds between the atmosphere and sensitive ecosystems. With the ability to simulate toxic pollutant processes in addition to the current photochemical oxidants and particulates, it is planned to transport the CMAQ model to a finer than urban scale to link with human exposure models.

New linkages with global models It is hoped that information from the urban and regional CMAQ applications and from global modeling applications can be bridged. CMAQ output, produced using state of the science techniques, can be used to benchmark or examine the parametric basis of process formulations in global models. In addition, global model output can be used to improve or enhance the initial and boundary conditions for regional and urban scale CMAQ simulations.

Modeling ecosystems Efforts to combine environmental modeling techniques to encompass an entire ecosystem is needed to address issues including (a) nutrient cycling through the atmosphere, water bodies, and soil and (b) acidic wet and dry deposition into sensitive ecosystems, including critical load analyses. With this ecosystem modeling approach, air quality issues can be studied in combination with other aspects of environmental health.

This is the Executive Summary of *Science Algorithms of the EPA Models-3 Community Multiscale Air Quality (CMAQ) Modeling System*, edited by D. W. Byun and J. K. S. Ching, 1999.

EPA/600/R-99/030

Chapter 1

INTRODUCTION TO THE MODELS-3 FRAMEWORK AND THE COMMUNITY MULTISCALE AIR QUALITY MODEL (CMAQ)

Jason Ching* **and Daewon Byun****
Atmospheric Modeling Division
National Exposure Research Laboratory
U.S. Environmental Protection Agency
Research Triangle Park, NC 27711

ABSTRACT

Models-3, a flexible software framework, and its Community Multiscale Air Quality (CMAQ) modeling system form a powerful third generation air quality modeling and assessment tool designed to support air quality modeling applications ranging from regulatory issues to science inquiries on atmospheric science processes. The CMAQ system can address tropospheric ozone, acid deposition, visibility, fine particulate and other air pollutant issues in the context of "one" atmosphere perspective where complex interactions between atmospheric pollutants and regional and urban scales are confronted. This CMAQ Science Document contains chapters that address specific scientific and technical issues involved in the development and application of Models-3/CMAQ system; collectively, it provides the scientific basis and point of reference for the state of the science captured in the June 1998 initial release of the CMAQ. This chapter provides an overview and context of each contributing chapter to the CMAQ system.

---

*On assignment from the National Oceanic and Atmospheric Administration, U.S. Department of Commerce. Corresponding author address: Jason Ching, MD-80, Research Triangle Park, NC 27711.
E-mail: Ching.Jason@epamail.epa.gov

**On assignment from the National Oceanic and Atmospheric Administration, U.S. Department of Commerce.

1.0 INTRODUCTION TO THE MODELS-3 FRAMEWORK AND THE COMMUNITY MULTISCALE AIR QUALITY MODEL (CMAQ)

Air quality simulation models are important tools for regulatory, policy, and environmental research communities. In the United States, the Clean Air Act provides a societal mandate to assess and manage air pollution levels to protect human health and the environment. The U.S. Environmental Protection Agency (USEPA) has established National Ambient Air Quality Standards (NAAQS), requiring the development of effective emissions control strategies for such pollutants as ozone, particulate matter, and nitrogen species. National and regional policies are needed for reducing and managing the amount and type of emissions that cause acid, nutrient and toxic pollutant deposition to ecosystems at risk and for enhancing the visual quality of the environment. Air quality models are used to develop emission control strategies to achieve these objectives. Optimal control strategies should be both environmentally protective and cost effective. Up to now, air quality model paradigms typically addressed individual pollutant issues separately. However, it is becoming increasingly evident that when pollutant issues are treated in isolation, the resulting control strategies may solve one set of problems but may lead to unexpected aggravation of other related pollutant issues. Pollutants in the atmosphere are subject to myriad transport processes and transformation pathways that control their composition and levels. Also, pollutant concentration fields are sensitive to the type and history of the atmospheric mixtures of different chemical compounds. Thus, modeled abatement strategies of pollutant precursors, such as volatile organic compounds (VOC) and NO_x, to reduce ozone levels may under a variety of conditions, cause an exacerbation of other air pollutants such as particulate matter or issues of acidic deposition.

The development of comprehensive air quality models started in the late seventies. The Urban Airshed Model (UAM) (Morris and Meyers, 1990) followed by the Regional Oxidant Model (ROM) (Lamb, 1983a, 1983b) provided Eulerian-based models for ozone, the former for urban and the latter for regional scale. Strategies for State Implementation Plans (SIPs) used ROM to provide boundary conditions for UAM simulations. Attention to acid deposition issues were addressed in the eighties with the development and evaluation of regional acid deposition models such as the Regional Acid Deposition Model (RADM) (Chang et al., 1987; Chang et al., 1990), the Acid Deposition and Oxidant Model (ADOM) (Venkatram et al., 1988), and the Sulfur Transport and Emissions Model (STEM) (Carmichael and Peters, 1984a, 1984b; Carmichael et al., 1991). Other major modeling systems included the Regional Lagrangian Modeling of Air Pollution model (RELMAP) (Eder et al., 1986), a Lagrangian framework system, and semi-empirical and statistical models. The genre of models of this period were designed to address specific air pollution issues such as ozone or acid deposition and to be applied under relatively prescriptive implementation guidance strategies. Thus, flexibility to deal with other issues, such as particulate matter or toxics, was very limited. Further, With the passage of the Clean Air Act Amendments of 1990 (CAAA-90), a wide range of additional issues were identified including visibility, fine and coarse particles, indirect exposure to toxic pollutants such as heavy metals, semi-volatile organic species, and nutrient deposition to water bodies. The direct response approach is to modify, adapt or extend current models to handle more complex implementations and issues but is both cumbersome and limiting.

Seeking a more strategic approach to handle the increased modeling requirements of the CAAA-90, more comprehensive modeling approaches appear to be needed. With projections for the increasing rapid pace of the development of computational capabilities at the start of the nineties, the opportunity arose for a strategic review of modeling approaches leading to design of a system that would both meet and keep pace with the increasing requirements on air quality modeling, of incorporating advances in state-of-science descriptions of atmospheric processes, as well as eliminate impediments of the current genre of models. The scope of such a system must be able to process great and diverse information from complicated emissions mixtures and complex distributions of sources, to modeling the complexities of atmospheric processes that transport and transform these mixtures in a dynamic environment that operates on a large range of time scales covering minutes to days and weeks. The corresponding spatial scales are commensurately large, ranging from local to continental scales. On these temporal and spatial scales, emissions from chemical manufacturing and other industrial activities, power generation, transportation, and waste treatment activities contribute to a variety of air pollution issues including visibility, ozone, particulate matter (PM), and acid, nutrient and toxic deposition. The residence times of pollutants in the atmosphere can extend to multiple days, therefore transport must be considered on at least a regional scale. NAAQS requirements and other goals for a cleaner environment vary over a range of time scales, from peak hourly to annual averages. These challenges suggest that more comprehensive approaches to air quality modeling are needed, and that assessments and pollution mitigation are achieved more successfully when the problems are viewed in a "one atmosphere" context that considers multiple pollutant issues. Further discussion of the needs for the third-generation air quality modeling system can be found in Dennis et al. (1996) and Dennis (1998).

To meet both the challenges posed by the CAAA-90 and the need to address the complex relationships between pollutants, the USEPA embarked upon the Models-3 project and developed the Community Multiscale Air Quality (CMAQ) system, an advanced air quality modeling system that addressed air quality from this "one atmosphere" multi-pollutant perspective. Based on its conceptual design, the high performance computational Models-3 framework serves to manage and orchestrate air quality simulations, using the CMAQ modeling system. The Models-3 framework is an advanced computational platform that provides a sophisticated and powerful modeling environment for science and regulatory communities. The framework provides tools used to develop and analyze emission control options, integrate related science components into a state-of-the-art quality modeling system, and apply graphical and analytical tools for facilitating model applications and evaluation. Descriptions of the Models-3 architecture are provided in **Chapter 2** and in Novak et al. (1998). CMAQ is a multi-pollutant, multiscale air quality model that contains state-of-science techniques for simulating all atmospheric and land processes that affect the transport, transformation, and deposition of atmospheric pollutants and/or their precursors on both regional and urban scales. It is designed as a science-based modeling tool for handling all the major pollutant issues (including photochemical oxidants, particulate matter, acidic, and nutrient deposition) holistically.

More than six years of investment and commitment from Federal staff and from scientists and model developers from the environmental and information communities were expended to develop the Models-3 framework and the CMAQ air quality modeling system. Models-3 CMAQ

was released to the public in June 1998. The science and model engineering concepts and progress of the project have been described in two peer-reviewed AWMA Transaction papers (Byun et al., 1995a; Coats et al., 1995) and others (Byun et al., 1995b, 1996, and 1998a; Ching et al., 1995). This release version of the Model-3 software is supported by the following documents under the overall heading "Third Generation Air Quality Modeling System":

- System Installation and Operations Manual. EPA/600/R-98/069a, National Exposure Research Laboratory, EPA, Research Triangle Park, NC
- Users Manual. EPA/600/R-98/069b, National Exposure Research Laboratory, Research Triangle Park, NC
- Tutorial. EPA/600/R-98/069c, National Exposure Research Laboratory, EPA, Research Triangle Park, NC
- Science Concepts of the Third Generation Air Quality Models: Project Report. In preparation. Edited by D.W. Byun and A. Hanna. National Exposure Research Laboratory, EPA, Research Triangle Park, NC
- Science Algorithms of the EPA Models-3 Community Multiscale Air Quality (CMAQ) Modeling System, Edited by D.W. Byun and J.K.S. Ching. National Exposure Research Laboratory, EPA, Research Triangle Park, NC (this document)

The project report "Science Concepts of the Third Generation Air Quality Models" summarizes the basic atmospheric science concepts and mathematical principles pertinent to the development of the third generation air quality modeling. This document discusses the key scientific features and options incorporated into the Models-3 CMAQ modeling system.

1.1 The Models-3 Emissions, Meteorology, and the CMAQ Modeling Systems

The structure of the Models-3/CMAQ system is shown in Figure 1-1. Orchestrated through the Models-3 system framework, the Community Multiscale Air Quality (CMAQ) modeling system incorporates output fields from emissions and meteorological modeling systems and several other data source through special interface processors into the CMAQ Chemical Transport Model (CCTM). CCTM then performs chemical transport modeling for multiple pollutants on multiple scales. With this structure, CMAQ retains a flexibility to substitute other emissions processing systems and meteorological models. One of the main objectives of this project was to provide an air quality modeling system with a "one atmosphere" modeling capability based mainly on the "first principles" description of the atmospheric system. CMAQ contains state-of-science parameterizations of atmospheric processes affecting transport, transformation, and deposition of such pollutants as ozone, particulate matter, airborne toxics, and acidic and nutrient pollutant species. With science in a continuing state of advancement and review, the modeling structure of CMAQ is designed to integrate and to test future formulations in an efficient manner, without requiring the development of a completely new modeling system. Contents of the CMAQ in the

June 1998 release version of Models-3 are summarized in Ching et al. (1998) and Byun et al. (1998b).

Currently, the Models-3 Emission Projection and Processing System (MEPPS) produces the emissions and the Fifth Generation Penn State University/ National Center for Atmospheric Research Mesoscale Model (MM5) provides the meteorological fields needed for the CCTM. They are considered to meet the present application needs for diverse air pollution problems in urban and regional scales. However, given the CMAQ paradigm, and other considerations, the emissions processing and meteorological modeling systems can be replaced with alternative processors.

Each of these three modeling systems are described briefly below, where associated chapters of this document are highlighted to provide directions to more in-depth discussions of these topics:

- The PSU/NCAR MM5 meteorological modeling system (Grell et al., 1994) generates the meteorological fields for CMAQ. MM5 is a complex, state-of-the-science community model, which is maintained by NCAR. MM5 is well-documented by its primary developers in technical notes and referenced journal articles. **Chapter 3** briefly describes the scientific aspects of MM5, including grid definitions, model physics, nesting and four-dimensional data assimilation.

- The MEPPS emission modeling system is based on the Geocoded Emission Modeling and Projection System (GEMAP) (Wilkinson et al., 1994) now known as the Emission Modeling System-95 (EMS-95). MEPPS processes emission inventory data, performs future projections (including control scenarios), and pre-processes data for use in the CMAQ model (**Chapter 4**). It provides speciated emissions consistent with CB-IV or RADM2 chemistry mechanisms.

- The CMAQ chemical transport modeling system (CCTM) is then used to perform model simulations for multiple pollutants and multiple scales with these input data (**Chapters 6, 7, 8, 9, 10 and 11**). The fundamental concepts used for the one-atmosphere dynamic modeling is described in **Chapter 5**. The techniques used for the management of CMAQ's source code are discussed in **Chapter 18**.

  The CMAQ modeling system also includes interface processors that process input data for the emission and meteorological modeling systems, and other processors that calculate photolysis rates, and develop initial and boundary conditions (**Chapters 4, 12, 13, and 14**). CMAQ also has an internal program control processor which is discussed in **Chapter 15**.

  Using the analysis routines provided in Models-3, the CMAQ output can be processed to provide process analysis information (**Chapter 16**) and/or analyzed further to provide aggregated statistical information (**Chapter 17**).

An important design requirements for CMAQ is that it addresses multiple scales and pollutants, which requires that governing equations and computational algorithms among the different systems should be consistent and compatible across the multiple scales. However, modeling assumptions used in various modeling systems may not be valid across all scales. For example, the atmospheric dynamics description in a meteorological model may have been optimized for application of certain scale or limited range of scales (e.g., global vs mesoscale vs complex terrain to urban). It is incumbent upon the user community to ensure the model component formulations are applicable to the range of scales upon which CMAQ is applied. The current version of MM5 and the CCTM is designed for regional to urban scales. Furthermore, when using nesting procedures to scale down from regional to urban scales and for avoiding feedback between the scales, one way nesting is recommended. In addition to the challenges of creating a multiscale air quality model, CMAQ's multi-pollutant capability cannot be achieved if the emissions modeling system does not provide appropriate precursor or pollutant emissions to the chemical transport model (CTM). The development of Models-3 and CMAQ overcome these hurdles by providing the flexibility to modify specific requirements (e.g., chemical mechanisms, model inputs, etc.), a generic coordinate system that ensures consistency across spatial scales, and user interfaces that can integrate alternative emissions or meteorological modeling systems.

1.2 CMAQ Interface Processors

The CMAQ modeling system includes interface processors to incorporate the outputs of the meteorology and emissions processors and to prepare the requisite input information for initial and boundary conditions and photolysis rates to the CCTM. Figure 1-1 illustrates the relationship and purpose of each of the CMAQ processors (and requisite interfaces) and their relation to the chemical transport modeling system. The arrows show the flow of data through the modeling system. Two additional functional features of the CMAQ system are included, one for process analysis, which is primarily for model diagnostic analyses, and a second one that is an aggregation methodology for estimating longer term averaged fields. Each of these processors is described briefly below, and the associated chapter numbers are also listed to note where detailed discussions can be found on the topics.

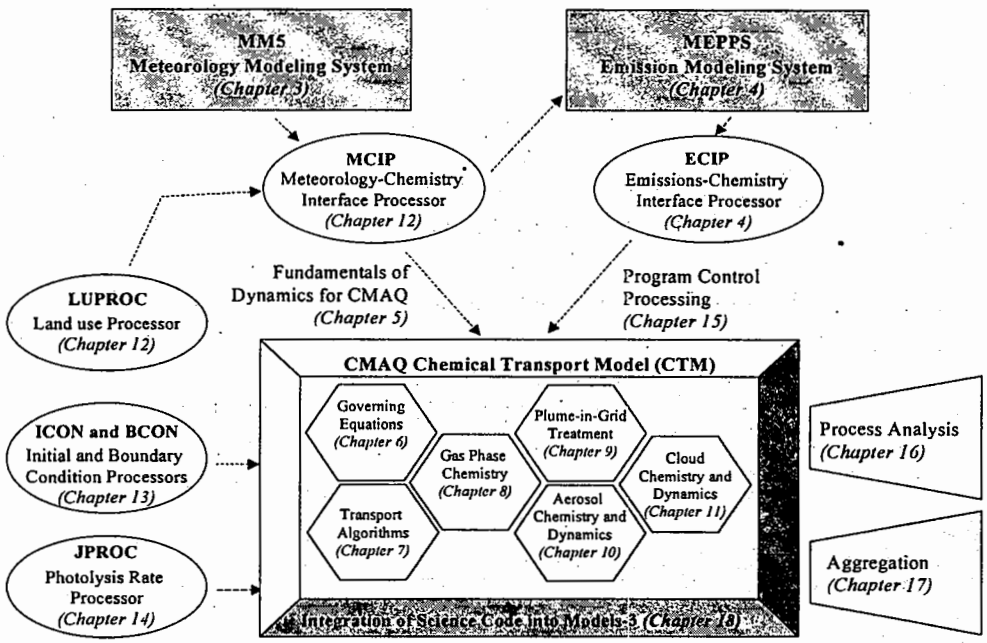

Figure 1-1. Emissions and Meteorological modeling systems and the CMAQ Chemical Transport Model and Interface Processor

- The Emission-Chemistry Interface Processor (ECIP) translates data from the MEPPS emission model for use in the CCTM. ECIP generates hourly three-dimensional emission data for CMAQ from the separate source type files produced by MEPPS, which include mobile, area, and point sources (**Chapter 4**). ECIP calculates the plume rise and initial vertical plume spread of point source emissions to determine the vertical level(s) of CCTM into which point source emissions should be introduced. Since meteorological conditions affect both point source plume rise and biogenic emissions, meteorological data from MCIP is also used in ECIP.

- The Meteorology-Chemistry Interface Processor (MCIP) translates and processes model outputs from the meteorology model for the CCTM (**Chapter 12**). MCIP interpolates the meteorological data if needed, converts between coordinate systems, computes cloud parameters, and computes surface and planetary boundary layer (PBL) parameters for the CCTM. MCIP uses landuse information from the landuse processor (LUPROC) to calculate the PBL and surface parameters.

- Initial Conditions and Boundary Conditions (ICON and BCON) provide concentration fields for individual chemical species for the beginning of a simulation and for the grids surrounding the modeling domain, respectively. The ICON and BCON processors (**Chapter 13**) use data provided from previous three-dimensional model simulations or

from clean-troposphere vertical profiles. Both the vertical profiles and modeled concentration fields have a specific chemical mechanisms associated with them, which are a function of how these files were originally generated.

- The photolysis processor (JPROC) calculates temporally varying photolysis rates (**Chapter 14**). JPROC requires vertical ozone profiles, temperature profiles, a profile of the aerosol number density, and the earth's surface albedo to produce the photolysis rates for the CCTM. JPROC uses this information in radiative transfer models to calculate the actinic flux needed for calculating photolysis rates. JPROC generates a lookup table of photo-dissociation reaction rates.

Each of these CMAQ interface processors incorporates raw data into CMAQ and performs functions such as calculating parameters and interpolating or converting data. Raw input data is currently specified in the source code for JPROC, LUPROC, ICON, and BCON. However, the interface processors in future releases of CMAQ will be modified to handle a more generalized set of raw input data, so that alternative data sets with varying resolutions or measurement units can be used.

1.3 The CMAQ Chemical Transport Model (CCTM)

The CCTM simulates the relevant and major atmospheric chemistry, transport and deposition processes involved throughout the modeling domains. The fundamental basis for CMAQ's one-atmosphere dynamics modeling is discussed in **Chapter 5**. Governing equations and model structure, including definitions of CMAQ's science process modules, are discussed in **Chapter 6**. The science options available to the user include the gas phase chemistry mechanisms, RADM2 and CB-IV, a set of numerical solvers for the mechanisms, options for horizontal and vertical advection schemes, algorithms for fine and coarse particulate matter predictions, photolysis rates, and a plume-in-grid approach. Through the Models-3 framework, CMAQ simulations can be developed using these different options without modifying source code. A general overview of these science process options is provided below along with a reference to the chapter(s) of this document where more scientific detail can be found.

- Advection and Diffusion (**Chapter 7**): Several advection methods are implemented in the CMAQ; these include a scheme by Bott (1989), a piecewise parabolic method (PPM) (Collela and Woodward, 1984), and the Yamartino-Blackman cubic algorithm. Options for computing subgrid vertical transport include eddy diffusion, and the Asymmetric Convective Model (ACM) (Pleim and Chang, 1992) applicable to convective conditions. Horizontal diffusion is modeled using a constant eddy diffusion coefficient. Numerical methods differ in the handling of advection of concentration fields.

- Gas Phase Chemistry (**Chapter 8**): CMAQ includes both the RADM2 and CB4 gas-phase chemical mechanisms. The CMAQ version of CB4 includes the most recent representation of isoprene chemistry and two additional variants of the RADM2 mechanism also contain the newer isoprene chemistry at two levels of detail. In addition,

CMAQ provides the capability to edit these mechanisms or to import a completely new mechanism by means of a generalized chemical mechanism processor. CMAQ also accounts for the formation of secondary aerosols and the reactions of pollutants in the aqueous phase, and aqueous reactions are simulated by means of the aqueous chemical mechanism incorporated in RADM. All CMAQ gas-phase mechanisms are linked to these processes to provide the capability to simulate multi-phase interactions.

Two chemistry solvers are available -- the Sparse Matrix Vectorized Gear (SMVGEAR) algorithm developed by Jacobson and Turco (1994) and the Quasi-Steady State Approximation (QSSA) method used in the Regional Oxidant Model. SMVGEAR is generally recognized as the more accurate of the two, but it is much slower than QSSA on non-vector computers.

- Plume-in-Grid (PinG) Modeling (**Chapter 9**): CMAQ includes algorithms to treat subgrid scale physical and chemical processes impacting pollutant species in plumes released from selected Major Elevated Point Source Emitters (MEPSEs). The PinG modules simulate plume rise and growth, and the relevant dynamic and chemical reaction processes of subgrid plumes. PinG can be used for the simulations at 36 km and 12 km resolutions, PinG is not invoked at 4 km resolutions and the MEPSE emissions are directly released into the CTM 3-D grid cells.

- Particle Modeling and Visibility (**Chapter 10**): One of the major advancements in CMAQ is the modeling of fine and coarse mode particles, with the use of the fine particle model described in Binkowski and Shankar (1995). CMAQ predicts hourly gridded concentrations of fine particle mass whose size is equal to or less that 2.5 microns in diameter ($PM_{2.5}$), speciated to sulfate, nitrate, ammonium, organics and aerosol water. Secondary sulfate is produced when hydroxyl radicals react with sulfur dioxide to produce sulfuric acid that either condenses to existing particles or nucleates to form new particles. CMAQ model output includes number densities for both fine and coarse modes. The modeling of aerosols in CMAQ also provides the capability to handle visibility, which is another CMAQ output. In another potential application, CMAQ can provide the basis for modeling the atmospheric transport and deposition of semi-volatile organic compounds (SVOC) with parameterizations for their rates of condensation to and/or volatilization from the modeled particles.

- Cloud processes (**Chapter 11 and 12**): Proper descriptions of clouds are essential in air quality modeling due to their critical role in atmospheric pollutant transport and chemistry processes. Clouds have both direct and indirect effects on the pollutant concentrations: they directly modify concentrations via aqueous chemical reactions, vertical mixing, and wet deposition removal processes, and they indirectly affect concentrations by altering radiative transmittances which affect photolysis rates and biogenic fluxes. CMAQ models deep convective clouds (Walcek and Taylor, 1986) and shallow clouds using the algorithms as implemented in RADM (Dennis et al., 1993) for 36 and 12 km resolutions. At 4 km resolution, the clouds are generally resolved, and explicit type cloud dominates.

- Photolysis Rates (**Chapter 14**): The photochemistry of air pollutants is initiated by photodissociation of smog precursors, which are driven by solar radiation. The amount of solar radiation is dependent on sun angle (time of day), season, latitude, and land surface characteristics, and is greatly affected by atmospheric scatterers and absorbers. Photolytic rates are also wavelength- and temperature-dependent. Within CCTM, temporally resolved 3-D gridded photolysis rates are interpolated from a lookup table generated by JPROC processor and corrected for cloud coverage.

1.4 Analysis of CMAQ Output

Air quality modeling simulations arise from modeling of complex atmospheric processes. It is important to assure and to understand the model results. Sensitivity tests are needed to detect problems in model formulations and to determine if the model is credible for assessing emission control strategies. A very powerful sensitivity analysis tool called process analysis is provided with CMAQ. Also, an aggregation technique is provided with CMAQ. Aggregation can be used to estimate seasonal or annual concentrations for pollutants from CMAQ simulations which are usually performed for shorter time periods due to time and computational limitations.

1.4.1 Process Analysis (Chapter 16)

Sensitivity analyses are needed to detect errors and uncertainties introduced into a model by the parameterization schemes and the input data. Results must also be analyzed to ensure that realistic values are obtained for the right reasons rather than through compensating errors among the science processes. Process Analysis techniques quantify the contributions of individual physical and chemical atmospheric processes to the overall change in a pollutant's concentration, revealing the relative importance of each process. Process analysis is particularly useful for understanding the effects from model or input changes. CMAQ provides the capability to perform process analyses using two different pieces of information: Integrated Process Rates (IPRs) and Integrated Reaction Rates (IRRs).

- The IPRs are obtained during a model simulation by computing the change in concentration of each species caused by physical processes (e.g., advection, diffusion, emissions), chemical reaction, aerosol production, and aqueous chemistry. Values provide only the *net* effect of each process. IPRs are particularly useful for identifying unexpectedly low or high process contributions which could be indicative of model errors.

- The IRR analysis involves the details of the chemical transformations. For gas-phase chemistry, the CCTM has been designed to compute not only the concentration of each species, but also the integral of the individual chemical reaction rates. IRR analyses have typically been used to understand the reasons for differences in model predictions obtained with different chemical mechanisms.

1.4.2 Aggregation (Chapter 17)

In support of studies mandated by the CAAA-90, CMAQ can be used to estimate deposition and air pollutant concentrations associated with specific levels of emissions. Assessment studies require estimates of ozone, acidic deposition, particulate matter as well as visibility, on seasonal and annual time frames. A statistical procedure called the "aggregation" has been developed and is provided for the CMAQ to derive the required seasonal and annual estimates. This methodology is an efficient technique and can be used instead of executing multiple CMAQ model runs for the intended period of averaging.

A typical CMAQ simulation provides hourly air quality fields for regional to urban scales for multi-day episodes, typically up to five days in duration. The new $PM_{2.5}$ standard includes an annual average value, so utilization of CMAQ for $PM_{2.5}$ will require the use aggregation techniques in order to estimate annual average $PM_{2.5}$ values. One such technique, initially developed for RADM wet deposition applications, was recently modified and successfully applied to $PM_{2.5}$ by Eder and LeDuc (1996). The approach utilizes visibility data as a surrogate for $PM_{2.5}$, and it will be applied to CMAQ on a continental scale (i.e., contiguous United States, southern Canada, and northern Mexico). Future efforts will be needed to validate this approach when a network of $PM_{2.5}$ samplers is deployed; also, aggregation approaches for mesoscale domains will need to be developed perhaps utilizing the method by Eder and LeDuc (1994).

1.5 Management of CMAQ Science Information Objects and Codes in Models-3

The CMAQ source code is managed through the Models-3 framework to make the CMAQ modeling system more efficient and easier to use by applying a program control processor, management and integration of source code, and implementing a modularity concept. These techniques also help users customize CMAQ for their own modeling applications without source code modifications.

1.5.1 Program Control Processors (Chapter 15)

Certain science information, such as grid and layer definitions and dimensions, chemical mechanisms, species list, model configurations, and episode (case) specification, is used repeatedly across the several process components in Models-3 CMAQ modeling system. Program control processors are a set of programs embedded in the Models-3 framework to handle these science information components and their codes. Program Control Processing (PCP) refers to setting up internal arrays, mappings of species names in the input processors, defining global parameters, and establishing linkages among processors in the CMAQ system. PCP allows users to define globally shared information on model components, and it uses that information to generate the global FORTRAN include files required for building a model in CMAQ.

1.5.2 CMAQ Code Integration (Chapter 18)

CMAQ's modularity facilitates efficient coordination of development work and management of the science codes. Chapter 18 describes the modularity concepts, code management method, and integration schemes of CMAQ science code with the Models-3 framework. Integrating the CMAQ code into the Models-3 framework is achieved by following a set of design, coding, and implementation standards that include:

- A standard subroutine interface at the module level
- The restriction of coding practices to avoid practices that can conceal data dependencies, hinder maintenance and foster hidden bugs
- The Models-3 Input/Output Applications Programming Interface (I/O API) (http://www.iceis.mcnc.org/EDSS/ioapi/index.html/), which contains standardized file I/O functions. The I/O API is an interface built on top of self-describing netCDF (http://www.unidata.ucar.edu/packages/netcdf/) files that are portable across most Unix platforms.

1.6 Post Release Studies and Near-Future Plans

1.6.1 CMAQ Evaluation Study

It is important to conduct extensive evaluation of the CMAQ. Subsequent to the initial release of the Models-3/CMAQ, the development team is engaged in a substantial program of evaluation. The scope of the effort includes analyses of the performance and veracity of each individual process module as well as the integrated air quality system. Findings from this evaluation can be incorporated into future releases of the CMAQ modeling system. The degree and rigor of this evaluation provides the basis for understanding the strengths or weaknesses of the current state-of-science in CMAQ. The evaluation of the initial release version of CMAQ is underway for three nested grids with 36, 12, and 4 km grid resolutions. With these results, CMAQ's performance can be evaluated on both the regional and urban scales. This model evaluation activity for CMAQ will be staged with the initial efforts to show relative performance against the RADM model, which has undergone extensive model evaluation efforts. Diagnostic evaluation will continue using databases from different regional studies such as the 1995 Southern Oxidant Study conducted in the vicinity of Nashville, TN and the 1995 NARSTO-NE study.

1.6.2 Testing Operational Configurations

CMAQ can be configured for a wide range of applications from science studies and investigations to regulatory applications. While the scientific community can take advantage of the CMAQ open system and flexibility to create alternative applications of CMAQ for research and development purposes, regulatory applications depend upon a standardized, evaluated form of CMAQ. The CMAQ evaluation program will provide the scientific benchmark needed for this. As science advances in CMAQ, future configurations of a more operational nature can also be periodically

re-benched as appropriate. As understanding of atmospheric processes improves, it is a natural tendency for models to become more complex and have increased computational demands. Efforts are underway to improve model computational efficiencies to compensate for this.

1.6.3 Extensions and Science Additions

Two major extensions are planned for the CMAQ modeling

- A version of the SAPRC-97 gas phase mechanism will be incorporated into CMAQ, in addition to the current CB-IV and RADM2 mechanisms available. The initial configuration of SAPRC will be in a fixed parameter mode, with a preset number of organic species. Another possible future implementation of SAPRC will allow the user to select from about 100 organic surrogate species in the semi-explicit SAPRC mechanism to construct a user-defined, smaller SAPRC mechanism. Another approach for representing gas-phase chemistry in CMAQ is also being developed. It will use a limited number reactive entities termed "morphecules" to include in the chemical reactions while using a much larger number of chemical species (singly or lumped) called allomorphs to provide extra chemical detail. This latter approach provides a means for including a much more detailed representation of atmospheric chemistry than conventional chemical mechanisms without significantly increasing computational burden, albeit at the expense of additional computer memory.

- A new emissions processor will be implemented which is called the Sparse Matrix Operator Kernel Emissions modeling system (SMOKE) (http://envpro.ncsc.org/products/). The linear operations used in emission processing can be represented as multiplications by matrices. Since most entries in these matrices are zeros, the SMOKE model formulates emissions modeling in terms of sparse matrix operations that require considerably less time to perform than current systems. Efficiency is enhanced even further when considering variations in emissions projections from base case scenarios by temporally modeling once per episode, calculating gridding matrices only once per grid, and calculating speciation matrices only once per chemical mechanism.

Development and testing of several science options is underway for incorporation into future releases of the CMAQ. These include an advanced surface-PBL linked system (Pleim and Xiu, 1995), optional meteorological processors such as the Regional Atmospheric Modeling System, RAMS, and an advanced 4-D Photolysis Rates Processor.

1.7 Opportunities and Encouragement for Long Term Extensions and Science Community Involvement

The Models-3/CMAQ concept is based on an open system design, we encourage the full participation and involvement of the scientific and modeling communities in the growth and use of Models-3 CMAQ. As described in this document, the Models-3 CMAQ system has flexibility for incorporating scientific and modeling advances into CMAQ processors, for testing of

alternative modeling techniques for science processes, and for extending its current capability to handle multimedia environmental issues. Additionally, the community of users should be vigilant in performing evaluations against improved databases and measurement technology to assess the realism of model performance and to measure the strengths and weaknesses of the current state of the-science as presented in the CMAQ modeling system. Some suggestions for extensions and community involvement are provided below, but certainly not limited to:

(1) Modeling airborne and deposition of atmospheric toxic pollutants: A key opportunity for CMAQ is the development of a modeling capability for toxic pollutants into the CMAQ chemical transport modeling system. Models of airborne toxic pollutant provide an important tool for understanding the transport and chemical pathways that are concerns to human exposure assessments and for risk assessments and its management. It also provides a powerful means to assess the exchange of toxic compounds between the atmosphere and sensitive ecosystems. However, developing such models is challenging. Air toxics arise from a wide variety of sources, which may have a wide range of chemical lifetimes and reactivity. Consequently, their toxicological impacts as well as their time-space distributions may be highly variable. These complex mixtures of reactive compounds can exhibit wide range and variability in physical properties and exist at various gas, liquid or particulate ambient metastates. Modeling paradigms might evolve from introducing gas-particulate partitioning of the semi-volatile species (Ching et al., 1997) to more fundamental modeling with detailed chemical mechanisms.

(2) Development of modeling capability to link with human exposure models: With the ability to simulate toxic pollutant processes in addition to the current photochemical oxidants and particulates, it is planned to transport the CMAQ model to a finer than urban scale to link with human exposure models. International efforts to determine and understand the etiology of adverse human effects of air pollutants, especially those that or associated with fine particles is underway. Modeled concentrations of air pollutant constituents at neighborhood scales when coupled with the limited numbers of sampling provide a powerful basis for driving human exposure models. With this necessary data, human exposure models provide a basis for the causality studies and for risk assessment research. Models have not yet been developed to predict the spatial and temporal distributions of the various causal pollutant classes under current consideration at the neighborhood scale. The downscaling requirements represent a great challenge to the scientific basis in current meteorological processors.

(3) Advanced data assimilation capability: As air quality modeling efforts extend to finer horizontal resolutions and time scales, it becomes increasingly important to make use of higher frequency asynoptic meteorological data such as satellite, radar wind profilers and NEXRAD. There is a need to develop and extend data assimilation techniques to these meteorological data sources. Improved methods for introducing cloud information into the CMAQ should also be investigated. Such fields have significant impact on chemical photolysis rates, the atmospheric and surface energy budgets, the stability and dispersive power of the boundary layer, and aqueous chemistry.

(4) Development of an air quality predictive mode: With further development of the emissions and meteorological modeling systems, plans include developing a predictive capability in the CMAQ modeling system. CMAQ is currently developed in retrospective mode for performing assessments and for implementation of the National Ambient Air Quality Standards (NAAQS). In principle, CMAQ may be extended to a forecast mode in order to provide air quality advisories for pollutants such as ozone and visibility and for operational support for issues such as smoke and PM/haze from prescribed fires. These capabilities will require the development and testing of day-specific emissions inventories and a real time data processing system for the meteorological mode.

(5) Up and downscale links to global scale models: New linkages with other areas of modeling, including scale and media, are envisioned. It is hoped that information from the urban and regional CMAQ applications and from global modeling applications can be bridged. Because CMAQ offers the state of science to simulate atmospheric process as realistically as possible at time scales commensurate with reality, CMAQ output can be used to benchmark or examine the parametric basis of process formulations in global models. From a downscale perspective, global model output can be used to improve or enhance the initial and boundary conditions in CMAQ regional and urban scale simulations.

(6) Ecosystem modeling: Efforts to combine environmental modeling techniques to encompass an entire ecosystem is needed to address issues including: (a) nutrient cycle modeling, which includes pathways through the atmosphere, water bodies, and soil; and (b) acidic wet and dry deposition into sensitive ecosystems, including critical load analyses. With this ecosystem modeling approach, air quality issues can be studied in combination with other aspects of environmental health. For example, nitrogen deposition can cause adverse nutrient loadings to ecosystems that can result in a reduction of water quality due to adverse biological responses. Further, toxic deposition can lead to adverse indirect human exposure from bioaccumulation through the food chain.

1.8 References

Binkowski, F.S., and U. Shankar, 1995: The Regional Particulate Model: Part I. Models description and preliminary results. *J.Geophys. Res.*, **100(D12)**: 26191-26209.

Bott, A., 1989: A positive definite advection scheme obtained by nonlinear renormalization of the advective fluxes, *Mon. Wea. Rev.* **117**: 1006-1015.

Byun D. W., A. Hanna, C. J. Coats, and D. Hwang, 1995a: Models-3 air quality model prototype science and computational concept development. Transactions of Air & Waste Management Association Specialty Conference on Regional Photochemical Measurement and Modeling Studies, Nov. 8-12, San Diego, CA. 1993, 197-212.

Byun, D. W., C. J. Coats, D. Hwang, S. Fine, T. Odman, A. Hanna and K. J. Galluppi, 1995b: Prototyping and implementation of multiscale air quality models for high performance computing. Mission Earth Symposium, Phoenix, AZ, April 9-13, 1993. 527-532.

Byun, D.W., D. Dabdub, S. Fine, A. F. Hanna, R. Mathur, M. T. Odman, A. Russell, E. J. Segall, J. H. Seinfeld, P. Steenkiste, and J. Young, 1996: Emerging Air Quality Modeling Technologies for High Performance Computing and Communication Environments, Air Pollution Modeling and Its Application XI, ed. S.E. Gryning and F. Schiermeier. 491-502.

Byun, D.W., J.K.S. Ching, J. Novak, and J. Young, 1997: Development and Implementation of the EPAís Models-3 Initial Operating Version: Community Multi-scale Air Quality (CMAQ) Model, 1998a: Twenty-Second NATO/CCMS International Technical Meeting on Air Pollution Modelling and Its Application, 2-6 June, 1997. Air Pollution Modeling and Its Application XII, ed. S.E. Gryning and N. Chaumerliac, Plenum Publishing Coorp. 357-368.

Byun, D.W., J. Young., G. Gipson., J. Godowitch., F. Binkowsk, S. Roselle, B. Benjey, J. Pleim, J.K.S. Ching., J. Novak, C. Coats, T. Odman, A. Hanna, K. Alapaty, R. Mathur, J. McHenry, U. Shankar, S. Fine, A. Xiu, and C. Jang, 1998b: Description of the Models-3 Community Multiscale Air Quality (CMAQ) model. Proceedings of the American Meteorological Society 78th Annual Meeting, Phoenix, AZ, Jan. 11-16, 1998: 264-268.

Carmichael G.R. and L.K. Peters, 1984a: An Eulerian transport/transformation/removal model for SO_2 and sulfate-I. Model development, *Atmos. Environ.* **18**: 937-952.

Carmichael G.R. and L.K. Peters, 1984b: An Eulerian transport/transformation/removal model for SO_2 and sulfate-II. Model calculation of SO_x transport in the Eastern United States, *Atmos. Environ.* **20**: 173-188.

Carmichael G.R., L.K. Peters, and R.D. Saylor, 1991: The STEM-II regional scale acid deposition and photochemical oxidant model-I. An overview of model development and applications, *Atmos. Environ.* **25A**: 2077-2090.

Chang, J.S., P.B. Middleton, W.R. Stockwell, C.J. Walcek, J.E. Pleim, H.H. Landsford, S. Madronich, F.S. Binkowski, N.L. Seaman, and D.R. Stauffer, 1990: "The Regional Acid Deposition Model and Engineering Model." NAPAP SOS/T Report 4, in *National Acid Precipitation Assessment Program: State of Science and Technology, Volume 1*. National Acid Precipitation Assessment Program, 722 Jacksn Place, N.W., Washington, D.C., September 1990.

Chang, J.S., R.A. Brost, I.S.A. Isaksen, S. Madronich, P. Middleton, W.R. Stockwell, and C.J. Walcek, 1987: A three-dimensional Eulerian acid deposition model: Physical concepts and formulation." *J. Geophy. Res.* **92**: 14681-14700.

Ching, J.K.S., D.W. Byun, A. Hanna, T. Odman, R. Mathur, C. Jang, J. McHenry, K. Galluppi, 1995: Design requirements for multiscale air quality models. Mission Earth Symposium, Phoenix, AZ, April 9-13 p532-538.

Ching, J.K.S., D.W. Byun, J. Young, F. Binkowsk., J. Pleim, S. Roselle, J. Godowitch, W. Benjey., and G. Gipson, 1998: Science features in Models-3 Community multiscale air quality system. Proceedings of the American Meteorological Society 78th Annual Meeting, Phoenix, AZ, Jan. 11-16, 1998: 269-273

Ching, J.K.S., Francis S. Binkowski, and O. Russell Bullock, Jr., 1997: Deposition of semivolatile toxic air pollutants to the Great Lakes: A regional modeling approach. In " Atmospheric Deposition of Contaminants to the Great Lakes and Coastal Waters, Ed by Joel Baker, SETAC Press. pp 293-304.

Coats, C. J., A.H. Hanna, D. Hwang, and D.W. Byun, 1995: Model engineering concepts for air quality models in an integrated environmental modeling system. Transactions of Air & Waste Management Association Specialty Conference on Regional Photochemical Measurement and Modeling Studies, Nov. 8-12, San Deigo, CA. 1993, 213-223.

Colella, P., and P. L. Woodward, 1984: The Piecewise Parabolic Method (PPM) for gas-dynamical simulations, *J. Comput. Phys.* **54**: 174-201.

Dennis, R, 1998: The Environmental Protection Agency's third generation air quality modeling system: An overall perspective. Proceedings of the American Meteorological Society 78th Annual Meeting, Phoenix, AZ, Jan. 11-16, 1998: 255-258.

Dennis, R.L., D.W. Byun, J.H. Novak, K.J. Galluppi, C.J. Coats, and M.A. Vouk, 1996: The next generation of integrated air quality modeling: EPA's Models-3. Atmospheric Environment, 30, No. 12, 1925-1938.

Eder, B.K., D.H. Coventry, C. Bollinger and T.L. Clark: RELMAP, 1986: A Regional Lagrangian Model of Air Pollution User's Guide. U.S. Environmental Protection Agency Report EPA/600/8-86/013, Research Triangle park, NC 146 pp.

Eder, B.K., J.M. Davis and P. Bloomfeld, 1994: An automatic classification scheme designed to better elucidate the dependence of ozone on meteorology. *J. Appl. Meteor*, **33**: 1182-1199.

Eder, B.K. and S. LeDuc, 1996: Can selected RADM simulations be aggregated to estimate annual concentrations of fine particulate matter? Reprint from the 11th Annual International Symposium on the Measurement of Toxic and Related Pollutants, May 7-10, 1996, RTP, NC 732-739.

Gillani, N.V., A. Biazar, Y. Wu, J. Godowitch, J. Ching, R. Imhoff, 1998: The Plume-in-Grid treatment of major elevated point source emissions in Models-3. 10th Joint Conference on Applications of Air Pollution Meteorology with AWMA, January 11-16, 1998, Phoenix, AZ, Amer. Meteorol. Soc., Boston, MA.

Grell, G.A., J. Dudhia, and D.R. Stauffer, 1993: A description of the Fifth-Generation Penn State/NCAR Mesoscale Model(MM5). NCAR Technical Note, NCAR/TN-398+IA

Jacobson M. and R.P. Turco, 1994: SMVGEAR: A Sparse-Matrix, vectorized Gear code for atmospheric models. *Atmos. Environ.* **28**: 273-284.

Jeffries, H. E. and S. Tonnesen, 1994: A comparison of two photochemical reaction mechanisms using mass balance and process analysis, *Atmos. Environ*, **28(18)**: 2991-3003.

Lamb, R.G., 1983a: *A Regional Scale (1000 km) Model of Photochemical Air Pollution, Part 1: Theoretical Formulation.* EPA-600/3-83-035, U.S. Environmental Protection Agency, Research Triangle Park, NC.

Lamb, R.G., 1983b: *A Regional Scale (1000 km) Model of Photochemical Air Pollution, Part 2: Input Processor Network Design.* EPA-600/3-84-085, U.S. Environmental Protection Agency, Research Triangle Park, NC.

Morris, R.E. and T.C. Meyers, 1990: *User's Guide for the Urban Airshed Model, Volume 1: User's Manual for UAM(CB-IV). EPA-450/4-90-007A.* U.S. Environmental Protection Agency, Research Triangle Park, NC.

Novak, J., J. Young, D.W. Byun, C. Coats, G. Walter, W. Benjey, G. Gipson, S. LeDuc, 1998: Models-3: A unifying framework for environmental modeling and assessments. Preprint Volume, 10th Joint AMS and A&WMA Conference on the Applications of Air Pollution Meteorology, Phoenix, AZ, Jan 11-16, 1998: 259-263.

Pleim J.E., and J.S. Chang, 1992: A non-local closure model in the convective boundary layer. *Atm Environ.*, **26A**: 965-981.

Pleim, J.E., and A. Xiu, 1995: Development and testing of a surface flux and planetary boundary layer model for application in mesoscale models, *J. Appl. Meteor.*, **34**:16-32.

Wilkinson, J.G., C.F. Loomis, D.E. McNally, R.A. Emigh, and T.W. Tesche, 1994: *Technical Formulation Document: SARMAP/LMOS Emissions Modeling System (EMS-95)*, Final Report, Lake Michigan Air Directors Consortium and the California Air Resources Board, AG-90/TS26 and AG-90/TS27, 120pp.

Venkatram, A.K. and P.K. Karamchandani, 1998: *The ADOM II Scavenging Module.* ENSR Consulting and Engineering Report 0780-004-205. Camarillo, CA.

This chapter is taken from *Science Algorithms of the EPA Models-3 Community Multiscale Air Quality (CMAQ) Modeling System*, edited by D. W. Byun and J. K. S. Ching, 1999.

Chapter 2

MODELS-3 ARCHITECTURE: A UNIFYING FRAMEWORK FOR ENVIRONMENTAL MODELING AND ASSESSMENT

Joan Novak* **and Sharon Leduc****
Atmospheric Modeling Division
National Exposure Research Laboratory
U.S. Environmental Protection Agency
Research Triangle Park, NC 27711

ABSTRACT

The Models-3 framework and Community Multiscale Air Quality (CMAQ) model were designed and built to function together. The CMAQ science is documented in the other chapters and this chapter is intended to provide science and technical details of the Models-3 framework which integrates the CMAQ. The Models-3 User Manual is available and useful for those who want operational details beyond the "big picture" provided in Chapter 2.

This chapter present the various components of the Models-3 framework (Dataset Manager, Program Manager, Science Manager, Study Planner, Strategy Manager, Model Builder, Source Code Manager, Framework Administrator, and Tool Manager). The Tool Manager provides access to third party applications for emissions processing, visualization, and analysis. The Framework Administrator provides the system administrator access to system lists and administrative functions in Models-3. Each of the other components is provided for developing, executing, and managing CMAQ applications.

The computer architecture, the client-server design, the object-oriented data base management system, and the graphical user interface are also addressed in this chapter, along with the design features of Models-3.

---

*On assignment from the National Oceanic and Atmospheric Administration, U.S. Department of Commerce. Corresponding author address: Joan Novak, MD-80, Research Triangle Park, NC 27711. Email: novak.joan@epamail.epa.gov

**On assignment from the National Oceanic and Atmospheric Administration, U.S. Department of Commerce.

2.0 MODELS-3 ARCHITECTURE: A UNIFYING FRAMEWORK FOR ENVIRONMENTAL MODELING AND ASSESSMENT

2.1 Introduction

Models-3 is a flexible software system designed to simplify the development and use of environmental assessment and decision support tools for a wide range of applications from regulatory and policy analysis to understanding the interactions of atmospheric chemistry and physics. The initial version of Models-3 contains a Community Multiscale Air Quality (CMAQ) (Byun, et al., 1997, and other chapters of this document) modeling system with capabilities for urban to regional scale air quality simulation of tropospheric ozone, acid deposition, visibility and fine particulate. The Models-3 framework provides an interface between the user and operational models, between the scientist and developing models, and between ever changing hardware and software platforms.

The concept of an integrated modeling and analysis framework (Novak, et al., 1995; Dennis, et al., 1996) was formulated in response to 1) problems and duplication of effort involved in maintaining the separate data pre-processing and post-processing software systems required for each model used to analyze different air quality pollutants or scales, 2) the difficulties States and industry encountered using more complex modeling systems, and 3) the large expense required to modify existing models to incorporate scientific advancements or to adapt the models to new domains. Based on technology advances in the National High Performance Computing and Communications program, Models-3 was designed to overcome these limitations and to serve as a community framework for continual advancement and use of environmental assessment tools. Capabilities and design features of the Models-3 framework provide more flexibility in data handling, modeling, visualization and analysis.

2.2 Overview of the Models-3 Framework

The Models-3 framework contains components that assist 1) the model user with air quality modeling studies and analysis of results, and 2) the model developer with creating, testing, and performing comparative analysis of new versions of air quality models. The major design goal is to simplify and integrate the development and use of complex environmental models, beginning with air quality and deposition models. The function of each framework component is described below.

2.2.1 Dataset Manager

Dataset Manager provides the user with the capability to register files for use with the modeling and analysis programs within the Models-3 framework. The registration process involves entering the location of the dataset (full path name) and metadata (information about the data such as spatial - temporal extent and resolution, source of data, time convention, units, etc.) into the Models-3 data base. Models-3 follows the Federal Geospatial Metadata Standard for metadata

content. The datasets may be located on any network-connected computer system known to the Models-3 system installed at the user's site. Once a dataset is registered, the user can search for the dataset based on its metadata information, file type, etc.

Dataset Manager allows the user to view the details of the selected dataset to ensure the correct one has been selected for use with an application. Dataset registration eliminates the need for the user to type the entire path name each time the dataset is used. Instead the user can highlight the dataset from a list of candidates that satisfy the search criteria specified by the user. Models-3 will automatically move selected data to the host where it is needed for a model execution. Dataset Manager also provides standard capabilities such as deleting, copying, archiving, and restoring files and metadata.

2.2.2 Program Manager

Program Manager allows the user to register, update, and search for executable programs and/or scripts to make them available for use in defining studies within the Study Planner component. During program registration, the user enters characteristics of the program into the framework including descriptive information on program function, input requirements, output specifications, runtime environment variables, target architecture and operating system. Once the program or script is registered, this executable can be used in Study Planner to sequence a series of executions which may depend on previous executions for input data. The user can access and execute programs that are not registered. However, registering programs ensures that all mandatory inputs have been specified and automatic naming and registration of output files is activated, to facilitate tracking output from numerous program executions. Recommended model configurations for standard domains are preregistered in the system, eliminating the need for the typical user to deal with the details of program registration.

2.2.3 Study Planner

Study Planner allows the user to define a study and control the execution of its associated processes. A study is a collection of plans and properties that are necessary to describe and perform one or more environmental modeling analyses. A plan is a collection of information defining dataset and program interdependencies and the sequence of execution of one or more programs. Study Planner gathers much of its information from the Program Manager and Dataset Manager registration data. The relationship between a program (node) and its required and optional datasets (links) is user-defined through the process of constructing and annotating a graphical diagram with simple drag-and-click mouse operations. Once a plan is constructed and its graphical diagram fully annotated with desired input datasets and options, the plan can be executed. User specified program options are entered by editing program environment variables.

Studies and associated plans are named entities that are saved in the system data base. Therefore, a typical user can start with an existing study plan provided by the model developer and simply change the dataset annotations by selecting, through a file browser, appropriate datasets needed

for execution. The Study Planner provides capabilities to create new studies, copy and modify existing studies, and delete existing studies.

2.2.4 Strategy Manager

Strategy Manager provides the capability to estimate point-, area-, and mobile-source emissions for future years and to determine the relative effectiveness of specified control scenarios. The user may adjust pollutant growth factors and emissions control factors to perform "what if" analyses for entire EPA regions, states, counties or for user-defined study areas. By applying estimated yearly emission growth factors from the Emissions Growth and Assessment System, control efficiency, rule effectiveness, and rule penetration factors to the EPA 1990 base year emissions inventory, the Strategy Manager provides estimates of future year (1991 - 2010) emissions for carbon monoxide, nitrogen oxide, particulate matter up to 10 microns, sulfur dioxide, and volatile organic compounds. Strategy Manager is based on EPA's Multiple Projection System. An input data processor is included to process the National Emissions Trend (NET) inventory (URL http://www.epa.gov/oar/oaqps/) data format.

2.2.5 Tool Manager

Tool Manager provides access to third-party applications (tools) that are registered with the Models-3 framework. Third-party applications that are currently available include Models-3 Emission Processing and Projection System (MEPPS), Vis5D, Text Editor, Package for Analysis and Visualization of Environmental Data (PAVE), SAS®, Arc/Info®, IBM Visualization Data Explorer™, DXDriver, and VisDriver. Tool Manager allows the user to add tools to the system that will help with the user's work. A file converter is included to convert between ASCII, SAS, and I/O API files.

2.2.5.1 Emissions Processing

The majority of the emissions processing needed to support air quality model applications can be prepared through minor modifications to pre-specified emissions plans in the Study Planner. However, for those users who need total flexibility in specifying details for emissions preparation, the Models-3 Emissions and Projection System (MEPPS) (Benjey and Moghari, 1996) is available for interactive processing of emissions. MEPPS provides capabilities to input and perform quality control on emission inventory data, and reformat and subset data for the user-specified modeling domain. The main emissions processing is performed by a significantly revised version of the Geocoded Emission Modeling and Projection (GEMAP) (Wilkinson and Emigh, 1994) system which requires the user to have Arc/Info® and SAS® licenses for operation. This Emissions Processor (EMPRO) transforms the annual county based emissions inventories into spatial and temporal resolutions that are consistent with the target model application, i.e. typically hourly gridded emissions for a selected domain. The processor also estimates mobile and biogenic emissions and performs chemical speciation consistent with the chemical mechanism in the target model. Mobile emission factors are calculated using Mobile 5a; biogenic emissions are calculated

using the Biogenic Emissions Inventory System (BEIS2). Finally, according to a user-specified criteria, an output processor merges the emissions files to provide the 2-D gridded files and a point source stack emissions file required for the model execution. The user is offered numerous choices for interactively changing parameters and reviewing results in all of the emissions components. The global science specifications created by the user in Science Manager are accessible from within MEPPS to ensure consistency when desired.

2.2.5.2 Visualization and Analysis Tools

Several freely available visualization tools are accessible from the Models-3 framework as well as commercial visualization and statistics packages, such as IBM Visualization Data Explorer™ and the SAS®. A graphical user interface component, VisDriver, provides an interface for finding and selecting Models-3 data files on local or remote hosts and launches visualization applications with Vis5D or PAVE. VisDriver performs requisite data conversions from the internal Models-3 data format to the data format required by these third party visualization packages. VisDriver also provides a data export capability to such formats as Advanced Visualization System (AVS™), Flow Analysis Software Toolkit (FAST™), and an ASCII spreadsheet. On-line help is available to assist the user with these visualization tools (http://www.epa.gov/asmdnerl/models3/vistutor/user/user-guide-00.htm/).

PAVE

The Package for Analysis and Visualization for Environmental data (PAVE), developed at the North Carolina Supercomputing Center of MCNC, allows the user to visualize 2-D multi-variate, gridded environmental data with smooth tile plots,3-D mesh plots, time series line and bar plots, vertical cross sections, wind vectors, and scatter plots. More information can be found at http://www.iceis.mcnc.org/EDSS/pave_doc/Pave.html.

Vis5D

Vis5D, a public domain package developed at the University of Wisconsin Space Science and Engineering Center, provides interactive visualization of large five-dimensional gridded datasets - the data are real numbers at each point of a grid that spans three space dimensions, one time dimension, and a dimension for enumerating multiple physical variables. Vis5D provides isosurfaces, contour line slices, colored slices, volume rendering of data in 3D, and rotation and animation of the 3D image in real time. There is also a feature for wind/trajectory tracing. More information can be found at http://www.ssec.wisc.edu/~billh/vis.html.

IBM Visualization Data Explorer

IBM Visualization Data Explorer™, a commercial visualization package, has been used to create custom visualizations to support diagnostic evaluation of the air quality models with visualization of multiple/nested grids, terrain following grids, grid cell time aggregate statistics such as

maximum ozone concentration and hours of non-compliance, comparison of measured aircraft data with model predictions along the path of flight, and detailed chemical analysis of the integrated reaction rates predicted over space and time in the air quality models. Other standard visualization capabilities for scalar and vector quantities, 2-D and 3-D graphs have also been integrated through the DXDriver interface.

2.2.6 Science Manager

Critical model specifications typically found hardwired in air quality model codes, such as details of the horizontal coordinate system, specification of horizontal grid dimensions, vertical layers, chemical mechanism specification (reactions and rate constants), etc. are treated as globally shared information in the Models-3 framework. Use of this global information enables more consistency throughout the system (i.e. emission, meteorological, and chemistry-transport components). Detailed specifications for these key science components are entered by the user only once using Science Manager graphical user interfaces. These specifications are saved as named entities in an object-oriented database accessible by all model components. A typical user would access and modify previously defined Science Manager components to define a new modeling domain.

The functionality of Science Manager, however, is targeted to the model developer to facilitate experimentation with new model components. For example, extensive research is done on improving photochemical mechanism specifications. One component of Science Manager enables the model developer to either edit an existing chemical mechanism or import a new set of chemical reactions, specify chemical species, molecular weights, etc. Both the Regional Acid Deposition Model, Version 2 (RADM-2) and the Carbon Bond-4 mechanisms are available in the Models-3/CMAQ framework and the State Air Pollution Research Center (SAPRC) chemical mechanism is being modified to fit within this paradigm to facilitate comparative studies with these chemical mechanisms. As long as the chemical species in any modified mechanisms are present in source emission profiles associated with Source Classification Codes (SCC), the chemical mechanism specification will propagate to the emission processing subsystem to enable generation of emission species consistent with the newly defined chemical mechanism.

2.2.7 Model Builder

The Models-3 framework facilitates the interchange of science components within a model, customization of the chemistry mechanism, and changes in the modeling domain, horizontal grid resolution, and vertical layering without the need for reprogramming. Modifying an existing model or building a new model is a two-step process. First, the model developer must use Science Manager to specify the horizontal coordinate system, horizontal grid dimensions, vertical layers, chemical mechanism, and select science modules for each class (i.e. advection, diffusion , cloud process, etc.) of science process to be included in the new model. Module selections are contained in a named configuration file. After the needed science components are specified, the

model developer uses Model Builder to select from available science specifications and configuration files to create a single custom model executable.

2.2.8 Source Code Manager

CMAQ source code is distributed with the Models-3 framework to provide the user flexibility to create a model for a user specified domain or to allow a user to build a new executable with a selected chemistry mechanism. Model Builder uses Source Code Manager to access appropriate source code to transform the user's selections into a working executable. Source Code Manager allows a user to retrieve a version of a source code file, modify it, and return it to the code archive after the change has been tested. Source code should only be modified by knowledgeable model developers. Source Code Manager is based on Concurrent Versions System (CVS)/Revision Control System (RCS) public domain software for code configuration management and tracks the history and version numbers for all source code changes. These version numbers become part of the history information associated with each output file.

2.2.9 Framework Administrator

The Framework Administrator subsystem menu allows the Models-3 system administrator to manipulate system lists and to access administrative functions of other Models-3 subsystems. System lists include users, hosts, device types, site IDs, file format types, compiler names, operating system names, platform names, and time zone names. Through this subsystem, only the authorized system administrator can set access controls for users, add or delete entries from the system lists, and maintain the integrity of controlled files.

2.3 Models-3 System Architecture

The Models-3 framework is designed as a three-tier client-server architecture with an object-oriented data base management system (OODBMS) ,ObjectStore™, to store persistent data (i.e. studies, horizontal grid definitions, metadata containing pointers to physical dataset locations , etc.). When the user brings up the Models-3 graphical user interface on user's desktop system, the user becomes a "client" requesting services from a "server". Several Models-3 servers act as "clients" requesting services from other Models-3 "servers". The client and server can be on the same machine or on separate machines giving the system scalability by either adding more client workstations with only slight impact on performance, or moving to faster and larger server machines. Each of the subsystem functions described in Section 2.2 is implemented as a server and can be can run on different machines. The Models-3 servers were initially developed on a Sun workstation using the Solaris 2.5.1 operating system (Models-3 Version 2.1). Models-3 is being ported to a Sun Solaris 2.6 operating system (Models-3 Version 2.2). The next server to be released for Models-3 will be SGI (late 1998). Models-3 Version 3 (summer 1999) will allow server to be a PC with a Windows NT® operating system.

This client-server architecture in conjunction with commercial cross-platform communications interface - ORBIX™ by Iona Technologies, Ltd. which is compliant with the Common Object Request Broker Architecture (CORBA) standard - and an OODBMS containing pointers to datasets distributed over the network enables transparent use of multiple computing platforms and access to data across the network. Figure 2-1 illustrates a possible configuration for multiple installations for Models-3 software. Each independent site must have at least one server to support the local OODBMS and Models-3 sessions. Each site can run autonomously. A two-server configuration is recommended at each installation: one to support emissions processing activities, and the second to support other client-server and model computations. Of course, additional servers will improve performance for larger applications and the current version of Models-3 also supports batch submissions of model executions to a supercomputer with job status reporting back to the framework through the standard Network Queuing Service (NQS). In the future, we envision maintaining a master database to foster sharing of data and to minimize duplication of effort.

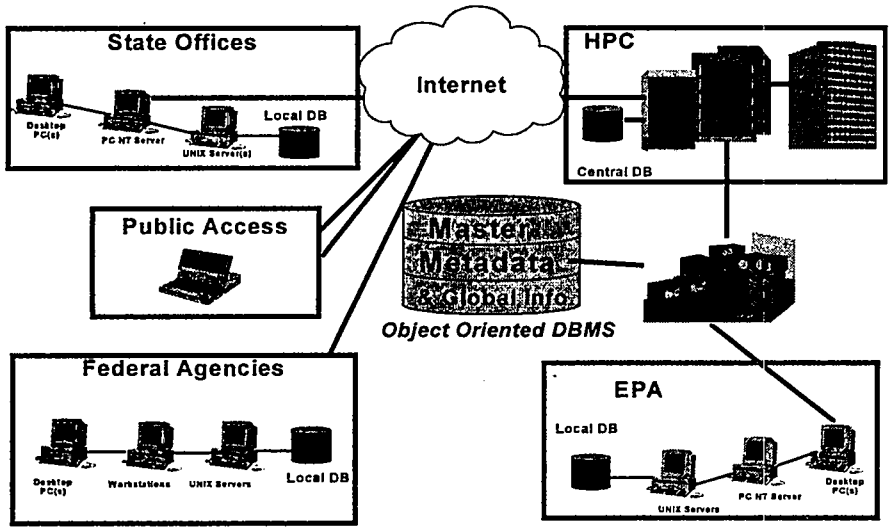

Figure 2-1. Seamless Computing and Data Management from PC to Scalable Parallel Computer

To adapt to ever changing hardware and software, the framework uses a layered interface design that isolates critical system components, thus minimizing the impact of hardware and software upgrades. Each layer, as seen in Figure 2, is connected to its adjacent layer(s) by a well specified interface thus easing the task of replacement if a more advanced component becomes available. Another key design choice is the use of an input/output application programming interface (I/O API) for the data access layer. This concept is implemented by using a standard FORTRAN or C callable library for all input/output in the air quality model codes. Thus I/O efficiencies can be improved by replacing this centralized library or new data types can be handled by adding new routines to the library.

The I/O API is layered on top of the netCDF standard data file format developed at the National Center for Atmospheric Research. This data format uses the underlying eXternal Data Representation (XDR), which is IEEE (Institute of Electrical and Electronics Engineers, Inc.) compliant and, therefore, enables cross-platform transfer of data without conversion. The Models-3 implementation conforms to the netCDF specification, but sets additional conventions for information stored in the file header. NetCDF is a self documenting file format that contains complete specifications (parameter names, units, etc) for the file contents. All netCDF records can be accessed via direct access methods to minimize data access times. When registering conforming programs, the Models-3 framework automatically writes execution history information to the file header record of each output file and to the OODBMS metadata associated with the output file. The history information, which establishes traceability of output datasets to the model that generates them, contains the date/time of model execution, the version numbers of the science process modules contained in the model executable, Science Manager specification names, host computing environment, and other pertinent information. Science Manager's global shared data objects and the netCDF format are the key aspects of building "plug compatible" science modules that conform to Models-3 guidelines.

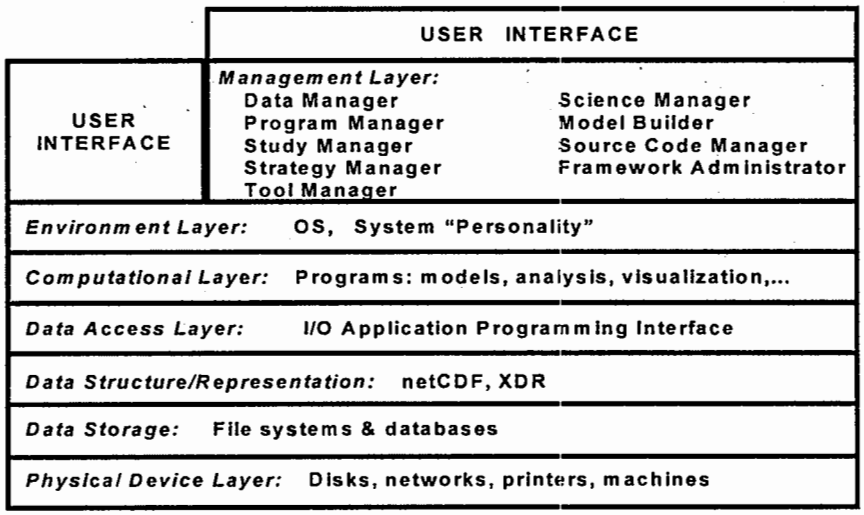

Figure 2-2. Architectural Layering: Flexibility for Future Change

2.4. Schedule and Future Plans

The Models-3 framework provides a unifying foundation for continual community evolvement of environmental modeling and assessment tools with possible extensions beyond the current air quality implementation. The use of the Models-3 framework for multimedia exposure and risk assessment is possible. A simple integration of the Hydrologic Simulation Program FORTRAN (HSPF) and the Chesapeake Bay Water Quality Model (CBWQM) in the Models-3 framework explored multimedia model linkage capabilities. Maintaining Models-3 framework to use emerging computing capabilities and transferring that capability to science researchers and environmental decision makers will continue to be the focus of the Models-3 effort.

2.5 References

Benjey, W.G., and N.M. Moghari. Functionality of an integrated emission preprocessing system for air quality modeling: the Models-3 emission processor. In *The Emissions Inventory: Programs & Progress*. VIP-56. Proceedings of a Specialty Conference, Research Triangle Park, NC, October 11-13, 1995. US Environmental Protection Agency, Research Triangle Park, NC, and Air & Waste Management Association, Pittsburgh, 463-471 (1996).

Byun, D., J. Young, J. Gipson, J. Godowitch, F. Binkowski, S. Roselle, B. Benjey, J. Pleim, J. Ching, J. Novak, C. Coats, T. Odman, A. Hanna, K. Alapaty, R. Mathur, J. McHenry, U. Shankar, S. Fine, A. Xiu, and C. Jang. Description of the Models-3 Community Multiscale Air Quality (CMAQ) model. Proceedings of the American Meterological Society 78th Annual Meeting, January 11-16, 1998, Phoenix, AZ.

Dennis, R.L., D.W. Byun, J.H. Novak, K.L. Galluppi, C.J. Coats, M.A. Vouk. The Next Generation of Integrated Air Quality Modeling: EPA's Models-3. *Atmospheric Environment*, Vol. 30, No.12, pp. 1925 - 1938, (1996).

Emission Inventory Improvement Program. URL http://www.epa.gov/oar/oaqps/eiip/

Novak, J.H., R.L. Dennis, D.W. Byun, J.E. Pleim, K.J. Galluppi, C.J. Coats, S. Chall, M.A. Vouk. EPA Third-generation Air Quality Modeling System, Volume 1: Concept. EPA 600/R95/084, National Exposure Research Laboratory, Research Triangle Park, NC, 55 pp. (1995).

Wilkinson, J.G., and Emigh, R.A. The Geocoded Emissions Modeling and Projections System (GEMAP): Advanced Training Workshop. Prepared for Environmental Protection Agency, Office of Research and Development, by Alpine Geophysics, Boulder, CO (1994).

This chapter is taken from *Science Algorithms of the EPA Models-3 Community Multiscale Air Quality (CMAQ) Modeling System*, edited by D. W. Byun and J. K. S. Ching, 1999.

EPA/600/R-99/030

Chapter 3

DEVELOPING METEOROLOGICAL FIELDS

Tanya L. Otte*
Atmospheric Modeling Division
National Exposure Research Laboratory
U. S. Environmental Protection Agency
Research Triangle Park, NC 27711

ABSTRACT

Meteorological data are important in many of the processes simulated in the Community Multiscale Air Quality (CMAQ) model included in the first release of the Models-3 framework. The meteorology model that has been selected and evaluated with CMAQ is the Fifth-Generation Pennsylvania State University/National Center for Atmospheric Research (NCAR) Mesoscale Model (MM5). All software in the Penn State/NCAR mesoscale modeling system has been dedicated to the public domain and is presently used for both research and operational purposes at many organizations worldwide. Improvements to MM5 within the meteorological community are ongoing, and these enhancements should be evaluated for their applicability to air quality modeling. Other meteorological models are being considered for compatibility with CMAQ but are not provided with the initial release. The application of MM5 with CMAQ is described in Chapter 3.

---

*On assignment from the National Oceanic and Atmospheric Administration, U.S. Department. of Commerce. Corresponding author address: Tanya L. Otte, MD-80, Research Triangle Park, NC 27711. Email: tlotte@hpcc.epa.gov

3.0 DEVELOPING METEOROLOGICAL FIELDS

3.1 Credits and Disclaimers for Use of MM5

The Fifth-Generation Pennsylvania State University/National Center for Atmospheric Research (NCAR) Mesoscale Model (MM5) was developed in cooperation with Penn State and the University Corporation for Atmospheric Research (UCAR). Penn State and UCAR make no proprietary claims, either statutory or otherwise, to this version and release of MM5, and they consider MM5 to be in the public domain for use by any person or entity without any fee or charge. Penn State and UCAR shall be credited in any publications that result from the use of MM5. The names "Penn State" and "UCAR" shall not be used or referenced in any advertising or publicity that endorses or promotes any products or commercial entity associated with or using MM5, or any derivative works thereof, without the written authorization of UCAR and Penn State.

MM5 is provided to the public by Penn State and UCAR on an "as is" basis, and any warranties, either express or implied, including but not limited to implied warranties of non-infringement, originality, merchantability, and fitness for a particular purpose, are disclaimed. Neither UCAR nor Penn State will be obligated to provide the user with any support, consulting, training, or assistance of any kind regarding the use, operation, and performance of MM5, nor will they be obligated to provide the user with any updates, revisions, new versions, error corrections, or "bug" fixes. In no event will UCAR and Penn State be liable for any damages, whatsoever, whether direct, indirect, consequential, or special, which may result from an action in contract, negligence, or other claim that arises out of or about the access, use, or performance of MM5, including infringement actions.

Data that are obtained from NCAR (e.g., global analyses and observations) are prepared and maintained by the Data Support Section, Scientific Computing Division, NCAR. NCAR is operated by UCAR and is sponsored by the National Science Foundation. Any published research that uses data from the NCAR archive shall credit the maintainers of the archive. In addition, the original source(s) of data shall be acknowledged.

3.2 Meteorology Model Pre-Processing

Before the meteorology model can be run, several smaller ("pre-processing") programs must be run to set up the domain for the simulation and to generate a set of initial and boundary conditions for the meteorology model. The pre-processing programs are briefly described in this section.

3.2.1 Defining the Simulation Domain (*TERRAIN*)

Domains for the meteorology simulations are defined by several primary parameters: number of grid points in each horizontal dimension, grid spacing, center latitude, center longitude, map projection (Mercator, Lambert conformal, or polar stereographic), and number of "nested" domains and their horizontal dimensions. (Some other user-specific parameters are also defined based on the primary parameters, as required.) These parameters are processed by a program that is executed only when a new domain location is required. This program, *TERRAIN*, makes use of high-resolution global terrain and land use data sets to create "static files" for the domain. The static files currently include values for each grid point for terrain height and land use specification (e.g., deciduous forest, desert, water). Future versions of *TERRAIN* may include additional diurnal, seasonal, and location-specific information. The *TERRAIN* program is thoroughly described by Guo and Chen (1994).

3.2.2 Processing the Meteorological Background Fields (*DATAGRID*)

After the simulation domain has been established, the program *DATAGRID* is run to process the meteorological background fields. *DATAGRID* generates first-guess fields for the model simulation by horizontally interpolating a larger-scale data set (global or regional coverage) to the simulation domain. *DATAGRID* interpolates the background fields to the simulation domain for times throughout the simulation period; these files are used ultimately to generate lateral boundary conditions for the coarse-domain simulations. (Nested domains obtain lateral boundary conditions from the coarse domain.) *DATAGRID* also processes the sea-surface temperature and snow files by interpolating the analyses to the simulation domain. Lastly, *DATAGRID* calculates map-scale factors and Coriolis parameters at each grid point to be used by MM5. The *DATAGRID* program is thoroughly described by Manning and Haagenson (1992).

3.2.3 Objective Analysis (*RAWINS*)

The program *RAWINS* performs an objective analysis by blending the first-guess fields generated by *DATAGRID* with upper-air and surface observations. There are four objective analysis techniques available in *RAWINS*. The following descriptions are taken largely from Dudhia et al. (1998).

- **The Cressman scheme** assigns a circular radius of influence to each observation. The weights associated with the observations decrease radially from the observation to the radius of influence. The first-guess (meteorological background) field at each grid point is adjusted by taking into account all observations that influence that grid point. (See Cressman, 1959.)

- **The Ellipse scheme** alters the Cressman circles for analyses of wind and relative humidity by elongating the circles along the wind flow. The eccentricity of the ellipses increases as wind speed increases. This scheme reduces to the Cressman scheme under light wind conditions. (See Benjamin and Seaman, 1985.)

- **The Banana scheme** alters the Cressman circles for analyses of wind and relative humidity by elongating the circles in the direction of the flow and curving the influence region along streamlines. The resulting influence region is banana-shaped. This scheme reduces to the ellipse scheme under straight-flow conditions, and it further reduces to the Cressman scheme under light wind conditions. (See Benjamin and Seaman, 1985.)

- **The Multiquadric Interpolation scheme** uses hyperboloid radial basis functions to perform objective analysis. This scheme takes much more time and memory than the Cressman-based schemes. This scheme must be used with caution in data-sparse regions and when more than 25% of the domain is water-covered. (See Nuss and Titley, 1994.)

In addition, *RAWINS* performs some data quality control checks and buddy checks with user-defined thresholds. The objective analysis is performed for a user-defined number of pressure surfaces (generally mandatory levels plus some additional surfaces). *RAWINS* is also used to prepare the analyses for the analysis nudging in the simulation model. The *RAWINS* program is thoroughly described by Manning and Haagenson (1992).

3.2.4 Setting the Initial and Boundary Conditions (*INTERP*)

The "standard" *INTERP* program sets the initial and boundary conditions for the meteorology simulation. The analyses from *RAWINS* are interpolated to MM5's staggered grid configuration and from their native vertical coordinate (pressure) to MM5's vertical coordinate (a terrain-following, pressure-based "sigma" coordinate). In addition, the state variables are converted as necessary, e.g., relative humidity to specific humidity. The analyses from one time (generally the first time analyzed by *RAWINS*) are interpolated by *INTERP* to provide MM5's initial conditions, while analyses from all times are interpolated to generate MM5's lateral boundary conditions.

INTERP can also be used for "one-way nesting," where the MM5 output from one model run is interpolated to provide initial and boundary conditions for the nested run. This is a "non-standard" use of the *INTERP* program, but it is commonly used to support air quality modeling.

3.3 The Meteorology Model (MM5)

The following subsections include brief summaries of the science and options that are available in MM5. Thorough descriptions of the standard MM5 options are found in Grell et al. (1994) and Dudhia et al. (1998). The source code for an early release of MM5 is documented in Haagenson et al. (1994). The Models-3 package does not include NCAR's most current release of MM5. MM5 user options have been tailored and expanded in the Models-3 release to support air quality modeling. Some of these options have not yet been accepted into the official version that is maintained by NCAR. Caution should be exercised when deviating from the version of MM5 that is included with Models-3. Refer to Section 3.5 for a summary of changes to MM5 for CMAQ.

3.3.1 Brief History

MM5 is the Fifth-Generation Penn State/NCAR Mesoscale Model. It has evolved from the model used by Anthes in the early 1970s, described by Anthes and Warner (1978). The improvements in MM5 over the previous version (MM4) include the option for non-hydrostatic physics, as well as more sophisticated explicit moisture, boundary layer processes, radiation, convective parameterization, among other improvements. Dudhia (1993) documented the major changes from MM4 to MM5. Starting with MM5 Version 2 (MM5v2), the software has been restructured to run on various hardware platforms in addition to the Cray, with emphasis placed on workstation-based MM5 simulations. The Cray version of MM5 provided on the Models-3 installation tape has been tested on the EPA's Cray C90. A workstation-based version of MM5 may be used with subsequent releases of Models-3.

3.3.2 Horizontal and Vertical Grid

The coordinate system for MM5 is (x, y, sigma-p). The x and y dimensions are a regular lattice of equally spaced points (delta-x = delta-y = horizontal grid spacing, in kilometers) forming rows and columns. Sigma is a terrain-following vertical coordinate that is a function of the pressure at the point on the grid (in hydrostatic runs) or the reference state pressure (in non-hydrostatic runs), the surface pressure at the grid point, and the pressure at the top of the model. Sigma varies from 1 at the surface to 0 at the top of the model. The influence of the terrain on the sigma structure diminishes with height, such that the sigma surfaces near the top of the model are nearly parallel.

The horizontal grid in MM5 has an Arakawa-B staggering of the velocity vectors with respect to the scalars (Arakawa and Lamb, 1977). The momentum variables (u- and v-components of wind and the Coriolis force) are on "dot" points, while all other variables (e.g., mass and moisture variables) are on "cross" points. The dot points form the regular lattice for the simulation

domain, while the cross points are offset by 0.5 grid point in both the x and y directions. Note that the interpolation of the variables to the staggered grid is done automatically within the *INTERP* program.

3.3.3 Prognostic Equations

MM5 is based on primitive physical equations of momentum, thermodynamics, and moisture. The state variables are temperature, specific humidity, grid-relative wind components, and pressure. In the prognostic equations, the state variables are mass-weighted with a modified surface pressure. MM5 can be run as either a hydrostatic or non-hydrostatic model. In the hydrostatic model, the state variables are explicitly forecast. In the non-hydrostatic model (Dudhia, 1993), pressure, temperature, and density are defined in terms of a reference state and perturbations from the reference state. MM5 is not mass-conserving in the non-hydrostatic mode. The vertical (sigma) coordinate is defined as a function of pressure. The model's prognostic equations are thoroughly discussed in Grell et al. (1994) and Dudhia et al. (1998).

3.3.3.1 Time Differencing

The hydrostatic and non-hydrostatic versions of MM5 use different time differencing schemes to filter the fast waves from the prognostic solutions in the model. In the non-hydrostatic model, a semi-implicit scheme based on Klemp and Wilhelmson (1978) is used to control the acoustic waves in the model solution. In the hydrostatic model, a split-explicit scheme based on Madala (1981) is used to control gravity waves in the model solution. The time differencing in MM5 is discussed at length in Grell et al. (1994) and Dudhia et al. (1998).

3.3.3.2 Lateral Boundary Conditions

There are five options for lateral boundary conditions in MM5: fixed, relaxation, time dependent, time and inflow/outflow dependent, and sponge. The lateral boundaries in MM5 consist of either the outer five grid points (relaxation and sponge options) or the outer grid point (all other options) on the horizontal perimeter of the simulation domain. (The outer four grid points are used for boundary conditions for "cross" point variables for the relaxation and sponge options.) The lateral boundary conditions for the coarse domain are derived from the background fields processed in *DATAGRID* and *INTERP*. When the one-way nest option is selected, the lateral boundary conditions for nested domains are interpolated from the simulation on the parent domain.

3.3.4 Model Physics

Several model physics options in MM5 are briefly noted below. The model physics options are further discussed and compared in Dudhia et al. (1998). The descriptions of the model physics options are largely taken from Dudhia et al. (1998), and other pertinent references are noted.

3.3.4.1 Radiation

There are five atmospheric radiation cooling schemes available in MM5.

- **The "None" option** applies no mean radiative tendency to the atmospheric temperature. This scheme is unrealistic for long-term simulations.
- **The Simple Cooling scheme** sets the atmospheric cooling rate strictly as a function of temperature. There is no cloud interaction or diurnal cycle.
- **The Surface Radiation scheme** is used with the "none" and "simple cooling" schemes. This scheme includes a diurnally varying shortwave and longwave flux at the surface for use in the ground energy budget. These fluxes are calculated based on atmospheric column-integrated water vapor and low/middle/high cloud fraction estimated from relative humidity.
- **The Dudhia Longwave and Shortwave Radiation scheme** is sophisticated enough to account for longwave and shortwave interactions with explicit cloud and clean air. This scheme includes surface radiation fluxes and atmospheric temperature tendencies. This scheme requires longer CPU time, but not much memory. (See Dudhia, 1989.)
- **The CCM2 Radiation scheme** includes multiple spectral bands in shortwave and longwave, but the clouds are treated simply as functions of relative humidity. This scheme is suitable for larger grid scales and probably more accurate for long time integration (e.g., climate modeling). It also provides radiative fluxes at the surface. (See Hack et al., 1993.)

3.3.4.2 Convective Parameterization

There are currently six convective parameterization schemes in MM5. There is also the option for no convective parameterization and an independent option for shallow convection. The convective parameterization schemes have been designed for use at various simulation scales, and they are not entirely interchangeable. For example, each scheme uses different assumptions for convective coverage on the sub-grid-scale and for the convective trigger function. The convective parameterization schemes also differ greatly in CPU usage and memory requirements.

- **The Anthes-Kuo scheme** is based on moisture convergence and is mostly applicable to larger grid scales (i.e., greater than 30 km). This scheme tends to produce more convective rainfall and less resolved-scale precipitation. This scheme uses a specified heating profile where moistening is dependent on relative humidity. (See Anthes, 1977.)

- **The Fritsch-Chappel scheme** is based on relaxation to a profile due to updraft, downdraft, and subsidence region properties. The convective mass flux removes 50% of the available buoyant energy in the relaxation time. There is a fixed entrainment rate. This scheme is suitable for 20-30 km scales due to the single cloud assumption and local subsidence. (See Fritsch and Chappel, 1980.)

- **The Arakawa-Schubert scheme** is a multi-cloud scheme that is otherwise similar to the Grell scheme (described below). This scheme is based on a cloud population, and it allows for entrainment into updrafts and the existence of downdrafts. This scheme is suitable for larger grid scales (i.e., greater than 30 km). This scheme can be computationally expensive compared to the other available schemes. (See Arakawa and Schubert, 1974.)

- **The Kain-Fritsch scheme** is similar to the Fritsch-Chappel scheme, but it uses a sophisticated cloud-mixing scheme to determine entrainment and detrainment. This scheme also removes all available buoyant energy in the relaxation time. (See Kain and Fritsch, 1990, 1993.)

- **The Betts-Miller scheme** is based on relaxation adjustment to a reference post-convective thermodynamic profile over a given period. This scheme is suitable for scales larger than 30 km. However, there is no explicit downdraft, so this scheme may not be suitable for severe convection. (See Betts, 1986; Betts and Miller, 1986, 1993; and Janjic, 1994.)

- **The Grell scheme** is based on rate of destabilization or quasi-equilibrium. This is a single-cloud scheme with updraft and downdraft fluxes and compensating motion that determines the heating and moistening profiles. This scheme is useful for smaller grid scales (e.g., 10-30 km), and it tends to allow a balance between the resolved scale rainfall and the convective rainfall. (See Grell et al., 1991; and Grell, 1993.)

- **The "no convective parameterization" option** (e.g., explicitly resolved convection on the grid scale) is also available. This option is generally used for simulations on domains with horizontal grid spacing smaller than 10 km.

- **The Shallow Convection scheme** is an independent option that handles non-precipitating clouds that are assumed to be uniform and to have strong entrainment, a small radius, and no downdrafts. This scheme is based on the Grell and Arakawa-Schubert schemes. There is also an equilibrium assumption between cloud strength and sub-grid boundary layer forcing.

3.3.4.3 Planetary Boundary Layer Processes

Four planetary boundary layer (PBL) parameterization schemes are available in MM5. These parameterizations are most different in the turbulent closure assumptions that are used. The PBL parameterization schemes also differ greatly in CPU usage.

- **The Bulk Formula scheme** is suitable for coarse vertical resolution in the PBL (i.e., greater than 250 m vertical grid sizes). This scheme includes two stability regimes.

- **The Blackadar scheme** is suitable for "high-resolution" PBL (e.g., five layers in the lowest kilometer and a surface layer less than 100 m thick). This scheme has four stability regimes; three stable and neutral regimes are handled with a first-order closure, while a free convective layer is treated with a non-local closure. (See Blackadar, 1979.)

- **The Burk-Thompson scheme** is suitable for coarse and high-resolution PBL. This scheme explicitly predicts turbulent kinetic energy for use in vertical mixing, based on a 1.5-order closure derived from the Mellor-Yamada formulas. (See Burk and Thompson, 1989.)

- **The Medium Range Forecast (MRF) model scheme** is suitable for high-resolution PBL. This scheme is computationally efficient. It is based on a Troen-Mahrt representation of the counter-gradient term and a first-order eddy diffusivity (K) profile in the well-mixed PBL. This scheme has been taken from the National Centers for Environmental Prediction's (NCEP's) MRF model. (See Hong and Pan, 1996.)

3.3.4.4 Surface Layer Processes

The surface layer processes with the Blackadar and MRF PBL schemes have been parameterized with fluxes of momentum, sensible heat, and latent heat, following Zhang and Anthes (1982). The energy balance equation is used to predict the changes in ground temperature using a single slab and a fixed-temperature substrate. The slab temperature is based on an energy budget, and the depth is assumed to represent the depth of the diurnal temperature variation (~10-20 cm). The 13 land use categories are used to seasonally define the physical properties at each grid point (e.g., albedo, available moisture, emissivity, roughness length, and thermal inertia).

A five-layer soil temperature model (Dudhia, 1996) is also available as an option in MM5. In this model, the soil temperature is predicted at layers of approximate depths of 1, 2, 4, 8, and 16 cm, with a fixed substrate below using a vertical diffusion equation. This scheme vertically resolves the diurnal temperature variation, allowing for more rapid response of surface temperature. This model can only be used in conjunction with the Blackadar and MRF PBL schemes.

In a subsequent release of CMAQ, the Pleim-Xiu land-surface scheme (Pleim and Xiu, 1995) may be included in MM5. The Pleim-Xiu scheme has been developed to address surface processes that can significantly impact air quality modeling, including evapotranspiration and soil moisture. Notable in the Pleim-Xiu scheme is the more careful treatment of the surface characteristics (particularly vegetation parameters) that are currently assigned to grid points based on land use specification, as well as a more detailed land use and soil type classification database.

3.3.4.5 Resolvable-Scale Microphysics Schemes

There are six resolvable-scale (explicit grid-scale) microphysics schemes in MM5. There is also an option for a "dry" model run. The microphysics schemes have been designed with varying degrees of complexity for different applications of the model. In addition, there are new prognostic output variables that are generated by the more sophisticated schemes. These microphysics schemes also differ greatly in CPU usage and memory requirements.

- **The Dry scheme** has no moisture prediction. Water vapor is set to zero. This scheme is generally used for sensitivity studies.

- **The Stable Precipitation scheme** generates non-convective precipitation. Large-scale saturation is removed and rained out immediately. There is no evaporation of rain or explicit cloud prediction.

- **The Warm Rain scheme** uses microphysical processes for explicit predictions of cloud and rainwater fields. This scheme does not consider ice phase processes. (See Hsie and Anthes, 1984.)

- **The Simple Ice scheme** adds ice phase processes to the warm rain scheme without adding memory. This scheme does not have supercooled water, and snow is immediately melted below the freezing level. (See Dudhia, 1989.)

- **The Mixed-Phase scheme** adds supercooled water to the simple ice scheme, and slow melting of snow is allowed. Additional memory was added to accommodate the ice and

snow. This scheme does not include graupel or riming processes. (See Reisner et al., 1993, 1998.)

- **The Mixed-Phase with Graupel scheme** adds graupel and ice number concentration prediction equations to the mixed-phase scheme. This scheme is suitable for cloud-resolving scales. (See Reisner et al., 1998.)

- **The NASA/Goddard Microphysics scheme** explicitly predicts ice, snow, graupel, and hail. This scheme is suitable for cloud-resolving scales. (See Tao and Simpson, 1993.)

3.3.5 Nesting

MM5 can simulate nested domains of finer resolutions within the primary simulation domain. In MM5, the software is configured to enable up to nine nests (ten domains) within a particular run. However, due to current hardware resources, the state of the science, numerical stability, and practicality, the number of domains in a simulation is generally limited to four or fewer.

Nesting can be accomplished by either a "one-way" or a "two-way" method. In one-way nesting, the coarse-resolution domain simulation is run independently of the nest. The coarse domain can then provide the initial and boundary conditions for its nest. In one-way nesting, each domain can be defined with independent terrain fields, and there are no feedbacks to the coarse domain from its nest. Note that the simulated meteorology at the same grid point in the coarse-resolution domain is likely to be different (if only slightly) from the nest in a one-way nest simulation.

Two-way interactive nesting (Zhang et al., 1986; Smolarkiewicz and Grell, 1992) allows for feedback to occur between the coarse-resolution domain and the nest throughout the simulation. The two domains are run simultaneously to enable this feedback, and terrain in the overlapping regions must be compatible to avoid mass inconsistencies and generation of numerical noise. The *TERRAIN* program automatically defines the terrain compatibility when the user specifies the two-way nesting interaction. When two-way nesting is used, the portion of the coarse-resolution domain that is simulated in the nest may reflect too much smaller-scale detail from the nest to be useful for the CMAQ simulations.

The nesting ratio between domains in MM5 is generally 3:1. (Some other mesoscale meteorology models allow for user-defined nest ratios.) For example, if the coarse domain is a 36-km resolution domain, its nest will be a 12-km resolution domain. This is strictly true for a two-way nest, but is largely held as a standard for the one-way nests in MM5. The nest ratio restricts the number of grid points in each dimension of the nest domains to a multiple of 3, plus 1.

3.3.6 Four-Dimensional Data Assimilation

The four-dimensional data assimilation (FDDA) scheme included in MM5 is based on Newtonian relaxation or "nudging". Nudging is a continuous form of FDDA where artificial (non-physical) forcing functions are added to the model's prognostic equations to nudge the solutions toward either a verifying analysis or toward observations. The artificial forcing terms are scaled by a nudging coefficient that is selected so that the nudging term will not dominate the prognostic equations. The nudging terms tend to be one order of magnitude smaller than the dominant terms in the prognostic equations and represent the inverse of the *e*-folding time of the phenomena captured by the observations.

There are two types of nudging in MM5: analysis nudging and observation nudging ("obs nudging"). Analysis nudging gently forces the model solution toward gridded fields. Analysis nudging can make use of three-dimensional analyses and some surface analyses. Analysis nudging is generally used for scales where synoptic and mesoalpha forcing are dominant. Obs nudging gently forces the model solution toward individual observations, with the influence of the observations spread in space and time. Obs nudging is better suited for assimilating high frequency, asynoptic data that may not otherwise be included in an analysis.

Nudging in MM5 is extensively discussed in Stauffer and Seaman (1990, 1994) and Stauffer et al. (1991). The data assimilation is generally used throughout the MM5 simulation period for air quality simulations. Three-dimensional analyses of wind, temperature, and moisture are assimilated, and only surface analyses of wind are assimilated, following Stauffer et al. (1991).

3.4 Meteorology Model Post-Processing

Since the output variables that are generated by an MM5 simulation are not always useful in their raw form, those variables must be converted into fields that are required by the chemistry and emission models. The conversion of MM5 output to useful fields for the other Models-3 programs is accomplished in the Meteorology Chemistry Interface Processor (MCIP), which is discussed in Chapter 12. MCIP computes variables that are useful to the subsequent models in Models-3, and it creates an output file written with the I/O API libraries in netCDF format that is standard in the Models-3/CMAQ modeling system.

3.5 Changes to the MM5 System's Software for Models-3

The version of MM5 included with the initial release of Models-3 is MM5 Version 2, Release 6. The system is complete with "bug fixes" included through October 1997. Only selected "bug fixes" and upgrades have been included beyond October 1997. (Including all of the changes to MM5 would have jeopardized testing and evaluation of CMAQ, which uses the MM5 output.)

The version of MM5 in the Models-3 release includes most of the science options in NCAR's current version. The omission of upgrades should not result in substandard or corrupted meteorological simulations.

The following is a summary of EPA-initiated changes that were made to the NCAR release of MM5 and its supporting software to support air quality modeling with CMAQ:

All Programs:

- Standardized the radius of the earth as 6370.997 km to be consistent with chemistry and emission models.

TERRAIN:

- Set terrain height over ocean to zero when using the 1-minute terrain database.
- Improved representation of urban areas along coasts.

INTERP:

- Increased loop indices and parameter sizes to accommodate 120-hour simulation.

MM5:

- Modified script and source code to enable analysis nudging on a one-way nested simulation.

3.6 References

Anthes, R. A., 1977: A cumulus parameterization scheme utilizing a one-dimensional cloud model. *Mon. Wea. Rev.*, **106**, 270–286.

Anthes, R. A., and T. T. Warner, 1978: Development of hydrodynamic models suitable for air pollution and other mesometeorological studies. *Mon. Wea. Rev.*, **106**, 1045–1078.

Arakawa, A., and V. R. Lamb, 1977: Computational design of the basic dynamical process of the UCLA general circulation model. *Methods in Computational Physics*, **17**, 173–265.

Arakawa, A., and W. H. Schubert, 1974: Interaction of a cumulus cloud ensemble with the large scale environment. Part I. *J. Atmos. Sci.*, **31**, 674–701.

Benjamin, S. G., and N. L. Seaman, 1985: A simple scheme for objective analysis in curved flow. *Mon. Wea. Rev.*, **113**, 1184–1198.

Betts, A. K., 1986: A new convective adjustment scheme: Part I: Observational and theoretical basis. *Quart. J. Roy. Meteor. Soc.*, **112**, 677–692.

Betts, A. K., and M. J. Miller, 1986: A new convective adjustment scheme. Part II: Single column tests using GATE wave, BOMEX, ATEX and Arctic air-mass data sets. *Quart. J. Roy. Meteor. Soc.*, **112**, 693–709.

Betts, A. K., and M. J. Miller, 1993: The Betts-Miller scheme. *The representation of cumulus convection in numerical models.* K. A. Emanuel and D. J. Raymond, Eds., Amer. Meteor. Soc., 246 pp.

Blackadar, A. K., 1979: High resolution models of the planetary boundary layer. Advances in Environmental Science and Engineering, 1, No. 1, Pfafflin and Ziegler, Eds., Gordon and Briech Sci. Publ., New York, 50–85.

Burk, S. D., and W. T. Thompson, 1989: A vertically nested regional numerical prediction model with second-order closure physics. *Mon. Wea. Rev.*, **117**, 2305–2324.

Cressman, G. P., 1959: An operational objective analysis system. *Mon. Wea. Rev.*, **87**, 367–374.

Dudhia, J., 1989: Numerical study of convection observed during the winter monsoon experiment using a mesoscale two-dimensional model. *J. Atmos. Sci.*, **46**, 3077–3107.

Dudhia, J., 1993: A nonhydrostatic version of the Penn State/NCAR mesoscale model: Validation tests and simulation of an Atlantic cyclone and cold front. *Mon. Wea. Rev.*, **121**, 1493–1513.

Dudhia, J., 1996: A multi-layer soil temperature model for MM5. Preprints, *The Sixth PSU/NCAR Mesoscale Model Users' Workshop*, Boulder, CO, Natl. Ctr. Atmos. Res.

Dudhia, J., D. Gill, Y.-R. Guo, D. Hansen, K. Manning, and W. Wang, 1998: PSU/NCAR mesoscale modeling system tutorial class notes (MM5 modeling system version 2). [Available from the National Center for Atmospheric Research, P. O. Box 3000, Boulder, CO 80307.]

Fritsch, J. M., and C. F. Chappel, 1980: Numerical prediction of convectively driven mesoscale pressure systems. Part I: Convective parameterization. *J. Atmos. Sci.*, **37**, 1722–1733.

Grell, G. A., Y.-H. Kuo, and R. Pasch, 1991: Semi-prognostic tests of cumulus parameterization schemes in the middle latitudes. *Mon. Wea. Rev.*, **119**, 5–31.

Grell, G. A., 1993: Prognostic evaluation of assumptions used by cumulus parameterizations. *Mon. Wea. Rev.*, **121**, 764–787.

Grell, G. A., J. Dudhia, and D. R. Stauffer, 1994: A description of the fifth-generation Penn State/NCAR mesoscale model (MM5). NCAR Tech. Note NCAR/TN-398+STR, 117 pp. [Available from the National Center for Atmospheric Research, P. O. Box 3000, Boulder, CO 80307.]

Guo, Y.-R., and S. Chen, 1994: Terrain and land use for the fifth-generation Penn State/NCAR mesoscale modeling system (MM5): Program TERRAIN. NCAR Tech. Note, NCAR/TN-397+IA, 119 pp. [Available from the National Center for Atmospheric Research, P. O. Box 3000, Boulder, CO 80307.]

Haagenson, P., J. Dudhia, D. Stauffer, and G. Grell, 1994: The Penn State/NCAR mesoscale model (MM5) source code documentation. NCAR Tech. Note, NCAR/TN-392+STR, 200 pp. [Available from the National Center for Atmospheric Research, P. O. Box 3000, Boulder, CO 80307.]

Hack, J. J., B. A. Boville, B. P. Briegleb, J. T. Kiehl, P. J. Rasch, and D. L. Williamson, 1993: Description of the NCAR community climate model (CCM2). NCAR Tech. Note, NCAR/TN-382+STR, 120 pp. [Available from the National Center for Atmospheric Research, P. O. Box 3000, Boulder, CO 80307.]

Hong, S.-Y., and H.-L. Pan, 1996: Nonlocal boundary layer vertical diffusion in a medium-range forecast model. *Mon. Wea. Rev.*, **124**, 2322–2339.

Hsie, E.-Y., and R. A. Anthes, 1984: Simulations of frontogenesis in a moist atmosphere using alternative parameterizations of condensation and precipitation. *J. Atmos. Sci.*, **41**, 2701–2716.

Janjic, Z. I., 1994: The step-mountain eta coordinate model: Further development of the convection, viscous sublayer, and turbulent closure schemes. *Mon. Wea. Rev.*, **122**, 927–945.

Kain, J. S., and J. M. Fritsch, 1990: A one-dimensional entraining/detraining plume model. *J. Atmos. Sci.*, **47**, 2784–2802.

Kain, J. S., and J. M. Fritsch, 1993: Convective parameterization for mesoscale models: The Kain-Fritsch scheme. *The representation of cumulus in mesoscale models*. K. A. Emanuel and D. J. Raymond, Eds., Amer. Meteor. Soc., 246 pp.

Klemp, J. B., and R. B. Wilhelmson, 1978: Simulations of three-dimensional convective storm dynamics. *J. Atmos. Sci.*, **35**, 1070–1096

Madala, R. V., 1981: Finite-difference techniques for vectorized fluid dynamics calculations. Edited by D. L. Book, Springer Verlag, New York.

Manning, K., and P. Haagenson, 1992: Data ingest and objective analysis for the PSU/NCAR modeling system: Programs DATAGRID and RAWINS. NCAR Tech. Note, NCAR/TN-396+IA, 209 pp. [Available from the National Center for Atmospheric Research, P. O. Box 3000, Boulder, CO 80307.]

Nuss, W. A., and D. W. Titley, 1994: Use of multiquadric interpolation in meteorological objective analysis. *Mon. Wea. Rev.*, **122**, 1611–1631.

Pleim, J. E., and A. Xiu, 1995: Development and testing of a surface flux and planetary boundary layer model for application in mesoscale models. *J. Appl. Meteor.*, **34**, 16–32.

Reisner, J., R. T. Bruintjes, and R. J. Rasmussen, 1993: Preliminary comparisons between MM5 NCAR/Penn State model generated icing forecasts and observations. Preprints, *Fifth Intl. Conf. on Aviation Weather Systems*, Vienna, VA, Amer. Meteor. Soc., 65–69.

Reisner, J., R. J. Rasmussen, and R. T. Bruintjes, 1998: Explicit forecasting of supercooled liquid water in winter storms using the MM5 mesoscale model. *Quart. J. Roy. Meteor. Soc.*, **124B**, 1071–1107.

Smolarkiewicz, P. K., and G. A. Grell, 1992: A class of monotone interpolation schemes. *J. Comp. Phys.*, **101**, 431–440.

Stauffer, D. R., and N. L. Seaman, 1990: Use of four-dimensional data assimilation in a limited-area mesoscale model. Part I: Experiments with synoptic-scale data. *Mon. Wea. Rev.*, **118**, 1250–1277.

Stauffer, D. R., N. L. Seaman, and F. S. Binkowski, 1991: Use of four-dimensional data assimilation in a limited-area mesoscale model. Part II: Effects of data assimilation within the planetary boundary layer. *Mon. Wea. Rev.*, **119**, 734–754.

Stauffer, D. R., and N. L. Seaman, 1994: Multiscale four-dimensional data assimilation. *J. Appl. Meteor.*, **33**, 416–434.

Tao, W.-K., and J. Simpson, 1993: Goddard cumulus ensemble model. Part I: Model description. *Terr., Atmos., and Oc. Sci.*, **4**, 35–72.

Zhang, D.-L., and R. A. Anthes, 1982: A high-resolution model of the planetary boundary layer -- Sensitivity tests and comparisons with SESAME-79 data. *J. Appl. Meteor.*, **21**, 1594–1609.

Zhang, D.-L., H.-R. Chang, N. L. Seaman, T. T. Warner, and J. M. Fritsch, 1986: A two-way interactive nesting procedure with variable terrain resolution. *Mon. Wea. Rev.*, **114**, 1330–1339.

This chapter is taken from *Science Algorithms of the EPA Models-3 Community Multiscale Air Quality (CMAQ) Modeling System*, edited by D. W. Byun and J. K. S. Ching, 1999.

EPA/600/R-99/030

Chapter 4

EMISSION SUBSYSTEM

William G. Benjey* and James M. Godowitch**
Atmospheric Modeling Division
National Exposure Research Laboratory
U.S. Environmental Protection Agency
Research Triangle Park, NC 27711

Gerald L. Gipson
Human Exposure and Atmospheric Sciences Division
National Exposure Research Laboratory
U.S. Environmental Protection Agency
Research Triangle Park, NC 27711

ABSTRACT

Chapter 4 provides a description of the Models-3 Emission Processing and Projection System (MEPPS) structure, scientific approach and the assumptions used in modeling and processing emission data in the Models-3 framework. The description includes emission data entry through the Inventory Data Analyzer (IDA) import and quality control checks; and the data flow and quality control used in loading emission inventory and meteorology data in the MEPPS Input Processor. The description of the main Emission Processor addresses the basis of spatial and temporal allocation procedures. The scientific models and assumptions used in modeling hourly mobile source and biogenic emissions are explained (Biogenic Emission Inventory System 2 and Mobile 5a, respectively). The rationale and assumptions are described which are used in the allocation and grouping of individual chemical species into "lumped species" in preparation for the lumped species chemical transformation mechanisms contained in the Community Multiscale Air Quality (CMAQ) model. The chapter also describes the procedures used by the Models-3 Emission Projection Processor to estimate emission data for use in modeling future air quality scenarios. Finally, the quality control report and output file options contained in the Output Processor are described.

---

*On assignment from the National Oceanic and Atmospheric Administration, U.S. Department of Commerce. Corresponding author address: Bill Benjey, MD-80. Research Triangle Park, NC 27711. E-mail: benjey@hpcc.epa.gov

**On assignment from the National Oceanic and Atmospheric Administration, U.S. Department of Commerce.

4.0 EMISSION SUBSYSTEM

The rationale for the Models-3 air quality emission processor is rooted in the need to estimate, organize, and process emission inventory data for regulatory and scientific analysis and modeling. Historically, air quality emission processing methods have been developed in an ad hoc manner, with each procedure specifically tuned to meet the need at hand, reflecting the various data information sources and estimation methodologies, as well as the uses of the data. The Models-3 air quality emission processor consolidates and simplifies the estimation, data handling, and linkage of the resulting data to air quality models. This section describes the purpose, origins, and scientific bases of the Models-3 Emission Projection and Processing System (MEPPS). Material is presented in the general sequence of emission processing. System requirements, system design ,and detailed user information for emission data processing are not addressed in this Volume. These items are described in Volume 7, Volume 8, and Volume 9B, respectively of the Models-3 documentation set. For example, processor names, environment variables, and flow diagrams are given in Chapter 6 of the *Models-3 Volume 9B: User Manual.*

4.1 Emission Inventory Processors

In the Models-3 framework, MEPPS imports, quality controls, and processes emission inventory data for either direct regulatory analysis or input to a chemical transport model. The MEPPS also models hourly biogenic emissions and mobile source emissions. The MEPPS is non-conforming within the framework because it is not an object-oriented component, and because it does not use the NetCDF Input/Output Applications Program Interface (I/O API) format internally. Processing is accomplished using a combination of FORTRAN, SAS®, and ARC/INFO® programs. The emission processor results are translated into the NetCDF I/O API format by the MEPPS Output Processor.

4.1.1 Discussion

The MEPPS builds on lessons from and functionalities of previous software developed for processing emission inventories. The capabilities and design decisions in MEPPS are placed in the context of emission inventory developments.

4.1.1.1 The Role of Emission Inventory Processing for Chemical Transport Modeling

Historically, there have been many air quality emission data bases which were compiled and used for the purposes of regulatory or scientific assessment of emissions, including spatial and temporal patterns and trends. As air quality chemical transport models (CTMs) were developed, each had its own specific format for input data, based either on the data structure used in the model and/or the format of the available data. Initially, CTMs were relatively simple and applied to one or a few point sources, such as emissions from an industrial stack. As CTMs for urban and regional scales - such as the Urban Airshed Model (Morris et al.,1992) - became more sophisticated, the level of detail needed for input emission data became increasingly more comprehensive and

detailed. It became necessary to include as complete an inventory as possible for the area of interest, including emissions from all diffuse as well as point sources at as great a degree of spatial and temporal resolution as possible. As the spatial and temporal resolution of the models has increased, so has the demand for detailed emission input data. Because of resource limitations on data gathering, the emission inventory information needed often substantially exceed the reported or observed emission data available. The result is development of a wide range of emission estimation and modeling techniques.

Emission inventory data are available from various sources, often state and local air pollution control agencies. The data are commonly compiled into annual emission inventories for specific areas to be analyzed and/or modeled. The spatial extent of an emission inventory may vary from plant-specific emission data to data for an entire country or more. Recent regional examples include the National Acid Precipitation Assessment Program 1985 National inventory (Saeger et al.,1989), the 1990 EPA Interim National Emission Inventory (U.S. EPA, 1993; U.S. EPA, 1994), and the 1990 Ozone Transport Assessment Group inventory (Ozone Transport Assessment Group, 1997). Most emission inventories are organized into four traditional general groups of emission types:

- Point sources, which are emission sources attributable to discrete emission points, usually a stack. The data include pollutant, source category code, stack parameters (height, diameter, exit velocity, temperature, flow rate), emissions, location coordinates, fuel, etc.

- Area sources, which are emission sources attributable to diffuse sources or areas, such as agricultural fields, large open mining operations, forests, or a combination of many point sources which are too small and numerous to account for individually (e.g., residences). Area source inventories are typically by county and include pollutant, source category code, emissions, location, coordinates, etc.

- Biogenic sources, which are often natural emissions from vegetation, soils, and lightning. Biogenic emissions are dependent on temperature, solar radiation, and land cover type. They are usually modeled hourly for specific days and locations.

- Mobile sources, which are emissions from vehicular traffic on roadways, aircraft, trains, shipping, and off-road mobile equipment. Mobile source emissions are dependent on the ambient temperature, road type, vehicle type and age, miles traveled, etc. These emissions are generally modeled for specific day and meteorology scenarios either by county or road segment (link-node data).

The techniques used to estimate emissions in compiling an emission inventory are based on extrapolation of limited direct measurements for point sources, and application of limited measurements or estimates to spatial surrogate data for area sources. Emissions which are dependent on environmental conditions (e.g., biogenic and mobile source emissions) are modeled to generate either portions of emission inventories or hourly data for direct use in air quality

modeling. The procedures used to process emission inventory data and to model and process mobile and biogenic source emission data are described in more detail in the following sections.

Point source and area source emission inventory data are usually included in annual emission inventories. Annual mobile and biogenic emissions are included if the inventory was intended for assessing annual totals or trends of emissions. If the inventory was prepared for modeling, only the annual "Vehicle Miles Traveled" by county or road segment and vegetation land cover may be provided. In order to accomplish episodic air quality modeling, it is necessary to model the hourly mobile and biogenic emissions for the episode-specific meteorological conditions.

The typical procedures used to prepare annual emission inventories for use in a CTM require temporal, spatial, and pollutant species allocation of the data. This is accomplished in a sequential manner. For regional modeling, initial "raw" emission inventory data files are very large, often several megabytes in size. The data files are subjected to a variety of data quality checks, depending upon the methodological sophistication and computing and time resources available. Typically, visual inspections of mapped locations, value range checks, cross-checks of sums, and routine computer checks for blank fields and valid data types are performed.

In order to reduce the size of emission data files, the data are often speciated first, depending upon the pollutants involved, then temporally allocated to hourly data, and then spatially allocated or "gridded" to a spatial domain with gridded cells of the resolution required by the CTM. At each step some of the detailed information, such as source category code and geographic coordinates, are dropped to reduce the file size. Hourly mobile source and biogenic emission data are modeled using the appropriate hourly meteorological data, and merged with point and area source data prior to speciation.

It is necessary to rerun the processing sequence in the event of an error, or for each new meteorological or day-specific scenario. Projections to future years require application of source-category-specific economic growth factors to a base year inventory to produce a projected annual inventory. The projected inventory is then processed through the entire emission processing sequence. Preparation of detailed regional emission inventory data for regional modeling using this traditional approach may take weeks or month.

4.1.1.2 Function and Place of the Emission Processor in the Models-3 Framework

The Models-3 framework is designed to contain conforming object-oriented modules that pass data in the NetCDF I/O API format, although non-conforming modules are accommodated at the cost of reduced functionality. The emission processing system is intended to ultimately be conforming. The initial version of MEPPS was derived from existing software and consequently is not a conforming object-oriented program in Models-3. However, it is integrated into the Models-3 framework and does take instructions and information from the system and provides emission data output in NetCDF IO/API format. Figure 4-1 provides a functional view of the Models-3 system. Processing of emission data is often a part of iterative air quality strategy

building, directly or indirectly, though the effect of emissions on air quality modeling results. Figure 4-2 is a simplified illustration of the location of MEPPS and other non-conforming components within the Models-3 framework. The main aspects of a study (including the principal emission processing options) are graphically defined in the high-level Models-3 Study Planner, and the resulting information is automatically passed to MEPPS as well as other portions of the system. Specifically, a study name is defined by the user by copying, modifying, and renaming an existing "template" emission study. For example, a tutorial emission study could be used as a template to define a new study. The new study is associated with input data sources, MEPPS processing and modeling modules and their primary options by annotating links and nodes in the specified emission study and plans. The pollutants of interest, the geographic domain, map projection, grid spatial resolution, chemical speciation mechanism, temporal resolution, and dates of interest (referred to as the "case") are defined in the Models-3 Science Manager and passed to the rest of the system including MEPPS. This approach allows the user to make primary specifications once, rather than separately to each of the system components and thus ensures consistency. Study Planner and Science Manager also aid in using the system to run multiple emission, projected emission, and emission control scenarios without frequent respecification of parameters. From a functional view, MEPPS generates emission data that reflect user-defined studies and cases, whether for regulatory analysis of emission data and/or for input to CTM runs and comparison with CTM results.

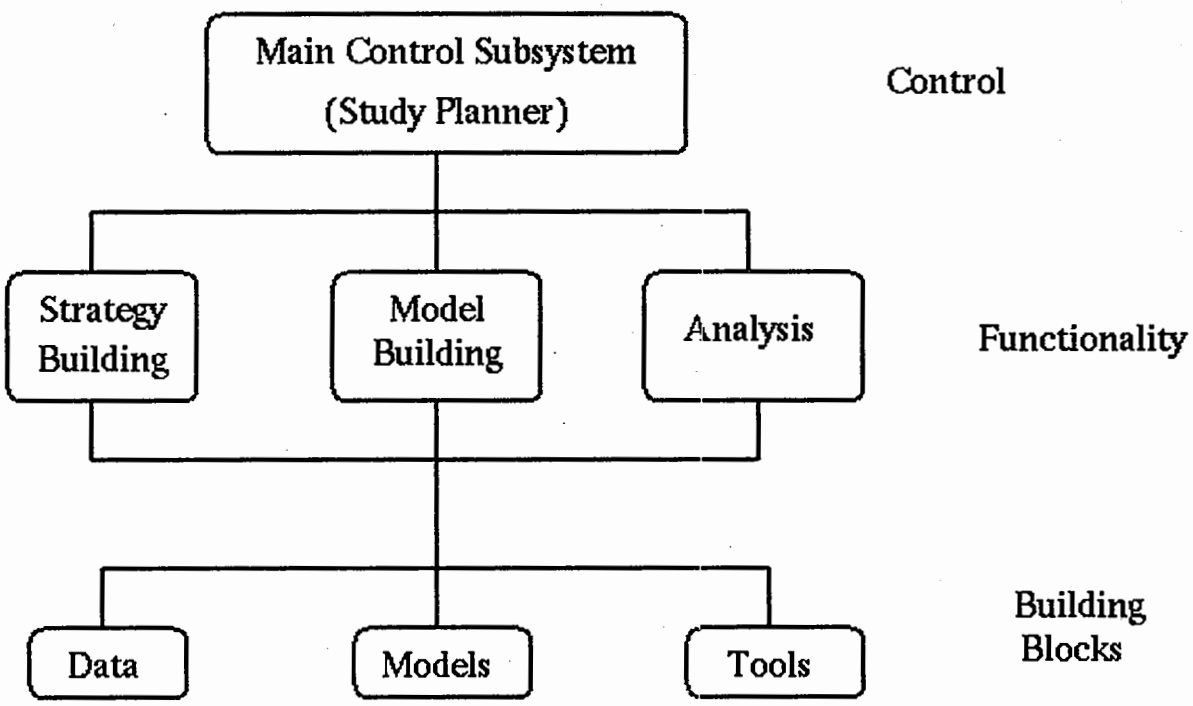

Figure 4-1 Functional View of the Models-3 System

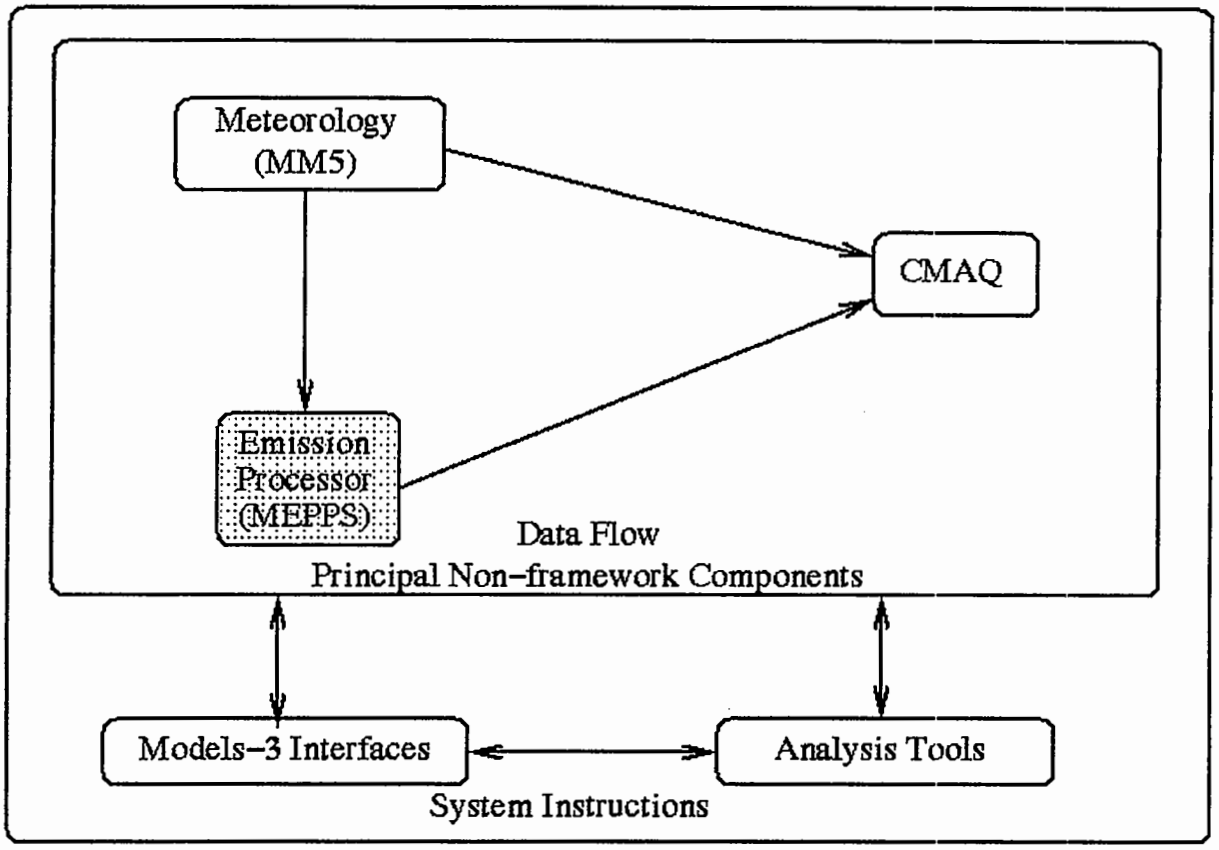

Figure 4-2 The location of MEPPS within the Models-3 Framework

The emission processing function of MEPPS requires that it be linked to the Models-3 framework, and to other processing, modeling, and analysis tools through the framework. MEPPS outputs data in the NetCDF I/O API format in order to link MEPPS to the Models-3 framework and other processing, modeling, and analysis modules. Figure 4-3 illustrates that information (grid, chemical mechanism, and case) user-specified in Models-3 Science Manager for a study is passed to other modules, including MEPPS. However, it is necessary to access the Parameter Window of MEPPS through the Tools Manager, to specific study name, grid, source (data source name), and case, and then return to the Study Planner to run the emission study. Direct access to MEPPS is through the Tools Manager and the emission projection and control functions are in Strategy Manager. New emission inventory data are imported and quality controlled through the Models-3 File Converter and its subsidiary Inventory Data Analyzer (IDA). The data are then imported directly into MEPPS through its internal Input Processor (INPRO). Meteorological information needed to estimate biogenic and mobile source emissions are provided to MEPPS from a meteorological model or dataset in the Models-3 system through

the Meteorology-Chemistry Interface Processor (MCIP). For regional-scale modeling, the current default meteorological model is Mesoscale Model 5 (MM5). The MEPPS processes emission data into speciated, spatially and temporally allocated hourly emission data for use in a Models-3 conforming CTM. The data are output as NetCDF I/O API files to the Emission-Chemistry Interface Processor (ECIP) which adjusts the format to that needed by the CTM. Emission data for large elevated point sources (large stack emissions) are also provided as I/O API files to the Plume Dynamics Module, and the plume rise algorithm.

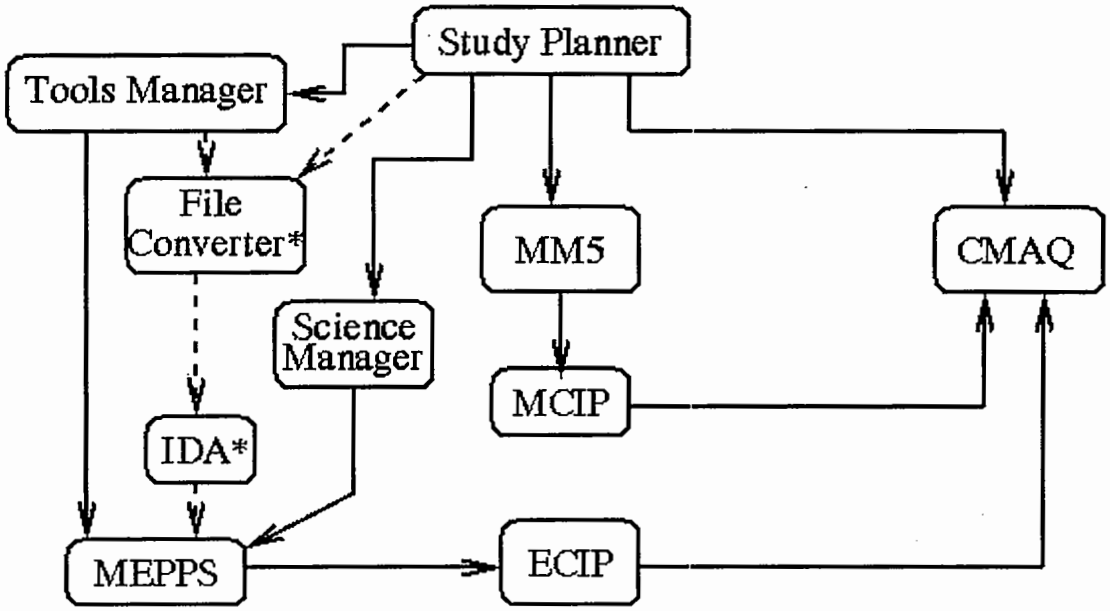

Where: MM5 is Mesoscale Model 5
CMAQ is Community Multiscale Air Quality Model
MEPPS is Models-3 Emission Processing and Projection System
MCIP is Meteorology-Chemistry Interface Processor
ECIP is Emissions-Chemistry Interface Processor
*IDA is Inventory Data Analyzer
*File Converter is generic to the Models-3 system
*IDA and File Converter are optional (used for new data)

Figure 4-3 Relationship of Principal Models-3 Framework Components

4.1.1.3 Rationale for the Basis of the Initial Version of MEPPS

In order to assure that an acceptable and functional emission inventory processor would be present in the initial release of Models-3 given time and resources available, it was decided that the emission processing module for the initial version would be based on software and methodologies available as of 1994. More advanced approaches being researched and developed then and now will be incorporated as soon as possible. The decision factors used in selecting

from existing emission processors were availability, cost, features (capabilities), hardware and software requirements, and operating characteristics. Table 4-1 lists the emission processing systems considered with respect to the principal evaluation factors.

Based on the evaluation, the Geocoded Emission Modeling and Projection System (GEMAP; Wilkinson et al.,1994), now known as the Emission Modeling System-95 (EMS-95), was selected as the basis of the initial emission processing system, although it is non-conforming (not in I/O API Net CDF) in the Models-3 system. The GEMAP was selected because it was readily available in the public domain; it was state-of-the-art at the time; there was no licensing cost (exclusive of GEMAP's internal use of SAS® and Arc/Info®); its code was modular and flexible; and it contained a geographic information system to perform spatial allocation of emission inventory data.

Other systems considered included the Emission Processing System (EPS), The Flexible Regional Emission Data System (FREDS), and the Sparse Matrix Operator Kernel Emission System (SMOKE). The EPS is used to process emission inventory data for the Urban Airshed Model (UAM; U.S. EPA, 1992). A recent adaptation of EPS by Environment Canada for regional use is called the Canadian Emission Processing System Version 1 (CEPS1.0) (Moran et al., 1998). Like GEMAP, EPS would be non-conforming code in the Models-3 framework, and would require design and development of interfaces with the Models-3 system and the addition of many features. However, EPS does not include flexible GIS-based gridding capability of GEMAP and was originally designed for urban scale air quality modeling as opposed to the multiscale (local to regional and national) air quality modeling capabilities of Models-3.

The FREDS has been used for regional air quality modeling during the past ten years in conjunction with the Regional Oxidant Model and Regional Acid Deposition Model (Modica et al., 1989). The FREDS code is run on a main-frame computer, and is "hard-wired" and difficult to change for different scenarios or grids. Consequently it lacks the modularity and flexibility needed to operate in the Model-3 framework.

Design and prototyping of SMOKE was just beginning when the design of the initial version of Models-3 was determined (Coats, 1995). The SMOKE, which is now being used in conjunction with UAM, could be modified to be fully compliant with the object-oriented Models-3 system. Additional analysis and quality control tools are being designed for SMOKE, and initial work has begun to adapt it to the Models-3 framework.

Table 4-1. Emission Processor Selection Factors for the Initial Public Release of Models-3

Factors	Emission Processing System (EPS)	Flexible Regional Emission Modeling System (FREDS)	Geocoded Emission Modeling and Projection System	Sparse Matrix Operator Kernel Emission (SMOKE) system
Acquisition Cost of Source Code[1]	None	None	None	N/A
Availability	Public domain	Public domain	Public domain	N/A
Degree of Development	Completed and in use	Completed and in use	Initial version being tested	Design and prototype beginning
Relative Flexibility for Modification to Models-3	Changes required recoding of modules to allow revised interfaces and external control - spatial allocation would be added	Changes required substantial recoding - many patches - relatively inflexible -spatial allocation would be added	Changes required recoding of modules to allow revised interfaces and external control - spatial allocation already present	N/A
Hardware Requirements	Work station with UNIX operating system	IBM Mainframe system	Work station with UNIX operation system	Unix-based machines, specifics not established
History (Operating Experience)	Established system used by EPA, state, and local agencies	Established system used by U.S. EPA in regional modeling programs	New system, used only with test data in California	N/A
Software Requirements	FORTRAN and SAS®	FORTRAN and SAS®	SAS® and ARC/INFO® licenses.	Unix-based, specifics not well established
Spatial Allocation Capability	Spatial allocation grids must be manually coded for each allocation scenario.	Spatial allocation grids must be manually coded for each allocation scenario.	ARC/INFO® allows flexible user-defined grid domains, spatial resolution and data overlays	Unknown

Since its selection, GEMAP/EMS-95 has been substantially modified and incorporated into MEPPS. Because of the changes, the GEMAP portion of MEPPS has been renamed the Emission Processor (EMPRO) module. Revisions were made to allow the software to be more generic and efficient in its operation, and new features were added. In general, new capabilities were written in FORTRAN and placed in modules outside of GEMAP. This was done to minimize rewriting of code in future when the GEMAP-based portion of the system is replaced.

MEPPS must include several basic functions. There are also many enhancements, detailed descriptions for which may be found in Volumes 7, 8, and 9 (System Requirements, System Design, and User Manual, respectively) of the Models-3 documentation set. The experience and design suggestions of personnel familiar with processing large emission inventories were used as important guidance in deciding which features to include in MEPPS. The design and implementation of MEPPS emphasized ease of use and efficiency within the overall design of the Models-3 system. The following paragraphs present a brief description of the principal functions included in MEPPS.

- Annual point and area source emission data from inventories are subset to the spatial domain of interest, spatially allocated to a grid, and temporally allocated. Area source emissions are spatially allocated using surrogate spatial coverages.

- Spatial allocation of each general type of air quality data (point, etc.) to grid cells is done by the GIS using a grid defined by the Science Manager module of Models-3.

- Modeled estimates of mobile source emissions are prepared on an hourly basis for periods of interest, usually several days. These estimates account for meteorological conditions using data from a meteorology model (such as MM5) that has been passed through the Models-3 meteorology-chemistry interface processor (MCIP). Hourly, grid-cell specific emission factors for different vehicle and roadway classifications are prepared with MM5 using vehicle miles traveled (VMT) data from an emission inventory.

- Modeled hourly estimates of biogenic source emissions are prepared on an hourly basis for periods of interest, using the Biogenic Emission Inventory System Version 2 (BEIS-2) and meteorology data from MCIP and land use coverages (see Section 4.2.4.1).

- Temporal allocation of emission data to hourly data for the period of interest is accomplished using source-type specific defaults or user-selected temporal allocation profiles.

- Disaggregation of gridded, temporally-allocated emission data of groups of chemical species to specific species (chemical speciation) is completed according to the users choice of chemical speciation mechanism (currently Carbon Bond 4 (CB-4) and RADM 2.0).

- Projection of emission inventory data to future years from a base-year inventory (1990) and application of controls is performed by the Models-3 Emission Projection Processor (MEPRO). Projected emission inventories are used to iteratively evaluate different emission scenarios caused by economic or emission control changes. Projected emission inventories are each processed by MEPPS for air quality modeling in the same way as the original, or "base" inventory.

- Merging of spatially and temporally-allocated, speciated files for point, area, mobile, and biogenic emission data into one emission data output file, and translation into NetCDF I/O API format are performed for use in the Models-3 system, including the chemical-transport model. Summary and quality control reports on the output data are also produced.

- User-defined point-source emission data are extracted and prepared for use in vertically-layered (three-dimensional) emission files to be used with the plume dynamics module of the Models-3 system.

4.1.2 General MEPPS Structure

The MEPPS is normally used as an integral part of the Models-3 framework from high-level menu-driven screens and pick-lists.

MEPPS in the Models-3 Framework

A user may define a study using the Study Planner within Models-3. The Study Planner specifies the name and description of a study, and defines data sources, models, and the relationship between them using a graphical interface. If a study includes processing of emission data, the sequence of processing operations, source file addresses and many options for processing are defined by the Study Planner and passed to MEPPS annotated to the study name. Specifications for spatial allocation grids, and definition of specific temporal cases are defined in the Science Manager. Existing studies, grids, work space directories, speciation mechanisms, source directories, and computer hosts must be selected from the MEPPS parameter window located through the MEPPS icon in the Tools Manager prior to running under the Study Planner. The MEPPS may also be directly accessed through the Tools Manager and run interactively via its SAS® interface windows. During direct access interactive operation, some features may be run individually in the background using an "interactive" batch mode selection, or a series of processes may be run together as a concatenated batch run.

The MEPPS shares an import File Convertor with the rest of the Models-3 framework. The File Convertor will import any ASCII, SAS®, or NetCDF I/O API file of format known to the user. SAS® data sets are used within EMPRO. The data are imported, converted, and subjected to basic quality control checks, including missing or out-of-range values. The data are then put through the Inventory Data Analyzer (IDA) for quality control and analysis specific to emission files,

including inventories (in one of four EPA formats), temporal allocation factors, control factors, vehicle miles traveled, and continuous emission monitoring (CEM) data. The data then go to the MEPPS Input Processor (INPRO) for final quality control and loading into EMPRO.

The Internal Components of MEPPS

The emission processor (MEPPS) includes several basic components (Figure 4-4): an emission data Input Processor (INPRO), a main Emission Processor (EMPRO), an Output Processor (OUTPRO), and a Models-3 Emission Projection Processor (MEPRO). The File Converter and IDA are not intrinsic parts of MEPPS. They are used to import, quality control, and convert the formats and units of data files of known format to the formats that are used in the Models-3 system, including emission inventories and related emission data files. The INPRO imports emission inventory data from IDA and meteorology files from MCIP, and prepares them for use in EMPRO. The EMPRO spatially and temporally allocates point and area source emission data to hourly gridded data. It is also used to model biogenic and mobile-source emission data using meteorological data generated by MM5 and processed by MCIP, as well as spatially and temporally allocates the data. The EMPRO then allocates (groups) the chemical species from the gridded temporally allocated emission files according to the user's selection of a chemical speciation mechanism. The speciated files then go to OUTPRO where they are merged (a two-dimensional file). Quality control is performed and summary reports are prepared in accordance with the user's choices. The user also may divide point sources into categories to separate very large sources (major-elevated point sources or MEPSE) and large sources (major sources) into separate output files, which may be placed in a three-dimensional emission output files to be allocated to vertical layers for CMAQ. The user defines what is MEPSE or major using a combination of pollutant-specific emission values and/or stack parameters (see Section 4.2.6). Remaining point sources are merged into the two-dimensional emission output file along with area, mobile, and biogenic source emission data. Output files are in NetCDF I/O API format. The MEPRO module projects emission inventory data to future years while applying controls. The projected emission data can be read by EMPRO for further processing if modeling of a projected case is desired

4.2 The MEPPS Emission Processing System

Although MEPPS is a significant advance in emission inventory data processing, it is continually being improved. The following sections describe the scientific rationale for the 1998 (first public release) version of the system.

This section describes the basis for emission processing procedures in MEPPS. For models developed independently of the Models-3 framework and incorporated into MEPPS, documentation for those models is referenced. MEPPS was developed to meet emission processing needs specified in *Models-3 Volume 7: Design Requirements* of the Models-3 documentation set, as amended. The design requirements for emission inventory processing are based on the emission data input requirements of chemical transport models, and on the needs of

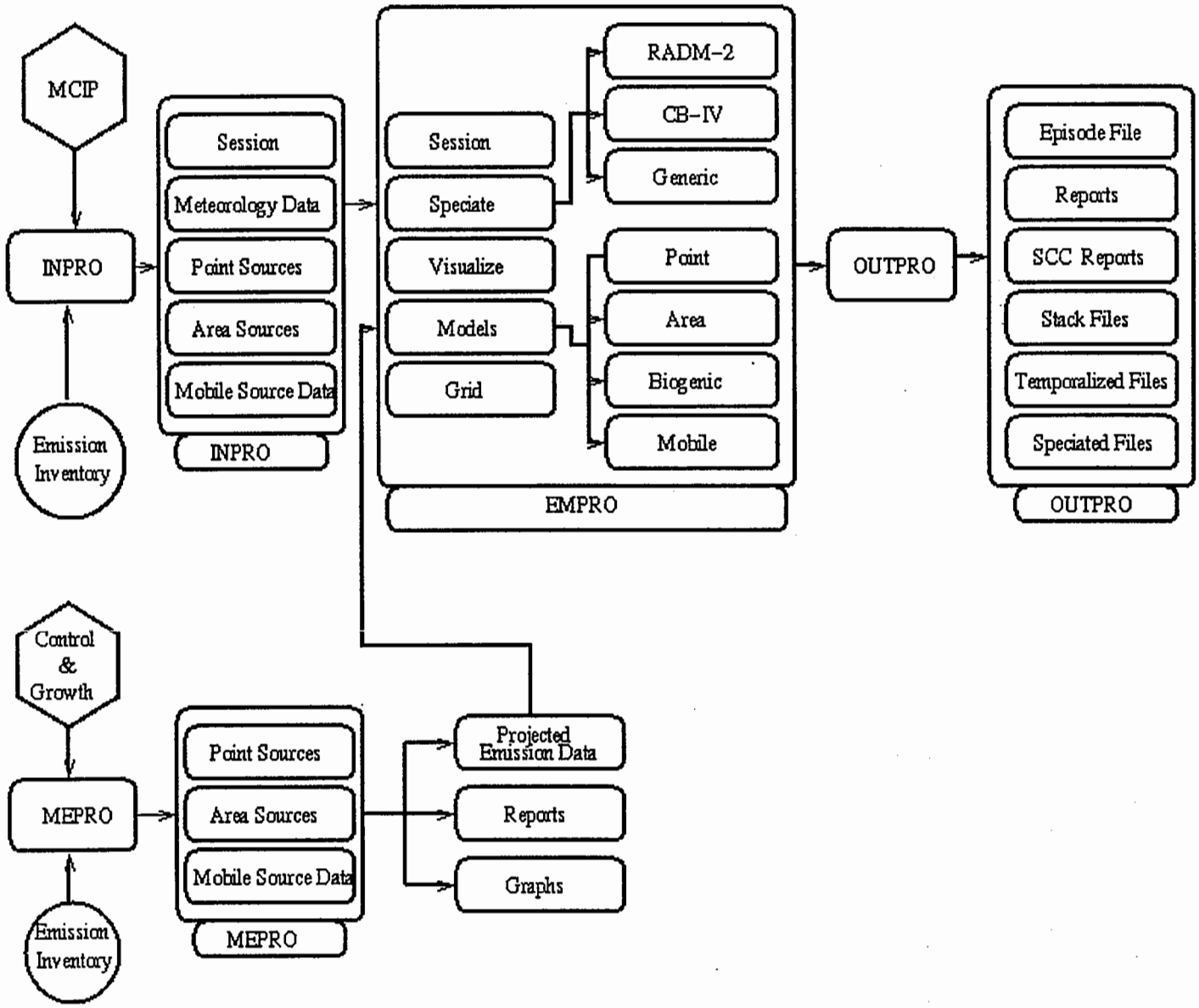

Figure 4-4 Functional Components of MEPPS

those who will use MEPPS to process emission data for both regulatory and scientific emission analysis as well as CMAQ data input. Two guiding principles were followed in the design and implementation of MEPPS. First, substantive changes to the existing GEMAP system were minimized because of a long-term goal to replace GEMAP with a more flexible, less costly (in terms of software licenses), and faster processor. Changes focused on improving the processing efficiency and correcting basic inadequacies of GEMAP. The second principle was to place new features and new emission processing developments outside of GEMAP to the extent possible, but within MEPPS. The resulting structure will make it easier to replace the GEMAP-based portion of MEPPS in the future.

MEPPS is usually run from the Models-3 Study Planner, although it can be run independently in interactive mode. Consequently, MEPPS is configured to run in a "batch" mode (from Study Planner for multi-day cases), and to accept Study Planner specifications for emission data processing and location of data sources. Some MEPPS processors that may be run when accessing MEPPS through the Tools Manager (such as file, grid, and case creation, deletion, or editing), will not function when MEPPS is accessed through the Study Planner. This provision avoids conflicts when these processes are specified from the Models-3 framework under Science Manager. The main components of MEPPS are each discussed in the following sections.

4.2.1 The Inventory Data Analyzer (IDA)

The IDA is an important enhancement to Models-3. It operates as an adjunct to the generic File Converter, which is described in Section 10.8 of the Models-3 User Manual (Volume 9b of the Models-3 documentation set). The File Converter is fully-compliant component of Models-3, applicable to the entire system, and provides file format and unit conversion for files imported into or exported from Models-3, including emission related files. The formats currently used in Models-3 and supported by the File Converter are NetCDF I/O API (gridded data), ASCII, and SAS®.

The IDA imports files from the File Converter and provides quality control and analysis tools specialized for reading, comparing, editing, and analyses of emission data . Quality control reports are generated including the results of the checks. Emission inventories that are in terms of annual, daily, or hourly emissions can be imported. The functionality of IDA is fully described in Section 6.2 of the User Manual. Specific quality control functions include the following:

- Range checks. Ranges accepted by IDA were taken from the range of values known to be correct in inventories currently in the system (1985, 1990, 1995). English units are used because most U. S. inventories are submitted with those units. Values outside of the validity ranges are considered incorrect. The validity ranges currently used in IDA for point-source stacks are:

Diameter	>0.5 and < 50 ft.
Diameter	< 0.2 * Height
Height	>1.0 and <1,250 ft.
Temperature	>50 and <2,000°F
Velocity	>1 and <1000 ft/sec
Flow rate	>1 and < 30,000,000 ft^3/sec and/or

Flow rate must not be more than 10 percent different from flow rate calculated from Velocity and Diameter.

- Sign checks. The system reports suspect signs based on the knowledge that particular parameters are always of a given sign (e.g., stack height are positive).

- Missing data checks. The system automatically fills missing data with Source Category Code-specific default data generated from the inventory being processed.

- Incorrect data checks. Data are corrected automatically when they can be computed based on specific mathematical relations between data elements (such as exit velocity for stack parameters).

- Completeness cross-checks are performed between the plant, stack, process, and emission hierarchy levels of point source inventories. Each level should be associated with data at the next lower and higher level. For example process data should be subsidiary to corresponding stack information, and superior to associated emission data. Specific quality control checks are provided for each level of point, area, and mobile source inventories.

- Location checks, which are applied to determine that the specified political unit (e.g., county) is valid in each case, and that latitude and longitude coordinates (for point sources) are not reversed or missing. Political unit identifiers are checked against a list within IDA. When point-source latitude and longitude coordinates are missing, they are currently assigned to the pseudo-center of the appropriate county. The missing values are usually associated with smaller point sources. This assignment procedure can result in over-representation at the county center. Work is planned to better distribute point sources reported without geographic coordinates.

- Some emission inventories do not include sulfate (SO_4) emission data, which are important in modeling of particulate matter. The IDA can approximate SO_4 emission data by multiplying the source-category specific ratios of SO_4 to sulfur dioxide (SO_2) taken from the 1985 National Acid Precipitation Assessment Program (NAPAP) inventory, with SO_2 values in another inventory. The NAPAP inventory is considered to contain the best separate national modeling estimates of both SO_2 and SO_4 emissions at this time. If an inventory contains SO_4 data, this approximation feature is not used. The SO_4 estimator is optional in IDA. However, it is applied automatically in INPRO if no SO_4 values are

present. With this method, SO_4 estimates were supplied for the 1990 and 1995 U.S. inventories included with the initial Models-3 release.

- Occasionally an emission inventory contains an error in particulate matter emission values such that the fine fraction ($PM_{2.5}$) emissions exceed the value of the coarser fraction emissions (PM_{10}) of which they are a part. In the absence of more specific data, or information that the coarser particulate emission (PM_{10}) are in error, IDA automatically computes a new $PM_{2.5}$ value using the 1990 national inventory ratio of $PM_{2.5}$ to PM_{10}, which is expressed as $PM_{2.5} = .2411\ PM_{10}$.

- Point source stack emission parameters are essential to plume rise calculations in modeling. However, the stack parameters often have erroneous or missing values in emission inventories. In addition to range checks, IDA addresses the problem in two ways:

  (1) IDA examines point source files for consistency between stack flow rate, velocity, and diameter. The following relationship is used to correct erroneous velocity and flow values:

  $$F = V * 0.785398 * D^2 \qquad (4\text{-}1)$$

  where:
  F is flow (cubic feet/second)
  V is velocity (feet/second)
  D is stack diameter (feet)

  (2) In the event that all or most stack parameters are missing for a given point source, IDA supplies default values which are computed by SCC from other point sources in the same emission inventory.

4.2.2 The MEPPS Input Processor (INPRO)

The INPRO includes the MEPPS processors used to establish an emission study, the grid directory structure, and time-specific cases. These items are usually defined using the Models-3 Science Manager, specified through the Study Planner in the Models-3 framework, and passed to INPRO, unless MEPPS is being operated through the Tools Manager.

<u>Import and Processing of Emission Inventories</u>

The INPRO serves as the principal data access point for MEPPS. Two primary sets of data manipulations are accomplished in INPRO to prepare the data for further study-specific processing in MEPPS:

- The emission inventory data are subsetted and imported for the grid specified in the main MEPPS window and (if necessary) created in Science Manager. The emission data are subset from the user-selected emission inventory for the kinds of emission sources (point, area, mobile) specified by the user. The INPRO accepts inventories from IDA in the NET or IDA inventory formats (see Section 10.8 of the User Manual). The user must be sure that any aggregated (not hourly) data in the inventory for biogenic and mobile source emissions (other than vehicle miles traveled) are deleted from the inventory before use. Otherwise, MEPPS will double-count these emissions because hourly biogenic and mobile source emissions are modeled during processing.

- The INPRO imports meteorological data specific to the spatial domain and temporal case defined in Science Manager and selected in the MEPPS main window, provided that the meteorological data have been previously generated. The data come from the Mesoscale Meteorology Model 5 (MM5), via MCIP. The MCIP converts MM5 output to NetCDF IO/API files containing information needed by the rest of the Models-3 system (see Section 7.3 of this volume and Section 2.3.1 of the User Manual). In MEPPS, meteorology data are needed to model hourly biogenic and mobile source emissions (Sections 4.2.4.1 and 4.2.4.2). The MEPPS uses four of the files provided by MCIP, named MET_CRO_2D_ xx, MET_CRO_3D_ xx, GRID_DOT_2D_ xx, and MET_DOT_3D_ xx. The terms "CRO" and "DOT" refer to the cross and dot points of grids, respectively, and the suffixes "xx" are study specific identifiers. Refer to Chapter 12 for the details of the grid system definitions.

ROG-to-TOG Adjustment

Emission inventories may reflect different assumptions or methodologies with respect to volatile organic compound (VOC) gases. They may be reported as VOC, reactive organic gases (ROG) or total organic gases (TOG). It is typical to require TOG for air quality modeling, whereas the VOCs comprising organic gases in many regional inventories are reported as ROG. This occurs because some emission measurement techniques do not capture all of the discrete hydrocarbon compounds in the emission stream. Since the hydrocarbon speciation profiles are based on total organic compounds, the measured value of the hydrocarbon must be adjusted to account for the missing hydrocarbon components for the emission measurements that fail to capture the total organic emission stream. This adjustment is included as an option when importing an inventory using INPRO. The default is "yes" - perform the adjustment. More details are given in the speciation discussion in Section 4.2.5.

4.2.3 Processing Procedure

A detailed description of the processing procedure is given in Chapter 6 of the *Models-3 Volume 9B: User Manual*. Briefly, EMPRO receives point- and area-source emission data from INPRO for use in biogenic- and mobile-source emission modeling. The general sequence of processing for all of the emission data is (1) spatial allocation, (2) temporal allocation, and (3) chemical

speciation. There are some variations in processing between the general types (point, area, biogenic, mobile) of emission data because of the spatial and temporal resolution available and method of estimation. The gridded, temporally allocated and speciated data are passed to OUTPRO where they are merged into output files in the NetCDF I/O API format.

4.2.3.1 Spatial Allocation of Emission Data

The emission inventory data are usually provided by discrete point sources or by political units (typically counties in the United States). In order to prepare the data for use in air quality models and for analysis by grid-oriented visualization tools such as PAVE, the data must be spatially allocated (gridded) on a map projection and rectangular grid. The map coordinate system, grid position and spatial resolution are defined from windows in the Models-3 framework Science Manager (Sections 7.1 and 7.2 of the *Models-3 Volume 9B: User Manual*), although the actual grid creation is performed by the ARC/Info program. The MEPPS is capable of using Lambert Conformal, Mercator, Albers, and Universal Transverse Mercator (UTM) map projections; and several datums including perfect sphere, NAD83, and Clarke. However, in order to maintain consistency with gridded MM5 meteorology data, a spherical datum must be used. The radius used for Models-3 applications is 6370.997 kilometers.

Aside from the spherical datum restriction, the gridding processor allows development of a variety of emission grid systems which are used in different aspects of air quality modeling studies, including emission processing and in CMAQ. The gridding processor is written in the ARC® Macro Language (AML®) of the Arc/Info® geographic information system (GIS). Grids are used in MEPPS to spatially disaggregate or aggregate emission estimates, using land use/land cover data, and area source spatial surrogate data. Surrogate data are needed to spatially distribute emission data because the exact location of emission sources totaled for a county, for example, are seldom known. For example, census tract population data are of higher spatial resolution than county boundaries, and therefore population distribution could be assumed to be directly proportional to the spatial distribution of dry cleaning establishments. Land use cover data, detailed road network maps, and many other kinds of spatial data may be used as spatial surrogates to locate different source types of emissions, if GIS coverages of these data are available. At this time MEPPS is provided with GIS coverages for political boundaries and land cover for North America, and detailed population data and road networks for the United States.

The primary input to the gridding processor consists of user-supplied data that are entered into windows or chosen from a pick-list in the Coordinate System and Grid windows of the Models-3 Science Manager. These data define the grid projection system, the origin of the grid, cell size, etc., which is then generated by Arc/Info® through MEPPS. The primary output of the gridding processor for MEPPS is an ARC® coverage which consists of the intersection of the political boundaries and the fixed grid.

Use of the Arc/Info® GIS as the key component in the gridding processor allows substantial flexibility in the definition and use of grids and surrogate data. It also allows MEPPS to

incorporate visualization methods for quality control and for managing and querying of the spatial emission data.

To generate the emission modeling grid structure, a political boundaries (state and county boundaries) Arc/Info® coverage named "counties" must already exist in the exact map projection that is intended for the emission modeling grid structure. Accordingly the counties coverage provided with MEPPS is in the Lambert Conformal projection. If inconsistent projections are used, the gridding processor produces unpredictable results. The processor produces three files that are used elsewhere in EMPRO:

- A running history of emission modeling grid structure changes.
- A list of the geographic location of each grid cell in the emissions modeling grid structure.
- The Arc/Info® coverage of the emission modeling grid structure.

The gridding processor supports the following subset of Arc/Info® map projections:

- UTM (Universal Transverse Mercator)
- Lambert (Lambert Conformal Conic)
- Albers (Albers Conic Equal Area)
- Geographic (actual latitude and longitude coordinates rather than a projection)
- State (State Plane Coordinate System)

For more information about the Arc/Info® map projections, refer to the following:

- *ARC/INFO® User's Guide: Map Projections & Coordinate Management, Concepts and Procedures.*
- *ARC/INFO® Command References: ARC® Command References, Commands J-Z.*

The UTM map projection is a specialized application of the Transverse Mercator projection. It is limited to use between the latitudes of 84° North and 80° South, and divides the earth into 60 longitudinally-defined zones (UTM zones 1-60) with each zone spanning 6°of longitude. UTM zone 1 starts at 180° West longitude and ends at 174° West longitude. UTM zone 2 starts at 174° West longitude and ends at 168° West longitude, and so on around the globe. Shape, area, direction, and distance errors are all minimized if a study area is within a single zone; however, error increases rapidly as study areas cross UTM zone boundaries.

The Lambert map projection is a projection of the earth onto a cone intersecting the earth along two parallels called standard parallels (for example 30° North and 60° North). The projection is good for large scale (continental or smaller), middle latitude (between 45° North and 45° South) study areas. Shapes are maintained on a small scale (state or smaller), and large shapes (countries, continents) are minimally distorted. Area and distance are maintained near the standard parallels, but area is reduced between the standard parallels and increased beyond the standard parallels; that is, the study area is accurately represented between the standard parallels.

Direction is accurate within the entire study area. CMAQ is currently tested and used with a Lambert conformal projection.

The Albers map projection is suitable for study domains where the east-west extent is greater than the north-south extent. Shape is minimally distorted near the standard parallels as long as the study domain's east-west extent is greater than the study domain's north-south extent. Area is accurate within the study domain. Direction is accurate only at the standard parallels and minimally distorted between the standard parallels. If the study area is in the middle latitudes (45° North to 45° South), distances are minimally distorted at and between the standard parallels. If the study area falls outside of the middle latitudes, distance error increases rapidly as the poles are approached.

The Geographic system is not a true map projection; instead it is a global reference system. It is supported as a map projection because geographic positioning (latitude and longitude) is the most widely used method of map location. The origin of the geographic global reference system is at 0° longitude (Meridian of Greenwich) and 0° latitude (equator). Directions in the northeast quadrant are measured in positive longitude degrees by positive latitude degrees. Directions in the northwest quadrant are measured in negative longitude degrees by positive latitude degrees. Directions in the southwest quadrant are measured in negative longitude degrees by negative latitude degrees. Directions in the southeast quadrant are measured in positive longitude degrees by negative latitude degrees.

The State system is also not a true map projection; instead it is a specialized coordinate system for the United States, Puerto Rico, and the United States Virgin Islands. The State system divides the aforementioned areas into a total of 120 zones of varying sizes. The map projection is inherent in each zone. The three map projections that are used in the State system are the Lambert Conic Conformal (for zones with where the east-west extent is greater than the north-south extent), Transverse Mercator (for zones where the north-south extent is greater than the east-west extent), and Oblique Mercator (used only for the Alaska Panhandle). Direction, distance, area, and shape errors vary with the map projection inherent in each zone; however, the zones have been designed so that error is reduced or eliminated as long as the study area falls entirely within a state plan zone.

The spatial allocation process grid description file (*$EMS_GRD/grd_desc.in*) references numerous data items that are used by the Grid Definition Model to prepare the emissions modeling grid structure. Table 4-2 lists the run description file data items that affect processing in the Grid Definition Model.

Table 4-2. Data Items That Affect the Gridding Processor

Variable Name	Menu Identifier	Type	Example	Description
gridid	Grid Id:	C	grid_a	directory name and grid identifier
griddesc	Description:	C	Tutorial 36km Resolution Grid	descriptive text for the emissions modeling grid
cell_loc	Cell Location: (S,E)	C	SOUTHWEST	location on/in the grid cell from which to make measurements (NORTH, NORTHEAST, EAST, SOUTHEAST, SOUTH, SOUTHWEST, WEST, NORTHWEST, CENTER)
utmzn	UTM zone: (S,E)	N	10	UTM zones for which the emissions modeling grid exists (1-60)
utmxorig	Origin X direction: (S,E)	N	-108000	southwest x corner origin (measured from the origin of the projection) of the emissions modeling domain (meters)
utmyorig	Origin Y direction: (S,E)	N	-1080000	southwest y corner origin (measured from the origin of the projection) of the emissions modeling domain (meters)
cellsizx	Cell size X direction: (S,E)	N	36000	x grid cell size (meters)
cellsizy	Cell size Y direction: (S,E)	N	36000	y grid cell size (meters)
xcells	Number of cells X direction: (S,E)	N	21	number of grid cells in the x direction
ycells	Number of cells Y direction (S,E)	N	21	number of grid cells in the y direction
zcells	Number of cells Z direction: (S)	N	10	number of grid cells in the z direction (currently not used by ARC/INFO)
projectn	Name: (S,E)	C	LAMBERT	projection name (LAMBERT, UTM, ALBERS, STATE, GEOGRAPHIC)

Table 4-2. Data Items That Affect the Gridding Processor

Variable Name	Menu Identifier	Type	Example	Description
projunit	Units: (S,E)	C	METERS	units used to make measurements in the selected projection (METERS, FEET, DD [decimal degrees])
xshift	X-shift: (E)	N	0.0	constant value to add to x input coordinates (value in *projunit* – typically 0.0)
yshift	Y-shift: (E)	N	0.0	constant value to add to y input coordinates (value in *projunit* – typically 0.0)
projzone	UTM zone: (S,E)	N	16	State Plane or UTM zone (used only when *projectn* is STATE or UTM -- see *ARC™ Command References, Commands J-Z; Table PROJECT-3 and Table PROJECT-4* for valid values)
fipszone	FIPS zone for state plane projection: (E)	N	3701	FIPS code for State Plane zone (used only when *projectn* is STATE -- see *ARC™ Command References, Commands J-Z; Table PROJECT-5* for valid values)
datum	Datum conversion name for projection: (S,E)	C	MM5 (Perfect sphere)	datum upon which input coordinates are based (used only when *projectn* is STATE -- NAD27, NAD83, UNKNOWN)
p_1sp_dd	1st standard parallel DD: (S,E)	N	30	degree of first standard parallel (only for *projectn* ALBERS or LAMBERT)
p_1sp_mm	1st standard parallel MM: (S,E)	N	0	minutes of first standard parallel (only for *projectn* ALBERS or LAMBERT)
p_1sp_ss	1st standard parallel SS: (S,E)	N	0.00	seconds of first standard parallel (only for *projectn* ALBERS or LAMBERT)

Table 4-2. Data Items That Affect the Gridding Processor

Variable Name	Menu Identifier	Type	Example	Description
p_2sp_dd	2nd standard parallel DD: (S,E)	N	60	degrees of second standard parallel (only for *projectn* ALBERS or LAMBERT)
p_2sp_mm	2nd standard parallel MM: (S,E)	N	0	minutes of second standard parallel (only for *projectn* ALBERS or LAMBERT)
p_2sp_ss	2nd standard parallel SS: (S,E)	N	0.00	seconds of second standard parallel (only for *projectn* ALBERS or LAMBERT)
p_cen_dd	Central meridian DD: (S,E)	N	-90	degrees of central meridian of projection (only for *projectn* ALBERS or LAMBERT)
p_cen_mm	Central meridian MM: (S,E)	N	0	minutes of central meridian of projection (only for *projectn* ALBERS or LAMBERT)
p_cen_ss	Central meridian SS: (S,E)	N	0.00	seconds of central meridian of projection (only for *projectn* ALBERS or LAMBERT)
p_lpo_dd	Latitude of projection origin DD: (S,E)	N	40	degrees of latitude from projection origin (only for *projectn* ALBERS or LAMBERT)
p_lpo_mm	Latitude of projection origin MM: (S,E)	N	0	minutes of latitude from projection origin (only for *projectn* ALBERS or LAMBERT)
p_lpo_ss	Latitude of projection origin SS: (S,E)	N	0.00	seconds of latitude from projection origin (only for *projectn* ALBERS or LAMBERT)
p_f_east	False easting: (E)	N	0.0	false easting (only for *projectn* ALBERS or LAMBERT -- meters)
p_fnorth	False northing: (E)	N	0.0	false northing (only for *projectn* ALBERS or LAMBERT -- meters)

Variable Name refers to the name as it is found in the SAS® data set *run_desc.ssd01* which can be found in the directory referenced by the UNIX environment variable *EMS_RUN* (see *Models-3 Volume 9B: User Manual*, Chapter 6). Menu Identifier refers to the descriptive text found on the grid definition window in Science Manager (S) or the EMPRO Grid Processor window (E) within MEPPS. Type refers to the variable type -- N is a numeric variable, and C is a character variable. Example gives an example of what might be entered for each data item. Description provides descriptive text about the data item, supported units, and a list of valid values that each data item recognizes -- valid values and units are listed in parentheses.

4.2.3.2 Temporal Allocation of Emission Data

Emission data that are based on annual, seasonal, weekly, or daily values must be temporally allocated (usually disaggregated) to hourly data for compatibility with the time scale of episodic air quality modeling. Generally, this procedure applies to regional inventories of point- and area-source emission data. Modeled emission data, such as biogenic- and mobile-source emissions are generated as hourly data for the time period of interest. Allocation of emission data from time periods greater than hourly (e.g., annual total, monthly total, weekly total), to hourly data is accomplished by use of seasonal, monthly, weekly, and daily diurnal temporal allocation factors to translate the data to daily total emission values. The daily values are then transformed into emission values for each hour of a typical day by using user-supplied or default temporal allocation profiles. The profiles assign proportions of the total daily emissions to each of the 24 hours of a typical day. Profiles are ideally source or source-category specific, but often are used for a range of similar source categories because of limited data on source category temporal variability. The majority of diurnal temporal source profiles have been developed for point sources, since more detailed reporting and monitoring exist for point sources, particularly large point sources, than for area sources which are spatially diverse and variable. Consequently are area source temporal allocation profiles tend to be less detailed and specific that point source temporal allocation profiles. Most of the temporal profiles used as defaults in MEPPS, were developed for the National Acid Rain Precipitation Assessment Program (NAPAP) (Fratt et al., 1990) and used in FREDS, with some more recent supplements (Moody et al., 1995).

In the EMPRO module of MEPPS, temporal allocation of point and area source category emission data is performed after spatial allocation of data in each main processor (point, area, biogenic, and mobile) and prior to speciation (see Chapter 6 of the Models-3 User Manual). This is transparent when running from Study Planner. If running in MEPPS under Tools Manager, the user may enter source category or source-specific daily or diurnal hourly temporal allocation data, or elect to use profiles computed by EMPRO (procedure described in the following sections) or use temporal allocation profiles based on those developed for use in the FREDS processors as supplemented. If a combination of emission inventory data at different temporal resolutions is used, EMPRO uses the most time-resolved (specific) data first, filling in with less time-specific data and applying temporal profiles as needed. If hourly, daily, and annual emission data are selected, EMPRO will provide hourly emission values taken from available data in the following order:

- Loading of hourly diurnal emission inventory (including Continuous Emission Monitoring (CEM) data);
- Loading and gridding of day-specific (daily) emission inventory data;
- Computing hourly emission data from annual or other longer-term emission inventory data.

Further details concerning temporal allocation are discussed as part of the following descriptions of the basis for processing each basic type of emission source.

4.2.3.3 Point Source Emission Data Processing

The point-source emission processor prepares gridded, temporally allocated point-source emission estimates suitable for speciation and reformatting for input to Models-3 framework for air quality modeling (e.g., CMAQ) (see Chapter 6 of the Models-3 User Manual). As previously indicated, the point-source emission processor does not compute basic emission estimates using emission factors and source-specific information. Instead, it reduces annual, point-source emission estimates to hourly, point source emissions estimates, unless the user is able to provide hourly emission data.

The point-source emission processor begins by establishing study-specific foundation emission estimates taken by INPRO from an user-specified emission inventory database. Foundation estimates (referred to as Foundation Files in MEPPS) are the basic annual emission inventory files imported to a processor (point, area, or mobile source) after quality control corrections have been applied and the data have been reduced to cover the study area only. After a point-source foundation file has been created, the processor spatially allocates the emission data into the spatial allocation grid structure, temporally allocates the emission estimates, and updates the hourly emission estimates derived from the foundation annual inventory with day-specific hourly emission estimates or hourly CEM data (if available). Usually, the point source-specific emission data are processed to files corresponding to the major hierarchical point-source data elements (i.e., Facility, Stack, Device, and Process), and translated to SAS® data sets.

Hourly emission estimates are computed using data from one of the following:

- Gridded emission estimates derived from annual emission inventory data by applying factors from source category-specific temporal allocation profiles
- Day and source-specific hourly emission data provided by the user
- Source-specific hourly CEM data.

Typically, the primary inputs to the point-source processor are the foundation emission annual estimates which are supplemented by available day-specific emission estimates. The primary output of the processor is the spatially and temporally allocated emission estimates.

<u>Computation of Point Source Emission Estimates</u>

The point-source emission processor treats emission estimates that have been prepared on one of the following bases: annual average; average day; or day-specific.

Day-Specific Emissions Estimates

Day-specific emission estimates are not computed by the MEPPS EMPRO point source processor. The user must supply any available day-specific emission estimates to the processor. Because day-specific emission estimates are more representative of actual conditions, they replace the hourly emission estimates derived from disaggregated annual emission data, when available. Day-specific emission data formats are made consistent with the internal formats of the SAS® data sets derived from other (e.g., annual) point-source emission data when imported through IDA.

CEM Hourly Emission Data

The CEM data are a subset of hourly emission data derived from continuous air pollutant concentration monitors attached to components of specific facilities, usually boilers or stacks of large point sources such as electric utilities. The data elements included are hourly emission rates for Carbon Monoxide (CO), nitrogen oxide, (NOx), and sulfur dioxide (SO_2). The CEM emission data are treated as hourly data imported to MEPPS via IDA. Electric utility CEM data are identified by specific source using their ORIS (Office of Regulatory Information Systems) identification number and are mapped to the corresponding point source identification number from an emission inventory. The CEM data are read in for a specified grid domain and day from a CEM dataset and substituted for hourly emission data derived from annual data. The CEM emission data are used in the format of data available for electric utility emissions provided by the U.S. EPA Acid Rain Division. The Acid Rain Division has electric utility CEM data for the United States for 1995 and 1996.

Spatial Allocation

Point sources are spatially allocated to an emission modeling grid by the geographic (latitude and longitude, UTM position) coordinates of a stack or by the geographic coordinates of the facility. The point-source emission data processor prepares an ASCII file of point-source identifiers and point-source geographic coordinate locations. The processor reads the ASCII file that was generated by the location processor, generates the appropriate ARC/INFO® coverages, and prepares two ASCII files:

- A file which contains point source identifiers and grid cell location; and
- A file which contains point-source identifiers and latitude/longitude coordinates. The process of assigning grid coordinates to point sources is an ARC/INFO® function; therefore, the underlying procedure follows the user documentation and proprietary code for the ARC/INFO® software.

Temporal Allocation

The EMPRO temporally allocates (produces hour-by-hour) foundation file emission estimates within each main emission processor (point, area, biogenic, and mobile emissions) based on operating schedule data that are provided in one of two ways. The operating schedule data may be passed into the MEPPS EMPRO module via an ASCII foundation file, which corresponds with the segment (process) level of point source inventory information. For point sources, the temporal factors may be assigned by the user at the segment (process) level of the EMPRO point source hierarchy. The hierarchy is closely aligned with that of regional emission inventories. Temporal allocation factors may be also be applied at the device level in the facility, stack, device hierarchy. Alternatively, default source-category-specific temporal allocation factors may be selected. These factors were used in a MEPPS predecessor, FREDS, and are referred to as FREDS temporal allocation factors. The point source hierarchy for temporal allocation factors in FREDS is: plant, point, temporal factors. Source-specific temporal allocation factors are typically not available for large regional modeling domains. Consequently, the default temporal allocation factors are commonly used in regional modeling, perhaps more than 90 percent of the time. Note that EMPRO temporally allocates foundation file emission estimates, but not day-specific emissions estimates since the latter are entered on an hour-by-hour basis.

EMPRO provides a variety of methods for identifying operating schedule data:

- Seasonal throughput fractions (winter [Dec, Jan, Feb], spring [Mar, Apr, May], summer [Jun, Jul, Aug], and fall [Sep, Oct, Nov])
- Hours per year in operation
- Days per year in operation;
- Weeks per year in operation;
- Days per week in operation; and
- Hours per day in operation.

Any, none, or all of the operating schedule data can be supplied. If no operating schedule data are supplied, EMPRO uses a default continuous operating schedule of 24 hours per day, 7 days per week, and 52 weeks per year; otherwise, EMPRO filters through a hierarchy of the operating schedule data to determine how to compute the temporal factors:

- Weekly temporal factor;
- Daily temporal factor; and
- 24 hourly temporal factors.

To determine the weekly temporal factor, EMPRO determines the number of days in the year of interest and divides that value by 7 days per week. For example, in a leap year, there are 29 days in February; therefore, the weekly temporal factor is 366 days/year ÷ 7 days/week).

EMPRO computes a daily temporal factor through a lookup table based on the value of average 8-hour work days (days per week in operation) which is passed into MEPPS through the ASCII foundation files. To determine the daily temporal factor, EMPRO examines the values for days,

hours per year (houryear), days per year (dayyear), and weeks respectively. If days has a valid value, EMPRO takes no further action to determine the days per week in operation for the source. If days does not have a valid value, EMPRO attempts to assign an operation code value to days by examining houryear, dayyear, and weeks respectively:

- houryear (hours per year in operation)

  if houryear > 0 and houryear <= 850 then days = 2,
  if houryear > 850 and houryear <= 1250 then days = 3,
  if houryear > 1250 and houryear <= 1670 then days = 4,
  if houryear > 1670 and houryear <= 2100 then days = 5,
  if houryear > 2100 and houryear <= 2500 then days = 6,
  if houryear > 2500 then days = 7;

- dayyear (days per year in operation)

  if dayyear > 0 and dayyear <= 110 then days = 2,
  if dayyear > 110 and dayyear <= 160 then days = 3,
  if dayyear > 160 and dayyear <= 210 then days = 4,
  if dayyear > 210 and dayyear <= 260 then days = 5,
  if dayyear > 260 and dayyear <= 315 then days = 6,
  if dayyear > 315 then days = 7;

- weeks (weeks per year in operation)

  if weeks > 0 and weeks <= 7 then days = 1,
  if weeks > 7 and weeks <= 13 then days = 2,
  if weeks > 13 and weeks <= 19 then days = 3,
  if weeks > 19 and weeks <= 26 then days = 4,
  if weeks > 26 and weeks <= 33 then days = 5,
  if weeks > 33 and weeks <= 39 then days = 6,
  if weeks > 39 then days = 7.

EMPRO computes an hourly temporal factor through a lookup table based on the value of hours (hours per day in operation) which is passed into EMPRO through the ASCII foundation files. If hours has a valid value, the value is used and no further action is taken to determine the hours per day in operation for the source. If hours does not have a valid value, EMPRO attempts to assign a value to hours by examining houryear, dayyear, and weeks respectively, using the above tables. If houryear, dayyear, or weeks has a valid value, then hours is assigned a value of 8, again based on an average work day of 8 hours. If hours or days cannot be assigned through the method described above, operation is assumed to be continuous and hours is assigned a value of 24, and days is assigned a value of 7. The following calculations are performed.

$$week_fac = daysinyear / 7 \quad (4\text{-}2)$$
$$day_sum^d = \sum dy_act_i^d,\ i = 1,\ldots 7 \quad (4\text{-}3)$$
$$day_fac_i = dy_act_i^d / day_sum^d,\ i = 1,\ldots 7 \quad (4\text{-}4)$$
$$hour_sum^h = \sum hr_act_i^h,\ i = 1, \ldots 24 \quad (4\text{-}5)$$
$$hrprof_i = hr_act_i^h / hour_sum^h,\ i = 1,\ldots 24 \quad (4\text{-}6)$$

where week_fac is the weekly temporal factor
daysinyear is the number of days in the year (365 or 366)
day_sum is the total relative activity for the week
dy_act is an array that contains relative daily activities
day_fac is the day of week temporal factor
hour_sum is the total relative activity for the day
hrprof is an array of hourly temporal factors
hr_act is an array that contains relative hourly activities
d is an index indicating which days per week in operation code (days) to use
h is an index indicating which hours per day in operation code (days) to use
i is the integer count that applies (e.g., 7 days or 24 hours)

EMPRO uses the temporal factors to allocate emission estimates to hourly values. Application of the temporal factors depends on the temporal basis (annual average, day-specific, average day) that emissions estimates were input to EMPRO.

- if the temporal basis code estt = "AA" (annual average) then

$$hremis_i = aceekg/(week_fac * day_fac * hrprof_i),\ i = 1,\ldots 24 \quad (4\text{-}7)$$

where hremis is the array of gridded, hourly emissions estimates (NO_X, TOG, CO, etc) (mass)
aceekg is the emission estimates (mass)
week_fac, day_fac, and hrprof are the weekly, daily and hourly temporal factors, respectively, computed by EMPRO

- if the temporal basis code estt = "AD" (average day) and (week_fac = 0 or day_fac = 0) then

$$hremis_i = 0.0,\ i = 1,\ldots 24 \quad (4\text{-}8)$$

- if the temporal basis code estt = "AD" (average day) and not (week_fac = 0 or day_fac = 0) then

$$hremis_i = aceekg * hrprof_i,\ i = 1,\ldots 24 \quad (4\text{-}9)$$

- if the temporal basis code estt = "DS" (day-specific) then

$$hremis_i = aceekg * prof_i,\ i = 1,\ldots 24 \qquad (4\text{-}10)$$

where prof is an array of day-specific, hourly temporal factors

4.2.3.4 Area Source Emission Data Processing

The area-source emission data processor prepares area-source emission estimates for speciation (lumped-model or discrete speciation) and reformatting for input to CMAQ or other Models-3 framework components. The area-source processor does not compute emission estimates from fundamental emission data. It reduces annual, county-wide emission estimates to emissions on an hourly, grid cell-by-grid cell basis. Most of the area source emission data processor is written in the SAS® programming language. The area-source spatial surrogates allocation component of the processor is written in the ARC® Macro Language (AML®). The primary inputs to the processor are the area-source emission estimates for the spatial domain of interest, and day-specific emission estimates (if available). The primary outputs are the spatially allocated, temporally resolved, emission estimates.

The processor begins with an area-source emission data base, extracted by INPRO from an emission inventory as an ASCII file and automatically converted to a SAS® file. The area-source processor updates the estimates with any available day-specific estimates, spatially allocates the emissions into the emission modeling grid, and temporally allocates the criteria emissions.

Emission Data Processing

This section discusses how area-source emission estimates are read into, manipulated by, and quality-assured by the area-source emission data processor. References are made to MEPPS source code where necessary to provide further details concerning area source emission allocation.
The processor uses county-wide area-source emission estimates, that have been prepared externally as part of an emission inventory, to produce spatially allocated, temporally resolved, pollutant emission estimates. To the extent that the inventory used includes small point sources in area source estimates, they are treated as area sources. All data provided as point sources, regardless of magnitude, are processed as point sources in EMPRO. The area-source emission data processor accommodates area-source emission estimates that have been prepared on the following bases: annual average; average day; or day-specific.

Day-specific emission data enter the area-source emission data processor during the temporal allocation step. Day-specific emission data are not computed by EMPRO. Like the foundation file emissions estimates, day-specific emission estimates are supplied from an external source to the emissions modeler. The day-specific emissions estimates replace the area-source emission estimates derived from annual inventory data because day-specific emission data are more representative of actual conditions.

Day-specific area-source emission estimates are summed to a daily total so that they are consistent with the internal formats of the SAS® data sets that maintain the other (e.g., derived from annual emission inventories) area-source emissions estimates, which are passed to EMS-95 on an hourly basis.

Spatial Allocation

Area-source emission estimates are allocated to a modeling domain through the application of spatial surrogates. In general, surrogates approximate the value of unknown quantities. For example, population can be used to estimate the number of gasoline service stations. A spatial surrogate not only helps estimate the value of an unknown quantity, but a spatial surrogate also helps locate the unknown quantity.

For each spatial surrogate, it is necessary to specify what data (categories of land use/land cover, population counts, housing counts, etc.) contribute to the surrogate. In EMPRO, county area, land cover, population (census), Federal Highway Administration major roadway, and TIGER/LINE roadway data for the United States are provided as ARC® coverages for use as surrogates. Others may be added by providing ARC® coverages generated external to MEPPS. County area, and less detailed population and land cover coverages are provided for Canada and Mexico. Each area source category must be assigned a unique spatial surrogate value by grid cell. After the appropriate files have been populated, EMPRO grids the necessary data sets according to the requirements of the user-defined spatial surrogates. Each area source category (asct) which has been assigned to a spatial surrogate (k) can be allocated to grid cells (l, m) through the application of Equation 4-11.

$$acee_{i,j,k',l,m} = acee_{i,j,k'} * ratio_{i,j,k,l,m} \quad (4\text{-}11)$$

where i is the index on states
j is the index on counties within the states
k is the spatial surrogate index
k' is the area source category index (directly related to k)
l is the x cell index
m is the y cell index
acee is the county-wide area source emissions estimate (mass)
ratio is the gridded surrogate ratio by state/county/surrogate/cell

Each surrogate is computed through the application of Equations 4-12 and 4-13.

$$surtot_{i,j,k} = \Sigma_l \, \Sigma_m \; attribute_{i,j,k,l,m} \quad (4\text{-}12)$$

$$ratio_{i,j,k,l,m} = attribute_{i,j,k,l,m} \, / \, surtot_{i,j,k} \quad (4\text{-}13)$$

where: i is the index on states
j is the index on counties within the states

k is the spatial surrogate index
l is the x cell index
m is the y cell index
surtot is the total value of a surrogate within specified (indexed) states and counties
attribute is the gridded value of the surrogate attribute by state/county/surrogate/cell
ratio is the gridded surrogate ratio for specified (indexed) states/counties/ surrogates/cells

In the case of census data or other area-based or length-based surrogate information, it is necessary to area-apportion or length-apportion the surrogate (such as population or housing) information prior to aggregation to the cell level. This is because the locale of interest crosses cell boundaries. The assumption is that the surrogate information (such as population or housing) has a constant density across the locale (in the case of population or housing data, a constant density across the census tract). Therefore, in some cases, it is necessary to apply Equations 4-14 through 4-16 prior to the application of Equations 4-12 and 4-13.

$$\text{arlg_tot}_{i,j,k} = \Sigma_l \Sigma_m \text{ arealeng}_{i,j,k,l,m} \quad (4\text{-}14)$$

$$\text{ap_ratio}_{i,j,k,l,m} = \text{arealeng}_{i,j,k,l,m} / \text{arlg_tot}_{i,j,k} \quad (4\text{-}15)$$

$$\text{attribute}_{i,j,l,m} = \text{attribute}_{i,j,k} * \text{ap_ratio}_{i,j,k,l,m} \quad (4\text{-}16)$$

where i is the index on states
j is the index on counties within the states
k is the locale of interest index (such as census tract or roadway)
l is the x cell index
m is the y cell index
arlg_tot is the total area or length of a locale of interest within specified (indexed) states and counties
arealeng is the gridded value of the specified (indexed) locale of interest by state/ county/surrogate/cell
ap_ratio is the gridded ratio of the locale of interest specified (by indices) states/ counties/locales/cell
attribute is the surrogate data (population, road length, etc.) for the area specified by indices.

As a check for Equations 4-14 through 4-16, the following must be true:

$$\Sigma_i \Sigma_j \Sigma_k \text{ ratio}_{i,j,k} = 1.0 \quad (4\text{-}17)$$

<u>Temporal Allocation</u>

Temporal allocation of area source emission data is performed in an identical manner as described for point source processing in Section 4.2.3.3, although it is almost always necessary to use default temporal allocation profiles. Please refer to that section for a discussion of temporal allocation of area sources.

4.2.4 Modeled Emission Data

Emission data from available emission inventories are spatially and temporally allocated as described in the preceding paragraphs. Many anthropogenic area and point sources of emissions vary little or predictably with time, and can reasonably be disaggregated for regional modeling. However, some emission data are highly variable, diurnally and seasonally, because they are dependent on environmental variables, such as temperature, humidity, and solar insolation. It is more accurate to model these kinds of emissions on an hourly basis for direct use in episodic air quality modeling. The two principal kinds of sources for which hourly emission data are normally modeled are mobile sources and biogenic sources. In both cases, MEPPS takes hourly meteorological data from MCIP output derived from MM5.

4.2.4.1 Biogenic Emissions

Hourly biogenic emission rates for biogenic VOC compounds (including isoprenes, monoterpenes, and soil NO) for each grid cell are estimated using the Biogenic Emission Inventory System, Version 2 (BEIS-2) within MEPPS. In order to estimate biogenic emissions for modeling, it is necessary to apply biogenic emission and biomass factors to a geographic distribution of land cover. The BEIS-2 was developed to fill this need separately from Models-3 as an improvement on BEIS-1 (Pierce et al., 1990; Geron et al., 1994), and has been used in conjunction with different air quality modeling systems, including the Regional Acid Deposition Model (RADM) (Pierce et al., in press), the Regional Oxidant Model (ROM), and now Models-3 CMAQ. Additional information concerning BEIS-2 can be found in the Emission Inventory Improvement Program report on Biogenic Sources Preferred Methods (EIIP, 1996) and Pierce et al. (1998). The BEIS-2 model applies emission flux factors specific to tree genera and agricultural crop types by geographic area for biogenic emission species in accordance with equation 4-18.

$$ER_i = \sum_j [A_j * EF * F_{ij}(S,T)] \qquad (4\text{-}18)$$

where: ER is the emission rate (in grams/sec/model cell)
i is the chemical species (e.g., isoprene, monoterpene)
j is the vegetation type
A is the vegetation area (meter^2) in a grid cell
EF is the emission factor (micrograms/gram of leaf biomass/hour), and
$F_{ij}(S,T)$ is an environment factor to account for solar radiation S and leaf temperature T

Vegetation emission flux factors were adapted from those compiled by Geron et al. (1994) for 77 tree genera. Emission flux factors for 16 agricultural crops were taken primarily from Lamb et al (1993), and the emission factors applied to 34 land cover types are from the work of Guenther et al. (1994). Emission flux factors by land cover type are used principally for Canada and the western United States where genus-level forest cover and agricultural crop data were not available. Biogenic emission flux factors for summer and winter conditions are given in Table 4-3 and Table 4-4, respectively. The vegetation classes are taken from the Biogenic Emission Land Use Database (BELD) (Kinnee et al., 1997), which in turn is drawn from other land cover data sets, with an emphasis on forest and agricultural land cover. Spatial resolution of the raw (original) land cover data is at the county-level for the United States and sub-province level for Canada. Emission flux factors are based on full leaf summer conditions normalized to leaf or soil temperatures of 30°C and photosynthetically active radiation (PAR) of 1000 micromoles/m^2/sec. For use in regional modeling, the mass of biogenic emissions are converted to moles by dividing the mass (grams-compound) by the molecular weight of the compound. The emission factors for tree genus and agricultural vegetation, and used in the Models-3 application of BEIS-2 are compiled by Pierce et al. (1998).

Table 4-3. Summer Biogenic Emission Flux Factors (μg-compound $m^{-2}hr^{-1}$) for Principal Biogenic Compounds by Vegetation Category

Vegetation or Land Cover Code	Isoprene	Terpene	Other VOCs	NO	Leaf Area Index (m^2 m^{-2})	Description
Abie	170.0	5100.0	2775.0	4.5	7	Abies (fir)
Acac	79.3	2380.0	1295.0	4.5	5	Acacia
Acer	42.5	680.0	693.7	4.5	5	Acer (maple)
Aesc	42.5	42.5	693.7	4.5	5	Aesculus (buckeye)
Aila	42.5	42.5	693.7	4.5	5	Ailanthus
Aleu	42.5	42.5	693.7	4.5	5	Aleurites (tung-oil tree)
Alfa	19.0	7.6	11.4	12.8	0	Alfalfa
Alnu	42.5	42.5	693.7	4.5	5	Alnus (European alder)
Amel	42.5	42.5	693.7	4.5	5	Amelanchier (serviceberry)
Asim	42.5	42.5	693.7	4.5	5	Asimina (pawpaw)
Avic	42.5	42.5	693.7	4.5	5	Avicennia (black mangrove)
Barl	7.6	19.0	11.4	256.7	0	Barley

Table 4-3. Summer Biogenic Emission Flux Factors (μg-compound $m^{-2}hr^{-1}$) for Principal Biogenic Compounds by Vegetation Category

Vegetation or Land Cover Code	Isoprene	Terpene	Other VOCs	NO	Leaf Area Index (m^2 m^{-2})	Description
Barr	0.0	0.0	0.0	0.0	0	Barren
Betu	42.5	85.0	693.7	4.5	5	Betula (birch)
Borf	910.0	713.0	755.0	4.5	5	Boreal forest (Guenther*)
Bume	42.5	42.5	693.7	4.5	5	Bumelia (gum bumelia)
Carp	42.5	680.0	693.7	4.5	5	Carpinus (hornbean)
Cary	42.5	680.0	693.7	4.5	5	Carya (hickory)
Casp	42.5	42.5	693.7	4.5	5	Castanopsis (chinkapin)
Cast	42.5	42.5	693.7	4.5	5	Castanea (chestnut)
Casu	29750.0	42.5	693.7	4.5	7	Casuarina (Austl pine)
Cata	42.5	42.5	693.7	4.5	5	Catalpa
Cedr	79.3	1269.3	1295.0	4.5	7	Cedrus (Deodar cedar)
Celt	42.5	85.0	693.7	4.5	5	Celtis (hackberry)
Cerc	42.5	42.5	693.7	4.5	5	Cercis (redbud)
Cham	170.0	340.0	2775.0	4.5	7	Chamaecyparis (prt-orford cedar)
Citr	42.5	680.0	693.7	4.5	5	Citrus (orange)
Cnif	745.4	1366.6	993.9	4.5	9	BEIS conifer forest
Conf	1550.0	1564.0	1036.0	4.5	6	Conifer forest (Guenther)
Corn	0.5	0.0	0.0	577.6	0	Corn
Coru	42.5	680.0	693.7	4.5	5	Cornus (dogwood)
Coti	42.5	42.5	693.7	4.5	5	Cotinus (smoke tree)
Cott	7.6	19.0	11.4	256.7	0	Cotton
Crat	42.5	42.5	693.7	4.5	5	Crataegus (hawthorn)
Cswt	1050.0	660.0	770.0	0.2	2	Herbaceous Wetlands (Guenther)
Desh	65.0	94.5	56.7	57.8	0	Desert shrub (Guenther)

Table 4-3. Summer Biogenic Emission Flux Factors (μg-compound $m^{-2}hr^{-1}$) for Principal Biogenic Compounds by Vegetation Category

Vegetation or Land Cover Code	Isoprene	Terpene	Other VOCs	NO	Leaf Area Index (m^2 m^{-2})	Description
Dios	42.5	42.5	693.7	4.5	5	Diospyros (persimmon)
Euca	29750.0	1275.0	693.7	4.5	5	Eucalyptus
Fagu	42.5	255.0	693.7	4.5	5	Fagus (american beech)
Frax	42.5	42.5	693.7	4.5	5	Fraxinus (ash)
Gled	42.5	42.5	693.7	4.5	5	Gleditsia (honey locust)
Gord	42.5	42.5	693.7	4.5	5	Gordonia (loblolly-bay)
Gras	56.2	140.5	84.3	57.8	0	Grass
Gymn	42.5	42.5	693.7	4.5	5	Gymnocladus (KY coffeetree)
Hale	42.5	42.5	693.7	4.5	5	Halesia (silverbell)
Harf	8730.0	436.0	882.0	4.5	5	Hardwood forest (Guenther)
Hay	37.8	94.5	56.7	12.8	0	Hay
Ilex	42.5	85.0	693.7	4.5	5	Ilex (holly)
Jugl	42.5	1275.0	693.7	4.5	5	Juglans (black walnut)
Juni	79.3	476.0	1295.0	4.5	7	Juniperus (east. red cedar)
Lagu	42.5	42.5	693.7	4.5	5	Laguncularia (white mangrove)
Lari	42.5	42.5	693.7	4.5	5	Larix (larch)
Liqu	29750.0	1275.0	693.7	4.5	5	Liquidambar (sweetgum)
Liri	42.5	85.0	693.7	4.5	5	Liriodendron (yellow poplar)
Macl	42.5	42.5	693.7	4.5	5	Maclura (osage-orange)
Magn	42.5	1275.0	693.7	4.5	5	Magnolia
Malu	42.5	42.5	693.7	4.5	5	Malus (apple)
Meli	42.5	42.5	693.7	4.5	5	Melia (chinaberry)
Mixf	11450.0	1134.0	1140.0	4.5	5	Mixed forest (Guenther)
Moru	42.5	85.0	693.7	4.5	5	Morus (mulberry)

Table 4-3. Summer Biogenic Emission Flux Factors (μg-compound $m^{-2}hr^{-1}$) for Principal Biogenic Compounds by Vegetation Category

Vegetation or Land Cover Code	Isoprene	Terpene	Other VOCs	NO	Leaf Area Index (m^2 m^{-2})	Description
Mscp	7.6	19.0	11.4	12.8	0	Misc crops
Nmxf	10150.0	1100.0	850.0	4.5	5	Northern Mixed Forest (Guenther)
Nyss	5950.0	255.0	693.7	4.5	5	Nyssa (blackgum)
Oak	3108.3	255.5	894.2	4.5	6	BEIS oak forest
Oats	7.6	19.0	11.4	256.7	0	Oats
Odcd	2112.4	368.8	871.8	4.5	6	BEIS other deciduous forest
Ofor	56.2	140.5	84.3	4.5	0	Open forest
Oksv	7350.0	100.0	600.0	4.5	2	Oak Savannah (Guenther)
Ostr	42.5	42.5	693.7	4.5	5	Ostrya (hophornbeam)
Othe	56.2	140.5	84.3	57.8	0	Other (unknown, assume grass)
Oxyd	42.5	255.0	693.7	4.5	5	Oxydendrum (sourwood)
Pacp	55.0	79.8	47.9	35.3	0	Pasture crop land (Guenther)
Past	56.2	140.5	84.3	57.8	0	Pasture
Paul	42.5	42.5	693.7	4.5	5	Paulownia
Pean	102.0	255.0	153.0	12.8	0	Peanuts
Pers	42.5	255.0	693.7	4.5	5	Persea (redbay)
Pice	23800.0	5100.0	2775.0	4.5	7	Picea (spruce)
Pinu	79.3	2380.0	1295.0	4.5	3	Pinus (pine)
Plan	42.5	42.5	693.7	4.5	5	Planera (water elm)
Plat	14875.0	42.5	693.7	4.5	5	Platanus (sycamore)
Popu	29750.0	42.5	693.7	4.5	5	Populus (aspen)
Pota	9.6	24.0	14.4	192.5	0	Potato
Pros	42.5	42.5	693.7	4.5	5	Prosopis (mesquite)
Prun	42.5	42.5	693.7	4.5	5	Prunus (cherry)

Table 4-3. Summer Biogenic Emission Flux Factors (μg-compound $m^{-2}hr^{-1}$) for Principal Biogenic Compounds by Vegetation Category

Vegetation or Land Cover Code	Isoprene	Terpene	Other VOCs	NO	Leaf Area Index (m^2 m^{-2})	Description
Pseu	170.0	2720.0	2775.0	4.5	7	Pseudotsuga (douglas fir)
Quer	29750.0	85.0	693.7	4.5	5	Quercus (oak)
Rang	37.8	94.5	56.7	57.8	0	Range
Rhiz	42.5	42.5	693.7	4.5	5	Rhizophora (red mangrove)
Rice	102.0	255.0	153.0	0.2	0	Rice
Robi	5950.0	85.0	693.7	4.5	5	Robinia (black locust)
Rye	7.6	19.0	11.4	12.8	0	Rye
Sabl	5950.0	42.5	693.7	4.5	5	Sabal (cabbage palmetto)
Sali	14875.0	42.5	693.7	4.5	5	Salix (willow)
Sapi	42.5	42.5	693.7	4.5	5	Sapium (chinese tallow tree)
Sass	42.5	42.5	693.7	4.5	5	Sassafras
Scru	37.8	94.5	56.7	57.8	0	Scrub
Scwd	2700.0	349.0	651.0	31.2	2	Scrub woodland (Guenther)
Sere	14875.0	42.5	693.7	4.5	5	Serenoa (saw palmetto)
Shrf	10750.0	530.0	910.0	4.5	5	Southeast/Western Deciduous Forest
Smxf	17000.0	1500.0	1250.0	4.5	4	Southeast Mixed Forest
Snow	0.0	0.0	0.0	0.0	0	Snow
Sor	42.5	42.5	693.7	4.5	5	Sorbus (mountain ash)
Sorg	7.8	19.5	11.7	577.6	0	Sorghum
Soyb	22.0	0.0	0.0	12.8	0	Soybean
Spin	1460.0	1983.0	1252.0	4.5	3	Southern pine (Guenther)
Swie	42.5	42.5	693.7	4.5	5	Swietenia (W. Indies mahogany)
Taxo	42.5	1275.0	693.7	4.5	5	Taxodium (cypress)
Thuj	170.0	1020.0	2775.0	4.5	7	Thuja (W. red cedar)

Table 4-3. Summer Biogenic Emission Flux Factors (μg-compound $m^{-2}hr^{-1}$) for Principal Biogenic Compounds by Vegetation Category

Vegetation or Land Cover Code	Isoprene	Terpene	Other VOCs	NO	Leaf Area Index (m^2 m^{-2})	Description
Tili	42.5	42.5	693.7	4.5	5	Tilia (basswood)
Toba	0.0	58.8	235.2	256.7	0	Tobacco
Tsug	79.3	158.7	1295.0	4.5	7	Tsuga (Eastern hemlock)
Tund	2411.7	120.6	150.7	0.2	0	Tundra
Ufor	1988.7	663.7	920.0	4.5	0	BEIS urban forest
Ugra	56.2	140.5	84.3	57.8	0	BEIS urban grass
Ulmu	42.5	42.5	693.7	4.5	5	Ulmus (American elm)
Uoth	0.0	0.0	0.0	0.0	0	BEIS other urban (barren)
Urba	408.6	161.9	200.5	12.5	0	BEIS urban (.2 grass/.2 forest)
Utre	5140.0	1000.0	959.0	4.5	5	Urban trees (.5 Harf/.5 Conf)
Vacc	42.5	42.5	693.7	4.5	5	Vaccinium (blueberry)
Wash	5950.0	42.5	693.7	4.5	5	Washingtonia (fan palm)
Wate	0.0	0.0	0.0	0.0	0	Water
Wcnf	4270.0	1120.0	1320.0	4.5	5	W Coniferous Forest (Guenther)
Wdcp	2550.0	663.0	2053.0	8.7	3	Woodland/crop land (Guenther)
Wetf	3820.0	923.0	1232.0	0.2	5	Wetland forest (Guenther)
Whea	15.0	6.0	9.0	192.5	0	Wheat
Wmxf	5720.0	620.0	530.0	4.5	4	Western Mixed Forest (Guenther)
Wwdl	525.0	250.0	360.0	4.5	3	Western Woodlands (Guenther)

*Guenther references biogenic emission factors taken from Guenther et al. (1994) using AVHRR (Advanced Very High Resolution Radiometer) satellite imagery.

Table 4-4. Winter Biogenic Emission Flux Factors (μg-compound $m^{-2}hr^{-1}$) for Principal Biogenic Compounds by Vegetation Category

Vegetation or Land Cover Code	Isoprene	Terpene	Other VOCs	NO	Leaf Area Index (m^2 m^{-2})	Description
Abie	170.0	5100.0	2775.0	4.5	7	Abies (fir)
Acac	0.0	0.0	0.0	4.5	5	Acacia
Acer	0.0	0.0	0.0	4.5	5	Acer (maple)
Aesc	0.0	0.0	0.0	4.5	5	Aesculus (buckeye)
Aila	0.0	0.0	0.0	4.5	5	Ailanthus
Aleu	0.0	0.0	0.0	4.5	5	Aleurites (tung-oil tree)
Alfa	0.0	0.0	0.0	12.8	0	Alfalfa
Alnu	0.0	0.0	0.0	4.5	5	Alnus (European alder)
Amel	0.0	0.0	0.0	4.5	5	Amelanchier (serviceberry)
Asim	0.0	0.0	0.0	4.5	5	Asiminia (pawpaw)
Avic	42.5	42.5	693.7	4.5	5	Avicennia (black mangrove)
Barl	0.0	0.0	0.0	256.7	0	Barley
Barr	0.0	0.0	0.0	0.0	0	Barren
Betu	0.0	0.0	0.0	4.5	5	Betula (birch)
Borf	640.0	706.0	634.0	4.5	6	Boreal forest (AVHRR/G.*)
Bume	42.5	42.5	693.7	4.5	5	Bumelia (gum bumelia)
Carp	0.0	0.0	0.0	4.5	5	Carpinus (hornbean)
Cary	0.0	0.0	0.0	4.5	5	Carya (hickory)
Casp	0.0	0.0	0.0	4.5	5	Castanopsis (chinkapin)
Cast	0.0	0.0	0.0	4.5	5	Castanea (chestnut)

Table 4-4. Winter Biogenic Emission Flux Factors (μg-compound $m^{-2}hr^{-1}$) for Principal Biogenic Compounds by Vegetation Category

Vegetation or Land Cover Code	Isoprene	Terpene	Other VOCs	NO	Leaf Area Index (m^2 m^{-2})	Description
Casu	29750.0	42.5	693.7	4.5	7	Casuarina (Austl pine)
Cata	0.0	0.0	0.0	4.5	5	Catalpa
Cedr	79.3	1269.3	1295.0	4.5	7	Cedrus (Deodar cedar)
Celt	0.0	0.0	0.0	4.5	5	Celtis (hackberry)
Cerc	0.0	0.0	0.0	4.5	5	Cercis (redbud)
Cham	170.0	340.0	2775.0	4.5	7	Chamaecyparis (prt-orford cedar)
Citr	42.5	680.0	693.7	4.5	5	Citrus (orange)
Cnif	0.0	1353.0	835.0	4.5	9	BEIS conifer forest
Conf	1400.0	1548.0	870.0	4.5	6	Conifer forest (AVHRR, G.)
Corn	0.0	0.0	0.0	577.6	0	Corn
Coru	0.0	0.0	0.0	4.5	5	Cornus (dogwood)
Coti	0.0	0.0	0.0	4.5	5	Cotinus (smoke tree)
Cott	0.0	0.0	0.0	256.7	0	Cotton
Crat	0.0	0.0	0.0	4.5	5	Crataegus (hawthorn)
Cswt	1050.0	660.0	770.0	0.2	1	Herbaceous Wetlands (AVHRR, G.)
Desh	0.0	0.0	0.0	57.8	0	Desert shrub (AVHRR, G.)
Dios	0.0	0.0	0.0	4.5	5	Diospyros (persimmon)
Euca	29750.0	1275.0	693.7	4.5	5	Eucalyptus
Fagu	0.0	0.0	0.0	4.5	5	Fagus (american beech)
Frax	0.0	0.0	0.0	4.5	5	Fraxinus (ash)

Table 4-4. Winter Biogenic Emission Flux Factors (μg-compound $m^{-2}hr^{-1}$) for Principal Biogenic Compounds by Vegetation Category

Vegetation or Land Cover Code	Isoprene	Terpene	Other VOCs	NO	Leaf Area Index (m^2 m^{-2})	Description
Gled	0.0	0.0	0.0	4.5	5	Gleditsia (honeylocust)
Gord	0.0	0.0	0.0	4.5	5	Gordonia (loblolly-bay)
Gras	0.0	0.0	0.0	57.8	0	Grass
Gymn	0.0	0.0	0.0	4.5	5	Gymnocladus (KY coffeetree)
Hale	0.0	0.0	0.0	4.5	5	Halesia (silverbell)
Harf	0.0	371.0	185.0	4.5	3	Hardwood forest (AVHRR, G.)
Hay	0.0	0.0	0.0	12.8	0	Hay
Ilex	42.5	85.0	693.7	4.5	5	Ilex (holly)
Jugl	0.0	0.0	0.0	4.5	5	Juglans (black walnut)
Juni	79.3	476.0	1295.0	4.5	7	Juniperus (east. red cedar)
Lagu	42.5	42.5	693.7	4.5	5	Laguncularia (white mangrove)
Lari	0.0	0.0	0.0	4.5	5	Larix (larch)
Liqu	0.0	0.0	0.0	4.5	5	Liquidambar (sweetgum)
Liri	0.0	0.0	0.0	4.5	5	Liriodendron (yellow poplar)
Macl	0.0	0.0	0.0	4.5	5	Maclura (osage-orange)
Magn	42.5	1275.0	693.7	4.5	5	Magnolia
Malu	0.0	0.0	0.0	4.5	5	Malus (apple)
Meli	0.0	0.0	0.0	4.5	5	Melia (chinaberry)

Table 4-4. Winter Biogenic Emission Flux Factors (μg-compound $m^{-2}hr^{-1}$) for Principal Biogenic Compounds by Vegetation Category

Vegetation or Land Cover Code	Isoprene	Terpene	Other VOCs	NO	Leaf Area Index (m^2 m^{-2})	Description
Mixf	0.0	1077.0	581.0	4.5	4	Mixed forest (AVHRR, G.)
Moru	0.0	0.0	0.0	4.5	5	Morus (mulberry)
Mscp	0.0	0.0	0.0	12.8	0	Misc crops
Nmxf	175.0	1100.0	850.0	4.5	1	Northern Mixed Forest (AVHRR, G.)
Nyss	0.0	0.0	0.0	4.5	5	Nyssa (blackgum)
Oak	0.0	217.0	188.0	4.5	6	BEIS oak forest
Oats	0.0	0.0	0.0	256.7	0	Oats
Ocdf	0.0	313.0	183.0	4.5	6	BEIS other deciduous forest
Ofor	0.0	0.0	0.0	4.5	0	Open forest
Oksv	0.0	100.0	200.0	4.5	1	Oak Savannah (AVHRR, Guen)
Ostr	0.0	0.0	0.0	4.5	5	Ostrya (hophornbeam)
Othe	0.0	0.0	0.0	57.8	0	Other (unknown, assume grass)
Oxyd	0.0	0.0	0.0	4.5	5	Oxydendrum (sourwood)
Pacp	0.0	0.0	0.0	35.3	0	Pasture cropland (AVHRR, G.)
Past	0.0	0.0	0.0	57.8	0	Pasture
Paul	0.0	0.0	0.0	4.5	5	Paulownia
Pean	0.0	0.0	0.0	12.8	0	Peanuts
Pers	42.5	255.0	693.7	4.5	5	Persea (redbay)
Pice	23800.0	5100.0	2775.0	4.5	7	Picea (spruce)
Pinu	79.3	2380.0	1295.0	4.5	3	Pinus (pine)

Table 4-4. Winter Biogenic Emission Flux Factors (μg-compound $m^{-2}hr^{-1}$) for Principal Biogenic Compounds by Vegetation Category

Vegetation or Land Cover Code	Isoprene	Terpene	Other VOCs	NO	Leaf Area Index (m^2 m^{-2})	Description
Plan	0.0	0.0	0.0	4.5	5	Planera (water elm)
Plat	0.0	0.0	0.0	4.5	5	Platanus (sycamore)
Popu	0.0	0.0	0.0	4.5	5	Populus (aspen)
Pota	0.0	0.0	0.0	92.15	0	Potato
Pros	0.0	0.0	0.0	4.5	5	Prosopis (mesquite)
Prun	0.0	0.0	0.0	4.5	5	Prunus (cherry)
Pseu	170.0	2720.0	2775.0	4.5	7	Pseudotsuga (douglas fir)
Quer	0.0	0.0	0.0	4.5	5	Quercus (oak)
Rang	0.0	0.0	0.0	57.8	0	Range
Rhiz	42.5	42.5	693.7	4.5	5	Rhizophora (red mangrove)
Rice	0.0	0.0	0.0	0.2	0	Rice
Robi	0.0	0.0	0.0	4.5	5	Robinia (black locust)
Rye	0.0	0.0	0.0	12.8	0	Rye
Sabl	5950.0	42.5	693.7	4.5	5	Sabal (cabbage palmetto)
Sali	0.0	0.0	0.0	4.5	5	Salix (willow)
Sapi	0.0	0.0	0.0	4.5	5	Sapium (chinese tallow tree)
Sass	0.0	0.0	0.0	4.5	5	Sassafras
Scru	0.0	0.0	0.0	57.8	0	Scrub
Scwd	0.0	332.0	332.0	31.2	2	Scrub woodland (AVHRR, G.)
Sere	14875.0	42.5	693.7	4.5	5	Serenoa (saw palmetto)
Shrf	0.0	0.0	0.0	4.5	0	SE/W Deciduous Forest (AVHRR, G.)

Table 4-4. Winter Biogenic Emission Flux Factors (μg-compound $m^{-2}hr^{-1}$) for Principal Biogenic Compounds by Vegetation Category

Vegetation or Land Cover Code	Isoprene	Terpene	Other VOCs	NO	Leaf Area Index (m^2 m^{-2})	Description
Smxf	0.0	1500.0	500.0	4.5	2	SE Mixed Forest (AVHRR, G.)
Snow	0.0	0.0	0.0	0.0	0	Snow
Sorb	0.0	0.0	0.0	4.5	5	Sorbus (mountain ash)
Sorg	0.0	0.0	0.0	577.6	0	Sorghum
Soyb	0.0	0.0	0.0	12.8	0	Soybean
Spin	0.0	1963.0	1052.0	4.5	3	Southern pine (AVHRR, G.)
Swie	42.5	42.5	693.7	4.5	5	Swietenia (W. Indies mahogany)
Taxo	42.5	1275.0	693.7	4.5	5	Taxodium (cypress)
Thuj	170.0	1020.0	2775.0	4.5	7	Thuja (W. red cedar)
Tili	0.0	0.0	0.0	4.5	5	Tilia (basswood)
Toba	0.0	0.0	0.0	256.7	0	Tobacco
Tsug	79.3	158.7	1295.0	4.5	7	Tsuga (Eastern hemlock)
Tund	0.0	0.0	0.0	0.2	0	Tundra
Ufor	0.0	631.0	469.0	4.5	0	BEIS urban forest
Ugra	0.0	0.0	0.0	57.8	0	BEIS urban grass
Ulmu	0.0	0.0	0.0	4.5	5	Ulmus (American elm)
Uoth	0.0	0.0	0.0	0.0	0	BEIS other urban (barren)
Urba	0.0	154.0	102.0	12.5	0	BEIS urban (.2 grass/.2 forest)
Utre	700.0	960.0	528.0	4.5	6	Urban tree (.5 Harf/.5 Conf)

Table 4-4. Winter Biogenic Emission Flux Factors (μg-compound $m^{-2}hr^{-1}$) for Principal Biogenic Compounds by Vegetation Category

Vegetation or Land Cover Code	Isoprene	Terpene	Other VOCs	NO	Leaf Area Index (m^2 m^{-2})	Description
Vacc	0.0	0.0	0.0	4.5	5	Vaccinium (blueberry)
Wash	5950.0	42.5	693.7	4.5	5	Washingtonia (fan palm)
Wate	0.0	0.0	0.0	0.0	0	Water
Wcnf	3500.0	1120.0	1200.0	4.5	5	Western Coniferous Forest (AVHRR, G.)
Wdcp	0.0	630.0	1047.0	8.7	2	Woodland/cropland (AVHRR, G.)
Wetf	0.0	877.0	628.0	0.2	3	Wetland forest (AVHRR, G.)
Whea	0.0	0.0	0.0	192.5	0	Wheat
Wmxf	0.0	620.0	330.0	4.5	3	Western Mixed Forest (AVHRR, G.)
Wwdl	0.0	250.0	360.0	4.5	3	Western Woodlands (AVHRR, G.)

* AVHRR/G. references biogenic emission factors from Guenther et al (1994) which used land use classifications from Advanced Very High Resolution Radiometer (AVHRR) satellite imagery.

The BEIS-2 applies environmental correction factors to account for the effect of leaf temperature and visible solar radiation on isoprene (Pierce et al.,1998). Specifically:

$$I = I_s * C_L * C_T \tag{4-19}$$

where: I is the adjusted isoprene emission flux,

I_S is the isoprene emission flux standardized to leaf temperature 30°C and PAR of 1000 micromoles/m^2/sec.

The light adjustment factor C_L is estimated by:

$$C_L = (\alpha c_{L1} PAR) / \sqrt{(1+\alpha^2 PAR2)} \tag{4-20}$$

where: $\alpha = 0.0027$, and $C_{L1} = 1.066$ are empirically derived coefficients. The leaf temperature adjustment factor C_T is derived from laboratory data and is computed using the following formula:

$$C_T = (\exp[c_{T1}(T-T_s)/RT_sT])/ (1+\exp[c_{T2}(T-T_m)/RT_sT]) \quad (4\text{-}21)$$

where: $C_{T1} = 95{,}000$ J mol^{-1}
T_s is the standardized temperature (303°K),
R is the ideal gas constant (8.314 °K mol^{-1}),
$C_{T2} = 230{,}000$ J mol^{-1}, and
$T_m = 314$°K.

PAR is computed as a function of height by:

$$PAR_z = PAR_0 (\exp[-0.42LAI_z]) \quad (4\text{-}22)$$

During March 1998, the factor used in BEIS-2 within Models-3 to convert solar radiation values from watts per square meter (W/m^2) to micromoles per square meter-second (μm/m^2-sec) was changed from 2.2982 to 2, based on Alados et al. (1996). This had the effect of reducing PAR by ~ 15 percent and isoprene emissions by ~ 5 percent based on limited simulation tests for the July 1995 ozone maximum period.

Emissions for VOCs other that isoprene are assumed to vary only as a function of leaf temperature in accordance with the following:

$$E = E_s * \exp[0.09 (T-T_s)] \quad (4\text{-}23)$$

where: E_s is the standardized emission flux for monoterpenes and other VOCs,
T is the leaf temperature in degrees Kelvin, and
T_s is the standardized temperature (303°K).

The soil NO emission flux factors used in BEIS-2 were adapted from Williams et al. (1992). For temperatures greater than 0°C, soil NO temperature corrections follow the formulation of Williams et al. As follows:

$$NO = NO_o * \exp[0.071(T-T_s)] \quad (4\text{-}24)$$

where NO is the adjusted soil NO emission flux,
NO_o is the emission flux standardized to a soil temperature T_s of 30° C, and
T is the soil temperature.

NO emissions at temperatures less than 0° C are set to zero. During March 1998, it was decided to cap the exponential increase of soil NO emissions with temperatures above 30°C, based on the findings of Yienger and Levy (1995).

The inclusion of BEIS-2 into MEPPS biogenic emission modeling required creating an efficient connection such that BEIS-2 is easy to use from within MEPPS, and also so that the input and output data related to BEIS-2 can take advantage of MEPPS and Models-3 data handling and analysis features. The changes included:

- BEIS-2 is now automatically invoked from MEPPS or the Study Planner when the user requests that biogenic emission factors be calculated. It is not necessary to work directly with the BEIS-2 software.

- Solar radiation and temperature input files are not directly supplied by the user when BEIS-2 is run. These meteorological data are supplied automatically from MCIP files for the case (time period) specified, presuming that MM5 and MCIP have been run for that period.

- Within MEPPS, BEIS-2 can now use ARC-INFO® generated grids and use gridded surrogate data to disaggregate county-level data to grid cells.

- BEIS-2 results are in terms of hourly emissions per grid cell within Models-3.

- Biogenic emission data are subject to the extended quality control and reporting features in MEPPS, and visualization using the ARC-INFO® based GIS-View feature.

The MEPPS uses BEIS-2 by allowing the user to assume summer, winter seasons, or access frost data in order to allow for the seasonal change in vegetative biomass. For summer and winter conditions, vegetation genus and emission factors for isoprene, monoterpene, other biogenic VOC emissions, emission factors for NO, and the leaf area index (LAI) are provided based on the work of Geron et al. (1994). Frost data include the federal identification protocol (FIPS) codes by state and county along with the biomass of the first and last day of summer. The MEPPS draws hourly temperature and solar radiation from MCIP for use in the biogenic processor. Land cover and vegetation are provided in gridded ARC/INFO coverage. The biogenic modeling input data are then provided to BEIS-2 and output as hourly gridded emission values of the VOCs isoprene, monoterpene, and "other" (unspecified); along with NO to the EMPRO speciation processor, where they are grouped with chemical species from other source types depending upon the conventions of either the CB4 or RADM2 speciation split factors (Section 4.2.5).

4.2.4.2 Mobile Source Emissions

Emissions from mobile sources to the air are established as one of the primary contributors to pollution problems in many localities. Unlike many anthropogenic emissions, mobile source emissions are strongly affected by the rapid variations of atmospheric temperature and anthropogenically-influenced, geographically-varying factors. Consequently, it is necessary to model hourly mobile emissions, rather than to temporally disaggregate annual totals. The capability to do this is in the MEPPS mobile-source emission processor. For gaseous emissions

the mobile source processor estimates hourly emissions of VOC total organic gases (TOG), carbon monoxide (CO), and oxides of nitrogen (NOx) from on-road mobile sources (vehicles). The processor, which is located in the EMPRO module of MEPPS, uses a combination of air temperature data at 1.5 m above the surface (provided by MM5 through MCIP), mobile source emission factors (computed by the EPA regulatory model Mobile 5a for gaseous emissions from on-road mobile sources), fleet vehicle type composition, road type, and traffic data in the form of vehicle miles traveled (VMT) to generate emission estimates. Vehicle emission controls, and Inspection and Maintenance programs may be accounted for in the user-defined input settings for Mobile 5a (U.S. EPA, 1991; U.S. EPA, 1996). The VMT data are usually available by county, or occasionally by specific road segments. The resulting county or road segment-specific hourly emissions are spatially allocated to the cells of a user-defined study grid. The gridded emission data are combined with corresponding species output from the mobile source particulate emission model, and allocated to different groups of lumped species for processing by the Speciation Processor (Section 4.2.5).

Emissions of particulate species (particulate matter less that 10 micrometer and 2.5 micrometers in diameter - PM_{10} and $PM_{2.5}$, respectively) from mobile sources are modeled analogously to gaseous emissions, using vehicle fleet composition, road type (urban or rural), and VMT data. The mobile particulate emission factors are modeled with PART5 (U.S. EPA, 1995), the particulate companion of Mobile 5a. Vehicle emission controls, Inspection and Maintenance programs, and use of reformulated fuel may be accounted for with the input settings of PART5. In addition input information for road silt content and precipitation is required. The particulate species modeled include lead, direct and indirect particulate sulfate (any remaining sulfur in fuel is assumed to be exhausted as gaseous SO_2), total exhaust particulate (sum of lead, direct sulfate, and carbon including soluble organic material and other remaining carbon), and (separately) soluble organic fraction (SOF) and a remainder carbon portion (RCP), which are added to the mobile source emission output file.

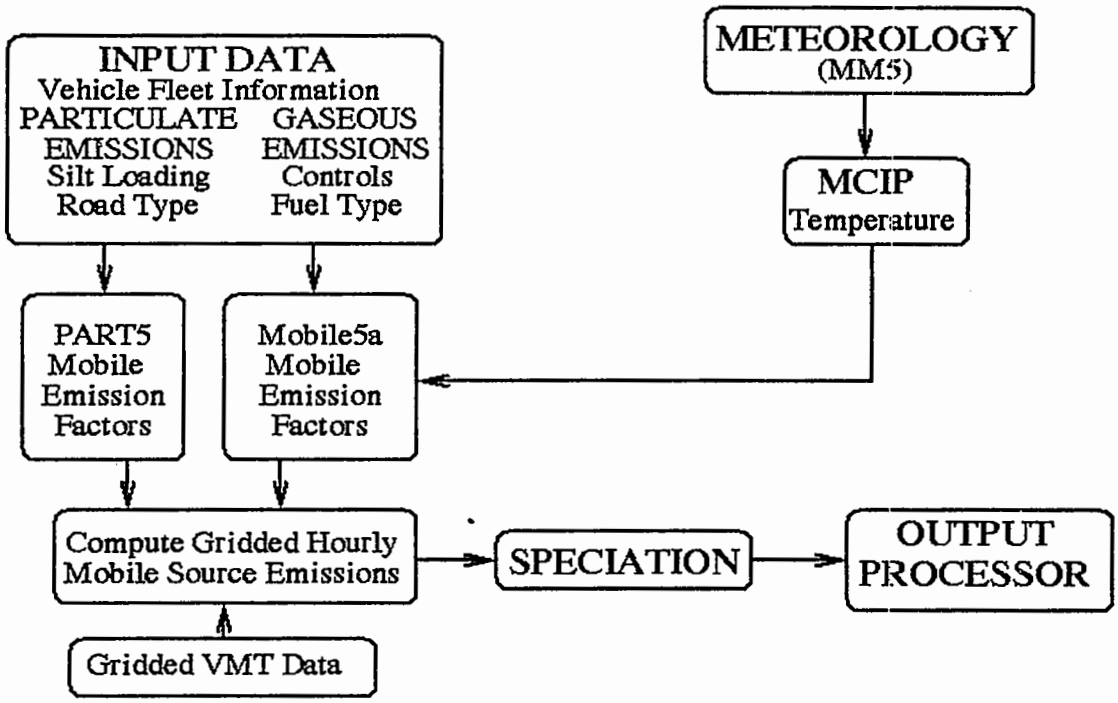

Figure 4-5 General Flow of Mobile Source Emission Modeling

The procedure by which mobile source emission data are estimated in MEPPS and flow diagrams for the process are given in Section 6.5.3.4 of the *Models-3 Volume 9B: User Manual.* Briefly, the sequence is as follows:

- VMT vehicle fleet data files are established for the study area (gridded spatial domain) of interest by either extracting county-level annual aggregate VMT data from the annual emission input files previously established by INPRO, or by loading "link-node" VMT data that are available for specific road segments (links) between nodes with geographic coordinates . The link-node data are generally available only for selected urban areas and dates in conjunction with special studies. The process is similar for VMT data which are occasionally available by quarter section (1/4 square mile) areas.

- ARC/INFO® spatial coverage files of surrogate data (Federal Highway Administration major highways, or United States Census Tiger Line road coverages are provided) are used to spatially allocate county-level aggregate VMT data to the cells of the gridded domain being used with a particular study. County area may also be used as a coarse surrogate coverage.

- Spatial allocation ratios are computed for use in assigning county-level VMT data to the surrogate coverages. The EMPRO calculates the proportion of road links or county area

in the spatial domain attributable to each grid cell overlain by the road link (FHA or TIGER/LINE) or county.

- Mobile source emission factors are computed using Mobile 5a and/or PART 5- U.S. EPA regulatory models. Mobile 5a requires user-defined information on driving operations, vehicle fleet and fuel use, and hourly ambient temperature data. PART 5 requires user-defined information on vehicle fleet and fuel use, emission controls, non-attainment, road dust silt content, moisture, and percent of unpaved roads by geographic area (usually county). Temperature and moisture data are from the MM5 model as processed by MCIP.

- Hourly mobile emissions are computed for each grid cell, with adjustments applied to VMT to indirectly reflect the effect of temperature on gaseous emissions, and moisture on re-entrained dust for particulate emissions.

- For mobile emissions of VOC, hourly gridded mobile emissions are speciated using either RADM 2.0 or CB-4 emission profile splits. Speciation is not needed for particulate emission data.

- The hourly, gridded, speciated mobile emission data are merged with gridded, speciated hourly area-source emission data in OUTPRO, and converted to NetCDF I/O API format, to provide a two dimensional emission data set acceptable to the chemical-transport model and other Models-3 framework applications.

The Mobile 5a Model

Detailed descriptions of Mobile 5a are available from EPA publications (US EPA 1991, US EPA 1996). An optional Mobile 5b has also been adopted (US EPA 1996) to accommodate slight modifications in Inspection and Modification credits for hybrid fuels. Both Mobile 5a and 5b are improvements in the Mobile 4.1 model (US EPA, July 1991). Mobile 6 is in development and is tentatively expected in late 1999. A new off-road mobile emission model is also due in late 1998. Portions of the following description of Mobile are adapted from Wilkinson et al (1994). The incorporation of Mobile 5a into MEPPS was extensively revised from its treatment in GEMAP, including:

- The application of Mobile 5a factors was revised to substantially reduce redundancy and computational space required. The application of Mobile 5a in GEMAP computed specific emission factors for individual state/counties by area type/road type and hour. The combinations of hour and road type were derived by mapping operating modes (percent of hot and cold starts) to the hours and road types that used them, causing a duplication of Mobile 5a runs and factors. It was necessary to recompute factors if there was a change in how the emission factors were used by hours or road type. The computed mobile emission factors were merged into permanent (for the processing run) emission

factor tables without regard to calendar year. In MEPPS, Mobile 5a emission factors are computed and stored by calendar year, state/county, and operating mode. Also, the system now has separate user-specified tables that allocate emission factors by hour and road type, using operating mode. The tables are used directly in the emission estimate calculation. In addition start and end times may now be specified for mobile emission runs rather than number of complete hours. This has also shortened the processing time for county-level mobile emission processing.

- Calculations were separated into county-level, link-node level, and land-survey level options, depending upon the spatial detail of VMT information available to the user.

- The ability to assign alias identification by state or county was added. This allows the user to assign the values in a Mobile input file for a given area to a similar area which lacks specific input data.

- Geographic coverages of major highways (from the Federal Highway Administration) and all roads (TIGER-Line data) were made available as surrogate data to allow better spatial allocation of mobile emissions.

- Mobile emission data are now subject to the additional quality control and ARC-INFO® based visualization capabilities in MEPPS.

Mobile 5a is an ANSI FORTRAN 77 computer program designed to estimate hydrocarbon (HC), carbon monoxide (CO), and oxides of nitrogen (NO_X) emission factors for gasoline-fueled and diesel-fueled highway motor vehicles. The computation methods that are embedded in Mobile 5a are based on the procedures that are presented in the *Compilation of Air Pollutant Emission Factors -- Volume XX: Highway Mobile Sources* (US EPA, 1995). Mobile 5a computes emissions factors for eight vehicle categories in two regions of the country (high-altitude and low-altitude). The eight vehicle categories include the following:

- LDGV – light-duty gasoline vehicles;
- LDGT1 -- light-duty gasoline trucks (up to 6000 pounds);
- LDGT2 -- light-duty gasoline trucks (6001 to 8500 pounds);
- HDGV – heavy-duty gasoline vehicles (over 8500 pounds);
- LDDV – light-duty diesel vehicles;
- LDDT – light-duty diesel trucks (0 to 8500 pounds);
- HDDV – heavy-duty diesel vehicles (over 8500 pounds); and
- MC -- motorcycles.

The Mobile 5a emission factors depend on various conditions including, but not limited to, ambient temperature, vehicle speed, operating modes, and vehicle mileage accrual rates. Much of the data required by Mobile 5a may be specified by the user through the Mobile input file. Mobile computes emissions factors for any year from 1960 to 2020. This date range is important for

mobile-source emission estimated projections, and for the application of regulatory control factors. Mobile version 5a.01 (which was modified for use in GEMAP/EMS-95 and later for MEPPS) is currently implemented in the EMPRO module of MEPPS. Consult the *User's Guide to MOBILE 5, EPA-AA-TEB-92-01* for further details on Mobile 5a. Mobile model documentation may be obtained from the EPA Office of Mobile Sources World Wide Web home page located at: **http://www.epa.gov/OMSWWW/models.htm**.

A comprehensive discussion of the technical formulation of Mobile 5a is found in the above references. This section contains a description of modifications to Mobile 5a for use in GEMAP and later in MEPPS. Mobile 5a was modified for use in EMS-95 to compute and report diurnal evaporative emissions factors (grams/mile) separately. The unmodified Mobile 5a model computes and reports diurnal evaporative emission factors as part of a composite evaporative emission factor. Also, Mobile 5a was modified to report a total non-diurnal evaporative emission factor. The total non-diurnal evaporative emission factor includes hot soak, crankcase blow-by, running losses, and resting losses. In the MEPPS EMPRO module, the Mobile SAS® table generators have been rewritten and segmented for greater computational efficiency, as have been the VMT and surrogate coverage grid processors and mobile source emission calculation procedures. The technical procedure and rationale are the same, but processing time is shortened by at least a factor of two for regional modeling of spatial domains.

The mobile-source emission processor relies on a SAS® lookup table to find appropriate emissions factors to compute the motor vehicle emission estimates. The SAS® lookup table is generated through iterative runs of Mobile 5a. The necessary number of runs of Mobile 5a is performed automatically, and is based on the standard Mobile ASCII input file supplied by the user. For urban scale modeling, an input file for one state may suffice. However, for regional modeling, multiple Mobile 5a ASCII input files can be concatenated to one file and run through the processor. This capability is necessary to handle study domains where motor vehicle activity differs spatially and temporally. For example, in a multiple-state study domain, it is unlikely that adjoining states have the same inspection and maintenance (I/M) program or the same vehicle fleet distribution (to name just two inputs to Mobile 5a). Differences in regional inputs to Mobile 5a such as I/M programs and vehicle fleet distributions result in different motor vehicle emissions factors. A concatenated input file template (based on example values used for the OTAG project) is provided which may be copied and edited. In MEPPS, the Mobile input file (*m5a.mv*) is located in the directory structure at:

$EMS_HOME*/project/*$EMS_PROJECT/raw_data/*$EMS_DOMAIN*/common/.

The only difference in the concatenated input file from the original input file is that the state title lines contain state (and where needed, county) FIPS identifier codes to identify the area for which each section of the Mobile 5a input file is applicable:

- FIPS state code -- Mobile input file applies to a state; or
- FIPS state code and FIPS county code -- Mobile input file applies to a particular county.

The mobile-source emission processor varies the vehicle speed and ambient temperature records of the user-supplied input file and runs Mobile for each variation. The Mobile source processor varies the vehicle speeds from 4 miles per hour to 64 miles per hour in increments of 2 miles per hour, although the user may adjust the increment (Mobile supports computation of emission factors for speeds between 2.5 MPH and 65 MPH). The mobile-source processor varies the minimum ambient temperature from 50° F to 110° F in increments of 2° F, and the mobile source processor varies the maximum ambient temperature from 50° F to 110° F in increments of 2° F (Mobile 5a supports computation of exhaust emissions factors for temperatures between 0° F and 110° F and evaporative emissions factors for temperatures between 40° F and 110° F). The vehicle speed and ambient temperature values can be set interactively in EMPRO under the mobile source model, using the "Generate Mobile Emission Factors" screen.

In MEPPS, the mobile-source processor generates two emission factor SAS® lookup tables. These are compact tables that contain the information held in seven generated SAS lookup tables in EMS-95. They are:

- State/area type/facility type diurnal emissions factors (I/M and non-I/M HC diurnal evaporative emissions factors for eight vehicle categories by state, minimum ambient temperature, maximum ambient temperature, and calendar year). The user specifies whether the operating mode varies by the hour of the day in the Temporal Allocation screen of the mobile emission model of EMPRO);

- State/area-type/facility-type non-diurnal emissions factors (I/M and non-I/M HC [evaporative and exhaust], CO [exhaust only], and NO_X [exhaust only] emissions factors for eight vehicle categories by state, area type [urban or rural], facility type [eg. interstate, collector, arterial, local], vehicle speed, ambient temperature, and calendar year. The user can interactively specify whether the operating mode varies by hour of the day when establishing temporal profiles in the Temporal Allocation screen of the mobile emission model of EMPRO.

Operating mode is an important variable in the computation of motor vehicle emissions factors. Attention is specifically called to operating mode because the mobile source processor uses up to four different operating mode mixes to compute emissions factors for the Mobile 5a lookup tables (refer to the Mobile 5a user's guide for further discussion of operating modes).

If area type/facility type records are to be used in the Mobile-generated lookup tables, the user must specify the mix of operating modes. The following example of operating mode mixes was used for the Lake Michigan Ozone Study: 5% PCCN, 12.1% PCHC, and 10.9% PCCC, where PCCN is percent VMT generated by non-catalyst vehicles in cold-start mode, PCHC is percent VMT generated by catalyst vehicles in hot-start mode, and PCCC is percent VMT generated by catalyst vehicles in cold-start mode. If hourly records are used in the Mobile-generated lookup tables, the user must define the operating mode mixes by time of day, consistent with Mobile 5a guidance. The following is an example of the use of four operating mode mixes:

- 0000 to 0700 operating mode is 12.9% PCCN, 7% PCHC, and 17% PCCC;
- 0700 to 0900 operating mode is 15% PCCN, 10% PCHC, and 15.4% PCCC;
- 0900 to 1600 operating mode is 5% PCCN, 12.1% PCHC, and 10.9% PCCC;
- 1600 to 1800 operating mode is 10.1% PCCN, 9.1% PCHC, and 13.9% PCCC;
- 1800 to 2200 operating mode is 5% PCCN, 12.1% PCHC, and 10.9% PCCC;
- 2200 to 0000 operating mode is 12.9% PCCN, 7% PCHC, and 17% PCCC.

As with the vehicle speeds and ambient temperatures, the operating mode mixes can be changed interactively on the Operating mode screen in THE MEPPS EMPRO module under Models, Mobile, Mobile Source.

The mobile source processor generates emission factors for the following area type (urban or rural) and facility type (interstate, local, etc.) combinations:

- rural/principal arterial - interstate
- urban/principal arterial - interstate
- rural/principal arterial - other
- urban/principal arterial - free/express-ways
- rural/minor arterial
- urban/principal arterial - other
- rural/major collector
- urban/collector
- rural/minor collector
- urban/minor arterial
- rural/local
- urban/local

As with vehicle speeds, ambient temperatures, and operating modes; area type/facility type combinations can be changed interactively using the "Generate Mobile Emission Factors" screen under EMPRO, Models, Mobile, Mobile Source to edit the ASCII input file . When changes are made, the same changes are automatically made to the SAS® data sets.

User Input Data

The mobile source emission processor requires user-defined specifications using interactive screens and an input file. While some of the specifications are required, some are not required. In each case, there is provision to import the data file through IDA or in the mobile source processor of MEPPS.

The principal input data ASCII files to the mobile source model include the following (environment variables are defined in Chapter 6 of the *Models 3 Volume 9B: User Manual*):

- On-network link-specific area type/facility type (*$EMS/onnet.mv)*

- On-network link-specific percentage of vehicles that fall under an I/M program *($EMS/onnetim.mv)*
- On-network link-specific daily or hourly VMT *($EMS/onnetvmt.mv)*;
- Hourly or daily, link-specific or area type/facility type-specific vehicle mix
- Off-network, area type/ facility type average speed *($EMS_LOC/offnetspd.mv)*
- Off-network, area type/facility type VMT *($EMS/offnvmt.mv)*;
- Off-network, area type/facility type-specific vehicle mix profile *($EMS_LOC/offvmix.mv)*
- Public land survey quarter sections area type/ facility type hourly or daily VMT, hourly speeds, and daily vehicle mix profile *($EMS/ofnvmtp.mv)*;
- Area type/facility type seasonal and daily adjustment factors *($EMS/adjstvmt.mv)*
- Area type/facility type hourly average speed profile *($EMS_CAT/spdadju.mv)*
- On-network, link-specific hourly or daily average speed *($EMS_GRD/onnetspd.mv)*
- Area type/facility type hourly VMT fractional profile *($EMS/fracvmtu.mv)*

If off-network VMT is to be used to compute emissions estimates (typical when county VMT data are taken from regional emission inventories), the mobile emission processor can assign VMT to grid cells using ARC/INFO® coverage files for either county area, Federal Highway Administration (FHA) major highways, or TIGER/LINE road data. These coverages for the contiguous United States are provided with MEPPS. Subsets of the coverages for the spatial domain of interest are extracted either when a grid is established or during mobile source processing.

If Public Land Survey Quarter Section-based VMT is to be used to compute emissions estimates, the mobile source emission processor requires an ARC/Info® export data set of the polygon-network system.

Gridding VMT

After the ASCII user input (foundation) data files have been read and checked, the user directs the mobile source emission processor to prepare the necessary network coverages (unless they were prepared when the grid was established). The on-network system is prepared from the user-provided ASCII input files. The off-network system is prepared via county boundary, FHA, or TIGER/LINE data file extracts. The polygon system is prepared from an ARC/INFO® export coverage. The networks are gridded by overlaying the emission modeling grid on the network coverages in much the same manner that the area source spatial surrogates are gridded. Each link in the networks (or area type/facility type polygon) are length (or area) apportioned to a grid cell in the emissions modeling domain. Once the networks have been gridded, the corresponding VMT can also be gridded. Equations 4-25 through 4-30 show how the on-network, off-network, and polygon VMT are gridded respectively.

$$lenratio_{i,j,k,l,m} = lengrid_{i,j,k,l,m} / lenpar_{i,j,k} \quad (4\text{-}25)$$

$$VMT_{i,j,k,l,m} = vmtorig_{i,j,k} * lenratio_{i,j,k,l,m} \quad (4\text{-}26)$$

$$cellpct_{i,j,a,f,l,m} = cellsum_{i,j,a,f,l,m} / ctysum_{i,j,a,f} \quad (4\text{-}27)$$

$$VMT_{i,j,a,f,l,m} = vmtorig_{i,j,a,f} * cellpct_{i,j,a,f,l,m} \quad (4\text{-}28)$$
$$areapct_{i,j,p,a,f,l,m} = areagrd_{i,j,p,a,f,l,m} / areapar_{i,j,p} \quad (4\text{-}29)$$
$$VMT_{i,j,p,a,f,l,m} = vmtorig_{i,j,p,a,f} * areapct_{i,j,p,a,f,l,m} \quad (4\text{-}30)$$

where lenratio is the percentage of a link in a given grid cell
lengrid is the length of a link in a given grid cell
lenpar is the total length of the link
VMT is the gridded VMT value
vmtorig is the original VMT
cellpct is the percent of the FHA or TIGER/Line-based area type/facility type roadway in a given cell
cellsum is the total length of FHA or TIGER/Line-based area type/facility type roadway in a given cell
ctysum is the total length of the FHA or TIGER/Line-based area type/facility type roadway in a county
areapct is the percent of the polygon-based area type/facility type roadway in a given cell
areagrd is the total length of the polygon-based area type/facility type roadway in a given cell
areapar is the total length of the polygon-based area type/facility type roadway in a county
i is the state index
j is the county index
k is the link index for on-network systems
l is the east-west grid cell index
m is the north-south grid cell index
a is the area type index for off-network systems
f is the facility type index for off-network systems
p is the polygon index for Public Land Survey Quarter Sections network systems.

For on-network and polygon VMT, the indices may also include an identifier for hour since polygon and on-network VMT can also be supplied on an hourly basis.

Apply Default Information

If the user supplies limited data to the mobile-source emission processor, it can apply a variety of default values to compute motor vehicle emissions estimates. These defaults include vehicle mix, speeds, VMT fractional profiles, and I/M vehicle percentages. If the user supplies limited data, the mobile-source emission processor applies the following defaults:

Default Vehicle Mix Profile

Vehicle Class	Percentage
LDGV	0.618
LDGT1	0.177
LDGT2	0.077
HDGV	0.035

LDDV	0.008
LDDT	0.002
HDDV	0.077
MC	0.008

Default Speed Profile

Area Type	Facility Type	Speed
0	1	60
0	4	56
0	6	56
0	7	54
0	8	40
0	9	35
1	1	60
1	2	59
1	4	55
1	5	30
1	6	55
1	9	30

Default Hourly VMT Fractional Profile

Emission Hour	1	2	3	4	5	6	7	8	9	10	11	12
Diurnal	0.000	0.000	0.000	0.000	0.000	0.129	0.021	0.100	0.095	0.095	0.166	0.199
Other	0.016	0.010	0.003	0.006	0.010	0.026	0.053	0.064	0.055	0.048	0.050	0.052

	13	14	15	16	17	18	19	20	21	22	23	24
Diurnal	0.079	0.116	0.000	0.000	0.000	0.000	0.000	0.000	0.000	0.000	0.000	0.000
Other	0.054	0.055	0.059	0.070	0.074	0.070	0.058	0.046	0.037	0.033	0.028	0.022

If the user does not specify what the percentage of vehicles are under an I/M program, the mobile source emission processor assumes that no vehicles are under an I/M program. The result is higher emission estimates.

The mobile source emission processor does not override user-supplied data. Default information are applied only when data are missing from the ASCII user input files.

Add Temperatures and Adjust VMT

Prior to computing the motor vehicle emission estimates, the mobile-source emission processor adds the gridded, hourly temperatures and adjusts the VMT to the specific modeling day. The temperature data are used to obtain the correct emission factor from the Mobile emission factors lookup tables. Through the application of Equations 4-31 through 4-34, the day-specific, diurnal and nondiurnal (other than full days), hourly VMT are computed, respectively.

$$dvmt_{i,j,l,h,m,n} = ddayvmt_{i,j,l,m,n} * adjday * adjmonth * dvmt_prof_{i,j,l,h} \quad (4\text{-}31)$$
$$ovmt_{i,j,l,h,m,n} = odayvmt_{i,j,l,m,n} * adjday * adjmonth * ovmt_prof_{i,j,l,h} \quad (4\text{-}32)$$
$$dvmt_{i,j,a,f,h,m,n} = ddayvmt_{i,j,a,f,m,n} * adjday * adjmonth * dvmt_prof_{i,j,a,f,h} \quad (4\text{-}33)$$
$$ovmt_{i,j,a,f,h,m,n} = odayvmt_{i,j,a,f,m,n} * adjday * adjmonth * ovmt_prof_{i,j,a,f,h} \quad (4\text{-}34)$$

where

dvmt is the diurnal VMT;
dayvmt is the total day diurnal VMT;
adjday is the day-specific VMT adjustment factor supplied through an ASCII input file;
adjmonth is the month-specific VMT adjustment factor supplied through an ASCII input file;
dvmt_prof is the hour-specific, diurnal VMT fractional profile factor;
ovmt is the nondiurnal VMT;
odayvmt is the total day nondiurnal VMT;
ovmt_prof is the hour-specific, nondiurnal VMT fractional profile factor;
i is the state index;
j is the county index;
h is the hour index;
l is the link identifier index;
a is the area type index;
f is the facility type index;
m is the east-west grid cell index; and
n is the north-south grid cell index.

Compute Motor Vehicle Emissions Estimates

The mobile source emission processor computes day-specific, gridded, hourly motor vehicle emissions estimates of VOC total organic gases (TOG), carbon monoxide (CO), and oxides of nitrogen (NO_X). The actual emission estimate computations performed and maintained in the MEPPS data base are as follows:

- TOG for gasoline (noncatalyst/catalyst composite) evaporative diurnal processes;
- TOG for gasoline (noncatalyst/catalyst composite) evaporative nondiurnal processes;
- TOG for gasoline (noncatalyst/catalyst composite) exhaust operations;
- NO_X for gasoline (noncatalyst/catalyst composite) exhaust operations;
- CO for gasoline (noncatalyst/catalyst composite) exhaust operations;
- TOG for diesel (noncatalyst/catalyst composite) exhaust operations;
- NO_X for diesel (noncatalyst/catalyst composite) exhaust operations; and
- CO for diesel (noncatalyst/catalyst composite) exhaust operations.

The mobile emission processor computes motor vehicle emissions estimates based on three types of VMT files:

- On-network VMT;
- Off-network VMT; and
- Public land survey quarter sections VMT.

The differences in the VMT types are:

- On-network VMT are network link-specific;
- Off-network VMT are county/area type/facility type-specific; and
- Public land survey quarter sections VMT are county/polygon/area type/facility type-specific.

The mobile-emission processor estimates motor vehicle emissions for all combinations of VMT. Regardless of the VMT type that is used to generate motor vehicle emission estimates, all motor-vehicle emission estimates have some degree of uncertainty. However, the most desirable motor-vehicle emissions estimates usually are generated from on-network, link-specific data, followed by public land survey quarter sections data, and finally off-network data. Motor vehicle emission estimates that are generated from on-network data are not more certain, but that they are more spatially representative.

Before the mobile-source emission processor computes the motor vehicle emission estimates, it computes a fleet composite emission factor. Equations 4-44 through 4-67 show how the processor computes the fleet composite emission factors. In all cases, the emission factors are extracted from the Mobile lookup tables based on the appropriate indices. Please refer to the section on generating the Mobile emission factors lookup tables earlier in this section for additional information.

If the user has provided non-I/M-specific VMT, the mobile source emission processor computes the fleet composite emission factors by vehicle classification for temperature and speeds combinations through the application of Equations 4-35 through 4-42.

$$hcdif_{s,t} = \Sigma_j hcdi_{j,s,t} * vmix_j \quad (4\text{-}35)$$
$$hcexf_{s,t} = \Sigma_j hcex_{j,s,t} * vmix_j \quad (4\text{-}36)$$
$$noxf_{s,t} = \Sigma_j noxx_{j,s,t} * vmix_j \quad (4\text{-}37)$$
$$coexf_{s,t} = \Sigma_j coex_{j,s,t} * vmix_j \quad (4\text{-}38)$$
$$hcevf_{s,t} = \Sigma_j hcev_{j,s,t} * vmix_j \quad (4\text{-}39)$$
$$dhcexf_{s,t} = \Sigma_j dhcex_{j,s,t} * vmix_j \quad (4\text{-}40)$$
$$dnoxf_{s,t} = \Sigma_j dnoxx_{j,s,t} * vmix_j \quad (4\text{-}41)$$
$$dcoexf_{s,t} = \Sigma_j dcoex_{j,s,t} * vmix_j \quad (4\text{-}42)$$

where: j is the vehicle classification index
s is the speed index
t is the temperature index
hcdif is the hydrocarbon diurnal fleet composite emission factor for all vehicle types (grams/mile)
hcdi is the non-I/M hydrocarbon diurnal emission factor (grams/mile)
vmix is the vehicle mix profile

hcexf is the hydrocarbon exhaust nondiurnal fleet composite emission factor for gasoline vehicles (grams/mile)
hcex is the non-I/M hydrocarbon exhaust nondiurnal emission factor for gasoline vehicles (grams/mile)
noxf is the oxides of nitrogen exhaust nondiurnal fleet composite emission factor for gasoline vehicles (grams/mile)
noxx is the non-I/M oxides of nitrogen exhaust nondiurnal emission factor for gasoline vehicles (grams/mile)
coexf is the carbon monoxide exhaust nondiurnal fleet composite emission factor for gasoline vehicles (grams/mile)
coex is the non-I/M carbon monoxide exhaust nondiurnal emission factor for gasoline vehicles (grams/mile)
hcevf is the hydrocarbon evaporative nondiurnal fleet composite emission factor for gasoline vehicles (grams/mile)
hcev is the non-I/M hydrocarbon evaporative nondiurnal emission factor for gasoline vehicles (grams/mile)
dhcexf is the hydrocarbon exhaust nondiurnal fleet composite emission factor for diesel vehicles (grams/mile)
dhcex is the non-I/M hydrocarbon exhaust nondiurnal emission factor for diesel vehicles (grams/mile)
dnoxf is the oxides of nitrogen exhaust nondiurnal fleet composite emission factor for diesel vehicles (grams/mile)
dnoxx is the non-I/M oxides of nitrogen exhaust nondiurnal emission factor for diesel vehicles (grams/mile)
dcoexf is the carbon monoxide exhaust nondiurnal fleet composite emission factor for diesel vehicles (grams/mile)
dcoex is the non-I/M carbon monoxide exhaust nondiurnal emission factor for diesel vehicles (grams/mile)

If the user has provided I/M-specific VMT data, the processor computes the fleet composite emission factors by vehicle category for temperature and speed combinations through the application of Equations 4-43 through 4-50.

$$hcdif_{s,t} = \Sigma_j\ ihcdi_{j,s,t} * vmix_j \quad (4\text{-}43)$$
$$hcexf_{s,t} = \Sigma_j\ ihcex_{j,s,t} * vmix_j \quad (4\text{-}44)$$
$$noxf_{s,t} = \Sigma_j\ inoxx_{j,s,t} * vmix_j \quad (4\text{-}45)$$
$$coexf_{s,t} = \Sigma_j\ icoex_{j,s,t} * vmix_j \quad (4\text{-}46)$$
$$hcevf_{s,t} = \Sigma_j\ ihcev_{j,s,t} * vmix_j \quad (4\text{-}47)$$
$$dhcexf_{s,t} = \Sigma_j\ idhcex_{j,s,t} * vmix_j \quad (4\text{-}48)$$
$$dnoxf_{s,t} = \Sigma_j\ idnoxx_{j,s,t} * vmix_j \quad (4\text{-}49)$$
$$dcoexf_{s,t} = \Sigma_j\ idcoex_{j,s,t} * vmix_j \quad (4\text{-}50)$$

where: ihcdi is the I/M hydrocarbon diurnal emission factor (grams/mile)

ihcex is the I/M hydrocarbon exhaust nondiurnal emission factor for gasoline vehicles (grams/mile)
inoxx is the I/M oxides of nitrogen exhaust nondiurnal emission factor for gasoline vehicles (grams/mile)
icoex is the I/M carbon monoxide exhaust nondiurnal emission factor for gasoline vehicles (grams/mile)
ihcev is the I/M hydrocarbon evaporative nondiurnal emission factor for gasoline vehicles (grams/mile)
idhcex is the I/M hydrocarbon exhaust nondiurnal emission factor for diesel vehicles (grams/mile)
idnoxx is the I/M oxides of nitrogen exhaust nondiurnal emission factor for diesel vehicles (grams/mile)
idcoex is the I/M carbon monoxide exhaust nondiurnal emission factor for diesel vehicles (grams/mile)

If the user has provided both I/M and non-I/M VMT data, the mobile source emission processor computes the fleet composite emission factors by vehicle category for temperature and speed combinations through the application of Equations 4-51 through 4-58 This set of equations can be applied only to on-network VMT data because the I/M percentages are input to the mobile source emission processor on a link-specific basis.

$$hcdif_{s,t} = \Sigma_j ((ihcdi_{j,s,t} * imvmt_l) + (hcdi_{j,s,t} * (1 - imvmt_l))) * vmix_j \quad (4\text{-}51)$$
$$hcexf_{s,t} = \Sigma j ((ihcex_{j,s,t} * imvmt_l) + (hcex_{j,s,t} * (1 - imvmt_l))) * vmix_j \quad (4\text{-}52)$$
$$noxf_{s,t} = \Sigma_j ((inoxx_{j,s,t} * imvmt_l) + (noxx_{j,s,t} * (1 - imvmt_l))) * vmix_j \quad (4\text{-}53)$$
$$coexf_{s,t} = \Sigma_j ((icoex_{j,s,t} * imvmt_l) + (coex_{j,s,t} * (1 - imvmt_l))) * vmix_j \quad (4\text{-}54)$$
$$hcevf_{s,t} = \Sigma_j ((ihcev_{j,s,t} * imvmt_l) + (hcev_{j,s,t} * (1 - imvmt_l))) * vmix_j \quad (4\text{-}55)$$
$$dhcexf_{s,t} = \Sigma_j ((idhcex_{j,s,t} * imvmt_l) + (dhcex_{j,s,t} * (1 - imvmt_l))) * vmix_j \quad (4\text{-}56)$$
$$dnoxf_{s,t} = \Sigma_j ((idnoxx_{j,s,t} * imvmt_l) + (dnoxx_{j,s,t} * (1 - imvmt_l))) * vmix_j \quad (4\text{-}57)$$
$$dcoexf_{s,t} = \Sigma_j ((idcoex_{j,s,t} * imvmt_l) + (dcoex_{j,s,t} * (1 - imvmt_l))) * vmix_j \quad (4\text{-}58)$$

where: imvmt is the fraction of vehicles that are under an I/M program; and
l is the link identifier index.

Many indices have been left out of Equations 4-35 through 4-58. The composite emission factors that are generated are gridded, hourly values. Because temperature is a gridded, hourly value, the temperature index *t* in Equations 4-31 through 4-54 implies that the composite emissions factor are gridded, hourly values.

Once the fleet composite emission factors have been computed, the mobile source emission processor computes the motor vehicle emission estimates through the application of Equations 4-59 through 4-66.

dhc_vee = hcdif * divmt * 10**-3 (4-59)
hc_xee = hcexf * ovmt * 10**-3 (4-60)
noxxee = noxf * ovmt * 10**-3 (4-61)
co_xee = coexf * ovmt * 10**-3 (4-62)
hc_vee = hcevf * ovmt * 10**-3 (4-63)
dhc_xee = dhcexf * ovmt * 10**-3 (4-64)
dnoxxee = dnoxf * ovmt * 10**-3 (4-65)
dco_xee = dcof * ovmt * 10**-3 (4-66)

where: dhc_vee is the gridded, hourly diurnal hydrocarbon emission estimate (kilograms)
divmt is the gridded, hourly diurnal VMT (miles)
hc_xee is the gridded, hourly exhaust hydrocarbon nondiurnal emission estimate for gasoline vehicles (kilograms)
ovmt is the gridded, hourly nondiurnal VMT (miles)
noxxee is the gridded, hourly exhaust oxides of nitrogen nondiurnal emission estimate for gasoline vehicles (kilograms)
co_xee is the gridded, hourly exhaust carbon monoxide nondiurnal emission estimate for gasoline vehicles (kilograms)
hc_vee is the gridded, hourly evaporative hydrocarbon nondiurnal emission estimate for gasoline vehicles (kilograms)
dhc_xee is the gridded, hourly exhaust hydrocarbon nondiurnal emission estimate for diesel vehicles (kilograms)
dnoxxee is the gridded, hourly exhaust oxides of nitrogen nondiurnal emission estimate for diesel vehicles (kilograms)
dco_xee is (the gridded, hourly exhaust carbon monoxide nondiurnal emission estimate for diesel vehicles (kilograms)

The mobile-source emission processor computes the final motor vehicle emission estimates file by summing the emission estimates computed by Equations 4-59 through 4-66 over each state identifier, county identifier, east-west grid cell identifier, north-south grid cell identifier, process type (EV for evaporative, EX for exhaust), technology type (1 for gasoline, 2 for diesel), and pollutant identifier (HC for hydrocarbon, CO for carbon monoxide, NO_X for oxides of nitrogen).

The PART5 Model

The current version of PART5 was released in 1995 by the U.S. EPA Office of Mobile Sources. The description given here is taken principally from the user's guide, *A Draft User's Guide to PART5: A Program for Calculating Particle Emissions from Motor Vehicles* (U.S. EPA, 1995b), which provides information in addition to that given in this section. The guide is available from the Office of Mobile Sources Internet web site at **http:www.epa.gov/omsw/models.htm** The PART5 is a FORTRAN program used to model emission factors needed to estimate emissions from gasoline and diesel powered on-road vehicles. It calculates particle emission factors in grams per mile for particle sizes 1 to 10 micrometers. The emission factors include

exhaust particulate matter and components, brake wear, tire wear, and re-entrained road dust. The program includes default data for most inputs, but allows user-supplied data for most items. The interactive aspects of running PART5, as it is provided by the Office of Mobile Sources, have been subsumed into MEPPS to allow the user to enter and edit data, specify program control flags, and run the model via a series of windows within the EMPRO mobile source processor.

Controls specified within PART5 may vary spatially and temporally. PART5 output report flags are not germane within MEPPS because the outputs are automatically processed with emissions from other emission sources in MEPPS internal format. They flags used include the following items:

- Vehicle fleet mix. The user may specify of whether default or user-supplied VMT vehicle fleet mixes are used. The VMT mix is the fraction of total VMT for all vehicles contributed to by each vehicle class. The default VMT is based on national averages and trends over the years. The trends reflect the sales shift from automobiles to light-duty trucks, and the increasing use of diesel engines in both light and heavy-duty trucks. VMT mix may vary spatially. The following are the descriptions of the vehicle classes and corresponding Federal Highway Administration (FHA) and gross vehicle weight (GVW) used in PART5.

Vehicle Class	FHA Class	GVW (lbs)
1 = LDGV (light-duty gasoline vehicle)		
2 = LDGT1 (light-duty gasoline truck, I)	1	<6000
3 = LDGT2 (light-duty gasoline truck II)	2A	6001-8500
4 = HDGV (heavy-duty gasoline truck)	2B-8B	>8500
5 = MC (motor cycle)		
6 = LDDV (light-duty diesel vehicle)	1	<6000
7 = LDDT (light-duty diesel truck)	2A	6001-8500
8 = 2BHDDV (class 2B heavy duty diesel vehicle)	2B	8501-10000
9 = LHDDV (light heavy-duty diesel vehicle)	3,4,5	10001-19500
10 = MHDDV (medium heavy-duty diesel vehicle)	6,7,8A	19501-33000
11 = HHDDV (heavy heavy-duty diesel vehicle)	8B	33000+
12 = BUSES (buses)		

- Mileage accumulation rates. The user may supply or use default mileage accumulation rates and vehicle registration distributions. The mileage accumulation rate is the expected number of miles that a typical vehicle (for each class) is expected to travel in a year, divided by 100,000. The rates must be provided for each vehicle type for each of 25 years (12 years for motor cycles).

- Inspection and maintenance. The user specifies whether an inspection and maintenance program is assumed for gasoline vehicle vehicles only.

- Reformulated gasoline. The specifies whether the use and effects of reformulated gasoline on particulate emissions are assumed. The effects are partially based on the sulfur content of gasoline used. An average sulfur weight percent of 0.034 is used for any gasoline used in all years prior to 2000. If reformulated gasoline is used for the year 2000 or later, the sulfur weight percent is assumed to be 0.0138.

The purpose of MEPPS is to estimate temporally and spatially-varying emission data on a gridded basis. This is consistent with some additional input data which PART5 requires be entered on spatial basis, which are defined as PART5 scenarios. In EMPRO mobile source processing the user is prompted to edit existing or new scenario data. The information includes:

- Region, calendar year, speed cycle (type of driving, ie. cruise), and average speed.

- Percent of unpaved road silt, paved road silt loading in gm /m^2, and optionally, the average number of wheels per vehicle. Modeled dust emission factor are highly sensitive to the unpaved road silt percentage which is extremely variable. Consequently, measured data are advised when possible.

- The number of days each year with greater than 0.01 inches of precipitation for use in modeling re-entrained dust. This is climatological average data. In the future, the emission processing system may be modified to use more spatially and temporally accurate modeled precipitation data by grid cell taken from MM5 and MCIP for the PART5 calculations.

- A scenario name may be applied. In MEPPS a FIPS code a geographic identifier is entered which is used to apply PART5 emission factors computed for the county level to the appropriate modeling grid cells.

- PART5 expects the user to define a maximum particle size cutoff (maximum allowed is 10 micrometers). In MEPPS the maximum size is defaulted to 10 micrometers to ensure that the full range of particle sizes are represented in the regional emission estimates.

- Average vehicle weight (lbs)

PART5 Emission Factors

The emission factors calculated by PART5 include the particulate pollutant compounds of lead, sulfate, soluble organic fraction particulate matter, remaining carbon portion particulate matter, and total exhausted particulate. The lead and sulfate are formed from the lead and sulfur contained in the fuel. The soluble organic fraction consists primarily of hydrocarbons coming

from unburned or partially burned fuel and lubricating oil. The remaining carbon portion consists of soot-like carbon (elemental carbon) and trace amounts of other components from the fuel and lubricating oil. The total exhaust particulate is the sum of these four categories. In addition to these categories of exhaust emissions, idle exhaust emissions (for heavy diesel vehicles only), brake wear, tire wear, fugitive dust, indirect sulfate, and gaseous sulfur dioxide are calculated by PART5.

The model calculates the emission factors for the 12 vehicle classes previously described and a fleet-wide average (estimated by VMT weighting of the emission factors for each of the 12 vehicle classes. The factors are composites of the emission factors for the 25+ years prior to the year of interest, in order to allow for the effects of older vehicles. The composite emission factor for each vehicle class is calculated by weighting the emission factor calculated for each model year by the travel fraction for that model year, and then summing the 25 weighted factors. The travel fraction of a model year is the fraction of VMT by a vehicle of that model year out of the total number of miles traveled by all model years' vehicles in that vehicle class.

$$EFCOMP_v = \sum_{m=1}^{25} EF_{m,v} * TF_{m,v} \qquad (4\text{-}67)$$

where: $EFCOMP_v$ is the composite emission factor for vehicle class v,
$EF_{m,v}$ is the emission factor for vehicle class v, model year m,
$TF_{m,v}$ is the travel fraction for vehicle class v, model year m.

The overall travel fraction of a vehicle class represents the fraction of the total number of VMT of that class of the total highway VMT by all 12 classes. The VMT fractions for each vehicle class are multiplied by the corresponding composite emission factors ($EFCOMP_v$), and the sum of the adjusted emission factors is reported as the emission factor for all vehicles.

$$EFALL = \Sigma\, EFCOMP_v * TFCLASS_v \qquad (4\text{-}68)$$

where: EFALL is the weighted emission factor for all vehicles,
$TFCLASS_v$ is the VMT of vehicle class v.

The emission factor for all vehicles, EFALL, represents the grams/mile of emissions

Lead Emission Factors for gasoline-fueled vehicles

Lead particulate emission factors for gasoline-fueled vehicles assume that almost all lead in the fuel is exhausted. Therefore, the emission factors (grams/mile) depend on the lead content of fuel and fuel economy of the vehicle (miles/gallon). The factors allow for the fact that the lead content of leaded fuel is much greater than for unleaded fuel. *The assumption is made that because diesel fuel has negligible lead content, the lead emissions from diesel vehicles will be negligible.* The

following formulae are used to compute lead emission factors for all gasoline-fueled automobiles and motorcycles, respectively.

$$LEAD_{m,v} = PLNOCT_{m,v} * VLNOCT_{m.v} + PUNOCT_{m,v} * VUNOCT_{m,v} + PLYSCT_{m,v} * VLYSCT_{m,v} + PUYSCT_{m,v,} * VUYSCT_{m,v} \quad (4\text{-}69)$$

where: m denotes a specified model year
v denotes a specified vehicle class
$LEAD_{m,v}$ is the lead particulate emissions for any given vehicle (grams/mile)
$PLNOCT_{m,v}$ is the emissions for a non-catalyst, leaded fuel vehicle (grams/mile)
$PUNOCT_{m,v}$ is the emissions for a non-catalyst, unleaded fuel vehicle (grams/mile)
$PLYSCT_{m,v}$ is the emissions for a catalyst, leaded fuel vehicle (grams/mile)
$PUYSCT_{m,v}$ is the emissions for a catalyst, unleaded fuel vehicle (grams/mile)
$VLNOCT_{m,v}$ is the emissions for a non-catalyst, leaded fuel vehicle (grams/mile)
$VUNOCT_{m,v}$ is the emissions for a non-catalyst, unleaded fuel vehicle (grams/mile)
$VLYSCT_{m,v}$ is the fraction of catalyst leaded fuel vehicles
$VUYSCT_{m,v}$ is the fraction of catalyst, unleaded fuel vehicles

The emission rate is adjusted for speed by the factor FEC such that:

$$CLEAD_{m,v} = FEC * LEAD_{m,v} \quad (4\text{-}70)$$

where: $CLEAD_{m,v}$ is the lead emissions for a vehicle of model year m and vehicle class v, which has been adjusted for the effect of speed (grams/mile)

FEC is $1/SCF_c$ (4-71)

SCF_c is the speed correction factor, based either transient driving cycle (c=1) or steady cruise driving cycle (c=2)

$$SCF_1 = 0.17930 + (0.038561 * SPEED_v) - (0.00041067 * SPEED_v^2) \quad (4\text{-}72)$$

$$SCF_2 = 0.26929 + (0.054607 * SPEED_v) - (0.00069818 * SPEED_v^2) \quad (4\text{-}73)$$

$SPEED_v$ is the average speed for vehicle class v (mph) - user input

Motorcycles do not have catalytic emission controls, therefore organic emission factors are not calculated and sulfate emission factors are deemed negligible. PART5 emission factors for motorcycles are almost entirely for lead particulate matter. The lead particulate emission factor for 2-stroke engines is 0.33 g/mi and for 4-stoke engines 0.046 grams/mile. For model years before 1978 there were 51 percent 4-stroke engines and 49 percent 2-stroke engines, computed as follows:

$$LEAD_{m,\ motorcycle} = [(0.49 * 0.33) + (0.51 * 0.046)] * PSL \quad (4\text{-}74)$$

For model years 1978 and later motorcycles are assumed to consist entirely of 4-stroke engines:

$$LEAD_{m,motorcycle} = 0.046 * PSL \quad (4\text{-}75)$$

where: PSL is the fraction of all particles that are emitted based on a specified upper particle size cutoff (10 micrometers running in MEPPS)

The specific derivations of the lead particulate emission formulae are given in Appendix 1 of the PART 5 user's guide (U.S. EPA, 1995b).

Sulfate Emission Factors for Gasoline-Fueled Vehicles

Particulate sulfate emission factors consist of direct and indirect sulfate material. The direct sulfate is exhausted as sulfuric acid, and the indirect sulfate is formed later in the atmosphere from exhausted SO_2. The indirect sulfate in the model is calculated based on the assumption that it consists entirely of ammonium sulfate and ammonium bisulfate. The direct sulfate, indirect sulfate, and gaseous sulfate emission factors are computed in PART5, and the emission factors reported as grams/mile traveled.

The direct sulfate from non-catalyst vehicles using leaded fuel (includes catalyst-equipped vehicles which are misfueled, making the catalyst ineffective) is calculated as:

$$DSULFN = .002, \text{ for speeds equal to or less than 19.6 mph} \quad (4\text{-}76)$$

$$DSULFN = .001, \text{ for speeds equal to or greater than 34.8 mph} \quad (4\text{-}77)$$

The direct sulfate from catalyst vehicles is calculated as :

$$DSULFC_{m,v} = [FRAC_{cat/no\ air}\ (.005) + FRAC_{cat/air}\ (.016)] \quad (4\text{-}78)$$

for speeds equal to or less than 19.6 mph

$$DSULFC_{m,v} = [FRAC_{ox/noair}\ (.005) + FRAC_{3w/noair}\ (.001) + FRAC_{ox/air}\ (.020) + FRAC_{3w/air}\ (.025)] \quad (4\text{-}79)$$

for speeds equal to or greater than 34.8 mph

For speeds between 19.6 and 34.8 mph, DSULFN and DSULFC are interpolated between Equations 4-76 and 4-77 and 4-78 and 4-79, respectively.

where: m denotes a specified model year
v denotes a specified vehicle class
$FRAC_{cat/noair}$ is the fraction of vehicles which are catalyst equipped with no air pump

$FRAC_{cat/air}$ is the fraction of vehicles which are catalyst equipped with an air pump
$FRAC_{ox/noair}$ is the fraction of vehicles which are oxygen catalyst equipped with no air pump
$FRAC_{3w/noair}$ is the fraction of vehicles which are 3-way catalyst equipped with no air pump
$FRAC_{ox/air}$ is the fraction of vehicles which are oxidation catalyst equipped with an air pump
$FRAC_{3w/air}$ is the fraction of vehicles which are 3-way catalyst equipped with air pump

The direct sulfate from all gasoline-fueled vehicles is computed as:

$$DSULF_{m,v} = CTLFRC_{m,v} * DSULFC_{m,v} + (1.0 - CTLFRC_{m,v}) * DSULFN \quad (4\text{-}80)$$

where: $CTLFRC_{m,v} = CATFCT_{m,v} (1-RMIS_{m,v})$ (4-81)
the fraction of the vehicle class that has an effective catalyst

The PART5 assumes that all sulfur in fuel is exhausted as either sulfate or gaseous sulfur dioxide (SO_2). Therefore when the direct sulfate emission factor is calculated, the remaining sulfur in the fuel is considered to be exhausted as SO_2. The amount of sulfur remaining in the fuel after the direct sulfate emission factor has been determined must be calculated to find the amount of sulfur exhausted as SO_2 (grams/mile).

The following equation is used to determine the fraction of sulfur in the fuel that has been directly converted to sulfate ($DSULF_{m,v}$ calculated in Equation 4-80 above). The equation calculates direct sulfate as a function of the fuel sulfur content, DCNVRT (the fraction of sulfur in the fuel that is converted to direct sulfate), and the fuel economy.

$$DSULF_{m,v} = 13.6078 * (1.0 + WATER) * FDNSTY * SWGHT * DCNVRT / FE_{m,v} \quad (4\text{-}82)$$

where: m denotes a given model year
v denotes a given vehicle class
$DSULF_{m,v}$ is the direct sulfate emission factor (grams/mile)
WATER is the weight ratio of seven water molecules to sulfate, 1.2857, based the estimate that at 50 percent humidity, seven water molecules bond with each sulfuric acid molecule
FDNSTY is the fuel density in lb/gal (6.09 pounds/gallon)
$FE_{m,v}$ is the fuel economy
SWGHT is the weight percent of sulfur content in fuel (.034, except for reformulated fuel phase II, for year 2000 and later .0138)
DNVRT is the percent of sulfur in the fuel that is directly converted into sulfate (2 percent)

13.6078 is a unit conversion factor equal to (453.592 * 3.0)/100, where 453. 592 is equal to the number of gram in a pound, 3.0 is the weight ratio of sulfate to sulfur, and division by 100 corrects for the weight percent of sulfur, SWGHT

If $DSULFC_{m,v}$ and DSULFN (from Equations 4-76 through 4-79) are substituted in Equation 4-82, one can solve for the fractions of sulfur in the fuel that are converted to sulfate separately for catalyst and noncatalyst vehicles:

$$FCNVRC_{m,v} = DSULFC_{m,v} * FE_{m,v} \quad / (13.6078 * (1.0 + WATER) * FDNSTY * SWGHT) \qquad (4\text{-}83)$$

$$FCNVRN_{m,v} = DSULFN * FE_{m,v} \quad / (13.6078 * (1.0 + WATER) * FDNSTY * SWGHT) \qquad (4\text{-}84)$$

where: $FCNVRC_{m,v}$ is the fraction of the percent of fuel that is directly converted into sulfate for catalyst equipped vehicles
$FCNVRN_{m,v}$ is the fraction of the percent of fuel that is directly converted into sulfate for non-catalyst vehicles

The gaseous sulfur emission factors, which are dependent on the above fractions, are calculated from the following equation:

$$SO2_{m,v} = 9.072 * FDNSTY * SWGHT * (1.0 - DCNVRT) / FE_{m,v} \qquad (4\text{-}85)$$

where: $SO2_{m,v}$ is the gaseous sulfur emission factor of a vehicle
9.072 is a unit conversion factor equal to (453.592 *2)/100, where 453.592 is the number of grams in a pound, 2 is the weight ratio of SO_2 to sulfur, and the division by 100 corrects for the weight percent of sulfur, SWGHT

Additional details concerning the calculation of gaseous sulfur emission factors are given in the PART5 user's guide (U.S. EPA, 1995b). In addition to direct sulfate and gaseous sulfate emission factors, PART5 estimates an indirect sulfate emission factor by assuming that a fraction of the gaseous sulfur dioxide emissions is later converted in the atmosphere to sulfate material. Based on ambient sulfur and sulfate measurements in 11 cities, it is estimated that 12 percent of all gaseous sulfur is converted to sulfate. Additional information on the calculation of indirect sulfate is given in the PART5 user's guide.

Sulfate Emission Factors for Diesel-Fueled Vehicles

For diesel-fueled vehicles, PART5 calculates sulfate emission factors again assuming that all sulfur in the fuel is exhausted as either sulfuric acid or gaseous sulfur dioxide. The direct sulfate emission factor (grams/mile) is calculated using the following equation:

$$DSULF_{m,v} = 13.6078 * (1.0 + WATER) * FDNSTY * SWGHTD * DCNVRT / FE_{m,v} \quad (4\text{-}86)$$

where: m is a specified model year
y is a specified vehicle class
$DSULF_{m,v}$ is the direct sulfate emission factor for a vehicle (grams/mile)
DCNVRT is the fraction of sulfur in the fuel that is converted directly to sulfate (2.0 percent

FDNSTY is the density of diesel fuel (7.11 pounds/gallon)
$FE_{m,v}$ is the fuel economy for a vehicle (miles/gallon)
SWGHTD is the weight percent of sulfur in diesel fuel (0.25 for high sulfur fuel, 0.05 for low sulfur fuel used in 1993 and later)
WATER is the weight ratio of seven water molecules to sulfate (1.2857)
13.6078 is a unit conversion factor equal to 493.592 * 3/100, where 493.592 is the number of grams in a pound, 3 is the weight ratio of sulfate to sulfur, and the division by 100 corrects for the weight percent of sulfur SWGHTD

The gaseous sulfur emission factor is calculated by the following equation:

$$SO2_{m,v} = 9.072 * FDNSTY * SWGHTD * (1.0 - DCNVRT) / FE_{m,v} \quad (Eq.4\text{-}87)$$

where:
$SO2_{m,v}$ is the sulfur emission factor (grams/mile) of a vehicle
9.072 is a unit conversion factor equal to (453.592 * 2/100) where 453.592 is the number of grams in a pound, 2 is the weight ratio of SO_2 to sulfur, and the division by 100 corrects for the weight percent of sulfur, SWGHTD

The indirect sulfate emission factor, consisting mainly of ammonium sulfate and ammonium bisulfate is calculated using the following equation:

$$ISULF_{m,v} = ICNVRT * SO2_{m,v} * (3/2) * AMNWGT \quad (4\text{-}88)$$

where:
$ISULF_{m,v}$ is the indirect sulfate emission factor of a vehicle (grams/mile)
ICNVRT is the fraction of SO_2 converted to sulfate in the atmosphere (12 percent)
3/2 is the weight ratio of SO_2 to sulfate
AMNWGT is the estimated weight ratio of the combination of ammonium bisulfate and ammonium sulfate in the atmosphere to sulfate (1.6)

Total Exhaust Particulate Emission Factors for Gasoline-Fueled Vehicles

The total exhaust particulate emission factors for light-duty gasoline fueled vehicles are calculated by summing lead, direct sulfate, and a carbon emission factor which includes soluble organic material and other remaining carbon. Table 4-5 presents a summary of the carbon emission factors by vehicle model year and type of technology.

Table 4-5. Carbon Emission Factors for Gasoline-Fueled Vehicles (grams/mile)

Vehicle Type/ Model Year	Leaded Fuel	Unleaded/ Catalyst Equipped (No air pump)	Unleaded/ Catalyst Equipped (with air pump)	Unleaded/ Non-catalyst equipped
Light-Duty Gasoline Vehicles				
pre-1970	.193	NA	NA	.030
1970-1974	.068	.0060	.0250	.030
1975-1980	.030	.0060	.0250	.030
1981 +	.017	.0043	.0043	.017
Light-Duty Gasoline Trucks I				
pre-1970	.193	NA	NA	.030
1970-1974	.068	.0060	.0250	.030
1975-1986	.030	.0060	.0250	.030
1987 +	.017	.0043	.0043	.017
Light-Duty Gasoline Trucks II				
pre-1979	.370	NA	NA	.054
1979-1986	.068	.0060	.0250	.030
1987 +	.030	.0043	.0043	.017
Heavy-Duty Gasoline Vehicles				
pre-1987	.370	.054	.054	.054
1987 +	.163	.054	.054	.054

Total Exhaust Particulate Emission Factors for Diesel-Fueled Vehicles

The total exhaust particulate emission factors are for diesel-fueled vehicle categories and model years ($EFDPM_{m,v}$). The emission factors for heavy-duty vehicles are in units of grams/brake-horsepower hour (g/BHP-hr), which are converted to grams/mile by PART5. The conversion factors and emission factors vary by model year. The emission factors for light-duty diesel vehicles are in units of grams/mile. The total exhaust emission factors given in Table 4-6 are based on high-sulfur fuel. The sulfur content in diesel fuel was reduced in 1993 by EPA regulatory requirements. Consequently, when a the specified calendar year is 1993 or later, PART5 will adjust the exhaust emission factors for lower sulfur fuel. Particulate emission factors for diesel-fueled vehicles are not adjusted for speed.

Table 4-6. Exhaust Particulate Emission Factors for Diesel-Fueled Vehicles

Vehicle Type/ Model Year Group	Exhaust Particulate Emission Factor
Light-Duty Diesel Vehicles (grams/mile)	
pre-1981	.700
1981	.259
1982-1984	.256
1985-1986	.255
1987	.134
1988-1990	.132
1991-1993	.131
1994-1995	.128
1996 +	.100
Light-Duty Diesel Trucks (grams/mile)	
pre-1981	.700
1981	.309
1982-1984	.354
1985-1986	.358
1987	.334
1988-1990	.291
1991-1993	.294
1994-1996	.130
1997 +	.109

Table 4-6. Exhaust Particulate Emission Factors for Diesel-Fueled Vehicles

Vehicle Type/ Model Year Group	Exhaust Particulate Emission Factor
Class 2B Heavy-Duty Diesel Vehicles (grams/brake horsepower-hour)	
pre-1988	.5156
1988-1990	.5140
1991-1993	.2873
1994 +	.1011
Light Heavy-Duty Diesel Vehicles (grams/brake horsepower-hour)	
pre-1988	.5156
1988-1990	.5140
1991-1993	.2873
1994 +	.1011
Medium Heavy-Duty Diesel Vehicles (grams/brake horsepower-hour)	
pre-1987	.6946
1988-1990	.4790
1991-1993	.2747
1994 +	.0948
Heavy Heavy-Duty Diesel Vehicles (grams/brake horsepower-hour)	
pre-1987	.6444
1988-1990	.4360
1991-1993	.2709
1994 +	.0836
Buses (grams/brake horsepower-hour)	
pre-1987	.6931
1988-1990	.4790
1991	.2772

Table 4-6. Exhaust Particulate Emission Factors for Diesel-Fueled Vehicles

Vehicle Type/ Model Year Group	Exhaust Particulate Emission Factor
1992 without traps	.1716
1992 with traps	.0257
1993 without traps	.1457
1998 with traps	.0240
1994 +	.0591

Soluble Organic Fraction and Remaining Carbon Portion Emission Factors for Diesel-Fueled Vehicles

The PART5 model calculates the Soluble Organic Fraction (SOF) emission factor as a fraction of the remaining mass, using the following equation:

$$SOF_{m,v,} = [EF_{m,v} - DSULF_{m,v}] * (fraction_{SOF,v}) \quad (4\text{-}89)$$

The Remaining Carbon Portion (RCP) is defined the remainder (everything else):

$$RCP_{m,v} = Ef_{m,v} - DSULF_{m,v} - SOF_{m,v} \quad (4\text{-}90)$$

where: m is the model year of a selected vehicle
v is the class of a selected vehicle
$SOF_{m,v}$ is the Soluble Organic Fraction of the exhaust particulate emission factor (grams/mile)
$RCP_{m,v}$ is the remaining carbon portion (elemental carbon) of the exhaust particulate emission factor (grams/mile)
$EF_{m,v}$ is $EFDPM_{m,v} * CF_{m,v}$, the exhaust particulate emission factor for a vehicle (grams/mile)
$EFDPM_{m,v}$ is the exhaust particulate emission factor for a vehicle (grams/Brake Horsepower-hour)
$CF_{m,v}$ is the conversion factor from grams/Brake Horsepower-hour to grams/mile (Brake Horsepower-hour/mile)
$fraction_{SOF,v}$ is the fraction of the non-sulfate portion (ie. the carbon portion) of the diesel exhaust particulate emission factor which is organic carbon for a vehicle (Brake Horsepower-hours/mile)

The Soluble Organic Fractions ($fraction_{SOF,v}$) for different vehicle classes are as follows (U.S. EPA, 1990):

- 0.18 for LDDVs (Light-Duty Diesel Vehicles)
- 0.50 for LDDT1s (Class 1 Light-Duty Diesel Trucks)
- 0.48 for LDDT2s (Class 2 Light-Duty Diesel Trucks)
- 0.51 for LHDDVs (Light Heavy-Duty Diesel Vehicles) and 2BHDDVs (Class 2B Heavy-Duty Diesel Vehicles)
- 0.44 for MHDDVs (Medium Heavy-Duty Diesel Vehicles) and BUSES
- 0.24 for HHDDVs (Heavy Heavy-Duty Diesel Vehicles)

Idle Emission Factors for Heavy Diesel-Fueled Vehicles

Idle emission factor data in grams/hour were collected from manufacturers for heavy-duty diesel vehicle classes only. Consequently, the idle emission factors are not included into the "all vehicles" emission category. The vehicle class emission factors are calculated by averaging together model-year-specific emission data, where the model-year-specific emission data are weighted by the estimated travel fraction of that model year within the vehicle class.

The idle emission factors are model-year-specific but the model year emission rates do not vary by vehicle class. Consequently, the same model year emission factors are used for all the heavy-duty diesel classes, and the differences between idle emission factors between classes reflects only the differing travel fractions between model years for a class. As a result, the emission factors reported for the smaller of the heavy-duty vehicle classes, such as 2BHDDV and LHDDV, may be over estimated. The base idle emission factors in PART5 for all heavy-duty diesel vehicles are as follows:

- 5.370 grams/hour for models prior to 1988
- 3.174 grams/hour for model years 1988-1990
- 1.860 grams/hour for model years 1991-1993
- 1.004 grams/hour for model year 1994 +

Re-entrained Dust from Unpaved Roads

Re-entrained road dust emission factors for PM_{10} (particulate matter less than 10 micrometers in size) in PART5 are estimated using an equation (4-91) based on ambient measurements. Because these measurements include particulate matter from brake wear, tailpipe exhaust, tire wear, and ambient background particulate matter concentrations, these factors must be subtracted from the unpaved road particulate emission factors before the latter factors can be applied. It is necessary to obtain a data base of unpaved and paved road types by county for regional modeling purposes. The MEPPS contains procedures and estimates for 1995 developed for EPA by calculating re-entrained emissions by the month at the state road-type level for the average vehicle fleet, and then allocated to the county road type by population for unpaved roads and by total VMT for paved roads. These procedures should be consulted for more details, such as the means of estimating unpaved and paved VMT data. The equation used to calculate PM_{10} from unpaved roads is as follows:

$$UNPVD = PSDUNP * 5.9 * (UNSILT/12.0) * (SPD/30.0) * (WEIGHT/3.0)^{0.7} * (VWHEEL/4.0)^{0.5} * (365-IPDAYS)/365 * 453.592 \quad (4\text{-}91)$$

where: UNPVD is the fleet average unpaved road dust emission factor (grams/mile)
PSDUNP is the fraction of particles less than or equal to the particle size cutoff (the cutoff is 10 micrometers in MEPPS)
UNSILT is the percent silt content of the surface material (user input)
SPD is the average vehicle speed in miles/hour (user input)
WEIGHT is the fleet average vehicle weight (user input in pounds)
VWHEEL is the fleet average number of wheels (user input, default is 4)
IPDAYS is the average number of precipitation days per year with greater than 0.01 inches of rain (user input - MEPPS contains climatological default data for 1995)
453.592 is the number of grams in a pound

Emission factors for brake and tire wear (in addition to exhaust emissions) must be calculated so that they may be subtracted from the unpaved road emission factors. The brake wear emission factor is assumed to be the same for all vehicle classes. It is set equal to:

$$BRAKE = 0.0128 * PSBRK \quad (4\text{-}92)$$

where: PSBRK is the fraction of particles less than or equal to the particle size cutoff. The emission factor 0.0128 grams/mile is taken from U.S. EPA, 1985c.

The tire wear emission factor is calculated using the following equation:

$$EFTIRE_v = 0.002 * PSTIRE * IVEHWL_v \quad (4\text{-}93)$$

where: v is a selected vehicle class
$EFTIRE_v$ is the tire wear emission factor
0.002 is the emission rate of airborne particulate matter from tire wear for light-duty vehicles (U.S. EPA, 1985)
PSTIRE is the fraction of particles less than or equal to the particle size cutoff
$IVEHWL_v$ is the average number of wheels on a vehicle of a given class, where LDGV=4, LDGT1,2=4, HDGV=6, MC=2, LDDV=4, LDDT=4, 2BHDDV=4, LHDDV=6, MHDDV=6,HHDDV=18, BUSES=4

Re-entrained Dust from Paved Roads

The PM_{10} emission factor for paved roads is estimated similarly to that for unpaved roads. The VMT data for paved roads may be developed following the procedures described in U. S. EPA, 1998. The equation used to estimated paved road re-entrained dust emission factors again is based on ambient measurements, and tailpipe, brake wear, and tire wear emission factors must be

subtracted prior to use of the paved road dust emission factor. The paved road emission factors are calculated by:

$$PAVED = PSDPVD * (PVSILT/2.0)^{0.65} * (WEIGHT/3.0)^{1.5} \quad (4\text{-}94)$$

where: PAVED is the fleet average paved road dust emission factor (grams/mile)
PSDPVD is the base emission factor for the particle size cutoff (10 micrometers in MEPPS)
PVSILT is the road surface silt loading (grams/square meter) (user input)
WEIGHT is the fleet average vehicle weight (input by the user in pounds)

Application in MEPPS

The PART5 model is a companion of Mobile5a in MEPPS. When running MEPPS interactively through the Tools Manager, the user is prompted to specify input data and options under EMPRO, Mobile Source Model. Standard lookup data files can be found in the Models-3 directory structure at /home/models3/datasets/nostudies/part5/. Default/example input data sets are included for the 1995 calendar year. When a study is created, the study input data are located at *$EMS_HOME*/project/*$EMS_PROJECT*/raw_data/*$EMS_DOMAIN*/common/.
If the user is processing mobile emission data using the Study Planner, it is necessary to ensure that the appropriate PART5 input data sets are in place first. This may be accomplished when using MEPPS interactively to establish MEPPS directory structure prior to running through Study Planner. If the data are in place, Study Planner will automatically process them.

When processing mobile particulate emission data, the input and output data of PART5 are assigned to and summed within each grid cell in the same fashion given in detail under the *Gridding VMT* discussion of the implementation of the Mobile 5a model (above).

4.2.5 Chemical Speciation of Emission Data

Chemical transport models, such as CMAQ, require that emission data be provided for either individual species or specific species groups or "lumped" species. This is necessary so that the atmospheric chemistry of pollutants may be more accurately modeled. However, an initial processing step is required because emission data are often reported for pollutants that are aggregates of many species, such as VOC. These aggregate pollutants must be split into their component species, or "speciated".

The speciation takes two forms, discrete and lumped-model.

In discrete speciation, a pollutant is split into the individual components which comprise the pollutant. For the organic pollutant TOG (total organic gas), the individual components which comprise the pollutant are dependent on a variety of factors including the process, fuel type, and device from which the emissions occurred. For example, TOG from the exhaust of automobile

may contain approximately fifty discrete organic compounds (benzene, methane, toluene, hexane, etc.), while TOG from degreasers may contain approximately seventy discrete organic compounds. NO_X (nitrogen oxides), which is related to combustion processes, is speciated (discrete) into NO and NO_2 (and sometimes HONO).

The discrete components in an emission stream are determined by a number of methods including source testing, surrogate application, and engineering knowledge of the process. Many sources have been inventoried and a compendium of species profiles has been assembled by the US EPA in *the Air Emissions Species Manual* (US EPA, 1988). The *Air Emissions Species Manual* contains a list of TOG and particulate matter (PM) species profiles to which a substantial number of emission sources have been assigned. A compendium of species profiles currently available is compiled in the US EPA *Speciate* database. The database is available on the *Air Chief* CD ROM, which is updated annually (US EPA, 1997). Each of the species profiles identifies the mass percent of the discrete compounds that comprise TOG and PM. Note that NO_X, SO_X (sulfur oxides), and CO (carbon monoxide) do not have source-specific speciation profiles. For all sources, NO_X is discretely speciated into NO and NO_2 (and sometimes HONO), and CO is treated explicitly. The speciation processor currently assumes that NOx is speciated to 95 percent NO and 5 percent NO_2, based on average observed values.

The MEPPS EMPRO speciation processor provides chemical speciation of hydrocarbons, oxides of nitrogen, and sulfur oxides. For example, aggregations of hydrocarbon species such as TOG are disaggregated to their component individual chemical species. The processor speciates the spatially and temporally allocated emission estimates that are prepared by the emission estimation processors and models (e.g., point source processor, mobile emission model). The speciation is accomplished using look-up tables of profiles containing source-category specific and specie-specific chemical split factors (percent of mass of source emissions attributable to each specie for a given source category). The general components of emission speciation processing are illustrated in Figure 4-6.

It is computationally prohibitive to model the chemistry of all discrete VOC compounds in the emissions stream in photochemical grid models. Therefore, individual organic species comprising Total Organic Gas are assigned to one or more model species (groups of species) according to the chemical mechanism that is being used. Thus, instead of modeling with a larger number of discrete compounds, the discrete compounds are lumped into a much smaller number of mechanism species. The rules for assigning the discrete compounds to the mechanism species are mechanism dependent and typically involve lumping in one of two ways: 1) lumping compounds with similar reactivity characteristics into a single mechanism species (the lumped molecule approach) or 2) assigning molecular fragments of an individual compound to one or more mechanism species on the basis of molecular structure (lumped structure approach). In Models-3, the lumping of discrete compounds to form mechanism species is carried out using tables of split factors that assign the discrete compounds to mechanism species. Currently, two mechanisms, the Regional Acid Deposition Model 2.0 (RADM2) and Carbon Bond 4 (CB-4) are available in Models-3. The user may also define lumping procedures for an alternative mechanism if the

assignment methods for that mechanism are known, or the user may create a modified version of the lumping procedure for one of the two mechanisms in Models-3.

In the CB-4 mechanism, discrete compounds are assigned to mechanism species on the basis of the compound's carbon bond structure (Gery et al.,1989). For instance, single carbon-carbon hydrocarbon bonds are assigned to a paraffin group (PAR), and carbon-carbon double bonds are assigned to an olefinic group (OLE). Thus, an individual discrete VOC could be dis-aggregated into more than one mechanism species depending on its structure. Descriptions of the CB-4 mechanism species are given in Table 4-8.

The RADM2 mechanism lumps discrete compounds on the basis of their prevalence in the atmosphere, common reactivity, and/or molecular weight (Stockwell et al., 1990). For RADM2, individual VOC compounds are first assigned to one of 32 lumped groups. The 32 lumped groups are then further reduced to 15 groups for increased computational efficiency. The relationship between the 32 and 15 lumped groups is shown in Table 4-9. The EMPRO does not include chemical or size fractionation of particulate matter, although size fractionation of particulate matter is planned in the future.

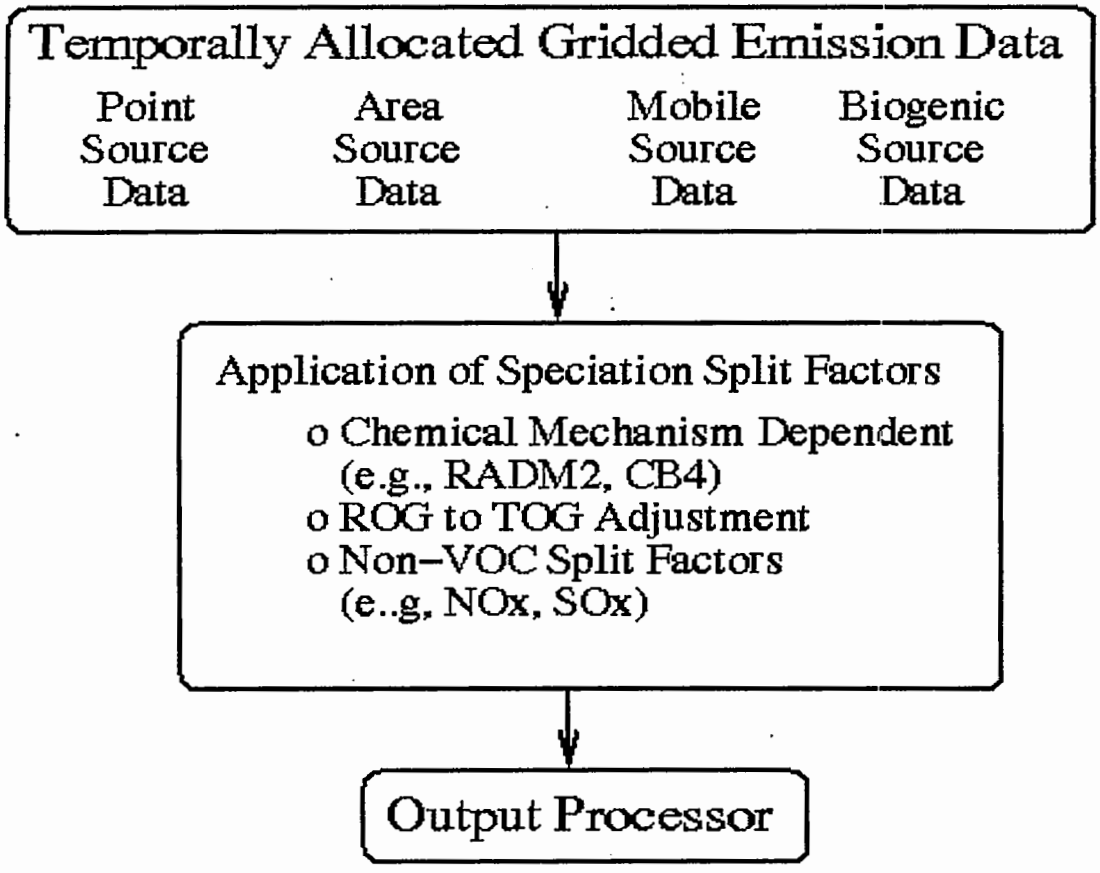

Figure 4-6 General Components of Emission Speciation Processing

Table 4-8. Carbon Bond-4 Lumped Species

CB4 Lumped Species Number	CB4 Lumped Species Code	Lumped Species Description
1	OLE	Olefinic carbon bond (C=C)
2	PAR	Paraffin carbon bond (C-C)
3	TOL	Toluene (C6H5-CH3)
4	XYL	Xylene (C6H4-(CH3)2)
5	FORM	Formaldehyde (CH2=O)
6	ALD2	High MW aldehydes (RCHO, R>H)
7	ETH	Ethene (CH2=CH2)
8	MEOH	Methanol (CH3OH)
9	ETOH	Ethanol (C2H5OH)
10	ISOP	Isoprene
11	NR	Non Reactives as methane
12	NO	Nitric Oxide
13	NO2	Nitrogen Dioxide
14	CO	Carbon Monoxide
15	SO2	Sulfur Dioxide
16	AERO	Aerosols (PM)

Table 4-9. RADM 2.0 Lumped Species Descriptions

RADM 2.0 32 Lumped Species	RADM 2.0 16 Lumped Species	Allocation Factor (fraction of one)	Reactivity Factor (ratio)	Description of the 32 RADM Lumped Species Before Grouping to 16 Lumped Species
1	CH4	1	1	Methane
2	ETH	1	1	Ethane
3	HC3	1	0.519	Propane
4	HC3	1	0.964	Alkanes (0.25-0.50)
5	HC5	1	0.956	Alkanes (0.50-1.00)
6	HC8	1	0.945	Alkanes (1.00-2.00)
7	HC8	1	1.141	Alkanes (>2.00)
8	HC8	0.91	1.101	Alkane/Aromatic Mix
8	XYL	0.09	1	Alkane/Aromatic Mix
9	OL2	1	1	Ethene
10	OLT	1	1	Propene
11	OLT	1	1	Alkenes (Primary)
12	OLI	1	1	Alkenes (Internal)
13	OLT	0.5	1	Alkenes (Prim/Int Mix)
13	OLI	0.5	1	Alkenes (Prim/Int Mix)
14	TOL	1	0.293	Benzene/Halobenzenes
15	TOL	1	1	Aromatics (<2 react)
16	XYL	1	1	Aromatics (>2 react)
17	CSL	1	1	Phenols and Cresols
18	OLT	0.5	1	Styrenes
18	TOL	0.5	1	Styrenes
19	HCHO	1	1	Formaldehyde
20	ALD	1	1	Higher Aldehydes
21	KET	1	0.253	Acetone
22	KET	1	1	Ketones

Table 4-9. RADM 2.0 Lumped Species Descriptions

RADM 2.0 32 Lumped Species	RADM 2.0 16 Lumped Species	Allocation Factor (fraction of one)	Reactivity Factor (ratio)	Description of the 32 RADM Lumped Species Before Grouping to 16 Lumped Species
23	ORA2	1	1	Organic Acids
24	HC3	1	0.343	Acetylene
25	HC3	1	0.078	Haloalkenes
26	.	1	1	Unreactive
27	HC3	1	0.404	Others (<0.25 react)
28	HC3	1	1.215	Others (0.25-0.5 react)
29	HC5	1	1.075	Others (0.5-1.0 react)
30	HC8	1	1.011	Others (>1.00 react)
31	.	1	1	Unidentified
32	.	1	1	Unassigned

In Models-3, the user initiates speciation by selecting the chemical mechanism to be used for a study in the Study Manager under the Models-3 framework, and within the MEPPS main window under Tools Manager. The procedure is explained in detail in Chapter 6 of *Models-3 Volume 9B: User Manual*. The speciation processor is written primarily in SAS®; however, it includes some FORTRAN programs. ARC/INFO® is not used in the speciation processor.

Speciation Processing in MEPPS

In MEPPS, speciated gaseous emissions can be calculated in either of two units – moles/hour or Kg/hour. (Particle emissions are always calculated as Kg/hr.) Emissions in moles are required by the Models-3 CMAQ, but some analyses require that emissions be expressed in mass per unit time. Emissions in mole and mass units are calculated using the following two generic equations:

$$chemest_{ij} = \Sigma_p \Sigma_m hr_{imp} * 1000 * rogtotog_{mp} * factor_{jmp} / divisor_{jmp} \qquad (4\text{-}95)$$

where: $chemest_{ij}$ is the gridded emissions estimate for hour i and mechanism species j (moles/hour)

hr_{imp} is the gridded hourly emission estimate of pollutant p (NOx, SOx, CO, PM, NH3, or ROG) for hour i and source category m (Kg /hr). The factor of 1000 is used to convert kilograms to grams.

$rogtotog_{mp}$ is a ROG to TOG conversion factor (discussed below)
$factor_{jmp}$ is a mole-based split factor to allocate total emissions of pollutant p from source category m to mechanism species j

$divisor_{jmp}$ is a second conversion factor to allocate total emissions of pollutant p from source category m to mechanism species j

and

$$estKg_{ij} = \Sigma_p \Sigma_m hr_{imp} * rogtotog_{mp} * xmass_{jmp} \quad (4\text{-}96)$$

where: $estKg_{ij}$ is the gridded emissions estimate for hour i and mechanism species j (Kg/hour)
hr_{imp} is the gridded hourly emission estimate of pollutant p (NOx, Sox, CO, PM, NH3, or ROG) for hour i and source category m (Kg /hr)
$rogtotog_{mp}$ is a ROG to TOG conversion factor (discussed below)
$xmass_{jmp}$ is a mass-based split factor to allocate total emissions of pollutant p from source category m to mechanism species j

These equations show that emissions for mechanism species are computed by summing the contributions of pollutants from the different source categories that emit that pollutant. As indicated previously, the assignment of a pollutant to a specific mechanism species usually mechanism dependent, although some assignments may be handled the same way in different mechanisms. In Equations 4-95 and 4-96, the terms $factor_{jmp}$, $divisor_{jmp}$, and $xmass_{jmp}$ are mechanism specific apportioning factors that will be defined further below. Note that, in some cases a pollutant will contribute to only one mechanism species, but in other cases a pollutant will contribute to more than on species. For example, emissions of ammonia are always assigned to a model species named NH3, but NOx is allocated between two mechanism species NO and NO2. The details of the allocation procedure for both the RADM2 and CB4 mechanisms will be described further below. First, however, the derivation and use of the $rogtotog_{mp}$ conversion factor is described.

ROG-to-TOG Adjustment

The ROG (Reactive organic gas) to TOG conversion portion of the speciation process is selected when the emission inventory is loaded by INPRO (see section 4.2.2). VOC substances deemed non-reactive (e.g., methane and ethane) are often excluded from inventories, and some emission measurement techniques do not capture all discrete compounds in an emission stream (e.g, formaldehyde). The ROG-to-TOG adjustment factor is used to account for those missing components. It is calculated using Equations 4-97 and 4-98:

$$mistog_m = \Sigma_k ntsrd_{k,m} \quad (4\text{-}97)$$

$$rogtotog_m = 1.0 / mistog_m \quad (4\text{-}98)$$

where: $mistog_i$ is the sum of mass fractions of the discrete VOC compounds deemed non-reactive or not included in an emission inventory for source category m (grams of missing compound per gram of TOG)

$ntsrd_{k,m}$ is the mass fraction of the missing or non-reactive compound k in the emission stream for source category m

$rogtotog_m$ is the ROG to TOG conversion factor

Note that the $rogtotog_{m,p}$ adjustment factor applies only to anthropogenic emissions of VOC, and thus the p subscript used in Equation 4-95 and 4-96 has been dropped here. In equations 4-95 and 4-96, $rogtotog_{m,p}$ is set to 1.0 for all pollutants other than ROG and also set to 1.0 when VOC emissions of biogenic origin are being computed.

Carbon Bond 4 (CB4) Speciation Factors

The CB-4 chemical mechanism is widely used in air quality model simulations of ozone concentrations at urban and regional spatial scales. As described in the introductory part of this section, the basis of the CB-4 mechanism is that reactivity of organic compounds in the atmosphere can reasonably be simulated by mechanism species that represent different carbon bond types. A detailed description of the CB-4 mechanism is contained in Section 8.2.1. The focus of the discussion here is on how the CB-4 apportioning factors used in Equations 4-95 and 4-96 are calculated. Since speciation of anthropogenic VOC emissions is done differently than for other pollutants, the discussion is divided into two subsections.

Anthropogenic VOC speciation. For the CB4 mechanism, the apportioning factor $divisor_{jmp}$ in equation 4-95 is set to 1.0 for all anthropogenic VOC emission calculations(i.e., it is essentially not used). The $factor_{jmp}$ term for anthropogenic VOC is set equal to a split factor term s_{jl} that is computed for a specified VOC emission profile l, which in turn is assigned to a source category m (i.e., an SCC or ASC). The split factor for each profile and mechanism species is computed as follows:

$$sf_{j,l} = \Sigma_k \; xmf_{k,l} / mw_k * xnum_{j,k} \quad (4\text{-}99)$$

where: $sf_{j,l}$ is a molar split factor for CB4 species j and VOC profile l (moles of CB4 species/gram of TOG)

$xmf_{k,l}$ is a mass fraction of discrete VOC compound k in VOC profile l (grams of discrete VOC/grams of TOG)

mw_k is the molecular weight of discrete VOC compound k (grams of discrete VOC/mole of discrete VOC)

$xnum_{j,k}$ is the moles of discrete VOC compound k assigned to CB4 species j (moles of CB4 species/mole of discrete VOC)

In Equation 4-96, the $xmass_{jmp}$ term apportions mass emissions to CB4 species for a given pollutant and source category. Analogous to the CB4 molar split factor defined above, the $xmass_{jmp}$ term is set equal to a mass split factor that apportions the mass of a discrete VOC compound according to the fraction of carbon atoms that is assigned to a mechanism species:

$$xmass_{j,l} = \Sigma_k \, (xmf_{k,l} * cn_j) \, / \, cn_k \qquad (4\text{-}100)$$

where: $xmass_{j,l}$ is the mass split factor for CB4 species j and VOC profile l (moles of CB4 species/gram of TOG)
$xmf_{k,l}$ is the mass fraction of discrete VOC compound k in VOC profile l (grams of discrete VOC/grams of TOG)
cn_j is the number of carbon atoms in CB4 species j
cn_k is the number of carbon atoms in discrete VOC compound k

Again, one VOC profile is assigned to each source category, and thus split factors are generated for each source category/mechanism species combination.

Other speciation. For pollutants and source categories other than anthropogenic VOC, the terms $factor_{jmp}$, $divisor_{jmp}$, and $xmass_{jmp}$ are simply assigned numeric values that determine the allocation of pollutant emissions. These are summarized in Table 4-10.

For all pollutants (except particles) in Table 4-10, the divisor corresponds to the molecular weight of the pollutant and is used in equation 4-76 to convert mass emissions of the pollutant to moles of pollutant. The two split factors $factor_{jmp}$, and $xmass_{jmp}$ are used to apportion the pollutant emissions to the mechanism species. A factor of 1.0 indicates a 1:1 correspondence. Factors different from one indicate a disaggregation or lumping of pollutant emissions into individual species.

CO and NH3 are treated explicitly in many air quality models, and therefore emissions of these compounds are not split into other components. Similarly, particle emissions are treated explicitly so no lumping or dis-aggregation is necessary for them either.

When SOx emissions are speciated, 97% of the SOx mass is treated as SO2. The remaining 3% of the SOx mass corresponds to SO4 (or SULF), but is dropped from further consideration. SO2 and SO4 emissions are treated as explicit species.

Table 4-10. CB4 Split Factors for Pollutants Other Than Anthropogenic VOC

Source Category	Pollutant	CB4 Species	$factor_{jmp}$	$divisor_{jmp}$	$xmass_{jmp}$
All	CO	CO	1.0	28.0	1.0
All	NH3	NH3	1.0	17.0	1.0
All	AERO	AERO	1.0	1.0	1.0
All	PM10	PM10	1.0	1.0	1.0
All	PM2_5	PM2_5	1.0	1.0	1.0
All except BIO	NOX	NO	0.62	30.0	0.62
All except BIO	NOX	NO2	0.05	46.0	0.05
All	SO2	SO2	1.0	64.0	1.0
All	SOX	SO2	0.97	64.0	0.97
All	SO4	SULF	1.0	96.0	1.0
BIO	NO	NO	1.0	30.0	1.0
BIO	Isoprene	ISOP	1.0	68.12	1.0
BIO	OVOC	NR	0.5	148.0	0.05
BIO	OVOC	OLE	0.5	148.0	0.10
BIO	OVOC	PAR	8.0	148.0	0.85
BIO	TERP	ALD2	1.5	136.23	0.3
BIO	TERP	OLE	0.5	136.23	0.1
BIO	TERP	PAR	6.0	136.23	0.6
BIO	TERP	TERPB	1.0	136.23	1.0

In MEPPS, it is assumed that NOx is composed of 95% NO and 5% NO2 (by mass). However, actual NOX composition can vary from 89%/11% to 95%/5%. In a few cases, a small percentage (<2%) of NOX emissions is assumed to be nitrous acid (HONO). Since NOx emissions are typically reported as NO2 mass, it is necessary to normalize the NOx emissions by the molecular weight of NO2. Hence, the molar split factors ($factor_{jmp}$) for NO and NO2 are calculated as follows:

$$sf_{NO} = xmf_{NO} * mw_{NO} / mw_{NO2} \quad (4\text{-}101)$$

$$sf_{NO2} = xmf_{NO2} * mw_{NO2} / mw_{NO2} \quad (4\text{-}102)$$

With a NOx composition of 95% NO (as NO2) and 5% NO2 by mass, the split factors for NO and NO2 become 0.62 and 0.05, respectively. The mass split factors are calculated in the same manner, and thus have the same values as for the molar split factors.

The speciation of biogenic emissions in CB4 is the same as used in the Regional Oxidant Model (EPA, 1989). Isoprene is treated as an explicit species and terpene emissions are speciated into 1.0 mole of OLE, 6.0 moles of PAR, and 3.0 moles of ALD2. Terpenes are also assigned to the model species TERPB for special processing in the aerosol module of the CMAQ. The apparent double counting of terpene emissions is accounted for in the CMAQ processing however. Finally, the category OVOC (other VOCs from biogenic sources) is apportioned to 1.0 mole of OLE, 8.5 moles of PAR, and 0.5 mole of NR. Here it assumed that number of carbon atoms in a OVOC molecule is 10.

RADM2 Speciation Factors

The RADM2 chemical mechanism was developed for and has been used principally in regional air quality simulations of sulfur dioxide (SO2) and oxides of nitrogen for acid rain assessment (Walters and Saegar, 1990). A detailed description of the RADM2 mechanism is given in section 8.2.2. The speciation procedure used for RADM2 is fully described in Walters and Saeger (1990), and will only be summarized here. This section focuses on how the RADM2 apportioning factors used in Equations 4-95 and 4-96 are calculated. Again, the discussion is divided into two subsections, one dealing with the speciation of anthropogenic VOC emissions and one with all other speciation.

Anthropogenic VOC speciation. The RADM2 mechanism requires that discrete organic VOC compounds be lumped into 15 mechanism species based on common reactivity and reaction products. As with the CB4 mechanism, the apportioning factor $divisor_{jmp}$ in Equation 4-95 is set to 1.0 for all anthropogenic VOC emission calculations, and thus is not used. Also as with the CB4 mechanism, The $factor_{jmp}$ term for anthropogenic VOC is set equal to a split factor term s_{jl} that is computed for a specified VOC emission profile l, which in turn is assigned to a source category m (i.e., an SCC or ASC). However, the RADM2 split factors are calculated using the following equation:

$$sf_{j,l} = \Sigma_k \; xmf_{k,l} * afac_{j,k} * rfac_{j,k} / mw_k \quad (4\text{-}103)$$

where: $sf_{j,l}$ is the molar split factor for RADM2 species j and VOC profile l (moles of RADM2 species/gram of TOG)

$xmf_{k,l}$ is the mass fraction of discrete VOC compound k in VOC profile l (grams of discrete VOC/grams of TOG)
$afac_{j,k}$ is the allocation factor listed in Table 4-6 for RADM2 species j and discrete VOC compound k

$rfac_{j,k}$ is the reactivity factor listed in Table 4-6 for RADM2 species j and discrete VOC compound k
mw_k is the molecular weight of discrete VOC compound k (grams of discrete VOC/mole of discrete VOC)

In the RADM2 speciation process, each discrete VOC compound is assigned to one of the 32 lumped species categories, and that assignment is used to further lumped to one of the 15 species in the condensed group. See Middleton et al. (1990) for information on how the allocation and reactivity factors are derived.

In Equation 4-96, the term $xmass_{jmp}$ apportions mass emissions to RADM2 species for a given pollutant and source category. Analogous to the RADM2 molar split factor defined above, the term $xmass_{jmp}$ is set equal to a mass split factor that apportions the mass of a discrete VOC compound according to the mass fraction of the discrete VOC compound in the emission stream and the mechanism specific allocation factor:

$$xmass_{j,l} = \Sigma_k \; xmf_{k,l} * afac_{k,l} \qquad (4\text{-}104)$$

where: $xmass_{j,l}$ is the mass split factor for RADM2 species j and and VOC profile l (moles of CB4 species/gram of TOG)
$xmf_{k,l}$ is the mass fraction of discrete VOC compound k in VOC profile *l* (grams of discrete VOC/grams of TOG)
$afac_{j,k}$ is the allocation factor listed in Table 4-6 for RADM2 species j and discrete VOC compound k

Other speciation. For pollutants and source categories other than anthropogenic VOC, the terms $factor_{jmp}$, $divisor_{jmp}$, and $xmass_{jmp}$ are simply assigned numeric variables that control the allocation of emissions, similar to what is done for the CB4 mechanism. The factors for RADM2 are summarized in Table 4-11.

Except for the biogenic categories, the contents of Table 4-11 are identical to those in Table 4-10 for the CB4 mechanism. Thus, the reader is referred to the corresponding CB4 section for information on those source category/pollutant combinations. The biogenic portions of the two tables are similar in that isoprene is treated as an explicit species in RADM2, and terpenes and other VOCs (OVOC) of biogenic origin are apportioned to mechanism species. In RADM2, terpenes are apportioned entirely to OLI (Middleton et al., 1990). As with the CB4 mechanism ,terpenes are also assigned to the model species TERPB for special processing in the aerosol

module of the CMAQ, but the apparent double counting of terpene emissions is accounted for in the CMAQ processing however. Finally, the assignment of other VOC species to RADM2 species is carried out in a manner analogous to that for CB4: 85% is assumed to correspond to slow reacting alkanes, 15% to fast reacting olefins, and 5% is assumed to be non-reactive. Thus, in RADM2 85% of the OVOC mass is assigned to the category containing the slowest reacting alkanes (category 27 in Table 4-6). The split factor is obtained by multiplying the mass fraction (.85) by the reactivity factor (0.404) to give a molar split factor of 0.343. The 10% of the mass of OVOC assumed to be reactive olefins is assigned to the OLI category. Both the mass and molar split factors for this compound are simply 0.1.

Table 4-11. RADM2 Split Factors for Pollutants Other Than Anthropogenic VOC

Source Category	Pollutant	CB4 Species	$factor_{jmp}$	$divisor_{jmp}$	$xmass_{jmp}$
All	CO	CO	1.0	28.0	1.0
All	NH3	NH3	1.0	17.0	1.0
All	AERO	AERO	1.0	1.0	1.0
All	PM10	PM10	1.0	1.0	1.0
All	PM2_5	PM2_5	1.0	1.0	1.0
All except BIO	NOX	NO	0.62	30.0	0.62
All except BIO	NOX	NO2	0.05	46.0	0.05
All	SO2	SO2	1.0	64.0	1.0
All	SOX	SO2	0.97	64.0	0.97
All	SO4	SULF	1.0	96.0	1.0
BIO	NO	NO	1.0	30.0	1.0
BIO	Isoprene	ISO	1.0	68.12	1.0
BIO	OVOC	HC3	0.343	148.0	0.85
BIO	OVOC	OLI	0.1	148.0	0.1
BIO	TERP	OLI	1.0	136.23	1.0
BIO	TERP	TERPB	1.0	136.23	1.0

4.2.6 Output Processor (OUTPRO)

The results of MEPPS processing must be in a form that is useful to the Models-3 framework and readily evaluated for the substantive content and quality of the data. The OUTPRO processes spatially and temporally allocated, speciated emission data files to prepare them for use by the

Models-3 framework and its components, including CMAQ. In addition, OUTPRO prepares many standard and user-defined emission summary reports. The processing includes the following items:

- Merging of temporally allocated point, area, biogenic, and mobile source emission data files.

- Merging of speciated point, area, biogenic, and mobile source emission data files .

- Merging of point, area, biogenic, and mobile source files into a consolidated two-dimensional emission file. Merging is optional; and data type files may be maintained and output separately.

- Preparation of three-dimensional point source emission files for use by the plume rise and Plume-in-Grid models available in CMAQ. The user may define groups of similar stacks by specifying percentage tolerance differences in different physical stack properties. In addition, the user may categorize minor, major, and major elevated point source emission (MEPSE) stacks by their emission rates and/or stack properties . The classification criteria are not pre-specified, but are set by the user. Specifically, any combination of emissions of specified pollutants in tons/day and/or physical stack parameters including height, diameter, flow rate, or exhaust velocity may be used to define a major or MEPSE point source. Generally, MEPSE stacks are the largest of point sources, such as electric utility stacks. Major point sources are usually somewhat smaller, but significant point sources. Source-specific information is necessary to classify MEPSE or major point sources. Smaller sources not classified as MEPSE or major point sources or without source-specific information are referred to as minor point sources, and are usually included with the surface area sources by OUTPRO, unless specified otherwise by the user.

- Conversion of output file format to NetCDF I/O API format. This allows other components of the Models-3 framework, including the CMAQ and visualization tools, to use the emission files. The CMAQ accepts the emission files and processes them for input to CMAQ using the Emission Chemical Input Processor (ECIP). The ECIP is described in Section 7.

- Preparation of summary reports of the processed emission files, including summaries by primary emission type (point, area, biogenic, mobile), by geographic area (grid area, grid cell, state, county, etc.), by source category code and groups of codes (tiers, or combinations of these items. In addition, the reports rank emission values by amount, type, geographic area, etc.

4.3 Models-3 Emission Projection Processor (MEPRO)

It is often necessary to iteratively project emissions and emission control combinations to future years in order to model future year ambient pollutant concentrations relative to regulatory standards. Consequently the Models-3 system includes a projection and control system, the Models-3 Emission Projection (MEPRO) processor to perform the necessary work. The MEPRO was developed from the Multiple Projection System (MPS). The MPS was originally designed as a stand-alone software tool to assist the EPA in projecting and tracking the "reasonable further progress" of regulatory emission reduction programs for criteria pollutants (Monroe et al., 1994). It may be invoked from Strategy Manager from the Models-3 framework or run separately. Because MPS was designed as a PC application using the Superbase® programming language, MEPRO must be run under an emulator (SoftWindows®) if it used in an UNIX operating system. Currently, MEPRO is more efficiently run on a PC workstation with a Windows NT® operating system. Figure 4-7 illustrates the relationship of MEPRO with the rest of MEPPS.

Using MEPRO, the user may edit regulatory control factors, control efficiency, rule penetration, rule effectiveness, as well as "across-the-board" emission adjustments and source category code-specific emission projections . Projected emission inventory data, and/or inventory data with revised emission controls and efficiencies are passed to EMPRO (in the /raw_data/*$EMS_DOMAIN*/common/ directory) for processing to the NetCDF I/O API format required for air quality modeling by CMAQ. Mobile source emissions are not projected in MEPRO. Instead, VMT is projected, and the projected mobile sources emissions are computed in the mobile source model of EMPRO.

The MEPRO will project emissions of NO_x, VOC, and CO for each year from 1991 through 2010, using the 1990 EPA inventory for the base year. The capability to project SO_2 and PM emission data may be provided in the future. Projections are by source category code of emissions for any area in the United States. The base year and the annual projection factors will be updated as new data become available. The annual growth factors for VOC, NO_x, and CO are taken from look-up tables containing economic growth factors by county for the United States. The growth factors are based on economic forecasts applied to specific source category codes by the Economic Growth Analysis System (EGAS) (US EPA, 1995a).

The EGAS system is a PC-based tool which uses a hierarchical three-tiered approach to generate growth factors. Tier 1 is the National Economic Tier. It includes an economic model by Regional Economic Models, Inc (REMI) (Treyz et al., 1994) which is primarily based on the Bureau of Labor Statistics (BLS) American Workforce 1992-2005 projections. After 2005, the BLS moderate growth labor force participation rates and the Census Bureau's middle population projections for the United States are used to forecast the labor force. The second tier is the Regional Economic Tier, the results of which are overlain on the Tier 1 results. The Regional Economic Tier contains separate economic models developed by REMI for each non-attainment area and attainment area of each state. The largest area addressed by one model is a state. The third tier is the Growth Factor Tier, which contains commercial, residential, industrial, and electric

utility models, and a VMT growth module. The commercial, residential, and industrial energy models were developed by the Argonne National Laboratory and were used in the National Acid Precipitation Assessment Program (Boyd et al., 1990). Electrical Utilities projection was accomplished using the Neural Network Electric Utility Model (EUMOD). The default economic projection tables from EGAS are based on U.S. Bureau of Labor Statistics forecasts. Projection factor tables based on forecasts by the Wharton School of Economics are provided as an option.

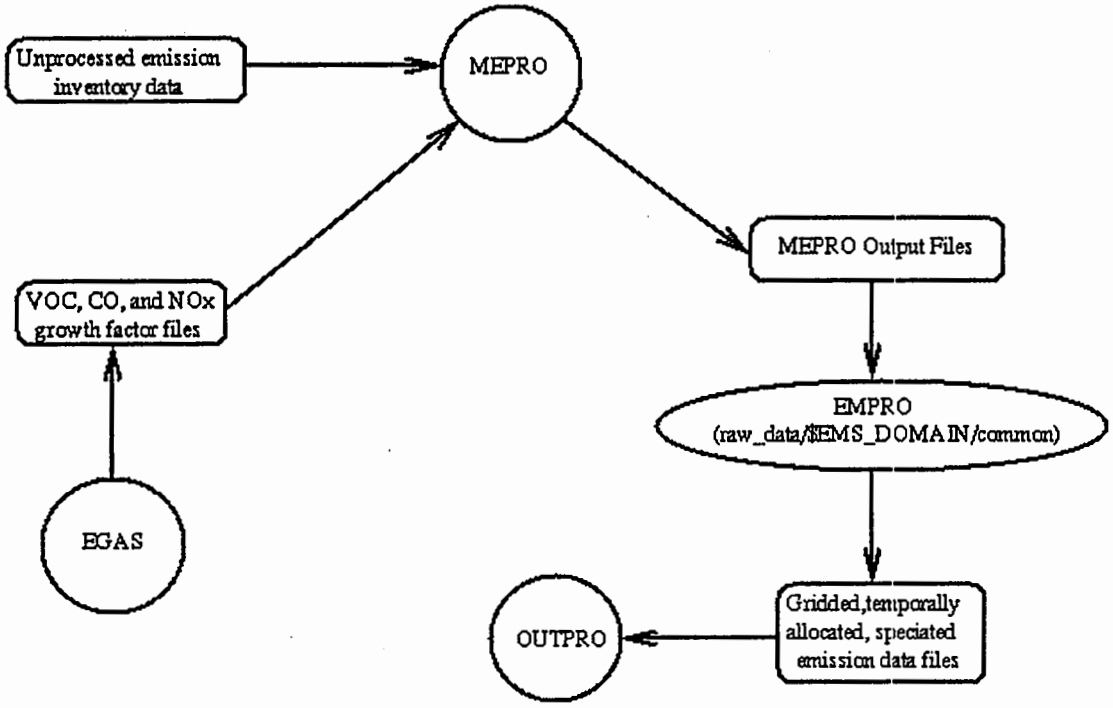

Figure 4-7 MEPRO Relationship to Other MEPPS Components

The method of applying regulatory and growth projection factors to point and area source emission data to obtain future year daily controlled emission data is summarized by Equation 4-105. Because MEPRO projects only the VMT data for mobile source emissions, the projection method is slightly different (Equation 4-106). The projected VMT data are passed to the EMPRO mobile-source emission model to be converted into projection mobile source emission data.

$$PCONE = DCONE * PGF * (1 + AF/100) * [1-(PCE * PRE * PRP)]/[1-(CE * RE * RP)] \quad (4\text{-}105)$$

where: PCONE is the point or area source future-year daily controlled emissions

DCONE is the base year daily-controlled emissions
PGF is the projected year growth factor (percent)
AF is the projected year emission adjustment factor (percent)
PCE is the projected year control efficiency
PRE is the projected year rule effectiveness
PRP is the projected year rule penetration
CE is the (adjusted) base year control efficiency
RE is the (adjusted) base year rule effectiveness
RP is the (adjusted) base year rule penetration

For mobile source data:

$$FPE = BVMT * EF * PGF * (1 + AF/100) \quad (4\text{-}106)$$

where: FPE is the future projected emissions (on-road mobile)
BVMT is the base VMT by vehicle class by facility class by year
EF is the emission factor
PGF is the projected year growth factor
AF is the projected year emission adjustment factor

Additional details for EGAS and MPS are given the references cited above.

4.4 Emission Processing Interface

An accurate characterization of the spatial and temporal variability of emissions at the surface and aloft is vital for realistic air quality grid modeling. The MEPPS creates separate emission files for surface area and elevated point sources for a particular domain and time period to be modeled. Consequently, an interface processor program was needed to efficiently consolidate these various emissions types into a single, hourly gridded data file for use in grid model simulations.

4.4.1 Overview of Key Features of ECIP

The Emission-Chemistry Interface Processor (ECIP) serves as the key link between the MEPPS system and the CMAQ Chemistry Transport Model (CCTM). The primary function of ECIP is to generate an hourly 3-dimensional (3-D) emission data file for the CCTM from the individual emission file types produced by the MEPPS.

The schematic diagram in Figure 4-8 shows the principal input files used to drive ECIP.
The notable elevated point sources were likely separated into major and MEPSE (Major Elevated Point Source Emissions) source groups, based on a user-specified emission rate criterion during MEPPS processing. The MEPSE group contains the largest point source emissions and is intended to be specially simulated by the CCTM Plume-in-Grid (PING) treatment. However, the PING treatment is an optional capability of the CCTM and when it is not exercised, the MEPSE

emission file must be processed by ECIP for the modeling scenario so that the significant emissions from these point sources are included in the 3-D emission data file with the other major point source emissions. Thus, this capability to include or omit the MEPSE emissions in ECIP allows for CCTM runs to be performed without PING or with the PING treatment, respectively, while not requiring separate runs of the MEPPS emissions system. A companion stack parameter file for each point source emission file is needed by ECIP for plume rise calculations. In addition, meteorological data files generated by MCIP are also required to run ECIP in order to simulate point source plume processes. The ECIP 3-D emission file displayed in Figure 4.6 contains the surface area anthropogenic and biogenic emissions, and the elevated emissions from major point sources and the MEPSEs, if appropriate. The 3-D emissions output file from ECIP is ready for direct input into the CCTM.

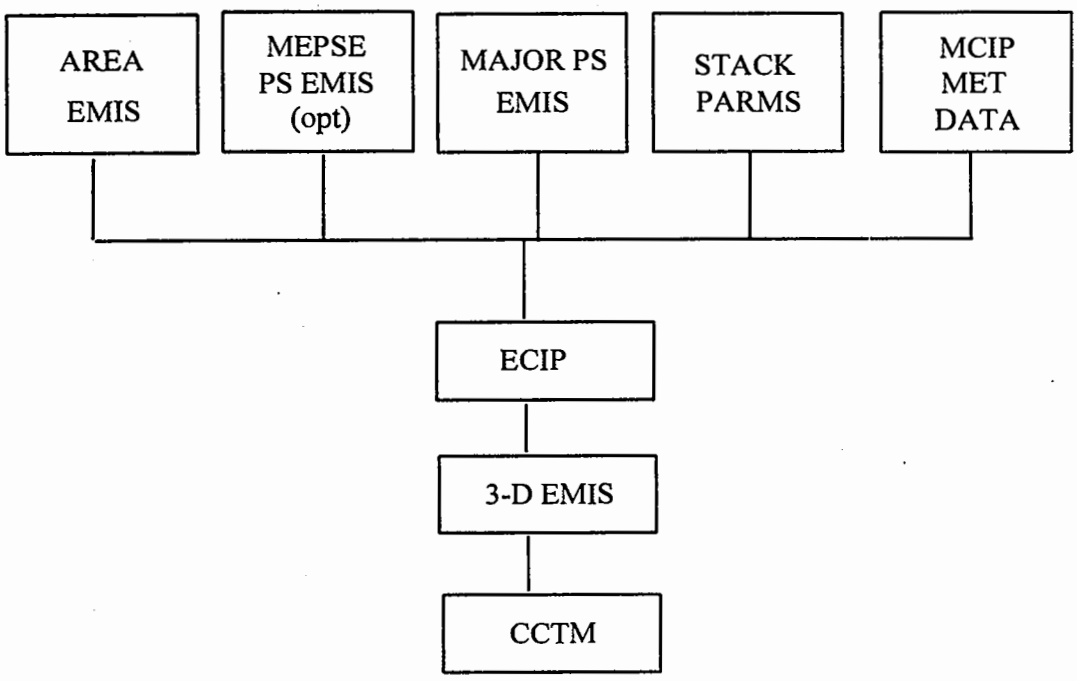

Figure 4-8 Schematic Flow Diagram of the Input Files and 3-D Emission Data File for CCTM generated by ECIP

A specific set of tasks is performed by ECIP for preparation of the 3-D emission file. The 2-D gridded area emissions are incorporated into the first model layer since they represent near-surface releases. In contrast, each elevated point source plume must be subjected to plume rise and initial vertical spread processes prior to the allocation of the plume emissions into the proper grid cells aloft. Another capability of ECIP can be applied in case the CCTM domain is smaller

than the emission domain. ECIP can perform "spatial windowing" of the emissions needed for a particular CCTM domain from a larger MEPPS emissions domain.

The methods used in ECIP to treat the processes impacting point source plumes are described in subsequent sections. While these approaches employ existing scientific techniques, it is recognized that other formulations exist. However, the modular design of the Models-3 coding structure allows for the implementation and application of alternative algorithms to treat a particular process.

4.4.2 Plume Rise of Point Source Emissions

The rise of a buoyant plume above stack height is strongly dependent upon the initial stack parameters and atmospheric vertical structure at the time of release. A realistic determination of the height of final plume rise is important to incorporating the plume emissions into the proper vertical layer(s) of the model. The initial buoyancy flux (F_b), which is a key parameter in plume rise formulas, is given by

$$F_b = \frac{g(T_s - T_a)(V_s d^2)}{4T_s} \tag{4-107}$$

where T_s and T_a are the stack exit temperature and ambient temperature at stack top, respectively. Other notable stack parameters in Equation 4-107 include the plume exit velocity (V_s) and stack diameter (d), while g is gravity. Clearly, the magnitude of F_b is greatly influenced by these stack exit parameters. For buoyant plumes, which exist for the vast majority of point sources, F_b is greater than zero since $T_s > T_a$. However, if $T_s < T_a$, then F_b is set to zero.

The vertical profile of wind and temperature also greatly impact plume rise. In particular, advances in the accuracy of plume rise estimates have resulted from taking into consideration the vertical variations in the thermal stability and wind structure which frequently display a strong height dependency in the atmosphere. A key atmospheric stability parameter (s) used to distinguish the different stability regimes aloft is defined by

$$s = (g/T_a)(d\theta/dz) \tag{4-108}$$

where $d\theta/dz$ is the vertical potential temperature gradient. The value of s is employed as a criterion to apply the appropriate stability-dependent plume rise formula. However, for the initial calculation of plume rise, the convective velocity scale (H_*) is used as an indicator variable to identify the particular stability regime and it is defined by

$$H_* = \frac{g}{T_s}\overline{wT} \tag{4-109}$$

where T_s is the 1.5m air temperature, and wT is the surface heat flux covariance. Unstable conditions are defined for $H_* > 0.03H_{*min}$, while stable conditions exit when $H_* < -0.03H_{*min}$. Neutral conditions occur for the range of values between these criteria. The default value of H_{*min} has been set to 10^{-4} m^2/s^3.

The layer-by-layer approach described by Turner (1985), as originally suggested by Briggs (1975), has been applied in ECIP for the determination of final plume rise (Δh) based on the stability of each vertical layer. This practical scheme takes advantage of the vertical resolution of the hourly, temperature and wind profiles and other 2-D meteorological parameters provided by the MM5 dynamic mesoscale meteorological model outputs as postprocessed through MCIP. The method, as outlined by Turner (1985), is an iterative approach which computes plume rise through each layer. An initial plume rise calculation is performed using meteorological variables derived at the stack top height with a stability-dependent plume rise formula at this level. Two methods, linear interpolation or a surface similarity scheme by Byun (1990), are available for deriving temperature and wind at stack height from the modeled profile values. For tall stacks, negligible differences were found in the derived values between these methods. If the projected effective plume rise height ($h_e = h_s + \Delta h$) exceeds the top of the layer containing the stack top, the amount of rise is limited to the height of the current layer top. Then residual buoyancy flux (F_R) is determined with an inverted form of the plume rise equation just applied. Using F_R, the procedure is repeated to determine the plume rise using the profile parameters for the next higher layer. This method is applied over successive layers until the buoyancy flux is completely exhausted. The plume rise ceases at the level where $F_b = 0$.

A set of analytical plume rise equations presented by Briggs (1984) for different atmospheric stabilities have been utilized in ECIP for all point sources. The various plume rise equations are provided below. The final effective plume centerline height (h_e) is found by adding the computed plume rise (Δh) to h_s.

4.4.2.1 Plume Rise Treatment for Stable Conditions

For stable atmospheric conditions, plume rise is taken from Briggs (1984) equation for bent-over plumes.

$$\Delta h = 2.6\left[\frac{F_b}{us}\right]^{1/3} \tag{4-110}$$

where u is the wind speed for the layer. Equation 4-88 is applied when $H_* < -0.03H_*$ for the initial plume rise computation at the stack, and when $s > 10^{-5}$ for subsequent layers in the current approach.

4.4.2.2 Plume Rise Treatment for Unstable Conditions

The plume rise formula proposed by Briggs (1984) during unstable conditions is given by

$$\Delta h = 3[F_b/u]^{3/5} H_*^{-2/5} \tag{4-111}$$

However, Briggs (1983) suggested a reasonable approximation for H_* which permits Equation 4-111 to be applied in the following form.

$$\Delta h = 30\,[F_b/u]^{3/5} \tag{4-112}$$

The rationale for the simplification is due to the lack of data for evaluation to justify a more complicated form. Equation 4-112 is applied with $H_* > 0.03H_{min}$ for the first plume rise computation at the stack and for higher layers for $s < 10^{-5}$.

4.4.2.3 Plume Rise Treatment for Neutral Conditions

The neutral formula developed by Briggs (1984) plume rise equation has been modified into the following expression.

$$\Delta h = 1.2[F_b/(u u_*^2)]^{3/5}[h_s + 1.3F_b/(u u_*^2)]^{2/5} \tag{4-113}$$

where u_* is the surface friction velocity. Equation 4-113 introduces minor differences from the other form. Equation 4-113 is a more computationally efficient form suggested by Briggs (1983, communication) since his original neutral formula requires iteration to solve. In the plume rise algorithm of ECIP, the neutral plume rise equation is also solved during other stability conditions in the layers aloft. A comparison between the two plume rise estimates is made and the lower value is selected before proceeding.

4.4.2.4 Special Conditions

For the cases when $F_b = 0$, plume rise can occur due to momentum provided by the exit velocity of the plume out of the stack. Therefore, a momentum rise formula (Turner, 1985) has also been implemented to consider these situations and is given by

$$\Delta h_m = 3d\ v_s/u \tag{4-114}$$

If Equation 4-114 is selected, no further plume rise computations are performed.

Another situation occurs when the stack is below the PBL height (z_i) under unstable conditions and the condition (h_s - z_i) < 200 m applies. A treatment for limited plume penetration above the PBL is determined when this situation is triggered. This condition most often occurs during the morning period. Since z_i is generally growing rapidly, this period is generally brief. To consider plume penetration of the overlying stable layer, a practical algorithm employed previously by Byun and Binkowski (1991) has been implemented based on Briggs (1984). If h_s is less than 200 m below z_i, then the following equation is solved.

$$z_b = 3.9[F_b/us]^{1/3} \tag{4-115}$$

If z_i is greater than z_b, , then the plume top height (z_t) is set to z_i and h_e is defined to be $2/3z_t$. However, plume penetration is permitted when $z_i < z_b$ in Equation 4-115. For this case, the plume top height is defined to be the height of the top of the next higher layer and the effective plume height is again computed as $2/3h_t$.

4.4.3 Method for the Treatment of Initial Vertical Plume Spread

Buoyancy-induced turbulence promotes plume expansion during the rise phase. A widely-used method from Briggs (1975) designates the vertical thickness of a plume to be equivalent to the amount of plume rise. With this method, the heights of the top and bottom of the plume are determined by

$$\begin{aligned} h_t &= h_s + 1.5\Delta h \\ h_b &= h_s - 0.5\Delta h \end{aligned} \tag{4-116}$$

where h_t and h_b are the heights of the plume top and bottom, respectively. Since the plume thickness is directly related to the amount of plume rise, this approach leads to rather thick plumes during the nocturnal period. Experimental plume dimension data suggest more limited vertical thickness for plumes during the nighttime hours. As an alternative, an empirical form has also been included. It is based on analyses of observed plume dimensions and vertical temperature gradients (Gillani, 1996 communication). He found the best-fit empirical result is given by

$$\sigma_z = Ae^{(-BdT/dz)} \tag{4-117}$$

where the standard deviation of plume depth (σ_z) is a function of the vertical temperature gradient (dT/dz) at h_e. Values for A and B are given by 10 and 117, respectively. A minimum value specified for σ_z is 3 m. With this method, h_t and h_b are determined to be $\pm 2.15\sigma_z$ above and below h_s, respectively. This approach provides for smaller plume thicknesses during the nocturnal period.

4.4.4 Vertical Allocation of Plume Emissions

Rather than dumping the entire emissions of a plume into a single layer, an approach has been developed to allow for the allocation of plume emissions into multiple layers since a plume can often span more than one layer. This situation occurs often as more vertical layers are used in the model since model layers are thinner.

Once h_t and h_b have been computed for each plume, these values, along with the heights of the model layer interfaces (z_z) are employed to determine the fractional amount of plume overlap across each layer. The method uses the fractional amount of the plume depth residing within a layer in order to weight the amount of plume emissions incorporated into a particular layer. If both h_t and h_b are contained within a particular layer, all the plume's emissions are allocated into one layer. As noted above, the number of layers receiving plume emissions is also dependent on the number of vertical layers in the model. A model configuration with fewer vertical layers generally implies greater layer thicknesses.

4.4.5 Generation of 3-D Emissions

Once the plume rise and plume partitioning functions have been performed, the emissions from each point source plume are transferred to the 3-D emission array which also contains the surface area emissions in the first layer. The 3-D emission array is written at an hourly interval for the entire simulation period to a data file in a format compatible for use in CCTM simulations.

4.5 Data Requirements

The following items are the data input requirements for operation of MEPPS. Those items that must be supplied by the user are marked (U). Those items that are fixed internal lookup tables, provided with Models-3, or that may be generated in MEPPS are marked (I).

- Complete annual (point, area, and mobile-source data by source category code) Regional, National, or international emission inventories are necessary for regional modeling. The inventories preferably should be in the ASCII format of the EPA National Emission Trends (NET) inventories. However, IDA allows import and conversion of any inventory with known fields formats in ASCII, SAS, or NetCDF format. Currently, the 1985 NAPAP, 1988 National Inventory, 1990 National Interim Inventory, and 1990 National Emission Trends (NET) inventories for criteria pollutants are included. Limited data for

southern Canada are available as a part of these inventories (I). Emission inventories for other areas, years, or pollutants must be supplied by the user (U).

- Existing hourly emission data, such as CEM data, may be used directly or substituted for hourly emission data derived by temporal disaggregation from annual emission inventories. The hourly data may be imported through the File Converter and IDA. The Models-3 system is includes 1995 CEM data in the SAS data set format provided by the US EPA Office of Acid Rain (I). Other hourly data must be supplied by the user if desired (U).

- Hourly meteorological data for surface temperature and solar radiation, in NetCDF I/O API format, (from MM5 processed via MCIP) must be available for modeling biogenic or mobile source emission data. If data files for the appropriate case area available, the user may select them in MEPPS or when running Study Planner. Otherwise, it is necessary to first run MM5 and output the meteorology files through MCIP (I).

- Chemical speciation profiles matched to source category codes are necessary for the speciation processor (I). These may be updated with new information.

- Temporal allocation profiles, by source category code, must be available to accomplish temporal allocation of emission data to hourly emission data (I). These may be updated with new information

- Geographic coverages for surrogate spatial allocation (gridding) of emission data. The user may supply additional coverages: Those supplied with MEPPS include (I):

  Political boundaries at the county level for North America
  Land-water boundaries and features for North America
  County-level population information for North America (with a gridded surrogate for Canada)
  Federal Highway Administration major highway coverage for the United States
  TIGER-LINE detail road coverage for the United States
  Land cover for North America. Currently is at county-scale for the United States and gridded at coarser resolution for Canada and Mexico. Land cover for the United States at one kilometer resolution is anticipated in 1999

- Species emission factors for biogenic emission modeling (I)

- Standard Mobile 5a model input information by political area (usually state and/or county), including vehicle fleet composition data, fuel type use by geographic area,

inspection and maintenance program information, etc, (U). A template with examples is provided for the user to edit.

- Road silt loading, geographic distribution of paved and unpaved roads, vehicle fleet composition data, fuel use data, and inspection and maintenance data are necessary as input to the PART5 mobile particulate model.

- Geographic, source category code-specific growth projection factors. These are provided for use with MEPRO (I).

- Source category and/or geographically specific emission control data, and regulatory factors including control efficiency, rule effectiveness, and rule penetration for use in MEPRO. These must be supplied by the user because controls are not standard, and in fact are a key variable in examining different emission scenarios (U).

4.6 Plans for Improvement

Plans for improvement of MEPPS may be divided into long and short-term improvements. The short-term improvements are those that are anticipated to be in the Models-3 release scheduled for the summer of 1999.

Short-term Improvements

- The IDA will be improved to consolidate and further automate much of the quality control processing, format and unit conversion, and data file manipulation. In particular, format templates of internal formats will be added to assist importing of emission data files into the system, and quality control for the CEM data will be enhanced.

- Although SAS® has proved to be a useful tool to date, increasing data handling requirements will likely overwhelm the data handling capabilities of SAS®. Therefore, it is necessary to convert MEPPS to a fully Models-3 framework compliant system in order to take full advantage of the or object-oriented data base architecture of the system (eg., Orbix®) to more efficiently manage very large amounts of data. The use of the Sparse Matrix Operator Kernel Emission (SMOKE) system, in conjunction with the Models-3 object-oriented architecture and expansion of existing functionality should substantially improve performance because relatively inefficient processing sequences will not be necessary, and it will not be necessary to manipulate all elements of large files for each operation. More information about SMOKE can be found in Coats et al. (1995). An initial (but not complete) version of SMOKE is planned for installation by summer 1999.

Long-term Improvements

- New mobile source emission estimation models are being developed by the U.S. EPA Office of Mobile Sources. They are scheduled for completion late summer of 1999. Mobile 6 will replace Mobile 5a and Mobile 5b, and an Off-road Mobile Source Model will be introduced. These models will be installed in MEPPS when they are available and resources allow.

- The MEPPS contains the split factor assignments for two common chemical speciation mechanisms, CB-4 and RADM 2, that may be selected by users. These speciation mechanisms will also be in SMOKE. There are plans to also install the split factor information and computational mechanisms necessary to use for the Statewide Air Pollution Research Center (SAPRC) (Carter, 1988), and eventually, code necessary to support the more complex Morphecule mechanism being developed at the University of North Carolina.

- Additional quality control and reporting capabilities will be added to SMOKE, equaling or surpassing those capabilities in currently in MEPPS.

- The emission data processing system could be enhanced to support nested grid structures. Currently, there is only limited support for nested grid structures and no support for multiscale grid structures. Under the current formulation, EMPRO (including the gridding processor) must be run consecutively for each grid structure that exists within the nested grid structure. Repetitive runs are inefficient, and computer resources are poorly utilized because certain areas in the modeling domain will be processed more than once. In addition, the gridding processor cannot generate rotated grids, which may be a limitation for some applications. If an air quality modeling study requires a rotated emission modeling grid, a knowledgeable ARC/INFO® user must prepare the grid independently from menu options provided in Model-3 and MEPPS.

- Tools such as NetCDF and the I/O API will evolve to directly accommodate geographic data references in their structure. This will allow manipulation of geographic data (gridding, for example) to be accomplished without the use of non-conforming commercial software tools now in Models-3 system.

4.7 References

Alados, I., I. Foyo-Moreno, and L. Alados-Arboledas, 1996: Photosynthetically Active Radiation: Measurements and Modeling, *Agri. and Forest Meteor.*, **78**, pp. 121-131.

Beck, L., L.A.. Bravo, B.L. Peer, M.L. Saeger, and Y. Yan, 1994: A Data Attributes Rating System, Presented at the International Conference on the Emission Inventory: Applications and Improvement, Raleigh, NC., November 1-3, 1994, 12 pp.

Boyd, G.A., E.C. Kokkelenberg, and M.H. Ross, 1990: Sectoral Electricity and Fossil Fuel Demand in U.S. Manufacturing: Development of the Industrial Regional Activity and Energy Demand (INRAD) Model, Argonne National Laboratory, Argonne, IL.

Briggs, G.A., 1975: Plume Rise Predictions. In: Lectures on Air Pollution and Environmental Impact Analyses, Workshop, Proceedings, Boston, MA, 1975, pp 59-111.

Briggs, G.A., 1983 communication: Plume rise equations used in EPA models. Meteorology Division, Environmental Sciences Research Lab., Research Triangle Park, NC.

Briggs, G.A., 1984: Plume Rise and Buoyancy Effects. In: Atmospheric Science and Power Production, D. R. Anderson, Ed., *DOE/TIC-27601 (DE84005177)*, Technical Information Center, U.S. DOE, Oak Ridge, TN, 850 pp.

Byun, D.W., 1990: On the Analytical Solutions of Flux-profile Relationships for the Atmospheric Surface Layer. *J. of Appl. Meteorol.*, **29**, No. 7, 652-657

Byun, D.W. and F.S. Binkowski, 1991: Sensitivity of RADM to Point Source Emissions Processing. Seventh AMS/AWMA Joint Conf. on Applications of Air Poll. Meteorol., New Orleans, LA, Jan. 14-18, 1991, Preprints, Amer. Meteorol. Soc., Boston, MA., 1991, pp. 70-73.

Carter, W.P.L., 1988: Documentation for the SAPRC Atmospheric Photochemical Mechanism Preparation and Emissions Processing Programs for Implementation in Airshed Models, Prepared for the California Air Resources Board, *Report A5-122-32.*

Coats, C.J., Jr., 1995: High Performance Algorithms in the Sparse Matrix Operator Kernel Emissions (SMOKE) Modeling System, Microelectronics Center of North Carolina, Environmental Systems Division, Research Triangle Park, NC, 6 pp.

E.H. Pechan and Associates, 1994: Industrial SO_2 and NO_x Tracking System, *EPA Contract No. 68-D1-0146*, 38 pp.

Emission Inventory Improvement Program (EIIP), 1996: Biogenic Sources Preferred Methods, Volume V, prepared for the EIIP Area Sources Committee by the Radian Corporation, Research Triangle Park, NC, 104 pp.

Fratt, D.B., D.F. Mudgett, and R.A. Walters, 1990: The 1985 NAPAP Emissions Inventory: Development of Temporal Allocation Factors, *EPA-600/7-89-010d*, U.S. Environmental Protection Agency, Office of Research and Development, Washington, D.C., 209 pp.

Geron, C.D., A.B. Guenther, and T.E. Pierce, 1994: An Improved Model for Estimating Emissions of Volatile Organic Compounds from Forests in the Eastern United States, *J. Geophys. Res.*, **99**, D6, pp. 12773-12791.

Gery, M.W., G.Z. Whitten, J.P. Killus, and M.C. Dodge, M.C., 1989: A Photochemical Kinetics Mechanism for Urban and Regional Scale Computer Models, *J. Geophys. Res.*, **94**, D10, 12295-12956.

Gillani, N.V., 1996: personal communication: Analyses results of plume data.

Guenther, A.B., P. Zimmermann, and M. Wildemuth, 1994: Natural Volatile Organic Compound Emission Rate Estimates for U.S. Woodland Landscapes, *Atmos. Environ.*, **28**, 1197-1210.

Kinnee, E., C. Geron, and T. Pierce, 1997: United States Land Use Inventory for Estimating Ozone Precursor Emissions, *Ecol. Appl.*, **7**, 46-58.

Middleton, P., W.R. Stockwell, and W.P.L. Carter, 1990: Aggregation and Analysis of Volatile Organic Compound Emissions for Regional Modeling, *Atmos. Environ.*, **24A**, pp. 1107-1133.

Modica, L.G., D.R. Dulleba, R.A. Walters, and J.E. Langstaff, 1989: Flexible Regional Emissions Data System (FREDS) Documentation for the 1985 NAPAP Emissions Inventory, *EPA-600/9-89-047*, U.S. Environmental Protection Agency, Research Triangle Park, NC, 574 pp.

Monroe, C.C., T.A. Dean, and W.R. Barnard, 1994: Multiple Projections System: Version 1.0 User's Manual, *EPA-600/R-94-085*, 70 pp.

Moody, T., J.D. Winkler, T. Wilson, and S. Kersteter, 1995: The Development and Improvement of Temporal Allocation Factor Files, *EPA-600/R-95-004*, 457 pp.

Moran, M.D., M.T. Scholtz, C.F. Slama, A. Dorkalam, A. Taylor, N.S. Ting, D. Davies, C. Sobkowicz, P.A. Makar, and S. Venkatesh, 1998: An Overview of CEPS1.0: Version 1.0 of the Canadian Emissions Processing System for Regional-Scale Air Quality Models, in the Proceedings of a Specialty Conference on Emission Inventory: Planning for the Future, Air and Waste Management Association, Pittsburgh, VIP-77, Volume I, 95-106.

Morris R.E., M.A. Yocke, T.C. Myers and V. Mirabella, 1992: Overview of the Variable-Grid Urban Airshed Model (UAM-V), Paper presented to the Air and Waste Mangement Association, 85th Annual Meeting, Kansas City, MO, June 21-26, 1992, 13 pp.

Ozone Transport Assessment Group, 1997: Emission Inventory Development Report (Draft), 3 Volumes.

Pierce, T.E., B.K. Lamb, and A.R. VanMeter, 1990: Development of a Biogenic Emissions Inventory System for Regional Scale Air Pollution Models, Paper presented to the Air and Waste Management Association, 83rd Annual Meeting, Pittsburgh, PA, June 24-29, 1990, 16 pp.

Pierce, T., C. Heron, L. Bender, R. Dennis, G. Tennyson, and A. Guenther, 1998: The Influence of Increased Isoprene Emissions on Regional Ozone Modeling, *J. Geophys. Res.*, in press.

Saeger, M., J. Langstaff, R. Walters, L. Modica, D. Zimmerman, D. Fratt, D. Dulleba, R. Ryan, J. Demmy, W. Tax., D. Sprague, D. Mudgett, and A.S. Werner, 1989: The 1985 NAPAP Emissions Inventory (Version 2): Development of the Annual Data and Modelers' Tapes, U.S. Environmental Protection Agency, Office of Research and Development, *EPA-600/7-89-012a*, 692 pp.

Stockwell, W.R., P. Middleton, and J.S. Chang, 1990: The Second Generation Regional Acid Deposition Model Chemical Mechanism for Regional Air Quality Modeling, *J. Geophys. Res.*, **95** (D10), pp. 16,343-16367.

Treyz, G. et al.: 1994: Model Documentation for the REMI EDFS-14 Forecasting and Simulation Model, Regional Economic Models, Inc., Amherst, MA.

Turner, D.B., 1985: Proposed Pragmatic Methods for Estimating Plume Rise and Plume Penetration through Atmospheric Layers. *Atmos. Environ.*, **19**, 1215-1218.

U.S. EPA, Office of Mobile Sources, 1985: Size Specific Total Particulate Emission Factors for Mobile Sources, *EPA-460/3-85-005*, 294 pp.

U.S. EPA, Office of Air Quality Planning and Standards, 1988: Air Species Manual: Volume 1, Volatile Organic Compound Species Profiles, *EPA-450/2-88-003a*, 492 pp.

U.S. EPA, Office of Research and Development, 1989: Development of the Regional Oxidant Model Version 2.1, *U.S. EPA Technical Report.*

U.S. EPA, Office of Mobile Sources, 1991: User's Guide to MOBILE 4.1 (Mobile Source Emission Factor Model), *EPA-AA-TEB-91-01*, 354 pp.

U.S. EPA, Office of Air Quality Planning and Standards, 1992: User's Guide for the Urban Airshed Model, Volume IV: User's Manual for the Emissions Preprocessor System 2.0, *EPA-450/4-90-007D(R)*, 497 pp.

U.S. EPA, Office of Air Quality Planning and Standards, 1993: Regional Interim Emission Inventories 1987-1991), *EPA-454/R-93-0212*, 54 pp.

U.S. EPA, Office of Air Qaulity Planning and Standards, 1994: Emissions Inventory for the National Particulate Matter Study, Final Draft, Prepared by E.H. Pechan, Inc., *EPA Contract No. 68-D3005, WA No. 0-10*, 83 pp.

U.S. EPA, Office of Air Quality Planning and Standards, 1995: Compilation of Air Pollutant Emission Factors: Volume II: Mobile Sources, AP-42, Fifth Edition, 293 pp.

U.S. EPA, Office of Research and Development, 1995a: Economic Growth Analysis System: User's Guide Version 3.0, *EPA-600/R-95-132b*, 89 pp.

U.S. EPA, Office of Mobile Sources, 1995b: Draft User's Guide to PART5: A Program for Calculating Particle Emissions from Motor Vehicles, *EPA-AA-AQAB-94-2*, 67 pp.

U.S. EPA, Office of Mobile Sources, 1996: User's Guide for MOBILE 5a (Mobile Source Emission Factor Model), *EPA-AA-TEB-92-01*, 176 pp.

U.S. EPA, Office of Air Quality Planning and Standards, 1997: Air CHIEF, Version 5 (Compact Disk containing air quality speciation profiles, emission factors, and other emission-related data), Research Triangle Park, NC.

U.S. EPA, Office of Air Quality Planning and Standards, 1998: National Air Pollutant Emission Trends Procedures Document, 1900-1996 Projections 1999-2010, *EPA-454/R-98-008*, 712 pp.

U.S. EPA, Office of Research and Development, 1995: Models-3: Volume 7, System Requirements (Draft) .

U.S. EPA, Office of Research and Development, 1995: Models-3: System Design (Draft).

Walters, R.A. and M.L. Saeger, 1990: The 1985 NAPAP Emissions Inventory: Development of Species Allocation Factors, *EPA-600/7-89-010f*, 470 pp.

Wilkinson, J.G., C.F. Loomis, D.E. McNally, R.A. Emigh, and T.W. Tesche, 1994: Technical Formulation Document: SARMAP/LMOS Emissions Modeling System (EMS-95), Final Report, Lake Michigan Air Directors Consortium and the California Air Resources Board, *AG-90/TS26 and AG-90/TS27*, 120 pp.

Williams, E., A. Guenther, and F. Fehsenfeld, 1992: An Inventory of Nitric Oxide Emissions from Soils in the United States, *J. Gaffes. Res.*, **97**, 7511-7519.

Yienger, J.J. and H. Levy II, 1995: Empirical Model of Global Soil-Biogenic Nox Emissions, *J. Gaffes. Res.*, **100**, No. D6, 11447-11464.

This chapter is taken from *Science Algorithms of the EPA Models-3 Community Multiscale Air Quality (CMAQ) Modeling System*, edited by D. W. Byun and J. K. S. Ching, 1999.

EPA/600/R-99/030

Chapter 5

FUNDAMENTALS OF ONE-ATMOSPHERE DYNAMICS FOR MULTISCALE AIR QUALITY MODELING

Daewon W. Byun*
Atmospheric Modeling Division
National Exposure Research Laboratory
U.S. Environmental Protection Agency
Research Triangle Park, NC 27711

ABSTRACT

This chapter provides essential information needed for the proper use of meteorological data in air quality modeling systems. Sources of meteorological data are diverse and many difficulties can arise while linking these with air quality models. To provide an integral view of atmospheric modeling, a robust and fully compressible governing set of equations for the atmosphere is introduced. Limitations of several simplifying assumptions on atmospheric dynamics are presented. Also, concepts of on-line and off-line coupling of meteorological and air quality models are discussed.

When the input meteorological data are recast with the proposed set of governing equations, chemical transport models can follow the dynamic and thermodynamic descriptions of the meteorological data closely. In addition, this chapter introduces a procedure to conserve mixing ratio of trace species even in the case meteorological data are not mass consistent. In summary, it attempts to bridge the information gap between dynamic meteorologists and air quality modelers by highlighting the implication of using different meteorological coordinates and dynamic assumptions for air quality simulations.

* On assignment from the National Oceanic and Atmospheric Administration, U.S. Department of Commerce. Corresponding author address: Daewon W. Byun, MD-80, Research Triangle Park, NC 27711. E-mail: bdx@hpcc.epa.gov

5.0 FUNDAMENTALS FOR ONE-ATMOSPHERE MODELING FOR MULTISCALE AIR QUALITY MODELING

To simulate weather and air quality phenomena realistically, adaptation of a one-atmosphere perspective based mainly on "first principles" description of the atmospheric system (Dennis, 1998) is necessary. The perspective emphasizes that the influence of interactions at different dynamic scales and among multi-pollutants cannot be ignored. For example, descriptions of processes critical to producing oxidants, acid and nutrient depositions, and fine particles are too closely related to treat separately. Proper modeling of these air pollutants requires that the broad range of temporal and spatial scales of multi-pollutant interactions be considered simultaneously. Several chapters (Chapters 4, 8, 9, 11 and 16) of this document present the one-atmosphere modeling perspective related with the multi-pollutant chemical interactions. Another key aspect of the one-atmosphere perspective is the dynamic description of the atmosphere. This is the focus of the present chapter.

Air quality modeling should be viewed as an integral part of atmospheric modeling and the governing equations and computational algorithms should be consistent and compatible. Previously, many atmospheric models have been built with limited atmospheric dynamics assumptions. To simplify the model development process, the governing equations were first simplified to match with the target problems, then computer codes were implemented. This approach enabled rapid development of models. However, we believe that dynamic assumptions and choice of coordinates should not precede the computational structure of the modeling system. To provide the scalability in describing dynamics, a fully compressible governing set of equations in a generalized coordinate system is preferable. Once the system is based on the fully compressible governing equations, simpler models can be built readily. The characteristics of the vertical coordinates and other simplifying assumptions need to be considered as well. For successful one-atmosphere simulations, it is imperative to have consistent algorithmic linkage between meteorological and chemical transport models (CTMs).

The present chapter addresses the issue of consistent description of physical processes across scales in meteorological and air quality modeling systems. It intends to provide appropriate background information to properly link air quality and meteorological models at a fundamental level. It deals with dynamic scalability issues, such as hydrostatic and nonhydrostatic modeling covering wide range of both temporal and spatial scales. Some of the contents are extracts from Byun (1999a and b) and others are complementary information to them. It includes mass correction methods, mass conservative temporal interpolation method, and the coupling paradigm for meteorology and chemical transport models.

5.1 Governing Equations and Approximations for the Atmosphere

In most weather prediction models, temperature and pressure, as well as moisture variables, are used to represent thermodynamics of the system. Often these thermodynamic parameters are represented with the advective form equations in meteorological models. Most of time, the

density is diagnosed as a byproduct of the simulation, usually through the ideal gas law. For multiscale air quality applications where the strict mass conservation is required, prognostic equations for the thermodynamic variables are preferably expressed in a conservative form similar to the continuity equation. Recently, Ooyama (1990) has proposed the use of prognostic equations for entropy and air density in atmospheric simulations by highlighting the thermodynamic nature of pressure. Entropy is a well-defined state function of the thermodynamic variables such as pressure, temperature, and density. Therefore, entropy is a field variable that depends only on the state of the fluid. The principle he uses is the separation of dynamic and thermodynamic parameters into their primary roles. An inevitable interaction between dynamics and thermodynamics occurs in the form of the pressure gradient force.

In this section, a set of governing equations for fully compressible atmosphere is presented. Here, density and entropy are used as the primary thermodynamic variables. For simplicity, a dry adiabatic atmosphere is considered. Most of the discussions in this section should be extensible for moist atmosphere if Ooyama's approach is followed.

5.1.1 Governing Equations in a Generalized Curvilinear Coordinate System

Using tensor notation, the governing set of equations for the dry atmosphere in a generalized curvilinear coordinate system can be written as:

$$\frac{\partial \hat{v}^j}{\partial t} + \hat{v}^k \hat{v}^j_{;k} + \hat{g}^{jk}\left(\frac{1}{\rho}\frac{\partial p}{\partial \hat{x}^k} + \frac{\partial \Phi}{\partial \hat{x}^k}\right) + 2\hat{\varepsilon}^{jkl}\Omega_k \hat{v}_l = \hat{F}^j_r \tag{5-1}$$

$$\frac{\partial(\rho\sqrt{\hat{\gamma}})}{\partial t} + \frac{\partial(\rho\sqrt{\hat{\gamma}}\hat{v}^j)}{\partial \hat{x}^j} = \hat{Q}_\rho = \sqrt{\hat{\gamma}}Q_\rho \tag{5-2}$$

$$\frac{\partial(\zeta\sqrt{\hat{\gamma}})}{\partial t} + \frac{\partial(\zeta\sqrt{\hat{\gamma}}\hat{v}^j)}{\partial \hat{x}^j} = \hat{Q}_\zeta = \sqrt{\hat{\gamma}}Q_\zeta \tag{5-3}$$

$$\frac{\partial(\varphi_i\sqrt{\hat{\gamma}})}{\partial t} + \frac{\partial(\varphi_i\sqrt{\hat{\gamma}}\hat{v}^j)}{\partial \hat{x}^j} = \hat{Q}_{\varphi_i} = \sqrt{\hat{\gamma}}Q_{\varphi_i} \tag{5-4}$$

where $\hat{v}^j$ and $\hat{v}_k$ are contravariant and covariant wind components, respectively, $\hat{v}^j_{;k}$ represents the covariant derivative of contravariant vector, $\hat{\varepsilon}^{jkl}$ is the Levi-Cevita symbol, Ω_k is the angular velocity of earth's rotation, $\hat{F}^j_r$ represents frictional forcing terms, $\sqrt{\hat{\gamma}}$ is the Jacobian of coordinate transformation, Φ is geopotential height, ρ is air density, and $\hat{g}^{jk}$ represents components of gravity vector in tensor form. Refer to Appendix 5A for the tensor primer and the derivation of the continuity equation in a generalized curvilinear coordinate system. φ_i represents trace species concentration, and ζ is (dry air) entropy per unit volume (entropy density), given as

$$\zeta = \rho C_{vd} \ln(\frac{T}{T_{oo}}) - \rho R_d \ln(\frac{\rho}{\rho_{oo}}) \tag{5-5}$$

where T is temperature, T_{oo} and ρ_{oo} are temperature and density of the reference atmosphere, respectively, at pressure p_{oo} = 1000 mb = 10^5 Pascal, C_{vd} is the specific heat capacity at constant volume, and R_d is the gas constant for dry air. The Q-terms represent sources and sinks of each conservative property. Although the source term for air density (Q_ρ) should be zero in an ideal case, it is retained here to capture the possible density error originating from numerical procedures in meteorological models. It is important to understand how this error term influences computations of other parameters such as vertical velocity component. Effects of the error term on trace gas simulation are discussed later.

To close the system we need to utilize the ideal gas law and the thermodynamic relations for temperature, entropy, pressure gradients, and density. Here, atmospheric pressure is treated as a thermodynamic variable that is fully defined by the density and entropy of the atmosphere. Then, pressure gradient terms can be computed using the thermodynamic relations with the density and entropy (e.g., Batchelor, 1967; Ooyama, 1990; DeMaria, 1995) in terms of the general vertical coordinate $s = \hat{x}^3$, as:

$$p = \rho R_d T \tag{5-6a}$$

$$\nabla_s p = \left(\frac{\partial p}{\partial \rho}\right)\nabla_s \rho + \left(\frac{\partial p}{\partial \zeta}\right)\nabla_s \zeta \tag{5-6b}$$

$$\frac{\partial p}{\partial s} = \left(\frac{\partial p}{\partial \rho}\right)\frac{\partial \rho}{\partial s} + \left(\frac{\partial p}{\partial \zeta}\right)\frac{\partial \zeta}{\partial s} \tag{5-6c}$$

$$\frac{\partial p}{\partial \rho} = \left(C_{pd} - \frac{\zeta}{\rho}\right)\frac{R_d T}{C_{vd}} \tag{5-6d}$$

$$\frac{\partial p}{\partial \zeta} = \frac{R_d T}{C_{vd}}, \tag{5-6e}$$

where C_{pd} is the specific heat capacity at constant pressure for dry air, and $\nabla_s = \hat{\mathbf{i}}\partial/\partial\hat{x}^1\big|_{s=const} + \hat{\mathbf{j}}\partial/\partial\hat{x}^2\big|_{s=const}$. For a conformal map projection, we can relate generalized meteorological curvilinear coordinates $(\hat{x}^1, \hat{x}^2, \hat{x}^3, \hat{t})$ to the reference rotated earth-tangential coordinates (x, y, z, t) as

$$\begin{cases} \hat{x}^1 = mx \\ \hat{x}^2 = my \\ \hat{x}^3 = s \\ \hat{t} = t \end{cases} \qquad \begin{cases} x = m^{-1}\hat{x}^1 \\ y = m^{-1}\hat{x}^2 \\ z = h(\hat{x}^1,\hat{x}^2,\hat{x}^3,\hat{t}) = h_{AGL}(\hat{x}^1,\hat{x}^2,\hat{x}^3,\hat{t}) + z_{sfc}(\hat{x}^1,\hat{x}^2) \\ t = \hat{t} \end{cases} \tag{5-7a, b}$$

where m is the map scale factor, z_{sfc} is the topographic height, and h is the geometric height, and h_{AGL} represents height above the ground (AGL). In the derivation of Equations 5-7a,b, we neglected the first-order variations of the map scale factor in x- and y-directions. The approximation establishes a quasi-orthogonality of the vertical coordinate to the horizontal plane on the confomal map. The covariant metric tensor, for example, and its determinant are given as

$$\hat{\gamma}_{jk} = \begin{bmatrix} m^{-2} + (\frac{\partial h}{\partial \hat{x}^1})^2 & (\frac{\partial h}{\partial \hat{x}^1})(\frac{\partial h}{\partial \hat{x}^2}) & (\frac{\partial h}{\partial \hat{x}^1})(\frac{\partial h}{\partial s}) \\ (\frac{\partial h}{\partial \hat{x}^1})(\frac{\partial h}{\partial \hat{x}^2}) & m^{-2} + (\frac{\partial h}{\partial \hat{x}^2})^2 & (\frac{\partial h}{\partial \hat{x}^2})(\frac{\partial h}{\partial s}) \\ (\frac{\partial h}{\partial \hat{x}^1})(\frac{\partial h}{\partial s}) & (\frac{\partial h}{\partial \hat{x}^2})(\frac{\partial h}{\partial s}) & (\frac{\partial h}{\partial s})^2 \end{bmatrix}, \tag{5-7c}$$

$$\hat{\gamma} = |\hat{\gamma}_{jk}| = \frac{1}{m^4}(\partial h / \partial s)^2. \tag{5-7d}$$

With above relations, one can rewrite the governing momentum equation, Equation 5-1, into the horizontal and vertical components of the curvilinear coordinates as (Byun, 1999a):

$$\frac{\partial \hat{\mathbf{V}}_s}{\partial t} + (\hat{\mathbf{V}}_s \bullet \nabla_s)\hat{\mathbf{V}}_s + \hat{v}^3 \frac{\partial \hat{\mathbf{V}}_s}{\partial s} + f\hat{\tau}_3 \times \hat{\mathbf{V}}_s$$

$$+m^2(\frac{1}{\rho}\nabla_s p + \nabla_s \Phi) - m^2\left(\frac{\partial s}{\partial z}\right)(\frac{1}{\rho}\frac{\partial p}{\partial s} + \frac{\partial \Phi}{\partial s})\nabla_s h = \hat{\mathbf{F}}_s \tag{5-8}$$

$$\frac{\partial \hat{v}^3}{\partial t} + (\hat{\mathbf{V}}_s \bullet \nabla_s)\hat{v}^3 + \hat{v}^3 \frac{\partial \hat{v}^3}{\partial s} + \hat{v}^k \hat{v}^j \frac{\partial^2 h}{\partial \hat{x}^k \partial \hat{x}^j}\left(\frac{\partial s}{\partial z}\right)$$

$$-m^2 \frac{\partial s}{\partial z}(\frac{1}{\rho}\nabla_s p + \nabla_s \Phi) \bullet \nabla_s h + |\nabla_z s|^2 (\frac{1}{\rho}\frac{\partial p}{\partial s} + \frac{\partial \Phi}{\partial s}) = \hat{F}_3 \tag{5-9}$$

where $\hat{\mathbf{V}}_s = \hat{v}^1\mathbf{i} + \hat{v}^2\mathbf{j}$, $\Phi(\hat{x}^1,\hat{x}^2,\hat{x}^3,\hat{t}) = gz$ represents the geopotential height, $\hat{\mathbf{F}}_s$ is the horizontal forcing vector, $\hat{\tau}_3$ is the vertical tangential basis vector and $\hat{F}_3$ is the forcing term in the momentum equation for $\hat{x}^3$ direction.

An alternative equation for the Cartesian vertical velocity component is given as:

$$\frac{\partial(\rho J_s w)}{\partial t} + m^2 \nabla_s \bullet \left(\frac{\rho J_s w \mathbf{V}_z}{m} \right) + \frac{\partial(\rho J_s w \hat{v}^3)}{\partial s}$$

$$+\rho J_s \left(\frac{m}{\rho} \frac{\partial p}{\partial s} + \frac{\partial \Phi}{\partial s} \right) \left(\frac{\partial s}{\partial z} \right) = \rho J_s \left(F_3 + \frac{w Q_\rho}{\rho} \right) \qquad (5\text{-}9')$$

where $\mathbf{V}_z = U\mathbf{i} + V\mathbf{j} = (\hat{v}^1 / m)\mathbf{i} + (\hat{v}^2 / m)\mathbf{j}$ is the horizontal wind vector represented in the Cartesian coordinate system, w is the vertical velocity component, J_s is the Jacobian for vertical coordinate transformation ($J_s = \left|\frac{\partial h}{\partial s}\right| = \frac{1}{g}\left|\frac{\partial \Phi}{\partial s}\right| = m^2 \sqrt{\hat{\gamma}}$), and F_3 is forcing term for the w-component. Note that the contravariant vertical velocity component is related to the Cartesian vertical velocity as:

$$\hat{v}^3 = \frac{ds}{dt} = \frac{\partial s}{\partial t} + \mathbf{V}_z \bullet \nabla_z s + w \left(\frac{\partial s}{\partial z} \right) = \frac{\partial s}{\partial t} + (-\frac{1}{g} \hat{\mathbf{V}}_s \bullet \nabla_s \Phi + w) \left(\frac{\partial s}{\partial z} \right), \qquad (5\text{-}10)$$

where $\nabla_z = \hat{\mathbf{i}} \partial / \partial x|_{z=const} + \hat{\mathbf{j}} \partial / \partial y|_{z=const}$.

The conservation equations for air density, entropy density, and tracer concentrations are found to be:

$$\frac{\partial(\rho J_s)}{\partial t} + m^2 \nabla_s \bullet \left(\frac{\rho J_s \hat{\mathbf{V}}_s}{m^2} \right) + \frac{\partial(\rho J_s \hat{v}^3)}{\partial s} = J_s Q_\rho \qquad (5\text{-}11)$$

$$\frac{\partial(\zeta J_s)}{\partial t} + m^2 \nabla_s \bullet \left(\frac{\zeta J_s \hat{\mathbf{V}}_s}{m^2} \right) + \frac{\partial(\zeta J_s \hat{v}^3)}{\partial s} = J_s Q_\zeta \qquad (5\text{-}12)$$

$$\frac{\partial(\varphi_i J_s)}{\partial t} + m^2 \nabla_s \bullet \left(\frac{\varphi_i J_s \hat{\mathbf{V}}_s}{m^2} \right) + \frac{\partial(\varphi_i J_s \hat{v}^3)}{\partial s} = J_s Q_{\varphi_i} \qquad (5\text{-}13)$$

5.1.2 Assumptions of Atmospheric Dynamics

In this subsection, several popular assumptions used in meteorological models are reviewed. Here, the dynamic and thermodynamic assumptions are discussed separately because they have been applied as independent approximations in many atmospheric models. However, readers should be aware of the inseparable nature of the dynamics and thermodynamics of the atmosphere. This study focuses on the impact of basic assumptions of the mass conservation issues and limits of applications in air quality applications.

5.1.2.1 Boussinesq Approximation

The crux of the Boussinesq approximation is that variation in density is important only when it is combined as a factor with the acceleration of gravity. Originally, it was applied for studying

shallow convection or boundary layer dynamics. Descriptions of the Boussinesq approximation can be found in the literature (e.g., Arya, 1988; Pielke, 1984; Stull, 1988; and Thunis and Bornstein, 1996). Although the Boussinesq approximation was originally developed for incompressible fluid, Dutton and Fichtl (1969) expanded the concept for anelastic deep convection applications. The results of the approximation lead to the following simplifications of the equations of motions in the planetary boundary layer (PBL):

(1) Flows can be treated essentially as solenoidal either in velocity field (incompressible) or in momentum field (anelastic).

(2) The equation of state for the fluctuating component is simplified because the ratio of fluctuating density to total density can be approximated by the ratio of temperature fluctuation to the reference temperature.

(3) Molecular properties including diffusivity are constant. These approximations are often used in air quality modeling to simplify the equations of motions and trace gas conservation equations. The effect of the Boussinesq approximation on mass continuity is in the limitation of the flow characteristics, such as incompressible or anelastic. For multiscale atmospheric studies, this approximation may be used only in the parameterization of the surface fluxes where the density can be treated essentially independent of height.

5.1.2.2 Nondivergent Flow Field Assumption

Essentially, this is an assumption about flow characteristics. The basis of this assumption is purely dynamic although an incompressible assumption leads to the nondivergent flow approximation. *A priori*, there is no connection with atmospheric thermodynamics. Therefore this assumption does not provide any information about the state variables, such as density, temperature, and pressure fields. For atmospheric applications, this approximation should be viewed as a result of the incompressible atmosphere assumption linked through the continuity equation of air. Because of the characteristics that the nondivergent velocity field can be expressed as the curl of a vector stream function, the field is also called solenoidal. Implications of this assumption on mass conservation of trace species are presented below in the description of the incompressible atmosphere assumption. In the generalized coordinate system, the nondivergent flow field is represented with following equation

$$\frac{1}{\sqrt{\hat{\gamma}}}\frac{\partial\left(\sqrt{\hat{\gamma}}\hat{v}^j\right)}{\partial\hat{x}^j}=0,\ j=1,2,3 \qquad (5\text{-}14)$$

This is somewhat different from the meteorological nondivergent flow field assumption in the Cartesian coordinate system, $\nabla \bullet \mathbf{V} = 0$. In the generalized meteorological coordinate system, Equation 14 can be rewritten as

$$\frac{\partial \hat{v}^j}{\partial \hat{x}^j} - 2m\hat{v}^j \frac{\partial m}{\partial \hat{x}^j} + \hat{v}^j \frac{\partial \ln J_s}{\partial \hat{x}^j} = 0 \qquad (5\text{-}14')$$

The two additional terms represent essentially the effects of the map projection and the gradient of the vertical Jacobian on the divergence of wind. For a small domain and for a coordinate whose vertical Jacobian is constant with respect to height (e.g., σ_z-coordinate), Equation 14' becomes identical to the nondivergent wind flow assumption used in a meteorological model. When the vertical Jacobian is a function of air density, the dependency of the wind on the density distribution cannot be ignored.

5.1.2.3 Incompressible Atmosphere Assumption

This is an assumption about the thermodynamic characteristics of air. The equation of state describes how density is affected by the changes in pressure and temperature fields. The incompressibility of air can be assumed (Batchelor, 1967) if:

$$\left|\frac{1}{\rho}\frac{d\rho}{dt}\right| << \frac{U}{L}, \qquad (5\text{-}15)$$

where U and L are the velocity and length scales, respectively, of the atmospheric motion.

As proposed in Byun (1999a), one can choose the density and the entropy as the two independent parameters of state. The total derivative of pressure with respect to time can be expressed as:

$$\frac{dp}{dt} = \left(\frac{\partial p}{\partial \rho}\right)\frac{d\rho}{dt} + \left(\frac{\partial p}{\partial \zeta}\right)\frac{d\zeta}{dt} \qquad (5\text{-}16)$$

Then, Equation 5-15 becomes the relation:

$$\frac{1}{\rho c_{sound}^2}\left|\frac{dp}{dt} - \left(\frac{\partial p}{\partial \zeta}\right)\frac{d\zeta}{dt}\right| << \frac{U}{L}, \qquad (5\text{-}17)$$

where c_{sound} is the speed of sound in the atmosphere, i.e., $c_{sound} = \sqrt{|\partial \rho / \partial p|}$. Batchelor (1967) stated that for Equation 5-17 to be satisfied, not only the difference between the two terms in the left hand side of Equation 5-17, but also the magnitude of each term should be small. When the condition

$$\left|\frac{1}{\rho c_{sound}^2}\frac{dp}{dt}\right| << \frac{U}{L} \qquad (5\text{-}18)$$

is satisfied, the change in the density of a material element due to pressure variations are negligible, that is, the fluid is behaving as if it were incompressible. By expanding the term $\frac{dp}{dt}$

in an Eulerian expression one can show that in order for the atmosphere to be treated as incompressible, the following conditions must be satisfied:

$$\frac{U^2}{c_{sound}^2} << 1; \qquad \frac{U_p^{\ 2}}{c_{sound}^2} << 1; \qquad \frac{gL}{c_{sound}^2} << 1, \tag{5-19}$$

where U_p is the phase speed of dominant atmospheric waves. The first condition states that the movement of air should have a Mach number much smaller than one, say 10%; the second condition states that energy-carrying waves should not propagate as fast as 10% of the speed of sound; and the last condition limits the vertical extent of motion to less than about one kilometer. Similarly, Dutton and Fichtl (1969) showed that the nondivergent wind relation is generally applicable up to half a kilometer above ground level through a scale analysis of the continuity equation. Because of these limitations, a meteorological model with incompressible flow approximation may not be suitable for multiscale air quality simulations that require descriptions of atmospheric motions over a wide range of temporal and spatial scales. The second condition:

$$\left| \frac{1}{\rho c_{sound}^2} \left(\frac{\partial p}{\partial \zeta} \right) \frac{d\zeta}{dt} \right| << \frac{U}{L} \tag{5-20}$$

means that variation of entropy due to internal heating or due to molecular conduction of heat into the element must be small. For adiabatic or pseudo-adiabatic atmosphere, Equation 5-20 is usually satisfied.

Basically, an incompressible atmosphere assumption is a shallow-water approximation for an adiabatic atmosphere. With the incompressibility assumption, the distinction between the continuity equation and its advective form becomes blurred. Consequently, concentrations in the form of either density or mixing ratio are often used indiscriminately in atmospheric diffusion equations. As presented above, the incompressible atmosphere assumption is a very restrictive approximation that disassociates linkage between the thermodynamics and dynamics of atmospheric motions. The incompressible atmosphere approximation simplifies the continuity equation of the air to the nondivergent wind component relation regardless of the type of vertical coordinates used. Compared with this, the atmosphere described with the hydrostatic pressure coordinate is not necessarily incompressible even for the hydrostatic atmosphere. Because the vertical layer is defined by the pressure surface, the hydrostatic approximation applied with the hydrostatic pressure coordinate system limits only the vertical propagation of sound waves and the atmosphere is not totally incompressible.

One might expect that as long as the wind field satisfies the nondivergent flow approximation, an air quality model would satisfy the pollutant species mass conservation. In the following, it is shown that this expectation is correct only when the air density field is perfectly mass consistent. As will be shown later in Equation 5-24, the trace species mass conservation is affected by the air density error term Q_ρ irrespective of whether or not the wind field is solenoidal. The implication is that a nondivergent wind field does not guarantee the mass conservation of

pollutant species as long as there is inconsistency in air density and wind fields. It is not a surprising statement, but in general this fact has not been actively addressed in air quality modeling studies. Because the nondivergent relation simply disassociates density and wind fields, it cannot be used to estimate the mass consistency error in the meteorological data set. On the other hand, the diagnostic relations applicable for the family of hydrostatic pressure coordinates based on total air density maintain the consistency in wind and air density fields.

5.1.2.4 Anelastic Atmosphere Assumption

Another popular limiting approximation applied in meteorological modeling is the anelastic assumption. It simplifies the continuity equation as a diagnostic relation for the momentum ($\rho_o \mathbf{V}$, where ρ_o is density of reference atmosphere) components as follows:

$$\nabla_s \bullet (\sqrt{\hat{\gamma}} \rho_o \hat{\mathbf{V}}_s) + \frac{\partial}{\partial s}(\sqrt{\hat{\gamma}} \rho_o \hat{v}^3) = 0 \qquad (5\text{-}21)$$

Ogura and Phillips (1962) and Dutton and Fitchl (1969) found that for deep atmospheric convection, if the characteristic vertical scale of motions is smaller than the atmospheric scale height, the anelastic assumption is satisfied. For shallow convection, the Boussinesq approximation allows us to treat the fluid as incompressible; for deep convection, the approximate continuity equation requires the momentum field to be solenoidal, and the expansion or contraction of parcels moving in the vertical is taken into account. Lipps and Hemler (1982) also performed a scale analysis to propose a set of approximate equations of motion which are anelastic when the time scale is larger than the inverse of Brunt-Väisäla frequency. The anelastic approximation leads to a divergent wind field, i.e.:

$$\nabla_s \bullet (\sqrt{\hat{\gamma}} \hat{\mathbf{V}}_s) + \frac{\partial(\sqrt{\hat{\gamma}} \hat{v}^3)}{\partial s} = -\sqrt{\hat{\gamma}}(\hat{\mathbf{V}}_s \bullet \nabla_s \ln \rho_o + \hat{v}^3 \frac{\partial}{\partial s} \ln \rho_o) \qquad (5\text{-}22)$$

Usually, the right hand side of Equation 5-22 does not vanish. Like the nondivergent wind field approximation, this assumption provides a diagnostic relation among wind components although it cannot be used to estimate the inconsistency in the total air density, ρ, and wind field data provided by a meteorological model. However, unlike the incompressible atmosphere assumption, the pressure, temperature and wind fields are not completely independent with the anelastic assumption. The distribution of pressure must be such that the wind fields predicted by the momentum equations continue to satisfy the anelastic relation (Gal-Chen and Somerville, 1975). For this reason, most anelastic meteorological models solve for the elliptic equation for the pressure that is derived from Equation 5-22. Refer to Nance and Durran (1994) for a recent review on the accuracy of anelastic meteorological modeling systems.

For air quality application, the anelastic approximation still requires use of a full continuity equation for the perturbation density component. However, most anelastic meteorological models do not solve for the perturbation air density directly. Therefore, one needs to infer it from other thermodynamic fields. Also, because the trace gas concentration depends on the total

density of air, not on just the reference density, it does not simplify the pollutant continuity equation and the concentration distribution represented in density units cannot be interchanged with trace species mixing ratio.

5.1.2.5 Hydrostatic Atmosphere Approximation

Perhaps one of the most popular assumptions of atmospheric dynamics used in meteorological models is the hydrostatic approximation. In the case of a hydrostatic atmosphere, the acceleration and the frictional force terms in the z-direction of the earth-tangential Cartesian coordinates are considered negligible. In earlier days of atmospheric modeling, the hydrostatic approximation was usually applied with the pressure coordinate. It is well known that the hydrostatic pressure coordinate applied to a hydrostatic atmosphere has a special property that simplifies the continuity equation into a solenoidal form and provides a diagnostic equation for the vertical velocity component. On the other hand, the geometric height coordinate was not used extensively for studying a hydrostatic atmosphere. Recently, Ooyama (1990) and DeMaria (1995) have presented a diagnostic vertical velocity equation. Extending this, a general diagnostic equation for the vertical velocity component can be obtained with the hydrostatic approximation for a coordinate whose Jacobian is independent of time (Byun, 1999a):

$$\frac{\partial}{\partial s}\left(\tilde{\rho} c_{sound}^2 \frac{\partial \hat{v}^3}{\partial s}\right) = -sign(\frac{\partial s}{\partial z}) g \left[m^2 \nabla_s \bullet \left(\frac{J_s \tilde{\rho} \hat{\mathbf{V}}_s}{m^2} \right) - J_s Q_\rho \right]$$

$$+ \frac{\partial}{\partial s}\left[(\frac{\partial p}{\partial \tilde{\rho}} Q_\rho + \frac{\partial p}{\partial \zeta} Q_\zeta) - m^2 \tilde{\rho} c_{sound}^2 \nabla_s \bullet \left(\frac{\hat{\mathbf{V}}_s}{m^2} \right) - \hat{\mathbf{V}}_s \bullet \nabla_s p \right] \qquad (5\text{-}23)$$

The diagnostic Equation 5-23 can be used to maintain mass consistency in meteorological data for air quality simulations.

It is worthwhile to note that the hydrostatic or nonhydrostatic atmospheric description, which is a characterization of the vertical motion, is rather independent from either the compressible/incompressible atmosphere or the anelastic atmosphere assumption, which is an approximation of the mass continuity equation. Choices of the assumptions from the two distinct groups have been used to simplify atmospheric motions, although some of the combinations, such as compressible but hydrostatic atmosphere, are rarely used in atmospheric studies.

5.2 Choice of Vertical Coordinate System for Air Quality Modeling

Figure 5-1 provides a pedigree of vertical coordinates used in many atmospheric models. Definitions of the coordinates are provided in Tables 5-1, 5-2 and 5-3. The hierarchy of classification is: (1) temporal dependency of coordinates, (2) base physical characteristic of coordinate variables, and (3) method of topography treatments. Application assumptions, such as hydrostatic or nonhydrostatic atmosphere approximations, are not part of the classification criteria. Isentropic coordinates are not included here because they are not suitable for the

regional and urban scale air quality simulation due to their inherent difficulties representing planetary boundary layer (PBL) structure. For larger-scale simulations, an isentropic coordinate system can serve as an interesting alternative (Arakawa et al., 1992). Also, there are new developments of hybrid coordinates that combine isentropic coordinates with other coordinates to mitigate the problem.

Many different types of vertical coordinates have been used for various meteorological simulations. For example, the geometric height is used to study boundary layer phenomenon because of its obvious advantage of relating near surface measurements with modeled results. Pressure coordinates are natural choices for atmospheric studies because many upper atmospheric measurements are made on pressure surfaces. Because most radiosonde measurements are based on hydrostatic pressure, one may prefer use of the pressure coordinate to study cloud dynamics. This idea of using the most appropriate vertical coordinate for describing a physical process is referred to as a generic coordinate concept (Byun et al., 1995). Several different generic coordinates can be used in a CTM for describing different atmospheric processes while the underlying model structure should be based on a specific coordinate consistent with the preprocessor meteorological model. The Models-3 Community Multiscale Air Quality (CMAQ) modeling system allows users to choose a specific coordinate without having to exchange science process modules (i.e., subroutines with physical parameterizations for describing atmospheric processes) which are written in their generic coordinates. The coordinate transformation is performed implicitly through the use of Jacobian within CMAQ.

Byun (1999a) discusses key science issues related to using a particular vertical coordinate for air quality simulations. They include a governing set of equations for atmospheric dynamics and thermodynamics, the vertical component of the Jacobian, the form of continuity equation for air, the height of a model layer (expressed in terms of geopotential height), and other special characteristics of a vertical coordinate for either hydrostatic or nonhydrostatic atmosphere applications. Tables 5-1, 5-2 and 5-3 summarize properties of the popular time-independent vertical coordinates (e.g., terrain-influenced height and the reference hydrostatic pressure coordinate systems) and the time-dependent terrain-influenced coordinate systems, respectively.

Not only the assumptions on atmospheric dynamics, but also the choice of coordinate can affect the characteristics of atmospheric simulations. For the time-independent vertical coordinates (z, p_o, *sigma-z*, *sigma-*p_o), the vertical Jacobians are also time-independent. Especially with the hydrostatic assumption, one can obtain a diagnostic equation for the vertical velocity component , which includes soundwaves together with meteorological signals. Further assumptions on flow characteristics, such as anelastic approximation, provide a simpler diagnostic equation for the nonsolenoidal air flow. For such cases, with or without the anelastic approximation, one can maintain trace species mass conservation in a CTM by using the vertical velocity field estimated from the diagnostic relation. The scheme works whether the horizontal wind components, temperature, and density field data are directly provided from a meteorological model or interpolated from hourly data at the transport time step. This suggests that the mass error can be estimated with the diagnostic relations that originate from one of the governing equations of the

preprocessor meteorological models. For a nonhydrostatic atmosphere, which does not have a special diagnostic relation for time independent coordinates, one should rely on the methods described below to account for the mass consistency errors.

For time dependent coordinates, the vertical Jacobians are also time dependent. In general, this makes it more difficult to derive a diagnostic relation from the continuity equation. However, for a coordinate with the Jacobian-weighted air density independent of height, a diagnostic equation for the vertical velocity is available when appropriate top and bottom boundary conditions are used. Vertical layers defined with this type of vertical coordinate are considered as material surfaces because mass continuity can be satisfied in a diagnostic fashion. Air particles are not expected to cross material surfaces during the advection process. An atmospheric model based on this type of coordinate may not have a mass consistency problem except for numerical reasons. The dynamic pressure coordinates based on true air density belong to this category, which includes such coordinates as π -coordinate, σ_π-coordinate, and the η -coordinate defined in conjunction with σ_π (See Table 5-3). A meteorological model using one of these coordinates will conserve mass within the limits of numerical errors expected from finite differencing and computer precision. For these coordinates, one can apply the same mass conservation procedure for both hydrostatic and nonhydrostatic cases. Note that the diagnostic relations obtained by appropriate choices of coordinates and assumptions on atmospheric dynamics allow estimation of the density error term in the continuity equation. This information can be used to reconstruct mass-consistent air density and wind fields that ensure mass conservation of pollutant species in air quality models.

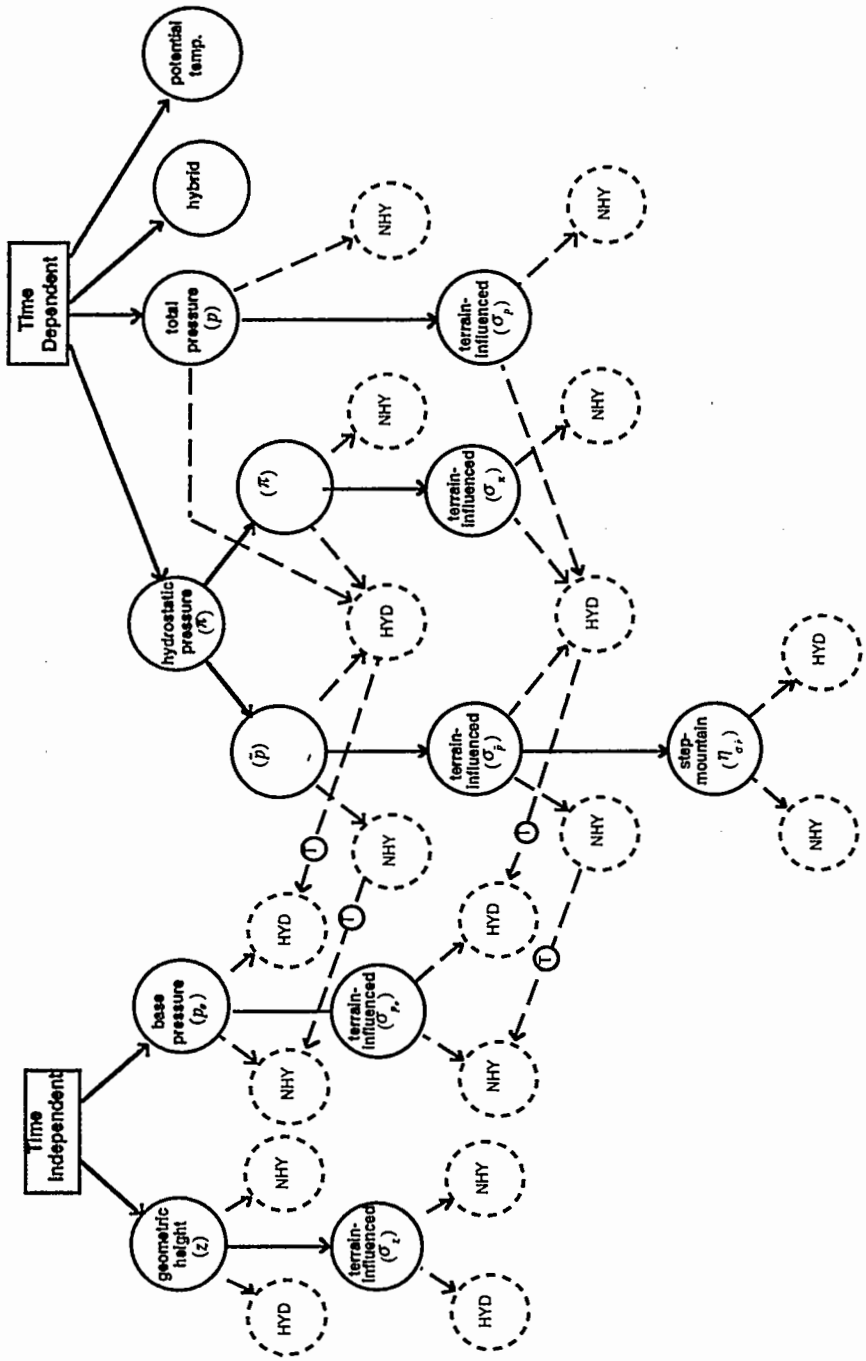

Figure 5-1. Pedigree of meteorological vertical coordinates. The encircled T symbol represents that the associated coordinates are identical when temporal dependency is ignored. Dashed-circles show that all the coordinates can be used for hydrostatic (HYD) and nonhydrostatic (NHY) application, regardless of the dynamic characteristics of the variables used to define vertical coordinates.

Table 5-1. Summary of Characteristics of the Geometric Height and Pressure Coordinate Systems. [Note: HYD and NHY stand for hydrostatic and nonhydrostatic applications, respectively. D( ) and P( ) symbols are assigned for diagnostic and prognostic formulas with equation numbers. ρ_o and $\tilde{\rho}$ are the reference and dynamic (time-dependent) hydrostatic pressure, respectively.]

Coordinate	vertical velocity	Vertical Jacobian	Geopotential height
geometric height (z)	NHY: w with P(5-9) or P(5-9') HYD: D(5-23)	$J_z = 1$ constant in $(\hat{x}^1, \hat{x}^2, \hat{x}^3, t)$	$\Phi = gz$
reference hydrostatic pressure (p_o) $\frac{\partial p_o}{\partial z} = -\rho_o(z)g$	NHY: P(5-9) or P(5-9') HYD: D(5-23)	$J_{p_o} = (\rho_o g)^{-1}$ constant in $(\hat{x}^1, \hat{x}^2, t)$	$\Phi = \Phi_{sfc} - \int_{p_{osfc}}^{p_o} \frac{dp_o'}{\rho_o}$
dynamic hydrostatic pressure (π), $\frac{\partial \pi}{\partial z} = -\rho(x,y,z,t)g$	$\hat{v}^3 = \dot{\pi} = -\int_{\pi_T}^{\pi} [m^2 \nabla_{\pi'} \bullet \left(\frac{\hat{\mathbf{V}}_{\pi}}{m^2}\right) - \frac{Q_\rho}{\rho}] d\pi'$ for both NHY & HYD	$J_\pi = (\rho g)^{-1}$ but, $\rho J_\pi = 1/g$ constant in $(\hat{x}^1, \hat{x}^2, \hat{x}^3, t)$	$\Phi = \Phi_{sfc} - \int_{\pi_{sfc}}^{\pi} \frac{d\pi'}{\rho}$
large-scale hydrostatic pressure $(\tilde{p})$, $\frac{\partial \tilde{p}}{\partial z} = -\tilde{\rho}(x,y,z,t)g$	NHY: P(5-9) or P(5-9') for perturbation component HYD: $\hat{v}^3 = \dot{\tilde{p}} = -\int_{\tilde{p}_T}^{\tilde{p}} [m^2 \nabla_{\tilde{p}} \bullet \left(\frac{\hat{\mathbf{V}}_{\tilde{p}}}{m^2}\right) - \frac{Q_\rho}{\tilde{\rho}}] d\tilde{p}$	$J_{\tilde{p}} = (\tilde{\rho} g)^{-1}$	$\Phi = \Phi_{sfc} - \int_{\tilde{p}_{sfc}}^{\tilde{p}} \frac{d\tilde{p}'}{\tilde{\rho}}$

Table 5-2. Summary of Time Independent Terrain-influenced Height and Reference Hydrostatic Pressure Coordinate Systems. [Note: D( ) and P( ) symbols are assigned for diagnostic and prognostic formulas with equation numbers, respectively, and '$\neq f()$' represents that the parameter is not dependent on the argument.]

Coordinate	Application	Vertical Momentum	Vertical Jacobian	Geopotential height
normalized geometric height (σ_z) $\sigma_z = \frac{z - z_{sfc}}{H - z_{sfc}}$	hydrostatic	D(5-23)	$J_{\sigma_z} = H - z_{sfc}$ $\neq f(\hat{x}^3, t)$	$\Phi = gz =$ $g[z_{sfc} + \sigma_z(H - z_{sfc})]$
	generalized hydrostatic	P(5-9) or, P(5-9') with Eq.(5-10)		
	non-hydrostatic			
terrain-influenced reference pressure (σ_{p_o}) $\sigma_{p_o} = \frac{p_o - p_T}{p_o(z_{sfc}) - p_T}$	hydrostatic	D(5-23)	$J_{\sigma_{p_o}} = \frac{p_o^*}{\rho_o(\hat{x}^3)g}$ $\neq f(t)$, $p_o^* = p_o(z_{sfc}) - p_T$	$\Phi = \Phi_{sfc} - \int_{\sigma_{p_o sfc}}^{\sigma_{p_o}} \frac{p_o^*}{\rho_o} d\sigma_{po}'$
	non-hydrostatic	P(5-9) or, P(5-9') with Eq.(5-10) for perturbation component		

Table 5-3. Summary of Characteristics of the Time Dependent Terrain-influenced Coordinate Systems.

Coordinate	Application	Vertical Momentum	Vertical Jacobian	Geopotential height
terrain-influenced hydrostatic pressure (σ_π) $\sigma_\pi = \frac{\pi - \pi_T}{\pi_{sfc} - \pi_T}$	hydrostatic	$\pi^* \dot{\sigma}_\pi \Big\|_{\sigma_{\pi T}}^{\sigma_\pi} = \int_{\sigma_{\pi T}}^{\sigma_\pi} [\pi^* \frac{Q_p}{\rho} - m^2 \nabla_{\sigma_\pi} \bullet \frac{\pi^* \hat{\mathbf{V}}_{\sigma_\pi}}{m^2}] \, d\sigma'_\pi$ $-(\sigma_\pi - \sigma_{\pi T}) \frac{\partial \pi^*}{\partial t}$	$\tilde{\rho} J_{\sigma_{\tilde{p}}} = \frac{\tilde{p}^*}{g}$ $\neq f(\hat{x}^3)$	$\Phi = \Phi_{sfc} - \int_{\sigma_{\tilde{p}sfc}}^{\sigma_{\tilde{p}}} \frac{\tilde{p}^*}{\tilde{\rho}} d\sigma_{\tilde{p}}'$
	non-hydrostatic		$\pi^* = \pi_{sfc} - \pi_T$ $\rho J_{\sigma_\pi} = \frac{\pi^*}{g}$ $\neq f(\hat{x}^3)$	$\Phi = \Phi_{sfc} - \int_{\sigma_{\pi sfc}}^{\sigma_\pi} \frac{\pi^*}{\tilde{\rho}} d\sigma_\pi'$
terrain-influenced large-scale hydrostatic pressure $(\sigma_{\tilde{p}})$	non-hydrostatic	P(5-9) or, P(5-9') with Eq.(5-10) for perturbation component when $\tilde{p}$ and $\tilde{\rho}$ given	$\tilde{\rho} J_{\sigma_{\tilde{p}}} = \frac{\tilde{p}^*}{g}$ $\neq f(\hat{x}^3)$	$\Phi = \Phi_{sfc} - \int_{\sigma_{\tilde{p}sfc}}^{\sigma_{\tilde{p}}} \frac{\tilde{p}^*}{\tilde{\rho}} d\sigma_{\tilde{p}}'$
step-mountain eta (η) with σ_π, $\eta = \sigma_\pi \eta_{sfc}$, $\eta_{sfc} = \frac{p_o(z_{sfc}) - p_T}{p_o(0) - p_T}$	hydrostatic	$\frac{\partial \pi^*}{\partial t} = \frac{1}{\eta_{sfc}} \int_0^{\eta_{sfc}} [\pi^* \frac{Q_p}{\rho} - m^2 \eta_{sfc} \nabla_\eta \bullet \frac{\pi^* \hat{\mathbf{V}}_\eta}{m^2 \eta_{sfc}}] \, d\eta'$ $\pi^* \dot{\eta} \Big\|_0^\eta = -\eta \frac{\partial \pi^*}{\partial t} + \int_0^\eta [\pi^* \frac{Q_p}{\rho} - m^2 \eta_{sfc} \nabla_\eta \bullet \frac{\pi^* \hat{\mathbf{V}}_\eta}{m^2 \eta_{sfc}}] \, d\eta'$	$J_\eta = \frac{\tilde{p}^*}{\tilde{\rho} g \eta_{sfc}}$ $\tilde{\rho} J_\eta \neq f(\hat{x}^3)$	$\Phi = \Phi_{sfc} - \int_{\eta_{sfc}}^{\eta} \frac{\tilde{p}^*}{\tilde{\rho} \eta_{sfc}} d\eta'$
	non-hydrostatic		$J_\eta = \frac{\pi^*}{\rho g \eta_{sfc}}$ $\rho J_\eta \neq f(\hat{x}^3)$	$\Phi = \Phi_{sfc} - \int_{\eta_{sfc}}^{\eta} \frac{\pi^*}{\rho \eta_{sfc}} d\eta'$
step-mountain ETA $(\eta_{\sigma_{\tilde{p}}})$ with $\sigma_{\tilde{p}}$, $\eta_{\sigma_{\tilde{p}}} = \sigma_{\tilde{p}} \eta_{sfc}$	non-hydrostatic	P(5-9) or, P(5-9') with Eq.(5-10) for perturbation component when $\dot{\eta}_{\sigma_{\tilde{p}}}$, $\tilde{\rho}$ provided	$J_\eta = \frac{\tilde{p}^*}{\tilde{\rho} g \eta_{sfc}}$	$\Phi = \Phi_{sfc} - \int_{\eta_{sfc}}^{\eta} \frac{\tilde{p}^*}{\tilde{\rho} \eta_{sfc}} d\eta'$

5.3 Coupling of Meteorology and Air Quality

Characteristics of air quality model simulations are heavily dependent on the quality of the meteorological data. Meteorological data for air quality can be provided either by diagnostic models, which analyze observations at surface sites and upper air soundings, or by dynamic models with or without four-dimensional data assimilation (FDDA). Readers are referred to Seaman (1999) for a state-of-science review on this topic. In the next section a dynamic modeling with FDDA approach, which is used in the Models-3 CMAQ system, is described.

5.3.1 Meteorological Data for Air Quality Modeling

Meteorological simulations are applied to drive a CTM for solving atmospheric diffusion equations for trace species. For regional scale simulations, whose problem size is continental scale or somewhat smaller, hydrostatic meteorological models have been used, usually with FDDA. For small scale simulations where topographic effects are important, nonhydrostatic or compressible atmospheric models are used. These differences in the assumptions used for atmospheric characterization affect air quality simulations greatly.

Meteorological data can be supplied by running dynamic models prognostically, or with the archived reanalysis data routinely available as a part of numerical weather forecasting for air quality simulations (Schulze and Turner, 1998). Currently, GCIP (GEWAX Continental-scale International Project) provides an archive of the Eta model reanalysis of surface and upper air fields at 48 km resolution (Leese, 1993; Kalany et al., 1996). Based on the success of GCIP, the National Center for Environmental Prediction (NCEP), NOAA, is planning to archive regional reanalysis at a higher resolution. Similarly, the Mesoscale Analysis and Prediction System/Rapid Update Cycle (MAPS/RUC) of the Forecast Systems Laboratory (FSL), NOAA, produces accurate and timely analyses and short-term forecasts at 40-60 km resolutions (Benjamin et al., 1995, 1998). The output data are archived at 1-3 hour intervals on 25-34 levels. These alternative data sources are promising because of the wealth of observation data used for the reanalysis and the availability of long-term meteorological characterization data suitable for seasonal or annual assessment studies.

5.3.2 Off-line and On-line Modeling Paradigms

Air quality models are run many times to understand the effects of emissions control strategies on the pollutant concentrations using the same meteorological data. A non-coupled prognostic model with FDDA can provide adequate meteorological data needed for such operational use. This is the so-called off-line mode air quality simulation. However, a successful air quality simulation requires that the key parameters in meteorological data be consistent. For example, to ensure the mass conservation of trace species, the density and velocity component should satisfy the continuity equation accurately. Details of this issue will be discussed below.

If air quality is solved as a part of the meteorology modeling, this data consistency problem would be much less apparent. Dynamic and thermodynamic descriptions of operational

meteorological models should be self-consistent, and necessary meteorological parameters are readily available at the finite time steps needed for the air quality process modules during the numerical integration. The ultimate goal within atmospheric community is the development of a fully integrated meteorological-chemical model (Seaman, 1995). This is the so-called on-line mode air quality simulation. There have been a few successful examples of integrating meteorology and atmospheric chemistry algorithms into a single computer program (e.g., Vogel et al., 1995). For certain research purposes, such as studying two-way interactions of radiation processes, the on-line modeling approach is needed. However, the conventional on-line modeling approach, where chemistry-transport code is imbedded in one system, exhibits many operational difficulties. For example, in addition to tremendously increasing the computer resource requirements, differences in model dynamics and code structures hinder development and maintenance of a fully coupled meteorological/chemical/emissions modeling system for use in routine air quality management.

Figure 5-2 shows structures of the on-line and off-line air quality modeling systems, respectively, commonly used at present time. Table 5-4 compares a few characteristics of on-line and off-line modeling paradigms. Each method has associated pros and cons. Therefore, in the future versions of the Models-3 CMAQ system, we intend to realize both on-line and off-line modes of operations through the use of an advanced input/output (I/O) applications programming interface (API) (Coats, 1996). Figure 5-3 provides a schematic diagram of the implementation idea. A proof-of-concept research effort using MM5 and a prototype version of CMAQ is underway (Xiu et al., 1998). However, to accomplish the goals of multiscale on-line/off-line modeling with one system, a full adaptation of the one-atmosphere concept is needed.

Development of the fully coupled chemistry-transport model to a meteorological modeling system requires a fundamental rethinking of the atmospheric modeling approach in general. Some of the suggested requirements for a next generation mesoscale meteorological model that can be used as a host of the on-line/off-line modeling paradigms are:

- **Scaleable dynamics and thermodynamics:** Use fully compressible form of governing set of equations and a flexible coordinate system that can deal with multiscale dynamics.

- **Unified governing set of equations:** Not only the weather forecasting, dynamics and thermodynamics research but also the air quality studies should rely on the same general governing set of equations describing the atmosphere.

- **Cell-based mass conservation:** As opposed to the simple conservation of domain total mass, cell-based conservation of the scalar (conserving) quantities is needed. Use of proper state variables, such as density and entropy, instead of pressure and temperature, and representation of governing equations in the conservation form rather than in the advective form are recommended.

- **State-of-the-art data assimilation method:** Not only the surface measurements and upper air soundings, but also other observation data obtained through the remote sensing and other in situ means must be included for the data assimilation.

- **Multiscale physics descriptions:** It has been known that certain parameterizations of physical processes, including clouds, used in present weather forecasting models are scale dependent. General parameterization schemes capable of dealing with a wide spectrum of spatial and temporal scales are needed.

The Weather Research & Forecasting (WRF) Modeling System (Dudhia et al., 1998), which is under development by scientists at NCAR and NOAA, could meet most of the above requirements. Therefore, the WRF modeling system has the potential to be the future meteorological model of the Models–3 CMAQ system to provide the multiscale on-line/off-line air quality modeling capability simultaneously.

Table 5-4. Comparison of On-line and Off-line Modeling Paradigms

	Off-line Modeling	**On-line Modeling**
Dynamic Consistency	• Need sophisticated interface processors • Need careful treatment of meteorology data in AQM	• Easier to accomplish, but must have proper governing equations. • Meteorology data available as computed
Process Interactions	• No two-way interactions between meteorology and air quality	• Two-way interaction • Small error in meteorological data will cause large problem in air quality simulation (positive feedback problem).
System Characteristics	• Systems maintained at different institutions • Modular at system level. Different algorithms can be mixed and tested • Large and diverse user base • Community Involvement	• Proprietary ownership • Expensive in terms of computer resource need (memory and CPU) • Unnecessary repeat of computations for control strategy study • Low flexibility • Limited user base • Legacy complex code, which hinders new development
Application Characteristics	• Easy to test new science concept • Efficient for emissions control study • Good for independent air quality process study	• Difficult to isolate individual effects • Excellent for studying feedback of met. and air quality

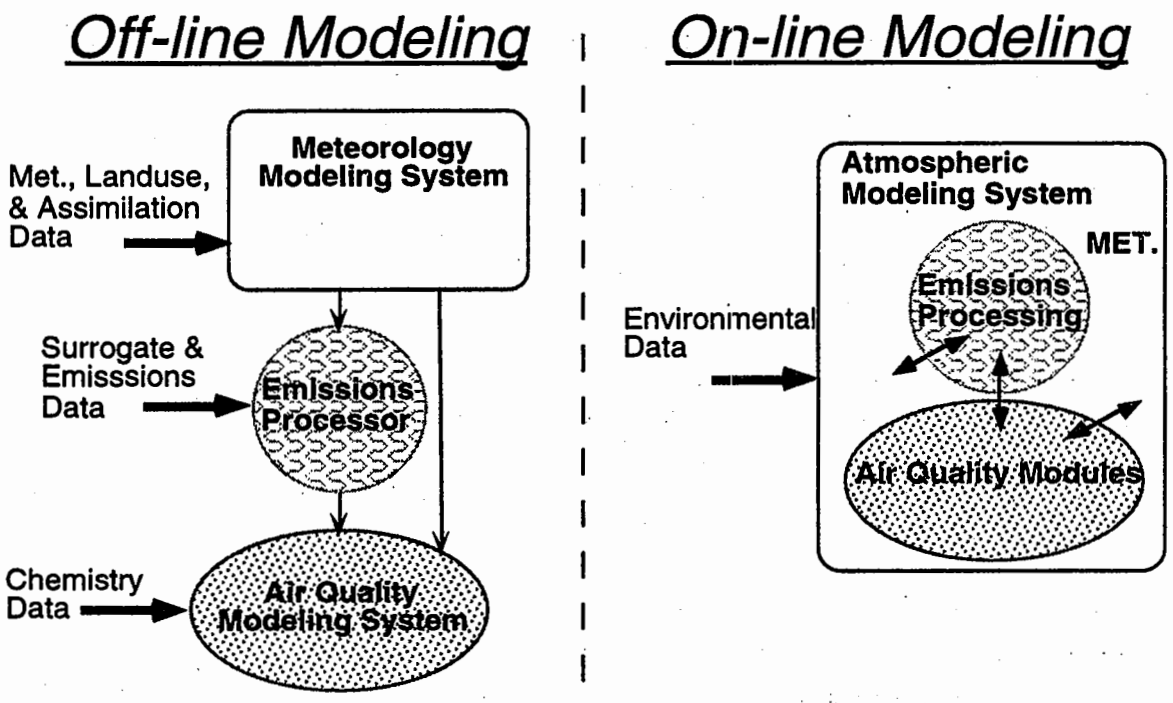

Figure 5-2. Current On-line and Off-line Air Quality Modeling Paradigms

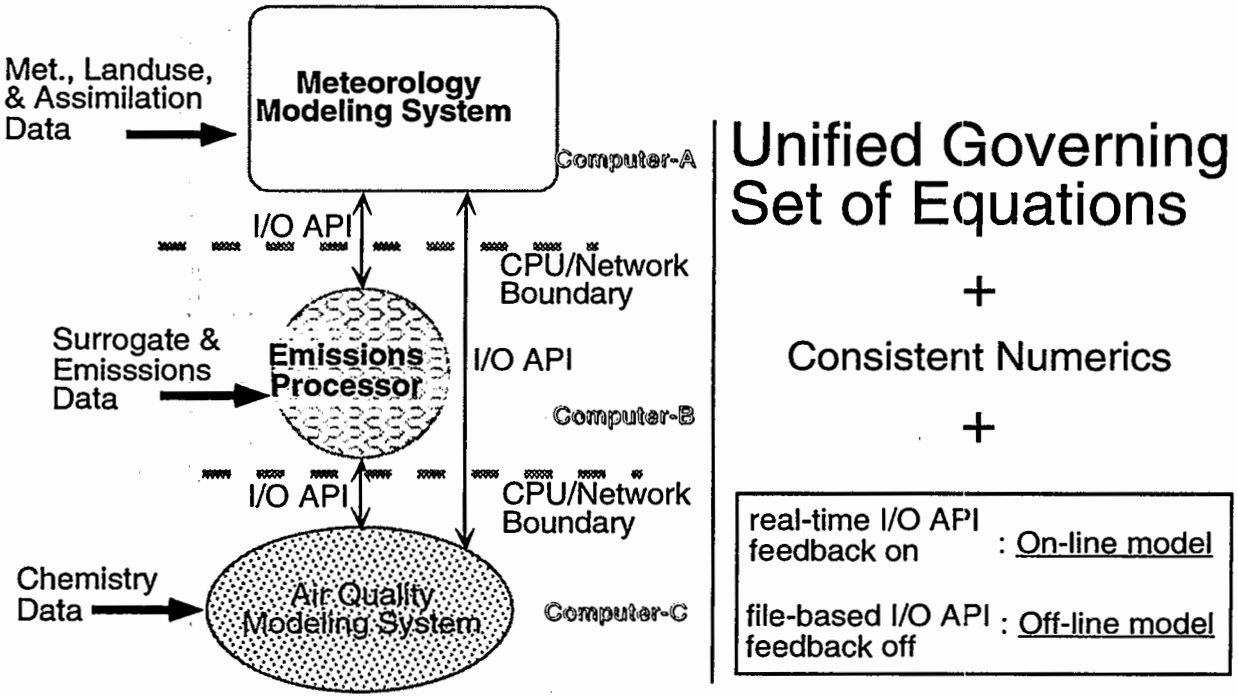

Figure 5-3. Proposed One-atmosphere Air Quality Modeling Paradigms. Double arrowhead lines represent possibility of two-way coupling. The coupling of independent modeling components is accomplished through the I/O API linking the cooperating executables.

5.4 Mass Conservation

For air quality simulations, mass conservation is the most important physical constraint. This is because it is unrealistic to have injection of primary pollutant mass through any other means than a real source emission process, and also because the little perturbations in the mass of both primary and secondary pollutants will jeopardize the correct simulation of reactions among trace species. Therefore, conserving mass of a passive primary trace species is a necessary property of an air quality model.

5.4.1 Mass Consistency in Meteorological Data

The main objective of many meteorological models has been to predict synoptic or mesoscale weather phenomena. Therefore, major design considerations are focused on such issues important for energy conservation, resolving a spectrum of different wavelengths, and energy cascade under nonlinear wave-wave interactions. Conservation of mass is not usually emphasized as the other constraints listed. Also, the predictive quantities are generally thermodynamic parameters, such as temperature and pressure. The conservation equation for air density is rarely solved directly in meteorological models because of little operational use of air density for weather forecasting and no direct measurements to compare. Usually it is estimated from the equation for the state of ideal gas or from a hydrostatic relation when hydrostatic assumptions are made. Even the predictive equations for the moisture variables are often written

in an advective form rather than a continuity equation form. On the other hand, air quality simulation relies mostly on the continuity equation. The success of a simulation is heavily dependent on the consistency of density and wind data (i.e., how well they satisfy the continuity equation).

The mass inconsistency in density and wind fields from a meteorological model is most likely caused by one or more of the following reasons:

1. Many meteorological models do not use the proposed ideal set of governing equations. A continuity equation for air is not used as one of the prognostic equations and air density is usually a diagnostic parameter in meteorological models.

2. The prognostic equation for temperature is often used to represent thermodynamics of the atmosphere. It is well known that temperature is not a good conserving parameter.

3. Removal of hydrometeors due to condensation or sublimation may subtract and add mass and heat to the moist atmosphere making the system nonadiabatic (thermodynamically irreversible) and not mass-conserving.

4. Numerical schemes used in meteorological models are designed to conserve energy, entropy, rather than the mass of air.

5. The FDDA and overall assimilation process, including the effects of Newtonian forcing terms in the momentum and temperature equations, may cause inadvertent modification of the energy balance and subsequent perturbation of air density resulting in mass conservation problems.

6. Heat, moisture and momentum flux exchanges at the surface-atmosphere interface may affect the air density distribution. Usually this effect is not significant as it is often neglected with the Boussinesq approximation.

7. Flux exchanges at the nesting boundaries for nested runs affect mass balance.

8. Energy and mass balance characteristics of cloud modules used influence air and moisture density fields.

9. Data output time steps are too large to capture the dynamic variations in the meteorological models. If temporally averaged data are provided from the meteorology model this problem can be minimized (Scamarock, 1998).

5.4.2 Techniques for Mass Conservation in Air Quality Models

As presented in Byun (1999b), species mixing ratios (c_i / ρ) is a useful conserved quantity for photochemical Eulerian air quality modeling, in particular. In limited area atmospheric modeling like an urban or a regional scale simulation, the total air mass in the simulation domain is subject

to the inflow conditions determined by large synoptic scale weather systems. In this situation, the conservation of pollutant mass in the modeling domain can be difficult unless the density and wind fields are perfectly mass consistent. When the mass inconsistency in the meteorological fields is expected, the conservation equation for mixing ratio must be used as a necessary condition to ensure exact conservation of pollutant mass. This is accomplished by replacing the right-hand-side term of Equation 5-11 with $Q_{c_i} = c_i \frac{Q_\rho}{\rho}$. Then, the conservation equation for pollutant species is rewritten as:

$$\frac{\partial(c_i J_s)}{\partial t} + m^2 \nabla_s \bullet \left(\frac{c_i J_s \hat{\mathbf{V}}_s}{m^2} \right) + \frac{\partial(c_i J_s \hat{v}^3)}{\partial s} = c_i J_s \frac{Q_\rho}{\rho} \tag{5-24}$$

This adjustment alone is not sufficient to conserve pollutant mass when the density error term is not small. Equation 5-24 shows that the correction term has the same form as a first-order chemical reaction whose reaction rate is determined by the normalized air density error term. Table 7-5 in Chapter 7 in this document summarizes correction methods discussed in Byun (1999b). Among these, the method based on the two-step procedure (i.e., solving the *lhs* of Equation 5-24 first followed by the mass correction step solving for *rhs*) is expected to be the most accurate:

$$(c_i J_s)^{cor} = \frac{(c_i J_s)^T}{(\rho J_s)^T} (\rho J_s)^{\text{int}}, \tag{5-25}$$

where superscripts *cor*, *int*, and *T* represent corrected, transported (advected), and interpolated quantities, respectively. It should be noted that J_s in Equation 5-25 must not be canceled out even for a coordinate with time independent J_s because the spatial variation of the Jacobian must be taken into account for the numerical advection. In the event the total air mass in the computational domain fluctuates, this correction procedure would affect air quality predictions. In general, the air quality prediction can be as good as the density prediction of the meteorological model. However, considering the nonlinear interactions of trace species in the chemical production/loss calculations, one could expect serious effects on air quality simulations when the quality of meteorology data is in doubt.

Byun (1999b) also provides an alternative method to deal with the mass inconsistency in meteorological data through the modification of wind field, while keeping the density field intact, before solving the species conservation equation. Assuming a modified wind field exists that eliminates the source term in the continuity equation for air, the relationship between the original and modified wind components is given as:

$$\hat{\mathbf{V}}_s^M = \hat{\mathbf{V}}_s + \frac{1}{2\alpha_1^2} \nabla_s \lambda \tag{5-26a}$$

$$\hat{v}^{3M} = \hat{v}^3 + \frac{1}{2\alpha_3^2}\frac{\partial\lambda}{\partial s} \qquad (5\text{-}26b)$$

where λ is the Lagrangian multiplier to be determined and α_1 and α_3 are the weights for the horizontal and vertical wind components. λ must satisfy the Poisson equation

$$m^2\nabla_s \bullet \left[\frac{\rho J_s}{2\alpha_1^2 m^2}\nabla_s\lambda\right] + \frac{\partial}{\partial s}[\frac{\rho J_s}{2\alpha_3^2}\frac{\partial\lambda}{\partial s}] = J_s Q_\rho, \qquad (5\text{-}27)$$

with the associated boundary conditions:

$\lambda = 0$ for flow-through boundaries; and

$\partial\lambda / \partial s = 0$ for impenetrable boundaries (i.e., at the topographic surface).

The modified wind components are subject to the same top and bottom boundary conditions imposed by the given coordinate system and dynamic assumptions.

The main difference in the two proposed correction methods, correction after advection versus correction of wind fields before advection, is practically philosophical. Should we process a CTM using meteorological data as supplied, then correct possible errors in the species concentrations, or should we modify the velocity field to be mass consistent before the computation of trace gas concentrations in the CTM? The answer to this question lies in whether the air quality modeling need is satisfied with simple mixing ratio conservation with the adjustment process or not. In case the source-receptor relation is important, it is preferable to maintain the linearity of transport process using the mass-consistent wind components, which have been modified at the expense of truthfulness of meteorological fields. In practice, a combination of both methods is needed. The mass consistency error in the meteorological data must be corrected before air quality simulations with the wind-field adjustment method and the mixing ratio correction method Equation 5-25 should be applied to compensate the numerical differences in advection processes between meteorological and air quality models.

5.4.3 Temporal Interpolation of Meteorological Data

Byun (1999b) discusses a mass-conservative temporal interpolation method to complement the mass inconsistency correction. Temporal interpolations of density and velocity data are often required in a CTM because the meteorological model output has a coarser temporal resolution than the transport time step (which is usually the synchronization time step for a CTM using a fractional time-step method).

The Jacobian and density at a time $t_\alpha = (1-\alpha)t_n + \alpha t_{n+1}$ between the two consecutive output time steps, t_n and t_{n+1}, are interpolated with linearity assumed:

$$(J_s)_\alpha = (1-\alpha)(J_s)_n + \alpha(J_s)_{n+1} \qquad (5\text{-}28a)$$

$$(\rho J_s)_\alpha = (1-\alpha)(\rho J_s)_n + \alpha(\rho J_s)_{n+1} \tag{5-28b}$$

where $0 \le \alpha \le 1$. It is obvious that the functional form of the Jacobian (which depends on a vertical coordinate) changes the characteristic of density interpolation. The premise used here is that the Jacobian is a fundamental quantity that determines the coordinate system. When the Jacobian is interpolated to define the vertical layers through linear interpolation, all other components involved in the mass conservation equation need to be interpolated accordingly. Wind components multiplied with the Jacobian-weighted density are interpolated linearly:

$$(\rho J_s \hat{\mathbf{V}}_s)_\alpha = (1-\alpha)(\rho J_s \hat{\mathbf{V}}_s)_n + \alpha(\rho J_s \hat{\mathbf{V}}_s)_{n+1} \tag{5-29a}$$

$$(\rho J_s \hat{v}^3)_\alpha = (1-\alpha)(\rho J_s \hat{v}^3)_n + \alpha(\rho J_s \hat{v}^3)_{n+1} \tag{5-29b}$$

and interpolated wind components are derived with:

$$(\hat{\mathbf{V}}_s)_\alpha = \frac{(\rho J_s \hat{\mathbf{V}}_s)_\alpha}{(\rho J_s)_\alpha} \tag{5-30a}$$

$$(\hat{v}^3)_\alpha = \frac{(\rho J_s \hat{v}^3)_\alpha}{(\rho J_s)_\alpha} \tag{5-30b}$$

However, the proposed scheme, Equation 5-28b, has a problem in such cases where the finite difference value of (ρJ_s) cannot approximate the linear interpolation of the time rate change of the quantity, $\frac{\partial(\rho J_s)}{\partial t}$, adequately. Usually, this tendency term is not available with the meteorological data. However, when the tendency is available or can be estimated with the diagnostic relations for certain meteorological coordinate systems, a different interpolation rule must be sought. Because the tendency term, not (ρJ_s) itself, is a component of the continuity equation, linear interpolation of the tendency may be more appropriate. Then, (ρJ_s) at the interpolation time step must be estimated in such a way that satisfies the continuity as well as the tendency term (Byun 1999b).

5.5 Conclusion

In this chapter I attempted to bridge the information gap between dynamic meteorologists and air quality modelers and to promote the proper use of meteorological information in air quality modeling studies. It highlights the importance of dynamic consistency in meteorological and air quality modeling systems. The effects of the common assumptions used for the atmospheric study on the mass conservation for trace species have been reviewed. Although meteorological data provided by operational meteorological models are usually self-consistent, air quality modelers need to evaluate the data for exact consistency before they can be used in air quality simulation. Minor adjustment of the meteorological data may be needed to assure mass conservation of trace gas species in CTMs. Also, characteristics of vertical coordinates have

been discussed. Certain coordinates provide diagnostic relations that can be used to maintain mass consistency in meteorological fields. When meteorological data are needed at sub-output time steps within CTM, the interpolation of the data should be done in such a way that the mass conservation and consistency in the thermodynamic variables are not compromised.

In addition, the on-line and off-line modeling concepts are discussed to provide design guidance for fully integrated meteorological-chemical models. To realize the noble goal of implementing the one-atmosphere modeling system, both the multi-pollutant chemistry and multiscale physics capability in meteorology are needed. The following are the features that make the CMAQ air quality model a suitable key component of an one-atmosphere modeling system:

- Flexible chemistry representations through a mechanism reader;
- Comprehensive list of atmospheric processes that are implemented;
- Modular coding structure and versatile data handling method;
- Capability to handle multiscale dynamics and thermodynamics;
- Fully compressible governing set of equations in generalized coordinates; and
- Robust mixing ratio conservation scheme, even with mass inconsistent meteorology data.

At present, we are encouraged by the efforts of the WRF meteorology model development groups that focus on issues such as choice of coordinates, grid staggering method, state variables in the governing equations (e.g., fully compressible), conservation properties (mass and energy) both in the model equations and numerics, modularity of code, data communication methods, and coding language. This entails continuous exchange of ideas between the Models-3 CMAQ and WRF modeling groups.

To achieve the true one-atmosphere modeling system, we must address multi-pollutant and multiscale processes that are typically broader than any one group (or institution) has expertise to address. The need is well summarized in Dennis (1998):

> Considering additional needs for emerging environmental problems such as coastal eutrophication and ecological damage issues related with cross-media purview, encompassing the one-atmosphere scope is needed. This means we have to work with a more complete one-atmosphere description to facilitate interactions within it as efficiently as broadly as possible. One potential answer is to foster a community modeling perspective and model system framework that is supported and used by a critical fraction of the scientific community.

5.6 References

Arakawa, A., C. R. Mechso, and C. S. Konor, 1992: An isentropic vertical coordinate model: Design and application to atmospheric frontogenesis studies. *Meteor. Atmos. Phys.* **50**, 31-45.

Arya, S. Pal, 1988: *Introduction to Micrometeorology.* Academic Press, Inc., 307 pp.

Batchelor, G. K., 1967: *An Introduction to Fluid Mechanics.* Cambridge University Press, 615 pp.

Benjamin, S.G., D. Kim, and T.W. Schlatter, 1995: The Rapid Update Cycle: A new mesoscale assimilation system in hybrid-theta-sigma coordinates at the National Meteorological Center. *Second International Symposium on Assimilation of Observations in Meteorology and Oceanography*, Tokyo, Japan, 13-17 March, 337-342.

Benjamin, S.G., J.M. Brown, K.J. Brunge, B.E. Schwarts, T.G. Smirnova, and T.L. Smith, 1998: The operational RUC-2. *16th Conference on Weather Analysis and Forecasting*, Phoenix, AZ, Amer. Meteor. Soc., 249-252.

Bishop, R. L. and S. I. Goldberg, 1968: Tensor Analysis on Manifolds. Dover Publications, Inc. New York.

Byun, D. W., 1999a: Dynamically consistent formulations in meteorological and air quality models for multiscale atmospheric applications: I. Governing equations in a generalized coordinate system. *J. Atmos. Sci.*, (in print)

Byun, D. W., 1999b: Dynamically consistent formulations in meteorological and air quality models for multiscale atmospheric applications: II. Mass conservation issues. *J. Atmos. Sci.*, (in print)

Byun D. W. , A.. Hanna, C. J. Coats, and D. Hwang, 1995a: Models-3 Air Quality Model Prototype Science and Computational Concept Development. *Trans. TR-24 Regional Photochemical Measurement and Modeling Studies*, San Diego, CA, of Air & Waste Management Association, 197-212.

Coats, C. J., cited 1996: The EDSS/Models-3 I/O Applications Programming Interface. MCNC Environmental Programs, Research Triangle Park, NC. [Available on-line from http://www.iceis.mcnc.org/EDSS/ioapi/H.AA.html.]

Defrise, P., 1964: Tensor Calculus in Atmospheric Mechanics. *Advances in Geophysics* **10**, 261-315.

DeMaria, M., 1995: Evaluation of a hydrostatic, height-coordinate formulation of the primitive equations for atmospheric modeling. *Mon. Wea. Rev.*, **123**, 3576-3589.

Dennis, R.L., 1998: The environmental protection agency's third generation air quality modeling system: an overall perspective. Proceedings of the American Meteorological Society 78th Annual Meeting, Phoenix, AZ, Jan. 11-16, 1998. 255-258.

Dudhia, J., D. Gill, J. Klemp, and W. Skamarock, 1998: WRF: Cuurrent status of model development and plans for the future. Preprints of the Eighth PSU/NCAR Mesoscale Model User's Workshop. Boulder, Colorado, 15-16 June, 1998.

Dutton, J. A., 1976: *The Ceaseless Wind, an Introduction to the Theory of Atmospheric Motion.* McGraw-Hill, 579 pp.

Dutton, J. A., and G. H. Fichtl, 1969: Approximate equations of motion for gases and liquids. *J. Atmos. Sci.*, **26**, 241-254.

Gal-Chen, T., and R. C. J. Somerville, 1975: On the use of coordinate transformations for the solution of the Navier-Stokes equations. *J. Comput. Phys.*, **17**, 209-228.

Kalany, E., and Co-authors, 1996: The NCEP/NCAR 40-year Reanalysis Project. *Bull. Amer. Meteor. Soc.*, **77**, 437-471.

Leese, J. A., 1993: Implementation Plan for the GEWEX Continental-Scale International Project (GCIP). Int. GEWEX Project Office #6, 148 pp. [Available from IGPO, 1100 Wayne Ave., Suite 1225, Silver Springs, MD 20910].

Lipps, F. B., and R. S. Hemler, 1982: A scale analysis of deep moist convection and some related numerical calculations. *J. Atmos. Sci.*, **39**, 2192-2210.

Nance, L. B., and D. R. Durran, 1994: A comparison of the accuracy of three anelastic systems and the pseudo-incompressible system. *J. Atmos. Sci.*, **51**, 3549-3565.

Ogura, Y., and N. W. Phillips, 1962: Scale analysis of deep and shallow convection in the atmosphere. *J. Atmos. Sci.*, **19**, 173-179.

Ooyama, K. V., 1990: A thermodynamic foundation for modeling the moist atmosphere. *J. Atmos. Sci.*, **47**, 2580-2593.

Pielke, R. A., 1984: *Mesoscale Meteorological Modeling*. Academic Press, 612 pp.

Scamarock, W. 1998: Personal communication.

Schulze, R. H., and D. B. Turner, 1998: Potential use of NOAA-archived meteorological observations to improve air dispersion model performance. *EM*, March 1998, 12-21.

Seaman, N. L, 1995: Status of meteorological pre-processors for air-quality modeling. *International Conf. on Particulate Matter*, Pittsburgh, PA, Air & Waste Management Association, 639-650.

Seaman, N.L., 1999: Meteorological modeling for air-quality assessments. (Submitted to *Atmos. Environ.*, 32, 87pp.)

Stull, R. B., 1988: *An Introduction to Boundary Layer Meteorology*. Kluwer Academic Publishers. 666 pp.

Thunis, P. and R. Bornstein, 1996: Hierarchy of mesoscale flow assumptions and equations. *J. Atmos. Sci.*, **53**, 380-397.

Vogel, B., F. Fiedler, and H. Vogel, 1995: Influence of topography and biogenic volatile organic compounds emission in the state of Baden-Wurttemberg on ozone concentrations during episodes of high air temperatures. *J. Geophys. Res.*, **100**, 22,907-22, 928.

Xiu, A., R. Mathur, C. Coats, and K. Alapaty, 1998: On the development of an air quality modeling system with integrated meteorology, chemistry, and emissions. *Proceedings of the International Symposium on Measurement of Toxic and Related Air Pollutants*, Research Triangle Park, North Carolina, 1-3 September, 1998. 144-152.

This chapter is taken from *Science Algorithms of the EPA Models-3 Community Multiscale Air Quality (CMAQ) Modeling System*, edited by D. W. Byun and J. K. S. Ching, 1999.

Appendix 5A. Tensor Primer and Derivation of the Continuity Equation in a Generalized Curvilinear Coordinate System

The Appendix 5A summarizes essential information needed for understanding the governing equations represented in tensor form. It includes tensor primer and derivation of the continuity equation in a generalized coordinate system. Readers are referred to classic references such as Dutton (1976), Defrise (1964), and Pielke (1984) for the details.

5A.1 Tensor Analysis in a Curvilinear Coordinate System

Cartesian coordinates are those curvilinear systems in which the positions of fluid elements are determined by their distance from intersecting planes. Although the Cartesian coordinates with orthogonal intersecting planes are specifically called rectangular, the adjective rectangular is often dropped. To represent formulations governing atmospheric phenomena in a coordinate system other than a rectangular Cartesian one, a tensor representation is often used. This generally involves determination of the unit vectors in the new system, determination of the components of a tensor with respect to theses unit vectors, and determination of the differential derivatives (e.g., divergence, curl, and gradient) of a tensor. All these quantities depend explicitly on the form of the new coordinate system and it is always convenient to express these quantities in a rectangular Cartesian coordinate system for comparison purposes.

In atmospheric modeling one is frequently led to adopt a curvilinear coordinate system other than the Cartesian coordinates depending on the problem under consideration. A general curvilinear coordinate system can be defined relative to a Cartesian system $\mathbf{x} = (x^1, x^2, x^3)$ represented by three families of curved surfaces

$$\hat{x}^i = \psi_i(x^1, x^2, x^3, t),\ i = 1,2,3 \qquad \text{(5A-1)}$$

Here, the symbols with carat (^) are used to denote a transformed curvilinear system. In vector form, it is given as:

$$\hat{\mathbf{x}} = \boldsymbol{\psi}(\mathbf{x}, t). \qquad \text{(5A-2)}$$

When the curvilinear system ψ is at rest relative to the rectangular Cartesian system, i.e., independent of time, $\hat{x}^i = \psi_i(x^1, x^2, x^3)$, then the system is called a Euclidean system. Here we assume that components of vector $\hat{\mathbf{x}}$, $(\hat{x}^1, \hat{x}^2, \hat{x}^3)$, are three independent, single-valued, and differentiable scalar point functions such that to every point of some region $\hat{\Re}$ of three-dimensional Euclidean space, there is a corresponding unique triple of values (x^1, x^2, x^3) in the Cartesian space $\Re$. In other words, the function ψ prescribes one and only one value of x and is such that the three coordinates are independent of each other. Also, we assume continuity of the function ψ. Then the new coordinates $\hat{\mathbf{x}}$ are called curvilinear and the surfaces $\hat{x}^1 = \psi_1 =$ constant, $\hat{x}^2 = \psi_2 =$ constant, $\hat{x}^3 = \psi_3 =$ constant are called coordinate surfaces. The curvilinear coordinates $(\hat{x}^1, \hat{x}^2, \hat{x}^3)$ should be independent, single-valued, and differentiable. As shown in

Figure 5A-1, the vector $\overrightarrow{OP}$ pointing a parcel of air enclosed by the boundary $\partial\Omega$ can be represented either in Cartesian or Euclidean curvilinear coordinate systems.

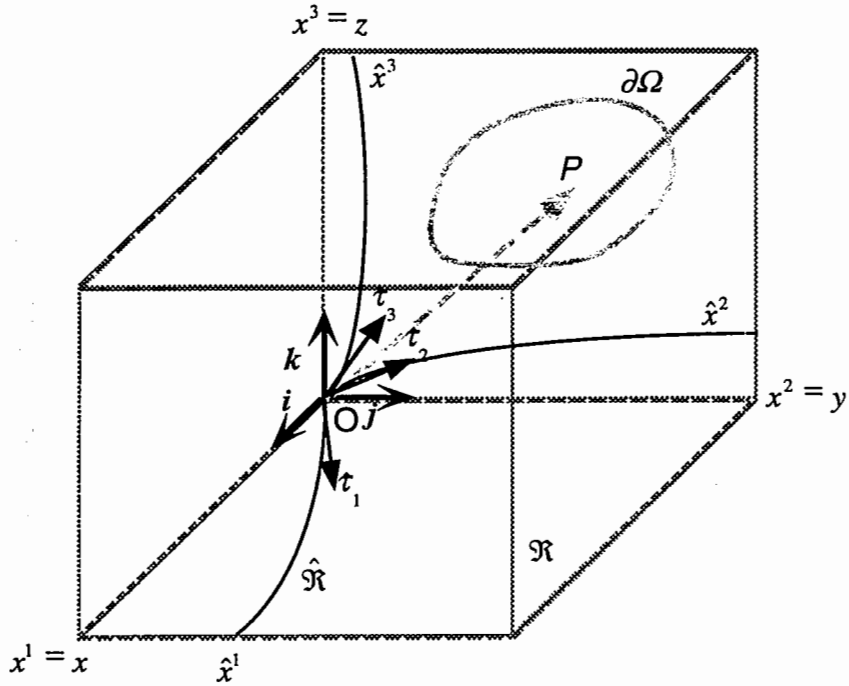

Figure 5A-1. Coordinates of the Cartesian and Curvilinear Coordinates. $\Re$ and $\hat{\Re}$ represent Cartesian and Euclidean spaces, respectively.

Note that the transformation involves with not only the spatial variables but also time as an independent variable. We need a tensor calculus in the four variables of space-time with regard to the coordinate transformations. Defrise (1964) used the term 'world tensor' to distinguish it from the time independent Euclidean tensor.

5A.2 Basis Vectors

In a rectangular coordinate system, directions of the basis vectors are constant in space. However, in a general curvilinear coordinates, directions of the basis vectors will vary from point to point and no one set of directions can be regarded as more natural than any other for the directions of base vectors to define the local base vectors. Usually, an upper index denotes contravariant, and a lower index denotes covariant tensors, respectively.

With the coordinates defined by Equation 5A-2, the chain rule provides the two expansions:

$$d\mathbf{x} = \frac{\partial \mathbf{x}}{\partial \hat{x}^j} d\hat{x}^j \qquad \text{(5A-3)}$$

$$d\hat{x}^i = \frac{\partial \hat{x}^i}{\partial x^j} dx^j = (\nabla \hat{x}^i) \bullet d\mathbf{x} \tag{5A-4}$$

Here, the Einstein summation convention (i.e., the repeated indices on two quantities that are multiplied by each other are summed over) has been implied. The symbol (•) represents the inner product. An inner product of two vectors yields a scalar that is invariant of the coordinate system. An inner product of two tensors results in contraction of the rank in the resulting tensor.

From Equations 5A-3 and 5A-4, we can form two distinct sets of basis vectors. One is the tangential vectors:

$$\hat{\boldsymbol{\tau}}_i = \frac{\partial \mathbf{x}}{\partial \hat{x}^j} \tag{5A-5}$$

that reveals the variation of the position vector as it traces out a curve in which $\hat{x}^j$ varies and the other two coordinates are constant. Hence $\hat{\boldsymbol{\tau}}_i$ is tangent to the curve along which only $\hat{x}^j$ varies. The other set of basis vectors is the normal vectors of the surfaces where $\hat{x}^i$ = constant:

$$\hat{\boldsymbol{\eta}}^i = \nabla \hat{x}^i \tag{5A-6}$$

While there could be many choices, the tangential ($\hat{\boldsymbol{\tau}}_i$) and normal ($\hat{\boldsymbol{\eta}}^i$) vectors are considered as a natural choice for the local basis vectors for the curvilinear coordinate system. Using Equations 5A-5 and 5A-6, one can show that:

$$\hat{\tau}_i \otimes \hat{\eta}^j = \delta_i^j = \begin{cases} 1 & i = j \\ 0 & i \neq j \end{cases} \tag{5A-7}$$

where δ_i^j is the Kronecker delta and the symbol $\otimes$ represents the outer product. Outer product of two tensors with rank r_1 and r_2 yields a tensor with rank (r_1+r_2).

A curvilinear system is not orthogonal when not all the off-diagonal components of $\hat{\eta}^i \otimes \hat{\eta}^j$ and $\hat{\tau}_i \otimes \hat{\tau}_j$ vanish. The orthogonal curvilinear coordinate system is often used for interesting engineering problems that can be described with simple geometric orthogonal coordinates, such as spherical, cylindrical coordinate systems. Usually, meteorological coordinates are not orthogonal and therefore, the vector calculus specific for the orthogonal curvilinear coordinates must not be used.

5A.3 Distance and Metric Tensor in a Curvilinear Coordinate System

The differential element of distance *ds* can be expressed in terms of the curvilinear coordinates as:

$$(ds)^2 = dx_i dx^i = \frac{\partial x^i}{\partial \hat{x}^j} d\hat{x}^j \frac{\partial x^i}{\partial \hat{x}^k} d\hat{x}^k = \frac{\partial x^i}{\partial \hat{x}^j} \frac{\partial x^i}{\partial \hat{x}^k} d\hat{x}^j d\hat{x}^k = \hat{\gamma}_{jk} d\hat{x}^j d\hat{x}^k \tag{5A-8}$$

$$\hat{\gamma}_{jk} = \frac{\partial x^i}{\partial \hat{x}^j}\frac{\partial x^l}{\partial \hat{x}^k} = \hat{\boldsymbol{\tau}}_j \otimes \hat{\boldsymbol{\tau}}_k \tag{5A-9}$$

Because of its obvious role in the measurement of distance, the quantity $\hat{\gamma}^{ik}$ is called the metric tensor. It is a symmetric tensor. As such, it has an inverse matrix $\hat{\gamma}^{ik}$, which will satisfy following condition:

$$\hat{\gamma}^{ik} = \frac{\partial \hat{x}^i}{\partial x^l}\frac{\partial \hat{x}^k}{\partial x^l} = \hat{\boldsymbol{\eta}}^i \otimes \hat{\boldsymbol{\eta}}^k \tag{5A-10}$$

$$\hat{\gamma}_{ij}\hat{\gamma}^{ik} = \delta_j^k = \begin{cases} 1 & j = k \\ 0 & j \neq k \end{cases} \tag{5A-11}$$

The Levi-Cevita symbol ε used in Equation 5-1 is an antisymmetric tensor defined as

$$\varepsilon^{ijk} = \begin{cases} 0 & \text{if } i = j,\ j = k,\ \text{or } i = k \\ 1 & \text{if } i,j,k \text{ are an even permutation of } 1,2,3 \\ -1 & \text{if } i,j,k \text{ are an odd permutation of } 1,2,3 \end{cases} \tag{5A-12}$$

Using the Levi-Cevita symbol, the cross vector product $\mathbf{A} = \mathbf{B} \times \mathbf{C}$ can be written as $A^l = \varepsilon^{ijk} B_j C_k$.

One of the uses of the metric tensor and its inverse is for converting a covariant tensor to a contravariant tensor, and vice versa. Another important usage of the metric tensor is the estimation of the Jacobian determinant of the transformation, which is defined as:

$$J = \sqrt{\hat{\gamma}} = \sqrt{\det(\hat{\gamma}_{ij})} = \sqrt{[\det(\hat{\gamma}^{ij})]^{-1}} \tag{5A-13}$$

where $J = \left|\{J_x^{\hat{x}}\}\right| = \left|\frac{\partial(x_1, x_2, x_3)}{\partial(\hat{x}_1, \hat{x}_2, \hat{x}_3)}\right|$. Note that the Jacobian matrix and the metric tensor are related as:

$$\hat{\gamma}_{ij} = \{J_x^{\hat{x}}\}^T \{J_x^{\hat{x}}\} \tag{5A-14}$$

A necessary and sufficient condition that $(\hat{x}^1, \hat{x}^2, \hat{x}^3)$ be orthogonal at every point in $\Re$ is that the components of the metric tensor vanish for $i \neq j$.

5A.4 Covariant Tensor and Contravariant Tensor

In this section, the covariant and contravariant tensor concepts are presented using a vector, which is a simple form of a tensor (i.e., a tensor of rank one). A distance in a Euclidean space can be represented in two corresponding sets of tangential basis vectors:

$$ds = d\hat{x}^j \hat{\tau}_j = dx^l \tau_l \tag{5A-15}$$

where

$$\hat{\tau}_j = \frac{\partial x^l}{\partial \hat{x}^j} \tau_l \tag{5A-16}$$

Any vector that transforms similarly to the tangential basis vector $\hat{\boldsymbol{\tau}}_j$ is called as a covariant vector. On the other hand, when a vector transforms like the local normal basis vectors $\hat{\boldsymbol{\eta}}^j$, we call it a contravariant vector:

$$\hat{v}^k = \frac{\partial \hat{x}^k}{\partial x^j} v^j, \tag{5A-17}$$

where v^j is the components of **V** with respect to the normal base vectors.

Since a vector **A** is invariant between coordinate systems, we can express it using either contravariant components (i.e., with the tangential basis vectors) or covariant components (i.e., with the normal basis vectors):

$$\mathbf{A} = A_j \hat{\eta}^j = A^l \hat{\tau}_l \tag{5A-18}$$

Using Equation 5A-7, one can readily find the covariant and contravariant components with:

$$A_j = \mathbf{A} \bullet \hat{\tau}_j \tag{5A-19a}$$

$$A^i = \mathbf{A} \bullet \hat{\eta}^i \tag{5A-19b}$$

5A.5 Derivatives, Total Derivative, and Divergence in Euclidean Coordinate

Covariant derivative of a contravariant vector is defined as:

$$\hat{V}^i_{;k} = \frac{\partial \hat{V}^i}{\partial \hat{x}^k} + \hat{\Gamma}^i_{kj} \hat{V}^j, \quad \hat{\Gamma}^i_{kj} = \frac{\partial \hat{x}^i}{\partial x^l} \frac{\partial^2 x^l}{\partial \hat{x}^k \partial \hat{x}^j}. \tag{5A-20}$$

Similarly, covariant derivative of a covariant vector is defined as:

$$\tilde{A}_{i;k} = \frac{\partial \tilde{A}^i}{\partial \tilde{x}^k} - \tilde{\Gamma}^l_{ki} \tilde{A}^l, \quad \tilde{\Gamma}^l_{ki} = \frac{\partial \tilde{x}^l}{\partial x^r} \frac{\partial^2 x^r}{\partial \tilde{x}^k \partial \tilde{x}^i}. \tag{5A-21}$$

The Christoffel symbol $\hat{\Gamma}^i_{kj}$ is not a tensor but it is an important quantity relating the derivatives in the curvilinear coordinate system with those in the original Cartesian coordinate system. Its relation with the metric tensor is:

$$\hat{\Gamma}^i_{kj} = \frac{1}{2}\hat{\gamma}^{jl}\left(\frac{\partial \gamma_{il}}{\partial \hat{x}^k} + \frac{\partial \gamma_{kl}}{\partial \hat{x}^i} - \frac{\partial \gamma_{ik}}{\partial \hat{x}^l}\right) \tag{5A-22}$$

Divergence of a contravariant vector $\hat{W}$, wind for example, can be expressed as:

$$\hat{W}^i_{;i} = \frac{\partial \hat{W}^i}{\partial \hat{x}^i} + \hat{\Gamma}^i_{ij}\hat{W}^j = \frac{\partial \hat{W}^i}{\partial \hat{x}^i} + \frac{\hat{W}^j}{\sqrt{\hat{\gamma}}}\frac{\partial \sqrt{\hat{\gamma}}}{\partial \hat{x}^j}$$

$$= \frac{1}{\sqrt{\hat{\gamma}}}\{\sqrt{\hat{\gamma}}\frac{\partial \hat{W}^i}{\partial \hat{x}^i} + \hat{W}^j\frac{\partial \sqrt{\hat{\gamma}}}{\partial \hat{x}^j}\} = \frac{1}{\sqrt{\hat{\gamma}}}\frac{\partial(\sqrt{\hat{\gamma}}\hat{W}^i)}{\partial \hat{x}^i} \tag{5A-23}$$

The total derivative of a covariant vector A is represented in a Cartesian coordinate as

$$\frac{d\mathbf{A}}{dt} = \frac{\partial \mathbf{A}}{\partial t} + \mathbf{v} \bullet \nabla \mathbf{A} = \frac{\partial A_i}{\partial t} + \hat{v}^j \frac{\partial A_i}{\partial \hat{x}^j} \tag{5A-24}$$

where $\mathbf{v} \bullet \nabla = v^l \frac{\partial}{\partial x^l} = \hat{v}^j \frac{\partial x^l}{\partial \hat{x}^j}\frac{\partial}{\partial x^l} = \hat{v}^j \frac{\partial}{\partial \hat{x}^j}$ was used. This expression is correct in any holonomic coordinate system where the covariant component A_i, metric tensor, velocity, and x^k all refer to the same system whether or not the coordinate system is time dependent.

5A.6 Continuity Equation in Generalized Curvilinear Coordinate System

Many practical coordinate systems used for atmospheric studies are time dependent. Consider the case when a volume element that confines the fluid moves with the fluid. Then, this is also the velocity of the fluid in the respective coordinate system. A direct conversion from the continuity equation expressed in a Cartesian coordinate system does not work because the divergence term should take into account for the time rate change of volume element as well the same for the time dependent curvilinear coordinates. In this situation, the Lie derivative concept (e.g., Bishop and Goldberg, 1968) becomes appropriate. A Lie derivative is obtained by differentiating a function with respect to the parameters along the moving frame of reference. Following Defrise (1964), one can show that a Lie derivative of a mass volume integral along the moving frame vanishes:

$$\mathcal{L}(\delta M) = 0 \tag{5A-25}$$

where $\delta M = \rho \delta V = \rho\sqrt{\hat{\gamma}}\delta\hat{V}$, $\delta V = \delta x^1 \delta x^2 \delta x^3$, and $\delta\hat{V} = \delta\hat{x}^1\delta\hat{x}^2\delta\hat{x}^3$. Therefore:

$$\delta\hat{V}\mathcal{L}(\rho\sqrt{\hat{\gamma}}) = \delta\hat{V}(\hat{v}^\mu \frac{\partial \rho\sqrt{\hat{\gamma}}}{\partial \hat{x}^\mu} + \rho\sqrt{\hat{\gamma}}\frac{\partial \hat{v}^\mu}{\partial \hat{x}^\mu})$$

$$= \delta\hat{V}\frac{\partial(\rho\sqrt{\hat{\gamma}}\hat{v}^\mu)}{\partial \hat{x}^\mu} = 0 \tag{5A-26}$$

where, index $\mu = 1,4$; $\hat{x}^4 = t$ and $\hat{v}^4 = 1$. Using the same notation convention, the contravariant velocity is defined as for the coordinates that moves with fluid:

$$\hat{v}^{\mu} = \frac{\partial \hat{x}^{\mu}}{\partial x^{\alpha}} v^{\alpha};\ \alpha, \mu = 1,4 \tag{5A-27}$$

Note that one cannot derive the same result by directly replacing the divergence term in the continuity equation for a Cartesian coordinate system because the volume element is dependent on time as well.

Alternatively, one can obtain Equation 5A-26 by a method based on the finite derivative of a volume integral with the application of the Leibnitz rule. This method of derivation helps to visualize the meaning of terms in the equation more clearly than the procedure based on the Lie derivative. Volume integral in a Cartesian coordinates is defined as:

$$F = \iiint_{\partial\Omega} f(x^1, x^2, x^3)\delta V \tag{5A-28}$$

where f is a conservative quantity, such as density or total kinetic energy. Equation 5A-28 can be rewritten in the curvilinear coordinate as:

$$F = \iiint_{\partial\Omega} f(\hat{x}^1, \hat{x}^2, \hat{x}^3)\sqrt{\hat{\gamma}}\delta\hat{V} \tag{5A-29}$$

For example, if f=1:

$$F = \iiint_{\partial\Omega} \delta V = V_{\partial\Omega} = \iiint_{\partial\Omega} \sqrt{\hat{\gamma}}\delta\hat{V} = \sqrt{\hat{\gamma}}\hat{V}_{\partial\Omega} \tag{5A-30}$$

The meaning of the metric becomes very clear–it is a measure of volume correction for the transformed coordinates.

$$F = \iiint_{\partial\Omega} f(\hat{x}^1, \hat{x}^2, \hat{x}^3)\sqrt{\hat{\gamma}}\delta\hat{V} = \iiint_{\partial\Omega} h(\hat{x}^1, \hat{x}^2, \hat{x}^3)\delta\hat{x}^1\delta\hat{x}^2\delta\hat{x}^3 \tag{5A-31}$$

where $h(\hat{x}^1, \hat{x}^2, \hat{x}^3) = f(\hat{x}^1, \hat{x}^2, \hat{x}^3)\sqrt{\hat{\gamma}}$ was used.

Consider a time derivative following the control volume. Applying a three-dimensional version of Leibnitz rule for the time differential of the integral, we get:

$$\left.\frac{\delta F}{\delta t}\right|_{\substack{following \\ volume}} = \frac{\delta}{\delta t}\iiint_{\partial\Omega} h(\hat{x}^1, \hat{x}^2, \hat{x}^3)\delta\hat{x}^1\delta\hat{x}^2\delta\hat{x}^3$$

$$= \iiint_{\partial\Omega} \left(\frac{\partial h}{\partial t}\right)_{\hat{x}^1, \hat{x}^2, \hat{x}^3} \delta\hat{x}^1\delta\hat{x}^2\delta\hat{x}^3$$

$$+\int_{\hat{x}_a^2}^{\hat{x}_b^2}\int_{\hat{x}_a^3}^{\hat{x}_b^3}\left[h(\hat{x}_b^1,\hat{x}^2,\hat{x}^3)\frac{d\hat{x}_b^1}{dt}-h(\hat{x}_a^1,\hat{x}^2,\hat{x}^3)\frac{d\hat{x}_a^1}{dt}\right]\delta\hat{x}^3\delta\hat{x}^2$$

$$+\int_{\hat{x}_a^1}^{\hat{x}_b^1}\int_{\hat{x}_a^2}^{\hat{x}_b^2}\left[h(\hat{x}^1,\hat{x}^2,\hat{x}_b^3)\frac{d\hat{x}_b^3}{dt}-h(\hat{x}^1,\hat{x}^2,\hat{x}_a^3)\frac{d\hat{x}_a^3}{dt}\right]\delta\hat{x}^2\delta\hat{x}^1$$

$$+\int_{\hat{x}_a^3}^{\hat{x}_b^3}\int_{\hat{x}_a^1}^{\hat{x}_b^1}\left[h(\hat{x}^1,\hat{x}_b^2,\hat{x}^3)\frac{d\hat{x}_b^2}{dt}-h(\hat{x}^1,\hat{x}_a^2,\hat{x}^3)\frac{d\hat{x}_a^2}{dt}\right]\delta\hat{x}^1\delta\hat{x}^3 \qquad \text{(5A-32)}$$

Then, using the following relation with the aid of Figure 5A-2:

$$\int_{\hat{x}_a^2}^{\hat{x}_b^2}\frac{\partial}{\partial\hat{x}^2}h\left(\left.\frac{d\hat{x}^2}{dt}\right|_{bd}\right)\delta\hat{x}^2=h(\hat{x}_b^2)\frac{d\hat{x}_b^2}{dt}-h(\hat{x}_a^2)\frac{d\hat{x}_a^2}{dt} \qquad \text{(5A-33)}$$

we obtain an integral equation:

$$\left.\frac{\delta F}{\delta t}\right|_{\substack{following\\volume}}=\iiint_{\partial\Omega}\left\{\frac{\partial h}{\partial t}+\frac{\partial}{\partial\hat{x}^1}\left(h\left.\frac{d\hat{x}^1}{dt}\right|_{bd}\right)+\frac{\partial}{\partial\hat{x}^2}\left(h\left.\frac{d\hat{x}^2}{dt}\right|_{bd}\right)+\frac{\partial}{\partial\hat{x}^3}\left(h\left.\frac{d\hat{x}^3}{dt}\right|_{bd}\right)\right\}\delta\hat{x}^1\delta\hat{x}^2\delta\hat{x}^3 \qquad \text{(5A-34)}$$

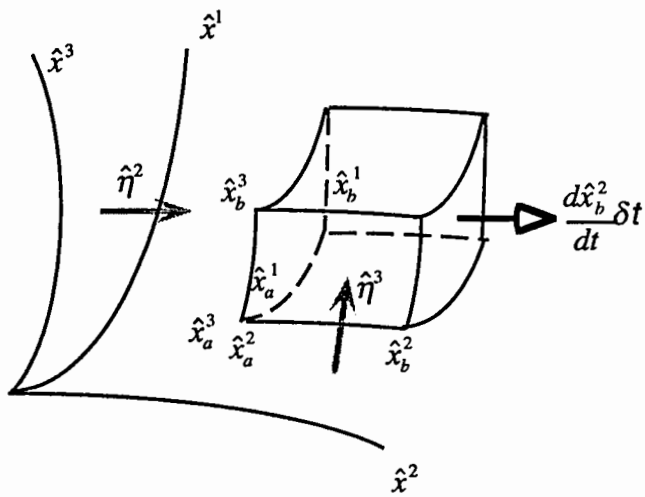

Figure 5A-2. Volume Element in a Curvilinear Coordinate System

When $f=\rho$ (density), then $F=\iiint_{\partial\Omega}\rho(x^1,x^2,x^3)\delta x^1\delta x^2\delta x^3=M$ = mass of the volume element.

Therefore, the conservation law states:

$$\left.\frac{\delta F}{\delta t}\right|_{\substack{following\\volume}} = \left.\frac{\delta M}{\delta t}\right|_{\substack{following\\volume}} = 0 \tag{5A-35}$$

Here, for example, $\left.\frac{d\hat{x}^2}{dt}\right|_{bd}$ is the velocity of the boundary of the volume element in the curvilinear coordinate $\hat{x}^2$. Because the volume element confines the fluid and moves with the fluid, this is velocity component of the fluid in the curvilinear coordinate $\hat{x}^2$. Then, we have

$$\iiint_{\partial\Omega}\left[\frac{\partial(\rho\sqrt{\hat{\gamma}})}{\partial t} + \frac{\partial(\rho\sqrt{\hat{\gamma}}\hat{v}^j)}{\partial\hat{x}^j}\right]\delta\hat{V} = 0 \tag{5A-36}$$

Since above integral should be satisfied for an arbitrarily infinitesimal volume element, we obtain the continuity equation in differential equation form for the time-dependent curvilinear coordinate as follows:

$$\frac{\partial(\rho\sqrt{\hat{\gamma}})}{\partial t} + \frac{\partial(\rho\sqrt{\hat{\gamma}}\hat{v}^j)}{\partial\hat{x}^j} = 0 \tag{5A-37}$$

EPA/600/R-99/030

Chapter 6

GOVERNING EQUATIONS AND COMPUTATIONAL STRUCTURE OF THE COMMUNITY MULTISCALE AIR QUALITY (CMAQ) CHEMICAL TRANSPORT MODEL

Daewon W. Byun* **and Jeffrey Young****
Atmospheric Modeling Division,
National Exposure Research Laboratory
U.S. Environmental Protection Agency
Research Triangle Park, NC 27711

M. Talat Odman***
MCNC-Environmental Programs
P.O. Box 12889, 3021 Cornwallis Road
Research Triangle Park, NC 27709-2889, USA

ABSTRACT

The chemical transport model (CTM) of the Models-3/CMAQ (Community Multiscale Air Quality) modeling system can be configured to follow the dynamics of the preprocessor meteorological model. A science process module in the CMAQ CTM is not specific to a coordinate system. The generality is accomplished through the use of the coordinate transformation Jacobian within the CMAQ CTM. In this chapter, we derive the governing diffusion equation in a generalized coordinate system, which is suitable for multiscale atmospheric applications. We describe the CMAQ system's modularity concepts, fractional time-step formulation, and key science processes implemented in the current version of the CMAQ CTM. We examine dynamic formulations of several popular Eulerian air quality models as emulated by the governing diffusion equations in the generalized coordinate system. Also, a nesting technique for the CMAQ CTM is introduced. Finally, because the amount of a substance in the atmosphere can be expressed in many different ways, we summarize the most popular expressions for concentration and their transformation relations.

*On assignment from the National Oceanic and Atmospheric Administration, U.S. Department of Commerce. Corresponding author address: Daewon W. Byun, MD-80, Research Triangle Park, NC 27711.
E-mail: bdx@hpcc.epa.gov
** On assignment from the National Oceanic and Atmospheric Administration, U.S. Department of Commerce.
*** Present Affiliation: Georgia Institute of Technology, Atlanta, GA.

6.0 GOVERNING EQUATIONS AND COMPUTATIONAL STRUCTURE OF THE COMMUNITY MULTISCALE AIR QUALITY (CMAQ) CHEMICAL TRANSPORT MODEL

In Chapter 5, "Fundamentals of Atmospheric Modeling ..." we discussed the fundamental set of equations for atmospheric dynamics and thermodynamics in a generalized coordinate system. In this Chapter, we investigate the diffusion equation for the trace species in the atmosphere in the generalized coordinate system and the computational structure of the Community Multiscale Air Quality chemical transport model (CMAQ CTM or, hereafter, CCTM).

One requirement of the CMAQ modeling system is to maintain a consistent description of the atmosphere for different meteorological and chemical transport models. This is a feature that is essential for spatial scalability. Various coordinate systems are used in atmospheric models. Selection of a suitable coordinate system is an important step of model formulation. There are numerous criteria to be considered in selecting a coordinate system, such as the dynamic characteristics it can handle and how well it can deal with curvature of the earth's surface and features of the terrain. Formulation of the models may vary substantially for different coordinate systems. If a CTM can be formulated and coded using a generalized coordinate system, it would be easy to switch from one coordinate to another depending on the application. The generalized coordinate concept is useful because a single CTM formulation can adapt to any of the coordinates commonly used in meteorological models. It is also desirable to compare the benefits of various coordinate systems and to be able to link the CTMs to meteorological models and databases in different coordinates.

Conformity of the coordinates to the physics of the problem is very important. Unlike a model with a fixed coordinate system, a generalized coordinate system allows use of generic coordinates for the specific science processes within a model. Although the model's overall structure is determined by the choice of a coordinate system, the individual science modules can still use their own generic coordinates that best suit the physical processes they model. This means that each science process can utilize the parameterizations based on the best coordinate to represent the problem. For example, the planetary boundary layer (PBL) parameterizations can be expressed in terms of geometric height, or dimensionless height scaled with PBL height, while for cloud physics, they can be represented in terms of pressure. The linkages between the generic coordinate parameterizations in the science processes and the governing conservation equation in the generalized coordinates are established through the application of appropriate coordinate transformation rules.

Here, we intend to provide a comprehensive and rational development of the governing conservation equation in generalized coordinates, which can be readily implemented in an Eulerian model. The operating assumptions used for the derivations are listed below (see Srivastava et al., 1995).

- **Assumption 1**: Pollutant concentrations are sufficiently small, such that their presence would not affect the meteorology to any detectable extent. Hence, the species

conservation equations can be solved independently of the Navier-Stokes and energy equations. The conditions which could invalidate this assumption are for cases where sufficient heat is generated by chemical reactions to influence the temperature of the medium or where an atmospheric layer become so concentrated with pollutants that absorption, reflection, and scattering of radiation alter the air flow (Seinfeld, 1986).

- **Assumption 2**: The velocities and concentrations of the various species in atmospheric flow are turbulent quantities and undergo turbulent diffusion. Because turbulent diffusion is much greater than molecular diffusion for most trace species, the latter can be ignored.

- **Assumption 3**: The metric tensor that defines the coordinate transformation rules is not a turbulent variable. This means that we can define the coordinates based on the Reynolds averaged quantities. The vertical grids will be defined incrementally between time steps when a time-dependent vertical coordinate is used.

- **Assumption 4**: The ergodic hypothesis holds for the ensemble averaging process. This means that the ensemble average of a property can be substituted with the time average of that property.

- **Assumption 5**: The turbulence is assumed stationary for the averaging time period of interest (say 30 minutes to one hour for atmospheic applications).

- **Assumption 6**: The source function (i.e., emissions of pollutants) is deterministic for all practical purposes and there is no turbulent component.

- **Assumption 7**: The effect of concentration fluctuation on the rate of chemical reaction is negligible, i.e., contributions of covariance effects among tracer species are neglected.

- **Assumption 8**: Because the large-scale motions of the atmosphere are quasi-horizontal with respect to the earth's surface, science processes can be separately represented in horizontal and vertical directions (i.e., quasi-orthogonal in transformed coordinates).

6.1 Derivation of the Atmospheric Diffusion Equation

In Chapter 5, we derived the species continuity equation in generalized coordinates. It is given as:

$$\frac{\partial(\varphi_i J_s)}{\partial t} + m^2 \nabla_s \bullet \left(\frac{\varphi_i J_s \hat{\mathbf{V}}_s}{m^2} \right) + \frac{\partial(\varphi_i J_s \dot{s})}{\partial s} = J_s Q_{\varphi_i} \qquad (6\text{-}1)$$

where φ_i is the trace species concentration in density units (e.g., kg m^{-3}), J_s is the vertical Jacobian of the terrain-influenced coordinate s, m is the map scale factor, $\hat{\mathbf{V}}_s$ and $\dot{s}$ are horizontal and vertical wind components in the generalized coordinates, and Q_{φ_i} is the source or sink term.

To make the instantaneous species continuity equation useful for air quality simulation, we need to derive the governing diffusion equation. This is done by decomposing the variables in Equation 6-1, except for the Jacobian and map scale factor, in terms of mean and turbulent components. The Reynolds decompositions of species concentration and mixing ratio are expressed as:

$$\varphi_i = \overline{\varphi}_i + \varphi_i" \tag{6-2a}$$

$$q_i = \overline{q}_i + q_i" \tag{6-2b}$$

$$\overline{\varphi}_i + \varphi_i" = \overline{q}_i\overline{\rho} + q_i"\overline{\rho} + \overline{q}_i\rho" + q_i"\rho" \tag{6-2c}$$

where $q_i = \dfrac{\varphi_i}{\rho}$ is the species mass mixing ratio and a stochastic quantity is decomposed into mean, $(\overline{\ })$, and turbulent, $(")$, components. Stationary turbulence assumption 5 implies that a turbulent component has a zero mean for the averaging period. Following Venkatram (1993), we can estimate the mean and turbulent components of species and air concentrations as

$$\overline{\varphi}_i \approx \overline{q}_i\overline{\rho} \tag{6-3a}$$

$$\varphi_i" = q_i"\overline{\rho} + \overline{q}_i\rho" + q_i"\rho" \tag{6-3b}$$

$$\frac{\overline{q_i"\rho"}}{\overline{q}_i\overline{\rho}} \approx \frac{\overline{\rho"^2}}{(\overline{\rho})^2} << 1 \tag{6-3c}$$

Without loss of generality, we redefine the terrain-influenced vertical coordinate s with a coordinate $\hat{x}^3$, whose value is increasing monotonically with height, as:

$$\hat{x}^3 = \xi = \begin{cases} s & (\textit{if } s \textit{ increases with height}) \\ 1-s & (\textit{if } s \textit{ decreases with height}) \end{cases} \tag{6-4}$$

The choice of a generalized vertical coordinate which increases monotonically with height simplifies the derivation of the governing equation and thus reduces the likelihood of making sign errors in the formulas and in computer codes. The transformation does not change the horizontal wind components or the Jacobian, which is always defined to be a positive quantity. Hereafter, the subscript s is replaced with ξ to reflect modification of the vertical coordinate. Subsequently, the vertical velocity is represented with $\hat{v}^3 = d\xi / dt = \dot{\xi}$, which is positive for upward motion.

Application of decomposition of velocity components in Equation 6-1 and ensemble averaging produces Reynolds flux terms in the mass conservation equation as:

$$\frac{\partial(\overline{\varphi}_i J_\xi)}{\partial t} + m^2 \nabla_\xi \bullet \left(\frac{\overline{(\overline{\varphi}_i + \varphi_i")(\overline{\hat{\mathbf{V}}}_\xi + \hat{\mathbf{V}}_\xi")} J_\xi}{m^2} \right)$$

$$+ \frac{\partial}{\partial \hat{x}^3} \left[\overline{(\overline{\varphi}_i + \varphi_i")(\overline{\hat{v}^3} + \hat{v}^3")} J_\xi \right] = J_\xi Q_{\varphi_i} \qquad (6\text{-}5)$$

where we used $J_\xi = \overline{J}_\xi$ and $Q_{\varphi_i} = \overline{Q}_{\varphi_i}$ based on Assumption 3 and Assumption 6, respectively. The Reynolds flux terms in Equation 6-5 can be approximated in terms of the mixing ratio as:

$$\overline{\varphi_i" \hat{\mathbf{V}}_\xi"} \approx \overline{\rho} \overline{q_i" \hat{\mathbf{V}}_\xi"} + \overline{q}_i \overline{\rho" \hat{\mathbf{V}}_\xi"} \approx \overline{\rho} \overline{q_i" \hat{\mathbf{V}}_\xi"} \qquad (6\text{-}6a)$$

$$\overline{\varphi_i" \hat{v}^3"} \approx \overline{\rho} \overline{q_i" \hat{v}^3"} + \overline{q}_i \overline{\rho" \hat{v}^3"} \approx \overline{\rho} \overline{q_i" \hat{v}^3"} \qquad (6\text{-}6b)$$

$$\overline{q}_i \overline{\rho" \hat{\mathbf{V}}_\xi"} << 1 \qquad (6\text{-}6c)$$

$$\overline{q}_i \overline{\rho" \hat{v}^3"} << 1 \qquad (6\text{-}6d)$$

in which we have neglected the second order perturbation terms based on the scale analysis of the equations. Equation 6-5 can be rewritten using Equations 6-3a-c and 6-6a-c to give:

$$\frac{\partial(\overline{\varphi}_i J_\xi)}{\partial t} + m^2 \nabla_\xi \bullet \left(\frac{\overline{\varphi}_i \overline{\hat{\mathbf{V}}}_\xi J_\xi}{m^2} \right) + \frac{\partial(\overline{\varphi}_i \overline{\hat{v}^3} J_\xi)}{\partial \hat{x}^3}$$

$$+ m^2 \nabla_\xi \bullet \left(\overline{\rho} \frac{\overline{q_i" \hat{\mathbf{V}}_\xi"} J_\xi}{m^2} \right) + \frac{\partial(\overline{\rho} \overline{q_i" \hat{v}^3"} J_\xi)}{\partial \hat{x}^3} = J_\xi Q_{\varphi_i} \qquad (6\text{-}7)$$

The turbulence flux terms can be parameterized using a simple closure scheme such as the eddy diffusion concept (K-theory):

$$\overline{q_i" \hat{u}_\xi"} = -\hat{K}^{1l} \frac{\partial \overline{q}_i}{\partial \hat{x}^l}; \; \overline{q_i" \hat{v}_\xi"} = -\hat{K}^{2l} \frac{\partial \overline{q}_i}{\partial \hat{x}^l}; \; \overline{q_i" \hat{v}^3"} = -\hat{K}^{3l} \frac{\partial \overline{q}_i}{\partial \hat{x}^l} \qquad (6\text{-}8)$$

where $\hat{K}^{jl}$ denotes the eddy diffusivity tensor in the transformed coordinate. The eddy diffusivity tensor for the generalized meteorological coordinates is related to the diffusivity tensor in Cartesian coordinates as:

$$\hat{K}^{kl} = \frac{\partial \hat{x}^k}{\partial x^i} \frac{\partial \hat{x}^l}{\partial x^j} K^{ij} \qquad (6\text{-}9)$$

If we postulate that the diffusivity tensor in Cartesian coordinates is diagonal (i.e., all the off-diagonal components vanish), then the eddy diffusivity tensor in the generalized meteorological coordinates becomes:

$$\hat{\mathbf{K}} = \begin{pmatrix} m^2 K_{xx} & 0 & m\frac{\partial \hat{x}^3}{\partial x} K_{xx} \\ 0 & m^2 K_{yy} & m\frac{\partial \hat{x}^3}{\partial y} K_{yy} \\ m\frac{\partial \hat{x}^3}{\partial x} K_{xx} & m\frac{\partial \hat{x}^3}{\partial y} K_{yy} & (\frac{\partial \hat{x}^3}{\partial x})^2 K_{xx} + (\frac{\partial \hat{x}^3}{\partial y})^2 K_{yy} + (\frac{\partial \hat{x}^3}{\partial z})^2 K_{zz} \end{pmatrix} \qquad (6\text{-}10)$$

where $K_{xx} = K^{11}$, $K_{yy} = K^{22}$, and $K_{zz} = K^{33}$ are the diagonal components of eddy diffusivity tensor in the Cartesian coordinate. To match with the computational grid, the gradient terms in Equation 6-10 must be rewritten in terms of the generalized coordinates $\hat{x}^3$ (defined based on height above ground $h_{AGL} = h - z_{sfc}$, where z_{sfc} represents the height of topography) using the appropriate chain rules, for example, $\frac{1}{m}\left(\frac{\partial A}{\partial x}\right)_z = \left(\frac{\partial A}{\partial \hat{x}^1}\right)_{\hat{x}^3} - \frac{\partial A}{\partial z}\left(\frac{\partial A}{\partial \hat{x}^3}\right)\left(\frac{\partial h}{\partial \hat{x}^1}\right)_{\hat{x}^3}$. When A = $\hat{x}^3$, we get

$$\hat{\mathbf{K}} = \begin{pmatrix} m^2 K_{xx} & 0 & -m^2 \frac{\partial \hat{x}^3}{\partial z}\frac{\partial h}{\partial \hat{x}^1} K_{xx} \\ 0 & m^2 K_{yy} & -m^2 \frac{\partial \hat{x}^3}{\partial z}\frac{\partial h}{\partial \hat{x}^2} K_{yy} \\ -m^2 \frac{\partial \hat{x}^3}{\partial z}\frac{\partial h}{\partial \hat{x}^1} K_{xx} & -m^2 \frac{\partial \hat{x}^3}{\partial z}\frac{\partial h}{\partial \hat{x}^2} K_{yy} & (\frac{\partial \hat{x}^3}{\partial z})^2 \left[\left(m\frac{\partial h}{\partial \hat{x}^1}\right)^2 K_{xx} + \left(m\frac{\partial h}{\partial \hat{x}^2}\right)^2 K_{yy} + K_{zz}\right] \end{pmatrix} \qquad (6\text{-}11).$$

Then the non-zero diffusion terms in Equation 6-7 can be parameterized with the eddy diffusion theory as follows:

$$m^2 \nabla_\xi \bullet \left(\bar{\rho} \frac{\overline{q_i'' \hat{\mathbf{V}}_\xi'' J_\xi}}{m^2} \right) = m^2 \frac{\partial}{\partial \hat{x}^1}\left[-\frac{\bar{\rho} J_\xi}{m^2} (\hat{K}^{11} \frac{\partial \bar{q}_i}{\partial \hat{x}^1} + \hat{K}^{13} \frac{\partial \bar{q}_i}{\partial \hat{x}^3}) \right]$$

$$+ m^2 \frac{\partial}{\partial \hat{x}^2}\left[-\frac{\bar{\rho} J_\xi}{m^2} (\hat{K}^{22} \frac{\partial \bar{q}_i}{\partial \hat{x}^2} + \hat{K}^{23} \frac{\partial \bar{q}_i}{\partial \hat{x}^3}) \right] \qquad (6\text{-}12)$$

and

$$\frac{\partial (\bar{\rho} \overline{q_i'' \hat{v}^{3''}} J_\xi)}{\partial \hat{x}^3} = \frac{\partial}{\partial \hat{x}^3}\left[-\bar{\rho} J_\xi (\hat{K}^{31} \frac{\partial \bar{q}_i}{\partial \hat{x}^1} + \hat{K}^{32} \frac{\partial \bar{q}_i}{\partial \hat{x}^2} + \hat{K}^{33} \frac{\partial \bar{q}_i}{\partial \hat{x}^3}) \right] \qquad (6\text{-}13)$$

Rewriting Equation 6-7 with Equations 6-12 and 6-13, and separating the diagonal and off-diagonal diffusion terms with an explicit description of the source terms, one can obtain the governing atmospheric diffusion equation in the generalized coordinates where the turbulent flux terms are expressed with the eddy diffusion theory:

$$\frac{\partial(\overline{\varphi}_i J_\xi)}{\partial t} + m^2 \nabla_\xi \bullet \left(\frac{\overline{\varphi}_i \overline{\hat{\mathbf{V}}}_\xi J_\xi}{m^2} \right) + \frac{\partial(\overline{\varphi}_i \overline{\hat{v}^3} J_\xi)}{\partial \hat{x}^3}$$

(a) (b) (c)

$$-m^2 \frac{\partial}{\partial \hat{x}^1}\left[\frac{\overline{\rho} J_\xi}{m^2}(\hat{K}^{11}\frac{\partial \overline{q}_i}{\partial \hat{x}^1})\right] - m^2 \frac{\partial}{\partial \hat{x}^2}\left[\frac{\overline{\rho} J_\xi}{m^2}(\hat{K}^{22}\frac{\partial \overline{q}_i}{\partial \hat{x}^2})\right] - \frac{\partial}{\partial \hat{x}^3}\left[\overline{\rho} J_\xi (\hat{K}^{33}\frac{\partial \overline{q}_i}{\partial \hat{x}^3})\right]$$

(d) (e)

$$-m^2 \frac{\partial}{\partial \hat{x}^1}\left[\frac{\overline{\rho} J_\xi}{m^2}(\hat{K}^{13}\frac{\partial \overline{q}_i}{\partial \hat{x}^3})\right] - m^2 \frac{\partial}{\partial \hat{x}^2}\left[\frac{\overline{\rho} J_\xi}{m^2}(\hat{K}^{23}\frac{\partial \overline{q}_i}{\partial \hat{x}^3})\right]$$

(f)

$$-\frac{\partial}{\partial \hat{x}^3}\left[\overline{\rho} J_\xi (\hat{K}^{31}\frac{\partial \overline{q}_i}{\partial \hat{x}^1} + \hat{K}^{32}\frac{\partial \overline{q}_i}{\partial \hat{x}^2})\right]$$

(g)

$$= J_\xi R_{\varphi_i}(\overline{\varphi}_1,\ldots,\overline{\varphi}_N) + J_\xi Q_{\varphi_i} + \left.\frac{\partial(\overline{\varphi}_i J_\xi)}{\partial t}\right|_{cld} + \left.\frac{\partial(\overline{\varphi}_i J_\xi)}{\partial t}\right|_{aero} + \left.\frac{\partial(\overline{\varphi}_i J_\xi)}{\partial t}\right|_{ping} \qquad (6\text{-}14)$$

(h) (i) (j) (k) (l)

The terms in Equation 6-14 are summarized as follows:

(a) time rate of change of pollutant concentration;
(b) horizontal advection;
(c) vertical advection;
(d) horizontal eddy diffusion (diagonal term);
(e) vertical eddy diffusion (diagonal term);
(f) off-diagonal horizontal diffusion;
(g) off-diagonal vertical diffusion;
(h) production or loss from chemical reactions;
(i) emissions;
(j) cloud mixing and aqueous-phase chemical production or loss;
(k) aerosol process; and

(l) plume-in-grid process.

Note that the dry deposition process can be included in the vertical diffusion process as a flux boundary condition at the bottom of the model layer.

Alternatively, we can express the turbulent flux terms in Equation 6-7 using the Reynolds flux terms defined as:

$$\overline{q_i''\hat{u}_\xi''} = \hat{F}^1_{q_i},\ \overline{q_i''\hat{v}_\xi''} = \hat{F}^2_{q_i},\ \overline{q_i''\hat{v}^3''} = \hat{F}^3_{q_i} \tag{6-15}$$

and the turbulent flux terms are related with the Cartesian counterpart using $\hat{F}^k_{q_i} = \frac{\partial \hat{x}^k}{\partial x^j} F^j_{q_i}$:

$$\hat{F}^1_{q_i} = mF^x_{q_i},\ \hat{F}^2_{q_i} = mF^y_{q_i},\ \hat{F}^3_{q_i} = (\frac{\partial \hat{x}^3}{\partial x})F^x_{q_i} + (\frac{\partial \hat{x}^3}{\partial y})F^y_{q_i} + (\frac{\partial \hat{x}^3}{\partial z})F^z_{q_i} \tag{6-16}$$

In comparison with Equation 6-14, the Reynolds flux terms shown in Equation 6-15 include the off-diagonal components. One can now rewrite the governing conservation equation for trace species equivalently to Equation 6-14 in terms of the Reynolds flux terms:

$$\begin{aligned}
&\frac{\partial(\overline{\varphi}_i J_\xi)}{\partial t} + m^2\nabla_\xi \bullet \left(\frac{\overline{\varphi}_i \overline{\hat{\mathbf{V}}}_\xi J_\xi}{m^2}\right) + \frac{\partial(\overline{\varphi}_i \overline{\hat{v}^3} J_\xi)}{\partial \hat{x}^3} \\
&\quad + m^2 \frac{\partial}{\partial \hat{x}^1}\left[\frac{\overline{\rho} J_\xi}{m^2}\hat{F}^1_{q_i}\right] + m^2 \frac{\partial}{\partial \hat{x}^2}\left[\frac{\overline{\rho} J_\xi}{m^2}\hat{F}^2_{q_i}\right] + \frac{\partial}{\partial \hat{x}^3}\left[\overline{\rho} J_\xi \hat{F}^3_{q_i}\right] \\
&\quad = J_\xi R_{\varphi_i}(\overline{\varphi}_1,\ldots,\overline{\varphi}_N) + J_\xi Q_{\varphi_i} + \left.\frac{\partial(\overline{\varphi}_i J_\xi)}{\partial t}\right|_{cld} + \left.\frac{\partial(\overline{\varphi}_i J_\xi)}{\partial t}\right|_{aero} + \left.\frac{\partial(\overline{\varphi}_i J_\xi)}{\partial t}\right|_{ping}
\end{aligned} \tag{6-17}$$

The governing equation can be simplified for a domain with gentle topography for which one may ignore all the terms involved with the horizontal gradients of the surface normal to the vertical coordinate. This forces the vertical diffusion terms in the curvilinear coordinate system to be identical to those of the orthogonal Cartesian coordinate system. Then the trace species conservation equation can be written in a simpler form:

$$\begin{aligned}
&\frac{\partial \varphi_i^*}{\partial t} + \hat{\nabla}_\xi \bullet \left[\varphi_i^* \overline{\hat{\mathbf{V}}}_\xi\right] + \frac{\partial(\varphi_i^* \overline{\hat{v}^3})}{\partial \hat{x}^3} + \hat{\nabla}_\xi \bullet \left[\overline{\rho}\sqrt{\hat{\gamma}}\hat{\mathbf{F}}_{q_i}\right] + \frac{\partial(\overline{\rho}\sqrt{\hat{\gamma}}\hat{F}^3_{q_i})}{\partial \hat{x}^3} \\
&\quad = \sqrt{\hat{\gamma}} R_{\varphi_i}(\overline{\varphi}_1,\ldots,\overline{\varphi}_N) + \sqrt{\hat{\gamma}} S_{\varphi_i} + \left.\frac{\partial(\varphi_i^*)}{\partial t}\right|_{cld} + \left.\frac{\partial(\varphi_i^*)}{\partial t}\right|_{ping} + \left.\frac{\partial(\varphi_i^*)}{\partial t}\right|_{aero}
\end{aligned} \tag{6-18}$$

where $\varphi_i^* = \sqrt{\hat{\gamma}}\overline{\varphi}_i = (J_\xi / m^2)\overline{\varphi}_i$. In writing Equation 6-18, we have explicitly identified terms to directly relate to science process modules implemented in the CMAQ. Equation 6-18 is similar to the conservation equation in the generalized coordinates as suggested by Toon et al. (1988).

6.2 Representation of Science Processes in CMAQ Modeling System

This section describes how the CMAQ modeling system is structured to accommodate many different science process modules that provide a one-atmosphere, multiscale and multi-pollutant modeling capability to the CMAQ system. First, we describe the modularity concepts and key science processes implemented in the current version of CMAQ. Then the governing fractional time-step formulation for each science process is presented.

6.2.1 Supporting Models and Interface Processors

Key supporting models for the current version of the CMAQ modeling system are the Mesoscale Model Version 5 (MM5) (Seaman et al., 1995)and Models-3 Emissions Processing and Projection System (MEPPS). The CMAQ modeling system is comprised of the main CMAQ chemical transport model (CCTM) and several interface processors that link other model input data to the CCTM. The Meteorology-Chemistry Interface Processor (MCIP) processes MM5 output to provide a complete set of meteorological data required for CCTM. MCIP is designed in such a way that other meteorological models can be linked with minimal effort. Initial and boundary conditions are generated with the ICON and BCON processors, respectively, and the Emissions-Chemistry Interface Processor (ECIP) combines area and point source emissions to generate three-dimensional gridded emissions data for CCTM. In addition, a plume dynamics model (PDM) is used to provide dimensions and positions of plumes from major elevated point-sources. The PDM data are used for driving the plume-in-grid processing in CCTM. A photolytic rate constant processor (JPROC) which is based on the RADM (Chang et al., 1987) approach, computes species specific photolysis rates for a set of predefined zenith angles, latitude, and altitudes. An alternative detailed-science version adopts state-of-the-science radiative transfer models that can take into account the total ozone column (TOMS data) and turbidity. Refer to Table 6-1 for the list of the interface processors in CMAQ and Figure 6-1 for the data linkage among these interface processors.

By assembling appropriate science modules available in the CMAQ system, users can build a specific CCTM's that may include all or some of the critical science processes, such as atmospheric transport, deposition, cloud mixing, emissions, gas- and aqueous-phase chemical transformations, and aerosol dynamics and chemistry. One of the features of CMAQ that distinguishes it from other air quality models is the hierarchical functional modularity of the science processor codes. We define the levels of modularity in the science model based on the granularity of the modeling components. The coarsest level of modularity is the distinction between the system framework and science models. The second level is the division of science sub-models (MM5, MEPPS, and CMAQ). The third level of modularity involves a driver module, processor modules, data provider modules, and a utility module (a collection of assisting

subroutines) in a CTM. While the emissions processing and the meteorology model are modular at the second level, the CCTM achieves the third-level of modularity by employing the operator splitting, or fractional time step, concept in the science processes. The next level of modularity is based on the computational functionality in a processor module, e.g., science parameterization, numerical solver, processor analysis, and input/output routines. The lowest meaningful modularization level is the isolation of sections of code that can benefit from machine dependent optimization.

6.2.2 Modularity Concept of CMAQ

To allow for both the continuous improvement of science and for the addition of new capabilities in a unified fashion, it is critical to have efficient modular schemes in the CMAQ design. Currently, the modularity within CMAQ is based mostly on the fractional time-step implementation of the science processes. This level of modularity involves the distinction of a driver, processor modules, data provider modules, and utility subroutines in CMAQ. We have chosen this method because it provides a natural disciplinary distinction for different science processes through which developments in specific research areas can readily be incorporated (Refer to Figure 6-2).

In some of the process modules, such as the aqueous-phase chemistry module, the science algorithms and numerical solvers are tightly linked. For other types of modules, the science parameterization components and numerical solvers have a looser association. In such cases the modularity can be defined either at the parameterization level, the numerical algorithm level, or both. For example, the module definition for the advection process is based on the numerical advection algorithm used. For the gas-phase chemistry process, the modularity is based on the ordinary differential equation numerical solvers. The chemistry mechanism description is generalized and the Models-3/CMAQ framework provides a straightforward method to link model species surrogate names with the species names in the data set. See Chapter 15 for details. The use of different chemical mechanisms is accommodated through the mechanism reader and generalized codes for setting up the production and loss terms of the chemistry reactions. Therefore, the CCTM does not require different gas-phase chemistry modules for different mechanisms.

The vertical diffusion process can be formulated using either local- or non-local-mixing parameterization schemes. The current classification of vertical diffusion modules is based on the process parameterization methods. The modularity of this process can be enhanced if we distinguish the method used for computing the vertical diffusivities for local-mixing. In this case, the modularity is defined at the level of data provider modules. The modularity level can be deepened further if we identify different numerical solution methods for the diffusion.

With the current version of CMAQ, the level of science modularity is subordinated by the way the science process codes are archived in the system. Here, we define a class as a collection of different modules for a given science process. The science classes are identified with the grouping

of the terms in the governing conservation equation, Equation 6-18. Currently, nine science process classes are defined in CCTM:

- **DRIVER** controls model data flows and synchronizes fractional time steps;
- **HADV** computes the effects of horizontal advection;
- **VADV** computes the effects of vertical advection;
- **ADJCON** adjusts mixing ratio conservation property of advection processes;
- **HDIFF** computes the effects of horizontal diffusion;
- **VDIFF** computes the effects of vertical diffusion and deposition;
- **CHEM** computes the effects of gas-phase chemical reactions;
- **CLOUD** computes the effects of aqueous-phase reactions and cloud mixing;
- **AERO** computes aerosol dynamics and size distributions; and
- **PING** computes the effects of plume chemistry.

CCTM does not have emissions as a separate science process because it can be either a part of the vertical diffusion or the gas-phase chemical reaction process. It is worthwhile to mention here that the current modular paradigm does not prevent establishment of combination of processes in a larger single module. For example, one can develop a module describing the vertical transport, chemistry, and emissions simultaneously when time scales of those processes become comparable. Users could experiment with the combination of modules to best fit to their problems at hand.

In addition to nine science process modules, CCTM includes two science process classes. The PHOT computes photolysis rates, and AERO_DEPV computes particle size-dependent dry deposition velocities. These are typical "data-provider" science process classes, which do not involve updating concentrations directly. There are some other classes that do not fall in any of the above definitions. We have grouped these auxiliary routines as the UTIL class, which is a collection of utility subroutines. As one can see, the current modularity of the CCTM is implemented more on a practical basis rather than by strictly following a design paradigm. One can also see that the present modularity definition of CMAQ is somewhat subjective. In the future we intend to allow definition of the modularity at the user-defined granularity level.

Figure 6-1 describes the key science process modules in CCTM and their data linkage with CMAQ's preprocessors, whose descriptions are available in other chapters. The only data dependencies among the CCTM science modules are the trace species concentration field as seen in the diagram and the model integration time step. Figure 6-2 shows the distinct data

dependencies within the CCTM. To facilitate modularity and to minimize data dependency in CCTM, we store concentrations in global memory while the environmental input data are obtained from random-access files and interpolated to the appropriate computational (synchronization) time step. This realizes the recommended "thin-interface" structure of the model:

- Common timing data are managed through the science process main subroutine's call arguments;
- Concentrations are the object of all process operations;
- Environmental data are provided through a standard I/O interface;
- Model structure data are provided through shared include files; and
- Standard physical constants are obtained from shared include files.

See Chapter 18 for further details on how the science codes are integrated in the Models-3 CMAQ system.

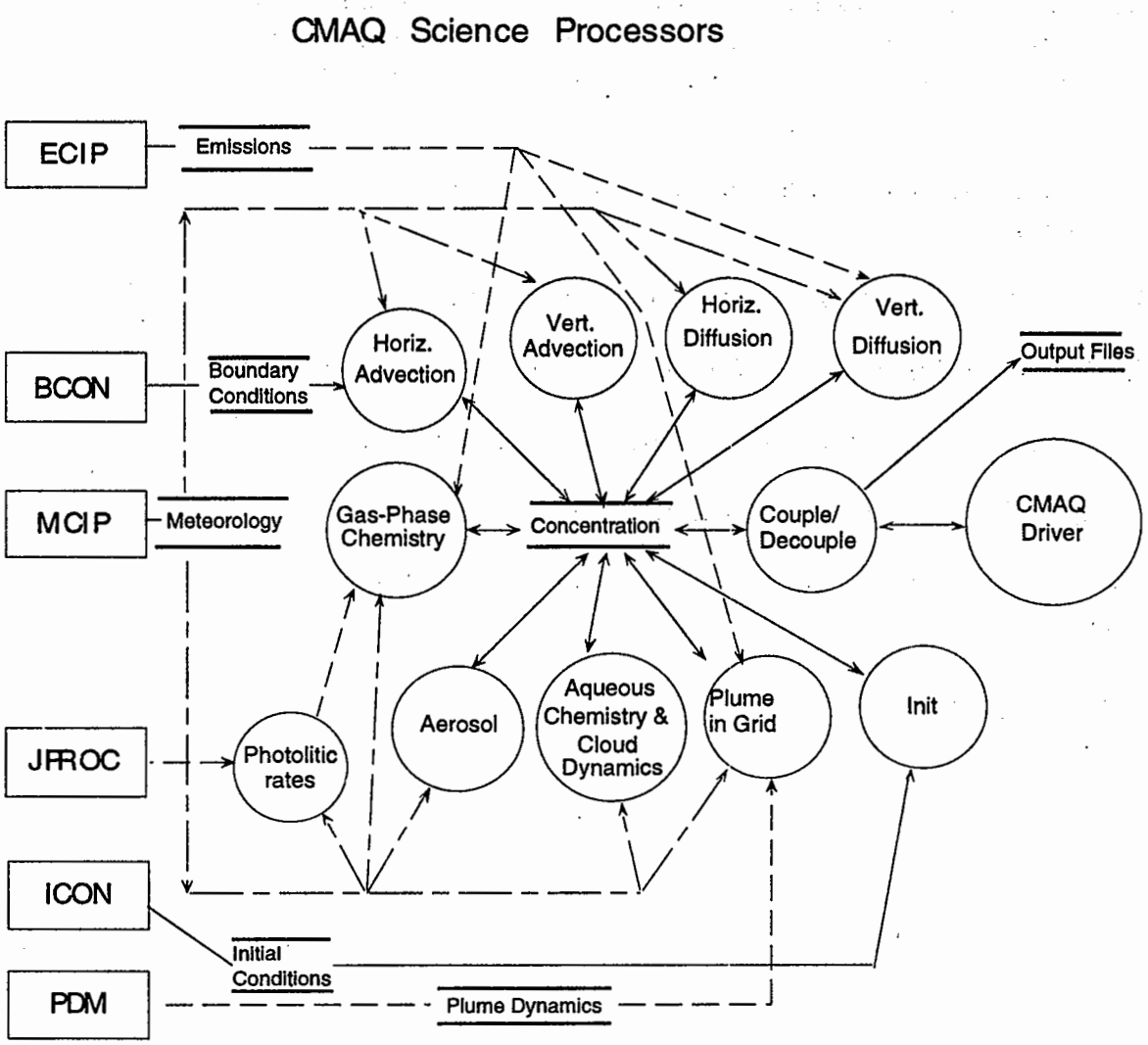

Figure 6-1. Science Process Modules in CMAQ. Interface processes are shown with rectangular boxes. Typical science process modules are updating the concentration field directly and the data-provider modules include routines to feed appropriate environmental input data to the science process modules. Driver module orchestrates the synchronization of numerical integration across the science processes. Concentrations are linked with solid lines and other environmental data with broken lines. (From Byun et al., 1998.)

Table 6-1. Interface Processors for the CMAQ Modeling System

Interface Processor	Description	Reference
ICON	Provides initial three-dimensional fields of trace species concentrations for modeling domain	Chapter 13
BCON	Provides concentrations of trace species for the boundary cells	Chapter 13
ECIP	Incorporates emissions from separate area and major point sources to generate hourly 3-D emissions input file	Chapter 3
MCIP	Processes the output of a meteorological model to provide the necessary meteorological data for CMAQ models	Chapter 12
JPROC	Computes photolysis rates for various altitudes, latitudes, and sun zenith angle	Chapter 14
PDM	Generates plume information needed to apply plume-in-grid (PinG) processing in CCTM	Chapter 9

6.2.3 Description of Science Processes

In this section we describe individual science processes, shown in Figure 6-1, associated with the groups of individual terms in the governing diffusion equation. Note that different concentration units are used for different science processes in CMAQ CTMs. Appendix 6A provides the relationships among the concentration units and their conversion factors from one unit to another.

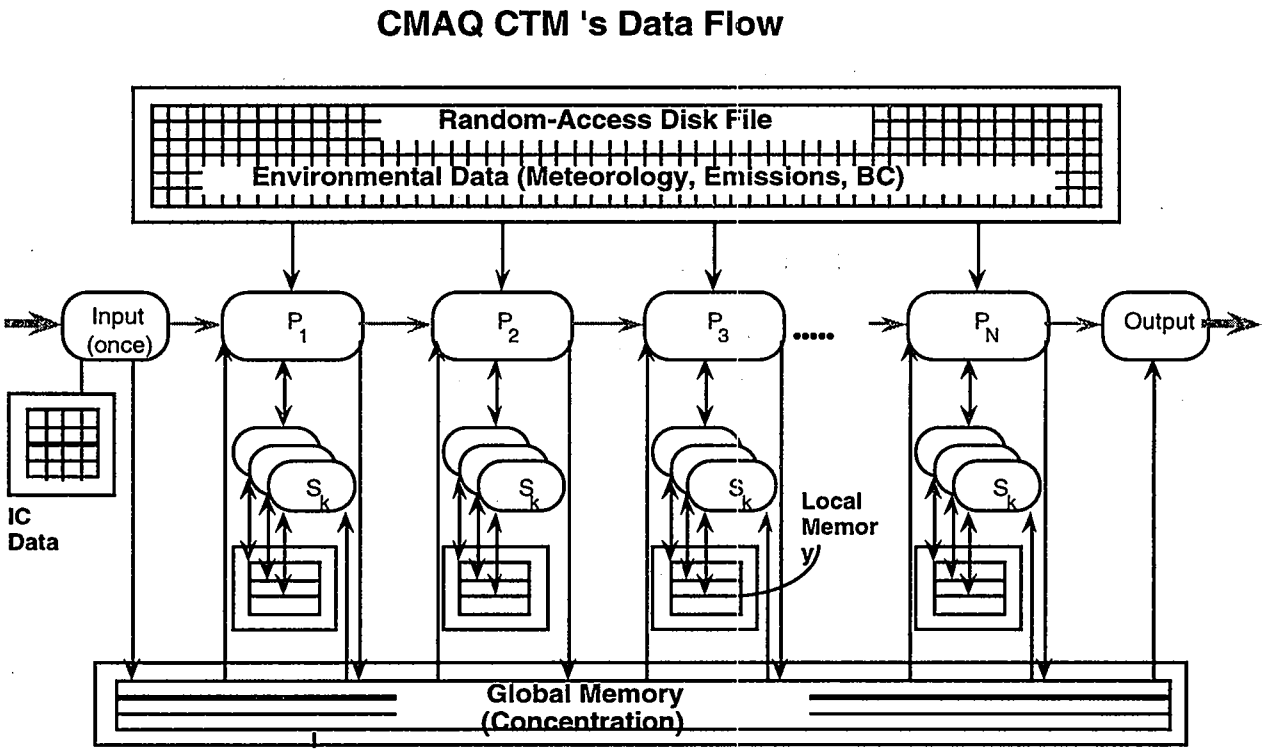

Figure 6-2. Data Dependencies Among Modules in CCTM. P and S_k represent a science process module and the related subroutines for the module, respectively. (From Byun et al., 1995.)

6.2.3.1 Driver Class for CCTM

The key function of the driver class module is hosting the science processors. It is responsible for coordinating model integration time (synchronizing fractional-time steps of science process call) and some input/output sequences. The driver structure of the current CCTM is given in Figure 6-3. A synchronization time step is used to ensure the global stability of the CCTM's numerical integration at the advection time step, which is based on a Courant number limit. Nesting requires finer synchronization time steps for the fine grid domain. The CCTM's process synchronization time steps are represented as integer seconds because the Models-3 I/O API can only handle integer seconds for I/O data. All the needed data are appropriately interpolated based on the synchronization time step. For maintaining numerical stability and for other reasons, an individual process module may have its own internal time steps. In general, each science process module uses the synchronization time step (Δt_{sync}) as the input time step of required environmental data. The global output time steps can be set differently from the

synchronization time step. Usually, the output time step (Δt_{out}) is set as one hour, but sub-hourly output down to the synchronization time step is possible.

Table 6-2. List of Science Process Subroutines Called by the CMAQ Driver

Subroutine	Science Class	Description
CGRID_MAP	UTIL	Sets up pointers for different concentration species: gas chemistry, aerosol, non-reactive, and tracer species
INITSCEN	INIT*	Initializes simulation time period, time stepping constants, and concentration arrays for the driver
ADVSTEP	DRIVER	Computes the model synchronization time step and number of repetitions for the output time step
COUPLE/ DECOUPLE	COUPLE*	Converts units and couples or de-couples concentration values with the density and Jacobian for transport
SCIPROC	DRIVER	Controls all of the physical and chemical processes for a grid (currently, two versions are available: symmetric and asymmetric around the chemistry processes)
XADV, YADV	HADV	Computes advection in horizontal plane (x- and y-directions)
ZADV	VADV	Computes advection in the vertical direction in the generalized coordinate system
ADJADV	ADJCON	Adjusts concentration fields to ensure mixing ratio conservation given mass consistency error in meteorology data
HDIFF	HDIFF	Computes horizontal diffusion
VDIFF	VDIFF	Computes vertical diffusion and deposition
CHEM	CHEM	Solves gas-phase chemistry
PING	PING	Computes effects of plume-in-grid process
AERO	AERO	Computes aerosol dynamics, particle formation, and deposition
CLDPRC	CLOUD	Computes cloud mixing and aqueous chemistry

*represents a process class that is part of DRIVER function.

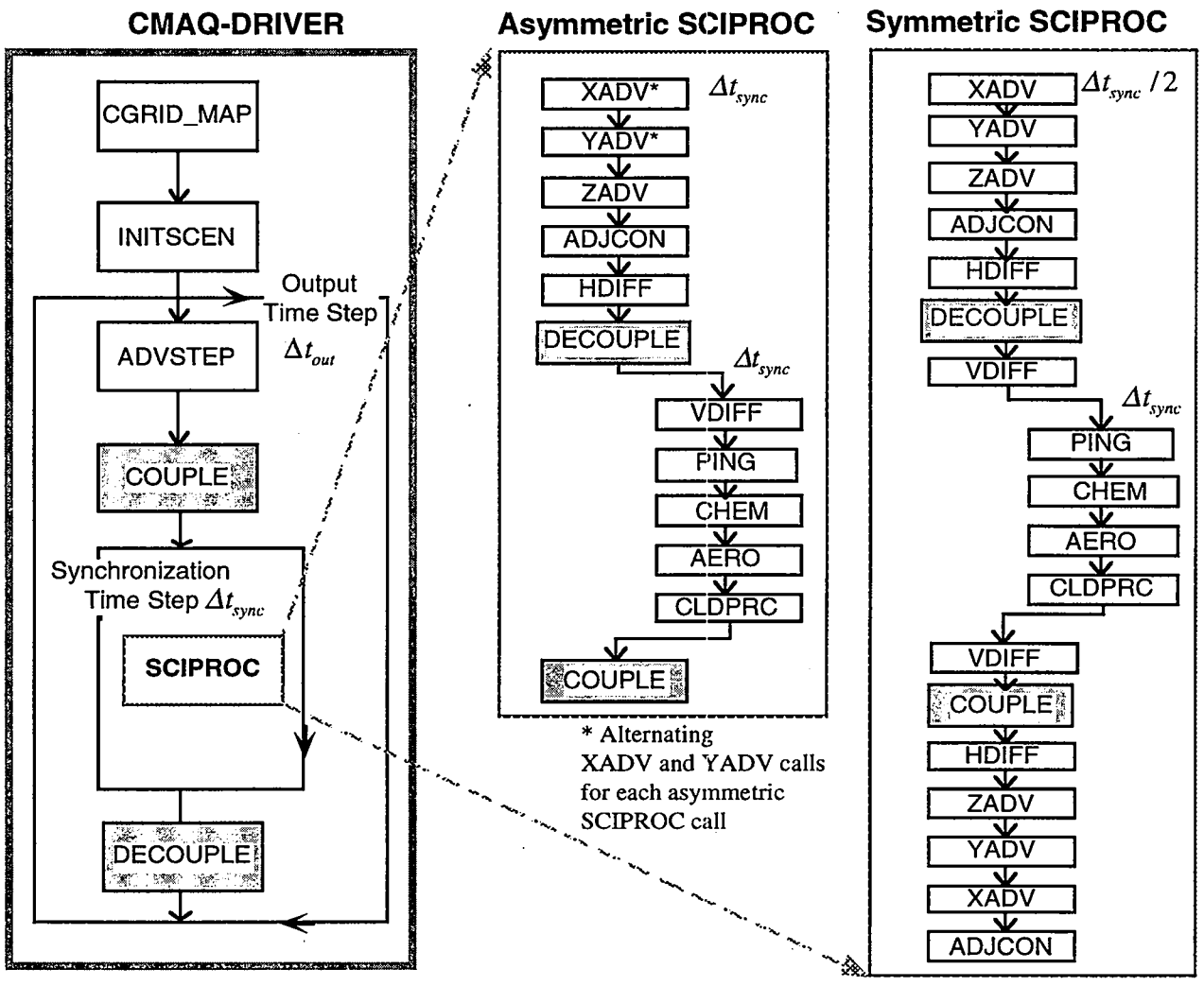

Figure 6-3. Driver Module and Its Science Process Call Sequence.
Both asymmetric and symmetric call sequences in SCIPROC are presented. Δt_{sync} and Δt_{out} are model synchronization and output time steps, respectively. Refer to Table 6-2 for the description of the subroutines.

The DRIVER program calls initialization routines to set up CCTM runs. It initializes the concentration field and checks if the input files, run time, and grid/coordinate information are consistent for a given scenario. Subroutines used for the initialization process are grouped into the INIT class. Usually, initial concentrations for gaseous species are in molar mixing ratio units (ppm) and aerosol species in density units (μg m^{-3}), the same as the output units of CMAQ. Also, DRIVER calls couple/decouple subroutines to convert concentration units for appropriate data processing. The pair of couple/decouple calls, which are available in the class COUPLE, limit the interchange of process modules between two different concentration units, such as density versus mixing ratio. The classes INIT and COUPLE are introduced just for the

convenience of code management from the point of view of science process modularity, and they should be considered as part of the DRIVER class modules.

6.2.3.2 Advection Processes for CCTM: HADV, VADV and ADJCON

For convenience, the advection process is divided into horizontal and vertical components. This distinction is possible because the mean atmospheric motion is mostly in horizontal planes. Usually the vertical motion is related with the interaction of dynamics and thermodynamics. The advection process relies on the mass conservation characteristics of the continuity equation:

$$\frac{\partial(\sqrt{\hat{\gamma}}\overline{\varphi}_i)}{\partial t} = -\nabla_\xi \bullet \left(\sqrt{\hat{\gamma}}\overline{\varphi}_i \overline{\hat{\mathbf{V}}}_\xi\right) - \frac{\partial(\sqrt{\hat{\gamma}}\overline{\varphi}_i \overline{\hat{v}^3})}{\partial \hat{x}^3} \tag{6-19}$$

Using the dynamically and thermodynamically consistent meteorology data from MCIP, we can maintain data consistency for air quality simulations at the synchronization time step. In case the meteorological data provided and the numerical advection algorithms are not exactly mass consistent, we need to solve a modified advection equation:

$$\frac{\partial(\sqrt{\hat{\gamma}}\overline{\varphi}_i)}{\partial t} = -\nabla_\xi \bullet \left(\sqrt{\hat{\gamma}}\overline{\varphi}_i \overline{\hat{\mathbf{V}}}_\xi\right) - \frac{\partial(\sqrt{\hat{\gamma}}\overline{\varphi}_i \overline{\hat{v}^3})}{\partial \hat{x}^3} + \overline{\varphi}_i \sqrt{\hat{\gamma}}\frac{Q_\rho}{\rho} \tag{6-20}$$

where Q_ρ is mass consistency error term (Byun, 1999). Equation 6-20 ensures conservation of mixing ratio, which is a necessary (though not sufficient) condition for preserving total tracer mass given significant fluctuations of density field in space and time. The equation shows that the correction term has the same form as a first-order chemical reaction whose reaction rate is determined by the mass consistency error (normalized with air density) in the meteorology data.

Modules in HADV class solve for the horizontal advection:

$$\frac{\partial(\sqrt{\hat{\gamma}}\overline{\varphi}_i)}{\partial t} = -\nabla_\xi \bullet \left(\sqrt{\hat{\gamma}}\overline{\varphi}_i \overline{\hat{\mathbf{V}}}_\xi\right) \tag{6-21}$$

and modules in VADV class solve for the vertical advection with boundary conditions $\overline{\hat{v}^3} = 0$ at the bottom and top of the model.

$$\frac{\partial(\sqrt{\hat{\gamma}}\overline{\varphi}_i)}{\partial t} = -\frac{\partial(\sqrt{\hat{\gamma}}\overline{\varphi}_i \overline{\hat{v}^3})}{\partial \hat{x}^3} \tag{6-22}$$

In simulating air quality, one of fundamental characteristic of the model application should be conservation of mass. Therefore, the modules in the ADJCON class solve for the mass correction term:

$$\frac{\partial(\sqrt{\hat{\gamma}}\overline{\varphi}_i)}{\partial t} = \overline{\varphi}_i \sqrt{\hat{\gamma}}\frac{Q_\rho}{\rho} \tag{6-23}$$

We wish to emphasize that the artificial distinction of advection modules between horizontal and vertical processes is not adequate and that all three modules (HADV, VADV, and ADJCON) should be considered as an integral unit for solving the physical advection process of trace species. The advection and mass adjustment algorithms are described in detail in Chapter 7.

6.2.3.3 Diffusion Process Classes for CCTM: HDIFF and VDIFF

For convenience the atmospheric diffusion process is divided into horizontal and vertical components. This distinction is needed because the vertical diffusion mostly represents the thermodynamic influence on the atmospheric turbulence by the air-surface energy exchange processes while the horizontal diffusion represents subgrid scale mixing due to the unresolved wind fluctuations. To handle the atmospheric diffusion processes in the generalized coordinates, we need to carefully examine the governing equation to properly set up the diffusion solver.

We start from the atmospheric diffusion equation in the same concentration units as used in advection:

$$\left.\frac{\partial \varphi_i^*}{\partial t}\right|_{diff} = \left.\frac{\partial\left(\sqrt{\hat{\gamma}}\overline{\rho}\overline{q}_i\right)}{\partial t}\right|_{diff} = -\hat{\nabla}_s \bullet \left[\sqrt{\hat{\gamma}}\overline{\rho}\hat{\mathbf{F}}_{q_i}\right] - \frac{\partial(\sqrt{\hat{\gamma}}\overline{\rho}\hat{F}^3_{q_i})}{\partial \hat{x}^3} + \sqrt{\hat{\gamma}}\overline{\rho}\left(\frac{Q_{\varphi_i}}{\overline{\rho}}\right) \qquad (6\text{-}24)$$

where $\varphi_i^* = \sqrt{\hat{\gamma}}\overline{\varphi}_i$, and the term $(Q_{\varphi_i} / \overline{\rho})$ is the time rate change of mass mixing ratio due to emissions of species i. Initially, it is assumed that we can decompose the diffusion into the horizontal and vertical components with respect to the curvilinear coordinates:

$$\left.\frac{\partial \varphi_i^*}{\partial t}\right|_{hdiff} = \left.\frac{\partial\left(\sqrt{\hat{\gamma}}\overline{\rho}\overline{q}_i\right)}{\partial t}\right|_{hdiff} = -\hat{\nabla}_\xi \bullet \left[\sqrt{\hat{\gamma}}\overline{\rho}\hat{\mathbf{F}}_{q_i}\right] \qquad (6\text{-}25)$$

$$\left.\frac{\partial \varphi_i^*}{\partial t}\right|_{vdiff} = \left.\frac{\partial\left(\sqrt{\hat{\gamma}}\overline{\rho}\overline{q}_i\right)}{\partial t}\right|_{vdiff} = -\frac{\partial(\sqrt{\hat{\gamma}}\overline{\rho}\hat{F}^3_{q_i})}{\partial \hat{x}^3} + \sqrt{\hat{\gamma}}\overline{\rho}\left(\frac{Q_{\varphi_i}}{\overline{\rho}}\right) \qquad (6\text{-}26)$$

Emissions can be included either in vertical diffusion or gas-phase chemistry module. If we can parameterize the turbulent fluxes directly in the curvilinear coordinates, we can implement HDIFF and VDIFF modules following Equations 6-25 and 6-26. When the turbulent fluxes are parameterized with eddy diffusion theory, the contributions of the off-diagonal (cross-directional) diffusion terms show up explicitly as shown in Equation 6-14:

$$\left.\frac{\partial \varphi_i^*}{\partial t}\right|_{cdiff} = \frac{\partial}{\partial \hat{x}^1}\left[\sqrt{\hat{\gamma}}\overline{\rho}(\hat{K}^{13}\frac{\partial \overline{q}_i}{\partial \hat{x}^3})\right] + \frac{\partial}{\partial \hat{x}^2}\left[\sqrt{\hat{\gamma}}\overline{\rho}(\hat{K}^{23}\frac{\partial \overline{q}_i}{\partial \hat{x}^3})\right]$$

$$+\frac{\partial}{\partial \hat{x}^3}\left[\sqrt{\hat{\gamma}}\overline{\rho}(\hat{K}^{31}\frac{\partial \overline{q}_i}{\partial \hat{x}^1}+\hat{K}^{32}\frac{\partial \overline{q}_i}{\partial \hat{x}^2})\right] \tag{6-27}$$

For a domain with a significant topographic feature, the module CDIFF must be implemented. However, the current CMAQ version does not include CDIFF module as the off-diagonal terms are often neglected in operational air quality models. In such a case, the HDIFF and VDIFF modules solve for diagonal terms (with respect to the curvilinear coordinates) as follows:

$$\left.\frac{\partial \varphi_i^*}{\partial t}\right|_{hdiff}=\frac{\partial}{\partial \hat{x}^1}\left[\sqrt{\hat{\gamma}}\overline{\rho}(\hat{K}^{11}\frac{\partial \overline{q}_i}{\partial \hat{x}^1})\right]+\frac{\partial}{\partial \hat{x}^2}\left[\sqrt{\hat{\gamma}}\overline{\rho}(\hat{K}^{22}\frac{\partial \overline{q}_i}{\partial \hat{x}^2})\right] \tag{6-25'}$$

$$\left.\frac{\partial \varphi_i^*}{\partial t}\right|_{vdiff}=\frac{\partial}{\partial \hat{x}^3}\left[\sqrt{\hat{\gamma}}\overline{\rho}(\hat{K}^{33}\frac{\partial \overline{q}_i}{\partial \hat{x}^3})\right] \tag{6-26'}$$

Compared with above formulations, let's consider the case that we approximate the quantity $\sqrt{\hat{\gamma}}\overline{\rho}$, which defines the computational grid, to be constant for the duration of synchronization time step for integrating the diffusion process with the fractional time-step method. Then, the problem becomes equivalent to solving for the diffusion equations in terms of the mass mixing ratio instead of density:

$$\left.\frac{\partial \overline{q}_i}{\partial t}\right|_{diff}=-\hat{\nabla}_\xi\bullet\left[\hat{\mathbf{F}}_{q_i}\right]-\frac{\partial(\hat{F}^3_{q_i})}{\partial \hat{x}^3}+\left(\frac{Q_{\varphi_i}}{\overline{\rho}}\right)-\hat{\mathbf{F}}_{q_i}\bullet\hat{\nabla}_\xi\left[\ln(\sqrt{\hat{\gamma}}\overline{\rho})\right]-\hat{F}^3_{q_i}\frac{\partial\left[\ln(\sqrt{\hat{\gamma}}\overline{\rho})\right]}{\partial \hat{x}^3} \tag{6-28}$$

If we rely on Equation 6-28 for representing the atmospheric diffusion process, the concentration must first be decoupled to obtain mass mixing ratio, q_i. Once the new mixing ratio is computed, it needs to be coupled with $\sqrt{\hat{\gamma}}\overline{\rho}$ to give the updated concentration in terms of φ_i^*. This means that the operator for the horizontal diffusion process should compute:

$$\left.\frac{\partial \overline{q}_i}{\partial t}\right|_{hdiff}=-\hat{\nabla}_\xi\bullet\left[\hat{\mathbf{F}}_{q_i}\right]-\hat{\mathbf{F}}_{q_i}\bullet\hat{\nabla}_\xi\left[\ln(\sqrt{\hat{\gamma}}\overline{\rho})\right] \tag{6-29}$$

and the vertical diffusion process should solve for:

$$\left.\frac{\partial \overline{q}_i}{\partial t}\right|_{vdiff}=-\frac{\partial(\hat{F}^3_{q_i})}{\partial \hat{x}^3}+\left(\frac{Q_{\varphi_i}}{\overline{\rho}}\right)-\hat{F}^3_{q_i}\frac{\partial\left[\ln(\sqrt{\hat{\gamma}}\overline{\rho})\right]}{\partial \hat{x}^3} \tag{6-30}$$

This approach is more convenient in numerically solving the flux-form turbulence mixing representation because most of the flux-based closure algorithms use parameterizations of turbulent fluxes in terms of conserving quantities, such as the mass mixing ratio, q_i. A considerable amount of meteorological and air quality literature on turbulence diffusion fails to clarify this important point. Especially for the case of multiscale applications, the representation of diffusion in terms of a conserving quantity is critical as shown by Venkatram (1993).

The effects of turbulence flux caused by the divergence of the grid boxes in the coordinate system need to be included in order to describe the turbulence exchange processes precisely. One can readily show that the coordinate-divergence term in Equation 6-30 vanishes for a mass conserving vertical coordinate. Similarly, when topographical features vary significantly and horizontal variations of the quantity $\sqrt{\hat{\gamma}}\bar{\rho}$ are large, one cannot neglect the last term in Equation 6-29. Chapter 7 of this document describes physical parameterization schemes and numerical algorithms for the horizontal and vertical diffusion processes in the CCTM.

One may wonder how deposition should be represented in the generalized coordinate system. In Eulerian air quality models, the deposition process affects the concentration in the lowest layer as a boundary flux condition. Considering the deposition process as the diffusion flux at the bottom of the model, we can relate the boundary condition in the generalized coordinate system to that of the Cartesian coordinate system as:

$$\hat{F}^3_{q_i}\Big|_{dep} = (\frac{\partial \hat{x}^3}{\partial x})F^x_{q_i}\Big|_{dep} + (\frac{\partial \hat{x}^3}{\partial y})F^y_{q_i}\Big|_{dep} + (\frac{\partial \hat{x}^3}{\partial z})F^z_{q_i}\Big|_{dep} = (\frac{\partial \hat{x}^3}{\partial z})F^z_{q_i}\Big|_{dep} \tag{6-31}$$

because $F^x_{q_i}\Big|_{dep}$ and $F^y_{q_i}\Big|_{dep}$ do not exist. Then, the effects of dry deposition on the species concentration is accounted for by the following relationship:

$$\frac{\partial \varphi^*_i}{\partial t}\Big|_{dep} = \frac{\partial\left(\sqrt{\hat{\gamma}}\bar{\rho}\bar{q}_i\right)}{\partial t}\Bigg|_{dep} = -\frac{\partial(\sqrt{\hat{\gamma}}\bar{\rho}\hat{F}^3_{q_i})}{\partial \hat{x}^3}\Bigg|_{dep} = -\frac{\partial}{\partial \hat{x}^3}\left(\sqrt{\hat{\gamma}}\bar{\rho}(\frac{\partial \hat{x}^3}{\partial z})F^z_{q_i}\right)_{dep}$$

$$\approx -\frac{-(\frac{\partial \hat{x}^3}{\partial z})_{dep}(\sqrt{\hat{\gamma}}\bar{\rho})\left(F^z_{q_i}\right)_{dep}}{(\Delta \hat{x}^3)_{dep}} = -\frac{v_d}{h_{dep}}(\sqrt{\hat{\gamma}}\bar{\rho})\bar{q}_i\Big|_{layer1} = -\frac{v_d}{h_{dep}}\varphi^*_i\Big|_{layer1} \tag{6-32}$$

where $h_{dep} = \left(\frac{\partial z}{\partial \hat{x}^3}\right)_{dep}(\Delta \hat{x}^3)_{dep}$ is the thickness of the lowest model layer in the geometric height coordinate. In the derivation of Equation 6-32, we assume that the deposition flux is constant in the lower part of the surface layer (i.e., a constant flux layer). Thus, the deposition velocities are computed at the middle (in terms of the generalized coordinate, ξ) of the lowest model layer at which the concentrations are represented. For the case in which the mass mixing ratio is used as the concentration variable for solving the diffusion equation, the deposition should be implemented as a boundary condition for the vertical diffusion (VDIFF) in the following manner:

$$\frac{\partial \bar{q}_i}{\partial t}\Big|_{dep} = -\frac{\partial(\hat{F}^3_{q_i})}{\partial \hat{x}^3}\Bigg|_{dep} = -\frac{\partial}{\partial \hat{x}^3}\left((\frac{\partial \hat{x}^3}{\partial z})F^z_{q_i}\right)_{dep} \tag{6-33}$$

Therefore, the bottom boundary condition for the VDIFF module is given as:

$$\left.\frac{\partial \overline{q}_i}{\partial t}\right|_{dep} = -\frac{\partial}{\partial \hat{x}^3}\left(\left(\frac{\partial \hat{x}^3}{\partial z}\right)F^z_{q_i}\right)_{dep} \approx -\frac{-\left(\frac{\partial \hat{x}^3}{\partial z}\right)_{bottom}\left(F^z_{q_i}\right)_{dep}}{(\Delta \hat{x}^3)_{dep}} = \frac{\left(F^z_{q_i}\right)_{dep}}{h_{dep}} = -\frac{v_d}{h_{dep}}\overline{q}_i\Big|_{layer1} \qquad (6\text{-}33')$$

Equations 6-32 and 6-33 show that we do not need to estimate contravariant deposition velocities if the deposition process is implemented as a bottom boundary condition in the generalized coordinate formulation.

In the current CCTM implementation, the concentration units for horizontal and vertical diffusion processes are density (coupled with Jacobian) and molar mixing ratio, $m_i = q_i \frac{M_{air}}{M_i}$, respectively. We have chosen m_i as the generic concentration unit for the vertical diffusion to coordinate with the emissions units in the data. Subsection 6.2.3.6 provides a detailed explanation for this. Therefore, HDIFF is placed outside and VDIFF is placed in between the pair of couple/decouple calls. Because the ratio of molecular weights are constant, equations for the vertical diffusion in terms of molar mixing ratio are equivalent to those in terms of mass mixing ratio, q_i. Refer to Chapter 7 for details of the computational algorithms for HDIFF and VDIFF.

6.2.3.4 Gas-phase Chemistry Process for CCTM

Instead of directly computing the time rate of change of φ_i^*, as is given by:

$$\left.\frac{\partial(\varphi_i^*)}{\partial t}\right|_{chem} = \sqrt{\hat{\gamma}}R_{\varphi_i}(\overline{\varphi}_1,\ldots,\overline{\varphi}_N) + \sqrt{\hat{\gamma}}Q_{\varphi_i} \qquad (6\text{-}34),$$

we need to decouple the Jacobian and air density in $\sqrt{\hat{\gamma}}\overline{\varphi}_i$ before computing gas-phase chemistry. This is useful because we can approximate that the computational grid remains constant for the duration of a synchronization time step, which is set by the Courant conditions for the fractional time step numerical integration schemes. Because the concentration unit required in the gas-phase chemistry is the volumetric mixing ratio, we rewrite the concentration φ_i^* as follows:

$$\varphi_i^* = \sqrt{\hat{\gamma}}\overline{\varphi}_i = \sqrt{\hat{\gamma}}\overline{\rho}\overline{q}_i\frac{M_{air}}{M_i}\frac{M_i}{M_{air}} = \overline{q}_i\frac{M_{air}}{M_i}\left[\sqrt{\hat{\gamma}}\overline{\rho}\frac{M_i}{M_{air}}\right]$$

$$= \overline{m}_i\left[\sqrt{\hat{\gamma}}\overline{\rho}\frac{M_i}{M_{air}}\right] \qquad (6\text{-}35)$$

where $\overline{m}_i = \overline{q}_i\frac{M_{air}}{M_i}$ is used as the definition of the volumetric or molar mixing ratio. The time rate of change of the volumetric mixing ratio due to the gas-phase chemistry is evaluated with the following equation:

$$\left.\frac{\partial \overline{m}_i}{\partial t}\right|_{chem} = \hat{R}_{m_i}(\overline{m}_1,\ldots,\overline{m}_N) + \hat{Q}_{m_i}(\overline{m}_i) \tag{6-36}$$

where $\hat{R}_{m_i}$ and $\hat{Q}_{m_i}$ represent chemistry reactions and source terms in molar mixing ratio units, respectively.

CMAQ employs generalized chemistry solvers, such as QSSA (Young et al., 1993) and SMVGEAR (Jacobson and Turco, 1994), which are designed to solve the nonlinear set of stiff ordinary equations presented in Equation 6-36. They can be applied independent of the coordinate and grid descriptions. To accommodate the need for modified or new chemical mechanisms, the CMAQ system is equipped with a generalized chemical mechanism processor. Refer to Chapter 8 for detailed description of numerical solvers used for gas-phase chemistry.

The Models-3 framework provides a mapping table to link chemistry mechanism species with surrogate species names in the initial and boundary condition files and emissions files. See Chapter 15 for details. When a new mechanism is used, appropriate emissions data must be supplied. It is possible to include emissions either in the gas-phase chemistry or in the vertical diffusion process. It is preferable that the emissions are interpolated with the same temporal interpolation schemes used in the transport processes.

6.2.3.5 Aerosol Process Class for CCTM

The fractional time step implementation solves for the effects of aerosol chemistry and dynamics on trace gas and aerosol species concentrations with:

$$\left.\frac{\partial \varphi_i^*}{\partial t}\right|_{aero} = \sqrt{\hat{\gamma}}R_{aero_i}(\overline{\varphi}_1,\ldots,\overline{\varphi}_N) + \sqrt{\hat{\gamma}}Q_{aero_i} - \hat{v}_g\frac{\partial \varphi_i^*}{\partial \xi} \tag{6-37}$$

where R_{aero_i} represents processes such as new particle formation and growth and depletion of existing particles. Q_{aero_i} stands for all the external sink and source terms, and $\hat{v}_g$ is the contravariant sedimentation velocity. The generic concentration units for the aerosol process are $[\mu g\ \ m^{-3}]$ (density) for aerosol mass and $[number\ \ m^{-3}]$ for aerosol particle number density. Because the aerosol process is called within the pair of couple/decouple calls, the input concentration is already decoupled and the following set of governing equations are solved in the aerosol process module:

$$\left.\frac{\partial \varphi_i}{\partial t}\right|_{aero} = R_{aero_i}(\overline{\varphi}_1,\ldots,\overline{\varphi}_N) + Q_{aero_i} - \hat{v}_g\frac{\partial \varphi_i}{\partial \xi} \tag{6-38}$$

The present implementation of the aerosol module in CCTM is derived from the Regional Particulate Model (Binkowski and Shankar, 1995). Here, primary particles are divided into two groups: fine particles and coarse particles. The fine particles result from combustion and secondary production processes and the coarse group is composed of materials such as wind-

blown dust and marine particles. The key scientific algorithms simulating aerosol processes for the CCTM are: (1) aerosol removal by size-dependent dry deposition; (2) aerosol-cloud droplet interaction and removal by precipitation; (3) new particle formation by binary homogeneous nucleation in a sulfuric acid/water vapor system; (4) the production of an organic aerosol component from gas-phase precursors; and (5) particle coagulation and condensation growth. Refer to Chapter 10 for details on aerosol process implemented in CCTM.

6.2.3.6 Emissions Process for CCTM

As mentioned earlier, the emissions process does not have its own science process class. Instead, it is included either in vertical diffusion or in the gas-phase chemistry process. In the governing conservation equations for the trace gases, the emissions process is represented simply as source terms.

If emissions data are given in the unit of time rate of change of mass, for example for particulate species, such as PM2.5 and PM10 in [$g\ s^{-1}$], they are expressed as:

$$Q_{\varphi_i} = \frac{E_i}{\delta V} = \frac{1}{\delta V}\overline{\frac{\partial(\varphi_i \delta V)}{\partial t}}\bigg|_{emis} = \frac{1}{\delta V}\overline{\frac{\partial(\rho q_i \delta V)}{\partial t}}\bigg|_{emis} \tag{6-39}$$

where δV is volume of the cell and $E_i = \overline{\frac{\partial(\varphi_i \delta V)}{\partial t}}\bigg|_{emis}$ represents the emissions rate into the cell. If the mass of air in the cell does not change for each time step (usually one hour), the concentration expression, either as the time rate of change of density or as the mass mixing ratio can be used. Otherwise, when the volume and density of a cell change substantially with time, the effect of change in air mass must be accounted for in determining the emissions rates.

For gaseous species, the time rate of change of E_I for each hour and each grid cell are provided in the three-dimensional emissions data files in molar units, (i.e., $mole\ \ s^{-1}$):

$$E_i = \left(\frac{M_{air}}{M_i}\frac{Q_{\varphi_i}}{\overline{\rho}}\right)\delta V \tag{6-40}$$

Emissions for gaseous species in molar units are preferred to those in mass units because molar units are the natural units for chemistry and mass units must be transformed into [$mole\ \ s^{-1}$] eventually for the gas-phase chemistry process. For gaseous species the molar mixing ratio and mass mixing ratio differ only by a simple multiplication factor, the ratio of molecular weights. However, for lumped species, the molecular weights are variable depending on the fractional compositions of the categorized hydrocarbon species in the emissions data. Therefore, transformation of emissions in mass units into the molar units for the lumped species can introduce misrepresentation of emissions amount. The data for the fractional compositions of the categorized hydrocarbon species are available in the emissions processor, Models-3 Emissions Projection and Processing System (MEPPS) (See Chapter 4). Thus, when emissions

data are processed in [$mole\ \ s^{-1}$] units, we do not have this conversion problem. Then the emissions process is represented as:

$$\left.\frac{\partial \overline{m}_i}{\partial t}\right|_{emiss} \approx \frac{M_{air}}{M_i}\frac{Q_{\varphi_i}}{\overline{\rho}} \tag{6-41}$$

An additional benefit is that the same transformation rule can be applied when emissions are included either in the vertical diffusion or in the chemistry.

6.2.3.7 Cloud Mixing and Aqueous-phase Chemistry (CLOUD) for CCTM

The rate of change in pollutant concentrations due to cloud processes is given by:

$$\left.\frac{\partial \overline{m}_i}{\partial t}\right|_{cld} = \left.\frac{\partial \overline{m}_i}{\partial t}\right|_{subcld} + \left.\frac{\partial \overline{m}_i}{\partial t}\right|_{rescld} \tag{6-42}$$

where subscripts *cld*, *subcld*, and *rescld* represent cloud, subgrid scale cloud, and resolved cloud, respectively. Although calls to the CLOUD module are made at every synchronization time step, the subgrid cloud effects are accounted for once an hour while the resolved cloud effects are impacted at each call. This is equivalent to assuming that the cloud life time of all sub-grid clouds is one hour. The effects of subgrid cloud processes, such as mixing (*mix*), scavenging (*scav*), aqueous-phase chemistry (*aqchem*), and wet deposition (*wdep*) on grid-average concentrations are parameterized with a "representative cloud" within the grid cell:

$$\left.\frac{\partial \overline{m}_i}{\partial t}\right|_{subcld} \sim f(mix,\ scav,\ aqchem,\ wdep) \tag{6-43}$$

where f represents a function of its arguments. We chose this expression because of the implicit nature of the algorithm representing the processes. For the resolved cloud, no additional cloud dynamics are considered in CMAQ and only effects of the scavenging and aqueous-phase chemistry are considered:

$$\left.\frac{\partial \overline{m}_i}{\partial t}\right|_{rescld} = \left.\frac{\partial \overline{m}_i}{\partial t}\right|_{scav} + \left.\frac{\partial \overline{m}_i}{\partial t}\right|_{aqchem} \tag{6-44}$$

See Chapter 11 for details of the cloud process descriptions.

6.2.3.8 Plume-in-Grid Process (PING) for CCTM

Anthropogenic precursors of the tropospheric loading of ozone, aerosols, and acidic species are largely emitted from major point sources, mobile sources, and urban-industrial area sources. In particular, inadequate spatial resolution of the major point source emissions can cause inaccurate predictions of air quality in regional and urban Eulerian air quality models. A plume-in-grid

(PinG) approach in CCTM provides a more realistic treatment of the subgrid scale physical and chemical processes for major elevated point source emitters (MEPSEs).

The PING module solves for:

$$\frac{\partial m_p}{\partial t} = \left.\frac{\partial m_p}{\partial t}\right|_{disp} + \left.\frac{\partial m_p}{\partial t}\right|_{emis} + \left.\frac{\partial m_p}{\partial t}\right|_{chem} + \left.\frac{\partial m_p}{\partial t}\right|_{dep} \tag{6-45}$$

where m_p is concentration of the subgrid plume (in molar mixing ratio) and the time-rate of change terms with subscripts *disp*, *emis*, *chem*, and *dep* represent effects of plume dispersion, point source emissions, plume chemistry, and dry deposition in the plume, respectively. The location and shape of plumes are determined by the PDM and plume chemistry is computed in the CCTM within plume subsections. When the subgrid scale phase of the plume simulation has been completed, the PING module updates grid scale concentrations with:

$$\left.\frac{\partial m_i}{\partial t}\right|_{ping} = \frac{\delta V_p}{\delta V}\frac{\partial (m_p - m_{ibg})}{\partial t} \tag{6-46}$$

where m_{ibg} is the back ground concentration and δV_p is the volume of plume in a grid cell with volume δV. Currently, only gaseous species are treated with the PING module. Readers are referred to Chapter 9 for the details. The work for the inclusion of particulates in the PING process has been started.

6.3 Equivalent Model Formulations for Different Vertical Coordinates

Because the CCTM is based on a generalized coordinate system, it is possible to emulate the governing equations of other popular Eulerian air quality models. For most urban and regional applications, the choice of horizontal map projection is handled with the map scale factors at the individual grid points. Therefore, there are no real differences in formulations in horizontal directions. One caveat is that the current CMAQ version is not tested with anholonomic coordinates, such as spherical coordinates. A few implementation details must be taken into account to accommodate the spherical coordinates. Most of the distinction of the dynamics is attributed to the choice of the vertical coordinate of the system.

The generalized governing conservation equation for trace species, written in the Reynolds flux form, is given in Equation 6-18. The same equation in eddy-diffusion form, in which the components of the eddy diffusivity tensor are represented in terms of those in Cartesian coordinates, is given below:

$$\frac{\partial}{\partial t}(J_\xi \overline{\varphi}_i) + m^2 \hat{\nabla}_\xi \bullet \left[\frac{J_\xi \overline{\varphi}_i}{m^2}\overline{\hat{\mathbf{V}}_\xi}\right] + \frac{\partial (J_\xi \overline{\varphi}_i \overline{\hat{v}^3})}{\partial \xi}$$

$$-m^2 \frac{\partial}{\partial \hat{x}^1}\left[\bar{\rho} J_\xi (K_{xx} \frac{\partial \bar{q}_i}{\partial \hat{x}^1})\right] - m^2 \frac{\partial}{\partial \hat{x}^2}\left[\bar{\rho} J_\xi (K_{yy} \frac{\partial \bar{q}_i}{\partial \hat{x}^2})\right]$$

$$-\frac{\partial}{\partial \xi}\left[\frac{\bar{\rho}}{J_\xi}[(\frac{\partial z_{sfc}}{\partial \hat{x}^1})^2 K_{xx} + (\frac{\partial z_{sfc}}{\partial \hat{x}^2})^2 K_{yy} + K_{zz}]\frac{\partial \bar{q}_i}{\partial \xi})\right]$$

$$= J_\xi\left[R_{\varphi_i}(\bar{\varphi}_1,\ldots,\bar{\varphi}_N) + Q_{\varphi_i}\right] + \left.\frac{\partial (J_\xi \bar{\varphi}_i)}{\partial t}\right|_{cld} + \left.\frac{\partial (J_\xi \bar{\varphi}_i)}{\partial t}\right|_{ping} + \left.\frac{\partial (J_\xi \bar{\varphi}_i)}{\partial t}\right|_{aero} \qquad (6\text{-}47)$$

In most popular air quality models, including the present implementation of the CCTM, the cross-terms from the off-diagonal components of the diffusivity tensor are neglected. Note that some models use wind components defined in Cartesian coordinates. The mass conservation characteristic of Equation 6-47 is heavily dependent on the quality of the wind data provided. In particular, depending on the dynamic assumptions used in atmospheric models, methods for estimating the contravariant vertical velocity component vary considerably. Refer to Chapter 5 for the details.

Formulations of other air quality models with popular meteorological vertical coordinates, such as z, σ_z, σ_{po}, and $\sigma_{\tilde{p}}$; and the step-mountain eta coordinate, η, can be obtained by substituting the appropriate vertical Jacobian in Equation 6-47. Refer to Table 6-3 for the coordinate definitions, associated Jacobians and contravariant vertical velocity components. Occasionally, one may find discrepancies in the governing equation between the one represented by Equation 6-47 and the one presented in the documentation of a specific model with the same vertical coordinates. Some of these can be attributed to the explicit representation of the dynamic characteristics and other idiosyncratic implementation practices used in those models. In the CCTM, the vertical coordinate is defined to increase with geometric height as given in Equation 6-4. This restriction simplifies interpretation of terms in the governing equations and eventually the computer coding of the algorithms. For example, the sign of the contravariant vertical velocity component is kept the same (i.e., positive value represents upward motion) across the different coordinate systems.

The terrain-influenced height coordinate σ_z has been used often for studying air quality especially with some simplifying conditions such as the Boussinesq approximation and anelastic assumption. For urban air quality simulations, there are a few examples of applying the σ_z coordinate defined with time and space dependent H (thickness of model), which is often related with the boundary layer height. The σ_z coordinate is used in air quality models, such as the Urban Airshed Model (UAM) (Scheffe and Morris, 1993), STEM-II (Carmichael et al., 1991), CIT (Harley et al., 1993), CALGRID (Yamartino et al., 1992), and others. The terrain-influenced reference pressure coordinate is used in SAQM (Chang et al., 1997), which is designed to be consistent with the nonhydrostatic MM5 meteorological model. The terrain-influenced time dependent hydrostatic pressure coordinate is used in RADM (Chang et al., 1987). It is the same coordinate used for MM4 or MM5 hydrostatic applications. Step-mountain eta coordinate is

used for NCEP's Eta meteorological model (Black, 1994, and Mesinger et al., 1988), but no operational air quality model using the eta coordinate is available.

Table 6-3. Vertical Coordinates and Associated Characteristics

CMAQ Coordinate $\hat{x}^3 = \xi$	Definition	Contravariant Vertical Velocity $\hat{v}^3$	Vertical Jacobian J_ξ	Remarks
Z		$w = \frac{dz}{dt}$	1	Geometric height
$\sigma_{\bar{z}}$	$\sigma_{\bar{z}} = H\frac{z - z_{sfc}}{H - z_{sfc}}$	$\frac{d\sigma_{\bar{z}}}{dt}$	$\frac{H - z_{sfc}}{H}$	H is the thickness of model and $\sigma_{\bar{z}}$ is the scaled height
σ_z	$\sigma_z = \frac{z - z_{sfc}}{H - z_{sfc}}$	$\frac{d\sigma_z}{dt}$	$H - z_{sfc}$	Nondimensional height, terrain-influenced
$1 - \sigma_{po}$	$\sigma_{po} = \frac{p_o - p_T}{p_{os} - p_T}$	$-\frac{d\sigma_{po}}{dt}$	$\frac{p_{os} - p_T}{\rho_o g}$	Nondimensional reference pressure
$1 - \sigma_{\tilde{p}}$	$\sigma_{\tilde{p}} = \frac{\tilde{p} - p_T}{\tilde{p}_s - p_T}$	$-\frac{d\sigma_{\tilde{p}}}{dt}$	$\frac{\tilde{p}_s - p_T}{\tilde{\rho} g}$	Nondimensional geostrophic pressure
$1 - \eta$	$\eta = \left(\frac{\pi - \pi_T}{\pi_s - \pi_T}\right)\eta_{sfc}$	$-\frac{d\eta}{dt}$	$\frac{\pi_s - \pi_T}{\tilde{\rho} g \eta_{sfc}}$	Step-mountain ETA $\eta_{sfc} = \left(\frac{p_o(z_{sfc}) - p_T}{p_o(0) - p_T}\right)$

6.4 Nesting Techniques

The nested grid CTM is needed to provide the required high resolution simulations. At present, Models-3 CMAQ allows only static grid nesting. In static grid nesting, finer grids (FGs) are placed (i.e., nested) inside coarser grids (CGs). The resolution and the extent of each grid are determined *a priori* and remain fixed throughout the CTM simulation. Static grid nesting conserves mass and preserves transport characteristics at the interfaces of grids with different resolutions (Odman et al., 1995). It allows for effective interaction between different scales with efficient use of computing resources. On the other hand, the nest domain is redefined during a simulation with the dynamic nesting. Both static and dynamic nesting techniques allow one-way or two-way exchange of information among FGs and the CG and periodically by independently simulating CTMs at each grid (coarse or nested) with its own time step. The dynamic nesting procedure is not implemented in the CMAQ system.

In one-way nesting, the primary concern is the mass conservation at the grid interface where boundary conditions are input to the FG using the CG solution. The advective flux at the inflow

boundaries of the FG is the flux as determined by the CG solution that passes through this interface. We also allow for time variation of the flux during the CG time step. This is performed by computing the departure point of the last particle passing through the interface for each FG time step. In the Lagrangian description, the mass crossing the interface is equal to the spatial integral of the concentration distribution between the departure point and the interface. Most flux-conserving advection schemes use the same Lagrangian concept to calculate the mass transfer between grid cells (e.g., Bott, 1989). During each FG time step, we meter into the FG the exact amount of mass that would have crossed the interface on the CG (Byun et al., 1996).

In two-way nesting, the concentrations are updated in each CG cell by averaging the concentrations of all the FG cells overlapping with the CG cell. Special care is required to assure strict mass conservation at the grid interface. The mass of some species (e.g., radicals) may no longer be conserved because, when advancing the FG solution, we perform nonlinear chemical transformations in addition to transport. However, the mass of the basic chemical elements such as sulfur, nitrogen, and carbon must be conserved. The FG solution is used to compute the flux of each element at the grid interface. When conservation principles are applied to the grid interface, as described above, the CG concentrations near the interface must be corrected (when the Courant stability limit is applied, only the first row of CG cells immediately outside the interface need correction). This is done by renormalizing the concentration of each species based on the assumption that the ratio of the species mass to element mass will remain the same before and after the correction. This method is similar to the renormalization procedure used to make slightly non-conservative chemical solvers strictly conservative. Alapaty et al. (1998) compares different spatial interpolation schemes used for the two-way nesting.

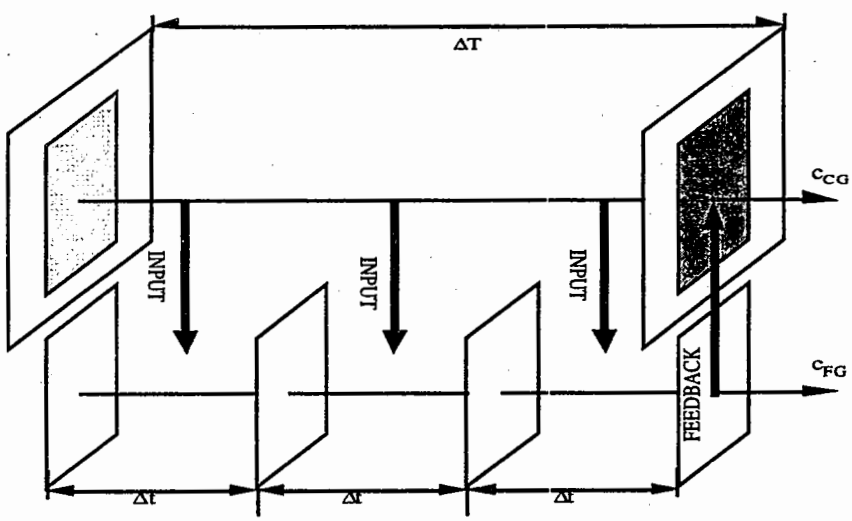

Figure 6-5. Static Grid Nesting Used in CMAQ System

The CCTM provides a static nesting (see Figure 6-5) capability while maintaining a high level of modularity by separately processing object codes for different grid domains and by enforcing the protocol that each module reads its required input data independently from others. The scheme

is also applicable for multiple and multi-level grid nesting. Multi-level nesting is a natural extension of the single static grid nesting. Figure 6-6 presents a schema for multi-level nesting, where three-levels are illustrated. The feedback processes update coarser grid concentrations at each synchronization time steps of the nest grids. The information about the grid is communicated to each process module through a set of FORTRAN include files specific to each grid domain during compilation time. This allows use of the same process modules for different grids. Customizing a nested model is as simple as preparing include files with grid dimensions for each grid and a driver with the appropriate process calling sequence.

As seen in Figure 6-6, the only difference between the one-way and two-way nesting is whether concentrations in coarser grid simulations are updated with the finer grid simulations through the feedback processors or not. Depending on the computer hardware and software configurations, one could build a nested CTM model with one executable collectively simulating all the FGs and CG, or with independent CTM executables for different grids that run simultaneously on multiple CPUs accessing common data through appropriate I/O API. The latter approach relies on the cooperating processors concept in a UNIX environment. As mentioned before, the current CMAQ version lacks a feedback module, which is necessary for the two-way nesting.

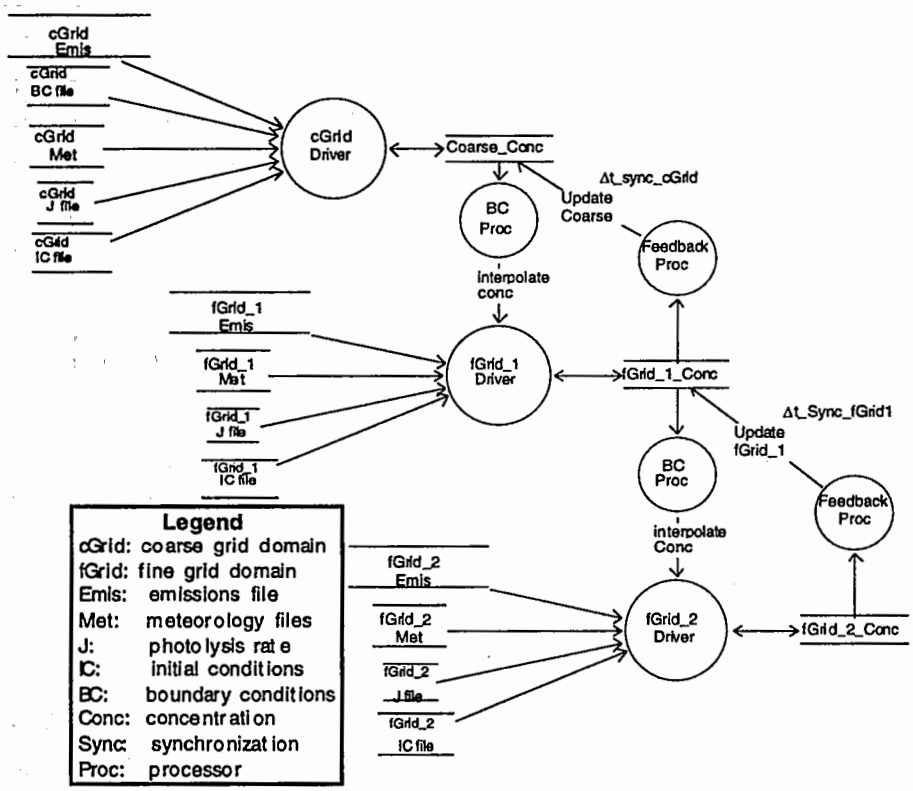

Figure 6-6. Schematics for Multi-level Nesting (three levels illustrated)

6.5 Summary

The CMAQ system achieves multi-pollutant and multiscale capabilities by combining several distinct modeling techniques. The generalized governing conservation equations of the CCTM allow transformation among various vertical coordinates (e.g., terrain-influenced geometric height, or pressure) and transformation among various horizontal coordinates, especially map projections (e.g., rectangular, Mercator, Lambert, and polar stereographic) by simple changes in a few scaling parameters defining the boundary domain, map origin, and orientation. Therefore, CMAQ can be configured to match the dynamic characteristics of the preprocessor meteorological models. The CMAQ system uses a nesting technique and a plume-in-grid approach to handle small scale air quality problems and subgrid scale plume dispersion and chemical reactions, respectively. The multi-pollutant capability is provided by a generalized mechanism reader and generalized chemistry solvers, linked cloud mixing and aqueous reaction processes, and aerosol modules. The CCTM code uses a modular structure that allows for the continuing improvement of the science and addition of new capabilities in a unified fashion. It provides a natural disciplinary distinction among different science processes through which developments in specific research areas can be readily incorporated.

As mentioned above, there remain a few implementation tasks, such as development of feed-back modules for two-way nesting and adaptation of anholonomic coordinates (e.g., latitude-longitude), which will provide additional functionalities in CCTM.

6.6 References

Alapaty, K., R. Mathur, and T. Odman, 1998: Intercomparison of spatial interpolation schemes for use in nested grid models. *Mon. Wea. Rev.* **126**, 243-249.

Binkowski, F. and U. Shankar, 1995: The regional particulate model, Part I: Model description and preliminary results. *J. Geophys. Res.*, **100**: 26191-26209.

Black, T., 1994: The new NMC mesoscale Eta model: Description and forecast examples. *Wea. Forecasting*, **9**, 265-278.

Bott, A., 1989: A positive definite advection scheme obtained by nonlinear renormalization of the advective fluxes. *Mon. Wea. Rev.* **117**, 1006-1015.

Byun D. W. , A. Hanna, C. J. Coats, and D. Hwang, 1995: Models-3 Air Quality Model Prototype Science and Computational Concept Development. *Trans. TR-24 Regional Photochemical Measurement and Modeling Studies*, 8-12 November 1993, San Diego, CA, Air & Waste Management Association. Pittsburgh, PA., 197-212.

Byun, D.W., D. Dabdub, S. Fine, A. F. Hanna, R. Mathur, M. T. Odman, A. Russell, E. J. Segall, J. H. Seinfeld, P. Steenkiste, and J. Young, 1996: Emerging Air Quality Modeling Technologies for High Performance Computing and Communication Environments, Air Pollution Modeling and Its Application XI, ed. S.E. Gryning and F. Schiermeier, 491-502.

Byun, D.W., J. Young., G. Gipson., J. Godowitch., F. Binkowsk, S. Roselle, B. Benjey, J. Pleim, J. Ching., J. Novak, C. Coats, T. Odman, A. Hanna, K. Alapaty, R. Mathur, J. McHenry, U. Shankar, S. Fine, A. Xiu, and C. Jang, 1998: Description of the Models-3 Community Multiscale Air Quality (CMAQ) model. Proceedings of the American Meteorological Society 78th Annual Meeting, Phoenix, AZ, Jan. 11-16, 1998. 264-268.

Byun, D. W., 1999: Dynamically consistent formulations in meteorological and air quality models for multi-scale atmospheric applications: II. Mass conservation issues. *J. Atmos. Sci.*, (in print).

Carmichael, G.R., L.K. Peters, and R.D. Saylor, 1991: The STEM-II regional scale acid deposition and photochemical oxidant model-I. An overview of model development and applications. *Atmos. Environ.* **25**, 2077-2090.

Chang, J.S., R.A. Brost, I.S.A. Isaksen, S. Madronich, P. Middleton, W.R. Stockwell, and C.J. Walcek, 1987: A three-dimensional Eulerian acid deposition model: Physical concepts and formulation, *J. of Geophys. Res.*, **92**, 14,681-700.

Chang J. S., S. Jin, Y. Li, M. Beauharnois, C.-H. Lu, H.-C. Huang, S. Tanrikulu, and J. DaMassa, 1997: *The SARMAP air quality model. Final Report*, SJVAQS/AUSPEX Regional Modeling Adaptation Project, 53 pp. [Available from California Air Resources Board, 2020 L Street, Sacramento, California 95814.]

Coats, C.J., cited 1996: The EDSS/Models-3 I/O Applications Programming Interface. MCNC Environmental Programs, Research Triangle Park, NC. [Available on-line from http://www.iceis.mcnc.org/EDSS/ioapi/H.AA.html.]

Harley, R.A., A.G. Russell, G.J. McRae, G.R. Cass, and J.H. Seinfeld. 1993: Photochemical modeling of the Southern California air quality study. *Envir. Sci. Technol.* **27**, 378-388.

Jacobson, M.Z. and R.P. Turco, 1994: SMVGEAR: A sparse-matrix vectorized Gear code for atmospheric models. *Atmos. Environ.* **20**, 3369-3385.

Mesinger, F., Z. I. Janjic, S. Nickovic, D. Gavrilov, and D. G. Deaven, 1988: The step-mountain coordinate: model description and performance for cases of Alpine lee cyclogenesis and for a case of Appalachian redevelopment. *Mon. Wea. Rev.*, **116**, 1493-1518.

Odman, M.T., R. Mathur, K. Alapaty, R.K. Srivastava, D.S. McRae, and R.J. Yamartino, 1995: Nested and adaptive grids for multiscale air quality modeling. U.S. EPA Workshop on Next Generation Models Computational Algorithms (NGEMCOM), Bay City, MI, June 1995.

Seaman, N. L., D. R. Stauffer, and A. M. Lario-Gibbs, 1995: A multiscale four-dimensional data assimilation system applied in the San Joaquin Valley during SARMAP. Part I: Modeling design and basic performance characteristics. *J. Appl. Meteor.*, **34**, 1739-1761.

Seinfeld, J.H., 1986: *Atmospheric Chemistry and Physics of Air Pollution*. Wiley-Interscience, New York.

Scheffe, R. D., and R. E. Morris, 1993: A review of the development and application of the Urban Airshed Model. *Atmos. Environ.*, **27B**, 23-39.

Srivastava, R.K., D.S. McRae, M.T. Odman, 1995: Governing Equations of Atmospheric Diffusion. Technical Report, MCNC [Available from MCNC-North Carolina Supercomputing Center, P.O. Box 12889, 3021 Cornwallis Rd. Research Triangle Park, NC 27709-2889.]

Schwartz, E. S. and P. Warneck, 1995: Units for use in atmospheric chemistry. *Pure & Appl. Chem.* **67**, Nos 8/9, 1377-1406.

Toon, O.B., R.P. Turco, D. Westphal, R. Malone, and M.S. Liu, 1988: A multidimensional model for aerosols: Description of computational analogs. *J. Atmos. Sci.*, **45**, 2123-2143.

Venkatram, A., 1993: The parameterization of the vertical dispersion of a scalar in the atmospheric boundary layer. *Atmos. Environ.* **27A**, 1963-1966.

Yamartino, R.J., J.S. Scire, G.R. Carmichael, and Y.S. Chang, 1992: The CALGRID mesoscale photochemical grid model - Part I. Model formulation, *Atmos. Environ.* **26A**, 1493-1512.

Young, J.O., E. Sills, D. Jorge, 1993: *Optimization of the Regional Oxidant Model for the Cray Y-MP*, EPA/600/R-94/065. [Available from U.S. Environmental Protection Agency, Research Triangle Park, NC 27711.]

This chapter is taken from *Science Algorithms of the EPA Models-3 Community Multiscale Air Quality (CMAQ) Modeling System*, edited by D. W. Byun and J. K. S. Ching, 1999.

Appendix 6A. Concentration Units Used for Air Quality Studies

As we have seen above, many different concentration units are used for air quality studies. In this section we summarize the relations among the concentration units and their conversion factors from one unit to another. For Models-3/CMAQ system we follow the International System of Units (Système International, SI) as a framework for units in the formulations. The fundamental assumption used here is that air and trace gases follow the ideal gas law, i.e.,

$$pV = vR_g T, \tag{6A-1}$$

where R_g is the universal gas constant $= 8.314510\ [J/(mol \bullet K)]$,
v is molar number,
V is volume of the gas $[m^3]$,
p is pressure $[Pa]$, and
T is temperature $[K]$.

There are many different ways to express the amount of substance in the atmosphere. We introduce most popular quantities and transformation relations among them are presented below.

Number Density, n

One way to express trace gas quantities is to count number of molecules in the unit volume. For example, number of molecules of air in the unit volume, n_{air}, is expressed as:

$$n_{air} = \frac{v_{air} N_A}{V} \tag{6A-2}$$

where v_{air} is number of moles of air,
N_A is the Avogadro's number $= 6.0221367 \times 10^{23}$, and
Similarly, number of molecules of trace gas per volume, i.e., number density of species n_i, is defined as:

$$n_i = \frac{v_i N_A}{V} = \frac{v_i N_A}{v_i R_g T / p_i} = \frac{p_i}{k_B T}\ [molecules\ \ m^{-3}] \tag{6A-3}$$

where v_i is number of moles of trace gas i in a given volume, and
$k_B = R_g / N_A$ is Bolzmann's constant
p_i is the partial pressure of species i.

Molar Density, c_i

The number of moles of air (c_{air}) and trace gas (c_i) normalized for a unit volume of air are simply defined as:

$$c_{air} = \frac{v_{air}}{V} \tag{6A-4a}$$

$$c_i = \frac{v_i}{V} \tag{6A-4b}$$

with the unit [$mole\ \ m^{-3}$]. Because the SI unit for the amount of substance is *mol*, this quantity can be used conveniently for expressing chemical relationships.

Partial Pressure, p_i

Although not used widely in atmospheric chemistry, the partial pressure has been playing an important role specifying thermodynamic properties of the atmosphere, especially for water vapor in the air. The Dalton's law states that the total pressure exerted by a mixture of gases is equal to the sum of the partial pressure exerted by each constituent at the given temperature and volume. Because we assume that each trace gas follows the ideal gas law, the partial pressure can be used to express the trace gas quantity. The partial pressure of atmospheric constituent gas is related to the number of moles per volume as:

$$p_i = \frac{v_i R_g T}{V} = c_i R_g T \tag{6A-5}$$

and the standard SI unit for the partial pressure is Pascal [Pa].

Molar Mixing Ratio, m_i

Often, the molar mixing ratio is used as a synonym for the volume mixing ratio, or the mole fraction of a substance in air. Basically it is a unitless quantity. However, it is customary to identify in terms of molar unit as [$mole/mole$]. Because the volume occupied by a mole of ideal gas at given pressure is the same regardless of the constituent, the mole fraction is essentially equal to the volume fraction. However, mole fraction is preferred because it does not require the implicit assumption of the ideality of the gases, and more importantly because it is applicable also to condensed-phase species (Schwartz and Warneck, 1995). For a given volume, the volume mixing ratio of a trace species is expressed in terms of concentration units defined above as:

$$m_i = \frac{v_i}{v_{air} + v_i} = \frac{c_i}{c_{air} + c_i} = \frac{p_i}{p}, \tag{6A-6}$$

where p is the total pressure.

Because $v_i << v_{air}$ for trace gases, Equation 6A-6 can be approximated as:

$$m_i \approx \frac{v_i}{v_{air}} = \frac{c_i}{c_{air}} = \frac{p_i}{p_{air}}$$

When dealing with trace gases in the real atmosphere, the contribution of moisture can be used in the definition of mixing ratio. Therefore, p_{air} represents total pressure of the atmosphere which includes vapor pressure of water while the contribution of other trace gases are neglected. Because the variation caused by the moisture can amount to several percent, some researchers prefer to use dry air when expressing trace gas mixing ratios. However, in the Models-3/CMAQ system, we use the trace gas mixing ratio with respect to the moist air because we rely on the continuity equation for the total air density to represent atmospheric mass conservation.

Mass Mixing Ratio, q_i

Mass mixing ratio is used often for describing transport process and is simply related with the volume mixing ratio as:

$$q_i = m_i \frac{M_i}{M_{air}} \tag{6A-7}$$

Density, φ_i

Concentrations of substances in air can be expressed in terms of amount of substance mass per volume of air, i.e. density. Density is a most popular unit for dynamic representation of atmospheric concentration because it is the operating units of the mass continuity equation. Density can be expressed in terms of other concentration units as:

$$\varphi_i = \frac{v_i M_i}{V} = c_i M_i = \frac{c_i}{c_{air}} c_{air} M_i$$

$$\approx (m_i \frac{M_i}{M_{air}})(c_{air} M_{air}) = q_i \rho_{air} \tag{6A-8}$$

Table 6A-1 provides cross-reference relationships among the concentration variables described. However, the individual process science area prefers to use certain specific units of decimal multiples of the SI unit suggested. We included the conversion factors among the concentration variables actually implemented in science process modules. Because it is convenient to express the conversion factors in terms of the dry air quantities, the virtual temperature is used in Table 6A-1.

Table 6A.1. Conversion formula among various trace gas concentration units used in the CMAQ system

	number density, N_i [$molecules/m^3$]	molar density, c_i [mol/m^3]	partial pressure, p_i [$Pascal$]	molar mixing ratio, m_i [$ppmV$]	mass mixing ratio, q_i [ppm]	density, φ_i [$\mu g/m^3$]
number density, N_i [$molecules/m^3$]	1	$N_i = (N_A)c_i$	$N_i = (k_B T)^{-1} p_i$	$N_i = 10^{-3} \bullet \left(N_A \frac{\rho_{air}}{M_{air}} \right) m_i$	$N_i = 10^{-3} \bullet \left(N_A \frac{\rho_{dr}}{M_i} \right) q_i$	$N_i = 10^{-6} \bullet \left(\frac{N_A}{M_i} \right) \varphi_i$
molar density, c_i [mol/m^3]	$c_i = (N_A)^{-1} N_i$	1	$c_i = (R_g T)^{-1} p_i$	$c_i = 10^{-3} \bullet \left(\frac{\rho_{air}}{M_{air}} \right) m_i$	$c_i = 10^{-3} \bullet \left(\frac{\rho_{air}}{M_i} \right) q_i$	$c_i = 10^{-6} \bullet (M_i)^{-1} \varphi_i$
partial pressure, p_i [$Pascal$]	$p_i = (k_B T) N_i$	$p_i = (R_g T) c_i$	1	$p_i = 10^{-6} \bullet (p) m_i$	$p_i = 10^{-6} \bullet \left(\frac{M_{air}}{M_i} p \right) q_i$	$p_i = 10^{-6} \bullet \left(\frac{R_g T}{M_i} \right) \varphi_i$
molar mixing ratio, m_i [$ppmV$]	$m_i = 10^3 \bullet \left(\frac{M_{air}}{\rho_{air} N_A} \right) N_i$	$m_i = 10^3 \bullet \left(\frac{M_{air}}{\rho_{air}} \right) c_i$	$m_i = 10^6 \bullet (p)^{-1} p_i$	1	$m_i = \left(\frac{M_{air}}{M_i} \right) q_i$	$m_i = 10^{-3} \bullet \left(\frac{M_{air}}{\rho_{air} M_i} \right) \varphi_i$
mass mixing ratio, q_i [ppm]	$q_i = 10^3 \bullet \left(\frac{M_i}{N_A \rho_{air}} \right) N_i$	$q_i = 10^3 \bullet \left(\frac{M_i}{\rho_{air}} \right) c_i$	$q_i = 10^6 \bullet \left(\frac{M_i}{p M_{air}} \right) p_i$	$q_i = \left(\frac{M_i}{M_{air}} \right) m_i$	1	$q_i = 10^3 \bullet (\rho_{air})^{-1} \varphi_i$
density, φ_i [$\mu g/m^3$]	$\varphi_i = 10^6 \bullet \left(\frac{M_i}{N_A} \right) N_i$	$\varphi_i = 10^6 \bullet (M_i) c_i$	$\varphi_i = 10^6 \bullet \left(\frac{M_i}{R_g T} \right) p_i$	$\varphi_i = 10^3 \bullet \left(\frac{\rho_{air} M_i}{M_{air}} \right) m_i$	$\varphi_i = 10^3 \bullet (\rho_{air}) q_i$	1

Note: Values for the Avogadro's constant (N_A) is 6.0221367x10^{23} [number/mol], the universal gas constant (R_g) is 8.314510 [$J/mol\text{-}K$], and the Boltzmann's constant (k_B) is defined with R_g / N_A. Molar mixing ratio is equivalent to volume mixing ratio and their units [ppmV], [ppb], and [ppt] are short hand notations for [μ mol mol^{-1}], [n mol mol^{-1}], and [p mol mol^{-1}], respectively. The unit for mass mixing ratio, [ppm], is a short hand for [10^{-6} kg kg^{-1}]. Both and may represent values for dry air or moisture air depending on applications. However, in one processing system, their usage should be consistent. M_{air} and M_i (molecular weight of species i) are in [g mol^{-1}] and ρ_{air} is in [kg m^{-3}].

EPA/600/R-99/030

EPA/600/R-99/030

Chapter 7

NUMERICAL TRANSPORT ALGORITHMS FOR THE COMMUNITY MULTISCALE AIR QUALITY (CMAQ) CHEMICAL TRANSPORT MODEL IN GENERALIZED COORDINATES

Daewon W. Byun,[*] Jeffrey Young,[**] and Jonathan Pleim[**]
Atmospheric Modeling Division
National Exposure Research Laboratory
U.S. Environmental Protection Agency
Research Triangle Park, NC 27711

M. Talat Odman[+] and Kiran Alapaty
MCNC-Environmental Programs
P.O. Box 12889, 3021 Cornwallis Road
Research Triangle Park, NC 27709-2889

ABSTRACT

The transport processes in the atmosphere primarily consist of advection and diffusion, except for the mixing of pollutants by the parameterized subgrid-scale clouds. In this chapter, numerical algorithms for advection, vertical diffusion, and horizontal diffusion implemented in the Community Multiscale Air Quality (CMAQ) chemical transport models are discussed. To provide the CMAQ system with multiscale capability, we have formulated the transport processes, both advection and diffusion, in conservation (i.e., flux) forms for the generalized coordinate system. Therefore the numerical transport algorithms implemented in CMAQ will function under a wide variety of dynamical situations and concentration distribution characteristics. Users can not only choose transport algorithms from optional modules available in CMAQ, but also are encouraged to experiment with their own algorithms to test different numerical schemes for air quality simulations.

---

[*]On assignment from the National Oceanic and Atmospheric Administration, U.S. Department of Commerce. Corresponding author address: Daewon W. Byun, MD-80, Research Triangle Park, NC 27711. E-mail: bdx@hpcc.epa.gov

[**]On assignment from the National Oceanic and Atmospheric Administration, U.S. Department of Commerce.

[+]Present Affiliation: Georgia Institute of Technology, Atlanta, GA.

7.0 NUMERICAL TRANSPORT ALGORITHMS FOR THE COMMUNITY MULTISCALE AIR QUALITY (CMAQ) CHEMICAL TRANSPORT MODEL IN GENERALIZED COORDINATES

In this chapter, we study numerical algorithms for the transport processes in a turbulent atmosphere. Many of the contents provided here are the results of a collaborative research project, the EPA's Cooperative Agreement CR822053-01 with MCNC-Environmental Programs (Exploratory Research on Air Quality Modeling Techniques: Research on Numerical Transport Algorithms for Air Quality Simulation Models), and other related in-house projects at EPA. Readers are referred to Alapaty et al. (1997), Byun (1999a, b), Byun and Lee (1999), and Odman (1998) for additional information.

In principal, the transport process consists of advection and diffusion that cause the movement and dispersion of pollutants in space and time. Transport of pollutants by the parameterized subgrid-scale cloud modules is not considered here. We have assumed that the transport of pollutants in the atmospheric turbulent flow field can be described by means of differential equations with appropriate initial and boundary conditions. In Eulerian air quality models, the transport process is modeled using numerical algorithms. These numerical algorithms for the advection and diffusion processes must satisfy several properties that are essential for making useful air quality simulations. As with all numerical methods, the numerical schemes for solving the transport equations must meet convergence conditions and correctly model the conservation, dissipation, and dispersion properties of the governing equations. A numerical scheme is said to be convergent if the solution approaches the true solution of the corresponding partial differential equation as the grid spacing and time-step size become infinitesimally small. Thus, a convergent numerical scheme can provide a numerical solution of any desired accuracy within finite precision bounds by reducing the grid spacing and the time-step size. For linear equations, consistency and stability are both necessary and sufficient conditions for convergence (Lax's equivalence theorem). In practice, machine precision and the computational resource availability limit the reduction of grid spacing and time-step size. Therefore, numerical errors associated with using limited grid spacing and time-step sizes must be of concern.

There have been many studies on the numerical advection algorithms used in air quality models. The reason it attracted so much attention is that the equation is hyperbolic in nature and spatial discretization of the solution generates a finite number of Fourier modes that travel at different speeds and leads to constructive and destructive interference. If the high wave-number Fourier modes are damped significantly, then numerical diffusion becomes prevalent. Solving the diffusion equation, on the other hand, is a lot safer because the stiffness matrix is diagonally dominant and the discretized solution is stable and sign preserving for a relatively wide range of conditions (Chock, 1999).

Transport processes are of central importance in turbulent flow studies, and in the literature there are numerous transport algorithms that have different numerical characteristics and varying degrees of accuracy and computational complexity. The skill needed here is to select appropriate numerical schemes that provide solutions with the desired accuracy at reasonable computational cost. This document does not intend to provide an extensive review of the transport algorithms used in air quality modeling. Instead, we describe several popular numerical schemes implemented in the Community Multiscale Air Quality Chemical Transport Model (CMAQ CTM or, hereafter, CCTM), expecting users to choose the algorithms appropriate to their own study objectives. We offer a few examples of good transport algorithms and present some key numerical characteristics users should look for. With this information, users can find the best algorithms through evaluation processes, and may even bring in their own algorithms to build a transport model for their applications. To provide the CMAQ system with the multiscale and multi-pollutant capabilities, we strive to incorporate schemes that can function under a wide variety of dynamic situations and distribution characteristics (e.g., distributions of different primary species and secondary species are quite distinct). Also, the schemes should be efficient in the use of computer time and storage. Selected numerical transport algorithms for horizontal and vertical advection and for vertical and horizontal diffusion are described below.

7.1 Numerical Advection Algorithms

Numerical advection algorithms for air quality models should satisfy several computational requirements.

- They should be free of mass conservation errors to accurately account for pollutant sources and sinks.
- They should have small numerical diffusion to minimize the spread of a signal in every direction and the smoothing of spatial gradients.
- They should also have small phase errors since disturbances that propagate at different speeds produce spurious oscillations.
- Given initial positive concentrations, the schemes should be positive-definite (i.e., they should not produce negative concentrations.
- They should be monotonic (i.e., they should not produce new extrema).

While it is essential that the schemes be positive-definite, this alone may not be sufficient because the monotonic property, for example, is just as desirable for air quality modeling.

Numerical algorithms have not been able to satisfy all the requirements listed above, and they are imperfect, with varying degrees of accuracy. Advection schemes with different properties introduce different errors, all of which are sources of uncertainty in air quality model predictions. Before recommending its use, it is critical to identify which of the computational properties a scheme possesses. Because an advection scheme with all the desired properties is not currently available, a user needs to select a scheme with the most desirable properties and greatest efficiency to meet the needs of the application.

7.1.1 Conservation Form Equation for Advection

The atmospheric advection process is expressed in conservation (flux) form as:

$$\left.\frac{\partial \varphi_i^*}{\partial t}\right|_{adv} = -\nabla_\xi \bullet \left(\varphi_i^* \overline{\hat{\mathbf{V}}}_\xi\right) - \frac{\partial(\varphi_i^* \overline{\hat{v}^3})}{\partial \hat{x}^3} \tag{7-1}$$

where φ_i^* is the concentration of trace species i coupled with the coordinate Jacobian. Refer to Chapters 5 and 6 for the definition of symbols used in Equation 7-1. For convenience, the advection process is decomposed into horizontal and vertical advection processes, with the fractional time-step implementation:

$$\left.\frac{\partial \varphi_i^*}{\partial t}\right|_{hadv} = -\nabla_\xi \bullet \left(\varphi_i^* \overline{\hat{\mathbf{V}}}_\xi\right) = -\frac{\partial(\varphi_i^* \overline{\hat{v}^1})}{\partial \hat{x}^1} - \frac{\partial(\varphi_i^* \overline{\hat{v}^2})}{\partial \hat{x}^2} \tag{7-2}$$

$$\left.\frac{\partial \varphi_i^*}{\partial t}\right|_{vadv} = -\frac{\partial(\varphi_i^* \overline{\hat{v}^3})}{\partial \hat{x}^3} \tag{7-3}$$

where $\overline{\hat{v}^1}$, $\overline{\hat{v}^2}$ and $\overline{\hat{v}^3}$ are contravariant components of wind velocity. Splitting of the three-dimensional (3-D) advection into the horizontal and vertical components will lead some difficulties, such as the representativeness of the mass continuity and setting up of proper boundary conditions for non-orthogonal horizontal and vertical directions when simulating a region with complex topography.

Many models further split the horizontal advection equation in two directions and solve for two one-dimensional equations, one in each direction, using the solution of one as the initial condition of the other. We refer to this scheme as a one-dimensional (1-D) algorithm. Others solve the two-dimensional (2-D) form directly. Although using 1-D schemes is very common, it has been found that problems can arise due to this additional splitting (Flatoy, 1993, and Odman and Russell, 1993). Although 2-D schemes may be more desirable in this regard, fewer have been tested and they are often more difficult to implement and less computationally efficient than 1-D schemes. Also, there are general conditions in which the splitting scheme is actually more stable

and accurate than the non-splitting case for higher-order approximations because the splitting scheme intrinsically contains cross-spatial derivatives whereas the non-splitting scheme would not (Leith, 1965). Yanenko (1971) has shown that time-splitting is second-order accurate if the one-component advection operators commute. Alternating the sequence of operations would be quasi-second-order accurate in the case of non-commutativity (Chock, 1999). Here, only 1-D schemes will be discussed. When using appropriately interpolated contravariant wind components, the 1-D advection in the generalized coordinate system is equivalent to the 1-D equation in the Cartesian coordinate system. Therefore, it is sufficient here to discuss advection algorithms in Cartesian coordinates.

The 1-D advection equation written in the Cartesian coordinate system is:

$$\frac{\partial \varphi}{\partial t} + \frac{\partial (u\varphi)}{\partial x} = 0 \tag{7-4}$$

Equation 7-4 is the flux (or conservation) form and the quantity $F_x = u\varphi$ is defined as the one-dimensional constituent flux. The flux form is a natural choice here because it is based on the continuity equation without any assumptions on the atmospheric dynamics. Maintaining the advection equation in flux form is key to providing transport schemes with multiscale and multi-pollutant capabilities. A flux-form discretization of Equation 7-4 with first-order accuracy in time results in:

$$\varphi_j^{n+1} = \varphi_j^n - \frac{\Delta t}{\Delta x_j}\left(F_{j+1/2}^n - F_{j-1/2}^n\right) \tag{7-5}$$

where $F_{j+1/2}^n$ and $F_{j-1/2}^n$ denote the advective fluxes through the faces of cell j, Δt is the time-step and $\Delta x_j = x_{j+1/2} - x_{j-1/2}$ is the horizontal grid spacing. To maintain numerical stability, and to accommodate other physical changes such as emissions input in a synchronized way, the time-step of 1-D advection should satisfy the Courant-Friedrich-Lewy (CFL) condition for hyperbolic equations:

$$\max_j(\beta_{j+1/2}) \le 1 \tag{7-6}$$

where $\beta_{j+1/2} = \left|u_{j+1/2}\right| \frac{\Delta t}{\Delta x_j}$ is the Courant number for advection. This condition should be viewed as a method defining a reference time scale for accommodating different physical processes in AQMs. If we do not consider the synchronization of mass injection to the cell through other physical processes, the CFL condition can be determined separately for individual advection schemes. For certain schemes the restriction can be significantly less than one. And for

advection alone, an implicit scheme may not have the Courant number restriction for stability (Chock, 1999).

7.1.2 Classification of Advection Schemes

Numerical advection schemes in the literature were developed using several different approaches (e.g., Chock and Dunker, 1983, and Chock, 1985, 1991). Following Rood (1987), we classify these schemes based on the methods used in their formulations. However, reviews in the literature may not capture the most recent developments in advection research. Depending on the methods used, the schemes may be classified as:

- Finite difference schemes;
- Finite volume schemes;
- Flux corrected schemes;
- Lagrangian Schemes;
- Finite element schemes; or
- Spectral schemes.

The distinction is somewhat arbitrary and only meant to convey the key intrinsic features of the scheme. Current trends in advection scheme development show a merging of the methods to take advantage of the most desirable properties of several schemes. For example, the Characteristic-Galerkin method (Childs and Morton, 1990) combines the best of the finite element and Lagrangian methods. Flux corrections are being used in the framework of finite element and spectral schemes (Löhner et al., 1987). Also, the classical finite difference schemes are being abandoned in favor of modern finite volume schemes. Refer to Odman (1998) for details of the classification.

7.1.3 Description of Advection Schemes in CCTM

In this section we describe the schemes that are available with the first release of the CCTM codes in the following order: the piecewise parabolic method (PPM), the Bott scheme (BOT), and the Yamartino-Blackman Cubic scheme (YAM).

Odman (1998) provides additional descriptions of the Smolarkiewicz scheme (SMO), the accurate space derivative scheme (ASD) (Chock,1991, and Dabdub and Seinfeld,1994), the flux-corrected transport, the semi-Lagrangian method, and the chapeau function scheme with Forester filter. These codes are not integrated into the CMAQ system yet, but along with other advection modules, will be added to the system in the near future.

To simplify the discussion, we will consider a uniform (i.e., constant $\Delta x = \Delta x_j$) and staggered grid (φ_j represents the grid cell average of the concentration, while $u_{j+1/2}$ is the advection velocity defined at grid cell interfaces). While discussing the finite-volume schemes (the piecewise parabolic method, the Bott scheme and the Yamartino scheme) below, we use the explicit flux formula presented in Equation 7-5. Further, a nondimensional coordinate η is defined as $\eta = (x - x_{j-1/2})/\Delta x$, so that, in grid cell j, $0 \le \eta \le 1$. Now, suppose that the concentration has a certain distribution $\varphi_j(\eta)$ in each grid cell. Depending on the direction of the velocity, the flux $F_{j+1/2}$ can be expressed as:

$$F_{j+1/2} = \begin{cases} \dfrac{\Delta x}{\Delta t} \displaystyle\int_{1-\beta_{j+1/2}}^{1} \varphi_j(\eta) d\eta, & u_{j+1/2} \ge 0 \\ \dfrac{\Delta x}{\Delta t} \displaystyle\int_{0}^{\beta_{j+1/2}} \varphi_{j+1}(\eta) d\eta, & u_{j+1/2} < 0 \end{cases} \tag{7-7}$$

where $\beta_{j+1/2}$ is the Courant number at the right boundary of grid cell j.

The conditions of high-order accuracy and freedom from spurious oscillations are difficult to be achieved simultaneously. The usual way to satisfy one of these conditions without significant violation of the other is to introduce a correction mechanism. Typically, this mechanism is provided by nonlinear flux-corrections, or by nonlinear filtering. In advection schemes, such adjustments are either applied implicitly through the solution or explicitly as a subsequent step to the linear solution. There is extensive literature on both solution algorithms (linear and nonlinear) and explicit nonlinear mechanisms.

7.1.3.1 Piecewise Parabolic Method (PPM)

In the piecewise parabolic method (Colella and Woodward, 1984) the concentration distribution is assumed to be parabolic in any given grid cell. In terms of the grid cell average concentration φ_j and the predicted values of the parabola at the left and right boundaries of the cell $\varphi_{L,j}$ and $\varphi_{R,j}$, this distribution can be written as:

$$\varphi_j(\eta) = \varphi_{L,j} + \eta\left[\left(\varphi_{R,j} - \varphi_{L,j}\right) + 6\left(\varphi_j^n - \frac{\varphi_{L,j} + \varphi_{R,j}}{2}\right)(1-\eta)\right] \tag{7-8}$$

Since the initial cell average is known, the construction of the parabola involves the determination of the edge values. First, an approximation to φ at $x_{j+1/2}$ is computed subject to the constraint

that its value is within the range of the values at the neighboring cells. For the uniform Δx_j, a first guess for $\varphi_{j+1/2}$ is estimated with:

$$c_{j+1/2} = \frac{7}{12}(c_j^n + c_{j+1}^n) - \frac{1}{12}(c_{j+2}^n + c_{j-1}^n) \tag{7-9}$$

In smooth parts of the solution away from extrema, $\varphi_{L,j+1} = \varphi_{R,j} = \varphi_{j+1/2}$ so that the distribution is continuous at $x_{j+1/2}$. In other parts, the cell boundary values are further modified so that φ is monotonic on each grid cell. This step introduces discontinuities at cell edges and yields a piecewise continuous global distribution for concentration. There are two cases where the edge values are modified. First, if φ_j is a local extremum, then the distribution is assumed to be constant instead of parabolic. The second case is when φ_j is between $\varphi_{L,j}$ and $\varphi_{R,j}$, but sufficiently close to one of the values so that the parabola may take on values outside the range, and lead to overshoots or undershoots. In this case, to make the distribution monotonic, one of the edge values is reset so that the derivative of $\varphi(\eta)$ is zero at the opposite edge.

The most distinctive feature of this monotonic scheme is that the nonlinear adjustments are purely geometric. The numerical diffusion introduced by this scheme may be slightly higher than in some other schemes discussed here, but its monotonic property is desirable for photochemical modeling purposes. The scheme has been used in meteorological modeling (e.g., Carpenter et al., 1990) and in air quality models (Odman et al., 1993) including the CCTM. The scheme can be modified so that, in the neighborhood of a discontinuity, it produces a narrower profile. This feature, known as steepening, avoids the smearing of sharp gradients. Though Carpenter et al. (1990) did not recommend steepening for meteorological modeling, this feature may be beneficial in air quality modeling practice, where steep gradients may occur in the vertical direction. However, it should be noted that steepening is of no value and the PPM reverts to a lower order method in the case of sharp spikes or extreme values in a single cell such as emissions from point sources.

7.1.3.2 Bott Scheme (BOT)

The numerical scheme introduced in Bott (1989) is a positive definite scheme with small numerical diffusion. The distribution of the concentration within the cell is represented by a polynomial of order l as:

$$\varphi_j(\eta) = \sum_{k=0}^{l} a_{j,k}\eta^k \tag{7-10}$$

The polynomial can be made area-preserving by requiring:

$$\varphi_{j+i} = \int_{i}^{i+1} \sum_{k=0}^{l} a_{j,k} \eta^k d\eta, \; i = 0, \pm 1, \pm 2, \ldots, \pm \frac{l}{2} \tag{7-11}$$

over a stencil of l+1 grid cells by varying the value of i. The solution to this linear system yields the coefficients $a_{j,k}$. The coefficients obtained this way for a quadratic (l=2) and quartic (l=4) together with those of the donor cell (or upwind) scheme, and Tremback's scheme with second-order polynomials (Tremback et al., 1987), are listed in Table 7-1.

Using Equation 7-7, integrating the polynomial of Equation 7-10 between appropriate limits, we arrive at a first estimate of the fluxes. Finally, to make the scheme positive-definite, the total outflux from cell j is limited by requiring that it should be positive and less than what the available mass in the cell would allow:

$$0 \le F_j^{\text{out}} \le \frac{\Delta x}{\Delta t} c_j \tag{7-12}$$

The outflux F_j^{out} is a combination of the boundary fluxes and its expression depends on the sign of the velocities. In the CCTM implementation, we used fourth-order polynomials as recommended by Bott (1989) except for the boundary cells. The scheme is receiving increasing attention in current air quality models because of its high accuracy and low computational cost.

Recently, a monotonic version of the scheme was also developed (Bott, 1992) and the time-splitting errors associated with the use of one-dimensional operators in multidimensional applications were reduced (Bott, 1993). Monotonicity is obtained by directly replacing the positive-definite flux limiter of the original approach by new monotone flux limiters as:

$$\begin{aligned} &\min\left(\varphi_{j-1}^n, \varphi_j^n\right) \le \varphi_j^{n+1} \le \max\left(\varphi_{j-1}^n, \varphi_j^n\right), \text{ if } u \ge 0 \\ &\min\left(\varphi_{j+1}^n, \varphi_j^n\right) \le \varphi_j^{n+1} \le \max\left(\varphi_{j+1}^n, \varphi_j^n\right), \text{ if } u < 0 \end{aligned} \tag{7-13}$$

Although the new flux limited Bott scheme yields monotonic results, there is an inherent mass conservation problem. This problem is directly related to the flux limiting that takes place. Near the leading edge of a sharp wave the use of second or higher order polynomials causes an underestimation of a certain advective flux, $F_{k-1/2}$. When this flux is not corrected it is less than $F_{k+1/2}$, and an undershoot occurs in cell k, as experienced with the original algorithm (Bott, 1989). The motivation for the monotone flux limitation is to avoid such undershoots. However, there are cases when the monotone flux limiter leaves the underestimated flux intact. Instead of increasing the underestimated flux, the limiter reduces the advective flux downwind, $F_{k+1/2}$, in order to avoid an undershoot in cell k. This eventually reduces the net flux out of the domain resulting in an accumulation of mass in the domain.

Table 7-1. Coefficients of the Polynomials Used in Each Scheme

	Donor Cell	Tremback-2	Bott-2	Bott-4
a_0	φ_j	φ_j	$-\frac{1}{24}(\varphi_{j+1}-26\varphi_j-\varphi_{j-1})$	$\frac{1}{1920}(9\varphi_{j+2}-116\varphi_{j+1}+2134\varphi_j-116\varphi_{j-1}+9\varphi_{j-2})$
a_1	—	$\frac{1}{2}(\varphi_{j+1}-\varphi_{j-1})$	$\frac{1}{2}(\varphi_{j+1}-\varphi_{j-1})$	$\frac{1}{48}(-5\varphi_{j+2}+34\varphi_{j+1}-34\varphi_{j-1}+5\varphi_{j-2})$
a_2	—	$\frac{1}{2}(\varphi_{j+1}-2\varphi_j+\varphi_{j-1})$	$\frac{1}{2}(\varphi_{j+1}-2\varphi_j+\varphi_{j-1})$	$\frac{1}{16}(-\varphi_{j+2}+12\varphi_{j+1}-22\varphi_j+12\varphi_{j-1}-\varphi_{j-2})$
a_3	—	—	—	$\frac{1}{12}(\varphi_{j+2}-2\varphi_{j+1}+2\varphi_{j-1}-9\varphi_{j-2})$
a_4	—	—	—	$\frac{1}{24}(\varphi_{j+2}-4\varphi_{j+1}+6\varphi_j-4\varphi_{j-1}+\varphi_{j-2})$

7.1.3.3 Yamartino-Blackman Cubic Scheme (YAM)

Yamartino (1993) presents another finite volume scheme where the interpolating polynomial is a cubic spline:

$$\varphi_j(\eta) = a_0 + a_1\eta + a_2\eta^2 + a_3\eta^3 \tag{7-14}$$

where
$$\begin{aligned} a_0 &= \varphi_j \\ a_1 &= d_j\,\Delta x \\ a_2 &= -\frac{1}{4}(\varphi_{j+1}-2\varphi_j+\varphi_{j-1}) + \frac{3\Delta x}{8}(d_{j+1}-d_{j-1}) \\ a_3 &= (\varphi_{j+1}-\varphi_{j-1}) - \frac{\Delta x}{6}(d_{j+1}+10d_j+d_{j-1}) \end{aligned} \tag{7-15}$$

The spline derivatives, d_j, are obtained from the tridiagonal system:

$$\alpha\, d_{j-1} + (1-2\alpha)\, d_j + \alpha\, d_{j+1} = \frac{\varphi_{j+1}-\varphi_{j-1}}{2\Delta x} \tag{7-16}$$

with α=0.22826. Note that a value of α=0 would correspond to explicit expressions of d_j.

The positivity of $\varphi_j(\eta)$ is ensured by various mechanisms. First, when φ_j is a local minimum, a donor-cell scheme is used instead of the cubic spline. Second, the spline is spectrally limited by the relation:

$$\left|\frac{a_k}{a_0}\right| \le \frac{\pi^k}{k!}, \quad k = 1,2,3. \tag{7-17}$$

Third, a mass conservative flux renormalization is applied, where the fluxes are normalized with the ratio for the upwind cell of the cell concentration (i.e., concentration at η=0) divided by the average concentration. Finally, a mildly diffusive filter is applied in an attempt to block the depletion of donor cells. Yamartino's scheme is not monotonic and can generate new maxima.

7.1.4 Treatment of Boundary Conditions

Mathematically, the advection equation is a first-order hyperbolic partial differential equation, so it accepts only inflow boundary conditions. Physically, the solution is not affected by the downwind concentrations, so no outflow boundary conditions should be imposed. In practice, however, some outflow boundary conditions have to be imposed. Often, the characteristics of a numerical advection scheme are affected by the boundary condition used.

In the CCTM, a positive-definite zero-flux outflow boundary condition with appropriate flow divergence restriction is used. The zero-flux divergence condition at the boundary (flux gradient out of the boundary cell is set equal to the flux gradient into the cell, i.e., $u_1(\varphi_1 - \varphi_0)/\Delta x = u_2(\varphi_2 - \varphi_1)/\Delta x)$ gives:

$$\varphi_0 = \max\left\{0,\ \varphi_1 - \frac{u_2}{u_1}(\varphi_2 - \varphi_1)\right\} \tag{7-18}$$

where φ_0, φ_1, and φ_2 represent concentrations outside the computational domain, at the boundary cell, and first cell of the inner domain, respectively. u_1 is wind at the outer boundary flux point and u_2 is wind at the inner boundary flux point. Refer to Figure 7-1 for the cell subscript definitions at the outflow boundary. To prevent spurious boundary flux situations that are often associated with the zero-flux divergence boundary condition, the following constraints are applied. When u_1 is sufficiently small (for example smaller than 10^{-3} m/s), or when the wind is divergent at the boundary cell (i.e., $u_1 \bullet u_2 < 0$), a zero concentration gradient at the outflow boundary (i.e., $\varphi_0 = \varphi_1$) is imposed. This boundary scheme can be used with any of the numerical advection algorithms implemented in CCTM.

On the other hand, Odman (1998) introduced a "no condition at outflow boundary" [sic], for Bott's scheme where the scheme is modified to remove the need for the concentration φ_0 at the downwind cell. A first-order polynomial (derived from φ_1 and φ_2) is used in Cell 1 to compute the flux out of the domain. A second-order polynomial (derived from φ_1, φ_2 and φ_3 is used in Cell 2 and a fourth-order polynomial is used in Cell 3. Mathematically, this condition is more correct than the others. However, the order of the polynomial is reduced to one at the boundary while the other conditions use a second-order polynomial to compute the flux out of the domain. Because of the lack of generality of this approach, we have not implemented Odman's boundary scheme in the CCTM. The improved positive-definite zero-flux outflow boundary condition scheme essentially reproduces his results without having to rely on the modified advection algorithms near boundary.

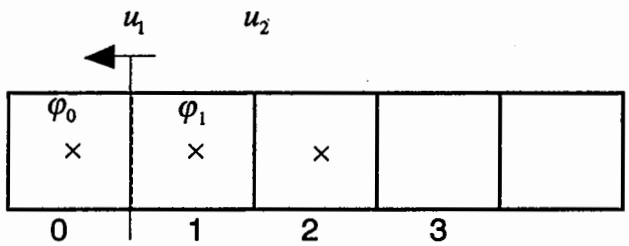

Figure 7-1. Outflow boundary condition. Cell 0 is outside the domain. Vertical solid line denotes the domain boundary and the vertical dotted lines denote the cell interfaces. The advection scheme computes concentrations for Cells 1, 2, 3, and so on.

7.1.5 Test of Algorithms with Idealized Linear Horizontal Flow Fields

Typically, the performances of advection schemes are measured and compared with each other using test cases with idealized flow fields. These ideal flow tests have analytic solutions and may be very useful for determining certain properties of the schemes. Odman (1998) provides some evaluation results identifying schemes with desirable properties. Here we summarize the results of the one-dimensional tests and rotating cone test. The evaluation and comparison of the schemes are based on the performance measures listed in Table 7-2. Again, readers are referred to Odman (1998) for the details of the analysis.

Table 7-2. Summary of Performance Measures Used to Test the Effects of Numerical Advection. φ_i^* and φ_i^{*e} methods and exact concentrations.[+]

Performance Measure	Formula	Description
peak ratio[&]	$\frac{\max(\varphi_i^*)}{\max(\varphi_i^{*e})}$	Measure of peak preservation (best when 1.0)
Background to peak ratio	$\frac{\min(\varphi_i^*)}{\max(\varphi_i^{*e})}$	Measure of ripples introduced by a non-monotonic scheme
mass ratio	$\frac{\sum(\varphi_i^*)}{\sum(\varphi_i^{*e})}$	Measure of mass conservation characteristic (best when 1.0)
Distribution ratio	$\frac{\sum(\varphi_i^*)^2}{\sum(\varphi_i^{*e})^2}$	Measure of shape retention (best when 1.0)
Average absolute error	$\frac{1}{N}\sum\lvert\varphi_i^* - \varphi_i^{*e}\rvert$	Measure of absolute difference (best when 0.0)
root-mean square error	$\sqrt{\frac{1}{N}\sum\left(\frac{\varphi_i^* - \varphi_i^{*e}}{\varphi_i^{*e}}\right)^2}$	Measure of distribution error (best when 0.0)

[+] To account for the total mass correctly, the concentration should be coupled with the Jacobian of the grid system
[&] Peak ratio alone is not a meaningful criteria unless the positions of the computed and actual peaks are also given.

7.1.5.1 Advection of One-Dimensional Pulses

Various tests have been conducted in the literature with pulses of different shapes advected with uniform velocity. We conducted tests using a Gaussian signal of exactly 8Δx width with 100 ppm peak advected from cell 25 to cell 75 in a 100-cell uniform grid domain. Background values were set at 5 ppm. Table 7-3 summarizes the value of various performance measures after advected the signal for a distance of 50Δx at a Courant number of 0.25 (i.e., after 200 time-steps). The Accurate Space Derivative (ASD) and Yamartino's schemes (YAM) preserved the peak height very well. However, the distribution ratio has a lower value for YAM, indicating distortions of the pulse's shape. For the same reason, the average and RMS errors are larger than those of the ASD. On all accounts, these two schemes perform much better than the other schemes in this test. Bott's scheme (BOT) ranks third overall, but large ripples are observed at leading and trailing edges of the pulse as indicated by the values below the background (as much as 4% of the peak height). When the monotonic limiter is used (BOT-M), the ripples are eliminated but the peak retention performance deteriorates. Also, a 2% increase in mass is observed. PPM is somewhat more diffusive than BOT-M. However, PPM performed better than BOT-M in minimizing the average absolute error and root mean square error and because it is intrinsically monotonic, did better in regard to shape retention as measured by the distribution ratio. Smolarkiewicz's scheme (SMO) displays poorer performance than the other schemes.

SMO produces ripples upwind from the pulse and leads to average and RMS errors larger than other schemes.

Table 7-3. Gaussian signal test (Abridged from Odman, 1998)

Scheme	ASD	BOT	BOT-M	PPM	SMO	YAM
Peak Ratio	0.99	0.87	0.74	0.69	0.61	0.98
Background	0.05	0.01	0.05	0.05	0.02	0.05
Mass Ratio	1.00	1.00	1.02	1.00	1.00	1.00
Distribution	0.99	0.93	0.83	0.79	0.66	0.92
Average Error	0.08	0.87	1.38	1.16	2.21	0.51
RMS Error	0.01	0.18	0.27	0.17	0.50	0.12

7.1.5.2 Rotating Cone Test

In this test, a cone-shaped puff is introduced into a rotational flow field and followed for a certain number of revolutions. The exact solution is a rigid-body rotation of the puff without any change to its original shape. Various errors can be revealed in this test. For example, numerical diffusion (or dissipation) manifests itself in the drop of the peak height during rotation. Also, by observing the location of the peak, one can determine the leading or lagging phase-speed errors.

A 32x32 grid is used for this test (i.e., $-16\Delta x \le x \le +16\Delta x$; $-16\Delta y \le y \le +16\Delta y$ $\Delta x = \Delta y$). A cone-shaped puff with peak concentration equal to 100 ppm and a base radius of $4\Delta x$ is initialized such that its peak is located at $[+8\,\Delta x, 0]$. Note that the peak is not initially at a grid-cell center but a cell corner (i.e., there are four cells around the peak with the same average concentration). The background concentration is set to 5 ppm. To obtain a counterclockwise rotation around an axis passing through the center of the domain, the wind field is defined as $u = -\omega y$ and $v = \omega x$. The angular velocity, ω, is adjusted so that the Courant number of approximately 0.28 at the location of the peak of the puff.

Table 7-4. Rotating Cone Test (Abridged from Odman, 1998)

Scheme	ASD	BOT	BOT-M	BOT2D	PPM	SMO	YAM
Peak Ratio	0.99	0.87	0.65	0.65	0.61	0.49	0.99
Background	0.06	0.03	0.06	0.06	0.06	0.02	0.06
Mass Ratio	1.00	1.00	1.02	1.02	1.00	1.00	1.00
Distribution	0.96	0.93	0.83	0.83	0.78	0.64	0.91
Average Error	0.18	0.46	0.76	0.76	0.54	1.60	0.33
RMS Error	0.05	0.16	0.30	0.30	0.18	0.51	0.13

ASD and YAM maintain the peak height and the overall shape of the cone better than the others. BOT performs third best in this test, but it yields non-monotonicity, which results in values below the background (as seen in a ring-shaped valley at the base of the cone). BOT-M and

PPM predict similar peak heights (65% and 61%, respectively), but the shape distortions look very different in each case. PPM has the worst peak clipping effect but the resulting shape has the smallest base span among the three schemes. SMO is clearly the most diffusive scheme; it also introduces a ripple upwind from the cone. Table 7-4 summarizes the performance measures at the end of two rotations. Since there is no shear in the flow field, BOT-M and the two-dimensional version of Bott's scheme (BOT2D) (Bott, 1993) produce identical results. Again, the mass conservation problem is revealed with BOT-M. BOT preserves 87% of the peak height (third best after ASD and YAM), but it leads to ripples with an amplitude of 3% of the original peak height. Performances of BOT-M and PPM are comparable in predicting the peak. But PPM produces the lower distribution ratio, smaller absolute average and RMS errors. Notice that the comparison results obtained from this test are very similar to those of the Gaussian signal test. Additional test results such as skew advection of a point-source plume and advection with shear flow are available in Odman (1998). Also, effects of density distribution on the numerical advection are studied with a set of linear flows in Byun and Lee (1999). The solvers integrated into the CCTM are BOT, PPM and YAM. Although ASD has very high accuracy except for the $2\Delta x$ wavelengths, ASD is neither strictly mass conservative nor monotonic. It is also the most CPU-intensive scheme (taking about 4-5 times longer than BOT). In addition to BOT's overall performance, results reported in Odman (1998) for a broad series of tests showed that BOT had the best computational performance of all the schemes tested. However, because of the concerns over the non-monotonicity about BOT and the mass conservation problem and diffusive nature of BOT-M, we chose PPM for a number of demonstration executions (Byun et al., 1998). Similar testing with BOT and YAM is underway. We intend to integrate other methods into the CCTM at a later time.

7.1.6 Vertical Advection

Algorithms in the CCTM for vertical advection are essentially the same as those for the one-dimensional horizontal algorithms. However, the vertical advection is performed in terms of the generalized vertical coordinate in CMAQ. The contravariant vertical velocity component is used as the transport wind for the irregular vertical grid spacing (usually expanding with altitude) represented in the generalized coordinate. For the irregular grid, the computational time-step should satisfy the CFL condition:

$$\Delta t \le \min_k \{ \frac{\Delta\xi_{k-1}}{\left|\hat{v}^3{}_{k-1/2}\right|}, \frac{\Delta\xi_k}{\left|\hat{v}^3{}_{k-1/2}\right|}, \frac{\Delta\xi_k}{\left|\hat{v}^3{}_{k+1/2}\right|}, \frac{\Delta\xi_{k+1}}{\left|\hat{v}^3{}_{k+1/2}\right|} \} \tag{7-19}$$

As in the case of Cartesian representation, we assume there is no mass exchange by advection (i.e., $\overline{\hat{v}^3} = 0$) at the top and bottom boundaries of the model. Therefore, there is no need to apply special algorithms for the boundary process. Because vertical grid spacing is usually irregular in

most air quality models, a scheme that can accommodate irregular spacing must be used for vertical advection. This means that numerical algorithms used to represent the vertical advection may be different from that used for horizontal advection. For example, when the ASD algorithm, which requires equal spacing in the computational domain, is used for horizontal advection, a numerical algorithm that allows irregular spacing (e.g., BOT and PPM) would need to be used for vertical advection.

7.1.7 Adjustment of Mass Conservation Error

Recently, Byun (1999a, b) has highlighted the importance of dynamic consistency in meteorological and air quality modeling for multiscale atmospheric applications. Mass consistency quantifies how well the density and wind fields satisfy the continuity equation for air. One of the fundamental requirements for the numerical transport algorithms used in air quality models is the conservation of trace species in the domain. Ideally, the input meteorological data for air quality simulations should be mass consistent. However, using numerical models with highly parameterized physical and cloud algorithms, inappropriate set of governing equations, misapplication of four-dimensional data assimilation (FDDA) schemes, or using incomplete objective analysis methods to characterize the atmosphere for a CTM could result in meteorological conditions that are not mass consistent. In this situation, even precisely mass conserving numerical algorithms may fail to conserve trace species mass in the domain. Preferably, the mass inconsistency must be minimized before air quality simulation using a suitable diagnostic relation or a variational wind field adjustment scheme as discussed in Byun (1999b) and in Chapter 5. For certain vertical coordinates with appropriate dynamic assumptions, the diagnostic methods can be used within the CTM to provide mass consistent wind data. This is accomplished usually by adjusting the vertical wind component for the advection process. However, the variational methods are applied during the meteorological data preparation stage, instead of inside CTMs, mostly due to the computational efficiency reasons.

Whether the meteorological data are mass consistent or not, Byun (1999b) has shown that the tracer mixing ratio must be conserved as a precondition for the tracer mass conservation. He has reported several adjustment schemes used in current air quality models and proposed a two-step time splitting numerical algorithm that satisfies the mixing ratio conservation equation. In the event the meteorological data are not mass consistent, the mixing-ratio conservation scheme is demonstrated to be useful for photochemical air quality models where chemical production and loss terms are computed using molar mixing ratio. For this purpose, Equation 7-1 should be modified as follows to conserve trace species:

$$\frac{\partial \varphi_i^*}{\partial t} = -\frac{\partial(\varphi_i^* \overline{\hat{u}})}{\partial \hat{x}^1} - \frac{\partial(\varphi_i^* \overline{\hat{v}})}{\partial \hat{x}^2} - \frac{\partial(\varphi_i^* \overline{\hat{v}^3})}{\partial \hat{x}^3} + \varphi_i^* \frac{Q_\rho}{\rho} \qquad (7\text{-}20)$$

where Q_ρ is the density error term for the meteorological data. This is a necessary condition for the tracer mass conservation. The total tracer mass of the domain is conserved only when the additional condition that total air mass of the domain is conserved, i.e.:

$$\iiint_{\partial\Omega} \frac{J_s}{m^2} Q_\rho dV = 0 \tag{7-21}$$

where $\partial\Omega$ represents the boundary of a computational domain. However, even this condition does not guarantee the cell base conservation of tracer mass except for the case of uniform mixing ratio, because $\iiint_{\partial\Omega} \varphi_i^* \frac{Q_\rho}{\rho} dV = \iiint_{\partial\Omega} q_i \frac{J_s}{m^2} Q_\rho dV \neq q_i \iiint_{\partial\Omega} \frac{J_s}{m^2} Q_\rho dV$ in general. Because of this, the correction methods should only be used for improving mass conservation characteristics of the numerical advection algorithms after the mass inconsistency is minimized . Nevertheless, if the objective is to maintain the property of cell-based mixing ratio conservation, the mass conservation error caused by the inconsistency in meteorology data ($\varphi_i^* \frac{Q_\rho}{\rho}$) can be corrected with:

$$(\varphi_i^*)^{cor} = (\varphi_i^*)^T \exp[\int \frac{Q_\rho}{\rho} dt] \tag{7-22}$$

where superscripts '*T*' and '*cor*' represent values after transport (advection) and after correction, respectively. Table 7-5 summarizes several adjustment methods reported in Byun (1999b). An adequate correction scheme for photochemical Eulerian AQMs should conserve the tracer mixing ratio at least even if wind and density fields are not mass consistent. The correction scheme proposed and labeled *A5* in Table 7-5 is expected to maintain conservation of mixing ratio up to machine precision. Correction schemes *A1* and *A2* ignore the effects of coordinate/grid structures during the advection process. For Cartesian coordinates where the Jacobian is uniform and constant with time, the scheme *A2* is equivalent to *A5*. For a steady-state flow, schemes *A3*, *A4*, and *A5* become identical. Note that all the correction algorithms in Table 7-5 become the same for a steady state flow with uniform density distribution in Cartesian coordinates.

Table 7-5. Trace Gas Mass Correction Schemes

Symbol	Correction Method	Mass correction algorithm
A0	No correction	
A1	Advection of unity	$\varphi_i^{cor} = \frac{\varphi_i^T}{\varphi_r^T}\varphi_r, \ \varphi_r = 1.0$
A2	Advection of air density	$\varphi_i^{cor} = \frac{\varphi_i^T}{\rho^T}\rho^{\text{int}}$
A3	Advection of $\rho J_\xi / m^2$ with anelastic approximation	$(\varphi_i J_\xi / m^2)^{cor} = (c_i J_\xi / m^2)^T \exp\left[\frac{(\rho J_\xi / m^2)_n - (\rho J_\xi / m^2)^T}{(\rho J_\xi / m^2)_n}\right]$
A4	Advection of $\rho J_\xi / m^2$ with finite differencing of tendency term	$(\varphi_i J_\xi / m^2)^{cor} = (\varphi_i J_\xi / m^2)^T \exp\left[\frac{(\rho J_\xi / m^2)^{\text{int}} - (\rho J_\xi / m^2)^T}{(\rho J_\xi / m^2)^{\text{int}}}\right]$
A5	Advection of $\rho J_\xi / m^2$ with two-step time splitting	$(\varphi_i J_\xi / m^2)^{cor} = \frac{(\varphi_i J_\xi / m^2)^T}{(\rho J_\xi / m^2)^T}(\rho J_\xi / m^2)^{\text{int}}$

(Note: Superscripts *cor*, *int*, and *T* represent corrected, interpolated, and advected quantities, respectively.)

Byun and Lee (1999) compared the performance of the correction algorithms under several idealized two-dimensional linear flows and different density fields. In addition, the linearity of the advection processes was studied to show how well the different precursors from same sources can be advected without losing their integrity. The characteristics of the correction procedures can be summarized as follows:

- The correction scheme fixes mass conservation errors due to the time splitting and numerical algorithms as well as the mass inconsistent meteorological data input.
- The correction scheme does not, however, improve inherent properties of the numerical advection scheme such as monotonicity, or numerical diffusion.
- In a budget study, such as in process analysis, the adjustment process must be considered as an integral part of the three-dimensional advection. Horizontal advection, vertical advection, and the mass correction step all together simulate the atmospheric advection process.

7.2 Vertical Mixing Algorithms

In this section, we describe turbulence closure schemes for the CCTM. We describe numerical algorithms for vertical mixing and dry deposition, and discuss the details of the mathematical representations, integration time-steps and solvers. Unless stated otherwise, the vertical structures of meteorological and chemical transport models are assumed to be the same. This is

desirable because the interpolation of meteorological quantities in vertical direction would alter the original turbulent flux exchange characteristics.

7.2.1 Closure Problem

Because of the stochastic nature of atmospheric motion, the primitive equations in the set describing the atmosphere are averaged to form a set of deterministic equations before they can be solved numerically. The decomposition of velocity components and concentrations into mean and turbulent terms and the application of ensemble averaging produces Reynolds flux terms in the species mass continuity equation. Introduction of the Reynolds flux terms generates a new problem set in which the number of unknowns is larger than the number of equations. This closure problem is caused by the attempt to represent nonlinear processes such as momentum advection using a linear decomposition such as the Reynolds decomposition. We describe some approaches on the closure of the Reynolds flux terms below.

7.2.1.1 Local Closure

Local closure assumes that turbulence is analogous to molecular diffusion, i.e., that an unknown turbulence flux at any point in space is parameterized by values of known quantities at the same point (Stull, 1988). First order closure retains the prognostic equations for only the mean variables such as wind, temperature, humidity, and trace gas concentrations while the second-order moments (Reynolds fluxes) are approximated. An example of a local closure scheme is the approximation of Reynolds flux terms using a gradient transport theory, or a mixing length theory resulting in an eddy diffusion method. One of the problems with the gradient transport theory is finding a rational basis for parameterizing the eddy diffusivity. Also, the theory fails when eddies larger than the grid size are present, like they are in a convective boundary layer.

The so-called one-and-a-half order closure retains the prognostic equations for the mean variables and adds equations for the variances of those variables. The set of one-and-a-half order equations is obtained by simplifying the full second-order turbulence equations. Instead of the velocity component variance equations, the turbulent kinetic energy (TKE) equation is often used. By including the variance equations, we have increased the number of unknowns that need to be parameterized compared to the first-order closure approach. However, the benefit is that the eddy diffusivity can be parameterized not only with the mean quantities but also with the TKE and the temperature variance which characterize turbulence intensity. However, if an air quality model is based on one-and-a-half order closure in a true sense, the prognostic equations of the variances for the tracer concentrations should be included explicitly. In practical Eulerian air quality models that deal with photochemical problems, additional prognostic variance equations for the tracer species are very expensive computationally. Also, the additional closure problem

must be dealt with by parameterizing the Reynolds average terms involved with the variances for tracer species. Therefore, the one-and-a-half order closure for an air quality model often actually means that the diffusion equations for the tracer species are formulated with first order closure, while eddy diffusivities (if gradient theory is applied for the closure) or turbulent fluxes (if non-local flux-based closure is used) are estimated with the TKE information from a meteorological model with one-and-a-half order schemes for wind, temperature, and humidity.

The set of second-order turbulence equations includes all the second moment terms. To derive these terms, parameterizations on a full set of third-order moments are required. Similar to the first-order case, the second-order closure approximates terms involving third moments. Several basic closure assumptions such as down-gradient diffusion, return to isotropy, and turbulent dissipation in the inertial subrange are used in the parameterization of the third moment terms. These parameterizations must be valid, especially, for the scales of the energy-containing eddies that are sensitive to atmospheric stability. Measurements of high-order moments in the real atmosphere are difficult because of large scatter in the direct flux measurements and because a long averaging time or a very large sample size of data is required because the events with a much lower probability of occurrence must be gathered to estimate higher-order moments using eddy-correlation methods. For air quality applications, especially for a complex chemical reaction system, the technique requires too many ad-hoc assumptions that cannot be confirmed by observations or other theoretical reasoning. In addition the second-order closure incurs a prohibitively high computational cost. As before, we can solve the first-order tracer diffusion equations with the variances and covariances for wind components, temperature, and humidity from the second-order meteorological models. For air quality applications, the true second-order closure formulation solves for the cross-species covariances explicitly. Some researchers have attempted second-order closure for simple chemical mechanisms with a limited number of photochemically reactive species. The introduction of additional parameterizations for the third-order moment terms among the tracer species themselves and wind components (about which we lack sufficient knowledge) and the added cost of solving for a large number of covariance terms make this scheme impractical and prohibitively costly for operational Eulerian photochemical models.

7.2.1.2 Non-local Closure

Non-local closure recognizes that larger-size eddies can transport fluid across finite distances before the smaller eddies have a chance to cause mixing. This advection-like concept is supported by observations of thermals rising with undiluted cores, finite size swirls of leaves or snow, and the organized circulation patterns sometimes visible from cloud photographs.

Two main approaches of non-local closure methods are the transilient turbulence theory and the spectral diffusion theory. Both allow a range of eddy sizes to contribute to the turbulent mixing process. The spectral diffusion theory attempts to simulate mixing process by transforming signals into a spectral space. For example, a spectral diffusion model of Otte and Wyngaard (1996) represents the mean variables within the planetary boundary layer (PBL) by a truncated series of Legendre polynomials. The first Legendre mode represents the layer average, and additional modes add structure to the vertical profiles. Only a few modes are necessary to resolve vertical profiles comparable to high resolution diffusion models. However, the need to fit a different number of spectral modes for each trace species makes the scheme less attractive for air quality application and thus it have not been considered here. The transilient turbulence theory (e.g., Stull, 1988) is a general representation of the turbulent flux exchange process. The Latin word transilient, meaning to jump over, is used since turbulent eddies that exist in the PBL can transport mass and momentum directly across several grid layers. A variety of mixing processes can be modeled with the transilient scheme depending on the form of the transilient matrix. Examples include complete mixing, top-down/bottom-up mixing, asymmetric convection mixing, small-eddy mixing, cloud top entrainment, a detraining updraft core, patchy turbulence, no turbulence, or eddies triggered by the surface layer. Non-local closure is most suitable for describing vertical turbulence mixing process, which should represent turbulent diffusion and atmospheric transport by eddies of different sizes simultaneously.

In the following, we describe only the first-order turbulent mixing schemes. The true one-and-a-half and the second-order closure schemes are not discussed here. We organize the description of vertical mixing algorithms based on the details of the turbulence parameterization; the eddy-diffusion form or the Reynolds-flux form. Both the eddy-diffusion and the Reynolds-flux forms are capable of accommodating information from higher order turbulence closure for momentum and other meteorological parameters such as potential temperature and humidity. The vertical diffusion modules in CMAQ will include two different ways of parameterizing the eddy diffusivity (using PBL similarity theory and using TKE) and three flux form non-local algorithms (Blackadar, ACM, and Transilient Turbulence).

7.2.2 Computing Vertical Mixing with the Eddy Diffusion Formulation: K-Theory

The eddy diffusion algorithm in the CCTM computes the following:

$$\left.\frac{\partial \varphi_i^*}{\partial t}\right|_{vdiff} = \frac{\partial}{\partial \hat{x}^3}\left[\sqrt{\hat{\gamma}}\,\overline{\rho}\left(\hat{K}^{33}\frac{\partial \overline{q}_i}{\partial \hat{x}^3}\right)\right] \tag{7-23}$$

where $\hat{K}^{33}$ is the contravariant vertical component of eddy diffusivity in the generalized coordinates. The contravariant eddy diffusivity is related to the diffusivities in Cartesian coordinates as:

$$\hat{K}^{33} = \left(\frac{\partial \hat{x}^3}{\partial x}\right)^2 K_{xx} + \left(\frac{\partial \hat{x}^3}{\partial y}\right)^2 K_{yy} + \left(\frac{\partial \hat{x}^3}{\partial z}\right)^2 K_{zz}$$
$$= J_\xi^{-2}\left[\left((m\frac{\partial h}{\partial \hat{x}^1})^2 + (m\frac{\partial h}{\partial \hat{x}^2})^2\right)K_H + K_{zz}\right] \qquad (7\text{-}24)$$

where $J_\xi^{-1} = \left|\frac{\partial \hat{x}^3}{\partial z}\right|$. Here we focus on the parameterization of the eddy diffusivity, K_{zz}, in a generic Cartesian vertical coordinate z (geometric height h). Parameterizations of the horizontal eddy diffusivity are described later. However, in the current CMAQ implementation, the term involving horizontal diffusivity K_H in Equation 7-24 for the estimation of $\hat{K}^{33}$ is neglected. Evaluation of the effects of this simplification is left for future work.

7.2.2.1 Parameterization of Vertical Eddy Diffusivity K_{zz} with PBL Similarity Theory

There are several eddy diffusivity parameterizations using different similarity theories. Since these are somewhat similar, we consider the formulations suggested by Businger et al. (1971) and Hass et al. (1991) to represent the turbulent process in the surface layer and mixed layer. Previous studies (Chang et al., 1987, and Hass et al., 1991) indicated that this type of formulation can represent turbulent mixing in air quality models adequately. With K-theory, we assume that trace species have non-dimensional profile characteristics similar to potential temperature, Θ, i.e., $K_{zz} = K_h$. We briefly describe the surface and boundary layer similarity theory used for the parameterization of eddy diffusivity for different stability regimes of the PBL below. The stability regime is defined with a nondimensional number z/L, where z is the height above the ground and L is the Monin-Obukhov length.

For the surface layer, the non-dimensional profile functions of the vertical gradient of Θ are expressed as:

$$\phi_h = \mathrm{Pr}_o(1 + \beta_h \frac{z}{L}) \quad \text{for moderately stable conditions } (1 \geq z/L \geq 0) \qquad (7\text{-}25a)$$

$$\phi_h = (1 - \gamma_h \frac{z}{L})^{-1/2} \quad \text{for unstable conditions } (z/L < 0) \qquad (7\text{-}25b)$$

where Pr_o is the Prandtl number for neutral stability and β_h and γ_h are coefficients of the profile functions determined through field experiments. In addition, following Holtslag et al. (1990) we

add a function for the very stable condition ($z/L \geq 1$) to extend the applicability of the surface layer similarity:

$$\phi_h = \mathrm{Pr}_o(\beta_h + \frac{z}{L}) \tag{7-25c}$$

Parameterizations for eddy diffusivity for the surface layer can be shown as:

$$K_h = \frac{ku_* z}{\phi_h(z/L)} \tag{7-26a}$$

where u_* is the surface friction velocity.

For the PBL (above the surface layer), eddy diffusivity is parameterized with:

$$K_h = \frac{ku_* z(1 - z/h)^{3/2}}{\phi_h(z/L)} \qquad \text{for } \frac{z}{L} > 0 \text{ (stable)} \tag{7-26b}$$

$$K_h = kw_* z(1 - z/h) \qquad \text{for } \frac{z}{L} < 0 \text{ (unstable)} \tag{7-26c}$$

In the above expressions, h is the depth of the boundary layer, k the Von Karman constant, and w_* the convective velocity. Refer to Chapter 12 for the method used to estimate the PBL height in the CMAQ modeling system.

These parameterizations for K_h are sensitive to the boundary-layer height (h) and surface-layer height. Therefore, when the vertical resolution is too coarse in the boundary layer, using a "representative" eddy diffusivity together with the mean-concentration gradient at the interface seems to be more appropriate for the estimation of the diffusive flux. In fact, the diffusive flux across the interface can be estimated more accurately with the mean diffusivity and mean concentration gradient than with local diffusivity and mean concentration gradient; the former has an error of $O[(\Delta\xi)^2]$ (at best) while the latter has an error of $O[\Delta\xi]$. To estimate the "representative" eddy diffusivity at the layer interface, integrated eddy diffusivity formulas are used as in RADM and CMAQ. They are summarized in the following equations (Byun and Dennis, 1995)

- <u>Surface Layer</u>

  (a) Stable conditions:

$$\overline{K}_h = \frac{1}{z_2 - z_1}\int_{z_1}^{z_2} \frac{ku_* z}{\mathrm{Pr}_o(1+\beta_h z/L)}dz = \frac{ku_*}{\mathrm{Pr}_o(z_2 - z_1)}\left[\frac{z_2 - z_1}{\beta_1} - \frac{1}{\beta_1}\left(\ln\frac{\beta_1 z_2 + 1}{\beta_1 z_1 + 1}\right)\right] \quad (7\text{-}27a)$$

where $\beta_1 = \dfrac{\beta_h}{\mathrm{Pr}_o L}$.

(b) Unstable conditions:

$$\overline{K}_h = \frac{1}{z_2 - z_1}\int_{z_1}^{z_2} \frac{ku_* z}{\mathrm{Pr}_o(1-\gamma_h z/L)}dz$$

$$= \frac{ku_*}{\mathrm{Pr}_o(z_2 - z_1)}\left[\frac{2(3\alpha z_2 - 2)(1+\alpha z_2)^{\frac{3}{2}}}{15\alpha^2} - \frac{2(3\alpha z_1 - 2)(1+\alpha z_1)^{\frac{3}{2}}}{15\alpha^2}\right] \quad (7\text{-}27b)$$

where $\alpha = -\gamma_h/L$.

- <u>Planetary Boundary Layer</u>

(a) Stable conditions:

$$\overline{K}_h = \frac{ku_*}{z_2 - z_1}\int_{z_1}^{z_2} \frac{z(1-z/h)^{3/2}}{\mathrm{Pr}_o(1+\beta_h z/L)}dz$$

$$= \left[\frac{r_2^5}{5} + \frac{a^2-1}{3}r_2^3 + (a^4 - a^2)r_2\right] - \left[\frac{r_1^5}{5} + \frac{a^2-1}{3}r_1^3 + (a^4 - a^2)r_1\right] \quad (7\text{-}27c)$$

$$= (a^6 - a^4)\left[\frac{1}{2a}\ln\frac{(a+r_2)|a-r_1|}{|a+r_2|(a+r_1)}\right]$$

where $r_1 = (1 - z_1/h)^{1/2}$, $r_2 = (1 - z_2/h)^{1/2}$, $a^2 = (1+\delta)/\delta$, and $\delta = \dfrac{\beta_h h}{\mathrm{Pr}_o L}$.

(b) Unstable conditions:

$$\overline{K}_h = \frac{kw_*}{z_2 - z_1}\int_{z_1}^{z_2}(z - \frac{z^2}{h})dz = kw_*[\frac{z_2 + z_1}{2} - \frac{z_2^2 + z_2 z_1 + z_1^2}{3h}] \quad (7\text{-}28)$$

In the free atmosphere above the mixed layer, turbulent mixing is parameterized using the formulation as implemented in RADM (Chang et al., 1987), in which vertical eddy diffusivities are represented as functions of the bulk Richardson number and wind shear in the vertical. This formulation can be written as:

$$K_h = K_o + S^2 \frac{Ri_c - Ri_B}{Ri_c} \tag{7-29}$$

where the Richardson number is defined as $Ri_B = \frac{g}{\Theta_o S^2} \frac{\Delta\Theta_k}{\Delta z_k}$, K_o is the background value set at 1 $m^2 s^{-1}$, and S is the vertical wind shear. Effects of the parameterization, Equation 7-29, on air quality simulation will be evaluated in near future. Furthermore, not much is known of the eddy diffusivity formulas for strong stable condition (i.e., $z/L > 1$) and therefore require further research in this area.

7.2.2.2 Estimation of Vertical Eddy Diffusivity Using Turbulent Kinetic Energy

Various forms of higher order closure schemes are becoming common in mesoscale meteorology models. Typically, such models are referred to as TKE models. The simplest form of a TKE model, which Mellor and Yamada (1974) referred to as level 2.5, has only one second order prognostic equation, for TKE itself. The next level up in complication is the true one-and-a-half order closure model, level 3 in Mellor and Yamada (1974) nomenclature, which in addition to TKE includes prognostic equations for the turbulent variances of other relevant quantities such as temperature and humidity. The TKE scheme in the latest version of MM5 can be run as either level 2.5 or level 3 where prognostic equations for temperature variance, moisture variance, and temperature-moisture covariance are added to the TKE equation (Burk and Thompson, 1989). Another similar form of a higher order closure model is known as TKE-ε, which has prognostic equations for TKE and the turbulent dissipation rate (ε). An example of this type of model is described by Alapaty et al (1996).

A common feature of TKE models, for level 2.5 or 3 or TKE-ε, is that the turbulent fluxes of momentum, heat, and moisture are represented as local gradient diffusion similar to Equation 7-23. It is this characteristic that distinguishes 1.5 order closure from true 2nd order closure where the flux covariances are explicitly represented by prognostic equations. Therefore, adaptation of a CTM to a meteorology model that includes TKE closure is essentially simple if the TKE fields are available to the CTM. Only a small part of the TKE model need be reproduced in the CTM, namely the parameterization of eddy diffusion coefficients based on quantities already produced in the meteorology model. For example, in the TKE-ε model of Alapaty et al. (1996), the governing TKE equations in Cartesian coordinates are:

$$\frac{\partial E}{\partial t} = -u\frac{\partial E}{\partial x} - v\frac{\partial E}{\partial y} - w\frac{\partial E}{\partial z} - \overline{u''w''}\frac{\partial u}{\partial z} - \overline{v''w''}\frac{\partial v}{\partial z}$$

$$+\frac{g}{\Theta}\overline{\theta''w''}-\frac{\partial}{\partial z}\left(\overline{w''E''}+\frac{1}{\rho}\overline{p''w''}\right)-\varepsilon \tag{7-30a}$$

$$\frac{\partial\varepsilon}{\partial t}=-u\frac{\partial\varepsilon}{\partial x}-v\frac{\partial\varepsilon}{\partial y}-w\frac{\partial\varepsilon}{\partial z}+\frac{c_1\varepsilon}{E}\left(-\overline{u''w''}\frac{\partial u}{\partial z}-\overline{v''w''}\frac{\partial v}{\partial z}+\frac{g}{\Theta}\overline{\theta''w''}\right)$$

$$-\frac{c_2\varepsilon^2}{E}-c_3\frac{\partial}{\partial z}\left(\overline{w''\varepsilon''}\right), \tag{7-30b}$$

where u, v are horizontal wind components;

E is the turbulent kinetic energy per unit mass;

z is height;

Θ_v is the virtual potential temperature;

ε is the rate of TKE dissipation;

$\overline{u''w''}$, $\overline{v''w''}$, and $\frac{g}{\Theta}\overline{\theta''w''}$ are turbulence fluxes of momentum components and heat flux;

ρ is the density; and

p'' is the fluctuating pressure.

The constants c_1, c_2, and c_3 can be estimated following Detering and Etling (1985). The first three terms on the right-hand-side of the first equation represent advection of turbulent kinetic energy, and the other terms, shear production, buoyancy production, turbulence transport and the dissipation, respectively. Similarly, the first three terms on the right-hand-side of the second equation represent advection of ε. The rest of the terms represent the net rate change of ε due to shear and buoyancy production, the rate change of ε related to the time-scale of turbulence, and the vertical transport, respectively. The coefficients of eddy viscosity for momentum and heat can be written as:

$$K_m=\frac{c_2E^2}{\varepsilon} \tag{7-31a}$$

$$K_h=K_m\frac{\phi_m(z/L)}{\phi_h(z/L)} \tag{7-31b}$$

where K_m and K_h are the eddy exchange coefficients for momentum and heat, respectively. E and ε need to be provided by meteorological models in their native coordinates, thus the parameterization does not depend on the grid spacing explicitly. Obviously, we are assuming here that the vertical layer structure in the CTM is compatible with that used in the preprocessor meteorological model. Once K_h is computed, chemical fluxes can be modeled assuming similarity

with heat flux using the same eddy diffusion numerical algorithm described below (section 7.2.3.1). The derivation of eddy coefficients in the Burk and Thompson (1989) model is algebraically more complex (see Mellor and Yamada, 1974, 1982) but based only on mean quantities plus TKE. Therefore, given the TKE fields, which are output automatically from MM5 when the Burk and Thompson (1989) option is invoked, K_h can be re-diagnosed within the CTM.

7.2.2.3 Numerical Algorithm for Vertical Eddy Diffusion Modules

As described in Chapter 5, the vertical eddy diffusion module must solve the following equation in terms of mixing ratio $\overline{q}$:

$$\left.\frac{\partial \overline{q}_i}{\partial t}\right|_{vdiff} = \frac{\partial}{\partial \hat{x}^3}(\hat{K}^{33}\frac{\partial \overline{q}_i}{\partial \hat{x}^3}) + \hat{K}^{33}\frac{\partial \ln(\sqrt{\hat{\gamma}}\overline{\rho})}{\partial \hat{x}^3}\frac{\partial \overline{q}_i}{\partial \hat{x}^3}, \tag{7-32}$$

where the vertical mixing is represented with the pure diffusion term and the turbulent flux exchange term, respectively.

<u>Numerical algorithm for the diffusion kernel</u>

In its generic form, the diffusion kernel solves for:

$$\frac{\partial q}{\partial t} = \frac{\partial}{\partial \xi}(K\frac{\partial q}{\partial \xi}) \tag{7-33}$$

where ξ is the generic vertical coordinate which increases with geometric height. To account for the loss process due to deposition in the lowest model layer (j=1), dry deposition flux is considered as the flux boundary condition at the surface, i.e.:

$$\left.\frac{\partial q_1}{\partial t}\right|_{dep} = -\frac{v_d}{h_{dep}}q_1 \tag{7-34}$$

where the geometric thickness of the lowest model layer is used for h_{dep}.

The diffusion equation can be discretized for level j $(1 < j < N)$ in a N-layer model and time-steps t^n and t^{n+1} as:

$$q_j^{n+1} = q_j^n + \frac{\Delta t}{\Delta \xi_j}\left[\frac{K_{j+1/2}}{\Delta \xi_{j+1/2}}\left(\vartheta(q_{j+1}^{n+1} - q_j^{n+1}) + (1-\vartheta)(q_{j+1}^n - q_j^n)\right)\right.$$

$$\left. - \frac{K_{j-1/2}}{\Delta \xi_{j-1/2}}\left(\vartheta(q_j^{n+1} - q_{j-1}^{n+1}) + (1-\vartheta)(q_j^n - q_{j-1}^n)\right)\right], \qquad (7\text{-}35a)$$

where ϑ is a time-step weighting factor and

$$\xi_{j+1/2} = (\xi_j + \xi_{j+1})/2;\ \Delta\xi_{j+1/2} = \xi_{j+1/2} - \xi_{j-1/2};\ \Delta\xi_{j+1} = \xi_{j+1} - \xi_j$$

For the lowest model layer, we need to account for the loss due to deposition process:

$$q_1^{n+1} = q_1^n + \frac{\Delta t}{\Delta \xi_1}\left[\frac{K_{1+\frac{1}{2}}}{\Delta \xi_{1+\frac{1}{2}}}\left(\vartheta(q_2^{n+1} - q_1^{n+1}) + (1-\vartheta)(q_2^n - q_1^n)\right)\right]$$

$$-\Delta t \frac{v_d}{h_{dep}}\left[\vartheta q_1^{n+1} + (1-\vartheta) q_1^n\right] \qquad (7\text{-}35b)$$

and for the top layer we have zero flux through the top boundary:

$$q_N^{n+1} = q_N^n - \frac{\Delta t}{\Delta \xi_N}\frac{K_{N-1/2}}{\Delta \xi_{N-1/2}}\left(\vartheta(q_N^{n+1} - q_{N-1}^{n+1}) + (1-\vartheta)(q_N^n - q_{N-1}^n)\right) \qquad (7\text{-}35c)$$

Depending on ϑ, the finite difference scheme is explicit (ϑ=0), semi-implicit (ϑ=1/2), or fully implicit (ϑ=1). In the current version of CMAQ, the semi-implicit (Crank-Nicholson) algorithm is implemented. Equations 7-35a-c can be rearranged to yield a matrix equation:

$$\mathbf{Aq} = \mathbf{b} \qquad (7\text{-}36)$$

where **A** is tridiagonal whose coefficients (sub-diagonal component a_j, diagonal component d_j, and super-diagonal component c_j) when j=1 are given as:

$$d_1 = 1 + \frac{\vartheta \Delta t}{\Delta \xi_1}\frac{K_{1\frac{1}{2}}}{\Delta \xi_{1\frac{1}{2}}} + \vartheta \Delta t \frac{v_d}{h_{dep}}$$

$$c_1 = -\frac{\vartheta \Delta t}{\Delta \xi_1}\frac{K_{1\frac{1}{2}}}{\Delta \xi_{1\frac{1}{2}}} \qquad (7\text{-}37a)$$

and for j=N:

$$a_N = -\frac{\vartheta \Delta t}{\Delta \xi_N} \frac{K_{N-\frac{1}{2}}}{\Delta \xi_{N-\frac{1}{2}}}$$

$$d_N = 1 + \frac{\vartheta \Delta t}{\Delta \xi_N} \frac{K_{N-\frac{1}{2}}}{\Delta \xi_{N-\frac{1}{2}}} \tag{7-37b}$$

and for $2 \le j \le N-1$:

$$a_j = -\frac{\vartheta \Delta t}{\Delta \xi_j} \frac{K_{j-\frac{1}{2}}}{\Delta \xi_{j-\frac{1}{2}}}$$

$$d_j = 1 + \frac{\vartheta \Delta t}{\Delta \xi_j} \left(\frac{K_{j+\frac{1}{2}}}{\Delta \xi_{j+\frac{1}{2}}} + \frac{K_{j-\frac{1}{2}}}{\Delta \xi_{j-\frac{1}{2}}} \right)$$

$$c_j = -\frac{\vartheta \Delta t}{\Delta \xi_j} \frac{K_{j+\frac{1}{2}}}{\Delta \xi_{j+\frac{1}{2}}} \tag{7-37c}$$

Coefficients of vector **b** are, for j=1 and N:

$$b_1 = \left(1 - \frac{(1-\vartheta)\Delta t}{\Delta \xi_1} \left[\frac{K_{1\frac{1}{2}}}{\Delta \xi_{1\frac{1}{2}}} \right] - (1-\vartheta)\Delta t \frac{v_d}{h_{dep}} \right) q_1^n + \left(\frac{(1-\vartheta)\Delta t}{\Delta \xi_1} \left[\frac{K_{1\frac{1}{2}}}{\Delta \xi_{1\frac{1}{2}}} \right] \right) q_2^n$$

$$b_N = \left(1 - \frac{(1-\vartheta)\Delta t}{\Delta \xi_N} \left[\frac{K_{N-\frac{1}{2}}}{\Delta \xi_{N-\frac{1}{2}}} \right] \right) q_N^n + \left(\frac{(1-\vartheta)\Delta t}{\Delta \xi_N} \left[\frac{K_{N-\frac{1}{2}}}{\Delta \xi_{N-\frac{1}{2}}} \right] \right) q_{N-1}^n \tag{7-37d}$$

and for $2 \le j \le N-1$:

$$b_j = \left(1 - \frac{(1-\vartheta)\Delta t}{\Delta\xi_j}\left[\frac{K_{j+\frac{1}{2}}}{\Delta\xi_{j+\frac{1}{2}}} + \frac{K_{j-\frac{1}{2}}}{\Delta\xi_{j-\frac{1}{2}}}\right]\right)q_j^n$$

$$+\left(\frac{(1-\vartheta)\Delta t}{\Delta\xi_j}\left[\frac{K_{j+\frac{1}{2}}}{\Delta\xi_{j+\frac{1}{2}}}\right]\right)q_{j+1}^n + \left(\frac{(1-\vartheta)\Delta t}{\Delta\xi_j}\left[\frac{K_{j-\frac{1}{2}}}{\Delta\xi_{j-\frac{1}{2}}}\right]\right)q_{j-1}^n \qquad (7\text{-}37e)$$

The numerical algorithm solving the tridiagonal system is based on the Thomas algorithm. Refer to Appendix 7A.1 for details of the algorithm and stability characteristics.

Numerical algorithm for the coordinate divergence kernel

The coordinate divergence kernel solves for

$$\frac{\partial q}{\partial t} = K\frac{\partial \ln(\sqrt{\hat{\gamma}\overline{p}})}{\partial \xi}\frac{\partial q}{\partial \xi} = V_{mix}\frac{\partial q}{\partial \xi} \qquad (7\text{-}38)$$

where $V_{mix} = K\frac{\partial \ln(\sqrt{\hat{\gamma}\overline{p}})}{\partial \xi}$. The differential equation is in advective from with the effective mass transfer velocity V_{mix}. It can be solved with a vertical advection code. Because most operational meteorological models rely on logarithmically spaced vertical layering based on *sigma-p* type coordinates, V_{mix} is expected to be small. Currently, this component is not implemented in CMAQ. However, a quantitative study is needed to assess the importance of this term.

Integration time-steps

According to Oran and Boris (1987), any numerical algorithm for the diffusion equation (with equal grid spacing) should produce the following quantitative properties:

- the total integral of $q(\xi,t)$ should be conserved;
- the amplitude $|q(\xi,t)|$ should decay monotonically;
- there should be no phase errors introduced by the algorithm (for equal grid spacing); and
- positivity should be preserved.

Although the numerical solver algorithm for the semi-implicit scheme is stable in the sense that the amplitude of the signal either decays or stays the same, the positivity condition may not be satisfied if we choose a large time-step for the integration, especially for signals with small wavelengths. For example, with equal grid spacing, we can use the Von Neuman stability analysis technique to demonstrate that some part of the short-wavelength spectrum shows a

negative amplitude when the time-step is too long. The semi-implicit scheme is positive definite given the rather stringent CFL condition, for a uniform vertical grid spacing:

$$\beta \equiv \frac{2\Delta t K}{(\Delta\xi)^2} < 1.0 \tag{7-39a}$$

For non-uniform grid spacing, we use the CFL condition:

$$\max\{\beta_j\} \equiv \max\left\{\frac{\Delta t}{\Delta\xi_j}\left(\frac{K_{j-1/2}}{\Delta\xi_{j-1/2}} + \frac{K_{j+1/2}}{\Delta\xi_{j+1/2}}\right)\right\} < 1.0 \tag{7-39b}$$

to ensure positive definiteness of the semi-implicit solution. The internal time-step for vertical diffusion is thus determined in CMAQ with the following equation:

$$\Delta t_{vdiff} = \min\{\Delta t_j\} \tag{7-40}$$

where $\Delta t_j = \Delta\xi_j\left(\frac{K_{j-1/2}}{\Delta\xi_{j-1/2}} + \frac{K_{j+1/2}}{\Delta\xi_{j+1/2}}\right)^{-1}$

7.2.3 Flux Form Representation of Vertical Mixing

Vertical mixing can be represented in flux form as:

$$\frac{\partial q}{\partial t} = -\frac{\partial F^{\xi}}{\partial \xi} - F^{\xi}\frac{\partial\left[\ln(\sqrt{\hat{\gamma}}\overline{\rho})\right]}{\partial \xi}, \tag{7-41}$$

where $F^{\xi} = \hat{F}^3_{q_i}$ is the turbulent flux represented in the generalized vertical coordinate ξ, whose value increases monotonically with geometric height. Here, the flux should be parameterized in ξ coordinate instead of the generic height coordinate. The cross directional (w.r.t. generalized coordinate) diffusion terms, as well as the flux divergence due to grid spacing (second term in Equation 7-41), are neglected.

Thus, the numerical solver kernel for the flux form vertical diffusion should solve for:

$$\frac{\partial q}{\partial t} = -\frac{\partial F^{\xi}}{\partial \xi} \tag{7-42}$$

when the source term is zero. The flux form representation is extremely useful in describing the algorithms based on non-local closure. Non-local closure recognizes that larger-size eddies can

transport fluid across distances longer than the grid increment before the smaller eddies have a chance to cause mixing (Stull, 1988).

To represent the turbulent mass exchange with the transilient parameterization, the boundary layer height must coincide with the height of layer interfaces of the vertical grid. For most situations, the index for the boundary layer top (L_p) is less than the total number of model layers (i.e., $L_p < N$). With the transilient turbulence formulation, the new values of the trace species mixing ratio q due to turbulent mixing for a layer j at a future time $(t + \Delta t)$ can be written as:

$$q_j(t + \Delta t) = \sum_{k=1}^{L_p} c_{jk}(t, \Delta t) q_k(t) \tag{7-43}$$

where c_{jk} are the components of a transilient matrix and subscripts j and k are indices of two different grid boxes (vertical layers) below boundary layer top in a column of atmosphere. If we consider turbulent mixing between grid boxes j and k, c_{jk} represents fraction of air mass ending in the grid box j that came from grid box k. The grid box j is considered as the "destination" box while grid box k is considered as the "source" box. Thus, the change in the tracer concentration due to turbulent mixing for grid box j at a time interval Δt is a simple matrix multiplication with concentration from the source cell. The transilient matrix representation is in fact applicable for any physical process that involves mass exchange among grid boxes in a column. For example, convective cloud mixing can be represented by a transilient matrix as well, similar to how mixing in a convective boundary layer is handled.

The mass conservation requirements provide constraints for the coefficients of the transilient matrix. The conservation of air mass requires that the sum over k of all mixing fractions be unity:

$$\sum_{k=1}^{L_p} c_{jk}(t, \Delta t) = 1 \tag{7-44}$$

and the conservation of trace gas amount requires that the sum over j of all mass-ratio weighted transilient coefficients be unity as well:

$$\sum_{k=1}^{L_p} \frac{\Delta \xi_j}{\Delta \xi_k} c_{jk}(t, \Delta t) = 1 \tag{7-45}$$

where $\Delta \xi_j / \Delta \xi_k$ represents the mass ratio (i.e., ratio of layer thicknesses for mixing ratio q) between the source and destination boxes. In order that transilient turbulence theory be useful, the coefficients should be determined using appropriate turbulent flux parameterizations.

Consider how the mixing coefficients are related with the turbulent flux representations. Because the transilient matrix describes the exchange of mass between grid boxes, the kinematic turbulent fluxes across the j-th level can be expressed, for a vertical layering with non-uniform grid spacing (Stull, 1993), for $2 \le j \le L_p$ as:

$$F_j(t,\Delta t) = F_{j-1}(t,\Delta t) + \frac{\Delta\xi_j}{\Delta t}\sum_{k=1}^{L_p} c_{jk}(t,\Delta t)[q_j(t) - q_k(t)] \tag{7-46a}$$

and for j=1 as:

$$F_1(t,\Delta t) = \frac{\Delta\xi_1}{\Delta t}\sum_{k=1}^{L_p} c_{1k}(t)[q_1(t) - q_k(t)] \tag{7-46b}$$

The concentration (mixing ratio) of the lowest model layer, taking into account the deposition flux, is:

$$\frac{\partial q_1}{\partial t} = -\frac{F_1 - F_s}{\Delta\xi_1} = -\frac{v_d}{h_{dep}}q_1 - \sum_{k=1}^{L_p}\frac{c_{1k}(t,\Delta t)}{\Delta t}[q_1(t) - q_k(t)] \tag{7-47}$$

where F_s is the flux at the surface.

The transilient turbulent representation, as shown in Equation 7-43, is an explicit expression in which the magnitudes of mixing coefficients depend on the numerical integration time-step. To use the transilient matrix representation as a general expression for the non-local turbulent closure methods, we need to relate Equation 7-43 with the semi-implicit representations of simple non-local closure algorithms such as in Blackadar (1978) and the Asymmetric Convection Model (Pleim and Chang, 1992). Using Blackadar's definition of m_{jk}, which is the fraction of mass exchange between two levels j and k per unit time, the turbulent fluxes at a given time t can be rewritten as:

$$F_j(t) = F_{j-1}(t) + \Delta\xi_j\sum_{k=1}^{L_p} m_{jk}(t)[q_j(t) - q_k(t)] \tag{7-48}$$

Note that $m_{jk} = c_{jk} / \Delta t$ for an explicit method. Substituting Equation 7-43 into the semi-implicit method, as in Equation 7-46, we get:

$$q_j^{n+1} = q_j^n - \frac{\Delta t}{\Delta\xi_j}\left[\vartheta(F_j^{n+1} - F_{j-1}^{n+1}) + (1-\vartheta)(F_j^n - F_{j-1}^n)\right] \tag{7-49}$$

resulting in a general matrix equation:

$$\mathbf{P}\mathbf{q}^{n+1} = \mathbf{R}\mathbf{q}^{n} \tag{7-50}$$

where the coefficients of **P** and **R** are given as:

$$p_{jj} = 1 + \vartheta \Delta t \sum_{\substack{k=1 \\ k \neq j}}^{L_p} m_{jk}\,;\; p_{\substack{jk \\ j \neq k}} = -\vartheta \Delta t m_{jk}$$

$$r_{jj} = 1 - (1-\vartheta)\Delta t \sum_{\substack{k=1 \\ k \neq j}}^{L_p} m_{jk}\,;\; r_{\substack{jk \\ j \neq k}} = (1-\vartheta)\Delta t m_{jk}$$

If the matrix **P** is nonsingular, we have a general expression for the transilient turbulence:

$$\mathbf{q}^{n+1} = \mathbf{P}^{-1}\mathbf{R}\mathbf{q}^{n} = \mathbf{C}\mathbf{q}^{n} \tag{7-51}$$

where $\mathbf{C}=\mathbf{P}^{-1}\mathbf{R}$.

The relationship between the coefficients of the transilient matrix and the mass exchange ratio among the grid boxes are somewhat complicated for the semi-implicit scheme. However, the semi-implicit scheme becomes attractive for the closure algorithms with sparse **P** matrix (i.e., when the matrix inversion is not so expensive) because it allows longer integration time-steps than the explicit method. In the following, we describe non-local flux-form atmospheric turbulence algorithms as a subset of the generalized transilient turbulence representations.

7.2.3.1 Blackadar Non-local Scheme

This scheme, first introduced by Blackadar (1978), has long been used as one of the PBL schemes in the Mesoscale Meteorology model generation 4 (MM4) and generation 5 (MM5). The Blackadar model is a simple non-local closure scheme designed to simulate vertical transport by large convective eddies during conditions of free convection. Therefore, this scheme is used only in the convective boundary layer and must be coupled with another scheme for non-convective conditions and above the boundary layer, such as K-theory. In general, the flux-form diffusion algorithm can be written for the lowest layer as:

$$\frac{\partial q_1}{\partial t} = -\frac{v_d}{h_{dep}} q_1 - \sum_{k=1}^{L_p} m_{1k}(t)[q_1(t) - q_k(t)] \tag{7-52a}$$

and for $2 \le j \le L_p$ as:

$$\frac{\partial q_j}{\partial t} = -\sum_{k=1}^{L_p} m_{jk}(t)[q_j(t) - q_k(t)] \tag{7-52b}$$

where m_{jk} is the rate of mass exchange between two grid boxes in a column of the atmosphere (below boundary layer top) per unit time. The convective mixing is assumed to be dominated by eddies of varying sizes but all having roots in the surface layer, each eddy exchanging a certain amount of its mass with the air around it as it ascends. The rate of change of mean potential temperature caused by the mass exchange in the mixed layer can be expressed as:

$$\frac{\partial \Theta}{\partial t} = M_u w(\xi)(\Theta_{sfc} - \Theta) \tag{7-53}$$

where $w(\xi)$ is a weight function that accounts for the variation of exchange rate with height.

The mass exchange rate, M_u, can be estimated from conservation of energy, which requires the heat flux at any level to satisfy the equation:

$$H = H_{sfc} - M_u \int_{\xi_{sfc}}^{\xi} C_{pd}\rho(\Theta_{sfc} - \Theta)w(\xi')J_\xi d\xi' \tag{7-54}$$

where H_{sfc} is the sensible heat flux leaving the surface layer and C_{pd} is the specific heat at constant pressure. When the integration limit is extended to the top of the boundary layer, where H is assumed to be zero, we can estimate M_u with:

$$M_u = H_{sfc} / \int_{\xi_{sfc}}^{\xi_h} C_{pd}\rho(\Theta_{sfc} - \Theta)w(\xi)J_\xi d\xi \tag{7-55}$$

Usually the weight function w is approximated to be unity in the mixed layer. With the Blackadar scheme, the mixing algorithm is represented for the lowest model layer by:

$$\frac{\partial q_1}{\partial t} = -\frac{v_d}{h_{dep}} q_1 - \sum_{k=1}^{L_p} M_u \frac{\Delta\xi_k}{\Delta\xi_1}[q_1(t) - q_k(t)] \tag{7-56a}$$

and for $2 \le j \le L_p$ by:

$$\frac{\partial q_j}{\partial t} = -M_u \frac{\Delta\xi_1}{\Delta\xi_j}[q_j(t) - q_1(t)] \tag{7-56b}$$

where we used $m_{1k} = M_u \frac{\Delta\xi_k}{\Delta\xi_1}$, $m_{j1} = M_u \frac{\Delta\xi_1}{\Delta\xi_j}$, and all other components of m_{jk} are zero.

Finite difference representations of the above equations are:

$$\frac{q_1^{n+1} - q_1^n}{\Delta t} = -\frac{v_d}{h_{dep}}[\vartheta q_1^{n+1} + (1-\vartheta)q_1^n] - \vartheta \frac{M_u}{\Delta\xi_1}\left[(\xi_h - \Delta\xi_1)q_1^{n+1} - \sum_{k=2}^{L_p} \Delta\xi_k q_k^{n+1}\right]$$

$$-(1-\vartheta)\frac{M_u}{\Delta\xi_1}\left[(\xi_h - \Delta\xi_1)q_1^n - \sum_{k=2}^{L_p} \Delta\xi_k q_k^n\right] \tag{7-57a}$$

where we used $\xi_h = \sum_{k=1}^{L_p} \Delta\xi_k$, and for $2 \le j \le L_p$:

$$\frac{q_j^{n+1} - q_j^n}{\Delta t} = -\vartheta M_u \frac{\Delta\xi_1}{\Delta\xi_j}(q_j^{n+1} - q_1^{n+1}) - (1-\vartheta)M_u \frac{\Delta\xi_1}{\Delta\xi_j}(q_j^n - q_1^n) \tag{7-57b}$$

After rearrangement, we obtain the following matrix equation:

$$\begin{pmatrix} d_1 & f_2 & \cdots & f_k & \cdots & f_{L_p} \\ e_2 & d_2 & 0 & 0 & \cdots & 0 \\ \vdots & 0 & \ddots & \cdots & \cdots & 0 \\ e_j & \vdots & \vdots & d_j & \vdots & \vdots \\ \vdots & 0 & 0 & 0 & \ddots & 0 \\ e_{L_p} & \cdots & 0 & 0 & 0 & d_{L_p} \end{pmatrix} \begin{pmatrix} q_1^{n+1} \\ q_2^{n+1} \\ \vdots \\ q_j^{n+1} \\ \vdots \\ q_{L_p}^{n+1} \end{pmatrix} = \begin{pmatrix} b_1 \\ b_2 \\ \vdots \\ b_j \\ \vdots \\ b_{L_p} \end{pmatrix} \tag{7-58}$$

where the elements are defined with:

$$d_1 = 1 + \vartheta \frac{v_d \Delta t}{h_{dep}} + \vartheta \frac{\Delta t M_u}{\Delta\xi_1}(\xi_h - \Delta\xi_1)$$

$$b_1 = \left[1 - (1-\vartheta)\frac{v_d \Delta t}{h_{dep}} - (1-\vartheta)\frac{\Delta t M_u}{\Delta\xi_1}(\xi_h - \Delta\xi_1)\right] q_1^n + (1-\vartheta)\frac{\Delta t M_u}{\Delta\xi_1}\sum_{k=2}^{L_p} \Delta\xi_k q_k^n$$

and for $2 \le j \le L_p$:

$$f_j = -\vartheta\left(\frac{\Delta t M_u}{\Delta\xi_j}\right)\Delta\xi_1$$

$$e_j = -\vartheta\left(\frac{\Delta t M_u}{\Delta\xi_1}\right)\Delta\xi_j$$

$$d_j = 1 + \vartheta\left(\frac{\Delta t M_u}{\Delta\xi_j}\right)\Delta\xi_1$$

$$b_j = \left[1-(1-\vartheta)\left(\frac{\Delta t M_u}{\Delta\xi_j}\right)\Delta\xi_1\right]q_j^n + (1-\vartheta)\left(\frac{\Delta t M_u}{\Delta\xi_j}\right)\Delta\xi_1 q_1^n$$

The numerical algorithm to solve the sparse matrix system is similar to the Thomas algorithm for the tridiagonal system. For the details of the numerical algorithm, refer to Appendix 7A.2.

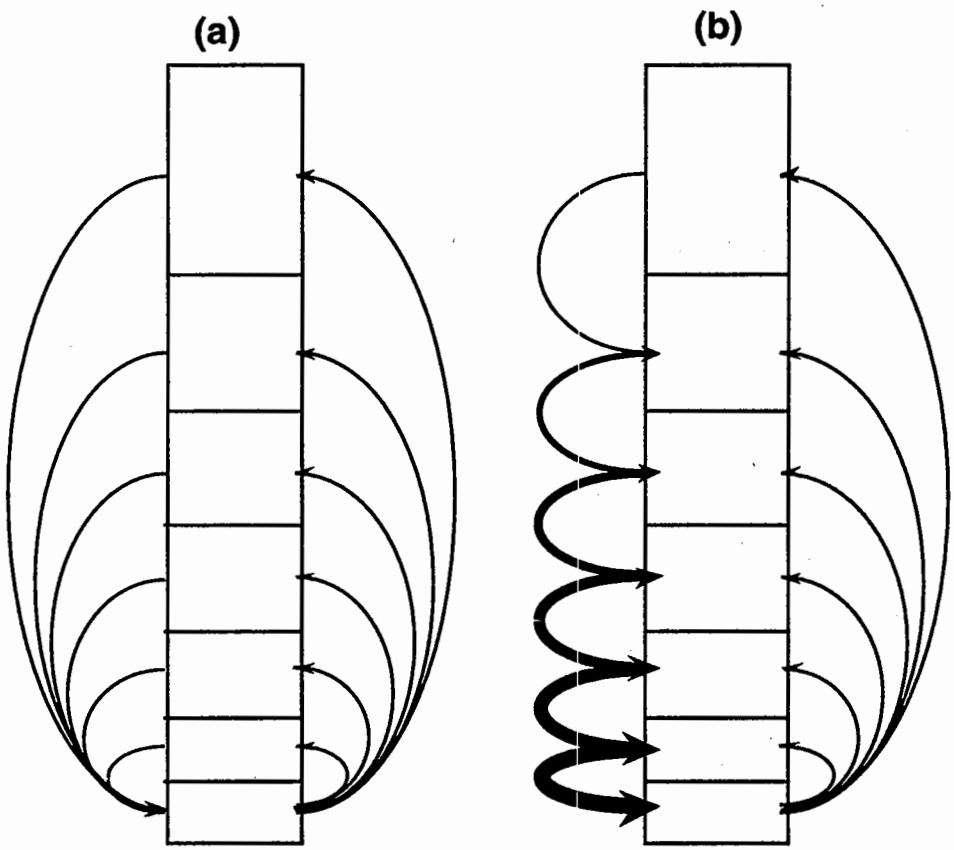

Figure 7-2. Schematics of the Blackadar Scheme (a) and the Asymmetric Convective Model (b)

7.2.3.2 Asymmetric Convective Mixing

The Asymmetric Convective Model (ACM), developed by Pleim and Chang (1992), is based on Blackadar's non-local closure scheme (Blackadar, 1978) but with a different scheme for

downward mixing in the convective boundary layer (CBL). Blackadar's scheme is based on the assumption that the turbulent mixing is isotropic (i.e., symmetric) in the CBL. However, observational evidence and large-eddy simulation modeling studies indicate that mixing processes in a convective boundary layer are essentially asymmetric (i.e., turbulence is anisotropic; Schumann, 1989) with fast upward buoyant plumes and slow broad compensatory subsidence. Therefore the direct, non-local downward transport of the Blackadar scheme is replaced with layer by layer subsidence which increases in mass flux as it descends, like a cascading waterfall (Figure 7-2). As with the Blackadar model, the ACM can only be used during convective conditions in the PBL. For other stability regimes, one needs to rely on other schemes such as K-theory.

Turbulent mixing in the PBL for any dynamic, or thermodynamic variables, or trace gas species concentrations can be represented in essentially the same way as in the above transilient parameterization. Also, the conceptual design of the ACM allows for considerable simplification. Because the mass influx to the lowest model layer is from the second layer only in ACM (refer to Figure 7-2), we can write the time rate change of mixing ratio as follows:

$$\frac{\partial q_1}{\partial t} = -\frac{v_d}{h_{dep}} q_1 - \frac{1}{\Delta\xi_1}[M_u(\xi_h - \xi_1)q_1(t) - M_{d2}\Delta\xi_2 q_2(t)] \tag{7-59a}$$

For $2 \le j \le L_p$:

$$\frac{\partial q_j}{\partial t} = M_u q_1 - M_{dj} q_j + M_{dj+1}\frac{\Delta\xi_{j+1}}{\Delta\xi_j} q_{j+1} \tag{7-59b}$$

where M_u represents upward mixing rate. M_{dj} represents downward mixing rate at layer j and is defined as:

$$M_{dj} = M_u \frac{\xi_h - \xi_{j-1}}{\Delta\xi_j} \tag{7-60}$$

The scheme can be represented in terms of transilient mixing rates (m_{jk}), as shown in general form in Equation 7-48:

$$\frac{\partial q_j}{\partial t} = -m_{j1}(q_j - q_1) - m_{j,j+1}(q_j - q_{j+1}) \tag{7-61}$$

Therefore, by equating Equations 7-59b and 7-61, we see that $m_{j1} = M_u \neq m_{1j}$, which shows that the transfer coefficients are asymmetric as expected, and $m_{j1} + m_{j,j+1} = M_{dj}$, which demonstrates a recursive relationship for M_{dj}:

$$M_{dj-1} = M_u + M_{dj}\frac{\Delta\xi_{j+1}}{\Delta\xi_j} \tag{7-62}$$

Finally, we rewrite the prediction equation in terms of the upward mixing rate:

$$\frac{\partial q_1}{\partial t} = -M_u\frac{\xi_h - \xi_1}{\Delta\xi_1}(q_1 - q_2) - \frac{v_d}{h_{dep}}q_1 \tag{7-63a}$$

and for $2 \le j \le L_p$:

$$\frac{\partial q_j}{\partial t} = M_u\left[q_1 - \left(\frac{\xi_h - \xi_{j-1}}{\Delta\xi_j}\right)q_j + \left(\frac{\xi_h - \xi_j}{\Delta\xi_{j+1}}\right)q_{j+1}\right] \tag{7-63b}$$

Note that this scheme does include the effects of vertical wind shear in generating turbulent mixing. The magnitude of the mixing rates of the transilient matrix is based on the conservation of sensible heat flux in the vertical direction:

$$M_u = H_{sfc} / \left[c_p\rho(\overline{\theta}_{sfc} - \theta_2)J_\xi(\xi_1 - \xi_h)\right] \tag{7-64}$$

Finite difference representations of the above equations are:

$$\begin{aligned}\frac{q_1^{n+1} - q_1^n}{\Delta t} = &-\left(\frac{v_d}{h_{dep}} + M_u\frac{\xi_h - \xi_1}{\Delta\xi_1}\right)[\vartheta q_1^{n+1} + (1-\vartheta)q_1^n] \\ &+ M_u\frac{\xi_h - \xi_1}{\Delta\xi_1}[\vartheta q_2^{n+1} + (1-\vartheta)q_2^n]\end{aligned} \tag{7-65a}$$

and for $2 \le j \le L_p$:

$$\begin{aligned}\frac{q_j^{n+1} - q_j^n}{\Delta t} = &M_u[\vartheta q_1^{n+1} + (1-\vartheta)q_1^n] \\ &-\left(\frac{\xi_h - \xi_{j-1}}{\Delta\xi_j}\right)[\vartheta q_j^{n+1} + (1-\vartheta)q_j^n] + \left(\frac{\xi_h - \xi_j}{\Delta\xi_{j+1}}\right)[\vartheta q_{j+1}^{n+1} + (1-\vartheta)q_{j+1}^n]\end{aligned} \tag{7-65b}$$

This results in a sparse matrix of the form:

$$\begin{pmatrix} d_1 & c_1 & \cdots & 0 & \cdots & 0 \\ e_2 & d_2 & c_2 & 0 & \cdots & 0 \\ \vdots & 0 & \ddots & \ddots & \cdots & 0 \\ e_j & \vdots & \vdots & d_j & c_j & \vdots \\ \vdots & 0 & 0 & 0 & \ddots & c_{L_p-1} \\ e_{L_p} & \cdots & 0 & 0 & 0 & d_{L_p} \end{pmatrix} \begin{pmatrix} q_1^{n+1} \\ q_2^{n+1} \\ \vdots \\ q_j^{n+1} \\ \vdots \\ q_{L_p}^{n+1} \end{pmatrix} = \begin{pmatrix} b_1 \\ b_2 \\ \vdots \\ b_j \\ \vdots \\ b_{L_p} \end{pmatrix}, \tag{7-66}$$

where:

$$d_1 = 1 + (\frac{v_d}{h_{dep}} + M_u \frac{\xi_h - \xi_1}{\Delta\xi_1})\vartheta\Delta t;$$

$$c_1 = -M_u \frac{\xi_h - \xi_1}{\Delta\xi_1}\vartheta\Delta t;$$

$$b_1 = [1 - (\frac{v_d}{h_{dep}} + M_u \frac{\xi_h - \xi_1}{\Delta\xi_1})(1-\vartheta)\Delta t]q_1^n + M_u \frac{\xi_h - \xi_1}{\Delta\xi_1}(1-\vartheta)\Delta t q_2^n;$$

$$e_j = -M_u \vartheta\Delta t;$$

$$d_j = 1 + M_u (\frac{\xi_h - \xi_j}{\Delta\xi_{j+1}})\vartheta\Delta t;$$

$$c_j = -M_u (\frac{\xi_h - \xi_j}{\Delta\xi_j})\vartheta\Delta t; \text{ and}$$

$$b_j = [1 - M_u \frac{\xi_h - \xi_{j-1}}{\Delta\xi_j})(1-\vartheta)\Delta t]q_j^n + M_u \frac{\xi_h - \xi_j}{\Delta\xi_{j+1}}(1-\vartheta)\Delta t q_{j+1}^n + M_u(1-\vartheta)\Delta t q_1^n.$$

The numerical algorithm solving the sparse matrix system is presented in Appendix 7A.3.

7.2.3.3 Transilient Turbulence Parameterization

The general computational paradigm for the transilient turbulence parameterization has been presented above. In order to use the transilient turbulence concept for mixing trace gases, one needs to know the mass exchange coefficient matrix. This is the closure problem with this parameterization. A couple of methods have been presented in the literature. One method is based on the TKE equation (Stull and Driedonks, 1987, and Raymond and Stull, 1990) and the other is the one based on non-local Richardson number (Zhang and Stull, 1992). In the following we describe briefly the TKE based scheme and discuss its associated difficulties.

The horizontally homogeneous form of the TKE equation, Equation 7-30a is given as:

$$\frac{\partial E}{\partial t} = -\overline{u''w''}\frac{\partial u}{\partial z} - \overline{v''w''}\frac{\partial v}{\partial z} + \frac{g}{\Theta_o}\overline{\theta''w''} - \varepsilon. \tag{7-67}$$

Note that the pressure and turbulent transport terms have been ignored. After normalizing with E, the non-local analogy of the finite difference form of Equation 7-67 can be written as:

$$\frac{\Delta_t E_{jk}}{E_{jk}} = \left[\frac{\left(-\overline{u''w''}\right)_{jk}}{E_{jk}}\left(\frac{\Delta u}{\Delta z}\right)_{jk} + \frac{\left(-\overline{v''w''}\right)_{jk}}{E_{jk}}\left(\frac{\Delta v}{\Delta z}\right)_{jk} + \frac{g}{\Theta_j}\frac{\left(\overline{\theta''w''}\right)_{jk}}{E_{jk}} - \frac{\varepsilon_{jk}}{E_{jk}}\right]\Delta_t t, \tag{7-68}$$

where the symbol Δ_t represents temporal change while Δ represents spatial gradient. To close the system, the unknown parameters are written in terms of known parameters by introducing three scaling parameters T_o, Ri_c, and D, which are the time scale of turbulence, the critical Richardson number, and dissipation factor, respectively. Thus, weighted kinematic fluxes can be written as:

$$\frac{\left(-\overline{u''w''}\right)_{jk}}{E_{jk}} = T_o\left(\frac{\Delta u}{\Delta z}\right)_{jk}, \tag{7-69a}$$

$$\frac{\left(-\overline{v''w''}\right)_{jk}}{E_{jk}} = T_o\left(\frac{\Delta v}{\Delta z}\right)_{jk}, \tag{7-69b}$$

$$\frac{\left(-\overline{\theta''w''}\right)_{jk}}{E_{jk}} = \frac{T_o}{Ri_c}\left(\frac{\Delta\Theta}{\Delta z}\right)_{jk}. \tag{7-69c}$$

Then Equation 7-68 can be rewritten as:

$$Y_{jk} = \frac{\Delta_t E_{jk}}{E_{jk}} = \frac{T_o \Delta_t t}{(\Delta z)_{jk}^2}\left[(\Delta u)_{jk}^2 + (\Delta v)_{jk}^2 - \frac{g}{Ri_c \Theta_j}(\Delta\Theta)_{jk}(\Delta z)_{jk}\right] - \frac{\varepsilon_{jk}\Delta_t t}{E_{jk}}. \tag{7-70}$$

To use Equation 7-70 for the generalized coordinate ξ, the corresponding layer heights $(\Delta z)_{jk}$ should be computed for $(\Delta\xi)_{jk}$.

Since we are dealing with fraction of masses that are coming from and going to different layers (i.e., $j \neq k$), Y_{jk} in the above equation is for off-diagonal elements only. Diagonal elements in Equation 7-70, Y_{jj}, represent mass of air that remain in each layer without interaction with other layers. Observations during convective conditions (Ebert et al., 1989) indicated that turbulent eddies cause a well-mixed rather than convectively overturned boundary layer. This requires

that the values of the mixing potential elements (Y_{jk}) should increase monotonically from the upper right-most element towards the main diagonal. Further, to account for the subgrid scale mixing in each layer, an independent parameter Y_{ref} was introduced. Thus, the diagonal elements can be written as:

$$Y_{jj} = MAX(Y_{j,j-1}, Y_{j,j+1}) + Y_{ref} \tag{7-71}$$

given values for T_o, Ri_c, and D. Usually, Y_{ref} is estimated based on observations (Stull, 1988). Finally, the off-diagonal elements of the transilient matrix are estimated with:

$$c_{jk} = \frac{Y_{jk}}{\|\mathbf{Y}\|_\infty} \tag{7-72}$$

where $\|\mathbf{Y}\|_\infty$ is the infinite norm of matrix $\mathbf{Y}$, $\max\{|\mathbf{Y}|\}$. The formulation presented in Raymond and Stull (1990) and Alapaty et al. (1997) includes the additional weighting based on the mass in the layer for irregularly spaced grids. However, we believe that Equation 7-72 should be valid even for irregularly spaced grids when the constraint Equation 7-45 is satisfied. Also, Stull (1993) states that the formulation Equation 7-72 causes too much mixing near the surface and inclusion of the mass weighting in the formulation exacerbates the problem further. The diagonal elements of the transilient matrix can be computed by rewriting Equation 7-44 as:

$$c_{jj} = 1 - \sum_{\substack{k=1 \\ k \neq j}}^{L_p} c_{jk} \tag{7-73}$$

Once the transilient matrix is determined, the concentration due to turbulent processes in the boundary layer can be estimated from Equation 7-43. The difficulties associated with this parameterization are:

- The scheme still depends on many free parameters (T_o, Ri_c, D, and Y_{ref}) and they control the behavior of the mixing algorithm; and
- The time-steps should be such that the trace species mixing ratio cannot be negative because Equation 7-43 is written in explicit form. Although explicit methods do not require matrix inversion, the time-step must be small enough to ensure positivity and numerical stability of the solution.

7.3 Horizontal Mixing Algorithms

Unfortunately, our understanding of horizontal turbulence is limited due to the lack of adequate turbulence measurements as well as the scale dependency of the problem. In earlier days of

atmospheric modeling, the horizontal diffusion process was often ignored because the numerical diffusion associated with the advection algorithms used was large. For problems with large scales, such as regional to global transport studies, the coarse grid resolutions did not require an explicit implementation of horizontal diffusion. However, with the advent of very accurate (i.e., less diffusive) numerical advection schemes and the emerging need for high resolution grids for urban scale problems, a good algorithm for horizontal diffusion is required. The skill needed is balancing numerical diffusion associated with the advection schemes with the added explicit diffusion to model horizontal diffusion in the atmosphere. A fundamental problem is that we do not know much about the expected magnitude of the actual horizontal diffusion. In this section we will describe the numerical algorithm for the horizontal diffusion implemented in the CMAQ system.

The horizontal diffusion process in the curvilinear coordinate system (See Equation 6-25' in Chapter 6) is given as:

$$\left.\frac{\partial c_i^*}{\partial t}\right|_{hdiff} = \left.\frac{\partial\left(\sqrt{\hat{\gamma}}\overline{\rho}\overline{q}_i\right)}{\partial t}\right|_{hdiff} = -\hat{\nabla}_s \bullet \left[\sqrt{\hat{\gamma}}\overline{\rho}\hat{\mathbf{F}}_{q_i}\right] \tag{7-74}$$

There are not many choices for the horizontal diffusion parameterizations. Frequently, the horizontal turbulent fluxes are parameterized using eddy diffusion theory. The contributions of the off-diagonal diffusion terms show up explicitly as in Equation 6-14 in Chapter 6. Often, these off-diagonal terms are neglected in air quality simulations, and in the CMAQ implementation, we solve for diagonal terms only:

$$\left.\frac{\partial c_i^*}{\partial t}\right|_{hdiff} = \frac{\partial}{\partial \hat{x}^1}\left[\sqrt{\hat{\gamma}}\overline{\rho}(\hat{K}^{11}\frac{\partial \overline{q}_i}{\partial \hat{x}^1})\right] + \frac{\partial}{\partial \hat{x}^2}\left[\sqrt{\hat{\gamma}}\overline{\rho}(\hat{K}^{22}\frac{\partial \overline{q}_i}{\partial \hat{x}^2})\right]. \tag{7-75}$$

The contravariant eddy diffusivity components are related to the Cartesian counterparts as $\hat{K}^{11} = mK_{xx}$ and $\hat{K}^{22} = mK_{yy}$. In practice, for Eulerian air quality modeling, we do not distinguish between eddy diffusivities in two different horizontal directions (i.e., $K_{xx} = K_{yy} = K_H$). For a Lagrangian simulation of atmospheric turbulence, the longitudinal (following the plume movement) and lateral (perpendicular to the plume movement) dispersion are treated differently according to characteristics from the isotropic turbulence analysis. Often the horizontal eddy diffusivity in the Cartesian coordinates is parameterized with the magnitude of the deformation in the gridded wind field. For that case, one must be careful whether the wind data are represented in Cartesian coordinates or in the transformed coordinates.

Unlike the vertical diffusion case, we do not separate the grid divergence term from the diffusion equation. An explicit solution method for Equation 7-75 is:

$$(\rho^*)^{n+1}_{l,m} q^{n+1}_{l,m} = (\rho^*)^n_{l,m} q^n_{l,m} + \frac{\Delta t}{(\Delta \hat{x}^1)^2}\left[(\rho^*)^n_{l+1,m}\overline{\hat{K}^{11}_{l+1,m}}(q^n_{l+1,m} - q^n_{l,m}) - (\rho^*)^n_{l,m}\overline{\hat{K}^{11}_{l,m}}(q^n_{l,m} - q^n_{l-1,m})\right]$$

$$+\frac{\Delta t}{(\Delta \hat{x}^2)^2}\left[(\rho^*)^n_{l,m+1}\overline{\hat{K}^{22}_{l,m+1}}(q^n_{l,m+1} - q^n_{l,m}) - (\rho^*)^n_{l,m}\overline{\hat{K}^{22}_{l,m}}(q^n_{l,m} - q^n_{l,m-1})\right], \qquad (7\text{-}76)$$

where $\overline{\hat{K}^{11}_{l,m}} = \frac{1}{2}(\hat{K}^{11}_{l,m+1} + \hat{K}^{11}_{l,m})$ and $\overline{\hat{K}^{22}_{l,m}} = \frac{1}{2}(\hat{K}^{22}_{l+1,m} + \hat{K}^{22}_{l,m})$. At the boundary cells, a zero-gradient boundary condition (Neumann) is applied. Because Equation 7-76 is an explicit scheme, the time-step should be chosen to prevent numerical instability and to maintain positivity. With an appropriate Courant number for horizontal diffusion, β_{hdiff}, the time-step can be determined with:

$$\Delta t|_{hdiff} = \beta_{hdiff}\frac{(\Delta x)^2}{\max\limits_{\forall(l,m)}(\hat{K}^{11}_{l,m}, \hat{K}^{22}_{l,m})}. \qquad (7\text{-}77)$$

At present β_{hdiff}= 0.3 and a uniform eddy diffusivity $K_H|_{\Delta x=4km}$ = 2000 m^2/s is used for the 4-km grid resolution. To compensate for larger grid sizes for coarser grids, the eddy diffusivity is modified to give:

$$K_H|_{\Delta x} = \frac{(4000)^2}{(\Delta x)^2} K_H|_{\Delta x=4km} \qquad (7\text{-}78)$$

where Δx is in meters.

Obviously, the above parameterization is too simple to be realistic in a variety of atmospheric conditions. Also, depending on the numerical advection algorithms chosen, the artificial diffusivity can be quite different. This calls for several in-depth studies on following two major issues:

(1) Quantification of realistic horizontal sub-grid scale diffusion.

The simplest approach is to assume a space independent diffusivity (e.g., K_h = 50 m^2/s). Smagorinsky (1963) formulated a horizontal diffusivity that accounts for diffusion due to distortion or stress in the horizontal wind field. For plumes which are several kilometers or more across, the Briggs (1973) parameterizations of horizontal diffusion define the diffusivity as a constant times the transport wind speed. The constant is usually based on the landuse (i.e.,

urban or rural) and the stability class (i.e., stable through unstable). However, it is difficult to quantify what the horizontal eddy diffusivity should be appropriate for a variety of atmospheric conditions without more detailed wind field and turbulence information.

(2) Maintaining appropriate horizontal diffusion in the presence of numerical diffusion.

Most methods for simulating advective transport in current models yield an effective numerical diffusivity much larger than physical horizontal diffusivities (Yamartino et al., 1992). Thus, the physical process may be outweighed by the numerical errors in the model. A re-assessment of this issue is required when the resolution of the model changes or when the method for simulating advection is updated. For idealized concentrations and wind fields distributions, we may be able to quantify the magnitude of the numerical diffusion in an advection scheme. However, for the more general applications, estimating the magnitude of numerical diffusion with a specific advection scheme is almost impossible. Refer to Odman (1997) for methodologies that quantify numerical diffusion errors associated with advection algorithms.

7.4 Conclusions

In this chapter, we have described numerical advection and diffusion algorithms. It has two purposes: to provide a description of the algorithms currently implemented in CCTM, and to describe the fundamental formulations that would guide future implementation of advection and diffusion modules. We encourage the development of algorithms in conservation (i.e., flux) forms to ensure compatibility of new modules with existing ones.

Because of the concerns over the non-monotonicity of BOT and YAM schemes and the mass conservation problem and diffusive nature of BOT-M, we have used PPM for a number of demonstration executions (Byun et al., 1998). Similar testing with BOT and YAM is underway. We intend to integrate other methods into the CCTM at a later time.

Also, we have identified several aspects in vertical and horizontal diffusion algorithms that require additional quantitative studies:

- Effects of the parameterization for the free troposphere;
- Importance of coordinate divergence term for vertical diffusion, in particular for the height-based constant coordinates;
- Characteristics among competing algorithms for the vertical diffusion, such as TKE and transilient turbulence schemes; and
- Practical and theoretical concerns with the horizontal diffusion algorithms.

7.5 References

Alapaty, K., R. Mathur, and D.W. Byun, 1996: A modeling study of vertical diffusion of passive and reactive tracers using local- and nonlocal-closure boundary layer schemes. Air Pollution Modeling and Its Application XI, ed. S.E. Gryning and F. Schiermeier. 433-442.

Alapaty, K.A., J.E. Pleim, S. Raman, D.S. Niyogi, and D.W. Byun. 1997: Simulation of atmospheric boundary layer processes using local- and nonlocal-closure schemes. *J. Applied Meteor.* Vol. **36.** 214-233.

Blackadar, A. K., 1978: Modeling pollutant transfer during daytime convection, *Preprints, Fourth Symposium on Atmospheric Turbulence, Diffusion, and Air Quality*, Reno, Am. Meteor. Soc., 443-447.

Bott, A., 1989: A positive definite advection scheme obtained by nonlinear renormalization of the advective fluxes. *Mon. Wea. Rev.* **117**, 1006-1015.

Bott, A., 1992: Monotone flux limitation in the area-preserving flux-form advection algorithm. *Mon. Wea. Rev.* **120**, 2592-2602.

Bott, A., 1993: The monotone area-preserving flux-form advection algorithm: reducing the time-splitting error in two-dimensional flow fields." *Mon. Wea. Rev.* **121**. 2637-2641.

Briggs, G. A., 1973: Diffusion estimates for small emissions. ATDL Contribution No. 79 [Available from Atmospheric Turbulence and Diffusion Laboratory, Oak Ridge, Tenn.]

Brooks, A. N., and T. J. R. Hughes, 1982: Streamline upwind/Petrov-Galerkin formulations for convection dominated flows with particular emphasis on the incompressible Navier-Stokes equations. *Comp. Meth. Appl. Mech. Eng.* **32**, 199-259.

Burk, S.D., and W.T. Thompson, 1989: A vertically nested regional numerical weather prediction model with second-order physics. *Mon. Wea. Rev.* **117**, 2305-2324.

Businger J. A., J. C. Wyngaard, Y. Izumi, and E. F. Bradley, 1971: Flux profile relationships in the atmospheric surface layer, *J. Atmos. Sci.*, **28**, 181-189.

Byun, D. W., 1999a: Dynamically consistent formulations in meteorological and air quality models for multi-scale atmospheric applications: I. Governing equations in a generalized coordinate system. *J. Atmos. Sci.*, (in print).

Byun, D. W., 1999b: Dynamically consistent formulations in meteorological and air quality models for multi-scale atmospheric applications: II. Mass conservation issues. *J. Atmos. Sci.*, (in print).

Byun, D. W., and R. L. Dennis, 1995: Design artifacts in Eulerian air quality models: Evaluation of the effects of layer thickness and vertical profile correction on surface ozone concentrations. *Atmos. Environ.*, **29**, 105-126.

Byun, D.W., and S.-M. Lee, 1999: Mass conservative numerical integration of trace species conservation equation: I Experiment with idealized two-dimensional flows. (in preparation)

Byun, D.W., J. Young., G. Gipson., J. Godowitch., F. Binkowsk., S. Roselle, B. Benjey, J. Pleim, J. Ching., J. Novak, C. Coats, T. Odman, A. Hanna, K. Alapaty, R. Mathur, J. McHenry, U. Shankar, S. Fine, A. Xiu, and C. Jang, 1998: Description of the Models-3 Community Multiscale Air Quality (CMAQ) model. Proceedings of the American Meteorological Society 78th Annual Meeting, Phoenix, AZ, Jan. 11-16, 1998.

Carpenter, R. L., K. K. Droegemeier, P. R. Woodward, and , C. E., Hane, 1990: Application of the piecewise parabolic method (PPM) to meteorological modeling. *Mon. Wea. Rev.* **118**, 586-612.

Chang, J.S., R.A. Brost, I.S.A. Isaksen, S. Madronich, P. Middleton, W.R. Stockwell, and C.J. Walcek, 1987: A three-dimensional Eulerian acid deposition model: Physical concepts and formulation, *J. of Geophys. Res.*, **92**, 14,681-700.

Childs, P. N., and K. W. Morton, 1990: Characteristic Galerkin methods for scalar conservation laws in one dimension. *SIAM J. Numer. Anal.* **27**, 553-594.

Chock, D. P., and A. M. Dunker, 1983: A comparison of numerical methods for solving the advection equation. *Atmos. Environ.* **17**(1), 11-24.

Chock, D. P., 1985: A comparison of numerical methods for solving the advection equation - II. *Atmos. Environ.* **19**(4), 571-586.

Chock, D. P., 1991: A comparison of numerical methods for solving the advection equation-III. *Atmos. Environ.* **25A**(5/6), 853-871.

Chock, D. P., 1999: Personal communication.

Colella, P., and , P. R. Woodward, 1984: The piecewise parabolic method (PPM) for gas-dynamical simulations. *J. Comp. Phys* **54**, 174-201.

Dabdub, D., and Seinfeld, J. H., 1994: Numerical advective schemes used in air quality models - sequential and parallel implementation. *Atmos. Environ.* **28**(20), 3369-3385.

Detering, H.W., and D. Etling, 1985: Application of E-ε turbulence model to the atmospheric boundary layer. *Bound.-Layer Meteor.,* **33**, 113-133.

Ebert, E.E., U. Schumann, and R. B. Stull, 1989: Nonlocal turbulence mixing in the convective boundary layer evaluated from large-eddy simulation. *J. Atmos. Sci.*, **46**, 2178-2207.

Flatoy, F., 1993: Balanced wind in advanced advection schemes when species with long lifetimes are transported. *Atmos. Environ.* **27A**(12), 1809-1819.

Hass, H., H.J. Jacobs, M. Memmescheimer, A. Ebel, and J.S. Change, 1991: Simulation of a wet deposition case in Europe using the European Acid Deposition Model (EURAD). *Air Pollution Modelling and Its Applications*, Vol. VIII (edited by van Dop H. and D.G. Steyn), Plenum Press, 205-213.

Holtslag, A. A., E. I. F. de Bruin, and H.-L. Pan, 1990: A high resolution air mass transformation model for short-range weather forecasting. *Mon. Weather Rev.*, **118**, 1561-1575.

Leith, C. C., 1965: Numerical simulation of the earth's atmosphere. A chapter *in Methods in Computational Physics. Vol. 4, Applications in Hydrodynamics*. p.1. ed., B. Alder, Academic Press, New York.

Löhner, R., K. Morgan, J. Peraire, and M. Vahdati, 1987: Finite element flux-corrected transport (FEM-FCT) for the Euler and Navier-Stokes Equations. *Finite Elements in Fluids. Vol. 7* . John Wiley & Sons. 105-121.

Mellor, G.L. and T. Yamada, 1974: A hierarchy of turbulence closure models for planetary boundary layers, *J. Atmos. Sci.*, **31**, 1791-1806.

Mellor, G.L. and T. Yamada, 1982: Development of a turbulence closure model for geophysical fluid problems. *Reviews of Geophysica and Space Physics*, **20**, 851-875.

Odman, M. T., 1997: A quantitative analysis of numerical diffusion introduced by advection algorithms in air quality models. *Atmos. Environ.* **31**, 1933-1940.

Odman, M. T., 1998: Research on Numerical Transport Algorithms for Air Quality Simulation Models. EPA Report. EPA/660/R-97/142. [Available from National Exposure Research Laboratory, U.S. Environmental Protection Agency, Research Triangle Park, NC 27711].

Odman, M. T., and A. G. Russell, 1993: A nonlinear filtering algorithm for multi-dimensional finite element pollutant advection schemes. *Atmos. Environ.* **27A**, 793-799.

Odman, M. T., A. Xiu, and D. W. Byun, 1995: Evaluating advection schemes for use in the next generation of air quality modeling systems, In *Regional Photochemical Measurement and Modeling Studies*, eds A.J. Ranzieri and P.A. Solomon, Vol. III, Air & Waste Management Association, Pittsburgh, PA. 1386-1401.

Oran, E., and J. Boris, 1987: Numerical Solution of Reactive Flow, New York, Elsevier.

Otte, M.J. and J.C. Wyngaard, 1996: A general framework for an "unmixed layer" PBL model. *J. Atmos. Sci.*, **53**, 2652-2670.

Pleim, J.E. and J. Chang, 1992: A non-local closure model for vertical mixing in the convective boundary layer. *Atmos. Envi.*, **26A**, 965-981.

Raymond, W.H. and R.B. Stull, 1990: Application of transilient turbulence theory to mesoscale numerical weather forecasting. *Mon. Weather Rev.*, **118**, 2471-2499.

Rood, R. B., 1987: Numerical advection algorithms and their role in atmospheric transport and chemistry models. *Rev. Geophysics* **25**(1), 71-100.

Schumann, U., 1989: Large-eddy simulation of turbulent diffusion with chemical reactions in the convective boundary layer. *Atmos. Envi.*, **26A**, 965-981.

Smagorinsky, J., 1983: General circulation experiments with the primitive equations: 1. The basic experiment. *Mon. Wea. Rev.* **91**, 99-164.

Stull, R. B., 1988: *An Introduction to Boundary Layer Meteorology*. Kluwer Academic, 666 pp.

Stull, R. B., 1993: Review of non-local mixing in turbulent atmosphere: Transilient turbulence theory. *Bound.-Layer Meteor.*, **62**, 21-96.

Stull, R. B., and A.G.M. Driedonk, 1987: Applications of the transilient turbulence parameterization to atmospheric boundary layer simulations. *Bound.-Layer Meteor.*, **40**, 209-239.

Tremback, G. J., Powell, J., Cotton, W. R. and Pielke, R. A., 1987: The forward-in-time upstream advection scheme: extension to higher orders. *Mon. Wea. Rev.* **115**, 540-555.

Yamartino, R. J., 1993: Nonnegative, conserved scalar transport using grid-cell-centered, spectrally constrained Blackman cubics for applications on a variable-thickness mesh. *Mon. Wea. Rev.* **121**, 753-763.

Yamartino, R.J., J.S. Scire, G.R. Carmichael, and Y.S. Chang, 1992: The CALGRID mesoscale photochemical grid model - Part I. Model formulation, *Atmos. Environ.* **26A**, 1493-1512.

Yanenko, N. N., 1971: *The Method of Fractional Steps*. Spring-Verlag, New York, 160pp.

Zhang, Q., and Stull, R. B. Stull, 1992: Alternative nonlocal descriptions of boundary-layer evolution. *J. Atmos. Sci.*, **49**, 2267-2281.

This chapter is taken from *Science Algorithms of the EPA Models-3 Community Multiscale Air Quality (CMAQ) Modeling System*, edited by D. W. Byun and J. K. S. Ching, 1999.

Appendix 7A Numerical Solvers for Diffusion Equations

In this appendix we describe numerical procedures for eddy diffusion, the Blackadar mixing scheme, and the asymmetric convective model.

7A.1 Stability of Tridiagonal Solver

The eddy diffusion formulation requires the solution of the linear equation

$$\mathbf{Aq} = \mathbf{b} \tag{7A-1}$$

where:

$$\mathbf{A} = \begin{pmatrix} d_1 & c_1 & 0 & 0 & \cdots & 0 \\ a_2 & d_2 & c_2 & 0 & \cdots & 0 \\ 0 & a_3 & d_3 & c_3 & \cdots & 0 \\ \vdots & \vdots & \vdots & \vdots & \vdots & \vdots \\ 0 & \cdots & 0 & a_{n-1} & d_{n-1} & c_{n-1} \\ 0 & \cdots & 0 & 0 & a_n & d_n \end{pmatrix};$$

$$\mathbf{q} = \begin{pmatrix} q_1 & q_2 & q_3 & \cdots & q_n \end{pmatrix}^T; \text{ and}$$

$$\mathbf{b} = \begin{pmatrix} b_1 & b_2 & b_3 & \cdots & b_n \end{pmatrix}^T.$$

The system Equation 7A-1 can be solved by the Thomas algorithm (Gaussian elimination of a tridiagonal matrix without pivoting) followed by back substitution. Assume that the following stage of the elimination has been reached:

$$\alpha_{j-1} q_{j-1} + c_{j-1} q_j = \beta_{j-1} \tag{7A-2a}$$

$$a_j q_{j-1} + d_j q_j + c_j q_{j+1} = b_j \tag{7A-2b}$$

where $\alpha_1 = d_1$ and $\beta_1 = b_1$.

For j=2,3,⋯n-1, eliminating q_{j-1} from Equations 7A-2a,b leads to:

$$\alpha_j q_j + c_j q_{j+1} = \beta_j \tag{7A-3a}$$

where

$$\alpha_j = d_j - \frac{a_j c_{j-1}}{\alpha_{j-1}} \tag{7A-3b}$$

$$\beta_j = b_j - \frac{a_j \beta_{j-1}}{\alpha_{j-1}} \tag{7A-3c}$$

The last pair of simultaneous equations are:

$$\alpha_{n-1} q_{n-1} + c_n q_n = \beta_{n-1} \tag{7A-4a}$$

$$a_n q_{n-1} + d_n q_n = b_n \tag{7A-4b}$$

Eliminating q_{n-1} gives:

$$\alpha_n q_n = \beta_n \tag{7A-5a}$$

and with Equation 7A-3a, we can obtain the solution by back substitution, i.e., $j = n\text{-}1, n\text{-}2, \cdots, 1$:

$$q_j = \frac{\beta_j + c_j q_{j+1}}{\alpha_j} \tag{7A-5b}$$

The algorithm described above is stable for the tridiagonal system if:

(i) $d_j > 0$, $a_j < 0$, and $c_j < 0$;
(ii) $d_j > -(a_{j+1} + c_{j-1})$ for j=1,2, ,$\cdots n$-1, defining $c_o = a_n = 0$; and
(iii) $d_j > -(a_j + c_j)$ for j=1,2, ,$\cdots n$-1, defining $a_1 = c_{n-1} = 0$.

The first two conditions ensure that the forward elimination is stable and the first and third conditions ensure that the back substitution is stable.

To prove that the forward elimination procedure is stable, it is necessary to show that the moduli of the multipliers $m_j = -a_j / \alpha_{j-1}$ used to eliminate q_1, q_2, ... are positive and less than or equal to one. From Equation 7A-2, we get:

$$\alpha_j = d_j + m_j c_{j-1} \tag{7A-6a}$$

and

$$m_{j+1} = -\frac{a_{j+1}}{\alpha_j} = \frac{-a_{j+1}}{d_j + m_j c_{j-1}} \tag{7A-6b}$$

Then, since $d_1 > -a_2 > 0 = c_o$:

$$0 < m_2 < -\frac{a_2}{d_1} < 1 \tag{7A-7a}$$

Similarly, we have:

$$0 < m_3 < \frac{-a_3}{d_2 + m_2 c_1} < \frac{-a_3}{d_2 + c_1} < \frac{-a_3}{-(a_3 + c_1) + c_1} = 1 \tag{7A-7b}$$

since $d_2 > -(a_3 + c_1)$. In this way, we can show that $0 < m_j < 1$ for j=1, 2, ···n-1.

For back substitution, we can write:

$$q_j = \frac{1}{\alpha_j}(\beta_j - c_j q_{j+1}) = p_{j+1} q_{j+1} + \frac{\beta_j}{\alpha_j} \tag{7A-8}$$

with $a_1 = c_{n-1} = 0$ for j=1, 2, ···n-1.

There will be no build-up of errors in the back substitution process if $|p_{j+1}| < 1$, where:

$$p_{j+1} = \frac{-c_j}{\alpha_j} = \frac{-c_j}{d_j + a_j p_j} \tag{7A-9a}$$

Now, $0 < p_2 = -c_1 / d_1 < 1$, since $a_1 = 0$ and $d_1 > -c_1$ by hypothesis. Then:

$$p_3 = \frac{-c_2}{d_2 + a_2 p_2} \tag{7A-9b}$$

As $-c_2 > 0$, $0 < p_2 < 1$, and $d_2 > -a_2 > 0$, it follows that:

$$0 < p_3 < \frac{-c_2}{d_2 + a_2} < \frac{-c_2}{-(a_2 + c_2) - a_2} = 1 \tag{7A-10}$$

Similarly, we can show that $0 < p_j < 1$ for j=1, 2,···n-1.

7A.2 Solver for Blackadar Scheme

The Blackadar scheme requires solving the sparse linear matrix equation **Aq=b** of the form

$$\mathbf{A} = \begin{pmatrix} d_1 & f_2 & f_3 & \cdots & f_{n-1} & f_n \\ e_2 & d_2 & 0 & 0 & \cdots & 0 \\ e_3 & 0 & d_3 & 0 & \cdots & 0 \\ \vdots & \vdots & \vdots & \vdots & \vdots & \vdots \\ e_{n-1} & \cdots & 0 & 0 & d_{n-1} & 0 \\ e_n & \cdots & 0 & 0 & 0 & d_n \end{pmatrix} \tag{7A-11}$$

The solver for this system uses a similar numerical procedure as for the tridiagonal system. The elements of the linear set of equations are related as follows:

$$d_1 q_1 + \sum_{j=2}^{n} f_j q_j = b_1 \tag{7A-12a}$$

and for $2 \le j \le n$:

$$e_j q_1 + d_j q_j = b_j \tag{7A-12b}$$

By substituting q_j with q_1 for each j, we get:

$$q_1 = \frac{b_1 - \sum_{j=2}^{n} b_j f_j / d_j}{d_1 - \sum_{j=2}^{n} e_j f_j / d_j} \tag{7A-13a}$$

and for $2 \le j \le n$:

$$q_j = (b_j - e_j q_1) / d_j \tag{7A-13b}$$

Note that Equation 7A-13b involves neither a forward nor a backward substitution loop.

7A.3 Solver for Asymmetric Convective Model (ACM)

The Asymmetric Convective Model requires solving the linear matrix equation **Aq=b** with a sparse matrix of the form:

$$\mathbf{A} = \begin{pmatrix} d_1 & c_2 & 0 & \cdots & 0 & 0 \\ e_2 & d_2 & c_2 & 0 & \cdots & 0 \\ e_3 & 0 & d_3 & c_3 & \cdots & 0 \\ \vdots & \vdots & \vdots & \vdots & \vdots & \vdots \\ e_{n-1} & \cdots & 0 & 0 & d_{n-1} & c_{n-1} \\ e_n & \cdots & 0 & 0 & 0 & d_n \end{pmatrix} \tag{7A-14}$$

The solver for this system is based on a numerical procedure similar to the tridiagonal solver. The relation among the variables q_i are given as:

$$d_1 q_1 + c_1 q_2 = b_1 \tag{7A-15a}$$

$$e_n q_1 + d_n q_n = b_n \tag{7A-15b}$$

and for $2 \le j \le n-1$:

$$e_j q_1 + d_j q_j + c_j q_{j+1} = b_j \tag{7A-15c}$$

Assume that the following stage of the elimination has been reached for $1 \le j \le n-1$:

$$\alpha_j q_1 + c_j q_{j+1} = \beta_j \tag{7A-16a}$$

where:

$$\alpha_j = e_j - \frac{d_j}{c_{j-1}} \alpha_{j-1} \tag{7A-16b}$$

$$\beta_j = b_j - \frac{d_j}{c_{j-1}} \beta_{j-1} \tag{7A-16c}$$

with $\alpha_1 = d_1$ and $\beta_1 = b_1$. From Equation 7A-16a for $j = n-1$ and Equation 7A-15b, q_1 is found to be:

$$q_1 = \frac{d_n \beta_{n-1} - b_n c_{n-1}}{d_n \alpha_{n-1} - e_n c_{n-1}} \tag{7A-17a}$$

and all other q_is are computed with:

$$q_{j+1} = \frac{\beta_j - \alpha_j q_1}{c_j} \tag{7A-17b}$$

for $1 \le j \le n-1$. The final substitution stage can be implemented either in a forward or backward sweep.

Chapter 8

GAS-PHASE CHEMISTRY

Gerald L. Gipson*
Human Exposure and Atmospheric Sciences Division
National Exposure Research Laboratory
U. S. Environmental Protection Agency
Research Triangle Park, NC 27711, USA

Jeffrey O. Young**
Atmospheric Modeling Division
National Exposure Research Laboratory
U.S. Environmental Protection Agency
Research Triangle Park, NC 27711, USA

ABSTRACT

This chapter describes the manner in which gas-phase chemistry is treated in the Models-3 Community Multiscale Air Quality (CMAQ) modeling system. The CMAQ system currently includes two chemical mechanisms -- RADM2 and CB4 -- with plans to incorporate a third -- the SAPRC97 mechanism -- in the near future. Each of these mechanisms is described, and the manner in which the first two are linked to the aqueous chemistry and aerosol formation processes is discussed. Enhanced isoprene chemistry that has been included in the RADM2 mechanism is also described, and procedures for entering new chemical mechanisms in the CMAQ system are addressed. The representation of reaction kinetics in the CMAQ system and the numerical modeling of gas-phase chemistry are also presented. The CMAQ system currently employs two numerical solvers, SMVGEAR and a variant of the QSSA method. The numerical procedures used in each are presented, and the relative computational efficiencies of each on different computing platforms are noted.

---

*Corresponding author address: Gerald L. Gipson, MD-80, Research Triangle Park, NC 27711. E-mail: ggb@hpcc.epa.gov

**On assignment from the National Oceanic and Atmospheric Administration, U.S. Department of Commerce.

8.0 GAS-PHASE CHEMISTRY

Since atmospheric chemistry plays a major role in many air pollution problems, the representation of chemical interactions among atmospheric constituents is often an essential element of an air quality model. All important chemical transformations relevant to the problem being studied must be included to make accurate predictions of ambient pollutant concentrations. Many atmospheric pollutants or their precursors are emitted as gases and interact primarily in the gaseous phase. However, some important atmospheric processes such as acid deposition and the formation of aerosols involve the interaction of constituents in the gas, liquid, and solid phases, so transformations taking place in all three phases often need to be represented. For computational efficiency, these processes are usually modeled separately. This approach has been adopted in the Chemical Transport Model (CTM) that is part of the Community Multiscale Air Quality (CMAQ) modeling system (hereafter referred to as the CCTM). This section addresses the modeling of gas-phase transformations alone in the CCTM. Descriptions of the linkages of gas-phase constituents with aerosols and with aqueous chemistry are discussed below and in Chapters 10 and 11, respectively. A potential future improvement to the CCTM would involve more closely coupling the chemical interactions taking place in all three phases. Nevertheless, the current formulation still enables the investigation and assessment of environmental problems using a multi-pollutant, one-atmosphere modeling concept.

Interactions in the gas-phase are represented in air quality models by means of chemical mechanisms. The CMAQ system currently includes two base chemical mechanisms that have been developed primarily to address issues associated with urban and regional scale ozone formation and acid deposition -- the CB4 (Gery et al., 1989) and RADM2 (Stockwell et al., 1990) mechanisms. Variants of these two mechanisms have been developed for the CMAQ system to provide the necessary linkages to the aerosol and aqueous chemistry processes. Current plans also call for adding a third mechanism -- the SAPRC-97 mechanism (Carter, 1997). Although these mechanisms should be adequate for many air pollution applications, it may be necessary to modify or even replace these mechanisms to address some issues. To facilitate changing mechanisms and adding new ones, the CMAQ system has been equipped with a generalized chemical mechanism processor. It must be emphasized, however, that supplemental data for other CMAQ processors may be required when one of the predefined mechanisms is modified or replaced. This is addressed in more detail section 8.2.5.

The remainder of this chapter addresses different aspects of the representation of gas-phase chemistry in the CMAQ system. The first section includes background information on chemical mechanisms and provides the rationale for including the predefined chemical mechanisms in the CMAQ system. The subsequent section describes the predefined chemical mechanisms as implemented in the CMAQ system and addresses adding new mechanisms or changing existing ones. This is followed by a description of reaction kinetics as it relates to the CCTM representation, and the final section describes the mathematical procedures used internally in the CCTM to solve the equations that arise from the mathematical representation of gas-phase chemistry.

8.1 Background

A chemical mechanism is a collection of reactions that transforms reactants into products, including all important intermediates. Chemical mechanisms developed for air quality modeling are highly condensed, parameterized representations of a true chemical mechanism. They include artificial species and operators, and many of the mechanism reactions are parameterizations of a large set of true atmospheric reactions. In some cases, mechanism reactions may include elements which have no physical significance (e.g., products with negative stoichiometry). While it would be difficult to design a generalized mechanism processor to handle all possible parameterizations used in various condensed mechanisms, some degree of generalization in the CMAQ system is achieved by using special conventions for entering chemical mechanisms. First, all reactions in the mechanism are treated as if they are elementary, and the stoichiometric coefficients for all reactants must be one. Since all reactions are assumed to be elementary, a reaction can have no more than three reactants. These conventions permit the reaction rate to be derived directly from the stoichiometric equation, thereby simplifying the mathematical representation of the reactions. Other conventions adopted for the CMAQ generalized mechanism processor are included in Section 8.3 and in Chapter 15.

Mechanism species can be divided into two categories: inorganic and organic. The number of important inorganic species is relatively small, and they are almost always represented explicitly in chemical mechanisms. The important inorganic species included in these mechanisms are ozone, nitric oxide, nitrogen dioxide, nitric acid, nitrous acid, hydrogen peroxide, sulfur dioxide, and several radicals formed through their interactions with other species. Although most of the chemical reactions involving these species are common to all mechanisms, some differences do exist. For example, some of the mechanisms omit a few reactions because they are normally minor pathways and thus do not affect modeling results significantly. Also, different rate constants may be used for some reactions, especially those that are photolytic. The representation of organic species usually differs more substantially, however. Some species in the mechanism represent real organic compounds, but others represent a mixture of several different compounds. The manner in which the grouping of organic compounds is carried out typically distinguishes one mechanism from another, and that is described next. In this chapter, the phrase *mechanism species* is used to refer to any species in the gas-phase mechanism, regardless of whether it is an explicit species or not.

Although explicit mechanisms have been developed for many organic compounds, the resultant number of reactions and species needed to represent their atmospheric chemistry is too large to model efficiently in photochemical grid models such as the CCTM. In addition, explicit mechanisms have not yet been developed for most organic compounds, thereby requiring that some reaction pathways be postulated. Thus, both compression and generalization are necessary when depicting organic reactions. Although chemical mechanisms differ in the manner in which organic species are represented, the mechanism developer usually chooses some distinguishable organic property to group similar organics into classes that reduce both the number of mechanism species and reactions. The three most common representations include the lumped structure

technique, the surrogate species approach, and the lumped species method. In the lumped structure approach, organic compounds are apportioned to one or more mechanism species on the basis of chemical bond type associated with individual carbon atoms (Whitten et al., 1980). In the surrogate species method, the chemistry of a single species is used to represent compounds of the same class (e.g., Lurmann et al., 1987). Generalized reactions are then written based on the hypothetical model species. The lumped species method is very similar to the surrogate species approach, but various mechanism parameters associated with a particular surrogate are adjusted to account for variations in the composition of the compounds being represented by the surrogate species (e.g., Carter, 1990, and Stockwell et al., 1990).

The construction of a compact chemical mechanism necessarily introduces varying levels of distortion, generalization, and omission in the representation of atmospheric chemistry (Jeffries, 1995). Although mechanisms are routinely tested using results obtained from environmental chamber experiments, the data are often insufficient to resolve uncertainties associated with some of the chemical representations. For example, Carter (1990) noted that much is unknown about several important reaction types, and that their representations "... continue to be largely speculative or are based on empirical models derived from fits to environmental chamber data." Further, rate constants for some reactions are either unknown completely, or significant disagreement exists as to their accuracy. Several studies have been conducted to compare different chemical mechanisms (e.g., Leone and Seinfeld, 1985; Hough, 1988; and Dodge, 1989). These comparisons revealed that the mechanisms often yield results that are similar for some species. This could indicate that the fundamental atmospheric chemistry is fairly well understood for these species, or that the mechanisms were derived from the same experimental kinetic or mechanistic data, which may or may not be accurate. Larger differences tend to occur for those species for which the atmospheric chemistry is more uncertain. Thus, it is often difficult to assess the relative merits of different mechanisms when applied to any one situation. Therefore, the CMAQ system includes the capability to use more than just one chemical mechanism.

Given the inherent uncertainties in existing chemical mechanisms, alternate approaches for representing gas-phase chemistry are needed. One approach being explored involves decreasing uncertainties associated with the simplifications that are introduced to reduce mechanism size. This approach is based on the concept that much of the information needed for an expanded chemical representation does not necessarily have to be included in the mechanism explicitly, but rather can be maintained in auxiliary variables linked to a relatively small number of core species that are included in the mechanism (Jeffries et al., 1993). Thus, it may be possible to expand chemical representations without greatly increasing the size of the basic mechanism, and this could be a future enhancement to the treatment of gas-phase chemistry in the CMAQ system.

8.2 Chemical Mechanisms in the CMAQ System

This section includes summary descriptions of the two basic chemical mechanisms included in the CMAQ system -- the CB4 (Gery et al., 1989) and the RADM2 (Stockwell et al., 1990). Since the SAPRC-97 mechanism (Carter, 1997) is to be added in the near future, some discussion of it is

also included. These mechanisms require that information be supplied to the CCTM in a form that is unique for each mechanism, and this is carried out in several sub-systems incorporated in the CMAQ system. These include the emissions processing system which generates emissions for key mechanism species; the initial conditions/boundary conditions processor that generates ambient starting and boundary concentrations for mechanism species; and the photolysis rate processor that produces mechanism specific photolysis rates. The reader is referred to the chapters describing those sub-systems for a description of the treatment of mechanistic data, and to the mechanism references for a more detailed description of each chemical mechanism.

In addition the base mechanisms, both the base CB4 and RADM2 mechanisms have been modified in the CMAQ system to provide necessary linkages for aerosol and aqueous chemistry processes, and the RADM2 mechanism has also been modified to create two new mechanism variants that include enhanced isoprene chemistry representations. Note that the existing sub-systems provide all of the necessary information for the extensions to the base mechanism. The modifications to the base mechanisms are discussed below in the section on mechanism extensions. Complete listings of all mechanisms currently available in the CMAQ system are included in Appendix 8A. The last portion of this section briefly discusses changing the base mechanism or their variants or adding new mechanisms to the CMAQ system.

8.2.1 CB4 Mechanism

The CB4 mechanism is a lumped structure type that is the fourth in a series of carbon-bond mechanisms, and differs from its predecessors notably in the detail of the organic compound representation. It has been used in models such as EPA's Empirical Kinetic Modeling Approach (EPA, 1989) and Regional Oxidant Model (Lamb, 1983), and in versions IV and V of the Urban Airshed Model (EPA, 1991 and SAI, 1993). The CMAQ implementation of the basic CB4 mechanism includes 36 species and 93 reactions, including 11 photolytic reactions.

The CB4 uses nine primary organic species (i.e., species emitted directly to the atmosphere as opposed to secondary organic species formed by chemical reaction in the atmosphere). Most of the organic species in the mechanism represent carbon-carbon bond types, but ethene (ETH), isoprene (ISOP) and formaldehyde (FORM) are represented explicitly. The carbon-bond types include carbon atoms that contain only single bonds (PAR), double-bonded carbon atoms (OLE), 7-carbon ring structures represented by toluene (TOL), 8-carbon ring structures represented by xylene (XYL), the carbonyl group and adjacent carbon atom in acetaldehyde and higher molecular weight aldehydes represented by acetaldehyde (ALD2), and non-reactive carbon atoms (NR). Many organic compounds are apportioned to the carbon-bond species based simply on the basis of molecular structure. For example, propane is represented by three PARs since all three carbon atoms have only single bonds, and propene is represented as one OLE (for the one carbon-carbon double bond) and one PAR (for the carbon atom with all single bonds). Some apportionments are based on reactivity considerations, however. For example, olefins with internal double bonds are represented as ALD2s and PARs rather than OLEs and PARs. Further, the reactivity of some compounds may be lowered by apportioning some of the carbon atoms to the non-reactive class

NR (e.g., ethane is represented as 0.4 PAR and 1.6 NR). Apportioning rules have been established for hundreds of organic compounds, and are built into the emissions processing sub-systems to produce the appropriate emission rates for the CB4 mechanism species.

The CB4 mechanism described by Gery et al. (1989) has undergone several changes since its publication. In 1991, the PAN rate constants were changed and a termination reaction between the XO2 operator and the HO2 radical were added. Subsequently, terminal reactions for the XO2N operator were also added. An updated CB4 isoprene chemistry mechanism based on the work of Carter (1996) was developed in 1996. All of these changes have been incorporated in the CMAQ version. It should also be noted that the original CB4 mechanism incorporated simple Arrhenius type rate constant expressions that were derived from more complex expressions for temperature and pressure dependent rate constants. Since the top of the CCTM domain may extend to heights that makes pressure dependencies important, the CMAQ version incorporates the original expressions rather than the derived ones.

8.2.2 RADM2 Mechanism

The RADM2 mechanism is a lumped species type that uses a reactivity based weighting scheme to adjust for lumping (Stockwell et al., 1990). It has evolved from the original RADM1 mechanism (Stockwell, 1986), and is employed in version 2 of the Regional Acid Deposition Model (Chang et al., 1987). The base mechanism as implemented in the CMAQ system contains 57 model species and 158 reactions, of which 21 are photolytic.

In RADM2, the primary organics are represented by 15 mechanism species, five of which are explicit because of their high emission rates or because of special reactivity considerations (methane, ethane, ethene, isoprene, and formaldehyde). The other ten represent groups of organic compounds aggregated on the basis of their reactivity with the hydroxyl radical (HO) and/or their molecular weights. To account for varying reactivities of the different organics that are lumped into a single group, emissions of each organic within a group are weighted by a reactivity factor (F) that is computed as the ratio of the fraction of emitted organic compound that reacts to the fraction of the mechanism species that reacts:

$$F = \frac{1 - \exp(-k_{\text{HO Emiss}} \int [\text{HO}]\, dt)}{1 - \exp(-k_{\text{HO Mech}} \int [\text{HO}]\, dt)} . \qquad (8\text{-}1)$$

The integral term is estimated from a daily average integrated HO radical concentration of 110 ppt min that was derived from RADM simulations (Stockwell et al., 1990). Note that F approaches unity if the reactivity of the emitted organic nearly equals that of the mechanism species or if the reactivities of both are very large. As with CB4, the RADM2 lumping and weighting rules have been built into the CMAQ emission processing system.

The implementation of the RADM2 mechanism in the CMAQ system is almost identical to that described by Stockwell et al. (1990), with only two minor modifications. First, the reaction of HO with cresol (CSL) was reformulated as follows to eliminate negative stoichiometry in the mechanism:

From: $HO + CSL \rightarrow 0.1\ HO_2 + 0.9\ XO_2 + 0.9\ TCO_3 - 0.9\ HO$ $\quad k_{HO+CSL}$;

To: $HO + CSL \rightarrow 0.1\ HO_2 + 0.9\ XO_2 + 0.9\ TCO_3$ $\quad k_{HO+CSL}$;

$HO + CSL \rightarrow CSL$ $\quad 0.9\ k_{HO+CSL}$.

(Note that negative stoichiometry is permitted in the CMAQ system, but was removed here for consistency with previous implementations of RADM2.) Second, the concentration of methane in the CCTM is assumed to be constant at 4.5×10^{13} molecules/cc. Thus, methane was removed as a reactant in the reaction of OH with methane and the corresponding rate constant changed from second-order to pseudo first-order using the assumed CCTM methane concentration.

8.2.3 SAPRC-97 Mechanism

The SAPRC-97 mechanism (Carter, 1997) employs the lumped surrogate species approach, but offers the capability to incorporate semi-explicit chemistry of selected organics. The SAPRC series of mechanisms evolved from the "ALW" mechanism of Atkinson et al. (1982). SAPRC-97 is similar to its predecessors SAPRC-90 and SAPRC-93, but incorporates improvements to aromatic chemistry and updates to reactions of many individual organic compounds. Although many of the reactions for organic compounds are generalized and incorporate non-explicit species, product yield coefficients and rate constants are tabulated for over 100 individual organic compounds. Thus, each of these organics can be modeled individually by including their semi-explicit chemistry in the mechanism. Due to computational constraints, however, the full set of organic compounds cannot be incorporated in an Eulerian model. For this situation, the mechanism is condensed by lumping individual organic compounds into groups with corresponding rate constants and product yield coefficients that have been weighted by mole fractions of the individual organics. The mole fractions are typically derived from emission inventory data used in the model simulation. Thus, unlike the previous mechanisms, the SAPRC-97 mechanism can potentially change with each application since new rate constants and product yield coefficients can be computed for each application.

The SAPRC-97 mechanism has been developed with supplemental software to facilitate constructing mechanisms of varying levels of condensation. Documentation of the procedures include three distinct levels of detail, differing primarily in the number of organic species that are included in the mechanism (Carter, 1988). Since no decisions have made on the form of the mechanism that will be added to the CMAQ system, listings for this mechanism are not included in Appendix 8A. Documentation will be provided when the CMAQ version is made available however.

8.2.4 Extended Mechanisms

Each gas-phase chemical mechanism has been linked to aqueous chemistry and to aerosol formation processes. Since these linkages required some modifications to the original gas-phase mechanisms, different versions of the same mechanism were created for modeling gas-phase chemistry alone or for modeling gas-phase chemistry with or without aerosols and/or aqueous chemistry. Different versions of the mechanisms are distinguished by means of a special naming convention. Gas-phase mechanisms that have not been modified are referred to by their base name (e.g., CB4, RADM2, and SAPRC when the latter is available). Mechanisms that have been modified to account for aerosol production have their names appended with "_AE", mechanisms modified for aqueous chemistry are appended with "_AQ", and mechanisms modified for both are appended with "_AE_AQ". Thus, CB4_AE_AQ refers to the CB4 gas-phase mechanism that has been modified to include linkages to both aerosols and aqueous chemistry. A second set of RADM2 gas-phase mechanisms that incorporates new isoprene chemistry has also been included in the CMAQ system. These mechanisms include either "_CIS1" or "_CIS4" in their names to denote that the mechanism incorporates enhanced isoprene chemistry. Methods used to develop the extended mechanisms are described below according to the three types of extensions: aerosol, aqueous chemistry, and isoprene chemistry.

8.2.4.1 Aerosol Extensions

A major pathway leading to the formation of aerosols is the oxidation of sulfur dioxide (SO_2) to sulfate, primarily by the gas-phase reaction of SO_2 with the hydroxyl radical (OH). All mechanisms in the CMAQ system incorporate this reaction. Because organics are represented differently in the base mechanisms, however, aerosol formed from the reactions of organic compounds must be handled somewhat differently. In the CCTM, organic aerosol formation is quantified using aerosol yields, i.e., μgm^{-3} of aerosol produced per ppm of organic reacted with OH, ozone or nitrate radical (NO_3). The yields used in the CCTM are those reported by Bowman et al. (1995) that were derived from the work of Pandis et al. (1992). These yields are given in terms of the SAPRC-90 chemical mechanism species, so some adjustments were required to adapt them to the CMAQ mechanisms. In the CMAQ system, aerosol production is assumed to occur from reactions involving five different generic organic groupings. Individual mechanism species are then mapped to these general groupings to obtain the aerosol yields. The five generic groups are defined as: 1) long-chain alkanes; 2) alkyl-substituted benzenes such as toluene and xylene; 3) cresol and phenols; 4) long-chain olefins; and 5) monoterpenes. Note that the aerosol yields vary significantly among these five groups, so it is important to map the organic species in each mechanism to the proper aerosol production group. The remainder of this section describes the mapping that is used for the CMAQ base mechanisms and how the aerosol production rates are determined from the gas-phase reactions. The derivation of the yields used in the CCTM and the manner in which they are used in the aerosol module are described in Chapter 10.

To apply the aerosol yields, the amount of reactant consumed by reaction must be determined for several mechanism species. In the CMAQ system, this is accomplished by using "counter" species

that have been added as products to those reactions involving the mechanism species of interest (e.g., Bowman et al., 1995). These counter species are essentially "dummy" species with no physical significance, and are not subjected to any other model process such as advection or diffusion. Thus, changes in their concentrations reflect the effect of chemical reaction alone. Also, their inclusion in the mechanisms does not affect basic gas-phase chemistry since they do not interact with any of the other species in the mechanism.

Special procedures are used in the CCTM to determine aerosol production from monoterpenes since their aerosol yields are relatively large and they are either lumped with other organic compounds into a single mechanism species or are apportioned among several mechanism species. The approach involves tracking the rate of reaction of monoterpenes separately from the rates of their mechanistic representation. The CMAQ emission processor generates emissions for monoterpenes as a unique species *in addition to* lumping or apportioning the emissions into the appropriate mechanism species. Whenever aerosols are being modeled, the unique monoterpene species is included in the mechanisms and is modeled as a separate species. As with the counter species, however, the monoterpene species is incorporated in the mechanisms such that it does not affect the basic gas-phase chemistry. This is described in more detail below. A potential future modification to the CMAQ system would involve incorporating a more explicit representation of monoterpenes in the base mechanisms that would eliminate the need for this special treatment and would also improve the chemical representation of these species in the gas-phase mechanisms (e.g., Stockwell et al., 1997).

- **RADM2_AE.** Much of the linkage between the RADM2 mechanism and aerosol formation is relatively straightforward. Aerosol production from SO2 and long-chain alkanes is derived from the amount of SO2 and HC8 reacted with OH, respectively. Similarly, aerosol production from alkyl-substituted benzenes is derived from the sum of the TOL and XYL reactions with OH. The production from phenols and cresols is based upon the sum of the CSL reactions with OH and NO_3. Thus, special counter species named SULAER, HC8AER, TOLAER, XYLAER, and CSLAER have been added to track these reactions.

  In the RADM2 mechanism, both monoterpenes and other olefinic compounds are lumped into the mechanism species OLI. As noted above, however, monoterpenes are modeled separately whenever aerosols are modeled. The monoterpenes are represented in the RADM2 mechanism by the species TERP, and the following reactions are added:

  TERP + HO → TERPAER + HO

  TERP + NO_3 → TERPAER + NO_3

  TERP + O_3 → TERPAER + O_3

These reactions use the same rate constants as the reaction of OLI with these species, and have the TERPAER counter species added to track the throughput of this reaction. Note that concentrations of the reactants OH, NO_3 and ozone are unaffected by these reactions since their production equals their loss.

The final pathway for aerosol production in the RADM2 mechanism is via reaction of long-chain olefins with OH, NO_3 and ozone. The RADM2 mechanism species OLI is used as the surrogate for long-chain olefins, and thus a counter species product named OLIAER is added to each of the reactions of OLI with OH, NO_3 and ozone. Since OLI includes both monoterpenes and other olefins, however, OLIAER tracks the reaction rate of both. The amount of long-chain olefins reacted is determined by subtracting the concentration of the counter species TERPAER from that of OLIAER. The yield of aerosols from long-chain olefins is then applied to this difference to obtain aerosol production by this pathway.

- **CB4_AE.** Since the CB4 gas-phase mechanism is structure-based, individual organic molecules are often disaggregated and assigned to more than one mechanism species. For example, long-chain alkenes are apportioned to both the PAR and OLE mechanism species. Thus, many of the organic mechanism species contain fragments of molecules, and the identity of the original contributing organic compound is lost. As a result, it is not possible to ascertain with certainty the amount of long-chain alkanes and alkenes reacting in the CB4 mechanism, and thus aerosol production via these pathways is omitted. The production of aerosols from the reactions of toluene, xylene, and cresol is included, however, by tracking the amounts of TOL, XYL, and CRES that react using the counter species TOLAER, XYLAER, and CSLAER. The manner in which aerosol production from monoterpenes is modeled is identical to that used in the RADM2 mechanism. Monoterpenes are modeled independently as the mechanism species TERP, with rate constants for the reactions of TERP with OH, O_3, and NO_3 set to the same values as those used in the RADM2 mechanism extension.

8.2.4.2 Isoprene Extensions

Over the past few years, the importance of isoprene in ozone formation has become a major concern. Its representation in the original gas-phase mechanisms was substantially condensed, partially because of computational resource considerations and partially due to significant uncertainties about the pathways of its reaction products. Recent mechanistic and environmental chamber studies have led to a greater understanding of its atmospheric chemistry and thus improved mechanistic representations (Carter and Atkinson, 1996). In the CMAQ system, two different levels of more detailed isoprene chemistry have been included in the RADM2 mechanism, and these are referred to as the one-product and the four-product Carter isoprene mechanisms (Carter, 1996). Both are condensed forms of the more detailed mechanism developed by Carter and Atkinson (1996). Since this detailed mechanism may be too large to use in full-scale Eulerian modeling studies, Carter condensed the detailed mechanism to two levels of

detail: one in which isoprene products are represented by four products, and one in which only one product is used. The four-product mechanism is the lesser condensed of the two, and includes the explicit representation of many of the isoprene's unique products (e.g., methacrolein, methyl vinyl ketone, and methacrolein's PAN analogue). The one-product form lumps the major products into a single species, thereby yielding a more compact albeit less explicit mechanism. As noted above, these two mechanisms are named RADM2_CIS4 and RADM2_CIS1, and both have been linked to aerosols and aqueous chemistry as well. It should also be noted that the isoprene chemistry incorporated in the CMAQ CB4 mechanism corresponds to the Carter 1-product form, but the 4-product form is not available for the CB4 mechanism in the CMAQ system

8.2.4.3 Aqueous Chemistry Extensions

The base RADM2 mechanism does not have to be modified to link it to the aqueous chemistry processes since the aqueous processes in the CMAQ system are similar to those incorporated in the original RADM model. As described in Chapter 15, other aspects of the linkages require a separate mechanism with a unique name. The linkages to aqueous chemistry do require some minor changes to the CB4 mechanism however. These changes were based on a variant of the CB4 mechanism developed for acid deposition modeling by Gery et al. (1987). In this version, the following product species that were omitted in the base CB4 mechanism are included: formic acid, acetic acid, peroxyacetic acid, and methylhydroperoxide (MHP). Since these species are products only, their inclusion in the mechanism does not affect the concentrations of any of the other mechanism species. It should be noted, however, that the concentration of MHP in this modified mechanism represents an upper limit for two reasons. First, known decomposition pathways for it are not included in the mechanism. Second, the production of MHP will be overstated since it is produced by an operator that includes radicals other than the methylperoxy radical (Gery et al., 1987).

8.2.5 Changing or Adding Mechanisms in CMAQ

As noted in the introduction to this chapter, the CMAQ system has been instrumented with a generalized chemical mechanism processor to facilitate making changes to existing mechanisms or adding new mechanisms. The procedures for altering or adding a new mechanism are described in EPA (1998), and will not be repeated here. It should be emphasized, however, that the addition of a new mechanism will likely require modifications to the previously mentioned subsystems that provide key mechanism-specific information, i.e., emissions, initial/boundary condition, and photolytic rate processors. Changes to an existing mechanism would also likely require modifications to these processing subsystems if new organic species are added or if an alternative organic grouping scheme is implemented. If changes are limited such that they affect only the reactions of intermediate and/or product species, however, these subsystems may not need to be changed at all, and the modifications can then be implemented solely within the generalized chemical mechanism processor. For example, the modifications to the base mechanisms to provide linkages to aerosol and aqueous chemistry and to expand isoprene chemistry that were described previously did not require any major changes to the other processors except to add a

photolysis rate for acrolein in the photolytic rate processor for the CIS1 and CIS4 versions of RADM2.

Although the CMAQ system provides a convenient tool for making mechanism changes, some caution should be exercised in modifying existing CMAQ mechanisms. The mechanisms currently in the CMAQ system have been evaluated outside of the CMAQ system using environmental chamber data and/or more detailed chemical mechanism representations. Any proposed changes to reactions or reactions rates that significantly affect model predictions should normally be subjected to similar independent testing before being introduced into the CMAQ system and subsequently used in modeling applications. Thus, it would be expected that the introduction of most changes to a mechanism in the CMAQ system would only be performed by a researcher who is experienced in atmospheric chemistry and is familiar with the base mechanism.. Finally, it should be noted that the existing CMAQ mechanisms are fully specified. In most instances, it will only be necessary for a user to choose one of the existing mechanisms for their application, and it will not be necessary to make any changes to that mechanism.

8.3 Reaction Kinetics

The rates of chemical reaction determine whether a species is formed or destroyed by gas-phase chemistry. Since the CMAQ system treats all reactions as if they are elementary, the laws of reaction kinetics can be used directly to develop mathematical expressions for the rates of each chemical reaction. This section describes the rate expressions and the forms of the rate constants that are used in those expressions, with special emphasis placed on the conventions used in the CMAQ system. The reader may also wish to refer to Chapter 15 and EPA (1998) for details on how mechanism data are entered in the CMAQ system.

8.3.1 Reaction Rates

The rate of a chemical reaction l (r_l) can be expressed as the product of a rate constant (k_l) and a term that is dependent on the concentrations of the reactants:

$$r_l = k_l f(\text{concentration}) \ . \tag{8-2}$$

For elementary reactions, the concentration dependent term is simply the product of reactant concentrations, and the rate of reaction takes one of the following forms:

$$r_l = \begin{cases} k_l C_1 & \text{for first-order reactions} \\ k_l C_1 C_2 & \text{for second-order reactions} \\ k_l C_1 C_2 C_3 & \text{for third-order reactions} \end{cases} \tag{8-3}$$

where C_1, C_2,and C_3 refer to the concentration of reactants 1, 2 and 3, respectively. Note that when a species reacts with itself, the concentration dependent term includes the species

concentration squared. Thus, the rate for the reaction $NO + NO + O_2 \rightarrow 2NO_2$ is equal to $k[NO][NO][O_2]$ and not $k[NO][O_2]$.

Several important ter-molecular reactions involve O_2 and/or N_2 which mediate those reactions by absorbing energy from exothermic bi-molecular reactions. When either N_2 or O_2 serves this role, the third body is usually referred to as "M", where $M = N_2 + O_2$. Since their concentrations are relatively stable in the atmosphere, some mechanism developers convert second- or third-order reactions that include these species to a reaction one order lower by multiplying the higher-order rate coefficient by the concentration of M, O_2, or N_2. The CMAQ convention is to include third-body reactants in the reaction rate calculations if they are explicitly shown in the reaction, and to omit them if they are not shown or included only as comments. For example, consider the bimolecular reaction: $O^1D + O_2 \rightarrow O^3P + O_2$. If the reaction is written in this form, the reaction is assumed to be second-order and the CCTM will use the appropriate concentration for O_2 in the rate computation. If the reaction is written as $O^1D \rightarrow O^3P$ (or as $O^1D \{+ O_2\} \rightarrow O^3P$, where here the braces denote a comment), the reaction rate will be assumed to be first-order and the CCTM will *not* include the O_2 concentration in the reaction rate calculation. In the latter case, the mechanism developer must specify a pseudo first-order rate constant for the reaction. The same convention also applies to H_2O.

8.3.2 Rate Constant Expressions

As shown in Equation 8-3, the rate of reaction is related to the concentration term by a constant of proportionality k_l. The rate constant k_l can take many forms depending upon the characteristics of the reaction. One important class of uni-molecular reactions involves the absorption of radiant energy and subsequent dissociation of the reactant into product species. The rate constants for these types of reactions are functions of the incident radiant energy and properties of the absorbing molecule, such as the absorption cross section and the quantum yield. In the CMAQ system, these rate constants are calculated by the photolytic rate processor, and the details of these calculations are described in Chapter 14. The remainder of the reactions are classified as thermal, and their rate constants are typically functions of temperature and sometimes pressure. The calculation of these rate constants is discussed below.

To facilitate incorporating rate constant information for thermal reactions, the CMAQ generalized mechanism processor (discussed in Chapter 15) has been designed to accept the standard rate constant expressions used in NASA (1997). Rate constant information is most often supplied in cms units (i.e., gas concentrations in molecules/cc and time in seconds), but some mechanisms use mixing ratio units (i.e, gas concentrations converted to mixing ratios in parts per million and time in minutes). The CMAQ generalized mechanism reader is designed to accept either, but they must be consistent throughout the mechanism (i.e., the same units must be used for all rate constant forms that can be expressed in either set of units). Some rate constant expressions (e.g., falloff expressions and other special forms discussed below) can be expressed only in cms units, however, and must always be in these units even when mixing ratio units are being used for all other types of rate constants. The CCTM will automatically perform the necessary units

conversions during the model simulation. Nevertheless, since the CMAQ domain typically extends through the entire troposphere, cms units are usually preferred because differences in number density differences with height are explicitly accounted for with those units.

Descriptions of the forms of rate constant expressions currently used in the CMAQ system are presented next.

- **Arrhenius Equation**. Many rate constants exhibit a temperature dependence that corresponds to the Arrhenius equation:

$$k = A\ e^{(-E/T)} \tag{8-4}$$

where A is the pre-exponential factor, E is the activation energy divided by the gas constant R, and T is the temperature in degrees Kelvin. For this form of reaction, either cms or mixing ratio units may be used, and only A and E need to be specified.

- **Temperature Dependent A-factors.** For some reactions, the temperature dependence of the pre-exponential factor can become significant, and the Arrhenius equation does not hold. These rate constant expressions can often be put in the following form that is available in the CMAQ system:

$$k = A\ (T/300)^B\ e^{(-E/T)} \tag{8-5}$$

where A, E, and T are defined as above, and B is an empirically derived constant that provides a best fit to the data (Pitts-Finlayson and Pitts, 1986). For this form, either set of units can be used, and only A, E and B need to be specified.

- **Falloff Expressions.** Several ter-molecular reactions exhibit pressure dependencies that can be significant when modeling atmospheric chemistry. These can be especially important when modeling from the troposphere through the stratosphere. In these cases, the rate constant increases with increasing pressure. In effect, the behavior of these reactions approaches second-order at high pressure and third-order at low pressure. Equation 8-6 gives an effective second-order rate constant for the falloff region between these two limits.

$$k = \frac{k_0[\mathrm{M}]}{1 + k_0[\mathrm{M}]/k_\infty}\ F_C^{\{1\ +\ [N^{-1}\log(k_0[\mathrm{M}]/k_\infty)]^2\}^{-1}} \tag{8-6}$$

In Equation 8-6, k_0 and k_∞ are the low- and high-pressure limiting rate constants, respectively, and are calculated using the temperature dependent A-factor form described above. The parameters F_C and N are also reaction specific, but for atmospheric conditions are very often 0.6 and 1.0 respectively (Finlayson-Pitts and Pitts, 1986). For this type of rate constant expression, A, E, and B must be specified for both k_0 and k_∞, and only cms

units are allowed. If the parameters N and Fc are not specified, the values listed above will be used.

- **Special Forms.** The following special rate constant forms are also in general use and have been included in the CMAQ system:

$$k = k_1 + k_2[\mathrm{M}] \tag{8-7}$$

$$k = k_0 + \left(\frac{k_3[\mathrm{M}]}{1 + k_3[\mathrm{M}]/k_2}\right) \tag{8-8}$$

$$k = A\ (1.0 + 0.6P) \tag{8-9}$$

Equation 8-7 is used for the rate constants of the reactions forming hydrogen peroxide from hydroperoxy radicals ($HO_2 + HO_2 \rightarrow H_2O_2$ and $HO_2 + HO_2 + H_2O \rightarrow H_2O_2$). Equation 8-8 is used for the reaction of the hydroxyl radical with nitric acid ($HO + HNO_3 \rightarrow NO_3 + H_2O$), and Equation 8-9 is used for the reaction of the hydroxyl radical with carbon monoxide ($HO + CO \rightarrow HO_2 + CO_2$). In these equations, k_0, k_1, k_2, and k_3 are calculated using the Arrhenius equation, and A and E must be specified for each, with A given in cms units. In Equation 8-9, P is the atmospheric pressure in atmospheres and A can be specified in either set of units.

- **Reverse Equilibria Forms.** The CMAQ system also includes a special reverse equilibrium form for first-order decomposition reactions. With these types of reactions, the equilibrium constant is input in a form similar to the Arrhenius equation. Thus, the rate constant can be expressed as follows:

$$k = k_f\ /\ A e^{(-E/T)} \tag{8-10}$$

In Equation 8-10, k_f is the rate constant for the forward reaction forming a species, and the denominator is an Arrhenius-like form for the equilibrium constant. These reaction rate coefficient types are used, for example, for the decomposition of pernitric acid and nitrogen pentoxide (i.e., HNO4 $\rightarrow HO_2 + NO_2$ and $N_2O_5 \rightarrow NO_2 + NO_3$). In the CMAQ system, A, E, and the corresponding forward reaction must be specified. Either set of units may be used with this form.

8.4 Mathematical Modeling

This section describes the mathematical modeling concepts used in the CCTM to simulate gas-phase chemical reactions. The first sub-section describes the fundamental equations that must be solved and some of the difficulties encountered in obtaining solutions to them. The next two sub-sections describe the two gas-phase chemistry solvers that are currently available in the CCTM. The last sub-section summarizes some of the important solver characteristics.

8.4.1 Governing Equations

As described in Chapter 5, operator splitting allows gas-phase chemistry to be de-coupled from physical processes such as advection, diffusion and deposition, and, as noted in the introduction to this chapter, gas-phase chemistry is modeled separately from aerosol formation and aqueous chemistry. As a consequence, continuity equations for each gas-phase mechanism species can be formulated and solved independently on a cell-by-cell basis. By using the kinetics laws for elementary reactions and applying a mass balance to each species, the following equation for the rate of change of each species concentration can be derived for a single cell:

$$\frac{dC_i}{dt} = P_i - L_i C_i \tag{8-11}$$

where

$$P_i = \sum_{l=1}^{m_i} \nu_{i,l} r_l \tag{8-12}$$

and

$$L_i C_i = \sum_{l=1}^{n_i} r_l \tag{8-13}$$

In Equations 8-11 through 8-13, C_i is the concentration of species i, $\nu_{i,l}$ is the stoichiometric coefficient for species i in reaction l, and r_l is the rate of reaction l. The sum $l = 1...m_i$ is over all reactions in which species i appears as a product, and the sum $l = 1...n_i$ is over all reactions in which species i appears as a reactant.

Equation 8-11 states that the change in species concentration is equal to the chemical production of that species minus its chemical loss, and it is the fundamental species continuity equation for gas-phase chemistry that is solved in the CCTM. If the concentration of species i is known at some particular time, its concentration can be computed at a later time by solving Equation 8-11. Since the production and loss terms contain references to other species concentrations, however, Equation 8-11 must be solved as part of a coupled set of ordinary differential equations.

It should also be noted that the CCTM contains an option for including emissions in either the vertical diffusion process or in gas-phase chemistry. When emissions are included in gas-phase chemistry, the fundamental form of the Equation 8-11 is not altered since an emission source term is simply a zeroth-order production rate. Thus, for the discussions that follow, the production term P_i is assumed to include an emission source term if species i is emitted and emissions are included in gas-phase chemistry.

The system of non-linear, ordinary differential equations (ODEs) arising from Equation 8-11 for N species can be expressed as follows:

$$\frac{dC_i}{dt} = P_i(\mathbf{c},t) - L_i(\mathbf{c},t)\,C_i = f_i(\mathbf{c},t) \quad i = 1,2,\ldots,N \tag{8-14a}$$

with the initial conditions:

$$\mathbf{c}(t_0) = \mathbf{c}_0 \tag{8-14b}$$

where $\mathbf{c}$ is the vector of species concentrations and N is the total number of species in the chemical mechanism. Numerical "marching" methods are typically employed to obtain approximate solutions for this class of problem. In these methods, the concentrations of all species are given at the starting point and a solution is computed at selected time intervals (i.e., time steps) using the right hand side of Equation 8-14a. Two sources of difficulty arise in obtaining numerical solutions to these equations as they apply to atmospheric chemistry problems. First, the system is nonlinear because the production and loss terms include second- and third-order reactions. Second, the system of equations is "stiff" because of the widely varying time scales of the chemical reactions and complex interactions among species. A stiff system can be described mathematically as one in which all the eigenvalues of the Jacobian matrix of Equation 8-14a are negative, and the ratio of the absolute values of the largest-to-smallest real parts of the eigenvalues is much greater than one. Systems are typically termed stiff if the latter ratio is greater than 10^4. For atmospheric chemistry problems, the ratio is often greater than 10^{10}, making the system very stiff (Gong and Cho, 1993).

The stiffness problem coupled with the fact that these equations must be solved for tens of thousands of cells in a typical modeling application require that special numerical methods be employed. The use of standard explicit methods is often precluded because relatively small time steps are required to maintain numerical stability and obtain accurate solutions. On the other hand, classical implicit methods that are both accurate and stable have not often been used because of high computational demands. As a result, several special techniques have been developed to obtain reasonably accurate solutions in a computationally efficient manner. At present, two solution techniques are available in the CCTM: the implicit Sparse-Matrix Vectorized Gear algorithm (SMVGEAR) and a variant of the explicit Quasi-Steady State Approximation (QSSA) method. Each of these is described in detail below. Although each of these techniques, as well as others that have been used in atmospheric chemistry models, have been designed to be computationally efficient, they still consume 50 to 90% of the total CPU time used in a model simulation. Thus, obtaining a numerical solution to Equation 8-14a,b is normally the most computationally intensive portion of the CCTM.

8.4.2 SMVGEAR

Numerical solvers based on the algorithm developed by Gear (1971b) have traditionally been used to obtain accurate solutions to stiff ODE problems. The technique is implicit in method, does not amplify errors from one step to another and incorporates automatic step size and error control. In fact, solvers based on this method have often been used to evaluate other faster solution methods for accuracy (e.g., Odman et al., 1992; Gong and Cho, 1993; Dabdub and Seinfeld, 1995; and Saylor and Ford, 1995). Past versions of this code have rarely been installed in Eulerian models, however, because of the high computational cost. Jacobson and Turco (1994) have modified the Gear algorithm to obtain considerable speedups on vector computers. The SMVGEAR algorithm is highly vectorized to improve computational performance on vector computers and it incorporates special sparse matrix techniques to increase computational efficiency. Further enhancements have been obtained by ordering the cells for processing. Each of these are described further below. Since the technique is based on Gear's original algorithm, it is briefly described first. For more details on the Gear method, the reader is referred to Gear (1971a) and Gear (1971b).

8.4.2.1 Standard Gear Algorithm

The Gear algorithm is one of a class of methods referred to as backward differentiation formulae (BDF). The generalized BDF that forms the basis for Gear's method can be expressed as follows:

$$\mathbf{c}_n = h\beta_0 \mathbf{f}(\mathbf{c}_n, t_n) + \sum_{j=1}^{p} \alpha_j \mathbf{c}_{n-j} \tag{8-15}$$

where n refers to the time step, h is the size of the time step, p is the assumed order, β_0 and α_j are scalar quantities that are functions of the order, and $\mathbf{f}(\mathbf{c}_n,t_n)$ is the vector of production and loss terms defined by the right hand side of Equation 8-14a. The method is implicit since concentrations at the desired time step n depend on values of the first derivatives contained in $\mathbf{f}(\mathbf{c}_n,t_n)$ that are functions of the concentrations at the same time. The order of the method corresponds to the number of concentrations at previous time steps that are incorporated in the summation on the right hand side of Equation 8-15.

To facilitate changing step size and estimating errors, the multi-step method in Equation 8-15 is transformed to a multi-value form in which information from only the previous step is retained, but information on higher order derivatives is now used (Gear, 1971b). In this formulation, the solution to Equation 8-14a,b is first approximated by predicting concentrations and higher order derivatives at the end of a time step for each species using the following matrix equation:

$$\mathbf{z}_{i,n,(0)} = \mathbf{B}\,\mathbf{z}_{i,n-1} \tag{8-16}$$

where $\mathbf{z}_i = [c_i, hc'_i, ..., hpc_i^{(p)}/p!]^T$, the subscript n,(0) refers to the prediction at the end of time step n, and the subscript n-1 refers to values obtained at the end of previous time step (or the initial conditions when $n = 1$). **B** is the Pascal triangle matrix, the columns of which contain the binomial coefficients:

$$\mathbf{B} = \begin{bmatrix} 1 & 1 & 1 & 1 & \cdots & 1 & 1 \\ & 1 & 2 & 3 & \cdots & p-1 & p \\ & & 1 & 3 & \cdots & & \\ & & & 1 & \cdots & & \\ & & & & \ddots & & \\ & 0 & & & & 1 & p \\ & & & & & & 1 \end{bmatrix} \tag{8-17}$$

The prediction obtained from Equation 8-16 is then corrected by solving for $\mathbf{z}_{i,n}$ such that the following relations hold for all species:

$$\mathbf{z}_{i,n} = \mathbf{z}_{i,n,(0)} + \mathbf{r}\,[hf_i(\mathbf{c}_n, t_n) - hc'_{i,n,(0)}] \tag{8-18}$$

In Equation 8-18, **r** is a vector of coefficients that is dependent on the order, but r_2, the element corresponding to the first derivative location in **z**, is always equal to one. Thus, the correct value of $c_{i,n}$ is obtained when the calculatcd value of $c'_{i,n}$ equals $f_i(\mathbf{c}_n, t_n)$ in Equation 8-18. An approximate solution for $c_{i,n}$ is obtained by applying Newton's method to the system of equations that correspond to the first equation in 8-18 for all species. This leads to the following corrector iteration equation:

$$\mathbf{c}_{n,(m+1)} = \mathbf{c}_{n,(m)} + [\mathbf{I} - h\beta_0\mathbf{J}]^{-1} r_1\,[h\mathbf{f}(\mathbf{c}_{n,(m)}, t_n) - h\delta\mathbf{c}_{n,(m)}] \tag{8-19}$$

where m refers to the Newton iteration number, the vector $\mathbf{f}(\mathbf{c}_n, t_n)$ is calculated using concentrations computed for the m-th iteration, $\delta\mathbf{c}$ is a vector containing the most recent estimates of first derivatives, **I** is the identity matrix, and **J** is the Jacobian matrix whose entries are defined as:

$$J_{ij} = \frac{\partial f_i(\mathbf{c}, t_n)}{\partial c_j} \qquad i,j = 1,2,...N \tag{8-20}$$

At the end of each iteration, the vector containing the first derivatives ($\delta\mathbf{c}$) is updated, but higher order derivatives in **z** need not be computed until convergence is achieved.

After convergence is achieved, the local truncation error for each species, e_i, is given by:

$$e_i = \frac{1}{p+2} h^{p+1} c_{i,n}^{(p+1)} + O(h^{p+2}) \tag{8-21}$$

The error is estimated in the algorithm by neglecting the $O(h^{p+2})$ term and approximating $h^{p+1}c_i^{(p+1)}$ from the backward difference of $h^p c_i^{(p)}/p!$ which can be calculated using the last components of the vectors $\mathbf{z}_{i,n(m)}$ and $\mathbf{z}_{i,n-1}$ defined above. These error estimates are used to control accuracy and to change both the time step size and the order of the method when warranted.

Although several variants of the basic Gear algorithm have been developed, the fundamental computational scheme can be described generically as follows. At the beginning of any integration interval, the order is set to one and the starting time step is either calculated or selected by the user. Each time step is initiated by predicting concentrations at the end of the time step using Equation 8-16. Corrector iterations are then carried out using Equation 8-19 until prescribed convergence criteria are achieved or non-convergence is deemed to have occurred. When convergence is achieved, the error is computed using the approximation for Equation 8-21. If the error is within prescribed limits, the solution for the step is accepted and the step size and order to be used in the next step are estimated. The size of the time step is estimated for the current order, the next lowest order, and the next highest order using error estimates derived from Equation 8-21 for the next step. From these, the largest time-step size and its corresponding order are then selected for use in the next step. If either the convergence or error test fails, the integration is restarted from the beginning of the failed time step after re-evaluating the Jacobian matrix, reducing the size of the time step, and/or lowering the order.

The individual operations described above are normally handled automatically in Gear algorithms. To reduce computational demands, the algorithms also utilize several empirically based rules. For example, the Jacobian matrix is only updated after a prescribed number of successful steps have been completed, if the order changes, or if a convergence or error test failure occurs. In the Newton iterations, progress towards convergence is monitored and the iterations halted if the progress is judged insufficient or if three complete iterations have been performed without convergence being achieved. To maintain numerical stability, changes to the size of the time step and the order are allowed no more than once every p+1 steps for a p-th order method.

8.4.2.2 Vectorized Gear Algorithm

Jacobson and Turco (1994) have modified the Gear algorithm to incorporate additional computational efficiencies that can achieve speedups on the order of 100 on vector computers. About half of the improvement is attributed to enhanced vectorization, and half to improved matrix operations. Because of the improved matrix operations, SMVGEAR also runs faster than traditional Gear solvers on non-vector machines, but the greatest benefit will be obtained with vector machines. The major enhancements incorporated in SMVGEAR are now described in more detail.

In the conventional application of the Gear-type algorithm, the method is applied to each grid cell individually. With this implementation, the length of the innermost loops in most computations corresponds to the number of species, which is typically on the order of 30 to 100. In SMVGEAR, the modeling domain is divided into blocks of cells, and the Gear algorithm is applied to each cell within a block simultaneously. With this structure, the length of the innermost loops for most calculations is equal to the number of cells in a block. Substantial improvements in vectorization can therefore be obtained if the block size is larger than the number of species. Jacobson and Turco (1994) found that a block size on the order of 500 cells achieves about 90% of the maximum vectorization speed on a Cray C-90 computer. The use of larger block sizes may not substantially increase computational speed and may incur some additional penalties. For example, memory requirements increase with increasing block size. Furthermore, the size of a time step in SMVGEAR is the same for each cell within a block and is based on the time-step estimate for the stiffest cell in the block. Limiting the block size can therefore reduce excess calculations that need to be performed for the less stiff cells. Jacobson (1995) also achieved computational savings by ordering the cells by stiffness before dividing them into blocks. Each block then tends to contain cells of similar stiffness, thereby reducing excess computations for some cells. Jacobson found excess computations were reduced by about a factor of two, and that these reductions more than offset the additional work incurred with calculating and sorting the cells by stiffness.

Much of the computational intensity associated with the Gear method arises from the matrix operations that are needed to perform the Newton iterations in the corrector step. Jacobson and Turco have introduced two techniques to improve the efficiency of these operations. First, all known cases of multiplication by zero in matrix multiplication and decomposition are eliminated. This is particularly beneficial for atmospheric chemistry problems since the Jacobian matrices are almost always sparse (i.e., they contain a large number of zero entries). However, decomposition techniques that are applied to these matrices often result in substantial fill-in, thereby reducing the benefits of employing sparse-matrix techniques. To maintain maximum sparsity after the decomposition operation, SMVGEAR orders the species in the Jacobian such that those with the fewest partial derivative terms are located in the top rows, and those with the most are in the bottom rows. At the very beginning of the program, the ordering is done and a symbolic decomposition is performed to identify multiplies by zero. Since the computations associated with the matrix operations are determined entirely by the structure of the chemical mechanism, it is necessary to do this only once and the results can then be applied to every cell uniformly.

The SMVGEAR algorithm has been implemented in the CCTM with minor changes to the original algorithm but extensive changes to the original computer code. The code changes arose from linking the algorithm to the generalized chemistry processor used in the CMAQ system, and developing a driver routine specific to the CCTM structure. The only significant change to the algorithm involved modifying the code to eliminate the possibility of obtaining negative concentrations. With the standard Gear algorithm, negative concentrations can occur when a species is rapidly depleted, although the magnitudes of these concentrations are extremely small. In the CCTM implementation, a lower bound on allowable concentrations is applied, and the rates

of change and the Jacobian matrix are modified to reflect that no changes in concentration are occurring when the lower bound is reached. Comparisons with the standard Gear algorithm show virtually no differences in species concentrations above the lower bound, but a small penalty in computational performance is incurred. Nevertheless, the approach insures a positive-definite solution.

The computational performance of SMVGEAR is also affected by the error tolerances used for the Newton iteration convergence tests and the local truncation error tests. Error control in SMVGEAR is similar to that used in LSODE (Hindmarsh, 1980). Both a relative and an absolute tolerance must be specified. In their discussion of ODE solvers, Byrne and Hindmarsh (1987) relate the relative error tolerance to the number of accurate digits and the absolute error tolerance to the noise level (i.e., the size of the largest concentration that can be neglected). If r is the number of accurate digits required, then Byrne and Hindmarsh suggest setting the relative tolerance to $10^{-(r+1)}$. The absolute error tolerances cannot be specified as generically because particular model applications may require different accuracies for the mechanismn species. In the CCTM implementation of SMVGEAR, the relative tolerance and absolute tolerances have been preset to 10^{-3} and 10^{-9} ppm, respectively. However, these values can be changed by the user relatively easily in the CCTM as described in EPA (1998).

8.4.3 QSSA Solver

The QSSA solver is a low order, explicit solver that exhibits good stability for stiff systems. Although less accurate than the Gear solver, it is still a reasonably accurate, fast solver that is especially suitable for large scale grid models. There are actually many versions of solvers that go by the name "QSSA" (e.g., Mathur et al., 1998). The solver developed for the CCTM is a predictor/corrector version based on the one developed by Lamb and used in the Regional Oxidant Model (Lamb, 1983, and Young et al., 1993).

The QSSA method originates from assuming integration time steps sufficiently small such that in Equation 8-11, the production and loss rate terms P_i and L_i can be considered constant. If the Jacobian is diagonally dominant, this assumption may be valid as $\Delta t \rightarrow 0$, and the time step solution at $t_{n+1} = t_n + \Delta t$ can be written formally as:

$$C_i = C_{i_\infty} + (C_{i_n} - C_{i_\infty})\, e^{-L_i \Delta t} \qquad (8\text{-}22)$$

where $C_{i_\infty} = P_i / L_i$ and C_{i_∞} is the solution at t_n.

The CCTM QSSA makes no *a priori* assumptions about reaction time scales. For example, there are no assumed steady states. However, the algorithm separates the numerical computation into either an Euler step, a fully explicit integration, or an asymptotic evaluation based on photochemical lifetimes estimated from an initial, predictor calculation of P_i and L_i. The cut-offs and equations for each predictor step are:

$$\begin{array}{lll} \text{Eulerstep:} & L_i \Delta t \le 0.01 & C_i = C_{i_n} + (P_i + L_i C_{i_n}) \\ \text{Explicit:} & 0.01 < L_i \Delta t < 10.0 & C_i = C_{i_\infty} + (C_{i_n} - C_{i_\infty}) e^{-} \\ \text{Asymptotic:} & L_i \Delta t \ge 10.0 & C_i = C_{i_\infty} \end{array} \tag{8-23}$$

The CMAQ QSSA algorithm proceeds in three stages: an optimal time step determination, a predictor evaluation, and a corrector evaluation. In the first stage, an optimal chemistry time step interval Δt is determined at time t_n based on a tolerance parameter, λ, such that

$$| C_i - C_{i_n} | \le \lambda C_{i_n} . \tag{8-24}$$

Substituting Equation 8-22 into 8-24 gives:

$$\Delta t \le -\frac{1}{L_i} \ln\left(1 - \lambda \frac{C_{i_n}}{| C_{i_\infty} - C_{i_n} |} \right) . \tag{8-25}$$

The algorithm attempts to weight the time step determination against species whose concentrations are very small compared to the primary oxidants. These usually include some of the fastest reacting radicals. The following quantity is defined as

$$C_{test} = [NO] + [NO_2] + [O_3] \tag{8-26}$$

Then the following quantity is computed for only those species that satisfy $C_\alpha > \varepsilon C_{test}$ ($\varepsilon = 0.01$):

$$\delta t_\alpha = -\frac{1}{L_\alpha} \ln\left(1 - \lambda \frac{C_{\alpha_n}}{| C_{\alpha_\infty} - C_{\alpha_n} |} \right) \tag{8-27}$$

If $L_\alpha = 0$,

$$\delta t_\alpha = \frac{\lambda C_{\alpha_n}}{P_\alpha} \tag{8-28}$$

The tolerance parameter λ is controlled by the rate at which the key NO species concentrations are changing; if they are changing too rapidly, the tolerance is tightened, otherwise it is relaxed:

$$\lambda = \begin{cases} 0.001, \text{ if } \dfrac{d[NO]}{dt} / [NO] \geq 0.5\% \text{ per minute} \\ 0.005, \text{ otherwise} \end{cases} \tag{8-29}$$

After determining a time scale for each species α, Δt is set to $\min\{\delta t_\alpha\}$. For computational efficiency, Δt is further constrained to be no less than one second and of course is also constrained to be no greater than the total integration time.

In the predictor step, the species concentrations are updated ($C_i \rightarrow C_i^*$) with the optimal time step using the Euler-step, explicit or asymptotic calculations described above. Once C_i^* is calculated, QSSA computes new production and loss rate coefficients P_i^* and L_i^*, respectively.

In the corrector step, the final production rate is set as the average of the initial and predictor values, $\tilde{P}_i = (P_i^* + P_i)/$, and the new concentration C_i for time $t_{n+1} = t_n + \Delta t$ is computed using the same cut-offs based on L_i that were determined in the predictor step:

$$\begin{aligned} &\text{Eulerstep:} && C_i = C_{i_n} + (\tilde{P}_i + L_i^* C_{i_n})\,\Delta t \\ &\text{Explicit:} && C_i = \tilde{P}_i / L_i^* + (C_{i_n} - \tilde{P}_i / L_i^*)\, e^{-L_i^* \Delta t} \\ &\text{Asymptotic:} && C_i = \tilde{P}_i / L_i^* \end{aligned} \tag{8-30}$$

The algorithm has been optimized for vector computers by moving the grid cell loops into the innermost position (Young et al., 1993) as is done in SMVGEAR described above. To minimize storage requirements, grid cell blocking has been implemented wherein blocks of cells are handed off to the solver in sequence. The CMAQ QSSA has also been optimized for the Cray T3D by utilizing various coding techniques aimed specifically at that architecture. Some of these optimizations are described in Chapter 19.

8.4.4 Summary

Gear type solvers have generally been considered the most accurate for gas chemistry, representing "exact solutions" (provided the controlling numerical tolerances are sufficiently tight). Until the advent of SMVGEAR, however, it has not been feasible to use these solvers in Eulerian models. SMVGEAR is designed to run optimally on high end vector computers such as the Cray C90, but its use on scalar machines may be impractical. Although less accurate, the QSSA solver may be more suitable for those types of computers.

The issue of accuracy versus computational speed is a continuing concern (Mathur et al., 1998), particularly since the availability of high-end machines like the Cray C90 is limited. The CMAQ QSSA solver presents a reasonable, numerically efficient alternative and, although not considered

as accurate as a Gear-type solver, may be sufficiently accurate for modeling, taking into consideration the uncertainties of the other numerical modeling components. Accuracy can be somewhat improved by using shorter integration steps in the solver, but then computational work mounts, defeating the purpose. For the CMAQ QSSA, accuracy will be compromised when the ODE system is very stiff and the system Jacobian strays from diagonal dominance. Nevertheless, the trade-off between solution efficiency and accuracy may still warrant its use in these cases.

Finally, both the SMVGEAR and the QSSA solvers have been incorporated in the CMAQ system with the predefined accuracy controls that were described in the previous two sections. Of course, these error controls can be changed by the user if desired, but that will of course affect both the prediction accuracy and the efficiency of obtaining a solution. Note also, that either solver can be used with any of the CMAQ chemical mechanisms that were described in section 8.2.

8.5 References

Atkinson R., Lloyd A. C. and Winges L. (1982) An updated chemical mechanism for hydrocarbon/NOx/SO2 photooxidations suitable for inclusion in atmospheric simulation models. *Atmos. Environ.*, **16**, 1,341-1,355.

Bowman F. M., Pilinis C., and Seinfeld J. (1995) Ozone and aerosol productivity of reactive. *Atmos. Environ.*, **29**, 579-589.

Byrne G. D. and Hindmarsh A. C. (1987) Stiff ODE solvers: a review of current and coming attractions. *J. Comput. Phys.* **70**, 1-62.

Carter W. P. L. (1988) Appendix C Documentation of the SAPRC Atmospheric Photochemical Mechanism Preparation and Emissions Processing Programs for Implementation in Airshed Models. Final Report for California Air Resources Board Contract No. A5-122-32.

Carter W. P. L. (1990) A detailed mechanism for the gas-phase atmospheric reactions of organic compounds. *Atmos. Environ.* **24A**, 481-515.

Carter W. P. L. (1996) Condensed atmospheric photooxidation mechanisms for isoprene. *Atmos. Environ.* **24**, 4,275-4,290.

Carter W. P. L. and Atkinson R. (1996) Development and evaluation of a detailed mechanism for the atmospheric reactions of isoprene and NOx. *Int. J. Chem. Kinet.* **28**, 497-530.

Carter W. P. L., Luo D. and Malkina I. L. (1997) Environmental Chamber Studies for Development of an Updated Photochemical Mechanism for Reactivity Assessment. Final Report for California Air Resources Board Contract No. 92-345, Coordinating Research Council, Inc., Project M-9 and National Renewable Energy Laboratory, Contract ZF-2-12252-07.

Chang J. S., Brost R. A. , Isaksen I. S. A., Madronich S., Middleton P., Stockwell W.R. and Waleck C.J. (1987) A three-dimensional Eulerian acid deposition model: physical concepts and formulation, *J. geophys. Res.*, **92**, 14,681 - 14,700.

Dabdub D. and Seinfeld J. H. (1995) Extrapolation techniques used in the solution of stiff ODEs associated with chemical kinetics of air quality models. *Atmos. Environ.* **29**, 403-410.

Dodge M.C. (1989) A comparison of three photochemical oxidant mechanisms, *J. geophys. Res.*, **94**, 5,121-5,136.

EPA (1989) Procedures for Applying City-specific EKMA. EPA-450/4-89-012.

EPA (1991) User's Guide for the Urban Airshed Model, Volume I: User's Manual for UAM (CB4). EPA-450/4-90-007a.

EPA (1998) EPA Third-Generation Air Quality Modeling System, Models-3 Volume 9b User Manual. EPA-600/R-98/069b.

Gear C. W. (1971a) *Numerical Initial Value Problems in Ordinary Differential Equations.* Prentice-Hall, Englewood Cliffs, NJ.

Gear C. W. (1971b) The automatic integration of ordinary differential equations. *Comm. ACM* **14**, 176-179.

Gery M. W., Morris R. E., Greenfield S. M., Liu M. K., Whitten G. Z., and Fieber J. L. (1987) Development of a Comprehensive Chemistry Acid Deposition Model (CCADM). Final Report for Interagency Agreement DW 14931498, U. S. Environmental Protection Agency and U. S. Department of Interior.

Gery M. W., Whitten G. Z., Killus J. P. and Dodge M. C. (1989) A photochemical kinetics mechanism for urban and regional scale computer modeling. *J. geophys. Res.* **94**, 12,925-12,956.

Gong W. and Cho H. R. (1993) A numerical scheme for the integration of the gas-phase chemical rate equations in three-dimensional atmospheric models. *Atmos. Environ.* **27A**, 2,147-2,160.

Hindmarsh A. C. (1980) LSODE and LSODI, two new initial value ordinary differential equation solvers. *ACM Newsl.* **15**, 10-11.

Hough A. (1988) An intercomparison of mechanisms for the production of photochemical oxidants. *J. geophys. Res.*, **93**, 3,789-3,812.

Jacobson M. and Turco R. P. (1994) SMVGEAR: A sparse-matrix, vectorized Gear code for atmospheric models. *Atmos. Environ.* **28**, 273-284.

Jacobson M. (1995) Computation of global photochemistry with SMVGEAR II. *Atmos. Environ.* **29**, 2,541-2,546.

Jeffries H. E. (1995) Photochemical Air Pollution. Chapter 5 in *Composition, Chemistry, and Climate of the Atmosphere*. Ed. H. B. Singh, Von Nostand-Reinhold, New York.

Jeffries H. E., Gery M. and Murphy K. (1993) Advanced Chemical Reaction Mechanisms and Solvers for Models-3. Progress Report for EPA Cooperative Agreement CR-820425.

Lamb, R.G. (1983) A Regional Scale (1000 km) Model of Photochemical Air Pollution. Part I - Theoretical Formulation. EPA-600/3-83-035, U. S. Environmental Protection Agency, Research Triangle Park, NC.

Leone J.A. and Seinfeld J.H. (1985) Comparative analysis of chemical reaction mechanisms for photochemical smog. *Atmos. Environ.*, **19**, 437-464.

Lurmann F. W., Carter W. P. L. and Coyner L. A. (1987) A Surrogate Species Chemical Reaction Mechanism for Urban Scale Air Quality Simulation Models Volume 1. EPA-600/3-87-014a.

Mathur R., Young J. O., Schere K. L., and Gipson G. L. (1998) A Comparison of Numerical Techniques for Solution of Atmospheric Kinetic Equations. *Atmos. Environ.*, **32**, 1,535-1,553.

NASA (1997). Chemical Kinetics and Photochemical Data for Use in Stratospheric Modeling Evaluation No. 12. JPL Publication 97-4, Jet Propulsion Laboratory, Pasedena, CA.

Odman, M. T., Kumar N. and Russell A. G. (1992) A comparison of fast chemical kinetic solvers for air quality modeling. *Atmos. Environ.* **26A**, 1,783-1,789.

Pandis S. N., Harley R. A., Cass G. R. and Seinfeld J. H.(1992) secondary aerosol formation and transport. *Atmos. Environ.* **26A**, 2,269-2,282.

Pitts-Finlayson B.J. and Pitts J.N. (1986) *Atmospheric Chemistry: Fundamentals and Experimental Techniques*, J. Wiley and Sons, New York.

SAI (1993) Systems Guide to the Urban Airshed Model (UAM-V). Systems Applications International, San Rafael, CA.

Saylor, R. D. and Ford G. D. (1995) On the comparison of numerical methods for the integration of kinetic equations in atmospheric chemistry and transport models. *Atmos. Environ.***29**, 2,585-2,593.

Stockwell W. R., Middleton P. and Chang J. S. and Tang X. (1990) The second generation regional acid deposition model chemical mechanism for regional air quality modeling. *J. geophys. Res.* **95** (d10), 16,343-16,367.

Stockwell W.R. (1986) A homogeneous gas phase mechanism for use in a regional acid deposition model, *Atmos. Environ.*, **20**, 1,615-1,632.

Stockwell W. R., Kirchner F., Kuhn M., and S. Seefeld (1997) A new mechanism for regional atmospheric chemistry modeling. *J. geophys. Res.* **102** (D22), 25,847-25,879.

Whitten G. Z., Hogo H. and Killus J. P. (1980) The carbon bond mechanism: a condensed kinetic mechanism for photochemical smog. *Envir. Sci. Technol.* **14**, 690-701.

Young J. O., Sills E., Jorge D. (1993) Optimization of the Regional Oxidant Model for the Cray Y-MP. EPA/600/R-94-065, U. S. Environmental protection Agency, Research Triangle Park, NC.

This chapter is taken from *Science Algorithms of the EPA Models-3 Community Multiscale Air Quality (CMAQ) Modeling System*, edited by D. W. Byun and J. K. S. Ching, 1999.

Appendix 8A Chemical Mechanisms Included in the CMAQ System

Table 8A-1. CB4 Mechanism Species List

Table 8A-2. RADM2 Mechanism Species List

Table 8A-3. CB4 Mechanism

Table 8A-4. CB4_AE Mechanism

Table 8A-5. CB4_AQ Mechanism

Table 8A-6. CB4_AE_AQ Mechanism

Table 8A-7. RADM2 and RADM2_AQ Mechanisms

Table 8A-8. RADM2_AE and RADM2_AE_AQ Mechanisms

Table 8A-9. RADM2_CIS1 and RADM2_CIS1_AQ Mechanisms

Table 8A-10. RADM2_CIS1_AE and RADM2_CIS1_AE_AQ Mechanisms

Table 8A-11. RADM2_CIS4 and RADM2_CIS4_AQ Mechanisms

Table 8A-12. RADM2_CIS4_AE and RADM2_CIS4_AE_AQ Mechanisms

Notes to Tables 8A-3 through 8A-12:

a) The mechanism listings are divided into two parts. The first lists the reactions and the second lists the rate constant expressions.

b) The parameters for the rate constants are given in cms units. Rate constants calculated in cms units for T=298 °K and P= 1 atm are shown in the rightmost column of these listings.

c) For photolytic reactions, photo table refers to the photolysis rates described in Chapter 14. The rate constant for all photolytic contains a zero entry in these tables, but is calculated in the CCTM as the product of the scale factor and the photolysis rate that is calculated by the CMAQ photolysis rate processor.

d) The falloff rate expression referred to in these tables is Equation 8-6 in Section 8.3.2.

Table 8A-1
CB4 Mechanism Species List

Nitrogen Species	
NO	Nitric oxide
NO2	Nitrogen dioxide
HONO	Nitrous acid
NO3	Nitrogen trioxide
N2O5	Nitrogen pentoxide
HNO3	Nitric acid
PNA	Peroxynitric acid
Oxidants	
O3	Ozone
H2O2	Hydrogen peroxide
Sulfur Species	
SO2	Sulfur dioxide
SULF	Sulfuric acid
Atomic Species	
O	Oxygen atom (triplet)
O1D	Oxygen atom (singlet)
Odd Hydrogen Species	
OH	Hydroxyl radical
HO2	Hydroperoxy radical
Carbon oxides	
CO	Carbon monoxide
Hydrocarbons	
PAR	Paraffin carbon bond (C-C)
ETH	Ethene (CH_2=CH_2)
OLE	Olefinic carbon bond (C=C)
TOL	Toluene (C_6H_4-CH_3)
XYL	Xylene (C_6H_5-$(CH_3)_2$)
ISOP	Isoprene
Carbonyls and phenols	
FORM	Formaldehyde
ALD2	Acetaldehyde and higher aldehydes
MGLY	Methyl glyoxal ($CH_3C(O)C(O)H$)
CRES	Cresol and higher molecular weight phenols
Organic nitrogen	
PAN	Peroxyacyl nitrate ($CH_3C(O)OONO_2$)
NTR	Organic nitrate
Organic Radicals	
C2O3	Peroxyacyl radical ($CH_3C(O)OO\cdot$)
ROR	Secondary organic oxy radical
CRO	Methylphenoxy radical

Operators

XO2	NO-to-NO_2 Operation
XO2N	NO-to-nitrate operation

Products of organics

TO2	Toluene-hydroxyl radical adduct
OPEN	High molecular weight aromatic oxidation ring fragment
ISPD	Products of isoprene reactions

Species added for aerosols

SULAER	Counter species for H_2SO_4 production
TOLAER	Counter species for toluene reaction
XYLAER	Counter species for xylene reaction
CSLAER	Counter species for cresol reaction
TERPAER	Counter species for terpene reaction
TERP	Monoterpenes

Species added for aqueous chemistry

FACD	Formic acid
AACD	Acetic and higer acids
PACD	Peroxy acetic acid
UMHP	Upper limit of methylhydroperoxide

Table 8A-2
RADM2 Mechanism Species List

Nitrogen Species	
NO	Nitric oxide
NO2	Nitrogen dioxide
HONO	Nitrous acid
NO3	Nitrogen trioxide
N2O5	Nitrogen pentoxide
HNO3	Nitric acid
HNO4	Peroxynitric acid
Oxidants	
O3	Ozone
H2O2	Hydrogen peroxide
Sulfur Species	
SO2	Sulfur dioxide
SULF	Sulfuric acid
Atomic Species	
O3P	Oxygen atom (triplet)
O1D	Oxygen atom (singlet)
Odd Hydrogen Species	
HO	Hydroxyl radical
HO2	Hydroperoxy radical
Carbon oxides	
CO	Carbon monoxide
Alkanes	
ETH	Ethane
HC3	Alkanes w/ $2.7\times10^{-13} > k_{OH} < 3.4\times10^{-12}$
HC5	Alkanes w/ $3.4\times10^{-12} > k_{OH} < 6.8\times10^{-12}$
HC8	Alkanes w/ $k_{OH} > 6.8\times10^{-12}$
Alkenes	
OL2	Ethene
OLT	Terminal olefins
OLI	Internal olefins
ISO	Isoprene
Aromatics	
TOL	Toluene and less reactive aromatics
XYL	Xylene and more reactive aromatics
CSL	Cresol and other hydroxy substituted aromatics
Carbonyls	
HCHO	Formaldehyde
ALD	Acetaldehyde and higher aldehydes
KET	Ketones
GLY	Glyoxal
MGLY	Methyl glyoxal
DCB	Unsaturated dicarbonyl
Organic nitrogen	
PAN	Peroxyacetyl nitrate and higher PANs
TPAN	$H(CO)CH{=}CHCO_3NO_2$
ONIT	Organic nitrate
Organic peroxides	
OP1	Methyl hydrogen peroxide
OP2	Higher organic peroxides
PAA	Peroxyacetic acid
Organic acids	
ORA1	Formic acid
ORA2	Acetic and higher acids
Peroxy radicals from alkanes	
MO2	Methyl peroxy radical
ETHP	Peroxy radical formed from ETH
HC3P	Peroxy radical formed from HC3
HC5P	Peroxy radical formed from HC5
HC8P	Peroxy radical formed from HC8
Peroxy radicals from alkenes	
OL2P	Peroxy radical formed from OL2P
OLTP	Peroxy radical formed from OLTP
OLIP	Peroxy radical formed from OLIP
Peroxy radicals from aromatics	
TOLP	Peroxy radical formed from TOL
XYLP	Peroxy radical formed from XYL
Peroxy radicals with carbonyl groups	
ACO3	Acetylperoxy radical
KETP	Peroxy radical formed from KET
TCO3	$H(CO)CH{=}CHCO_3$
Peroxy radicals involving nitrogen	
XO2	NO-to-NO_2 Operator
XNO2	NO-to-nitrate operator
OLN	NO3-alken adduct
Species added for aerosols	
SULAER	Counter species for H_2SO_4 production
HC8AER	Counter species for HC8 reaction
OLIAER	Counter species for OLI reaction
TOLAER	Counter species for toluene reaction
XYLAER	Counter species for xylene reaction
CSLAER	Counter species for cresol reaction
TERPAER	Counter species for terpene reaction
TERP	Monoterpenes

Table 8A-3. CB4 Mechanism

```
 Reaction List
>-----------------------------------------------------------------------<
{  1} NO2    + hv              -->          NO     +        O
{  2} O      + [O2]            -->          O3
{  3} O3     + NO              -->          NO2
{  4} O      + NO2             -->          NO
{  5} O      + NO2             -->          NO3
{  6} O      + NO              -->          NO2
{  7} O3     + NO2             -->          NO3
{  8} O3     + hv              -->          O
{  9} O3     + hv              -->          O1D
{ 10} O1D    + [N2]            -->          O
{ 11} O1D    + [O2]            -->          O
{ 12} O1D    + [H2O]           -->    2.000*OH
{ 13} O3     + OH              -->          HO2
{ 14} O3     + HO2             -->          OH
{ 15} NO3    + hv              -->    0.890*NO2    + 0.890*O      + 0.110*NO
{ 16} NO3    + NO              -->    2.000*NO2
{ 17} NO3    + NO2             -->          NO     +        NO2
{ 18} NO3    + NO2             -->          N2O5
{ 19} N2O5   + [H2O]           -->    2.000*HNO3
{ 20} N2O5                     -->          NO3    +        NO2
{ 21} NO     + NO     + [O2]   -->    2.000*NO2
{ 22} NO     + NO2    + [H2O]  -->    2.000*HONO
{ 23} OH     + NO              -->          HONO
{ 24} HONO   + hv              -->          OH     +        NO
{ 25} HONO   + OH              -->          NO2
{ 26} HONO   + HONO            -->          NO     +        NO2
{ 27} OH     + NO2             -->          HNO3
{ 28} OH     + HNO3            -->          NO3
{ 29} HO2    + NO              -->          OH     +        NO2
{ 30} HO2    + NO2             -->          PNA
{ 31} PNA                      -->          HO2    +        NO2
{ 32} PNA    + OH              -->          NO2
{ 33} HO2    + HO2             -->          H2O2
{ 34} HO2    + HO2    + [H2O]  -->          H2O2
{ 35} H2O2   + hv              -->    2.000*OH
{ 36} H2O2   + OH              -->          HO2
{ 37} CO     + OH              -->          HO2
{ 38} FORM   + OH              -->          HO2    +        CO
{ 39} FORM   + hv              -->    2.000*HO2    +        CO
{ 40} FORM   + hv              -->          CO
{ 41} FORM   + O               -->          OH     +        HO2    +        CO
{ 42} FORM   + NO3             -->          HNO3   +        HO2    +        CO
{ 43} ALD2   + O               -->          C2O3   +        OH
{ 44} ALD2   + OH              -->          C2O3
{ 45} ALD2   + NO3             -->          C2O3   +        HNO3
{ 46} ALD2   + hv              -->          XO2    + 2.000*HO2    +        CO
                                     +      FORM
{ 47} C2O3   + NO              -->          NO2    +        XO2    +        FORM
                                     +      HO2
{ 48} C2O3   + NO2             -->          PAN
{ 49} PAN                      -->          C2O3   +        NO2
{ 50} C2O3   + C2O3            -->    2.000*XO2    + 2.000*FORM   + 2.000*HO2
{ 51} C2O3   + HO2             -->    0.790*FORM   + 0.790*XO2    + 0.790*HO2
                                     + 0.790*OH
{ 52} OH                       -->          XO2    +        FORM   +        HO2
{ 53} PAR    + OH              -->    0.870*XO2    + 0.130*XO2N   + 0.110*HO2
                                     + 0.110*ALD2   + 0.760*ROR    - 0.110*PAR
```

Table 8A-3. CB4 Mechanism

```
{ 54} ROR                    -->   1.100*ALD2  + 0.960*XO2   + 0.940*HO2
                                 - 2.100*PAR   + 0.040*XO2N  + 0.020*ROR
{ 55} ROR                    -->         HO2
{ 56} ROR    + NO2           -->         NTR
{ 57} OLE    + O             -->   0.630*ALD2  + 0.380*HO2   + 0.280*XO2
                                 + 0.300*CO    + 0.200*FORM  + 0.020*XO2N
                                 + 0.220*PAR   + 0.200*OH
{ 58} OLE    + OH            -->         FORM  +       ALD2  +       XO2
                                 +       HO2   -       PAR
{ 59} OLE    + O3            -->   0.500*ALD2  + 0.740*FORM  + 0.330*CO
                                 + 0.440*HO2   + 0.220*XO2   + 0.100*OH
                                 -       PAR
{ 60} OLE    + NO3           -->   0.910*XO2   + 0.090*XO2N  +       FORM
                                 +       ALD2  -       PAR   +       NO2
{ 61} ETH    + O             -->         FORM  + 0.700*XO2   +       CO
                                 + 1.700*HO2   + 0.300*OH
{ 62} ETH    + OH            -->         XO2   + 1.560*FORM  +       HO2
                                 + 0.220*ALD2
{ 63} ETH    + O3            -->         FORM  + 0.420*CO    + 0.120*HO2
{ 64} TOL    + OH            -->   0.080*XO2   + 0.360*CRES  + 0.440*HO2
                                 + 0.560*TO2
{ 65} TO2    + NO            -->   0.900*NO2   + 0.900*HO2   + 0.900*OPEN
                                 + 0.100*NTR
{ 66} TO2                    -->         CRES  +       HO2
{ 67} CRES   + OH            -->   0.400*CRO   + 0.600*XO2   + 0.600*HO2
                                 + 0.300*OPEN
{ 68} CRES   + NO3           -->         CRO   +       HNO3
{ 69} CRO    + NO2           -->         NTR
{ 70} XYL    + OH            -->   0.700*HO2   + 0.500*XO2   + 0.200*CRES
                                 + 0.800*MGLY  + 1.100*PAR   + 0.300*TO2
{ 71} OPEN   + OH            -->         XO2   + 2.000*CO    + 2.000*HO2
                                 +       C2O3  +       FORM
{ 72} OPEN   + hv            -->         C2O3  +       HO2   +       CO
{ 73} OPEN   + O3            -->   0.030*ALD2  + 0.620*C2O3  + 0.700*FORM
                                 + 0.030*XO2   + 0.690*CO    + 0.080*OH
                                 + 0.760*HO2   + 0.200*MGLY
{ 74} MGLY   + OH            -->         XO2   +       C2O3
{ 75} MGLY   + hv            -->         C2O3  +       HO2   +       CO
{ 76} ISOP   + O             -->   0.750*ISPD  + 0.500*FORM  + 0.250*XO2
                                 + 0.250*HO2   + 0.250*C2O3  + 0.250*PAR
{ 77} ISOP   + OH            -->   0.912*ISPD  + 0.629*FORM  + 0.991*XO2
                                 + 0.912*HO2   + 0.088*XO2N
{ 78} ISOP   + O3            -->   0.650*ISPD  + 0.600*FORM  + 0.200*XO2
                                 + 0.066*HO2   + 0.266*OH    + 0.200*C2O3
                                 + 0.150*ALD2  + 0.350*PAR   + 0.066*CO
{ 79} ISOP   + NO3           -->   0.200*ISPD  + 0.800*NTR   +       XO2
                                 + 0.800*HO2   + 0.200*NO2   + 0.800*ALD2
                                 + 2.400*PAR
{ 80} XO2    + NO            -->         NO2
{ 81} XO2    + XO2           -->
{ 82} XO2N   + NO            -->         NTR
{ 83} SO2    + OH            -->         SULF  +       HO2
{ 84} SO2                    -->         SULF
{ 85} XO2    + HO2           -->
{ 86} XO2N   + HO2           -->
{ 87} XO2N   + XO2N          -->
{ 88} XO2N   + XO2           -->
{ 89} ISPD   + OH            -->   1.565*PAR   + 0.167*FORM  + 0.713*XO2
                                 + 0.503*HO2   + 0.334*CO    + 0.168*MGLY
                                 + 0.273*ALD2  + 0.498*C2O3
{ 90} ISPD   + O3            -->   0.114*C2O3  + 0.150*FORM  + 0.850*MGLY
```

Table 8A-3. CB4 Mechanism

```
                                  + 0.154*HO2    + 0.268*OH     + 0.064*XO2
                                  + 0.020*ALD2   + 0.360*PAR    + 0.225*CO
{ 91} ISPD  + NO3            -->    0.357*ALD2   + 0.282*FORM   + 1.282*PAR
                                  + 0.925*HO2    + 0.643*CO     + 0.850*NTR
                                  + 0.075*C2O3   + 0.075*XO2    + 0.075*HNO3
{ 92} ISPD  + hv             -->    0.333*CO     + 0.067*ALD2   + 0.900*FORM
                                  + 0.832*PAR    + 1.033*HO2    + 0.700*XO2
                                  + 0.967*C2O3
{ 93} ISOP  + NO2            -->    0.200*ISPD   + 0.800*NTR    +        XO2
                                  + 0.800*HO2    + 0.200*NO     + 0.800*ALD2
                                  + 2.400*PAR
>-----------------------------------------------------------------------<


Rate Expression                                                    Rate Constant
==============================================================================
k(  1) uses photo table NO2_CBIV88       , scaled by 1.00000E+00   {0.00000E+00}
k(  2) is a falloff expression using:                              {1.37387E-14}
   k0   =  6.0000E-34 * (T/300)**(-2.30)
   kinf =  2.8000E-12 * (T/300)**( 0.00)
   F =  0.60,  n =  1.00
k(  3) =  1.8000E-12 * exp( -1370.0/T)                             {1.81419E-14}
k(  4) =  9.3000E-12                                               {9.30000E-12}
k(  5) is a falloff expression using:                              {1.57527E-12}
   k0   =  9.0000E-32 * (T/300)**(-2.00)
   kinf =  2.2000E-11 * (T/300)**( 0.00)
   F =  0.60,  n =  1.00
k(  6) is a falloff expression using:                              {1.66375E-12}
   k0   =  9.0000E-32 * (T/300)**(-1.50)
   kinf =  3.0000E-11 * (T/300)**( 0.00)
   F =  0.60,  n =  1.00
k(  7) =  1.2000E-13 * exp( -2450.0/T)                             {3.22581E-17}
k(  8) uses photo table NO2_CBIV88       , scaled by 5.30000E-02   {0.00000E+00}
k(  9) uses photo table O3O1D_CBIV88     , scaled by 1.00000E+00   {0.00000E+00}
k( 10) =  1.8000E-11 * exp(   107.0/T)                             {2.57757E-11}
k( 11) =  3.2000E-11 * exp(    67.0/T)                             {4.00676E-11}
k( 12) =  2.2000E-10                                               {2.20000E-10}
k( 13) =  1.6000E-12 * exp(  -940.0/T)                             {6.82650E-14}
k( 14) =  1.4000E-14 * exp(  -580.0/T)                             {1.99920E-15}
k( 15) uses photo table NO2_CBIV88       , scaled by 3.39000E+01   {0.00000E+00}
k( 16) =  1.3000E-11 * exp(   250.0/T)                             {3.00805E-11}
k( 17) =  2.5000E-14 * exp( -1230.0/T)                             {4.03072E-16}
k( 18) is a falloff expression using:                              {1.26440E-12}
   k0   =  2.2000E-30 * (T/300)**(-4.30)
   kinf =  1.5000E-12 * (T/300)**(-0.50)
   F =  0.60,  n =  1.00
k( 19) =  1.3000E-21                                               {1.30000E-21}
k( 20) = k( 18) / Keq,  where Keq =  2.700E-27 * exp( 11000.0/T)   {4.36029E-02}
k( 21) =  3.3000E-39 * exp(   530.0/T)                             {1.95397E-38}
k( 22) =  4.4000E-40                                               {4.39999E-40}
k( 23) is a falloff expression using:                              {6.69701E-12}
   k0   =  6.7000E-31 * (T/300)**(-3.30)
   kinf =  3.0000E-11 * (T/300)**(-1.00)
   F =  0.60,  n =  1.00
k( 24) uses photo table NO2_CBIV88       , scaled by 1.97500E-01   {0.00000E+00}
k( 25) =  6.6000E-12                                               {6.60000E-12}
k( 26) =  1.0000E-20                                               {1.00000E-20}
k( 27) is a falloff expression using:                              {1.14885E-11}
   k0   =  2.6000E-30 * (T/300)**(-3.20)
   kinf =  2.4000E-11 * (T/300)**(-1.30)
   F =  0.60,  n =  1.00
```

Table 8A-3. CB4 Mechanism

```
k( 28) is a special rate expression of the form:                    {1.47236E-13}
   k = k0 + {k3[M] / (1 + k3[M]/k2)}, where
   k0 =  7.2000E-15 * exp(   785.0/T)
   k2 =  4.1000E-16 * exp(  1440.0/T)
   k3 =  1.9000E-33 * exp(   725.0/T)
k( 29) =  3.7000E-12 * exp(   240.0/T)                              {8.27883E-12}
k( 30) is a falloff expression using:                               {1.48014E-12}
   k0   =  2.3000E-31 * (T/300)**(-4.60)
   kinf =  4.2000E-12 * (T/300)**( 0.20)
   F =  0.60,  n =  1.00
k( 31) = k( 30) / Keq,  where Keq =  2.100E-27 * exp( 10900.0/T)   {9.17943E-02}
k( 32) =  1.3000E-12 * exp(   380.0/T)                              {4.65309E-12}
k( 33) =  5.9000E-14 * exp(  1150.0/T)                              {2.79783E-12}
k( 34) =  2.2000E-38 * exp(  5800.0/T)                              {6.23927E-30}
k( 35) uses photo table HCHOmol_CBIV88  , scaled by 2.55000E-01    {0.00000E+00}
k( 36) =  3.1000E-12 * exp(  -187.0/T)                              {1.65514E-12}
k( 37) =  1.5000E-13 * (1.0 + 0.6*Pressure)                         {2.40000E-13}
k( 38) =  1.0000E-11                                                {1.00000E-11}
k( 39) uses photo table HCHOrad_CBIV88  , scaled by 1.00000E+00    {0.00000E+00}
k( 40) uses photo table HCHOmol_CBIV88  , scaled by 1.00000E+00    {0.00000E+00}
k( 41) =  3.0000E-11 * exp( -1550.0/T)                              {1.65275E-13}
k( 42) =  6.3000E-16                                                {6.30000E-16}
k( 43) =  1.2000E-11 * exp(  -986.0/T)                              {4.38753E-13}
k( 44) =  7.0000E-12 * exp(   250.0/T)                              {1.61972E-11}
k( 45) =  2.5000E-15                                                {2.50000E-15}
k( 46) uses photo table ALD_CBIV88      , scaled by 1.00000E+00    {0.00000E+00}
k( 47) =  3.4900E-11 * exp(  -180.0/T)                              {1.90766E-11}
k( 48) =  2.6300E-12 * exp(   380.0/T)                              {9.41356E-12}
k( 49) =  2.0000E+16 * exp(-13500.0/T)                              {4.23268E-04}
k( 50) =  2.5000E-12                                                {2.50000E-12}
k( 51) =  6.5000E-12                                                {6.50000E-12}
k( 52) =  1.1000E+02 * exp( -1710.0/T)                              {3.54242E-01}
k( 53) =  8.1000E-13                                                {8.10000E-13}
k( 54) =  1.0000E+15 * exp( -8000.0/T)                              {2.19325E+03}
k( 55) =  1.6000E+03                                                {1.60000E+03}
k( 56) =  1.5000E-11                                                {1.50000E-11}
k( 57) =  1.2000E-11 * exp(  -324.0/T)                              {4.04572E-12}
k( 58) =  5.2000E-12 * exp(   504.0/T)                              {2.82173E-11}
k( 59) =  1.4000E-14 * exp( -2105.0/T)                              {1.19778E-17}
k( 60) =  7.7000E-15                                                {7.70000E-15}
k( 61) =  1.0000E-11 * exp(  -792.0/T)                              {7.01080E-13}
k( 62) =  2.0000E-12 * exp(   411.0/T)                              {7.94340E-12}
k( 63) =  1.3000E-14 * exp( -2633.0/T)                              {1.89105E-18}
k( 64) =  2.1000E-12 * exp(   322.0/T)                              {6.18715E-12}
k( 65) =  8.1000E-12                                                {8.10000E-12}
k( 66) =  4.2000E+00                                                {4.20000E+00}
k( 67) =  4.1000E-11                                                {4.10000E-11}
k( 68) =  2.2000E-11                                                {2.20000E-11}
k( 69) =  1.4000E-11                                                {1.40000E-11}
k( 70) =  1.7000E-11 * exp(   116.0/T)                              {2.50901E-11}
k( 71) =  3.0000E-11                                                {3.00000E-11}
k( 72) uses photo table HCHOrad_CBIV88  , scaled by 9.04000E+00    {0.00000E+00}
k( 73) =  5.4000E-17 * exp(  -500.0/T)                              {1.00858E-17}
k( 74) =  1.7000E-11                                                {1.70000E-11}
k( 75) uses photo table HCHOrad_CBIV88  , scaled by 9.64000E+00    {0.00000E+00}
k( 76) =  3.6000E-11                                                {3.60000E-11}
k( 77) =  2.5400E-11 * exp(   407.6/T)                              {9.97368E-11}
k( 78) =  7.8600E-15 * exp( -1912.0/T)                              {1.28512E-17}
k( 79) =  3.0300E-12 * exp(  -448.0/T)                              {6.73819E-13}
k( 80) =  8.1000E-12                                                {8.10000E-12}
k( 81) =  1.7000E-14 * exp(  1300.0/T)                              {1.33359E-12}
```

Table 8A-3. CB4 Mechanism

```
k( 82) =  8.1000E-12                                                {8.10000E-12}
k( 83) =  4.3900E-13 * exp(   160.0/T)                              {7.51005E-13}
k( 84) =  1.3600E-06                                                {1.36000E-06}
k( 85) =  7.6700E-14 * exp(  1300.0/T)                              {6.01684E-12}
k( 86) =  7.6700E-14 * exp(  1300.0/T)                              {6.01684E-12}
k( 87) =  1.7300E-14 * exp(  1300.0/T)                              {1.35712E-12}
k( 88) =  3.4500E-14 * exp(  1300.0/T)                              {2.70640E-12}
k( 89) =  3.3600E-11                                                {3.36000E-11}
k( 90) =  7.1100E-18                                                {7.11000E-18}
k( 91) =  1.0000E-15                                                {1.00000E-15}
k( 92) uses photo table ACROLEIN        , scaled by 3.60000E-03     {0.00000E+00}
k( 93) =  1.4900E-19                                                {1.49000E-19}
=============================================================================
```

Table 8A-4. CB4_AE Mechanism

```
Reaction List
>-----------------------------------------------------------------------------------------<
{  1} NO2      + hv                 -->          NO       +        O
{  2} O        + [O2]               -->          O3
{  3} O3       + NO                 -->          NO2
{  4} O        + NO2                -->          NO
{  5} O        + NO2                -->          NO3
{  6} O        + NO                 -->          NO2
{  7} O3       + NO2                -->          NO3
{  8} O3       + hv                 -->          O
{  9} O3       + hv                 -->          O1D
{ 10} O1D      + [N2]               -->          O
{ 11} O1D      + [O2]               -->          O
{ 12} O1D      + [H2O]              -->    2.000*OH
{ 13} O3       + OH                 -->          HO2
{ 14} O3       + HO2                -->          OH
{ 15} NO3      + hv                 -->    0.890*NO2      + 0.890*O        + 0.110*NO
{ 16} NO3      + NO                 -->    2.000*NO2
{ 17} NO3      + NO2                -->          NO       +        NO2
{ 18} NO3      + NO2                -->          N2O5
{ 19} N2O5     + [H2O]              -->    2.000*HNO3
{ 20} N2O5                          -->          NO3      +        NO2
{ 21} NO       + NO       + [O2]    -->    2.000*NO2
{ 22} NO       + NO2      + [H2O]   -->    2.000*HONO
{ 23} OH       + NO                 -->          HONO
{ 24} HONO     + hv                 -->          OH       +        NO
{ 25} HONO     + OH                 -->          NO2
{ 26} HONO     + HONO               -->          NO       +        NO2
{ 27} OH       + NO2                -->          HNO3
{ 28} OH       + HNO3               -->          NO3
{ 29} HO2      + NO                 -->          OH       +        NO2
{ 30} HO2      + NO2                -->          PNA
{ 31} PNA                           -->          HO2      +        NO2
{ 32} PNA      + OH                 -->          NO2
{ 33} HO2      + HO2                -->          H2O2
{ 34} HO2      + HO2      + [H2O]   -->          H2O2
{ 35} H2O2     + hv                 -->    2.000*OH
{ 36} H2O2     + OH                 -->          HO2
{ 37} CO       + OH                 -->          HO2
{ 38} FORM     + OH                 -->          HO2      +        CO
{ 39} FORM     + hv                 -->    2.000*HO2      +        CO
{ 40} FORM     + hv                 -->          CO
{ 41} FORM     + O                  -->          OH       +        HO2      +        CO
{ 42} FORM     + NO3                -->          HNO3     +        HO2      +        CO
{ 43} ALD2     + O                  -->          C2O3     +        OH
{ 44} ALD2     + OH                 -->          C2O3
{ 45} ALD2     + NO3                -->          C2O3     +        HNO3
{ 46} ALD2     + hv                 -->          XO2      + 2.000*HO2      +        CO
                                        +       FORM
{ 47} C2O3     + NO                 -->          NO2      +        XO2      +        FORM
                                        +       HO2
{ 48} C2O3     + NO2                -->          PAN
{ 49} PAN                           -->          C2O3     +        NO2
{ 50} C2O3     + C2O3               -->    2.000*XO2      + 2.000*FORM     + 2.000*HO2
{ 51} C2O3     + HO2                -->    0.790*FORM     + 0.790*XO2      + 0.790*HO2
                                        + 0.790*OH
{ 52} OH                            -->          XO2      +        FORM     +        HO2
{ 53} PAR      + OH                 -->    0.870*XO2      + 0.130*XO2N     + 0.110*HO2
                                        + 0.110*ALD2      + 0.760*ROR      - 0.110*PAR
{ 54} ROR                           -->    1.100*ALD2      + 0.960*XO2      + 0.940*HO2
                                        - 2.100*PAR       + 0.040*XO2N     + 0.020*ROR
```

Table 8A-4. CB4_AE Mechanism

```
{ 55} ROR                    -->        HO2
{ 56} ROR      + NO2         -->        NTR
{ 57} OLE      + O           -->  0.630*ALD2    + 0.380*HO2     + 0.280*XO2
                                + 0.300*CO      + 0.200*FORM    + 0.020*XO2N
                                + 0.220*PAR     + 0.200*OH
{ 58} OLE      + OH          -->        FORM    +       ALD2    +       XO2
                                +       HO2     -       PAR
{ 59} OLE      + O3          -->  0.500*ALD2    + 0.740*FORM    + 0.330*CO
                                + 0.440*HO2     + 0.220*XO2     + 0.100*OH
                                -       PAR
{ 60} OLE      + NO3         -->  0.910*XO2     + 0.090*XO2N    +       FORM
                                +       ALD2    -       PAR     +       NO2
{ 61} ETH      + O           -->        FORM    + 0.700*XO2     +       CO
                                + 1.700*HO2     + 0.300*OH
{ 62} ETH      + OH          -->        XO2     + 1.560*FORM    +       HO2
                                + 0.220*ALD2
{ 63} ETH      + O3          -->        FORM    + 0.420*CO      + 0.120*HO2
{ 64} TOL      + OH          -->  0.080*XO2     + 0.360*CRES    + 0.440*HO2
                                + 0.560*TO2     +       TOLAER
{ 65} TO2      + NO          -->  0.900*NO2     + 0.900*HO2     + 0.900*OPEN
                                + 0.100*NTR
{ 66} TO2                    -->        CRES    +       HO2
{ 67} CRES     + OH          -->  0.400*CRO     + 0.600*XO2     + 0.600*HO2
                                + 0.300*OPEN    +       CSLAER
{ 68} CRES     + NO3         -->        CRO     +       HNO3    +       CSLAER
{ 69} CRO      + NO2         -->        NTR
{ 70} XYL      + OH          -->  0.700*HO2     + 0.500*XO2     + 0.200*CRES
                                + 0.800*MGLY    + 1.100*PAR     + 0.300*TO2
                                +       XYLAER
{ 71} OPEN     + OH          -->        XO2     + 2.000*CO      + 2.000*HO2
                                +       C2O3    +       FORM
{ 72} OPEN     + hv          -->        C2O3    +       HO2     +       CO
{ 73} OPEN     + O3          -->  0.030*ALD2    + 0.620*C2O3    + 0.700*FORM
                                + 0.030*XO2     + 0.690*CO      + 0.080*OH
                                + 0.760*HO2     + 0.200*MGLY
{ 74} MGLY     + OH          -->        XO2     +       C2O3
{ 75} MGLY     + hv          -->        C2O3    +       HO2     +       CO
{ 76} ISOP     + O           -->  0.750*ISPD    + 0.500*FORM    + 0.250*XO2
                                + 0.250*HO2     + 0.250*C2O3    + 0.250*PAR
{ 77} ISOP     + OH          -->  0.912*ISPD    + 0.629*FORM    + 0.991*XO2
                                + 0.912*HO2     + 0.088*XO2N
{ 78} ISOP     + O3          -->  0.650*ISPD    + 0.600*FORM    + 0.200*XO2
                                + 0.066*HO2     + 0.266*OH      + 0.200*C2O3
                                + 0.150*ALD2    + 0.350*PAR     + 0.066*CO
{ 79} ISOP     + NO3         -->  0.200*ISPD    + 0.800*NTR     +       XO2
                                + 0.800*HO2     + 0.200*NO2     + 0.800*ALD2
                                + 2.400*PAR
{ 80} XO2      + NO          -->        NO2
{ 81} XO2      + XO2         -->
{ 82} XO2N     + NO          -->        NTR
{ 83} SO2      + OH          -->        SULF    +       HO2     +       SULAER
{ 84} SO2                    -->        SULF    +       SULAER
{ 85} XO2      + HO2         -->
{ 86} XO2N     + HO2         -->
{ 87} XO2N     + XO2N        -->
{ 88} XO2N     + XO2         -->
{ 89} ISPD     + OH          -->  1.565*PAR     + 0.167*FORM    + 0.713*XO2
                                + 0.503*HO2     + 0.334*CO      + 0.168*MGLY
                                + 0.273*ALD2    + 0.498*C2O3
{ 90} ISPD     + O3          -->  0.114*C2O3    + 0.150*FORM    + 0.850*MGLY
                                + 0.154*HO2     + 0.268*OH      + 0.064*XO2
```

Table 8A-4. CB4_AE Mechanism

```
                                          + 0.020*ALD2     + 0.360*PAR      + 0.225*CO
 { 91} ISPD    + NO3                 -->   0.357*ALD2     + 0.282*FORM     + 1.282*PAR
                                          + 0.925*HO2      + 0.643*CO       + 0.850*NTR
                                          + 0.075*C2O3     + 0.075*XO2      + 0.075*HNO3
 { 92} ISPD    + hv                  -->   0.333*CO       + 0.067*ALD2     + 0.900*FORM
                                          + 0.832*PAR      + 1.033*HO2      + 0.700*XO2
                                          + 0.967*C2O3
 { 93} ISOP    + NO2                 -->   0.200*ISPD     + 0.800*NTR      +        XO2
                                          + 0.800*HO2      + 0.200*NO       + 0.800*ALD2
                                          + 2.400*PAR
 { 94} TERP    + OH                  -->          TERPAER +        OH
 { 95} TERP    + NO3                 -->          TERPAER +        NO3
 { 96} TERP    + O3                  -->          TERPAER +        O3
 >-------------------------------------------------------------------------------------<


Rate Expression                                                          Rate Constant
 ==========================================================================================
 k(  1) uses photo table NO2_CBIV88       , scaled by 1.00000E+00    {0.00000E+00}
 k(  2) is a falloff expression using:                                {1.37387E-14}
    k0   =  6.0000E-34 * (T/300)**(-2.30)
    kinf =  2.8000E-12 * (T/300)**( 0.00)
    F =  0.60,  n =  1.00
 k(  3) =  1.8000E-12 * exp( -1370.0/T)                               {1.81419E-14}
 k(  4) =  9.3000E-12                                                 {9.30000E-12}
 k(  5) is a falloff expression using:                                {1.57527E-12}
    k0   =  9.0000E-32 * (T/300)**(-2.00)
    kinf =  2.2000E-11 * (T/300)**( 0.00)
    F =  0.60,  n =  1.00
 k(  6) is a falloff expression using:                                {1.66375E-12}
    k0   =  9.0000E-32 * (T/300)**(-1.50)
    kinf =  3.0000E-11 * (T/300)**( 0.00)
    F =  0.60,  n =  1.00
 k(  7) =  1.2000E-13 * exp( -2450.0/T)                               {3.22581E-17}
 k(  8) uses photo table NO2_CBIV88       , scaled by 5.30000E-02    {0.00000E+00}
 k(  9) uses photo table O3O1D_CBIV88     , scaled by 1.00000E+00    {0.00000E+00}
 k( 10) =  1.8000E-11 * exp(   107.0/T)                               {2.57757E-11}
 k( 11) =  3.2000E-11 * exp(    67.0/T)                               {4.00676E-11}
 k( 12) =  2.2000E-10                                                 {2.20000E-10}
 k( 13) =  1.6000E-12 * exp(  -940.0/T)                               {6.82650E-14}
 k( 14) =  1.4000E-14 * exp(  -580.0/T)                               {1.99920E-15}
 k( 15) uses photo table NO2_CBIV88       , scaled by 3.39000E+01    {0.00000E+00}
 k( 16) =  1.3000E-11 * exp(   250.0/T)                               {3.00805E-11}
 k( 17) =  2.5000E-14 * exp( -1230.0/T)                               {4.03072E-16}
 k( 18) is a falloff expression using:                                {1.26440E-12}
    k0   =  2.2000E-30 * (T/300)**(-4.30)
    kinf =  1.5000E-12 * (T/300)**(-0.50)
    F =  0.60,  n =  1.00
 k( 19) =  1.3000E-21                                                 {1.30000E-21}
 k( 20) = k( 18) / Keq,  where Keq =  2.700E-21 * exp( 11000.0/T)     {4.36029E-08}
 k( 21) =  3.3000E-39 * exp(   530.0/T)                               {1.95397E-38}
 k( 22) =  4.4000E-40                                                 {4.39999E-40}
 k( 23) is a falloff expression using:                                {6.69701E-12}
    k0   =  6.7000E-31 * (T/300)**(-3.30)
    kinf =  3.0000E-11 * (T/300)**(-1.00)
    F =  0.60,  n =  1.00
 k( 24) uses photo table NO2_CBIV88       , scaled by 1.97500E-01    {0.00000E+00}
 k( 25) =  6.6000E-12                                                 {6.60000E-12}
 k( 26) =  1.0000E-20                                                 {1.00000E-20}
 k( 27) is a falloff expression using:                                {1.14885E-11}
    k0   =  2.6000E-30 * (T/300)**(-3.20)
```

Table 8A-4. CB4_AE Mechanism

```
    kinf =  2.4000E-11 * (T/300)**(-1.30)
    F =  0.60,  n =  1.00
k( 28) is a special rate expression of the form:                    {1.47236E-13}
    k = k0 + {k3[M] / (1 + k3[M]/k2)}, where
    k0 =  7.2000E-15 * exp(   785.0/T)
    k2 =  4.1000E-16 * exp(  1440.0/T)
    k3 =  1.9000E-33 * exp(   725.0/T)
k( 29) =  3.7000E-12 * exp(   240.0/T)                              {8.27883E-12}
k( 30) is a falloff expression using:                               {1.48014E-12}
    k0   =  2.3000E-31 * (T/300)**(-4.60)
    kinf =  4.2000E-12 * (T/300)**( 0.20)
    F =  0.60,  n =  1.00
k( 31) = k( 30) / Keq,  where Keq =  2.100E-27 * exp( 10900.0/T)    {9.17943E-02}
k( 32) =  1.3000E-12 * exp(   380.0/T)                              {4.65309E-12}
k( 33) =  5.9000E-14 * exp(  1150.0/T)                              {2.79783E-12}
k( 34) =  2.2000E-38 * exp(  5800.0/T)                              {6.23927E-30}
k( 35) uses photo table HCHOmol_CBIV88  , scaled by 2.55000E-01    {0.00000E+00}
k( 36) =  3.1000E-12 * exp(  -187.0/T)                              {1.65514E-12}
k( 37) =  1.5000E-13 * (1.0 + 0.6*Pressure)                         {2.40000E-13}
k( 38) =  1.0000E-11                                                {1.00000E-11}
k( 39) uses photo table HCHOrad_CBIV88  , scaled by 1.00000E+00    {0.00000E+00}
k( 40) uses photo table HCHOmol_CBIV88  , scaled by 1.00000E+00    {0.00000E+00}
k( 41) =  3.0000E-11 * exp( -1550.0/T)                              {1.65275E-13}
k( 42) =  6.3000E-16                                                {6.30000E-16}
k( 43) =  1.2000E-11 * exp(  -986.0/T)                              {4.38753E-13}
k( 44) =  7.0000E-12 * exp(   250.0/T)                              {1.61972E-11}
k( 45) =  2.5000E-15                                                {2.50000E-15}
k( 46) uses photo table ALD_CBIV88      , scaled by 1.00000E+00    {0.00000E+00}
k( 47) =  3.4900E-11 * exp(  -180.0/T)                              {1.90766E-11}
k( 48) =  2.6300E-12 * exp(   380.0/T)                              {9.41356E-12}
k( 49) =  2.0000E+16 * exp(-13500.0/T)                              {4.23268E-04}
k( 50) =  2.5000E-12                                                {2.50000E-12}
k( 51) =  6.5000E-12                                                {6.50000E-12}
k( 52) =  1.1000E+02 * exp( -1710.0/T)                              {3.54242E-01}
k( 53) =  8.1000E-13                                                {8.10000E-13}
k( 54) =  1.0000E+15 * exp( -8000.0/T)                              {2.19325E+03}
k( 55) =  1.6000E+03                                                {1.60000E+03}
k( 56) =  1.5000E-11                                                {1.50000E-11}
k( 57) =  1.2000E-11 * exp(  -324.0/T)                              {4.04572E-12}
k( 58) =  5.2000E-12 * exp(   504.0/T)                              {2.82173E-11}
k( 59) =  1.4000E-14 * exp( -2105.0/T)                              {1.19778E-17}
k( 60) =  7.7000E-15                                                {7.70000E-15}
k( 61) =  1.0000E-11 * exp(  -792.0/T)                              {7.01080E-13}
k( 62) =  2.0000E-12 * exp(   411.0/T)                              {7.94340E-12}
k( 63) =  1.3000E-14 * exp( -2633.0/T)                              {1.89105E-18}
k( 64) =  2.1000E-12 * exp(   322.0/T)                              {6.18715E-12}
k( 65) =  8.1000E-12                                                {8.10000E-12}
k( 66) =  4.2000E+00                                                {4.20000E+00}
k( 67) =  4.1000E-11                                                {4.10000E-11}
k( 68) =  2.2000E-11                                                {2.20000E-11}
k( 69) =  1.4000E-11                                                {1.40000E-11}
k( 70) =  1.7000E-11 * exp(   116.0/T)                              {2.50901E-11}
k( 71) =  3.0000E-11                                                {3.00000E-11}
k( 72) uses photo table HCHOrad_CBIV88  , scaled by 9.04000E+00    {0.00000E+00}
k( 73) =  5.4000E-17 * exp(  -500.0/T)                              {1.00858E-17}
k( 74) =  1.7000E-11                                                {1.70000E-11}
k( 75) uses photo table HCHOrad_CBIV88  , scaled by 9.64000E+00    {0.00000E+00}
k( 76) =  3.6000E-11                                                {3.60000E-11}
k( 77) =  2.5400E-11 * exp(   407.6/T)                              {9.97368E-11}
k( 78) =  7.8600E-15 * exp( -1912.0/T)                              {1.28512E-17}
k( 79) =  3.0300E-12 * exp(  -448.0/T)                              {6.73819E-13}
```

Table 8A-4. CB4_AE Mechanism

```
k( 80) =  8.1000E-12                                                {8.10000E-12}
k( 81) =  1.7000E-14 * exp(  1300.0/T)                              {1.33359E-12}
k( 82) =  8.1000E-12                                                {8.10000E-12}
k( 83) =  4.3900E-13 * exp(   160.0/T)                              {7.51005E-13}
k( 84) =  1.3600E-06                                                {1.36000E-06}
k( 85) =  7.6700E-14 * exp(  1300.0/T)                              {6.01684E-12}
k( 86) =  7.6700E-14 * exp(  1300.0/T)                              {6.01684E-12}
k( 87) =  1.7300E-14 * exp(  1300.0/T)                              {1.35712E-12}
k( 88) =  3.4500E-14 * exp(  1300.0/T)                              {2.70640E-12}
k( 89) =  3.3600E-11                                                {3.36000E-11}
k( 90) =  7.1100E-18                                                {7.11000E-18}
k( 91) =  1.0000E-15                                                {1.00000E-15}
k( 92) uses photo table ACROLEIN        , scaled by 3.60000E-03     {0.00000E+00}
k( 93) =  1.4900E-19                                                {1.49000E-19}
k( 94) =  1.0700E-11 * exp(   549.0/T)                              {6.75269E-11}
k( 95) =  3.2300E-11 * exp(  -975.0/T)                              {1.22539E-12}
k( 96) =  7.2900E-15 * exp( -1136.0/T)                              {1.61125E-16}
==============================================================================
```

Table 8A-5. CB4_AQ Mechanism

```
 Reaction List
>-----------------------------------------------------------------------<
{  1} NO2    + hv              -->          NO     +        O
{  2} O      + [O2]            -->          O3
{  3} O3     + NO              -->          NO2
{  4} O      + NO2             -->          NO
{  5} O      + NO2             -->          NO3
{  6} O      + NO              -->          NO2
{  7} O3     + NO2             -->          NO3
{  8} O3     + hv              -->          O
{  9} O3     + hv              -->          O1D
{ 10} O1D    + [N2]            -->          O
{ 11} O1D    + [O2]            -->          O
{ 12} O1D    + [H2O]           -->    2.000*OH
{ 13} O3     + OH              -->          HO2
{ 14} O3     + HO2             -->          OH
{ 15} NO3    + hv              -->    0.890*NO2    + 0.890*O      + 0.110*NO
{ 16} NO3    + NO              -->    2.000*NO2
{ 17} NO3    + NO2             -->          NO     +        NO2
{ 18} NO3    + NO2             -->          N2O5
{ 19} N2O5   + [H2O]           -->    2.000*HNO3
{ 20} N2O5                     -->          NO3    +        NO2
{ 21} NO     + NO     + [O2]   -->    2.000*NO2
{ 22} NO     + NO2    + [H2O]  -->    2.000*HONO
{ 23} OH     + NO              -->          HONO
{ 24} HONO   + hv              -->          OH     +        NO
{ 25} HONO   + OH              -->          NO2
{ 26} HONO   + HONO            -->          NO     +        NO2
{ 27} OH     + NO2             -->          HNO3
{ 28} OH     + HNO3            -->          NO3
{ 29} HO2    + NO              -->          OH     +        NO2
{ 30} HO2    + NO2             -->          PNA
{ 31} PNA                      -->          HO2    +        NO2
{ 32} PNA    + OH              -->          NO2
{ 33} HO2    + HO2             -->          H2O2
{ 34} HO2    + HO2    + [H2O]  -->          H2O2
{ 35} H2O2   + hv              -->    2.000*OH
{ 36} H2O2   + OH              -->          HO2
{ 37} CO     + OH              -->          HO2
{ 38} FORM   + OH              -->          HO2    +        CO
{ 39} FORM   + hv              -->    2.000*HO2    +        CO
{ 40} FORM   + hv              -->          CO
{ 41} FORM   + O               -->          OH     +        HO2    +        CO
{ 42} FORM   + NO3             -->          HNO3   +        HO2    +        CO
{ 43} ALD2   + O               -->          C2O3   +        OH
{ 44} ALD2   + OH              -->          C2O3
{ 45} ALD2   + NO3             -->          C2O3   +        HNO3
{ 46} ALD2   + hv              -->          XO2    + 2.000*HO2    +        CO
                                       +    FORM
{ 47} C2O3   + NO              -->          NO2    +        XO2    +        FORM
                                       +    HO2
{ 48} C2O3   + NO2             -->          PAN
{ 49} PAN                      -->          C2O3   +        NO2
{ 50} C2O3   + C2O3            -->    2.000*XO2    + 2.000*FORM   + 2.000*HO2
{ 51} C2O3   + HO2             -->    0.790*FORM   + 0.790*XO2    + 0.790*HO2
                                       + 0.790*OH   + 0.210*PACD
{ 52} OH                       -->          XO2    +        FORM   +        HO2
{ 53} PAR    + OH              -->    0.870*XO2    + 0.130*XO2N   + 0.110*HO2
                                       + 0.110*ALD2 + 0.760*ROR    - 0.110*PAR
```

Table 8A-5. CB4_AQ Mechanism

```
{ 54} ROR                    -->   1.100*ALD2  + 0.960*XO2   + 0.940*HO2
                                 - 2.100*PAR   + 0.040*XO2N  + 0.020*ROR
{ 55} ROR                    -->         HO2
{ 56} ROR    + NO2           -->         NTR
{ 57} OLE    + O             -->   0.630*ALD2  + 0.380*HO2   + 0.280*XO2
                                 + 0.300*CO    + 0.200*FORM  + 0.020*XO2N
                                 + 0.220*PAR   + 0.200*OH
{ 58} OLE    + OH            -->         FORM  +       ALD2  +       XO2
                                 +       HO2   -       PAR
{ 59} OLE    + O3            -->   0.500*ALD2  + 0.740*FORM  + 0.330*CO
                                 + 0.440*HO2   + 0.220*XO2   + 0.100*OH
                                 + 0.200*FACD  + 0.200*AACD  -       PAR
{ 60} OLE    + NO3           -->   0.910*XO2   + 0.090*XO2N  +       FORM
                                 +       ALD2  -       PAR   +       NO2
{ 61} ETH    + O             -->         FORM  + 0.700*XO2   +       CO
                                 + 1.700*HO2   + 0.300*OH
{ 62} ETH    + OH            -->         XO2   + 1.560*FORM  +       HO2
                                 + 0.220*ALD2
{ 63} ETH    + O3            -->         FORM  + 0.420*CO    + 0.120*HO2
                                 + 0.400*FACD
{ 64} TOL    + OH            -->   0.080*XO2   + 0.360*CRES  + 0.440*HO2
                                 + 0.560*TO2
{ 65} TO2    + NO            -->   0.900*NO2   + 0.900*HO2   + 0.900*OPEN
                                 + 0.100*NTR
{ 66} TO2                    -->         CRES  +       HO2
{ 67} CRES   + OH            -->   0.400*CRO   + 0.600*XO2   + 0.600*HO2
                                 + 0.300*OPEN
{ 68} CRES   + NO3           -->         CRO   +       HNO3
{ 69} CRO    + NO2           -->         NTR
{ 70} XYL    + OH            -->   0.700*HO2   + 0.500*XO2   + 0.200*CRES
                                 + 0.800*MGLY  + 1.100*PAR   + 0.300*TO2
{ 71} OPEN   + OH            -->         XO2   + 2.000*CO    + 2.000*HO2
                                 +       C2O3  +       FORM
{ 72} OPEN   + hv            -->         C2O3  +       HO2   +       CO
{ 73} OPEN   + O3            -->   0.030*ALD2  + 0.620*C2O3  + 0.700*FORM
                                 + 0.030*XO2   + 0.690*CO    + 0.080*OH
                                 + 0.760*HO2   + 0.200*MGLY
{ 74} MGLY   + OH            -->         XO2   +       C2O3
{ 75} MGLY   + hv            -->         C2O3  +       HO2   +       CO
{ 76} ISOP   + O             -->   0.750*ISPD  + 0.500*FORM  + 0.250*XO2
                                 + 0.250*HO2   + 0.250*C2O3  + 0.250*PAR
{ 77} ISOP   + OH            -->   0.912*ISPD  + 0.629*FORM  + 0.991*XO2
                                 + 0.912*HO2   + 0.088*XO2N
{ 78} ISOP   + O3            -->   0.650*ISPD  + 0.600*FORM  + 0.200*XO2
                                 + 0.066*HO2   + 0.266*OH    + 0.200*C2O3
                                 + 0.150*ALD2  + 0.350*PAR   + 0.066*CO
{ 79} ISOP   + NO3           -->   0.200*ISPD  + 0.800*NTR   +       XO2
                                 + 0.800*HO2   + 0.200*NO2   + 0.800*ALD2
                                 + 2.400*PAR
{ 80} XO2    + NO            -->         NO2
{ 81} XO2    + XO2           -->
{ 82} XO2N   + NO            -->         NTR
{ 83} SO2    + OH            -->         SULF  +       HO2
{ 84} SO2                    -->         SULF
{ 85} XO2    + HO2           -->         UMHP
{ 86} XO2N   + HO2           -->
{ 87} XO2N   + XO2N          -->
{ 88} XO2N   + XO2           -->
{ 89} ISPD   + OH            -->   1.565*PAR   + 0.167*FORM  + 0.713*XO2
                                 + 0.503*HO2   + 0.334*CO    + 0.168*MGLY
                                 + 0.273*ALD2  + 0.498*C2O3
```

Table 8A-5. CB4_AQ Mechanism

```
{ 90} ISPD  + O3          -->  0.114*C2O3  + 0.150*FORM  + 0.850*MGLY
                             + 0.154*HO2   + 0.268*OH    + 0.064*XO2
                             + 0.020*ALD2  + 0.360*PAR   + 0.225*CO
{ 91} ISPD  + NO3         -->  0.357*ALD2  + 0.282*FORM  + 1.282*PAR
                             + 0.925*HO2   + 0.643*CO    + 0.850*NTR
                             + 0.075*C2O3  + 0.075*XO2   + 0.075*HNO3
{ 92} ISPD  + hv          -->  0.333*CO    + 0.067*ALD2  + 0.900*FORM
                             + 0.832*PAR   + 1.033*HO2   + 0.700*XO2
                             + 0.967*C2O3
{ 93} ISOP  + NO2         -->  0.200*ISPD  + 0.800*NTR   +        XO2
                             + 0.800*HO2   + 0.200*NO    + 0.800*ALD2
                             + 2.400*PAR
>-----------------------------------------------------------------------<


Rate Expression                                                    Rate Constant
==============================================================================
k(  1) uses photo table NO2_CBIV88      , scaled by 1.00000E+00   {0.00000E+00}
k(  2) is a falloff expression using:                             {1.37387E-14}
   k0   =  6.0000E-34 * (T/300)**(-2.30)
   kinf =  2.8000E-12 * (T/300)**( 0.00)
   F =  0.60,  n =  1.00
k(  3) =  1.8000E-12 * exp( -1370.0/T)                            {1.81419E-14}
k(  4) =  9.3000E-12                                              {9.30000E-12}
k(  5) is a falloff expression using:                             {1.57527E-12}
   k0   =  9.0000E-32 * (T/300)**(-2.00)
   kinf =  2.2000E-11 * (T/300)**( 0.00)
   F =  0.60,  n =  1.00
k(  6) is a falloff expression using:                             {1.66375E-12}
   k0   =  9.0000E-32 * (T/300)**(-1.50)
   kinf =  3.0000E-11 * (T/300)**( 0.00)
   F =  0.60,  n =  1.00
k(  7) =  1.2000E-13 * exp( -2450.0/T)                            {3.22581E-17}
k(  8) uses photo table NO2_CBIV88      , scaled by 5.30000E-02   {0.00000E+00}
k(  9) uses photo table O3O1D_CBIV88    , scaled by 1.00000E+00   {0.00000E+00}
k( 10) =  1.8000E-11 * exp(   107.0/T)                            {2.57757E-11}
k( 11) =  3.2000E-11 * exp(    67.0/T)                            {4.00676E-11}
k( 12) =  2.2000E-10                                              {2.20000E-10}
k( 13) =  1.6000E-12 * exp(  -940.0/T)                            {6.82650E-14}
k( 14) =  1.4000E-14 * exp(  -580.0/T)                            {1.99920E-15}
k( 15) uses photo table NO2_CBIV88      , scaled by 3.39000E+01   {0.00000E+00}
k( 16) =  1.3000E-11 * exp(   250.0/T)                            {3.00805E-11}
k( 17) =  2.5000E-14 * exp( -1230.0/T)                            {4.03072E-16}
k( 18) is a falloff expression using:                             {1.26440E-12}
   k0   =  2.2000E-30 * (T/300)**(-4.30)
   kinf =  1.5000E-12 * (T/300)**(-0.50)
   F =  0.60,  n =  1.00
k( 19) =  1.3000E-21                                              {1.30000E-21}
k( 20) = k( 18) / Keq,  where Keq =  2.700E-27 * exp( 11000.0/T)  {4.36029E-02}
k( 21) =  3.3000E-39 * exp(   530.0/T)                            {1.95397E-38}
k( 22) =  4.4000E-40                                              {4.39999E-40}
k( 23) is a falloff expression using:                             {6.69701E-12}
   k0   =  6.7000E-31 * (T/300)**(-3.30)
   kinf =  3.0000E-11 * (T/300)**(-1.00)
   F =  0.60,  n =  1.00
k( 24) uses photo table NO2_CBIV88      , scaled by 1.97500E-01   {0.00000E+00}
k( 25) =  6.6000E-12                                              {6.60000E-12}
k( 26) =  1.0000E-20                                              {1.00000E-20}
k( 27) is a falloff expression using:                             {1.14885E-11}
   k0   =  2.6000E-30 * (T/300)**(-3.20)
   kinf =  2.4000E-11 * (T/300)**(-1.30)
```

Table 8A-5. CB4_AQ Mechanism

```
   F =  0.60,  n =  1.00
k( 28) is a special rate expression of the form:                    {1.47236E-13}
   k = k0 + {k3[M] / (1 + k3[M]/k2)}, where
   k0 =  7.2000E-15 * exp(   785.0/T)
   k2 =  4.1000E-16 * exp(  1440.0/T)
   k3 =  1.9000E-33 * exp(   725.0/T)
k( 29) =  3.7000E-12 * exp(   240.0/T)                              {8.27883E-12}
k( 30) is a falloff expression using:                               {1.48014E-12}
   k0   =  2.3000E-31 * (T/300)**(-4.60)
   kinf =  4.2000E-12 * (T/300)**( 0.20)
   F =  0.60,  n =  1.00
k( 31) = k( 30) / Keq,  where Keq =  2.100E-27 * exp( 10900.0/T)   {9.17943E-02}
k( 32) =  1.3000E-12 * exp(   380.0/T)                              {4.65309E-12}
k( 33) =  5.9000E-14 * exp(  1150.0/T)                              {2.79783E-12}
k( 34) =  2.2000E-38 * exp(  5800.0/T)                              {6.23927E-30}
k( 35) uses photo table HCHOmol_CBIV88  , scaled by 2.55000E-01    {0.00000E+00}
k( 36) =  3.1000E-12 * exp(  -187.0/T)                              {1.65514E-12}
k( 37) =  1.5000E-13 * (1.0 + 0.6*Pressure)                         {2.40000E-13}
k( 38) =  1.0000E-11                                                {1.00000E-11}
k( 39) uses photo table HCHOrad_CBIV88  , scaled by 1.00000E+00    {0.00000E+00}
k( 40) uses photo table HCHOmol_CBIV88  , scaled by 1.00000E+00    {0.00000E+00}
k( 41) =  3.0000E-11 * exp( -1550.0/T)                              {1.65275E-13}
k( 42) =  6.3000E-16                                                {6.30000E-16}
k( 43) =  1.2000E-11 * exp(  -986.0/T)                              {4.38753E-13}
k( 44) =  7.0000E-12 * exp(   250.0/T)                              {1.61972E-11}
k( 45) =  2.5000E-15                                                {2.50000E-15}
k( 46) uses photo table ALD_CBIV88      , scaled by 1.00000E+00    {0.00000E+00}
k( 47) =  3.4900E-11 * exp(  -180.0/T)                              {1.90766E-11}
k( 48) =  2.6300E-12 * exp(   380.0/T)                              {9.41356E-12}
k( 49) =  2.0000E+16 * exp(-13500.0/T)                              {4.23268E-04}
k( 50) =  2.5000E-12                                                {2.50000E-12}
k( 51) =  6.5000E-12                                                {6.50000E-12}
k( 52) =  1.1000E+02 * exp( -1710.0/T)                              {3.54242E-01}
k( 53) =  8.1000E-13                                                {8.10000E-13}
k( 54) =  1.0000E+15 * exp( -8000.0/T)                              {2.19325E+03}
k( 55) =  1.6000E+03                                                {1.60000E+03}
k( 56) =  1.5000E-11                                                {1.50000E-11}
k( 57) =  1.2000E-11 * exp(  -324.0/T)                              {4.04572E-12}
k( 58) =  5.2000E-12 * exp(   504.0/T)                              {2.82173E-11}
k( 59) =  1.4000E-14 * exp( -2105.0/T)                              {1.19778E-17}
k( 60) =  7.7000E-15                                                {7.70000E-15}
k( 61) =  1.0000E-11 * exp(  -792.0/T)                              {7.01080E-13}
k( 62) =  2.0000E-12 * exp(   411.0/T)                              {7.94340E-12}
k( 63) =  1.3000E-14 * exp( -2633.0/T)                              {1.89105E-18}
k( 64) =  2.1000E-12 * exp(   322.0/T)                              {6.18715E-12}
k( 65) =  8.1000E-12                                                {8.10000E-12}
k( 66) =  4.2000E+00                                                {4.20000E+00}
k( 67) =  4.1000E-11                                                {4.10000E-11}
k( 68) =  2.2000E-11                                                {2.20000E-11}
k( 69) =  1.4000E-11                                                {1.40000E-11}
k( 70) =  1.7000E-11 * exp(   116.0/T)                              {2.50901E-11}
k( 71) =  3.0000E-11                                                {3.00000E-11}
k( 72) uses photo table HCHOrad_CBIV88  , scaled by 9.04000E+00    {0.00000E+00}
k( 73) =  5.4000E-17 * exp(  -500.0/T)                              {1.00858E-17}
k( 74) =  1.7000E-11                                                {1.70000E-11}
k( 75) uses photo table HCHOrad_CBIV88  , scaled by 9.64000E+00    {0.00000E+00}
k( 76) =  3.6000E-11                                                {3.60000E-11}
k( 77) =  2.5400E-11 * exp(   407.6/T)                              {9.97368E-11}
k( 78) =  7.8600E-15 * exp( -1912.0/T)                              {1.28512E-17}
k( 79) =  3.0300E-12 * exp(  -448.0/T)                              {6.73819E-13}
k( 80) =  8.1000E-12                                                {8.10000E-12}
```

Table 8A-5. CB4_AQ Mechanism

```
k( 81) =  1.7000E-14 * exp(  1300.0/T)                          {1.33359E-12}
k( 82) =  8.1000E-12                                            {8.10000E-12}
k( 83) =  4.3900E-13 * exp(   160.0/T)                          {7.51005E-13}
k( 84) =  1.3600E-06                                            {1.36000E-06}
k( 85) =  7.6700E-14 * exp(  1300.0/T)                          {6.01684E-12}
k( 86) =  7.6700E-14 * exp(  1300.0/T)                          {6.01684E-12}
k( 87) =  1.7300E-14 * exp(  1300.0/T)                          {1.35712E-12}
k( 88) =  3.4500E-14 * exp(  1300.0/T)                          {2.70640E-12}
k( 89) =  3.3600E-11                                            {3.36000E-11}
k( 90) =  7.1100E-18                                            {7.11000E-18}
k( 91) =  1.0000E-15                                            {1.00000E-15}
k( 92) uses photo table ACROLEIN        , scaled by 3.60000E-03 {0.00000E+00}
k( 93) =  1.4900E-19                                            {1.49000E-19}
================================================================================
```

Table 8A-6. CB4_AE_AQ Mechanism

```
 Reaction List
>-------------------------------------------------------------------------------------<
{  1} NO2      + hv                  -->          NO       +        O
{  2} O        + [O2]                -->          O3
{  3} O3       + NO                  -->          NO2
{  4} O        + NO2                 -->          NO
{  5} O        + NO2                 -->          NO3
{  6} O        + NO                  -->          NO2
{  7} O3       + NO2                 -->          NO3
{  8} O3       + hv                  -->          O
{  9} O3       + hv                  -->          O1D
{ 10} O1D      + [N2]                -->          O
{ 11} O1D      + [O2]                -->          O
{ 12} O1D      + [H2O]               -->    2.000*OH
{ 13} O3       + OH                  -->          HO2
{ 14} O3       + HO2                 -->          OH
{ 15} NO3      + hv                  -->    0.890*NO2      + 0.890*O        + 0.110*NO
{ 16} NO3      + NO                  -->    2.000*NO2
{ 17} NO3      + NO2                 -->          NO       +        NO2
{ 18} NO3      + NO2                 -->          N2O5
{ 19} N2O5     + [H2O]               -->    2.000*HNO3
{ 20} N2O5                           -->          NO3      +        NO2
{ 21} NO       + NO       + [O2]     -->    2.000*NO2
{ 22} NO       + NO2      + [H2O]    -->    2.000*HONO
{ 23} OH       + NO                  -->          HONO
{ 24} HONO     + hv                  -->          OH       +        NO
{ 25} HONO     + OH                  -->          NO2
{ 26} HONO     + HONO                -->          NO       +        NO2
{ 27} OH       + NO2                 -->          HNO3
{ 28} OH       + HNO3                -->          NO3
{ 29} HO2      + NO                  -->          OH       +        NO2
{ 30} HO2      + NO2                 -->          PNA
{ 31} PNA                            -->          HO2      +        NO2
{ 32} PNA      + OH                  -->          NO2
{ 33} HO2      + HO2                 -->          H2O2
{ 34} HO2      + HO2      + [H2O]    -->          H2O2
{ 35} H2O2     + hv                  -->    2.000*OH
{ 36} H2O2     + OH                  -->          HO2
{ 37} CO       + OH                  -->          HO2
{ 38} FORM     + OH                  -->          HO2      +        CO
{ 39} FORM     + hv                  -->    2.000*HO2      +        CO
{ 40} FORM     + hv                  -->          CO
{ 41} FORM     + O                   -->          OH       +        HO2      +        CO
{ 42} FORM     + NO3                 -->          HNO3     +        HO2      +        CO
{ 43} ALD2     + O                   -->          C2O3     +        OH
{ 44} ALD2     + OH                  -->          C2O3
{ 45} ALD2     + NO3                 -->          C2O3     +        HNO3
{ 46} ALD2     + hv                  -->          XO2      + 2.000*HO2      +        CO
                                         +        FORM
{ 47} C2O3     + NO                  -->          NO2      +        XO2      +        FORM
                                         +        HO2
{ 48} C2O3     + NO2                 -->          PAN
{ 49} PAN                            -->          C2O3     +        NO2
{ 50} C2O3     + C2O3                -->    2.000*XO2      + 2.000*FORM     + 2.000*HO2
{ 51} C2O3     + HO2                 -->    0.790*FORM     + 0.790*XO2      + 0.790*HO2
                                         + 0.790*OH       + 0.210*PACD
{ 52} OH                             -->          XO2      +        FORM     +        HO2
{ 53} PAR      + OH                  -->    0.870*XO2      + 0.130*XO2N     + 0.110*HO2
                                         + 0.110*ALD2     + 0.760*ROR      - 0.110*PAR
{ 54} ROR                            -->    1.100*ALD2     + 0.960*XO2      + 0.940*HO2
                                         - 2.100*PAR      + 0.040*XO2N     + 0.020*ROR
```

Table 8A-6. CB4_AE_AQ Mechanism

```
{ 55} ROR                    -->        HO2
{ 56} ROR      + NO2         -->        NTR
{ 57} OLE      + O           -->  0.630*ALD2    + 0.380*HO2     + 0.280*XO2
                                + 0.300*CO      + 0.200*FORM    + 0.020*XO2N
                                + 0.220*PAR     + 0.200*OH
{ 58} OLE      + OH          -->        FORM    +       ALD2    +       XO2
                                +       HO2     -       PAR
{ 59} OLE      + O3          -->  0.500*ALD2    + 0.740*FORM    + 0.330*CO
                                + 0.440*HO2     + 0.220*XO2     + 0.100*OH
                                + 0.200*FACD    + 0.200*AACD    -       PAR
{ 60} OLE      + NO3         -->  0.910*XO2     + 0.090*XO2N    +       FORM
                                +       ALD2    -       PAR     +       NO2
{ 61} ETH      + O           -->        FORM    + 0.700*XO2     +       CO
                                + 1.700*HO2     + 0.300*OH
{ 62} ETH      + OH          -->        XO2     + 1.560*FORM    +       HO2
                                + 0.220*ALD2
{ 63} ETH      + O3          -->        FORM    + 0.420*CO      + 0.120*HO2
                                + 0.400*FACD
{ 64} TOL      + OH          -->  0.080*XO2     + 0.360*CRES    + 0.440*HO2
                                + 0.560*TO2     +       TOLAER
{ 65} TO2      + NO          -->  0.900*NO2     + 0.900*HO2     + 0.900*OPEN
                                + 0.100*NTR
{ 66} TO2                    -->        CRES    +       HO2
{ 67} CRES     + OH          -->  0.400*CRO     + 0.600*XO2     + 0.600*HO2
                                + 0.300*OPEN    +       CSLAER
{ 68} CRES     + NO3         -->        CRO     +       HNO3    +       CSLAER
{ 69} CRO      + NO2         -->        NTR
{ 70} XYL      + OH          -->  0.700*HO2     + 0.500*XO2     + 0.200*CRES
                                + 0.800*MGLY    + 1.100*PAR     + 0.300*TO2
                                +       XYLAER
{ 71} OPEN     + OH          -->        XO2     + 2.000*CO      + 2.000*HO2
                                +       C2O3    +       FORM
{ 72} OPEN     + hv          -->        C2O3    +       HO2     +       CO
{ 73} OPEN     + O3          -->  0.030*ALD2    + 0.620*C2O3    + 0.700*FORM
                                + 0.030*XO2     + 0.690*CO      + 0.080*OH
                                + 0.760*HO2     + 0.200*MGLY
{ 74} MGLY     + OH          -->        XO2     +       C2O3
{ 75} MGLY     + hv          -->        C2O3    +       HO2     +       CO
{ 76} ISOP     + O           -->  0.750*ISPD    + 0.500*FORM    + 0.250*XO2
                                + 0.250*HO2     + 0.250*C2O3    + 0.250*PAR
{ 77} ISOP     + OH          -->  0.912*ISPD    + 0.629*FORM    + 0.991*XO2
                                + 0.912*HO2     + 0.088*XO2N
{ 78} ISOP     + O3          -->  0.650*ISPD    + 0.600*FORM    + 0.200*XO2
                                + 0.066*HO2     + 0.266*OH      + 0.200*C2O3
                                + 0.150*ALD2    + 0.350*PAR     + 0.066*CO
{ 79} ISOP     + NO3         -->  0.200*ISPD    + 0.800*NTR     +       XO2
                                + 0.800*HO2     + 0.200*NO2     + 0.800*ALD2
                                + 2.400*PAR
{ 80} XO2      + NO          -->        NO2
{ 81} XO2      + XO2         -->
{ 82} XO2N     + NO          -->        NTR
{ 83} SO2      + OH          -->        SULF    +       HO2     +       SULAER
{ 84} SO2                    -->        SULF    +       SULAER
{ 85} XO2      + HO2         -->        UMHP
{ 86} XO2N     + HO2         -->
{ 87} XO2N     + XO2N        -->
{ 88} XO2N     + XO2         -->
{ 89} ISPD     + OH          -->  1.565*PAR     + 0.167*FORM    + 0.713*XO2
                                + 0.503*HO2     + 0.334*CO      + 0.168*MGLY
                                + 0.273*ALD2    + 0.498*C2O3
{ 90} ISPD     + O3          -->  0.114*C2O3    + 0.150*FORM    + 0.850*MGLY
```

Table 8A-6. CB4_AE_AQ Mechanism

```
                                        + 0.154*HO2      + 0.268*OH       + 0.064*XO2
                                        + 0.020*ALD2     + 0.360*PAR      + 0.225*CO
{ 91} ISPD    + NO3                 -->   0.357*ALD2     + 0.282*FORM     + 1.282*PAR
                                        + 0.925*HO2      + 0.643*CO       + 0.850*NTR
                                        + 0.075*C2O3     + 0.075*XO2      + 0.075*HNO3
{ 92} ISPD    + hv                  -->   0.333*CO       + 0.067*ALD2     + 0.900*FORM
                                        + 0.832*PAR      + 1.033*HO2      + 0.700*XO2
                                        + 0.967*C2O3
{ 93} ISOP    + NO2                 -->   0.200*ISPD     + 0.800*NTR      +        XO2
                                        + 0.800*HO2      + 0.200*NO       + 0.800*ALD2
                                        + 2.400*PAR
{ 94} TERP    + OH                  -->          TERPAER +        OH
{ 95} TERP    + NO3                 -->          TERPAER +        NO3
{ 96} TERP    + O3                  -->          TERPAER +        O3
>-------------------------------------------------------------------------------------<


Rate Expression                                                        Rate Constant
 ==============================================================================
 k(  1) uses photo table NO2_CBIV88       , scaled by 1.00000E+00   {0.00000E+00}
 k(  2) is a falloff expression using:                              {1.37387E-14}
    k0   =  6.0000E-34 * (T/300)**(-2.30)
    kinf =  2.8000E-12 * (T/300)**( 0.00)
    F =  0.60,  n =  1.00
 k(  3) =  1.8000E-12 * exp( -1370.0/T)                             {1.81419E-14}
 k(  4) =  9.3000E-12                                               {9.30000E-12}
 k(  5) is a falloff expression using:                              {1.57527E-12}
    k0   =  9.0000E-32 * (T/300)**(-2.00)
    kinf =  2.2000E-11 * (T/300)**( 0.00)
    F =  0.60,  n =  1.00
 k(  6) is a falloff expression using:                              {1.66375E-12}
    k0   =  9.0000E-32 * (T/300)**(-1.50)
    kinf =  3.0000E-11 * (T/300)**( 0.00)
    F =  0.60,  n =  1.00
 k(  7) =  1.2000E-13 * exp( -2450.0/T)                             {3.22581E-17}
 k(  8) uses photo table NO2_CBIV88       , scaled by 5.30000E-02   {0.00000E+00}
 k(  9) uses photo table O3O1D_CBIV88     , scaled by 1.00000E+00   {0.00000E+00}
 k( 10) =  1.8000E-11 * exp(   107.0/T)                             {2.57757E-11}
 k( 11) =  3.2000E-11 * exp(    67.0/T)                             {4.00676E-11}
 k( 12) =  2.2000E-10                                               {2.20000E-10}
 k( 13) =  1.6000E-12 * exp(  -940.0/T)                             {6.82650E-14}
 k( 14) =  1.4000E-14 * exp(  -580.0/T)                             {1.99920E-15}
 k( 15) uses photo table NO2_CBIV88       , scaled by 3.39000E+01   {0.00000E+00}
 k( 16) =  1.3000E-11 * exp(   250.0/T)                             {3.00805E-11}
 k( 17) =  2.5000E-14 * exp( -1230.0/T)                             {4.03072E-16}
 k( 18) is a falloff expression using:                              {1.26440E-12}
    k0   =  2.2000E-30 * (T/300)**(-4.30)
    kinf =  1.5000E-12 * (T/300)**(-0.50)
    F =  0.60,  n =  1.00
 k( 19) =  1.3000E-21                                               {1.30000E-21}
 k( 20) = k( 18) / Keq,  where Keq =  2.700E-27 * exp( 11000.0/T)   {4.36029E-02}
 k( 21) =  3.3000E-39 * exp(   530.0/T)                             {1.95397E-38}
 k( 22) =  4.4000E-40                                               {4.39999E-40}
 k( 23) is a falloff expression using:                              {6.69701E-12}
    k0   =  6.7000E-31 * (T/300)**(-3.30)
    kinf =  3.0000E-11 * (T/300)**(-1.00)
    F =  0.60,  n =  1.00
 k( 24) uses photo table NO2_CBIV88       , scaled by 1.97500E-01   {0.00000E+00}
 k( 25) =  6.6000E-12                                               {6.60000E-12}
 k( 26) =  1.0000E-20                                               {1.00000E-20}
 k( 27) is a falloff expression using:                              {1.14885E-11}
```

Table 8A-6. CB4_AE_AQ Mechanism

```
   k0   =  2.6000E-30 * (T/300)**(-3.20)
   kinf =  2.4000E-11 * (T/300)**(-1.30)
   F =  0.60,  n =  1.00
k( 28) is a special rate expression of the form:                    {1.47236E-13}
   k = k0 + {k3[M] / (1 + k3[M]/k2)}, where
   k0 =  7.2000E-15 * exp(   785.0/T)
   k2 =  4.1000E-16 * exp(  1440.0/T)
   k3 =  1.9000E-33 * exp(   725.0/T)
k( 29) =  3.7000E-12 * exp(   240.0/T)                              {8.27883E-12}
k( 30) is a falloff expression using:                               {1.48014E-12}
   k0   =  2.3000E-31 * (T/300)**(-4.60)
   kinf =  4.2000E-12 * (T/300)**( 0.20)
   F =  0.60,  n =  1.00
k( 31) = k( 30) / Keq,  where Keq =  2.100E-27 * exp( 10900.0/T)    {9.17943E-02}
k( 32) =  1.3000E-12 * exp(   380.0/T)                              {4.65309E-12}
k( 33) =  5.9000E-14 * exp(  1150.0/T)                              {2.79783E-12}
k( 34) =  2.2000E-38 * exp(  5800.0/T)                              {6.23927E-30}
k( 35) uses photo table HCHOmol_CBIV88  , scaled by 2.55000E-01     {0.00000E+00}
k( 36) =  3.1000E-12 * exp(  -187.0/T)                              {1.65514E-12}
k( 37) =  1.5000E-13 * (1.0 + 0.6*Pressure)                         {2.40000E-13}
k( 38) =  1.0000E-11                                                {1.00000E-11}
k( 39) uses photo table HCHOrad_CBIV88  , scaled by 1.00000E+00     {0.00000E+00}
k( 40) uses photo table HCHOmol_CBIV88  , scaled by 1.00000E+00     {0.00000E+00}
k( 41) =  3.0000E-11 * exp( -1550.0/T)                              {1.65275E-13}
k( 42) =  6.3000E-16                                                {6.30000E-16}
k( 43) =  1.2000E-11 * exp(  -986.0/T)                              {4.38753E-13}
k( 44) =  7.0000E-12 * exp(   250.0/T)                              {1.61972E-11}
k( 45) =  2.5000E-15                                                {2.50000E-15}
k( 46) uses photo table ALD_CBIV88      , scaled by 1.00000E+00     {0.00000E+00}
k( 47) =  3.4900E-11 * exp(  -180.0/T)                              {1.90766E-11}
k( 48) =  2.6300E-12 * exp(   380.0/T)                              {9.41356E-12}
k( 49) =  2.0000E+16 * exp(-13500.0/T)                              {4.23268E-04}
k( 50) =  2.5000E-12                                                {2.50000E-12}
k( 51) =  6.5000E-12                                                {6.50000E-12}
k( 52) =  1.1000E+02 * exp( -1710.0/T)                              {3.54242E-01}
k( 53) =  8.1000E-13                                                {8.10000E-13}
k( 54) =  1.0000E+15 * exp( -8000.0/T)                              {2.19325E+03}
k( 55) =  1.6000E+03                                                {1.60000E+03}
k( 56) =  1.5000E-11                                                {1.50000E-11}
k( 57) =  1.2000E-11 * exp(  -324.0/T)                              {4.04572E-12}
k( 58) =  5.2000E-12 * exp(   504.0/T)                              {2.82173E-11}
k( 59) =  1.4000E-14 * exp( -2105.0/T)                              {1.19778E-17}
k( 60) =  7.7000E-15                                                {7.70000E-15}
k( 61) =  1.0000E-11 * exp(  -792.0/T)                              {7.01080E-13}
k( 62) =  2.0000E-12 * exp(   411.0/T)                              {7.94340E-12}
k( 63) =  1.3000E-14 * exp( -2633.0/T)                              {1.89105E-18}
k( 64) =  2.1000E-12 * exp(   322.0/T)                              {6.18715E-12}
k( 65) =  8.1000E-12                                                {8.10000E-12}
k( 66) =  4.2000E+00                                                {4.20000E+00}
k( 67) =  4.1000E-11                                                {4.10000E-11}
k( 68) =  2.2000E-11                                                {2.20000E-11}
k( 69) =  1.4000E-11                                                {1.40000E-11}
k( 70) =  1.7000E-11 * exp(   116.0/T)                              {2.50901E-11}
k( 71) =  3.0000E-11                                                {3.00000E-11}
k( 72) uses photo table HCHOrad_CBIV88  , scaled by 9.04000E+00     {0.00000E+00}
k( 73) =  5.4000E-17 * exp(  -500.0/T)                              {1.00858E-17}
k( 74) =  1.7000E-11                                                {1.70000E-11}
k( 75) uses photo table HCHOrad_CBIV88  , scaled by 9.64000E+00     {0.00000E+00}
k( 76) =  3.6000E-11                                                {3.60000E-11}
k( 77) =  2.5400E-11 * exp(   407.6/T)                              {9.97368E-11}
k( 78) =  7.8600E-15 * exp( -1912.0/T)                              {1.28512E-17}
```

Table 8A-6. CB4_AE_AQ Mechanism

```
k( 79) =  3.0300E-12 * exp(  -448.0/T)                          {6.73819E-13}
k( 80) =  8.1000E-12                                            {8.10000E-12}
k( 81) =  1.7000E-14 * exp(  1300.0/T)                          {1.33359E-12}
k( 82) =  8.1000E-12                                            {8.10000E-12}
k( 83) =  4.3900E-13 * exp(   160.0/T)                          {7.51005E-13}
k( 84) =  1.3600E-06                                            {1.36000E-06}
k( 85) =  7.6700E-14 * exp(  1300.0/T)                          {6.01684E-12}
k( 86) =  7.6700E-14 * exp(  1300.0/T)                          {6.01684E-12}
k( 87) =  1.7300E-14 * exp(  1300.0/T)                          {1.35712E-12}
k( 88) =  3.4500E-14 * exp(  1300.0/T)                          {2.70640E-12}
k( 89) =  3.3600E-11                                            {3.36000E-11}
k( 90) =  7.1100E-18                                            {7.11000E-18}
k( 91) =  1.0000E-15                                            {1.00000E-15}
k( 92) uses photo table ACROLEIN        , scaled by 3.60000E-03 {0.00000E+00}
k( 93) =  1.4900E-19                                            {1.49000E-19}
k( 94) =  1.0700E-11 * exp(   549.0/T)                          {6.75269E-11}
k( 95) =  3.2300E-11 * exp(  -975.0/T)                          {1.22539E-12}
k( 96) =  7.2900E-15 * exp( -1136.0/T)                          {1.61125E-16}
==============================================================================
```

Table 8A-7. RADM2 and RADM2_AQ Mechanisms

```
 Reaction List
>-------------------------------------------------------------------------<
{  1} NO2    + hv                 -->          O3P    +        NO
{  2} O3     + hv                 -->          O1D
{  3} O3     + hv                 -->          O3P
{  4} HONO   + hv                 -->          HO     +        NO
{  5} HNO3   + hv                 -->          HO     +        NO2
{  6} HNO4   + hv                 -->          HO2    +        NO2
{  7} NO3    + hv                 -->          NO
{  8} NO3    + hv                 -->          NO2    +        O3P
{  9} H2O2   + hv                 -->    2.000*HO
{ 10} HCHO   + hv                 -->          CO
{ 11} HCHO   + hv                 -->          HO2    +        HO2    +        CO
{ 12} ALD    + hv                 -->          MO2    +        HO2    +        CO
{ 13} OP1    + hv                 -->          HCHO   +        HO2    +        HO
{ 14} OP2    + hv                 -->          ALD    +        HO2    +        HO
{ 15} PAA    + hv                 -->          MO2    +        HO
{ 16} KET    + hv                 -->          ACO3   +        ETHP
{ 17} GLY    + hv                 -->    0.130*HCHO   + 1.870*CO
{ 18} GLY    + hv                 -->    0.450*HCHO   + 1.550*CO     + 0.800*HO2
{ 19} MGLY   + hv                 -->          ACO3   +        HO2    +        CO
{ 20} DCB    + hv                 -->    0.980*HO2    + 0.020*ACO3   +        TCO3
{ 21} ONIT   + hv                 -->    0.200*ALD    + 0.800*KET    +        HO2
                                     +        NO2
{ 22} O3P    + [M]     + [O2]      -->          O3
{ 23} O3P    + NO2                 -->          NO
{ 24} O1D    + [N2]                -->          O3P
{ 25} O1D    + [O2]                -->          O3P
{ 26} O1D    + [H2O]               -->    2.000*HO
{ 27} O3     + NO                  -->          NO2
{ 28} O3     + HO                  -->          HO2
{ 29} O3     + HO2                 -->          HO
{ 30} HO2    + NO                  -->          NO2    +        HO
{ 31} HO2    + NO2                 -->          HNO4
{ 32} HNO4                         -->          HO2    +        NO2
{ 33} HO2    + HO2                 -->          H2O2
{ 34} HO2    + HO2     + [H2O]     -->          H2O2
{ 35} H2O2   + HO                  -->          HO2
{ 36} NO     + HO                  -->          HONO
{ 37} NO     + NO      + [O2]      -->    2.000*NO2
{ 38} O3     + NO2                 -->          NO3
{ 39} NO3    + NO                  -->    2.000*NO2
{ 40} NO3    + NO2                 -->          NO     +        NO2
{ 41} NO3    + HO2                 -->          HNO3
{ 42} NO3    + NO2                 -->          N2O5
{ 43} N2O5                         -->          NO2    +        NO3
{ 44} N2O5   + [H2O]               -->    2.000*HNO3
{ 45} HO     + NO2                 -->          HNO3
{ 46} HO     + HNO3                -->          NO3
{ 47} HO     + HNO4                -->          NO2
{ 48} HO     + HO2                 -->
{ 49} HO     + SO2                 -->          SULF   +        HO2
{ 50} CO     + HO                  -->          HO2
{ 51} HO                           -->          MO2
{ 52} ETH    + HO                  -->          ETHP
{ 53} HC3    + HO                  -->    0.830*HC3P   + 0.170*HO2    + 0.009*HCHO
                                     + 0.075*ALD    + 0.025*KET
{ 54} HC5    + HO                  -->          HC5P   + 0.250*XO2
{ 55} HC8    + HO                  -->          HC8P   + 0.750*XO2
{ 56} OL2    + HO                  -->          OL2P
{ 57} OLT    + HO                  -->          OLTP
```

Table 8A-7. RADM2 and RADM2_AQ Mechanisms

```
{ 58} OLI   + HO          -->        OLIP
{ 59} TOL   + HO          -->  0.750*TOLP  + 0.250*CSL   + 0.250*HO2
{ 60} XYL   + HO          -->  0.830*XYLP  + 0.170*CSL   + 0.170*HO2
{ 61} CSL   + HO          -->  0.100*HO2   + 0.900*XO2   + 0.900*TCO3
{ 62} CSL   + HO          -->        CSL
{ 63} HCHO  + HO          -->        HO2   +       CO
{ 64} ALD   + HO          -->        ACO3
{ 65} KET   + HO          -->        KETP
{ 66} GLY   + HO          -->        HO2   + 2.000*CO
{ 67} MGLY  + HO          -->        ACO3  +       CO
{ 68} DCB   + HO          -->        TCO3
{ 69} OP1   + HO          -->  0.500*MO2   + 0.500*HCHO  + 0.500*HO
{ 70} OP2   + HO          -->  0.500*HC3P  + 0.500*ALD   + 0.500*HO
{ 71} PAA   + HO          -->        ACO3
{ 72} PAN   + HO          -->        HCHO  +       NO3   +       XO2
{ 73} ONIT  + HO          -->        HC3P  +       NO2
{ 74} ISO   + HO          -->        OLTP
{ 75} ACO3  + NO2         -->        PAN
{ 76} PAN                 -->        ACO3  +       NO2
{ 77} TCO3  + NO2         -->        TPAN
{ 78} TPAN                -->        TCO3  +       NO2
{ 79} MO2   + NO          -->        HCHO  +       HO2   +       NO2
{ 80} HC3P  + NO          -->  0.750*ALD   + 0.250*KET   + 0.090*HCHO
                             + 0.036*ONIT  + 0.964*NO2   + 0.964*HO2
{ 81} HC5P  + NO          -->  0.380*ALD   + 0.690*KET   + 0.080*ONIT
                             + 0.920*NO2   + 0.920*HO2
{ 82} HC8P  + NO          -->  0.350*ALD   + 1.060*KET   + 0.040*HCHO
                             + 0.240*ONIT  + 0.760*NO2   + 0.760*HO2
{ 83} OL2P  + NO          -->  1.600*HCHO  +       HO2   +       NO2
                             + 0.200*ALD
{ 84} OLTP  + NO          -->        ALD   +       HCHO  +       HO2
                             +       NO2
{ 85} OLIP  + NO          -->        HO2   + 1.450*ALD   + 0.280*HCHO
                             + 0.100*KET   +       NO2
{ 86} ACO3  + NO          -->        MO2   +       NO2
{ 87} TCO3  + NO          -->        NO2   + 0.920*HO2   + 0.890*GLY
                             + 0.110*MGLY  + 0.050*ACO3  + 0.950*CO
                             + 2.000*XO2
{ 88} TOLP  + NO          -->        NO2   +       HO2   + 0.170*MGLY
                             + 0.160*GLY   + 0.700*DCB
{ 89} XYLP  + NO          -->        NO2   +       HO2   + 0.450*MGLY
                             + 0.806*DCB
{ 90} ETHP  + NO          -->        ALD   +       HO2   +       NO2
{ 91} KETP  + NO          -->        MGLY  +       NO2   +       HO2
{ 92} OLN   + NO          -->        HCHO  +       ALD   + 2.000*NO2
{ 93} HCHO  + NO3         -->        HO2   +       HNO3  +       CO
{ 94} ALD   + NO3         -->        ACO3  +       HNO3
{ 95} GLY   + NO3         -->        HNO3  +       HO2   + 2.000*CO
{ 96} MGLY  + NO3         -->        HNO3  +       ACO3  +       CO
{ 97} DCB   + NO3         -->        HNO3  +       TCO3
{ 98} CSL   + NO3         -->        HNO3  +       XNO2  + 0.500*CSL
{ 99} OL2   + NO3         -->        OLN
{100} OLT   + NO3         -->        OLN
{101} OLI   + NO3         -->        OLN
{102} ISO   + NO3         -->        OLN
{103} OL2   + O3          -->        HCHO  + 0.400*ORA1  + 0.420*CO
                             + 0.120*HO2
{104} OLT   + O3          -->  0.530*HCHO  + 0.500*ALD   + 0.330*CO
                             + 0.200*ORA1  + 0.200*ORA2  + 0.230*HO2
                             + 0.220*MO2   + 0.100*HO
{105} OLI   + O3          -->  0.180*HCHO  + 0.720*ALD   + 0.100*KET
```

Table 8A-7. RADM2 and RADM2_AQ Mechanisms

```
                                    + 0.230*CO     + 0.060*ORA1   + 0.290*ORA2
                                    + 0.260*HO2    + 0.140*HO     + 0.310*MO2
{106} ISO    + O3            -->      0.530*HCHO   + 0.500*ALD    + 0.330*CO
                                    + 0.200*ORA1   + 0.200*ORA2   + 0.230*HO2
                                    + 0.220*MO2    + 0.100*HO
{107} HO2    + MO2           -->          OP1
{108} HO2    + ETHP          -->          OP2
{109} HO2    + HC3P          -->          OP2
{110} HO2    + HC5P          -->          OP2
{111} HO2    + HC8P          -->          OP2
{112} HO2    + OL2P          -->          OP2
{113} HO2    + OLTP          -->          OP2
{114} HO2    + OLIP          -->          OP2
{115} HO2    + KETP          -->          OP2
{116} HO2    + ACO3          -->          PAA
{117} HO2    + TOLP          -->          OP2
{118} HO2    + XYLP          -->          OP2
{119} HO2    + TCO3          -->          OP2
{120} HO2    + OLN           -->          ONIT
{121} MO2    + MO2           -->      1.500*HCHO   +        HO2
{122} MO2    + ETHP          -->      0.750*HCHO   +        HO2    + 0.750*ALD
{123} MO2    + HC3P          -->      0.840*HCHO   + 0.770*ALD    + 0.260*KET
                                    +        HO2
{124} MO2    + HC5P          -->      0.770*HCHO   + 0.410*ALD    + 0.750*KET
                                    +        HO2
{125} MO2    + HC8P          -->      0.800*HCHO   + 0.460*ALD    + 1.390*KET
                                    +        HO2
{126} MO2    + OL2P          -->      1.550*HCHO   + 0.350*ALD    +        HO2
{127} MO2    + OLTP          -->      1.250*HCHO   + 0.750*ALD    +        HO2
{128} MO2    + OLIP          -->      0.890*HCHO   + 0.725*ALD    +        HO2
                                    + 0.550*KET
{129} MO2    + KETP          -->      0.750*HCHO   + 0.750*MGLY   +        HO2
{130} MO2    + ACO3          -->          HCHO     + 0.500*HO2    + 0.500*MO2
                                    + 0.500*ORA2
{131} MO2    + TOLP          -->          HCHO     + 0.170*MGLY   + 0.160*GLY
                                    + 0.700*DCB    + 2.000*HO2
{132} MO2    + XYLP          -->          HCHO     + 0.450*MGLY   + 0.806*DCB
                                    + 2.000*HO2
{133} MO2    + TCO3          -->      0.500*HCHO   + 0.445*GLY    + 0.055*MGLY
                                    + 0.500*ORA2   + 0.025*ACO3   + 0.460*HO2
                                    + 0.475*CO     +        XO2
{134} MO2    + OLN           -->      1.750*HCHO   + 0.500*HO2    +        ALD
                                    +        NO2
{135} ETHP   + ACO3          -->          ALD      + 0.500*HO2    + 0.500*MO2
                                    + 0.500*ORA2
{136} HC3P   + ACO3          -->      0.770*ALD    + 0.260*KET    + 0.500*HO2
                                    + 0.500*MO2    + 0.500*ORA2
{137} HC5P   + ACO3          -->      0.410*ALD    + 0.750*KET    + 0.500*HO2
                                    + 0.500*MO2    + 0.500*ORA2
{138} HC8P   + ACO3          -->      0.460*ALD    + 1.390*KET    + 0.500*HO2
                                    + 0.500*MO2    + 0.500*ORA2
{139} OL2P   + ACO3          -->      0.800*HCHO   + 0.600*ALD    + 0.500*HO2
                                    + 0.500*MO2    + 0.500*ORA2
{140} OLTP   + ACO3          -->          ALD      + 0.500*HCHO   + 0.500*HO2
                                    + 0.500*MO2    + 0.500*ORA2
{141} OLIP   + ACO3          -->      0.725*ALD    + 0.550*KET    + 0.140*HCHO
                                    + 0.500*HO2    + 0.500*MO2    + 0.500*ORA2
{142} KETP   + ACO3          -->          MGLY     + 0.500*HO2    + 0.500*MO2
                                    + 0.500*ORA2
{143} ACO3   + ACO3          -->      2.000*MO2
{144} ACO3   + TOLP          -->          MO2      + 0.170*MGLY   + 0.160*GLY
```

Table 8A-7. RADM2 and RADM2_AQ Mechanisms

```
                                    + 0.700*DCB   +       HO2
{145} ACO3   + XYLP          -->          MO2   + 0.450*MGLY  + 0.806*DCB
                                    +       HO2
{146} ACO3   + TCO3          -->          MO2   + 0.920*HO2   + 0.890*GLY
                                    + 0.110*MGLY  + 0.050*ACO3  + 0.950*CO
                                    + 2.000*XO2
{147} ACO3   + OLN           -->          HCHO  +       ALD   + 0.500*ORA2
                                    +       NO2   + 0.500*MO2
{148} OLN    + OLN           -->    2.000*HCHO  + 2.000*ALD   + 2.000*NO2
{149} XO2    + HO2           -->          OP2
{150} XO2    + MO2           -->          HCHO  +       HO2
{151} XO2    + ACO3          -->          MO2
{152} XO2    + XO2           -->
{153} XO2    + NO            -->          NO2
{154} XNO2   + NO2           -->          ONIT
{155} XNO2   + HO2           -->          OP2
{156} XNO2   + MO2           -->          HCHO  +       HO2
{157} XNO2   + ACO3          -->          MO2
{158} XNO2   + XNO2          -->
>-----------------------------------------------------------------------<


Rate Expression                                                    Rate Constant
==============================================================================
k(  1) uses photo table NO2_RADM88       , scaled by 1.00000E+00   {0.00000E+00}
k(  2) uses photo table O3O1D_RADM88     , scaled by 1.00000E+00   {0.00000E+00}
k(  3) uses photo table O3O3P_RADM88     , scaled by 1.00000E+00   {0.00000E+00}
k(  4) uses photo table HONO_RADM88      , scaled by 1.00000E+00   {0.00000E+00}
k(  5) uses photo table HNO3_RADM88      , scaled by 1.00000E+00   {0.00000E+00}
k(  6) uses photo table HNO4_RADM88      , scaled by 1.00000E+00   {0.00000E+00}
k(  7) uses photo table NO3NO_RADM88     , scaled by 1.00000E+00   {0.00000E+00}
k(  8) uses photo table NO3NO2_RADM88    , scaled by 1.00000E+00   {0.00000E+00}
k(  9) uses photo table H2O2_RADM88      , scaled by 1.00000E+00   {0.00000E+00}
k( 10) uses photo table HCHOmol_RADM88   , scaled by 1.00000E+00   {0.00000E+00}
k( 11) uses photo table HCHOrad_RADM88   , scaled by 1.00000E+00   {0.00000E+00}
k( 12) uses photo table ALD_RADM88       , scaled by 1.00000E+00   {0.00000E+00}
k( 13) uses photo table MHP_RADM88       , scaled by 1.00000E+00   {0.00000E+00}
k( 14) uses photo table HOP_RADM88       , scaled by 1.00000E+00   {0.00000E+00}
k( 15) uses photo table PAA_RADM88       , scaled by 1.00000E+00   {0.00000E+00}
k( 16) uses photo table KETONE_RADM88    , scaled by 1.00000E+00   {0.00000E+00}
k( 17) uses photo table GLYform_RADM88   , scaled by 1.00000E+00   {0.00000E+00}
k( 18) uses photo table GLYmol_RADM88    , scaled by 1.00000E+00   {0.00000E+00}
k( 19) uses photo table MGLY_RADM88      , scaled by 1.00000E+00   {0.00000E+00}
k( 20) uses photo table UDC_RADM88       , scaled by 1.00000E+00   {0.00000E+00}
k( 21) uses photo table ORGNIT_RADM88    , scaled by 1.00000E+00   {0.00000E+00}
k( 22) =  6.0000E-34 * (T/300)**(-2.30)                            {6.09302E-34}
k( 23) =  6.5000E-12 * exp(   120.0/T)                             {9.72293E-12}
k( 24) =  1.8000E-11 * exp(   110.0/T)                             {2.60365E-11}
k( 25) =  3.2000E-11 * exp(    70.0/T)                             {4.04730E-11}
k( 26) =  2.2000E-10                                               {2.20000E-10}
k( 27) =  2.0000E-12 * exp( -1400.0/T)                             {1.82272E-14}
k( 28) =  1.6000E-12 * exp(  -940.0/T)                             {6.82650E-14}
k( 29) =  1.1000E-14 * exp(  -500.0/T)                             {2.05452E-15}
k( 30) =  3.7000E-12 * exp(   240.0/T)                             {8.27883E-12}
k( 31) is a falloff expression using:                              {1.39058E-12}
   k0   =  1.8000E-31 * (T/300)**(-3.20)
   kinf =  4.7000E-12 * (T/300)**(-1.40)
   F =  0.60,  n =  1.00
k( 32) = k( 31) / Keq,  where Keq =  2.100E-27 * exp( 10900.0/T)   {8.62399E-02}
k( 33) is a special rate expression of the form:                   {3.01634E-12}
   k = k1 + k2[M], where
```

Table 8A-7. RADM2 and RADM2_AQ Mechanisms

```
   k1 =  2.2000E-13 * exp(   620.0/T)
   k2 =  1.9000E-33 * exp(   980.0/T)
k( 34) is a special rate expression of the form:                    {6.78905E-30}
   k = k1 + k2[M], where
   k1 =  3.0800E-34 * exp(  2820.0/T)
   k2 =  2.6600E-54 * exp(  3180.0/T)
k( 35) =  3.3000E-12 * exp(  -200.0/T)                              {1.68671E-12}
k( 36) is a falloff expression using:                               {4.87144E-12}
   k0   =  7.0000E-31 * (T/300)**(-2.60)
   kinf =  1.5000E-11 * (T/300)**(-0.50)
   F =  0.60,  n =  1.00
k( 37) =  3.3000E-39 * exp(   530.0/T)                              {1.95397E-38}
k( 38) =  1.4000E-13 * exp( -2500.0/T)                              {3.18213E-17}
k( 39) =  1.7000E-11 * exp(   150.0/T)                              {2.81225E-11}
k( 40) =  2.5000E-14 * exp( -1230.0/T)                              {4.03072E-16}
k( 41) =  2.5000E-12                                                {2.50000E-12}
k( 42) is a falloff expression using:                               {1.26440E-12}
   k0   =  2.2000E-30 * (T/300)**(-4.30)
   kinf =  1.5000E-12 * (T/300)**(-0.50)
   F =  0.60,  n =  1.00
k( 43) = k( 42) / Keq,  where Keq =  1.100E-27 * exp( 11200.0/T)    {5.47034E-02}
k( 44) =  2.0000E-21                                                {2.00000E-21}
k( 45) is a falloff expression using:                               {1.14885E-11}
   k0   =  2.6000E-30 * (T/300)**(-3.20)
   kinf =  2.4000E-11 * (T/300)**(-1.30)
   F =  0.60,  n =  1.00
k( 46) is a special rate expression of the form:                    {1.47236E-13}
   k = k0 + {k3[M] / (1 + k3[M]/k2)}, where
   k0 =  7.2000E-15 * exp(   785.0/T)
   k2 =  4.1000E-16 * exp(  1440.0/T)
   k3 =  1.9000E-33 * exp(   725.0/T)
k( 47) =  1.3000E-12 * exp(   380.0/T)                              {4.65309E-12}
k( 48) =  4.6000E-11 * exp(   230.0/T)                              {9.95294E-11}
k( 49) is a falloff expression using:                               {8.88848E-13}
   k0   =  3.0000E-31 * (T/300)**(-3.30)
   kinf =  1.5000E-12 * (T/300)**( 0.00)
   F =  0.60,  n =  1.00
k( 50) =  1.5000E-13 * (1.0 + 0.6*Pressure)                         {2.40000E-13}
k( 51) =  2.8300E+01 * (T/300)**( 2.00) * exp( -1280.0/T)           {3.80672E-01}
k( 52) =  1.2330E-12 * (T/300)**( 2.00) * exp(  -444.0/T)           {2.74210E-13}
k( 53) =  1.5900E-11 * exp(  -540.0/T)                              {2.59669E-12}
k( 54) =  1.7300E-11 * exp(  -380.0/T)                              {4.83334E-12}
k( 55) =  3.6400E-11 * exp(  -380.0/T)                              {1.01696E-11}
k( 56) =  2.1500E-12 * exp(   411.0/T)                              {8.53916E-12}
k( 57) =  5.3200E-12 * exp(   504.0/T)                              {2.88684E-11}
k( 58) =  1.0700E-11 * exp(   549.0/T)                              {6.75269E-11}
k( 59) =  2.1000E-12 * exp(   322.0/T)                              {6.18715E-12}
k( 60) =  1.8900E-11 * exp(   116.0/T)                              {2.78943E-11}
k( 61) =  4.0000E-11                                                {4.00000E-11}
k( 62) =  9.0000E-01 * k( 61)                                       {3.60000E-11}
k( 63) =  9.0000E-12                                                {9.00000E-12}
k( 64) =  6.8700E-12 * exp(   256.0/T)                              {1.62197E-11}
k( 65) =  1.2000E-11 * exp(  -745.0/T)                              {9.85020E-13}
k( 66) =  1.1500E-11                                                {1.15000E-11}
k( 67) =  1.7000E-11                                                {1.70000E-11}
k( 68) =  2.8000E-11                                                {2.80000E-11}
k( 69) =  1.0000E-11                                                {1.00000E-11}
k( 70) =  1.0000E-11                                                {1.00000E-11}
k( 71) =  1.0000E-11                                                {1.00000E-11}
k( 72) =  6.1650E-13 * (T/300)**( 2.00) * exp(  -444.0/T)           {1.37105E-13}
k( 73) =  1.5500E-11 * exp(  -540.0/T)                              {2.53137E-12}
```

Table 8A-7. RADM2 and RADM2_AQ Mechanisms

```
k( 74) =  2.5500E-11 * exp(   409.0/T)                    {1.00601E-10}
k( 75) =  2.8000E-12 * exp(   181.0/T)                    {5.13974E-12}
k( 76) =  1.9500E+16 * exp(-13543.0/T)                    {3.57235E-04}
k( 77) =  4.7000E-12                                      {4.70000E-12}
k( 78) =  1.9500E+16 * exp(-13543.0/T)                    {3.57235E-04}
k( 79) =  4.2000E-12 * exp(   180.0/T)                    {7.68378E-12}
k( 80) =  4.2000E-12 * exp(   180.0/T)                    {7.68378E-12}
k( 81) =  4.2000E-12 * exp(   180.0/T)                    {7.68378E-12}
k( 82) =  4.2000E-12 * exp(   180.0/T)                    {7.68378E-12}
k( 83) =  4.2000E-12 * exp(   180.0/T)                    {7.68378E-12}
k( 84) =  4.2000E-12 * exp(   180.0/T)                    {7.68378E-12}
k( 85) =  4.2000E-12 * exp(   180.0/T)                    {7.68378E-12}
k( 86) =  4.2000E-12 * exp(   180.0/T)                    {7.68378E-12}
k( 87) =  4.2000E-12 * exp(   180.0/T)                    {7.68378E-12}
k( 88) =  4.2000E-12 * exp(   180.0/T)                    {7.68378E-12}
k( 89) =  4.2000E-12 * exp(   180.0/T)                    {7.68378E-12}
k( 90) =  4.2000E-12 * exp(   180.0/T)                    {7.68378E-12}
k( 91) =  4.2000E-12 * exp(   180.0/T)                    {7.68378E-12}
k( 92) =  4.2000E-12 * exp(   180.0/T)                    {7.68378E-12}
k( 93) =  6.0000E-13 * exp( -2058.0/T)                    {6.01030E-16}
k( 94) =  1.4000E-12 * exp( -1900.0/T)                    {2.38307E-15}
k( 95) =  6.0000E-13 * exp( -2058.0/T)                    {6.01030E-16}
k( 96) =  1.4000E-12 * exp( -1900.0/T)                    {2.38307E-15}
k( 97) =  1.4000E-12 * exp( -1900.0/T)                    {2.38307E-15}
k( 98) =  2.2000E-11                                      {2.20000E-11}
k( 99) =  2.0000E-12 * exp( -2923.0/T)                    {1.09940E-16}
k(100) =  1.0000E-11 * exp( -1895.0/T)                    {1.73099E-14}
k(101) =  3.2300E-11 * exp(  -975.0/T)                    {1.22539E-12}
k(102) =  5.8100E-13                                      {5.81000E-13}
k(103) =  1.2000E-14 * exp( -2633.0/T)                    {1.74559E-18}
k(104) =  1.3200E-14 * exp( -2105.0/T)                    {1.12933E-17}
k(105) =  7.2900E-15 * exp( -1136.0/T)                    {1.61125E-16}
k(106) =  1.2300E-14 * exp( -2013.0/T)                    {1.43295E-17}
k(107) =  7.7000E-14 * exp(  1300.0/T)                    {6.04038E-12}
k(108) =  7.7000E-14 * exp(  1300.0/T)                    {6.04038E-12}
k(109) =  7.7000E-14 * exp(  1300.0/T)                    {6.04038E-12}
k(110) =  7.7000E-14 * exp(  1300.0/T)                    {6.04038E-12}
k(111) =  7.7000E-14 * exp(  1300.0/T)                    {6.04038E-12}
k(112) =  7.7000E-14 * exp(  1300.0/T)                    {6.04038E-12}
k(113) =  7.7000E-14 * exp(  1300.0/T)                    {6.04038E-12}
k(114) =  7.7000E-14 * exp(  1300.0/T)                    {6.04038E-12}
k(115) =  7.7000E-14 * exp(  1300.0/T)                    {6.04038E-12}
k(116) =  7.7000E-14 * exp(  1300.0/T)                    {6.04038E-12}
k(117) =  7.7000E-14 * exp(  1300.0/T)                    {6.04038E-12}
k(118) =  7.7000E-14 * exp(  1300.0/T)                    {6.04038E-12}
k(119) =  7.7000E-14 * exp(  1300.0/T)                    {6.04038E-12}
k(120) =  7.7000E-14 * exp(  1300.0/T)                    {6.04038E-12}
k(121) =  1.9000E-13 * exp(   220.0/T)                    {3.97533E-13}
k(122) =  1.4000E-13 * exp(   220.0/T)                    {2.92919E-13}
k(123) =  4.2000E-14 * exp(   220.0/T)                    {8.78758E-14}
k(124) =  3.4000E-14 * exp(   220.0/T)                    {7.11376E-14}
k(125) =  2.9000E-14 * exp(   220.0/T)                    {6.06762E-14}
k(126) =  1.4000E-13 * exp(   220.0/T)                    {2.92919E-13}
k(127) =  1.4000E-13 * exp(   220.0/T)                    {2.92919E-13}
k(128) =  1.7000E-14 * exp(   220.0/T)                    {3.55688E-14}
k(129) =  1.7000E-14 * exp(   220.0/T)                    {3.55688E-14}
k(130) =  9.6000E-13 * exp(   220.0/T)                    {2.00859E-12}
k(131) =  1.7000E-14 * exp(   220.0/T)                    {3.55688E-14}
k(132) =  1.7000E-14 * exp(   220.0/T)                    {3.55688E-14}
k(133) =  9.6000E-13 * exp(   220.0/T)                    {2.00859E-12}
k(134) =  1.7000E-14 * exp(   220.0/T)                    {3.55688E-14}
```

Table 8A-7. RADM2 and RADM2_AQ Mechanisms

```
k(135) =  3.4000E-13 * exp(   220.0/T)                          {7.11376E-13}
k(136) =  1.0000E-13 * exp(   220.0/T)                          {2.09228E-13}
k(137) =  8.4000E-14 * exp(   220.0/T)                          {1.75752E-13}
k(138) =  7.2000E-14 * exp(   220.0/T)                          {1.50644E-13}
k(139) =  3.4000E-13 * exp(   220.0/T)                          {7.11376E-13}
k(140) =  3.4000E-13 * exp(   220.0/T)                          {7.11376E-13}
k(141) =  4.2000E-14 * exp(   220.0/T)                          {8.78758E-14}
k(142) =  4.2000E-14 * exp(   220.0/T)                          {8.78758E-14}
k(143) =  1.1900E-12 * exp(   220.0/T)                          {2.48981E-12}
k(144) =  4.2000E-14 * exp(   220.0/T)                          {8.78758E-14}
k(145) =  4.2000E-14 * exp(   220.0/T)                          {8.78758E-14}
k(146) =  1.1900E-12 * exp(   220.0/T)                          {2.48981E-12}
k(147) =  4.2000E-14 * exp(   220.0/T)                          {8.78758E-14}
k(148) =  3.6000E-16 * exp(   220.0/T)                          {7.53221E-16}
k(149) =  7.7000E-14 * exp(  1300.0/T)                          {6.04038E-12}
k(150) =  1.7000E-14 * exp(   220.0/T)                          {3.55688E-14}
k(151) =  4.2000E-14 * exp(   220.0/T)                          {8.78758E-14}
k(152) =  3.6000E-16 * exp(   220.0/T)                          {7.53221E-16}
k(153) =  4.2000E-12 * exp(   180.0/T)                          {7.68378E-12}
k(154) =  4.2000E-12 * exp(   180.0/T)                          {7.68378E-12}
k(155) =  7.7000E-14 * exp(  1300.0/T)                          {6.04038E-12}
k(156) =  1.7000E-14 * exp(   220.0/T)                          {3.55688E-14}
k(157) =  4.2000E-14 * exp(   220.0/T)                          {8.78758E-14}
k(158) =  3.6000E-16 * exp(   220.0/T)                          {7.53221E-16}
==============================================================================
```

Table 8A-8. RADM2_AE and RADM2_AE_AQ Mechanisms

```
Reaction List
>-----------------------------------------------------------------------------------------<
{  1} NO2      + hv                  -->          O3P      +        NO
{  2} O3       + hv                  -->          O1D
{  3} O3       + hv                  -->          O3P
{  4} HONO     + hv                  -->          HO       +        NO
{  5} HNO3     + hv                  -->          HO       +        NO2
{  6} HNO4     + hv                  -->          HO2      +        NO2
{  7} NO3      + hv                  -->          NO
{  8} NO3      + hv                  -->          NO2      +        O3P
{  9} H2O2     + hv                  -->    2.000*HO
{ 10} HCHO     + hv                  -->          CO
{ 11} HCHO     + hv                  -->          HO2      +        HO2      +        CO
{ 12} ALD      + hv                  -->          MO2      +        HO2      +        CO
{ 13} OP1      + hv                  -->          HCHO     +        HO2      +        HO
{ 14} OP2      + hv                  -->          ALD      +        HO2      +        HO
{ 15} PAA      + hv                  -->          MO2      +        HO
{ 16} KET      + hv                  -->          ACO3     +        ETHP
{ 17} GLY      + hv                  -->    0.130*HCHO     + 1.870*CO
{ 18} GLY      + hv                  -->    0.450*HCHO     + 1.550*CO       + 0.800*HO2
{ 19} MGLY     + hv                  -->          ACO3     +        HO2      +        CO
{ 20} DCB      + hv                  -->    0.980*HO2      + 0.020*ACO3     +        TCO3
{ 21} ONIT     + hv                  -->    0.200*ALD      + 0.800*KET      +        HO2
                                         +        NO2
{ 22} O3P      + [M]      + [O2]     -->          O3
{ 23} O3P      + NO2                 -->          NO
{ 24} O1D      + [N2]                -->          O3P
{ 25} O1D      + [O2]                -->          O3P
{ 26} O1D      + [H2O]               -->    2.000*HO
{ 27} O3       + NO                  -->          NO2
{ 28} O3       + HO                  -->          HO2
{ 29} O3       + HO2                 -->          HO
{ 30} HO2      + NO                  -->          NO2      +        HO
{ 31} HO2      + NO2                 -->          HNO4
{ 32} HNO4                           -->          HO2      +        NO2
{ 33} HO2      + HO2                 -->          H2O2
{ 34} HO2      + HO2      + [H2O]    -->          H2O2
{ 35} H2O2     + HO                  -->          HO2
{ 36} NO       + HO                  -->          HONO
{ 37} NO       + NO       + [O2]     -->    2.000*NO2
{ 38} O3       + NO2                 -->          NO3
{ 39} NO3      + NO                  -->    2.000*NO2
{ 40} NO3      + NO2                 -->          NO       +        NO2
{ 41} NO3      + HO2                 -->          HNO3
{ 42} NO3      + NO2                 -->          N2O5
{ 43} N2O5                           -->          NO2      +        NO3
{ 44} N2O5     + [H2O]               -->    2.000*HNO3
{ 45} HO       + NO2                 -->          HNO3
{ 46} HO       + HNO3                -->          NO3
{ 47} HO       + HNO4                -->          NO2
{ 48} HO       + HO2                 -->
{ 49} HO       + SO2                 -->          SULF     +        HO2      +        SULAER
{ 50} CO       + HO                  -->          HO2
{ 51} HO                             -->          MO2
{ 52} ETH      + HO                  -->          ETHP
{ 53} HC3      + HO                  -->    0.830*HC3P     + 0.170*HO2      + 0.009*HCHO
                                         + 0.075*ALD      + 0.025*KET
{ 54} HC5      + HO                  -->          HC5P     + 0.250*XO2
{ 55} HC8      + HO                  -->          HC8P     + 0.750*XO2      +        HC8AER
{ 56} OL2      + HO                  -->          OL2P
{ 57} OLT      + HO                  -->          OLTP
```

Table 8A-8. RADM2_AE and RADM2_AE_AQ Mechanisms

```
{ 58} OLI     + HO                 -->          OLIP     +        OLIAER
{ 59} TOL     + HO                 -->   0.750*TOLP      + 0.250*CSL      + 0.250*HO2
                                   +          TOLAER
{ 60} XYL     + HO                 -->   0.830*XYLP      + 0.170*CSL      + 0.170*HO2
                                   +          XYLAER
{ 61} CSL     + HO                 -->   0.100*HO2       + 0.900*XO2      + 0.900*TCO3
                                   +          CSLAER
{ 62} CSL     + HO                 -->          CSL
{ 63} HCHO    + HO                 -->          HO2      +        CO
{ 64} ALD     + HO                 -->          ACO3
{ 65} KET     + HO                 -->          KETP
{ 66} GLY     + HO                 -->          HO2      + 2.000*CO
{ 67} MGLY    + HO                 -->          ACO3     +        CO
{ 68} DCB     + HO                 -->          TCO3
{ 69} OP1     + HO                 -->   0.500*MO2       + 0.500*HCHO     + 0.500*HO
{ 70} OP2     + HO                 -->   0.500*HC3P      + 0.500*ALD      + 0.500*HO
{ 71} PAA     + HO                 -->          ACO3
{ 72} PAN     + HO                 -->          HCHO     +        NO3      +        XO2
{ 73} ONIT    + HO                 -->          HC3P     +        NO2
{ 74} ISO     + HO                 -->          OLTP
{ 75} ACO3    + NO2                -->          PAN
{ 76} PAN                          -->          ACO3     +        NO2
{ 77} TCO3    + NO2                -->          TPAN
{ 78} TPAN                         -->          TCO3     +        NO2
{ 79} MO2     + NO                 -->          HCHO     +        HO2      +        NO2
{ 80} HC3P    + NO                 -->   0.750*ALD       + 0.250*KET      + 0.090*HCHO
                                   + 0.036*ONIT          + 0.964*NO2      + 0.964*HO2
{ 81} HC5P    + NO                 -->   0.380*ALD       + 0.690*KET      + 0.080*ONIT
                                   + 0.920*NO2           + 0.920*HO2
{ 82} HC8P    + NO                 -->   0.350*ALD       + 1.060*KET      + 0.040*HCHO
                                   + 0.240*ONIT          + 0.760*NO2      + 0.760*HO2
{ 83} OL2P    + NO                 -->   1.600*HCHO      +        HO2      +        NO2
                                   + 0.200*ALD
{ 84} OLTP    + NO                 -->          ALD      +        HCHO     +        HO2
                                   +          NO2
{ 85} OLIP    + NO                 -->          HO2      + 1.450*ALD      + 0.280*HCHO
                                   + 0.100*KET           +        NO2
{ 86} ACO3    + NO                 -->          MO2      +        NO2
{ 87} TCO3    + NO                 -->          NO2      + 0.920*HO2      + 0.890*GLY
                                   + 0.110*MGLY          + 0.050*ACO3     + 0.950*CO
                                   + 2.000*XO2
{ 88} TOLP    + NO                 -->          NO2      +        HO2      + 0.170*MGLY
                                   + 0.160*GLY           + 0.700*DCB
{ 89} XYLP    + NO                 -->          NO2      +        HO2      + 0.450*MGLY
                                   + 0.806*DCB
{ 90} ETHP    + NO                 -->          ALD      +        HO2      +        NO2
{ 91} KETP    + NO                 -->          MGLY     +        NO2      +        HO2
{ 92} OLN     + NO                 -->          HCHO     +        ALD      + 2.000*NO2
{ 93} HCHO    + NO3                -->          HO2      +        HNO3     +        CO
{ 94} ALD     + NO3                -->          ACO3     +        HNO3
{ 95} GLY     + NO3                -->          HNO3     +        HO2      + 2.000*CO
{ 96} MGLY    + NO3                -->          HNO3     +        ACO3     +        CO
{ 97} DCB     + NO3                -->          HNO3     +        TCO3
{ 98} CSL     + NO3                -->          HNO3     +        XNO2     + 0.500*CSL
                                   + 0.500*CSLAER
{ 99} OL2     + NO3                -->          OLN
{100} OLT     + NO3                -->          OLN
{101} OLI     + NO3                -->          OLN      +        OLIAER
{102} ISO     + NO3                -->          OLN
{103} OL2     + O3                 -->          HCHO     + 0.400*ORA1     + 0.420*CO
                                   + 0.120*HO2
```

Table 8A-8. RADM2_AE and RADM2_AE_AQ Mechanisms

```
{104} OLT     + O3          -->  0.530*HCHO    + 0.500*ALD     + 0.330*CO
                                 + 0.200*ORA1    + 0.200*ORA2    + 0.230*HO2
                                 + 0.220*MO2     + 0.100*HO
{105} OLI     + O3          -->  0.180*HCHO    + 0.720*ALD     + 0.100*KET
                                 + 0.230*CO      + 0.060*ORA1    + 0.290*ORA2
                                 + 0.260*HO2     + 0.140*HO      + 0.310*MO2
                                 +       OLIAER
{106} ISO     + O3          -->  0.530*HCHO    + 0.500*ALD     + 0.330*CO
                                 + 0.200*ORA1    + 0.200*ORA2    + 0.230*HO2
                                 + 0.220*MO2     + 0.100*HO
{107} HO2     + MO2         -->         OP1
{108} HO2     + ETHP        -->         OP2
{109} HO2     + HC3P        -->         OP2
{110} HO2     + HC5P        -->         OP2
{111} HO2     + HC8P        -->         OP2
{112} HO2     + OL2P        -->         OP2
{113} HO2     + OLTP        -->         OP2
{114} HO2     + OLIP        -->         OP2
{115} HO2     + KETP        -->         OP2
{116} HO2     + ACO3        -->         PAA
{117} HO2     + TOLP        -->         OP2
{118} HO2     + XYLP        -->         OP2
{119} HO2     + TCO3        -->         OP2
{120} HO2     + OLN         -->         ONIT
{121} MO2     + MO2         -->  1.500*HCHO    +       HO2
{122} MO2     + ETHP        -->  0.750*HCHO    +       HO2     + 0.750*ALD
{123} MO2     + HC3P        -->  0.840*HCHO    + 0.770*ALD     + 0.260*KET
                                 +       HO2
{124} MO2     + HC5P        -->  0.770*HCHO    + 0.410*ALD     + 0.750*KET
                                 +       HO2
{125} MO2     + HC8P        -->  0.800*HCHO    + 0.460*ALD     + 1.390*KET
                                 +       HO2
{126} MO2     + OL2P        -->  1.550*HCHO    + 0.350*ALD     +       HO2
{127} MO2     + OLTP        -->  1.250*HCHO    + 0.750*ALD     +       HO2
{128} MO2     + OLIP        -->  0.890*HCHO    + 0.725*ALD     +       HO2
                                 + 0.550*KET
{129} MO2     + KETP        -->  0.750*HCHO    + 0.750*MGLY    +       HO2
{130} MO2     + ACO3        -->         HCHO   + 0.500*HO2     + 0.500*MO2
                                 + 0.500*ORA2
{131} MO2     + TOLP        -->         HCHO   + 0.170*MGLY    + 0.160*GLY
                                 + 0.700*DCB     + 2.000*HO2
{132} MO2     + XYLP        -->         HCHO   + 0.450*MGLY    + 0.806*DCB
                                 + 2.000*HO2
{133} MO2     + TCO3        -->  0.500*HCHO    + 0.445*GLY     + 0.055*MGLY
                                 + 0.500*ORA2    + 0.025*ACO3    + 0.460*HO2
                                 + 0.475*CO      +       XO2
{134} MO2     + OLN         -->  1.750*HCHO    + 0.500*HO2     +       ALD
                                 +       NO2
{135} ETHP    + ACO3        -->         ALD    + 0.500*HO2     + 0.500*MO2
                                 + 0.500*ORA2
{136} HC3P    + ACO3        -->  0.770*ALD     + 0.260*KET     + 0.500*HO2
                                 + 0.500*MO2     + 0.500*ORA2
{137} HC5P    + ACO3        -->  0.410*ALD     + 0.750*KET     + 0.500*HO2
                                 + 0.500*MO2     + 0.500*ORA2
{138} HC8P    + ACO3        -->  0.460*ALD     + 1.390*KET     + 0.500*HO2
                                 + 0.500*MO2     + 0.500*ORA2
{139} OL2P    + ACO3        -->  0.800*HCHO    + 0.600*ALD     + 0.500*HO2
                                 + 0.500*MO2     + 0.500*ORA2
{140} OLTP    + ACO3        -->         ALD    + 0.500*HCHO    + 0.500*HO2
                                 + 0.500*MO2     + 0.500*ORA2
{141} OLIP    + ACO3        -->  0.725*ALD     + 0.550*KET     + 0.140*HCHO
```

Table 8A-8. RADM2_AE and RADM2_AE_AQ Mechanisms

```
                                        + 0.500*HO2      + 0.500*MO2      + 0.500*ORA2
{142} KETP    + ACO3              -->          MGLY      + 0.500*HO2      + 0.500*MO2
                                        + 0.500*ORA2
{143} ACO3    + ACO3              -->    2.000*MO2
{144} ACO3    + TOLP              -->          MO2       + 0.170*MGLY     + 0.160*GLY
                                        + 0.700*DCB       +        HO2
{145} ACO3    + XYLP              -->          MO2       + 0.450*MGLY     + 0.806*DCB
                                        +        HO2
{146} ACO3    + TCO3              -->          MO2       + 0.920*HO2      + 0.890*GLY
                                        + 0.110*MGLY      + 0.050*ACO3     + 0.950*CO
                                        + 2.000*XO2
{147} ACO3    + OLN               -->          HCHO      +        ALD     + 0.500*ORA2
                                        +        NO2       + 0.500*MO2
{148} OLN     + OLN               -->    2.000*HCHO      + 2.000*ALD      + 2.000*NO2
{149} XO2     + HO2               -->          OP2
{150} XO2     + MO2               -->          HCHO      +        HO2
{151} XO2     + ACO3              -->          MO2
{152} XO2     + XO2               -->
{153} XO2     + NO                -->          NO2
{154} XNO2    + NO2               -->          ONIT
{155} XNO2    + HO2               -->          OP2
{156} XNO2    + MO2               -->          HCHO      +        HO2
{157} XNO2    + ACO3              -->          MO2
{158} XNO2    + XNO2              -->
{159} TERP    + HO                -->          TERPAER +        HO
{160} TERP    + NO3               -->          TERPAER +        NO3
{161} TERP    + O3                -->          TERPAER +        O3
>-------------------------------------------------------------------------------------<
```

```
Rate Expression                                                        Rate Constant
=========================================================================================
k(  1) uses photo table NO2_RADM88       , scaled by 1.00000E+00    {0.00000E+00}
k(  2) uses photo table O3O1D_RADM88     , scaled by 1.00000E+00    {0.00000E+00}
k(  3) uses photo table O3O3P_RADM88     , scaled by 1.00000E+00    {0.00000E+00}
k(  4) uses photo table HONO_RADM88      , scaled by 1.00000E+00    {0.00000E+00}
k(  5) uses photo table HNO3_RADM88      , scaled by 1.00000E+00    {0.00000E+00}
k(  6) uses photo table HNO4_RADM88      , scaled by 1.00000E+00    {0.00000E+00}
k(  7) uses photo table NO3NO_RADM88     , scaled by 1.00000E+00    {0.00000E+00}
k(  8) uses photo table NO3NO2_RADM88    , scaled by 1.00000E+00    {0.00000E+00}
k(  9) uses photo table H2O2_RADM88      , scaled by 1.00000E+00    {0.00000E+00}
k( 10) uses photo table HCHOmol_RADM88   , scaled by 1.00000E+00    {0.00000E+00}
k( 11) uses photo table HCHOrad_RADM88   , scaled by 1.00000E+00    {0.00000E+00}
k( 12) uses photo table ALD_RADM88       , scaled by 1.00000E+00    {0.00000E+00}
k( 13) uses photo table MHP_RADM88       , scaled by 1.00000E+00    {0.00000E+00}
k( 14) uses photo table HOP_RADM88       , scaled by 1.00000E+00    {0.00000E+00}
k( 15) uses photo table PAA_RADM88       , scaled by 1.00000E+00    {0.00000E+00}
k( 16) uses photo table KETONE_RADM88    , scaled by 1.00000E+00    {0.00000E+00}
k( 17) uses photo table GLYform_RADM88   , scaled by 1.00000E+00    {0.00000E+00}
k( 18) uses photo table GLYmol_RADM88    , scaled by 1.00000E+00    {0.00000E+00}
k( 19) uses photo table MGLY_RADM88      , scaled by 1.00000E+00    {0.00000E+00}
k( 20) uses photo table UDC_RADM88       , scaled by 1.00000E+00    {0.00000E+00}
k( 21) uses photo table ORGNIT_RADM88    , scaled by 1.00000E+00    {0.00000E+00}
k( 22) =  6.0000E-34 * (T/300)**(-2.30)                             {6.09302E-34}
k( 23) =  6.5000E-12 * exp(   120.0/T)                              {9.72293E-12}
k( 24) =  1.8000E-11 * exp(   110.0/T)                              {2.60365E-11}
k( 25) =  3.2000E-11 * exp(    70.0/T)                              {4.04730E-11}
k( 26) =  2.2000E-10                                                {2.20000E-10}
k( 27) =  2.0000E-12 * exp( -1400.0/T)                              {1.82272E-14}
k( 28) =  1.6000E-12 * exp(  -940.0/T)                              {6.82650E-14}
k( 29) =  1.1000E-14 * exp(  -500.0/T)                              {2.05452E-15}
```

Table 8A-8. RADM2_AE and RADM2_AE_AQ Mechanisms

```
k( 30) =  3.7000E-12 * exp(   240.0/T)                          {8.27883E-12}
k( 31) is a falloff expression using:                           {1.39058E-12}
   k0   =  1.8000E-31 * (T/300)**(-3.20)
   kinf =  4.7000E-12 * (T/300)**(-1.40)
   F =  0.60,  n =  1.00
k( 32) = k( 31) / Keq,  where Keq =  2.100E-27 * exp( 10900.0/T)  {8.62399E-02}
k( 33) is a special rate expression of the form:                {3.01634E-12}
   k = k1 + k2[M], where
   k1 =  2.2000E-13 * exp(   620.0/T)
   k2 =  1.9000E-33 * exp(   980.0/T)
k( 34) is a special rate expression of the form:                {6.78905E-30}
   k = k1 + k2[M], where
   k1 =  3.0800E-34 * exp(  2820.0/T)
   k2 =  2.6600E-54 * exp(  3180.0/T)
k( 35) =  3.3000E-12 * exp(  -200.0/T)                          {1.68671E-12}
k( 36) is a falloff expression using:                           {4.87144E-12}
   k0   =  7.0000E-31 * (T/300)**(-2.60)
   kinf =  1.5000E-11 * (T/300)**(-0.50)
   F =  0.60,  n =  1.00
k( 37) =  3.3000E-39 * exp(   530.0/T)                          {1.95397E-38}
k( 38) =  1.4000E-13 * exp( -2500.0/T)                          {3.18213E-17}
k( 39) =  1.7000E-11 * exp(   150.0/T)                          {2.81225E-11}
k( 40) =  2.5000E-14 * exp( -1230.0/T)                          {4.03072E-16}
k( 41) =  2.5000E-12                                            {2.50000E-12}
k( 42) is a falloff expression using:                           {1.26440E-12}
   k0   =  2.2000E-30 * (T/300)**(-4.30)
   kinf =  1.5000E-12 * (T/300)**(-0.50)
   F =  0.60,  n =  1.00
k( 43) = k( 42) / Keq,  where Keq =  1.100E-27 * exp( 11200.0/T)  {5.47034E-02}
k( 44) =  2.0000E-21                                            {2.00000E-21}
k( 45) is a falloff expression using:                           {1.14885E-11}
   k0   =  2.6000E-30 * (T/300)**(-3.20)
   kinf =  2.4000E-11 * (T/300)**(-1.30)
   F =  0.60,  n =  1.00
k( 46) is a special rate expression of the form:                {1.47236E-13}
   k = k0 + {k3[M] / (1 + k3[M]/k2)}, where
   k0 =  7.2000E-15 * exp(   785.0/T)
   k2 =  4.1000E-16 * exp(  1440.0/T)
   k3 =  1.9000E-33 * exp(   725.0/T)
k( 47) =  1.3000E-12 * exp(   380.0/T)                          {4.65309E-12}
k( 48) =  4.6000E-11 * exp(   230.0/T)                          {9.95294E-11}
k( 49) is a falloff expression using:                           {8.88848E-13}
   k0   =  3.0000E-31 * (T/300)**(-3.30)
   kinf =  1.5000E-12 * (T/300)**( 0.00)
   F =  0.60,  n =  1.00
k( 50) =  1.5000E-13 * (1.0 + 0.6*Pressure)                     {2.40000E-13}
k( 51) =  2.8300E+01 * (T/300)**( 2.00) * exp( -1280.0/T)       {3.80672E-01}
k( 52) =  1.2330E-12 * (T/300)**( 2.00) * exp(  -444.0/T)       {2.74210E-13}
k( 53) =  1.5900E-11 * exp( -540.0/T)                           {2.59669E-12}
k( 54) =  1.7300E-11 * exp(  -380.0/T)                          {4.83334E-12}
k( 55) =  3.6400E-11 * exp(  -380.0/T)                          {1.01696E-11}
k( 56) =  2.1500E-12 * exp(   411.0/T)                          {8.53916E-12}
k( 57) =  5.3200E-12 * exp(   504.0/T)                          {2.88684E-11}
k( 58) =  1.0700E-11 * exp(   549.0/T)                          {6.75269E-11}
k( 59) =  2.1000E-12 * exp(   322.0/T)                          {6.18715E-12}
k( 60) =  1.8900E-11 * exp(   116.0/T)                          {2.78943E-11}
k( 61) =  4.0000E-11                                            {4.00000E-11}
k( 62) =  9.0000E-01 * k( 61)                                   {3.60000E-11}
k( 63) =  9.0000E-12                                            {9.00000E-12}
k( 64) =  6.8700E-12 * exp(   256.0/T)                          {1.62197E-11}
k( 65) =  1.2000E-11 * exp(  -745.0/T)                          {9.85020E-13}
```

Table 8A-8. RADM2_AE and RADM2_AE_AQ Mechanisms

```
k( 66) =  1.1500E-11                                                    {1.15000E-11}
k( 67) =  1.7000E-11                                                    {1.70000E-11}
k( 68) =  2.8000E-11                                                    {2.80000E-11}
k( 69) =  1.0000E-11                                                    {1.00000E-11}
k( 70) =  1.0000E-11                                                    {1.00000E-11}
k( 71) =  1.0000E-11                                                    {1.00000E-11}
k( 72) =  6.1650E-13 * (T/300)**( 2.00) * exp(  -444.0/T)               {1.37105E-13}
k( 73) =  1.5500E-11 * exp(  -540.0/T)                                  {2.53137E-12}
k( 74) =  2.5500E-11 * exp(   409.0/T)                                  {1.00601E-10}
k( 75) =  2.8000E-12 * exp(   181.0/T)                                  {5.13974E-12}
k( 76) =  1.9500E+16 * exp(-13543.0/T)                                  {3.57235E-04}
k( 77) =  4.7000E-12                                                    {4.70000E-12}
k( 78) =  1.9500E+16 * exp(-13543.0/T)                                  {3.57235E-04}
k( 79) =  4.2000E-12 * exp(   180.0/T)                                  {7.68378E-12}
k( 80) =  4.2000E-12 * exp(   180.0/T)                                  {7.68378E-12}
k( 81) =  4.2000E-12 * exp(   180.0/T)                                  {7.68378E-12}
k( 82) =  4.2000E-12 * exp(   180.0/T)                                  {7.68378E-12}
k( 83) =  4.2000E-12 * exp(   180.0/T)                                  {7.68378E-12}
k( 84) =  4.2000E-12 * exp(   180.0/T)                                  {7.68378E-12}
k( 85) =  4.2000E-12 * exp(   180.0/T)                                  {7.68378E-12}
k( 86) =  4.2000E-12 * exp(   180.0/T)                                  {7.68378E-12}
k( 87) =  4.2000E-12 * exp(   180.0/T)                                  {7.68378E-12}
k( 88) =  4.2000E-12 * exp(   180.0/T)                                  {7.68378E-12}
k( 89) =  4.2000E-12 * exp(   180.0/T)                                  {7.68378E-12}
k( 90) =  4.2000E-12 * exp(   180.0/T)                                  {7.68378E-12}
k( 91) =  4.2000E-12 * exp(   180.0/T)                                  {7.68378E-12}
k( 92) =  4.2000E-12 * exp(   180.0/T)                                  {7.68378E-12}
k( 93) =  6.0000E-13 * exp( -2058.0/T)                                  {6.01030E-16}
k( 94) =  1.4000E-12 * exp( -1900.0/T)                                  {2.38307E-15}
k( 95) =  6.0000E-13 * exp( -2058.0/T)                                  {6.01030E-16}
k( 96) =  1.4000E-12 * exp( -1900.0/T)                                  {2.38307E-15}
k( 97) =  1.4000E-12 * exp( -1900.0/T)                                  {2.38307E-15}
k( 98) =  2.2000E-11                                                    {2.20000E-11}
k( 99) =  2.0000E-12 * exp( -2923.0/T)                                  {1.09940E-16}
k(100) =  1.0000E-11 * exp( -1895.0/T)                                  {1.73099E-14}
k(101) =  3.2300E-11 * exp(  -975.0/T)                                  {1.22539E-12}
k(102) =  5.8100E-13                                                    {5.81000E-13}
k(103) =  1.2000E-14 * exp( -2633.0/T)                                  {1.74559E-18}
k(104) =  1.3200E-14 * exp( -2105.0/T)                                  {1.12933E-17}
k(105) =  7.2900E-15 * exp( -1136.0/T)                                  {1.61125E-16}
k(106) =  1.2300E-14 * exp( -2013.0/T)                                  {1.43295E-17}
k(107) =  7.7000E-14 * exp(  1300.0/T)                                  {6.04038E-12}
k(108) =  7.7000E-14 * exp(  1300.0/T)                                  {6.04038E-12}
k(109) =  7.7000E-14 * exp(  1300.0/T)                                  {6.04038E-12}
k(110) =  7.7000E-14 * exp(  1300.0/T)                                  {6.04038E-12}
k(111) =  7.7000E-14 * exp(  1300.0/T)                                  {6.04038E-12}
k(112) =  7.7000E-14 * exp(  1300.0/T)                                  {6.04038E-12}
k(113) =  7.7000E-14 * exp(  1300.0/T)                                  {6.04038E-12}
k(114) =  7.7000E-14 * exp(  1300.0/T)                                  {6.04038E-12}
k(115) =  7.7000E-14 * exp(  1300.0/T)                                  {6.04038E-12}
k(116) =  7.7000E-14 * exp(  1300.0/T)                                  {6.04038E-12}
k(117) =  7.7000E-14 * exp(  1300.0/T)                                  {6.04038E-12}
k(118) =  7.7000E-14 * exp(  1300.0/T)                                  {6.04038E-12}
k(119) =  7.7000E-14 * exp(  1300.0/T)                                  {6.04038E-12}
k(120) =  7.7000E-14 * exp(  1300.0/T)                                  {6.04038E-12}
k(121) =  1.9000E-13 * exp(   220.0/T)                                  {3.97533E-13}
k(122) =  1.4000E-13 * exp(   220.0/T)                                  {2.92919E-13}
k(123) =  4.2000E-14 * exp(   220.0/T)                                  {8.78758E-14}
k(124) =  3.4000E-14 * exp(   220.0/T)                                  {7.11376E-14}
k(125) =  2.9000E-14 * exp(   220.0/T)                                  {6.06762E-14}
k(126) =  1.4000E-13 * exp(   220.0/T)                                  {2.92919E-13}
```

Table 8A-8. RADM2_AE and RADM2_AE_AQ Mechanisms

```
k(127) =  1.4000E-13 * exp(   220.0/T)                                  {2.92919E-13}
k(128) =  1.7000E-14 * exp(   220.0/T)                                  {3.55688E-14}
k(129) =  1.7000E-14 * exp(   220.0/T)                                  {3.55688E-14}
k(130) =  9.6000E-13 * exp(   220.0/T)                                  {2.00859E-12}
k(131) =  1.7000E-14 * exp(   220.0/T)                                  {3.55688E-14}
k(132) =  1.7000E-14 * exp(   220.0/T)                                  {3.55688E-14}
k(133) =  9.6000E-13 * exp(   220.0/T)                                  {2.00859E-12}
k(134) =  1.7000E-14 * exp(   220.0/T)                                  {3.55688E-14}
k(135) =  3.4000E-13 * exp(   220.0/T)                                  {7.11376E-13}
k(136) =  1.0000E-13 * exp(   220.0/T)                                  {2.09228E-13}
k(137) =  8.4000E-14 * exp(   220.0/T)                                  {1.75752E-13}
k(138) =  7.2000E-14 * exp(   220.0/T)                                  {1.50644E-13}
k(139) =  3.4000E-13 * exp(   220.0/T)                                  {7.11376E-13}
k(140) =  3.4000E-13 * exp(   220.0/T)                                  {7.11376E-13}
k(141) =  4.2000E-14 * exp(   220.0/T)                                  {8.78758E-14}
k(142) =  4.2000E-14 * exp(   220.0/T)                                  {8.78758E-14}
k(143) =  1.1900E-12 * exp(   220.0/T)                                  {2.48981E-12}
k(144) =  4.2000E-14 * exp(   220.0/T)                                  {8.78758E-14}
k(145) =  4.2000E-14 * exp(   220.0/T)                                  {8.78758E-14}
k(146) =  1.1900E-12 * exp(   220.0/T)                                  {2.48981E-12}
k(147) =  4.2000E-14 * exp(   220.0/T)                                  {8.78758E-14}
k(148) =  3.6000E-16 * exp(   220.0/T)                                  {7.53221E-16}
k(149) =  7.7000E-14 * exp(  1300.0/T)                                  {6.04038E-12}
k(150) =  1.7000E-14 * exp(   220.0/T)                                  {3.55688E-14}
k(151) =  4.2000E-14 * exp(   220.0/T)                                  {8.78758E-14}
k(152) =  3.6000E-16 * exp(   220.0/T)                                  {7.53221E-16}
k(153) =  4.2000E-12 * exp(   180.0/T)                                  {7.68378E-12}
k(154) =  4.2000E-12 * exp(   180.0/T)                                  {7.68378E-12}
k(155) =  7.7000E-14 * exp(  1300.0/T)                                  {6.04038E-12}
k(156) =  1.7000E-14 * exp(   220.0/T)                                  {3.55688E-14}
k(157) =  4.2000E-14 * exp(   220.0/T)                                  {8.78758E-14}
k(158) =  3.6000E-16 * exp(   220.0/T)                                  {7.53221E-16}
k(159) =  1.0000E+00 * k( 58)                                           {6.75269E-11}
k(160) =  1.0000E+00 * k(101)                                           {1.22539E-12}
k(161) =  1.0000E+00 * k(105)                                           {1.61125E-16}
==============================================================================
```

Table 8A-9. RADM2_CIS1 and RADM2_CIS1_AQ Mechanisms

```
Reaction List
>-------------------------------------------------------------------------------------------------<
{  1} NO2      + hv                    -->        O3P      +       NO
{  2} O3       + hv                    -->        O1D
{  3} O3       + hv                    -->        O3P
{  4} HONO     + hv                    -->        HO       +       NO
{  5} HNO3     + hv                    -->        HO       +       NO2
{  6} HNO4     + hv                    -->        HO2      +       NO2
{  7} NO3      + hv                    -->        NO
{  8} NO3      + hv                    -->        NO2      +       O3P
{  9} H2O2     + hv                    -->   2.000*HO
{ 10} HCHO     + hv                    -->        CO
{ 11} HCHO     + hv                    -->        HO2      +       HO2      +       CO
{ 12} ALD      + hv                    -->        MO2      +       HO2      +       CO
{ 13} OP1      + hv                    -->        HCHO     +       HO2      +       HO
{ 14} OP2      + hv                    -->        ALD      +       HO2      +       HO
{ 15} PAA      + hv                    -->        MO2      +       HO
{ 16} KET      + hv                    -->        ACO3     +       ETHP
{ 17} GLY      + hv                    -->   0.130*HCHO     + 1.870*CO
{ 18} GLY      + hv                    -->   0.450*HCHO     + 1.550*CO       + 0.800*HO2
{ 19} MGLY     + hv                    -->        ACO3     +       HO2      +       CO
{ 20} DCB      + hv                    -->   0.980*HO2      + 0.020*ACO3     +       TCO3
{ 21} ONIT     + hv                    -->   0.200*ALD      + 0.800*KET      +       HO2
                                         +        NO2
{ 22} O3P      + [M]      + [O2]       -->        O3
{ 23} O3P      + NO2                   -->        NO
{ 24} O1D      + [N2]                  -->        O3P
{ 25} O1D      + [O2]                  -->        O3P
{ 26} O1D      + [H2O]                 -->   2.000*HO
{ 27} O3       + NO                    -->        NO2
{ 28} O3       + HO                    -->        HO2
{ 29} O3       + HO2                   -->        HO
{ 30} HO2      + NO                    -->        NO2      +       HO
{ 31} HO2      + NO2                   -->        HNO4
{ 32} HNO4                             -->        HO2      +       NO2
{ 33} HO2      + HO2                   -->        H2O2
{ 34} HO2      + HO2      + [H2O]      -->        H2O2
{ 35} H2O2     + HO                    -->        HO2
{ 36} NO       + HO                    -->        HONO
{ 37} NO       + NO       + [O2]       -->   2.000*NO2
{ 38} O3       + NO2                   -->        NO3
{ 39} NO3      + NO                    -->   2.000*NO2
{ 40} NO3      + NO2                   -->        NO       +       NO2
{ 41} NO3      + HO2                   -->        HNO3
{ 42} NO3      + NO2                   -->        N2O5
{ 43} N2O5                             -->        NO2      +       NO3
{ 44} N2O5     + [H2O]                 -->   2.000*HNO3
{ 45} HO       + NO2                   -->        HNO3
{ 46} HO       + HNO3                  -->        NO3
{ 47} HO       + HNO4                  -->        NO2
{ 48} HO       + HO2                   -->
{ 49} HO       + SO2                   -->        SULF     +       HO2
{ 50} CO       + HO                    -->        HO2
{ 51} HO                               -->        MO2
{ 52} ETH      + HO                    -->        ETHP
{ 53} HC3      + HO                    -->   0.830*HC3P     + 0.170*HO2      + 0.009*HCHO
                                         + 0.075*ALD      + 0.025*KET
{ 54} HC5      + HO                    -->        HC5P     + 0.250*XO2
{ 55} HC8      + HO                    -->        HC8P     + 0.750*XO2
{ 56} OL2      + HO                    -->        OL2P
{ 57} OLT      + HO                    -->        OLTP
```

Table 8A-9. RADM2_CIS1 and RADM2_CIS1_AQ Mechanisms

```
{ 58} OLI      + HO                 -->        OLIP
{ 59} TOL      + HO                 -->  0.750*TOLP     + 0.250*CSL      + 0.250*HO2
{ 60} XYL      + HO                 -->  0.830*XYLP     + 0.170*CSL      + 0.170*HO2
{ 61} CSL      + HO                 -->  0.100*HO2      + 0.900*XO2      + 0.900*TCO3
{ 62} CSL      + HO                 -->        CSL
{ 63} HCHO     + HO                 -->        HO2      +       CO
{ 64} ALD      + HO                 -->        ACO3
{ 65} KET      + HO                 -->        KETP
{ 66} GLY      + HO                 -->        HO2      + 2.000*CO
{ 67} MGLY     + HO                 -->        ACO3     +       CO
{ 68} DCB      + HO                 -->        TCO3
{ 69} OP1      + HO                 -->  0.500*MO2      + 0.500*HCHO     + 0.500*HO
{ 70} OP2      + HO                 -->  0.500*HC3P     + 0.500*ALD      + 0.500*HO
{ 71} PAA      + HO                 -->        ACO3
{ 72} PAN      + HO                 -->        HCHO     +       NO3      +       XO2
{ 73} ONIT     + HO                 -->        HC3P     +       NO2
{ 74} ACO3     + NO2                -->        PAN
{ 75} PAN                           -->        ACO3     +       NO2
{ 76} TCO3     + NO2                -->        TPAN
{ 77} TPAN                          -->        TCO3     +       NO2
{ 78} MO2      + NO                 -->        HCHO     +       HO2      +       NO2
{ 79} HC3P     + NO                 -->  0.750*ALD      + 0.250*KET      + 0.090*HCHO
                                        + 0.036*ONIT     + 0.964*NO2      + 0.964*HO2
{ 80} HC5P     + NO                 -->  0.380*ALD      + 0.690*KET      + 0.080*ONIT
                                        + 0.920*NO2      + 0.920*HO2
{ 81} HC8P     + NO                 -->  0.350*ALD      + 1.060*KET      + 0.040*HCHO
                                        + 0.240*ONIT     + 0.760*NO2      + 0.760*HO2
{ 82} OL2P     + NO                 -->  1.600*HCHO     +       HO2      +       NO2
                                        + 0.200*ALD
{ 83} OLTP     + NO                 -->        ALD      +       HCHO     +       HO2
                                        +       NO2
{ 84} OLIP     + NO                 -->        HO2      + 1.450*ALD      + 0.280*HCHO
                                        + 0.100*KET      +       NO2
{ 85} ACO3     + NO                 -->        MO2      +       NO2
{ 86} TCO3     + NO                 -->        NO2      + 0.920*HO2      + 0.890*GLY
                                        + 0.110*MGLY     + 0.050*ACO3     + 0.950*CO
                                        + 2.000*XO2
{ 87} TOLP     + NO                 -->        NO2      +       HO2      + 0.170*MGLY
                                        + 0.160*GLY      + 0.700*DCB
{ 88} XYLP     + NO                 -->        NO2      +       HO2      + 0.450*MGLY
                                        + 0.806*DCB
{ 89} ETHP     + NO                 -->        ALD      +       HO2      +       NO2
{ 90} KETP     + NO                 -->        MGLY     +       NO2      +       HO2
{ 91} OLN      + NO                 -->        HCHO     +       ALD      + 2.000*NO2
{ 92} HCHO     + NO3                -->        HO2      +       HNO3     +       CO
{ 93} ALD      + NO3                -->        ACO3     +       HNO3
{ 94} GLY      + NO3                -->        HNO3     +       HO2      + 2.000*CO
{ 95} MGLY     + NO3                -->        HNO3     +       ACO3     +       CO
{ 96} DCB      + NO3                -->        HNO3     +       TCO3
{ 97} CSL      + NO3                -->        HNO3     +       XNO2     + 0.500*CSL
{ 98} OL2      + NO3                -->        OLN
{ 99} OLT      + NO3                -->        OLN
{100} OLI      + NO3                -->        OLN
{101} OL2      + O3                 -->        HCHO     + 0.400*ORA1     + 0.420*CO
                                        + 0.120*HO2
{102} OLT      + O3                 -->  0.530*HCHO     + 0.500*ALD      + 0.330*CO
                                        + 0.200*ORA1     + 0.200*ORA2     + 0.230*HO2
                                        + 0.220*MO2      + 0.100*HO
{103} OLI      + O3                 -->  0.180*HCHO     + 0.720*ALD      + 0.100*KET
                                        + 0.230*CO       + 0.060*ORA1     + 0.290*ORA2
                                        + 0.260*HO2      + 0.140*HO       + 0.310*MO2
```

Table 8A-9. RADM2_CIS1 and RADM2_CIS1_AQ Mechanisms

```
{104} HO2     + MO2      -->        OP1
{105} HO2     + ETHP     -->        OP2
{106} HO2     + HC3P     -->        OP2
{107} HO2     + HC5P     -->        OP2
{108} HO2     + HC8P     -->        OP2
{109} HO2     + OL2P     -->        OP2
{110} HO2     + OLTP     -->        OP2
{111} HO2     + OLIP     -->        OP2
{112} HO2     + KETP     -->        OP2
{113} HO2     + ACO3     -->        PAA
{114} HO2     + TOLP     -->        OP2
{115} HO2     + XYLP     -->        OP2
{116} HO2     + TCO3     -->        OP2
{117} HO2     + OLN      -->        ONIT
{118} MO2     + MO2      -->  1.500*HCHO     +       HO2
{119} MO2     + ETHP     -->  0.750*HCHO     +       HO2     + 0.750*ALD
{120} MO2     + HC3P     -->  0.840*HCHO     + 0.770*ALD     + 0.260*KET
                           +       HO2
{121} MO2     + HC5P     -->  0.770*HCHO     + 0.410*ALD     + 0.750*KET
                           +       HO2
{122} MO2     + HC8P     -->  0.800*HCHO     + 0.460*ALD     + 1.390*KET
                           +       HO2
{123} MO2     + OL2P     -->  1.550*HCHO     + 0.350*ALD     +       HO2
{124} MO2     + OLTP     -->  1.250*HCHO     + 0.750*ALD     +       HO2
{125} MO2     + OLIP     -->  0.890*HCHO     + 0.725*ALD     +       HO2
                           + 0.550*KET
{126} MO2     + KETP     -->  0.750*HCHO     + 0.750*MGLY    +       HO2
{127} MO2     + ACO3     -->        HCHO     + 0.500*HO2     + 0.500*MO2
                           + 0.500*ORA2
{128} MO2     + TOLP     -->        HCHO     + 0.170*MGLY    + 0.160*GLY
                           + 0.700*DCB      + 2.000*HO2
{129} MO2     + XYLP     -->        HCHO     + 0.450*MGLY    + 0.806*DCB
                           + 2.000*HO2
{130} MO2     + TCO3     -->  0.500*HCHO     + 0.445*GLY     + 0.055*MGLY
                           + 0.500*ORA2     + 0.025*ACO3    + 0.460*HO2
                           + 0.475*CO       +       XO2
{131} MO2     + OLN      -->  1.750*HCHO     + 0.500*HO2     +       ALD
                           +       NO2
{132} ETHP    + ACO3     -->        ALD      + 0.500*HO2     + 0.500*MO2
                           + 0.500*ORA2
{133} HC3P    + ACO3     -->  0.770*ALD      + 0.260*KET     + 0.500*HO2
                           + 0.500*MO2      + 0.500*ORA2
{134} HC5P    + ACO3     -->  0.410*ALD      + 0.750*KET     + 0.500*HO2
                           + 0.500*MO2      + 0.500*ORA2
{135} HC8P    + ACO3     -->  0.460*ALD      + 1.390*KET     + 0.500*HO2
                           + 0.500*MO2      + 0.500*ORA2
{136} OL2P    + ACO3     -->  0.800*HCHO     + 0.600*ALD     + 0.500*HO2
                           + 0.500*MO2      + 0.500*ORA2
{137} OLTP    + ACO3     -->        ALD      + 0.500*HCHO    + 0.500*HO2
                           + 0.500*MO2      + 0.500*ORA2
{138} OLIP    + ACO3     -->  0.725*ALD      + 0.550*KET     + 0.140*HCHO
                           + 0.500*HO2      + 0.500*MO2     + 0.500*ORA2
{139} KETP    + ACO3     -->        MGLY     + 0.500*HO2     + 0.500*MO2
                           + 0.500*ORA2
{140} ACO3    + ACO3     -->  2.000*MO2
{141} ACO3    + TOLP     -->        MO2      + 0.170*MGLY    + 0.160*GLY
                           + 0.700*DCB      +       HO2
{142} ACO3    + XYLP     -->        MO2      + 0.450*MGLY    + 0.806*DCB
                           +       HO2
{143} ACO3    + TCO3     -->        MO2      + 0.920*HO2     + 0.890*GLY
                           + 0.110*MGLY     + 0.050*ACO3    + 0.950*CO
```

Table 8A-9. RADM2_CIS1 and RADM2_CIS1_AQ Mechanisms

```
                                          + 2.000*XO2
{144} ACO3      + OLN                 -->         HCHO      +       ALD       + 0.500*ORA2
                                          +       NO2       + 0.500*MO2
{145} OLN       + OLN                 -->   2.000*HCHO      + 2.000*ALD       + 2.000*NO2
{146} XO2       + HO2                 -->         OP2
{147} XO2       + MO2                 -->         HCHO      +       HO2
{148} XO2       + ACO3                -->         MO2
{149} XO2       + XO2                 -->
{150} XO2       + NO                  -->         NO2
{151} XNO2      + NO2                 -->         ONIT
{152} XNO2      + HO2                 -->         OP2
{153} XNO2      + MO2                 -->         HCHO      +       HO2
{154} XNO2      + ACO3                -->         MO2
{155} XNO2      + XNO2                -->
{156} ISO       + HO                  -->         ISO_RO2   + 0.079*XO2
{157} ISO_RO2   + NO                  -->   0.088*ONIT      + 0.912*NO2       + 0.912*HO2
                                          + 0.912*ISOPROD   + 0.629*HCHO
{158} ISO_RO2   + HO2                 -->         OP2
{159} ISO_RO2   + ACO3                -->   0.500*HO2       + 0.500*MO2       + 0.500*ORA2
                                          +       ISOPROD
{160} ISO_RO2   + MO2                 -->   0.500*HCHO      + 0.500*HO2       +       ISOPROD
{161} ISO       + O3                  -->   0.600*HCHO      + 0.650*ISOPROD   + 0.390*ORA1
                                          + 0.270*HO        + 0.070*HO2       + 0.070*CO
                                          + 0.200*XO2       + 0.200*ACO3      + 0.150*ALD
{162} ISO       + O3P                 -->   0.750*ISOPROD   + 0.250*ACO3      + 0.250*HCHO
                                          + 0.250*MO2
{163} ISO       + NO3                 -->         ISON_RO2
{164} ISON_RO2  + NO                  -->         NO2       + 0.800*ALD       + 0.800*ONIT
                                          + 0.800*HO2       + 0.200*ISOPROD   + 0.200*NO2
{165} ISON_RO2  + HO2                 -->         ONIT
{166} ISON_RO2  + ACO3                -->   0.500*HO2       + 0.500*MO2       + 0.500*ORA2
                                          +       ALD       +       ONIT
{167} ISON_RO2  + MO2                 -->   0.500*HCHO      + 0.500*HO2       +       ALD
                                          +       ONIT
{168} ISOPROD   + HO                  -->   0.500*ACO3      + 0.500*IP_RO2    + 0.200*XO2
{169} IP_RO2    + NO                  -->         NO2       +       HO2       + 0.590*CO
                                          + 0.550*ALD       + 0.250*HCHO      + 0.080*GLY
                                          + 0.340*MGLY      + 0.630*KET
{170} IP_RO2    + HO2                 -->         OP2
{171} IP_RO2    + ACO3                -->   0.500*HO2       + 0.500*MO2       + 0.500*ORA2
                                          + 0.500*ALD       + 0.500*KET
{172} IP_RO2    + MO2                 -->   0.500*HCHO      + 0.500*HO2       + 0.500*ALD
                                          + 0.500*KET
{173} ISOPROD   + O3                  -->   0.268*HO        + 0.100*HO2       + 0.114*ACO3
                                          + 0.054*MO2       + 0.070*XO2       + 0.155*CO
                                          + 0.146*HCHO      + 0.020*ALD       + 0.010*GLY
                                          + 0.850*MGLY      + 0.090*KET       + 0.462*ORA1
{174} ISOPROD   + hv                  -->   0.970*ACO3      + 0.333*HO2       + 0.700*MO2
                                          + 0.200*HCHO      + 0.333*CO        + 0.067*ALD
                                          + 0.033*KET
{175} ISOPROD   + NO3                 -->   0.075*ACO3      + 0.075*HNO3      + 0.643*CO
                                          + 0.282*HCHO      + 0.925*ONIT      + 0.282*ALD
                                          + 0.925*HO2       + 0.925*XO2
>-------------------------------------------------------------------------------------------<

Rate Expression                                                          Rate Constant
==============================================================================
k(  1) uses photo table NO2_RADM88       , scaled by 1.00000E+00    {0.00000E+00}
k(  2) uses photo table O3O1D_RADM88     , scaled by 1.00000E+00    {0.00000E+00}
k(  3) uses photo table O3O3P_RADM88     , scaled by 1.00000E+00    {0.00000E+00}
```

Table 8A-9. RADM2_CIS1 and RADM2_CIS1_AQ Mechanisms

```
k(  4) uses photo table HONO_RADM88      , scaled by 1.00000E+00    {0.00000E+00}
k(  5) uses photo table HNO3_RADM88      , scaled by 1.00000E+00    {0.00000E+00}
k(  6) uses photo table HNO4_RADM88      , scaled by 1.00000E+00    {0.00000E+00}
k(  7) uses photo table NO3NO_RADM88     , scaled by 1.00000E+00    {0.00000E+00}
k(  8) uses photo table NO3NO2_RADM88    , scaled by 1.00000E+00    {0.00000E+00}
k(  9) uses photo table H2O2_RADM88      , scaled by 1.00000E+00    {0.00000E+00}
k( 10) uses photo table HCHOmol_RADM88   , scaled by 1.00000E+00    {0.00000E+00}
k( 11) uses photo table HCHOrad_RADM88   , scaled by 1.00000E+00    {0.00000E+00}
k( 12) uses photo table ALD_RADM88       , scaled by 1.00000E+00    {0.00000E+00}
k( 13) uses photo table MHP_RADM88       , scaled by 1.00000E+00    {0.00000E+00}
k( 14) uses photo table HOP_RADM88       , scaled by 1.00000E+00    {0.00000E+00}
k( 15) uses photo table PAA_RADM88       , scaled by 1.00000E+00    {0.00000E+00}
k( 16) uses photo table KETONE_RADM88    , scaled by 1.00000E+00    {0.00000E+00}
k( 17) uses photo table GLYform_RADM88   , scaled by 1.00000E+00    {0.00000E+00}
k( 18) uses photo table GLYmol_RADM88    , scaled by 1.00000E+00    {0.00000E+00}
k( 19) uses photo table MGLY_RADM88      , scaled by 1.00000E+00    {0.00000E+00}
k( 20) uses photo table UDC_RADM88       , scaled by 1.00000E+00    {0.00000E+00}
k( 21) uses photo table ORGNIT_RADM88    , scaled by 1.00000E+00    {0.00000E+00}
k( 22) =  6.0000E-34 * (T/300)**(-2.30)                             {6.09302E-34}
k( 23) =  6.5000E-12 * exp(   120.0/T)                              {9.72293E-12}
k( 24) =  1.8000E-11 * exp(   110.0/T)                              {2.60365E-11}
k( 25) =  3.2000E-11 * exp(    70.0/T)                              {4.04730E-11}
k( 26) =  2.2000E-10                                                {2.20000E-10}
k( 27) =  2.0000E-12 * exp( -1400.0/T)                              {1.82272E-14}
k( 28) =  1.6000E-12 * exp(  -940.0/T)                              {6.82650E-14}
k( 29) =  1.1000E-14 * exp(  -500.0/T)                              {2.05452E-15}
k( 30) =  3.7000E-12 * exp(   240.0/T)                              {8.27883E-12}
k( 31) is a falloff expression using:                               {1.39058E-12}
   k0   =  1.8000E-31 * (T/300)**(-3.20)
   kinf =  4.7000E-12 * (T/300)**(-1.40)
   F =  0.60,  n =  1.00
k( 32) = k( 31) / Keq,  where Keq =  2.100E-27 * exp( 10900.0/T)    {8.62399E-02}
k( 33) is a special rate expression of the form:                    {3.01634E-12}
   k = k1 + k2[M], where
   k1 =  2.2000E-13 * exp(   620.0/T)
   k2 =  1.9000E-33 * exp(   980.0/T)
k( 34) is a special rate expression of the form:                    {6.78905E-30}
   k = k1 + k2[M], where
   k1 =  3.0800E-34 * exp(  2820.0/T)
   k2 =  2.6600E-54 * exp(  3180.0/T)
k( 35) =  3.3000E-12 * exp(  -200.0/T)                              {1.68671E-12}
k( 36) is a falloff expression using:                               {4.87144E-12}
   k0   =  7.0000E-31 * (T/300)**(-2.60)
   kinf =  1.5000E-11 * (T/300)**(-0.50)
   F =  0.60,  n =  1.00
k( 37) =  3.3000E-39 * exp(   530.0/T)                              {1.95397E-38}
k( 38) =  1.4000E-13 * exp( -2500.0/T)                              {3.18213E-17}
k( 39) =  1.7000E-11 * exp(   150.0/T)                              {2.81225E-11}
k( 40) =  2.5000E-14 * exp( -1230.0/T)                              {4.03072E-16}
k( 41) =  2.5000E-12                                                {2.50000E-12}
k( 42) is a falloff expression using:                               {1.26440E-12}
   k0   =  2.2000E-30 * (T/300)**(-4.30)
   kinf =  1.5000E-12 * (T/300)**(-0.50)
   F =  0.60,  n =  1.00
k( 43) = k( 42) / Keq,  where Keq =  1.100E-27 * exp( 11200.0/T)    {5.47034E-02}
k( 44) =  2.0000E-21                                                {2.00000E-21}
k( 45) is a falloff expression using:                               {1.14885E-11}
   k0   =  2.6000E-30 * (T/300)**(-3.20)
   kinf =  2.4000E-11 * (T/300)**(-1.30)
   F =  0.60,  n =  1.00
k( 46) is a special rate expression of the form:                    {1.47236E-13}
```

Table 8A-9. RADM2_CIS1 and RADM2_CIS1_AQ Mechanisms

```
   k = k0 + {k3[M] / (1 + k3[M]/k2)}, where
   k0 =  7.2000E-15 * exp(   785.0/T)
   k2 =  4.1000E-16 * exp(  1440.0/T)
   k3 =  1.9000E-33 * exp(   725.0/T)
k( 47) =  1.3000E-12 * exp(   380.0/T)                          {4.65309E-12}
k( 48) =  4.6000E-11 * exp(   230.0/T)                          {9.95294E-11}
k( 49) is a falloff expression using:                           {8.88848E-13}
   k0   =  3.0000E-31 * (T/300)**(-3.30)
   kinf =  1.5000E-12 * (T/300)**( 0.00)
   F =  0.60,  n =  1.00
k( 50) =  1.5000E-13 * (1.0 + 0.6*Pressure)                     {2.40000E-13}
k( 51) =  2.8300E+01 * (T/300)**( 2.00) * exp( -1280.0/T)       {3.80672E-01}
k( 52) =  1.2330E-12 * (T/300)**( 2.00) * exp(  -444.0/T)       {2.74210E-13}
k( 53) =  1.5900E-11 * exp(  -540.0/T)                          {2.59669E-12}
k( 54) =  1.7300E-11 * exp(  -380.0/T)                          {4.83334E-12}
k( 55) =  3.6400E-11 * exp(  -380.0/T)                          {1.01696E-11}
k( 56) =  2.1500E-12 * exp(   411.0/T)                          {8.53916E-12}
k( 57) =  5.3200E-12 * exp(   504.0/T)                          {2.88684E-11}
k( 58) =  1.0700E-11 * exp(   549.0/T)                          {6.75269E-11}
k( 59) =  2.1000E-12 * exp(   322.0/T)                          {6.18715E-12}
k( 60) =  1.8900E-11 * exp(   116.0/T)                          {2.78943E-11}
k( 61) =  4.0000E-11                                            {4.00000E-11}
k( 62) =  9.0000E-01 * k( 61)                                   {3.60000E-11}
k( 63) =  9.0000E-12                                            {9.00000E-12}
k( 64) =  6.8700E-12 * exp(   256.0/T)                          {1.62197E-11}
k( 65) =  1.2000E-11 * exp(  -745.0/T)                          {9.85020E-13}
k( 66) =  1.1500E-11                                            {1.15000E-11}
k( 67) =  1.7000E-11                                            {1.70000E-11}
k( 68) =  2.8000E-11                                            {2.80000E-11}
k( 69) =  1.0000E-11                                            {1.00000E-11}
k( 70) =  1.0000E-11                                            {1.00000E-11}
k( 71) =  1.0000E-11                                            {1.00000E-11}
k( 72) =  6.1650E-13 * (T/300)**( 2.00) * exp(  -444.0/T)       {1.37105E-13}
k( 73) =  1.5500E-11 * exp(  -540.0/T)                          {2.53137E-12}
k( 74) =  2.8000E-12 * exp(   181.0/T)                          {5.13974E-12}
k( 75) =  1.9500E+16 * exp(-13543.0/T)                          {3.57235E-04}
k( 76) =  4.7000E-12                                            {4.70000E-12}
k( 77) =  1.9500E+16 * exp(-13543.0/T)                          {3.57235E-04}
k( 78) =  4.2000E-12 * exp(   180.0/T)                          {7.68378E-12}
k( 79) =  4.2000E-12 * exp(   180.0/T)                          {7.68378E-12}
k( 80) =  4.2000E-12 * exp(   180.0/T)                          {7.68378E-12}
k( 81) =  4.2000E-12 * exp(   180.0/T)                          {7.68378E-12}
k( 82) =  4.2000E-12 * exp(   180.0/T)                          {7.68378E-12}
k( 83) =  4.2000E-12 * exp(   180.0/T)                          {7.68378E-12}
k( 84) =  4.2000E-12 * exp(   180.0/T)                          {7.68378E-12}
k( 85) =  4.2000E-12 * exp(   180.0/T)                          {7.68378E-12}
k( 86) =  4.2000E-12 * exp(   180.0/T)                          {7.68378E-12}
k( 87) =  4.2000E-12 * exp(   180.0/T)                          {7.68378E-12}
k( 88) =  4.2000E-12 * exp(   180.0/T)                          {7.68378E-12}
k( 89) =  4.2000E-12 * exp(   180.0/T)                          {7.68378E-12}
k( 90) =  4.2000E-12 * exp(   180.0/T)                          {7.68378E-12}
k( 91) =  4.2000E-12 * exp(   180.0/T)                          {7.68378E-12}
k( 92) =  6.0000E-13 * exp( -2058.0/T)                          {6.01030E-16}
k( 93) =  1.4000E-12 * exp( -1900.0/T)                          {2.38307E-15}
k( 94) =  6.0000E-13 * exp( -2058.0/T)                          {6.01030E-16}
k( 95) =  1.4000E-12 * exp( -1900.0/T)                          {2.38307E-15}
k( 96) =  1.4000E-12 * exp( -1900.0/T)                          {2.38307E-15}
k( 97) =  2.2000E-11                                            {2.20000E-11}
k( 98) =  2.0000E-12 * exp( -2923.0/T)                          {1.09940E-16}
k( 99) =  1.0000E-11 * exp( -1895.0/T)                          {1.73099E-14}
k(100) =  3.2300E-11 * exp(  -975.0/T)                          {1.22539E-12}
```

Table 8A-9. RADM2_CIS1 and RADM2_CIS1_AQ Mechanisms

```
k(101) =  1.2000E-14 * exp( -2633.0/T)                                  {1.74559E-18}
k(102) =  1.3200E-14 * exp( -2105.0/T)                                  {1.12933E-17}
k(103) =  7.2900E-15 * exp( -1136.0/T)                                  {1.61125E-16}
k(104) =  7.7000E-14 * exp(  1300.0/T)                                  {6.04038E-12}
k(105) =  7.7000E-14 * exp(  1300.0/T)                                  {6.04038E-12}
k(106) =  7.7000E-14 * exp(  1300.0/T)                                  {6.04038E-12}
k(107) =  7.7000E-14 * exp(  1300.0/T)                                  {6.04038E-12}
k(108) =  7.7000E-14 * exp(  1300.0/T)                                  {6.04038E-12}
k(109) =  7.7000E-14 * exp(  1300.0/T)                                  {6.04038E-12}
k(110) =  7.7000E-14 * exp(  1300.0/T)                                  {6.04038E-12}
k(111) =  7.7000E-14 * exp(  1300.0/T)                                  {6.04038E-12}
k(112) =  7.7000E-14 * exp(  1300.0/T)                                  {6.04038E-12}
k(113) =  7.7000E-14 * exp(  1300.0/T)                                  {6.04038E-12}
k(114) =  7.7000E-14 * exp(  1300.0/T)                                  {6.04038E-12}
k(115) =  7.7000E-14 * exp(  1300.0/T)                                  {6.04038E-12}
k(116) =  7.7000E-14 * exp(  1300.0/T)                                  {6.04038E-12}
k(117) =  7.7000E-14 * exp(  1300.0/T)                                  {6.04038E-12}
k(118) =  1.9000E-13 * exp(   220.0/T)                                  {3.97533E-13}
k(119) =  1.4000E-13 * exp(   220.0/T)                                  {2.92919E-13}
k(120) =  4.2000E-14 * exp(   220.0/T)                                  {8.78758E-14}
k(121) =  3.4000E-14 * exp(   220.0/T)                                  {7.11376E-14}
k(122) =  2.9000E-14 * exp(   220.0/T)                                  {6.06762E-14}
k(123) =  1.4000E-13 * exp(   220.0/T)                                  {2.92919E-13}
k(124) =  1.4000E-13 * exp(   220.0/T)                                  {2.92919E-13}
k(125) =  1.7000E-14 * exp(   220.0/T)                                  {3.55688E-14}
k(126) =  1.7000E-14 * exp(   220.0/T)                                  {3.55688E-14}
k(127) =  9.6000E-13 * exp(   220.0/T)                                  {2.00859E-12}
k(128) =  1.7000E-14 * exp(   220.0/T)                                  {3.55688E-14}
k(129) =  1.7000E-14 * exp(   220.0/T)                                  {3.55688E-14}
k(130) =  9.6000E-13 * exp(   220.0/T)                                  {2.00859E-12}
k(131) =  1.7000E-14 * exp(   220.0/T)                                  {3.55688E-14}
k(132) =  3.4000E-13 * exp(   220.0/T)                                  {7.11376E-13}
k(133) =  1.0000E-13 * exp(   220.0/T)                                  {2.09228E-13}
k(134) =  8.4000E-14 * exp(   220.0/T)                                  {1.75752E-13}
k(135) =  7.2000E-14 * exp(   220.0/T)                                  {1.50644E-13}
k(136) =  3.4000E-13 * exp(   220.0/T)                                  {7.11376E-13}
k(137) =  3.4000E-13 * exp(   220.0/T)                                  {7.11376E-13}
k(138) =  4.2000E-14 * exp(   220.0/T)                                  {8.78758E-14}
k(139) =  4.2000E-14 * exp(   220.0/T)                                  {8.78758E-14}
k(140) =  1.1900E-12 * exp(   220.0/T)                                  {2.48981E-12}
k(141) =  4.2000E-14 * exp(   220.0/T)                                  {8.78758E-14}
k(142) =  4.2000E-14 * exp(   220.0/T)                                  {8.78758E-14}
k(143) =  1.1900E-12 * exp(   220.0/T)                                  {2.48981E-12}
k(144) =  4.2000E-14 * exp(   220.0/T)                                  {8.78758E-14}
k(145) =  3.6000E-16 * exp(   220.0/T)                                  {7.53221E-16}
k(146) =  7.7000E-14 * exp(  1300.0/T)                                  {6.04038E-12}
k(147) =  1.7000E-14 * exp(   220.0/T)                                  {3.55688E-14}
k(148) =  4.2000E-14 * exp(   220.0/T)                                  {8.78758E-14}
k(149) =  3.6000E-16 * exp(   220.0/T)                                  {7.53221E-16}
k(150) =  4.2000E-12 * exp(   180.0/T)                                  {7.68378E-12}
k(151) =  4.2000E-12 * exp(   180.0/T)                                  {7.68378E-12}
k(152) =  7.7000E-14 * exp(  1300.0/T)                                  {6.04038E-12}
k(153) =  1.7000E-14 * exp(   220.0/T)                                  {3.55688E-14}
k(154) =  4.2000E-14 * exp(   220.0/T)                                  {8.78758E-14}
k(155) =  3.6000E-16 * exp(   220.0/T)                                  {7.53221E-16}
k(156) =  2.5400E-11 * (T/300)**( 1.00) * exp(   407.6/T)               {9.90719E-11}
k(157) =  4.2000E-12 * (T/300)**( 1.00) * exp(   181.2/T)               {7.66335E-12}
k(158) =  7.7000E-14 * (T/300)**( 1.00) * exp(  1298.3/T)               {5.96598E-12}
k(159) =  8.4000E-14 * (T/300)**( 1.00) * exp(   221.4/T)               {1.75402E-13}
k(160) =  3.4000E-14 * (T/300)**( 1.00) * exp(   221.4/T)               {7.09961E-14}
k(161) =  7.8600E-15 * (T/300)**( 1.00) * exp( -1912.2/T)               {1.27569E-17}
```

Table 8A-9. RADM2_CIS1 and RADM2_CIS1_AQ Mechanisms

```
k(162) =  3.6000E-11                                                {3.60000E-11}
k(163) =  3.0300E-12 * (T/300)**( 1.00) * exp(  -447.9/T)           {6.69552E-13}
k(164) =  4.2000E-12 * (T/300)**( 1.00) * exp(   181.2/T)           {7.66335E-12}
k(165) =  7.7000E-14 * (T/300)**( 1.00) * exp(  1298.3/T)           {5.96598E-12}
k(166) =  8.4000E-14 * (T/300)**( 1.00) * exp(   221.4/T)           {1.75402E-13}
k(167) =  3.4000E-14 * (T/300)**( 1.00) * exp(   221.4/T)           {7.09961E-14}
k(168) =  3.3600E-11                                                {3.36000E-11}
k(169) =  4.2000E-12 * (T/300)**( 1.00) * exp(   181.2/T)           {7.66335E-12}
k(170) =  7.7000E-14 * (T/300)**( 1.00) * exp(  1298.3/T)           {5.96598E-12}
k(171) =  8.4000E-14 * (T/300)**( 1.00) * exp(   221.4/T)           {1.75402E-13}
k(172) =  3.4000E-14 * (T/300)**( 1.00) * exp(   221.4/T)           {7.09961E-14}
k(173) =  7.1100E-18                                                {7.11000E-18}
k(174) uses photo table ACROLEIN        , scaled by 3.60000E-03     {0.00000E+00}
k(175) =  1.0000E-15                                                {1.00000E-15}
==========================================================================
```

Table 8A-10. RADM2_CIS1_AE and RADM2_CIS1_AE_AQ Mechanisms

```
Reaction List
>------------------------------------------------------------------------------------------<
{  1} NO2      + hv                  -->        O3P      +       NO
{  2} O3       + hv                  -->        O1D
{  3} O3       + hv                  -->        O3P
{  4} HONO     + hv                  -->        HO       +       NO
{  5} HNO3     + hv                  -->        HO       +       NO2
{  6} HNO4     + hv                  -->        HO2      +       NO2
{  7} NO3      + hv                  -->        NO
{  8} NO3      + hv                  -->        NO2      +       O3P
{  9} H2O2     + hv                  -->   2.000*HO
{ 10} HCHO     + hv                  -->        CO
{ 11} HCHO     + hv                  -->        HO2      +       HO2      +       CO
{ 12} ALD      + hv                  -->        MO2      +       HO2      +       CO
{ 13} OP1      + hv                  -->        HCHO     +       HO2      +       HO
{ 14} OP2      + hv                  -->        ALD      +       HO2      +       HO
{ 15} PAA      + hv                  -->        MO2      +       HO
{ 16} KET      + hv                  -->        ACO3     +       ETHP
{ 17} GLY      + hv                  -->   0.130*HCHO    + 1.870*CO
{ 18} GLY      + hv                  -->   0.450*HCHO    + 1.550*CO       + 0.800*HO2
{ 19} MGLY     + hv                  -->        ACO3     +       HO2      +       CO
{ 20} DCB      + hv                  -->   0.980*HO2     + 0.020*ACO3     +       TCO3
{ 21} ONIT     + hv                  -->   0.200*ALD     + 0.800*KET      +       HO2
                                        +        NO2
{ 22} O3P      + [M]      + [O2]     -->        O3
{ 23} O3P      + NO2                 -->        NO
{ 24} O1D      + [N2]                -->        O3P
{ 25} O1D      + [O2]                -->        O3P
{ 26} O1D      + [H2O]               -->   2.000*HO
{ 27} O3       + NO                  -->        NO2
{ 28} O3       + HO                  -->        HO2
{ 29} O3       + HO2                 -->        HO
{ 30} HO2      + NO                  -->        NO2      +       HO
{ 31} HO2      + NO2                 -->        HNO4
{ 32} HNO4                           -->        HO2      +       NO2
{ 33} HO2      + HO2                 -->        H2O2
{ 34} HO2      + HO2      + [H2O]    -->        H2O2
{ 35} H2O2     + HO                  -->        HO2
{ 36} NO       + HO                  -->        HONO
{ 37} NO       + NO       + [O2]     -->   2.000*NO2
{ 38} O3       + NO2                 -->        NO3
{ 39} NO3      + NO                  -->   2.000*NO2
{ 40} NO3      + NO2                 -->        NO       +       NO2
{ 41} NO3      + HO2                 -->        HNO3
{ 42} NO3      + NO2                 -->        N2O5
{ 43} N2O5                           -->        NO2      +       NO3
{ 44} N2O5     + [H2O]               -->   2.000*HNO3
{ 45} HO       + NO2                 -->        HNO3
{ 46} HO       + HNO3                -->        NO3
{ 47} HO       + HNO4                -->        NO2
{ 48} HO       + HO2                 -->
{ 49} HO       + SO2                 -->        SULF     +       HO2      +       SULAER
{ 50} CO       + HO                  -->        HO2
{ 51} HO                             -->        MO2
{ 52} ETH      + HO                  -->        ETHP
{ 53} HC3      + HO                  -->   0.830*HC3P    + 0.170*HO2      + 0.009*HCHO
                                        + 0.075*ALD     + 0.025*KET
{ 54} HC5      + HO                  -->        HC5P     + 0.250*XO2
{ 55} HC8      + HO                  -->        HC8P     + 0.750*XO2      +       HC8AER
{ 56} OL2      + HO                  -->        OL2P
{ 57} OLT      + HO                  -->        OLTP
```

Table 8A-10. RADM2_CIS1_AE and RADM2_CIS1_AE_AQ Mechanisms

```
{ 58} OLI      + HO                 -->        OLIP     +       OLIAER
{ 59} TOL      + HO                 -->  0.750*TOLP     + 0.250*CSL      + 0.250*HO2
                                        +       TOLAER
{ 60} XYL      + HO                 -->  0.830*XYLP     + 0.170*CSL      + 0.170*HO2
                                        +       XYLAER
{ 61} CSL      + HO                 -->  0.100*HO2      + 0.900*XO2      + 0.900*TCO3
                                        +       CSLAER
{ 62} CSL      + HO                 -->        CSL
{ 63} HCHO     + HO                 -->        HO2      +       CO
{ 64} ALD      + HO                 -->        ACO3
{ 65} KET      + HO                 -->        KETP
{ 66} GLY      + HO                 -->        HO2      + 2.000*CO
{ 67} MGLY     + HO                 -->        ACO3     +       CO
{ 68} DCB      + HO                 -->        TCO3
{ 69} OP1      + HO                 -->  0.500*MO2      + 0.500*HCHO     + 0.500*HO
{ 70} OP2      + HO                 -->  0.500*HC3P     + 0.500*ALD      + 0.500*HO
{ 71} PAA      + HO                 -->        ACO3
{ 72} PAN      + HO                 -->        HCHO     +       NO3      +       XO2
{ 73} ONIT     + HO                 -->        HC3P     +       NO2
{ 74} ACO3     + NO2                -->        PAN
{ 75} PAN                           -->        ACO3     +       NO2
{ 76} TCO3     + NO2                -->        TPAN
{ 77} TPAN                          -->        TCO3     +       NO2
{ 78} MO2      + NO                 -->        HCHO     +       HO2      +       NO2
{ 79} HC3P     + NO                 -->  0.750*ALD      + 0.250*KET      + 0.090*HCHO
                                        + 0.036*ONIT     + 0.964*NO2      + 0.964*HO2
{ 80} HC5P     + NO                 -->  0.380*ALD      + 0.690*KET      + 0.080*ONIT
                                        + 0.920*NO2      + 0.920*HO2
{ 81} HC8P     + NO                 -->  0.350*ALD      + 1.060*KET      + 0.040*HCHO
                                        + 0.240*ONIT     + 0.760*NO2      + 0.760*HO2
{ 82} OL2P     + NO                 -->  1.600*HCHO     +       HO2      +       NO2
                                        + 0.200*ALD
{ 83} OLTP     + NO                 -->        ALD      +       HCHO     +       HO2
                                        +       NO2
{ 84} OLIP     + NO                 -->        HO2      + 1.450*ALD      + 0.280*HCHO
                                        + 0.100*KET      +       NO2
{ 85} ACO3     + NO                 -->        MO2      +       NO2
{ 86} TCO3     + NO                 -->        NO2      + 0.920*HO2      + 0.890*GLY
                                        + 0.110*MGLY     + 0.050*ACO3     + 0.950*CO
                                        + 2.000*XO2
{ 87} TOLP     + NO                 -->        NO2      +       HO2      + 0.170*MGLY
                                        + 0.160*GLY      + 0.700*DCB
{ 88} XYLP     + NO                 -->        NO2      +       HO2      + 0.450*MGLY
                                        + 0.806*DCB
{ 89} ETHP     + NO                 -->        ALD      +       HO2      +       NO2
{ 90} KETP     + NO                 -->        MGLY     +       NO2      +       HO2
{ 91} OLN      + NO                 -->        HCHO     +       ALD      + 2.000*NO2
{ 92} HCHO     + NO3                -->        HO2      +       HNO3     +       CO
{ 93} ALD      + NO3                -->        ACO3     +       HNO3
{ 94} GLY      + NO3                -->        HNO3     +       HO2      + 2.000*CO
{ 95} MGLY     + NO3                -->        HNO3     +       ACO3     +       CO
{ 96} DCB      + NO3                -->        HNO3     +       TCO3
{ 97} CSL      + NO3                -->        HNO3     +       XNO2     + 0.500*CSL
                                        + 0.500*CSLAER
{ 98} OL2      + NO3                -->        OLN
{ 99} OLT      + NO3                -->        OLN
{100} OLI      + NO3                -->        OLN      +       OLIAER
{101} OL2      + O3                 -->        HCHO     + 0.400*ORA1     + 0.420*CO
                                        + 0.120*HO2
{102} OLT      + O3                 -->  0.530*HCHO     + 0.500*ALD      + 0.330*CO
                                        + 0.200*ORA1     + 0.200*ORA2     + 0.230*HO2
```

Table 8A-10. RADM2_CIS1_AE and RADM2_CIS1_AE_AQ Mechanisms

```
                                    + 0.220*MO2      + 0.100*HO
{103} OLI      + O3          -->    0.180*HCHO      + 0.720*ALD      + 0.100*KET
                                    + 0.230*CO       + 0.060*ORA1     + 0.290*ORA2
                                    + 0.260*HO2      + 0.140*HO       + 0.310*MO2
                                    +       OLIAER
{104} HO2      + MO2         -->           OP1
{105} HO2      + ETHP        -->           OP2
{106} HO2      + HC3P        -->           OP2
{107} HO2      + HC5P        -->           OP2
{108} HO2      + HC8P        -->           OP2
{109} HO2      + OL2P        -->           OP2
{110} HO2      + OLTP        -->           OP2
{111} HO2      + OLIP        -->           OP2
{112} HO2      + KETP        -->           OP2
{113} HO2      + ACO3        -->           PAA
{114} HO2      + TOLP        -->           OP2
{115} HO2      + XYLP        -->           OP2
{116} HO2      + TCO3        -->           OP2
{117} HO2      + OLN         -->           ONIT
{118} MO2      + MO2         -->    1.500*HCHO      +       HO2
{119} MO2      + ETHP        -->    0.750*HCHO      +       HO2      + 0.750*ALD
{120} MO2      + HC3P        -->    0.840*HCHO      + 0.770*ALD      + 0.260*KET
                                    +       HO2
{121} MO2      + HC5P        -->    0.770*HCHO      + 0.410*ALD      + 0.750*KET
                                    +       HO2
{122} MO2      + HC8P        -->    0.800*HCHO      + 0.460*ALD      + 1.390*KET
                                    +       HO2
{123} MO2      + OL2P        -->    1.550*HCHO      + 0.350*ALD      +       HO2
{124} MO2      + OLTP        -->    1.250*HCHO      + 0.750*ALD      +       HO2
{125} MO2      + OLIP        -->    0.890*HCHO      + 0.725*ALD      +       HO2
                                    + 0.550*KET
{126} MO2      + KETP        -->    0.750*HCHO      + 0.750*MGLY     +       HO2
{127} MO2      + ACO3        -->           HCHO     + 0.500*HO2      + 0.500*MO2
                                    + 0.500*ORA2
{128} MO2      + TOLP        -->           HCHO     + 0.170*MGLY     + 0.160*GLY
                                    + 0.700*DCB      + 2.000*HO2
{129} MO2      + XYLP        -->           HCHO     + 0.450*MGLY     + 0.806*DCB
                                    + 2.000*HO2
{130} MO2      + TCO3        -->    0.500*HCHO      + 0.445*GLY      + 0.055*MGLY
                                    + 0.500*ORA2     + 0.025*ACO3     + 0.460*HO2
                                    + 0.475*CO       +       XO2
{131} MO2      + OLN         -->    1.750*HCHO      + 0.500*HO2      +       ALD
                                    +       NO2
{132} ETHP     + ACO3        -->           ALD      + 0.500*HO2      + 0.500*MO2
                                    + 0.500*ORA2
{133} HC3P     + ACO3        -->    0.770*ALD       + 0.260*KET      + 0.500*HO2
                                    + 0.500*MO2      + 0.500*ORA2
{134} HC5P     + ACO3        -->    0.410*ALD       + 0.750*KET      + 0.500*HO2
                                    + 0.500*MO2      + 0.500*ORA2
{135} HC8P     + ACO3        -->    0.460*ALD       + 1.390*KET      + 0.500*HO2
                                    + 0.500*MO2      + 0.500*ORA2
{136} OL2P     + ACO3        -->    0.800*HCHO      + 0.600*ALD      + 0.500*HO2
                                    + 0.500*MO2      + 0.500*ORA2
{137} OLTP     + ACO3        -->           ALD      + 0.500*HCHO     + 0.500*HO2
                                    + 0.500*MO2      + 0.500*ORA2
{138} OLIP     + ACO3        -->    0.725*ALD       + 0.550*KET      + 0.140*HCHO
                                    + 0.500*HO2      + 0.500*MO2      + 0.500*ORA2
{139} KETP     + ACO3        -->           MGLY     + 0.500*HO2      + 0.500*MO2
                                    + 0.500*ORA2
{140} ACO3     + ACO3        -->    2.000*MO2
{141} ACO3     + TOLP        -->           MO2      + 0.170*MGLY     + 0.160*GLY
```

Table 8A-10. RADM2_CIS1_AE and RADM2_CIS1_AE_AQ Mechanisms

				+ 0.700*DCB	+	HO2	
{142}	ACO3	+ XYLP	-->	MO2	+ 0.450*MGLY	+ 0.806*DCB	
				+ HO2			
{143}	ACO3	+ TCO3	-->	MO2	+ 0.920*HO2	+ 0.890*GLY	
				+ 0.110*MGLY	+ 0.050*ACO3	+ 0.950*CO	
				+ 2.000*XO2			
{144}	ACO3	+ OLN	-->	HCHO	+	ALD	+ 0.500*ORA2
				+ NO2	+ 0.500*MO2		
{145}	OLN	+ OLN	-->	2.000*HCHO	+ 2.000*ALD	+ 2.000*NO2	
{146}	XO2	+ HO2	-->	OP2			
{147}	XO2	+ MO2	-->	HCHO	+	HO2	
{148}	XO2	+ ACO3	-->	MO2			
{149}	XO2	+ XO2	-->				
{150}	XO2	+ NO	-->	NO2			
{151}	XNO2	+ NO2	-->	ONIT			
{152}	XNO2	+ HO2	-->	OP2			
{153}	XNO2	+ MO2	-->	HCHO	+	HO2	
{154}	XNO2	+ ACO3	-->	MO2			
{155}	XNO2	+ XNO2	-->				
{156}	TERP	+ HO	-->	TERPAER	+	HO	
{157}	TERP	+ NO3	-->	TERPAER	+	NO3	
{158}	TERP	+ O3	-->	TERPAER	+	O3	
{159}	ISO	+ HO	-->	ISO_RO2	+ 0.079*XO2		
{160}	ISO_RO2	+ NO	-->	0.088*ONIT	+ 0.912*NO2	+ 0.912*HO2	
				+ 0.912*ISOPROD	+ 0.629*HCHO		
{161}	ISO_RO2	+ HO2	-->	OP2			
{162}	ISO_RO2	+ ACO3	-->	0.500*HO2	+ 0.500*MO2	+ 0.500*ORA2	
				+ ISOPROD			
{163}	ISO_RO2	+ MO2	-->	0.500*HCHO	+ 0.500*HO2	+	ISOPROD
{164}	ISO	+ O3	-->	0.600*HCHO	+ 0.650*ISOPROD	+ 0.390*ORA1	
				+ 0.270*HO	+ 0.070*HO2	+ 0.070*CO	
				+ 0.200*XO2	+ 0.200*ACO3	+ 0.150*ALD	
{165}	ISO	+ O3P	-->	0.750*ISOPROD	+ 0.250*ACO3	+ 0.250*HCHO	
				+ 0.250*MO2			
{166}	ISO	+ NO3	-->	ISON_RO2			
{167}	ISON_RO2	+ NO	-->	NO2	+ 0.800*ALD	+ 0.800*ONIT	
				+ 0.800*HO2	+ 0.200*ISOPROD	+ 0.200*NO2	
{168}	ISON_RO2	+ HO2	-->	ONIT			
{169}	ISON_RO2	+ ACO3	-->	0.500*HO2	+ 0.500*MO2	+ 0.500*ORA2	
				+ ALD	+	ONIT	
{170}	ISON_RO2	+ MO2	-->	0.500*HCHO	+ 0.500*HO2	+	ALD
				+ ONIT			
{171}	ISOPROD	+ HO	-->	0.500*ACO3	+ 0.500*IP_RO2	+ 0.200*XO2	
{172}	IP_RO2	+ NO	-->	NO2	+	HO2	+ 0.590*CO
				+ 0.550*ALD	+ 0.250*HCHO	+ 0.080*GLY	
				+ 0.340*MGLY	+ 0.630*KET		
{173}	IP_RO2	+ HO2	-->	OP2			
{174}	IP_RO2	+ ACO3	-->	0.500*HO2	+ 0.500*MO2	+ 0.500*ORA2	
				+ 0.500*ALD	+ 0.500*KET		
{175}	IP_RO2	+ MO2	-->	0.500*HCHO	+ 0.500*HO2	+ 0.500*ALD	
				+ 0.500*KET			
{176}	ISOPROD	+ O3	-->	0.268*HO	+ 0.100*HO2	+ 0.114*ACO3	
				+ 0.054*MO2	+ 0.070*XO2	+ 0.155*CO	
				+ 0.146*HCHO	+ 0.020*ALD	+ 0.010*GLY	
				+ 0.850*MGLY	+ 0.090*KET	+ 0.462*ORA1	
{177}	ISOPROD	+ hv	-->	0.970*ACO3	+ 0.333*HO2	+ 0.700*MO2	
				+ 0.200*HCHO	+ 0.333*CO	+ 0.067*ALD	
				+ 0.033*KET			
{178}	ISOPROD	+ NO3	-->	0.075*ACO3	+ 0.075*HNO3	+ 0.643*CO	
				+ 0.282*HCHO	+ 0.925*ONIT	+ 0.282*ALD	
				+ 0.925*HO2	+ 0.925*XO2		

Table 8A-10. RADM2_CIS1_AE and RADM2_CIS1_AE_AQ Mechanisms

```
>-----------------------------------------------------------------------------------------------<

Rate Expression                                                                    Rate Constant
==============================================================================================
k(  1) uses photo table NO2_RADM88       , scaled by 1.00000E+00    {0.00000E+00}
k(  2) uses photo table O3O1D_RADM88     , scaled by 1.00000E+00    {0.00000E+00}
k(  3) uses photo table O3O3P_RADM88     , scaled by 1.00000E+00    {0.00000E+00}
k(  4) uses photo table HONO_RADM88      , scaled by 1.00000E+00    {0.00000E+00}
k(  5) uses photo table HNO3_RADM88      , scaled by 1.00000E+00    {0.00000E+00}
k(  6) uses photo table HNO4_RADM88      , scaled by 1.00000E+00    {0.00000E+00}
k(  7) uses photo table NO3NO_RADM88     , scaled by 1.00000E+00    {0.00000E+00}
k(  8) uses photo table NO3NO2_RADM88    , scaled by 1.00000E+00    {0.00000E+00}
k(  9) uses photo table H2O2_RADM88      , scaled by 1.00000E+00    {0.00000E+00}
k( 10) uses photo table HCHOmol_RADM88   , scaled by 1.00000E+00    {0.00000E+00}
k( 11) uses photo table HCHOrad_RADM88   , scaled by 1.00000E+00    {0.00000E+00}
k( 12) uses photo table ALD_RADM88       , scaled by 1.00000E+00    {0.00000E+00}
k( 13) uses photo table MHP_RADM88       , scaled by 1.00000E+00    {0.00000E+00}
k( 14) uses photo table HOP_RADM88       , scaled by 1.00000E+00    {0.00000E+00}
k( 15) uses photo table PAA_RADM88       , scaled by 1.00000E+00    {0.00000E+00}
k( 16) uses photo table KETONE_RADM88    , scaled by 1.00000E+00    {0.00000E+00}
k( 17) uses photo table GLYform_RADM88   , scaled by 1.00000E+00    {0.00000E+00}
k( 18) uses photo table GLYmol_RADM88    , scaled by 1.00000E+00    {0.00000E+00}
k( 19) uses photo table MGLY_RADM88      , scaled by 1.00000E+00    {0.00000E+00}
k( 20) uses photo table UDC_RADM88       , scaled by 1.00000E+00    {0.00000E+00}
k( 21) uses photo table ORGNIT_RADM88    , scaled by 1.00000E+00    {0.00000E+00}
k( 22) =  6.0000E-34 * (T/300)**(-2.30)                             {6.09302E-34}
k( 23) =  6.5000E-12 * exp(   120.0/T)                              {9.72293E-12}
k( 24) =  1.8000E-11 * exp(   110.0/T)                              {2.60365E-11}
k( 25) =  3.2000E-11 * exp(    70.0/T)                              {4.04730E-11}
k( 26) =  2.2000E-10                                                {2.20000E-10}
k( 27) =  2.0000E-12 * exp( -1400.0/T)                              {1.82272E-14}
k( 28) =  1.6000E-12 * exp(  -940.0/T)                              {6.82650E-14}
k( 29) =  1.1000E-14 * exp(  -500.0/T)                              {2.05452E-15}
k( 30) =  3.7000E-12 * exp(   240.0/T)                              {8.27883E-12}
k( 31) is a falloff expression using:                               {1.39058E-12}
   k0   =  1.8000E-31 * (T/300)**(-3.20)
   kinf =  4.7000E-12 * (T/300)**(-1.40)
   F =  0.60,  n =  1.00
k( 32) = k( 31) / Keq,  where Keq =  2.100E-27 * exp( 10900.0/T)    {8.62399E-02}
k( 33) is a special rate expression of the form:                    {3.01634E-12}
   k = k1 + k2[M], where
   k1 =  2.2000E-13 * exp(   620.0/T)
   k2 =  1.9000E-33 * exp(   980.0/T)
k( 34) is a special rate expression of the form:                    {6.78905E-30}
   k = k1 + k2[M], where
   k1 =  3.0800E-34 * exp(  2820.0/T)
   k2 =  2.6600E-54 * exp(  3180.0/T)
k( 35) =  3.3000E-12 * exp(  -200.0/T)                              {1.68671E-12}
k( 36) is a falloff expression using:                               {4.87144E-12}
   k0   =  7.0000E-31 * (T/300)**(-2.60)
   kinf =  1.5000E-11 * (T/300)**(-0.50)
   F =  0.60,  n =  1.00
k( 37) =  3.3000E-39 * exp(   530.0/T)                              {1.95397E-38}
k( 38) =  1.4000E-13 * exp( -2500.0/T)                              {3.18213E-17}
k( 39) =  1.7000E-11 * exp(   150.0/T)                              {2.81225E-11}
k( 40) =  2.5000E-14 * exp( -1230.0/T)                              {4.03072E-16}
k( 41) =  2.5000E-12                                                {2.50000E-12}
k( 42) is a falloff expression using:                               {1.26440E-12}
   k0   =  2.2000E-30 * (T/300)**(-4.30)
   kinf =  1.5000E-12 * (T/300)**(-0.50)
```

Table 8A-10. RADM2_CIS1_AE and RADM2_CIS1_AE_AQ Mechanisms

```
   F =  0.60,  n =  1.00
k( 43) = k( 42) / Keq,  where Keq =  1.100E-27 * exp( 11200.0/T)  {5.47034E-02}
k( 44) =  2.0000E-21                                              {2.00000E-21}
k( 45) is a falloff expression using:                             {1.14885E-11}
   k0   =  2.6000E-30 * (T/300)**(-3.20)
   kinf =  2.4000E-11 * (T/300)**(-1.30)
   F =  0.60,  n =  1.00
k( 46) is a special rate expression of the form:                  {1.47236E-13}
   k = k0 + {k3[M] / (1 + k3[M]/k2)}, where
   k0 =  7.2000E-15 * exp(   785.0/T)
   k2 =  4.1000E-16 * exp(  1440.0/T)
   k3 =  1.9000E-33 * exp(   725.0/T)
k( 47) =  1.3000E-12 * exp(   380.0/T)                            {4.65309E-12}
k( 48) =  4.6000E-11 * exp(   230.0/T)                            {9.95294E-11}
k( 49) is a falloff expression using:                             {8.88848E-13}
   k0   =  3.0000E-31 * (T/300)**(-3.30)
   kinf =  1.5000E-12 * (T/300)**( 0.00)
   F =  0.60,  n =  1.00
k( 50) =  1.5000E-13 * (1.0 + 0.6*Pressure)                       {2.40000E-13}
k( 51) =  2.8300E+01 * (T/300)**( 2.00) * exp( -1280.0/T)         {3.80672E-01}
k( 52) =  1.2330E-12 * (T/300)**( 2.00) * exp(  -444.0/T)         {2.74210E-13}
k( 53) =  1.5900E-11 * exp(  -540.0/T)                            {2.59669E-12}
k( 54) =  1.7300E-11 * exp(  -380.0/T)                            {4.83334E-12}
k( 55) =  3.6400E-11 * exp(  -380.0/T)                            {1.01696E-11}
k( 56) =  2.1500E-12 * exp(   411.0/T)                            {8.53916E-12}
k( 57) =  5.3200E-12 * exp(   504.0/T)                            {2.88684E-11}
k( 58) =  1.0700E-11 * exp(   549.0/T)                            {6.75269E-11}
k( 59) =  2.1000E-12 * exp(   322.0/T)                            {6.18715E-12}
k( 60) =  1.8900E-11 * exp(   116.0/T)                            {2.78943E-11}
k( 61) =  4.0000E-11                                              {4.00000E-11}
k( 62) =  9.0000E-01 * k( 61)                                     {3.60000E-11}
k( 63) =  9.0000E-12                                              {9.00000E-12}
k( 64) =  6.8700E-12 * exp(   256.0/T)                            {1.62197E-11}
k( 65) =  1.2000E-11 * exp(  -745.0/T)                            {9.85020E-13}
k( 66) =  1.1500E-11                                              {1.15000E-11}
k( 67) =  1.7000E-11                                              {1.70000E-11}
k( 68) =  2.8000E-11                                              {2.80000E-11}
k( 69) =  1.0000E-11                                              {1.00000E-11}
k( 70) =  1.0000E-11                                              {1.00000E-11}
k( 71) =  1.0000E-11                                              {1.00000E-11}
k( 72) =  6.1650E-13 * (T/300)**( 2.00) * exp(  -444.0/T)         {1.37105E-13}
k( 73) =  1.5500E-11 * exp(  -540.0/T)                            {2.53137E-12}
k( 74) =  2.8000E-12 * exp(   181.0/T)                            {5.13974E-12}
k( 75) =  1.9500E+16 * exp(-13543.0/T)                            {3.57235E-04}
k( 76) =  4.7000E-12                                              {4.70000E-12}
k( 77) =  1.9500E+16 * exp(-13543.0/T)                            {3.57235E-04}
k( 78) =  4.2000E-12 * exp(   180.0/T)                            {7.68378E-12}
k( 79) =  4.2000E-12 * exp(   180.0/T)                            {7.68378E-12}
k( 80) =  4.2000E-12 * exp(   180.0/T)                            {7.68378E-12}
k( 81) =  4.2000E-12 * exp(   180.0/T)                            {7.68378E-12}
k( 82) =  4.2000E-12 * exp(   180.0/T)                            {7.68378E-12}
k( 83) =  4.2000E-12 * exp(   180.0/T)                            {7.68378E-12}
k( 84) =  4.2000E-12 * exp(   180.0/T)                            {7.68378E-12}
k( 85) =  4.2000E-12 * exp(   180.0/T)                            {7.68378E-12}
k( 86) =  4.2000E-12 * exp(   180.0/T)                            {7.68378E-12}
k( 87) =  4.2000E-12 * exp(   180.0/T)                            {7.68378E-12}
k( 88) =  4.2000E-12 * exp(   180.0/T)                            {7.68378E-12}
k( 89) =  4.2000E-12 * exp(   180.0/T)                            {7.68378E-12}
k( 90) =  4.2000E-12 * exp(   180.0/T)                            {7.68378E-12}
k( 91) =  4.2000E-12 * exp(   180.0/T)                            {7.68378E-12}
k( 92) =  6.0000E-13 * exp( -2058.0/T)                            {6.01030E-16}
```

Table 8A-10. RADM2_CIS1_AE and RADM2_CIS1_AE_AQ Mechanisms

```
k( 93) =  1.4000E-12 * exp( -1900.0/T)                    {2.38307E-15}
k( 94) =  6.0000E-13 * exp( -2058.0/T)                    {6.01030E-16}
k( 95) =  1.4000E-12 * exp( -1900.0/T)                    {2.38307E-15}
k( 96) =  1.4000E-12 * exp( -1900.0/T)                    {2.38307E-15}
k( 97) =  2.2000E-11                                      {2.20000E-11}
k( 98) =  2.0000E-12 * exp( -2923.0/T)                    {1.09940E-16}
k( 99) =  1.0000E-11 * exp( -1895.0/T)                    {1.73099E-14}
k(100) =  3.2300E-11 * exp(  -975.0/T)                    {1.22539E-12}
k(101) =  1.2000E-14 * exp( -2633.0/T)                    {1.74559E-18}
k(102) =  1.3200E-14 * exp( -2105.0/T)                    {1.12933E-17}
k(103) =  7.2900E-15 * exp( -1136.0/T)                    {1.61125E-16}
k(104) =  7.7000E-14 * exp(  1300.0/T)                    {6.04038E-12}
k(105) =  7.7000E-14 * exp(  1300.0/T)                    {6.04038E-12}
k(106) =  7.7000E-14 * exp(  1300.0/T)                    {6.04038E-12}
k(107) =  7.7000E-14 * exp(  1300.0/T)                    {6.04038E-12}
k(108) =  7.7000E-14 * exp(  1300.0/T)                    {6.04038E-12}
k(109) =  7.7000E-14 * exp(  1300.0/T)                    {6.04038E-12}
k(110) =  7.7000E-14 * exp(  1300.0/T)                    {6.04038E-12}
k(111) =  7.7000E-14 * exp(  1300.0/T)                    {6.04038E-12}
k(112) =  7.7000E-14 * exp(  1300.0/T)                    {6.04038E-12}
k(113) =  7.7000E-14 * exp(  1300.0/T)                    {6.04038E-12}
k(114) =  7.7000E-14 * exp(  1300.0/T)                    {6.04038E-12}
k(115) =  7.7000E-14 * exp(  1300.0/T)                    {6.04038E-12}
k(116) =  7.7000E-14 * exp(  1300.0/T)                    {6.04038E-12}
k(117) =  7.7000E-14 * exp(  1300.0/T)                    {6.04038E-12}
k(118) =  1.9000E-13 * exp(   220.0/T)                    {3.97533E-13}
k(119) =  1.4000E-13 * exp(   220.0/T)                    {2.92919E-13}
k(120) =  4.2000E-14 * exp(   220.0/T)                    {8.78758E-14}
k(121) =  3.4000E-14 * exp(   220.0/T)                    {7.11376E-14}
k(122) =  2.9000E-14 * exp(   220.0/T)                    {6.06762E-14}
k(123) =  1.4000E-13 * exp(   220.0/T)                    {2.92919E-13}
k(124) =  1.4000E-13 * exp(   220.0/T)                    {2.92919E-13}
k(125) =  1.7000E-14 * exp(   220.0/T)                    {3.55688E-14}
k(126) =  1.7000E-14 * exp(   220.0/T)                    {3.55688E-14}
k(127) =  9.6000E-13 * exp(   220.0/T)                    {2.00859E-12}
k(128) =  1.7000E-14 * exp(   220.0/T)                    {3.55688E-14}
k(129) =  1.7000E-14 * exp(   220.0/T)                    {3.55688E-14}
k(130) =  9.6000E-13 * exp(   220.0/T)                    {2.00859E-12}
k(131) =  1.7000E-14 * exp(   220.0/T)                    {3.55688E-14}
k(132) =  3.4000E-13 * exp(   220.0/T)                    {7.11376E-13}
k(133) =  1.0000E-13 * exp(   220.0/T)                    {2.09228E-13}
k(134) =  8.4000E-14 * exp(   220.0/T)                    {1.75752E-13}
k(135) =  7.2000E-14 * exp(   220.0/T)                    {1.50644E-13}
k(136) =  3.4000E-13 * exp(   220.0/T)                    {7.11376E-13}
k(137) =  3.4000E-13 * exp(   220.0/T)                    {7.11376E-13}
k(138) =  4.2000E-14 * exp(   220.0/T)                    {8.78758E-14}
k(139) =  4.2000E-14 * exp(   220.0/T)                    {8.78758E-14}
k(140) =  1.1900E-12 * exp(   220.0/T)                    {2.48981E-12}
k(141) =  4.2000E-14 * exp(   220.0/T)                    {8.78758E-14}
k(142) =  4.2000E-14 * exp(   220.0/T)                    {8.78758E-14}
k(143) =  1.1900E-12 * exp(   220.0/T)                    {2.48981E-12}
k(144) =  4.2000E-14 * exp(   220.0/T)                    {8.78758E-14}
k(145) =  3.6000E-16 * exp(   220.0/T)                    {7.53221E-16}
k(146) =  7.7000E-14 * exp(  1300.0/T)                    {6.04038E-12}
k(147) =  1.7000E-14 * exp(   220.0/T)                    {3.55688E-14}
k(148) =  4.2000E-14 * exp(   220.0/T)                    {8.78758E-14}
k(149) =  3.6000E-16 * exp(   220.0/T)                    {7.53221E-16}
k(150) =  4.2000E-12 * exp(   180.0/T)                    {7.68378E-12}
k(151) =  4.2000E-12 * exp(   180.0/T)                    {7.68378E-12}
k(152) =  7.7000E-14 * exp(  1300.0/T)                    {6.04038E-12}
k(153) =  1.7000E-14 * exp(   220.0/T)                    {3.55688E-14}
```

Table 8A-10. RADM2_CIS1_AE and RADM2_CIS1_AE_AQ Mechanisms

```
k(154) =  4.2000E-14 * exp(   220.0/T)                                {8.78758E-14}
k(155) =  3.6000E-16 * exp(   220.0/T)                                {7.53221E-16}
k(156) =  1.0000E+00 * k( 58)                                         {6.75269E-11}
k(157) =  1.0000E+00 * k(100)                                         {1.22539E-12}
k(158) =  1.0000E+00 * k(103)                                         {1.61125E-16}
k(159) =  2.5400E-11 * (T/300)**( 1.00) * exp(   407.6/T)             {9.90719E-11}
k(160) =  4.2000E-12 * (T/300)**( 1.00) * exp(   181.2/T)             {7.66335E-12}
k(161) =  7.7000E-14 * (T/300)**( 1.00) * exp(  1298.3/T)             {5.96598E-12}
k(162) =  8.4000E-14 * (T/300)**( 1.00) * exp(   221.4/T)             {1.75402E-13}
k(163) =  3.4000E-14 * (T/300)**( 1.00) * exp(   221.4/T)             {7.09961E-14}
k(164) =  7.8600E-15 * (T/300)**( 1.00) * exp( -1912.2/T)             {1.27569E-17}
k(165) =  3.6000E-11                                                  {3.60000E-11}
k(166) =  3.0300E-12 * (T/300)**( 1.00) * exp(  -447.9/T)             {6.69552E-13}
k(167) =  4.2000E-12 * (T/300)**( 1.00) * exp(   181.2/T)             {7.66335E-12}
k(168) =  7.7000E-14 * (T/300)**( 1.00) * exp(  1298.3/T)             {5.96598E-12}
k(169) =  8.4000E-14 * (T/300)**( 1.00) * exp(   221.4/T)             {1.75402E-13}
k(170) =  3.4000E-14 * (T/300)**( 1.00) * exp(   221.4/T)             {7.09961E-14}
k(171) =  3.3600E-11                                                  {3.36000E-11}
k(172) =  4.2000E-12 * (T/300)**( 1.00) * exp(   181.2/T)             {7.66335E-12}
k(173) =  7.7000E-14 * (T/300)**( 1.00) * exp(  1298.3/T)             {5.96598E-12}
k(174) =  8.4000E-14 * (T/300)**( 1.00) * exp(   221.4/T)             {1.75402E-13}
k(175) =  3.4000E-14 * (T/300)**( 1.00) * exp(   221.4/T)             {7.09961E-14}
k(176) =  7.1100E-18                                                  {7.11000E-18}
k(177) uses photo table ACROLEIN        , scaled by 3.60000E-03       {0.00000E+00}
k(178) =  1.0000E-15                                                  {1.00000E-15}
==============================================================================
```

Table 8A-11. RADM2_CIS4 and RADM2_CIS4_AQ Mechanisms

```
Reaction List
>-----------------------------------------------------------------------------------------------<
{  1} NO2      + hv                    -->        O3P      +       NO
{  2} O3       + hv                    -->        O1D
{  3} O3       + hv                    -->        O3P
{  4} HONO     + hv                    -->        HO       +       NO
{  5} HNO3     + hv                    -->        HO       +       NO2
{  6} HNO4     + hv                    -->        HO2      +       NO2
{  7} NO3      + hv                    -->        NO
{  8} NO3      + hv                    -->        NO2      +       O3P
{  9} H2O2     + hv                    -->  2.000*HO
{ 10} HCHO     + hv                    -->        CO
{ 11} HCHO     + hv                    -->        HO2      +       HO2      +       CO
{ 12} ALD      + hv                    -->        MO2      +       HO2      +       CO
{ 13} OP1      + hv                    -->        HCHO     +       HO2      +       HO
{ 14} OP2      + hv                    -->        ALD      +       HO2      +       HO
{ 15} PAA      + hv                    -->        MO2      +       HO
{ 16} KET      + hv                    -->        ACO3     +       ETHP
{ 17} GLY      + hv                    -->  0.130*HCHO     + 1.870*CO
{ 18} GLY      + hv                    -->  0.450*HCHO     + 1.550*CO       + 0.800*HO2
{ 19} MGLY     + hv                    -->        ACO3     +       HO2      +       CO
{ 20} DCB      + hv                    -->  0.980*HO2      + 0.020*ACO3     +       TCO3
{ 21} ONIT     + hv                    -->  0.200*ALD      + 0.800*KET      +       HO2
                                          +        NO2
{ 22} O3P      + [M]      + [O2]       -->        O3
{ 23} O3P      + NO2                   -->        NO
{ 24} O1D      + [N2]                  -->        O3P
{ 25} O1D      + [O2]                  -->        O3P
{ 26} O1D      + [H2O]                 -->  2.000*HO
{ 27} O3       + NO                    -->        NO2
{ 28} O3       + HO                    -->        HO2
{ 29} O3       + HO2                   -->        HO
{ 30} HO2      + NO                    -->        NO2      +       HO
{ 31} HO2      + NO2                   -->        HNO4
{ 32} HNO4                             -->        HO2      +       NO2
{ 33} HO2      + HO2                   -->        H2O2
{ 34} HO2      + HO2      + [H2O]      -->        H2O2
{ 35} H2O2     + HO                    -->        HO2
{ 36} NO       + HO                    -->        HONO
{ 37} NO       + NO       + [O2]       -->  2.000*NO2
{ 38} O3       + NO2                   -->        NO3
{ 39} NO3      + NO                    -->  2.000*NO2
{ 40} NO3      + NO2                   -->        NO       +       NO2
{ 41} NO3      + HO2                   -->        HNO3
{ 42} NO3      + NO2                   -->        N2O5
{ 43} N2O5                             -->        NO2      +       NO3
{ 44} N2O5     + [H2O]                 -->  2.000*HNO3
{ 45} HO       + NO2                   -->        HNO3
{ 46} HO       + HNO3                  -->        NO3
{ 47} HO       + HNO4                  -->        NO2
{ 48} HO       + HO2                   -->
{ 49} HO       + SO2                   -->        SULF     +       HO2
{ 50} CO       + HO                    -->        HO2
{ 51} HO                               -->        MO2
{ 52} ETH      + HO                    -->        ETHP
{ 53} HC3      + HO                    -->  0.830*HC3P     + 0.170*HO2      + 0.009*HCHO
                                          + 0.075*ALD      + 0.025*KET
{ 54} HC5      + HO                    -->        HC5P     + 0.250*XO2
{ 55} HC8      + HO                    -->        HC8P     + 0.750*XO2
{ 56} OL2      + HO                    -->        OL2P
{ 57} OLT      + HO                    -->        OLTP
```

Table 8A-11. RADM2_CIS4 and RADM2_CIS4_AQ Mechanisms

```
{ 58} OLI      + HO      -->        OLIP
{ 59} TOL      + HO      -->  0.750*TOLP     + 0.250*CSL      + 0.250*HO2
{ 60} XYL      + HO      -->  0.830*XYLP     + 0.170*CSL      + 0.170*HO2
{ 61} CSL      + HO      -->  0.100*HO2      + 0.900*XO2      + 0.900*TCO3
{ 62} CSL      + HO      -->        CSL
{ 63} HCHO     + HO      -->        HO2      +       CO
{ 64} ALD      + HO      -->        ACO3
{ 65} KET      + HO      -->        KETP
{ 66} GLY      + HO      -->        HO2      + 2.000*CO
{ 67} MGLY     + HO      -->        ACO3     +       CO
{ 68} DCB      + HO      -->        TCO3
{ 69} OP1      + HO      -->  0.500*MO2      + 0.500*HCHO     + 0.500*HO
{ 70} OP2      + HO      -->  0.500*HC3P     + 0.500*ALD      + 0.500*HO
{ 71} PAA      + HO      -->        ACO3
{ 72} PAN      + HO      -->        HCHO     +       NO3      +       XO2
{ 73} ONIT     + HO      -->        HC3P     +       NO2
{ 74} ACO3     + NO2     -->        PAN
{ 75} PAN                -->        ACO3     +       NO2
{ 76} TCO3     + NO2     -->        TPAN
{ 77} TPAN               -->        TCO3     +       NO2
{ 78} MO2      + NO      -->        HCHO     +       HO2      +       NO2
{ 79} HC3P     + NO      -->  0.750*ALD      + 0.250*KET      + 0.090*HCHO
                             + 0.036*ONIT     + 0.964*NO2      + 0.964*HO2
{ 80} HC5P     + NO      -->  0.380*ALD      + 0.690*KET      + 0.080*ONIT
                             + 0.920*NO2      + 0.920*HO2
{ 81} HC8P     + NO      -->  0.350*ALD      + 1.060*KET      + 0.040*HCHO
                             + 0.240*ONIT     + 0.760*NO2      + 0.760*HO2
{ 82} OL2P     + NO      -->  1.600*HCHO     +       HO2      +       NO2
                             + 0.200*ALD
{ 83} OLTP     + NO      -->        ALD      +       HCHO     +       HO2
                             +       NO2
{ 84} OLIP     + NO      -->        HO2      + 1.450*ALD      + 0.280*HCHO
                             + 0.100*KET      +       NO2
{ 85} ACO3     + NO      -->        MO2      +       NO2
{ 86} TCO3     + NO      -->        NO2      + 0.920*HO2      + 0.890*GLY
                             + 0.110*MGLY     + 0.050*ACO3     + 0.950*CO
                             + 2.000*XO2
{ 87} TOLP     + NO      -->        NO2      +       HO2      + 0.170*MGLY
                             + 0.160*GLY      + 0.700*DCB
{ 88} XYLP     + NO      -->        NO2      +       HO2      + 0.450*MGLY
                             + 0.806*DCB
{ 89} ETHP     + NO      -->        ALD      +       HO2      +       NO2
{ 90} KETP     + NO      -->        MGLY     +       NO2      +       HO2
{ 91} OLN      + NO      -->        HCHO     +       ALD      + 2.000*NO2
{ 92} HCHO     + NO3     -->        HO2      +       HNO3     +       CO
{ 93} ALD      + NO3     -->        ACO3     +       HNO3
{ 94} GLY      + NO3     -->        HNO3     +       HO2      + 2.000*CO
{ 95} MGLY     + NO3     -->        HNO3     +       ACO3     +       CO
{ 96} DCB      + NO3     -->        HNO3     +       TCO3
{ 97} CSL      + NO3     -->        HNO3     +       XNO2     + 0.500*CSL
{ 98} OL2      + NO3     -->        OLN
{ 99} OLT      + NO3     -->        OLN
{100} OLI      + NO3     -->        OLN
{101} OL2      + O3      -->        HCHO     + 0.400*ORA1     + 0.420*CO
                             + 0.120*HO2
{102} OLT      + O3      -->  0.530*HCHO     + 0.500*ALD      + 0.330*CO
                             + 0.200*ORA1     + 0.200*ORA2     + 0.230*HO2
                             + 0.220*MO2      + 0.100*HO
{103} OLI      + O3      -->  0.180*HCHO     + 0.720*ALD      + 0.100*KET
                             + 0.230*CO       + 0.060*ORA1     + 0.290*ORA2
                             + 0.260*HO2      + 0.140*HO       + 0.310*MO2
```

Table 8A-11. RADM2_CIS4 and RADM2_CIS4_AQ Mechanisms

```
{104} HO2     + MO2          -->        OP1
{105} HO2     + ETHP         -->        OP2
{106} HO2     + HC3P         -->        OP2
{107} HO2     + HC5P         -->        OP2
{108} HO2     + HC8P         -->        OP2
{109} HO2     + OL2P         -->        OP2
{110} HO2     + OLTP         -->        OP2
{111} HO2     + OLIP         -->        OP2
{112} HO2     + KETP         -->        OP2
{113} HO2     + ACO3         -->        PAA
{114} HO2     + TOLP         -->        OP2
{115} HO2     + XYLP         -->        OP2
{116} HO2     + TCO3         -->        OP2
{117} HO2     + OLN          -->        ONIT
{118} MO2     + MO2          -->  1.500*HCHO     +       HO2
{119} MO2     + ETHP         -->  0.750*HCHO     +       HO2      + 0.750*ALD
{120} MO2     + HC3P         -->  0.840*HCHO     + 0.770*ALD      + 0.260*KET
                                 +       HO2
{121} MO2     + HC5P         -->  0.770*HCHO     + 0.410*ALD      + 0.750*KET
                                 +       HO2
{122} MO2     + HC8P         -->  0.800*HCHO     + 0.460*ALD      + 1.390*KET
                                 +       HO2
{123} MO2     + OL2P         -->  1.550*HCHO     + 0.350*ALD      +       HO2
{124} MO2     + OLTP         -->  1.250*HCHO     + 0.750*ALD      +       HO2
{125} MO2     + OLIP         -->  0.890*HCHO     + 0.725*ALD      +       HO2
                                 + 0.550*KET
{126} MO2     + KETP         -->  0.750*HCHO     + 0.750*MGLY     +       HO2
{127} MO2     + ACO3         -->        HCHO     + 0.500*HO2      + 0.500*MO2
                                 + 0.500*ORA2
{128} MO2     + TOLP         -->        HCHO     + 0.170*MGLY     + 0.160*GLY
                                 + 0.700*DCB      + 2.000*HO2
{129} MO2     + XYLP         -->        HCHO     + 0.450*MGLY     + 0.806*DCB
                                 + 2.000*HO2
{130} MO2     + TCO3         -->  0.500*HCHO     + 0.445*GLY      + 0.055*MGLY
                                 + 0.500*ORA2     + 0.025*ACO3     + 0.460*HO2
                                 + 0.475*CO       +       XO2
{131} MO2     + OLN          -->  1.750*HCHO     + 0.500*HO2      +       ALD
                                 +       NO2
{132} ETHP    + ACO3         -->        ALD      + 0.500*HO2      + 0.500*MO2
                                 + 0.500*ORA2
{133} HC3P    + ACO3         -->  0.770*ALD      + 0.260*KET      + 0.500*HO2
                                 + 0.500*MO2      + 0.500*ORA2
{134} HC5P    + ACO3         -->  0.410*ALD      + 0.750*KET      + 0.500*HO2
                                 + 0.500*MO2      + 0.500*ORA2
{135} HC8P    + ACO3         -->  0.460*ALD      + 1.390*KET      + 0.500*HO2
                                 + 0.500*MO2      + 0.500*ORA2
{136} OL2P    + ACO3         -->  0.800*HCHO     + 0.600*ALD      + 0.500*HO2
                                 + 0.500*MO2      + 0.500*ORA2
{137} OLTP    + ACO3         -->        ALD      + 0.500*HCHO     + 0.500*HO2
                                 + 0.500*MO2      + 0.500*ORA2
{138} OLIP    + ACO3         -->  0.725*ALD      + 0.550*KET      + 0.140*HCHO
                                 + 0.500*HO2      + 0.500*MO2      + 0.500*ORA2
{139} KETP    + ACO3         -->        MGLY     + 0.500*HO2      + 0.500*MO2
                                 + 0.500*ORA2
{140} ACO3    + ACO3         -->  2.000*MO2
{141} ACO3    + TOLP         -->        MO2      + 0.170*MGLY     + 0.160*GLY
                                 + 0.700*DCB      +       HO2
{142} ACO3    + XYLP         -->        MO2      + 0.450*MGLY     + 0.806*DCB
                                 +       HO2
{143} ACO3    + TCO3         -->        MO2      + 0.920*HO2      + 0.890*GLY
                                 + 0.110*MGLY     + 0.050*ACO3     + 0.950*CO
```

Table 8A-11. RADM2_CIS4 and RADM2_CIS4_AQ Mechanisms

```
                                                  + 2.000*XO2
{144} ACO3      + OLN                    -->          HCHO      +        ALD       + 0.500*ORA2
                                                  +        NO2      + 0.500*MO2
{145} OLN       + OLN                    -->    2.000*HCHO      + 2.000*ALD       + 2.000*NO2
{146} XO2       + HO2                    -->          OP2
{147} XO2       + MO2                    -->          HCHO      +        HO2
{148} XO2       + ACO3                   -->          MO2
{149} XO2       + XO2                    -->
{150} XO2       + NO                     -->          NO2
{151} XNO2      + NO2                    -->          ONIT
{152} XNO2      + HO2                    -->          OP2
{153} XNO2      + MO2                    -->          HCHO      +        HO2
{154} XNO2      + ACO3                   -->          MO2
{155} XNO2      + XNO2                   -->
{156} ISO       + HO                     -->          ISO_RO2   + 0.079*XO2
{157} ISO_RO2   + NO                     -->    0.088*ONIT      + 0.912*NO2       + 0.912*HO2
                                                + 0.362*ISOPROD  + 0.230*MACR      + 0.320*MVK
                                                + 0.629*HCHO     + 0.079*XO2
{158} ISO_RO2   + HO2                    -->          OP2
{159} ISO_RO2   + ACO3                   -->    0.500*HO2       + 0.500*MO2       + 0.500*ORA2
                                                + 0.362*ISOPROD  + 0.230*MACR      + 0.320*MVK
                                                + 0.629*HCHO
{160} ISO_RO2   + MO2                    -->    0.500*HCHO      + 0.500*HO2       + 0.362*ISOPROD
                                                + 0.230*MACR     + 0.320*MVK       + 0.629*HCHO
{161} ISO       + O3                     -->    0.600*HCHO      + 0.390*MACR      + 0.160*MVK
                                                + 0.390*ORA1     + 0.270*HO        + 0.070*HO2
                                                + 0.070*CO       + 0.200*XO2       + 0.200*MCO3
                                                + 0.150*ALD      + 0.100*ISOPROD
{162} ISO       + O3P                    -->    0.750*ISOPROD    + 0.250*MCO3      + 0.250*HCHO
                                                + 0.250*MO2
{163} ISO       + NO3                    -->          ISON_RO2
{164} ISON_RO2  + NO                     -->          NO2       + 0.800*ALD       + 0.800*ONIT
                                                + 0.800*HO2      + 0.200*ISOPROD   + 0.200*NO2
{165} ISON_RO2  + HO2                    -->          ONIT
{166} ISON_RO2  + ACO3                   -->    0.500*HO2       + 0.500*MO2       + 0.500*ORA2
                                                +        ALD     +        ONIT
{167} ISON_RO2  + MO2                    -->    0.500*HCHO      + 0.500*HO2       + 0.500*ALD
                                                + 0.500*ONIT
{168} MACR      + HO                     -->    0.500*MCO3      + 0.500*MACR_RO2
{169} MACR_RO2  + NO                     -->          NO2       +        HO2       + 0.840*KET
                                                + 0.840*CO       + 0.150*HCHO      + 0.150*MGLY
{170} MACR_RO2  + HO2                    -->          OP2
{171} MACR_RO2  + ACO3                   -->    0.500*HO2       + 0.500*MO2       + 0.500*ORA2
                                                + 0.840*KET      + 0.840*CO        + 0.150*HCHO
                                                + 0.150*MGLY
{172} MACR_RO2  + MO2                    -->    0.650*HCHO      + 0.500*HO2       + 0.840*KET
                                                + 0.840*CO       + 0.150*MGLY
{173} MACR      + O3                     -->    0.630*ORA1      + 0.210*HO        + 0.110*HO2
                                                + 0.110*CO       + 0.200*HCHO      + 0.100*XO2
                                                + 0.100*ACO3
{174} MACR      + hv                     -->    0.660*HO2       + 0.330*MCO3      + 0.670*CO
                                                + 0.670*HCHO     + 0.670*ACO3      + 0.340*HO
                                                + 0.340*XO2
{175} MACR      + NO3                    -->    0.500*MCO3      + 0.500*HNO3      + 0.500*CO
                                                + 0.500*HO2      + 0.500*ONIT      + 0.500*XO2
{176} MVK       + HO                     -->          MVK_RO2
{177} MVK_RO2   + NO                     -->          NO2       + 0.700*ALD       + 0.700*XO2
                                                + 0.700*ACO3     + 0.300*HCHO      + 0.300*MGLY
                                                + 0.300*HO2
{178} MVK_RO2   + HO2                    -->          OP2
{179} MVK_RO2   + ACO3                   -->    0.500*HO2       + 1.200*MO2       + 0.500*ORA2
```

Table 8A-11. RADM2_CIS4 and RADM2_CIS4_AQ Mechanisms

```
                                          + 0.700*ALD      + 0.300*HCHO     + 0.300*MGLY
{180} MVK_RO2   + MO2                 -->   0.800*HCHO     + 0.500*HO2      + 0.700*ALD
                                          + 0.700*MO2      + 0.300*MGLY
{181} MVK       + O3                  -->   0.670*ORA1     + 0.160*HO       + 0.110*HO2
                                          + 0.110*CO       + 0.950*MGLY     + 0.100*HCHO
                                          + 0.050*XO2      + 0.050*ACO3
{182} MVK       + hv                  -->   0.700*ISOPROD  + 0.700*CO       + 0.300*MO2
                                          + 0.300*MCO3
{183} MPAN                            -->         MCO3     +       NO2
{184} MCO3      + NO                  -->         NO2      +       HCHO     +       ACO3
{185} MCO3      + NO2                 -->         MPAN
{186} MCO3      + HO2                 -->         PAA
{187} MCO3      + MO2                 -->   2.250*HCHO     + 0.500*HO2      + 0.500*MO2
{188} MCO3      + ACO3                -->   2.000*MO2      +       HCHO
{189} MCO3      + MCO3                -->   2.000*MO2      + 2.000*HCHO
{190} ISOPROD   + HO                  -->   0.313*ACO3     + 0.687*IP_RO2
{191} IP_RO2    + NO                  -->         NO2      +       HO2      + 0.610*CO
                                          + 0.270*ALD      + 0.030*HCHO     + 0.180*GLY
                                          + 0.210*MGLY     + 0.700*KET
{192} IP_RO2    + HO2                 -->         OP2
{193} IP_RO2    + ACO3                -->   0.500*HO2      + 0.500*MO2      + 0.500*ORA2
                                          + 0.500*ALD      + 0.500*KET
{194} IP_RO2    + MO2                 -->   0.500*HCHO     + 0.500*HO2      + 0.500*ALD
                                          + 0.500*KET
{195} ISOPROD   + O3                  -->   0.476*HO       + 0.072*HO2      + 0.168*MO2
                                          + 0.237*ACO3     + 0.100*XO2      + 0.243*CO
                                          + 0.218*HCHO     + 0.062*ALD      + 0.278*KET
                                          + 0.031*GLY      + 0.653*MGLY     + 0.044*ORA1
{196} ISOPROD   + hv                  -->   1.216*CO       + 0.434*ALD      + 0.350*HCHO
                                          + 0.216*KET      + 1.216*HO2      + 0.784*ACO3
{197} ISOPROD   + NO3                 -->   0.668*CO       + 0.332*HCHO     + 0.332*ALD
                                          +       ONIT     +       HO2      +       XO2
>-------------------------------------------------------------------------------------------<


Rate Expression                                                    Rate Constant
==============================================================================
k(  1) uses photo table NO2_RADM88       , scaled by 1.00000E+00   {0.00000E+00}
k(  2) uses photo table O3O1D_RADM88     , scaled by 1.00000E+00   {0.00000E+00}
k(  3) uses photo table O3O3P_RADM88     , scaled by 1.00000E+00   {0.00000E+00}
k(  4) uses photo table HONO_RADM88      , scaled by 1.00000E+00   {0.00000E+00}
k(  5) uses photo table HNO3_RADM88      , scaled by 1.00000E+00   {0.00000E+00}
k(  6) uses photo table HNO4_RADM88      , scaled by 1.00000E+00   {0.00000E+00}
k(  7) uses photo table NO3NO_RADM88     , scaled by 1.00000E+00   {0.00000E+00}
k(  8) uses photo table NO3NO2_RADM88    , scaled by 1.00000E+00   {0.00000E+00}
k(  9) uses photo table H2O2_RADM88      , scaled by 1.00000E+00   {0.00000E+00}
k( 10) uses photo table HCHOmol_RADM88   , scaled by 1.00000E+00   {0.00000E+00}
k( 11) uses photo table HCHOrad_RADM88   , scaled by 1.00000E+00   {0.00000E+00}
k( 12) uses photo table ALD_RADM88       , scaled by 1.00000E+00   {0.00000E+00}
k( 13) uses photo table MHP_RADM88       , scaled by 1.00000E+00   {0.00000E+00}
k( 14) uses photo table HOP_RADM88       , scaled by 1.00000E+00   {0.00000E+00}
k( 15) uses photo table PAA_RADM88       , scaled by 1.00000E+00   {0.00000E+00}
k( 16) uses photo table KETONE_RADM88    , scaled by 1.00000E+00   {0.00000E+00}
k( 17) uses photo table GLYform_RADM88   , scaled by 1.00000E+00   {0.00000E+00}
k( 18) uses photo table GLYmol_RADM88    , scaled by 1.00000E+00   {0.00000E+00}
k( 19) uses photo table MGLY_RADM88      , scaled by 1.00000E+00   {0.00000E+00}
k( 20) uses photo table UDC_RADM88       , scaled by 1.00000E+00   {0.00000E+00}
k( 21) uses photo table ORGNIT_RADM88    , scaled by 1.00000E+00   {0.00000E+00}
k( 22) =  6.0000E-34 * (T/300)**(-2.30)                            {6.09302E-34}
k( 23) =  6.5000E-12 * exp(   120.0/T)                             {9.72293E-12}
k( 24) =  1.8000E-11 * exp(   110.0/T)                             {2.60365E-11}
```

Table 8A-11. RADM2_CIS4 and RADM2_CIS4_AQ Mechanisms

```
k( 25) =  3.2000E-11 * exp(    70.0/T)                                {4.04730E-11}
k( 26) =  2.2000E-10                                                  {2.20000E-10}
k( 27) =  2.0000E-12 * exp( -1400.0/T)                                {1.82272E-14}
k( 28) =  1.6000E-12 * exp(  -940.0/T)                                {6.82650E-14}
k( 29) =  1.1000E-14 * exp(  -500.0/T)                                {2.05452E-15}
k( 30) =  3.7000E-12 * exp(   240.0/T)                                {8.27883E-12}
k( 31) is a falloff expression using:                                 {1.39058E-12}
   k0   =  1.8000E-31 * (T/300)**(-3.20)
   kinf =  4.7000E-12 * (T/300)**(-1.40)
   F =  0.60,  n =  1.00
k( 32) = k( 31) / Keq,  where Keq =  2.100E-27 * exp( 10900.0/T)  {8.62399E-02}
k( 33) is a special rate expression of the form:                      {3.01634E-12}
   k = k1 + k2[M], where
   k1 =  2.2000E-13 * exp(   620.0/T)
   k2 =  1.9000E-33 * exp(   980.0/T)
k( 34) is a special rate expression of the form:                      {6.78905E-30}
   k = k1 + k2[M], where
   k1 =  3.0800E-34 * exp(  2820.0/T)
   k2 =  2.6600E-54 * exp(  3180.0/T)
k( 35) =  3.3000E-12 * exp(  -200.0/T)                                {1.68671E-12}
k( 36) is a falloff expression using:                                 {4.87144E-12}
   k0   =  7.0000E-31 * (T/300)**(-2.60)
   kinf =  1.5000E-11 * (T/300)**(-0.50)
   F =  0.60,  n =  1.00
k( 37) =  3.3000E-39 * exp(   530.0/T)                                {1.95397E-38}
k( 38) =  1.4000E-13 * exp( -2500.0/T)                                {3.18213E-17}
k( 39) =  1.7000E-11 * exp(   150.0/T)                                {2.81225E-11}
k( 40) =  2.5000E-14 * exp( -1230.0/T)                                {4.03072E-16}
k( 41) =  2.5000E-12                                                  {2.50000E-12}
k( 42) is a falloff expression using:                                 {1.26440E-12}
   k0   =  2.2000E-30 * (T/300)**(-4.30)
   kinf =  1.5000E-12 * (T/300)**(-0.50)
   F =  0.60,  n =  1.00
k( 43) = k( 42) / Keq,  where Keq =  1.100E-27 * exp( 11200.0/T)  {5.47034E-02}
k( 44) =  2.0000E-21                                                  {2.00000E-21}
k( 45) is a falloff expression using:                                 {1.14885E-11}
   k0   =  2.6000E-30 * (T/300)**(-3.20)
   kinf =  2.4000E-11 * (T/300)**(-1.30)
   F =  0.60,  n =  1.00
k( 46) is a special rate expression of the form:                      {1.47236E-13}
   k = k0 + {k3[M] / (1 + k3[M]/k2)}, where
   k0 =  7.2000E-15 * exp(   785.0/T)
   k2 =  4.1000E-16 * exp(  1440.0/T)
   k3 =  1.9000E-33 * exp(   725.0/T)
k( 47) =  1.3000E-12 * exp(   380.0/T)                                {4.65309E-12}
k( 48) =  4.6000E-11 * exp(   230.0/T)                                {9.95294E-11}
k( 49) is a falloff expression using:                                 {8.88848E-13}
   k0   =  3.0000E-31 * (T/300)**(-3.30)
   kinf =  1.5000E-12 * (T/300)**( 0.00)
   F =  0.60,  n =  1.00
k( 50) =  1.5000E-13 * (1.0 + 0.6*Pressure)                           {2.40000E-13}
k( 51) =  2.8300E+01 * (T/300)**( 2.00) * exp( -1280.0/T)             {3.80672E-01}
k( 52) =  1.2330E-12 * (T/300)**( 2.00) * exp(  -444.0/T)             {2.74210E-13}
k( 53) =  1.5900E-11 * exp(  -540.0/T)                                {2.59669E-12}
k( 54) =  1.7300E-11 * exp(  -380.0/T)                                {4.83334E-12}
k( 55) =  3.6400E-11 * exp(  -380.0/T)                                {1.01696E-11}
k( 56) =  2.1500E-12 * exp(   411.0/T)                                {8.53916E-12}
k( 57) =  5.3200E-12 * exp(   504.0/T)                                {2.88684E-11}
k( 58) =  1.0700E-11 * exp(   549.0/T)                                {6.75269E-11}
k( 59) =  2.1000E-12 * exp(   322.0/T)                                {6.18715E-12}
k( 60) =  1.8900E-11 * exp(   116.0/T)                                {2.78943E-11}
```

Table 8A-11. RADM2_CIS4 and RADM2_CIS4_AQ Mechanisms

```
k( 61) =  4.0000E-11                                                    {4.00000E-11}
k( 62) =  9.0000E-01 * k( 61)                                           {3.60000E-11}
k( 63) =  9.0000E-12                                                    {9.00000E-12}
k( 64) =  6.8700E-12 * exp(   256.0/T)                                  {1.62197E-11}
k( 65) =  1.2000E-11 * exp(  -745.0/T)                                  {9.85020E-13}
k( 66) =  1.1500E-11                                                    {1.15000E-11}
k( 67) =  1.7000E-11                                                    {1.70000E-11}
k( 68) =  2.8000E-11                                                    {2.80000E-11}
k( 69) =  1.0000E-11                                                    {1.00000E-11}
k( 70) =  1.0000E-11                                                    {1.00000E-11}
k( 71) =  1.0000E-11                                                    {1.00000E-11}
k( 72) =  6.1650E-13 * (T/300)**( 2.00) * exp(  -444.0/T)               {1.37105E-13}
k( 73) =  1.5500E-11 * exp(  -540.0/T)                                  {2.53137E-12}
k( 74) =  2.8000E-12 * exp(   181.0/T)                                  {5.13974E-12}
k( 75) =  1.9500E+16 * exp(-13543.0/T)                                  {3.57235E-04}
k( 76) =  4.7000E-12                                                    {4.70000E-12}
k( 77) =  1.9500E+16 * exp(-13543.0/T)                                  {3.57235E-04}
k( 78) =  4.2000E-12 * exp(   180.0/T)                                  {7.68378E-12}
k( 79) =  4.2000E-12 * exp(   180.0/T)                                  {7.68378E-12}
k( 80) =  4.2000E-12 * exp(   180.0/T)                                  {7.68378E-12}
k( 81) =  4.2000E-12 * exp(   180.0/T)                                  {7.68378E-12}
k( 82) =  4.2000E-12 * exp(   180.0/T)                                  {7.68378E-12}
k( 83) =  4.2000E-12 * exp(   180.0/T)                                  {7.68378E-12}
k( 84) =  4.2000E-12 * exp(   180.0/T)                                  {7.68378E-12}
k( 85) =  4.2000E-12 * exp(   180.0/T)                                  {7.68378E-12}
k( 86) =  4.2000E-12 * exp(   180.0/T)                                  {7.68378E-12}
k( 87) =  4.2000E-12 * exp(   180.0/T)                                  {7.68378E-12}
k( 88) =  4.2000E-12 * exp(   180.0/T)                                  {7.68378E-12}
k( 89) =  4.2000E-12 * exp(   180.0/T)                                  {7.68378E-12}
k( 90) =  4.2000E-12 * exp(   180.0/T)                                  {7.68378E-12}
k( 91) =  4.2000E-12 * exp(   180.0/T)                                  {7.68378E-12}
k( 92) =  6.0000E-13 * exp( -2058.0/T)                                  {6.01030E-16}
k( 93) =  1.4000E-12 * exp( -1900.0/T)                                  {2.38307E-15}
k( 94) =  6.0000E-13 * exp( -2058.0/T)                                  {6.01030E-16}
k( 95) =  1.4000E-12 * exp( -1900.0/T)                                  {2.38307E-15}
k( 96) =  1.4000E-12 * exp( -1900.0/T)                                  {2.38307E-15}
k( 97) =  2.2000E-11                                                    {2.20000E-11}
k( 98) =  2.0000E-12 * exp( -2923.0/T)                                  {1.09940E-16}
k( 99) =  1.0000E-11 * exp( -1895.0/T)                                  {1.73099E-14}
k(100) =  3.2300E-11 * exp(  -975.0/T)                                  {1.22539E-12}
k(101) =  1.2000E-14 * exp( -2633.0/T)                                  {1.74559E-18}
k(102) =  1.3200E-14 * exp( -2105.0/T)                                  {1.12933E-17}
k(103) =  7.2900E-15 * exp( -1136.0/T)                                  {1.61125E-16}
k(104) =  7.7000E-14 * exp(  1300.0/T)                                  {6.04038E-12}
k(105) =  7.7000E-14 * exp(  1300.0/T)                                  {6.04038E-12}
k(106) =  7.7000E-14 * exp(  1300.0/T)                                  {6.04038E-12}
k(107) =  7.7000E-14 * exp(  1300.0/T)                                  {6.04038E-12}
k(108) =  7.7000E-14 * exp(  1300.0/T)                                  {6.04038E-12}
k(109) =  7.7000E-14 * exp(  1300.0/T)                                  {6.04038E-12}
k(110) =  7.7000E-14 * exp(  1300.0/T)                                  {6.04038E-12}
k(111) =  7.7000E-14 * exp(  1300.0/T)                                  {6.04038E-12}
k(112) =  7.7000E-14 * exp(  1300.0/T)                                  {6.04038E-12}
k(113) =  7.7000E-14 * exp(  1300.0/T)                                  {6.04038E-12}
k(114) =  7.7000E-14 * exp(  1300.0/T)                                  {6.04038E-12}
k(115) =  7.7000E-14 * exp(  1300.0/T)                                  {6.04038E-12}
k(116) =  7.7000E-14 * exp(  1300.0/T)                                  {6.04038E-12}
k(117) =  7.7000E-14 * exp(  1300.0/T)                                  {6.04038E-12}
k(118) =  1.9000E-13 * exp(   220.0/T)                                  {3.97533E-13}
k(119) =  1.4000E-13 * exp(   220.0/T)                                  {2.92919E-13}
k(120) =  4.2000E-14 * exp(   220.0/T)                                  {8.78758E-14}
k(121) =  3.4000E-14 * exp(   220.0/T)                                  {7.11376E-14}
```

Table 8A-11. RADM2_CIS4 and RADM2_CIS4_AQ Mechanisms

```
k(122) =  2.9000E-14 * exp(   220.0/T)                                {6.06762E-14}
k(123) =  1.4000E-13 * exp(   220.0/T)                                {2.92919E-13}
k(124) =  1.4000E-13 * exp(   220.0/T)                                {2.92919E-13}
k(125) =  1.7000E-14 * exp(   220.0/T)                                {3.55688E-14}
k(126) =  1.7000E-14 * exp(   220.0/T)                                {3.55688E-14}
k(127) =  9.6000E-13 * exp(   220.0/T)                                {2.00859E-12}
k(128) =  1.7000E-14 * exp(   220.0/T)                                {3.55688E-14}
k(129) =  1.7000E-14 * exp(   220.0/T)                                {3.55688E-14}
k(130) =  9.6000E-13 * exp(   220.0/T)                                {2.00859E-12}
k(131) =  1.7000E-14 * exp(   220.0/T)                                {3.55688E-14}
k(132) =  3.4000E-13 * exp(   220.0/T)                                {7.11376E-13}
k(133) =  1.0000E-13 * exp(   220.0/T)                                {2.09228E-13}
k(134) =  8.4000E-14 * exp(   220.0/T)                                {1.75752E-13}
k(135) =  7.2000E-14 * exp(   220.0/T)                                {1.50644E-13}
k(136) =  3.4000E-13 * exp(   220.0/T)                                {7.11376E-13}
k(137) =  3.4000E-13 * exp(   220.0/T)                                {7.11376E-13}
k(138) =  4.2000E-14 * exp(   220.0/T)                                {8.78758E-14}
k(139) =  4.2000E-14 * exp(   220.0/T)                                {8.78758E-14}
k(140) =  1.1900E-12 * exp(   220.0/T)                                {2.48981E-12}
k(141) =  4.2000E-14 * exp(   220.0/T)                                {8.78758E-14}
k(142) =  4.2000E-14 * exp(   220.0/T)                                {8.78758E-14}
k(143) =  1.1900E-12 * exp(   220.0/T)                                {2.48981E-12}
k(144) =  4.2000E-14 * exp(   220.0/T)                                {8.78758E-14}
k(145) =  3.6000E-16 * exp(   220.0/T)                                {7.53221E-16}
k(146) =  7.7000E-14 * exp(  1300.0/T)                                {6.04038E-12}
k(147) =  1.7000E-14 * exp(   220.0/T)                                {3.55688E-14}
k(148) =  4.2000E-14 * exp(   220.0/T)                                {8.78758E-14}
k(149) =  3.6000E-16 * exp(   220.0/T)                                {7.53221E-16}
k(150) =  4.2000E-12 * exp(   180.0/T)                                {7.68378E-12}
k(151) =  4.2000E-12 * exp(   180.0/T)                                {7.68378E-12}
k(152) =  7.7000E-14 * exp(  1300.0/T)                                {6.04038E-12}
k(153) =  1.7000E-14 * exp(   220.0/T)                                {3.55688E-14}
k(154) =  4.2000E-14 * exp(   220.0/T)                                {8.78758E-14}
k(155) =  3.6000E-16 * exp(   220.0/T)                                {7.53221E-16}
k(156) =  2.5400E-11 * (T/300)**( 1.00) * exp(   407.6/T)             {9.90719E-11}
k(157) =  4.2000E-12 * (T/300)**( 1.00) * exp(   181.2/T)             {7.66335E-12}
k(158) =  7.7000E-14 * (T/300)**( 1.00) * exp(  1298.3/T)             {5.96598E-12}
k(159) =  8.4000E-14 * (T/300)**( 1.00) * exp(   221.4/T)             {1.75402E-13}
k(160) =  3.4000E-14 * (T/300)**( 1.00) * exp(   221.4/T)             {7.09961E-14}
k(161) =  7.8600E-15 * (T/300)**( 1.00) * exp( -1912.2/T)             {1.27569E-17}
k(162) =  3.6000E-11                                                  {3.60000E-11}
k(163) =  3.0300E-12 * (T/300)**( 1.00) * exp(  -447.9/T)             {6.69552E-13}
k(164) =  4.2000E-12 * (T/300)**( 1.00) * exp(   181.2/T)             {7.66335E-12}
k(165) =  7.7000E-14 * (T/300)**( 1.00) * exp(  1298.3/T)             {5.96598E-12}
k(166) =  8.4000E-14 * (T/300)**( 1.00) * exp(   221.4/T)             {1.75402E-13}
k(167) =  3.4000E-14 * (T/300)**( 1.00) * exp(   221.4/T)             {7.09961E-14}
k(168) =  1.8600E-11 * (T/300)**( 1.00) * exp(   176.1/T)             {3.33618E-11}
k(169) =  4.2000E-12 * (T/300)**( 1.00) * exp(   181.2/T)             {7.66335E-12}
k(170) =  7.7000E-14 * (T/300)**( 1.00) * exp(  1298.3/T)             {5.96598E-12}
k(171) =  8.4000E-14 * (T/300)**( 1.00) * exp(   221.4/T)             {1.75402E-13}
k(172) =  3.4000E-14 * (T/300)**( 1.00) * exp(   221.4/T)             {7.09961E-14}
k(173) =  1.3600E-15 * (T/300)**( 1.00) * exp( -2113.5/T)             {1.12330E-18}
k(174) uses photo table ACROLEIN        , scaled by 3.60000E-03       {0.00000E+00}
k(175) =  1.5000E-12 * (T/300)**( 1.00) * exp( -1726.0/T)             {4.54753E-15}
k(176) =  4.1400E-12 * (T/300)**( 1.00) * exp(   452.9/T)             {1.87990E-11}
k(177) =  4.2000E-12 * (T/300)**( 1.00) * exp(   181.2/T)             {7.66335E-12}
k(178) =  7.7000E-14 * (T/300)**( 1.00) * exp(  1298.3/T)             {5.96598E-12}
k(179) =  8.4000E-14 * (T/300)**( 1.00) * exp(   221.4/T)             {1.75402E-13}
k(180) =  3.4000E-14 * (T/300)**( 1.00) * exp(   221.4/T)             {7.09961E-14}
k(181) =  7.5100E-16 * (T/300)**( 1.00) * exp( -1519.7/T)             {4.54966E-18}
k(182) uses photo table ACROLEIN        , scaled by 1.11000E-02       {0.00000E+00}
```

Table 8A-11. RADM2_CIS4 and RADM2_CIS4_AQ Mechanisms

```
k(183) =  1.6000E+16 * (T/300)**( 1.00) * exp(-13486.0/T)          {3.52536E-04}
k(184) =  4.2000E-12 * (T/300)**( 1.00) * exp(   181.2/T)          {7.66335E-12}
k(185) =  2.8000E-12 * (T/300)**( 1.00) * exp(   181.2/T)          {5.10890E-12}
k(186) =  7.7000E-14 * (T/300)**( 1.00) * exp(  1298.3/T)          {5.96598E-12}
k(187) =  9.6000E-13 * (T/300)**( 1.00) * exp(   221.4/T)          {2.00460E-12}
k(188) =  1.1900E-12 * (T/300)**( 1.00) * exp(   221.4/T)          {2.48486E-12}
k(189) =  1.1900E-12 * (T/300)**( 1.00) * exp(   221.4/T)          {2.48486E-12}
k(190) =  3.3600E-11                                               {3.36000E-11}
k(191) =  4.2000E-12 * (T/300)**( 1.00) * exp(   181.2/T)          {7.66335E-12}
k(192) =  7.7000E-14 * (T/300)**( 1.00) * exp(  1298.3/T)          {5.96598E-12}
k(193) =  8.4000E-14 * (T/300)**( 1.00) * exp(   221.4/T)          {1.75402E-13}
k(194) =  3.4000E-14 * (T/300)**( 1.00) * exp(   221.4/T)          {7.09961E-14}
k(195) =  7.1100E-18                                               {7.11000E-18}
k(196) uses photo table ACROLEIN        , scaled by 3.60000E-03    {0.00000E+00}
k(197) =  1.0000E-13                                               {1.00000E-13}
==================================================================================
```

Table 8A-12. RADM2_CIS4_AE and RADM2_CIS4_AE_AQ Mechanisms

Reaction List

```
>-----------------------------------------------------------------------------------------------<
{  1} NO2      + hv                    -->        O3P      +       NO
{  2} O3       + hv                    -->        O1D
{  3} O3       + hv                    -->        O3P
{  4} HONO     + hv                    -->        HO       +       NO
{  5} HNO3     + hv                    -->        HO       +       NO2
{  6} HNO4     + hv                    -->        HO2      +       NO2
{  7} NO3      + hv                    -->        NO
{  8} NO3      + hv                    -->        NO2      +       O3P
{  9} H2O2     + hv                    -->   2.000*HO
{ 10} HCHO     + hv                    -->        CO
{ 11} HCHO     + hv                    -->        HO2      +       HO2      +       CO
{ 12} ALD      + hv                    -->        MO2      +       HO2      +       CO
{ 13} OP1      + hv                    -->        HCHO     +       HO2      +       HO
{ 14} OP2      + hv                    -->        ALD      +       HO2      +       HO
{ 15} PAA      + hv                    -->        MO2      +       HO
{ 16} KET      + hv                    -->        ACO3     +       ETHP
{ 17} GLY      + hv                    -->   0.130*HCHO    + 1.870*CO
{ 18} GLY      + hv                    -->   0.450*HCHO    + 1.550*CO       + 0.800*HO2
{ 19} MGLY     + hv                    -->        ACO3     +       HO2      +       CO
{ 20} DCB      + hv                    -->   0.980*HO2     + 0.020*ACO3     +       TCO3
{ 21} ONIT     + hv                    -->   0.200*ALD     + 0.800*KET      +       HO2
                                             +       NO2
{ 22} O3P      + [M]       + [O2]      -->        O3
{ 23} O3P      + NO2                   -->        NO
{ 24} O1D      + [N2]                  -->        O3P
{ 25} O1D      + [O2]                  -->        O3P
{ 26} O1D      + [H2O]                 -->   2.000*HO
{ 27} O3       + NO                    -->        NO2
{ 28} O3       + HO                    -->        HO2
{ 29} O3       + HO2                   -->        HO
{ 30} HO2      + NO                    -->        NO2      +       HO
{ 31} HO2      + NO2                   -->        HNO4
{ 32} HNO4                             -->        HO2      +       NO2
{ 33} HO2      + HO2                   -->        H2O2
{ 34} HO2      + HO2       + [H2O]     -->        H2O2
{ 35} H2O2     + HO                    -->        HO2
{ 36} NO       + HO                    -->        HONO
{ 37} NO       + NO        + [O2]      -->   2.000*NO2
{ 38} O3       + NO2                   -->        NO3
{ 39} NO3      + NO                    -->   2.000*NO2
{ 40} NO3      + NO2                   -->        NO       +       NO2
{ 41} NO3      + HO2                   -->        HNO3
{ 42} NO3      + NO2                   -->        N2O5
{ 43} N2O5                             -->        NO2      +       NO3
{ 44} N2O5     + [H2O]                 -->   2.000*HNO3
{ 45} HO       + NO2                   -->        HNO3
{ 46} HO       + HNO3                  -->        NO3
{ 47} HO       + HNO4                  -->        NO2
{ 48} HO       + HO2                   -->
{ 49} HO       + SO2                   -->        SULF     +       HO2      +       SULAER
{ 50} CO       + HO                    -->        HO2
{ 51} HO                               -->        MO2
{ 52} ETH      + HO                    -->        ETHP
{ 53} HC3      + HO                    -->   0.830*HC3P    + 0.170*HO2      + 0.009*HCHO
                                             + 0.075*ALD   + 0.025*KET
{ 54} HC5      + HO                    -->        HC5P     + 0.250*XO2
{ 55} HC8      + HO                    -->        HC8P     + 0.750*XO2      +       HC8AER
{ 56} OL2      + HO                    -->        OL2P
{ 57} OLT      + HO                    -->        OLTP
```

Table 8A-12. RADM2_CIS4_AE and RADM2_CIS4_AE_AQ Mechanisms

```
{ 58} OLI      + HO                 -->        OLIP      +       OLIAER
{ 59} TOL      + HO                 -->  0.750*TOLP      + 0.250*CSL      + 0.250*HO2
                                         +      TOLAER
{ 60} XYL      + HO                 -->  0.830*XYLP      + 0.170*CSL      + 0.170*HO2
                                         +      XYLAER
{ 61} CSL      + HO                 -->  0.100*HO2       + 0.900*XO2      + 0.900*TCO3
                                         +      CSLAER
{ 62} CSL      + HO                 -->        CSL
{ 63} HCHO     + HO                 -->        HO2       +       CO
{ 64} ALD      + HO                 -->        ACO3
{ 65} KET      + HO                 -->        KETP
{ 66} GLY      + HO                 -->        HO2       + 2.000*CO
{ 67} MGLY     + HO                 -->        ACO3      +       CO
{ 68} DCB      + HO                 -->        TCO3
{ 69} OP1      + HO                 -->  0.500*MO2       + 0.500*HCHO     + 0.500*HO
{ 70} OP2      + HO                 -->  0.500*HC3P      + 0.500*ALD      + 0.500*HO
{ 71} PAA      + HO                 -->        ACO3
{ 72} PAN      + HO                 -->        HCHO      +       NO3      +       XO2
{ 73} ONIT     + HO                 -->        HC3P      +       NO2
{ 74} ACO3     + NO2                -->        PAN
{ 75} PAN                           -->        ACO3      +       NO2
{ 76} TCO3     + NO2                -->        TPAN
{ 77} TPAN                          -->        TCO3      +       NO2
{ 78} MO2      + NO                 -->        HCHO      +       HO2      +       NO2
{ 79} HC3P     + NO                 -->  0.750*ALD       + 0.250*KET      + 0.090*HCHO
                                         + 0.036*ONIT     + 0.964*NO2      + 0.964*HO2
{ 80} HC5P     + NO                 -->  0.380*ALD       + 0.690*KET      + 0.080*ONIT
                                         + 0.920*NO2      + 0.920*HO2
{ 81} HC8P     + NO                 -->  0.350*ALD       + 1.060*KET      + 0.040*HCHO
                                         + 0.240*ONIT     + 0.760*NO2      + 0.760*HO2
{ 82} OL2P     + NO                 -->  1.600*HCHO      +       HO2      +       NO2
                                         + 0.200*ALD
{ 83} OLTP     + NO                 -->        ALD       +       HCHO     +       HO2
                                         +      NO2
{ 84} OLIP     + NO                 -->        HO2       + 1.450*ALD      + 0.280*HCHO
                                         + 0.100*KET      +       NO2
{ 85} ACO3     + NO                 -->        MO2       +       NO2
{ 86} TCO3     + NO                 -->        NO2       + 0.920*HO2      + 0.890*GLY
                                         + 0.110*MGLY     + 0.050*ACO3     + 0.950*CO
                                         + 2.000*XO2
{ 87} TOLP     + NO                 -->        NO2       +       HO2      + 0.170*MGLY
                                         + 0.160*GLY      + 0.700*DCB
{ 88} XYLP     + NO                 -->        NO2       +       HO2      + 0.450*MGLY
                                         + 0.806*DCB
{ 89} ETHP     + NO                 -->        ALD       +       HO2      +       NO2
{ 90} KETP     + NO                 -->        MGLY      +       NO2      +       HO2
{ 91} OLN      + NO                 -->        HCHO      +       ALD      + 2.000*NO2
{ 92} HCHO     + NO3                -->        HO2       +       HNO3     +       CO
{ 93} ALD      + NO3                -->        ACO3      +       HNO3
{ 94} GLY      + NO3                -->        HNO3      +       HO2      + 2.000*CO
{ 95} MGLY     + NO3                -->        HNO3      +       ACO3     +       CO
{ 96} DCB      + NO3                -->        HNO3      +       TCO3
{ 97} CSL      + NO3                -->        HNO3      +       XNO2     + 0.500*CSL
                                         + 0.500*CSLAER
{ 98} OL2      + NO3                -->        OLN
{ 99} OLT      + NO3                -->        OLN
{100} OLI      + NO3                -->        OLN       +       OLIAER
{101} OL2      + O3                 -->        HCHO      + 0.400*ORA1     + 0.420*CO
                                         + 0.120*HO2
{102} OLT      + O3                 -->  0.530*HCHO      + 0.500*ALD      + 0.330*CO
                                         + 0.200*ORA1     + 0.200*ORA2     + 0.230*HO2
```

Table 8A-12. RADM2_CIS4_AE and RADM2_CIS4_AE_AQ Mechanisms

```
                                        + 0.220*MO2      + 0.100*HO
{103} OLI      + O3                 -->   0.180*HCHO     + 0.720*ALD      + 0.100*KET
                                        + 0.230*CO       + 0.060*ORA1     + 0.290*ORA2
                                        + 0.260*HO2      + 0.140*HO       + 0.310*MO2
                                        +       OLIAER
{104} HO2      + MO2                -->         OP1
{105} HO2      + ETHP               -->         OP2
{106} HO2      + HC3P               -->         OP2
{107} HO2      + HC5P               -->         OP2
{108} HO2      + HC8P               -->         OP2
{109} HO2      + OL2P               -->         OP2
{110} HO2      + OLTP               -->         OP2
{111} HO2      + OLIP               -->         OP2
{112} HO2      + KETP               -->         OP2
{113} HO2      + ACO3               -->         PAA
{114} HO2      + TOLP               -->         OP2
{115} HO2      + XYLP               -->         OP2
{116} HO2      + TCO3               -->         OP2
{117} HO2      + OLN                -->         ONIT
{118} MO2      + MO2                -->   1.500*HCHO     +       HO2
{119} MO2      + ETHP               -->   0.750*HCHO     +       HO2      + 0.750*ALD
{120} MO2      + HC3P               -->   0.840*HCHO     + 0.770*ALD      + 0.260*KET
                                        +       HO2
{121} MO2      + HC5P               -->   0.770*HCHO     + 0.410*ALD      + 0.750*KET
                                        +       HO2
{122} MO2      + HC8P               -->   0.800*HCHO     + 0.460*ALD      + 1.390*KET
                                        +       HO2
{123} MO2      + OL2P               -->   1.550*HCHO     + 0.350*ALD      +       HO2
{124} MO2      + OLTP               -->   1.250*HCHO     + 0.750*ALD      +       HO2
{125} MO2      + OLIP               -->   0.890*HCHO     + 0.725*ALD      +       HO2
                                        + 0.550*KET
{126} MO2      + KETP               -->   0.750*HCHO     + 0.750*MGLY     +       HO2
{127} MO2      + ACO3               -->         HCHO     + 0.500*HO2      + 0.500*MO2
                                        + 0.500*ORA2
{128} MO2      + TOLP               -->         HCHO     + 0.170*MGLY     + 0.160*GLY
                                        + 0.700*DCB      + 2.000*HO2
{129} MO2      + XYLP               -->         HCHO     + 0.450*MGLY     + 0.806*DCB
                                        + 2.000*HO2
{130} MO2      + TCO3               -->   0.500*HCHO     + 0.445*GLY      + 0.055*MGLY
                                        + 0.500*ORA2     + 0.025*ACO3     + 0.460*HO2
                                        + 0.475*CO       +       XO2
{131} MO2      + OLN                -->   1.750*HCHO     + 0.500*HO2      +       ALD
                                        +       NO2
{132} ETHP     + ACO3               -->         ALD      + 0.500*HO2      + 0.500*MO2
                                        + 0.500*ORA2
{133} HC3P     + ACO3               -->   0.770*ALD      + 0.260*KET      + 0.500*HO2
                                        + 0.500*MO2      + 0.500*ORA2
{134} HC5P     + ACO3               -->   0.410*ALD      + 0.750*KET      + 0.500*HO2
                                        + 0.500*MO2      + 0.500*ORA2
{135} HC8P     + ACO3               -->   0.460*ALD      + 1.390*KET      + 0.500*HO2
                                        + 0.500*MO2      + 0.500*ORA2
{136} OL2P     + ACO3               -->   0.800*HCHO     + 0.600*ALD      + 0.500*HO2
                                        + 0.500*MO2      + 0.500*ORA2
{137} OLTP     + ACO3               -->         ALD      + 0.500*HCHO     + 0.500*HO2
                                        + 0.500*MO2      + 0.500*ORA2
{138} OLIP     + ACO3               -->   0.725*ALD      + 0.550*KET      + 0.140*HCHO
                                        + 0.500*HO2      + 0.500*MO2      + 0.500*ORA2
{139} KETP     + ACO3               -->         MGLY     + 0.500*HO2      + 0.500*MO2
                                        + 0.500*ORA2
{140} ACO3     + ACO3               -->   2.000*MO2
{141} ACO3     + TOLP               -->         MO2      + 0.170*MGLY     + 0.160*GLY
```

Table 8A-12. RADM2_CIS4_AE and RADM2_CIS4_AE_AQ Mechanisms

```
                                        + 0.700*DCB      +       HO2
{142} ACO3      + XYLP          -->         MO2      + 0.450*MGLY     + 0.806*DCB
                                      +     HO2
{143} ACO3      + TCO3          -->         MO2      + 0.920*HO2      + 0.890*GLY
                                        + 0.110*MGLY   + 0.050*ACO3     + 0.950*CO
                                        + 2.000*XO2
{144} ACO3      + OLN           -->         HCHO     +       ALD      + 0.500*ORA2
                                      +     NO2      + 0.500*MO2
{145} OLN       + OLN           -->   2.000*HCHO     + 2.000*ALD      + 2.000*NO2
{146} XO2       + HO2           -->         OP2
{147} XO2       + MO2           -->         HCHO     +       HO2
{148} XO2       + ACO3          -->         MO2
{149} XO2       + XO2           -->
{150} XO2       + NO            -->         NO2
{151} XNO2      + NO2           -->         ONIT
{152} XNO2      + HO2           -->         OP2
{153} XNO2      + MO2           -->         HCHO     +       HO2
{154} XNO2      + ACO3          -->         MO2
{155} XNO2      + XNO2          -->
{156} TERP      + HO            -->         TERPAER  +       HO
{157} TERP      + NO3           -->         TERPAER  +       NO3
{158} TERP      + O3            -->         TERPAER  +       O3
{159} ISO       + HO            -->         ISO_RO2  + 0.079*XO2
{160} ISO_RO2   + NO            -->   0.088*ONIT     + 0.912*NO2      + 0.912*HO2
                                        + 0.362*ISOPROD + 0.230*MACR    + 0.320*MVK
                                        + 0.629*HCHO   + 0.079*XO2
{161} ISO_RO2   + HO2           -->         OP2
{162} ISO_RO2   + ACO3          -->   0.500*HO2      + 0.500*MO2      + 0.500*ORA2
                                        + 0.362*ISOPROD + 0.230*MACR    + 0.320*MVK
                                        + 0.629*HCHO
{163} ISO_RO2   + MO2           -->   0.500*HCHO     + 0.500*HO2      + 0.362*ISOPROD
                                        + 0.230*MACR   + 0.320*MVK      + 0.629*HCHO
{164} ISO       + O3            -->   0.600*HCHO     + 0.390*MACR     + 0.160*MVK
                                        + 0.390*ORA1   + 0.270*HO       + 0.070*HO2
                                        + 0.070*CO     + 0.200*XO2      + 0.200*MCO3
                                        + 0.150*ALD    + 0.100*ISOPROD
{165} ISO       + O3P           -->   0.750*ISOPROD  + 0.250*MCO3     + 0.250*HCHO
                                        + 0.250*MO2
{166} ISO       + NO3           -->         ISON_RO2
{167} ISON_RO2  + NO            -->         NO2      + 0.800*ALD      + 0.800*ONIT
                                        + 0.800*HO2    + 0.200*ISOPROD  + 0.200*NO2
{168} ISON_RO2  + HO2           -->         ONIT
{169} ISON_RO2  + ACO3          -->   0.500*HO2      + 0.500*MO2      + 0.500*ORA2
                                      +     ALD      +       ONIT
{170} ISON_RO2  + MO2           -->   0.500*HCHO     + 0.500*HO2      + 0.500*ALD
                                        + 0.500*ONIT
{171} MACR      + HO            -->   0.500*MCO3     + 0.500*MACR_RO2
{172} MACR_RO2  + NO            -->         NO2      +       HO2      + 0.840*KET
                                        + 0.840*CO     + 0.150*HCHO     + 0.150*MGLY
{173} MACR_RO2  + HO2           -->         OP2
{174} MACR_RO2  + ACO3          -->   0.500*HO2      + 0.500*MO2      + 0.500*ORA2
                                        + 0.840*KET    + 0.840*CO       + 0.150*HCHO
                                        + 0.150*MGLY
{175} MACR_RO2  + MO2           -->   0.650*HCHO     + 0.500*HO2      + 0.840*KET
                                        + 0.840*CO     + 0.150*MGLY
{176} MACR      + O3            -->   0.630*ORA1     + 0.210*HO       + 0.110*HO2
                                        + 0.110*CO     + 0.200*HCHO     + 0.100*XO2
                                        + 0.100*ACO3
{177} MACR      + hv            -->   0.660*HO2      + 0.330*MCO3     + 0.670*CO
                                        + 0.670*HCHO   + 0.670*ACO3     + 0.340*HO
                                        + 0.340*XO2
```

Table 8A-12. RADM2_CIS4_AE and RADM2_CIS4_AE_AQ Mechanisms

```
{178} MACR     + NO3                 -->   0.500*MCO3      + 0.500*HNO3      + 0.500*CO
                                         + 0.500*HO2       + 0.500*ONIT      + 0.500*XO2
{179} MVK      + HO                  -->         MVK_RO2
{180} MVK_RO2  + NO                  -->         NO2       + 0.700*ALD       + 0.700*XO2
                                         + 0.700*ACO3      + 0.300*HCHO      + 0.300*MGLY
                                         + 0.300*HO2
{181} MVK_RO2  + HO2                 -->         OP2
{182} MVK_RO2  + ACO3                -->   0.500*HO2       + 1.200*MO2       + 0.500*ORA2
                                         + 0.700*ALD       + 0.300*HCHO      + 0.300*MGLY
{183} MVK_RO2  + MO2                 -->   0.800*HCHO      + 0.500*HO2       + 0.700*ALD
                                         + 0.700*MO2       + 0.300*MGLY
{184} MVK      + O3                  -->   0.670*ORA1      + 0.160*HO        + 0.110*HO2
                                         + 0.110*CO        + 0.950*MGLY      + 0.100*HCHO
                                         + 0.050*XO2       + 0.050*ACO3
{185} MVK      + hv                  -->   0.700*ISOPROD   + 0.700*CO        + 0.300*MO2
                                         + 0.300*MCO3
{186} MPAN                           -->         MCO3      +       NO2
{187} MCO3     + NO                  -->         NO2       +       HCHO      +       ACO3
{188} MCO3     + NO2                 -->         MPAN
{189} MCO3     + HO2                 -->         PAA
{190} MCO3     + MO2                 -->   2.250*HCHO      + 0.500*HO2       + 0.500*MO2
{191} MCO3     + ACO3                -->   2.000*MO2       +       HCHO
{192} MCO3     + MCO3                -->   2.000*MO2       + 2.000*HCHO
{193} ISOPROD  + HO                  -->   0.313*ACO3      + 0.687*IP_RO2
{194} IP_RO2   + NO                  -->         NO2       +       HO2       + 0.610*CO
                                         + 0.270*ALD       + 0.030*HCHO      + 0.180*GLY
                                         + 0.210*MGLY      + 0.700*KET
{195} IP_RO2   + HO2                 -->         OP2
{196} IP_RO2   + ACO3                -->   0.500*HO2       + 0.500*MO2       + 0.500*ORA2
                                         + 0.500*ALD       + 0.500*KET
{197} IP_RO2   + MO2                 -->   0.500*HCHO      + 0.500*HO2       + 0.500*ALD
                                         + 0.500*KET
{198} ISOPROD  + O3                  -->   0.476*HO        + 0.072*HO2       + 0.168*MO2
                                         + 0.237*ACO3      + 0.100*XO2       + 0.243*CO
                                         + 0.218*HCHO      + 0.062*ALD       + 0.278*KET
                                         + 0.031*GLY       + 0.653*MGLY      + 0.044*ORA1
{199} ISOPROD  + hv                  -->   1.216*CO        + 0.434*ALD       + 0.350*HCHO
                                         + 0.216*KET       + 1.216*HO2       + 0.784*ACO3
{200} ISOPROD  + NO3                 -->   0.668*CO        + 0.332*HCHO      + 0.332*ALD
                                         +       ONIT      +       HO2       +       XO2
>-------------------------------------------------------------------------------------------<


Rate Expression                                                          Rate Constant
==============================================================================
k(  1) uses photo table NO2_RADM88       , scaled by 1.00000E+00   {0.00000E+00}
k(  2) uses photo table O3O1D_RADM88     , scaled by 1.00000E+00   {0.00000E+00}
k(  3) uses photo table O3O3P_RADM88     , scaled by 1.00000E+00   {0.00000E+00}
k(  4) uses photo table HONO_RADM88      , scaled by 1.00000E+00   {0.00000E+00}
k(  5) uses photo table HNO3_RADM88      , scaled by 1.00000E+00   {0.00000E+00}
k(  6) uses photo table HNO4_RADM88      , scaled by 1.00000E+00   {0.00000E+00}
k(  7) uses photo table NO3NO_RADM88     , scaled by 1.00000E+00   {0.00000E+00}
k(  8) uses photo table NO3NO2_RADM88    , scaled by 1.00000E+00   {0.00000E+00}
k(  9) uses photo table H2O2_RADM88      , scaled by 1.00000E+00   {0.00000E+00}
k( 10) uses photo table HCHOmol_RADM88   , scaled by 1.00000E+00   {0.00000E+00}
k( 11) uses photo table HCHOrad_RADM88   , scaled by 1.00000E+00   {0.00000E+00}
k( 12) uses photo table ALD_RADM88       , scaled by 1.00000E+00   {0.00000E+00}
k( 13) uses photo table MHP_RADM88       , scaled by 1.00000E+00   {0.00000E+00}
k( 14) uses photo table HOP_RADM88       , scaled by 1.00000E+00   {0.00000E+00}
k( 15) uses photo table PAA_RADM88       , scaled by 1.00000E+00   {0.00000E+00}
k( 16) uses photo table KETONE_RADM88    , scaled by 1.00000E+00   {0.00000E+00}
```

Table 8A-12. RADM2_CIS4_AE and RADM2_CIS4_AE_AQ Mechanisms

```
k( 17) uses photo table GLYform_RADM88  , scaled by 1.00000E+00   {0.00000E+00}
k( 18) uses photo table GLYmol_RADM88   , scaled by 1.00000E+00   {0.00000E+00}
k( 19) uses photo table MGLY_RADM88     , scaled by 1.00000E+00   {0.00000E+00}
k( 20) uses photo table UDC_RADM88      , scaled by 1.00000E+00   {0.00000E+00}
k( 21) uses photo table ORGNIT_RADM88   , scaled by 1.00000E+00   {0.00000E+00}
k( 22) =  6.0000E-34 * (T/300)**(-2.30)                           {6.09302E-34}
k( 23) =  6.5000E-12 * exp(   120.0/T)                            {9.72293E-12}
k( 24) =  1.8000E-11 * exp(   110.0/T)                            {2.60365E-11}
k( 25) =  3.2000E-11 * exp(    70.0/T)                            {4.04730E-11}
k( 26) =  2.2000E-10                                              {2.20000E-10}
k( 27) =  2.0000E-12 * exp( -1400.0/T)                            {1.82272E-14}
k( 28) =  1.6000E-12 * exp(  -940.0/T)                            {6.82650E-14}
k( 29) =  1.1000E-14 * exp(  -500.0/T)                            {2.05452E-15}
k( 30) =  3.7000E-12 * exp(   240.0/T)                            {8.27883E-12}
k( 31) is a falloff expression using:                             {1.39058E-12}
   k0   =  1.8000E-31 * (T/300)**(-3.20)
   kinf =  4.7000E-12 * (T/300)**(-1.40)
   F =  0.60,  n =  1.00
k( 32) = k( 31) / Keq,  where Keq =  2.100E-27 * exp( 10900.0/T)  {8.62399E-02}
k( 33) is a special rate expression of the form:                  {3.01634E-12}
   k = k1 + k2[M], where
   k1 =  2.2000E-13 * exp(   620.0/T)
   k2 =  1.9000E-33 * exp(   980.0/T)
k( 34) is a special rate expression of the form:                  {6.78905E-30}
   k = k1 + k2[M], where
   k1 =  3.0800E-34 * exp(  2820.0/T)
   k2 =  2.6600E-54 * exp(  3180.0/T)
k( 35) =  3.3000E-12 * exp(  -200.0/T)                            {1.68671E-12}
k( 36) is a falloff expression using:                             {4.87144E-12}
   k0   =  7.0000E-31 * (T/300)**(-2.60)
   kinf =  1.5000E-11 * (T/300)**(-0.50)
   F =  0.60,  n =  1.00
k( 37) =  3.3000E-39 * exp(   530.0/T)                            {1.95397E-38}
k( 38) =  1.4000E-13 * exp( -2500.0/T)                            {3.18213E-17}
k( 39) =  1.7000E-11 * exp(   150.0/T)                            {2.81225E-11}
k( 40) =  2.5000E-14 * exp( -1230.0/T)                            {4.03072E-16}
k( 41) =  2.5000E-12                                              {2.50000E-12}
k( 42) is a falloff expression using:                             {1.26440E-12}
   k0   =  2.2000E-30 * (T/300)**(-4.30)
   kinf =  1.5000E-12 * (T/300)**(-0.50)
   F =  0.60,  n =  1.00
k( 43) = k( 42) / Keq,  where Keq =  1.100E-27 * exp( 11200.0/T)  {5.47034E-02}
k( 44) =  2.0000E-21                                              {2.00000E-21}
k( 45) is a falloff expression using:                             {1.14885E-11}
   k0   =  2.6000E-30 * (T/300)**(-3.20)
   kinf =  2.4000E-11 * (T/300)**(-1.30)
   F =  0.60,  n =  1.00
k( 46) is a special rate expression of the form:                  {1.47236E-13}
   k = k0 + {k3[M] / (1 + k3[M]/k2)}, where
   k0 =  7.2000E-15 * exp(   785.0/T)
   k2 =  4.1000E-16 * exp(  1440.0/T)
   k3 =  1.9000E-33 * exp(   725.0/T)
k( 47) =  1.3000E-12 * exp(   380.0/T)                            {4.65309E-12}
k( 48) =  4.6000E-11 * exp(   230.0/T)                            {9.95294E-11}
k( 49) is a falloff expression using:                             {8.88848E-13}
   k0   =  3.0000E-31 * (T/300)**(-3.30)
   kinf =  1.5000E-12 * (T/300)**( 0.00)
   F =  0.60,  n =  1.00
k( 50) =  1.5000E-13 * (1.0 + 0.6*Pressure)                       {2.40000E-13}
k( 51) =  2.8300E+01 * (T/300)**( 2.00) * exp( -1280.0/T)         {3.80672E-01}
k( 52) =  1.2330E-12 * (T/300)**( 2.00) * exp(  -444.0/T)         {2.74210E-13}
```

Table 8A-12. RADM2_CIS4_AE and RADM2_CIS4_AE_AQ Mechanisms

```
k( 53) =  1.5900E-11 * exp(  -540.0/T)                                  {2.59669E-12}
k( 54) =  1.7300E-11 * exp(  -380.0/T)                                  {4.83334E-12}
k( 55) =  3.6400E-11 * exp(  -380.0/T)                                  {1.01696E-11}
k( 56) =  2.1500E-12 * exp(   411.0/T)                                  {8.53916E-12}
k( 57) =  5.3200E-12 * exp(   504.0/T)                                  {2.88684E-11}
k( 58) =  1.0700E-11 * exp(   549.0/T)                                  {6.75269E-11}
k( 59) =  2.1000E-12 * exp(   322.0/T)                                  {6.18715E-12}
k( 60) =  1.8900E-11 * exp(   116.0/T)                                  {2.78943E-11}
k( 61) =  4.0000E-11                                                    {4.00000E-11}
k( 62) =  9.0000E-01 * k( 61)                                           {3.60000E-11}
k( 63) =  9.0000E-12                                                    {9.00000E-12}
k( 64) =  6.8700E-12 * exp(   256.0/T)                                  {1.62197E-11}
k( 65) =  1.2000E-11 * exp(  -745.0/T)                                  {9.85020E-13}
k( 66) =  1.1500E-11                                                    {1.15000E-11}
k( 67) =  1.7000E-11                                                    {1.70000E-11}
k( 68) =  2.8000E-11                                                    {2.80000E-11}
k( 69) =  1.0000E-11                                                    {1.00000E-11}
k( 70) =  1.0000E-11                                                    {1.00000E-11}
k( 71) =  1.0000E-11                                                    {1.00000E-11}
k( 72) =  6.1650E-13 * (T/300)**( 2.00) * exp(  -444.0/T)               {1.37105E-13}
k( 73) =  1.5500E-11 * exp(  -540.0/T)                                  {2.53137E-12}
k( 74) =  2.8000E-12 * exp(   181.0/T)                                  {5.13974E-12}
k( 75) =  1.9500E+16 * exp(-13543.0/T)                                  {3.57235E-04}
k( 76) =  4.7000E-12                                                    {4.70000E-12}
k( 77) =  1.9500E+16 * exp(-13543.0/T)                                  {3.57235E-04}
k( 78) =  4.2000E-12 * exp(   180.0/T)                                  {7.68378E-12}
k( 79) =  4.2000E-12 * exp(   180.0/T)                                  {7.68378E-12}
k( 80) =  4.2000E-12 * exp(   180.0/T)                                  {7.68378E-12}
k( 81) =  4.2000E-12 * exp(   180.0/T)                                  {7.68378E-12}
k( 82) =  4.2000E-12 * exp(   180.0/T)                                  {7.68378E-12}
k( 83) =  4.2000E-12 * exp(   180.0/T)                                  {7.68378E-12}
k( 84) =  4.2000E-12 * exp(   180.0/T)                                  {7.68378E-12}
k( 85) =  4.2000E-12 * exp(   180.0/T)                                  {7.68378E-12}
k( 86) =  4.2000E-12 * exp(   180.0/T)                                  {7.68378E-12}
k( 87) =  4.2000E-12 * exp(   180.0/T)                                  {7.68378E-12}
k( 88) =  4.2000E-12 * exp(   180.0/T)                                  {7.68378E-12}
k( 89) =  4.2000E-12 * exp(   180.0/T)                                  {7.68378E-12}
k( 90) =  4.2000E-12 * exp(   180.0/T)                                  {7.68378E-12}
k( 91) =  4.2000E-12 * exp(   180.0/T)                                  {7.68378E-12}
k( 92) =  6.0000E-13 * exp( -2058.0/T)                                  {6.01030E-16}
k( 93) =  1.4000E-12 * exp( -1900.0/T)                                  {2.38307E-15}
k( 94) =  6.0000E-13 * exp( -2058.0/T)                                  {6.01030E-16}
k( 95) =  1.4000E-12 * exp( -1900.0/T)                                  {2.38307E-15}
k( 96) =  1.4000E-12 * exp( -1900.0/T)                                  {2.38307E-15}
k( 97) =  2.2000E-11                                                    {2.20000E-11}
k( 98) =  2.0000E-12 * exp( -2923.0/T)                                  {1.09940E-16}
k( 99) =  1.0000E-11 * exp( -1895.0/T)                                  {1.73099E-14}
k(100) =  3.2300E-11 * exp(  -975.0/T)                                  {1.22539E-12}
k(101) =  1.2000E-14 * exp( -2633.0/T)                                  {1.74559E-18}
k(102) =  1.3200E-14 * exp( -2105.0/T)                                  {1.12933E-17}
k(103) =  7.2900E-15 * exp( -1136.0/T)                                  {1.61125E-16}
k(104) =  7.7000E-14 * exp(  1300.0/T)                                  {6.04038E-12}
k(105) =  7.7000E-14 * exp(  1300.0/T)                                  {6.04038E-12}
k(106) =  7.7000E-14 * exp(  1300.0/T)                                  {6.04038E-12}
k(107) =  7.7000E-14 * exp(  1300.0/T)                                  {6.04038E-12}
k(108) =  7.7000E-14 * exp(  1300.0/T)                                  {6.04038E-12}
k(109) =  7.7000E-14 * exp(  1300.0/T)                                  {6.04038E-12}
k(110) =  7.7000E-14 * exp(  1300.0/T)                                  {6.04038E-12}
k(111) =  7.7000E-14 * exp(  1300.0/T)                                  {6.04038E-12}
k(112) =  7.7000E-14 * exp(  1300.0/T)                                  {6.04038E-12}
k(113) =  7.7000E-14 * exp(  1300.0/T)                                  {6.04038E-12}
```

Table 8A-12. RADM2_CIS4_AE and RADM2_CIS4_AE_AQ Mechanisms

```
k(114) =  7.7000E-14 * exp(  1300.0/T)                                  {6.04038E-12}
k(115) =  7.7000E-14 * exp(  1300.0/T)                                  {6.04038E-12}
k(116) =  7.7000E-14 * exp(  1300.0/T)                                  {6.04038E-12}
k(117) =  7.7000E-14 * exp(  1300.0/T)                                  {6.04038E-12}
k(118) =  1.9000E-13 * exp(   220.0/T)                                  {3.97533E-13}
k(119) =  1.4000E-13 * exp(   220.0/T)                                  {2.92919E-13}
k(120) =  4.2000E-14 * exp(   220.0/T)                                  {8.78758E-14}
k(121) =  3.4000E-14 * exp(   220.0/T)                                  {7.11376E-14}
k(122) =  2.9000E-14 * exp(   220.0/T)                                  {6.06762E-14}
k(123) =  1.4000E-13 * exp(   220.0/T)                                  {2.92919E-13}
k(124) =  1.4000E-13 * exp(   220.0/T)                                  {2.92919E-13}
k(125) =  1.7000E-14 * exp(   220.0/T)                                  {3.55688E-14}
k(126) =  1.7000E-14 * exp(   220.0/T)                                  {3.55688E-14}
k(127) =  9.6000E-13 * exp(   220.0/T)                                  {2.00859E-12}
k(128) =  1.7000E-14 * exp(   220.0/T)                                  {3.55688E-14}
k(129) =  1.7000E-14 * exp(   220.0/T)                                  {3.55688E-14}
k(130) =  9.6000E-13 * exp(   220.0/T)                                  {2.00859E-12}
k(131) =  1.7000E-14 * exp(   220.0/T)                                  {3.55688E-14}
k(132) =  3.4000E-13 * exp(   220.0/T)                                  {7.11376E-13}
k(133) =  1.0000E-13 * exp(   220.0/T)                                  {2.09228E-13}
k(134) =  8.4000E-14 * exp(   220.0/T)                                  {1.75752E-13}
k(135) =  7.2000E-14 * exp(   220.0/T)                                  {1.50644E-13}
k(136) =  3.4000E-13 * exp(   220.0/T)                                  {7.11376E-13}
k(137) =  3.4000E-13 * exp(   220.0/T)                                  {7.11376E-13}
k(138) =  4.2000E-14 * exp(   220.0/T)                                  {8.78758E-14}
k(139) =  4.2000E-14 * exp(   220.0/T)                                  {8.78758E-14}
k(140) =  1.1900E-12 * exp(   220.0/T)                                  {2.48981E-12}
k(141) =  4.2000E-14 * exp(   220.0/T)                                  {8.78758E-14}
k(142) =  4.2000E-14 * exp(   220.0/T)                                  {8.78758E-14}
k(143) =  1.1900E-12 * exp(   220.0/T)                                  {2.48981E-12}
k(144) =  4.2000E-14 * exp(   220.0/T)                                  {8.78758E-14}
k(145) =  3.6000E-16 * exp(   220.0/T)                                  {7.53221E-16}
k(146) =  7.7000E-14 * exp(  1300.0/T)                                  {6.04038E-12}
k(147) =  1.7000E-14 * exp(   220.0/T)                                  {3.55688E-14}
k(148) =  4.2000E-14 * exp(   220.0/T)                                  {8.78758E-14}
k(149) =  3.6000E-16 * exp(   220.0/T)                                  {7.53221E-16}
k(150) =  4.2000E-12 * exp(   180.0/T)                                  {7.68378E-12}
k(151) =  4.2000E-12 * exp(   180.0/T)                                  {7.68378E-12}
k(152) =  7.7000E-14 * exp(  1300.0/T)                                  {6.04038E-12}
k(153) =  1.7000E-14 * exp(   220.0/T)                                  {3.55688E-14}
k(154) =  4.2000E-14 * exp(   220.0/T)                                  {8.78758E-14}
k(155) =  3.6000E-16 * exp(   220.0/T)                                  {7.53221E-16}
k(156) =  1.0000E+00 * k( 58)                                           {6.75269E-11}
k(157) =  1.0000E+00 * k(100)                                           {1.22539E-12}
k(158) =  1.0000E+00 * k(103)                                           {1.61125E-16}
k(159) =  2.5400E-11 * (T/300)**( 1.00) * exp(   407.6/T)               {9.90719E-11}
k(160) =  4.2000E-12 * (T/300)**( 1.00) * exp(   181.2/T)               {7.66335E-12}
k(161) =  7.7000E-14 * (T/300)**( 1.00) * exp(  1298.3/T)               {5.96598E-12}
k(162) =  8.4000E-14 * (T/300)**( 1.00) * exp(   221.4/T)               {1.75402E-13}
k(163) =  3.4000E-14 * (T/300)**( 1.00) * exp(   221.4/T)               {7.09961E-14}
k(164) =  7.8600E-15 * (T/300)**( 1.00) * exp( -1912.2/T)               {1.27569E-17}
k(165) =  3.6000E-11                                                    {3.60000E-11}
k(166) =  3.0300E-12 * (T/300)**( 1.00) * exp(  -447.9/T)               {6.69552E-13}
k(167) =  4.2000E-12 * (T/300)**( 1.00) * exp(   181.2/T)               {7.66335E-12}
k(168) =  7.7000E-14 * (T/300)**( 1.00) * exp(  1298.3/T)               {5.96598E-12}
k(169) =  8.4000E-14 * (T/300)**( 1.00) * exp(   221.4/T)               {1.75402E-13}
k(170) =  3.4000E-14 * (T/300)**( 1.00) * exp(   221.4/T)               {7.09961E-14}
k(171) =  1.8600E-11 * (T/300)**( 1.00) * exp(   176.1/T)               {3.33618E-11}
k(172) =  4.2000E-12 * (T/300)**( 1.00) * exp(   181.2/T)               {7.66335E-12}
k(173) =  7.7000E-14 * (T/300)**( 1.00) * exp(  1298.3/T)               {5.96598E-12}
k(174) =  8.4000E-14 * (T/300)**( 1.00) * exp(   221.4/T)               {1.75402E-13}
```

Table 8A-12. RADM2_CIS4_AE and RADM2_CIS4_AE_AQ Mechanisms

```
k(175) =  3.4000E-14 * (T/300)**( 1.00) * exp(   221.4/T)          {7.09961E-14}
k(176) =  1.3600E-15 * (T/300)**( 1.00) * exp( -2113.5/T)          {1.12330E-18}
k(177) uses photo table ACROLEIN        , scaled by 3.60000E-03    {0.00000E+00}
k(178) =  1.5000E-12 * (T/300)**( 1.00) * exp( -1726.0/T)          {4.54753E-15}
k(179) =  4.1400E-12 * (T/300)**( 1.00) * exp(   452.9/T)          {1.87990E-11}
k(180) =  4.2000E-12 * (T/300)**( 1.00) * exp(   181.2/T)          {7.66335E-12}
k(181) =  7.7000E-14 * (T/300)**( 1.00) * exp(  1298.3/T)          {5.96598E-12}
k(182) =  8.4000E-14 * (T/300)**( 1.00) * exp(   221.4/T)          {1.75402E-13}
k(183) =  3.4000E-14 * (T/300)**( 1.00) * exp(   221.4/T)          {7.09961E-14}
k(184) =  7.5100E-16 * (T/300)**( 1.00) * exp( -1519.7/T)          {4.54966E-18}
k(185) uses photo table ACROLEIN        , scaled by 1.11000E-02    {0.00000E+00}
k(186) =  1.6000E+16 * (T/300)**( 1.00) * exp(-13486.0/T)          {3.52536E-04}
k(187) =  4.2000E-12 * (T/300)**( 1.00) * exp(   181.2/T)          {7.66335E-12}
k(188) =  2.8000E-12 * (T/300)**( 1.00) * exp(   181.2/T)          {5.10890E-12}
k(189) =  7.7000E-14 * (T/300)**( 1.00) * exp(  1298.3/T)          {5.96598E-12}
k(190) =  9.6000E-13 * (T/300)**( 1.00) * exp(   221.4/T)          {2.00460E-12}
k(191) =  1.1900E-12 * (T/300)**( 1.00) * exp(   221.4/T)          {2.48486E-12}
k(192) =  1.1900E-12 * (T/300)**( 1.00) * exp(   221.4/T)          {2.48486E-12}
k(193) =  3.3600E-11                                               {3.36000E-11}
k(194) =  4.2000E-12 * (T/300)**( 1.00) * exp(   181.2/T)          {7.66335E-12}
k(195) =  7.7000E-14 * (T/300)**( 1.00) * exp(  1298.3/T)          {5.96598E-12}
k(196) =  8.4000E-14 * (T/300)**( 1.00) * exp(   221.4/T)          {1.75402E-13}
k(197) =  3.4000E-14 * (T/300)**( 1.00) * exp(   221.4/T)          {7.09961E-14}
k(198) =  7.1100E-18                                               {7.11000E-18}
k(199) uses photo table ACROLEIN        , scaled by 3.60000E-03    {0.00000E+00}
k(200) =  1.0000E-13                                               {1.00000E-13}
==============================================================================
```

Chapter 9

PLUME-IN-GRID TREATMENT OF MAJOR POINT SOURCE EMISSIONS

N. V. Gillani
Earth System Science Laboratory
University of Alabama in Huntsville
Huntsville, Alabama 35899

James M. Godowitch*
Atmospheric Modeling Division
National Exposure Research Laboratory
U.S. Environmental Protection Agency
Research Triangle Park, North Carolina 27711

ABSTRACT

A plume-in-grid (PinG) technique has been developed to more realistically treat the dynamic and chemical processes impacting selected, major point source pollutant plumes in the Community Multiscale Air Quality (CMAQ) modeling system. The principal science algorithms include a Plume Dynamics Model (PDM) and a Lagrangian reactive plume code. The PDM processor simulates plume rise, horizontal and vertical plume growth, and transport of each plume section during the subgrid scale phase. It generates a data file of this information for use by the PinG module. In contrast to the traditional Eulerian grid modeling method of instantly mixing the emissions from each point source into an entire grid cell volume, the PinG module simulates the relevant physical and chemical processes during a subgrid scale phase which allows each plume section to expand in a realistic manner and to evolve chemically. The PinG module is fully integrated into the CMAQ Chemical Transport Model (CCTM) in order to utilize the grid concentrations as boundary conditions and it provides a feedback of the plume pollutants to the grid model concentration field at the proper time and grid location. The technical approaches and the model formulation of the relevant processes treated by this plume-in-grid approach are described. The capabilities and limitations of the initial version of PinG are also discussed and selected results from a test application for a single point source are briefly described.

---

*On assignment from the National Oceanic and Atmospheric Administration, U.S. Department of Commerce. Corresponding author address: James M. Godowitch, MD-80, Research Triangle Park, NC 27711. E-mail: jug@hpcc.epa.gov

9.0 PLUME-IN-GRID TREATMENT OF MAJOR POINT SOURCE EMISSIONS

9.1 Introduction

Significant emissions of anthropogenic nitrogen oxides (NO_x) and sulfur oxides (SO_x) are released from individual elevated point sources into the atmosphere at various levels. These major point source emissions are distributed throughout the U.S. The physical dimensions of their plumes are relatively small initially and expand at finite growth rates. This diffusion-limited nature of plumes is in sharp contrast to the traditional method applied in Eulerian photochemical grid modeling, which has been to uniformly and instantly mix point source emissions into the entire volume of a model grid cell. Depending on the meteorological conditions, however, pollutant plumes may require up to several hours to grow to the typical size of a regional model grid cell. Since the horizontal grid resolution of regional scale domains for Eulerian models has generally been 20-30 km or greater, a real-world pollutant plume may remain a subgrid scale feature at current regional model grid resolutions for a substantial time period and considerable distance after release. Thus, the widely-used grid modeling approach inadequately treats subgrid scale plume transport and diffusion.

There are also important implications on the chemical processes in models due to the inability of large grid cells to adequately resolve a major point source plume. As a real-world plume gradually grows, it concurrently evolves chemically as it entrains surrounding ambient air often richer in volatile organic compounds (VOCs). However, these dynamic and chemical processes of plumes are neglected when large point source emissions are instantly diluted into large grid cells with other anthropogenic area emissions, which may actually be separated spatially from a plume. The effect is that the simultaneous availability of NO_x and VOC's in a large grid cell prematurely initiates rapid photochemistry leading to distortion in the spatial and temporal features of secondary species concentrations. This overdilution of point source emissions and the subsequent distortion of chemical processes contribute to model uncertainty. Consequently, it has been recognized that a realistic, subgrid scale modeling approach is needed which simulates the relevant physical and chemical processes impacting this notable class of large point source emissions, and in particular, that has the capability of properly resolving the spatial scale of plumes and their growth.

There are approaches which have been applied in attempts to resolve fine scale emissions in regional grid models. These have included uniform, nested grid modeling (Odman and Russell, 1991; Chang et al., 1993), non-uniform grid modeling (Mathur et al., 1992), and the plume-in-grid modeling (PinG) technique. The nested grid (telescoping) modeling approach employs the same Eulerian model and simulations are performed with progressively finer-mesh grid sizes within a domain to better resolve small scale emission features. While an advantage of this approach is the use of a single model algorithm, a disadvantage is the successively higher computational burden as the grid cell size is reduced in order to resolve major emission sources. Efforts to implement and apply the plume-in-grid technique, in particular, have been performed by Seigneur et al. (1983) in a version of the Urban Airshed Model (UAM-PARIS), by Morris et al.

(1992) in the UAM-V model, by Kumar and Russell (1996) in the Urban-Regional Model (URM), and by Myer et al. (1996) in the SAQM (SARMAP Air Quality Model) model. Briefly, each of these PinG efforts simulate multiple plumes or puffs in a domain with no interaction between individual plumes. Seigneur et al. (1983) employed a rectangular plume cross-section divided into vertically well-mixed plume cells exhibiting varying widths to maintain equal pollutant mass among the cells. It was applied to an urban domain with a 4 km grid cell size. The other efforts employ an elliptical plume section divided into concentric rings, except for the Kumar and Russell (1996) PinG. Plume material in an outermost elliptic ring or shell is sequentially transferred to the grid model as it attains the grid size. In the treatment by Kumar and Russell, the plume was returned to the grid model after one hour. The general result of applications from these PinG implementations was that noticeable differences were found primarily within or near the grid cells containing the major point sources and negligible impact was found far downwind. This finding is to be expected since these formulations seemed to focus on the plume-core chemistry only in an early phase of plume chemical evolution with the feedback of plume pollutants occurring rather quickly to the grid model.

A cooperative research and development effort was undertaken to design and implement a plume-in-grid (PinG) capability in the Models-3 CMAQ Chemical Transport Model (CCTM) in order to address the need for an improved approach to treat major point source emissions. The current PinG approach has been designed to be suitable for the largest, isolated point source emissions with grid resolutions of regional modeling domains, where the subgrid scale error in the representation of these sources is expected to be greatest without a PinG treatment. An important consideration is to be able to spatially resolve a pollutant plume and to adequately simulate physical expansion so that the chemical evolution can occur gradually.
Therefore, the objectives with this PinG technique are to provide an improved characterization of the near-source pollutant field from the subgrid scale plume concentrations and to also generate better regional pollutant concentrations downwind due to the feedback of the PinG concentrations to the gridded domain. Consequently, when the PinG approach is applied to the largest point source emissions in a regional, coarse-grid domain, improved initial and boundary conditions are anticipated for use with subsequent simulations for a subdomain of the same grid resolution or for fine-mesh nested domains that also need the regional gridded concentration fields.

In this chapter, the conceptual design of the PinG approach is discussed. The key modeling components are a Plume Dynamics Model (PDM) and a Lagrangian reactive plume model designated as the PinG module since it is fully integrated and coupled with the CCTM Eulerian grid model. The PDM has been developed to serve as a processor program to generate plume dimensions, plume position information and related parameters needed by the PinG module. The descriptions of the mathematical formulations and numerical techniques contained in these modeling components are also presented. Their solutions form the basis of the physical-chemical simulations of subgrid scale plumes as implemented in the principal algorithms of the PinG modeling components.

9.2 Overview of the Conceptual Framework of the Plume-in-Grid Treatment

The PinG technique is intended for the largest point sources, designated as major elevated point source emissions (MEPSEs), which are isolated from notable area emission sources. A complete description of the various criteria available to classify a point source as a MEPSE is provided in the emission processing system in chapter 4. In the context of photochemical modeling, the NO_x emission rate is a useful criterion to classify a major point source as a MEPSE from the thousands of individual major point sources in an inventory. Based on a NO_x emission rate criterion of 50 tons/day as a lower limit, Figure 9-1 depicts the group of fewer than 100 MEPSEs in a 36 km gridded domain covering the eastern US with emission rates greater than this criterion. The MEPSE sources are situated away from major metropolitan emission source areas. It reveals that numerous MEPSEs are distributed throughout the Ohio River and Tennessee River valley regions. Since the current PinG technique also relies on linear superposition of MEPSE plumes for determining the impact on grid concentration, the relatively isolated MEPSEs located in these remote rural environments also provide for the lowest likelihood of plume-plume interactions.

An important feature of a PinG treatment is that it must be able to reproduce the various stages in the chemical evolution found in a large, rural point source plume. Based on daytime experimental field study plume data, Gillani and Wilson (1980) documented three distinct stages, as displayed in Figure 9-2, in the chemical evolution of ozone (O_3) in a pollutant plume from a high NO_x source. The O_3 data measured across a plume at different downwind distances in Figure 9-2 illustrate ozone evolution in a large NO_x point source plume. Although NO_x was not obtained, it would display a similar variation to SO_2 shown in Figure 9-2. During the first stage, the relatively fresh plume is dominated by primary NO_x emissions and an O_3 deficit exists in the plume due to titration by very high NO concentrations. The chemistry in stage 1 is mostly inorganic and VOC-limited since MEPSE plumes generally exhibit low VOC emissions. The second stage represents a transition in the chemistry with rapid production of O_3 along the plume edges and some O_3 recovery in the plume core. Plume growth from dispersion processes allows for entrainment of background air which generally contains a richer supply of ambient VOC concentrations. Consequently, this promotes rapid photochemical O_3 production which leads to the characteristically higher O_3 concentrations observed at the edges of a plume during this stage. Figure 9-2 reveals that stage 2 certainly exhibits considerable subgrid scale plume structure in species concentrations. Therefore, the proper simulation of plume chemistry throughout stage 2 is a key phase for a realistic, overall characterization of plume chemical evolution. In fact, full completion of stage 2 is an important requirement for a chemical criterion during the PinG simulation before the plume pollutants are transferred to the grid system. In stage 3, the plume is chemically mature and substantially diluted. In this mature stage, the broad plume would also exhibit a high VOC/NO_x ratio, low NO_x concentrations, and O_3 concentrations in excess of background levels. In the modeling system, background (boundary) concentrations are provided from a CCTM grid cell containing the subgrid scale plume section.

The chemical evolution, as described above, for a large MEPSE plume in the eastern US generally may take up to several hours to reach full maturity even during the daytime period. The

photochemical cycle is strongly influenced by the plume growth rate, particularly the rate of horizontal spread, with stage 3 achieved when a typical MEPSE plume attains a width of about 30 km during the daytime period. In addition, the time period to reach chemical maturity is also a function of the emission rate. There is a range of emission rates even within a MEPSE group. For example, particular MEPSE plume with lower NO_x emissions is expected to exhibit a faster chemical evolution than a MEPSE with a higher emission rate, assuming other factors being the same. Nevertheless, during the subgrid scale simulation period, the plume may travel a considerable distance downwind (i.e. several model grid cells) of its source location in the daytime planetary boundary layer (PBL) during the summer before reaching a width comparable to the grid cell size.

The conceptual design of the Models-3 PinG is illustrated in Figure 9-3. PinG components simulate the relevant processes impacting the hourly emission rate of all pollutant species during the subgrid scale phase and it provides a feedback, or "handover", of the modeled plume species concentrations at an appropriate handover time ($t_{H/O}$) to the CCTM grid framework. The PinG module operates in a Lagrangian modeling framework to simulate the dynamics and kinetics in a moving plume section during the subgrid scale phase whose duration depends primarily upon source strength, plume growth rate, chemical composition of the background CCTM grid concentrations, and sunlight. The PinG module simulates the plume processes concurrently during the simulation of the CCTM grid model.

The PinG module contains a series of rectangular plume cross-sections, each of which are composed of a contiguous, crosswind array of plume cells with the depth of each cell extending vertically from plume bottom to a top height. As displayed in Figure 9-3a, the vertical depth of the single-layer plume model may be elevated initially, however, it eventually extends from the surface to the PBL height (z_i). This one-layer plume structure in the initial PinG module also presents a limitation under high wind speed shear conditions since this situation cannot be modeled adequately. While strong speed shears are more frequent during the nocturnal period, the vertical extent of a plume is also generally confined, which lessens the possible impact of speed shear. Nevertheless, this condition is identified and appropriately handled by the PinG components.

9.3 Formulation of the Plume-in-Grid Modeling Components

9.3.1 Description of the Plume Dynamics Model

The PDM was developed to serve as a processor program in order to provide data needed for the CCTM/PinG simulation. Therefore, the PDM and the PinG module are closely linked through the PDM data file. The key processes simulated by the PDM include plume rise, plume transport, and plume dispersion of each MEPSE plume cross-section. The PDM also specifies when a particular plume section is to be transferred to the grid model based on an indicator flag which communicates to the PinG module when this process is to be performed. The PDM is capable of simultaneously treating up to 100 MEPSEs in a single simulation with the impact on

computational time a function of the number of MEPSEs simulated. In addition, the maximum simulation period is currently limited to 24 hours. Therefore, a single simulation of the CCTM with PinG is also limited to a 24-hour time period.

9.3.1.1 Aspects of Plume Rise of MEPSE Sources

The plume rise treatment implemented in PDM contains the same algorithms applied in the Emissions-Chemistry Interface Processor (ECIP). A detailed discussion of the plume rise equations and treatment has been provided in section 4.4.2 of chapter 4 on the MEPPS system and therefore is not repeated herein.

The plume rise algorithms handle the entire diurnal cycle since plume sections are released hourly throughout the 24 hour cycle. The temporal variation of the final effective plume height for hourly MEPSE plume releases is illustrated in Figure 9-4. In this case, a diurnal variation in the final plume height is evident with lower plume rise occurring at night believed to be due in part to stronger wind speeds. The plume height increases during the morning period as the PBL height grows and the relatively high values found in the afternoon display little variation until the end of the daytime period.

A notable feature of MEPSE plumes also revealed in Figure 9-4 is the rather significant height often attained by this class of point sources. Statistics of the stack parameters from MEPSE and non-MEPSE groups of major point sources were determined. A comparison indicates notable differences in certain stack parameters between these source groups. The average values from a MEPSE group containing 84 stacks compared to the other major point source class containing 6539 stacks show a stack height of 207 m versus 45 m , a stack velocity of 20 m/s versus 12.5 m/s , a stack diameter of 7.5 m versus 2.3 m, a stack exit temperature of 410° K versus 424° K, and a stack exit flow rate of 908 m^3/s versus 105 m^3/s, respectively. Clearly, these results indicate why MEPSE plume heights attain higher levels than most point sources. In general, MEPSE stacks are considerably higher and their plumes exhibit greater buoyancy flux due primarily to greater physical dimensions which contribute to higher plume rise heights.

9.3.1.2 Plume Dispersion Methods

A key aspect of modeling a subgrid scale reactive plume, as noted earlier, is the importance of realistically specifying plume dimensions during travel time downwind. Practical methods have been applied in the initial version of PDM to determine the horizontal and vertical dimensions of each Lagrangian plume section throughout its life cycle.

Each rectangular plume cross-section has a width (W_p) and an overall height from plume bottom to top denoted by H_p. The traditional dispersion parameters in the horizontal (σ_y) and vertical (σ_z) have been employed in order to derive these plume dimensions. In the current version, the plume width and plume height values are determined according to

$$W_p = a\sigma_y \tag{9-1a}$$

$$H_p = h_T - h_b \tag{9-1b}$$

where **a** has been set to 3.545 which is obtained from $2(\pi)^{1/2}$, an adjustment parameter from an elliptical shape to the rectangular plume. The top and bottom heights of each plume cross-section are denoted by h_T and h_b , respectively. The methods used to determine values for the parameters in Equations 9-1a and 9-1b are discussed next.

During the plume rise phase, a plume experiences initial growth due to buoyancy-induced turbulence. To account for this process, practical methods have been used to determine initial values for the dispersion parameters. The initial value of σ_y is computed according an expression suggested in Irwin (1979), as advanced by Pasquill (1976), given by

$$\sigma_{yo} = \Delta h/3.5 \tag{9-2}$$

In Equation 9-2, the initial value is a function of the plume rise (Δh) above the stack top.

Two methods have been installed to prescribe an initial vertical plume thickness. The widely used approach advanced by Briggs (1975) is to define H_p to be equivalent to the amount of plume rise (Δh). This method can result in a rather thick plume when there is considerable plume rise, particularly, at night when experimental evidence suggests nocturnal plumes may be relatively thin. Consequently, an optional approach provided as an experimental alternative has been included. It consists of an empirical form developed by Gillani (1996) which is based on analyses of observed plume data taken during a field study (Gillani et al., 1981). His regression analyses produced an expression given by

$$\sigma_{zo} = Ae^{(-BdT/dz)} \tag{9-3}$$

where dT/dz is the vertical ambient temperature gradient at the plume centerline height and the best-fit values for A and B are 15 and 117, respectively. A minimum σ_{zo} value is set to 3 m. Then, the initial H_p is determined from SZ0FA times σ_{zo}. SZ0FA is a user-specified input parameter for a PDM simulation and it is currently set to 3.545.

Atmospheric turbulence and wind direction shear contribute to lateral plume growth during travel downwind. During the daytime convective period, the turbulence component is often dominant, although directional shear across the PBL also has an important role in contributing to plume

spread with travel distance. In contrast, turbulence is generally weak at night, and horizontal plume expansion may be dominated by wind direction shear over a plume's depth. Thus, the composite horizontal (lateral) dispersion parameter (σ_y) can be defined by

$$\sigma_y^2 = \sigma_{yt}^2 + \sigma_{ys}^2 + \sigma_{yo}^2 \tag{9-4}$$

where the turbulence (σ_{yt}) and direction shear (σ_s) terms may both contribute to horizontal plume growth after the initial plume spread.

A general form for σ_{yt} can be expressed by

$$\sigma_{yt} = \sigma_v T f(T/\tau_L) \tag{9-5}$$

where σ_v is the standard deviation of the lateral wind (v) component, T is travel time, and τ_L is the Lagrangian time scale. Although various expressions for the function, $f(t/\tau_L)$, have emerged (e.g., Draxler, 1976; Irwin, 1983), the following form from Weil (1985;1988) and applied by others (eg.,Venkatram, 1988) has been adopted.

$$f = \frac{1}{(1 + T/2\tau_L)^{1/2}} \tag{9-6}$$

This form is advantageous since it fits dispersion at both the short ($t < \tau_L$) and also long travel times ($t >> \tau_L$). Since the Lagrangian time scale is small relative to the plume section travel times which are often several hours, the expressions above reveal the familiar relation that σ_{yt} increases with the square root of travel time. Therefore, the following form according to Weil (1988) at long travel times, which has been examined by Clarke et al. (1983), is given by

$$\sigma_{yt}^2 = 2\sigma_v^2 \tau_L T \tag{9-7}$$

The above equation also displays the square root of time increase for the lateral dispersion parameter. Using modeled meteorological parameters from data files generated by MCIP, methods have been incorporated to determine the key parameters needed to solve the above expressions for σ_{yt}. Values for σ_v and τ_L are computed with a set of formulas presented in Hanna et al. (1982) and Hanna (1984), respectively, for various stability conditions based on Monin-Obhukov length (L) limits. For unstable conditions with $L < 0$

$$\sigma_v = u_*(12 - 0.5z_i/L)^{1/3} \tag{9-8}$$

$$\tau_L = 0.15z_i/\sigma_v \tag{9-9}$$

where z_i is the PBL height and u_* is the surface friction velocity. Under stable conditions defined by $L > 0$,

$$\sigma_v = 1.3u_*(1 - z/z_i) \tag{9-10}$$

$$\tau_L = 0.07z_i/\sigma_v(z/z_i)^{0.5} \tag{9-11}$$

and z is the height of the plume centerline. For neutral conditions ($L = 0$), values are determined by

$$\sigma_v = 1.3e^{(-2fz/u_*)} \tag{9-12}$$

$$\tau_L = 0.5z/\sigma_v(1 + 15fz/u_*) \tag{9-13}$$

where f is the Coriolis parameter. Using σ_v and τ_L values, the contribution from the turbulence component is computed incrementally from the derivative of Equation 9-7 and solved at each time step. The turbulence term is accumulated with time. Other semi-empirical methods available in PDM provide an alternative set of parameterizations for σ_v as provided by Weil (1988), Nieuwstadt(1984), and Arya(1984) for the different stability regimes, which may be selected from an input option when exercising PDM.

Wind direction shear due to turning of the wind over the vertical extent of a plume can also provide an important contribution to horizontal plume growth. While turbulence often dominates in the daytime PBL, direction shear during the nocturnal period is the principal mechanism for lateral plume expansion since turbulence is generally weak. An expression by Pasquill (1979) has been applied for all conditions to derive the direction shear term and is given by

$$\sigma_{ys}^2 = \alpha\Delta\theta^2X^2 \tag{9-14}$$

where α is 0.03, X is distance traveled by a plume section over a particular time interval, and $\Delta\theta$ is the wind direction difference (radians) over the vertical extent of the plume. The shear and turbulence terms are combined to solve for the total σ_y^2 in Equation 9-4.

After the initial plume thickness has been determined, the treatment for σ_z differs based on whether the plume height is above or below the PBL height. When the plume centerline height is above z_i, then the following expression from Gillani (1996) is applied to determine σ_z.

$$\sigma_z^2 = \sigma_{zo}^2 \frac{(1 + bT^{0.5})}{(1 + bT_o^{0.5})} \tag{9-15}$$

where b is 2.3 and T is travel time. Equation 9-15 is applied for T < 4 hours. At longer travel times, σ_z is set to zero for plumes existing above the PBL in the free atmosphere.

When a plume section is inside the PBL, the parameterization for the vertical plume dispersion parameter can be expressed by the same general form as σ_{yt}.

$$\sigma_z = \sigma_w \, T \, f(T/\tau_{Lz}) \tag{9-16}$$

As before, T is the travel time, and f has the same functional form as used for σ_{yt} although it now contains the Lagrangian time scale in the vertical (τ_{Lz}). The standard deviation of the vertical wind component (σ_w) is computed from the following expressions as given by Weil (1988) for unstable conditions and from Venkatram et al (1984) for neutral/stable conditions, respectively.

$$\sigma_w = 0.6 w_* \qquad (\textit{convective case}) \tag{9-17}$$

$$\sigma_w = 1.3 u_* (1 - z/z_i)^{3/4} \qquad \textit{neutral/stable} \tag{9-18}$$

The MCIP data files provide values for the fraction velocity (u_*), the convective velocity scale (w_*) and z_i. The plume centerline height is represented by z. The value of τ_{Lz} is computed from the following expressions by Hanna et al. (1982) for unstable and by Venkatram et al. (1984) for neutral/stable conditions.

$$\tau_{Lz} = 0.15 \frac{z_i}{\sigma_w} [1 - e^{-5z/z_i}] \qquad (\textit{unstable}) \tag{9-19}$$

In the latter expression, the length scale (l) is derived according to Venkatram et al. (1984).

An example application of these methods from a PDM simulation for a plume released at night from a MEPSE tall stack is shown in Figure 9-5. It shows the plume remains rather narrow and it

$$\tau_{Lz} = \frac{l}{\sigma_w} \qquad (neutral/stable) \tag{9-20}$$

stays elevated during the night. However, once the PBL grows beyond the plume height during the morning period, the plume thickness expands to fill the entire PBL with the plume top height matching z_i until it reaches a maximum height. The temporal variation of the plume width for the same example case is displayed in Figure 9-6. It shows that since the plume has a limited vertical extent at night, the plume width increases at a relatively slow rate as sufficient direction shear existed over the plume depth to cause lateral spreading. During the daytime, however, horizontal plume expansion occurs at a faster rate due to both greater turbulence and shear contributions. For a regional grid cell size of 36 km, the plume width for this release reached the physical grid size during the mid-morning hour. These results and other simulation results obtained from a daytime release versus observed values (Godowitch et al., 1995) provide preliminary evidence that these methods give a realistic depiction of the temporal behavior of the magnitudes of plume width and depth. Additional cases have also been exercised, although results are not shown herein, in order to assess the robustness and capability of the algorithms for different days. An extensive evaluation of these dispersion methods in PDM is planned against field study data obtained in the vicinity of major point sources in the Nashville, Tennessee area during the Southern Oxidant Study experimental period in the summer of 1995.

9.3.1.3 Plume Transport

With the updated plume top and bottom heights, the mean wind components are determined by averaging the winds over the layers spanned by the plume from h_b to h_T. This approach is currently applicable because of the single vertical layer structure of the current PinG module. The mean plume transport speed is used to determine an updated plume centerline position over the time interval. In addition, the positions of the plume edges at the bottom and top are also found in order to derive grid indices for later use in applying the proper grid cell concentrations for boundary conditions of each plume section.

9.3.2 Formulation of the Plume-in-Grid Module

9.3.2.1 Overview of the Plume Conceptual Framework

The Lagrangian plume model described originally by Gillani (1986) provided the conceptual basis for the Models-3 PinG module. However, the computer algorithms in the CCTM/ PinG have been rewritten to contain updated methods for the key processes to be described in a later section.

In a modeling framework, a PinG plume cross-section can be described as a semi-infinite vertical slab moving along a Lagrangian trajectory with a mean wind flow. A plume cross-section is considered rectangular with a vertical height (H_p) and a width (W_p). Temporally, plume spread in the vertical and horizontal is specified by growth rates dH_p/dt and dW_p/dt, respectively. A plume cross-section is discretized laterally into an array of attached plume cells or pillars with the same H_p at time t, as depicted in Figure 9-7. Each plume section consists of N plume cells (currently, N = 10) with the width of each cell being equal. With respect to the plume centerline, there are N_L cells on the left side and N_R cells to the right side, such that

$$\begin{aligned} W_p &= \sum_{i=1}^{N_L} w_{Li} + \sum_{i=1}^{N_R} w_{Ri} \\ N &= N_L + N_R \end{aligned} \tag{9-21}$$

Currently, $N_L = N_R$ as L and R refer to the cells on the left and right sides, respectively. With respect to the plume centerline, the right side of the plume section expands to the right and the left side expands to the left. The width (w_i) of each plume cell is given by

$$(w_i)_{L/R} = (y_{i+1} - y_i)_{L/R} \tag{9-22}$$

where y values represent distances from the plume centerline position. Normalization of the plume cell widths is performed such that as the plume expands laterally, each cell width increases in the same proportion as the overall plume width. Thus, since the individual cell width is normalized with respect to the total plume width, the result is a transformed moving crosswind gridded array which is invariant with respect to time. The transformed crosswind coordinate (η) of the model is given by

$$\eta_i = \frac{y_i}{W_p} \tag{9-23}$$

and $d\eta_i/dt$ is zero. Therefore, although W_p and y_i are time dependent, η_i remains constant during a simulation. Additionally, although the fractional width of the cells across the plume section in the PinG has been prescribed to be equal in the current setup of the module, the algorithms have been generalized to allow for unequal plume cell widths and a different number of cells on the left and right sides of the plume centerline as described in Gillani (1986).

9.3.2.2 Formulation of the Plume Mass Balance Equation

The relevant processes, as noted in Figure 9-7, have been incorporated into the plume equation for the mass balance of individual species. They include dilution and entrainment due to vertical plume expansion, dilution and entrainment/detrainment due to horizontal plume expansion, lateral diffusion, gas-phase chemistry, surface removal, and surface emission.

The subscript i denotes plume cell i (left or right of the plume centerline), subscript j denotes species j, and superscript t denotes a particular time. Thus, C^t_{ji} is the concentration of species j in cell i at time t, and m^t_{ji} is mass of species j in cell i at time t. In the following derivation of the terms of the mass balance equation for any species j in cell i, the subscript j is omitted for convenience; also, the equations and terms do not show "L" or "R" representing a left or right plume cell, since the equation and terms apply similarly to both sides. Consequently, consider the mass balance of (left or right) cell i (for species j) corresponding to the its expansion during a small time interval dt.

$$\partial m_i = (\partial m_i)_{Disp} + (\partial m_i)_{Emis} + (\partial m_i)_{Chem} + (\partial m_i)_{Dep} \tag{9-24}$$

Now, the following expression is also applicable for the plume cell mass.

$$\partial m_i = m_i^{t+dt} - m_i^t = C_i^{t+dt} l H_p^{t+dt} W_p^{t+dt} - C_i^t l H_p^t W_p^t \tag{9-25}$$

Herein the alongwind dimension in the downwind direction (l = Udt) is prescribed, which is determined from the initial mean transport speed (U) over the time interval dt.

Mathematical expressions are presented in subsequent sections for the updated concentration of species j in cell i due to the action of the individual processes during time interval dt. In the current version of PinG, only surface emissions after plume touchdown are included in the emission term since (non-MEPSE) point-source emissions into grid cells (above the lowest cell layer) neighboring the MEPSE plume are released uniformly into the entire emission grid cell and impact the MEPSE plume only through the boundary conditions. Surface removal is due to dry deposition at the ground. Gas-phase chemistry is included with the full chemical mechanisms of the CCTM in the chemistry term. In the future, the PinG will be adapted to employ the same aerosol module used by the CCTM. No wet processes are treated in the initial PinG version. The current approach to address limitations in the initial version of PinG is to transfer the plume over to the grid solution whenever conditions exist (e.g., precipitation) which the PinG treatment cannot adequately accommodate. This issue will be addressed in more detail in the section on plume handover.

9.3.2.3 Treatment of Plume Expansion and Diffusion Processes

Dispersion affects the mass balance of a plume cell as a result of dilution and entrainment/detrainment processes related to the lateral and vertical expansion of a plume cross-section during a time interval dt, as well as mass diffusion which impacts cell concentrations as a result of concentration gradients between adjacent cells. The dispersion processes can be expressed by

$$(\partial m_i)_{Disp} = (\partial m_i)_{Dil/E/D} + (\partial m_i)_{Dif} \tag{9-26}$$

where the first term on the right side of Equation 9-26 represents the dilution / entrainment / detrainment processes and the last term is the eddy diffusion process.

The relationships developed herein apply to cells on either side of the plume centerline, since the only difference occurs in their application when different boundary conditions occur at each edge.

$$(\partial m_i)_{Dil/E/D} = (m_i^{t+dt} - m_i^t)_{Dil/E/D} \tag{9-27}$$

refers to the change of mass in plume cell i (for any transported species j) during dt as a result of dilution and entrainment/detrainment. The changes due to just the horizontal and vertical exchange processes can be expressed by

$$m_i^{t+dt} = m_i^t + (\partial m_i)_{Latdil/E/D} + (\partial m_i)_{Vertdil/E/D} \tag{9-28}$$

where Latdil refers to horizontal (lateral) dilution. In practice, the lateral dilution/ entrainment/detrainment term in Equation 9-28 is determined and then the last term is solved.

The lateral dilution term in Equation 9-28 is given by

$$(\partial m_i)_{Latdil/E/D} = lH_p^t(C_{i+1}^t \partial y_{i+1} - C_i^t \partial y_i) \tag{9-29}$$

However, the following relationship also exists.

$$\partial y_i = \eta_i \partial W_p \tag{9-30}$$

since η is invariant. Therefore, Equation 9-29 can be revised to the following form.

$$(\partial m_i)_{LatdilI/E/D} = lH_p^t(\eta_{i+1}C_{i+1}^t - \eta_i C_i^t)\partial W_p \tag{9-31}$$

At this time, (i.e., after lateral dilution/entrainment/detrainment) the width of a plume cell is w_i^{t+dt}. With the cell widths remaining unchanged, plume vertical expansion occurs (i.e., in the up and down direction for an elevated plume, and up only after plume touchdown). Let C_a^{t+dt} and C_b^{t+dt} denote the concentrations of species j above and below plume cell i, respectively, for the elevated plume case. C_a and C_b represent the CCTM grid concentrations at t+dt. Once the plume becomes surface-based, only C_a is relevant. The equation for the vertical dilution term is given by

$$(\partial m_i)_{VertdilI/E/D} = lw_i^{t+dt}(C_a^{t+dt}\partial H_a + C_b^{t+dt}\partial H_b) \tag{9-32}$$

where the changes in H_a and H_b denote plume vertical expansion of the upper and lower plume boundaries, respectively. An assumption is made that

$$\partial H_a = \partial H_b = 0.5\partial H_p \tag{9-33}$$

for an elevated plume cross-section, and after a plume reaches the surface

$$\begin{aligned} \partial H_a &= \partial H_p \\ \partial H_b &= 0 \end{aligned} \tag{9-34}$$

are applicable. Equation 9-32 can be rewritten accordingly as

$$(\partial m_i)_{VertdilI/E/D} = lw_i^{t+dt}C_*^{t+dt}\partial H_p \tag{9-35}$$

where

$$\begin{aligned} C_*^{t+dt} &= (C_a + C_b) && (\textit{elevated plume}) \\ C_*^{t+dt} &= C_a^{t+dt} && (\textit{surface-based plume}) \end{aligned} \tag{9-36}$$

for an elevated plume and a plume bottom at the surface, respectively. The combination of Equations 9-31 and 9-35 produces the following form.

$$(\partial m^{t})_{Dil/E/D} = lH_p^t \partial W_p(\eta_{i+1}C_{i+1}^t - \eta_i C_i^t) + l\partial H_p w_i^{t+dt} C_*^{t+dt} \tag{9-37}$$

However, by substituting the next expression,

$$(\partial m_i)_{Dil/E/D} = C_i^{t+dt} lH_p^{t+dt} w_i^{t+dt} - C_i^t lH_p^t w_i^t \tag{9-38}$$

and rearranging, the concentration after the total dilution/entrainment/detrainment step is

$$C_i^{t+dt} = C_i H_p^t \frac{w_i^t}{H_p^{t+dt}} w_i^{t+dt} + \frac{H_p^t}{H_p^{t+dt}} \frac{\partial W_p}{w_i^{t+dt}} (\eta_{i+1}C_{i+1}^t - \eta_i C_i^t) + \frac{\partial H_p}{H_p^{t+dt}} C_*^{t+dt} \tag{9-39}$$

The first term on the right-side is related to the dilution effect and the next two terms are the lateral and vertical entrainment/detrainment effects, respectively. The subsequent expressions are also applicable.

$$\begin{aligned} w_i^t &= y_{i+1}^t - y_i^t = W_p(\eta_{i+1} - \eta_i) \\ w_i^{t+dt} &= W_p^{t+dt}(\eta_{i+1} - \eta_i) = (\eta_{i+1} - \eta_i)(W_p + \partial W_p) \\ H_p^{t+dt} &= H_p^t + \partial H_p \end{aligned} \tag{9-40}$$

By substituting the above expressions into Equation 9-39, and rearranging gives

$$C_i^{t+dt} = C_i^t \frac{(H_p W_p)^t}{(H_p W_p)^{t+dt}} + \frac{\partial H_p}{H_p^{t+ddt}} C_*^{t+dt} + \frac{H_p^t}{H_p^{t+dt}} \frac{\partial W_p}{W_p} \frac{(\eta_{i+1}C_{i+1}^t - \eta_i C_i^t)}{(\eta_{i+1} - \eta_i)} \tag{9-41}$$

However, Equation 9-41 can be simplified and re-written as

$$C_i^{t+dt} = \frac{1}{1+\lambda_H}\left((\lambda_H C_*^{t+dt} + \frac{1}{1+\lambda_W}[(C_i^t + \frac{\lambda_w}{\eta_{i+1} - \eta_i}(\eta_{i+1}C_{i+1}^t - \eta_i C_i^t)]\right) \tag{9-42}$$

where

$$\lambda_H = \frac{\partial H_p}{H_p} \quad , \quad \lambda_W = \frac{\partial W_p}{W_p} \tag{9-43}$$

When applying Equation 9-42, certain boundary conditions must be specified. In particular, if

$$\begin{aligned} i = 1 \quad ; \quad & \eta_i = \eta_1 = 0 \\ i = N_L \, , \, i = N_R \quad ; \quad & C_{i+1} = C_{bg}^{t+dt} \end{aligned} \tag{9-44}$$

where C_{bg}^{t+dt} and C_*^{t+dt} are the particular grid cell concentrations from the CCTM solution for the current time step.

In the execution of the CCTM/PinG, both the grid-cell and plume-cell concentrations are updated by numerical integration of the corresponding mass balance equations from time t to t+dt, where dt is the CCTM advection time step (MSTEP). The sequence is that CCTM performs this integration and updates the concentration field first, generating C^{t+dt} in each grid cell, before PinG is called to do the same. PinG performs the integration in a fractional step approach; first for plume dispersion (step 1) then for the surface emission and removal processes (step 2), and finally for plume chemistry (step 3). The chemistry integration is actually performed in smaller chemistry time steps, internally determined for the plume cells by the chemical solver, in sequence, until the integration is completed for the time interval dt. The emission/removal step is implemented in a single integration time step. The dispersion step is performed sequentially in subtime steps until dt is reached. The PinG dispersion time step is constrained by a restriction when applying Equation 9-42 arising from the fact that, in a given time step, the location after expansion of the inner interface of a given plume cell (i.e. y_i^{t+dt}) cannot pass beyond the location of the outer interface of that cell at the start of the ex expansion. Therefore, the following constraint applies.

$$y_i^{t+dt} \leq y_{i+1}^t \quad , \quad 2 \leq i \leq N_{L,R} \tag{9-45}$$

This criterion requires that the following limit for the PinG time step must be satisfied.

$$\partial t_{disp} \leq \frac{(\eta_{i+1} - \eta_i)}{\eta_i} \frac{1}{\lambda_W^*} \tag{9-46}$$

$$\lambda_W^* = \frac{1}{W_p} \frac{dW_p}{dt} \tag{9-47}$$

It should also be noted that λ_W^* is related to λ_w according to

$$\lambda_w = \int_t^{t+dt} \lambda_w^* dt \tag{9-48}$$

During the model simulation, W_p (t) and dW_p/dt are provided to the PinG module from the PDM data file. Thus, λ_W^* is determined directly, and λ_W can also be computed using the plume widths from time t and t+dt.

The dispersion step is not complete without inclusion of the diffusion term. The diffusion equation of a species concentration for any plume cell i may be expressed by

$$\frac{\partial C_i}{\partial t} = \frac{\partial}{\partial y}(K_y \frac{\partial C_i}{\partial y}) \tag{9-49}$$

where K_y is the horizontal eddy diffusion coefficient. It can be expressed by

$$K_y = \frac{1}{2} \frac{d}{dt}(\sigma_y^2) \tag{9-50}$$

By applying the relationship between σ_y and W_p in Equation 9-1, the following form for K_y can be derived.

$$K_y = \frac{W_p^2}{a^2} \lambda_w^* \tag{9-51}$$

Numerical integration of a form like Equation 9-49 is solved with the Crank-Nicholson method in which centered differencing is used for both time and space derivatives to solve the diffusion equation. This technique provided stable numerical solutions compared to an explicit method. The resulting finite-difference equation is then solved by matrix decomposition of the coefficient-matrix into upper and lower (LU) triangular matrices. For convenience in setting up the matrix form of the finite difference diffusion equation for all plume cross-section cells, a set of simultaneous equations is developed which are written in a vector-matrix form for solving by LU decomposition.

The derivation of the set of equations is provided. By averaging Equation 9-49 in time to obtain $\partial C/\partial t$ at $t+\partial t$, and using center-differencing to solve for $\partial^2 C/\partial y^2$, simplification leads to

$$C_{i-1}^{k+1}[-\frac{K_y\partial t}{(y_{i+1}-y_i)(y_{i+1}-y_{i-1})}] + C_i^{k+1}[1+\frac{K_y\partial t}{(y_{i+1}-y_i)(y_{i+2}-y_i)}] + \frac{K_y\partial t}{(y_{i+1}-y_i)(y_{i+1}-y_{i-1})}]$$
$$+ C_{i+1}^{k+1}[-\frac{K_y\partial t}{(y_{i+1}-y_i)(y_{i+2}-y_i)}] = C_{i-1}^{k}\frac{K_y\partial t}{(y_{i+1}-y_i)(y_{i+1}-y_{i-1})}]$$

$$+ C_i^{k}[1 - \frac{K_y\partial t}{(y_{i+1}-y_i)(y_{i+2}-y_i)} - \frac{K_y\partial t}{y_{i+1}-y_i)(y_{i+1}-y_{i-1})}] + C_{i+1}^{k}[\frac{K_y\partial t}{(y_{i+1}-y_i)(y_{i+2}-y_i)}]$$

(9-52)

where small k is used as a time index for time t, and k+1 represents $t+\partial t$, i is the index to the left edge of plume cell i, and y is the distance from the new reference position at the left background location of the plume cross-section. By using the relationship that $y_i = \eta_i W_p$, the following relations can be defined.

$$\alpha_i = \frac{K_y\partial t}{W_p^2}\frac{1}{(\eta_{i+1}-\eta_i)(\eta_{i+1}-\eta_{i-1})} \tag{9-53}$$

$$\gamma_i = \frac{K\partial t}{W_p^2}\frac{1}{(\eta_{i+1}-\eta_i)(\eta_{i+2}-\eta_i)} \tag{9-54}$$

$$\beta_i = \alpha_i + \gamma_i \tag{9-55}$$

By substituting the above expressions into Equation 9-52, the following formula is obtained.

$$-\alpha_i C_{i-1}^{k+1} + (1+\beta_i)C_i^{k+1} - \gamma_i C_{i+1}^{k+1} = \alpha_i C_{i-1}^{k} + (i-\beta_i)C_i^{k} + \gamma_i C_{i+1}^{k} \tag{9-56}$$

Equation 9-56 represents a system of simultaneous equations in the form,

$$Ax = b \tag{9-57}$$

where, $x = (C_i^{k+1} + \ldots C_{N+2}^{k+1})^t$ and N is the total number of plume cells. Additionally, the expression, A = I - G, is defined where A is a square matrix of size (N+1)x(N+2), and b = $(I+G)C^k$. In these expressions, I is the identity matrix, and G is a tridiagonal matrix of the form, G = tridiag (α, β, γ), and is of size (N+2)x(N+2). Subsequently, the simultaneous system of equations given by Equation 9-57 is solved using LU decomposition.

The boundary conditions are also included in the above system of equations since N+2 is used. Appropriate boundary conditions are provided by the CCTM grid concentrations for the right and left edges of each plume cross-section. At left edge boundary, $\alpha_1 = \beta_1 = \gamma_1$ and $b_1 = C_1 = C_{bg}^{L}$. At the right edge boundary, α_{N+2}, β_{N+2}, and γ_{N+2} are zero which leads to $b_{n+2} = C_{N+2} = C_{bg}^{R}$.

9.3.2.4 Surface Area Emissions and Dry Deposition

During the PinG simulation, surface emissions are injected into individual surface-based plume cells. The surface emissions, contained in layer 1 values of the 3-D emissions file which is also employed by the CCTM, are used in all plume cells of a plume cross-section. For each grid cell, there is an emission rate for certain species (q_j). In particular, a MEPSE plume cross-section passes over such gridded surface emissions. Consequently, the change in concentration of plume cell i during a time step from surface emissions is

$$\partial C_i^j = k_j \frac{q_j}{\Delta x \Delta y} \frac{\partial t}{H_p} \tag{9-58}$$

where k_j herein is an appropriate species-specific factor for the conversion of concentration from a mass unit to the appropriate volume unit.

Since the PinG formulation is composed of a single vertical layer, it was not designed to have the capability to properly ingest other elevated point-source emissions into the MEPSE plume cross-section. As long as such an along-path, point-source emission remain at a relatively low value, the impact on the MEPSE concentration field is assumed to be felt through background entrainment of the expanding MEPSE plume. If the other point source emission was ingested, of course, such entrained mass is currently dispersed instantaneously throughout the vertical extent of the plume. For this reason, when point-source emissions larger than a critical value are encountered by the MEPSE plume, the current logic is to handover the MEPSE plume to the grid solution.

Dry deposition is a sink term and occurs at the bottom of each plume cell based on the deposition velocity concept.

$$\frac{\partial C_i^j}{\partial t} = - \frac{V_d^j}{H_p} C_i^j \tag{9-59}$$

where C_i^j denotes the concentration of species j and the species-specific deposition velocity (V_d^j) values are available from a gridded data file. The same deposition velocity is applied to all cells of a plume section using the V_d values from the grid cell in which the plume centerline is located.

9.3.2.5 Gas-phase Chemistry of Plumes

A gas-phase chemistry mechanism implemented in the CCTM is also invoked by the PinG module. The current mechanisms include the RADM2 and carbon bond (CB-4) chemical mechanisms. Details about these chemical mechanisms are provided in section 8. In addition, there is a separate PinG module version for each chemical solver (i.e., SMVGEAR and QSSA). Minor revisions were needed in the PinG versions of the solver codes to customize them to deal with the plume concentration array whose dimensionality differs from the CCTM gridded concentration array. Nevertheless, the PinG gas photochemistry treatment is identical to that of the CCTM. Since only gas-phase plume chemistry has currently been implemented, when conditions conducive to extensive aqueous chemistry are encountered, a plume section is transferred to the CCTM grid system, as discussed in the handover section below. Future plans include implementation of the existing CCTM aerosol module into PinG so that it also has the capability to treat aerosol and particulate species.

9.3.2.6 Plume Initialization

The initialization of each plume cross-section is the first key procedure performed at the start of its simulation. The PinG initialization of a new MEPSE release occurs when a plume cross-section width reaches a minimum width. The width criterion is a user-specified variable and it is specified for the PDM simulation. A flag indicator variable in the PDM file communicates to PinG when a plume cross-section is ready to be initialized. The current minimum width for

initialization of a MEPSE plume section has tentatively been set at 2 km. At initialization, it is assumed that the lateral concentration distribution across the plume section of the primary emission species exhibits a Gaussian shape. For all other species, initial concentrations have been set to a machine minimum-value (ie. 10^{-30}).

The lateral concentration distribution of the primary species in the plume cells (i.e., "initial condition" of the plume concentration field) is given by

$$C_{ij}(0) = k_j \frac{q_j}{UH_p} \frac{1}{2\pi\sigma_y} \exp[-0.5(y_i^*/\sigma_y)^2] \tag{9-60}$$

where, y^* is $(y_i - y_o)$, the distance of the outer edge of cell i from the plume centerline, and U is the mean transport speed, q_j is the MEPSE emission rate of species j, and k_j is the appropriate species specific mass-to-volume conversion factor.

In PinG, it is assumed that the MEPSE emissions are at an hourly resolution, and that we are performing plume simulations of hourly releases. The assumption is made that the emission rate (q_j) remains constant over the hour. Consequently, at the handover time, the transformed mass impacted by the various plume dynamic and chemical processes corresponding to one hour of emission is released to the grid solution.

9.3.2.7 Methodology for Plume Feedback to the Eulerian Grid

When the subgrid scale phase of a plume section simulation has been completed, the plume material is ready for transfer to the CCTM grid. The total concentration of each species in any plume cell is composed of a component equal to the background concentration, and an additional component consisting of the plume concentration, which differs from the background grid level. In performing the handover, the conceptual basis is that only the plume component is related to the corresponding MEPSE emissions. Thus, the feedback is restricted to the plume contribution. Additionally, since hourly plume releases are simulated from each MEPSE source in PinG, and since the assumption has been made that each such hourly emission remains constant for the full hour, the current practice is to handover the contents of a plume section corresponding to a full hour release. Thus, for each plume species,

$$m_P = V_p(\overline{C_p} - \overline{C_{bg}}) \tag{9-61}$$

where average values for the plume and background grid concentrations are employed. The average plume concentration (C_p) of each species is determined from all plume cells. The background grid value (C_{bg}) represents the average of the CCTM grid-cell concentrations on

each side of the plume for all appropriate layers over the vertical extent of the plume. The handover plume mass is distributed into the column of cells up to H_p in which the plume centerline is located at the handover time. The feedback of plume mass represents an adjustment to the CCTM grid cell concentrations from an average concentration (C_{adj}). From a mass balance perspective,

$$\overline{C_{adj}}V_G = (\overline{C_p} - \overline{C_{bg}})V_p \tag{9-62}$$

where V_G is the CCTM grid cell volume. The plume volume (V_p) is determined from

$$V_p = W_p H_p (U\Delta t) \tag{9-63}$$

where U is the mean horizontal wind speed, Δt is a 1-hour interval and $U\Delta t$ corresponds to the alongwind dimension (Δx_p) spanned by the plume section. In a similar fashion, the grid volume impacted by the plume is given by

$$V_G = \Delta x_G \Delta y_G (Z_G^t - Z_G^b) \tag{9-64}$$

where Δx_G and Δy_G are the horizontal grid cell sizes, and Z_G^t and Z_G^b are the heights of the top and bottom of the model layers spanned by the plume.

Substituting the above expression into Equation 9-62 yields:

$$\overline{C_{adj}} = (\overline{C_p} - \overline{C_{bg}})\frac{H_p W_p \Delta x_p}{V_G} \tag{9-65}$$

In the initial release version of PinG when plume handover is triggered, an entire hour's worth of plume release in its transformed state is transferred to the appropriate column of grid cells during a CCTM advection time step. In the future, the intention is to incrementally transfer the same plume excess to the impacted grid cells over a one hour period of model time steps. In this manner, the continuous emissions after being treated in PinG would be transferred during a one hour period following the handover time.

PinG simulations are primarily intended for the coarse-grid, regional modeling grid sizes with the horizontal resolution (Δ) of nominally 20-40 km. Daytime MEPSE plumes reach or are close to chemical maturity when the plume width attains these grid sizes. However, PinG simulations at

finer grid sizes are possible, however, test runs have not been performed but are needed in order to assess the benefits of this approach at urban grid cell sizes. As the primary purpose of PinG is to improve the subgrid-scale treatment of large point-source plumes, the key handover size criterion based on plume width relative to grid cell size has been prescribed according to

$$\frac{W_p}{\Delta} \geq \gamma_{cr} \tag{9-66}$$

The default value for γ_{cr} is 1.0. Therefore, when a plume section width attains the grid cell size, a flag indicator variable generated by PDM triggers PinG to perform the handover process. Currently, the CCTM system is operated in a 1-way nesting mode, as multiple nested grids are not performed in a single simulation. Consequently, PinG is not equipped to handle the movement of a plume from a larger to a finer gridded domain within the same simulation.

Ideally, plume handover also occurs when the plume has also reached chemical maturation when concentration differences within the plume become rather small. A chemical criterion also incorporated into PinG involves a default condition recognizing chemical maturation. It is based on an average plume concentration ratio of O_3/O_x ,where $O_x = O_3 + NO_2$ denotes the principal oxidant species using concentrations from all cells in a plume section. This ratio is employed as a surrogate indicator of plume chemical age. The specific chemical maturation criterion is:

$$\frac{\overline{O_3}}{\overline{O_x}} \geq r_{chem} \tag{9-67}$$

where r_{chem} represents the critical value. The default value has been set at 0.99. Tests have indicated this value to be a good indicator corresponding to a chemically-mature stage 3 plume.

The use of O_3 / O_x as a surrogate for plume age is not common compared to NO_x / NO_y where NO_y includes all the reactive oxides of nitrogen. However, NO_x/NO_y has not been applied as a chemical criterion because injection of fresh emissions from large point sources has been observed to suddenly decrease the chemical age of the background which leads to "premature" activation of the chemical criterion. Experience from testing with the first chemical criterion has proved it to be more satisfactory.

In the initial version of the Models-3 PinG , additional criteria are needed which can also trigger plume handover to the Eulerian grid cells. As the PinG module is upgraded in the future, the these criteria may be avoided.

The next two criteria are related to non-MEPSE emissions in the immediate vicinity of a MEPSE plume cross-section.

Urban Criterion

PinG currently does not have the facility to injest different surface emissions into individual plume cells. Such a condition is likely to be encountered by a MEPSE plume after touch-down when it passes over an urban-industrial area with a very inhomogeneous spatial distribution of emissions. Gillani and Pleim (1996) have identified such "urban" areas based on the following criterion pertaining to the emissions of NO_x.

$$f_q\ (NO_x) > 10^{12} \quad molecules/cm^2/s \tag{9-68}$$

This condition denotes a fairly high NO_x surface emission flux (f_q). The critical value of 10^{12} chosen by Gillani and Pleim (1996) was based on an emission inventory with a horizontal spatial resolution of about 20 km. For such a grid size, this condition corresponds to an emission rate of about 0.3 kg/s. Thus, the selected "urban" emissions handover criterion is:

$$q_{NOx} \geq 0.3 \quad kg/s \tag{9-69}$$

The above condition must be satisfied to trigger plume section handover, and the plume bottom must also be at the ground for this criterion to activate.

Point-source Emissions Criterion

The initial PinG version does not possess multiple vertical layer resolution of the plume. Thus, if a plume section entrains the elevated concentration of a primary species in a background grid cell from a fresh NO_x emission from a non-MEPSE major point source, such entrained mass is instantaneously mixed vertically throughout the MEPSE plume. If the non-MEPSE point source emission is large enough, the related error of its treatment in the MEPSE plume relative to its treatment in the gridded solution becomes large. Thus, it is advantageous to handover the MEPSE plume under this circumstance. A handover criterion of 3.33×10^{-6} ppm/s has been set which corresponds to about 2 ppb/10 minutes. If the new non-MEPSE point-source emissions in the immediate vicinity of the MEPSE plume are large enough to raise the average background concentration (left/right and vertically-averaged over MEPSE plume height) by more than 2 ppb in 10 minutes, then handover is also triggered.

Precipitation Criterion

PinG has no facility to handle wet removal of the plume. Consequently, if the total (convective and non-convective) precipitation rate in the cell containing the MEPSE centroid exceeds a critical value, a plume handover is also triggered. Currently, the default value of this critical precipitation rate is 0.00008 cm/s or about 0.3 cm/hr.

Excessive Wind-Shear Criterion

Since the plume treatment is PinG is based on a Lagrangian simulation for a single vertical layer, there is no facility to properly treat the effect of wind shear. When excessive speed wind shear over the vertical extent of the plume exceeds a critical value, plume section handover will occur on the basis that the treatment of such wind shear will be better treated in the multi-layer grid model.

Domain Boundary Criterion

Finally, a MEPSE plume section is transferred to grid cell in which the centroid of the MEPSE is located if it is about to exit the gridded domain. Otherwise the plume concentration contribution cannot be accounted for if the plume travels beyond the model domain boundary.

In all handover cases considered above, the entire MEPSE plume section is transferred. There is a particular condition in which only a top portion of the plume may be handed over, while the remaining part of the plume continues to be simulated. This type of premature partial handover is forced because PinG does not possess adequate vertical resolution, and also because the plume simulation in PinG is based on a Lagrangian approach. This condition arises when the plume is well-mixed throughout the daytime PBL, and the PBL height decreases significantly along the path of the plume, for whatever reason. In reality, in such a case, the plume would be split between an upper portion above the PBL and a lower portion remaining within the PBL. The two portions could then experience very diverse stability and flow conditions which cannot be accommodated in the current version of PinG.

The approach is that once the PBL height begins to decrease, and it decreases by more than 15% of the previous z_i, the plume section is handed over. However, the lower portion continues to be simulated. If the decrease in z_i is temporary and it later begins to increase again, the remaining simulated plume would expand vertically just as if it was the full plume. When z_i continues to decrease, as during the evening transition period, then the partial handover would continue incrementally as the PBL decreases by each 15% segment until the nocturnal mixing height is reached, at which time the remaining plume is also handed over. In this manner, PinG does not continue to simulate the well-mixed daytime plume into the night. This approach avoids the Lagrangian simulation of the deep night-time plume which frequently experiences substantial wind shear conditions related to nocturnal jets and inertial oscillations.

The situation is different for a fresh MEPSE release into the nocturnal stable layer above the shallow mixing layer. Such a plume is likely to be thin in the vertical and, therefore, not very likely experience excessive shearing conditions. In our Lagrangian approach, therefore, PinG will generally simulate fresh nighttime plume sections which do not experience excessive shear because of their limited vertical extent.

9.3.2.8 Test Application of the Plume-in-Grid Modeling Approach

The schematic diagram in Figure 9-8 shows how the PDM and PinG fit into the overall Models-3 CMAQ system of science programs. Since PDM serves as a processor program, it is exercised in advance of the CCTM/PinG simulation. PDM requires the MEPSE stack parameter file generated by the MEPPS emissions system, and a set of meteorological data files prepared by MCIP from an MM5 simulation. The details of these input files which are needed to perform a PDM simulation are described in the Models-3 user guide (EPA, 1998). Input and output parameters for the PDM processor are also defined in the user guide.

The PinG module is an integral part of the CCTM, as depicted in Figure 9-8, and it is invoked by the CCTM driver program along with the other science processes. In the sequence of processes, PinG is called just before the grid model performs the gas-chemistry step. Consequently, when PinG completes a time step, the CCTM driver calls the chemistry to undertake gas-photochemistry on the 3-D gridded array. When PinG is being exercised, it needs data files generated by ECIP, MCIP, PDM and also the MEPSE emission file from MEPPS processing. The PinG module also generates a plume concentration file containing the species concentrations in each plume cell for each plume cross-section. Since the PinG concentration file is a Models-3 specific format, it can be viewed in a visualization software package designed for such data files. In addition, an effort is planned to visualize both the plume and grid concentrations on the same display.

The plume-in-grid algorithms were exercised for a single MEPSE within a 36 km gridded domain. The plume cell O_3 concentrations in Figure 9-9 are for various times from a selected plume section released during the early afternoon. The PinG module simulated 10 plume cells in this plume section, with the concentrations on each edge of the cross-section at various times being the CCTM gridded values used as background conditions. It is evident that the modeled O_3 concentrations displays the same chemical stages described earlier. A significant ozone deficit exists in the narrow plume for 1-2 hours after release. As the plume expanded, the O_3 concentration gradually recovers and exhibits higher O_3 in some cells outside the plume core of the cross-section at 15:30 than the grid value at each edge or in the plume core. This represents stage 2 of plume chemical evolution. Eventually, stage 3 was attained as all plume cell O_3 concentrations exceeded the CCTM concentrations on each side of the plume with the maximum excess of about 10 ppb in this case. Shortly after 1730 LST, the last time displayed in Figure 9-9 for this plume section, it was transferred to the CCTM grid system. Therefore, this plume section

was active in the subgrid phase about 5 hours in this case. Once the feedbeack of a plume section occurs, PinG no longer simulates it which reduces computational time.

The results of this test case and others not described herein are encouraging since they compare rather favorably in a qualitative sense with observed concentrations (not shown) across the same MEPSE plume at about the same time. Nevertheless, an extensive evaluation of the PinG is planned for several case study days with plume data for various species obtained during the Southern Oxidant Study 1995 experimental intensive program conducted in the Nashville, Tennessee area. The evaluation will assess the capability of the PinG components to treat pollutant plumes and determine the impacts on the regional grid concentrations.

9.4 Summary

A plume-in-grid technique has been developed for use in the Models-3 Community Multiscale Air Quality modeling system. The key algorithms include a plume dynamics Model (PDM) processor designed to generate a data file for use in the PinG module simulation. The PinG module has been fully integrated into the CCTM Eulerian grid model to provide a more refined, realistic treatment of the physical and chemical processes impacting selected major point source emissions during a subgrid scale plume phase in a regional model application. The initial release version is limited to performing gas-phase photochemistry within the plumes. A future PinG version is expected to include an aerosol and particulate modeling capability. Test simulation results have been conducted and qualitative results are encouraging regarding the treatment of plume growth and plume concentrations. However, a rigorous diagnostic evaluation of the various processes is planned using the 1995 Southern Oxidant Study-Nashville experimental plume data. Future advancements and refinements of the initial plume-in-grid algorithms are anticipated and upgraded algorithms will be reflected in upcoming releases.

9.5 References

Arya, P., 1984: Parametric relations for the atmospheric boundary layer. Boundary-Layer Meteorol.,30, 57-73.

Briggs, G.A., 1975: Plume rise predictions. In: Lectures on Air Pollution and Environmental Impact Analyses, Workshop Proceeding, Boston, MA, 1975, pp 59-111.

Chang, J.S., K.H. Chang, and S. Jin, 1993: Two-way and one-way nested SARMAP air quality model. International Conf. on Regional Photochemical Measurement & Modeling Studies, November 8-12, San Diego, CA, A&WMA, Pittsburgh, PA.

Clarke, J.F., J. Ching, J.M. Godowitch, 1983: Lagrangian and eulerian time scales relationships and plume dipsersion from the Tennessee Plume Study. Sixth Symp. on Turbulence and Diffusion, March 22-25, 1983, Amer. Meteorol. Soc., Boston, MA.

Draxler, R.R, 1976: Determination of atmospheric diffusion parameters. Atmos. Environ., 10, 99-105.

EPA, 1998: Models-3 Volume 9b: User Manual, EPA-600/R-98/069b, U.S. Environmental Protection Agency, Research Triangle Park, NC 27711.

Gillani, N.V. and W.E. Wilson, 1980: Formation and transport of ozone and aerosols in power plant plumes. Ann. N.Y. Acad. Sci., 338, 276-296.

Gillani, N.V., S. Kohli, and W.E. Wilson, 1981: Gas-to-particle conversion of sulfur in power plant plumes: I: Parameterization of the conversion rate for moderately polluted ambient conditions. Atmos. Environ., 15, 2293-2313.

Gillani, N.V. and J. E. Pleim, 1996: Subgrid scale features of anthropogenic emissions of NOx and VOC in the context of regional eulerian models. Atmos. Environ., 30, 2043-2059.

Gillani, N.V., 1986: Ozone Formation in pollutant plumes: A reactive plume model with arbitrary crosswind resolution. U.S. Environmental Protection Agency, EPA-600/3-86-051, Research Triangle Park, NC, 85 pp.

Gillani, N.V., 1996: Personal communication.

Godowitch, J.M., J. Ching, and N.V. Gillani, 1995: A treatment for Lagrangian transport and diffusion of subgrid scale plumes in an eulerian grid framework. Eleventh Symp. on Boundary Layers & Turb., March 27-31, Charlotte, NC, Amer. Meteorol. Soc., Boston, MA, 86-89.

Hanna, S.R., G.A. Briggs, and R.P. Hosker, 1982: Handbook on atmospheric diffusion, U.S. DOE, DOE/TIC-11223, DE82002045, National Technical Info. Center, Springfield, VA.

Hanna, S.R., 1984: Applications in air pollution modeling, Chap. 7, Atmos. Turb. & Air Poll. Modeling, Ed. F.T.M. Nieuwstadt and H. van Dop, D. Reidel Publishing Co., Kluwer Academic Publishers, Hingham, MA.

Hicks, B.B., 1985: Behavior of turbulence statistics in the convective boundary layer. J. of Clim. and Applied Meteorology. 24, 607-614.

Irwin, J.S., 1979: Scheme for estimating dispersion parameters as a function of release height, EPA-600/4-79-062, Research Triangle Park, NC., 56 pp.

Irwin, J.S., 1983: Estimating plume dispersion - a comparison of several sigma schemes. J. Clim. And Appl. Meteorol., 22, 92-114.

Kumar, N. and A.G. Russell, 1996: Development of a computationally efficient, reactive sub-grid scale plume model and the impact in the northeastern United State using increasing levels of chemical detail. J. of Geophys. Res., 101, 16737-16744.

Mathur, R., L.K. Peters, and R.D. Saylor, 1992: Sub-grid presentation of emission source clusters in regional air quality modeling. Atmos. Environ., 26A, 3219-3238.

Morris, R.E. M.A. Yocke, T.C. Myers, and V. Mirabella, 1992: Overview of the variable-grid Urban Airshed Model (UAM-V) 85th Annual Meeting of the A&WMA, June 21-26, 1992, Kansas City, MO., AWMA, Pittsburgh, PA.

Myer, T.C., P.D. Guthrie and S.Y. Wu, 1996: The implementation of a plume-in-grid module in the SARMAP air quality model (SAQM). SYSAPP-96-06, Systems Applications International, Inc., Available from Technical Support Div., California Air Resources Board, Sacramento CA.

Niewstadt, F.T.M., 1984: Some aspects of the turbulent stable boundary layer. Boundary-Layer Meteorol., 30, 31-55.

Odman, M. T. and A.G. Russell, 1991: Multiscale modeling of pollutant transport and chemistry. J. of Geophys. Res., 96, D4, 7363-7370.

Pasquill, F., 1976: Atmospheric dispersion parameters in Gaussian plum modeling: Part II. Possible requirements for change in the Turner workbook values. EPA-600/4-76-030b, US EPA, Research Triangle Park, NC , 53 pp.

Pasquill, F., 1979: Atmospheric dispersion modeling. J. of the Air Poll. Contrl. Assoc., 29, 117-119.

Seigneur, C., T.W. Tesche, P.M. Roth, and M.K. Liu, 1983: On the treatment of point source emissions in urban air quality. Atmos. Environ., 17(9), 1655-1676.

Turner, D.B., T. Chico and J.A. Catalano, 1986: TUPOS - a multiple source gaussian dispersion algorithm using on-site turbulence data. U.S. Environmental Protection Agency, EPA/600/8-86-010, National Technical Information Center, Springfield, VA.

Venkatram, A., D. Strimaitis, D. Cicristofaro, 1984: A semiempirical model to estimate dispersion of evelated releases in the stable boundary layer. Atmos. Environ., 18, 923-928.

Venkatram, A. 1988: Dispersion in the stable boundary layer. Chapter 5, In Lectures on Air Pollution Modeling, A. Venkatram abd J. Wyngaard, Eds., Amer. Meteorol. Soc., Boston, MA., 1988.

Weil, J.C., 1988: Dispersion in the convective boundary layer. Chapter 4, In Lectures on Air Pollution Modeling, A. Venkatram and J. Wyngaard, Eds., Amer. Meteorol. Soc., Boston, MA., 1988.

This chapter is taken from *Science Algorithms of the EPA Models-3 Community Multiscale Air Quality (CMAQ) Modeling System*, edited by D. W. Byun and J. K. S. Ching, 1999.

Locations of MEPSE Sources

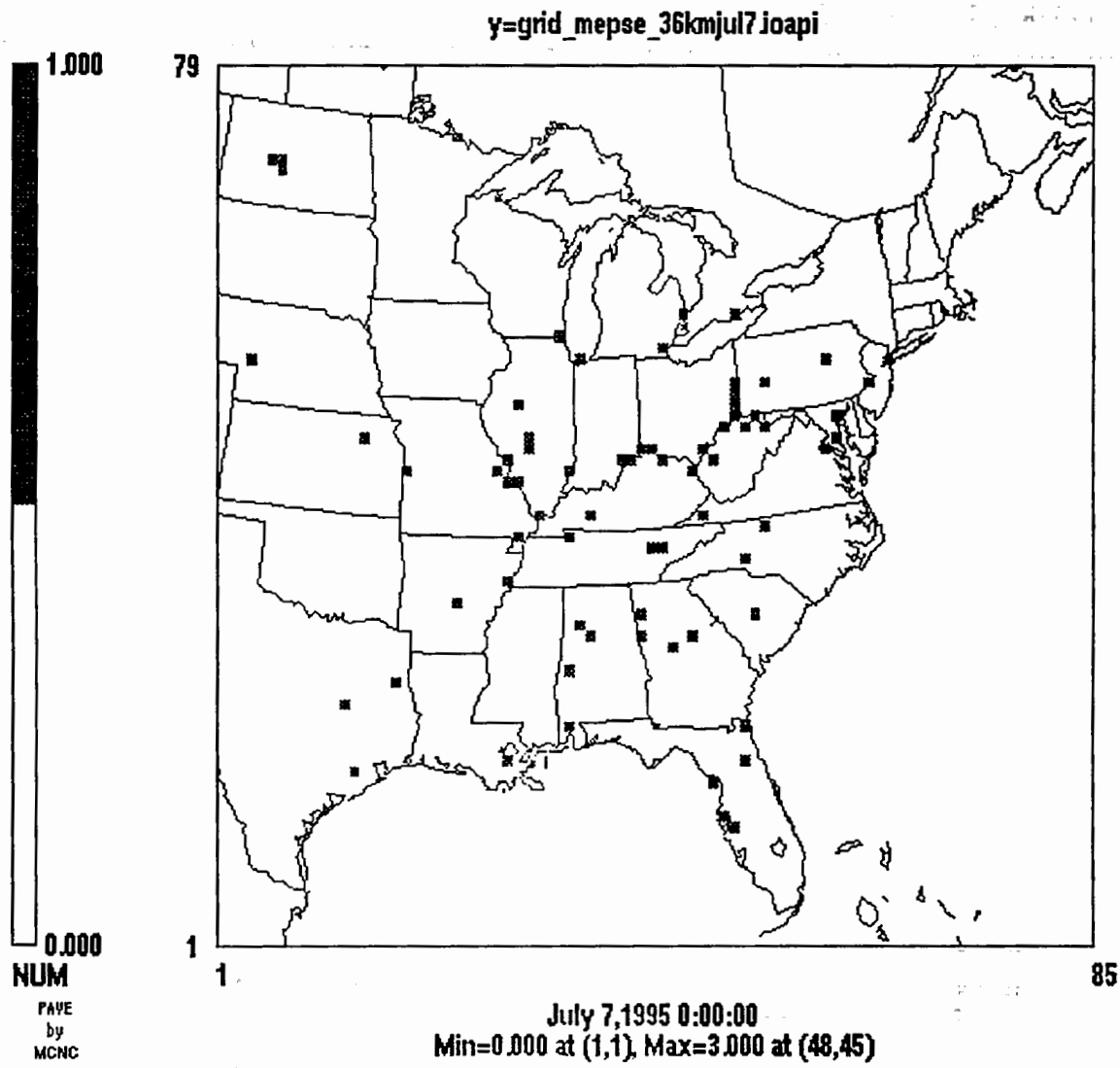

Figure 9-1 Location of MEPSEs depicted in individual grid cells.

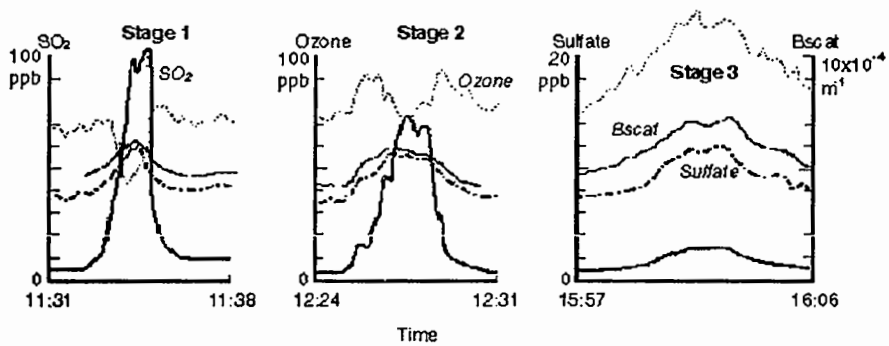

Figure 9-2. Chemical stages of a plume are depicted by aircraft plume data of SO2, ozone, sulfate, and aerosol scattering coefficient (Bscat) from crosswind traverses through a large MEPSE plume. Measurements are from the daytime period of the 23 August 1978 Tennessee Plume Study experiment. (Adapted from Gillani et al, 1981)

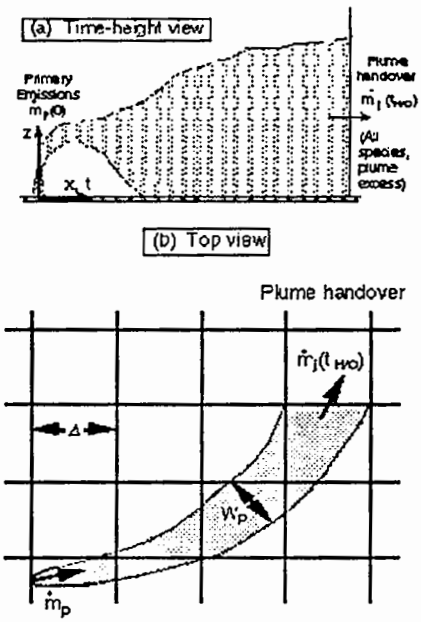

Figure 9-3. Schematics of the a) time-height view and b) top view of the modeling concept of the subgrid scale plume in the Models-3 PinG approach.

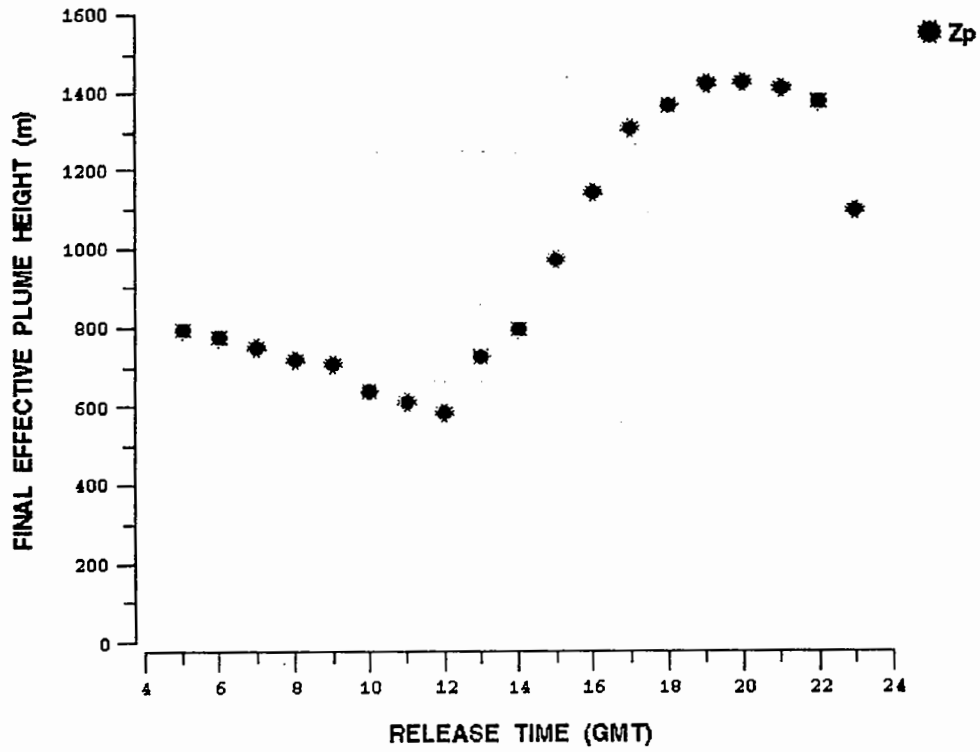

Figure 9-4. Example of the final plume height after plume rise for hourly releases from a MEPSE 300 m stack height.

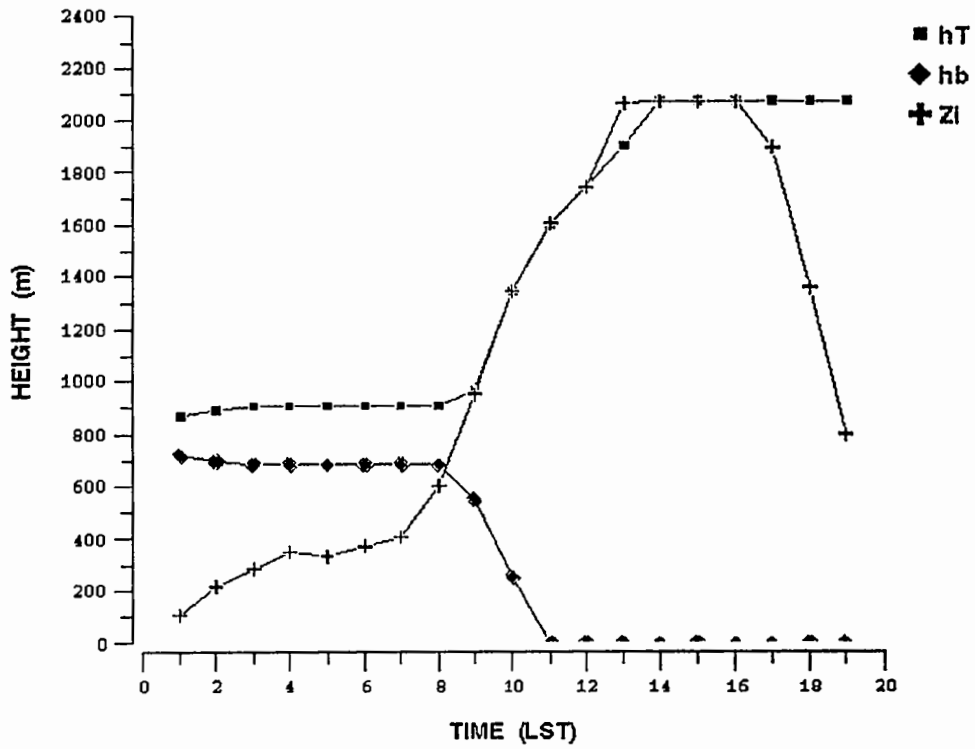

Figure 9-5. Time variation of the plume bottom (hb) and top (hT) heights and the PBL height (Zi) for a nocturnal release.

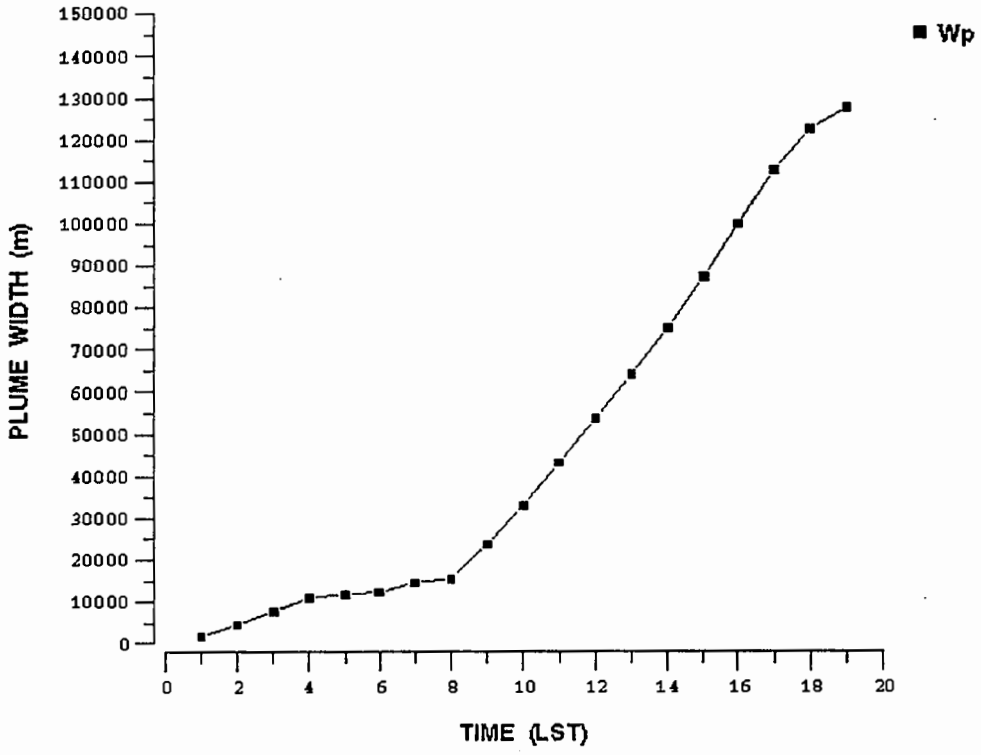

Figure 9-6. Time variation of plume width (Wp) from a nocturnal plume release. A plume width of about 30 km is achieved during the morning period about 10 hours after release.

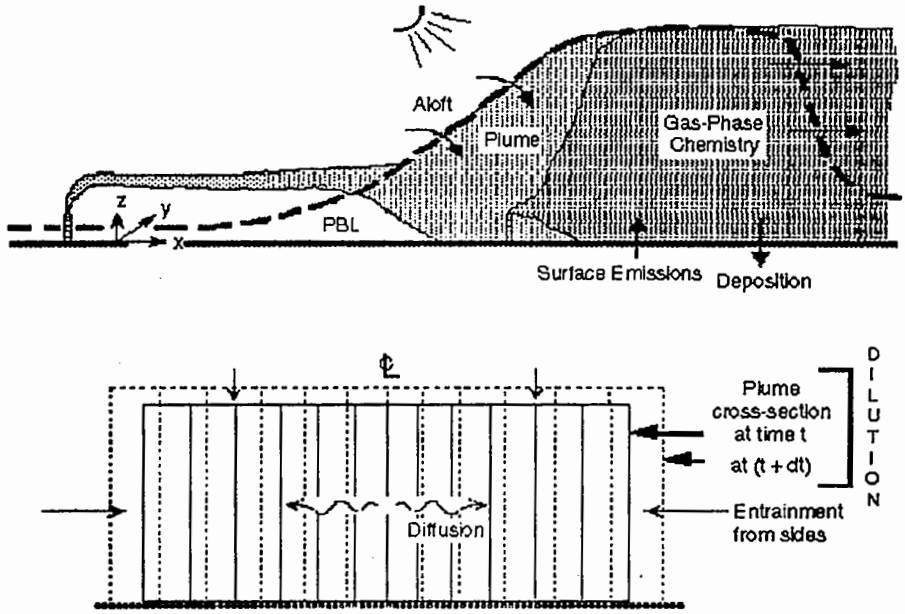

Figure 9-7. An illustration of the PinG module formulation depicting the relevant processes; a) time-height view and b) cross-sectional view.

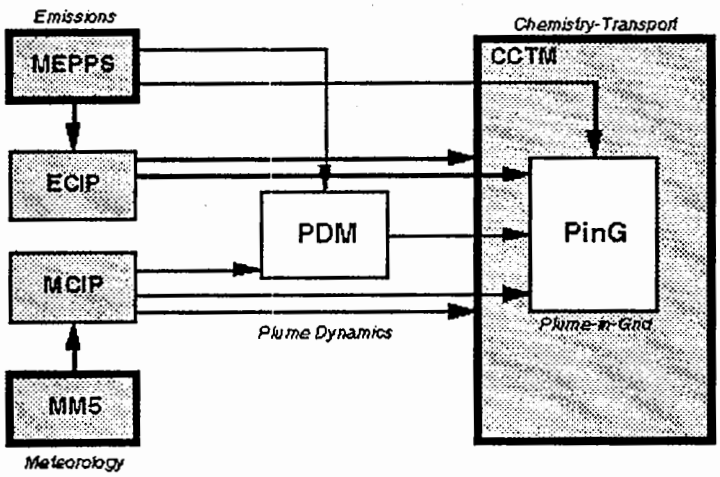

Figure 9-8. Flow diagram of the PDM processor and PinG module with associated programs in the Models-3 CMAQ system.

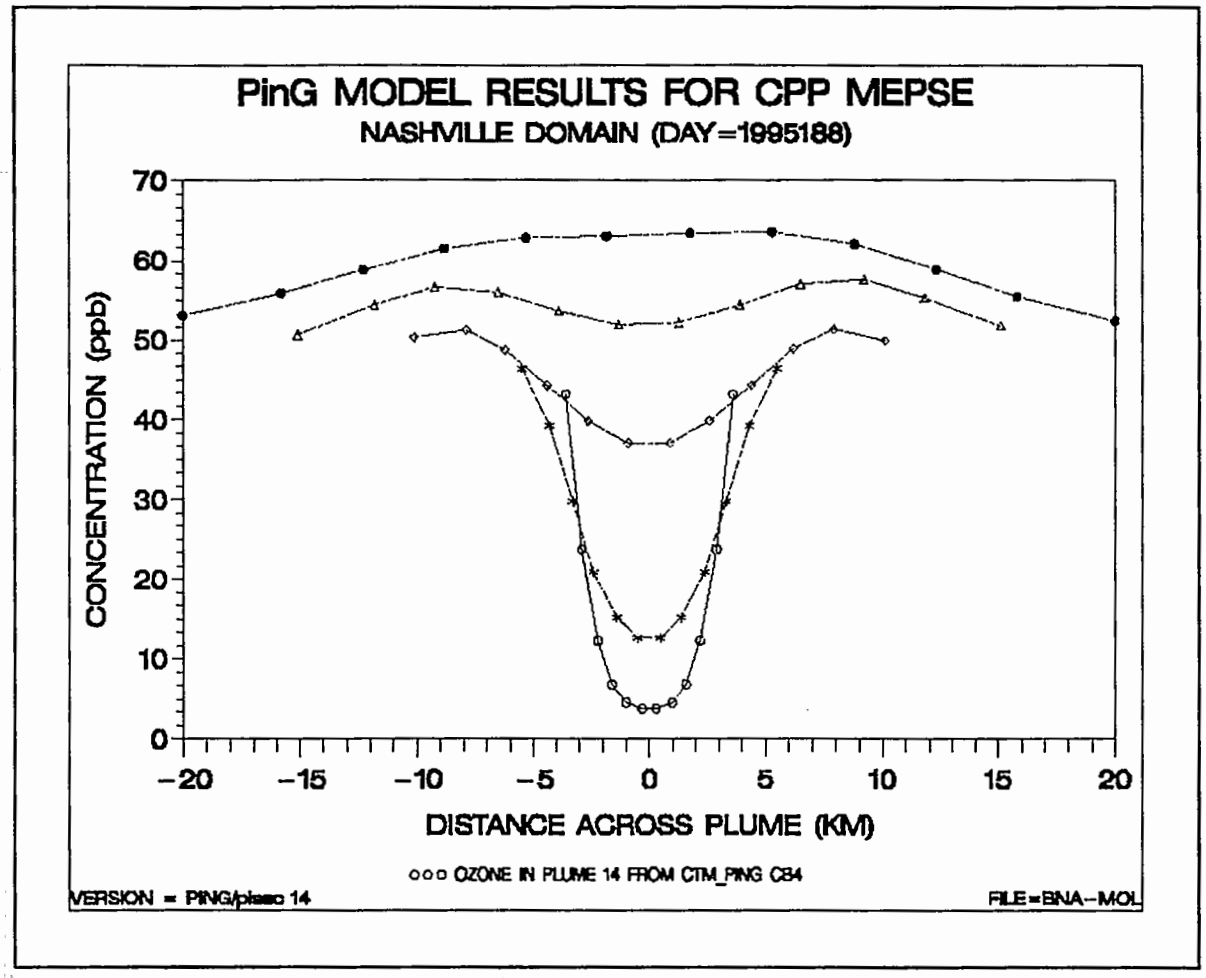

Figure 9-9 Plume ozone concentrations in an expanding cross-section in the subgrid scale plume phase at various times (o - 14:00, * - 14:30, ◊ - 15:30, ▵ - 15:30, • - 17:30). Plume section was released at 13:00. Symbol at each edge is the grid boundary concentration.

EPA/600/R-99/030

Chapter 10

AEROSOLS IN MODELS-3 CMAQ

Francis S. Binkowski*
Atmospheric Modeling Division
National Exposure Research Laboratory
U.S. Environmental Protection Agency
Research Triangle Park, North Carolina 27711

ABSTRACT

The aerosol module of the CMAQ is designed to be an efficient and economical depiction of aerosol dynamics in the atmosphere. The approach taken represents the particle size distribution as the superposition of three lognormal subdistributions, called modes. The processes of coagulation, particle growth by the addition of new mass, particle formation, etc. are included. Time stepping is done with analytical solution to the differential equations for the conservation of number and species mass conservation. The module considers both $PM_{2.5}$ and PM_{10} and includes estimates of the primary emissions of elemental and organic carbon, dust and other species not further specified. Secondary species considered are sulfate, nitrate, ammonium, water and organic from precursors of anthropogenic and biogenic origin. Extinction of visible light by aerosols represented by two methods, a parametric approximation to Mie extinction and an empirical approach based upon field data. The algorithms describing cloud interactions are also included in this chapter.

*On assignment from the National Oceanic and Atmospheric Administration, U.S. Department of Commerce. Corresponding author address: Francis S. Binkowski, MD-80, Research Triangle Park, NC 27711. E-mail: fzb@hpcc.epa.gov

10.0 AEROSOLS IN MODELS-3 CMAQ

Inclusion of aerosol particles in an air quality model presents several challenges. Among these are the differences between the physical characteristics of gases and particles. In treating gases in an air quality model, the size of the gas molecules is not usually of primary importance. In contrast, particle size is of primary importance. The interaction between condensing vapors and the target particle depends in an important way on the particle size in relation to the mean free path in the atmosphere. For gases, once the concentration is known, the corresponding number of molecules is known. This is not the case for particles. Thus, including aerosol particles in an air quality model means choosing how the total number, total mass, and size distribution of the particles is represented. Once this choice is made, then important physical and chemical processes involving particles must be represented. Particles may be emitted into the air by natural processes such as wind blowing dust from a desert. Human activities may disturb the soil to allow wind to blow soil particles off the ground. Sea salt particles come into the atmosphere by wind driven waves on the sea surface. Volcanic activity is another source of particles for both the troposphere and the stratosphere. Particles can be made in the atmosphere directly from chemical reaction. The most important example of this is the transformation of sulfur dioxide, a by-product of fossil fuel combustion, into sulfate particles. Hydroxyl radicals attack the sulfur dioxide and make sulfuric acid that then may nucleate in the presence of water vapor and ammonia to produce new particles. If there are particles already present in the atmosphere, the new sulfate may condense on the existing particles or nucleate to form new particles depending upon conditions which are only recently beginning to be understood. Reactions of organic precursors such as natural monoterpenes and anthropogenic organic species with ozone and other oxidants or radicals make new species that condense on existing particles or make new particles depending upon conditions. Combustion sources emit particles composed of mixtures of organic carbon and elemental carbon. The exact mixture of organic and elemental carbon is a strong function of the conditions of combustion. Once these particles are in the air, they may grow by condensing of species upon them as has already been mentioned. For a large group of particles made in the air, i.e., secondary particles, growth may be related to relative humidity because of water condensing on the particles. Another gas-particle interaction is the chemical equilibration of species within or on the surface of a particle with gases and vapors within the air. Unlike gases, particles coagulate, e.g., collide and form a particle whose mass and volume are the sums of the masses and volumes of the colliding particles. Thus, adding particles to an air quality model means adding a new set of physical processes.

In designing the aerosol component of CMAQ the following assumptions were made. Any representation of particles had to be consistent with observations of particles. The representation had to be mathematically and numerically efficient to minimize computer time. And finally the representation had to be usable for regional to urban simulations. These assumptions led to a choice of two methods. The first method would be to model particle behavior in set of bins of increasing size. This approach is quite popular and is described originally by Gelbard et. al. (1980) and more recently by Jacobson (1997). The second approach, the one chosen for implementation in CMAQ, is to follow Whitby (1978) and model the particles as a superposition of lognormal subdistributions called modes. The sectional method using the discrete size bins requires a large number of bins to capture the size distribution. If one wishes to model several

chemical components then the number of components is multiplied by the number of bins. This leads to a very large number of variables that must be added to an air quality model to capture particle behavior. In the modal approach, using the three modes suggested by Whitby(1978), only three integral properties of the distribution, the total particle number concentration, the total surface area concentration, and the total mass concentration of the individual chemical components in each of the three mode. The current approach differs from that taken by Binkowski and Shankar (1995) where the sixth moment was chosen as a third in integral property in place of the second moment. That moment as chosen because of a mathematical simplification (see Whitby and McMurry, 1997). The mathematical simplifications of the modal method allow analytical solutions to be used for the aerosol dynamics. The current approach uses numerical quadratures to calculate all of the coagulation terms. The numerical quadratures were compared with the analytical expressions exhibited in Whitby et al. (1991) and are accurate to six decimal places. The choice of using numerical quadratures was made to reduce the memory requirements associated with a variable geometric standard deviation and because the second moment unlike the sixth moment does not have an analytical form.

The aerosol component of the CMAQ is derived from the Regional Particulate Model (RPM) (Binkowski and Shankar, 1995) which in, turn, is based upon the paradigm of the Regional Acid Deposition Model (RADM), an Eulerian framework model (Chang et al., 1990). The particles are divided into two groups, which are fine particles and coarse particles. These groups generally have separate source mechanisms and chemical characteristics. The fine particles result from combustion processes and chemical production of material that then condenses upon existing particles or forms new particles by nucleation. The coarse group is composed of material such as wind-blown dust and marine particles (sea salt). The anthropogenic component of the coarse particles is most often identified with industrial processes. The common EPA nomenclature used in air quality refers to $PM_{2.5}$ (particles with diameters less than 2.5 μm) and PM_{10} (particles with diameters less than 10μm). Note that PM_{10} includes $PM_{2.5}$. Thus, in the present context, coarse particles are those with diameters between 2.5 and 10 μm. Then, the mass of the coarse particles is the difference between the masses in PM_{10} and $PM_{2.5}$.

As already noted, the aerosol particle size distribution is modeled using the concepts developed by Whitby (1978). That is, $PM_{2.5}$ is treated by two interacting subdistributions or modes. The coarse particles form a third mode. Conceptually within the fine group, the smaller (nuclei or Aitken), *i*-mode represents fresh particles either from nucleation or from direct emission, while the larger (accumulation), *j*-mode represents aged particles. Primary emissions may also be distributed between these two modes. The two modes interact with each other through coagulation. Each mode may grow through condensation of gaseous precursors; each mode is subject to wet and dry deposition. Finally, the smaller mode may grow into the larger mode and partially merge with it. These processes are described in the following subsections. The chemical species treated in the aerosol component are fine species sulfates, nitrates, ammonium, water, anthropogenic and biogenic organic carbon, elemental carbon, and other unspecified material of anthropogenic origin. The coarse-mode species include sea salt, wind-blown dust, and other unspecified material of anthropogenic origin. Because atmospheric transparency or visual range is an important air quality related value, the aerosol component also calculates estimates of visual range and aerosol extinction coefficient.

10.1 Aerosol Dynamics

The particle dynamics of this aerosol distribution are described fully in Whitby et al. (1991) and Whitby and McMurry 1997); therefore, only a brief summary of the method is given here.

(Note: In the following equations repeated subscripts are not summed.)

10.1.1 Modal Definitions

Given a lognormal distribution defined as

$$n(\ln D) = \frac{N}{\sqrt{2\pi}\,\ln\sigma_g}\exp\left[-0.5\left(\frac{\ln\frac{D}{D_g}}{\ln\sigma_g}\right)^2\right], \tag{10-1}$$

where N is the particle number concentration, D the particle diameter, and D_g and σ_g the geometric mean diameter and standard deviation of the distribution, respectively. The kth moment of the distribution is defined as

$$M_k = \int_{-\infty}^{\infty} D^k n(\ln D)\,\mathrm{d}(\ln D) \tag{10-2}$$

with the result

$$M_k = N\,D_g^k \exp\left[\frac{k^2}{2}\ln^2\sigma_g\right]. \tag{10-3}$$

M_0 is the total number, N, of aerosol particles within the mode suspended in a unit volume of air. For $k = 2$, the moment is proportional to the total particulate surface area within the mode per unit volume of air. For $k = 3$, the moment is proportional to the total particulate volume within the mode per unit volume of air. The constant of proportionality between M_2 and surface area is π; the constant of proportionality between M_3 and volume is $\pi/6$. Note that the geometric standard deviation is the same no matter which moment is selected. M_3 is determined from the nine distinct fine aerosol species (including water) listed in Table 10-1 as follows:

$$M_{3i} = \sum_{n=1}^{n_{max}} \frac{\varphi_i^n}{\frac{\pi}{6}\rho_n} \tag{10-4a}$$

$$M_{3j} = \sum_{n=1}^{n_{max}} \frac{\varphi_j^n}{\frac{\pi}{6}\rho_n} \tag{10-4b}$$

where φ_i^n and φ_j^n are the species mass concentrations of the nth species in each mode in [$\mu g\ m^{-3}$], ρ_n is the average density of the nth species. The third moment for the coarse mode is

obtained in a similar manner. Given a value of third moment concentration and number concentration, the geometric mean standard deviation and the geometric mean diameter for each mode is diagnosed from

$$\ln^2\sigma_g = \frac{1}{3}\left(2\ln(M_3) - 3\ln(N)\right) - \ln(M_2) \tag{10-5a}$$

$$D_g^3 = \frac{M_3}{N\exp\left[\frac{9}{2}\ln^2\sigma_g\right]} . \tag{10-5b}$$

The prediction equations for number, second moment and species mass are given in Section 10.1.4.

10.1.2 New Particle Production by Nucleation

The CMAQ aerosol component has a choice of two particle production mechanisms, those of Harrington and Kreidenweis (1998a,b) and Kulmala et al. (1998). Both of these methods predict the rate of increase of the number of particles, J, (in number per unit volume per unit time) by the nucleation from sulfuric acid vapor. In order to predict the rate of increase on new mass and new second moment an assumption about particle size is necessary. Following work by Weber et al. (1997), it is assumed that the new particles are 3.5 nm in diameter. Weber et al. reported measurements of the concentration of particles that are in the size range 2.7 to 4.nm. For simplicity we have chosen 3.5 nm as a representative diameter.

Using either of these methods, the production rate of new particle mass [$\mu g\ m^{-3}\ s^{-1}$] is then

$$\frac{d\,Mass}{dt} = \frac{\pi}{6}\rho d_{3.5}^3 J \tag{10-6a}$$

and that for number [$m^{-3}\ s^{-1}$] is

$$\frac{d\,Num}{dt} = J \tag{10-6b}$$

and that for second moment [$m^2\ m^{-3}$ s-1] is

$$\frac{d\,M_2}{dt} = d_{3.5}^2 J \tag{10-6c}$$

where $d_{3.5}$ is the diameter of the 3.5 nm particle and ρ is the density of the particle (taken as sulfuric acid) at ambient relative humidity (Nair and Vohra, 1975).

10.1.3 Primary Emissions

The EPA emission inventory for $PM_{2.5}$ and PM_{10} does not currently contain information about neither size distribution nor chemical speciation. In the CMAQ work, the assumption is that the major part of $PM_{2.5}$ particulate mass emissions are in the accumulation mode with a small fraction in the Aitken mode; i.e. a fraction of 0.999 of $PM_{2.5}$ is assumed to be in the accumulation mode and the remaining fraction, 0.001, is assigned to the Aitken mode. Sensitivity studies will be conducted to evaluate this assumption. In order to estimate the emissions rate for number and second moment from the mass emissions rate an assumed mass size distribution is required. It is convenient to express the emission rate for number, E_0, and that for second moment E_2 in terms of a total emissions rate for third moment. This is shown schematically as follows where E_n is the mass emissions rate for species n and ρ_n is the density for that species

$$E_{3n} = \left(\frac{6}{\pi}\right)\left(\frac{E_n}{\rho_n}\right) \tag{10-7a}$$

$$E_0 = \frac{\sum_n E_{3n}}{D_{gv}^3 \exp\left(-\frac{9}{2}\ln^2\sigma_g\right)} \tag{10-7b}$$

$$E_2 = \frac{\sum_n E_{3n}}{D_{gv} \exp\left(-\frac{1}{2}\ln^2\sigma_g\right)} \tag{10-7c}$$

where the sum is taken over all emitted species.

In Equation 10-7b,c, E_0 and E_2 schematically represent the emissions rates for the various modes. In Section 10.1.4, the nomenclature used to represent the emissions rate for number for each of the three modes will be respectively E_{0i}, E_{0j}, and E_{0cor}.

We have chosen values of 0.3 μm for the geometric mean diameter for mass, D_{gv}, and 2.0 for the geometric standard deviation, σ_g for the accumulation mode. The corresponding values for the Aitken mode are 0.03 μm and 1.7, and those for the coarse mode are 6 μm and 2.2.

The current emissions inventory estimates that 90% of PM_{10} is fugitive dust, and that 70% of this dust consists of $PM_{2.5}$ particles. The paradigm adopted for the CMAQ is that fugitive dust is a coarse mode phenomenon with a tail that overlaps the $PM_{2.5}$ range. Therefore, 90% of PM_{10} emissions are assigned entirely to the coarse mode species ASOIL. Sulfate emissions are treated differently in CMAQ than in RPM. In RPM sulfate emissions were treated as particles and distributed between the Aitken and accumulation modes. In CMAQ, the photochemical module has sulfate emissions incorporated into the chemical solver. Thus, the production rate for sulfuric

acid will include direct emissions of sulfate. This rate is passed from the photochemical module to the aerosol module. Assigning fractional amounts of emitted $PM_{2.5}$ and PM_{10} to the specific species in Table 10-1 is a matter of ongoing discussions with those responsible for preparing the national emissions inventory.

10.1.4 Numerical Solvers

The numerical solvers for the two fine particle modes in the Models-3 aerosol component have been modified from those in RPM, which followed from Whitby et al. (1991). The major difference is that the RPM solvers linearized the quadratic term for intramodal coagulation in the equation for modal number concentration. The new solvers in CMAQ retain this quadratic term.

The number concentrations for the Aitken and accumulation modes are denoted as N_i and N_j respectively. Intramodal coagulation coefficients are functions only of the geometric mean diameters and geometric standard deviations for each mode and are denoted as F_{0ii} and F_{0jj}.

Similarly, the intermodal coagulation coefficient for coagulation between the Aitken and accumulation modes is F_{0ij}. For simplicity the following coefficients are defined.

For the Aitken mode:

$a_i = F_{0ii}$, $b_i = N_j F_{0ij}$, and

$c_i = \frac{d\,Num}{dt} + E_{0i}$, with $\frac{d\,Num}{dt}$ from (10-6b);

and for the accumulation mode:

$a_j = F_{0jj}$, and $c_j = E_{0j}$

The emissions rates for number concentration are E_{0i} and E_{0j} and are set to values determined for each mode from Equation 10-7b.

We may now write for the particle number concentrations

$$\frac{\partial N_i}{\partial t} = c_i - a_i N_i^2 - b_i N_i \text{ ; and} \qquad (10\text{-}8a)$$

$$\frac{\partial N_j}{\partial t} = c_j - a_j N_j^2. \qquad (10\text{-}8b)$$

Equation 10-8a, a Riccati type equation and Equation 10-8b, a logistics type equation, have different analytical solutions depending upon whether c_i and c_j are zero or nonzero. These analytic solutions are used in the CMAQ solver with the coefficients being held constant over one model time step. In discussing the analytical solutions to Equations 10-8a and b, subscripts will be omitted for simplicity

The solution to Equation 10-8a for $c_i \neq 0$ is of the form

$$N(t) = \frac{r_1 + r_2 P \exp(\hat{D}t)}{a\left[1 + P \exp(\hat{D}t)\right]}$$

where

$$\hat{D} = \left(b^2 + 4ac\right)^{\frac{1}{2}}, r_1 = \frac{2ac}{b + \hat{D}}, r_2 = -\frac{b + \hat{D}}{2}, P = -\left(\frac{r_1 - a\,N(t_0)}{r_2 - a\,N(t_0)}\right).$$

For $c_i = 0$, the solution to Equation 10-8a is of the form

$$N(t) = \frac{bN(t_0)\exp(-bt)}{b + aN(t_0)\left[1 - \exp(-bt)\right]}.$$

The solution to Equation 10-8b when $c_j \neq 0$ is of the same form as that to Equation 10-8a except $b = 0$. The solution when $c_j = 0$, known as Smoluchowski's solution, is:

$$N(t) = \frac{N(t_0)}{1 + aN(t_0)t}.$$

The equations for the prediction of second moment, M_2, in the Aitken and accumulation modes are both of the form

$$\frac{\partial M_2}{\partial t} = P_2 - L_2 M_2;$$

with solutions of the form

$$M_2(t) = \frac{P_2}{L_2} + \left[M_2(t_0) - \frac{P_2}{L_2}\right]\exp(-L_2 t).$$

In these equations, production of second moment is denoted by P_2 and loss by L_2 .For the Aitken mode, the production term includes the rate of second moment increase by new particle formation from Equation 10-6c, condensational growth (Equation 7a of Binkowski and Shankar, 1995) and by primary emissions from Equation 10-7c. The loss term accounts for the loss of second moment by intramodal coagulation, as well as including the transfer of second moment to the accumulation mode by intermodal coagulation. For the accumulation mode, the production term includes the transfer of second moment by intermodal coagulation, condensational growth (Equation 7b of Binkowski and Shankar, 1995) and the contribution of primary emissions from Equation 10-7c. The loss term accounts for intramodal coagulation.

It is important to note that the history variable in CMAQ is the modal surface area, which, as already noted, is π time the second moment. For convenience, however, within the internal aerosol subroutines, the second moment is the treated. Before returning to the main CMAQ routines, the second moment is multiplied by π. That is why species number 23 and 24 in Table 10-1 are identified as modal surface areas. It is also important to note that the surface area predicted by CMAQ is the surface area for *spherical* particles and may not represent the true surface area available in nonspherical particles or in porous particles such as carbon soot. Empirical correction factors may be needed for use of CMAQ surface area predictions in certain applications.

The equations for mass concentration of species n may be written as:

$$\frac{\partial \varphi_i^n}{\partial t} = P_i^n - L_i \varphi_i^n; \text{ and} \tag{10-9a}$$

$$\frac{\partial \varphi_j^n}{\partial t} = P_j^n, \tag{10-9b}$$

where $P_i^n = \phi_i^n + E_i^n + R^n \Omega_i$ and $L_i = N_i N F_{3ij} / M_{3i}$

with $\phi_i^n = \frac{d\,Mass}{dt}$ from Equation 10-6a, when n denotes sulfate, and where E_i^n and E_j^n are the emission rates and R^n is the gas-phase production rate for species n. The factors Ω_i and Ω_j, defined by Equations A17 and A18 of Binkowski and Shankar (1995) represent the fractional apportionment of condensing species. F_{3ij} is the coagulation coefficient for the third moment.

Note that the loss of mass in Equation 10-9a is a gain of mass in Equation 10-9b. This represents the transfer of mass by intermodal coagulation. There is no such transfer of number in Equations 10-8a,b because of the convention that when a smaller particle coagulates with a larger particle there is a loss of number from the population of smaller particles, but no gain of number in the population of larger particles. There is, however, a transfer of mass. Equations 10-9a and b have an analytic solution holding the coefficients constant for the time step of the form:

$$\varphi(t) = \frac{P}{L} + \left[\varphi(t_0) - \frac{P}{L}\right] \exp\left(-Lt\right).$$

The solution to Equation 10-9b are by an Euler forward step once again holding the production terms constant over that time step.

The equation for the prediction of coarse mode mass is

$$\frac{\partial \varphi_{cor}^n}{\partial t} = E_{cor}^n,$$

The solution is by an Euler forward step. The equation for coarse mode number is similar because coagulation is ignored for the coarse mode, and is also solved by an Euler forward step.

10.1.5 Mode Merging by Renaming

In Binkowski and Shankar (1995), the Aitken mode diameters grew over the simulation period to become as large as those in the accumulation mode. While this is probably true in nature, it violates the modeling paradigm that two modes of distinct size ranges always exist. This phenomenon can be modeled by mode merging as follows. The Aitken mode approaches the accumulation mode by small increments over any model time step when particle growth and nucleation are occurring. Thus, an algorithm is needed that transfers number and mass concentration from the Aitken mode to the accumulation mode when the Aitken mode forcing exceeds the accumulation mode forcing and the number of particles in the accumulation mode is no larger than that in the Aitken mode.

This algorithm is formulated as follows (Binkowski et al., 1996). When Equation 10-10 is satisfied, the diameter of overlap, $\overset{*}{d}$, for the modal number distributions can be calculated exactly. Given this diameter, the fraction of the total number of Aitken mode particles greater than this diameter is easily calculated from the complementary error function

$$F_{num} = 0.5\left[1 + \mathrm{erfc}\,(x_{num})\right] \text{ , where} \qquad (10\text{-}10a)$$

$$x_{num} = \frac{\ln\left(\overset{*}{d}/d_{gni}\right)}{\sqrt{2}\ln\left(\sigma_{gi}\right)}$$

and d_{gni} is the geometric mean diameter for the Aitken mode number distribution.

The number concentration corresponding to these particles is transferred to the accumulation mode, a processes denoted here as renaming the particles. A similar process is used to transfer mass (third moment) concentration and surface area (second moment) concentration from the Aitken to the accumulation mode using the complementary error function corresponding to the third moment.

$$F_k = 0.5\left[1 + \mathrm{erfc}\,(x_k)\right] , \qquad (10\text{-}10b)$$

$$\text{where } x_k = x_{num} - \frac{k\ln\left(\sigma_{gi}\right)}{\sqrt{2}} .$$

For numerical stability, the transfer of number and mass is limited so that no more than one half of the Aitken mode mass may be transferred at any given time step.

This is accomplished by requiring that $\dfrac{3\ln\left(\sigma_{gi}\right)}{\sqrt{2}} \le x_{num}$.

The fraction of the total number and surface area (k= 2) and mass (k=3) remaining in the Aitken mode is calculated from the error function of the overlap diameters as:

$$\Phi_{num} = 0.5\left[1 + \text{erf}\,(x_{num})\right] \tag{10-10c}$$

$$\Phi_k = 0.5\left[1 + \text{erf}(x_k)\right] \tag{10-10d}$$

Using these fractions, Aitken and accumulation mode number and mass concentrations are updated as

$$N_j = N_j + F_{num} N_i \tag{10-11a}$$

$$\varphi_j^n = \varphi_j^n + F_3 \varphi_i^n \tag{10-11b}$$

$$M_{2\,j} = M_{2\,j} + F_2 M_{2i} \tag{10-11c}$$

$$N_i = \Phi_{num} N_i \tag{10-11d}$$

$$\varphi_i^n = \Phi_3 \varphi_i^n \tag{10-11e}$$

$$M_{2i} = \Phi_2 M_{2i} \tag{10-11f}$$

This method of particle renaming is analogous to the procedure discussed by Jacobson (1997) where particles are reassigned in the moving center concept of a bin model. When the particles grow beyond the boundaries of their size bin, they are reassigned to a larger bin and averaged with the new bin.

10.2 Aerosol Dry Deposition

The rate of dry deposition of particle zeroth and third moment to the earth's surface provides the lower boundary condition for the vertical diffusion of aerosol number and species mass, respectively. The method of doing this follows the RPM approach with the following exceptions. In RPM total fine mass was deposited. In CMAQ the species mass in each mode is deposited separately using the dry deposition velocity for the third moment. The impaction term is omitted for the coarse mode particles in both the zeroth and third moment dry deposition velocities. See Binkowski and Shankar (1995) Equations A25 through A34 for details.

10.3 Cloud Processing of Aerosols

Clouds are formed when the relative humidity reaches a value at which existing aerosol particles are activated. That is, they pass through a potential barrier and grow rapidly from a few micrometers to several micrometers to become cloud droplets (cloud nucleation). Soluble gases are then dissolved into the cloud droplets where aqueous-phase chemical equilibria and reactions occur. The attack on dissolved sulfur dioxide by hydrogen peroxide produces a dissolved sulfate species (oxidation of Sulfur (IV) to Sulfur (VI)). Because these processes are very complex in detail and occur at subgrid scale, most cloud modeling in mesoscale meteorological models and

in air quality models uses simplified parametric approaches to model the effect of clouds rather than modeling the clouds directly. This approach was used in RADM and RPM and is applied in the first version of CMAQ.

The assumptions for aerosol behavior in clouds are:

- The Aitken (i) mode forms interstitial aerosol which is scavenged by the cloud droplets. All three integral properties of the Aitken mode respond to in-cloud scavenging.
- The accumulation (j) mode forms cloud condensation nuclei and thus is distributed as aerosol within the cloud water. Mass and number in this mode may be lost through precipitation. Mass but not number is increased by in-cloud scavenging of the Aitken mode.
- All new sulfate mass produced by aqueous production is added to the accumulation mode, but the number of accumulation mode particles is unchanged as is the geometric standard deviation, σ_g, of the accumulation mode processes (cf Leaitch, 1996 for cumulus clouds).
- The assumption about the accumulation mode geometric standard deviation means that the surface area of the accumulation mode is reconstucted from the new mass and new number in the accumulation mode at the end of the cloud lifetime.
- The aerosol is mixed vertically by the same mechanisms mixing other species. The wet removal of aerosol is proportional to wet removal of sulfate (See Chapter 11).

The limitations are:

- The cloud process modules are similar to those of RPM and RADM with cloud droplet number concentrations being modeled by an empirical fit to data from Bower and Choularton (1992).
- Cloud droplet size distributions are lognormal with σ_g set to 1.2. Using the cloud liquid water content and the cloud droplet number concentration, the geometric mean cloud droplet diameter, d_g, can be calculated.

The mathematical approach begins with an extension (Binkowski and Shankar, 1994; Shankar and Binkowski, 1994) of Slinn's (1974) two-step model as used by Chaumerliac (1984).

The in-cloud scavenging of interstitial Aitken mode number, surface area and mass concentration, y_{ak}, may be represented by:

$$\frac{dy_{ak}}{dt} = -\alpha_k y_{ak} \qquad (10\text{-}12)$$

with solution (10-13)

$$y_{ak}\left(t+\tau_{cld}\right) = y_{ak}(0)\exp\left(-\alpha_k \tau_{cld}\right)$$

where α_k (k = 0,2,3) is the attachment rate for interstitial aerosol concentration. The attachment rate is assumed to be held constant over the cloud lifetime τ_{cld}. The initial values $y_{ak}(0)$ are determined after cloud mixing (see Equations 11-4 and 11-5).

The cloud water aerosol concentration is represented by

$$\frac{dy_{ck}}{dt} = \delta_{k3}\left(\alpha_k y_{ak} + P\right) - \beta\delta_{k0} y_{ck},\ k \neq 2 \qquad (10\text{-}14)$$

where β is the precipitation removal rate, and P is the production of new sulfate mass by aqueous chemistry. The first Kronecker delta indicates that only mass (k=3) is increased for the accumulation mode by chemical production and in-cloud scavenging. The second Kronecker delta indicates that only number (k=0) is removed by the precipitation removal term in this form. Mass is removed explicitly in the cloud processor.

The attachment rates, α_k, using the form recommended by Pruppacher and Keltt (1978) and including an enhancement factor for the settling velocity of the cloud droplets, v_{dc} are given by:

$$\alpha_k = 2\pi m_{1c}\hat{D}_{pk}\left(1 + 0.5\,Pe_k^{1/3}\right),\ k = 0,2,3; \qquad (10\text{-}15)$$

Where

$$m_{1c} = N_c d_{dg}\exp\left[\frac{1}{2}\ln^2\left(\sigma_{dg}\right)\right]. \qquad (10\text{-}16)$$

N_c and d_d are the cloud droplet number concentration and geometric mean diameter respectively.

$$Pe_k = \frac{v_{dc} d_d}{\hat{D}_{pk}} \text{ is a Peclet number.} \qquad (10\text{-}17)$$

The polydisperse diffusivity is given by

$$\hat{D}_{pk} = \left(\frac{k_b T}{3\pi\upsilon\rho_{air} D_g}\right) \times$$

$$\left\{\exp\left(\frac{(-2k+1)}{2}\ln^2\sigma_g\right) + 1.246 Kn_g \exp\left(\frac{(-4k+4)}{2}\ln^2\sigma_g\right)\right\}$$

and is the same form as that for dry deposition algorithm (see Binkowski and Shankar, 1995, Equation A29). (10-18)

The precipitation removal rate for number is given by

$$\beta = \frac{1}{\tau_{cld}}\left(\frac{[\delta SO_4]_{wetdep}}{[SO_4]_{init} + [SO_4]_{scav} + [\delta SO_4]_{prod}}\right) \quad (10\text{-}19)$$

where τ_{cld} is the cloud lifetime, $[\delta SO_4]_{wetdep}$ is the change in sulfate concentration due to precipitation loss, and $[SO_4]_{init}$ is the sulfate concentration at the beginning of the cloud lifetime, $[SO_4]_{scav}$ is the amount of sulfate added from in-cloud scavenging of Aitken mode sulfate; $[\delta SO_4]_{prod}$ is the amount of new sulfate produced by aqueous chemistry.

10.4 Aerosol Chemistry

The aerosol chemical species are listed in Table 10-1. The secondary species sulfate is produced by chemical reaction of hydroxyl radical on sulfur dioxide to produce sulfuric acid that may condense on existing particles or nucleate to form new particles. Emissions of fresh primary sulfate are treated in the gas-phase chemistry component, and this contributes to the total change in sulfate from the chemistry component. This is a change from RPM where primary sulfate emissions were treated as a source of new mass and new particle number. Other inorganic species such as (ammonia and nitric acid) are equilibrated with the aerosols.

An assumption of the model is that organics influence neither the water content nor the ionic strength of the system; however, this assumption may not be valid for many atmospheric aerosols. Although much progress has been made (e.g. Saxena et al., 1995; Saxena and Hildemann, 1996), sufficient basic data are not yet available to treat the system in a more complete and correct way. Over continental North America for $PM_{2.5}$, sea salt and soil particles are not considered in the equilibria. Thus, for the initial release of CMAQ, only the equilibrium of the sulfate, nitrate, ammonium and water system is considered. The equilibria and the associated constants are based upon Kim et al. (1993a) and shown in Table 10-3.

The aerosol water content is computed using the ZSR method (see Kim et al., 1993a) from:

$$W = \sum_n \frac{M_n}{m_{n0}(a_w)} \quad (10\text{-}20)$$

where W is the aerosol liquid water content [kg m^{-3}], M_n is the atmospheric concentration of the nth species [moles m^{-3}], and m_{n0} is the molality [moles kg^{-3}], of the nth species at a value of water activity (fractional relative humidity) of a_w. The values for the molality as a function of water activity are calculated from laboratory data from Giauque et al. (1960), Tang and Munkelwitz (1994), and Nair and Vohra (1975). The ZSR method is used in a somewhat different way than usual. The water content of sulfate aerosols depends strongly upon the ionic ratio of ammonium to sulfate. This ratio varies from zero for sulfuric acid to 2.0 for ammonium sulfate with intermediate values of 1.0 for ammonium bisulfate, and 1.5 for letovicite. The usual method would span this range with a single expression; however, Spann and Richardson (1985) have shown that this is not correct. They proposed a modification which resulted in a correction term. A very similar result is obtained by using the ZSR method between the ranges of the ionic

ratio of sulfuric acid to ammonium bisulfate, ammonium bisulfate to letovicite, and letovicite to ammonium sulfate. The binary activity coefficients are computed using Pitzer's method and the Bromley method is used for the multicomponent activity coefficients in the aqueous solution (see Kim et al., 1993a) for details.

Two regimes of ammonium to sulfate ionic ratio are considered. The ammonia deficient regime (in which the ionic ratio of ammonium to total sulfate ion is less than two) leads to an acidic aerosol system with very low concentrations of dissolved nitrate ion which depend very strongly on ambient relative humidity. The second regime is one in which the ammonium to sulfate ratio exceeds two, the sulfate is completely neutralized, and there is excess ammonia. If there is nitric acid vapor in the system, it will dissolve in the aqueous particles along with the excess ammonia and produce abundant nitrate.

For cases when the relative humidity is so low that the aerosol liquid water content comprises less than 20 percent of the total aerosol mass, and the ionic ratio of ammonium to sulfate is greater than two, "dry ammonium nitrate" aerosol is calculated with the following equilibrium relationship:

$$NH_4NO_3(s) \Leftrightarrow NH_3(g) + HNO_3(g) \qquad (10\text{-}21)$$

The value of the equilibrium constant is taken from Mozurkewich (1993) as noted in Table 10-2.

Precursors of anthropogenic organic aerosol (such as alkanes, alkenes, and aromatics) react with hydroxyl radicals, ozone, and nitrate radicals to produce condensable material. Monoterpenes react in a similar manner to produce biogenic organic aerosol species. The rates of production of sulfuric acid and the organic species are passed from the photochemical component to the aerosol component. The formation rates of aerosol mass (in terms of the reaction rates of the precursors) are taken from Pandis et al. (1992). These factors are given in Table 10-3.

10.5 Visibility

Visibility is usually defined to mean the furthest distance one can see and identify an object in the atmosphere. For a detailed presentation on the concepts of visibility, see Malm (1979). In a perfectly clean atmosphere composed only of nonabsorbent gases, the only process restricting visibility during daylight is the scattering of solar radiation from the molecules of the gases. This is known as Rayleigh scattering. Scattering is usually represented by a scattering coefficient. If absorption is also occurring in addition to scattering, an absorption coefficient may also be defined. The sum of the scattering and absorption coefficients is called the extinction coefficient. If absorption is not occurring, the extinction coefficient is defined to be equal to the scattering coefficient. The visibility in an atmosphere in which Rayleigh scattering is the only optical process active may be taken as a reference. A useful index for quantifying the impairment of visibility by the presence of atmospheric aerosol particles is the deciview (Pitchford and Malm, 1994). The deciview index, *deciV*, is given as

$$deciV = 10 \ln \left(\frac{\beta_{ext}}{0.01} \right) \tag{10-22}$$

where the value of 0.01 [km^{-1}] is taken as a standard value for Rayleigh extinction. The aerosol extinction coefficient, β_{ext} [km^{-1}], must be calculated from ambient aerosol characteristics such as index of refraction, volume concentration and size distribution.

The extinction coefficient at a wavelength of λ for aerosol may be expressed as

$$\beta_{ext} = \frac{3\pi}{2\lambda} \int_{-\infty}^{\infty} \frac{Q_{ext}}{\alpha} \frac{dV}{d\ln\alpha} d\ln\alpha , \tag{10-23}$$

where the particle distribution is given in a lognormal form as

$$\frac{dV}{d\ln\alpha} = V_T \left(\frac{A}{\pi}\right)^{1/2} \exp\left[- A \ln^2\left(\frac{\alpha}{\alpha_V}\right)\right] , \tag{10-24}$$

where $\alpha = \frac{\pi D}{\lambda}$, $\alpha_V = \frac{\pi D_{gv}}{\lambda}$, $A = \frac{1}{2 \ln^2 \sigma_g}$.

V_T is the total particle volume concentration, Q_{ext}, the Mie extinction efficiency factor, is a function of α and the index of refraction of the particles. Willeke and Brockmann (1977) showed that the behavior of the extinction coefficient is a smooth function of the geometric mean diameter for the volume distribution D_{gv}, and the index of refraction. This smooth characteristic implies that an accurate approximation to the Mie efficiency can be used in its place to reduce a very computationally intensive task. The method of Evans and Fournier (1990), a highly accurate approximation, is used to calculate Q_{ext}.

Because routine measurements of aerosol species mass concentrations are often available, but particle size distribution information is not, an additional method of calculating extinction has also been included. This is an empirical approach known as reconstructed extinction. The method is explained by Malm et al. (1994). The formula used here is a slight modification of their Equation 12 (Sisler, 1998).

$$\begin{aligned} \beta_{ext} \text{ [1/km]} = {} & 0.003 * f(rh) * \{ \text{[ammonium sulfate] + [ammonium nitrate] } \} \\ & + 0.004 * \text{[organic mass}\} \\ & + 0.01 * \text{[Light Absorbing Carbon] + } 0.001 * \text{[fine soil]} \\ & + 0.0006 * \text{[coarse mass]} \end{aligned} \tag{10-25}$$

In implementing this method, ammonium sulfate and ammonium nitrate were taken as the sum of ammonium, plus sulfate, plus nitrate. Organic mass was taken as the sum of all organic species. Light absorbing carbon was taken as elemental carbon. Fine soil was taken as the unspeciated portion of $PM_{2.5}$ emitted species, and the coarse mass term was not implemented in CMAQ at this time. The reason for not implementing coarse mass was that the uncertainty in the emissions was deemed to be too large at the present time. The relative humidity correction, f(rh), is

obtained from a table of corrections with entries at one- percent intervals. The methodology for the corrections is given in Malm et al. (1994).

10.6 Summary

The CMAQ aerosol component is a major extension of the RPM. Addition of the coarse mode and primary emissions now allow both $PM_{2.5}$ and PM_{10} to be treated. Ongoing work will improve the representation of the production of secondary organic aerosol (SOA) material by including a version of the method of Pankow (1994a,b) as discussed by Odum et al. (1996). This method, based upon laboratory experiments, calculates the yield of SOA as a function of the amount of organic material already in the particle phase.

Kleeman et al. (1997) have shown that various source types have size and species information that may be looked upon as a source signature. This assumes the availability of such source characteristics for the entire modeling domain. As noted in Section 10.1.3, there are ongoing discussions with those responsible for the national emissions inventory. As more information becomes available, identification of source signatures may be possible for a larger domain than the Los Angeles area, and an effort similar to Kleeman et al. (1997), albeit using a modal approach, might be undertaken. Other planned improvements for primary particles are the inclusion of marine aerosol as well as a better treatment of fugitive dust.

Future plans also include an intensive effort to evaluate the CMAQ aerosol component using atmospheric observations from selected field studies in which aerosol particles were observed. Comparison with routine visual range observations during the field study periods will provide an additional method of evaluation.

10.7 References

Binkowski F. S., and U. Shankar, The regional particulate model 1. Model description and preliminary results. *J. Geophys. Res.*, 100, D12, 26191-26209, 1995.

Binkowski F. S., and U. Shankar, Development of an algorithm for the interaction of a distribution of aerosol particles with cloud water for use in a three-dimensional eulaeian air quality model, Presentation at the Fourth International Aerosol Conference, Los Angeles, CA, Aug. 29 - Sept. 2, 1994.

Binkowski, F. S., S. M. Kreidenweis, D. Y. Harrington, and U. Shankar, Comparison of new particle formation mechanisms in the regional particulate model, Presentataion at the Fifteenth Annual Conference of the American Association for Aerosol Research, Orlando Florida, October 14-18, 1996.

Bower, K. N. and T. W. Choularton, A parameterisation of the effective radius of ice free clouds for use in global climate models. *Atmos. Res.*, 27, 305-339, 1992.

Bowman, F. M., C. Pilinis, and J. H. Seinfeld, Ozone and aerosol productivity of reactive organics, *Atmos. Environ.*, 29, 579-589, 1995.

Chang, J. S., F. S. Binkowski, N. L. Seaman, D. W. Byun, J. N. McHenry, P. J. Samson, W. R. Stockwell, C. J. Walcek, S. Madronich, P. B. Middleton, J. E. Pleim, and H. L. Landsford, The regional acid deposition model and engineering model, NAPAP SOS/T Report 4, in National Acid Precipitation Assessment Program, Acidic Deposition: State of Science and Technology, Volume I, Washington, D.C., 1990.

Chaumerliac, N., *Evaluation des Termes de Captation Dynamique dans un Modele Tridimensionel à Mesoechelle de Lessivage de L'Atmosphere,* Thèse Présentée à L'Université de Clermont II, U.E.R. de Recherche Scientifique et Technique, 1984.

Evans, T. N. and G. R. Fournier, Simple approximation to extinction efficiency valid over all size ranges. *Appl. Optics*, 29, 4666-4670, 1990.

Gelbard, F., Y. Tambour, and J. H. Seinfeld, Sectional representations for simulating aerosol dynamics. Jour.of Colloid and Interface. Sci., 76, 541-556, 1980.

Giauque, W. F., E. W. Hornung, J.E. Kunzler, and T. R. Rubin, The thermodynamics of aqueous sulfuric acid solutions and hydrates from 15 to 300 K, *J. Amer. Chem. Soc.*, 82, 62-67, 1960.

Harrington, D. Y. and S. M. Kreidenweis, Simulations of sulfate aerosol dynamics: Part I model description, *Atmos. Environ.*, 32, 1691-1700, 1998a.

Harrington, D. Y. and S. M. Kreidenweis, Simulations of sulfate aerosol dynamics: Part II model intercomparison, *Atmos. Environ.*, 1701-1709, 1998b.
Jacobson, M.Z. Development and application of a new air pollution modeling system-II. Aerosol module structure and design, *Atmos. Environ.*, 31, 131-144, 1997.

Kim,Y. P., J. H. Seinfeld, and P. Saxena, Atmospheric gas-aerosol equilibrium I. Thermodynamic model, *Aerosol Sci. and Technol.*, 19, 157-181, 1993a.

Kim,Y. P., J. H. Seinfeld, and P. Saxena, Atmospheric gas-aerosol equilibrium II. Analysis of common approximations and activity coefficient calculation methods, *Aerosol Sci. and Technol.*, 19, 182-198, 1993b.

Kleeman, M.J., G.R. Cass and A. Eldering, Modeling the airborne particle complex as a source-oriented external mixture. J. Geophys. Res., 102, 21355-21372, 1997.

Kulmala, M. , A. Laaksonen, and Liisa Pirjola, Parameterization for sulfuric acid/water nucleation rates. *J. Geophys. Res.*,103, 8301-8307, 1998.

Leaitch, W. R., Observations pertaining to the effect of chemical transformation in cloud on the anthropogenic aerosol size distribution, *Aerosol Sci. and Technol.*, Vol. 25, pp 157-173, 1996.

Malm, W. C., Considerations in the measurements of visibility, *J. Air Pollution Control Assoc.*, 29, 1042-1052, 1979.

Malm, W. C., J. F. Sisler, D. Huffman, R. A. Eldred, and T. A. Cahill, Spatial and seasonal trends in particle concentration and optical extinction in the United States, *J. Geophys. Res.*, 99, 1347-1370, 1994.

McElroy, M. W., R. C. Carr, D. S. Ensor, and G. R. Markowski, Size distribution of fine particles from coal combustion, *Science*, 215, 13-19, 1982.

Middleton, P. B. and C. S. Kiang, A kinetic model for the formation and growth of secondary sulfuric acid particles, *J. Aerosol Sci.*, 9, 359-385, 1978.

Mozurkewich, M. The dissociation constant of ammonium nitrate and its dependence on temperature, relative humidity, and particle size. *Atmos. Environ.*, 27A, 261-270, 1993.

Nair, P. V. N. and K. G. Vohra, Growth of aqueous sulphuric acid droplets as a function of relative humidity, *J. Aerosol Sci.*, 6, 265-271, 1975.

Odum, J. R., T. Hoffman, F. Bowman, D. Collins, R.C. Flagan, and J.H Seinfeld, Gas/particle partitioning and secondary organic aerosol yields. *Environ. Sci. Technol.*, 30, 2580-2585, 1996.

Pandis, S. N., R. A. Harley, G. R. Cass, and J. H. Seinfeld, Secondary organic aerosol formation and transport, *Atmos. Environ.*, 26A, 2269-2282, 1992.

Pankow, J. F., An absorption model of gas/particle partitioning of organic compounds in the atmosphere. *Atmos. Environ.*, 28, 185-188, 1994a.

Pankow, J.F., An absorption model of gas/particle partitioning involved in the formation of secondary organic aerosol, *Atmos. Environ.*, 28, 189-193, 1994b.

Pitchford, M. L. and W. C. Malm, Development and applications of a standard visual index, *Atmos. Environ.*, 28, 1049 - 1054, 1994.

Pratsinis, S. E., Simultaneous aerosol nucleation, condensation, and coagulation in aerosol reactors, *J. Colloid Interface Science, 124,* 417-427, 1988.

Pruppacher, H. R. and J. D. Klett, *Microphysics of Clouds and Precipitation*, Reidel, Dordrecht, Holland, 1978.

Saxena, P. and L. Hildemann, Water-soluble organics in atmospheric particles: a critical review of the literature and application of thermodynamics to identify candidate compounds, *J. Atmos. Chem.*, 24, 57-109, 1996.

Saxena, P., L. M. Hildemann, P. H. McMurry, and J. H. Seinfeld, Organics alter hygroscopic behavior of atmospheric particles, *J. Geophys. Res.*, 100, 18755 - 18770, 1995.

Seinfeld, J. H., *Atmospheric Chemistry and Physics of Air Pollution*, Wiley, New York, 1986.

Shankar, U. and F. S. Binkowski, Sulfate aerosol wet deposition in a three-dimensional Eulerian air quality modeling framework, Presentation at the Fourth International Aerosol Conference, Los Angeles, CA, Aug. 29 - Sept. 2, 1994.

Sisler, J. Personal Communication

Slinn, W. G. N., Rate-limiting aspects of in-cloud scavenging, *J. Atmos. Sci.*, 31, 1172-1173, 1974.

Spann, J. F. and C. B. Richardson, Measurement of the water cycle in mixed ammonium acid sulfate particles, *Atmos. Environ.*, 19, 919-825, 1985.

Tang, I.N. and H.R. Munkelwitz, Water activities, densities, and refractive indices of aqueous sulfates and sodium nitrate droplets of atmospheric importance, *J. Geophys. Res.*, 99, 18801-18808, 1994.

Van Dingenen, R. and F. Raes, Determination of the condensation accommodation coefficient of sulfuric acid on water-sulfuric acid aerosol, *Aerosol Sci. Technol.*, 15, 93-106, 1991.

Weber, R.J., J.J. Marti, P.H. McMurry, F.L. Eisele, D.J. Tanner, and A. Jefferson, Measurements of new particle formation and ultrafine partilce growth rates at a clean continental site. *J. Geophys. Res.*,102, 4375-4385, 1998.

Wesely, M. L., D. R. Cook, R. L. Hart, and R. E. Speer, Measurement and parameterization of particulate sulfur dry deposition over grass. *J. Geophys. Res.*, 90, 2131-2143, 1985.

Wexler, A. S., F. W. Lurmann, and J. H. Seinfeld, Modeling urban and regional aerosols: I. Model development, *Atmos. Envion.*, 28, 531-546, 1994.

Whitby, K. T., The physical characteristics of sulfur aerosols, *Atmos. Environ.*, 12, 135-159, 1978.

Whitby, E. R.and P. H. McMurry, Modal aerosol dynamics modeling, *Aerosol Sci. and Technol.*, 27, 673-688, 1997.

Whitby, E. R., P. H. McMurry, U. Shankar, and F. S. Binkowski, *Modal Aerosol Dynamics Modeling*, Rep. 600/3-91/020, Atmospheric Research and Exposure Assessment Laboratory, U.S. Environmental Protection Agency, Research Triangle Park, N.C., (NTIS PB91-161729/AS), 1991.

Willeke, K. and J. E. Brockmann, Extinction coefficients for multimodal atmospheric particle size distributions, *Atmos. Environ.*, 11, 995 - 999, 1977.

Youngblood, D.A. and S.M. Kreidenweis, *Further development and testing of a bimodal aerosol dynamics model*. Colorado State University, Department of Atmospheric Sciences Report No. 550, 1994.

This chapter is taken from *Science Algorithms of the EPA Models-3 Community Multiscale Air Quality (CMAQ) Modeling System*, edited by D. W. Byun and J. K. S. Ching, 1999.

Table 10-1 Aerosol Species Concentrations

Units: mass [$\mu g\ m^{-3}$], number [$\#\ m^{-3}$]

{ a1}	ASO4 J	Accumulation mode sulfate mass
{ a2}	ASO4I	Aitken mode sulfate mass
{ a3}	ANH4J	Accumulation mode ammonium mass
{ a4}	ANH4I	Aitken mode ammonium mass
{ a5}	ANO3J	Accumulation mode nitrate mass
{ a6}	ANO3I	Aitken mode aerosol nitrate mass
{ a7}	AORGAJ	Accumulation mode anthropogenic secondary organic mass
{ a8}	AORGAI	Aitken mode anthropogenic secondary organic mass
{ a9}	AORGPAJ	Accumulation mode primary organic mass
{a10}	AORGPAI	Aitken mode mode primary organic mass
{a11}	AORGBJ	Accumulation mode secondary biogenic organic mass
{a12}	AORGBI	Aitken mode biogenic secondary biogenic organic mass
{a13}	AECJ	Accumulation mode elemental carbon mass
{a14}	AECI	Aitken mode elemental carbon mass
{a15}	A25J	Accumulation mode unspecified anthropogenic mass
{a16}	A25I	Aitken mode unspecified anthropogenic mass
{a17}	ACORS	Coarse mode unspecified anthropogenic mass
{a18}	ASEAS	Coarse mode marine mass
{a19}	ASOIL	Coarse mode soil-derived mass
{a20}	NUMATKN	Aitken mode number
{a21}	NUMACC	Accumulation mode number
{a22}	NUMCOR	Coarse mode number
{a23}	SRFATKN	Aitken mode surface area
{a24}	SRFACC	Accumulation mode surface area
{a25}	AH2OJ	Accumulation mode water mass
{a26}	AH2OI	Aitken mode water mass

Table 10-2. Equilibrium Relations and Constants
(Kim et al., 1993a)

Equilibrium Relation	Constant	K(298.15)	a	b	Units
$HSO_4^-(aq) \Leftrightarrow H^+(aq) + SO_4^{2-}(aq)$	$\frac{[H^+][SO_4^{2-}]\gamma_{H^+}\gamma_{SO_4^{2-}}}{[HSO_4^-]\gamma_{HSO_4^{2-}}}$	1.015E-02	8.85	25.14	mol / kg
$NH_3(g) \Leftrightarrow NH_3(aq)$	$\frac{[NH_3(aq)]\gamma_{NH_3}}{P_{NH_3}}$	57.639	13.79	-5.39	mol / kg atm
$NH_3(aq) + H_2O(aq) \Leftrightarrow NH_4^+(aq) + OH^-(aq)$	$\frac{[NH_4^+][OH^-]\gamma_{NH^+}\gamma_{OH^-}}{[NH_3(aq)]\gamma_{NH_3}a_w}$	1.805E-05	-1.50	26.92	mol / kg
$HNO_3(g) \Leftrightarrow H^+(aq) + NO_3^-(aq)$	$\frac{[H^+][NO_3^-]\gamma_{H^+}\gamma_{NO_3^-}}{P_{HNO_3}}$	2.511E06	29.17	16.83	mol^2 / kg^2 atm
$NH_4NO_3(s) \Leftrightarrow NH_3(g) + HNO_3(g)$	$P_{NH_3}P_{HNO_3}$	5.746E-17#	-74.38#	6.12#	atm^2
$H_2O(aq) \Leftrightarrow H^+(aq) + OH^-(aq)$	$\frac{[H^+][OH^-]\gamma_{H^+}\gamma_{OH^-}}{a_w}$	1.010E-14	-22.52	26.92	mol^2 / kg^2

The constants a and b are used in the following to adjust for ambient temperature

$$K = K(T_0)\exp\left[a\left(\frac{T_0}{T} - 1\right) + b\left(1 + \ln\left(\frac{T_0}{T}\right) - \frac{T_0}{T}\right), T_0 = 298.15\ [K]\right]$$

These values are only used by Kim et al. (1993a,b). The values used in the CMAQ are from Mozurkewich (1993):

$$K = \exp\left(118.87 - \frac{24084}{T} - 6.025\ \ln\ (T)\right)$$

where Mozurkevich reports in nanobars squared. This yields a value for the equilibrium constant of 43.11 [nb^2] at 298.15 K.

Table 10-3. Organic Aerosol Yields in Terms of Amount of Precursor Reacted (From Pandis et al. (1992) and Bowman et al. (1995))

Gas-Phase Organic Species	**Aerosol Yield [$\mu g\ m^{-3}$ / ppm(reacted)]**
C8 and higher alkanes	380
Anthropogenic internal alkenes	247
monoterpenes	740
toluene	424
xylene	342
cresol	221

EPA/600/R-99/030

Chapter 11

CLOUD DYNAMICS AND CHEMISTRY

Shawn J. Roselle[*] and Francis S. Binkowski[**]
Atmospheric Modeling Division
National Exposure Research Laboratory
U.S. Environmental Protection Agency
Research Triangle Park, North Carolina 27711

ABSTRACT

Chapter 11 describes the cloud module that is currently incorporated into CMAQ. This module simulates the physical and chemical processes of clouds that are important in air quality simulations. Clouds affect pollutant concentrations by vertical-convective mixing, scavenging, aqueous chemistry, and removal by wet deposition. The CMAQ cloud module includes parameterizations for sub-grid convective precipitating and non-precipitating clouds and grid-scale resolved clouds. Cloud effects on both gas-phase species and aerosols are simulated by the cloud module.

---

[*]On assignment from the National Oceanic and Atmospheric Administration, U.S. Department of Commerce. Corresponding author address: Shawn J. Roselle, MD-80, Research Triangle Park, NC 27711. E-mail: sjr@hpcc.epa.gov

[**]On assignment from the National Oceanic and Atmospheric Administration, U.S. Department of Commerce.

11.0 CLOUD DYNAMICS AND CHEMISTRY

11.1 Background

Clouds play an important role in boundary layer meteorology and air quality. Convective clouds transport pollutants vertically, allowing an exchange of air between the boundary layer and the free troposphere. Cloud droplets formed by heterogeneous nucleation on aerosols grow into rain droplets through condensation, collision, and coalescence. Clouds and precipitation scavenge pollutants from the air. Once inside the cloud or rain water, some compounds dissociate into ions and/or react with one another through aqueous chemistry (i.e., cloud chemistry is an important process in the oxidation of sulfur dioxide to sulfate). Another important role for clouds is the removal of pollutants trapped in rain water and its deposition onto the ground. Clouds can also affect gas-phase chemistry by attenuating solar radiation below the cloud base which has a significant impact on the photolysis reactions.

The Models-3/CMAQ cloud model incorporates many of these cloud processes. The model includes parameterizations for several types of clouds, including sub-grid convective clouds (precipitating and non-precipitating) and grid-scale resolved clouds. It includes an aqueous chemistry model for sulfur, and includes a simple mechanism for scavenging.

11.2 Model Description

The cloud model can be divided into two main components, including the sub-grid cloud model (*subcld*) and the resolved cloud model (*rescld*). For large horizontal grid resolutions, the grid size will be larger than the size of a typical convective cloud, requiring a parameterization for these sub-grid clouds. The sub-grid cloud scheme simulates convective precipitating and non-precipitating clouds. The second component of the cloud model considers clouds which occupy the entire grid cell and have been "resolved" by the meteorological model. The rate of change in pollutant concentrations ($\overline{m_i}$) due to cloud processes is given by:

$$\left.\frac{\partial \overline{m_i}}{\partial t}\right|_{cld} = \left.\frac{\partial \overline{m_i}}{\partial t}\right|_{subcld} + \left.\frac{\partial \overline{m_i}}{\partial t}\right|_{rescld} \tag{11-1}$$

The terms on the right-hand side of Equation 11-1 are solved separately at different times. The influence of sub-grid clouds are instituted once an hour while the resolved clouds impact concentrations every synchronization timestep. Each subcomponent of the cloud model is described in detail below.

11.2.1 Subgrid Convective Cloud Scheme

$$\left.\frac{\partial \overline{m_i}}{\partial t}\right|_{subcld} \sim f\left(mixing, scav, aqchem, wetdep\right) \tag{11-2}$$

The current sub-grid cloud scheme in CMAQ was derived from the diagnostic cloud model in RADM version 2.6 (Dennis et al., 1993; Walcek and Taylor, 1986; Chang, et al., 1987; Chang, et al., 1990). Seaman (1998) noted that most convective parameterizations are based on the assumption that "the area of an updraft is small compared to the area of the grid cell" and most parameterizations can be used at grid resolutions a small as 12 km (Wang and Seaman, 1997). In CMAQ, subgrid clouds are considered only for horizontal grid resolutions on the order of 12 km or more. Seaman (1998) also pointed to a study by Weisman et al. (1997) that showed that explicit cloud models can resolve convection for resolution finer than 5 km. Within CMAQ, for resolutions of 4 km or less, vertical convection is assumed to be resolved at the grid level; therefore, the resolved cloud model will be the only cloud scheme used at small grid scales.

The effects of sub-grid clouds on grid-averaged concentrations are parameterized by modeling the mixing, scavenging, aqueous chemistry, and wet deposition of a "representative cloud" within the grid cell. For all sub-grid clouds, a 1-hour lifetime (τ_{cld}) has been assumed. Sub-grid clouds can be either precipitating or non-precipitating, and the non-precipitating subgrid clouds are further categorized as pure fair weather (PFW) clouds and non-precipitating clouds coexisting (CNP) with precipitating clouds.

The subgrid cloud model determines if precipitating or nonprecipitating clouds exist over each grid cell. Precipitating clouds are simulated when the meteorological preprocessor (currently the Mesoscale Model version 5 or MM5, Grell et al., 1994) indicates precipitation from its convective cloud model. The CMAQ implementation differs from the RADM in that only the convective precipitation amounts from MM5 are used to drive the subgrid precipitating cloud. RADM used the total precipitation (convective and nonconvective precipitation) to drive the subgrid cloud model. In CMAQ, the nonconvective precipitation is used in the resolved cloud model. Nonprecipitating clouds are modeled if the moisture and temperature profiles support the development of a cloud (Dennis et al., 1993). Nonprecipitating clouds are modeled only when the relative humidity of the source level is above 70% and the calculated cloud base is below 1500 m for PFW clouds or 3000 m for CNP clouds. For both precipitating and nonprecipitating cloud types, the geometry of the cloud (base, top, and spatial extent) are determined next. The cloud base is calculated by lifting a parcel of air from the cloud source level (the level between the surface and 650 mb with the highest equivalent potential temperature) to the lifting condensation level (LCL). The cloud top calculation depends upon the cloud type and atmospheric stability. For precipitating clouds in unstable conditions, the cloud top is found by following the moist adiabatic lapse rate from the cloud base up to the level where it becomes cooler than the surrounding environment. For precipitating clouds under stable conditions, the cloud top is set as the first layer above the cloud base in which the relative humidity falls below

65%, but limited to less than the 600 mb height. For nonprecipitating clouds, further restrictions are placed on the cloud top. The cloud top calculation for nonprecipitating clouds uses the same relative humidity criterion as the precipitating clouds, but the cloud top is allowed to extend up to 500 mb for CNP clouds and only to 1500 m for PFW clouds. If the atmosphere is unstable, the nonprecipitating cloud top may be reduced in height if the parcel method calculated a lower cloud top. The fractional cloud coverage calculations depend on cloud type and have been described thoroughly by Dennis et al. (1993). For precipitating clouds, the model uses a parameterization similar to approach of Kuo (1974). The fractional coverage parameterization for the nonprecipitating clouds is based on relative humidity.

The convective cloud simulated by the sub-grid cloud model is considered to be composed of air transported vertically-from below the cloud, entrained from above the cloud (for precipitating clouds), and entrained from the sides of the cloud. Concentrations of pollutants for each layer of the cloud are calculated by:

$$\overline{m_i}^{cld}(z) = f_{ent}\left[(1 - f_{side})\overline{m_i}^{down} + f_{side}\,\overline{m_i}(z)\right] + (1 - f_{ent})\overline{m_i}^{up} \quad (11\text{-}3)$$

where f_{side} is the fraction of entraining air originating from the side of the cloud. For nonprecipitating clouds, no entrainment of air from above the cloud is allowed and therefore f_{side}=1. The entrainment, f_{ent}, is calculated by iteratively solving conservation and thermodynamic equations (Dennis et al., 1993; Chang et al, 1990,1987; and Walcek and Taylor, 1986). The terms $\overline{m_i}^{up}$ and $\overline{m_i}^{down}$ represent the above and below cloud concentrations, respectively. Once the cloud volume has been determined, vertically-averaged cloud temperature, pressure, liquid water content, total water content, and pollutant concentrations, are computed with liquid water content (W_c) as the weighting function (gives the most weight to the layers with the highest liquid water content). Thus, the average pollutant concentrations within the cloud are calculated by:

$$\overline{m_i^{cld}} = \frac{\int_{z_{cbase}}^{z_{ctop}} \overline{m_i}^{cld}(z) W_c(z)\,dz}{\int_{z_{cbase}}^{z_{ctop}} W_c(z)\,dz} \quad (11\text{-}4)$$

With the averages over the cloud volume, the processes of scavenging, aqueous chemistry, and wet deposition are considered. The final step in cloud mixing is the reapportioning of mass back into individual layers. This is accomplished using cloud fractional coverage, initial in-cloud concentrations, final in-cloud concentration, and the initial vertical concentration profile. For

precipitating clouds, the average pollutant concentration for the grid cell within the cloud layers is computed by:

$$\overline{m_i}(z,t_0+\tau_{cld}) = \overline{m_i^{cld}}(z,t_0)\left[\frac{\overline{m_i^{cld}}(t_0+\tau_{cld})}{\overline{m_i^{cld}}(t_0)}\right]cfrac + \overline{m_i}(z,t_0)\left[1-cfrac\right] \tag{11-5}$$

where *cfrac* is the fractional cloud coverage. There are variations on this equation for below cloud, above cloud, and for nonprecipitating clouds.

11.2.1.1 Scavenging and Wet Deposition

Pollutant scavenging is calculated by two methods, depending upon whether the pollutant participates in the cloud water chemistry and on the liquid water content. (1) For those pollutants that are absorbed into the cloud water and participate in the cloud chemistry (and provided that the liquid water content is > 0.01 g/m^3), the amount of scavenging depends on Henry's law constants, dissociation constants, and cloud water pH. (2) For pollutants which do not participate in aqueous chemistry (or for all water-soluble pollutants when the liquid water content is below 0.01 g/m^3), the model uses the Henry's Law equilibrium equation to calculate ending concentration and deposition amounts. The rate of change for in-cloud concentrations (m_i^{cld}) for each pollutant (i) following the cloud timescale (τ_{cld}) is given by:

$$\left.\frac{\partial \overline{m_i^{cld}}}{\partial t}\right|_{scav} = \overline{m_i^{cld}}\left(\frac{e^{-\alpha_i \tau_{cld}}-1}{\tau_{cld}}\right) \tag{11-6}$$

where α_i is the scavenging coefficient for the pollutant. For subgrid convective clouds, τ_{cld} is 1 hour and for grid resolved clouds it is equal to the CMAQ's synchronization timestep. For gases, the scavenging coefficient is given by:

$$\alpha_i = \frac{1}{\tau_{washout}\left(1+\frac{TWF}{H_i}\right)} \tag{11-7}$$

where H_i is the Henry's Law coefficient for the pollutant, *TWF* is the total water fraction given by:

$$TWF = \frac{\rho_{H_2O}}{\overline{W}_T RT}. \tag{11-8}$$

where ρ_{H2O} is the density of water, $\overline{W}_T$ is the mean total water content (kg/m^3), R is the Universal gas constant, and T is the in-cloud air temperature (K). The washout time, $\tau_{washout}$ represents the amount of time required to remove all of the water from the cloud volume at the specified precipitation rate (P_r),
and is given by:

$$\tau_{washout} = \frac{\overline{W}_T \Delta z_{cld}}{\rho_{H_2O} P_r} \tag{11-9}$$

Here, Δz_{cld} is the cloud thickness.

The accumulation mode and coarse mode aerosols are assumed to be completely absorbed by the cloud and rain water. Therefore, the scavenging coefficients for these two aerosol modes are simply a function of the washout time:

$$\alpha_i = \frac{1}{\tau_{washout}} \tag{11-10}$$

The Aitken mode aerosols are treated as interstitial aerosol and are slowly absorbed into the cloud/rain water. This process is discussed in detail in the aerosol chapter (Chapter 10).

The wet deposition algorithms in CMAQ were taken from the RADM (Chang et al., 1987). In the current implementation, deposition is accumulated over 1-hour increments before being written to the output file. The wet deposition amount of chemical species i ($wdep_i$) depends upon the precipitation rate (P_r) and the cloud water concentration (m_i^{cld}):

$$wdep_i = \int_0^{\tau_{cld}} \overline{m}_i^{cld} P_r dt \tag{11-11}$$

Deposition amounts are accumulated for each of the modeled species, but the user specified which species are written to the output file. This is handled in the Program Control Processor (see Chapter 15).

11.2.1.2 Aqueous Chemistry

The aqueous chemistry model evolved from the original RADM model (Chang et al., 1987; and Walcek and Taylor, 1986). The model considers the absorption of chemical compounds into the cloud water; the amount that gas-phase species absorb into the cloud water depends on thermodynamic equilibrium, while accumulation-mode aerosols are considered to have been the nucleation particles for cloud droplet formation and are 100% absorbed into the cloud water. Then the model calculates the dissociation of compounds into ions, oxidation of S(IV) to S(VI), and wet deposition. The species that participate in the aqueous chemistry are given in Table 11-

1. This version of the aqueous chemistry model differs from Walcek's scheme in that it tracks contributions from gases and aerosols separately. It also considers the scavenging of interstitial aerosols, and it allows for variable-length cloud time scales.

Table 11-1. List of Species Considered in the Aqueous Chemistry Model

Gases	Aerosols
SO_2	$SO_4^=$ (Aitken & accumulation)
HNO_3	NH_4^+ (Aitken & accumulation)
N_2O_5	NO_3^- (Aitken, accumulation, & coarse)
CO_2	Organics (Aitken & accumulation)
NH_3	Primary (Aitken, accumulation, & coarse)
H_2O_2	$CaCO_3$
O_3	$MgCO_3$
formic acid	NaCl
methyl hydrogen peroxide	Fe^{3+}
peroxy acetic acid	Mn^{2+}
H_2SO_4	KCl
	Number (Aitken, accumulation, & coarse)

11.2.2 Resolved Cloud Scheme

At any grid resolution, clouds may be resolved by the MM5, which could include stratus, cumulus, or cirrus type clouds. The resolved clouds have been simulated by the MM5 to cover the entire grid cell. No additional cloud dynamics are considered in CMAQ for this cloud type since any convection and/or mixing would have been resolved and considered in the vertical wind fields provided by MM5. A resolved cloud horizontally covers the entire grid cell and vertically extends over the whole depth of the layer, thus $\overline{m_i}^{cld}$ and $\overline{m_i}$ are equivalent in resolved clouds. These clouds are activated in MM5 when the humidity is high enough for water vapor to condense, and then MM5 computes cloud and rain water amounts according to any of several microphysical submodels. Using the total of the condensed cloud water and rain water reported by MM5, the CMAQ resolved cloud model then considers scavenging, aqueous chemistry, and wet deposition. The average liquid water content $\overline{W_c}$ in a model layer (z) for the resolved cloud is given by:

$$\overline{W_C}(z) = \left[Q_C(z) + Q_R(z)\right]\rho(z) \tag{11-12}$$

where $Q_C(z)$ is the cloud water mixing ratio (kg/kg), $Q_R(z)$ is the rain water mixing ratio (kg/kg), $\rho(z)$ is the air density (kg/m^3). Precipitation amounts for resolved cloud layers, $P_r(z)$, are derived using the MM5 non-convective precipitation amounts (R_n), apportioned into individual model layers with the vertical profile of condensed liquid water as follows:

$$P_r(z) = R_n \left[\frac{\overline{W_c}(z)}{\int \overline{W_c}(z) dz} \right] \tag{11-13}$$

Once quantities for precipitation rate, liquid water content, etc. have been calculated, then the scavenging, aqueous chemistry, and wet deposition are solved using the same procedures as in the subgrid clouds.

$$\left. \frac{\partial \overline{m_i}}{\partial t} \right|_{rescld} = \left. \frac{\partial \overline{m_i}}{\partial t} \right|_{scav} + \left. \frac{\partial \overline{m_i}}{\partial t} \right|_{aqchem} \tag{11-14}$$

Several assumptions have been made in the current implementation of the resolved cloud model. (1) The lifetime of the resolved cloud computations varies based on the synchronization timestep of CMAQ. (2) Following the method of operator splitting, the effect of the resolved clouds on pollutant concentrations occurs at the end of the cloud lifetime, thus no exchange between layers is permitted during the cloud life-cycle. (3) The pollutants, cloud water, and rain water are uniformly distributed within the grid cell. Because of the separation of MM5 from CMAQ, we do not have the information to do precipitation fluxes. Even if a complete cloud precipitation model was developed within CMAQ, there is no guarantee that it would be consistent with what was done in MM5.

11.3 Conclusions

One of the concepts for Models-3 was that multiple modules may exist for each physical process of the air quality model. The implementation described here is the first module available for modeling cloud physics and chemistry. Other subgrid cloud models (i.e., the Kain-Fritsch (1990, 1993) and Betts-Miller (1986)) are under consideration and may be included as optional modules for CMAQ. In addition, a more detailed resolved cloud model is under development which will include a microphysical submodel for following the evolution of the cloud (i.e., cloud droplet formation, growth of rain droplets, and descent through model layers to the ground). It will also consider resolved cloud lifetimes which extend beyond the CMAQ synchronization timestep, thus maintaining the partition between gas and aqueous-phase pollutants during the gas-phase chemistry calculations. The current implementation of the cloud model in CMAQ will be evaluated using available datasets and will be used as a reference for evaluating future cloud modules for CMAQ.

11.4 References

Betts, A.K. and M.J. Miller, 1986. A new convective adjustment scheme. Part II: Single column tests using GATE wave, BOMEX, ATEX, and arctic air- mass data sets. *Quarterly J. Roy. Meteor. Soc.*, **112**, 693-709.

Chang, J.S., R.A. Brost, I.S.A. Isaksen, S. Madronich, P. Middleton, W.R. Stockwell, and C.J. Walcek, 1987. A three-dimensional Eulerian acid deposition model: Physical concepts and formation. *J. Geophys. Res.*, **92**, 14681-14700.

Chang, J.S., P.B. Middleton, W.R. Stockwell, C.J. Walcek, J.E. Pleim, H.H. Lansford, F.S. Binkowski, S. Madronich, N.L. Seaman, D.R. Stauffer, D. Byun, J.N. McHenry, P.J. Samson, H. Hass., 1990. The regional acid deposition model and engineering model, *Acidic Deposition: State of Science and Technology,* Report 4, National Acid Precipitation Assessment Program.

Dennis, R.L., J.N. McHenry, W.R. Barchet, F.S. Binkowski, and D.W. Byun, 1993. Correcting RADM's sulfate underprediction: Discovery and correction of model errors and testing the corrections through comparisons against field data, *Atmos. Environ.*, **26A**(6), 975-997.

Grell, G.A., J. Dudhia, and D.R. Stauffer, 1994. A description of the fifth generation Penn State/NCAR mesoscale model (MM5). NCAR Tech. Note NCAR/TN-398+STR, 138 pp.

Kain, J.S. and J.M. Fritsch, 1990. A one-dimensional entraining/detraining plume model and its application in convective parameterization. *J. Atmos. Sci*, **47**, 2784-2802.

Kain, J.S. and J.M. Fritsch, 1993. Convective parameterization for mesoscale models: The Kain-Fritsch scheme. *The Representation of Cumulus Convection in Numerical Models, Meteor. Monogr.*, **46**, Amer. Meteor. Soc., 165-170.

Kuo, H.L., 1974. Further studies of the parameterization of the influence of cumulus convection on large-scale flow, *J. Atmos. Sci.*, **31**, 1232-1240.

Seaman, N.L., 1988. Meteorological Modeling for Air-Quality Assessments: A NARSTO Review Paper, *Submitted to Atmos. Environ.*

Walcek, C.J. and G.R. Taylor, 1986. A theoretical method for computing vertical distributions of acidity and sulfate production within cumulus clouds, *J. Atmos. Sci* **43**, 339-355.

Wang, W. and N.L. Seaman, 1997. A comparison study of convective parameterization schemes in a mesoscale model. *Mon. Wea. Rev.*, **125**, 252-278.

Weisman, L.M., W.C. Skamarock and J.B. Klemp, 1997. The resolution dependence of explicitly modeled convective systems, *Mon. Wea. Rev.*, **125**, 527-548.

This chapter is taken from *Science Algorithms of the EPA Models-3 Community Multiscale Air Quality (CMAQ) Modeling System*, edited by D. W. Byun and J. K. S. Ching, 1999.

EPA/600/R-99/030

Chapter 12

METEOROLOGY-CHEMISTRY INTERFACE PROCESSOR (MCIP) FOR MODELS-3 COMMUNITY MULTISCALE AIR QUALITY (CMAQ) MODELING SYSTEM

Daewon W. Byun* and Jonathan E. Pleim**
Atmospheric Modeling Division
National Exposure Research Laboratory
U.S. Environmental Protection Agency
Research Triangle Park, NC 27711

Ruen Tai Tang
Dyntel Corporation
Research Triangle Park, NC 27711

Al Bourgeois
Lockheed Martin/U.S. EPA Scientific Visualization Center
Research Triangle Park, NC 27711

ABSTRACT

The Meteorology-Chemistry Interface Processor (MCIP) links meteorological models such as MM5 with the Chemical Transport Model (CTM) of the Models-3 Community Multiscale Air Quality (CMAQ) modeling system to provide a complete set of meteorological data needed for air quality simulations. Because most meteorological models are not built for air quality modeling purpose, MCIP deals with issues related to data format translation, conversion of units of parameters, diagnostic estimations of parameters not provided, extraction of data for appropriate window domains, and reconstruction of meteorological data on different grid and layer structures. To support the multiscale generalized coordinate implementation of the CMAQ CTM, MCIP provides appropriate dynamic meteorological parameters to allow mass-consistent air quality computations. The current implementation of MCIP links MM5 meteorological data to CMAQ CTM. Because its code has a streamlined modular computational structure, adapting the system to other inputs only require inclusion of a reader module and coordinate related routines specific for the meteorological model.

* On assignment from the National Oceanic and Atmospheric Administration, U.S. Department of Commerce. Corresponding author address: Daewon W. Byun, MD-80, Research Triangle Park, NC 27711. E-mail: bdx@hpcc.epa.gov

** On assignment from the National Oceanic and Atmospheric Administration, U.S. Department of Commerce.

12.0 METEOROLOGY-CHEMISTRY INTERFACE PROCESSOR (MCIP) FOR MODELS-3 COMMUNITY MULTISCALE AIR QUALITY (CMAQ) MODELING SYSTEM

12.1 Introduction

Models-3 Community Multiscale Air Quality (CMAQ) modeling system is a next generation modeling system designed to handle research and application issues for multiscale (urban and regional) and multi-pollutant (oxidants, acid deposition, and particulates) air quality problems. Its Chemical Transport Model (CTM) uses a generalized coordinate system. To accommodate meteorological inputs from a variety of meteorological models using different coordinate systems, CMAQ CTM (CCTM) requires information about the coordinates and grid as well as the meteorological data. The Meteorology-Chemistry Interface Processor (MCIP) links a meteorological model with CCTM to provide a complete set of meteorological data needed for air quality simulation. Because most meteorological models are not built for air quality modeling purposes, MCIP takes care of many issues related to data format translation, conversion of units of parameters, diagnostic estimations of parameters not provided, extraction of data for appropriate window domains, and reconstruction of meteorological data on different horizontal and vertical grid resolutions through interpolations as needed. Considering these functions, it is not difficult to see that MCIP is a key processor in the Models-3 CMAQ system.

In the Models-3 CMAQ system, the role of MCIP is further expanded to enforce consistency among the meteorological variables. The consistency among meteorological parameters and the way they are utilized in a CTM greatly influence the success of air quality simulations. This issue becomes a dominant concern for the CCTM, which uses a generalized coordinate system, because it should be able to deal with data from different meteorological models that may or may not use fully compressible formulations (or assumptions on the atmospheric dynamics such as hydrostatic or nonhydrostatic approximation). Chapters 5 and 6 of this science document provide detailed descriptions on the generalized coordinate system.

CMAQ's MCIP provides similar functions as the meteorological preprocessor for Regional Acid Deposition Model (RADM) (Chang et al., 1987, 1990). MCIP's code has a streamlined computational structure, incorporating many of the physical and dynamical algorithms necessary to prepare meteorological inputs used by CMAQ. Some of the planetary boundary layer (PBL) parameterizations are extensively updated subroutines of the RADM's meteorological preprocessor which was described in Byun and Dennis (1995). MCIP is highly modularized to accommodate data from different meteorological models. This versatility is accomplished by allowing incorporation of a different set of input modules for a specific meteorological model. At present, two sets of input modules are available. One links to the output of Pensylvania State University/National Center for Atmospheric Research (PSU/NCAR) Mesoscale Modeling System Generation 5 (MM5) with CCTM and the other links to meteorological data already in the Models-3 input/output applications programming interface (I/O API) format. MM5 can be run either in hydrostatic mode using a time dependent terrain-following hydrostatic pressure coordinate, or in nonhydrostatic mode using a time independent terrain-following reference pressure coordinate. For the details on how MM5 simulations are conducted and how the reference state is determined, refer to Seaman et al. (1995), Seaman and Stauffer (1993), Dudhia (1993), Grell et al. (1994), Stauffer and Seaman (1993), Tesche and McNally (1993), and Haagenson et al. (1994). To

characterize past atmospheric conditions properly, MM5 is usually run with Four Dimensional Data Assimilation (FDDA) for air quality simulations. It incorporates the results of intensive meteorological observations into the model simulations so that the uncertainties associated with meteorological input for a CTM are minimized (Stauffer and Seaman, 1993; Seaman et al., 1995). Different output data generated by the different options, such as dynamics cloud parameterization and surface-PBL algorithms used for the operation of MM5 operation, can be handled by MCIP accordingly.

This chapter provides a detailed description of the functions and data flow of MCIP and formulations used for estimating parameters diagnostically. Although this chapter mainly describes the current implementation of MCIP written for MM5, it also provides key information necessary to build different MCIP versions for other meteorological models. It is hoped that developers of different MCIP versions can concentrate their efforts to read in data files from different meteorological models with minimal modifications for diagnostic routines and output processes. Section 12-1 describes basic functions and data dependency of MCIP. Section 12-2 deals with meteorological data types, coordinates, and grids. Section 12-3 contains descriptions of diagnostic algorithms used for estimating parameters necessary for air quality simulation and Section 12-4 describes additional parameters needed for the generalized coordinate system. Section 12-5 provides key operational operational details, such as building and executing MCIP including how to set up grids/domains and environmental variables for different runtime options. Refer to Figure 12-1 for the structure of the contents of the present chapter.

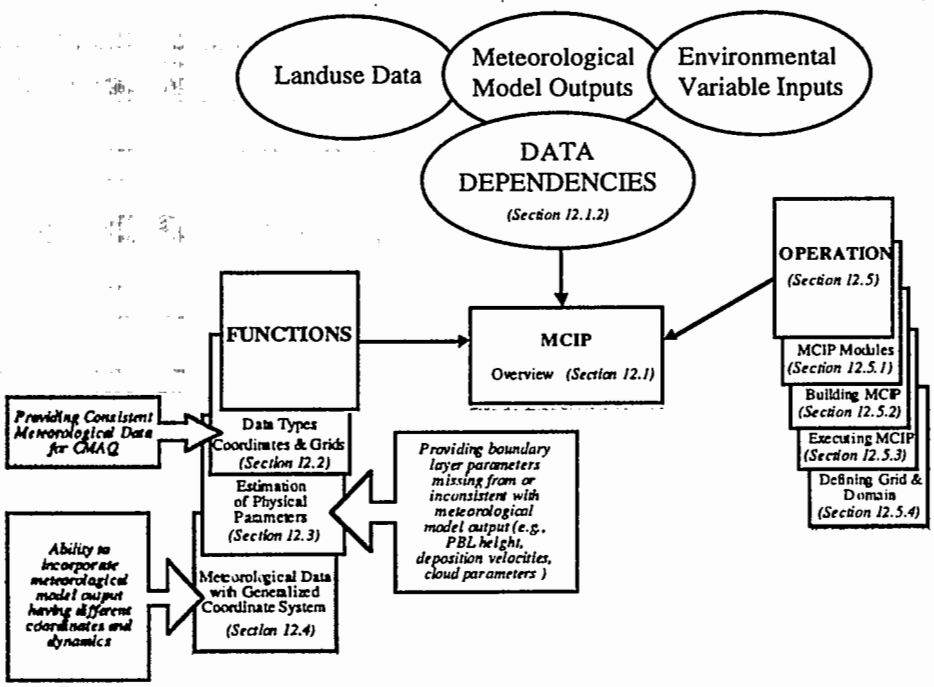

Figure 12-1. Contents and Structure of Chapter 12

12.1.1 MCIP Functions

One of MCIP's functions is to translate meteorological parameters from the output of a mesoscale model (e.g., MM5) to the Models-3 I/O API format (Coats, 1996), which is required for operations of Models-3 CMAQ processors. Some other necessary parameters not available from the meteorological model are estimated with appropriate diagnostic algorithms in the program. The key functions of MCIP are summarized below.

Reading in meteorological model output files:

The EPA-enhanced MM5 version (Pleim et al., 1997) generates not only the standard MM5 output but also several additional files that contain detailed PBL, cloud, and surface parameters. MCIP reads these files and stores the information in the memory for further processing. Essential header information is passed to the Models-3 I/O API file header.

Extraction of meteorological data for CTM window domain:

In general, the CCTM uses a smaller computational domain than MM5. Also, MM5 predictions in the cells near the boundary may not be adequate for use in air quality simulation. Therefore, MCIP extracts only the portion of the MM5 output data which falls within the CCTM's main domain and boundary cells.

Interpolation of coarse meteorological model output for finer grid:

When user requests meteorological data on a finer resolution grid than that simulated in the meteorological model, MCIP interpolates profile data using simple bilinear interpolation.

Collapsing of meteorological profile data if coarse vertical resolution data is requested:

MCIP performs a mass-weighted averaging of data in the vertical direction. For example, 30-layer meteorological data may be lumped into 15 layers, or 6 layers for the CCTM.

Computation or passing through surface and PBL parameters:

Depending on the user options, MCIP either passes through surface and PBL parameters simulated by the meteorology model directly or diagnoses them using the mean wind, temperature, and humidity profiles, surface data, and detailed landuse information available.

Diagnosing of cloud parameters:

When important parameters needed for processing cloud effects in the CCTM are not provided by the meteorological model, MCIP diagnoses cloud information (i.e., cloud top, base, liquid water content, and coverage) using a simple convective parameterization. The information can be used in the CCTM to process aqueous-phase chemistry and cloud mixing as well as to modulate photolysis rates that reflect the effects of cloud.

Computation of species-specific dry deposition velocities:

MCIP computes dry deposition velocities for important gaseous species using either diagnosed PBL parameters or the surface/PBL information passed through from the meteorological model.

Generation of coordinate dependent meteorological data for the generalized coordinate CCTM simulation:

Many of the coordinate-related functions traditionally treated in a CTM have been incorporated as a part of the MCIP functions. This change was necessary to maintain modularity of the CCTM regardless of the coordinates used and to eliminate many coordinate-dependent processor modules in the CCTM. By incorporating dynamically consistent interpolation methods and associated subroutines in the CCTM, the dynamic and thermodynamic consistencies among the meteorological data can be maintained even after the temporal interpolations.

Output meteorological data in Models-3 I/O API format:

MCIP writes the bulk of its two- and three-dimensional meteorological and geophysical output data in a transportable binary format using the Models-3 input/output applications program interface (I/O API) library.

12.1.2 MCIP's Data Dependency

MCIP processes meteorological model output files in order to provide environmental data needed for the other computational subsystems in Models-3 CMAQ. Landuse data is also required to generate additional meteorological information needed for air quality simulations. MCIP utilizes this and profiles of temperature, moisture, and wind components to estimate parameters for the turbulence and surface exchange characteristics. When the meteorological model computes all the necessary information, it can be passed through the MCIP as well. The inputs for MCIP consist of operational inputs and meteorological model output files. These inputs are described below.

12.1.2.1 Environmental Variable Inputs

The user can select a computational path among the internal process options and define parameters in MCIP output files by specifying several UNIX environmental variables. These settings allow MCIP to be configured to fit a particular meteorological model simulation and to follow process steps requested by the user. First, it defines the mode of meteorological model run to check if the meteorology data linked have been generated using options compatible with the MCIP. Then it assigns filenames of meteorology model output files, defines CTM model window domain offset coordinates in terms of the meteorological model grid definition, determines simulation time and duration of the MCIP, and assigns appropriate landuse data file type. Refer to Section 12-5 and Table 12-10 for the details of the UNIX environmental variables used in MCIP for these settings.

12.1.2.2 Meteorology Model Outputs

It is anticipated that MCIP will include a unique set of reader modules for a variety of meteorological models. Most of the idiosyncrasies of meteorological data from a specific meteorological model should be resolved in this module. They include the number of files, information on the data such as where they are stored and in what format, etc. In the following, we provide a description of the output files from MM5 as an example.

Standard MM5 output

The standard MM5 time-stepped grid-domain output contains most of the key meteorological data written by the MM5 subroutine OUTTAP. Each time-step includes a header record. This header is read by MCIP at each time-step, but only the header from the first time-step is used and the subsequent headers are ignored. Data following each header consist of two- and three-dimensional arrays. The time-step interval for the meteorological data is taken from the header record on the first time-step.

EPA-added MM5 output

EPA and MCNC added two more output files for additional information to facilitate air quality modeling. One includes additional two-dimensional boundary layer parameters and flux values and the other contains the detailed Kain-Fritsch (Kain and Fritsch, 1993) cloud data file, which describes locations and cloud lifetimes of convective clouds. Currently, only the first file is used to process CMAQ dry deposition module options and the second file is not actively used because

the CCTM does not yet support a corresponding aqueous-phase Kain-Fritsch cloud mixing module.

12.1.2.3 Landuse Data

MCIP requires landuse data that define surface characteristics in order to compute dry deposition velocities and other PBL parameters. Depending on the PBL and dry deposition modules desired, the needs for landuse data vary. The RADM dry deposition algorithm (Wesely, 1989) needs 11-category fractional landuse data. On the other hand, the new CMAQ deposition algorithm requires cell-averaged parameters defining surface exchange characteristics (i.e., landuse dependent parameters). The latter algorithm assumes that the landuse dependent subgrid effects are processed in the meteorology modeling system. To avoid incorrect averaging of the land-surface parameters, it distinguishes a dominant water cell from other landuse types.

Table 12-1. Relations Among MM5, CMAQ/RADM, and USGS Landuse Categories

MM5	MM5 Category	MCIP	CMAQ/RADM Category	USGS	USGS Category
1	Urban Land	1	Urban Land	1	Urban/built up
2	Agriculture Land	2	Agriculture	2	Dry cropland & pasture
				3	Irrigated cropland & pasture
				4	Mixed dryland/irrigated pasture
3	Range-Grassland	3	Range	7	Grassland
				8	Shrubland
				9	Mixed shrubland/grassland
				10	Chaparral
4	Deciduous Forest	4	Deciduous Forest	12	Broadleaf deciduous forest
				16	Deciduous coniferous forest
5	Coniferous Forest	5	Coniferous Forest	13	Evergreen coniferous forest
				14	Sub alpine forest
				17	Evergreen broadleaf
6	Mixed Forest/Wet Land	6	Mixed Forest and Wet Land	6	Woodland/cropland mosaic
				15	Mixed forest
7	Water	7	Water	18	Water
8	Marsh or Wet Land	9	Nonforest Wet Land	19	Herbaceous
				20	Forested wetlands
9	Desert	11	Rock, Open Shrub	21	Barren or sparsely vegetated
10	Tundra	8	Barren Land	22	Shrub & brush tundra
				23	Herbaceous tundra
				24	Bare ground tundra
				25	Wet tundra
				26	mixed tundra
11	Permanent Ice	7	Water	27	Perennial snowfields or glaciers
12	Tropical Forest	3*	Range*		
13	Savannah	3	Range	11	Savannah
None		10	Mixed Agriculture/Range Land	5	Grassland/cropland mosaic

* Mapping "Tropical Forest" to "Range" is not appropriate in most locations.

Currently, MCIP accepts four different types of landuse data. Two types of landuse input (one from MM5 directly, or the other from TERRAIN, a preprocessor for MM5 system) contain 13-category data. The third one is a preprocessed landuse data set in an ASCII file. Recently, we added a landuse processor (LUPROC) for the USGS vegetation information (described below) to improve landuse data quality. For the case of MM5, the percentages of MM5's 13 landuse category are transformed into the CMAQ/RADM's 11-category fractions in the landuse reader module. The USGS vegetation category is also transformed into the 11-category fractions. Table 12-1 provides the conversion rules for landuse types from MM5 13-category, and USGS 27 (http://edcwww.cr.usgs.gov/landdaac/glcc/ nadoc1_1.html) category to CMAQ/RADM's 11-category. The USGS North America land cover characteristics data base has 1-km nominal spatial resolution and is based on 1-km AVHRR data spanning April 1992 through March 1993. This data base has been adapted to the CMAQ's base map projection which uses Lambert conformal projection with origins at latitude 40° N and longitude 90° W.

Landuse Processor (LUPROC)

CMAQ's Landuse Processor (LUPROC) is a special processor that provides a high-resolution landuse data base for the system. MCIP requires landuse data that define surface characteristics to compute dry deposition and other PBL parameters. Depending on the PBL and dry deposition modules desired, the needs for the landuse data are somewhat different.

LUPROC windows out the landuse data for the user-defined domain and converts percentages of 27 vegetation categories in the database into the fractional landuse data in RADM's 11-category. The output of the LUPROC should have the same resolution as the CCTM domain and the LUPROC domain should include the boundary cells in addition to the CCTM's computational domain. In the near future, MM5 will be upgraded to allow use of the USGS land cover characteristic data as an option. When the CMAQ dry deposition algorithm is used and necessary PBL parameters are provided by the MM5 directly, LUPROC will not be needed.

12.1.3 Computational Structure

The MCIP data flow diagram, Figure 12-2, shows the key processing sequences. First, MCIP executes the one-time processes such as: reading the header, processing other operational information for the meteorological output, reading appropriate landuse data, and generating time independent MCIP output files. Then, MCIP loops through the time stepped (hourly or sub-hourly depending on the meteorology data) input data from a meteorology model performing the functions described above. The processing sequence of MCIP is summarized below:

- GETMET: reads and extracts meteorology data from standard MM5 output for the CCTM window domain, converts variables into SI units and process special files (e.g., two-dimensional surface/PBL data and Kain-Fritsch cloud files);
- PBLPKG/PBLSUB: computes PBL parameters using diagnostic method if desired;
- BCLDPRC_AK: computes diagnostic convective cloud parameters if needed;
- SOLAR: computes solar radiation parameters;
- RADMDRY/M3DDEP: computes dry deposition velocities; and

- METCRO_OUT & METDOT_OUT: computes additional meteorology data required for the generalized CTM, interpolates mean profile data into finer grid resolution if needed, and output Models-3 I/O API meteorology files.

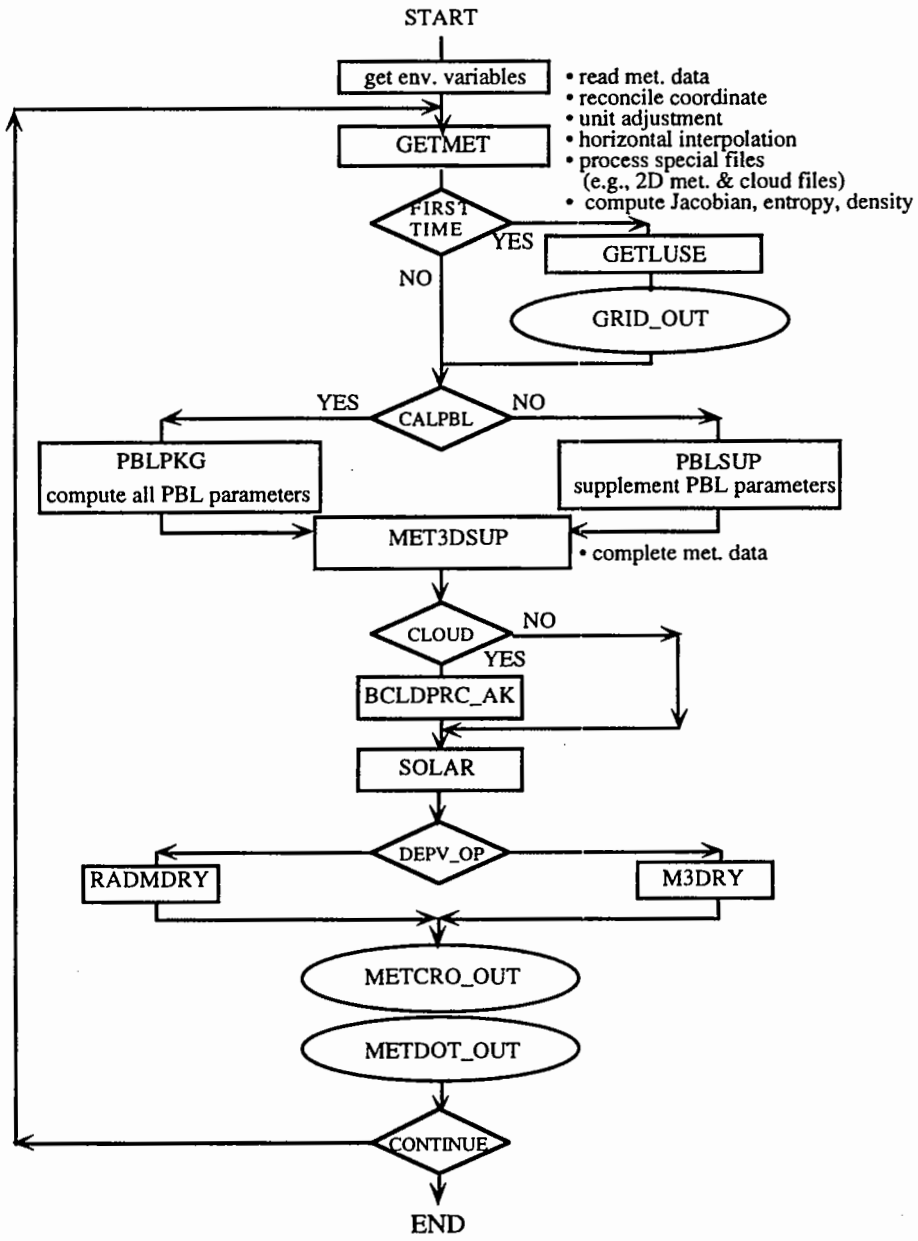

Figure 12-2. Flow Chart of MCIP Showing Key Data Processing Sequence.

12.2 Data Types, Coordinates, and Grids

MCIP's essential role is to provide consistent meteorological data for the CMAQ modeling system. Therefore, it is very important to understand the vertical coordinate used in the meteorological modeling system. For example, MM5 can be used either in hydrostatic mode, in which the hydrostatic pressure (time dependent) is used to define the terrain-influenced vertical coordinate, or in nonhydrostatic mode, where a reference hydrostatic pressure (time independent) in a normalized height form is used as the vertical coordinate. Many parts of current MCIP code deal with these differences in the vertical coordinate specifically. In the following we provide technical information related with coordinates and grids used in MCIP.

12.2.1 Meteorological Data Types

Many different combinations of approximations are used for describing the atmosphere in meteorological models. Therefore, classification of MCIP output parameters based on detailed classification of vertical coordinate types (such as geometric height, pressure, terrain-following coordinates, etc.), and their application approximations (such as hydrostatic and nonhydrostatic), can be exceedingly complex for the CTM with generalized coordinate implementation. Unlike previous use of detailed classification of meteorological coordinates for determining meteorological data type, we classify the coordinate types mainly based on the temporal dependency of the Jacobians (explained later). The benefit of this distinction is obvious. For example, a height coordinate which is time independent may require only a time constant file for describing the vertical coordinate while a dynamic pressure coordinate requires several parameters related with the coordinate description that needs to be stored in a time dependent file.

A similar distinction is made based on the need for describing data in different horizontal positions, such as flux-point data for horizontal wind components and cross-point for most other scalar parameters. For MM5, two horizontal wind components are defined at so-called 'dot' points while all other scalar values are at 'cross' points, following Arakawa-*E* grid definition. Refer to Figure 12-3 for the definitions of Arakawa *C*-grid and *E*-grid (Mesinger and Arakawa, 1976). For the CCTM, certain flux data are defined on the Arakawa *C*-grid in which the flux points are not collocated in $\hat{x}^1$- and $\hat{x}^2$-directions. Therefore, MCIP interpolates MM5's dot-point wind components linearly and multiplies the result with the two-point averaged density to provide the flux-point momentum component data. Both the flux-point and dot point data require array sizes larger than the cross-point data by one cell in each horizontal direction.

CMAQ utilizes contravariant wind components, instead of the regular wind components, to advect tracer species. Figure 12-4 shows that the east-west component of the contravariant wind field, $\hat{u}$, is placed at the $\hat{x}^1$-direction flux points (marked with the square symbol) and the north-south ($\hat{x}^2$-direction) component of the contravariant wind field, $\hat{v}$, is placed at the $\hat{x}^2$-direction flux points (marked with the triangle symbol). The vertical wind component is defined at the full-layer height.

The Models-3 I/O API requires individual data components to have exactly the same temporal and spatial dimensions in a file. Because the flux-point data and dot-point data both need additional column or row positions, we can combine them together in a so-called DOT file, which is larger than the CRO file by one cell for each horizontal direction. It is important to note that because the

flux points are different from the dot-points, they must be shifted by a half cell east or north (depending on whether they are square-point or triangle-point flux values) for graphical visualization of the flux-point parameters.

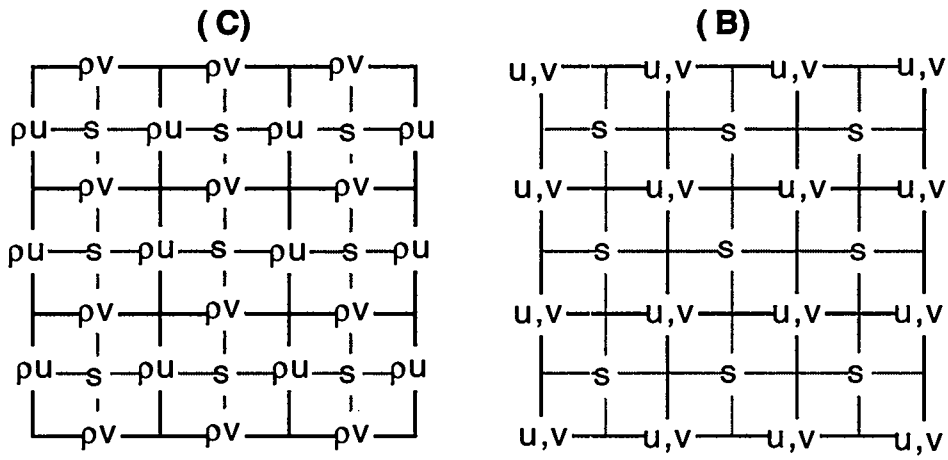

Figure 12-3. Two Different Grid Point Definitions, Arakawa *C*- and *B*-grids, Used in MCIP. *u* and *v* are horizontal wind components, *s* represents a scalar quantity, and ρ is density of air. For MM5, p^* is used instead of ρ.

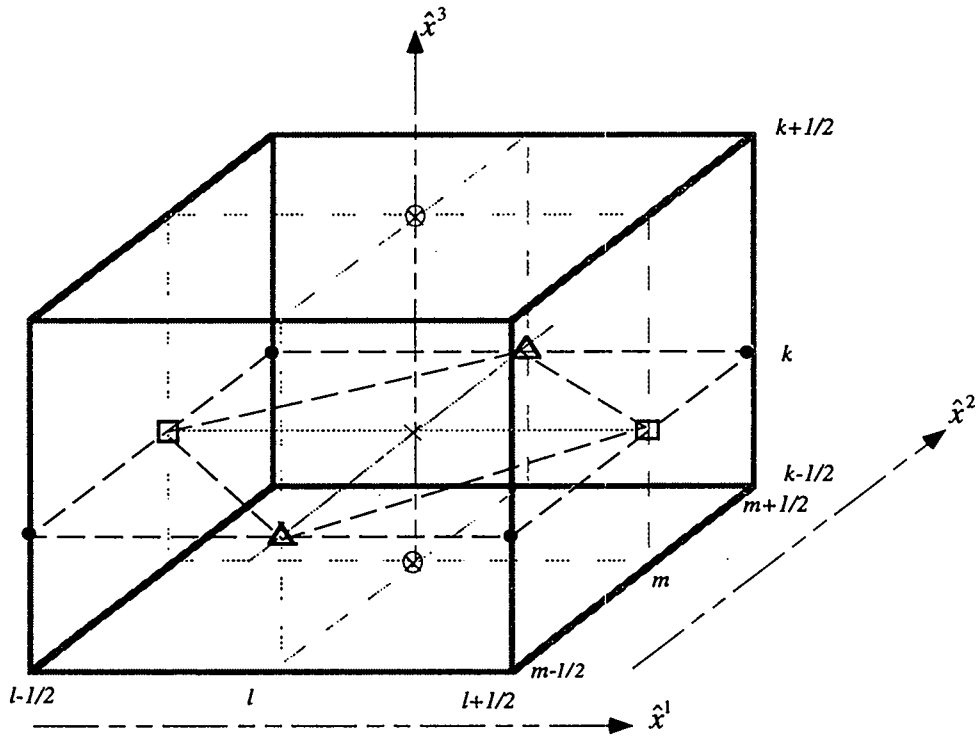

Figure 12-4. Computational Grid Points and Corresponding Indices Used in MCIP. Markers are for dot points (●), cross points (×), x-direction flux points (□), y-direction flux points (△), and vertical cross point at layer interface (⊗).

Furthermore, when these two flux components are assigned to form vectors in a visualization program like PAVE (Thorpe, 1996), the starting points of the vectors in the visualization are relocated at the dot-points although the two components are actually not collocated there.

Data for the boundary cells are defined with a special I/O API boundary data type. Depending on the need to describe boundary mass flux accurately, one may want to have a boundary domain with *NTHIK* cells (see Figure 12-5). The boundary grid is represented as the external perimeter to the main grid. This perimeter is *NTHIK* cells wide (where you may use a negative *NTHIK* to indicate an internal perimeter as used by such air quality modeling systems ROM and RADM). The boundary array is dimensioned in terms of the sizes of the arrays surrounding the main domain. Current Models-3 CMAQ system uses *NTHIK*=1 throughout the system components.

Finally, the dimensionality of the parameters (i.e., whether they contain three-dimensional or two-dimensional information) is used to distinguish the data type of meteorological parameters. In vertical direction, we define half and full layer positions based on the values of the generalized vertical coordinate, ($\hat{x}^3$). Vertical wind component and flux values are examples of the full-layer parameters. Although full-layer data require one more data point vertically, often the flux values at the bottom boundary (i.e., at the lowest full-layer) are zero. Therefore, we do not need to use additional data types for these, as long as we save the non-zero lowest full-layer data in a corresponding two-dimensional data type file separately. (Refer to Table 12-2 for dimensions used for each grid points.) Because a file represents a set of data with the same data type (with only a few exceptions) in the Models-3 system, locating meteorological parameters from an appropriate I/O API file is relatively easy. Table 12-3 summarizes the possible data types for the meteorological parameters. Depending on the choice of coordinates and grids, some of data types may not be relevant. For example, the current version of MCIP does not use GRID_DOT_3D and MET_DOT_2D data types. Appendix 12A provides the list of MCIP output parameters in each data file.

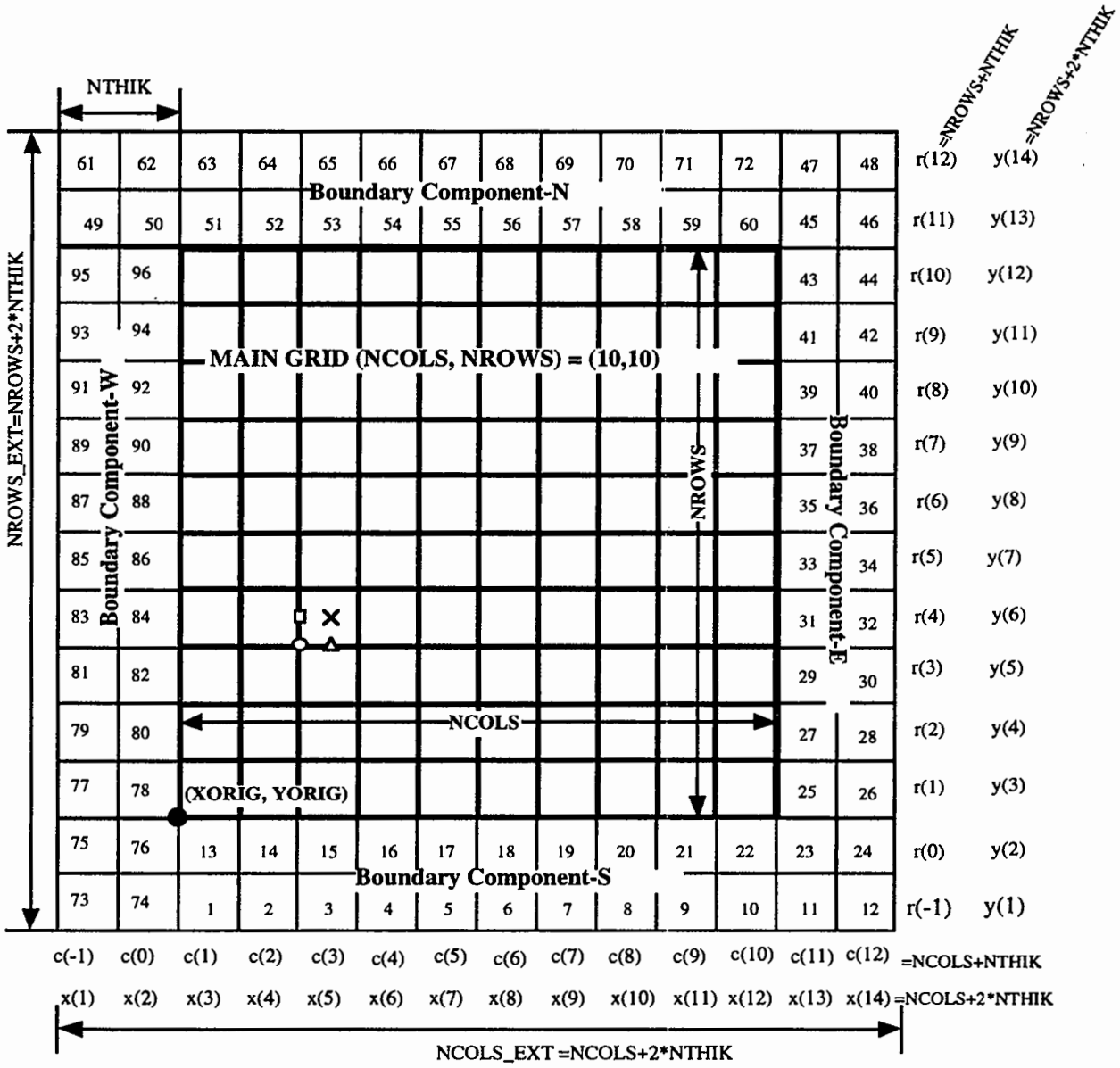

Note: Individual boundary component grids are treated as a I/O API 2-D file
S(1:NCOLS+NTHIK, 1-NTHIK:0)
E(NCOLS+1:NCOLS+NTHIK, 1:NROWS+NTHIK)
N(1-NTHIK:NCOLS, NROWS+1:NROWS+NTHIK)
W(1-NTHIK:0, 1-NTHIK:NROWS)

Figure 12-5. Grid Data Structure for Models-3/CMAQ Showing Main Grid and Boundary Components. Here *NTHIK*=2, *NCOLS*=10, *NROWS*=10 are used for the illustration.

Table 12-2. Dimensions and Indices for Grid Points used in MCIP and CCTM

	Dot-Point *(start: end)* *dimension* *index*	Cross-Point *(start: end)* *dimension* *index*	$\hat{x}^1$-direction Flux Point	$\hat{x}^2$-direction Flux Point	Full-Layer *(start: end)* *dimension* *index*	Half-Layer *(start: end)* *dimension* *index*
$\hat{x}^1$	(1:NCOLS+1) NCOLS+1 $l\pm1/2$	(1:NCOLS) NCOLS l	(1:NCOLS+1) NCOLS+1 $l\pm1/2$	(1:NCOLS) NCOLS l	N/A	N/A
$\hat{x}^2$	(1:NROWS+1) NROWS+1 $m\pm1/2$	(1:NROWS) NROWS m	(1: NROWS) NROWS m	(1: NROWS +1) NROWS+1 $m\pm1/2$	N/A	N/A
$\hat{x}^3$	N/A	N/A	N/A	N/A	(0:NLAYS) NLAYS+1 $k\pm1/2$	(1:NLAYS) NLAYS k

Table 12-3. Classification of Meteorological Data Types in the CMAQ System.
Data types GRID_DOT_3D and MET_DOT_2D (in gray color) are not used in CMAQ currently.

Time Independent		Time Dependent	
GRID_CRO_2D	GRID_CRO_3D	MET_CRO_2D	MET_CRO_3D
GRID_DOT_2D	GRID_DOT_3D	MET_DOT_2D	MET_DOT_3D
GRID_BDY_2D	GRID_BDY_3D	MET_BDY_2D	MET_BDY_3D

12.2.2 Coordinates

12.2.2.1 Horizontal Coordinates and Grid

MCIP can be configured with horizontal coordinates based on conformal map projections, such as Lambert Conformal, Polar Sterographic, and Mercator. Table 12-4 summarizes the necessary information for the description of the conformal map projections as defined in Models-3 I/O API. To generate I/O API files, which require exact definitions of the grid and coordinate system, users need to provide all the necessary map projection information in addition to vertical coordinate and layering definitions. The Models-3 CMAQ system uses square cells for the horizontal grid representation. A modeling domain is defined with the integer multiples of the square cells in E-W (column-wise) and N-S (row-wise) directions. Although a rectangular cell shape can be handled by the I/O API, the fractional time splitting approach used for the modularization of CTM processes requires use of square grid to maintain the accuracy of the finite differencing algorithms consistently. The effect of different horizontal coordinate is reflected in the values of the map scale

factor. Because of the need to couple the map scale factor (m) with other state variables and wind components, MCIP provides map scale factor for both the dot- and cross-points.

Table 12-4. Map Scale Factors and Parameters Defining Horizontal Coordinates in Models-3 I/O API (Coats, 1996)

Coordinate	ID in Models-3 I/O API	Map Parameters	Map Scale (m)	Note
lat.-long.	LATGRD3=1	N/A	N/A $m = 1$	$(\hat{x}^1, \hat{x}^2)$=(long,lat) are in degrees
Lambert	LAMGRD3=2	$P_\alpha = \phi_1 \leq P_\beta = \phi_2$ two latitudes that determine the projection cone. $P_\gamma = \lambda_o$, central meridian	$m = \frac{\sin(\pi/2-\phi_1)}{\sin(\pi/2-\phi)}\left[\frac{\tan(\pi/4-\phi/2)}{\tan(\pi/4-\phi_1/2)}\right]^n$ $n = \ln\left[\frac{\sin(\pi/2-\phi_2)}{\sin(\pi/2-\phi_1)}\right]$ $\bullet\left[\ln\left(\frac{\tan(\pi/4-\phi_2/2)}{\tan(\pi/4-\phi_1/2)}\right)\right]^{-1}$	$(\hat{x}^1{}_{cent}, \hat{x}^2{}_{cent}) = (\lambda_o, \phi_o)$ for the center of coordinate system. $(\hat{x}^1, \hat{x}^2)$are in meters
Mercator	MERGRD3=3	$P_\alpha = \phi_o$, $P_\beta = \lambda_o$: latitude longitude of coordinate origin within the tangent circle. P_γ: angle between cylinder axis and the North polar axis	$m = \frac{\cos\phi_o}{\cos\phi}$	$(\hat{x}^1{}_{cent}, \hat{x}^2{}_{cent}) = (\lambda_o, \phi_o)$ for the center of coordinate system. $(\hat{x}^1, \hat{x}^2)$are in meters
Stereo-graphic	STEGRD3=4	$P_\alpha = \phi_o$, $P_\beta = \lambda_o$: latitude and longitude of the point of tangency. P_γ: angle from true north to $\hat{x}^2$-axis	$m = \frac{1+\sin\phi_o}{1+\sin\phi}$	$(\hat{x}^1{}_{cent}, \hat{x}^2{}_{cent}) = (\lambda_o, \phi_o)$ for the center of coordinate system. $(\hat{x}^1, \hat{x}^2)$are in meters
UTM	UTMGRD3=5	P_α is the UTM zone P_β, P_γ not used	$m = 1$	$(\hat{x}^1{}_{cent}, \hat{x}^2{}_{cent})$ are offset from the UTM coordinate origin. $(\hat{x}^1, \hat{x}^2)$are in meters

12.2.2.2 Vertical Coordinates and Grid

The Models-3 CMAQ system allows many popular vertical coordinates used in meteorological models. We expect that the Models-3 I/O API will be extended to include several other vertical coordinates. The I/O API follows the definitions of vertical coordinates as used in meteorological models. However, in CMAQ the vertical coordinates are redefined to increase monotonically with height. This precaution is needed because the CMAQ code is expected to handle generalized coordinate system. We found that this constraint in the vertical coordinate is extremely useful for

the implementation of CTM in the generalized coordinate system by removing possible sign errors wherever vertical differentiations are involved. For example, the Jacobian information for a coordinate can be directly used to replace some of the derivatives involved with the generalized vertical coordinate. This internal change does not require redefinition of the vertical coordinates in the MCIP output files. The impact of this constraint is limited to an include file that defines the coordinates and vertical layers. In a typical Models-3 operation, this include file is automatically generated by the system framework through the use of the coordinate/grid manager. In the following two typical application examples are presented; one for the time dependent coordinate and the other for time independent coordinate.

Time dependent hydrostatic sigma-pressure coordinate

For the MM5 system, this coordinate is used when the hydrostatic option is chosen. In general, this coordinate can be used not only for the hydrostatic atmosphere simulations but also for nonhydrostatic cases. For example, when a regional scale hydrostatic meteorological model provides hydrostatic values, the same coordinate can be used in a nonhydrostatic nested model as described by Jaung (1992). In MCIP implementation, we should view this coordinate as an example of processing meteorological data with a dynamic vertical coordinate definition rather than an example of a hydrostatic coordinate.

The CCTM utilizes a generalized coordinate system that allows construction of the vertical layering consistent with the meteorological coordinate used. However, to maintain the vertical coordinate definition monotonically increasing with height, the coordinate definition for the CCTM has been modified as:

$$\hat{x}^3 = \xi \equiv 1 - \sigma_{\tilde{p}}\,;\ \sigma_{\tilde{p}} = \frac{\tilde{p} - p_T}{\tilde{p}_s - p_T} = \frac{\tilde{p} - p_T}{\tilde{p}^*} \tag{12-1}$$

where $\tilde{p}(\hat{x}^1, \hat{x}^2, \hat{x}^3, t)$ is the hydrostatic pressure, p_T is the pressure at the model top which is held constant, $\tilde{p}_s(\hat{x}^1, \hat{x}^2, t)$ is the surface pressure, and $\tilde{p}^* = \tilde{p}_s - p_T$. Because the pressure used in the definition of the vertical coordinate is in hydrostatic balance, we have:

$$\frac{\partial \tilde{p}}{\partial z} = -\tilde{\rho} g \tag{12-2}$$

The Jacobian is then defined as:

$$J_{\hat{x}^3} \equiv \left| \frac{\partial \hat{x}^3}{\partial z} \right|^{-1} = \left| -\frac{1}{\tilde{p}^*} \frac{\partial \tilde{p}}{\partial z} \right|^{-1} = \frac{\tilde{p}^*}{\tilde{\rho} g}, \tag{12-3}$$

and it is time dependent because the surface pressure and air density are time dependent.

Time independent reference hydrostatic sigma-pressure coordinate

In MM5 this coordinate is specifically used for the simulation of the nonhydrostatic atmosphere. The layer structure is entirely different from the case when hydrostatic option is used. The

coordinates defined with this option are time independent and have very similar characteristic to those of the normalized geometric height coordinates. The only difference is that the vertical layer thickness is defined with a nonlinear function of the geometric height. Here, we should view this coordinate as an example of processing meteorological data with time independent vertical coordinate.

The terrain-following reference hydrostatic pressure (σ_{p_o}) coordinate, again in a monotonically increasing form, is given as:

$$\hat{x}^3 = \xi \equiv 1 - \sigma_{p_o} \; ; \; \sigma_{p_o} = \frac{p_o - p_T}{p_{os} - p_T} = \frac{p_o - p_T}{p_{os}^*} \tag{12-4}$$

where $p_o(\hat{x}^1, \hat{x}^2, \hat{x}^3)$ is the hydrostatic pressure of the reference atmosphere, p_T is the pressure at the model top, $p_{os}(\hat{x}^1, \hat{x}^2)$ is the reference surface pressure which is determined by the topographic height z_s, and $p_o^* = p_{os} - p_T$.

Because the reference atmosphere is in hydrostatic balance, we have:

$$\frac{\partial p_o}{\partial z} = -\rho_o g \tag{12-5}$$

The Jacobian is then defined as:

$$J_{\hat{x}^3} \equiv \left| \frac{\partial \hat{x}^3}{\partial z} \right|^{-1} = \left| -\frac{1}{p_o^*} \frac{\partial p_o}{\partial z} \right|^{-1} = \frac{p_o^*}{\rho_o g} \tag{12-6}$$

and it is time independent because it is a function of the time-independent surface pressure and the density of the reference atmosphere. Here, the vertical coordinate z represents a height above the lowest point in a modeling domain, or the mean sea level (MSL) height if there is no place lower than the MSL. Usually, this type of vertical coordinate accompanies with a simple description of reference temperature profile of the base state. For example, in MM5 the base temperature profile is defined with a simple expression:

$$T_o(z) = T_{os} + A \ln\left(\frac{p_o(z)}{p_{oo}} \right) \tag{12-7}$$

where the reference values are chosen such that T_{os} is a sea level reference temperature in K, p_{oo} = 1000 mb = 10^5 Pascal, and A, which is set to be 50 K, is a measure of atmospheric lapse rate represented in temperature difference for the e-folding depth. With Equations 12-5 and 12-7 and the Equation of State, we could relate the reference pressure in terms of height z in a differential equation:

$$\frac{d\ln p_o(z)}{dz} = -\frac{g}{R}\frac{1}{[T_{os} - A\ln(p_{oo})] + A\ln(p_o(z))} \tag{12-8}$$

which can be readily solved for $p_o(z)$ by the separation-of-variables technique. The solution is a quadratic equation in terms of $\ln p_o$. For typical tropospheric conditions, the base pressure can be related with the geometric height by taking the positive square root term:

$$p_o(z) = \exp\left[\frac{-b + \sqrt{b^2 - 2Ac}}{A}\right] \tag{12-9}$$

where $b = T_{os} - A(\ln p_{oo})$, and $c = \frac{g}{R}z - [\frac{1}{2}A(\ln p_{oo})^2 + b(\ln p_{oo})]$.

Equation 12-9 shows that $p_o(z)$ is a monotonic, but nonlinear, function of z.

12.2.3 Modification of Grid Structure

In CMAQ, the horizontal and vertical coordinate information (such as the map projection parameters) for CTM simulation domains are required to be exactly the same as (or a derivative of) the master coordinates used in the meteorological model simulation. However, the horizontal grid structures of the CTM domains can be redefined depending on the need for air quality simulations. Here, the concept of grid family is introduced. It is as a set of grid domain specifications with the following properties:

1. the same coordinate origin and map projection;
2. a window domain for the parent domain; or
3. a nest (multi-stage) domain from a window or the parent domain.

The Models-3 I/O API file header helps to describe the horizontal grid and coordinates unambiguously to position the background map correctly and to provide relations among the members (multi-stage nesting domains) of the grid family. Only with a limited manner, the user is allowed to modify the grids in the vertical directions because of the concern that *ad hoc* interpolation may destroy the integrity of the meteorological data.

12.2.3.1 Windowing

The windowing functions in MCIP extract MM5 output for a CCTM window domain. As a rule of thumb, a CCTM uses a smaller computational domain than the domain used by meteorological models, because predictions in the cells near the boundaries may not be suitable for use in air quality simulation. Therefore, MCIP extracts only the portion of the MM5 output data which falls within the CTM's main domain and boundary cells. The CTM domain should be located at least four or five cells inside the MM5 domain to minimize the boundary effects. MCIP can, however, generate output for the CMAQ domain as large as 2 cells smaller than the meteorology domain, because it generates files for the boundary cells with *NTHIK*=1. (Note in MM5 terminology, it

may seem like the CMAQ domain is smaller by three because a DOT point concept is used in MM5 system for the grid definition.)

Limitation on the number of horizontal cells (to 120 cells) of the meteorology grid is coming from the MCIP's parameters defined in MCIPPARM.EXT:

```
 PARAMETER ( MAXI    = 120,        ! MET domain size in N-S dir.
&            MAXJ    = 120 )       ! MET domain size in E-W dir.
```

When the meteorology data has larger dimensions, MAXI and MAXJ should be modified accordingly. Also, there could be some limitations with reader routines specific for meteorology models. Because these reader modules are essentially foreign codes, there is no easy way to generalize the input process of the meteorological data. Refer to Figure 12-6, which shows the relation among the meteorology domain, the window domain for meteorological data extraction, and the CTM main and boundary domains.

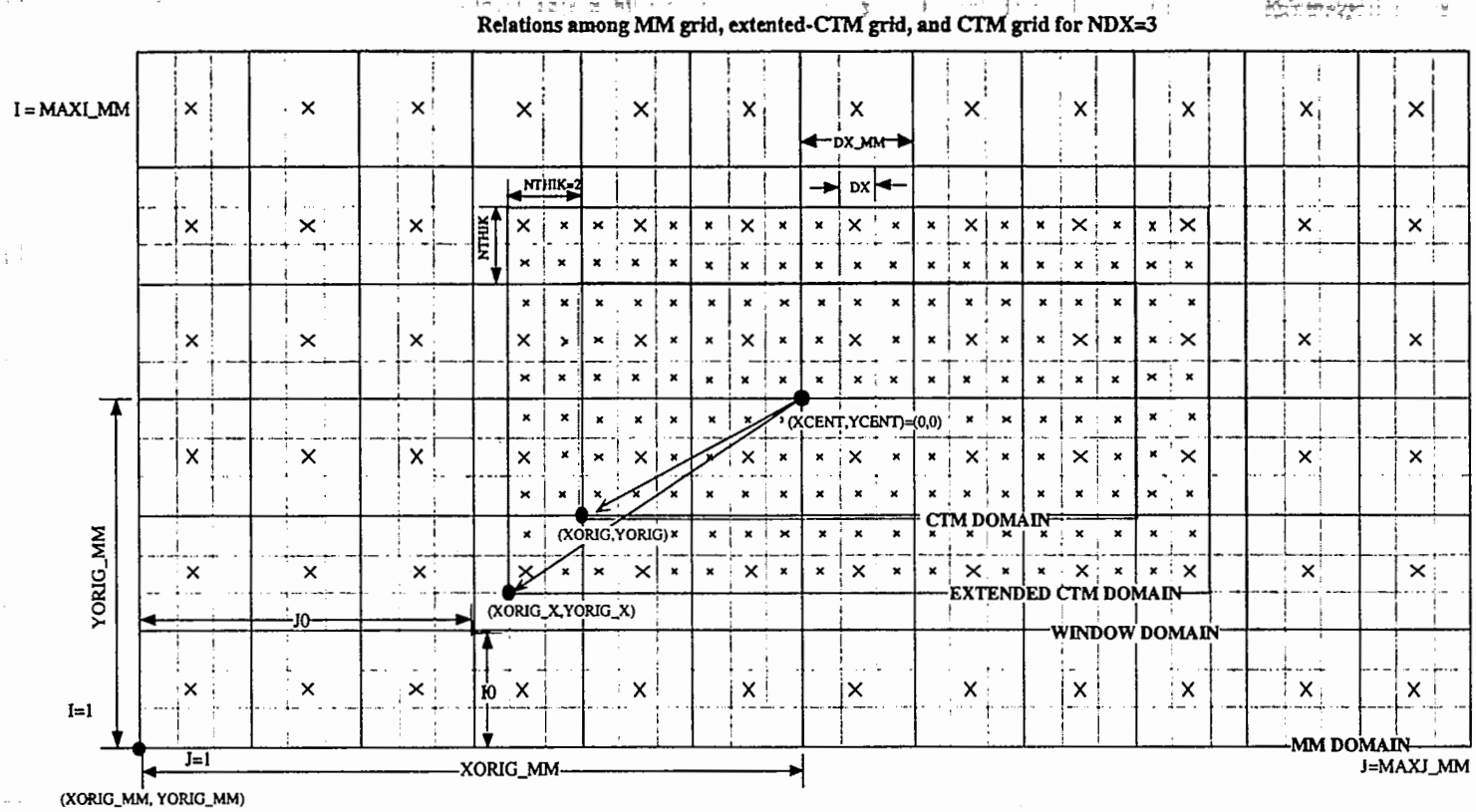

Figure 6. Relations among the meteorology domain, window domain for data extraction, and CTM's main and boundary domains.

12.2.3.2 Horizontal Interpolation

A horizontal interpolation function is provided to help users generate higher resolution data than the input meteorological data. This function is used when higher resolution emissions data is available but the detailed variations in meteorological fields can be neglected. This option is useful only when the surface and PBL parameters are diagnosed in MCIP. If interpolation is desired, *NDX* (defined in MCIPPARM.EXT) must be modified before the MCIP is compiled so that data arrays are dimensioned properly. When interpolation is desired, MCIP copies contiguous grid cell values from the coarse grid to the fine grid and then performs a two-dimensional bilinear interpolation on the three-dimensional data. The interpolated temperature profile is updated using fine resolution landuse data to reflect land-sea boundaries in the profile appropriately. The interpolated temperature, moisture, and wind components profiles, together with the detailed landuse data, are used to estimate surface and PBL parameters for the finer resolution. The user should be reminded that this procedure generates higher resolution meteorological data without enhanced physics, thus the newly generated data may have consistency problems. Therefore, such interpolation should be used sparingly for cases such as testing higher resolution emissions data with a finer resolution CTM. The procedure is never meant to replace or minimize the need for higher resolution meteorological model runs. It should be noted that the interpolated temperature and moisture profiles result in different estimations of cloud parameters (such as cloud bottom and top heights, fractions, liquid water contents) as determined by the diagnostic Anthes-Kuo cloud routine.

12.2.3.3 Vertical Layer Collapsing

A vertical collapsing function is supplied to generate a smaller data set for testing CTM in a smaller computer system. If desired, MCIP collapses MM5 profile data for the coarse vertical resolution data as defined by the user. MCIP performs a mass-weighted averaging of data in the vertical direction. For example, 30-layer MM5 data may be averaged into 15 or 6 CTM layers. During the collapsing procedure, the layer description is modified accordingly. The resulting profile may have consistency problems. This option is usually used to generate meteorology data for a system test-run for code debugging and development purposes. It is also appropriate to study the effects of the vertical resolution in air quality simulation such as presented in Byun and Dennis (1995). Refer to Table 12-5 as an example for the layer collapsing.

Defining the vertical layering structure for the CMAQ system requires consideration of several factors. Depending on the layer definitions used, the model results will be affected considerably. The implications of the layer definition are pervading across the entire system. For example, to determine mass exchange between the boundary layer and free troposphere, a good resolution near the boundary layer top is preferable. Also, different cloud parameterizations may perform differently, depending on the layering structure. Aerodynamic resistance, which influences dry deposition velocities, is a function of layer thickness and the boundary layer stability. For emissions processing, the layer thickness affects the plume rises from major stacks. Also, the vertical extent of the area emission effects is limited by the thickness of the lowest model layer for the CCTM. Although 6-layer vertical grid definition is provided with the tutorial simulation examples, we do not recommend it to be used for regulatory applications because of the difficulties in simulating certain processes, such as dry deposition under stable atmospheric conditions.

Current limitation on the number of vertical layers to 30 comes from one of the MCIP's parameters defined in MCIPPARM.EXT:

```
PARAMETER ( MAXK    =  30 )       ! MET number of layers
```

When a meteorological data has more number of layers, the parameter MAXK should be increased accordingly. Collapsing is done automatically when the COORD.EXT file (see Models-3 CMAQ User's Guide for the details) for the output grid has smaller number of layers than the input grid.

Table 12-5. An example of layer collapsing from 15 to 6 σ-layers. Full and half σ-levels and standard heights are provided to show relations between the two vertical grid systems. (adapted from Byun and Dennis, 1995)

Level Index(15)	Level Index(6)	σ-Level Full(15)	σ-Level Half(15)	Standard Height (m) Full(15)	Standard Height (m) Half(15)
15		0.0		16069	
			0.05		13712
14	6	0.1		11998	
			0.15		10649
13		0.2		9512	
			0.25		8513
12		0.3		7621	
			0.35		6813
11	5	0.4		6073	
			0.45		5390
10		0.5		4754	
			0.55		4159
9		0.6		3600	
			0.65		3071
8	4	0.7		2570	
			0.74		2187
7		0.78		1818	
			0.81		1550
6		0.84		1289	
	3		0.865		1077
5		0.89		868	
			0.91		705
4		0.93		544	
	2		0.945		425
3		0.96		307	
			0.97		230
2		0.98		152	
	1		0.985		114
1		0.99		76	
			0.995		38
0	0	1.0		0	

12.3 Estimation of Physical Parameters

MCIP's essential role is to provide consistent meteorological data for the CMAQ modeling system. However, the meteorological models used for air quality study may not provide important boundary layer parameters at all, or may predict those at very coarse temporal resolution, or may only compute a subset of the needed parameters. In such a case, it becomes necessary to estimate remaining meteorological parameters using certain diagnostic methods. MCIP allows either the direct pass through of the PBL parameters provided by MM5, or they can be computed from the mean profiles of temperature, humidity and momentum together with the surface landuse data. In the following, we explain the diagnostic methods used in MCIP. Note that the approaches introduced here may not be consistent with MM5 directly and therefore may produce somewhat different spatial distribution patterns for certain parameters. Basically, the diagnostic routines treat meteorological model outputs as the pseudo radiosonde observations.

When desired, MCIP estimates key parameters for cloud distributions based on Anthes-Kuo parameterization. They include precipitation rate, cloud fraction, and cloud base and top heights. MCIP also provides estimated dry deposition velocities for various chemical species in the RADM and carbon bond 4 (CB-4) mechanisms.

12.3.1 PBL Parameters

Depending on the user option, MCIP either passes through MM5 predicted surface and PBL parameters or estimates them us the MM5 profile data and detailed landuse information. The algorithms used for the diagnostic computation of PBL parameters are provided below.

12.3.1.1 Surface Flux Related Parameters

We utilize a diagnostic method based on similarity theory to estimate the turbulence flux related parameters. When the meteorological model uses very high vertical resolution and the thickness of lowest model layer is less than 20 m, we can utilize the surface similarity theory to determine turbulence parameters for both stable and unstable atmosphere.

For the computation of the surface layer parameters, MCIP utilizes analytical solutions suggested by Byun (1990) to minimize the needs for numerical iterations in solving the flux-profile relations. The method has been reviewed and successfully applied in several surface layer studies (e.g., Hess, 1992; Lo, 1993 and 1995). Also, a weather research model, the Advanced Regional Prediction System (ARPS) (Xue et al., 1995) utilizes it in the description of the surface layer. The algorithm is summarized below.

The nondimensional surface layer profile functions for momentum (ϕ_m) and potential temperature (ϕ_h) are defined as:

$$\frac{kz}{u_*}\frac{\partial U}{\partial z} = \phi_m(\frac{z}{L}) \qquad (12\text{-}10a)$$

$$\frac{kz}{\theta_*}\frac{\partial \Theta}{\partial z} = \phi_h(\frac{z}{L}) \tag{12-10b}$$

where U and Θ are the horizontal wind speed and potential temperature in the boundary layer, respectively, u_* is the friction velocity, and θ_* is the temperature scale representing the surface heat flux (covariance of potential temperature and wind fluctuations) divided by the friction velocity. L is the Monin-Obukhov length defined as:

$$L = \frac{\Theta_o u_*^2}{kg\theta_*} \tag{12-11}$$

The similarity functional forms proposed by Businger et al. (1971) are used in MCIP as follows: For moderately stable conditions ($1 \geq z/L \geq 0$) we have:

$$\phi_m = 1 + \beta_m \frac{z}{L} \tag{12-12a}$$

$$\phi_h = \mathrm{Pr}_o(1 + \beta_h \frac{z}{L}), \tag{12-12b}$$

where Pr_o is the Prandtl number for neutral stability and β_m and β_h are the coefficients determined through field experiments. Refer to Table 12-6 for the values of these coefficients used in MCIP. For unstable conditions ($z/L < 0$), we have:

$$\phi_m = (1 - \gamma_m \frac{z}{L})^{-1/4} \tag{12-13a}$$

$$\phi_h = (1 - \gamma_h \frac{z}{L})^{-1/2} \tag{12-13b}$$

where γ_m and γ_h are coefficients of the profile functions. In addition, we added a function for the very stable condition ($z/L \geq 1$) to extend the applicability of the surface layer similarity following Holtslag et al. (1990):

$$\phi_m = \beta_m + \frac{z}{L} \tag{12-14a}$$

$$\phi_h = \mathrm{Pr}_o(\beta_h + \frac{z}{L}) \tag{12-14b}$$

To estimate surface turbulence fluxes with the layered data from a meteorological model, we utilize the integrated flux-profile relationships: For ($z/L < 1$) we have profile functions represented as a modified logarithmic functions, when integrated from the height of the roughness length (z_o),

$$U(z) = \frac{u_*}{k}\left[\ln\frac{z}{z_o} - \psi_m(\frac{z}{L},\frac{z_o}{L})\right] \tag{12-15a}$$

$$\Delta\Theta(z) = \frac{\mathrm{Pr}_o\,\theta_*}{k}\left[\ln\frac{z}{z_o} - \psi_h(\frac{z}{L},\frac{z_o}{L})\right] \tag{12-15b}$$

and for strongly stable conditions, ($z/L \geq 1$), we use direct integration of the profile functions:

$$U(z) = \frac{u_*}{k}\left[\beta_m \ln\frac{z}{z_o} + \frac{z - z_o}{L}\right] \tag{12-16a}$$

$$\Delta\Theta(z) = \frac{\mathrm{Pr}_o\,\theta_*}{k}\left[\beta_h \ln\frac{z}{z_o} + \frac{z - z_o}{L}\right] \tag{12-16b}$$

The ψ functions are given by (e.g., Paulson 1970), for moderately stable conditions ($1 \geq z/L \geq 0$):

$$\psi_m(\frac{z}{L}) = -\beta_m\frac{z - z_o}{L} \tag{12-17a}$$

$$\psi_h(\frac{z}{L}) = -\beta_h\frac{z - z_o}{L} \tag{12-17b}$$

and for unstable conditions:

$$\psi_m(\frac{z}{L}) = 2\ln\left(\frac{1+x}{1+x_o}\right) + \ln\left(\frac{1+x^2}{1+x_o^2}\right) - 2\tan^{-1}(x) + 2\tan^{-1}(x_o) \tag{12-18a}$$

$$\psi_h(\frac{z}{L}) = 2\ln\left(\frac{1+y}{1+y_o}\right), \tag{12-18b}$$

where $x = (1-\gamma_m\frac{z}{L})^{1/4}$, $x_o = (1-\gamma_m\frac{z_o}{L})^{1/4}$, and

$$y = (1-\gamma_h\frac{z}{L})^{1/2},\ y_o = (1-\gamma_h\frac{z_o}{L})^{1/2}.$$

One important fact to note here is that although the similarity functions for stable conditions, Equations 12-12a-b and 12-14a-b, are continuous at $z/L = 1$, their integrated profiles are not continuous.

The flux profile relations described above are used to relate the Monin-Obukhov stability parameters with the readily computable bulk Richardson number Ri_b:

$$Ri_b = \frac{g(z-z_o)}{\Theta_o}\frac{\Delta\Theta}{U^2} \tag{12-19}$$

For moderately stable conditions ($1 > z/L \geq 0$), we have:

$$\zeta = \frac{\left(\frac{z}{z-z_o}\right)\ln\frac{z}{z_o}}{2\beta_h(\beta_m Ri_b - 1)}\left[-(2\beta_h Ri_b - 1) - \left(1 + \frac{4(\beta_h - \beta_m)Ri_b}{\mathrm{Pr}_o}\right)^{1/2}\right] \tag{12-20}$$

and for strongly stable conditions, ($z/L \geq 1$), we can derive a similar solution following the same procedure as described in Byun (1990) to give:

$$\zeta = \frac{\beta_m\left(\frac{z}{z-z_o}\right)\ln\frac{z}{z_o}}{\mathrm{Pr}_o - Ri_b}\left[-(\frac{1}{2} - Ri_b) + \left((\frac{1}{2} - Ri_b)^2 + (\mathrm{Pr}_o - Ri_b)Ri_b\right)^{1/2}\right] \tag{12-21}$$

Given a positive bulk Richardson number, one should use both Equations 12-20 and 12-21 to compute ζ and choose the value in the correct range between the moderately stable and strongly stable conditions.

For unstable conditions, we use an efficient analytical approximation by Byun (1990), for $(Q_b^3 - P_b^2) \geq 0$,

$$\zeta \approx \left(\frac{z}{z-z_o}\right)\ln\left(\frac{z}{z_o}\right)\left[-2\sqrt{Q_b}\cos(\frac{\theta_b}{3}) + \frac{1}{3\gamma_m}\right] \tag{12-22}$$

and for $(Q_b^3 - P_b^2) < 0$,

$$\zeta \approx \left(\frac{z}{z-z_o}\right)\ln\left(\frac{z}{z_o}\right)\left[-(T_b + \frac{Q_b}{T_b}) + \frac{1}{3\gamma_m}\right] \tag{12-23}$$

where $s_b = \frac{Ri_b}{\mathrm{Pr}_o}$;

$$Q_b = \frac{1}{9}\left[\frac{1}{\gamma_m^2} + 3\frac{\gamma_h}{\gamma_m}s_b^2\right];$$

$$P_b = \frac{1}{54}\left[-\frac{2}{\gamma_m^3} + \frac{9}{\gamma_m}(-\frac{\gamma_h}{\gamma_m} + 3)s_b^2\right];$$

$$\theta_b = \arccos\left(\frac{P_b}{\sqrt{Q_b^3}}\right); \text{ and}$$

$$T_b = \left[\sqrt{P_b^2 - Q_b^3} + P_b\right]^{1/3}.$$

The above equations are used to estimate friction velocity, u_*, by estimating the bulk Richardson number using the layered meteorological data:

$$u_* = \frac{kU(1)}{\ln(z/z_o) - \Psi_m(z/L) + \Psi_m(z_o/L)} \tag{12-24}$$

Heat flux can be found by using the temperature scale estimated with:

$$H = -\rho C_p u_* \theta_* \tag{12-25}$$

where

$$\theta_* = \frac{k[\Theta_1 - \Theta_s]}{\mathrm{Pr}_o[\ln(z_1/z_o) - \Psi_h(z_1/L) + \Psi_h(z_o/L)]} \tag{12-26}$$

There have been several suggestions for the coefficients of the surface layer profile functions. For example, Businger et al. (1971) suggested:

$$\beta_m = 4.7,\ \beta_h = 6.35,\ \gamma_m = 15.0,\ \gamma_h = 9.0,\ \mathrm{Pr}_o = 0.74$$

with the von Karman constant value of 0.35. On the other hand, Högström (1988) reanalyzed the experimental data used for the determination of the similarity functions and suggested use of:

$$\beta_m = 6.0,\ \beta_h = 8.21,\ \gamma_m = 19.3,\ \gamma_h = 11.6,\ \mathrm{Pr}_o = 0.95$$

with the von Karman constant value of 0.40. In the current version of MCIP, the latter set of coefficient values are used (refer to Table 12-6).

Moisture flux is found by using similar method as the potential temperature:

$$E = -\rho u_* q_*, \tag{12-27}$$

where mixing ratio scale, q_*, is determined with an equation similar to Equation 12-26 for given $\Delta q = q_1 - q_s$ (q_1 and q_s are the mixing ratios at the lowest model layer and at the surface, respectively).

12.3.1.2 Estimation of Surface Fluxes Using PBL Profile Functions

Occasionally meteorological models use the lowest model layer thicker than 40 m or so. Under this condition, it becomes difficult to believe that the lowest layer always belongs to the surface layer all the time, especially for very stable conditions. To avoid this limitation, MCIP estimates surface heat, momentum and moisture flux transfer parameters from MM5 surface wind and temperature by using the boundary layer similarity profiles proposed by Byun (1991). In this section, we describe the methods used in MCIP for estimating surface fluxes when the thickness of the lowest model layer is too thick to rely on the surface layer similarity. The intention is to provide a diagnostic method that can estimate the surface fluxes even when the lowest model layer extends above the surface layer. It is difficult to expect that a layer with 40 m thick, for example, continuously belongs to the surface layer though out a day.

Table 12-6. Parametric Constants Used to Describe the PBL in MCIP

Parameter	Symbol	Value
von Karman constant	K	0.4
Coefficient in stable profile function for momentum	β_m	6.0
Coefficient in stable profile function for heat (scalar)	β_h	8.21
Coefficient in unstable profile function for momentum	γ_m	19.30
Coefficient in unstable profile function for heat (scalar)	γ_h	11.60
Prandtl number for neutral stability	Pr_o	0.95
Critical Richardson Number	Ri_{cr}	0.25
Maximum bulk Richardson number	max(Ri_B)	0.70
Minimum bulk Richardson number	min(Ri_B)	-4.75
Minimum magnitude of Monin-Obukhov length	abs(L)	4.0
Scale height ratio for neutral stability	λ_o	0.07
Zilitinkevich c_h	c_h	0.80
Neutral value of similarity function for wind component parallel to surface stress	$A(0)$	1.70
Neutral value of similarity function for wind component normal to surface stress	$B(0)$	4.50
Reference height	z_r	10 m

The wind and temperature predicted by a meteorological grid model represent layer averaged values. In order to simplify computation of the surface fluxes, we apply the assumption that the predicted wind for the lowest model layer has the same direction as the surface stress (i.e., $u_m^2 + v_m^2 \approx U_m^2$, where u_m and v_m are latitudinal and longitudinal components of the first layer mean wind on the map and U_m is the layer mean wind speed in the direction of surface stress). Applying the PBL momentum profile functions of Byun (1991) and integrating them vertically from z_O (roughness length) to the top of the lowest CTM layer ($z_{F1} \leq h$), one can obtain wind and potential temperature profiles in the form:

$$U_m = \frac{u_*}{k} P_u(\mu, \eta_o, \eta_F), \tag{12-28}$$

$$\Theta_m - \Theta_o = \frac{\mathrm{Pr}_o \theta_*}{k} P_\theta(\mu, \eta_o, \eta_F) \tag{12-29}$$

where $\eta_o = \frac{z_o}{h}$, $\eta_F = \frac{z_{F1}}{h}$, and $\mu = \frac{h}{L}$. For a detailed description of the notation used, refer to Byun (1991) and Byun and Dennis (1995). Initially, the atmospheric stability (μ) is approximated by the analytical solutions of flux-profile relationships described earlier. Then, we compute μ, u_*, and θ_* using Equations 12-28 and 12-29, with the Newton-Raphson iteration. Equation 12-29 is then used to estimate temperatures at heights 1.5 m and 10 m in MCIP.

12.3.1.3 Utilization of Sub-grid Scale Landuse Information

Accurate description of atmospheric turbulence is one of the important elements in modeling the deposition of pollutants. For Eulerian air quality models, grid-average surface roughness based on sub-grid scale landuse information has played an important role in the characterization of the surface condition, which in turn determines intensity of turbulence in the atmosphere. To represent the atmospheric deposition process utilizing the available sub-grid landuse information, Walcek et al. (1986) introduced a method to estimate friction velocity for each landuse patch, which is used in the calculation of the subgrid-scale aerodynamic resistance. Also, several estimation methods have been proposed for the effective roughness length for use in meteorological grid models. Compared with the latter methods that estimate the representative grid values for the given sub-grid information, Walcek et al. (1986) emphasized the description of the sub-grid flux estimation by introducing a somewhat *ad hoc*, but useful assumption. They assumed that the quantity Uu_* is constant both for the cell averaged parameters and for the individual landuse patches, i.e.:

$$Uu_* = U_j u_{*_j} = \text{constant}, \tag{12-30}$$

where the non-subscripted variables refer to grid-averaged values while the *j*-subscripted values refer to the corresponding quantities over individual landuse types. Equation 12-30 is an intuitive expression of the often observed condition that where wind speed is high, the turbulence is low, and vice versa, under similar pressure gradient forcing. Strict validity of Equation 12-30 could be controversial, however, this approach is more realistic than those that assume constant wind or constant friction velocity. In the dimensional analysis point of view, the condition is a statement about the conservation of kinematic energy in the presence of surface friction. A derivation leading to Equation 12-30 is provided below using a combination of the surface layer similarity and the mixing length theories.

The momentum flux is related with mean wind gradient as:

$$-\overline{(u''w'')}_s = u_*^2 = K_m \frac{\partial U}{\partial z} \tag{12-31}$$

and the eddy diffusivity for momentum is given by:

$$K_m = \frac{k u_* z}{\phi_m(z/L)} \tag{12-32}$$

When we apply assumptions such as steady state flow and horizontal homogeneity of the each landuse patch, the momentum conservation equation can be simplified to give:

$$U\frac{\partial U}{\partial z} + \frac{\partial \overline{u''w''}}{\partial z} = -\frac{1}{\rho}\nabla_z p \tag{12-33}$$

Coriolis forcing is neglected in deriving Equation 12-33 because we are dealing with only the sub-grid scale variation of momentum field.

The right hand side of Equation 12-33 represents the pressure gradient forcing imposed over the grid and is therefore not dependent on sub-grid representation. Within the surface layer, which is treated as a constant flux layer, Equation 12-33 is further simplified to give:

$$U\frac{\partial U}{\partial z} = -\frac{1}{\rho}\nabla_z p = const. \tag{12-34}$$

Combining Equations 12-31, 12-32 and 12-34, one obtains

$$U u_* \frac{\phi_m(z/L)}{kz} = const. \tag{12-35}$$

For the atmosphere at neutral stability, $\phi_m = 1$, and the same expression should be applicable for each landuse patch. Then, Equation 12-35 becomes identical to Equation 12-30 at a given reference height $z = z_r$.

In addition to Equation 12-30, Walcek et al. (1986) assumed that the surface roughness length can be averaged as

$$z_o = \exp\left[\sum f_j \ln z_{oj}\right], \tag{12-36}$$

where f_j's are fractions of different landuse types in a grid cell. Walcek et al. (1986) stated that Equation 12-36 conforms to a logarithmic wind profile. In reality, however, Equation 12-36 can be derived from a simple geometric averaging and it does not produce a logarithmic wind profile. On the other hand, Mason (1987) suggest an averaging method based on the logarithmic wind profile by introducing a blending height (l_b) concept:

$$\left(\ln\frac{l_b}{z_o}\right)^2 = \left[\sum \frac{f_j}{\ln(l_b/z_{oj})^2}\right]^{-1}. \tag{12-37}$$

Although this approach is a practical averaging method of the roughness length, this by itself cannot be used to estimate landuse-dependent friction velocities. Therefore, here we compare several other roughness length averaging schemes that satisfy both Equation 12-30 and the logarithmic wind profile function for the neutral condition:

$$U(z_r) = \frac{u_*}{k} \ln \frac{z_r}{z_o} \tag{12-38a}$$

and

$$U_j(z_r) = \frac{u_{*j}}{k} \ln \frac{z_r}{z_{oj}} \tag{12-38b}$$

where z_r is the reference height. The objective is to compute landuse specific friction velocities from the cell average wind and friction velocity values while providing a consistent averaging scheme for the roughness length. The simplest method for estimating the grid average values from the sub-grid scale information is using the linear summation with the fractional weight:

$$< x >= \sum_j f_j x_j, \tag{12-39}$$

where x_j is a physical quantity and $\sum f_j = 1$. Because $U_j u_{*j}$ = constant, one can rewrite Equation 12-30 with Equation 12-39 as follows:

$$U u_* = U_j u_{*j} = \sum_j f_j U_j u_{*j} =< U u_* > \tag{12-40}$$

If the surface wind is a quantity that follows Equation 12-39, a relation between the grid average and sub-grid landuse dependent roughness lengths can be found as:

$$z_o = z_r \exp\left[-\frac{\left(\sum f_j u_{*j} \ln(z_r / z_{oj})\right)^2}{\sum f_j u_{*j}^2 \ln(z_r / z_{oj})} \right] \tag{12-41}$$

In order for the expression to be useful, u_{*j} in Equation 12-41 should be eliminated. From Equations 12-38a-b and 12-40, a simple relation for u_{*j} is found in terms of known quantities:

$$u_{*j} = u_* \left[\frac{\ln(z_r / z_o)}{\ln(z_r / z_{oj})} \right]^{1/2} \tag{12-42}$$

Substituting Equation 12-42 into Equation 12-41, we obtain a simple relation for the effective roughness length that satisfies both the logarithmic wind profile and the linearly-additive wind speed assumptions under the approximation, Equation 12-30:

$$z_o = z_r \exp\left[-\left(\sum f_j \sqrt{\ln(z_r / z_{oj})}\right)^2\right] \tag{12-43}$$

The reference height z_r needs to be within the regime where the log-linear wind profile can be satisfied. This means that it should be far away from z_o, but still within the surface layer. In the current MCIP, we are using z_r=10m. The new method conserves wind speed and $U_j u_{*j}$ under the linear summation (Equation 12-39). With this assumption the turbulence momentum flux (u_*^2) can be summed linearly when it is scaled with the factor $\left[\ln(z_r / z_o)/\ln(z_r / z_{oj})\right]$. Depending on the degree of inhomogeneity, this factor can be substantially different from unity, making less consistent with the expectation that fluxes from different patches can be summed up. One may expect that Equation 12-43 is sensitive to the choice of reference height z_r; however, the average roughness length is not strongly sensitive to the reasonable value of z_r between 1 to 10 m.

An alternative approach to the linearly-additive wind speed assumption is to assume that the sub-grid scale momentum flux can be summed linearly:

$$u_*^2 = \sum_j f_j u_{*j}^2 = < u_*^2 > \tag{12-44}$$

Using Equation 12-39 and the logarithmic wind profiles, one can find:

$$\frac{1}{\left[\ln(z_r / z_o)\right]^2} = \sum_j f_j \frac{(U_j / U)^2}{\left[\ln(z_r / z_{oj})\right]^2} \tag{12-45}$$

In order that Equation 12-45 to be useful, (U_j / U) should be expressed in terms of z_o, z_{oj}, and z_r. This is accomplished by dividing Equation 12-38a with Equation 12-38b and substituting (u_* / u_{*j}) with Equation 12-30 to get:

$$\frac{U_j}{U} = \left[\frac{\ln(z_r / z_{oj})}{\ln(z_r / z_o)}\right]^{1/2} \tag{12-46}$$

This leads to an averaging method for the sub-grid scale roughness length:

$$z_o = z_r \exp\left[-\left(\sum_j \frac{f_j}{\ln(z_r / z_{oj})}\right)^{-1}\right] \tag{12-47}$$

Another popular assumption is that at the reference height (or blending height) the drag coefficients representing the individual landuse patches in a cell can be summed linearly, i.e.:

$$C_D \equiv \frac{u_*^2}{U^2} = \sum_j f_j C_{Dj} = < C_D > \tag{12-48}$$

Unlike the two other assumptions introduced, this assumption does not depend on Equation 12-30. The resulting equation for average roughness length is then identical to Equation 12-37.

$$z_o = z_r \exp\left[-\left(\sum_j \frac{f_j}{\left[\ln(z_r / z_{oj})\right]^2}\right)^{-1/2}\right] \qquad (12\text{-}37')$$

Although the assumption in Equation 12-48 has been used often in the literature, it is not intuitive that the sub-grid drag coefficients can be added linearly. The drag coefficient simply quantifies the turbulence exchange characteristic of a landuse patch. By using this assumption together with the Equation 12-30, one can readily show that:

$$C_D = \sum_j f_j C_{Dj} = \sum_j f_j \frac{u_{*j}^2}{U_j^2} = \frac{1}{u_*^2 U^2} \sum_j f_j u_{*j}^4 = \frac{< u_*^4 >}{u_*^2 U^2} \qquad (12\text{-}49)$$

It is difficult to expect that u_*^4 is a physical quantity that can be added linearly. In MCIP, we have implemented both Equations 12-43 and 12-47 as a user option. Results of the comparison of the two recommended methods should be available as the model evaluation project progresses.

12.3.1.4 Boundary Layer Heights

Boundary layer height is a key parameter that determines the domain of atmospheric turbulence in which pollutants disperse. It is used as a fundamental scaling parameter for the similarity theory in the description of atmospheric diffusion characteristics. Estimating PBL height has been one of the key functions of meteorological pre-processors for air quality models. Below, we summarize PBL height estimation algorithms used in MCIP.

Unstable conditions

MCIP estimates the PBL height using the vertical profiles of potential temperature and the bulk Richardson number with an algorithm similar to the one reported in Holtslag et al. (1995). The bulk Richardson number of each model layer with respect to the surface is given as:

$$(Ri_B)^k = g \frac{z_H^k (\Theta_H^k - \Theta_o)}{\Theta_o (U_H^k)^2} \qquad (12\text{-}50)$$

where subscript H represents values at the layer middle (i.e., half sigma level).

First, the index of the PBL top (k_{PBL}) is determined at the layer when Ri_B first becomes larger than max(Ri_B). Then the proration factor of the bulk Richardson number relative to max(Ri_B) is computed with:

$$f_{Ri_B} = \min\left\{1, \frac{\max(Ri_B) - (Ri_B)^{k_{PBL}-1}}{(Ri_B)^{k_{PBL}} - (Ri_B)^{k_{PBL}-1}}\right\} \qquad (12\text{-}51)$$

where $\max(Ri_B)$=0.7 (refer to Table 12-6). Depending on the value of f_{Ri_B}, the index k_{PBL} and f_{Ri_B} are modified as follows:

for $f_{Ri_B} > 0.5$, $f'_{Ri_B} = f_{Ri_B} - 0.5$; $k'_{PBL} = k_{PBL}$, and

for $f_{Ri_B} < 0.5$, $f'_{Ri_B} = f_{Ri_B} + 0.5$; $k'_{PBL} = k_{PBL} - 1$.

Once the fraction and index for the PBL top are determined, we estimate the initial PBL height with:

$$h_{PBL} = f'_{Ri_B} z_F^{k'_{PBL}-1/2} + (1 - f'_{Ri_B}) z_F^{k'_{PBL}-3/2} \tag{12-52}$$

The above proration procedure ensures gradual increase of PBL height. Without the procedure, the resolution of PBL height is limited by the layer thickness of the model. In the RADM preprocessor, the PBL height is determined simply at the layer where the potential temperature first becomes warmer than the surface temperature for convective conditions. Compared with the RADM method, the present method takes into account effects of the wind shear as well.

Stable conditions

For stable conditions, the PBL height is determined by the maximum of the PBL height computed with above method and the stable boundary layer height given by the Zilitinkevich's (1989) formula:

$$h_{PBL} = \frac{1}{2}\left[-\frac{kc_h^2 L}{\lambda_o} + \sqrt{\left(\frac{kc_h^2 L}{\lambda_o}\right)^2 + 4ku_* c_h^2 \frac{L}{f}} \right] \tag{12-53}$$

Limiting PBL heights

Unlike the PBL height estimation algorithms based on temporal integration of surface heat flux (e.g., Carson, 1973; Betts, 1973; Driedonks, 1981), the above diagnostic algorithm could predict temporally disconnected PBL heights when the hourly meteorological data change abruptly. To minimize this effect, following limits on the PBL height are imposed.

1. Compare with PBL height for neutral conditions, and take maximum except for the tropical areas:

$$h'_{PBL} = \max\{h_{PBL},\ \lambda_o \frac{u_*}{f}\} \tag{12-54}$$

2. Compare with the urban boundary layer height, which is approximated with:

$$h_{UBL} = (1 - f_{urban}) h_{PBLmin} + f_{urban} h_{UBLmin} \tag{12-55}$$

where f_{urban} is the fraction of urban landuse in a cell. In MCIP, the minimum PBL height for urban area and other landuse types are set to be h_{UBLmin}=300 m and h_{PBLmin}=50 m. Then, take a maximum of the two to reflect the effect of urban landuse:

$$h'_{PBL} = \max\{h_{PBL},\ h_{UBL}\} \tag{12-56}$$

This step is introduced to apply the urban landuse classification, which is consistent with the one used for the emission processing, for the determination of the PBL height.

3. Limit the PBL height with a maximum value (h_{PBLmax}=3000 m) in case the temperature profile does not have a capping inversion:

$$h'_{PBL} = \min\{h_{PBL},\ h_{PBLmax}\}. \tag{12-57}$$

12.3.1.5 Aerodynamic Resistances

Aerodynamic resistance describes the ability of the atmospheric turbulence to transport pollutant to the surface for the deposition. In this regard, it may well be described with the probability concept. If 100 particles, say, are at height 20m, how many of them can reach the surface to be available for deposition during a given time interval? Or, what is the transport rate of particles in the air to the surface? The ratio represents the maximum potential deposition rate of particles subjected to atmospheric turbulence. However, even those particles which arrive at the surface may not all be deposited because of other resistances, which usually are parameterized using characteristics of surface and gaseous elements.

There have been many efforts to compare different formulations for dry deposition velocities. While there are a lot of uncertainties in describing atmospheric processes, the different aerodynamic resistance formulas in the literature are mainly originated from the differences in the applications and approximations of the same PBL theories and formulas. Among the components involved in atmospheric resistance computation, formulations for aerodynamic resistance have the least controversy. To compute the aerodynamic resistance, the parameterization of the eddy diffusivity for the PBL should be known. The eddy-diffusivity formulations used in the derivation of aerodynamic resistance are discussed below.

<u>Eddy diffusivity formulations</u>

The similarity theory suggests that eddy diffusivity in the surface layer for heat flux is given by:

$$K_h = \frac{k u_* z}{\phi_h(z/L)} \tag{12-58}$$

The profile function ϕ_h is defined in Equations 12-12b and 12-13b. Eddy diffusivity in the PBL (above the surface layer) (Brost and Wyngaard 1978) is given as:

$$K_h = \frac{ku_* z(1 - z/h_{PBL})^{3/2}}{\phi_h(z/L)} \tag{12-59a}$$

for stable atmosphere ($z/L > 0$), and as:

$$K_h = kw_* z(1 - \frac{z}{h_{PBL}}) \tag{12-59b}$$

for unstable atmosphere ($z/L \leq 0$), where the convective velocity scale w_* is defined as

$$w_* = \left[-\frac{g}{\Theta_o} h_{PBL} u_* \theta_* \right]^{1/3} \tag{12-60}$$

Aerodynamic resistance formulations

We often characterize the ability of turbulent atmosphere to carry pollutants to the vegetation or other surface elements using the aerodynamic resistance concept. Certain meteorological models may use the resistance representation of surface exchange processes in lieu of the conventional bulk aerodynamic methods and the aerodynamic resistance is available as a part of meteorological data with other PBL parameters. Conversely, there are models that do not predict resistances and related parameters needed. In such cases, we need to estimate it using PBL parameters and profiles of state variables.

The aerodynamic resistance (R_a) and sub-layer resistance (R_b) are parameterized in terms of friction velocity and surface roughness (Walcek, 1987; Chang et al., 1987 and 1990; Wesely, 1989; Wesely and Hicks, 1977). Although some consider the estimation of aerodynamic resistance as an integral part of the dry deposition velocity computation, we treat the aerodynamic resistance as an independent element that characterizes the effects of atmospheric turbulence. Here, we provide a set of integrated equations, which allow robust estimation of aerodynamic resistance compared with the method based on the nonintegrated form, which sometimes provides negative fluxes for unstable conditions. Refer to Byun and Dennis (1995) for details.

General formulation for the aerodynamic resistance at the deposition height z_{dep} (where concentration is represented) is divided into two components; the resistance in the surface layer (whose top is at z_{SL}, height of the surface layer) and the resistance in the PBL above the surface layer:

$$R_a = \int_{z_o}^{z} \frac{dz}{K_z(z)} = \int_{z_o}^{z_{SL}} \frac{dz}{K_z(z)} + \int_{z_{SL}}^{z_{dep}} \frac{dz}{K_z(z)} = R_{aSL} + R_{aPBL} \tag{12-61}$$

(a) For stable conditions:

$$R_{aSL} = \frac{\Pr_o}{ku_*}\left[\ln(\frac{z_{SL}}{z_o}) + \beta_h \frac{z_{SL} - z_o}{L}\right] \tag{12-62a}$$

$$R_{aPBL} = \frac{\Pr_o}{ku_*}\left[\frac{2(\beta+1)}{\sqrt{1-\eta_{dep}}} - \frac{2(\beta+1)}{\sqrt{1-\eta_{SL}}} + \ln\left|\frac{(-1+\sqrt{1-\eta_{dep}})(1+\sqrt{1-\eta_{SL}})}{(1+\sqrt{1-\eta_{dep}})(-1+\sqrt{1-\eta_{SL}})}\right|\right], \tag{12-62b}$$

where $\beta = \beta_h \frac{h_{PBL}}{L}$, $\eta_{dep} = \frac{z_{dep}}{h_{PBL}}$ and $\eta_{SL} = \frac{z_{SL}}{h_{PBL}}$.

(b) For unstable conditions:

$$R_{aSL} = \frac{\Pr_o}{ku_*}\left[\ln\left|\frac{(-1+\sqrt{1+\gamma_h z_{SL}/L})(1+\sqrt{1+\gamma_h z_o/L})}{(1+\sqrt{1+\gamma_h z_{SL}/L})(-1+\sqrt{1+\gamma_h z_o/L})}\right|\right] \tag{12-63a}$$

$$R_{aPBL} = \frac{1}{kw_*}\ln\left[\frac{\eta_{dep}(1-\eta_{SL})}{\eta_{SL}(1-\eta_{dep})}\right]. \tag{12-63b}$$

12.3.2 Dry Deposition Velocities

The term dry deposition represents a complex sequence of atmospheric phenomena resulting in the removal of pollutants from the atmosphere to the surface of the earth. The rate of transfer of pollutants between the air and exposed surfaces is controlled by a wide range of chemical, physical, and biological factors, which vary in their relative importance according to the nature and state of the surface, characteristics of the pollutant, and the strength of turbulence in the atmosphere. The complexity of the individual processes involved and the variety of possible interactions among them prohibits simple generalization of the process. Nevertheless, a "deposition velocity," analogous to a gravitational falling speed is of considerable use. In practice, the knowledge of dry deposition velocities enables fluxes to be estimated from airborne concentrations. Two dry deposition estimation methods, that from Wesely (1989) currently as implemented in CMAQ, and the new Models-3/CMAQ approach are presented.

12.3.2.1 RADM Method

The RADM dry deposition module in MCIP calculates deposition velocities of sixteen chemical species (Table 12-7). It requires various ancillary 2-D meteorology fields such as the PBL height, mixing scale velocities, Monin-Obukov length, etc. They are usually estimated from horizontal wind components, temperature and humidity profiles. The dry deposition flux of each chemical species from the atmosphere to surface is calculated in the CCTM by multiplying the concentration in the lowest model layer with the dry deposition velocity. The dry deposition velocity (V_d) is computed from the resistance-in-series method;

$$V_d = (R_a + R_b + R_c)^{-1} \tag{12-64}$$

where R_a is the aerodynamic resistance, R_b is the quasi-laminar boundary layer resistance, and R_c is the canopy (surface) resistance. Refer to Figure 12-7. V_d is usually estimated from a series of resistances to vertical transfer and surface uptake. Aerodynamic resistance (R_a) is a function of turbulent transfer in the atmospheric surface layer and can be estimated in several ways depending on the instrumentation used or parameterizations provided.

The canopy resistances (R_c) for SO_2 and O_3 are estimated from available measurements as a function of season, insolation, surface wetness, and land type (Walcek et al., 1986; Shieh et al., 1979; Fowler, 1978). The surface resistances for all other gaseous species, due to the lack of extensive measurements, are qualitatively scaled to the SO_2 and O_3 surface resistances according to their reactivity and solubility. The surface resistance for particulate sulfate is parameterized in terms of stability and friction velocity in the surface layer (Wesely, 1989), based on limited studies that do not include water surfaces. In CMAQ this method only applies to the treatment of surrogate gas-phase representation of sulfate species. Size dependent deposition velocities for particle depositions are estimated inside the CCTM's aerosol module. See Chapter 10 of this document and Binkwoski and Shankar (1995) for details.

The laminar sub-layer resistance (R_b) depends on the landuse specific friction velocity and molecular characteristics of gases. Using the landuse dependent friction velocity or the cell average friction velocity, R_b's for heat (R_{bh}) and trace gases (R_{bx}) are estimated with the Schmidt number (Sc):

$$R_{bh} = \frac{2}{ku_*} Sc^{2/3} \qquad \text{(for heat)} \tag{12-65a}$$

$$R_{bx} = \frac{2}{ku_*} Sc_x^{2/3} \qquad \text{(for trace gas species)} \tag{12-65b}$$

where Schmidt number is defined as the kinematic viscosity of air ($\nu = 0.146\ cm^2 s^{-1}$) divided by molecular diffusivity (i.e., $Sc = \nu / D_g$ for heat and $Sc_x = \nu / D_{gx}$ for trace gases). Here, ν is kinematic viscosity of air; D_g is molecular diffusivity of air (heat); and D_{gx} is molecular diffusivity of trace species. For heat, the molecular thermal diffusivity (D_g) is 0.206 $cm^2 s^{-1}$; for water vapor, molecular diffusivity (D_{gw}) is 0.244 $cm^2 s^{-1}$; and, for ozone molecular diffusivity (D_{gO3}) is 0.159 $cm^2 s^{-1}$ (molecular diffusivities of other chemical species are included in the model).

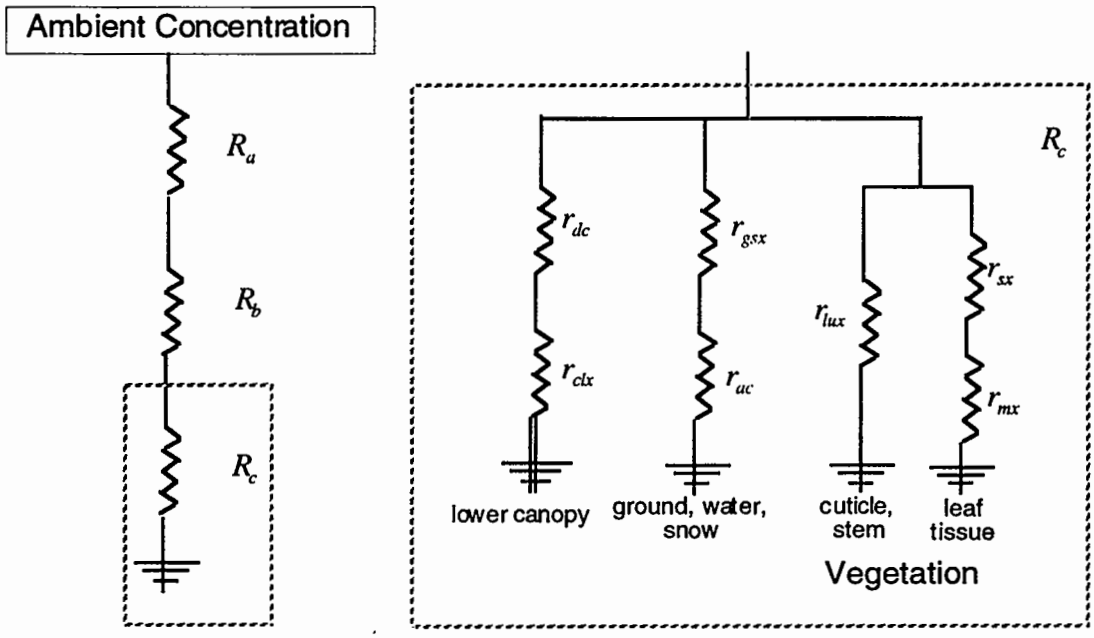

Figure 12-7. Schematic Diagram of Pathway Resistances Used in RADM Dry Deposition Model Resistances with subscript x are for different chemical species.

R_c represents the canopy resistance defined as:

$$R_c = \left(\frac{1}{r_{sx} + r_{mx}} + \frac{1}{r_{lux}} + \frac{1}{r_{dc} + r_{clx}} + \frac{1}{r_{ac} + r_{gsx}} \right)^{-1} \tag{12-66}$$

where r_{sx} = stomatal resistance;
r_{mx} = mesophyl resistance;
r_{lux} = resistance of the outer surface of leaves in the upper canopy;
r_{dc} = resistance for the gas transfer affected by buoyant convection in canopy;
r_{clx} = lower canopy resistance (uptake pathways at the leaves, twig, etc.);
r_{ac} = resistance that depends on the canopy height; and
r_{gsx} = resistance of soil, leaf litter, and other ground materials.

Stomatal resistance for water is obtained using following equation:

$$r_{sw} = r_{s\min} \left(1 + \left[\frac{200}{0.1 + G_{sw}} \right]^2 \right) \left(\frac{400}{T_c(40 - T_c)} \right) \tag{12-67}$$

where r_{sw} = stomatal resistance for water;
$r_{s\min}$ = minimum stomatal resistance for water, specified in Table 12-7;

T_c = surface air temperature in the canopy in Celsius temperature; and
G_{sw} =- solar radiation reaching at the canopy in W/m^2 unit.

Then stomatal resistance for trace gas species is obtained with:

$$r_{sx} = r_{sw} \frac{D_{gw}}{D_{gx}} \tag{12-68}$$

where D_{gw} is the molecular diffusivity of water. Ratio of molecular diffusivity of water to that of each trace species is provided in Table 12-7.

The mesophyl resistance is parameterized as:

$$r_{mx} = \left(\frac{H_{*x}}{3000} + 100 f_{ox} \right)^{-1} \tag{12-69}$$

where H_{*x} is Henry's gas constant (in mole atm^{-1})for the species, and f_{ox} is the reaction intensity factor.

Both the Henry's gas constants and reaction intensity factors are provided in Table 12-7 as well. r_{lux} is related with the upper canopy resistance for water (r_{lu}) which is provided in Table 2 of Wesely (1989) as:

$$r_{lux} = r_{luw} (10^{-5} H_{*x} + f_{ox})^{-1} \tag{12-70}$$

r_{dc} is parameterized in terms of the available solar radiation and the slope of local terrain:

$$r_{dc} = 100[1 + 1000(G_{sw} + 10)^{-1}](1 + 1000\theta)^{-1} \tag{12-71}$$

where θ is the slope of local terrain in radians. r_{clx} and r_{gsx} are estimated based on the respective resistance values for SO_2 and O_3 as follows:

$$r_{clx} = \left(\frac{H_{*x}}{10^5 r_{clS}} + \frac{f_{ox}}{r_{clO}} \right)^{-1} \tag{12-72a}$$

$$r_{gsx} = \left(\frac{H_{*x}}{10^5 r_{gsS}} + \frac{f_{ox}}{r_{gsO}} \right)^{-1} \tag{12-72b}$$

where subscript S and O are for SO_2 and O_3, respectively. All of these values, and r_{uc} (the resistance that depends on the canopy height) are landuse dependent and listed in Table 2 of Wesely (1989).

Table 12-7. Gaseous Species Treated in RADM Dry Deposition Module and Their Properties Relevant to Estimating Resistance Components as Implemented in MCIP (Modified from Wesely, 1989.)

Gaseous species	Symbol	D_{gw} / D_{gx}	H_{*x} (mole atm^{-1})	f_{ox}
Sulfur dioxide	SO_2	1.9	1.0X10^5	0.0
Sulfate	SO_4	-	-	-
Nitrogen dioxide	NO_2	1.6	0.01	0.1
Nitric oxide	NO	1.3	0.002	0.0
Ozone	O_3	1.6	0.01	1.0
Nitric acid vapor	HNO_3	1.9	1.0X10^{14}	0.0
Hydrogen peroxide	H_2O_2	1.4	1.0X10^5	1.0
Acetaldehyde	ALD	1.6	15.0	0.0
Formaldehyde	$HCHO$	1.3	6.0X10^3	0.0
Methyl hydroperoxide	OP	1.6	240.0	0.1
Peroxyacetic acid	PAA	2.0	540.0	0.1
Formic acid	ORA	1.6	4.0X10^6	0.0
Ammonia	NH_3	1.0	2.0X10^4	0.0
Peroxyacetyl nitrate	PAN	2.6	3.6	0.1
Nitrous acid	$HONO$	1.6	1.0X10^5	0.1
Carbon monoxide	CO	1.2	0.001	0.0

12.3.2.2 Models-3/CMAQ Dry Deposition Model

The Models-3/CMAQ dry deposition (M3DDEP) module estimates dry deposition velocities according to the same electrical resistance analog represented by Equation 12-64. M3DDEP uses common components with the new land-surface model that has recently been added to MM5. Specifically, the aerodynamic resistance and the canopy or bulk stomatal resistance are the same as those used in the modified MM5 (MM5PX) for computing evapotranspiration. Since the land surface scheme includes soil moisture and has an indirect nudging scheme for improving soil moisture estimates, the resulting stomatal resistance estimates should be better than those achieved with a stand alone dry deposition model. Pleim and Xiu (1995) give a description of an early prototype of the land surface model which is now coupled to MM5. Pleim et al (1996) and Pleim et al. (1997) briefly describe the dry deposition model and some studies comparing model results to field measurements of surface fluxes and PBL heights. The description which follows here is partially drawn from these sources.

When using the M3DDEP option in the CMAQ system the aerodynamic resistance, as well as the bulk stomatal resistance (r_{stbw}; discussed below) is provided to MCIP from the MM5PX. Note that these parameters are computed as part of the land surface model in the MM5PX and are not available from the standard MM5. In MM5PX the aerodynamic resistance R_a is computed assuming similarity with heat flux such that:

$$R_a = \rho C_p\left(\Theta_g - \Theta_1\right)/H - R_{bh} \tag{12-73}$$

where R_{bh} is the quasi-laminar resistance for heat (defined in Equation 12-65a), Θ_g and Θ_1 are potential temperature of the ground surface and the air, respectively, in the lowest model layer, and H is the sensible heat flux defined in Equation 12-25. If the sensible heat flux is very small (as during transition periods) the surface layer theory for neutral conditions is used as follows:

$$R_a = \frac{\mathrm{Pr}_o}{ku_*}\ln\left(\frac{z_1}{z_o}\right) \quad \text{for } |H/(\rho\, C_p)| < 10^{-15}\ [\mathrm{K\ m\ s^{-1}}] \tag{12-74}$$

where z_1 is the height of model layer 1 and z_o is the roughness length. The heat and momentum fluxes are derived from flux-profile relationships as in the MM5 (see Grell et al., 1995). The quasi-laminar boundary layer resistance accounts for diffusive transfer across a thin laminar layer adjacent to surfaces. Because of the no-slip condition, turbulent eddies cannot penetrate to a surface. Therefore, there exists a thin layer of non-turbulent air where molecular diffusion is the primary mechanism for transfer. While this concept is not relevant for momentum, it is relevant for any quantity that directly interacts with the surface such as heat, moisture, and chemical deposition. Therefore, for these quantities, the addition of a resistance based on molecular diffusion is necessary. Deposition layer resistance varies by the transported quantity because of differences in molecular diffusivity, which is defined earlier in Equations 12-65a and b.

The total surface resistance to dry deposition (R_s) has several components including bulk stomatal resistance (r_{stb}), dry cuticle resistance (r_{cut}), wet cuticle resistance (r_{cw}), ground resistance (r_g), and in-canopy aerodynamic resistance (r_{lc}):

$$R_s = \left[\frac{f_v}{r_{stb}} + LAI\left(\frac{f_v(1-f_w)}{r_{cut}} + \frac{f_v f_w}{r_{cw}}\right) + \frac{1-f_v}{r_g} + \frac{f_v}{r_{lc}+r_g}\right]^{-1} \tag{12-75}$$

Bulk stomatal resistance (r_{stb}), vegetation fractional coverage (f_v), leaf area index (LAI) and fractional leaf area wetness (f_w) are all provided by MM5PX since the same parameters are used in the land surface scheme. Figure 12-8 shows a schematic representation of Equation 12-75. Note that r_{stb}, as output from MM5PX, is already a combination of stomatal resistance on a leaf area basis r_{st}, mesophyl resistance r_m, and LAI as described below. A key component of the land surface model in the MM5PX is the parameterization of the bulk stomatal resistance that is used to compute evapotranspiration. The bulk stomatal resistance for water vapor is read in to MCIP from MM5PX and adjusted for chemical dry deposition in the M3DDEP model by weighting with the ratio of molecular diffusivities for water vapor and the chemical species:

$$r_{stbc} = \frac{D_{gw}}{D_{gx}} r_{stbw}. \tag{12-76}$$

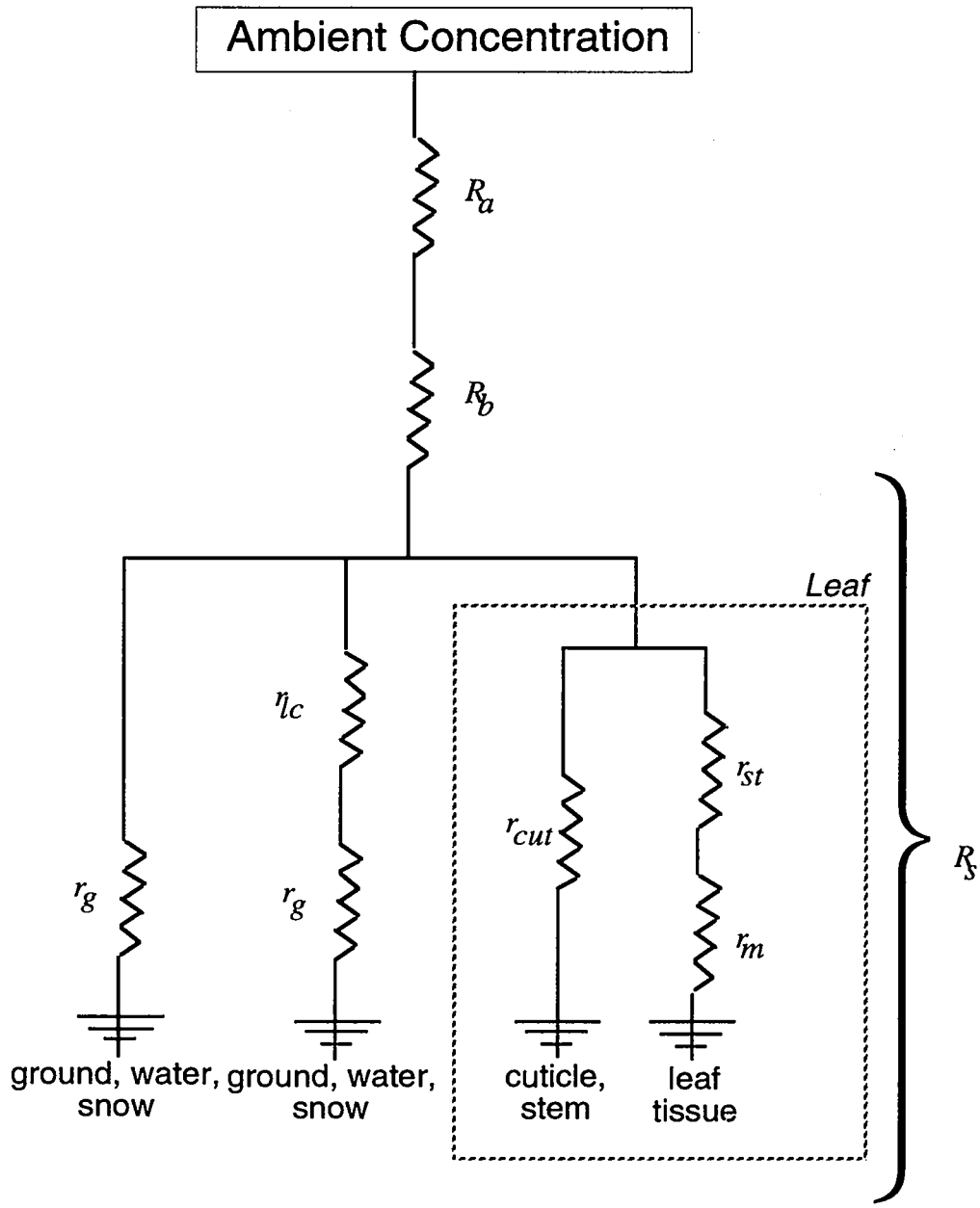

Figure 12-8. Schematic Diagram of Pathway Resistances Used in Models-3/CMAQ Dry Deposition Model.

In general, the bulk stomatal resistance is related to leaf based stomatal resistance as:

$$r_{stb} = \frac{P_s}{LAI}(r_{st} + r_m) \tag{12-77}$$

where P_s is a shelter factor to account for shading in denser canopies. For water vapor and many chemical species, such as O_3 and SO_2, r_m is assumed to be zero, however, for many less soluble

species a non-zero value should be used. The shelter factor is given by: $P_s = 0.3\ LAI + 0.7$ with a minimum of $P_s = 1.0$. Leaf scale stomatal resistance, computed as:

$$r_{st} = \frac{r_{st\,\min}}{F_1(PAR)F_2(w_2)F_3(RH_s)F_4(T_a)} \tag{12-78}$$

depends on four functions of environmental factors which influence stomatal function, and the minimum stomatal resistance ($r_{st\,min}$) which depends on vegetative species. The minimum stomatal resistance is a bulk parameter which reflects the maximum conductance of a leaf per unit area under unstressed conditions (well watered, full sunlight, and optimal temperature and humidity). This parameter is specified in the model according to vegetation type. The key to the model's ability to simulate stomatal conductance in real world conditions is the four environmental stress functions, $F_{1\text{-}4}$ in Equation 12-78. This kind of stomatal model, with independent empirical stress functions, is often called a Jarvis-type model after Jarvis (1976). Specifically, the land surface model in MM5PX is based on Noilhan and Planton (1989) (hereafter referred to as NP89) with many subsequent modifications. The radiation stress function is:

$$F_1 = \frac{1+f}{f + r_{st\,\min}/r_{st\,\max}} \tag{12-79}$$

with $f = 0.55\dfrac{2R_G}{R_{GL}}$ where $r_{st\,max}$ is maximum stomatal resistance which is an arbitrarily large number (5000 s/m), R_G is solar radiation at the surface and the 0.55 factor is an approximation for the photosynthetically active portion, and R_{GL} is a limit value of 30 W/m^2 for forest and 100 W/m^2 for crops according to NP89. The only difference from the F_1 in NP89 is that the dependence on LAI has been removed since the effects of leaf shading within the canopy are now accounted for by the shelter factor in Equation 12-77. Therefore, the F_1 as defined here represents the effects of sunlight on an individual leaf rather than the integrated effect on a canopy. The functions of root zone soil moisture and air temperature (F_2 and F_4) were modified to follow the form of logistic curves as suggested by Avissar et al. (1985). Logistic curves are "S"-shaped and therefore good for representing a smooth transition from one state to another. Also, logistic curves can be defined with varying degrees of abruptness, from an almost linear transition to an almost threshold behavior, and can be altered while maintaining differentiability. The function of root zone soil moisture (w_2) is:

$$F_2 = 1/\left(1 + \exp\left[-5.0\left(w_{af} + b_w\right)\right]\right) \tag{12-80}$$

where the available soil moisture fraction is:

$$w_{af} = \frac{w_2 - w_{wlt}}{w_{fc} - w_{wlt}}$$

and the half point of the function (where $F_2 = 0.5$) is:

$$b_w = \left(w_{fc} - w_{wlt}\right)/3 + w_{wlt}$$

where w_{wlt} is the wilting point and w_{fc} is the field capacity. All soil moisture values (w) are in volumetric fraction. In many previous models, including NP89, Jacquemin and Noilhan (1990), Wetzel and Chang (1988), Mihailocic et al. (1993), Sellers et al. (1986), and Avissar et al (1985), the function of air humidity (F_3) is expressed in terms of vapor pressure deficit between the inside of the leaf, assumed to be saturated at leaf temperature, and ambient air humidity ($vpd = e_s(T_s)-e_a$). However, recent advances in plant physiology research have led to a new generation of stomatal models based on leaf photosynthesis (Sellers et al., 1997) in which stomatal conductance ($g_{st} = 1/r_{st}$) is a linear function of relative humidity at the leaf surface (Collatz et al., 1991):

$$g_{st} = g'_{st} RH_s + b \qquad (12\text{-}81)$$

where g'_{st} is the stomatal conductance at $RH_s = 1$ and b is the minimum stomatal conductance at $RH_s = 0$. Clearly, it makes more sense that stomata react to the humidity at the surface of the leaf rather than the ambient air humidity at some height above the canopy. Although, a physical mechanism for this linear relationship to leaf surface RH has not been determined, experimental data shows it to be a very good fit (Ball et al., 1987). Since leaf surface relative humidity is neither an easily measured nor a modeled quantity, it must be computed from other parameters. According to the electrical analog, the humidity at the leaf surface (q_l) is an intermediate potential between the ambient air humidity (q_a) and the leaf interior humidity, $q_s(T_s)$, where T_s is surface temperature and q_s is saturation humidity (see Figure 12-9 for the schematics of the derivation). Assuming constant flux from the ambient air to the leaf interior, the relative humidity at the leaf surface ($RH_s = q_l/q_s(T_s)$) can be represented as:

$$RH_s = \frac{q_a g_a + q_s g_{st}}{(g_{st} + g_a) q_s} \qquad (12\text{-}82)$$

where g_a is the air conductance ($1/(R_a+R_{bw})$) and q_s is short hand for $q_s(T_s)$. If we assume that b in Equation 12-81 is small compared to g_{st}, which will be true in all but the driest conditions, and g'_{st} is the result of Equation 12-78 without the effects of humidity ($g'_{st} = F_3/r_{st}$), then RH_s is the solution of a quadratic equation which can be computed, once all the other components of Equation 12-78 have been determined. F_3 is equal to RH_s but with a minimum imposed at 0.25.

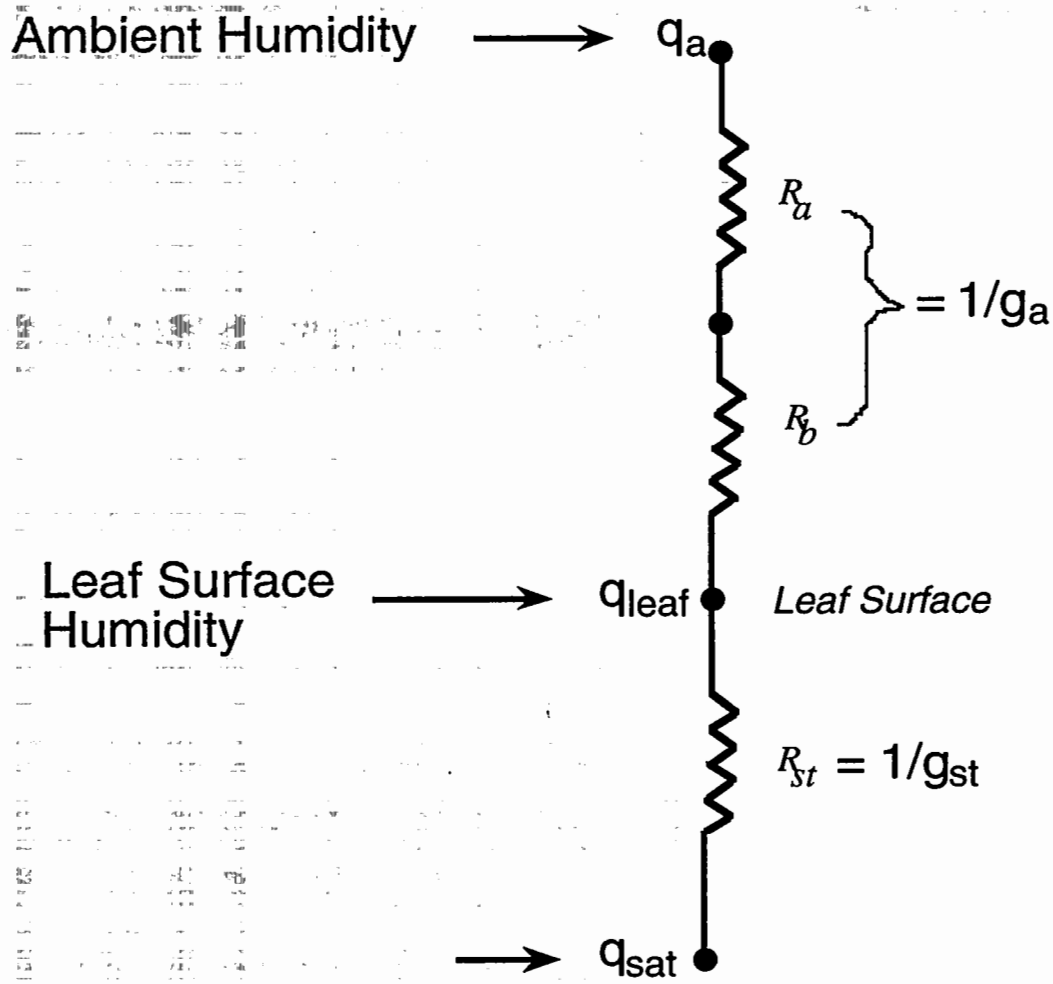

Figure 12-9. Derivation of Leaf Surface Relative Humidity

The fourth environmental stress function (F_4) is related to ambient temperature. Again, we deviate from the NP89 formulation which used a quadratic function peaking at the optimal temperature of 298 K. Instead, we followed the method of Avissar et al. (1985) which results in a function with a plateau over a range of optimal temperatures, the idea being that temperature (T_a) inhibits stomatal function only at extremes of heat or cold. F_4 is defined as:

$$F_4 = 1/\left(1 + \exp\left[a_T\left(T_a - b_T\right)\right]\right) \qquad (12\text{-}83)$$

where a_T = -0.41 and b_T = 282.05 K for $T_a \leq 302.15$ K and a_T =1.18 and b_T = 314 K for $T_a >$ 302.15 K. Note that the high side of the function extends into higher temperatures than suggested by Avissar et al. (1985) who used a b_T = 307.95. The current function is very similar to the function used by Rochette et al. (1991) and is close to the high side of the NP89 F_4 function.

Resistances for all of the non-stomatal dry deposition pathways in the M3DDEP module of MCIP are similar to the dry deposition model developed for the Acid Deposition and Oxidant Model

(ADOM) by Pleim et al. (1984) and later evaluated and modified by Padro et al. (1991). As in ADOM, surface resistances to ground and leaf cuticles are scaled relative to the most well measured chemical species such as SO_2 and O_3. The term used for the scaling factor: *relative reactivity* has caused considerable confusion since many users try to find a chemical definition for this parameter. This factor has no chemical definition but is simply meant to be a relative scaling factor for the removal rate of different species at the ground or cuticle surfaces. It is assumed that the relative propensity to deposit to different surfaces is similar, so that the same scaling factor can be used for ground and cuticles:

$$r_g = r_{go} A_o/A \tag{12-84a}$$

$$r_{cut} = r_{cuto} A_o/A \tag{12-84b}$$

where r_{go} *and* r_{cuto} are the ground and cuticle resistances, respectively, for the reference chemical species (usually SO_2 or O_3) and A_o and A are the relative reactivities for the reference species and the modeled species, respectively.

One improvement from the original ADOM model is the inclusion of an in-canopy aerodynamic resistance which is added in series to the ground resistance for the vegetated portion of the modeled area (f_v) according to Erissman et al. (1994):

$$r_{lc} = 14\ LAI\ h_c / u_* \tag{12-85}$$

where h_c is the height of the canopy. For wet or partially wet canopies (f_w), the surface resistance to wet cuticle is estimated as:

$$r_{cw} = r_{cwo} K_H / \alpha^* \tag{12-86}$$

where K_H is the nondimensional Henry's law constant and α^* is an aqueous dissociation factor. The empirical factor (r_{cwo}) is set to 2.4×10^8 s m^{-1}, which is similar to Wesely (1989). For O_3, r_{cw} is set to 1250 s m^{-1} based on field measurements. The *pH* of the canopy water can be specified to compute α^* for species such as SO_2 and NH_3 which readily dissociate. The canopy wetness fraction (f_w) is provided by the surface model in MM5PX. For deposition to open water, the ground resistance is replaced by a water surface resistance according to Slinn et al. (1978):

$$r_{gw} = K_H /(4.8e\text{-}4\ \alpha^*\ u_*) \tag{12-87}$$

The parameters needed for the non-stomatal part of this model are quite uncertain for many chemical species. Our latest estimation of these parameters for the species in the RADM2 chemical mechanism for which dry deposition is considered to be an important process are presented in Table 12-8. The Henry's law coefficients in Table 12-8 are in non-dimensional form as the ratio of gas- to aqueous-phase.

Molecular diffusivity and Henry's law have the least amount of uncertainty since these have definite chemical definitions and can be experimentally determined. Relative reactivity, however,

is less well defined and is estimated according to experimental and modeling studies in the published literature . The only organic species for which dry deposition is considered significant are the aldehydes, peroxides, and acids, all of which are soluble in water. For these organic lumped species the numbers for reactivity are merely educated guesses.

Table 12-8. Chemical Dependent Parameters for M3DDEP

Species	*Diff (cm2/s)*	*α^* (dimensionless)*	*Reactivity (dimensionless)*	*Henry's law[&] (K_H) (dimensionless)*
SO_2	0.1509	1000.0	8.00	0.04
NO_2	0.1656	1.0	2.00[@]	3.5
O_3	0.1594	10.0	16[@]	2.0
H_2O_2	0.2402	1.0	30[@]	4.e-7
HNO_3	0.1628	1.0e9	800[@]	2.7e-7
NH_3	0.2626	1.0e5	10.0	6.6e-4
PAN	0.0938[#]	1.0	4.0	0.01
NO	0.1877[#]	1.0	2.0[+]	23.
HCHO	0.1877[#]	1.0	10.0[+]	4.E-6
ALD	0.1525[#]	1.0	10.0[+]	2.7e-3[#]
OP	0.1525[#]	1.0	10.0[+]	1.7e-4[#]
PAA	0.1220[#]	1.0	20.0[+]	7.6e-5[#]
ORA	0.1525[#]	1.0	20.0[+]	1.0e-8[#]
HONO	0.1525[#]	1.0	20.0[+]	4.1e-7[#]
CO	0.2033[#]	1.0	5.0	40.

[@] Updates based on literature review
[#] Diff and H based on Wesely (1989) same as RADM
[+] Estimated
[&] gaseous phase value/aqueous phase value

The dissociation factor (α^*) is simply defined as the ratio of the effective Henry's law coefficient to the actual Henry's law coefficient. In this case, the effective coefficient is meant to include both aqueous dissociation and aqueous reactions. The α^*s for SO_2 and NH_3 are particularly important since their solubilities are greatly effected by dissociation, which is a strong function of *pH* for both species. Therefore, the model enables the user to specify the *pH* of the rainwater wetting the canopy and let the model compute α^* rather than use the default values in Table 12-7. The α^* for O_3 is also important since O_3 is only slightly soluble so any enhancement can have a large effect. The value of 10 for O_3 is meant to account for, very approximately, aqueous reactions such as the oxidation of *S(IV)* to *S(VI)*. Clearly, all of these parameters are quite uncertain and subject to revision.

The main advantage of the M3DDEP model over the many similar models previously used in air quality modeling is the coupling to the land surface model for description of the stomatal pathway. This is a very important feature for certain chemical species, particularly O_3 and SO_2, which have

been shown experimentally to have a strong stomatal pathway components. Several studies with this model have demonstrated its ability to realistically simulate both latent heat flux, with a large fraction from evapotranspiration, and ozone dry deposition, over corn and soybeans (Pleim et al., 1996; Pleim et al., 1997). These studies are continuing and are being extended to other chemical species (SO_2), and land-use types (deciduous and coniferous forests).

12.3.3 Cloud Parameters and Solar Radiation

Cloud information is developed and used in many different ways throughout the Models-3 CMAQ system. For example, MM5 includes parameterizations related with subgrid convective clouds, grid resolved cloud water and microphysics, and cloud effects on radiation. The CCTM needs cloud information for photolysis, convective transport, and aqueous chemistry. Therefore, MCIP has an important role in providing cloud information to CTMs by either propagating information from upstream processors (MM5) or by parameterization.

MCIP has multiple cloud parameterizations and functions depending on the options selected. There are currently two main options related to MM5 runs, either the standard MM5 version 2.6 which does not include cloud cover and radiation parameters in its output, and MM5PX which does. Later versions of MM5 (2.7, 2.8, and 2.9) also output these additional parameters. However, when MM5v2.6 or earlier versions are used, it is necessary to compute these parameters in MCIP. Incident solar radiation at the surface is an important output from MCIP since it is used to estimate biogenic emissions in the emissions processor.

Another cloud function in MCIP is to diagnose cloud information (such as cloud top, cloud base, liquid water content, and cloud coverage) which is passed to the CCTM to adjust actinic fluxes for computation of photolysis rates. This function is executed regardless of the choice of the MM5 version used. In addition, grid resolved cloud water and rain water are propagated through MCIP from the MM5 output to CMAQ for use in aqueous chemistry and for photolysis calculations at the 4 km grid resolution.

12.3.3.1 Cloud Coverage

The fractional cloud coverage scheme currently used in MCIP is the same as used in MM5PX and similar to the scheme used in the standard MM5. Cloud cover fraction (f_c^k) above the boundary layer is computed at each vertical model level k, according to Geleyn et al. (1982), as:

$$f_c^k = \left[\frac{RH^k - RH_c}{1 - RH_c} \right]^2 \qquad (12\text{-}88)$$

where RH_c is the critical relative humidity defined as a function of σ as:

$$RH_c = 1 - 2\sigma_c(1 - \sigma_c)[1 + 1.732(\sigma_c - 0.5)]$$

where $\sigma_c = p^k / p^{k_{PBL}}$.

We have modified the Geleyn scheme to avoid the overprediction of clouds in well-mixed boundary layers. Within the convective boundary layer (CBL) when $RH > RH_c$ the cloud cover is estimate by:

$$f_c^k = 0.34 \frac{RH^k - RH_c}{1 - RH_c} \tag{12-89}$$

where the critical relative humidity (RH_c) within the CBL is set to be 0.98. The factor 0.34 is from the suggestion that convective mixing induced clouds within the CBL should not exceed the fractional area of the updrafts at top of CBL, which large eddy simulations estimate to be about 34% (Schumann, 1989; Wyngaard and Brost, 1984) when inactive clouds are disregarded. The resulting layered cloud fractions, from Equations 12-88 and 12-89, are used for both functions; namely, to be used in the surface radiation calculation when these parameters are not read from MM5, and to derive the cloud parameters needed for the photolysis calculations.

For the surface radiation calculation, the layered cloud cover fractions are aggregated into the same three broad vertical cloud layers (low, middle, and high) as in MM5, assuming maximum overlap. Each layer is defined by pressure such that the low layer is between 97 and 80 kPa, the middle layer is between 80 and 45 kPa and the high layer is above 45 kPa. These three cloud layer fractions are then used in the radiation calculation described in this section (12.3.3.2).

The photolysis model requires cloud information in a different form. For the sake of consistency, these parameters are estimated from the same layer resolved fractional coverage described above (Equations 12-88 and 12-89). The photolysis model assumes a single uniform, vertically mixed cloud layer. Therefore, the required parameters are; cloud top, cloud base, cloud fractional coverage, and average liquid water content. Cloud top and base layers (k_{top} and k_{base}) are determined by looking up and down from level of maximum coverage to where the fractional coverage first becomes 50% of the maximum. The layer average cloud cover is then computed from the volume averaging of layer cloud fractions between k_{top} and k_{base}:

$$f_c^{Tot} = \sum_{k_{base}}^{k_{top}} f_c^k \Delta z_F^k \Big/ \sum_{k_{base}}^{k_{top}} \Delta z_F^k \tag{12-90}$$

Once the base, top, and fraction of the cloud layer are determined, the average liquid water content of the cloud is computed assuming convective characteristics as described by Walcek and Taylor (1986), Chang et al. (1987), and Chang et al. (1990). The lifted condensation level is assumed to be at the cloud base, defined as the bottom boundary of cloud layer k_{base}, where the air is saturated at the model's ambient temperature. The in-cloud liquid water profile (q_c) is then computed as a fraction of the adiabatic liquid water profile (q_{ad}):

$$q_c = \alpha q_{ad} \tag{12-91}$$

where $\alpha = 0.7\exp\left[\left(p - p_{lcl}\right)/8\right] + 0.2$ and p_{lcl} is the pressure (in KPa) at the lifting condensation level according to Warner (1970). The layer liquid cloud water values are then vertically averaged in the same way as fractional coverage (Equation 12-90).

12.3.3.2 Computation of Solar Radiation Components

To meet air quality modeling needs, MCIP outputs several parameters related with radiation at the surface including: incident surface shortwave radiation (R_{grnd}), absorbed surface shortwave radiation (G_{sw}), net long wave radiation at the ground (G_{lw}), total net radiation at the ground (R_{net}), and surface albedo (A). These radiation components are used in several CMAQ processors. For example, photosynthetically active radiation (PAR), which is needed for the biogenic emissions processing, is estimated with $PAR = 0.55R_{grnd}$. Depending on which version of MM5 is used, surface radiation parameters are either passed through from MM5 or computed in MCIP. The computation of surface radiation parameters in MCIP is identical to the surface radiation option in MM5, as described in Grell et al. (1995), except that the dependence on zenith angle is added to the land use specified albedo (A_{lu}) such that:

$$A = A_{lu} + 0.1\left[\exp\left(0.00386Z^{3/2}\right) - 1.0\right] \qquad (12\text{-}92)$$

where Z is zenith angle in degrees.

Note that MCIP computations of surface radiation parameters, which essentially replicate MM5, are a stop gap measure for use with MM5v2.6 which does not output these values. All later versions of MM5 do output these parameters which will be read and passed through by MCIP as is now done for the MM5PX option. It will be preferable in future applications of Models-3 to directly propagate the radiation parameters from MM5 to CMAQ so that the more sophisticated radiation models now available in MM5 can be used. The currently used surface radiation option includes effects of clouds, aerosols, and water vapor on radiation but neglects radiation effects on the atmosphere. Therefore, many future applications may utilize either the Dudhia radiation scheme (Dudhia, 1989) or the CCM2 scheme (Hack et al., 1993) which include atmospheric radiation effects. See Chapter 3, section 3.3.4.1, for description of MM5 radiation options.

12.4 Meteorological Data for CCTM with Generalized Coordinate System

One feature of the CMAQ system that is distinct from other Eulerian air quality modeling systems is its ability to incorporate meteorological models with various different coordinates and dynamics. This functionality is achieved by recasting meteorological parameters in terms of the variables used in the governing set of equations for the fully compressible atmosphere in generalized coordinate system (Byun, 1999a). Key dynamic and thermodynamic parameters are estimated for the given coordinates in such a way to ensure consistencies among the meteorological data. The consistency can be maintained throughout CCTM simulations when appropriate temporal interpolation methods are used.

12.4.1 Thermodynamic Variables: Pressure, Density and Entropy

To facilitate mass-consistent interpolation among the thermodynamic variables, the governing set of equations for the fully compressible atmosphere is used in the CMAQ system. The system includes prognostic equations for entropy and air density as suggested by Ooyama (1990). The algorithms used for estimating the thermodynamic parameters are presented below. For a detailed discussion on the governing set of equations and mass-consistent interpolation algorithm, refer to Byun (1999a and b).

12.4.1.1 Pressure, Density of Air and Density of Water Vapor

Like most of the other meteorological models, MM5 does not use a predictive equation for air density. Instead, air density is estimated with the equation of state using predicted pressure and temperature. For a terrain-influenced pressure coordinate, when it is applied for hydrostatic atmosphere, the hydrostatic pressure ($\tilde{p}$) can be computed with $\tilde{p}^*$ available from MM5.

$$p = \tilde{p} = p_T + \sigma_{\tilde{p}} \tilde{p}^* \tag{12-93}$$

The total pressure (p) in the terrain-influenced reference pressure coordinate (applied for a nonhydrostatic atmosphere in MM5) is the sum of the reference pressure and perturbation pressure:

$$p = p_o + p_p = \sigma p_o^* + p_T + p_p \tag{12-94}$$

Once p is known, virtual temperature (T_v) and density of the (moist) air are computed with:

$$T_v = \frac{T}{1 + (\frac{m_w}{m_d} - 1)\frac{p_w}{p}}, \tag{12-95}$$

where m_w and m_d are the molecular weights of water vapor and dry air, respectively , and

$$\rho = \frac{p}{R_d T_v}. \tag{12-96}$$

The water vapor partial pressure (p_v) can be found from the vapor mixing ratio (r) supplied by MM5 using the following equation:

$$p_v = r\frac{R_v}{R_d}p_d. \tag{12-97}$$

Then, the density of water vapor is simply given as:

$$\rho_v = \frac{r}{1+r}\rho. \tag{12-98}$$

12.4.1.2 Entropy

In the CMAQ system, entropy is treated as one of the key thermodynamic parameters. Because its conservation equation follows similar continuity equation for air density, entropy can be interpolated using the same interpolation scheme as air density. Then, we can reconstruct temperature and pressure for the intermediate time steps from the interpolated densities (for air and water) and entropy. This type of interpolation will maintain mass consistency among the thermodynamic variables for air quality applications. Using the density of moist air and density of water vapor obtained above, the entropy for moist air can be computed with:

$$\zeta = (\rho_d C_{vd} + \rho_v C_{vv})\ln(\frac{T}{T_{oo}}) + \rho_v \Lambda_{oo} - \rho_d R_d \ln(\frac{\rho_d}{\rho_{doo}}) - \rho_v R_v \ln(\frac{\rho_v}{\rho_{v*o}}), \tag{12-99}$$

where $\rho_d = \rho - \rho_v$, p_{oo}=10^5 Pascal, Λ_{oo} is the specific entropy of saturated vapor, $\rho_{d_{oo}}$ is the density of reference dry air, and ρ_{v*o} is the density of reference state water vapor saturated over water at reference temperature T_{oo}, 273.15 K. The integral constants are computed following Ooyama (1990):

$$\rho_{d_{oo}} = \frac{p_{oo}}{R_d T_{oo}} \tag{12-100}$$

$$\Lambda_{oo} = \Lambda(T_{oo}) = R_v T_{oo} \left.\frac{d\ln E(T_c)}{dT_c}\right|_{T_{oo}} \tag{12-101}$$

$$\rho_{v*o} = \rho_{v*}(T_{oo}) = \left.\frac{E(T_c)}{R_v T}\right|_{T_{oo}}, \tag{12-102}$$

where $T_c = T - 273.15$.

For the basic formulation of the saturation vapor pressure approximation, we use the AERK formula recommended by Alduchov and Eskridge (1996):

$$E(T_c) = ae^{bT_c/(c+T_c)} \tag{12-103a}$$

$$\frac{d\ln E(T_c)}{dT_c} = \frac{bc}{(c+T_c)^2}, \tag{12-103b}$$

where a=610.94, b=17.625, c=243.04 and $E(T_c)$ is in Pascal. With this information we can evaluate the integration constants, and thus the entropy using Equation 12-99.

12.4.2 Vertical Jacobian and Layer Height

In the CCTM, Jacobian is used for the definition of vertical and horizontal coordinates/grid system at every model synchronization time step. The Jacobian characterizes the coordinate transformation and is treated as one of the fundamental parameters defining grid structure of the CTM. Depending on the horizontal map projections and vertical coordinates, the physical characteristics of the Jacobian change.

12.4.2.1 Jacobian for Coordinate Transformation

The vertical Jacobian defines the coordinate transformation rules. For a vertical coordinate $\hat{x}^3 = \xi$, where ξ is a monotonically increasing function of height, the Jacobian is related with the geopotential height, $\Phi = gz$, as:

$$J_\xi = \frac{1}{g}\left|\frac{\partial\Phi}{\partial\xi}\right| = \frac{1}{g}\frac{\partial\Phi}{\partial\xi} \tag{12-104}$$

Sigma-$\tilde{p}$, time dependent coordinate

For hydrostatic application of MM5, the vertical coordinate is the same as the terrain-influenced sigma-$\tilde{p}$ coordinate, whose vertical Jacobian is defined as

$$J_{\sigma_p} = \frac{\tilde{p}^*(x,y,t)}{\tilde{\rho}g} \tag{12-105}$$

Note that Equations 12-3 and 12-105 are identical although CMAQ uses monotonically increasing coordinate ξ and MM5 uses monotonically decreasing sigma-$\tilde{p}$ coordinate.

Using the Equation of State and the definition of the sigma-$\tilde{p}$ coordinate, the vertical Jacobian can be obtained using the temperature and surface pressure from MM5.

Jacobian at half sigma-level is estimated for $1 \le k \le K$ with:

$$\left(J_{\sigma_p}\right)_H^k = \frac{R_{air}\tilde{p}^* \bullet T_{vH}^k}{g(\sigma_H^k\tilde{p}^* + p_T)}, \tag{12-106}$$

where K is the number of model layer (i.e., *NLAYS* in Models-3 I/O API), and Jacobian at full sigma-level is computed for $1 \le k \le K$-1 with:

$$\left(J_{\sigma_{\tilde{p}}}\right)_F^{k+1/2} = \frac{R_{air}\tilde{p}^* \bullet (T_{vH}^{k+1} + T_{vH}^{k})}{2g(\sigma_F^{k+1/2}\tilde{p}^* + p_T)} \tag{12-107}$$

and, at the surface (k=1/2) with:

$$\left(J_{\sigma_{\tilde{p}}}\right)_F^{k=1/2} = \frac{R_{air}\tilde{p}^* \bullet T_{vs}}{g(\sigma_F^{k=1/2}\tilde{p}^* + p_T)}, \tag{12-108}$$

where we have used T_{vs} to represent the virtual air temperature at the surface.

For the thirty layer MM5 sigma-$\tilde{p}$ coordinate, whose sigma value for the top of first layer is set 0.995 (i.e., about 38 m in the standard atmosphere), the reference temperature is estimated from the average between the skin temperature (T_g) and air temperature at the lowest model layer. The virtual air temperature at the surface is computed with the assumption that the relative humidity at the surface is the same as the relative humidity at the middle of first layer.

Time independent coordinate

For the nonhydrostatic application of MM5, we use the terrain-following sigma-p_o coordinate whose vertical Jacobian is defined as:

$$J_{\sigma_{p_o}} = \frac{p_o^*(x,y)}{\rho_o g} \tag{12-109}$$

Again, Equations 12-6 and 12-109 are identical although CMAQ uses monotonically increasing coordinate ξ and MM5 uses monotonically decreasing coordinate. Using the Equation of State for the reference hydrostatic atmosphere and the definition of the sigma-p_o coordinate, the vertical Jacobian can be obtained using the temperature and surface pressure from MM5. Jacobian at half σ-height is estimated for $1 \le k \le K$ with:

$$\left(J_{\sigma_{p_o}}\right)_H^k = \frac{R_{air}p_o^* \bullet \left[T_{os} + A\ln(\frac{\sigma_H^k p_o^* + p_T}{p_{oo}})\right]}{g(\sigma_H^k p_o^* + p_T)} \tag{12-110}$$

and Jacobian at full σ-height is computed for $0 \le k \le K$ with:

$$\left(J_{\sigma_{p_o}}\right)_F^{k+1/2} = \frac{R_{air}p_o^* \bullet \left[T_{os} + A\ln(\frac{\sigma_F^{k+1/2} p_o^* + p_T}{p_{oo}})\right]}{g(\sigma_F^{k+1/2} p_o^* + p_{oT})} \tag{12-111}$$

The Jacobian does not depend on MM5 data except for the topographic height and sigma-layer definition.

Total Jacobian

The total Jacobian ($\sqrt{\hat{\gamma}} \equiv J_\xi / m^2$) is used in the governing equations for the CCTM. The trace species concentrations are coupled with the total Jacobian. Because of the need to couple with both the trace species concentrations (defined at the layer middle) and vertical flux variables (defined at the layer interface), total Jacobians at the half and full level values are stored in the MET_CRO_3D file. The total Jacobian at the surface, $\left(J_{\sigma_p}\right)_F^{k=1/2}$ divided by the map scale factor squared, is stored in the MET_CRO_2D file. For hydrostatic applications of MM5 the Jacobian varies with time and for nonhydrostatic applications it is constant with time. Although we could have saved some file space by distinguishing this feature, the Jacobians are stored in MET_CRO_3D and MET_CRO_2D files to maintain the compatibility of data structure for both time-dependent and time-independent coordinate systems.

For use in the mass-conserving temporal interpolation, Jacobian weighted densities at the half-levels defined for $1 \le k \le K$ as:

$$(J_\xi \rho / m^2)_H^k = (J_\xi / m^2)_H^k \bullet (\rho)_H^k \qquad (12\text{-}112a)$$

$$(J_\xi \rho_v / m^2)_H^k = (J_\xi / m^2)_H^k \bullet (\rho_v)_H^k \qquad (12\text{-}112b)$$

are stored in the MET_CRO_3D file. Like density, the Jacobian weighted entropy at the layer middle is obtained for $1 \le k \le K$ with:

$$(J_\xi \zeta / m^2)_H^k = (J_\xi / m^2)_H^k \bullet (\zeta)_H^k \qquad (12\text{-}113)$$

They are stored in the MET_CRO_3D file as the Jacobian-weighted total air density and water vapor density, and entropy, respectively.

12.4.2.2 Layer Heights

In CMAQ, layer heights are computed using the basic definition of the geopotential height in terms of Jacobian instead of relying on the coordinate-specific analytic equations, such as a hypsometric equation for a hydrostatic coordinate. The height above mean sea level (MSL) is defined in terms of the vertical Jacobian as:

$$\hat{z} = \Phi / g = \hat{z}_s + \int_{\xi_s}^{\xi} J_\xi d\xi' \qquad (12\text{-}114)$$

The layer heights at the interface and middle of the layers above the ground level (AGL) are computed with:

$$z_F^{k+1/2} = \hat{z}_F^{k+1/2} - \hat{z}_s = \int_{\xi_s}^{\xi_F^{k+1/2}} J_\xi d\xi' \cong \sum_{j=1}^{k} J_{\xi H}^{j}(\xi_F^{j+1/2} - \xi_F^{j-1/2}) \tag{12-115a}$$

for $1 \le k \le K+1$, where

$$z_F^{k+1/2}\Big|_{k=0} = 0 \tag{12-115b}$$

and for $2 \le k \le K$ with:

$$z_H^k = \hat{z}^k - \hat{z}_s = \int_{\xi_s}^{\xi_H^k} J_\xi d\xi'$$

$$\cong z_H^1 + \sum_{j=2}^{k} \frac{1}{2}(J_{\xi H}^{j} + J_{\xi H}^{j-1})(\xi_H^j - \xi_H^{j-1}) \tag{12-116a}$$

where

$$z_H^1 = \frac{1}{2}(J_{\xi H}^{1} + J_{\xi F}^{1/2})(\xi_H^1 - \xi_F^{1/2}) \tag{12-116b}$$

Note that both $z_F^{k+1/2}$ and z_H^k are stored either in the GRID_CRO_3D file for the time independent vertical coordinate, or in the file MET_CRO_3D for time dependent one. Because $z_F^{k+1/2}\Big|_{k=0}$ is always zero for the terrain-influenced coordinates, it is not stored in any of MCIP files.

12.4.3 Contravariant Velocity Components

The generalized CCTM requires a set of contravariant velocity components to simulate numerical advection. Contravariant velocity components are scaled components of the wind vectors for the transformed coordinates. When the true velocity components (i.e., wind components for earth-tangential coordinates) are predicted in a meteorological model, they need to be transformed accordingly.

12.4.3.1 Horizontal Wind Components

MM5 predicts horizontal wind velocity components defined on the spherical earth in the coupled form with the surface pressure scale p^*. First, we need to de-couple the surface pressure scale as follows:

$$U^{l+1/2,m+1/2} = (p^* U)^{l+1/2,m+1/2} / (p^*)^{l+1/2,m+1/2} \tag{12-117a}$$

$$V^{l+1/2,m+1/2} = (p^* V)^{l+1/2,m+1/2} / (p^*)^{l+1/2,m+1/2} \tag{12-117b}$$

for $0 \le l \le L$ and $0 \le m \le M$, where L is the number of columns and M is the number of rows for the rectangular modeling domain. In the expression, p^* represents either $\tilde{p}^*$ or p_o^* depending on the hydrostatic/nonhydrostatic option in MM5. The value p^* at the dot-point is approximated with:

$$(p^*)^{l+1/2,m+1/2} = \frac{1}{4}[(p^*)^{l,m} + (p^*)^{l+1,m} + (p^*)^{l+1,m+1} + (p^*)^{l,m+1}] \tag{12-118}$$

The next step is to compute the contravariant components $u_\xi = mU$ and $v_\xi = mV$ at the dot-point:

$$(u_\xi)^{l+1/2,m+1/2} = m^{l+1/2,m+1/2} U^{l+1/2,m+1/2} \tag{12-119a}$$

$$(v_\xi)^{l+1/2,m+1/2} = m^{l+1/2,m+1/2} V^{l+1/2,m+1/2} \tag{12-119b}$$

Because the Jacobian-mass weighted contravariant wind components are needed for the mass consistent interpolation, we estimate these quantities at the square-point (flux point) for $\hat{x}^1$-direction and at the triangle-point (flux point) for $\hat{x}^2$-direction, respectively:

$$(\frac{\rho J_\xi}{m^2} u_\xi)^{l+1/2,m+1} \cong \frac{1}{4}[(\frac{\rho J_\xi}{m^2})^{l,m+1} + (\frac{\rho J_\xi}{m^2})^{l+1,m+1}][(u_\xi)^{l+1/2,m+1/2} + (u_\xi)^{l+1/2,m+3/2}] \tag{12-120a}$$

$$(\frac{\rho J_\xi}{m^2} v_\xi)^{l+1,m+1/2} \cong \frac{1}{4}[(\frac{\rho J_\xi}{m^2})^{l+1,m} + (\frac{\rho J_\xi}{m^2})^{l+1,m+1}][(v_\xi)^{l+1/2,m+1/2} + (v_\xi)^{l+3/2,m+1/2}] \tag{12-120b}$$

Both of these parameters, together with the contravariant wind components u_ξ and v_ξ at the DOT points, are stored in the MET_DOT_3D file.

12.4.3.2 Vertical Wind Component

In most meteorological models with terrain-influenced coordinates, the contravariant vertical velocity components are not computed directly because of the complex representation of the divergence term in the generalized coordinate system. In the generalized coordinate system, the prognostic equation for the vertical component contains Christoffel-symbols-of-the-second-type terms that make the equation not only complicated but also make conservation of momentum or kinetic energy difficult (Byun, 1999a). To circumvent this difficulty, some meteorological models use the prognostic equations of motion for the true vertical wind component.

For the MM5 hydrostatic application, the terrain-influenced hydrostatic pressure coordinate allows diagnostic computation of the contravariant vertical velocity. The continuity equation for air density becomes a diagnostic equation for this application. Here, the expressions are written with the normalized vertical coordinate, which increases with geometric height, $\xi \equiv 1 - \sigma_{\tilde{p}}$. By selecting the integration limits as $\xi = 0$ to 1, (i.e., $\sigma_{\tilde{p}s} = 1$ to $\sigma_{\tilde{p}T} = 0$) and using the boundary conditions at the top and bottom $\dot{\xi} = \hat{v}^3 = 0$, the tendency term can be computed with:

$$\frac{\partial(\rho J_\xi)}{\partial t} = \frac{\partial \tilde{p}^*}{\partial t} = \int_0^1 [\tilde{p}^* \frac{Q_\rho}{\rho} - m^2 \nabla_\xi \bullet \frac{\tilde{p}^* \hat{\mathbf{V}}_\xi}{m^2}]\, d\xi \tag{12-121}$$

This equation predicts time rate change of the hydrostatic pressure component whose vertical gradient is in balance with gravitational acceleration. In the geometric height coordinate, this equation does not exist. However, the height coordinate does not require surface pressure tendency to close the system because the coordinate is time independent. Because the hydrostatic pressure coordinate $\xi \equiv 1 - \sigma_{\tilde{p}}$ is a material coordinate, the mass continuity equation can also be used to estimate contravariant vertical velocity component by integrating the wind divergence term either from the bottom to a level ξ or from the top to ξ.

$$\dot{\xi} = \frac{1}{\rho J_\xi} \int_0^\xi [J_\xi Q_\rho - m^2 \nabla_\xi \bullet \frac{\rho J_\xi \hat{\mathbf{V}}_\xi}{m^2}]\, d\xi - \frac{\xi}{\rho J_\xi} \frac{\partial(\rho J_\xi)}{\partial t} \tag{12-122a}$$

$$\dot{\xi} = \frac{1}{\rho J_\xi} \int_{\xi_T}^\xi [J_\xi Q_\rho - m^2 \nabla_\xi \bullet \frac{\rho J_\xi \hat{\mathbf{V}}_\xi}{m^2}]\, d\xi - \frac{(\xi - \xi_T)}{\rho J_\xi} \frac{\partial(\rho J_\xi)}{\partial t} \tag{12-122b}$$

where $\xi_T = 1$.

For other coordinates that do not have diagnostic relations, the contravariant vertical velocity component should be estimated using standard coordinate transformation

$$\dot{\xi} = \hat{v}^3 = \frac{\partial \xi}{\partial t} + (-m\mathbf{V}_\xi \bullet \nabla_\xi h_T + w)\left(\frac{\partial \xi}{\partial z}\right) \tag{12-123}$$

where h_T is the height of the coordinate surface and w is the regular vertical component of wind. For nonhydrostatic MM5 applications, $\xi \equiv 1 - \sigma_{p_o}$ is the corresponding vertical coordinate in CMAQ. Equation 12-122a can be rewritten as:

$$\dot{\xi} = -\dot{\sigma}_{po} = [\frac{\sigma_{po}}{p_o^*} \frac{\partial p_o^*}{\partial \hat{x}^1}](mU) + [\frac{\sigma_{po}}{p_o^*} \frac{\partial p_o^*}{\partial \hat{x}^2}](mV) + \frac{\rho_o g}{p_o^*} w \tag{12-124}$$

Like the horizontal momentum components, we need the Jacobian-mass weighted contravariant vertical wind for the mass consistent interpolation. The quantity is computed with the thickness-weighted density as:

$$(\frac{\rho J_\xi}{m^2} \dot{\xi})^{k+1/2} \cong \left[f_z^{k+1/2} (\frac{\rho J_\xi}{m^2})^k + (1 - f_z^{k+1/2})(\frac{\rho J_\xi}{m^2})^{k+1} \right] \bullet \dot{\xi}^{k+1/2} \tag{12-125}$$

where $f_z^{k+1/2} = (z_F^{k+1/2} - z_H^k)/(z_H^{k+1} - z_H^k)$. Note that $(\frac{\rho J_\xi}{m^2} \dot{\xi})$ is defined at the layer interfaces. It is zero at the earth's surface (no-penetration boundary condition) and therefore not included in the

output. It also vanishes at the top of the modeled atmosphere. The quantity $(\frac{\rho J_\xi}{m^2}\dot{\xi})$ is stored in the MET_CRO_3D file from k=1 to K (i.e., *NLAYS*) with the variable name (WHAT_JD).

12.4.4 Mass Consistent Temporal Interpolation of Meteorological Parameters

In the CCTM, the temporal interpolations of meteorological data are needed because the output frequency of the meteorological data is usually much coarser than the synchronization time step of the chemistry-transport model. Consistency in meteorological parameters such as, Jacobian, density of air (total), density of water vapor, entropy (or temperature), and pressure are important for the science modules in the CCTM.

Here, we recommend interpolation schemes for density and velocity fields that maintain mass consistency. First, the Jacobian and density at a time $t_\alpha = (1-\alpha)t_n + \alpha t_{n+1}$ between the two consecutive output time steps, t_n and t_{n+1}, are expected to be interpolated with:

$$(J_\xi)_\alpha = (1-\alpha)(J_\xi)_n + \alpha(J_\xi)_{n+1} \tag{12-126}$$

$$(\rho J_\xi)_\alpha = (1-\alpha)(\rho J_\xi)_n + \alpha(\rho J_\xi)_{n+1} \tag{12-127}$$

where $0 \le \alpha \le 1$. The Models-3 I/O API provides a convenient function call (INTERP3) for the linear interpolation of grid variables. The premise used here is that the Jacobian is a fundamental quantity that determines the coordinate system. Density of water vapor (ρ_v) and entropy should follow the same interpolation rule (Equation 12-127). Then densities and entropy at t_n are computed with

$$(\rho)_\alpha = \frac{(\rho J_\xi)_\alpha}{(J_\xi)_\alpha};\ (\rho_v)_a = \frac{(\rho_v J_\xi)_\alpha}{(J_\xi)_\alpha};\ (\zeta)_\alpha = \frac{(\zeta J_\xi)_\alpha}{(J_\xi)_\alpha} \tag{12-128}$$

It is obvious that the functional form of the Jacobian (which depends on a vertical coordinate) changes the characteristic of density interpolation. For nonhydrostatic MM5 runs, where the Jacobian is constant with time, the density is simply interpolated linearly with time.

When the density tendency term is available from the meteorological model, or can be computed from diagnostic relations for certain choice of vertical coordinate system, one can use a piecewise cubic spline interpolation method for (ρJ_s):

$$(\rho J_s)_\alpha = a\alpha^3 + b\alpha^2 + c\alpha + d \tag{12-129}$$

where $a = \Delta t\left(\frac{\partial(\rho J_s)}{\partial t}\right)_{n+1} + \Delta t\left(\frac{\partial(\rho J_s)}{\partial t}\right)_n - 2\left[(\rho J_s)_{n+1} - (\rho J_s)_n\right]$

$$b = 3[(\rho J_s)_{n+1} - (\rho J_s)_n] - 2\Delta t\left(\frac{\partial(\rho J_s)}{\partial t}\right)_n - \Delta t\left(\frac{\partial(\rho J_s)}{\partial t}\right)_{n+1}$$

$$c = \Delta t\left(\frac{\partial(\rho J_s)}{\partial t}\right)_n$$

$$d = (\rho J_s)_n$$

The density of water vapor (ρ_v) and entropy should be interpolated with the same method. The density of dry air from the total air density can be obtained by subtracting ρ_v from ρ. The interpolated temperature is computed with:

$$T = T_{oo} \exp \frac{\zeta + \rho_d R_d \ln(\rho_d / \rho_{do}) + \rho_v R_v \ln(\rho_v / \rho_{vo})}{\rho_d C_{vd} + \rho_v C_{vv}} \tag{12-130}$$

and entropy can be computed with Equation 12-99. The interpolated pressure is computed with the ideal gas law,

$$p = (\rho_d R_d + \rho_v R_v)T \tag{12-131}$$

Next, wind components multiplied with the Jacobian-weighted density are interpolated linearly and the interpolated wind components are obtained by dividing the results with $(\rho J_s)_\alpha$:

$$(\rho J_s \hat{\mathbf{V}}_s)_\alpha = (1-\alpha)(\rho J_s \hat{\mathbf{V}}_s)_n + \alpha(\rho J_s \hat{\mathbf{V}}_s)_{n+1} \tag{12-132a}$$

$$(\rho J_s \hat{v}^3)_\alpha = (1-\alpha)(\rho J_s \hat{v}^3)_n + \alpha(\rho J_s \hat{v}^3)_{n+1} \tag{12-132b}$$

$$(\hat{\mathbf{V}}_s)_\alpha = \frac{(\rho J_s \hat{\mathbf{V}}_s)_\alpha}{(\rho J_s)_\alpha} \tag{12-133a}$$

$$(\hat{v}^3)_\alpha = \frac{(\rho J_s \hat{v}^3)_\alpha}{(\rho J_s)_\alpha} \tag{12-133b}$$

When density and wind data are not collocated, the above procedure may incur spatial interpolation errors.

12.4.5 Optional Conversion of Nonhydrostatic Data to Hydrostatic Meteorological Data for MM5

There may be a special situation when a hydrostatic CTM run is desired while the MM5 run is made with the nonhydrostatic option. In such a case one may want to redefine the nonhydrostatic coordinate into hydrostatic one while keeping the profile data as provided. In spite of many theoretical problems with this kind of data conversion, MCIP provides an option to convert the

nonhydrostatic coordinate into the hydrostatic pressure coordinate. Use of this option is not recommended for scientifically rigorous computations. However, this is a useful option for certain purposes such as code development and testing of a hydrostatic CTM.

Nonhydrostatic and hydrostatic coordinates can be compared in terms of the atmospheric pressure. Pressure in a hydrostatic MM5 run is defined in Equation 12-93 while the same in a hydrostatic MM5 is defined in Equation 12-94. Then, the difference in the nonhydrostatic and hydrostatic pressures is:

$$p^{*} = p_o^{*} - \sigma^{-1}(p - \tilde{p}) + \sigma^{-1} p_p \qquad (12\text{-}134)$$

If we force the hydrostatic pressure to be that of nonhydrostatic coordinate, i.e., $p \approx \tilde{p}$ at the surface, the time dependent surface pressure, p_s^{*}, can be estimated with:

$$p^{*} \approx p_o^{*} + p_p(\sigma_H^1) \qquad (12\text{-}134')$$

where $\sigma_F^{1/2} = \sigma_s = 1$ is used. Here, the perturbation pressure at the surface is assumed to be that of layer 1 because the real surface perturbation pressure is not provided by the nonhydrostatic MM5. One can redefine the vertical coordinate to be hydrostatic with the time dependent surface pressure. The difficulty of converting nonhydrostatic meteorology data into hydrostatic data is not in the estimation of pressure surfaces, but rather in the representativeness of profile data because of the change in the layer definitions.

12.5 Operation of MCIP

Because MCIP is a Models-3 conformant processor, it needs to be compiled and executed using a Models-3 build command (m3bld) with a configuration file. It requires the grid-domain object include files to define output domain and resolution. In most cases, the user does not need to define input data domains and resolutions because reader modules can extract the information from file headers. MCIP code structure, compilation and execution procedures are discussed below. Additional operational information for preparing MCIP through Models-3 system framework can be found in Chapter 7 of the EPA Third-Generation Air Quality Modeling System User Manual. Also, the User Manual Tutorial for the initial public release of Models-3 provides step-by-step instructions for running MCIP with a set of sample examples.

12.5.1 MCIP Modules

MCIP code is archived with CVS (Concurrent Version System) (Cederqvist, 1993) in the Models-3/CMAQ system. Currently, eleven module classes are defined for MCIP. The classification makes it convenient to customize MCIP code for special situations. For example, when different meteorological inputs and process options are needed to link with the CCTM, appropriate modules from different classes can be used. Refer to Table 12-9 for the details of module descriptions and associated source code.

12.5.2 Building MCIP

The MCIP code conforms to the Models-3 coding standard. It is designed to be compiled using m3bld with a configuration file. Refer to Appendix 12C for a sample MCIP configuration file. The user needs to retrieve the source code (main program, associated subroutines for selected modules, and include files) appropriate to the user's choice of optional modules through the CVS system. There are four kinds of include files for this processor. Three include file types, Models-3 I/O API include files, MCIP's global include files, and MCIP module specific include files, are fixed. The fourth include file type describes dimensional information of the input meteorology data and, as an exception, must be edited to match the number of vertical layers in the input.

The parameter MAXK in MCIPPARM.EXT may need to be changed large enough to accomodate the dimensions of the number of layers for the meteorological data. Horizontal domain information is obtained from the header of MM5 files automatically. MCIP expects that include files for the CTM grid/domain domain (HGRD.EXT, VGRD.EXT, COORD.EXT), for which the data will be extracted, are provide by the user. Vertical collapsing is done automatically when the number of layers in VGRD.EXT is less than the number of layers in input data and the coordinate interface values match as shown in Table 12-5. When a few lowest input model layers are collapsed into one for the output, only diagnostic option can be used because the surface flux values and aerodynamic resistance passed through are no longer valid due to the change in the thickness of the lowest layer. The M3DDEP option must not be used when collapsing the lowest model layers and doing so will be violating the parameteric values passed through from the meteorological model.

Table 12-9. MCIP Module Definitions and Associated Source Code

Class	Module	Description	Source Code
driver	mcip	controls main computational flow	mcip.F, initx.F
input	mm5	reads in MM5 output files	getmet_mm5.F, readmm1.F, readmm2.F, getgist.F, MM5INPUT.EXT, MM5HEADER.EXT
	m3	reads in MCIP output files	getmet_m3.F
	fakemet	generates meteorology fields for idealized flow field study	getmet_m3fake.F
	rams	reads in RAMS I/O API output files	*not available*
landuse	m3radm	reads in landuse data in RADM dry deposition category	getluse.F
pbl	pblpkg	computes PBL parameters	pblpkg.F, pblpwr.F, sfcflux.F, slflux.F
drydep	radmdd	computes dry deposition velocities using Wesely's RADM method	radmdry.F, DDEPSPC.EXT
	cmaqdd	computes dry deposition velocities using Pleim's CMAQ method	*not available*
cloud	radmkuo	computes cloud parameters using convective column assumption	bcldprc_ak.F
solar	solar_px	computes solar radiation using the algorithm implemented in MM5-PX version	solar.F, transm.F
met3d	m3sup	computes supplemental three-dimensional variables needed for CMAQ	layht.F, verthat.F, vertnhy.F, verthyd.F, jacobi.F, met3dsup.F
output	stnd	generates MCIP output for standard variable lists	comheader.F, gridout.F, metcro.F, metdot.F
util	util	collection of utility subroutines	bilin2d.F, bilin3d.F, cvbdx.F, collapx.F, cvmgp.F, cvmgz.F, ratint.F, errmsg.F, sanity.F
icl	icl	MCIP specific include files	CONST_mete.EXT, CONST_pbl.EXT, FILES3_MCIP.EXT, GROUTCOM.EXT, INFILES_MCIP.EXT, LRADMDAT.EXT, MCIPCOM.EXT, MCIPPARM.EXT, MCOUTCOM.EXT, MDOUTCOM.EXT

12.5.3 Executing MCIP

12.5.3.1 Run Script Command File

As with other interfaces, an execution run script is used to define key environmental variables prescribing run-time characteristics and linkage between logical file names specified in the codes and actual files for input and output. A sample script for MCIP execution can be retrieved from the CVS archive and edited for the user's particular application. The user may modify environmental variables for choosing different processing options and for defining input and output files. Refer to the APPENDIX D for a sample MCIP run script. For processing MM5 output, MCIP may not need to be co-resident with MM5 if its output files are in IEEE binary format. MCIP can be run on any UNIX computer for processing meteorological data in Models-3 I/O API format.

Input parameters METROW, METCOL, and METLAY are defined through the UNIX environmental variable list. These are used to check if the input meteorology data have correct dimensions as expected. Within MCIP, the actual values will be picked up from header information of MM5 data file. When offset values (I0, J0) are inconsistent with the information in MM5 header and in COORD.EXT, MCIP suggests a new set of (I0, J0) or (XORIG, YORIG) values. Make sure to set NDEP to correspond to the number of lowest input layers being collapsed into the lowest output model layer, so aerodynamic resistances are computed accordingly.

12.5.3.2 Input Files for MM5 Data Processing

Logical names of input files are described below:

- MMOUT_DOMAIN#: This standard MM5 file contains gridded hourly (or sub-hourly) two- and three-dimensional meteorological data covering the entire MM5 domain.

- MDL3_DOMAIN#: This is optional EPA added MM5 output that contains file contains PBL parameters needed when the pass-through option is chosen.

- LAND_CRO_2D_##KM: This is LUPROC output that contains 11-category fractional land-use data covering the entire MM5 domain. If USGS North American land/vegetation characteristic data base used as input to LUPROC is not enough to cover the desired domain, dominant landuse file LANDUSE_DOMAIN# from TERRAIN, a preprocessor for MM5 system, can be used.

12.5.3.3 Input Files for I/O API Meteorological Data Processing

MCIP can be used to extract meteorology data for a smaller window domain, to collapse number of layers, or to process meteorological data already in I/O API format further. It treats gridded input meteorological data as pseudo profiles for temperature, moisture and wind components. Required I/O API meteorological inputs for this option are; GRID_CRO_2D, GRID_DOT_2D, MET_CRO_2D, MET_CRO_3D, and MET_DOT_3D files. Because it does not use boundary files as its input, the output domain can be as large as (NCOLS-2)x(NROWS-2) for windowing or layer collapsing process. This option can be used to generate interpolated meteorology data for higher resolution grid than the original input as well.

Table 12-10. MCIP Environmental Variables

Environmental Variables	Description	Note
METLAY	number of layers in input meteorology data	should be larger than or equal to CTM NLAYS
METCOL	column (east-west) direction cell dimension in input meteorology data	should be larger than CTM NCOLS
METROW	row (south-north) direction cell dimension in input meteorology data	should be larger than CTM NROWS
I0	location of CTM domain origin offset in row direction = ROW_OFFSET	offset should be counted based on the input grid definition
J0	location of CTM domain origin offset in column direction = COL_OFFSET	offset should be counted based on the input grid definition
LUTYPE	file type for landuse data	1: TERRAIN binary 13 category
		2: preprocessed ASCII 11 category
		3: MM5 dominant landuse category
		4: use landuse in GRIDCRO2D
		5: use USGS I/O API landuse file
I0LUSE	location of CTM domain origin offset in row direction w.r.t. landuse data origin	offset should be counted based on the input grid definition. For LUTYPE 4 & 5, I0LUSE is not used
J0LUSE	location of CTM domain origin offset in column direction w.r.t. landuse data origin	offset should be counted based on the input grid definition. For LUTYPE 4 & 5, J0LUSE is not used
LCALCPBL	flag for estimating PBL parameters of not	TRUE: re-compute PBL parameters
		FALSE: pass through from MM5
LSLFLUX	flag for similarity algorithms	TRUE: use surface layer similarity
		FALSE: use PBL similarity
LM3DDEP	flag for dry deposition algorithm	TRUE: use CMAQ dry deposition
		FALSE: use RADM dry deposition

Table 12-10. MCIP Environmental Variables (continued)

Environmental Variables	Description	Note
LWIND	flag for wind field correction	0 (default): no correction
		+/- 1,2,3 wind field correction options (TBD)
LCALCCLD	flag for cloud algorithm	TRUE: compute cloud parameters
		FALSE: pass through from MM5
LHYDOUT	flag for hydrostatic output	TRUE: forces hydrostatic data output with approximations
		FALSE: pass through from MM5
CRO_FTYPE DOT_FTYPE	flag for I/O API file type	1 (default): time dependent
		0 (special): time independent
LSANITY	flag for checking ranges of output parameters	TRUE: check
		FALSE: do not check
BMAX	Maximum boost rate for urban area	2 (default): 100% increase when urban and water areas are coexisting
JUDATE	Julian date for the start time	(yyyyddd)
HSTRT	start hour	(hh)
HTOSKIP	number of hours to skip MCIP process	(hh)
HTORUN	number of hours to run	(hhh)
NDEP	number of deposition layers	1 (default)
GRDNAM	grid/domain name for MCIP output files	
EXECUTION_ID	user defined execution ID	
SCENFILE	user defined file path	
IOAPI_CHECK_HEADERS	flag for checking I/O API file headers	FALSE (default)

Table 12-11. MCIP File Linkage

Environmental Variables	Description	Note
MM51	Input filename for MM51 data file	for mm5 input module
MM52	Input filename for MM52 data file	for mm5 input module
LU13	Input filename for TERRAIN binary landuse	applicable for LUTYPE = 1
LUSE	input filename for I/O API landuse file	applicable for LUTYPE = 4 or 5
GRID_CRO_2D	input filename for GRID_CRO_2D	for m3 input module
GRID_DOT_2D	input filename for GRID_DOT_2D	for m3 input module
MET_CRO_2D	input filename for MET_CRO_2D	for m3 input module
MET_CRO_3D	input filename for MET_CRO_3D	for m3 input module
MET_DOT_3D	input filename for MET_DOT_3D	for m3 input module
GRID_BDY_2D_G1	output filename for GRID_BDY_2D	
GRID_BDY_3D_G1	output filename for GRID_BDY_3D	
GRID_CRO_2D_G1	output filename for GRID_CRO_2D	
GRID_CRO_3D_G1	output filename for GRID_CRO_3D	
GRID_DOT_2D_G1	output filename for GRID_DOT_2D	
MET_CRO_2D_G1	output filename for MET_CRO_2D	
MET_CRO_3D_G1	output filename for MET_CRO_3D	
MET_DOT_3D_G1	output filename for MET_DOT_3D	

12.5.4 Defining Grid and Domain for MCIP

12.5.4.1 MM5 Grid and Domain Definitions

MM5 may output as many as nine grid domains (one coarse grid and up to eight nested grid domains) per MM5 execution. The MM5 developers took the approach of compiling MM5 with the appropriate dimensions for each study being performed. On the other hand, MCIP processes output meteorological data one grid domain at a time. It needs to be compiled explicitly for each grid domain. For multiple scale MM5 model runs, usually MM5 users have to define all the multi-level nest domains together with the coarse "mother" grid. The complication in defining MM5 domains as the Models-3 domain objects is caused by somewhat inauthentic use of the left-hand coordinate system and dot-point grid/domain definitions in MM5. For the details on how to define MM5 domains, users are recommended to read MM5 User's Guide. In the following, we uses a set of multi-level MM5 domains listed in Table 12-12 as the examples of the discussion.

Table 12-12. An Example Set of Multi-level Nesting MM5 Domains
(Note that (I, J) in MM5 corresponds to (ROW, COL) in CMAQ system.)

MM5 Domain No. (N)	Resolution ($\Delta x=\Delta y$)	Dimensions *(IX,JX) = (ROWS+1,COLS+1)*	Origin Relative to Base Grid *(I_11,J_11)*	Origin Relative to Immediate Parent grid ($ROW_{offset}+1, COL_{offset}+1$)
1	108km	(41,61)	(1,1)	(1,1)
2	36km	(67,82)	(9,24)	(9,24)
3	12km	(82,100)	(19.333333,35.333333)	(32,35)
4	04km	(100,82)	(21.444444,41.555555)	(20,57)

a) Definitions for MM5 108 km mother grid (N=1)

In MM5, the grid is defined with the number of dot points. Therefore, to use MM5's grid definitions, for Models-3/CMAQ's cross-point grid definitions, we need to use following

$$\text{NCOLS} = \text{JX} - 1 = 61\text{-}1 = 60 \tag{12-138a}$$

$$\text{NROWS} = \text{IX} - 1 = 41\text{-}1 = 40. \tag{12-138b}$$

For this grid, no "parent grid" is defined. Origins should be defined with the formula that is specific to MM5's method of grid/domain definition. Note that we require the MM5 mother domain's number of cells in horizontal directions (i.e., NCOLS and NROWS) to be even numbers, so that the dimensions of the four quadrants relative to the center of the coordinates are identical (Refer to Figure 12-9). The origin of the coarse MM5 grid is defined with

$$(x_{orig}, y_{orig}) = (-\frac{N_{cols}}{2} * \Delta x, -\frac{N_{rows}}{2} * \Delta y) \tag{12-139}$$

Because it is the mother grid of the grid family, offsets should be set to zero:

$$(COL_{offset}, ROW_{offset}) = (0,0) \tag{12-140}$$

Currently this domain is defined with resolution of 108km (see Table 12-12).

b) Definitions for MM5 36 km first-level nest grid/domain (N=2)

For this grid, the MM5 108km domain defined above is used as the "parent grid." For the nested domains, NCOLS and NROWS can be either even or odd numbers:

$$\text{NCOLS} = \text{JX} - 1 = 67\text{-}1 = 66 \tag{12-141a}$$

$$\text{NROWS} = \text{IX} - 1 = 82\text{-}1 = 81. \tag{12-141b}$$

Because the left-most and bottom corner of the nest 36km domain is defined with $(I_{1,1}, J_{1,1})$ in MM5, we need to convert this information into $(COL_{offset}, ROW_{offset})$ using following equation:

$$(COL_{offset}, ROW_{offset}) = (J_{1,1} - 1, I_{1,1} - 1) \tag{12-142}$$

Note that MM5 uses left-hand coordinate system, so that the index positions for $(I_{1,1}, J_{1,1})$ are reversed with those for the Models-3/CMAQ's $(COL_{offset}, ROW_{offset})$. In the following case, the general equation for computing the offset numbers from $(I_{1,1}, J_{1,1})$ of the MM5 domains will be presented. The coordinates of the origin is computed with:

$$(x_{orig}, y_{orig}) = (x_{orig}^{parent} + COL_{offset}\Delta x^{parent}, y_{orig}^{parent} + ROW_{offset}\Delta y^{parent}) \tag{12-143}$$

c) Definitions for MM5 12 km and 4 km nest grid/domains (N=3, 4)

For the third, 12km domain (N=3),we have:

$$NCOLS = JX - 1 = 100-1 = 99 \quad (12\text{-}144a)$$

$$NROWS = IX - 1 = 82-1 = 81 \quad (12\text{-}144b)$$

and MM5 36km domain is used as the parent grid. Also, for the fourth 4 km domain (N=4), we have:

$$NCOLS = JX - 1 = 82-1 = 81 \quad (12\text{-}145a)$$

$$NROWS = IX - 1 = 100-1 = 99 \quad (12\text{-}145b)$$

and MM5 12km domain is used as the parent grid. Usually, the offset values will be known to the Models-3/CMAQ users.

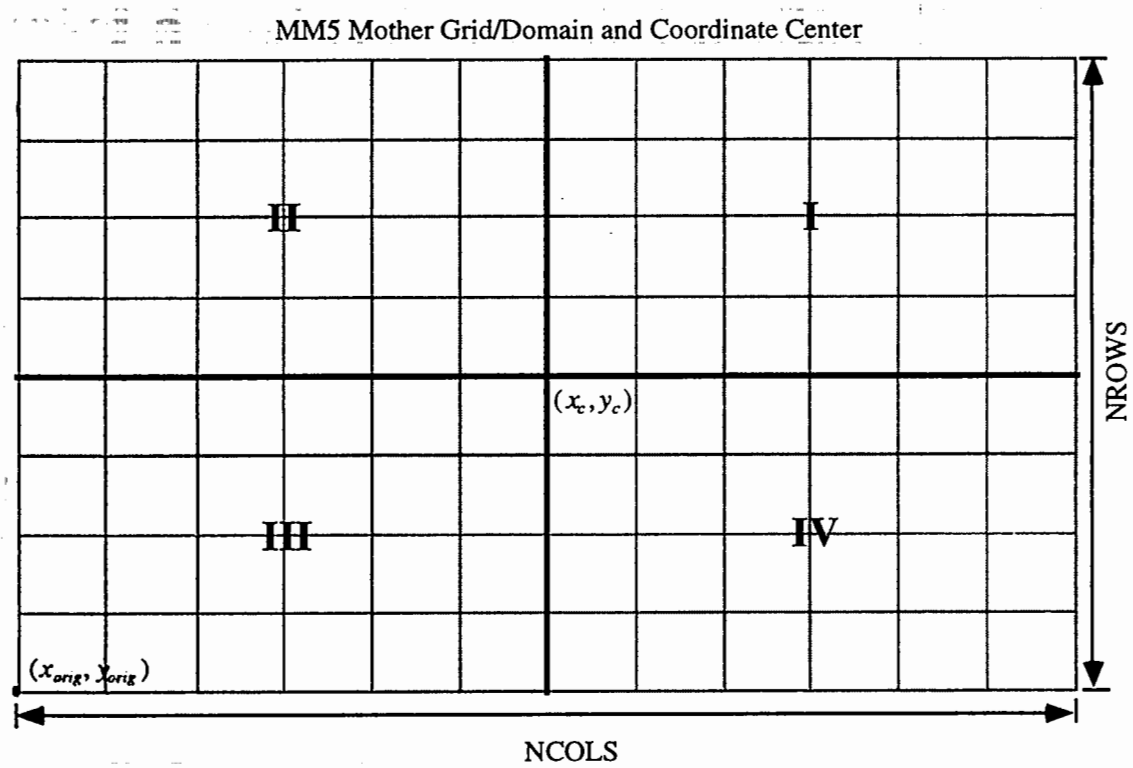

Figure 12-10. A Schematic of the MM5 Mother Grid Definitions.

Because MM5's mother grid is defined from the coordinate center and grows outward, the numbers of columns and rows for each quadrants relative to the coordinate center should be the same, i.e., NCOLS and NROWS for the MM5 mother grid should be even numbers. In case the offset information is not known a priori, one needs to compute the offset values using the header

information in the MM5 output files. To use the information correctly, we need to know how the MM5 nest domain's left-most and bottom corner $(I_{1,1}, J_{1,1})$ is defined. In MM5, all the nest domains are defined relative to the mother grid, and $(I_{1,1}, J_{1,1})$ provides the offset information of the nest domains in terms of the mother grid's resolution. The formula linking a nest MM5's domain $(I_{1,1}, J_{1,1})$ and Models-3/CMAQ's offset values $(COL_{offset}, ROW_{offset})$ are given for $N \geq 2$ as:

$$(J_{1,1}, I_{1,1})_N = \left(\left[1 + \sum_{k=2}^{N} \frac{(COL_{offset})_k}{(\Delta x^{parent} / \Delta x)^{k-2}} \right], \left[1 + \sum_{k=2}^{N} \frac{(ROW_{offset})_k}{(\Delta y^{parent} / \Delta y)^{k-2}} \right] \right) \tag{12-146}$$

where $(\Delta x^{parent} / \Delta x) = 3$ for the current MM5 application example. Because our objective is to help users to find out $(COL_{offset}, ROW_{offset})$ for the nest grid, we need to rewrite Equation 12-146 for $(COL_{offset}, ROW_{offset})$. Assuming we know all the coarser grid/domains offset values, $(COL_{offset}, ROW_{offset})$ for the current nesting level $N \geq 2$ can be found as:

$$(COL_{offset})_N = (\Delta x^{parent} / \Delta x)^{N-2} \left[(J_{1,1})_N - 1 - \sum_{k=2}^{N-1} \frac{(COL_{offset})_k}{(\Delta x^{parent} / \Delta x)^{k-2}} \right] \tag{12-147a}$$

$$(ROW_{offset})_N = (\Delta y^{parent} / \Delta y)^{N-2} \left[(I_{1,1})_N - 1 - \sum_{k=2}^{N-1} \frac{(ROW_{offset})_k}{(\Delta y^{parent} / \Delta y)^{k-2}} \right] \tag{12-147b}$$

Although Equations 12-147 a and b look somewhat complicated, one can readily compute offset numbers for Models-3 CMAQ's grid/domain definitions for the example set of domains defined in Table 12-11 as follows:

$$\left[(COL_{offset}), (ROW_{offset}) \right]_{N=2} = [(24-1), (9-1)] = [23, 8] \tag{12-148a}$$

$$\left[(COL_{offset}), (ROW_{offset}) \right]_{N=3} = \left[3[(35\frac{1}{3} - 1) - 3^0 * 23], 3[(19\frac{1}{3} - 1) - 3^0 * 8] \right]$$

$$= [34, 31] \tag{12-148b}$$

$$\left[(COL_{offset}), (ROW_{offset}) \right]_{N=4} = \left[3^2[(41\frac{5}{9} - 1) - \frac{23}{3^0} - \frac{34}{3}], 3^2[(21\frac{4}{9} - 1) - \frac{8}{3^0} - \frac{31}{3}] \right]$$

$$= [56, 19] \tag{12-148c}$$

Most of the time, the above MM5 domain definitions are provided by the MM5 modelers and Models-3/CMAQ users do not have to re-compute them.

12.5.4.2 CMAQ Grid Definitions

The horizontal grid structure used for the MM5 serves as the parent grid for the CCTM domains. To define a CCTM grid, number of cells to be excluded from the parent domain must be

determined. It is recommended that the CCTM grid be smaller than its parent MM5 grid by at least 4 grid cells (preferably by 6 grids) to avoid the possible numerical reflection problems at boundaries of MM5 domain. Once the offset values are known, (x_{orig}, y_{orig}) of the nest domain can be computed using Equation 12-143. Refer to Appendix 12B for other examples of other CCTM nest domain definitions.

12.5.5 Extension of MCIP for Other Meteorological Models

The current release version of MCIP can only process MM5 output in binary format or previous MCIP output in I/O API format. To realize the one-atmosphere concept for meteorological and air quality modeling, CMAQ utilizes generalized coordinates. One advantage of the generalized coordinate system is that a single CTM can adapt to any of the coordinate systems and dynamics commonly used in meteorological modeling. Because most meteorological models are not originally designed for air quality studies, they lack characteristics that are required for air quality modeling. Consistencies in dynamic descriptions of atmosphere, physical parameterizations, and numerical algorithms, where applicable, in meteorological and chemistry-transport models are critical in determining the quality of air pollutant simulations. This issue becomes more critical with high resolution air quality study where nonhydrostatic meteorological models must be used.

MCIP is the key processor allowing the consistent linkage between meteorological models and CMAQ. Currently, different meteorological models are used by different atmospheric modeling groups forming their own respective user communities. It is because these meteorological models are applicable for a limited range of spatial and temporal scales. To expand the user base of the Models-3 CMAQ system and to promote the one-atmosphere community modeling paradigm, it is essential to continuously develop MCIP modules for several popular mesoscale meteorological models such as RAMS, ARPS, HOTMAC, and others.

To build a version of MCIP for processing a set of meteorological model output, several issues involved with different dynamics and coordinates must be considered. They are; (1) compatibility of governing set of equations and state variables used, (2) scale limitations in subgrid scale parameterizations such as cloud, turbulence, and surface exchange processes, and (3) consistency in numerical algorithms and discretization methods. Before designing MCIP modules for other meteorological model, developers should identify the structure, format, and frequency of data as well as their impact on the processing structure of MCIP. MCIP expects time dependent meteorological data in a structured grid system as the input. As this moment, there is no provision for handling irregularly spaced data structure either from observations or from a meteorological modeling system with unstructured adaptive (fixed or dynamic) grid structure, such as the one used in OMEGA system (Bacon et al., 1996). If there is need for including these data, object analysis tools must be used to prepare data in a structured grid system.

The essential information related to the coordinates and dynamic assumptions used in meteorological models is captured in MCIP. Dynamic and thermodynamic state variables are recast into the fully compressible system as described in Chapter 5 of this volume.

It is important to know the processing sequence and associated data structures used in the current MCIP code. Major processing steps in MCIP can be summarized as follows: (1) Grid, coordinate, and information on atmospheric dynamics are used to compute Jacobian and layer heights; (2) State

variables in meteorological models are recast into density and entropy; (3) Contravariant wind components are computed; (4) necessary two-dimensional parameters are diagnosed; and (5) Some of two- and three-dimensional parameters are passed through. Figure 12-11 shows corresponding data structures used at different phases. Input phase uses arrays with dimensions covering the full meteorology domain ('F-arrays'), processing phase uses arrays for extended domain covering both the CMAQ and boundary domains ('X-arrays'). During the output phase, the information in X-arrays are separated into the CMAQ and boundary domains for respective data types described in Table 12-3.

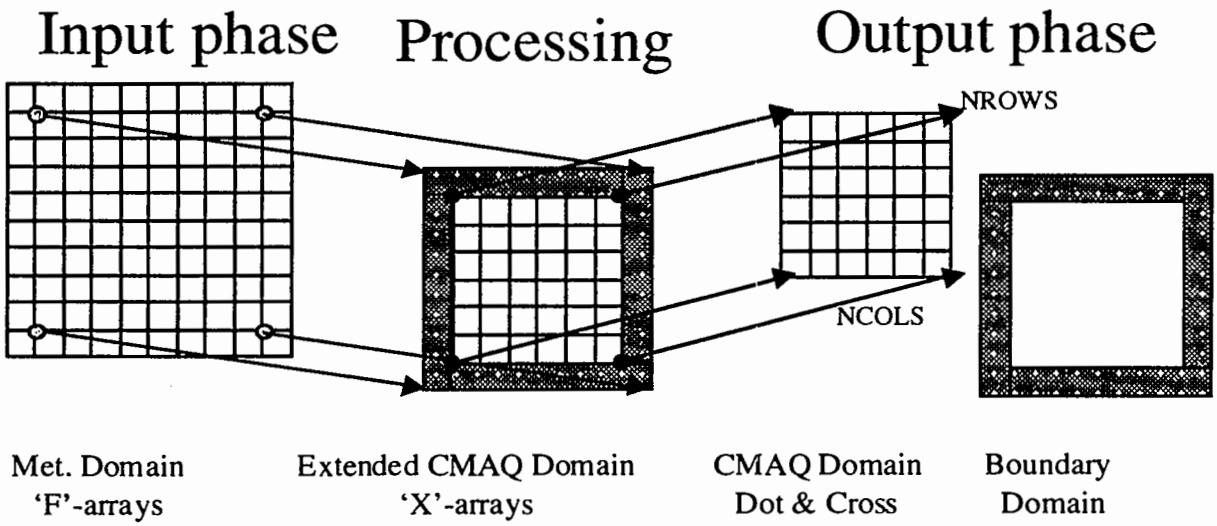

Figure 12-11. Data Structures Corresponding to Input, Processing, and Output Phases of MCIP Processing

12.6 Concluding Remarks

MCIP is a key processor linking meteorological models to the CMAQ modeling system. Its major roles are:

1. To read meteorological data from a meteorological model and converts them in Models-3 I/O API format.

2. To provide all the necessary meteorological parameters for air quality simulations. When necessary, PBL parameters and other derived quantities are computed using gridded meteorology data and high-resolution fractional land use information.

3. To support multiscale generalized coordinate implementation of the CCTM.

Current implementation of MCIP is mainly for linking MM5 output to CCTM. Reader modules to Regional Atmospheric Modeling System (RAMS) (Pielke et al., 1992), will be added. Users who wish to link other meteorological models may need to modify and introduce appropriate input modules.

12.7 References

Alduchov, O. A. and R. E. Eskridge, 1996: Improved Magnus form approximation of saturation pressure. *J. Appl. Meteorol.*, **35**, 601-609.

Anthes, R. A., E. Y. Hsie and Y.H Kuo, 1987: Description of the Penn State/NCAR Mesoscale Model version 4 (MM4). NCAR Technical Note, NCAR/TN-282+STR, National Center for Atmospheric Research, Boulder, CO. 66pp.

Avissar, R., P. Avissar, Y. Hahrer, and B. A. Bravdo, 1985: A model to simulate response of plant stomata to environmental conditions. *Ag. and Forest Meteorol.*, **34**, 21-29.

Bacon, D. P., Z. Boybeyi, P.R. Boris, T. J. Dunn, M. Hall, R. A. Sarma, S. Young, and J. Zack, 1996: An overview of the operational Multi-sclae Environmental model with Grid Adaptivity. *Proc. of the 15th Conf. on Wea. Anal. and Forecasting*, Norfolk, VA, August 19-23, 1996, American Meteorological Soc., Boston, MA.

Ball, J. T., I. E., Woodrow, and J. A. Berry, 1987: A model predicting stomatal conductance and its contribution to the control of photosythesis under different environmental conditions. In *Progress in photosynthesis Research, Vol. IV* (ed. J. Biggins), pp. 221-234. Martinus Nijhof Publishers, Dordrecht.

Betts, A. K., 1973: Non-precipitating cumulus convection and its parameterization. *Quart. J. Roy. Meteorol. Soc.* **99**, 178-196.

Binkowski, F.S. and U. Shankar, 1995: The Regional Particulate Model. 1. Model description and preliminary results. *J. Geophys. Res.*, **100 D12**, 26191-26209.

Blackadar, A. K., 1978: Modeling pollutant transfer during daytime convection, *Preprints, Fourth Symposium on Atmospheric Turbulence, Diffusion, and Air Quality*, Reno, Am. Meteor. Soc., 443-447.

Brost R. A. and J. C. Wyngaard, 1978: A model study of the stably stratified planetary boundary layer. *J. Atmos. Sci.*, **35**, 1427-1440.

Businger J. A., J. C. Wyngaard, Y. Izumi, and E. F. Bradley, 1971: Flux profile relationships in the atmospheric surface layer, *J. Atmos. Sci.*, **28**, 181-189.

Byun, D. W., 1990: On the analytical solutions of flux-profile relationships for the atmospheric surface layer, *J. Appl. meteorol.*, **29**, 652-657.

Byun, D. W., 1991: Determination of similarity functions of the resistance laws for the planetary boundary layer using surface-layer similarity functions, *Boundary Layer Meteorol.*, **57**, 17-48.

Byun, D.W., 1999a: Dynamically consistent formulations in meteorological and air quality models for multiscale atmospheric applications: I. Governing equations in generalized coordinate System. *J. Atmos. Sci.*, (in print)

Byun, D.W., 1999b: Dynamically consistent formulations in meteorological and air quality models for multiscale atmospheric applications: II. Mass conservation issues. *J. Atmos. Sci.*, (in print)

Byun, D. W., and R.L. Dennis, 1995: Design artifacts in Eulerian air quality models: Evaluation of the effects of layer thickness and vertical profile correction on surface ozone concentrations. Atmospheric Environment, **29**, No. 1, 105-126.

Carson, D. J., 1973: The development of a dry inversion-capped convectively unstable boundary layer. *Quart. J. Roy. Meteorol. Soc.* **99**, 450-467.

Cederqvist, P., 1993: *Version Management with CVS*, Signum Support AB, Linkoping, Sweden. 168pp.

Chang, J.S., R.A. Brost, I.S.A. Isaksen, S. Madronich, P. Middleton, W.R. Stockwell, and C.J. Walcek, 1987: A three-dimensional Eulerian acid deposition model: Physical concepts and formulation, *J. of Geophys. Res.*, **92**, 14,681-700.

Chang, J.S., P.B. Middleton, W.R. Stockwell, C.J. Walcek, J.E. Pleim, H.H. Lansford, S. Madronich, N.L. Seaman, D.R. Stauffer, F.S. Binkwski, D. Byun, J.N. McHenry, H. Hass, and P.J. Samson, 1990: The Regional Acid Deposition Model and Engineering Model, NAPAP report 4.

Coats, C. J., cited 1996: The EDSS/Models-3 I/O Applications Programming Interface. MCNC Environmental Programs, Research Triangle Park, NC. [Available on-line from http://www.iceis.mcnc.org/EDSS/ioapi/H.AA.html.]

Collatz, G. J., C. Grivet, J. T. Ball, and J. A. Berry, 1991: Physiological and environmental regulation of stomatal conductance, photosynthesis and transpiration: a model that includes a laminar boundary layer. *Ag. and Forest Meteorol.*, **54**, 107-136.

Driedonks, A. G. M., 1981: Dynamics of the well-mixed atmospheric boundary layer. De Bilt KNMI Sci. Rep. WR 81-2, 189pp.

Dudhia, J., 1989: Numerical study of convection observed during the Winter Monsoon Experiment using a mesoscale two-dimensional model. *J. Atmos. Sci.*, **46**, 3077-3107.

Dudhia, J., 1993: A nonhydrostatic version of the Penn State-NCAR mesoscale model: Validation tests and simulation of an Atlantic cyclone and cold front, *Mon. Wea. Rev.*, 121, 1493-1513.

Erisman, J. W., A. van Pul, and P. Wyers, 1994: Parameterization of surface resistance for the quantification of atmospheric deposition of acidifying pollutants and ozone. *Atmos. Environ.* **28**, 2595-2607.

Fowler, D., 1978: Dry deposition of SO_2 on agricultural crops, *Atmos. Environ.*, 12, 369-373.

Fritsch, J.M., and C.F. Chappell, 1980: Numerical prediction of convectively driven mesoscale pressure systems, 1, Convective parameterization, *J. Atmos. Sci.*, **37**, 1722-1733.

Geleyn, J.-F., A. Hense, and H.-J. Preuss, 1982: A comparison of model-generated radiation fields with satellite measurements. *Beitr. Phys. Atmos.*, **55**, 253-286.

Grell, G.A., J. Dudhia, and D.R. Stauffer, 1994: A Description of the Fifth-Generation PENN STATE/NCAR Mesoscale Model (MM5), NCAR Technical Note, NCAR/TN-398+*STR*, National Center for Atmospheric Research, Boulder, Colorado, 138pp

Haagenson, P. L., J. Dudhia, D. R. Stauffer, and G. A. Grell, 1994: The Penn State-NCAR mesoscale model (MM5) source code document, *NCAR/TN-392+STR*, National Center for Atmospheric Research, Boulder, Colorado.

Hack, J. J., B. A. Boville, B. P. Briegleb, J. T. Kiehl, P. J. Rasch, and D. L. Williamson, 1993: Description of the NCAR community climate model (CCM2). NCAR Tech. Note, NCAR/TN-382+STR, 120 pp. [Available from the National Center for Atmospheric Research, P.O. Box 3000, Boulder, CO 80307.]

Hess, G. D., 1992: Observations and scaling of the atmospheric boundary layer. *Aus. Meteorol. Mag.* **41**, 79-99.

Högström, U., 1988: Non-dimensional wind and temperature profiles in the atmospheric surface layers: a re-evaluation. *Boundary-Layer Meteor.*, **42**, 55-78.

Holtslag, A. A., E. I. F. de Bruin, and H.-L. Pan, 1990: A high resolution air mass transformation model for short-range weather forecasting. *Mon. Weather Rev.*, **118**, 1561-1575.

Holtslag, A.A.M., E.V. Meijgaard, and W.C. DeRooy, 1995: A comparison of boundary layer diffusion schemes in unstable conditions over land, Boundary-Layer Meteor., **76**, 69-95.

Jarvis, P. G., 1976: The interpretation of the variation of leaf water potential and stomatal conductance found in canopies in the field. *Phil. Trans. Royal Meteorol. Soc. of London, Series B,* **273**, 593-610.

Jacquemin B. and J. Noilhan, 1990: Sensitivity study and validation of a land surface parameterization using the HAPEX-MOBILHY data set. *Bound.-Layer Meteorol.,* **52**, 93-134.

Jaung, H.-M. H., 1992: A spectral fully compressible nonhydrostatic mesoscale model in hydrostatic sigma coordinates: Formulations and preliminary results. *Meteor. Atmos. Phys.*, **50**, 75-88.

Kain, J. S., and J. M. Fritsch, 1993: Convective paramterization for mesoscale models: The Kain-Fritsch scheme. *Jthe representation of cumulus in mesoscale models.*, K.A. Emanuel and D.J. Raymond, Eds., Amer. Meteor. Soc., 246pp.

Lo, A. K., 1993: The direct calculation of fluxes and profiles in the marine surface layer using measurements from a single atmospheric level. *J. Appl. Meteorol.*, **32**, 1890-1990.

Lo, A. K., 1995: Determination of zero-plane displacement and roughness length of a forest canopy using profiles of limited height. *Boundary-Layer Meteorol.*, **75**, 381-402.

Madronich, S., 1987: Intercomparison of NO2 photodissociation and UV radiometer measurements, *Atmos.Environ.*, **21**, 569-578.

Mason, P.J., 1987: The formation of areally-averaged roughness lengths. *Q.J.R. Meteorol. Soc.*, **106**, 351-366.

Mesinger, F. and A. Arakawa, 1976: Numerical methods used in atmospheric models. In: Global Atmospheric Research Programme (GARP), Joint Organization Committee, GARP Publication Series, No. 17, Aug., 1976: [Available from WMO Secretariat, Geneva].

Mihailovic, D. T., R. A. Pielke, B. Rajkovic, L. J. Tsengdar, and M. Jeftic, 1993: A resistance representation of schemes for evaporation from bare and partly plant-covered surfaces for use in atmospheric models. *J. Appl. Meteorol.*, **32**, 1038-1054.

Noilhan, J. and S. Planton, 1989: A simple parameterization of land surface processes for meteorological models. *Mon. Wea. Rev.*, **117**, 536-549.

Ooyama, K. V., 1990: A thermodynamic foundation for modeling the moist atmosphere. *J. Atmos. Sci.*, **47**, 2580-2593.

Padro, J., G. den Hartog, and H. H. Neumann, 1991: An investigation of the ADOM dry deposition module using summertime O_3 measurements above a deciduous forest, *Atmos. Environ.*, **25A**, 1689-1704.

Paulson, C. A., 1970: The mathematical representation of wind speed and temperature profile in the unstable atmospheric surface layer. *J. Appl. Meteor.*, **9**, 857-861.

Pielke, R. A., W. R. Cotton, R. L. Walko, C. J. Tremback, M. E. Nicholls, M. D. Moran, D. A. Wesley., T. J. Lee, and J. H. Copeland, 1992: A comprehensive meteorological modeling system–RAMS. *Meteor. Atmos. Phys.*, **49**, 69-91.

Pleim, J. , A. Venkatram, and R. Yamartino, 1984: ADOM/TADAP Model Development Program, Volume 4, The Dry Deposition Module. ERT P-B980-520, Prepared for OME, AES of Canada and the Umweltbundesamt, Germany.

Pleim, J. E. and A. Xiu, 1995: Development and testing of a surface flux and planetary boundary layer model for application in mesoscale models, *J. Appl. Meteor.*, **34**, 16-32.

Pleim, J. E. , A. Xiu, P. L. Finkelstein, and J. F. Clarke, 1997: Evaluation of a coupled land-surface and dry deposition model through comparison to field measurements of surface heat, moisture, and ozone fluxes, Proceedings of the 12th Symposium on Boundary Layers and Turbulence, July 28-August 1, 1997, Vancouver, BC.

Pleim, J. E., J. F. Clarke, P. L. Finkelstein, E. J. Cooter, T. G. Ellestad, A. Xiu, and W. M. Angevine, 1996: Comparison of measured and modeled surface fluxes of heat, moisture and

chemical dry deposition. In: Air Pollution Modeling and its Application XI, Ed: Gryning and Schiermeier, Plenum Press, New York.

Rochette, P., Desjardins, R. L., Dwyer, L. M., Stewart, D. W., Pattey, E., and Dubé, P. A., 1991: Estimation of maize canopy conductance by scaling up leaf stomatal conductance. *Ag. and Forest Meteorol.*, **54**, 241-262.

Schumann, U., 1989: Large-eddy simulation of turbulent diffusion with chemical reactions in the convective boundary layer. *Atmos. Environ.*, **23**, 1713-1727.

Seaman, N. L., D. R. Stauffer, and A. M. Lario-Gibbs, 1995: A multiscale four-dimensional data assimilation system applied in the San Joaquin Valley during SARMAP. Part I: Modeling design and basic performance characteristics, *J. Appl. Meteor.*, **34**, 1739-1761.

Seaman, N. L., and D. R. Stauffer, 1995: Simulation of the thermal structure of the San Joaquin Valley during SJVAQS/AUSPEX/SARMAP using MM5 with four-dimensional data assimilation, paper presented at the AWMA conference, Regional Photochemical Measurement and Modeling Studies, November 8-12, San Diego, Calif., 1993.

Sellers, P. J., Y. Mintz, Y. C. Sud, and A. Dalcher, 1986: A simple biosphere model (SiB) for use within general circulation models. *J. Atmos. Sci.*, **43,** 505-531.

Sellers, P. J., R. E. Dickinson, D. A. Randall, A. K. Betts, F. G. Hall, J. A. Berry, G. J. Collatz, A. S. Denning, H. A. Mooney, C. A. Nobre, N. Sato, C. B. Field, and A, Henderson-Sellers, 1997: Modeling the exchanges of energy, water, and carbon between continents and the atmosphere. *Science*, **275**, 502-509.

Sheih, C.M., M.L. Wesely, and B. B. Hicks, 1979: Estimated dry deposition velocities of sulfur over the eastern United States and surrounding regions, *Atmos. Environ.*, **13**, 1361-1368.

Sirois, A., and L.A. Barrie, 1988: An estimate of the importance of dry deposition as a pathway of acidic substances from the atmosphere to the biosphere in eastern Canada, *Tellus*, **40B**, 59-80.

Slinn, W. G. N., L. Hasse, B. B. Hicks, A. W. Hogan, D. Lal, P. S. Liss, K. O. Munnice, G. A. Sehmel, and O. Vittori, 1978: Some aspects of the transfer of atmospheric trace constituents past the air-sea interface. *Atmos. Environ.* **12**, 2055-2087.

Stauffer, D. R., and N. L. Seaman, 1993: Evaluation of multiscale four-dimensional data assimilation techniques developed and tested in MM5 during SJVAQS/AUSPEX/ SARMAP, paper presented at the AWMA conference, Regional Photochemical Measurement and Modeling Studies, November 8-12, San Diego, Calif., 1993.

Tesche, T. W., and D. McNally, 1993: Operational evaluation of the SARMAP meteorological model (SMM1) for episode 1: 3-6 August, 1990, Alpine Geophysics, Crested Butte, CO.

Thorpe, S., cited 1996: PAVE User Guide. MCNC Environmental Programs, Research Triangle Park, NC. [Available on-line from http://www.iceis.mcnc.org/ EDSS/pave_doc/SCCS/s.Pave.html.]

Voldner, E.C., L.A. Barrie, and A. Sirois, 1986: A literature survey of dry deposition of oxides of sulfur and nitrogen with emphasis on long-range transport modelling in North America, *Atmos.Environ.*, **20**, 2101-2123.

Walcek, C.J., 1987: A theoretical estimate of O3 and H2O2 dry deposition over the northeast United States, *Atmos.Environ.*, **21**, 2649-2659.

Walcek, C.J., R. A. Brost, J. S. Chang, and M. L. Wesely, 1986: SO2, sulfate and HNO3 deposition velocities computed using regional landuse and meteorological data, *Atmos.Environ.*, **20**, 949-964.

Walcek, C.J., and G.R. Taylor, 1986: A theoretical method for computing vertical distributions of acidity and sulfate production within cumulus clouds, *J.Atmos.Sci.*, **43**, 339-355.

Warner, J., 1970: On steady-state one-dimensional models of cumulus convection, *J. Atmos. Sci.*, **27**, 1035-1040.

Wesely, M. L., 1989: Parameterization of surface resistances to gaseous dry deposition in regional-scale numerical models, *Atmos.Environ.*, **23**, 1293-1304.

Wesely, M. L., and B. B. Hicks, 1977: Some factors that affect the deposition rates of sulfur dioxide and similar gases on vegetation, *J. Air Pollut. Control. Assoc.*, **27**, 1110-1116.

Wesely, M. L., D. R. Cook, R. L. Hart, and R. E. Speer, 1985: Measurements and parameterization of particulate sulfur dry deposition over grass, *J. Geophys. Res.*, **90**, 2131-2143.

Wetzel, P. J., and J.-T. Chang, 1988: Evapotranspiration from nonuniform surfaces: a first approach for short-term numerical weather prediction. *Mon. Wea. Rev.*, **116**, 600-621.

Wojcik, G.S., and J.S. Chang, 1996: An Eulerian modeling study of anthropogenic sulfur budgets and lifetimes for Eastern North America, *submitted to J.Atmos.Chem.*

Wyngaard, J. and Brost, J.C. and R. A. Brost, 1984: Top-down and bottom-up diffusion of a scalar in the convective boundary layer. *J. Atmos. Sci.*, **41**, 102-112.

Xue, M., K. Droegemeier, V. Vong, A. Shapiro, and K. Brewster, 1995: ARPS Version 4.0 User's Guide. Center for the Analysis and Prediction of Storms, Univ. of Oklahoma, 380 pp. [Available from Center for the Analysis and Prediction of Storms, Univ. of Oklahoma, Norman, OK 73019].

Zilitinkevich S. S., 1989: Velocity profiles, the resistance law and the dissipation rate of mean flow kinetic energy in a neutrally and stably stratified planetary boundary layer. *Bound. Layer Met.*, **46**, 367-387.

This chapter is taken from *Science Algorithms of the EPA Models-3 Community Multiscale Air Quality (CMAQ) Modeling System*, edited by D. W. Byun and J. K. S. Ching, 1999.

Appendix 12A MCIP Output Data

MCIP writes the bulk of its two- and three-dimensional meteorology and geophysical output data in a transportable binary format using a tailored Models-3 input/output applications program interface (I/O API) library. Depending on whether the meteorological vertical coordinate is time dependent or not, the temporal characteristics of certain variables that belong to GRID data types and MET data types may differ. For example, when the meteorological coordinate is σ_p, which is time dependent, Jacobian is also time dependent. On the other hand for σ_{po} coordinate, Jacobian is time independent. However we are using a consistent list of meteorological variables for both hydrostatic and nonhydrostatic coordinates for as the standard output. Tables 12A-1 through 12A-6 provide lists of variables in each data type.

Table 12A1. Variables in GRIDCRO2D

Variable Name	Unit	Description
LAT	DEGREES	latitude (south negative)
LON	DEGREES	longitude (west negative)
MSFX2	(M/M)**2	squared map-scale factor (CROSS)
HT	M	terrain elevation
ZZERO	M	roughness length
PRSFC0	Pascal	surface pressure difference of reference atmosphere
JACOBS0	M	total Jacobian at surface
LUSE_URBA	fraction (0-1)	landuse for URBAN_LAND
LUSE_AGRI	fraction (0-1)	landuse for AGRICILTURE
LUSE_RANG	fraction (0-1)	landuse for RANGE
LUSE_DECI	fraction (0-1)	landuse for DECIDUOUS_FOREST
LUSE_CONI	fraction (0-1)	landuse for CONIFEROUS_FOREST
LUSE_MIXF	fraction (0-1)	landuse for MIXFOREST_WETLND
LUSE_WATE	fraction (0-1)	landuse for WATER
LUSE_BARR	fraction (0-1)	landuse for BARREN_LAND
LUSE_NONE	fraction (0-1)	landuse for NONFOREST_WETLND
LUSE_MIXA	fraction (0-1)	landuse for MIXAGRI_RANGE
LUSE_DECI	fraction (0-1)	landuse for URBAN_LAND
LUSE_ROCK	fraction (0-1)	landuse for ROCKY_OPENSHRUB

Table 12A2. Variables in GRIDDOT2D

Variable Name	Unit	Description
LAT	DEGREES	latitude (south negative)
LON	DEGREES	longitude (west negative)
MSFD2	(M/M)**2	squared map-scale factor (DOT)

Table 12A3. Variables in GRIDCRO3D

Variable Name	Unit	Description
DENS0	KG/M**3	density of reference atmosphere
ENTRP0	J/K/M**3	entropy density of reference atmosphere
JACOB0F	M	total Jacobian at layer face
JACOB0M	M	total Jacobian at layer middle
TEMP0	K	temperature of reference atmosphere
PRES0	Pascal	pressure of reference atmosphere
X3HT0F	M	height of layer face (top) of reference atmosphere
X3HT0M	M	height of layer middle of reference atmosphere

Table 12A4. Variables in METCRO3D

Variable Name	Unit	Description
JACOBF	M	total Jacobian at layer face
JACOBM	M	total Jacobian at layer middle
DENSA_J	KG/M**2	Jacobian weighted total air density
DENSW_J	KG/M**2	Jacobian weighted density of vapor
ENTRP_J	J/K/M**2	Jacobian weighted entropy of moist air
WHAT_JD	KG/(M*S)	J & Density weighted vertical contra-W
QC	KG/KG	cloud water mixing ratio
QR	KG/KG	rain water mixing ratio
QV	KG/KG	water vapor mixing ratio
TA	K	air temperature
PRES	Pascal	pressure
DENS	KG/M**3	total density of air
WWIND	M/S	true W component of wind
ZH	M	mid-layer height above ground
ZF	M	full-layer height above ground
JDRATE	KG/M**2/S	time rate change of Jacob*Density

Table 12A5. Variables in METDOT3D

Variable Name	Unit	Description
UWIND	M/S	U-comp. of true wind at dot point
VWIND	M/S	V-comp. of true wind at dot point
UHAT_JD	KG/(M*S)	(contra_U*Jacobian*Density) at square point
VHAT_JD	KG/(M*S)	(contra_V*Jacobian*Density) at triangle point

Table 12A6. Variables in METCRO2D

Variable Name	Unit	Description
PRSFC	Pascal	surface pressure
JACOBS	M	total Jacobian at surface
DENSAS	KG/M**3	air density at surface
WSTAR	M/S	convective velocity scale
RIB	NODIM	bulk Richardson number
PBL	M	PBL height
ZRUF	M	surface roughness length
MOLI	1/M	inverse of Monin-Obukhov length
HFX	WATTS/M**2	sensible heat flux
QFX	WATTS/M**2	latent heat flux
MOLI	1/M	inverse of Monin-Obukhov length
RADYNI	M/S	inverse of aerodynamic resistance
RBNDYI	M/S	inverse of laminar bnd layer resistance
RSTOMI	M/S	bulk stomatal resistance for water
TEMPG	K	skin temperature at ground
TEMP10	K	air temperature at 10 m
TEMP1P5	K	air temperature at 1.5 m
SURF2	EMPTY	surface parameter 1
ALBEDO	NODIM	surface albedo
FSOIL	WATTS/M**2	heat flux in soil layers
GLW	WATTS/M**2	longwave radiation at ground
GSW	WATTS/M**2	solar radiation absorbed at ground
RGRND	WATTS/M**2	solar radiation reaching surface
RNET	WATTS/M**2	net radiation .
RN	CM	accumulated nonconvective hourly precip.
RC	CM	accumulated convective hourly precip.
CFRACH	Fraction	fraction of high cloud
CFRACM	Fraction	fraction of middle cloud
CFRACL	Fraction	fraction of low cloud
CFRAC	Fraction	total cloud fraction
CLDT	M	cloud top layer height
CLDB	M	cloud bottom layer height
WBAR	G/M**3	liquid water content of cloud
VD_XXXX	M/S	dry deposition velocity for species XXXX

Note: List of deposition velocities

```
VD_SO2    :"M/S"      ; deposition velocity for species SO2
VD_SULF   :"M/S"      ; deposition velocity for species SULF
VD_NO2    :"M/S"      ; deposition velocity for species NO2
VD_NO     :"M/S"      ; deposition velocity for species NO
VD_O3     :"M/S"      ; deposition velocity for species O3
VD_HNO3   :"M/S"      ; deposition velocity for species HNO3
VD_H2O2   :"M/S"      ; deposition velocity for species H2O2
VD_ALD    :"M/S"      ; deposition velocity for species ALD
VD_HCHO   :"M/S"      ; deposition velocity for species HCHO
VD_OP     :"M/S"      ; deposition velocity for species OP
VD_ORA    :"M/S"      ; deposition velocity for species ORA
VD_NH3    :"M/S"      ; deposition velocity for species NH3
VD_PAN    :"M/S"      ; deposition velocity for species PAN
VD_HONO   :"M/S"      ; deposition velocity for species HONO
VD_CO     :"M/S"      ; deposition velocity for species CO
```

Appendix 12B Examples of Nest Domain Definitions for CMAQ system

12B.1 Grid Domain Definitions for the Models-3 CMAQ Tutorial Study

Table 12B-1. Origins for the TUTORIAL MM5 domain, MCIP landuse domain, and CTM domains. Note that (x,y) corresponds to (COL,ROW) in CMAQ. MCIP landuse domain is smaller by one cell around than the original MM5 domain. Also, the CTM domain removes three cells around from the original MM5 domain. Origin is measured from the center of Base 108 km domain located at 90W and 40N.

Resolution ($\Delta x=\Delta y$)	Origin for original MM5 Domain (x_{orig}, y_{orig})	Origin for MCIP Landuse Domain (x_{orig}, y_{orig})	Origin for CTM Domain (x_{orig}, y_{orig})
108km	(-3996×10^3, -2808×10^3)	N/A	N/A
36km	(432×10^3, -432×10^3)	(468×10^3, -396×10^3)	(540×10^3, -324×10^3)
12km	(972×10^3, -36×10^3)	(984×10^3, -24×10^3)	(1008×10^3, 0×10^3)
04km	(1200×10^3, 120×10^3)	(1204×10^3, 124×10^3)	(1212×10^3, 132×10^3)

Table 12B-2. Offset Definitions for the Tutorial MM5 Nest Domains

MM5 Domain	Resolution (km)	NCOLS	NROWS	Col. Offset from Parent Domain, D1	Row Offset from Parent Domain, D1	Col. Offset for nest	Row Offset for nest
D1	108	74	52	0	0	0	0
D2	36	36	36	41	22	41	22
D3	12	39	36	47	26.666666	15	11
D4	4	36	36	48.666666	28.111111	19	13

Table 12B-3. Dimensions of Set of MM5, MCIP, and CTM Domains for Each Grid Resolution for the Tutorial Study

Resolution	MM5 NCOLS	MM5 NROWS	MCIP NCOLS	MCIP NROWS	CTM NCOLS	CTM NROWS
108	74	52	N/A	N/A	N/A	N/A
36	36	36	34	34	30	30
12	39	36	37	34	33	30
4	36	36	34	34	30	30

12B.2Grid Domain Definitions for the Models-3 CMAQ Demonstration Study

Table 12B-4. Origins for the CMAQ demonstration MM5 domain, MCIP landuse domain, and CTM domains. Note that (x,y) corresponds to (COL,ROW) in CMAQ. MCIP landuse domain is smaller by one cell around than the original MM5 domain. Also, the CTM domain removes three cells around from the original MM5 domain. Origin is measured from the center of Base 108 km domain located at 90W and 40N.

Resolution ($\Delta x=\Delta y$)	Origin for original MM5 Domain (x_{orig}, y_{orig})	Origin for MCIP Landuse Domain (x_{orig}, y_{orig})	Origin for CTM Domain (x_{orig}, y_{orig})
108km	(-3996×10^3, -2808×10^3)	N/A	N/A
36km	(-1080×10^3, -1728×10^3)	(-1044×10^3, -1692×10^3)	(-864×10^3, -1512×10^3)
12km	(486×10^3, -216×10^3)	(480×10^3, -204×10^3)	(540×10^3, -144×10^3)
04km	(1140×10^3, 24×10^3)	(1144×10^3, 28×10^3)	(1164×10^3, 48×10^3)

Table 12B-5. Offset Definitions for the CMAQ Demonstration MM5 Nest Domains

MM5 Domain	Resolution (km)	NCOLS	NROWS	Col. Offset from Parent Domain, D1	Row Offset from Parent Domain, D1	Col. Offset for nest	Row Offset for nest
D1	108	74	52	0	0	0	0
D2	36	87	81	27	22	27	10
D3	12	102	84	42.333333	25	43	42
D4	4	87	105	48.555556	27.222222	56	20

Table B6. Dimensions of Set of MM5, MCIP, and CTM Domains for Each Grid Resolution for the CMAQ Demonstration Study

Resolution	MM5 NCOLS	MM5 NROWS	MCIP NCOLS	MCIP NROWS	CTM NCOLS	CTM NROWS
108	74	52	N/A	N/A	N/A	N/A
36	87	81	85	79	75	69
12	102	84	100	82	90	72
4	87	105	85	103	75	93

Appendix 12C Sample MCIP Configuration File

```
// RCS file, release, date & time of last delta, author, state, [and locker]
// $Header: /project/work/rep/MCIP/src/sunOS5/sun_m3_12.cfg,v 1.1.1.1 1997/10/13 17:38:23 yoj
Exp $

// what(1) key, module and SID; SCCS file; date and time of last delta:
// @(#)sun_m3_12.cfg  1.1 /project/mod3/MCIP/doc/bldrun/sunOS5/SCCS/s.sun_m3_12.cfg 14 Jun
1997 15:41:54

// This is a configuration file for
   model mcip_m3_12;

// f77_flags  "-e -Nl200 -fast -O4";
   f77_flags  "-e -g -C";

// link_flags "-fast -O4";
   link_flags "-e -g -C";

  libraries  "-L${M3TOOLS}/IOAPI/src_lib/SunOS5 -lm3io \
              -L${M3TOOLS}/netCDF/SunOS5 -lnetcdf";

// global { verbose | parse_only | compile_all | one_step | clean_up } ...

   global verbose;

// shared include files ////////////////////////////////////////////////

// Models-3 I/O API permanent includes
   include SUBST_IOPARMS     $M3TOOLS/IOAPI/includes/PARMS3.EXT;
   include SUBST_IOFDESC     $M3TOOLS/IOAPI/includes/FDESC3.EXT;
   include SUBST_IODECL      $M3TOOLS/IOAPI/includes/IODECL3.EXT;

// Models-3 global constants for this processor
   include SUBST_CONST       $M3MODEL/ICL/src/fixed/const/CONST.EXT;

// Models-3 grid definitions
   include SUBST_HGRD_ID     $M3MODEL/ICL/src/grid/D_12_15/HGRD_21X21.EXT;
   include SUBST_VGRD_ID     $M3MODEL/ICL/src/grid/D_12_15/VGRD.EXT;
   include SUBST_COORD_ID    $M3MODEL/ICL/src/grid/D_12_15/COORD_21X21.EXT;

// Models-3 I/O API files for this processor
   include SUBST_INFILES     $M3MODEL/MCIP/src/icl/icl/INFILES_MCIP.EXT;
   include SUBST_FILES       $M3MODEL/MCIP/src/icl/icl/FILES3_MCIP.EXT;

   include SUBST_MET_CONST   $M3MODEL/MCIP/src/icl/icl/CONST_mete.EXT;
   include SUBST_PBL_CONST   $M3MODEL/MCIP/src/icl/icl/CONST_pbl.EXT;
```

```
// MCIP parameters
   include SUBST_MPARM      $M3MODEL/MCIP/src/icl/icl/MCIPPARM.EXT;
   include SUBST_MCMMN      $M3MODEL/MCIP/src/icl/icl/MCIPCOM.EXT;
   include SUBST_MGOUT      $M3MODEL/MCIP/src/icl/icl/GROUTCOM.EXT;
   include SUBST_MCOUT      $M3MODEL/MCIP/src/icl/icl/MCOUTCOM.EXT;
   include SUBST_MDOUT      $M3MODEL/MCIP/src/icl/icl/MDOUTCOM.EXT;
   include SUBST_LRADM      $M3MODEL/MCIP/src/icl/icl/LRADMDAT.EXT;

////////////////////////////////////////////////////////////////////////////

// the mcip driver class
   module mcip development;

// the landuse class
   module m3radm development;

// the input class
   module m3 development;

// the met3d class
   module m3sup development;

// the pbl class
   module pblpkg development;

// the drydep class
   module radmdd development;

// the cloud class
   module radmkuo development;

// the util class
   module util development;

// the output class
   module stnd development;
```

Appendix 12D Sample MCIP Run Script

```
#! /bin/csh -f

# RCS file, release, date & time of last delta, author, state, [and locker]
# $Header: /project/work/rep/MCIP/src/sunOS5/sun_m3_12.q,v 1.1.1.1 1997/10/13 17:38:23 yoj
Exp $

# what(1) key, module and SID; SCCS file; date and time of last delta:
# @(#)sun_m3_12.q     1.2 /project/mod3/MCIP/doc/bldrun/sunOS5/SCCS/s.sun_m3_12.q 19 Jun 1997
08:26:34

# for Sun Sparc 20, UltraSparc 2
# method: sun_m3_12.q >&! sun_m3_12.log &

# QSUB -r sun_m3_12
# QSUB -eo -o /work/you/your_directory/sun_m3.log
# QSUB -lM 8Mw
# QSUB -lT 1800

 date; set timestamp; cat sun_m3_12.cfg; echo "    "; set echo

 setenv M3HOME /home/models3
 setenv M3DATA $M3HOME/datasets

#-----------------------------------------------------------
#  set executable
#-----------------------------------------------------------
 set EXEC = mcip_m3_12

#-----------------------------------------------------------
#  set base directory
#-----------------------------------------------------------
#set BASE = /work/you/your_directory
 set BASE = $cwd

#-----------------------------------------------------------
#  set working directories
#-----------------------------------------------------------
 set MCIPDIR = $BASE
 set OUTDIR  = $cwd

#-----------------------------------------------------------
#  set input data directories
#-----------------------------------------------------------
 set DATADIR = $M3HOME/datasets/nostudies

#-----------------------------------------------------------
```

```
#  (METROW,METCOL,METLAY) is (ROWS, COLS, LAYS) for MM5 data
#-----------------------------------------------------------------
 setenv METROW 25
 setenv METCOL 25
 setenv METLAY 15

#-----------------------------------------------------------------
#  (I0, J0):  The left bottom loc. of CTM domain in MET terms
#             In CTM terms, I0 = ROW_OFFSET, J0 = COL_OFFSET
#-----------------------------------------------------------------
 setenv I0 1
 setenv J0 1

#-----------------------------------------------------------------
#  LUTYPE:  Filetype for Landuse data:
#               1:  BINARY 13 category directly from TERRAIN
#               2:  Preprocessed ASCII 11 category
#               3:  Use MM5 internal dominant landuse category
#               4:  Use M3 landuse fractions available in GRIDCRO2D
#-----------------------------------------------------------------
 setenv LUTYPE 4

#-----------------------------------------------------------------
#  (I0LUSE, J0LUSE):  The left bottom loc. of CTM domain in
#             LAND USE DATA GRID terms
#-----------------------------------------------------------------
 setenv I0LUSE 1
 setenv J0LUSE 1

#-----------------------------------------------------------------
#  If LCALCPBL is:  TRUE,  Recompute PBL values
#                   FALSE, Read PBL values from MM52
#-----------------------------------------------------------------
 setenv LCALCPBL T

#-----------------------------------------------------------------
#  If LSLFLUX is:   TRUE,  Use only surface layer similarity
#                   FALSE, Use PBL similarity
#-----------------------------------------------------------------
 setenv LSLFLUX F

#-----------------------------------------------------------------
#  If LM3DDEP is:   TRUE,  Use Models-3 D. Dep routtine
#                   FALSE, Use RADM D. Dep. routine
#-----------------------------------------------------------------
 setenv LM3DDEP F

#-----------------------------------------------------------------
#  If LCALCCLD is:  TRUE:  Recompute CLOUD values
```

```
#                    FALSE: Read CLOUD values from MM52
#-------------------------------------------------------------
 setenv LCALCCLD T

#-------------------------------------------------------------
#  If LSANITY is:   TRUE:  check range of output parameters
#                   FALSE: do not check range of paramters
#-------------------------------------------------------------
 setenv LSANITY T

#-------------------------------------------------------------
#  JUDATE :  INITIAL JULIAN STUDY DATE (YYDDD)
#  HSTRT  :  STARTING HOUR OF JUDATE FOR STUDY
#  HTORUN :  NUMBER OF HOURS TO USE FROM MM5
#  HTOSKIP:  NUMBER OF HOURS TO SKIP FIRST
#-------------------------------------------------------------
# 88218 00 0 2  ! John's data
# 88216 12 0 49 ! Dave's data
# 88214 12 10 108 ! Daewon's data
 setenv JUDATE 88209
 setenv HSTRT 00
 setenv HTOSKIP 00
 setenv HTORUN  25
#setenv HTORUN 108

#-------------------------------------------------------------
#   input file linkage
#  MM51:  Filename for MM51 datafile
#  MM52:  Filename for MM52 datafile (NA if none)
#  LU13:  Filename for LU13 datafile (binary from TERRAIN)
#-------------------------------------------------------------
#setenv MM51 $INDIR/MM51_es80
#setenv MM52 $INDIR/MM52_es80
#setenv LU13 $INDIR/LU80
#setenv LUSE $DATADIR/LU11_80
#setenv LUSE /work/bdx/metpp/newmcip/input/LU11_80

#-------------------------------------------------------------
#   number of iterations for vertical wind correction
#    (Use 0, +/- 1,2,3,..)
#-------------------------------------------------------------
 setenv IWIND 0

#-------------------------------------------------------------
#   number of deposition layers (default = 1)
#             (for layer collapsing, it could be 2, or 3)
#-------------------------------------------------------------
 setenv NDEP 1
```

```
#-----------------------------------------------------------------
#  GRDNAM:  Grid Name (User Defined)
#-----------------------------------------------------------------
 setenv GRDNAM TUTOR12

#-----------------------------------------------------------------
#  EXECUTION_ID        (User Defined)
#-----------------------------------------------------------------
 setenv EXECUTION_ID  MCIP_BETA

#-----------------------------------------------------------------
#  SCENFILE: file path(User Defined)
#-----------------------------------------------------------------
#setenv SCENFILE    $BASE/

#-----------------------------------------------------------------
#  If IOAPI_CHECK_HEADERS is:  TRUE,  Check the headers
#                              FALSE, Do NOT check headers
#-----------------------------------------------------------------
 setenv IOAPI_CHECK_HEADERS F
#setenv LOGFILE mcip.log

#-----------------------------------------------------------------
#  Remove any previously generated output files
#-----------------------------------------------------------------
#/bin/rm GRID_* MET_*
#/bin/rm ../output/GRID_* ../output/MET_*

#-----------------------------------------------------------------
#  Set up input files
#-----------------------------------------------------------------
 setenv GRID_CRO_2D  $DATADIR'/GRIDCRO2D_TUT12'
 setenv GRID_DOT_2D  $DATADIR'/GRIDDOT2D_TUT12'
 setenv MET_CRO_2D   $DATADIR'/METCRO2D_TUT12'
 setenv MET_CRO_3D   $DATADIR'/METCRO3D_TUT12'
 setenv MET_DOT_3D   $DATADIR'/METDOT3D_TUT12'

#-----------------------------------------------------------------
#  Set up output files
#-----------------------------------------------------------------

 setenv GRID_BDY_2D_G1  $OUTDIR'/GRIDBDY2D_tut12'
 setenv GRID_BDY_3D_G1  $OUTDIR'/GRIDBDY3D_tut12'
 setenv GRID_CRO_2D_G1  $OUTDIR'/GRIDCRO2D_tut12'
 setenv GRID_CRO_3D_G1  $OUTDIR'/GRIDCRO3D_tut12'
 setenv GRID_DOT_2D_G1  $OUTDIR'/GRIDDOT2D_tut12'
 setenv MET_BDY_2D_G1   $OUTDIR'/METBDY2D_tut12'
 setenv MET_BDY_3D_G1   $OUTDIR'/METBDY3D_tut12'
```

```
 setenv MET_CRO_2D_G1    $OUTDIR'/METCRO2D_tut12'
 setenv MET_CRO_3D_G1    $OUTDIR'/METCRO3D_tut12'
 setenv MET_DOT_3D_G1    $OUTDIR'/METDOT3D_tut12'

#-----------------------------------------------------------
#  Execute MCIP
#-----------------------------------------------------------
#cdbx "$EXEC -g -x"; exit
# ja
#/opt/SUNWspro/bin/debugger "$MCIPDIR/$EXEC";  exit
 $MCIPDIR/$EXEC
# ja -cshlt

 exit()
#-----------------------------------------------------------
#  Move output to proper directory
#-----------------------------------------------------------
#/bin/mv GRID* ../output1/
#/bin/mv MET*  ../output1/
```

EPA/600/R-99/030

Chapter 13

THE INITIAL CONCENTRATION AND BOUNDARY CONDITION PROCESSORS

Gerald L. Gipson*
Human Exposure and Atmospheric Sciences Division
National Exposure Research Laboratory
U. S. Environmental Protection Agency
Research Triangle Park, NC 27711, USA

ABSTRACT

This chapter describes the two processors in the Community Multiscale Air Quality (CMAQ) modeling system that generate the initial concentrations and boundary conditions that are required by the CMAQ Chemical Transport Model (CCTM). The major emphasis is on the functionality incorporated in those processors – the initial condition (ICON) and boundary condition (BCON) processors. The chapter describes how each processor can be used to generate initial concentrations and boundary conditions from one of two sources – from predefined default vertical profiles or from other CMAQ simulation results when model nesting is being performed. A description of generating initial and boundary concentrations for special tracer species is also included. The procedures that are used in both processors for interpolating in both the horizontal and vertical directions are described. A description of methods for converting initial and boundary concentrations from one chemical mechanism form to another is also presented. Finally, the manner in which each processor is applied within the Models-3/CMAQ framework is addressed.

*Corresponding author address: Gerald L. Gipson, MD-80, Research Triangle Park, NC 27711. E-mail: ggb@hpcc.epa.gov

13.0 THE INITIAL CONCENTRATION AND BOUNDARY CONDITION PROCESSORS

13.1 Introduction

The solution of partial and ordinary differential equations that arise in air quality models requires both initial concentrations (ICs) and boundary conditions (BCs). This chapter describes the Community Multiscale Air Quality (CMAQ) modeling system processors that generate these quantities. In the discussions that follow, they will be referred to as the ICON and BCON processors, respectively. The ICs and BCs generated by these two processors are used by the CMAQ Chemical Transport Model (hereafter referred to as the CCTM). For ICs, the CCTM requires that the concentrations of all model species within each grid cell in the modeling domain be specified for the start of the simulation. Concentrations of all model species at the boundaries of the modeling domain throughout the simulation are required as BCs to the CCTM. The emphasis in this chapter is on how the ICs and BCs are generated rather than on how they are used in the CCTM. The reader is referred to Chapter 5 for a discussion of the latter.

The ICON and BCON processors have been designed to process data as automatically as possible. Users should be aware of certain operational assumptions that are employed by the two processors and the CCTM to insure that their applications are performed in the intended manner, however. The discussion below begins with a brief overview of the processors and their relationship to the CCTM. Several topics that address the various aspects of the IC/BC processing are then presented, including the input sources, spatial interpolation, species processing, and mechanism conversions. The last section provides a brief overview of how the ICON and BCON processors are applied.

13.2 Overview of the ICON and BCON Processors

The ICON and BCON processors generate ICs and BCs for individual model species, which include gas-phase mechanism species, aerosols, nonreactive species and tracer species. The techniques for selecting and processing species data will be discussed in more detail below. It is important to emphasize at the outset, however, that it is not necessary for the ICON and BCON processors to generate ICs and BCs for every species that is being modeled. The CCTM will attempt to extract ICs and BCs for each species being modeled from the input files. If a species is not found on the file, the CCTM will automatically set its ICs and BCs to a minimum threshold limit (i.e., a nominal zero). Any data on an IC or BC file for a species that is not being modeled will simply be ignored by the CCTM. Therefore, the user is encouraged to check the ICON, BCON, and CCTM output logs to insure that the ICs and BCs are being set in the intended manner.

The ICON processor generates species concentrations for every cell in the modeling domain, whereas the BCON processor generates species concentrations for the cells immediately surrounding the modeling domain. At present, the thickness of the boundary cells is limited to

one, which is the thickness required for all the transport algorithms currently included as part of the CCTM (e.g., see Chapter 7). The reader is referred to Chapters 6 and 7 for a description of the CMAQ conventions used in establishing modeling domains and their boundary cells.

Both the ICON and BCON processors write the output ICs and BCs to standard Models-3 Input/Output Application Programmer Interface (I/O API) files: 3-dimensional gridded files for the ICs and 3-dimensional boundary files for the BCs. The opening, formatting, and writing of these files are handled automatically by the ICON and BCON processors. It should be noted, however, that the IO/API has a limit of 120 output variables (i.e., number of species) for any one IO/API file. If the number of output variables exceeds the IO/API maximum, the ICON and BCON processors will generate up to two additional files to hold the outputs. If more than 360 output variables are needed, however, code modifications will need to be made to the ICON and BCON processors and the CCTM to accommodate the additional variables.

13.3 Input Sources

The ICON and BCON processors generate IC and BC files from one of three input sources. The first is a time invariant set of vertical concentration profiles. The second source of input data consists of existing Models-3 IO/API 3-dimensional concentration files, normally generated by the CCTM. The final source of IC and BC data involves the generation of special tracer species concentrations used to test numerical transport algorithms. Each of these will be discussed below. It should be added, however, that the ICON/BCON processors can be bypassed if the user desires to use a different method. The only requirement is that the IC and BC files that are eventually fed to the CCTM must be standard Models-3 IO/API gridded concentration and boundary concentration files. The reader is referred to IO/API documentation for a description of the structure and format of those files (EPA, 1998).

13.3.1 Time Invariant Concentration Profiles

This section describes the manner in which the ICON and BCON processors generate ICs and BCs from predefined, vertical concentration profiles. The CMAQ system contains a set of predefined profiles that can be used to generate the requisite ICs and BCs. These profiles give species concentrations as a function of height, and are spatially independent for the ICON processor and only minimally spatially dependent for the BCON processor. Both the ICON and BCON profile data are time independent. Since these data are not highly resolved, they are typically used when no other information about ICs and BCs is available. It should also be noted that the predefined profile files can be replaced by user developed profile data provided that the replacement files are in the same format as the predefined files. The discussion below begins with a description of the predefined profile data, and is followed by a description of how the user can prepare replacement data.

The default IC and BC profiles have been developed for the RADM2 chemical mechanism and the terrain following sigma-p coordinate system (see Chapter 6 for a discussion of CMAQ coordinate

types). Both the IC and BC profiles are intended to represent relatively clean air conditions in the eastern-half of the United States, and have been formulated from available measurements and results obtained from modeling studies. Thus, they do not represent any specific time period. Although profiles for other chemical mechanisms and vertical coordinate systems are not currently available in the CMAQ system, it may still be possible to use the predefined profiles for these cases. Special procedures are included with the ICON and BCON processors to allow conversion from one vertical resolution and/or chemical mechanism to another. These procedures will be described in sections 13.4.2 and 13.6, respectively.

The predefined profile data are stored in ASCII files in the CMAQ system. Table 13-1 contains a listing of the CMAQ predefined IC profile file. Note that line numbers have been added to the listing for reference. The first three lines contain informational text that is not used by the ICON processor. Line 4 contains the number of vertical layers and the number of species for which profiles have been developed, followed by the vertical coordinate values of the sigma-p levels. The fifth line is blank and is ignored by the ICON processor. Lines 6 through 46 contain vertical profiles for 43 different RADM2 gas-phase species. The species name is given in the first column, followed by mixing ratios (in ppm) for each layer. The first entry for a species corresponds to the lowest layer, whereas the last entry corresponds to the uppermost layer. Lines 47 through 52 contain analogous information for key aerosol species. The units for ASO4I, ASO4J, and ASOIL are $\mu g/m^3$, and the units for NUMATKN, NUMACC, and NUMCOR are number/m^3.

Table 13-2 contains a listing of the corresponding predefined BC profile file. The format for this file is similar to that for the IC file, except that one set of profiles is input for each of the four different boundaries of the modeling domain (i.e., north, east, south and west). The BCON processor uses the appropriate set of profiles to generate the BCs at each edge of the modeling domain. Again, line five is blank and is ignored by the BCON processor.

As indicated above, the user can replace a CMAQ predefined profile file with one of their own provided the same file format is used. As noted in the discussion above, none of the first three text lines nor the fifth line in either file is used. Thus, those lines can contain any information or be blank, but they must be present in the file. The remaining data lines are read in FORTRAN list-directed format, so it is not necessary to align the data by columns. The only formatting requirement is that all inputs be separated by commas or by one or more blanks. The species names must not exceed 16 characters and must not contain any blanks. Also, it is not necessary that a six-layer vertical resolution be used, but at least one layer must be present and no more than 30 are allowed. Note that the number of layer heights on line 4 must be one greater than the actual number of layers used. These layer heights must correspond to the heights of the layer interfaces (i.e., not the mid-layer heights), and the first entry for any profile must be for the lowest level (i.e., ground-level). The input mixing ratios, however, are interpreted as layer average values as opposed to values at the layer interfaces. Finally, note that the BC vertical profile data for each edge begins with a line that contains the edge name. Although the processors do not require that these names be specified explicitly, a line corresponding to the edge name line must

be included and the processors expect the data for each edge to be input in the order shown in Table 13-2 (i.e., north, east, south, and west).

13.3.2 CCTM Concentration files

Both the ICON and BCON processors can be configured to generate ICs and BCs from existing Models-3 IO/API 3-dimensional, gridded, concentration files. This situation typically arises when performing a nested model simulation and modeling results are available for a coarser grid. Unlike the predefined profile files described above, the CCTM concentration files are both temporally and spatially resolved, necessitating some additional processing procedures. (The subject of spatial interpolation is described in section 13.4.) It should be added, however, that it is not necessary to use the ICON processor for a model continuation run (i.e., a run in which a model simulation is started at the exact same time that a previous one ended and the same modeling domain is being used). In such cases the CMAQ IO/API concentration file from the previous run may be used directly as the input IC file to the CCTM. However, it will still be necessary to generate a BC input file.

Since ICs are required only for the start of a model simulation, the ICON processor will generate ICs for only one time step. BCs are required throughout a simulation, however, so the user must prescribe the period of record for which to produce outputs. One set of BCs will be generated at each time step for that period of record. To illustrate, consider the case in which a model simulation has been performed for a coarse grid for a 24-hour period of record using 1-hour time steps (i.e., the model concentrations were predicted at hourly intervals). The IO/API gridded concentration file for the coarse grid will then contain species concentrations for 25 time steps, one for the start of the simulation (i.e., the ICs for that simulation) and 24 time steps corresponding to the model predictions at each hour. Now assume that it is desired to generate ICs and BCs for a nested model simulation for the same time period. The user would select the first time step for the ICON output, and the ICON processor would generate ICs for that time step only. For the BCON processor, the period of record for the output BCs would be obtained by selecting the same starting time and setting the duration for outputs at 24 hours. This selection would produce 25 time steps on the output file, one for the start and 24 for each of the subsequent simulation hours. The manner in which the time controls are set is described in the Models-3 User Manual (EPA, 1998).

13.3.3 Tracer Species

The ICON and BCON processors also contain the capability to generate ICs and BCs for special tracer species that can be used to investigate the accuracy of the various transport and diffusion algorithms available in the CCTM system. This capability has been included primarily to facilitate the evaluation of alternative algorithms, and thus would not likely be used in most air quality modeling applications.

ICs and BCs can be generated for eight different tracers. Each one can be used to examine different properties of transport algorithms, and thus can be selected individually for output. They are chosen by including specially defined tracer names in the list of model species. The defined names and a brief description of each tracer species follow. (Note that the ICs for these tracers can be viewed with one of the visualization tools to examine the patterns more closely.)

- IC1_BC0: All ICs in the modeling domain are set to 1.0 and all BCs are set to 0.0.
- IC1_BC1: All ICs in the modeling domain are set to 1.0 and all BCs are set to 1.0.
- IC0_BC1: All ICs in the modeling domain are set to 0.0 and all BCs are set to 1.0.
- STREET: Within any horizontal cross-section of cells, IC cell concentrations are set to either 1.0 or 0.0 such that the overall domain pattern resembles a street grid. All BCs are set to zero.
- CHKBRD: Within any horizontal cross-section of cells, IC cell concentrations are set to either 1.0 or 0.0 such that the overall domain pattern resembles a checkerboard. All BCs are set to zero.
- SPOS_A: ICs and BCs are set such that a concentration mound is centered at cell (10,10) in the modeling domain, and the concentration profile is defined below.
- SPOS_B: ICs and BCs are set such that a concentration mound is centered at cell (10,10) in the modeling domain, and the concentration profile is defined below.
- SPOS_C: ICs and BCs are set such that a concentration mound is centered at cell (10,10) in the modeling domain, and the concentration profile is defined below.

$$h_s = \frac{a^2}{a^2 + (x-x_r)^2 + (y-y_r)^2} \tag{13-1}$$

The last three tracer species are designed for superposition tests of transport algorithms. The base shape of the concentration mounds is described by the Witch of Agnesi surface:where a is the radius of the mound, x_r and y_r define the position of the peak of the mound, and h_s is the height of the mound. In the ICON and BCON processors, a is set to 3 and (x_r, y_r) to (10,10).

The three tracer signals h_A, h_B, and h_C for SPOS_A, SPOS_B, and SPOS_C are then defined as follows:

$$h_A = q_{\max} (1 + h_s) + q_{\min} , \tag{13-2a}$$

$$h_B = 2 q_{\max} (1 + h_s) - q_{\min} , \tag{13-2b}$$

$$h_C = - q_{\max} (1 + h_s) + 2 q_{\min} , \tag{13-2c}$$

where $q_{\max}$ and $q_{\min}$ determine the amplitude and background values of the signals, and both are set to 50 in the ICON and BCON processor. With these signals, the addition of mounds B and C will yield mound A. Thus, the degree to which h_A - (h_B+ h_C) differs from zero in an advection test provides a measure of the nonlinearity of the advection algorithm.

13.4 Spatial Interpolation

Both the ICON and BCON processors are designed to account for differences in spatial resolution between the input files and the IC/BC output files on an automatic basis. As described in Chapter 6, the CMAQ system is designed to handle different types of horizontal and vertical coordinate systems. All of the data required to completely specify the horizontal and vertical grid structure are contained in three INCLUDE files that are generated by the Models-3 framework: COORD.EXT, HGRD.EXT, and VGRD.EXT. When the CCTM is compiled (or built), these three files are included with the source code, thereby providing the CCTM with all of the necessary information on the grid structure that is being used. Both the ICON and BCON processors operate in a similar fashion, and thus both processors must be built with the same three INCLUDE files that are used to build the CCTM that will eventually use the ICs and BCs. Grid information on the IC/BC inputs is extracted from the input files themselves, so no additional information is required for them. Note that either the horizontal and vertical coordinates for the input file may be of a different type than that for the output file, or they may be of the same type but have different extents or resolutions.

13.4.1 Horizontal Interpolation

Horizontal interpolation is required when a CCTM concentration file is being used as input to either ICON or BCON and the horizontal coordinate system of the input file differs from that needed for the output file. Such cases typically arise when ICs and BCs are being generated for a nested modeling domain that has a finer resolution than a coarser, outer domain. Note that no horizontal interpolation is necessary if both the input and output domains have the same structure or if the time invariant profiles are being used to generate the ICs and BCs.

Disparities in horizontal grid structure are handled by mapping each vertical column of output cells to a corresponding column of input cells. The vertical concentration profiles corresponding

to the input column of cells are then used as the vertical profiles for the output column of cells. Note that some vertical interpolation may also be required as described in the next section. The horizontal mapping is done on the basis of cell proximity. The ground-level latitudes and longitudes at the center of each vertical column of cells are first calculated for both the input and output domains. These computed values are then used to find which input column is closest to each output column. Since the ICON and BCON can compute latitude and longitude for any of the available CMAQ map projections, the horizontal grid coordinate of the input and output files do not have to be the same type.

13.4.2 Vertical Interpolation

In some applications, the ICON and BCON may be required to generate ICs and BCs for a vertical grid system that is different from the one used for the input file. The CCTM is capable of handling several different vertical grid structures (e.g., sigma-p, sigma-z, pressure, etc.), and each of those grid types can have different vertical resolutions (i.e., different numbers of vertical layers or different spacings with the same number of layers). If the vertical structure of the input and output grids is identical (i.e., both are of the same type and have the same vertical resolution), then the processing of input data to output data is routine because of the one-to-one correspondence of the vertical layers. If the vertical grid types or resolutions are different, however, the ICON and BCON will convert from the input to the output vertical structure in most cases. Conversions from one resolution to another can be performed using either profile data or CCTM concentration files, but conversions from one grid type to another can only be performed when using CCTM concentration files. Both the ICON and BCON processors assume that the vertical grid-type of the profile data is the same as the required output structure, and thus no conversions can be performed in that case. The two different vertical interpolation cases that can be performed by the ICON and BCON processors are described next.

Identical Vertical Grid Types, Different Resolutions. When the input and output vertical grid types are the same but vertical resolutions are different, both ICON and BCON will derive ICs or BCs by linear interpolation using the layer heights contained in the input files and those contained in the COORD.EXT INCLUDE file. These heights are in the units of the vertical coordinate system (e.g., sigma-p, sigma-z, pressure, etc.) rather than height above ground level as measured in distance units such as feet or meters. The vertical resolution of the input IC/BC data can be either greater than or less than the output resolution. Linear interpolation is performed using layer heights that correspond to the middle of the layers. Output concentrations are not always interpolated for the bottommost and topmost layers, however. Output concentrations for all layers with mid-layer heights less than the bottommost mid-layer height in the input file will be set equal to the concentration of that bottommost layer. Similarly, output concentrations for all layers above the input topmost mid-layer height will be set equal to the concentration of the topmost layer.

Different Vertical Grid Types. A complete switch of vertical coordinate types can be carried out when the following two conditions are met: 1) the input IC/BC data are in standard Models-3

IO/API files and 2) the gridded 3-dimensional meteorological files that contain the mid-layer heights for both vertical coordinate systems are also available (see Chapter 12 for a description of these meteorological files). When these conditions are met, the ICON and BCON processors will use linear interpolation to convert from one coordinate system to another. The interpolation is performed in exactly the same manner as described in the previous paragraph, except that the mid-layer heights are taken from the 3-dimensional meteorological files which give the mid-layer heights in meters above ground level for both the input IC/BC data and the output IO/API files. Thus, the meteorological data files containing the layer heights in meters above ground level must be available for *both the input and output grids* before the ICON and BCON processors can be used.

13.5 ICON/BCON Species Processing

The selection of species that are to be modeled and thus require ICs and BCs is controlled by the Program Control Processor (PCP). A detailed description of that processor is contained in Chapter 15, and will not be repeated here. A brief overview of some of the relationships between the PCP and the ICON/BCON processors is presented here to facilitate the description of species processing, however.

The species that are to be modeled in a CCTM simulation are determined when the user invokes the PCP in the Models-3 framework to select a gas phase chemical mechanism, whether or not aerosols are to be included, and whether to include other nonreactive and/or tracer species. The Models-3 framework generates four INCLUDE files that contain the names of all species that are to be modeled -- GC_SPC.EXT, AE_SPC.EXT, NR_SPC.EXT, and TR_SPC.EXT (collectively referred to below as the SPC INCLUDE files). The Models-3 framework also allows the user to invoke special treatment of the ICs and BCs for individual species by defining special surrogate names and providing corresponding scale factors for the calculation of ICs (EPA, 1998). The Models-3 framework generates four INCLUDE files that contain this information -- GC_ICBC.EXT, AE_ICBC.EXT, NR_ICBC.EXT, and TR_ICBC.EXT (collectively referred to below as the ICBC INCLUDE files). Note that some of these files may not contain any entries depending on the user's selection, but all files will be generated by the framework. Just as both the SPC and ICBC INCLUDE files must be included when the CCTM is built, they must also be included when the ICON and BCON processors are built.

The SPC INCLUDE files contain the names of all species to be modeled and will therefore require ICs and BCs in the CCTM. The ICON/BCON processors use the information in both the SPC and the ICBC INCLUDE files to determine which species data should be extracted from the input file and be subsequently written to the output file. The ICON and BCON processors also include an option to convert from one chemical mechanism to another. Since it represents a special option with its own unique rules, it is described separately in section 13.6. The subsequent discussion focuses on the treatment of individual species for two cases - one with and one without associated surrogate names.

Consider first the case in which a surrogate name is not specified. This situation occurs when a model species (i.e., one whose name is included in one of the SPC INCLUDE files) does not have a surrogate name assigned to it. In this case, the ICON and BCON processors simply check to see if the input file contains data for a species with the exact same name as the model species name. If none is found, ICs and BCs are not generated for that species. If a match is found, the data for that species are extracted from the input file, processed, and written to the IC and BC output files.

The assignment of a surrogate name to a particular species complicates the processing slightly. Surrogate names in the CMAQ system arise at least in part from the generalized treatment of the chemical mechanisms and the fact that species names are not "hardwired" in the CMAQ system. Their primary function is to link a model species with data that are associated with a species of a different name. Two examples are presented to illustrate potential uses.

The first example illustrates how surrogates can be used to provide simple links from one species to another. First, suppose a series of CMAQ model simulations had been performed using the CMAQ system standard RADM2 mechanism in which formaldehyde is named HCHO. Thus, all of the data for that species will be associated with the name HCHO in the CMAQ system data files. Now consider that a researcher wants to make use of that data but will be using their own version of the RADM2 mechanism in which formaldehyde is named FORM. To use the older modeling data, the researcher could either change the formaldehyde name in the chemical mechanism to conform to the original RADM2 name or assign the surrogate HCHO for FORM. In the latter case, both the ICON/BCON processors and the CCTM are designed to extract IC/BC data using the surrogate name in place the model species name. This will be explained in more detail further below.

The second example of using a surrogate name illustrates how scale factors can be used with surrogates. Suppose a researcher is experimenting with a new chemical mechanism which divides a particular species PAR into two new species, PAR1 and PAR2. Further, suppose the researcher wants to use existing CMAQ model simulations with the PAR species to generate ICs and BCs for both PAR1 and PAR2. The researcher will assume that 25% of the PAR IC/BC concentrations will be assigned to PAR1 and 75% to PAR2. To effect this in the CMAQ modeling system, the researcher can assign the species surrogate name PAR to *both* PAR1 and PAR2, and assign 0.25 to the ICBC scale factor for PAR1 species and 0.75 to the ICBC scale factor for PAR2. The ICON/BCON processors and CCTM will use this information to compute the proper ICs and BCs for the two species PAR1 and PAR2 from the input PAR values. The procedures followed by both the ICON/BCON and the CCTM are described next.

The introduction of surrogate names for IC and BC species affects the manner in which both the ICON/BCON processors and the CCTM operate. Consider first the processing that takes place in the ICON/BCON processors. Each species in the SPC INCLUDE files is selected for processing individually. If a surrogate name is assigned to that species, the IC/BC input files are examined to see if the surrogate name is included with the inputs. If the surrogate name is on the input file, the

data corresponding to that name are extracted from the input file, processed and output *under the surrogate name*. Further, the ICBC scale factors are not applied in the ICON and BCON. If the surrogate name is not found on the input data file, the ICON/BCON processors will then check the input file using the model species name as if no surrogate name had existed. Again, if a match is found using the model species name, the corresponding data are extracted and output *under the model species name*. If the input file does not contain any data under the surrogate name or the model species name, then no IC/BC data are generated for that particular model species.

Now consider processing in the CCTM when surrogate names are used for ICs/BCs. The CCTM processes each species in the SPC INCLUDE files individually. If a surrogate name is specified for the model species and it is found on the IC/BC input files, the CCTM extracts the data for that name, applies the scale factor to those data, and then assigns the scaled concentrations to the ICs and BC concentrations for the model species. If the surrogate species name is not found on the input IC/BC files, the input file is checked using the model species name contained in the SPC INCLUDE files. If data for that model species are found, then the data are extracted and used directly as ICs and BCs (i.e., no scale factors are applied). If data for the species are not found on the input file, the ICs and BCs are set to the lower threshold limits.

For most routine applications, users need not concern themselves with surrogate mapping issues. The ICON and BCON processors are designed to generate the appropriate ICs and BCs with minimal user interaction, *provided the correct input files and include files are used with the processors*. Both the ICON and the BCON processors generate a species map on the output log that reports the relationship between the input and output IC and BC species. The user can check these logs to insure that the desired species mapping has been performed. Further, the CCTM's output log lists those species for which the lower threshold limits are used, and these should be checked to insure that the ICs/BCs for an important species have not been omitted.

13.6 Mechanism Conversions

The vertical profile data and the CCTM concentration file data that were described above normally correspond to one gas-phase, chemical mechanism. For example, the predefined, vertical profile data presently in the CMAQ system were developed for the RADM2 chemical mechanism. The capability to convert from one gas phase chemical mechanism to another has been included in the ICON and BCON processors, however. It should be emphasized that there is not always a definite correspondence between chemical mechanism species, and it is usually necessary to make several assumptions to make such conversions. This is particularly true for organic species that may be defined differently in two mechanisms. Nevertheless, some simple mechanism conversion capabilities have been included for those cases in which approximations are acceptable for converting from one mechanism to another.

A special routine to generate ICs and BCs for the CB4 chemical mechanism from RADM2 gas-phase mechanism inputs is included as part of the ICON and BCON processor options. At present, no other "hardwired" conversion routines are available in the system, but it is conceivable

that some could be added in the future as more chemical mechanisms are added to the CMAQ system. No conversion from CB4 to RADM2 format has been included because the carbon bond lumping technique makes it difficult to disaggregate mechanism species into their original chemical compounds. For a description of these two mechanisms, the reader is referred to Chapter 8. The hardwired RADM2 to CB4 conversion procedures that are used are the same as for the generalized conversion processor that is described next.

As a convenience for the user, a generalized mechanism conversion processor has also been included in both the ICON and BCON processors. This conversion procedure requires the user to generate an ASCII input file that contains mechanism conversion rules. Thus, the user is responsible for defining how the mechanism conversion is to be performed. An example file showing the conversion from RADM2 to CB4 is included in Table 13-3. The file contains the expressions that are used to convert the ICs and BCs from one mechanism form to another. The ICs and BCs for the CB4 species (i.e., those on the left hand side of the equal sign) are computed from the RADM2 species concentrations (i.e., those on the right hand side of the equal sign) according to the equations shown. As is evident, there is a simple one-to-one correspondence for most species and lumping only occurs for relatively few species. It should also be noted that no conversions will be performed for those species that are not included in the input file, and thus no ICs or BCs will be generated for them. As mentioned previously, the user is advised to review the species map on the ICON/BCON output log to insure that the conversions are being done as intended. Finally, it should be added that the mechanism conversion option applies only to the gas phase chemistry species. Aerosol, nonreactive and tracer species will be processed in the standard way, regardless of whether a mechanism conversion is being performed.

The format for the mechanism conversion rules is relatively simple. Species names must be 16 characters or less and not contain any blanks. Only one species is permitted on the left-hand side of the equation, and the species name should correspond to a name in the output mechanism. The equal sign must be present, and at least one species name must appear to the right of it. Coefficients for species are allowed on the right-hand side only, and they can be in either integer, real, or exponential format. They must always be followed by an asterisk to indicate multiplication. For expressions involving lumping of species, only addition is allowed and it is indicated by a plus sign. Line-wrap is allowed so that a single lumping rule can span more than one line. Each conversion rule must conclude with a semicolon, and the last command must be "END;". Finally, the input files are read in a free form input that generally ignores white spaces between species names, coefficients, operators and line terminators.

13.7 ICON/BCON Applications

This section provides an overview of how the ICON and BCON processors are applied in practice. Applications are normally carried out in two steps: compilation (or building) and execution. As mentioned earlier, when the ICON and BCON executables are built, the grid INCLUDE files for the modeling domain must be included. In addition, the user must select four modules that determine the ICON/BCON processing routines to incorporate when the executable

is built. Two modules must always be present: *icon* (or *bcon* in the case of the BCON processor) and *icl*. These two modules contain processing routines that are common to all applications. One of the following three modules must be chosen to include the routines to process the specific input source: 1) *profile* for using a time invariant vertical concentration profile contained in an ASCII file, 2) *m3conc* for processing a CMAQ IO/API concentration file, or 3) *tracer* for generating special tracer species ICs and BCs. Finally, one of three modules must also be selected to control the mechanism conversion procedure: 1) *noop* for no mechanism conversion, 2) *radm2_to_cb4* for a CMAQ predefined RADM2 to CB4 conversion, or 3) *user_defined* to process a user generated ASCII file (e.g., Table 13-3) containing mechanism conversion rules that are used to generate ICs and BCs for one mechanism using input concentrations for a different mechanism.

The second step involves running the processors with all necessary input files assigned and the time control parameters set. Both are provided to the processors by means of environment variables. The input and output files are assigned by means of predefined logical file names. The ICON processor requires a starting date and time in the Models-3 conventional time stamp format. The BCON processor requires both a starting date and time and a run duration parameter.

For detailed information on compiling and running these processors, the reader is referred to the Models-3 User Manual (EPA, 1998).

13.8 References

EPA, 1998. *Models-3 Volume 9b: User Manual*, Draft EPA report, U. S. Environmental Protection Agency, Research Triangle Park, N.C.

This chapter is taken from *Science Algorithms of the EPA Models-3 Community Multiscale Air Quality (CMAQ) Modeling System*, edited by D. W. Byun and J. K. S. Ching, 1999.

Table 13-1. CMAQ Predefined Vertical Profiles for Initial Concentrations

```
1 Optional boundary condition: The vertical coordinate of the model to
2 generate these b.c. is the terrain-following sigma coordinate. The number of
3 sigma  layers and defined sigma levels are listed below.
4 6      47   1.00  0.98  0.93  0.84  0.60  0.30  0.00
5
6 SO2        0.300E-03  0.200E-03  0.100E-03  0.100E-03  0.200E-04  0.100E-04
7 SULF       0.150E-03  0.150E-03  0.100E-03  0.100E-03  0.200E-04  0.100E-04
8 NO2        0.200E-04  0.200E-04  0.100E-04  0.000E+00  0.000E+00  0.000E+00
9 NO         0.200E-04  0.200E-04  0.100E-04  0.000E+00  0.000E+00  0.000E+00
10 O3        0.350E-01  0.350E-01  0.400E-01  0.500E-01  0.600E-01  0.700E-01
11 HNO3      0.500E-04  0.500E-04  0.500E-04  0.500E-04  0.700E-04  0.100E-03
12 H2O2      0.100E-02  0.100E-02  0.150E-02  0.100E-02  0.800E-03  0.200E-03
13 ALD       0.300E-04  0.350E-04  0.300E-04  0.200E-04  0.200E-04  0.100E-04
14 HCHO      0.250E-03  0.250E-03  0.250E-03  0.200E-03  0.100E-03  0.500E-04
15 OP1       0.250E-06  0.250E-06  0.250E-06  0.200E-06  0.100E-06  0.500E-07
16 OP2       0.300E-07  0.350E-07  0.300E-07  0.200E-07  0.200E-07  0.100E-07
17 PAA       0.300E-04  0.300E-04  0.300E-04  0.250E-04  0.200E-04  0.150E-04
18 ORA1      0.100E-05  0.100E-05  0.500E-06  0.500E-06  0.500E-06  0.000E+00
19 ORA2      0.100E-05  0.100E-05  0.500E-06  0.500E-06  0.500E-06  0.000E+00
20 NH3       0.100E-03  0.100E-03  0.300E-04  0.200E-04  0.200E-04  0.100E-04
21 N2O5      0.000E+00  0.000E+00  0.000E+00  0.000E+00  0.000E+00  0.000E+00
22 NO3       0.000E+00  0.000E+00  0.000E+00  0.000E+00  0.000E+00  0.000E+00
23 PAN       0.200E-04  0.200E-04  0.100E-04  0.100E-04  0.100E-04  0.000E+00
24 HC3       0.400E-04  0.400E-04  0.320E-04  0.120E-04  0.400E-05  0.000E+00
25 HC5       0.400E-04  0.400E-04  0.320E-04  0.120E-04  0.400E-05  0.000E+00
26 HC8       0.200E-04  0.200E-04  0.160E-04  0.600E-05  0.200E-05  0.000E+00
27 ETH       0.000E+00  0.000E+00  0.000E+00  0.000E+00  0.000E+00  0.000E+00
28 CO        0.800E-01  0.800E-01  0.800E-01  0.700E-01  0.650E-01  0.500E-01
29 OL2       0.500E-05  0.300E-05  0.200E-05  0.100E-05  0.100E-05  0.000E+00
30 OLT       0.200E-06  0.200E-06  0.100E-06  0.000E+00  0.000E+00  0.000E+00
31 OLI       0.100E-06  0.100E-06  0.000E+00  0.000E+00  0.000E+00  0.000E+00
32 TOL       0.100E-05  0.100E-05  0.100E-05  0.100E-05  0.000E+00  0.000E+00
33 XYL       0.200E-06  0.200E-06  0.100E-06  0.000E+00  0.000E+00  0.000E+00
34 ACO3      0.100E-08  0.100E-08  0.100E-08  0.100E-08  0.100E-08  0.100E-08
35 TPAN      0.100E-07  0.100E-07  0.100E-07  0.100E-07  0.100E-07  0.100E-07
36 HONO      0.100E-08  0.100E-08  0.100E-08  0.100E-08  0.100E-08  0.100E-08
37 HNO4      0.200E-08  0.200E-08  0.200E-08  0.200E-08  0.200E-08  0.200E-08
38 KET       0.300E-04  0.350E-04  0.300E-04  0.200E-04  0.200E-04  0.100E-04
39 GLY       0.250E-06  0.250E-06  0.250E-06  0.200E-06  0.100E-06  0.500E-07
40 MGLY      0.250E-06  0.250E-06  0.250E-06  0.200E-06  0.100E-06  0.500E-07
41 DCB       0.250E-06  0.250E-06  0.250E-06  0.200E-06  0.100E-06  0.500E-07
42 ONIT      0.200E-04  0.200E-04  0.160E-04  0.600E-05  0.200E-05  0.000E+00
43 CSL       0.100E-08  0.100E-08  0.100E-08  0.100E-08  0.100E-08  0.100E-08
44 ISO       0.250E-05  0.250E-05  0.250E-05  0.250E-05  0.250E-05  0.250E-05
45 HO        0.000E+00  0.000E+00  0.000E+00  0.000E+00  0.000E+00  0.000E+00
46 HO2       0.000E+00  0.000E+00  0.000E+00  0.000E+00  0.000E+00  0.000E+00
47 ASO4I     4.810E-02  3.207E-02  1.603E-02  1.603E-02  3.207E-03  1.603E-03
48 ASO4J     1.154E+00  7.696E-01  3.848E-01  3.848E-01  7.696E-02  3.848E-02
49 NUMATKN   1.437E+10  9.583E+09  4.791E+09  4.791E+09  9.583E+08  4.791E+08
```

Table 13-1. CMAQ Predefined Vertical Profiles for Initial Concentrations

50	NUMACC	4.110E+08	2.740E+08	1.370E+08	1.370E+08	2.740E+07	1.370E+07
51	ASOIL	1.000E+00	8.000E-01	4.000E-01	4.000E-01	8.000E-02	4.000E-02
52	NUMCOR	1.740E+04	1.392E+04	6.960E+03	6.960E+03	1.392E+03	6.960E+02

Table 13-2. CMAQ Predefined Vertical Profiles for Boundary Conditions

```
1 Optional boundary condition: The vertical coordinate of the model to
2 generate these b.c. is the terrain-following sigma coordinate. The number of
3 sigma layers and defined sigma levels are listed below.
4 6      47   1.00  0.98  0.93  0.84  0.60  0.30  0.00
5
6  North
7
8 SO2        0.300E-03  0.200E-03  0.100E-03  0.100E-03  0.200E-04  0.100E-04
9 SULF       0.150E-03  0.150E-03  0.100E-03  0.100E-03  0.200E-04  0.100E-04
10 NO2       0.200E-04  0.200E-04  0.100E-04  0.000E+00  0.000E+00  0.000E+00
11 NO        0.200E-04  0.200E-04  0.100E-04  0.000E+00  0.000E+00  0.000E+00
12 O3        0.350E-01  0.350E-01  0.400E-01  0.500E-01  0.600E-01  0.700E-01
13 HNO3      0.500E-04  0.500E-04  0.500E-04  0.500E-04  0.700E-04  0.100E-03
14 H2O2      0.100E-02  0.100E-02  0.150E-02  0.100E-02  0.800E-03  0.200E-03
15 ALD       0.300E-04  0.350E-04  0.300E-04  0.200E-04  0.200E-04  0.100E-04
16 HCHO      0.250E-03  0.250E-03  0.250E-03  0.200E-03  0.100E-03  0.500E-04
17 OP1       0.250E-06  0.250E-06  0.250E-06  0.200E-06  0.100E-06  0.500E-07
18 OP2       0.300E-07  0.350E-07  0.300E-07  0.200E-07  0.200E-07  0.100E-07
19 PAA       0.300E-04  0.300E-04  0.300E-04  0.250E-04  0.200E-04  0.150E-04
20 ORA1      0.100E-05  0.100E-05  0.500E-06  0.500E-06  0.500E-06  0.000E+00
21 ORA2      0.100E-05  0.100E-05  0.500E-06  0.500E-06  0.500E-06  0.000E+00
22 NH3       0.100E-03  0.100E-03  0.300E-04  0.200E-04  0.200E-04  0.100E-04
23 N2O5      0.000E+00  0.000E+00  0.000E+00  0.000E+00  0.000E+00  0.000E+00
24 NO3       0.000E+00  0.000E+00  0.000E+00  0.000E+00  0.000E+00  0.000E+00
25 PAN       0.200E-04  0.200E-04  0.100E-04  0.100E-04  0.100E-04  0.000E+00
26 HC3       0.400E-04  0.400E-04  0.320E-04  0.120E-04  0.400E-05  0.000E+00
27 HC5       0.400E-04  0.400E-04  0.320E-04  0.120E-04  0.400E-05  0.000E+00
28 HC8       0.200E-04  0.200E-04  0.160E-04  0.600E-05  0.200E-05  0.000E+00
29 ETH       0.000E+00  0.000E+00  0.000E+00  0.000E+00  0.000E+00  0.000E+00
30 CO        0.800E-01  0.800E-01  0.800E-01  0.700E-01  0.650E-01  0.500E-01
31 OL2       0.500E-05  0.300E-05  0.200E-05  0.100E-05  0.100E-05  0.000E+00
32 OLT       0.200E-06  0.200E-06  0.100E-06  0.000E+00  0.000E+00  0.000E+00
33 OLI       0.100E-06  0.100E-06  0.000E+00  0.000E+00  0.000E+00  0.000E+00
34 TOL       0.100E-05  0.100E-05  0.100E-05  0.100E-05  0.000E+00  0.000E+00
35 XYL       0.200E-06  0.200E-06  0.100E-06  0.000E+00  0.000E+00  0.000E+00
36 ACO3      0.100E-08  0.100E-08  0.100E-08  0.100E-08  0.100E-08  0.100E-08
37 TPAN      0.100E-07  0.100E-07  0.100E-07  0.100E-07  0.100E-07  0.100E-07
38 HONO      0.100E-08  0.100E-08  0.100E-08  0.100E-08  0.100E-08  0.100E-08
39 HNO4      0.200E-08  0.200E-08  0.200E-08  0.200E-08  0.200E-08  0.200E-08
40 KET       0.300E-04  0.350E-04  0.300E-04  0.200E-04  0.200E-04  0.100E-04
41 GLY       0.250E-06  0.250E-06  0.250E-06  0.200E-06  0.100E-06  0.500E-07
42 MGLY      0.250E-06  0.250E-06  0.250E-06  0.200E-06  0.100E-06  0.500E-07
43 DCB       0.250E-06  0.250E-06  0.250E-06  0.200E-06  0.100E-06  0.500E-07
44 ONIT      0.200E-04  0.200E-04  0.160E-04  0.600E-05  0.200E-05  0.000E+00
45 CSL       0.100E-08  0.100E-08  0.100E-08  0.100E-08  0.100E-08  0.100E-08
46 ISO       0.250E-05  0.250E-05  0.250E-05  0.250E-05  0.250E-05  0.250E-05
47 HO        0.000E+00  0.000E+00  0.000E+00  0.000E+00  0.000E+00  0.000E+00
48 HO2       0.000E+00  0.000E+00  0.000E+00  0.000E+00  0.000E+00  0.000E+00
```

Table 13-2. CMAQ Predefined Vertical Profiles for Boundary Conditions

49 ASO4I	2.405E-02	2.405E-02	1.603E-02	1.603E-02	3.207E-03	1.603E-03
50 ASO4J	5.772E-01	5.772E-01	3.848E-01	3.848E-01	7.696E-02	3.848E-02
51 NUMATKN	7.187E+09	7.187E+09	4.791E+09	4.791E+09	9.583E+08	4.791E+08
52 NUMACC	2.055E+08	2.055E+08	1.370E+08	1.370E+08	2.740E+07	1.370E+07
53 ASOIL	5.000E-01	5.000E-01	4.000E-01	4.000E-01	8.000E-01	3.000E-01
54 NUMCOR	8.750E+03	8.750E+03	7.000E+03	7.000E+03	1.400E+03	5.250E+02
55 East						
56						
57 SO2	0.000E+00	0.000E+00	0.000E+00	0.000E+00	0.000E+00	0.000E+00
58 SULF	0.200E-03	0.200E-03	0.200E-03	0.200E-03	0.200E-04	0.100E-04
59 NO2	0.100E-04	0.100E-04	0.000E+00	0.000E+00	0.000E+00	0.000E+00
60 NO	0.000E+00	0.000E+00	0.000E+00	0.000E+00	0.000E+00	0.000E+00
61 O3	0.300E-01	0.350E-01	0.400E-01	0.500E-01	0.600E-01	0.700E-01
62 HNO3	0.500E-04	0.500E-04	0.500E-04	0.500E-04	0.500E-04	0.150E-03
63 H2O2	0.200E-02	0.200E-02	0.200E-02	0.200E-02	0.150E-02	0.150E-02
64 ALD	0.400E-04	0.400E-04	0.400E-04	0.400E-04	0.400E-04	0.400E-04
65 HCHO	0.250E-03	0.250E-03	0.250E-03	0.200E-03	0.150E-03	0.100E-03
66 OP1	0.250E-06	0.250E-06	0.250E-06	0.200E-06	0.150E-06	0.100E-06
67 OP2	0.400E-07	0.400E-07	0.400E-07	0.400E-07	0.400E-07	0.400E-07
68 PAA	0.500E-04	0.500E-04	0.500E-04	0.500E-04	0.500E-04	0.500E-04
69 ORA1	0.150E-05	0.500E-06	0.500E-06	0.500E-06	0.500E-06	0.500E-06
70 ORA2	0.150E-05	0.500E-06	0.500E-06	0.500E-06	0.500E-06	0.500E-06
71 NH3	0.500E-04	0.500E-04	0.500E-04	0.200E-04	0.200E-04	0.200E-04
72 N2O5	0.000E+00	0.000E+00	0.000E+00	0.000E+00	0.000E+00	0.000E+00
73 NO3	0.000E+00	0.000E+00	0.000E+00	0.000E+00	0.000E+00	0.000E+00
74 PAN	0.100E-04	0.100E-04	0.100E-04	0.100E-04	0.100E-04	0.100E-04
75 HC3	0.120E-04	0.120E-04	0.120E-04	0.800E-05	0.400E-05	0.400E-05
76 HC5	0.120E-04	0.120E-04	0.120E-04	0.800E-05	0.400E-05	0.400E-05
77 HC8	0.600E-05	0.600E-05	0.600E-05	0.400E-05	0.200E-05	0.200E-05
78 ETH	0.000E+00	0.000E+00	0.000E+00	0.000E+00	0.000E+00	0.000E+00
79 CO	0.800E-01	0.800E-01	0.800E-01	0.750E-01	0.700E-01	0.650E-01
80 OL2	0.000E+00	0.000E+00	0.000E+00	0.000E+00	0.000E+00	0.000E+00
81 OLT	0.000E+00	0.000E+00	0.000E+00	0.000E+00	0.000E+00	0.000E+00
82 OLI	0.000E+00	0.000E+00	0.000E+00	0.000E+00	0.000E+00	0.000E+00
83 TOL	0.000E+00	0.000E+00	0.000E+00	0.000E+00	0.000E+00	0.000E+00
84 XYL	0.000E+00	0.000E+00	0.000E+00	0.000E+00	0.000E+00	0.000E+00
85 ACO3	0.100E-08	0.100E-08	0.100E-08	0.100E-08	0.100E-08	0.100E-08
86 TPAN	0.100E-07	0.100E-07	0.100E-07	0.100E-07	0.100E-07	0.100E-07
87 HONO	0.100E-08	0.100E-08	0.100E-08	0.100E-08	0.100E-08	0.100E-08
88 HNO4	0.200E-08	0.200E-08	0.200E-08	0.200E-08	0.200E-08	0.200E-08
89 KET	0.400E-04	0.400E-04	0.400E-04	0.400E-04	0.400E-04	0.400E-04
90 GLY	0.250E-06	0.250E-06	0.250E-06	0.200E-06	0.150E-06	0.100E-06
91 MGLY	0.250E-06	0.250E-06	0.250E-06	0.200E-06	0.150E-06	0.100E-06
92 DCB	0.250E-06	0.250E-06	0.250E-06	0.200E-06	0.150E-06	0.100E-06
93 ONIT	0.600E-05	0.600E-05	0.600E-05	0.400E-05	0.200E-05	0.200E-05
94 CSL	0.100E-08	0.100E-08	0.100E-08	0.100E-08	0.100E-08	0.100E-08
95 ISO	0.250E-05	0.250E-05	0.250E-05	0.250E-05	0.250E-05	0.250E-05
96 HO	0.000E+00	0.000E+00	0.000E+00	0.000E+00	0.000E+00	0.000E+00
97 HO2	0.000E+00	0.000E+00	0.000E+00	0.000E+00	0.000E+00	0.000E+00

Table 13-2. CMAQ Predefined Vertical Profiles for Boundary Conditions

98	ASO4I	3.207E-02	3.207E-02	3.207E-02	3.207E-02	3.207E-03	1.603E-03
99	ASO4J	7.696E-01	7.696E-01	7.696E-01	7.696E-01	7.696E-02	3.848E-02
100	NUMATKN	9.583E+09	9.583E+09	9.583E+09	9.583E+09	9.583E+08	4.791E+08
101	NUMACC	2.740E+08	2.740E+08	2.740E+08	2.740E+08	2.740E+07	1.370E+07
102	ASOIL	8.000E-01	8.000E-01	8.000E-01	8.000E-01	8.000E-02	4.000E-02
103	NUMCOR	1.392E+04	1.392E+04	1.392E+04	1.392E+04	1.392E+03	6.960E+02
104	South						
105							
106	SO2	0.000E+00	0.000E+00	0.000E+00	0.000E+00	0.000E+00	0.000E+00
107	SULF	0.200E-03	0.200E-03	0.200E-03	0.100E-03	0.500E-04	0.200E-04
108	NO2	0.100E-04	0.100E-04	0.000E+00	0.000E+00	0.000E+00	0.000E+00
109	NO	0.100E-04	0.100E-04	0.000E+00	0.000E+00	0.000E+00	0.000E+00
110	O3	0.300E-01	0.350E-01	0.400E-01	0.500E-01	0.600E-01	0.700E-01
111	HNO3	0.500E-04	0.500E-04	0.500E-04	0.500E-04	0.500E-04	0.150E-03
112	H2O2	0.200E-02	0.200E-02	0.200E-02	0.200E-02	0.150E-02	0.100E-02
113	ALD	0.400E-04	0.400E-04	0.400E-04	0.400E-04	0.400E-04	0.500E-05
114	HCHO	0.250E-03	0.250E-03	0.250E-03	0.200E-03	0.150E-03	0.100E-03
115	OP1	0.250E-06	0.250E-06	0.250E-06	0.200E-06	0.150E-06	0.100E-06
116	OP2	0.400E-07	0.400E-07	0.400E-07	0.400E-07	0.400E-07	0.500E-08
117	PAA	0.100E-03	0.100E-03	0.100E-03	0.100E-03	0.500E-04	0.500E-04
118	ORA1	0.150E-05	0.500E-06	0.500E-06	0.500E-06	0.500E-06	0.500E-06
119	ORA2	0.150E-05	0.500E-06	0.500E-06	0.500E-06	0.500E-06	0.500E-06
120	NH3	0.500E-04	0.500E-04	0.500E-04	0.300E-04	0.200E-04	0.200E-04
121	N2O5	0.000E+00	0.000E+00	0.000E+00	0.000E+00	0.000E+00	0.000E+00
122	NO3	0.000E+00	0.000E+00	0.000E+00	0.000E+00	0.000E+00	0.000E+00
123	PAN	0.100E-04	0.100E-04	0.100E-04	0.100E-04	0.100E-04	0.100E-04
124	HC3	0.120E-04	0.120E-04	0.120E-04	0.400E-05	0.400E-05	0.400E-05
125	HC5	0.120E-04	0.120E-04	0.120E-04	0.400E-05	0.400E-05	0.400E-05
126	HC8	0.600E-05	0.600E-05	0.600E-05	0.200E-05	0.200E-05	0.200E-05
127	ETH	0.000E+00	0.000E+00	0.000E+00	0.000E+00	0.000E+00	0.000E+00
128	CO	0.700E-01	0.700E-01	0.700E-01	0.700E-01	0.650E-01	0.550E-01
129	OL2	0.000E+00	0.000E+00	0.000E+00	0.000E+00	0.000E+00	0.000E+00
130	OLT	0.000E+00	0.000E+00	0.000E+00	0.000E+00	0.000E+00	0.000E+00
131	OLI	0.000E+00	0.000E+00	0.000E+00	0.000E+00	0.000E+00	0.000E+00
132	TOL	0.000E+00	0.000E+00	0.000E+00	0.000E+00	0.000E+00	0.000E+00
133	XYL	0.000E+00	0.000E+00	0.000E+00	0.000E+00	0.000E+00	0.000E+00
134	ACO3	0.100E-08	0.100E-08	0.100E-08	0.100E-08	0.100E-08	0.100E-08
135	TPAN	0.100E-07	0.100E-07	0.100E-07	0.100E-07	0.100E-07	0.100E-07
136	HONO	0.100E-08	0.100E-08	0.100E-08	0.100E-08	0.100E-08	0.100E-08
137	HNO4	0.200E-08	0.200E-08	0.200E-08	0.200E-08	0.200E-08	0.200E-08
138	KET	0.400E-04	0.400E-04	0.400E-04	0.400E-04	0.400E-04	0.500E-05
139	GLY	0.250E-06	0.250E-06	0.250E-06	0.200E-06	0.150E-06	0.100E-06
140	MGLY	0.250E-06	0.250E-06	0.250E-06	0.200E-06	0.150E-06	0.100E-06
141	DCB	0.250E-06	0.250E-06	0.250E-06	0.200E-06	0.150E-06	0.100E-06
142	ONIT	0.600E-05	0.600E-05	0.600E-05	0.200E-05	0.200E-05	0.200E-05
143	CSL	0.100E-08	0.100E-08	0.100E-08	0.100E-08	0.100E-08	0.100E-08
144	ISO	0.250E-05	0.250E-05	0.250E-05	0.250E-05	0.250E-05	0.250E-05
145	HO	0.000E+00	0.000E+00	0.000E+00	0.000E+00	0.000E+00	0.000E+00
146	HO2	0.000E+00	0.000E+00	0.000E+00	0.000E+00	0.000E+00	0.000E+00

Table 13-2. CMAQ Predefined Vertical Profiles for Boundary Conditions

ASO4I	3.207E-02	3.207E-02	3.207E-02	1.603E-02	3.207E-03	1.603E-03
ASO4J	7.696E-01	7.696E-01	7.696E-01	3.848E-01	7.696E-02	3.848E-02
NUMATKN	9.583E+09	9.583E+09	9.583E+09	4.791E+09	9.583E+08	4.791E+08
NUMACC	2.740E+08	2.740E+08	2.740E+08	1.370E+08	2.740E+07	1.370E+07
ASOIL	8.000E-01	8.000E-01	8.000E-01	4.000E-01	8.000E-02	4.000E-02
NUMCOR	1.400E+04	1.400E+04	1.400E+04	7.000E+03	1.400E+03	7.000E+02
West						
SO2	0.300E-03	0.200E-03	0.200E-03	0.100E-03	0.000E+00	0.000E+00
SULF	0.300E-03	0.200E-03	0.200E-03	0.100E-03	0.000E+00	0.000E+00
NO2	0.100E-03	0.100E-03	0.100E-03	0.500E-04	0.000E+00	0.000E+00
NO	0.500E-04	0.500E-04	0.500E-04	0.200E-04	0.000E+00	0.000E+00
O3	0.350E-01	0.400E-01	0.450E-01	0.500E-01	0.600E-01	0.700E-01
HNO3	0.500E-03	0.500E-03	0.500E-03	0.500E-03	0.200E-03	0.100E-03
H2O2	0.200E-02	0.200E-02	0.200E-02	0.200E-02	0.800E-03	0.200E-03
ALD	0.400E-04	0.400E-04	0.400E-04	0.400E-04	0.400E-04	0.500E-05
HCHO	0.400E-03	0.400E-03	0.400E-03	0.400E-03	0.100E-03	0.500E-04
OP1	0.400E-06	0.400E-06	0.400E-06	0.400E-06	0.100E-06	0.500E-07
OP2	0.400E-07	0.400E-07	0.400E-07	0.400E-07	0.400E-07	0.500E-08
PAA	0.250E-04	0.250E-04	0.250E-04	0.250E-04	0.200E-04	0.100E-04
ORA1	0.250E-05	0.250E-05	0.250E-05	0.250E-05	0.500E-06	0.500E-06
ORA2	0.250E-05	0.250E-05	0.250E-05	0.250E-05	0.500E-06	0.500E-06
NH3	0.300E-03	0.300E-03	0.300E-03	0.200E-03	0.100E-03	0.500E-04
N2O5	0.000E+00	0.000E+00	0.000E+00	0.000E+00	0.000E+00	0.000E+00
NO3	0.000E+00	0.000E+00	0.000E+00	0.000E+00	0.000E+00	0.000E+00
PAN	0.100E-03	0.100E-03	0.100E-03	0.500E-04	0.100E-04	0.100E-04
HC3	0.800E-04	0.800E-04	0.800E-04	0.600E-04	0.800E-05	0.400E-05
HC5	0.800E-04	0.800E-04	0.800E-04	0.600E-04	0.800E-05	0.400E-05
HC8	0.400E-04	0.400E-04	0.400E-04	0.300E-04	0.400E-05	0.200E-05
ETH	0.000E+00	0.000E+00	0.000E+00	0.000E+00	0.000E+00	0.000E+00
CO	0.800E-01	0.800E-01	0.800E-01	0.800E-01	0.650E-01	0.500E-01
OL2	0.100E-04	0.100E-04	0.500E-05	0.500E-05	0.100E-05	0.000E+00
OLT	0.200E-05	0.100E-05	0.500E-06	0.300E-06	0.000E+00	0.000E+00
OLI	0.100E-05	0.200E-06	0.100E-06	0.000E+00	0.000E+00	0.000E+00
TOL	0.100E-04	0.500E-05	0.500E-05	0.300E-05	0.000E+00	0.000E+00
XYL	0.300E-05	0.200E-05	0.400E-06	0.400E-06	0.000E+00	0.000E+00
ACO3	0.100E-08	0.100E-08	0.100E-08	0.100E-08	0.100E-08	0.100E-08
TPAN	0.100E-07	0.100E-07	0.100E-07	0.100E-07	0.100E-07	0.100E-07
HONO	0.100E-08	0.100E-08	0.100E-08	0.100E-08	0.100E-08	0.100E-08
HNO4	0.200E-08	0.200E-08	0.200E-08	0.200E-08	0.200E-08	0.200E-08
KET	0.400E-04	0.400E-04	0.400E-04	0.400E-04	0.400E-04	0.500E-05
GLY	0.400E-06	0.400E-06	0.400E-06	0.400E-06	0.100E-06	0.500E-07
MGLY	0.400E-06	0.400E-06	0.400E-06	0.400E-06	0.100E-06	0.500E-07
DCB	0.400E-06	0.400E-06	0.400E-06	0.400E-06	0.100E-06	0.500E-07
ONIT	0.400E-04	0.400E-04	0.400E-04	0.300E-04	0.400E-05	0.200E-05
CSL	0.100E-08	0.100E-08	0.100E-08	0.100E-08	0.100E-08	0.100E-08
ISO	0.250E-05	0.250E-05	0.250E-05	0.250E-05	0.250E-05	0.250E-05
HO	0.000E+00	0.000E+00	0.000E+00	0.000E+00	0.000E+00	0.000E+00
HO2	0.000E+00	0.000E+00	0.000E+00	0.000E+00	0.000E+00	0.000E+00

Table 13-2. CMAQ Predefined Vertical Profiles for Boundary Conditions

196	ASO4I	4.810E-02	3.207E-02	3.207E-02	1.603E-02	3.207E-03	1.603E-03
197	ASO4J	1.154E+00	7.696E-01	7.696E-01	3.848E-01	7.696E-02	3.848E-02
198	NUMATKN	1.437E+10	9.583E+09	9.583E+09	4.791E+09	9.583E+08	4.791E+08
199	NUMACC	4.110E+08	2.740E+08	2.740E+08	1.370E+08	2.740E+07	1.370E+07
200	ASOIL	1.000E+00	8.000E-01	8.000E-01	4.000E-01	8.000E-02	4.000E-02
201	NUMCOR	1.750E+04	1.400E+04	1.400E+04	7.000E+03	1.400E+03	7.000E+02

Table 13-3. Example RADM2 to CB4 Conversion Rules

```
NO2   =        NO2 ;
  NO    =        NO ;
  O     =        O3P;
  O3    =        O3 ;
  NO3   =        NO3;
  O1D   =        O1D;
  OH    =        HO ;
  HO2   =        HO2 ;
  N2O5  =        N2O5;
  HNO3  =        HNO3;
  HONO  =        HONO;
  PNA   =        HNO4;
  H2O2  =        H2O2;
  CO    =        CO;
  SO2   =        SO2;
  SULF  =        SULF;
  PAN   =        PAN;
  FACD  =        ORA1;
  AACD  =        ORA2;
  PACD  =        PAA;
  UMHP  =        OP1;
  MGLY  =        MGLY;
  OPEN  =        DCB;
  CRES  =        CSL;
  FORM  =        HCHO + 1.0 * GLY;
  ALD2  = 1.0 * ALD  + 2.0 * OLI;
  PAR   = 0.4 * ETH  + 2.9 * HC3  + 4.8 * HC5  +
          7.9 * HC8  + 0.8 * OLT  + 0.8 * OLI  +
          3.9 * KET;
  OLE   =        OLT;
  TOL   =        TOL;
  ISOP  =        ISO;
  ETH   =        OL2;
  XYL   =        XYL;
  TERP  =        TERP;
 END;
```

EPA/600/R-99/030

Chapter 14

PHOTOLYSIS RATES FOR CMAQ

Shawn J. Roselle,[*] Kenneth L. Schere,[**] and Jonathan E. Pleim[**]
Atmospheric Modeling Division
National Exposure Research Laboratory
U.S. Environmental Protection Agency
Research Triangle Park, North Carolina 27711

Adel F. Hanna
MCNC-North Carolina Supercomputing Center
Research Triangle Park, North Carolina 27709

ABSTRACT

The method for calculating photodissociation reaction rates (photolysis rates) for CMAQ is described in this chapter. The description includes the photolysis rate preprocessor (JPROC) and CMAQ subroutine PHOT. JPROC produces a clear-sky photolysis rate look-up table. The look-up table consists of photolysis rates at various altitudes, latitudes, and hour angles. The look-up table is recalculated for each simulation day and is dependent upon the chemical mechanism. Within CMAQ, photolysis rates for individual grid cells are interpolated from the look-up table in subroutine PHOT. PHOT also uses a parameterization to correct the clear-sky photolysis rates for cloud cover.

---

[*]On assignment from the National Oceanic and Atmospheric Administration, U.S. Department of Commerce. Corresponding author address: Shawn Roselle, MD-80, Research Triangle Park, NC 27711. E-mail: sjr@hpcc.epa.gov

[**]On assignment from the National Oceanic and Atmospheric Administration, U.S. Department of Commerce.

14.0 PHOTOLYSIS RATES FOR CMAQ

14.1 Background

Many chemical reactions in the atmosphere are initiated by the photodissociation of numerous trace gases. These photodissociative reactions are responsible for most of the smog buildup detrimental to humans, animals, plant life and materials. In order to accurately model and predict the effects of air pollution, good photodissociation reaction rate (or photolysis rate) estimates must be made.

Photodissociation is the conversion of solar radiation into chemical energy to activate and dissociate chemical species. Examples of species that photodissociate include many important trace constituents of the troposphere such as NO_2, O_3, HCHO, CH_3CHO, HONO, the NO_3 radical, and H_2O_2 (also see Table 14.1). The simulation accuracy of the entire chemical system is highly dependent upon the accuracy of photolysis rates, which are the primary sources of radicals in the troposphere. Photolysis rates (min^{-1}), sometimes called J-values, are computed for photodissociation reaction (i) by

$$J_i = \int_{\lambda_1}^{\lambda_2} F(\lambda)\sigma_i(\lambda)\phi_i(\lambda)d\lambda \qquad (14\text{-}1)$$

where, $F(\lambda)$ is the actinic flux (photons cm^{-2} min^{-1} nm^{-1}), $\sigma_i(\lambda)$ the absorption cross section for the molecule undergoing photodissociation (cm^2 $molecule^{-1}$), $\phi_i(\lambda)$ the quantum yield of the photolysis reaction (molecules $photon^{-1}$), and λ the wavelength (nm). Absorption cross sections and quantum yields are functions of wavelength, and may also be functions of temperature and pressure; they are unique to species and reactions. Laboratory experiments measuring the absorption cross sections and quantum yields. have been conducted for many species that photodissociate in the troposphere. Actinic flux is a radiometric quantity that measures the spectral radiance integrated over all solid angles per unit area. The spherical receiving surface distinguishes the actinic flux from the more commonly measured irradiance, which is the radiance falling on a horizontal surface. Thus, the actinic flux can be called spherical spectral irradiance. The actinic flux changes with time of day, longitude, latitude, altitude, and season, and is governed by the astronomical and geometrical relationships between the sun and the earth. It is greatly affected by the earth's surface albedo as well as by various atmospheric scatterers and absorbers. Hence, correct model calculation of the temporal and spatial variation of the actinic flux is critical to obtaining accurate photolysis rates for regional and mesoscale episodic photochemical modeling.

The current approach taken for setting photolysis rates in the Models-3/CMAQ framework follows that of the Regional Acid Deposition Model (RADM) (Chang et al., 1987). It includes two stages of processing: (1) a table of clear-sky photolysis rates is calculated for specified

heights, latitudes, and hours from local noon; and (2) photolysis rates are interpolated from the table within the CMAQ Chemistry Transport Model (CCTM) based on grid cell location and the model time, and are corrected for cloud cover. This approach is computationally efficient and has been shown by Madronich (1987) to give clear-sky photolysis rates within the uncertainty of the surface-based measurements.

14.2 Preprocessor JPROC: Calculate Clear-sky Photolysis Rate Table

Preprocessor JPROC calculates a table of clear-sky photolysis rates (or J-values) for a specific date. The table is dimensioned by latitude, altitude, and time. Currently, J-values are calculated for 6 latitudinal bands (10°N, 20°N, 30°N, 40°N, 50°N, and 60°N), 7 altitudes (0 km, 1 km, 2 km, 3 km, 4 km, 5 km, and 10 km), and ±9 hours from local noon (0 h, 1 h, 2 h, 3 h, 4 h, 5 h, 6 h, 7 h, and 8 h). There is a separate table for each photolysis reaction. In order to compute the photolysis rates using Equation 14.1, the actinic flux, absorption cross section, and quantum yield must be determined as a function of wavelength.

The delta-Eddington two-stream radiative transfer model (Joseph et al., 1976; Toon et al., 1989) is used for computing the actinic flux. The two-stream approximations are limited in application to cases where the scatter is not highly anisotropic. In computing the actinic flux, a description of the extraterrestrial radiation, aerosol, ozone absorption, oxygen absorption in the Schumann-Runge Bands, Rayleigh scattering (WMO, 1985) and surface albedo are provided to the radiation model.

Extraterrestrial radiation is specified by a user input file. JPROC is flexible enough to use any extraterrestrial radiation data distribution specified by the user. However, the wavelength distribution of the extraterrestrial radiation data is important because this is also the distribution that will be used in the integration of Equation 14.1. Therefore, the user should choose a wavelength distribution that resolves the features that are important to the photolysis reactions of interest. A modified WMO extraterrestrial radiation data distribution (Chang, et al., 1990) is used as input to JPROC, which has a variable wavelength resolution ranging from 1 nm to 10 nm.

The O_2 and O_3 absorption cross section data are specified by user input files, but it is recommended that the most recent NASA data (DeMore et al., 1994) be used in the calculations. Vertical ozone profiles are set by interpolating seasonal profiles from a user input file, and if total ozone column data are available (such as data measured by the Total Ozone Mapping Spectrometer (TOMS) instrument aboard the sun-synchronous polar orbiting Nimbus satellite), then the interpolated vertical profiles are uniformly rescaled so that the profiles integrated total ozone column value matches the measured total ozone column data. TOMS data are archived and available at the National Satellite Service Data Center (NSSDC) in the form of digital daily maps with a resolution of 1 degree latitude by 1.25 degrees longitude. The TOMS data are averaged over each latitudinal band in JPROC. Nimbus-7 TOMS data are available for years 1978 through 1993; Meteor-3 TOMS data are available for 1991-1994; ADEOS TOMS data are

available for 1996-1997; and Earth Probe TOMS data are available for 1996-1998. These data can be downloaded from site *http://jwocky.gsfc.nasa.gov*.

The albedo data given by Demerjian et al. (1980), which have been used extensively in radiative transfer models, are given as a function of wavelength and are used in the current version of JPROC. Currently, a single vertical profile of aerosol attenuation coefficients (Elterman, 1968) is used in JPROC. An effort is underway to incorporate predicted aerosol parameters from CMAQ into the photolysis rate calculations.

Several factors in JPROC depend on the vertical profiles of temperature and pressure, including ozone absorption and the absorption cross sections and quantum yields for individual photolysis reactions. JPROC interpolates seasonal profiles of temperature and pressure. We use the same vertical profile data that are used in the RADM (Chang et al., 1987).

Absorption cross section and quantum yield data are specified by the user through input files. Input files depend on the chemical mechanism selected by the user in the Program Control Processor (see Chapter 15). The original sets of cross section/quantum yield data published with the Carbon Bond Mechanism IV (Gery et al., 1989), the Regional Acid Deposition Model mechanism version 2 (RADM2) (Stockwell et al., 1990), and the SAPRC mechanism (Carter, 1990) are available for use in JPROC. However, users can deviate from these standard sets to test other data, including the revisions suggested by NASA (DeMore et al., 1994). Table 14.1 lists the photolysis reactions for the RADM2 mechanism.

14.3 Subroutine PHOT: Table Interpolation and Cloud Attenuation

Subroutine PHOT within the CCTM has two basic functions, including interpolation of the clear-sky photolysis rate table and application of a cloud correction factor to the clear-sky values. The interpolation step is fairly simple. For each grid cell, the latitude, height, and time from local noon are determined and used to interpolate clear-sky values from the photolysis rate table. The cloud correction step is a little more complicated. The method used to correct for cloud cover in PHOT was taken from RADM (Chang et al., 1987; Madronich, 1987). The correction of clear-sky values depends on whether the location is below, above, or within the cloud. The below cloud photolysis rate (J_{below}) is calculated as:

$$J_{below} = J_{clear}[1 + cfrac(1.6 t_r \cos(\theta) - 1)] \qquad (14\text{-}2)$$

where cfrac is the cloud coverage fraction (cloud fraction is interpolated from hourly data for each grid cell), θ is the zenith angle, and t_r is the cloud transmissivity. Below cloud photolysis rates will be lower than the clear-sky values due to the reduced transmission of radiation through the cloud. The cloud transmissivity is calculated by:

$$t_r = \frac{5 - e^{-\tau_{cld}}}{4 + 3\tau_{cld}(1 - f)} \tag{14-3}$$

where f is the scattering phase function asymmetry factor (assumed to be 0.86) and τ_{cld} is the cloud optical depth. We have replaced the cloud optical depth equation in RADM with one taken from Stephens (1978). The original RADM equation for τ_{cld} required an estimate of the cloud droplet radius, which is not readily available. In RADM, the cloud droplet radius was assumed to be 10μm. The empirical formula for τ_{cld} from Stephens (1978):

$$\log(\tau_{cld}) = 0.2633 + 1.7095 \ln[\log(W)] \tag{14-4}$$

is only a function of liquid water path (W), where W=LΔz (g/m^2), L is the liquid water content (g/m^3), and Δz is the cloud thickness. The above cloud top factor (F_a) is calculated as:

$$J_{above} = J_{clear}[1 + cfrac(\alpha_i(1 - t_r)\cos(\theta)] \tag{14-5}$$

This equation allows for enhancement of photolysis rates above the cloud due to the reflected radiation from the cloud. It also includes a reaction dependent coefficient (α_i) which allows for further above cloud enhancements (Chang et al., 1987). Within the cloud, the cloud correction factor is a simple linear interpolation of the below cloud factor at cloud base to the above cloud factor at cloud top. Once computed, the below, above, and within cloud factor are used to scale the clear sky photolysis rates to account for the presence of clouds. In the current implementation, all cloud types (including clouds composed of ice crystals) are treated the same using the above outlined procedure.

14.4 Summary

The current method for calculating photolysis rates in CMAQ, which was derived from RADM, uses a preprocessor to compute a look-up table and a subroutine within the chemistry transport model to interpolate J-values and apply a cloud-cover correction. Other approaches and enhancements are being developed and tested. One enhancement to be added in the future is the dynamic link between aerosol predictions and photolysis rate calculations. Another is to replace the two-stream model with a more comprehensive multi-stream radiative transfer model (Stamnes et al., 1988). Other absorption cross section and quantum yield data will be added or updated using the DeMore et al. (1997) revisions.

14.5 References

Carter, W.P.L., 1990: A detailed mechanism for the gas-phase atmospheric reactions of organic compounds, *Atmos. Environ.*, **24(A)**, 481-518.

Chang, J.S., R.A. Brost, I.S.A. Isaksen, S. Madronich, P. Middleton, W.R. Stockwell, and C.J. Walcek, 1987: A three-dimensional eulerian acid deposition model: physical concepts and formulation, *J. Geophys. Res.* **92 (D12)**: 14681-14700.

Chang, J.S., P.B. Middleton, W.R. Stockwell, C.J. Walcek, J.E. Pleim, H.H. Lansford, F.S. Binkowski, S. Madronich, N.L. Seaman, D.R. Stauffer, D. Byun, J.N. McHenry, P.J. Samson, H. Hass, 1990: The regional acid deposition model and engineering model, Acidic Deposition: State of Science and Technology, Report 4, National Acid Precipitation Assessment Program.

Demerjian, K.L., K.L. Schere, J.T. Peterson, 1980: Theoretical estimates of actinic (spherically integrated) flux and photolytic rate constants of atmospheric species in the lower troposphere. *Advances in Environmental Science and Technology*, Vol. 10, by John Wiley & Sons, Inc., 369-459.

DeMore, W.B., S.P. Sander, D.M. Golden, R.F. Hampson, M.J. Kurylo, C.J. Howard, A.R. Ravishankara, C.E. Kolb, and M.J. Molina, 1994: Chemical Kinetics and Photochemical Data for Use in Stratospheric Modeling: Evaluation Number 11, JPL Pub. 94-26. Pasadena, CA: National Aeronautics and Space Administration, Jet Propulsion Laboratory.

DeMore, W.B., S.P. Sander, D.M. Golden, R.F. Hampson, M.J. Kurylo, C.J. Howard, A.R. Ravishankara, C.E. Kolb, and M.J. Molina, 1997: Chemical Kinetics and Photochemical Data for Use in Stratospheric Modeling: Evaluation Number 12, JPL Pub. 97-4. Pasadena, CA: National Aeronautics and Space Administration, Jet Propulsion Laboratory.

Elterman, L, 1968: UV, Visible, and IR Attenuation for Altitudes to 50 km; AFCRL-68-0153. Bedford, MA: Air Force Cambridge Res. Lab.

Gery, M.W., G.Z. Whitten, J.P. Killus, M.C. Dodge, 1989: A photochemical mechanism for urban and regional scale computer modeling, *J. Geophys. Res.*, **94**, 12925-12956.

Joseph, J.H., W.J. Wiscombe, and J.A. Weinman, 1976: The delta-Eddington approximation for radiative flux transfer, *J. Atmos. Sci.*, **33**, 2452-2459.

Madronich, S, 1987: Photodissociation in the Atmosphere: 1. Actinic flux and the effects of ground reflections and clouds, *J. Geophys. Res.* **92 (D8)**: 9740-9752.

Stamnes, K., S. Tsay, W. Wiscombe, and K. Jayaweera, 1988: Numerically stable algorithm for discrete-ordinate-method radiative transfer in multiple scattering and emitting layered media, *Appl. Opt.*, **27**, 2502-2509.

Stephens, G.L., 1978: Radiation profiles in extended water clouds. II.: Parameterization schemes, *J. Atmos. Sci.* **35**: 2123-2132.

Stockwell, W.R., P. Middleton, and J.S. Chang, 1990: The second generation regional acid deposition model chemical mechanism for regional air quality modeling, *J. Geophys. Res.* **95 (D10)**: 16343-16367.

Toon, O.B., C.P. Mckay, and T.P. Ackerman, 1989: Rapid calculation of radiative heating rates and photodissociation rates in inhomogeneous multiple scattering atmospheres, *J. Geophys. Res.*, **94**, 16287-16301.

World Meteorological Organization, 1986: "Atmospheric Ozone 1985: Assessment of Our Understanding of the Processes Controlling its Present Distribution and Change"; WMO Rep. No. 16; Global Ozone Research and Monitoring Project, Geneva, Switzerland.

This chapter is taken from *Science Algorithms of the EPA Models-3 Community Multiscale Air Quality (CMAQ) Modeling System*, edited by D. W. Byun and J. K. S. Ching, 1999.

Table 14-1. RADM2 Photolysis Reactions (Adapted from Stockwell et al., 1990.)

Reaction	Description
$O_3 + h\nu \rightarrow O_2 + O^1D$	Ozone Photolysis to O^1D
$O_3 + h\nu \rightarrow O_2 + O^3P$	Ozone Photolysis to O^3P
$NO_2 + h\nu \rightarrow NO + O^3P$	Nitrogen Dioxide Photolysis
$NO_3 + h\nu \rightarrow NO + O_2$	Nitrate Photolysis to NO
$NO_3 + h\nu \rightarrow NO_2 + O^3P$	Nitrate Photolysis to NO_2
$HONO + h\nu \rightarrow OH + NO$	Nitrous Acid Photolysis
$HNO_3 + h\nu \rightarrow OH + NO_2$	Nitric Acid Photolysis
$HNO_4 + h\nu \rightarrow HO_2 + NO_2$	Pernitric Acid Photolysis
$H_2O_2 + h\nu \rightarrow OH + OH$	Hydrogen Peroxide Photolysis
$HCHO + h\nu \rightarrow H + HCO$	Formaldehyde Photolysis to Radicals
$HCHO + h\nu \rightarrow H_2 + CO$	Formaldehyde Photolysis to Molecular Hydrogen
$CH_3CHO + h\nu\ (+2O_2) \rightarrow CH_3OO + HO_2 + CO$	Acetaldehyde Photolysis
$CH_3COCH_3 + h\nu \rightarrow CH_3 + CH_3CO$	Acetone Photolysis
$CH_3COC_2H_5 + h\nu \rightarrow ACO_3 + ETH$	Methyl Ethyl Ketone Photolysis
$HCOCHO + h\nu \rightarrow HCHO + CO$	Glyoxal Photolysis to Formaldehyde
$HCOCHO + h\nu \rightarrow 2CO + H_2$	Glyoxal Photolysis to Molecular Hydrogen
$CH_3COCHO + h\nu \rightarrow ACO_3 + HO_2 + CO$	Methyl Glyoxal Photolysis
$HCOCH{=}CHCHO + h\nu \rightarrow 0.98HO_2 + TCO_3 + 0.02ACO_3$	Unsaturated Dicarbonyl Photolysis
$CH_3OOH + h\nu \rightarrow CH_2O + OH + HO_2$	Methyl Hydrogen Peroxide Photolysis
$CH_3ONO_2 + h\nu \rightarrow 0.2ALD + 0.8KET + HO_2 + NO_2$	Organic Nitrate Photolysis
$C_3H_4O + h\nu \rightarrow$ products	Acrolein Photolysis

EPA/600/R-99/030

Chapter 15

PROGRAM CONTROL PROCESSING IN MODELS-3

Jeffrey Young*
Atmospheric Modeling Division
National Exposure Research Laboratory
U.S. Environmental Protection Agency
Research Triangle Park, NC 27711

ABSTRACT

Based on user choices and input, the Models-3 framework creates objects and include files that control the complete problem domain under which a CMAQ model is built and executed. The general concepts underlying the definition of these objects and the creation of the include files are discussed.

*On assignment from the National Oceanic and Atmospheric Administration, U.S. Department of Commerce. Corresponding author address: Jeffrey Young, MD-80, Research Triangle Park, NC 27711. E-mail: yoj@hpcc.epa.gov

15.0 PROGRAM CONTROL PROCESSING IN MODELS-3

Program control processing (PCP) refers to setting up internal arrays and mappings, global parameters, and data linkages to establish the complete problem domain in which the programs, or "models," in the Community Multiscale Air Quality (CMAQ) system are built and executed. Controlled by user choices, the Models-3 framework carries out this processing automatically and provides the key to modularity and ensures uniform, consistent internal dimensioning, looping parameters and solver data in the compiled codes for all the CMAQ system models. Thus, modularity and consistency in establishing the computational domain and chemical mechanism for any particular application of the CMAQ system are assured by PCP. Modelers can easily and relatively safely carry out many different applications at different scales, or with different chemistry, or different solvers. Model developers can readily study the effects of different schemes and determine optimal implementations of the science and codes. PCP helps to establish a true "one-atmosphere" approach to modeling.

PCP involves both the Models-3 framework's graphical user interface and specialized processors that are launched from the framework. In the Models-3 framework, a user selects the computational grid and domain characteristics, the vertical layer structure, and the chemical mechanism to be used in building (compiling and linking) a model (an executable). How these choices get transformed automatically into compiled code is discussed in the following sections. This chapter focuses on the CMAQ Chemical Transport Model (CCTM) since the CCTM requires the most extensive use of PCP. However, some or all of the user choices made to set up a particular CCTM determine the particular application characteristics for all of the supporting processors (or "models"). In addition to the CCTM, CMAQ is comprised of eight additional processors as follows:

- The Models-3 emissions processing and projection system (MEPPS), described in Chapter 4.
- The emissions-chemistry interface processor (ECIP), described in Chapter 4.
- The plume-in-grid dynamics processor (PDM), described in Chapter 9.
- The meteorology-chemistry input processor (MCIP), described in Chapter 12.
- The land-use processor (LUPROC), described in Chapter 12.
- The initial and boundary conditions processors (ICON and BCON), described in Chapter 13.
- The photolytic J-value processor (JPROC), described in Chapter 14.
- The process analysis processor (PROCAN), described in Chapter 16. PROCAN is launched by the Models-3 framework and its execution is transparent to the user. The outputs from PROCAN are used to control CCTM diagnostic outputs (see Section 15.3.1 below).

Building a particular model in the Models-3/CMAQ system requires the creation of Fortran include files that populate the model's codes to set the specific computational grid and domain characteristics, the vertical layer structure, the chemical mechanism, and (for the CCTM) the process analysis to be used for the particular model. Once these model configuration objects are set by the user in the Models-3 Science Manager, the Models-3 framework automatically generates the required global Fortran include files. The use of global Fortran include files, the notion of "Global Name Table Data," and the design concepts that govern this implementation are discussed in Chapter 18, Sections 18.5 and 18.7.

15.1 Domain Configuration

The computational domain configuration data are contained in three include files:

- HGRD.EXT - The horizontal grid dimensions in terms of the number of grid cell columns and rows and the number of grid cells for which the computational domain boundary is extended for boundary data. The number of these perimeter boundary cells is also specified.
- VGRD.EXT - The vertical layer dimensions as the number of vertical layers. This include file also contains declarations for the layer surface and layer center arrays.
- COORD.EXT - The domain coordinate data:
  - The map projection type (Lambert, Mercator, Stereographic, UTM, or latitude-longitude).
  - The map projection parameters.
  - The center of the grid's coordinate system with respect to the "mother grid" or parent grid (usually the main grid from the meteorology pre-processing).
  - The horizontal grid cell sizes in meters.
  - The vertical layer type. There are 7 currently defined:
    1. σ_p coordinates.
    2. $\sigma_{p(0)}$ coordinates.
    3. σ_z coordinates.
    4. η_p coordinates.
    5. Pressure coordinates.
    6. Z coordinates (meters above ground).
    7. H coordinates (meters above mean sea level).
  - The units of the top vertical layer value.
  - The value of the top vertical layer variable.
  - The units of the vertical layer surface values.
  - The list of vertical layer surface values.
  - The list of vertical layer surface values converted to values monotonically increasing with altitude.
  - The grid name used for header description data in I/O API files (discussed in Section 15.2).

15.2 Input/Output Applications Programming Interface

Input and output data access for the CMAQ system is accomplished mainly through the Input/Output Applications Programmer's Interface (I/O API) sub-system [1]. The CMAQ system implementation of the I/O API is described in Chapter 18, Section 18.3. In order to access I/O API files and use other I/O API functions, it is necessary to specify the required declarations and parameters. Some or all of the following include files are needed in each subroutine that uses the I/O API:

- PARMS3.EXT - I/O API dimensioning parameters, file type and file characteristic parameters, coordinate system and map projection parameters, and vertical layer parameters.
- FDESC3.EXT - Fortran common blocks that contain a complete I/O API file description. The data in these common blocks are loaded from an I/O API file when opened and read. These data must be supplied from the user subroutine when an I/O API file is opened for writing.
- IODECL3.EXT - Declarations and usage comments for I/O API functions and routines.
- XSTAT3.EXT - Exit codes for the I/O API M3EXIT function. Generally, M3EXIT is called from any subroutine that produces a fatal error during I/O API access.

15.3 Other CCTM Configuration Control

15.3.1 CCTM Process Analysis

The Models-3/CMAQ system provides a diagnostic tool that allows a user to probe into the way the science processing is actually being executed in the CCTM. The process analysis tool optionally provides two types of information, which are termed Integrated Process Rates (IPR) and Integrated Reaction Rates (IRR). Note that these diagnostic tools apply only for the CCTM and not for the other models. The reader is referred to Chapter 16 for the details, but briefly the IPR processing captures the changes to the concentration field for different species, or groupings of species, for each individual science process modeled. The IRR processing focuses on the gas-phase chemistry and allows a detailed examination of various characteristics of the chemical mechanism implemented in the CCTM for the chosen scenario. The data produced by these tools are collected in I/O API output files, which can be further processed or examined using the visualization tools.

The CCTM requires three include files, even if neither IPR nor IRR processing is selected.[1] These include files are automatically generated from PROCAN, and the Models-3 framework then incorporates them in the CCTM build process. The three IPR/IRR include files are:

[1] If process analysis is not requested while building a CCTM model executable, the Models-3 framework automatically supplies the include files.

- PA_CTL.EXT - The declarations and values of the two flags that determine if IPR or IRR (or both) processing is to be performed.

- PA_CTM.EXT - Declarations and parameters that define the domain, output file descriptions, arrays and dimensions, IPR and IRR loop variables, and named common blocks for computational data.

- PA_DAT.EXT - Data statements containing values for the variables needed to fill in the common blocks in PA_CTM.EXT.

15.3.2 CCTM Fixed Data

The Models-3/CMAQ system can deal with other types of global include files and reference them from a user-supplied full path to build a model. The following three categories of global include files apply to the CCTM. The other processor models (MCIP, ECIP, etc.) also have include files in this category, but not as extensively.

- FILES_CTM.EXT - The set of logical file names used in the current CCTM implementation. The include file contains data statements for the file names as variables used in the codes and values for the variables. The values are character strings that are UNIX environment variable values set in the scripts launched by the Models-3 framework to run the models.

- CONST.EXT, CONST3_RADM.EXT - These include files contain parameter statements to define basic and frequently used air quality and meteorological modeling physical and mathematical constants. Inclusion of these files in the model codes helps to assure consistency in the science calculations across all the processes and modules.

- BLKPRM_500.EXT - Computational blocking: For computational efficiency and reduced memory requirements, operations may be performed on groups of grid cells (a block of cells) at a time. This include file provides convenient definitions to use 500-cell blocking.

- GRID_DECL.EXT - Declarations for the dimensions and species classes offsets in the main concentration array. See Chapter 18, Section 18.2.2 for details.

- EMISPRM.chem.EXT, EMISPRM.vdif.EXT - These two include files contain the declarations that control in which process the emissions sources are injected; either the vertical diffusion process of the gas-phase chemistry solver process. By using a C pre-processor (cpp) #ifdef directive, one or the other include file is actually included when the code is compiled. The cpp directive is set by the user during the model building phase. The reader is referred to Chapter 18, Section 18.5 for more details.

15.4 Generalized Chemistry

15.4.1 Design

In the past, a particular chemical mechanism was generally "hardwired" into a chemical transport model with mechanism parameters and variables embedded in the solver codes. Implementing even minor changes incurred a high potential for code and consistency errors. Additionally, some mechanism changes necessitated extensive coding changes, requiring careful tracing through all the mechanism dependencies. Worse, not finding these dependencies led to errors that were not necessarily detected. The Models-3/CMAQ system employs a generalized chemical mechanism processor (MP), also called the "mechanism reader," which greatly simplifies the task of implementing or altering gas-phase chemical mechanisms and provides the capability of easily and safely using different mechanisms in the CMAQ system.

MP reads an ASCII file that contains a symbolic description of a gas-phase chemical mechanism, and generates three ASCII Fortran source files. The input ASCII file is called a *mechanism description*, or simply, "mechanism."

The ASCII mechanism description file is formatted according to a simple set of rules in a free-form format similar to the approaches used by Jeffries et al. [2] and Gery and Crouse [3]. The types of reactions that are supported are described below in Section 15.4.3, and the specific formats are described in the Models-3 User Manual, Appendix M [4].

The Fortran files that are generated are incorporated as include files in the CMAQ Fortran codes. They consist of:

- Fortran named common blocks that declare parameters and explicitly dimensioned arrays associated with gas chemistry kinetic and photolytic reactions.
- Fortran data statements that fill in the common block arrays with actual values determined from the input ASCII mechanism file.

The common blocks and the data statements files are global and are used in all the codes that require gas chemistry information.

Another file that is generated from the mechanism description file by MP, which is transparent to the user, is a species list found in the mechanism description. This file is used by the framework to generate all the gas chemistry species global include files that are required in the model codes.

In order to implement the mechanism reader's capabilities, the CMAQ system requires generalized gas-phase chemistry solvers. At present, there are two such solvers available, SMVGEAR and QSSA, which are described in detail in Chapter 8. The use of generalized solvers precludes some code optimizations that can increase performance, but significantly facilitates implementing new or altered chemical mechanisms.

15.4.2 Operation

The CMAQ system accounts for chemistry in three forms: gas phase, aerosols (liquid and solid phase), and the aqueous phase. Therefore, the Models-3 framework controls certain aspects of how the model species are treated in a model simulation and provides linkages between species in different phases. Setting up the linkages is accomplished by means of a series of four species tables in a spread sheet format that are filled out by the user. These tables also allow the user to control some aspects of the simulation and generated outputs and provide links to data such as emissions, initial and boundary concentrations, and dry deposition velocities that are generated by the CMAQ input processors. The mechanism definition and species tables become objects that the Models-3 framework stores in its database. Therefore if a required chemical mechanism already exists in the database as a predefined mechanism, the user does not have to enter any mechanism data into the framework.

Since different gas-phase chemical mechanisms can be used in the CMAQ system and these mechanisms may employ different species names, it is necessary to supply the linkages among the gas-phase species, the fixed aerosol species, and the species that participate in aqueous-phase chemistry. Similarly, it is also necessary to link the gas-phase species to emissions, deposition velocities, and to aqueous-phase scavenging. In addition, the species tables allow the user to select which species concentrations are written to the output files and whether or not they are to be advected or diffused. In the same manner, most of these linkages must be established for aerosol, non-reactive, and possibly tracer species.

The methodology used to establish links between species names involves the concept of surrogate names. Surrogate names are used to provide linkages between model species within the CCTM and to link the model species to those that represent data provided by other CMAQ processors. For example the emissions-chemistry interface processor, ECIP, that links the Models-3 emissions processing and projection system (MEPPS) with the CCTM could write a species named XXX that represents xxx emissions rates. However, the CCTM that uses xxx may have the corresponding model species named YYY. Using the surrogate name concept, emissions species XXX gets mapped to model species YYY. The reader is referred to the Models-3 User Manual [4] for more details on the implementation of the set of predefined surrogate names used in the current version.

An additional feature that can be applied to any of the surrogate species linkages is the application of a multiplicative, or scale factor. The user can set the factor to be other than unity (the default) to easily modify some model input data related to the selected species and process linkage. For example, this could be used to test the effect of changing the deposition velocity for a certain species, or to modify initial or boundary conditions data. Also, the factors can be set to modify certain data between model species groups within the CCTM, such as in the gas-phase to aerosol linkage.

These linkages are set by the user and are distributed among the four tables that establish the linkages among gas-phase, aerosols, non-reactive, and (possibly) tracer species. Non-reactive species are gas-phase, but do not participate in gas-phase reactions. Optional tracer species are

inert and may have special, user-defined initial and boundary concentrations as well as emissions sources. The reader is referred to the Models-3 User Manual [4] for more details and a complete description of the species tables.

The following is a list of the linkages set up in the current implementation of the Models-3/CMAQ system. The linkages take place with respect to the CCTM or model species name; the surrogate names and flags point to this name.

1. Model species molecular weight.
2. Emissions species surrogate name.
3. Emissions species scale factor.
4. Initial and boundary concentrations species surrogate name.
5. Initial and boundary concentrations species scale factor.
6. Deposition velocity species surrogate name.
7. Deposition velocity species scale factor.
8. Gas-phase to aerosol linkage species surrogate name.
9. Gas-phase to aqueous-phase linkage species surrogate name.
10. Gas-phase aqueous scavenging linkage species surrogate name.
11. Gas-phase aqueous scavenging linkage species scale factor.
12. Aerosol to aqueous-phase linkage species surrogate name.
13. Aerosol aqueous scavenging linkage species surrogate name.
14. Aerosol aqueous scavenging linkage species scale factor.
15. Non-reactive to aerosol linkage species surrogate name.
16. Non-reactive to aqueous-phase linkage species surrogate name.
17. Non-reactive aqueous scavenging linkage species surrogate name.
18. Non-reactive aqueous scavenging linkage species scale factor.
19. Model species flag for participation in the advection processes.
20. Model species flag for participation in the diffusion processes.
21. Model species flag for inclusion in the concentration output file.
22. Model species flag for inclusion in the dry deposition output file.
23. Model species flag for inclusion in the wet deposition output file.
24. Tracer species - similar linkages to any of the above.

It should be noted that items 1 - 7 and 19 - 23 apply to all of the four groups of species (gas phase, aqueous phase, solid and liquid aerosols).

15.4.3 Supported Reaction Types

In this section we describe the types of gas-phase chemical reactions supported by the generalized mechanism processor, MP, in the current version of the Models-3/CMAQ system. The reader is referred to Chapter 8 for a description of the available mechanisms.

The gas-phase mechanism description file is a list of mechanism reactions. The mechanism reactions list consists of lines of symbolic descriptions of elementary reactions among modeled chemical species, followed by a rule-based symbolic description of the reaction rate expression for that reaction. The reader is referred to Chapter 8 for mechanism description examples.

These mechanism reaction lists are generally "free-form," in that spacing of the symbols on the page is not important (except, perhaps for readability), and reaction descriptions may span many lines if necessary. Liberal use of comments is facilitated by allowing for comment lines and comments embedded within the reaction lines. In addition, each reaction may be labeled for subsequent reference. The photolysis reactions are given labels for a specific photolytic table reference. These tables are generated by the J-value processor and are used in the CCTM for the gas-phase chemistry processing. Currently, there are 10 different rate constant expressions available for thermal reactions, including Arrhenius-type expressions and the class of so-called fall-off reactions (**Type f**, below). New expressions can be added, as necessary.

The type of reaction rate expressions that can be calculated are:

Type 1 :	$k = A$	
Type 2 :	$k = A(T/300)^B$,	where $T =$ temperature in deg K.
Type 3 :	$k = Ae^{(-C/T)}$,	where $C = E_a / R$, E_a is the activation energy, and R is the gas constant.
Type 4 :	$k = A(T/300)^B e^{(-C/T)}$	
Type 5 :	$k = k_r = k_f / Ae^{(-C/T)}$,	where k_f is any previously defined forward reaction.
Type 6 :	$k = Ak_n$,	where k_n refers to the nth reaction.
Type 7 :	$k = A(1.0 + 0.6P)$,	where $P =$ pressure in atmospheres.
Type 8:	$\mathbf{k = k_0 + \frac{k_3[M]}{1 + \frac{k_3[M]}{k_2}}}$,	where k_0, k_2, and k_3 are **Type 3**.
Type 9:	$k = k_1 + k_2[M]$,	where k_1 and k_2 are **Type 3**.
Type f:	$k = k = \frac{k_0[M]}{1 + k_0[M]/k_i} F^G$	

where k_0 and k_i may be **Type 1, 2, 3,** or **4**,
$G = \{1 + [\ln(k_0 [M] / k_i) / n]^2\}^{-1}$,
$F = 0.6$ (usually), and
$n = 1.0$ (usually).

15.4.4 Mechanism Parsing Rules

The mechanism description file that MP reads must follow a set of format rules in order to describe the reactions listed above. Generally, reserved ASCII characters and keywords on one line (which may wrap around the page) represent parts of a reaction, including species reactants and products, stoichiometric coefficients and rate expressions. In addition, labels are supported, which function to allow one reaction to refer to another and to fix photolytic reaction table names for photolytic reactions. As mentioned above, the reader is referred to Chapter 8 for mechanism description examples. Also, Appendix M of the Models-3 User Manual contains a complete description of these formats.

15.4.5 Chemical Species Include Files

As described above, MP reads and processes the mechanism description file, and one of the outputs it generates is a file that contains the list of chemical species found in the mechanism. The Models-3 framework reads this species file to initialize the gas-phase species table in a format similar to a spreadsheet, which the user completes by inserting data such as molecular weights, surrogate names and factors, and processing flags. The initial set-up presented to the user consists of all blank entries in each spreadsheet cell, but with the first column filled in with the species found in the MP-generated species file. Thus all the species in the mechanism are listed in the order in which they were found in the mechanism description file. The top row is also filled in with category headers that are related to the linkages described above and that determine the framework-generated Fortran include files to be used in the codes.

There are three additional tables that are initialized for aerosols, non-reactive and tracer species. They do not have the first column set up, but the first row is set as in the gas-phase table. It is up to the user to fill in the first column, as with all the other spreadsheet cells. Appendix M of the Models-3 User Manual describes the details of how to enter data into these tables.

The following sections describe all the standard include files that are generated from the species tables and the behavior of the models when accessing the data declared in the include files.

15.4.5.1 Gas-Phase Reactions

The gas-phase reactions data are required in the CCTM by the gas-phase chemistry solvers and the subroutine PHOT, which calculates the photolysis rate constants. These data are also required in JPROC, the processor model that calculates the table-based photolysis rates (see Chapter 14). There are two include files associated with this data:

- RXCM.EXT - contains all the declarations, parameter statements and array definitions associated with the gas-phase chemistry reactions. This file also contains three named common blocks for memory allocation of the data from RXDT.EXT.
- RXDT.EXT - contains data statements associated with the parameters and arrays declared in RXCM.EXT. These data fill the arrays in the named common blocks in RXCM.EXT.

The CCTM driver program must include both of these files in its declaration section. The subroutines in the gas-phase chemistry solver process module must include only the common block file, RXCM.EXT. That goes for the subroutine PHOT, as well. PHOT is called from the gas-phase chemistry "class-driver," the top-level subroutine (see Section 18.2.2 in Chapter 18). The CCTM driver, by including both files, causes the common blocks to be loaded with the necessary data used by all the modules that need the chemistry data, including the process analysis module, PROCAN.

The remaining sections describe the global include files associated with the four species tables. As mentioned above, these files are automatically generated by the Models-3 framework, according to the user-specified linkages and flags, and are targeted for inclusion in all model routines that require the specific chemistry data in them. For additional details the reader is referred to the Models-3 User Manual [4]. Each of the include files contains declarations and parameter statements for the loop index and array dimensioning for each particular species group. If a particular species group is not used (e.g., aerosols or tracers), the include file contains declarations and parameter statements that set the species loop counter to zero and its array dimensioning parameter to one, thus maintaining complete generality and modularity within the codes. In addition, by setting the dimensioning value to one (Fortran does not allow zero), the compiled codes do not waste memory, a typical problem when coding in Fortran with some pre-determined maximum dimension to hopefully account for all cases.

15.4.5.2 Model Species

The framework generates four model species include files that together contain the names and molecular weights of all the chemical species available globally to the model.

The model species include files are:

- GC_SPC.EXT - gas-phase model species names and molecular weights.
- AE_SPC.EXT - aerosol species names and molecular weights.
- NR_SPC.EXT - non-reactive species names and molecular weights.
- TR_SPC.EXT - tracer species names and molecular weights.

The next three sections describe include files that are associated with data access by the CCTM from external files. The data are referenced from I/O API files by means of file variable names that are contained in headers in each of the files.

15.4.5.3 Emissions

The CCTM reads the emissions data from an I/O API file produced by ECIP using the surrogate name concept discussed above. The data are read by file variable names (surrogates) and stored in arrays that are linked to the corresponding model species names.

The CCTM has the option of emissions sources injected as part of the vertical diffusion process or as part of the chemistry solver process, where the injected sources are treated as part of the chemical production terms. To read source emissions data into the CCTM for processing either in the vertical diffusion or in the gas-phase chemistry modules, the following include files are required:

- GC_EMIS.EXT - gas-phase emissions surrogate species names with scale factors and indices that point to the positions of the species in the model species name table (in GC_SPC.EXT).
- AE_EMIS.EXT - aerosol emissions surrogate species names with scale factors and indices that point to the positions of the species in the model species name table (in AE_SPC.EXT).
- NR_EMIS.EXT - non-reactive emissions surrogate species names with scale factors and indices that point to the positions of the species in the model species name table (in NR_SPC.EXT).
- TR_EMIS.EXT - tracer emissions surrogate species names with scale factors and indices that point to the positions of the species in the model species name table (in TR_SPC.EXT).

15.4.5.4 Initial and Boundary Conditions

For both the initial and boundary concentrations the CCTM reads I/O API input data by variable name reference. The processing first checks to see if the model species name is on the file and reads the data associated with that name. If the model species name is not on the file, it checks for the surrogate name. If that, too is not available, the input value is set to a minimum value ("model zero"). Additional information on initial and boundary conditions and how they are implemented in the Models-3/CMAQ system can be found in Chapter 14.

- GC_ICBC.EXT - gas-phase initial and boundary conditions surrogate species names with scale factors and indices that point to the positions of the species in the model species name table (in GC_SPC.EXT).
- AE_ICBC.EXT - aerosol initial and boundary conditions surrogate species names with scale factors and indices that point to the positions of the species in the model species name table (in AE_SPC.EXT).
- NR_ICBC.EXT - non-reactive initial and boundary conditions surrogate species names with scale factors and indices that point to the positions of the species in the model species name table (in NR_SPC.EXT).
- TR_ICBC.EXT - tracer initial and boundary conditions surrogate species names with scale factors and indices that point to the positions of the species in the model species name table (in TR_SPC.EXT)

15.4.5.5 Dry Deposition

The following include files are used to read in dry deposition velocities from an I/O API file produced by the meteorology-chemistry input processor, MCIP. Using the surrogate name concept discussed above, the data are read by file variable names (surrogates) and stored in arrays that are linked to the corresponding model species names.

- GC_DEPV.EXT - gas-phase deposition velocity surrogate species names with scale factors and indices that point to the positions of the species in the model species name table (in GC_SPC.EXT).

- AE_DEPV.EXT - aerosol deposition velocity surrogate species names with scale factors and indices that point to the positions of the species in the model species name table (in AE_SPC.EXT).

- NR_DEPV.EXT - non-reactive deposition velocity surrogate species names with scale factors and indices that point to the positions of the species in the model species name table (in NR_SPC.EXT).

- TR_DEPV.EXT - tracer deposition velocity surrogate species names with scale factors and indices that point to the positions of the species in the model species name table (in TR_SPC.EXT).

15.4.5.6 Wet Scavenging

In both the scavenging and the cross-phase linkages it is necessary to set up a mapping from the gas-phase species to the generic species names that are associated with aerosols and aqueous-phase chemistry and to the names of species that are absorbed by cloud and rain water. Because of the generality with respect to the gas-phase species names, these generic names are set in the subroutines associated with aerosols, aqueous chemistry, and removal by in-cloud and precipitation scavenging. They are linked to the model species names by employing the surrogate name concept described above.

- GC_SCAV.EXT - gas-phase scavenging surrogate species names with scale factors and indices that point to the positions of the species in the model species name table (in GC_SPC.EXT).

- AE_SCAV.EXT - aerosol scavenging surrogate species names with scale factors and indices that point to the positions of the species in the model species name table (in AE_SPC.EXT).

- NR_SCAV.EXT - non-reactive scavenging surrogate species names with scale factors and indices that point to the positions of the species in the model species name table (in NR_SPC.EXT).

- TR_SCAV.EXT - tracer scavenging surrogate species names with scale factors and indices that point to the positions of the species in the model species name table (in TR_SPC.EXT).

15.4.5.7 Cross-Phase Linkage

- GC_G2AE.EXT - surrogate names for gas-phase model species that participate in aerosol chemistry with scale factors and indices that point to the positions of the species in the model species name table (in GC_SPC.EXT).
- GC_G2AQ.EXT - surrogate names for gas-phase model species that participate in aqueous-phase chemistry with scale factors and indices that point to the positions of the species in the model species name table (in GC_SPC.EXT).
- AE_A2AQ.EXT - surrogate names for aerosol species that participate in aqueous-phase chemistry with scale factors and indices that point to the positions of the species in the model species name table (in AE_SPC.EXT).
- NR_N2AE.EXT - surrogate names for non-reactive species that participate in aerosol chemistry with scale factors and indices that point to the positions of the species in the model species name table (in NR_SPC.EXT).
- NR_N2AQ.EXT - surrogate names for non-reactive species that participate in aqueous-phase chemistry with scale factors and indices that point to the positions of the species in the model species name table (in NR_SPC.EXT).
- TR_T2AE.EXT - surrogate names for tracer species that participate in aerosol chemistry with scale factors and indices that point to the positions of the species in the model species name table (in TR_SPC.EXT).
- TR_T2AQ.EXT - surrogate names for tracer species that participate in aqueous-phase chemistry with scale factors and indices that point to the positions of the species in the model species name table (in TR_SPC.EXT).

15.4.5.8 Operational Choices

The Models-3 framework provides the capability of allowing the user to control how some of the processing is carried out with respect to the chemical species in the CCTM. The following lists describe the include files that the framework generates for the various processes:

1. **Advected species:** In order to save memory storage or to minimize computation, the user may choose not to advect certain modeled species such as some radicals. In general, the special "counter species" used in a mechanism should not be advected.
    - GC_ADV.EXT - names of gas-phase model species that are advected and indices that point to the positions of the species in the model species name table (in GC_SPC.EXT).

- AE_ADV.EXT - names of aerosol species that are advected and indices that point to the positions of the species in the model species name table (in AE_SPC.EXT).
- NR_ADV.EXT - names of non-reactive species that are advected and indices that point to the positions of the species in the model species name table (in NR_SPC.EXT).
- TR_ADV.EXT - names of tracer species that are advected and indices that point to the positions of the species in the model species name table (in TR_SPC.EXT).

2. **Species that undergo diffusive processes:** The comment above, for advected species, applies also to diffused species.

- GC_DIFF.EXT - names of gas-phase model species that are diffused and indices that point to the positions of the species in the model species name table (in GC_SPC.EXT).
- AE_DIFF.EXT - names of aerosol species that are diffused and indices that point to the positions of the species in the model species name table (in AE_SPC.EXT).
- NR_DIFF.EXT - names of non-reactive species that are diffused and indices that point to the positions of the species in the model species name table (in NR_SPC.EXT).
- TR_DIFF.EXT - names of tracer species that are diffused and indices that point to the positions of the species in the model species name table (in TR_SPC.EXT).

3. **Species that are saved to the dry deposition output file:** Generally, all the dry deposition species that are modeled would be saved to the output file, but a user might elect to reduce the number and save only a subset.

- GC_DDEP.EXT - names of gas-phase model species that are written to the dry deposition output file and indices that point to the positions of the species in the model species name table (in GC_SPC.EXT).
- AE_DDEP.EXT - names of aerosol species that are written to the dry deposition output file and indices that point to the positions of the species in the model species name table (in AE_SPC.EXT).
- NR_DDEP.EXT - names of non-reactive species that are written to the dry deposition output file and indices that point to the positions of the species in the model species name table (in NR_SPC.EXT).
- TR_DDEP.EXT - names of tracer species that are written to the dry deposition output file and indices that point to the positions of the species in the model species name table (in TR_SPC.EXT).

4. **Species that are saved to the wet deposition output file:** See the comment in item 3.

- GC_WDEP.EXT - names of gas-phase model species that are written to the wet deposition output file and indices that point to the positions of the species in the model species name table (in GC_SPC.EXT).
- AE_WDEP.EXT - names of aerosol species that are written to the wet deposition output file and indices that point to the positions of the species in the model species name table (in AE_SPC.EXT).

- NR_WDEP.EXT - names of non-reactive species that are written to the wet deposition output file and indices that point to the positions of the species in the model species name table (in NR_SPC.EXT).
- TR_WDEP.EXT - names of tracer species that are written to the wet deposition output file and indices that point to the positions of the species in the model species name table (in TR_SPC.EXT).

5. **Species that are saved to the concentration output file:** See the comment in item 3.

- GC_CONC.EXT - names of gas-phase model species that are written to the concentration output file and indices that point to the positions of the species in the model species name table (in GC_SPC.EXT).
- AE_CONC.EXT - names of aerosol species that are written to the concentration output file and indices that point to the positions of the species in the model species name table (in AE_SPC.EXT).
- NR_CONC.EXT - names of non-reactive species that are written to the concentration output file and indices that point to the positions of the species in the model species name table (in NR_SPC.EXT).
- TR_CONC.EXT - names of tracer species that are written to the concentration output file and indices that point to the positions of the species in the model species name table (in TR_SPC.EXT).

15.4.5.9 Tracer Species

The use of tracer species is purely user-determined. An application with tracers can provide the modeler with insights into how the model is simulating various physical processes, like advection or diffusion. If tracer species are to be modeled, the user must have created the special table entries appropriate to the application. In addition special data, such as emissions or initial and boundary tracer concentrations, must be created in the corresponding I/O API files. The specialized data creation is outside the scope of the Models-3 framework and must be carried out by the user in conjunction with the application that is being modeled.

15.6 Conclusion

In this chapter we have described how PCP helps to establish modularity and consistency for particular applications of models in the CMAQ system. The Models-3 framework processing, through PCP, enables model developers and model users to study the effects of different implementations of the science and codes or to execute different applications at various scales with different chemical mechanisms or with different numerical solvers. The design and implementation of the concepts in the program control processing helps to establish a true "one-atmosphere" approach to modeling.

15.7 References

[1] "The EDSS/Models-3 I/O API" http://sage.mcnc.org/products/I/O API/

[2] Jeffries H. E. (1990), "User's Guide to Photochemical Kinetics Simulation System PC-PKSS Software Version 3," Chapel Hill, N.C. 27514

[3] Gery M. W. and R. R. Crouse (1990), "User's Guide for Executing OZIPR," EPA/600/8-90/069, U. S. Environmental protection Agency, Research Triangle Park, NC 27711

[4] EPA Third-Generation Air Quality Modeling System Models-3 Volume 9b, User Manual, Appendices, June 1998, EPA-600/R-98/069(b)

This chapter is taken from *Science Algorithms of the EPA Models-3 Community Multiscale Air Quality (CMAQ) Modeling System*, edited by D. W. Byun and J. K. S. Ching, 1999.

EPA/600/R-99/030

Chapter 16

PROCESS ANALYSIS

Gerald L. Gipson*
Human Exposure and Atmospheric Sciences Division
National Exposure Research Laboratory
U. S. Environmental Protection Agency
Research Triangle Park, NC 27711

ABSTRACT

The implementation of process analysis techniques in the Models-3 Community Multiscale Air Quality (CMAQ) modeling system is described in this chapter. These techniques can be used in Eulerian photochemical models such as the CMAQ Chemical Transport Model (CCTM) to obtain information that provides insights into how model predictions are obtained. This type of information is particularly useful when modeling nonlinear systems such as atmospheric photochemistry. The two techniques available in the CMAQ system – integrated process rate (IPR) analysis and integrated reaction rate analysis (IRR) -- are each described. The manner in which IPR analysis can be used to determine the relative contributions of individual physical and chemical processes is presented. Descriptions of how to employ IRR analysis to elucidate important chemical pathways and to identify key chemical characteristics are included. Finally, the procedures used to apply each technique in the CMAQ system are also described.

*Corresponding author address: Gerald L. Gipson, MD-80, Research Triangle Park, NC 27711. E-mail: ggb@hpcc.epa.gov

16.0 PROCESS ANALYSIS

A major function of air pollution models is to predict the spatial and temporal distributions of ambient air pollutants and other species. For complex Eulerian grid models, output concentration fields of these species are determined by solving systems of partial differential equations. These equations define the time-rate of change in species concentrations due to a series of physical and chemical processes (e.g., emissions, chemical reaction, horizontal advection, etc.). Since most grid models are configured to output only the concentration fields that reflect the cumulative effect of all processes, information about the impact of individual processes is usually not available. Grid models can be configured to provide quantitative information on the effects of the chemical reactions and other atmospheric processes that are being simulated, however (Pleim, 1990; Jeffries and Tonnesen, 1994; Jang et al., 1995a,b). This type of information has been used to develop various process analyses that provide descriptions of how a model obtained its predictions. This chapter provides background information on these methods and describes how process analysis is implemented in the Models-3 Community Multiscale Air Quality (CMAQ) modeling system.

Although process analysis does not have to be included in a grid model application, it can provide supplemental information that can be quite useful in assessing a model's performance. Quantifying the contributions of individual processes to model predictions provides a fundamental explanation of the reasons for a model's predictions and shows the relative importance of each process. This information can be useful in identifying potential sources of error in the model formulation or its inputs. It can also be useful in interpreting model outputs, particularly with respect to understanding differences in model predictions that occur from a change to the model itself or to its input. Further, information provided from the chemical process analysis can be used to determine important characteristics of different chemical mechanisms. This is particularly useful for investigating mechanistic differences under different chemical regimes (e.g., VOC versus NO_x limiting conditions).

The inclusion of process analysis in a model application is generally carried out in two steps. First, the model itself is "instrumented" (i.e., additional code or modules are added to the model) to produce supplemental outputs about the contributions of individual processes and different chemical reaction pathways to the model predictions. These data are then used with the concentration fields in postprocessing operations to provide quantitative explanations of the factors affecting a model's predictions. Although several specific postprocessing techniques have been developed to reveal particular model features (e.g., Jeffries and Tonnesen, 1994; Jang et al., 1995a,b), process analysis data can be extracted and analyzed in many different ways. The implementation of process analysis in the CMAQ system has been structured to facilitate data extraction for subsequent model analysis. Although the main focus of this chapter is on data extraction techniques, some example process analyses are also presented to illustrate particular applications.

For purposes of discussion, it is convenient to separate process analysis into two parts: integrated process rate (IPR) analysis and integrated reaction rate (IRR) analysis. The first deals with the effects of all the physical processes and the *net* effect of chemistry on model predictions. IRR analysis deals with the details of the chemical transformations that are described in the model's chemical mechanism. In general, IPR analyses are generally much easier to apply and understand than IRR analyses since the latter typically requires a fairly thorough understanding of atmospheric chemistry. Thus, the discussion below describes each analysis method separately, starting with IPR analyses. Users not familiar with atmospheric chemistry details may wish to omit the sections on IRR analysis. It should be added that either analysis method can be applied independently of the other.

The CMAQ implementation of process analysis includes a flexible user interface that allows the user to request only those particular outputs that are needed for model analysis. The information generated for both IPR analysis and IRR analysis is controlled by the Process Analysis Control Program (PACP). The PACP processes user-specified commands to instrument the CMAQ Chemical Transport Model (hereafter referred to as the CCTM) to generate the specific outputs that are selected by the user. As a consequence, the PACP must be invoked before configuring a CCTM and running a simulation. The details of how the PACP works and the syntax for the commands are covered in the Models-3 User Manual (EPA, 1998), and they will not be repeated in their entirety here. Nevertheless, some of the command syntax and some simple examples are presented in the discussions that follow to illustrate how the PACP is used to set up a particular process analysis.

16.1 Integrated Process Rate Analysis

The governing equation for Eulerian models is the species continuity equation. Application of the continuity equation to a group of chemically reactive species results in a system of partial differential equations (PDEs) that gives the time-rate of change in species concentration as a function of the rates of change due to various chemical and physical processes that determine the ambient species concentrations. As noted in the introduction, the concentration fields that are the numerical solutions to these PDEs reveal only the net effects of all processes. This section is concerned with how the contributions of individual processes are determined and used in process analyses. The first two subsections deal with the calculation and use of IPRs in general. The last two subsections describe the CMAQ implementation of IPR analysis and the use of the PACP to set up an IPR analysis.

16.1.1 Computation of Integrated Process Rates

All Eulerian models utilize the technique of operator splitting. As a result, it is relatively easy to obtain quantitative information about the contribution of individual processes to total concentrations. In operator splitting, solutions to the system of PDEs are obtained by separating the continuity equation for each species into several simpler PDEs or ordinary differential equations (ODEs) that give the impact of only one or two processes. These simpler PDEs or

ODEs are then solved separately to arrive at the final concentration. To illustrate, consider the simple case of two-dimensional horizontal advection of a single species in the absence of any other processes, for which the governing equation can be expressed as follows:

$$\frac{\partial c}{\partial t} + \frac{\partial (uc)}{\partial x} + \frac{\partial (vc)}{\partial y} = 0 \ , \tag{16-1}$$

where c is the species concentration, and u and v are the x- and y-components of the wind velocity vector, respectively. With operator splitting, this 2-dimensional equation is split into two 1-dimensional operators, one for each direction:

$$\frac{\partial c}{\partial t} + \frac{\partial (uc)}{\partial x} = 0 \tag{16-2a}$$

and

$$\frac{\partial c}{\partial t} + \frac{\partial (vc)}{\partial y} = 0 \ . \tag{16-2b}$$

These two equations are then solved sequentially, with the solution to the first being used as the initial condition for the second. The solution to the second equation then represents the final solution and gives the net effect of 2-dimensional advection.

The final solution for the example presented above can also be represented as follows:

$$c(t + \Delta t) = c(t) + (\Delta c)_x + (\Delta c)_y \ , \tag{16-3}$$

where $c(t+\Delta t)$ is the final solution, $c(t)$ is the initial condition for the 2-dimensional problem, and $(\Delta c)_x$ and $(\Delta c)_y$ are the changes in concentration produced by each of the 1-dimensional operators. $(\Delta c)_x$ and $(\Delta c)_y$ give the impact of each operator in moving from the initial to the final concentration and are equivalent to the results obtained by integrating the process rates individually. Hence the term integrated process rates is used to describe them. Note that they can be computed with little additional work since they are simply equal to the difference between the final and initial concentrations for each operator.

From the above example, it should be evident that a general mathematical representation of IPRs for individual processes can be expressed as follows:

$$(\Delta c)_n = \int_t^{t+\Delta t} L_n \, dt \ , \tag{16-4}$$

where $(\Delta c)_n$ is the change in a species' concentration due to operator n, L_n is the differential operator associated with a process, and Δt is the model synchronization time step (which is

equivalent to Δt_{sync} in Chapter 6). Refer to Chapter 6 for a discussion of the various time steps used in CMAQ. The integration in equation (16-4) is performed by the model regardless of whether it has been instrumented for process analysis. Thus, it is only necessary to save the $(\Delta c)_n$ to obtain process analysis capabilities. In a few cases, however, models may be structured such that one operator deals with two or three processes simultaneously. In those cases, the $(\Delta c)_n$ obtained after the integration would represent the compound effect of all of those processes and it would not be possible to discern the impacts of the individual processes. Normally, the only way that information could be obtained would be to integrate the process rates separately. In some instances, however, it may still be possible to isolate the impacts of the individual processes without performing additional integrations. For example, the CCTM treats vertical diffusion, emissions, and dry deposition simultaneously in one operator, but the amount of material deposited by dry deposition is tabulated and the amount of material that is emitted is known. As a consequence, mass balance techniques can be used to compute the contribution of each process subsequent to the simultaneous integration of the process rates without separately integrating each process rate. Thus, the IPRs that are available for process analysis are to some degree determined by the underlying structure of the photochemical model that is being used and by the effort that is invested in separating individual components when processes are coupled in a single operator.

Analogous to equation (16-3), the concentration at the end of a time step can be expressed as follows:

$$c(t+\Delta t) = c(t) + \sum_{n=1}^{N} (\Delta c)_n \ , \qquad (16\text{-}5)$$

where the model is assumed to have N operators. It should be noted that most IPRs can be either positive or negative since most processes can cause concentrations to either increase or decrease. Further, it should also be evident that the IPRs in the above expression are additive. Thus, for example, the IPRs for horizontal advection and vertical advection could be summed to give one IPR that represents the net impact of the two advection processes. The differential operators (L_n) themselves are most often nonlinear, however. Because of these nonlinearities, the magnitude of the IPRs for most processes would change if the order of the model's operators was altered or even if only one of the operators was changed. Thus, the additive property for IPRs holds only for a particular application of the model.

16.1.2 Example IPR Analyses

The tabulation and subsequent output of IPRs provide the user with quantitative information on the effects of individual processes, and these can be examined and depicted in a number of ways. Figures 16-1 and 16-2 contain two types of displays that were developed to depict process contribution data graphically (Jeffries, 1996). Figure 16-1 is a time series plot showing both predicted concentrations and integrated process rates. This type of plot shows the hourly variations at a cell (or group of cells if the data are aggregated) of a predicted species

concentration and the change in concentration caused by each process (i.e., the IPRs). Plots of this type illustrate the variations in process contributions during the simulation period. Figure 16-2 shows process contributions and total concentrations for different model formulations, in this case, different grid resolutions. Here the data have been aggregated over several cells and hours, but could be developed for a single cell or time period just as well. This figure highlights how cumulative process contributions are altered by the different model formulations. For a more thorough discussion of how this type of data can be used to assist in the evaluation of a model's performance, the reader is referred to Jang et al. (1995a and 1995b) and to Pleim (1990).

16.1.3 Implementation of IPR Analysis in the CMAQ System

The previous section illustrated that instrumenting a model for process analysis involves providing the capability to capture IPRs. Since an IPR can be calculated for every combination of process and species, the amount of output data that can be generated is substantial. As a consequence, the PACP has been designed to allow substantial flexibility in selecting the particular IPRs for output. This is accomplished primarily by allowing the user to choose only those particular species/process combinations that are of interest. Additional control and flexibility are provided by including the ability to produce lumped IPRs, by allowing special species families to be defined, and by providing controls to limit the size of the modeling domain for which outputs are generated. These will be illustrated in the examples presented below.

The physical processes that are simulated in the CCTM and hence are available for IPR analysis are shown in Table 16-1. As will be illustrated below, these processes are referenced in the PACP by the codes shown in the first column. The procedure for selecting specific IPRs for output is species oriented. Hence, a user selects a species and then indicates which processes will be included in the IPR output. The species are referenced by their model names. In addition, the user may also define a family of species that is a linear combination of the model species (e.g., defining NOx as the sum of NO and NO_2) and extract IPRs for the family. This can be useful in saving disk space occupied by the output IPR files when information about individual members of a family is not needed.

It should be apparent from Table 16-1 that IPRs for some species will always be zero (e.g., those species not emitted always have zero IPRs for that process). Thus, the size of the output file can be minimized by not extracting those IPRs. The PACP also contains an option that allows the user to limit the amount of output data by extracting IPR outputs for only part of the modeling domain. Currently, the user is restricted to selecting a single, contiguous block of cells within the domain for the IPR outputs. The block is defined relative to the modeling domain by selecting a starting and ending column, row and level. A possible future enhancement would be to provide a graphical interface to allow the user to select any particular cell or group of cells within the domain.

The CCTM model has been instrumented to write the IPRs to an output file at the same time as the output concentration files are written. Thus, the IPR outputs represent the cumulative impact

of the process integrations over the entire output time interval. Process contributions over shorter time intervals can be obtained by increasing the frequency of writing outputs of both the concentration fields and the IPRs. Finally, the IPR output files are standard Models-3 IO/API gridded files, and can be viewed with the Models-3 visualization tools described in Models-3 User Manual (EPA, 1998).

16.1.4 Use of the PACP to set up an IPR Analysis

This section illustrates how the PACP can be used to generate the IPR data for an analysis. Details on formatting inputs and using the PACP are contained in the Models-3 User Manual (EPA, 1998). This section borrows from that discussion to illustrate how the PACP is used. The user selects and controls the form of the IPR output data by means of a PACP command file. A few predefined command files are available to set up an analysis, or users can generate their own files to customize their analyses. A command file consists of a series of commands and definitions that contain instructions for generating IPR outputs. The commands are input in a free form format to facilitate encoding, and they contain special keywords that have specific meaning to the PACP. The commands related to IPR analysis have been divided into two groups: Global commands and IPR output commands. A description of the commands within each group will be presented first, followed by an example illustrating how these commands are used. In the description that follows, the syntax for each command is given first, with bold type used for PACP keywords and normal type used for user supplied input. Alternative inputs are separated by vertical bars and completely optional inputs are enclosed in curly braces.

Global Commands:

OUTPUT_DOMAIN = {**LOCOL**[n_1] + **HICOL**[n_2] + **LOROW**[n_3] + **HIROW**[n_4] + **LOLEV**[n_5] + **HILEV**[n_6]};

The OUTPUT_DOMAIN command provides the capability to limit the IPR output data to only one portion of the modeling domain. The n_i in brackets are numbers that define the bounds of the output domain relative to the number of columns, rows, and vertical levels in the modeling domain. Thus, for example, the value for n_1 must be greater than or equal to one and less than or equal to the number of columns in the domain. If this command is included, at least one domain specifier must be present, and the end of the domain is used for any that are missing. If the command is omitted entirely, output is generated for the entire domain.

DEFINE FAMILY familyname = {c_1*}species$_1$ {+ {c_2*}species$_2$ + ...};

The DEFINE FAMILY command is used to define a group of species as members of a family. The user specified "familyname"

must be unique, and can be referenced in subsequent commands. The c_i are numerical coefficients that default to one if not specified; "$species_i$" are the names of individual model species.

ENDPA;

The ENDPA command signifies the end of the command input in the PACP command file.

IPR Output Command:

IPR_OUTPUT species|familyname|**ALL** {= $pcode_1$ + $pcode_2$ + ...};

The IPR_OUTPUT command defines specific IPR outputs to be generated during a CMAQ simulation. A species name, family name, or the keyword ALL must follow the IRR_OUTPUT keyword. The keyword ALL refers to all model species. IPRs are generated for the selected species or family, and they are controlled by the specified values of $pcode_i$, where $pcode_i$ corresponds to one of the process codes listed in Table 16-1. If no process codes are specified, IPRs will be generated for every process. The output variables that are generated are named either species_$pcode_i$ or familyname_$pcode_i$

A listing of an example PACP command file is contained in Exhibit 16-1. To facilitate the discussion that follows, the commands have been numbered, although this is not required by the PACP. (Note that all information enclosed by curly braces in a command file is treated as comments.) Each numbered line represents a command, and the input for each command is terminated by a semicolon. This particular set of commands causes the CCTM to generate several individual IPRs for a special user-defined sub-domain. Each of the commands is described below.

Command 1 is used to restrict the process analysis output to a subset of the modeling domain. As noted above, output would be generated for the entire computational domain if the OUTPUT_DOMAIN were omitted. Since keywords for columns and rows are not present, the PACP default is to include all rows and columns in the modeling domain. The keywords "LOLEV" and "HILEV" restrict the output for the vertical level to layers 1 through 2. Thus, the net effect of this command is to limit the IPR output to all cells within the first two vertical levels of the modeling domain.

Commands 2 and 3 are used to define families of species. The species names to the right of the equal sign are model species. The effect of the numerical coefficients in the definition of the VOC

families is to convert the units of the IPRs for individual organics from ppm to ppmC. As will be seen, these "defined" family names are referenced in subsequent commands.

Commands 4 through 8 actually cause IPR outputs to be generated. As described above, IPRs are generated for the species and the processes that are referenced by means of the codes listed in Table 16-1. Since no process codes are specified in commands 4 and 5, IPRs will be generated for each of the twelve processes in Table 16-1 for the families NOX and VOC (i.e., a total of 24 IPRs). Command 6 causes three IPRs to be generated for species O3, one each for total transport, chemistry, and clouds. Command 7 causes an IPR for vertical diffusion to be generated for every model species. The last command signifies the end of the command inputs.

The CCTM will generate the IPR output data in a form comparable to the output concentration files. Hence, the data are written to standard Models-3 IO/API gridded data files. The units of the IPR data are normally the same as those for the species concentration data (i.e., ppm for gas-phase species and either $\mu g/m^3$ or number/m^3 for aerosols). As described in the example of creating the family VOC with units of ppmC, however, different output units can be created using special family definitions.

The example just described was formulated primarily to illustrate how IPR commands are structured to collect IPR information during a model simulation. In general, the particular data that are collected for process analysis would be determined by the needs of the study, and thus it is difficult to define a "default" process analysis. Nevertheless, a minimal process analysis for studying ozone formation might involve collecting the process contributions for NOx, VOC, and for ozone. The example in Exhibit 16-1 could be used as the starting point for such an analysis. Commands 4 and 5 capture all the IPRs for NOx and VOC. Command 6 could be modified to capture all IPRs for ozone as well. Since it would not normally be necessary to capture vertical diffusion IPRs for all species, command 7 could be dropped. Of course, the user would still be required to define the domain for outputs (command 1) and to define the VOC family for the mechanism that is being used (command 3). Thus, commands 1 through 5 with command 6 modified to collect all IPRs for ozone would provide some very basic process analysis information on the formatio of ozone during a simulation.

16.2 Integrated Reaction Rate Analysis

The second major component of process analysis is IRR analysis. It is applied to investigate gas-phase chemical transformations that are simulated in the model. Its primary use to date has been to help explain how ambient ozone is formed in the chemical mechanisms that are used in photochemical models (e.g., Jeffries and Tonnesen, 1994; Tonnesen and Jeffries, 1994). Thus, the CMAQ implementation of IRR analysis currently addresses only gas-phase reactions. Nevertheless, the concepts should be adaptable to the modules simulating aerosol formation and aqueous chemistry as well, and this is an area for future enhancement in the CCTM. The remainder of this section describes how the IRRs are calculated and generated in the CMAQ system.

16.2.1 Computation of Integrated Reaction Rates

As described in Chapter 8, the simulation of atmospheric chemistry is a key component of a photochemical air quality model. The operator splitting techniques that are used in Eulerian photochemical models typically result in a set of nonlinear, coupled, ordinary differential equations (ODEs) that describe chemical interactions in the gas-phase. Solutions to these ODEs are obtained using numerical solvers to compute species concentrations as a function of time. Again, these computed concentrations show only the net effect of chemical transformations. As has been done for physical processes, a technique has been developed to provide quantitative information on individual chemical transformations (Jeffries and Tonnesen, 1994). Since the technique involves integrating the rates of the individual chemical reaction, the method is termed integrated reaction rate analysis.

As was noted in section 8.3.1, the mathematical expression for the rate of a chemical reaction takes one of the forms of equation set 8-3. The reaction rate is used to compute the change in species concentration that is caused by the reaction. Mathematically, this can be expressed as follows:

$$M_l(t+\Delta t) = M_l(t) + \int_t^{t+\Delta t} r_l \, dt \, , \qquad (16\text{-}6)$$

where M_l refers to the integrated reaction rate (IRR) for reaction l, Δt is the model synchronization time step used by the chemical solver, and r_l is the rate of reaction l corresponding to one of the forms of equation set 8-3. The value of M_l represents the total throughput of the reaction, and can be used with the appropriate stoichiometry to determine the amount of an individual species that is produced or consumed by the reaction. For example, assume the IRR for the reaction A + B → 2C is 20 ppb for a given time period. Then, the amount of A and B consumed in that time period by this reaction is 20 ppb, and correspondingly, the amount of C produced is 40 ppb. Further, the net change in a species concentration due to all chemical reactions is equivalent to the sum of all its production terms less the sum of all its loss terms. As a consequence, the contribution of each reaction to the change in concentration of any species is directly available from the IRRs. With this information, it is possible to identify the important chemical pathways that affect species concentrations and thereby unravel the complex chemical interactions that are being simulated.

As described in Chapter 8-4, the chemistry solvers used in air quality models typically employ marching methods that compute species concentrations at the end of a time step given the concentrations at the beginning of the step. Since the solvers adjust the time steps to maintain stability and accuracy, the reaction rates should not vary too greatly over a given time step. As a consequence, it is possible to use a fairly simple numerical integration technique to compute the IRRs. The technique used in the CCTM is the same the one used by Jeffries and Tonnesen (1994) -- the trapezoid rule. With this method, the IRRs are computed as follows:

$$M_l(t+\Delta t) = M_l(t) + \frac{1}{2}[r_l(t) + r_l(t+\Delta t)] \ . \tag{16-7}$$

Thus, the IRRs are simply computed from the values of the reaction rates at the beginning and the end of each chemistry integration time step. As the chemistry solver marches through time, the variable M_l accumulates the IRRs over the simulation period. Although an IRR could be accumulated for the entire simulation, more information can be gained on how the mechanistic processes vary with time if the accumulated IRRs are periodically output and the value of M_l is reset to zero. In the CCTM, the IRR output is synchronized with the outputs for the concentration fields and the integrated process rates. Thus, just like the IPRs, the IRRs that are output represent the integral of the reaction rates over the output time interval.

16.2.2 Example IRR Analyses

Most IRR analysis performed to date has been devoted to studying mechanistic processes that affect tropospheric ozone formation. One method that has been used involves analyzing two important, interacting cycles: the OH radical cycle and the NO_x oxidation cycle. This section contains a brief discussion of these cycles and other important chemical parameters to illustrate how integrated reaction rate analysis can be used to understand different chemical pathways. For more comprehensive discussions, the reader is referred to Jeffries (1995), Jeffries and Tonnesen (1994), and Tonnesen and Jeffries (1994).

Ozone is formed in the atmosphere via the photochemical cycle

$$NO_2 + h\nu \rightarrow NO + O(^3P) \tag{R1}$$

$$O(^3P) + O_2 \rightarrow O_3 \tag{R2}$$

$$NO + O_3 \rightarrow NO_2 \ . \tag{R3}$$

If these were the only reactions taking place in the atmosphere, an equilibrium condition would be established that would determine the ozone concentration. These levels are almost always lower than what is observed in the atmosphere because of other interactions (Seinfeld, 1998). The presence of free radicals can alter the ozone production rate through the following reactions that are competitive with R3:

$$HO_2 + NO \rightarrow NO_2 + OH \tag{R4}$$

$$RO_2 + NO \rightarrow NO_2 + RO \ . \tag{R5}$$

In these reactions, NO_2 is produced in reactions that do not consume ozone, thereby introducing a process by which ozone can accumulate. Furthermore, these reactions are radical propagation reactions since a hydroxyl radical (OH) is produced from the hydroperoxy radical (HO_2) and an

alkoxy radical (RO) is produced from an alkylperoxy radical (RO_2). These product radicals are then available to participate in other reactions, some of which lead to the regeneration of the peroxy radicals. Thus, the production of ozone can be viewed as an autocatalytic process since O_3 can be produced without the loss of its precursor NO_2. In the atmosphere, however, ozone production is limited by termination reactions that remove either radicals or NO_2 from the system.

The ozone formation process has been represented by means of a schematic diagram, shown in Figure 16-3a, that consists of two interacting cycles (Jeffries, 1995). The top portion of the figure is the OH reaction cycle which consists of the three principal categories of reactions involving radicals: initiation, propagation, and termination. Radical initiation reactions are almost always photolytic reactions that generate "new" radicals. Examples include the photolysis of formaldehyde, hydrogen peroxide and ozone . Radical propagation reactions include reactions such as R4 and R5 in which NO is converted to NO_2 but no radicals are lost. Many reactions in which organic compounds are oxidized also propagate radicals. The termination reactions remove radicals through the formation of stable products. The bottom portion of Figure 16-3a represents the NO_x oxidation cycle. As with the radical cycle, processes in this cycle are classified as either initiation, propagation, or termination. The initiation process for NO_x corresponds to emissions of NO_x, and the termination process corresponds to reactions in which NO_x is converted to stable products. The NO_x cycle is connected to the radical cycle by means of the propagation steps that convert NO to NO_2.

One form of an IRR analysis that can be conducted involves using the IRRs to develop quantitative information about the various initiation, propagation, and termination processes. Figure 16-3b shows a cycle diagram similar to Figure 16-3a in which the IRRs have been used to compute the numerical values that are shown. These values include net throughput for several parameters that serve to further characterize the state of the reacting system. For example, the fraction of OH that is regenerated by the chemical reactions (0.776 in Figure 16-3b) can be determined from the amount of OH that reacts (142.7 ppb) and the amount that is re-created (110.8 ppb). This is directly related to the OH chain length parameter (4.46) which corresponds to the average number of times each new OH is cycled until it is removed from the system. An analogous chain length parameter (5.13) can be calculated for the NO_x oxidation cycle in the form of the NO chain length. The longer these chain lengths, the greater the potential for O_3 formation per unit of NO_x emissions. Other parameters such as the "NO oxidations per VOC consumed" [$(NO \rightarrow NO_2)/VOC = 1.71$] and "$O_3$ produced per O^3P generated by NO_2 photolysis" ($[O_3]_p/[O^3P] = 0.951$) further quantify the relative efficiency of ozone production, the former being particularly useful in providing a measure of the reactivity of the organic compounds.

These types of analyses are particularly useful for comparing model results that are obtained using different chemical mechanisms or that are obtained at different locations with the same chemical mechanism. Other types of IRR analyses can provide other information as well. For example, IRRs have been used to allocate the total production of O_3 to the individual VOCs, to examine individual characteristics of various chemical mechanisms such as yields of radicals from different organics, and to quantify other entities such as the production and loss of odd-oxygen (O_x), which

can serve as surrogate for tracking the formation of ozone (Jeffries and Tonnesen, 1994; Tonnesen and Jeffries, 1994). It can be expected that many other types of IRR analyses will be developed, especially as newer and possibly more complex chemical mechanisms are developed and used in models.

16.2.3 Implementation of IRR Analysis the CMAQ system

As described in Chapter 8, the CMAQ system is designed to treat chemical mechanisms in a generalized manner. Since a specific chemical mechanism is not embedded in the CCTM, a comparable generalized method is needed to link IRR analysis with the chemical mechanism. The technique that has been incorporated in the CMAQ system is one that provides the user with the capability to formulate and then generate particular chemical parameters of interest. Presumably, these parameters would be chosen to reveal special properties of the mechanism and/or to be used in generating photochemical cycle diagrams such as Figure 16-3b. To illustrate, a special PACP command file has been prepared for the RADM2 mechanism. For reference, a listing of the RADM2 mechanism is contained in Exhibit 16-2, and the reader is referred to the Models-3 User Manual for a detailed explanation of the mechanism format. For purposes of the discussion that follows, it is sufficient to note that reaction labels are enclosed in "<" and ">" and precede each reaction, and that the reactants and products in each reaction are model species. Both the reaction labels and the species names will be referenced in PACP commands.

Table 16-2 lists the chemical parameters that are produced in this example IRR analysis for the RADM2 mechanism. Most of these parameters could also be generated for other chemical mechanisms, although the specific calculations that would have to be performed would necessarily differ because of differences in the mechanisms. The parameters in Table 16-2 are computed as simple, linear combinations of the IRRs that are calculated for each chemical reaction. The domain controls that are specified for the integrated process rate outputs apply to IRR outputs as well. Thus, both the IPR and IRR data will be generated for the same domain and written to output files at the same time intervals. Similarly, the IRR output files are standard Models-3 IO/API gridded files, and can be used with the standard Models-3 visualization tools. In addition, a special visualization tool that can generate "default" cycle diagrams similar to Figure 16-3b is available and is described in Models-3 User Manual (EPA, 1998). Note, however, that the IPR and IRR outputs are written to separate files.

One of the advantages of generating IRR data in the form of chemical parameters is that the output file storage requirements can often be minimized. Note that there are fewer IRR parameters in Table 16-2 than there are species in most mechanisms. The major disadvantage to this approach is that new or different parameters cannot be computed without rerunning a model simulation. As a consequence, the CMAQ implementation of IRR analysis also contains the option to capture the complete set of IRRs rather than chemical parameters when a model is run. With this option, one IRR is generated for each chemical reaction, and these IRRs can then be manipulated in postprocessing routines to form any particular chemical parameter of interest. Thus, it would be anticipated that the chemical parameters such as those in Table 16-2 would be

generated in fairly routine model applications, whereas IRRs for each reaction would be generated for exploratory analyses. The form of the outputs is controlled by the PACP commands that are described next.

16.2.4 Use of the PACP to set up an IRR Analysis

As with IPR analysis, the IRR outputs that are generated by the CCTM are controlled by commands and special operators that are processed by the PACP. The global commands that were described in the IPR section also apply to the IRR output. Thus, family names created with the DEFINE FAMILY may also be used with several of the IRR commands and operators. Before describing how the commands are used to construct an IRR analysis, a brief description of each IRR command and operator is first presented. These are divided into three groups: IRR global definitions, IRR operators and IRR output commands. Again, the same syntax conventions are used, i.e., PACP keywords and symbols are in bold type, user supplied values are in normal type, alternative inputs are separated by vertical bars, and completely optional inputs are enclosed in braces.

IRR Global Definitions:

IRR_TYPE = FULL|PARTIAL|NONE;

The IRR_TYPE command defines the type of IRR analysis. With the type set to FULL, IRRs for each reaction will be calculated and written to the IRR output file, and all other IRR commands will be ignored. IRR_TYPE set to PARTIAL indicates that the IRR commands following this command are to be processed to produced user defined IRR outputs. Type set to NONE causes all other IRR commands to be ignored and no IRR output to be generated. If the command is omitted, type PARTIAL is assumed.

DEFINE CYCLE cyclename = $species_1$;

The DEFINE CYCLE command is used to compute the net of all chemical production and loss of a species involved in more than one cyclical reaction set. Thus, this quantity is computed by summing the IRRs for all reactions in which a species is consumed, and then subtracting that sum from the sum of the IRRs for all reactions in which the species is produced. The "cyclename" is a user defined name that must be unique, and can be referenced in subsequent IRR_OUTPUT commands.

DEFINE RXNSUM sumname = $\{\pm\}\{c_1*\}$<$rxlabl_1$> $\{\pm\{c_2*\}$ <$rxlabl_2$> $\pm \ldots\}$;

The RXSUM command is used to compute a linear combination of IRRs for individual reactions that can then be referenced in a subsequent IRR_OUTPUT command; "sumname" is user defined and must be unique. The linear combination of IRRs is defined according to the expressions following the equal signs that specify the reaction IRRs to sum. The "$rxlabl_i$" is the reaction label that is used by the generalized mechanism to identify each reaction and is enclosed in "<" and ">". The "c_i" are optional numerical coefficients that default to one if not specified.

IRR Output Operators:

PROD[$species_1$] {**FROM**[$species_2$] {**AND**|**OR** [$species_3$] }}

The production operator (PROD) is used to compute the total production of a species by summing the IRRs of all reactions in which $species_1$ appears as a product. The optional qualifiers FROM, AND, and OR restrict the sum to include only those reactions in which $species_2$ and/or $species_3$ are reactants; "$species_1$" can be any gas-phase mechanism species or a family of gas-phase species that was defined using the DEFINE FAMILY command as described in the IPR section; "$species_2$" or $species_3$" may also be the keyword HV to restrict the selection to photolytic reactions.

NETP[$species_1$] {**FROM**[$species_2$] {**AND**|**OR** [$species_3$] }}

The net production operator (NETP) is very similar to the production operator PROD since it is used to compute the production of a species. Whereas the PROD operator includes every reaction in which species occurs as a product, the NETP operator includes only those reactions in which the net production of $species_1$ is greater than zero. Thus, if $species_1$ appears as both a reactant and a product with equal stoichiometry in a reaction, the PROD operator will include it but the NETP operator will not. This operator is useful for getting the net production of a family, for example, by eliminating those reactions in which the net effect of the reaction on the family concentration is zero. The qualifiers FROM, AND and OR restrict the inclusion of reactions to those in which $species_2$ and/or $species_3$ are reactants.

LOSS[$species_1$] {**AND**|**OR** [$species_2$] }

The loss operator (LOSS) is used to compute the total loss of a species by summing the IRRs of all reactions in which $species_1$ appears as a reactant. The optional qualifier AND restricts the sum to include only those reactions in which both $species_1$ and $species_2$ are reactants. Similarly, the OR qualifier includes all reactions in which either "$species_1$" or "$species_2$" appears as a reactant. The "$species_1$" or "$species_2$" can be any gas-phase species in the mechanism, a family name that includes only gas-phase mechanism species, or the keyword HV to restrict the selection of reactions to those that are photolytic.

NETL[$species_1$] {**AND**|**OR** [$species_2$] }}

The net loss operator (NETL) is very similar to the loss operator since it is used to compute the loss of a species. However, it includes only those reactions in which there is a net loss of "$species_1$" and/or "$species_2$" . Thus, if $species_1$ appears as both a reactant and a product with equal stoichiometry in the reaction, the NETL operator will not include it in summing the loss of that species, whereas the LOSS operator will include the IRR for that reaction. This operator is useful for getting the net loss of a family of species.

NET[$species_1$]

The net operator (NET) is very similar to the CYCLE definition since it gives the net of the production and the loss of a species for all reactions in which "$species_1$" appears either as reactant or a product; "$species_1$" may be any gas-phase, mechanism species or any family consisting wholly of gas-phase mechanism species.

IRR Output Commands:

IRR_OUTPUT irrname = {c_1*}op_1|cyclname{$qual_1$}|sumname{$qual_1$}|<$rxlabl_1$>
{ ± {c_2*}op_2|cyclname{$qual_2$}|sumname{$qual_2$}|<$rxlabl_2$> + ...};

The IRR_OUTPUT command defines a specific IRR output to be generated during a CCTM simulation. It is constructed by specifying a linear combination of IRR operators, IRR global definitions, or IRRs for specified reactions. Each individual term in the combination must include either one of the five IRR operators just described (i.e., op_i), a cycle name, a reaction sum name, or a reaction label enclosed in "greater than" and "less than" signs. The

optional qualifiers ($qual_i$) for cyclename or reaction sum name can be either POSONLY or NEGONLY. With these qualifiers, the defined quantity is included as a term only when it is positive or negative, respectively. If the name is not qualified, the quantity is included regardless of sign. The numerical coefficients for each term (c_i) are assumed to be one unless they are explicitly included. The irrname that is supplied by the user will be assigned as the variable name in the IO/API IRR output file.

DESCRIPTION = 'description';

The description command is provided to allow the user to specify a long description of the output variable that will be included on the IO/API IRR output name. If a description is not specified for an IRR_OUTPUT variable, the irrname (or short name) will be used in the output file. If the description command is used, it should be located immediately following the IRR_OUTPUT command to which it applies.

Before describing how these commands are actually used, some additional comments are warranted. First, the specification of any particular IRR output might be accomplished in several different ways. For example, the net production of a species could be obtained using a CYCLE definition, a RXNSUM definition, a NET operator, or simply specifying the appropriate sum of IRRs directly in the IRR_OUTPUT command (i.e., via reaction labels). Although the user is free to choose any particular approach, some computational efficiencies may be achieved by using the CYCLE and RXNSUM definitions. The CCTM has been constructed to compute these quantities just once, and then use them whenever they are referenced in an output command. Conversely, operator quantities are recomputed every time they are referenced. Thus, it is more efficient to use the RXNSUM and CYCLE commands when they can be referenced several different times in IRR_OUTPUT commands. Second, the NETP and NETL operators are probably most useful for computing the production and loss of species families. When these operators are used, a reaction is not included in the sum if there is no net loss or production of a family member in the reaction. Thus, all reactions are eliminated from the computations when a member of a family is formed from another member of the same family and there is no net impact on the family concentration. Finally, the sign conventions employed in the CMAQ process analysis need to be defined. IRRs for individual chemical reactions are always positive. Since IRRs can be subtracted when computing CYCLE, RXNSUM, and NET quantities, the result can be either positive or negative. The production and loss operators always produce positive values, however, since individual IRRs are always summed in their computation.

To illustrate how these PACP commands are used to generate IRR output data, two examples are presented. The first illustrates how to capture IRRs for each reaction. The second demonstrates

how PACP commands are used to compute the special chemical parameters in Table 16-2 for the RADM2 chemical mechanism.

Exhibit 16-3 contains the PACP commands for the first example that corresponds to a full IRR analysis since IRRs will be calculated for each and every reaction. This option is invoked by the first command that specifies that the IRR analysis type is FULL . Since no OUTPUT_DOMAIN command is present, the IRR outputs will be generated for every cell in the modeling domain.

Exhibit 16-4 shows the PACP commands for the example IRR analysis that has been set up for the RADM2 chemical mechanism. In a PACP command file, all lines that start with an exclamation point (!) in the first column are comments. To facilitate the discussion below, comment lines have been used to block the IRR commands into special groups. The first four groups contain global commands or definitions. All blocks after the first four contain the IRR commands that generate the particular parameters listed in Table 16-2.

The commands in the first group simply define the type of IRR analysis and the domain for which the IRR outputs are to be generated. The second group includes family definitions. These commands are of the same form as described for IPRs. The remaining two groups of commands define chemical cycles and reaction sums that are subsequently referenced in IRR_OUTPUT commands. As noted above, the cycle commands give the net production or loss of a species by all chemical reactions. Several of the reaction sums that are defined here are also cycles in that they generate the net effect of a few reactions on the production or loss of a few particular species. Most of the others are used to define special quantities. For example, the defined RXNSUM newMO2 in Exhibit 16-4 corresponds to the production of new MO2, where new refers to an initiation reaction for the radical MO2. As is apparent from the IRR_OUTPUT commands in the subsequent blocks, the cycle and reaction-sum names are referenced fairly frequently.

All of the remaining blocks of commands in Exhibit 16-4 contain the commands for IRR outputs. Again, one IRR output is generated for each IRR_OUTPUT command, and the outputs that are produced correspond to the chemical parameters listed in Table 16-2. As indicated above, each output is generated by the defined linear combination of predefined cycles, reaction sums, special IRR operators, and/or specified reaction IRRs referenced by reaction label. It should be evident that these commands are mechanism specific and require analysis of the mechanism itself to formulate. Thus, this particular PACP command file would not be applicable to any mechanism other than the RADM2. It should also be apparent that other important chemical parameters could be formulated and generated in an analogous manner. In fact, this command file can be used as the starting point for adding to or modifying some of the selected chemical parameters.

As with IPR outputs, the CCTM will generate the IRR output data in a form comparable to the output concentration files. That is, the data are contained in standard Models-3 IO/API gridded data files. The IRR outputs are linear combinations of individual reaction throughput, and thus have the same units as the gas-phase species concentrations (i.e., ppms). However, it should be

remembered that these are throughputs calculated by integrating reaction rates over the output time interval, and not simply abundances at a particular time.

16.3 Conclusion

Process Analysis is a diagnostic method for evaluating the inner workings of a model. Although specific types of techniques have been performed and used in the past, new ways of examining and analyzing process data are likely to be developed and used in the future. As a consequence, the emphasis in the CMAQ implementation of process analysis has been placed on providing easy methods of extracting key process data from the CCTM simulations. The CMAQ implementation also provides tools to allow users to customize their analyses. These tools are designed to be easy to use and not require coding changes to the model.

As noted previously, a process analysis is set up by using the PACP before constructing and running a CCTM simulation. Both IPR and IRR data can be gathered during a simulation, but each are written to separate output files. To collect both sets of output during a single simulation requires that the PACP command file contain both the IPR commands and the IRR commands. Although the IPR and IRR examples have been presented separately, both sets of outputs can be produced with a single file containing both sets of commands. Recall, however, that the OUTPUT_DOMAIN applies to both the IPR outputs and the IRR outputs. Thus, IPR and IRR data cannot be generated for different parts of the domain in the same simulation.

The PACP program performs a substantial amount of error checking. The program will check for the proper syntax of the input commands and perform some logic checking. For example, it checks to make sure that all species referenced in IRR commands are gas-phase mechanism species and that the members of defined families are either all gas-phase species or all aerosol species. As is apparent from Exhibit 16-4, however, the inputs for a comprehensive IRR analysis can be fairly extensive. As a consequence, the PACP produces an output report that summarizes what IRR and IPR outputs are being requested. One of its major functions is to report on the effects of the special IRR operators that are used in the PACP command file. A user may wish to review this report before proceeding to run the CCTM to insure that the desired outputs will be generated. The reader is referred to the Models-3 User Manual (EPA, 1998) for an example output report.

Finally, the default configuration for the CCTM is to omit process analysis outputs entirely. Thus, no process analysis will be generated in this configuration. Any process analysis must be set up in the Science Manager of the Models-3 framework. The reader is referred to the Models-3 User Manual (EPA, 1998) for details on how this is done.

16.4 References

Jang, J. C., H. E. Jeffries, D. Byun, and J. E. Pleim, 1995a. "Sensitivity of Ozone to Model Grid Resolution - I. Application of High-resolution Regional Acid Deposition Model", *Atmospheric Environment*, Volume 29, No. 21, 3085-3100.

Jang, J. C., H. E. Jeffries, and S. Tonnesen, 1995b. "Sensitivity of Ozone to Model Grid Resolution - II. Detailed Process Analysis for Ozone Chemistry", *Atmospheric Environment*, Volume 29, No. 21, 3101-3114..

Jeffries, H. E., 1995. "Photochemical Air Pollution," Chapter 9 in *Composition, Chemistry, and Climate of the Atmosphere*, Ed. H. B. Singh, Van Nostand-Reinhold, New York, N.Y.

Jeffries, H.E., 1996. "Ozone Chemistry and Transport", presentation to the FACA subcommittee for Ozone, Particulate Matter and Regional Haze Implementation, March 21, Alexandria, Va.

Jeffries, H. E. and S. Tonnesen, 1994. "A Comparison of Two Photochemical Reaction Mechanisms Using Mass Balance and Process Analysis", *Atmospheric Environment*, Volume 28, No. 18, 2991-3003.

Pleim, J.E., 1990. *Development and Application of New Modeling Techniques for Mesoscale Atmospheric Chemistry*, Ph.D. Thesis, State University of new York at Albany, Albany, New York.

Seinfeld, J. H. and S. N. Pandis, 1998. *Atmospheric Chemistry and Physics, From Air Pollution to Climate Change*, John Wiley and Sons, New York, New York.

Tonnesen, S. and H. E. Jeffries, 1994. "Inhibition of Odd Oxygen Production in the Carbon Bond Four and Generic Reaction Set Mechanisms", *Atmospheric Environment*, Volume 28, No. 7, 1339-1349.

This chapter is taken from *Science Algorithms of the EPA Models-3 Community Multiscale Air Quality (CMAQ) Modeling System*, edited by D. W. Byun and J. K. S. Ching, 1999.

Table 16-1.
CCTM Processes and PACP Codes

PACP Code	Process Description
XADV	Advection in the E-W direction
YADV	Advection in the N-S direction
ZADV	Vertical advection
ADJC	Mass adjustment for advection
HDIF	Horizontal diffusion
VDIF	Vertical diffusion
EMIS	Emissions
DDEP	Dry deposition
CHEM	Chemistry
AERO	Aerosols
CLDS	Cloud processes and aqueous chemistry
PING	Plume-in-grid

Note: The following process codes can also be used in the PACP.

XYADV	Sum of XADV and YADV
XYZADV	Sum of XADV, YADV, and ZADV
TOTADV	Sum of XADV, YADV, ZADV, and ADJC
TOTDIF	Sum of HDIF and VDIF
TOTTRAN	Sum of XADV, YADV, ZADV, ADJC, HDIF and VDIF

Table 16-2.
Chemical Parameters Used in Default IRR Analysis

{1}	Production of Odd Oxygen (Ox)
{2}	Loss of Odd Oxygen (Ox)
{3}	Production of NOz from NOx
{4}	Production of NOx from NOz
{5}	Production of new OH from O1D
{6}	Production of new OH other than from O1D
{7}	Production of new HO2
{8}	Total production of HO2
{9}	Production of new RO2
{10}	Total Production of RO2
{11}	Loss of CO and CH4 by reaction with OH
{12}	Production of OH from HO2
{13}	Production of NO2 from HO2
{14}	Production of NO2 from RO2
{15}	Production of PAN and TPAN
{16}	Net Production of organic nitrates
{17}	Loss of VOCs by reaction with OH
{18}	Loss of OH by reaction with organics
{19}	Net Production or Loss of HNO3
{20}	Loss of HCHO by reaction with OH
{21}	Loss of isoprene by reaction with OH
{22}	Production of new HO2 from HCHO
{23}	Production of HO2 from PAN
{24}	Production of HO2 from RO2 and NO
{25}	Production of HO2 from RO2 reacting with RO2
{26}	Production of RO2 from OH
{27}	Production of HNO3 from NO2 reacting with OH
{28}	Production of new OH from H2O2
{29}	Production of new OH from organic peroxides
{30}	Production of OH from HONO
{31}	Termination of OH
{31}	Termination of HO2
{31}	Termination of HO2 by reaction with RO2
{34}	Termination of RO2
{35}	Termination of RO2 by reaction with HO2
{36}	Termination of RO2 by reaction with RO2
{37}	Loss of OH by reaction with daughter VOCs

Exhibit 16-1.
Example PACP Command File for IPR Analysis

```
{1} OUTPUT_DOMAIN = LOLEV[1] + HILEV[2];

{2} DEFINE FAMILY NOX    = NO + NO2;

{3} DEFINE FAMILY VOC    =  2.0*ETH + 2.9*HC3 + 4.8*HC5 + 7.9*HC8
                            + 2.0*OL2  + 3.8*OLT +
                            4.8*OLI + 5.0*ISO + 7.1*TOL + 8.9*XYL
                            + 1.0*HCHO + 2.4*ALD;

{4} IPR_OUTPUT NOX;

{5} IPR_OUTPUT VOC;

{6} IPR_OUTPUT O3 = TOTTRAN + CHEM + CLDS;

{7} IPR_OUTPUT ALL = VDIF;

{8} ENDPA;
```

Exhibit 16-2. Listing of the RADM2 Chemical Mechanism

```
REACTIONS [cm]

< P1> NO2          =      O3P     +    NO                 # 1.0  /<NO2_RADM88>;
< P2> O3           =      O1D                             # 1.0  /<O3O1D_RADM88>;
< P3> O3           =      O3P                             # 1.0  /<O3O3P_RADM88>;
< P4> HONO         =      HO      +    NO                 # 1.0  /<HONO_RADM88>;
< P5> HNO3         =      HO      +    NO2                # 1.0  /<HNO3_RADM88>;
< P6> HNO4         =      HO2     +    NO2                # 1.0  /<HNO4_RADM88>;
< P7> NO3          =      NO                              # 1.0  /<NO3NO_RADM88>;
< P8> NO3          =      NO2     +    O3P                # 1.0  /<NO3NO2_RADM88>;
< P9> H2O2         = 2.0* HO                              # 1.0  /<H2O2_RADM88>;
<P10> HCHO         =      CO                              # 1.0  /<HCHOmol_RADM88>;
<P11> HCHO         =      HO2     +    HO2     +    CO    # 1.0  /<HCHOrad_RADM88>;
<P12> ALD          =      MO2     +    HO2     +    CO    # 1.0  /<ALD_RADM88>;
<P13> OP1          =      HCHO    +    HO2     +    HO    # 1.0  /<MHP_RADM88>;
<P14> OP2          =      ALD     +    HO2     +    HO    # 1.0  /<HOP_RADM88>;
<P15> PAA          =      MO2     +    HO                 # 1.0  /<PAA_RADM88>;
<P16> KET          =      ACO3    +    ETHP               # 1.0  /<KETONE_RADM88>;
<P17> GLY          = 0.13*HCHO + 1.870*CO                  # 1.0  /<GLYform_RADM88>;
<P18> GLY          = 0.45*HCHO + 1.550*CO + 0.800*HO2      # 1.0  /<GLYmol_RADM88>;
<P19> MGLY         =      ACO3    +     HO2    +    CO    # 1.0  /<MGLY_RADM88>;
<P20> DCB          = 0.98*HO2 +  0.020*ACO3    +   TCO3   # 1.0  /<UDC_RADM88>;
<P21> ONIT         = 0.20*ALD +  0.800*KET + HO2 + NO2    # 1.0  /<ORGNIT_RADM88>;
<  1> O3P + O2 + M =      O3                              # 6.0E-34^-2.3;
<  2> O3P + NO2    =      NO                              # 6.5E-12   @ -120.0;
<  3> O1D + N2     =      O3P                             # 1.8E-11   @ -110.0;
<  4> O1D + O2     =      O3P                             # 3.2E-11   @ -70.0;
<  5> O1D + H2O    = 2.0* HO                              # 2.20E-10;
<  6> O3  +   NO   =      NO2                             # 2.00E-12  @1400.0;
<  7> O3  +   HO   =      HO2                             # 1.60E-12  @ 940.0;
<  8> O3  +   HO2  =      HO                              # 1.10E-14  @ 500.0;
<  9> HO2 +   NO   =      NO2     +    HO                 # 3.70E-12  @ -240.0;
< 10> HO2 +   NO2  =     HNO4                      # 1.8E-31^-3.2 &4.7E-12^-1.4;
< 11> HNO4         =      HO2     +    NO2           # 2.1E-27 @ -10900.0 *E< 10>;
< 12> HO2 + HO2    =      H2O2         %3 # 2.20E-13@-620.0  & 1.90E-33@-980.0;
< 13> HO2 + HO2 + H2O =   H2O2         %3 # 3.08E-34@-2820.0 & 2.66E-54@-3180.0;
< 14> H2O2 + HO       =   HO2                            # 3.300E-12  @ 200.0;
< 15> NO  +  HO     =      HONO            # 7.0E-31^-2.6 &1.5E-11^-0.5;
< 16> NO  +  NO  + O2 = 2.0*NO2                           # 3.300E-39 @ -530.0;
< 17> O3  +  NO2    =      NO3                            # 1.4000E-13 @ 2500.0;
< 18> NO3 +  NO     =    2.0*NO2                          # 1.7000E-11 @ -150.0;
< 19> NO3 +  NO2    =       NO      +    NO2               # 2.5000E-14  @ 1230.0;
< 20> NO3 +  HO2    =       HNO3                           # 2.5000E-12;
< 21> NO3 +  NO2    =       N2O5                  # 2.2E-30^-4.3 &1.5E-12^-0.5;
< 22> N2O5          =       NO2     +    NO3      # 1.10E-27 @ -11200.0 *E<21>;
< 23> N2O5 + H2O    =     2.0*HNO3                 # 2.00E-21;
< 24> HO  +  NO2    =       HNO3                   # 2.6E-30^-3.2 &2.4E-11^-1.3;
< 25> HO  +  HNO3   =       NO3       %2 #7.2E-15@-785&4.1E-16@-1440&1.9E-33@-725;
< 26> HO  +  HNO4   =       NO2                            # 1.3000E-12 @ -380.0;
< 27> HO  +  HO2    =                                      # 4.6000E-11  @ -230.0;
< 28> HO  +  SO2    = SULF  +  HO2 + SULAER      # 3.0E-31^-3.3 &1.5E-12^0.0;
< 29> CO  +  HO     =       HO2                 %1 #1.5000E-13;
< 30> HO            =       MO2     (X 300 SQUARED)        # 28.3^2   @ 1280.0;
< 31> ETH +  HO     =       ETHP    (X 300 SQUARED)        # 1.233E-12^2 @ 444.0;
< 32> HC3 +  HO     =  0.83*HC3P + 0.17*HO2 +  0.009*HCHO  + 0.075*ALD
                     + 0.025*KET                           # 1.59E-11  @ 540.0;
< 33> HC5 +  HO     =      HC5P  +  0.250*XO2               # 1.73E-11  @ 380.0;
< 34> HC8 +  HO     =      HC8P  +  0.750*XO2 + HC8AER      # 3.64E-11  @ 380.0;
< 35> OL2 +  HO     =      OL2P                             # 2.15E-12  @ -411.0;
< 36> OLT +  HO     =      OLTP                             # 5.32E-12  @ -504.0;
< 37> OLI +  HO     =      OLIP  + OLIAER                   # 1.07E-11  @ -549.0;
```

Exhibit 16-2. Listing of the RADM2 Chemical Mechanism

```
< 38> TOL +  HO     = 0.75*TOLP + 0.250*CSL + 0.250*HO2
                      + TOLAER                          # 2.10E-12  @ -322.0;
< 39> XYL +  HO     = 0.83*XYLP + 0.170*CSL + 0.170*HO2
                      + XYLAER                          # 1.89E-11  @ -116.0;
< 40> CSL +  HO     = 0.10*HO2  + 0.900*XO2 + 0.900*TCO3
                      + CSLAER                          # 4.00E-11;
<40a> CSL +  HO     =     CSL                           # 0.9*K<40>;
< 41> HCHO + HO     =     HO2      +     CO             # 9.0000E-12;
< 42> ALD +  HO     =     ACO3                          # 6.8700E-12 @ -256.0;
< 43> KET +  HO     =     KETP                          # 1.2000E-11 @ 745.0;
< 44> GLY +  HO     =     HO2  +  2.000*CO              # 1.1500E-11;
< 45> MGLY + HO     =     ACO3     +     CO             # 1.7000E-11;
< 46> DCB +  HO     =     TCO3                          # 2.8E-11;
< 47> OP1 +  HO     = 0.5*MO2 + 0.500*HCHO +0.500*HO    # 1.0000E-11;
< 48> OP2 +  HO     = 0.5*HC3P + 0.500*ALD + 0.500*HO   # 1.0000E-11;
< 49> PAA +  HO     =     ACO3                          # 1.0000E-11;
< 50> PAN +  HO     =     HCHO + NO3 + XO2 (x 300 sq)   # 6.1650E-13^2  @ 444.0;
< 51> ONIT + HO     =     HC3P     +     NO2            # 1.5500E-11  @ 540.0;
< 52> ISO +  HO     =     OLTP                          # 2.5500E-11  @ -409.0;
< 53> ACO3 + NO2    =     PAN                           # 2.8000E-12  @ -181.0;
< 54> PAN           =     ACO3     +     NO2            # 1.9500E+16  @ 13543.0;
< 55> TCO3 + NO2    =     TPAN                          # 4.7000E-12;
< 56> TPAN          =     TCO3     +     NO2            # 1.9500E+16  @ 13543.0;
< 57> MO2 +  NO     =     HCHO     +     HO2    +     NO2   # 4.2000E-12  @ -180.0;
< 58> HC3P + NO     = 0.75*ALD  +  0.25*KET + 0.09*HCHO + 0.036*ONIT
                    + 0.964*NO2 +  0.964*HO2            # 4.2000E-12  @ -180.0;
< 60> HC5P + NO     = 0.38*ALD + 0.69*KET + 0.08*ONIT
                    +  0.92*NO2 + 0.92*HO2              # 4.2000E-12  @ -180.0;
< 62> HC8P + NO     = 0.35*ALD + 1.06*KET + 0.04*HCHO
                    + 0.24*ONIT + 0.76*NO2 +   0.76*HO2 # 4.2000E-12  @ -180.0;
< 64> OL2P + NO     = 1.6*HCHO + HO2 + NO2 + 0.20*ALD   # 4.2000E-12  @ -180.0;
< 65> OLTP + NO     =     ALD  + HCHO + HO2 + NO2       # 4.2000E-12  @ -180.0;
< 66> OLIP + NO     =     HO2 + 1.45*ALD +  0.28*HCHO
                    +  0.1*KET   +      NO2             # 4.2000E-12  @ -180.0;
< 67> ACO3 + NO     =     MO2     +     NO2             # 4.2000E-12  @ -180.0;
< 68> TCO3 + NO     =     NO2 + 0.920*HO2 +  0.890*GLY  + 0.110*MGLY
                    + 0.050*ACO3 +  0.950*CO  +  2.000*XO2
                                                        # 4.2000E-12  @ -180.0;
< 69> TOLP + NO     =     NO2 +  HO2 +  0.17*MGLY
                    +   0.16*GLY +   0.70*DCB           # 4.2000E-12  @ -180.0;
< 70> XYLP + NO     =  NO2 + HO2 + .45*MGLY + .806*DCB  # 4.2000E-12  @ -180.0;
< 71> ETHP + NO     =  ALD  +   HO2 +    NO2            # 4.2000E-12  @ -180.0;
< 72> KETP + NO     =  MGLY +      NO2  +      HO2      # 4.2000E-12  @ -180.0;
< 73> OLN  + NO     =  HCHO    +    ALD +    2.0*NO2    # 4.2000E-12  @ -180.0;
< 74> HCHO + NO3    =  HO2     +     HNO3    +     CO    # 6.000E-13   @ 2058.0;
< 75> ALD +  NO3    =  ACO3    +     HNO3                # 1.400E-12   @ 1900.0;
< 76> GLY +  NO3    =  HNO3     +    HO2 +  2.000*CO     # 6.000E-13   @ 2058.0;
< 77> MGLY + NO3    =  HNO3     +    ACO3    +    CO     # 1.400E-12   @ 1900.0;
< 78> DCB +  NO3    =  HNO3     +    TCO3                # 1.400E-12   @ 1900.0;
< 79> CSL +  NO3    =  HNO3    +   XNO2  + 0.500*CSL
                    + 0.500*CSLAER                      # 2.200E-11;
< 80> OL2 +  NO3    =  OLN                              # 2.000E-12   @ 2923.0;
< 81> OLT +  NO3    =  OLN                              # 1.000E-11   @ 1895.0;
< 82> OLI +  NO3    =  OLN + OLIAER                     # 3.230E-11   @ 975.0;
< 83> ISO +  NO3    =  OLN                              # 5.810E-13;
< 84> OL2 +  O3     =  HCHO + 0.400*ORA1 + 0.420*CO
                    + 0.120*HO2                         # 1.200E-14   @ 2633.0;
< 85> OLT +  O3     = 0.53*HCHO + 0.500*ALD +  0.33*CO  + 0.20*ORA1
                    + 0.20*ORA2 + 0.23*HO2 +  0.22*MO2 +  0.10*HO
                                                        # 1.3200E-14  @ 2105.0;
< 86> OLI +  O3     = 0.18*HCHO + 0.72*ALD +  0.10*KET  + 0.23*CO  + 0.06*ORA1
```

Exhibit 16-2. Listing of the RADM2 Chemical Mechanism

```
                    + 0.29*ORA2 + 0.26*HO2 +  0.14*HO + 0.31*MO2
                    + OLIAER                                  # 7.2900E-15  @ 1136.0;
< 87> ISO +  O3     = 0.53*HCHO + 0.500*ALD +  0.33*CO  +  0.20*ORA1
                    + 0.20*ORA2 + 0.23*HO2 +  0.22*MO2 +  0.10*HO
                                                            # 1.230E-14  @ 2013.0;
< 88> HO2 +  MO2    =    OP1                                # 7.700E-14  @ -1300.0;
< 89> HO2 +  ETHP   =    OP2                                # 7.700E-14  @ -1300.0;
< 90> HO2 +  HC3P   =    OP2                                # 7.700E-14  @ -1300.0;
< 91> HO2 +  HC5P   =    OP2                                # 7.700E-14  @ -1300.0;
< 92> HO2 +  HC8P   =    OP2                                # 7.700E-14  @ -1300.0;
< 93> HO2 +  OL2P   =    OP2                                # 7.700E-14  @ -1300.0;
< 94> HO2 +  OLTP   =    OP2                                # 7.700E-14  @ -1300.0;
< 95> HO2 +  OLIP   =    OP2                                # 7.700E-14  @ -1300.0;
< 96> HO2 +  KETP   =    OP2                                # 7.700E-14  @ -1300.0;
< 97> HO2 +  ACO3   =    PAA                                # 7.700E-14  @ -1300.0;
< 98> HO2 +  TOLP   =    OP2                                # 7.700E-14  @ -1300.0;
< 99> HO2 +  XYLP   =    OP2                                # 7.700E-14  @ -1300.0;
<100> HO2 +  TCO3   =    OP2                                # 7.700E-14  @ -1300.0;
<101> HO2 +  OLN    =    ONIT                               # 7.700E-14  @ -1300.0;
<102> MO2 +  MO2    = 1.5*HCHO   +    HO2                   # 1.90E-13   @ -220.0;
<103> MO2 +  ETHP   = 0.75*HCHO   +    HO2 +  0.75*ALD      # 1.40E-13   @ -220.0;
<104> MO2 +  HC3P   = 0.84*HCHO + 0.770*ALD +  0.260*KET
                    + 1.000*HO2                             # 4.20E-14 @ -220.0;
<105> MO2 +  HC5P   = 0.77*HCHO + 0.41*ALD +  0.75*KET
                    + 1.000*HO2                             # 3.40E-14  @ -220.0;
<106> MO2 +  HC8P   = 0.80*HCHO + 0.46*ALD +  1.39*KET
                    + 1.000*HO2                             # 2.90E-14  @ -220.0;
<107> MO2 +  OL2P   = 1.55*HCHO + 0.350*ALD +  HO2          # 1.40E-13   @ -220.0;
<108> MO2 +  OLTP   = 1.25*HCHO + 0.750*ALD +  HO2          # 1.40E-13   @ -220.0;
<109> MO2 +  OLIP   = 0.89*HCHO + 0.725*ALD +  HO2
                    + 0.55*KET                              # 1.70E-14  @ -220.0;
<110> MO2 +  KETP   = 0.75*HCHO + 0.750*MGLY + HO2          # 1.70E-14  @ -220.0;
<111> MO2 +  ACO3   =  HCHO + 0.5*HO2 +  0.5*MO2
                    + 0.50*ORA2                             # 9.60E-13  @ -220.0;
<112> MO2 +  TOLP   =  HCHO + 0.17*MGLY + 0.16*GLY
                    +  0.70*DCB  +  2.0*HO2                 # 1.70E-14  @ -220.0;
<113> MO2 +  XYLP   =  HCHO + 0.45*MGLY + 0.806*DCB
                    + 2.000*HO2                             # 1.70E-14  @ -220.0;
<114> MO2 +  TCO3   = .50*HCHO + 0.445*GLY +  0.055*MGLY
                    + 0.50*ORA2 + 0.025*ACO3 + 0.460*HO2
                    +  0.475*CO  +  XO2                     # 9.60E-13  @ -220.0;
<138> MO2 +  OLN    =  1.75*HCHO + 0.50*HO2 + ALD + NO2     # 1.70E-14  @ -220.0;
<115> ETHP + ACO3   =  ALD + 0.5*HO2 +  0.5*MO2
                    + 0.5* ORA2                             # 3.40E-13  @ -220.0;
<116> HC3P + ACO3   =  .77*ALD + 0.26* KET +  0.5*HO2
                    + 0.50*MO2 +  0.5*ORA2                  # 1.00E-13  @ -220.0;
<117> HC5P + ACO3   = 0.41*ALD + 0.75*KET +  0.5*HO2
                    + 0.50*MO2 +  0.5*ORA2                  # 8.40E-14  @ -220.0;
<118> HC8P + ACO3   = 0.46*ALD + 1.39*KET +  0.5*HO2
                    + 0.50*MO2 +  0.5*ORA2                  # 7.20E-14  @ -220.0;
<119> OL2P + ACO3   = 0.80*HCHO + 0.6*ALD +  0.5*HO2
                    + 0.5*MO2 +  0.5*ORA2                   # 3.40E-13  @ -220.0;
<120> OLTP + ACO3   =  ALD + 0.5*HCHO + 0.5*HO2
                    + 0.5*MO2 +  0.5*ORA2                   # 3.40E-13  @ -220.0;
<121> OLIP + ACO3   = 0.725*ALD + 0.55*KET +  0.14*HCHO
                    + 0.5*HO2 +  0.50*MO2  + 0.5*ORA2       # 4.20E-14   @ -220.0;
<122> KETP + ACO3   =  MGLY + 0.5*HO2 +  0.5*MO2
                    + 0.5*ORA2                              # 4.20E-14   @ -220.0;
<123> ACO3 + ACO3   =  2.0*MO2                              # 1.19E-12  @ -220.0;
<124> ACO3 + TOLP   =  MO2 + 0.170*MGLY + 0.16*GLY
                    +  0.70*DCB  +    HO2                   # 4.20E-14   @ -220.0;
```

Exhibit 16-2. Listing of the RADM2 Chemical Mechanism

```
<125> ACO3 + XYLP =  MO2 + 0.45*MGLY + 0.806*DCB
                  +   HO2                          # 4.20E-14   @ -220.0;
<126> ACO3 + TCO3 =  MO2 + 0.92*HO2 +  0.89*GLY
                  +  0.11*MGLY + 0.05*ACO3 + 0.95*CO
                  + 2.0*XO2                        # 1.19E-12  @ -220.0;
<139> ACO3 + OLN  =  HCHO +  ALD +  0.5*ORA2
                  +  NO2 +  0.5* MO2               # 4.20E-14   @ -220.0;
<140> OLN +  OLN  = 2.0*HCHO + 2.0*ALD +  2.0*NO2  # 3.60E-16  @ -220.0;

<127> XO2 +  HO2  =    OP2                         # 7.70E-14  @ -1300.0;
<128> XO2 +  MO2  =    HCHO   +     HO2            # 1.70E-14  @ -220.0;
<129> XO2 +  ACO3 =    MO2                         # 4.20E-14   @ -220.0;
<130> XO2 +  XO2  =                                # 3.60E-16  @ -220.0;
<131> XO2 +  NO   =    NO2                         # 4.2000E-12  @ -180.0;
<132> XNO2 + NO2  =    ONIT                        # 4.2000E-12  @ -180.0;
<133> XNO2 + HO2  =    OP2                         # 7.70E-14  @ -1300.0;
<134> XNO2 + MO2  =    HCHO   +     HO2            # 1.70E-14  @ -220.0;
<135> XNO2 + ACO3 =    MO2                         # 4.20E-14   @ -220.0;
<136> XNO2 + XNO2 =                                # 3.60E-16  @ -220.0;
<AE1> TERP + HO    = TERPAER + HO                  # 1.0*K<37>;
<AE1> TERP + NO3   = TERPAER + NO3                 # 1.0*K<82>;
<AE1> TERP + O3    = TERPAER + O3                  # 1.0*K<86>;

endmech
```

Exhibit 16-3. Example PACP Command File for a Full IRR Analysis

```
IRR_TYPE = FULL;

ENDPA;
```

Exhibit 16-4. Example PACP Commands for a Partial IRR Analysis

```
!*************************************************************************
!  Example PACP Command File illustrating Partial IRR Analysis
!*************************************************************************


!=========================================================================
! IRR type and domain commands
!=========================================================================

IRRTYPE = PARTIAL;

OUTPUT_DOMAIN = LOLEV[1] + HILEV[2];


!=========================================================================
! Family Definitions
!=========================================================================
DEFINE FAMILY OX     = O3 + NO2 + 2*NO3 + O3P +O1D + PAN + HNO4 + 3*N2O5 +
                       TPAN + OLN + HNO3 + ONIT;
DEFINE FAMILY NOZ    = PAN + TPAN + HONO + HNO4 + NO3 + N2O5 + ONIT +
                       OLN + HNO3;
DEFINE FAMILY NOX    = NO + NO2;
DEFINE FAMILY VOCA   = OL2 + OLI + OLT + ISO;
DEFINE FAMILY RO2    = MO2 + ETHP + HC3P + HC5P + HC8P + OL2P +
                       OLTP + OLIP + TOLP + XYLP + ACO3 + KETP +
                       TCO3 + XO2 + XNO2;
DEFINE FAMILY VOC    = {CH4 +} CO + ETH + HC3 + HC5 + HC8 + OL2 + OLT +
                       OLI + ISO + TOL + CSL + XYL + HCHO + ALD + KET +
                       GLY + MGLY + DCB;
DEFINE FAMILY dauHC = CSL + KET + GLY + MGLY + DCB + OP1 + OP2 +
                       PAA + PAN + ONIT;


!=========================================================================
! Cycle Definitions
!=========================================================================
DEFINE CYCLE PANcyc  = PAN;
DEFINE CYCLE TPANcyc = TPAN;
DEFINE CYCLE HONOcyc = HONO;
DEFINE CYCLE HNO4cyc = HNO4;


!=========================================================================
! Reaction Sum Definitions
!=========================================================================
DEFINE RXNSUM NO3cyc        = < 17> - < P7> - < P8> - < 18> - < 19>;
DEFINE RXNSUM N2O5cyc       = < 21> - < 22>;
DEFINE RXNSUM H2O2_OHcyc    = < P9> - < 12> - < 13>;
DEFINE RXNSUM HNO3_OHcyc    = < P5> - < 24>;
DEFINE RXNSUM OP1_OHcyc     = <P13> - < 88>;
DEFINE RXNSUM OP2_OHcyc     = <P14> - < 89> - < 90> - < 91> - < 92> -
                              < 93> - < 94> - < 95> - < 96> - < 97> -
                              < 98> - < 99> - <100>{ - <101>};
DEFINE RXNSUM PAA_OHcyc     = <P15> - < 97>;
DEFINE RXNSUM HNO4_HO2cyc   = < P6> + < 11> - < 10>;
DEFINE RXNSUM OP2_HO2cyc    = <P14> - < 89> - < 90> - < 91> - < 92> -
                              < 93> - < 94> - < 95> - < 96> - < 97> -
                              < 98> - < 99> - <100> {- <101>} - <127> -
                              <133>;
```

Exhibit 16-4. Example PACP Commands for a Partial IRR Analysis

```
DEFINE RXNSUM HOXcyc        = <  7> - <  8>;
DEFINE RXNSUM newMO2        = <P12> + 0.22*< 85> + 0.31*< 86> + 0.22*< 87>;
DEFINE RXNSUM newACO3       = <P16> + <P19> + 0.02*<P20> + < 77>;
DEFINE RXNSUM newETHP       = <P16>;
DEFINE RXNSUM newTCO3       = <P20> + < 78>;
DEFINE RXNSUM PAN_ACO3cyc   = < 54> - < 53>;
DEFINE RXNSUM TPAN_TCO3cyc  = < 56> - < 55>;
!DEFINE RXNSUM propRO2_NO    = <67> + 4.05*<68> + 1.5*<126>;

!=====================================================================
! IRR_OUTPUT 1: OX Production
!=====================================================================
IRR_OUTPUT OXprod = NETP[OX];

DESCRIPTION = 'OX Production';

!=====================================================================
! IRR_OUTPUT 2: OX Loss
!=====================================================================
IRR_OUTPUT OXloss =  NETL[OX];

DESCRIPTION = 'OX Loss';


!=====================================================================
! IRR_OUTPUT 3: Production of NOZ from NOX
!=====================================================================
IRR_OUTPUT NOZfromNOX =  PANcyc[POSONLY] +
                        TPANcyc[POSONLY] +
                        HONOcyc[POSONLY] +
                        HNO4cyc[POSONLY] +
                         NO3cyc[POSONLY] +
                        N2O5cyc[POSONLY] +
                              < 24> + 0.036*< 58> + 0.08*< 60> +
                        0.024*< 62> +       <132>;
DESCRIPTION = 'NOZ produced from NOX';


!=====================================================================
! IRR_OUTPUT 4: Production of NOX from NOZ
!=====================================================================
IRR_OUTPUT NOXfromNOZ =  PANcyc[NEGONLY] +
                        TPANcyc[NEGONLY] +
                        HONOcyc[NEGONLY] +
                        HNO4cyc[NEGONLY] +
                         NO3cyc[NEGONLY] +
                        N2O5cyc[NEGONLY] +
                             < P5> +       <P21> +       < 51> +
                             < 73> +       <138> +       <139> +
                         2.0*<140>;

DESCRIPTION = 'NOX produced from NOZ';


!=====================================================================
! IRR_OUTPUT 5: Production of new OH from O1D
!=====================================================================
IRR_OUTPUT OHfromO1D = PROD [HO] FROM [O1D];
```

Exhibit 16-4. Example PACP Commands for a Partial IRR Analysis

```
DESCRIPTION = 'OH produced from O1D';


!=====================================================================
! IRR_OUTPUT 6: Production of new OH other than from O1D
!=====================================================================
IRR_OUTPUT newOH =   0.1*< 85> +  0.14*< 86> +   0.1*< 87> +
                     2*H2O2_OHcyc[POSONLY]  +
                     HNO3_OHcyc[POSONLY]  +
                        HONOcyc[NEGONLY]  +
                      OP1_OHcyc[POSONLY]  +
                      OP2_OHcyc[POSONLY]  +
                      PAA_OHcyc[POSONLY];

DESCRIPTION = 'new OH';


!=====================================================================
! IRR_OUTPUT 7: Production of new HO2
!=====================================================================
IRR_OUTPUT newHO2 =      2.0*<P11> +       <P12> +   0.8*<P18> +
                             <P19> +  0.98*<P20> +       <P21> +
                             < 74> +       < 76> +  0.12*< 84> +
                         0.23*< 85> +  0.26*< 86> +  0.23*< 87> +
                         OP1_OHcyc[POSONLY] +
                         OP2_HO2cyc[POSONLY] +
                         HNO4_HO2cyc[POSONLY];
DESCRIPTION = 'new HO2';


!=====================================================================
! IRR_OUTPUT 8: Total Production of HO2
!=====================================================================
IRR_OUTPUT totalHO2 =    2.0*<P11> +       <P12> +   0.8*<P18> +
                             <P19> +  0.98*<P20> +       <P21> +
                             < 74> +       < 76> +  0.12*< 84> +
   {HO2new}              0.23*< 85> +  0.26*< 86> +  0.23*< 87> +
                           OP1_OHcyc[POSONLY] +
                          OP2_HO2cyc[POSONLY] +
                         HNO4_HO2cyc[POSONLY] +

  {HO2propbyOH}         PROD[HO2] FROM  [HO] AND [VOC] +

  {HO2viaRO2_NO}        PROD[HO2] FROM  [NO] AND [RO2] +

  {HO2byRO2_RO2}        PROD[HO2] FROM [RO2] AND [RO2] +

  {otherOH}             HOXcyc[POSONLY];

DESCRIPTION = 'total HO2';


!=====================================================================
! IRR_OUTPUT 9: Production of new RO2
!=====================================================================
IRR_OUTPUT newRO2 =   newMO2  +
                      newACO3 +
                      newETHP +
                      newTCO3 +
```

Exhibit 16-4. Example PACP Commands for a Partial IRR Analysis

```
                    PAN_ACO3cyc[POSONLY] +
                    TPAN_TCO3cyc[POSONLY];

DESCRIPTION = 'new RO2';

!=================================================================
! IRR_OUTPUT 10: Total Production of RO2
!=================================================================
IRR_OUTPUT TotalRO2 = newMO2  +
                      newACO3 +
{newRO2}              newETHP +
                      newTCO3 +
                      PAN_ACO3cyc[POSONLY] +
                      TPAN_TCO3cyc[POSONLY] +

{prcpRO2_OH}          PROD[RO2] FROM [HO] AND [VOC] +
                             < 30> +   0.5*< 47> +   0.5*<48> +
                             < 50> +       < 51> +

{propRO2_NO}          PROD[RO2] FROM [NO];

DESCRIPTION = 'Total RO2';

!=================================================================
! IRR_OUTPUT 11: Loss of CO & CH4 by reaction with OH
!=================================================================
IRR_OUTPUT Loss_CO_CH4 =     < 30> +
                        LOSS [CO];

DESCRIPTION = 'Loss of CO & CH4';

!=================================================================
! IRR_OUTPUT 12: Production of OH from HO2
!=================================================================
IRR_OUTPUT HO2toOH =  HOXcyc[NEGONLY] +
                      <9> +
                      2.0*H2O2_OHcyc[POSONLY];

DESCRIPTION = 'HO2 to OH';

!=================================================================
! IRR_OUTPUT 13: Production of NO2 from HO2
!=================================================================
IRR_OUTPUT NO2fromHO2 = <  9>;

DESCRIPTION = 'NO2 FROM HO2';

!=================================================================
! IRR_OUTPUT 14: Production of NO2 from RO2
!=================================================================
IRR_OUTPUT NO2fromRO2 =        < 57> + 0.964*< 58> + 0.92*< 60> +
                         0.76*< 62> +       < 64> +      < 65> +
                               < 66> +       < 67> +      < 68> +
                               < 69> +       < 70> +      < 71> +
                               < 72> +       < 73> +      <131>;
```

Exhibit 16-4. Example PACP Commands for a Partial IRR Analysis

```
DESCRIPTION = 'NO2 FROM HO2';


!=====================================================================
! IRR_OUTPUT 15: Production of PAN and TPAN
!=====================================================================
IRR_OUTPUT prodPAN_TPAN = PANcyc + TPANcyc;

DESCRIPTION = 'Production of PAN and TPAN';


!=====================================================================
! IRR_OUTPUT 16: Net Production of organic nitrates
!=====================================================================
IRR_OUTPUT netONIT = NET[ONIT];

DESCRIPTION = 'Net production of ONIT';

!=====================================================================
! IRR_OUTPUT 17: Loss of VOCs by reaction with OH
!=====================================================================
IRR_OUTPUT lossOH_HC = LOSS[VOC] AND [HO]     +
                       < 30> + < 47> + < 48> +
                       < 49> + < 50> + < 51>;

DESCRIPTION = 'Loss of HC plus OH';

!=====================================================================
! IRR_OUTPUT 18: Loss of OH by reaction with inorganics
!=====================================================================
IRR_OUTPUT lossOH_INORG = <  7> + < 14> + < 15> +
                          < 24> + < 25> + < 26> +
                          < 27>;

DESCRIPTION = 'Loss of OH with iorganics';


!=====================================================================
! IRR_OUTPUT 19: Net production or loss of HNO3
!=====================================================================
IRR_OUTPUT netHNO3 = NET[HNO3];

DESCRIPTION = 'Net change in HNO3';





!=====================================================================
! IRR_OUTPUT 20: Loss of HCHO by reaction with OH
!=====================================================================
IRR_OUTPUT lossHCHO_OH = LOSS[HCHO] AND [HO];

DESCRIPTION = 'Reaction OH HCHO with OH';


!=====================================================================
! IRR_OUTPUT 21: Loss of isoprene by reaction with OH
!=====================================================================
```

Exhibit 16-4. Example PACP Commands for a Partial IRR Analysis

```
IRR_OUTPUT lossISO_OH = LOSS[ISO] AND [HO];

DESCRIPTION = 'Reaction of ISO with OH';

!=================================================================
! IRR_OUTPUT 22:  Production of new HO2 from HCHO
!=================================================================
IRR_OUTPUT newHO2fromHCHO = PROD[HO2] FROM [HCHO] AND [hv];

DESCRIPTION = 'New HO2 from HCHO';


!=================================================================
! IRR_OUTPUT 23: Production of HO2 from PAN
!=================================================================
IRR_OUTPUT HO2fromPAN = PAN_ACO3cyc[POSONLY];

DESCRIPTION = 'HO2 from PAN';

!=================================================================
! IRR_OUTPUT 24: Production of HO2 from RO2 and NO
!=================================================================
IRR_OUTPUT HO2fromRO2_NO = PROD[HO2] FROM [NO] AND [RO2];

DESCRIPTION = 'HO2 from RO2 and NO';

!=================================================================
! IRR_OUTPUT 25: Production of HO2 from RO2 and RO2
!=================================================================
IRR_OUTPUT HO2fromRO2_RO2 = PROD[HO2] FROM [RO2] AND [RO2];

DESCRIPTION = 'HO2 from RO2 and RO2';

!=================================================================
! IRR_OUTPUT 26: Production of RO2 from OH
!=================================================================
IRR_OUTPUT RO2fromOH = PROD[RO2] FROM [HO];

DESCRIPTION = 'RO2 from OH';

!=================================================================
! IRR_OUTPUT 27: Production of HNO3 from OH + NO2
!=================================================================
IRR_OUTPUT HNO3fromOH_NO2 = < 24>;

DESCRIPTION = 'HNO3 from OH + NO2';

!=================================================================
! IRR_OUTPUT 28: Production of new OH from H2O2
!=================================================================
IRR_OUTPUT newOH_H2O2 = 2*H2O2_OHcyc[POSONLY];

DESCRIPTION = 'new OH from H2O2';
```

Exhibit 16-4. Example PACP Commands for a Partial IRR Analysis

```
!=====================================================================
! IRR_OUTPUT 29: Production of new OH from organic peroxides
!=====================================================================
IRR_OUTPUT newOH_OP1 =  OP1_OHcyc[POSONLY] +
                        OP2_OHcyc[POSONLY] +
                        PAA_OHcyc[POSONLY];

DESCRIPTION = 'new OH from OP1 OP2 PAA';


!=====================================================================
! IRR_OUTPUT 30: Production of OH from HONO
!=====================================================================
IRR_OUTPUT newOHfromHONO = HONOcyc[NEGONLY];

DESCRIPTION = 'new OH from HONO';


!=====================================================================
! IRR_OUTPUT 31: OH Termination
!=====================================================================
IRR_OUTPUT OHterm = < 25> + <26> + <27> + < 50> +
                    HNO3_OHcyc[NEGONLY] +
                       HONOcyc[POSONLY];

DESCRIPTION = 'OH Termination';

!=====================================================================
! IRR_OUTPUT 32: HO2 Termination
!=====================================================================
IRR_OUTPUT HO2term =     < 20> + < 27> + <101> +
                    2 *  H2O2_OHcyc[NEGONLY] +
                         HNO4_HO2cyc[NEGONLY];

DESCRIPTION = 'HO2 Termination';









!=====================================================================
! IRR_OUTPUT 33: Termination of HO2 by reaction with RO2
!=====================================================================
IRR_OUTPUT termHO2_RO2 =   OP1_OHcyc[NEGONLY] +
                          OP2_HO2cyc[NEGONLY] +
                           PAA_OHcyc[NEGONLY];

DESCRIPTION = 'HO2 term with RO2';

!=====================================================================
! IRR_OUTPUT 34: RO2 Termination
!=====================================================================
IRR_OUTPUT termRO2 = .036*<58> + .08*<60> + .24*<62> + .03*<68> +
                     PAN_ACO3cyc[NEGONLY] +
                         TPANcyc[POSONLY];
```

Exhibit 16-4. Example PACP Commands for a Partial IRR Analysis

```
DESCRIPTION = 'RO2 Termination';


!=====================================================================
! IRR_OUTPUT 35: Termination of RO2 by reaction with with HO2
!=====================================================================
IRR_OUTPUT termRO2_HO2 =  OP1_OHcyc[NEGONLY] +
                          OP2_OHcyc[NEGONLY] +
                          PAA_OHcyc[NEGONLY];

DESCRIPTION = 'RO2 Termination with HO2';

!=====================================================================
! IRR_OUTPUT 36: Termination of RO2 by reaction with RO2
!=====================================================================
IRR_OUTPUT termRO2_RO2 =    <102> + <103> + <104> + <105> + <106> +
                            <107> + <108> + <109> + <110> + <111> +
                     1.515 * <114> + <115> + <116> + <117> +
                            <118> + <119> + <120> + <121> + <122> +
                     1.030 * <126> + 0.500 * <138> +
                     0.500 * <139>;

DESCRIPTION = 'RO2 Termination with RO2';


!=====================================================================
! IRR_OUTPUTs 37: Loss of OH by reaction with daughter VOCs
!=====================================================================
IRR_OUTPUT dauHC_OH = LOSS [HO] AND [dauHC];

DESCRIPTION = 'OH + daughter HC';


ENDPA;
```

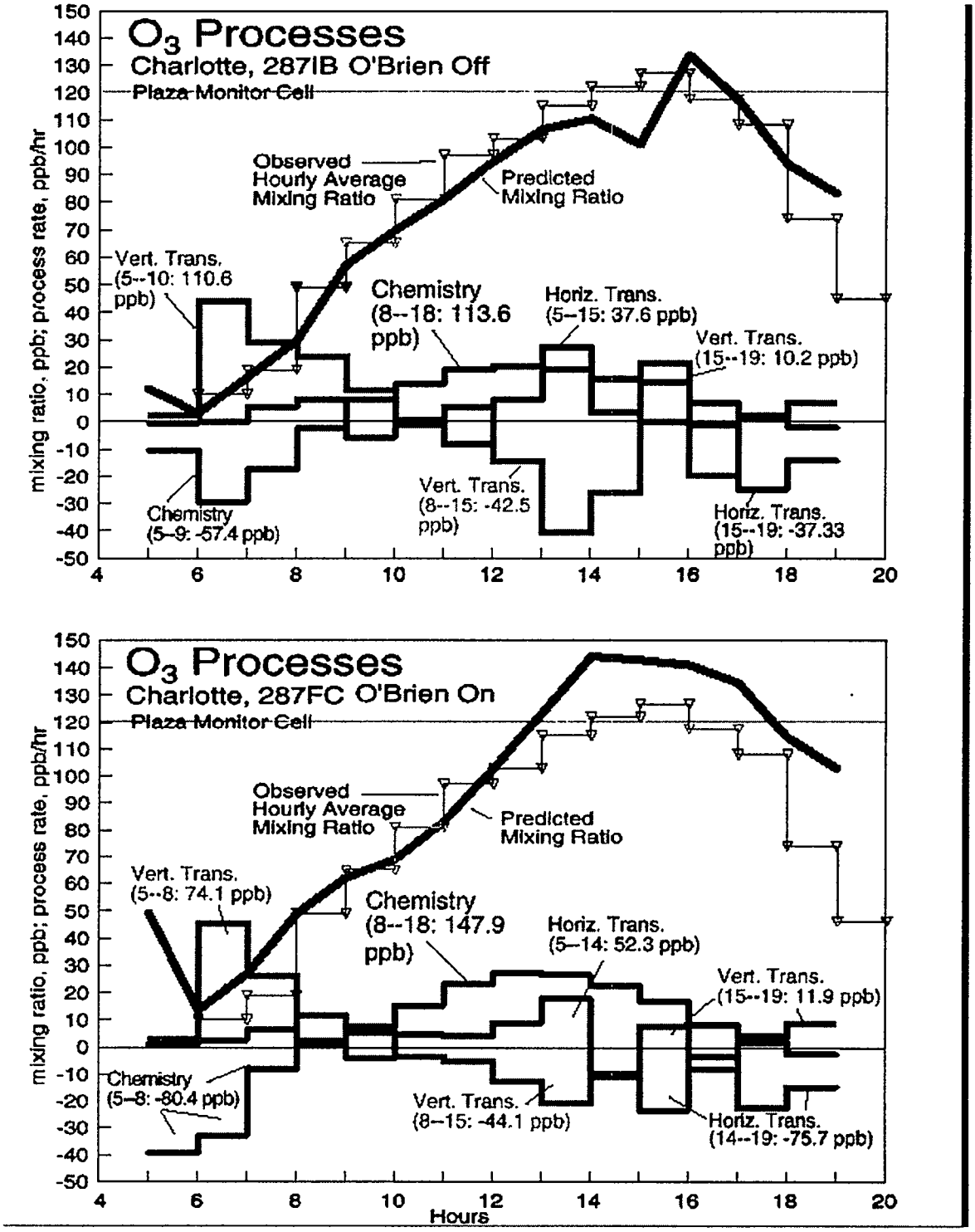

Figure 16-1. Example process analyses showing contributions of individual processes to model predicted concentrations (Source: Jeffries, 1996).

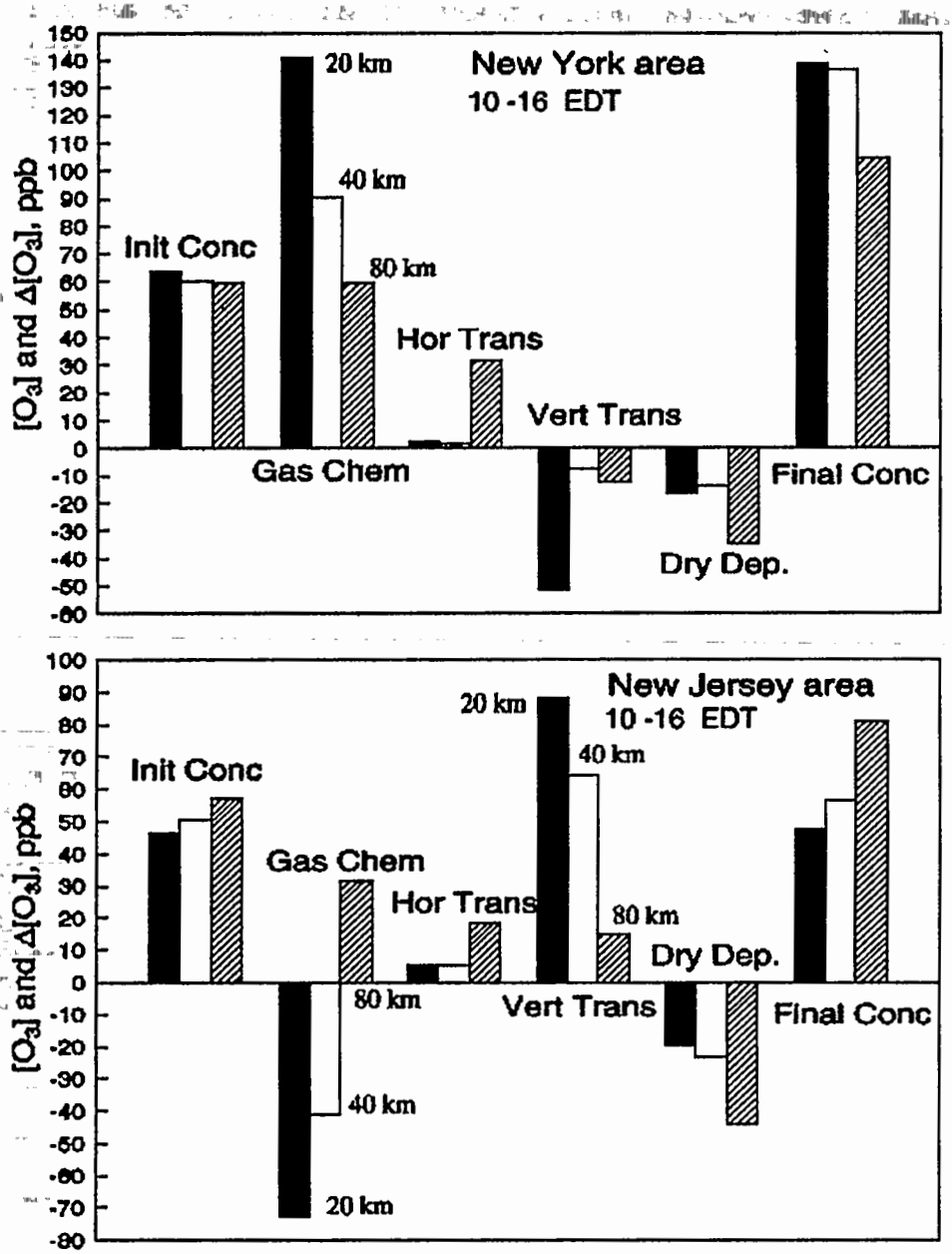

Figure 16-2. Example Process Analyses showing model predicted concentrations and process contributions for different model configurations (Source: Jeffries, 1996).

Photochemical Air Pollution

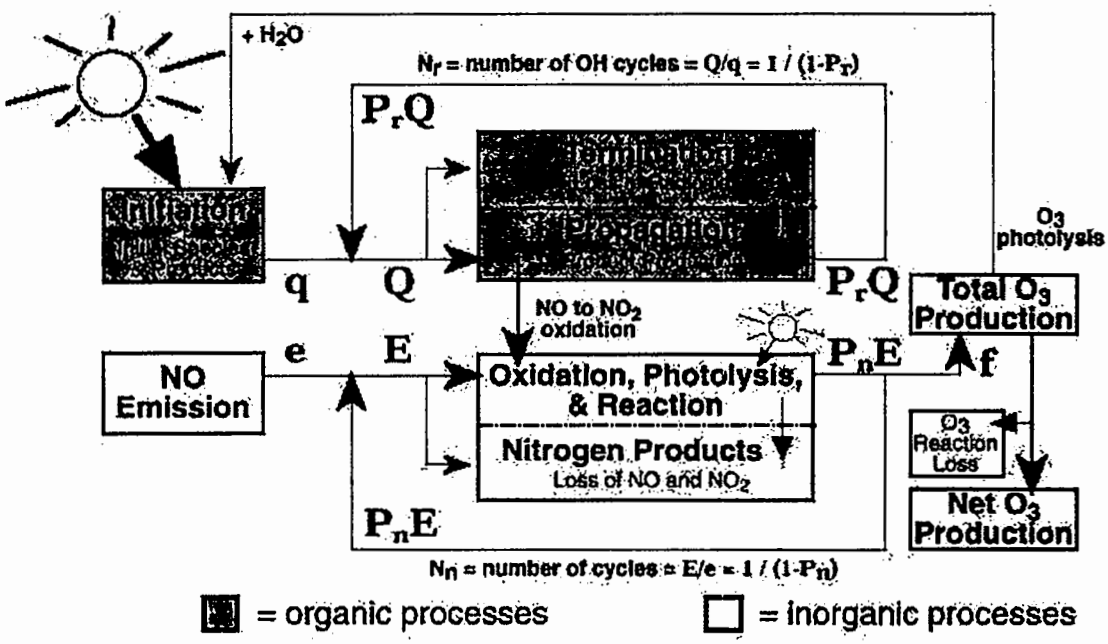

Figure 16-3a. Schematic of OH reaction with NO oxidation cycles (Source: Jeffries, 1996).

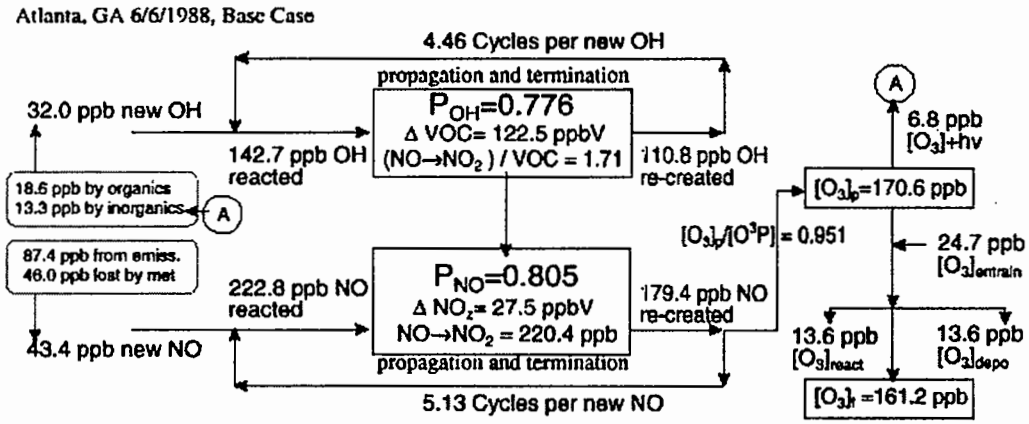

Figure 16-3b. Example photochemical cycle throughputs derived from integrated reaction rates (Source: Jeffries, 1995).

EPA/600/R-99/030

Chapter 17

AN AGGREGATION AND EPISODE SELECTION SCHEME DESIGNED TO SUPPORT MODELS-3 CMAQ

Richard D. Cohn
Analytical Sciences, Inc.
Durham, NC 27713

Brian K. Eder* and Sharon K. LeDuc**
Atmospheric Modeling Division
National Exposure Research Laboratory
Research Triangle Park, NC 27711

ABSTRACT

In support of studies mandated by the 1990 Clean Air Act Amendments, the Models-3 Community Multiscale Air Quality (CMAQ) model can be used to estimate pollutant concentrations and deposition associated with specified emission levels. Assessment studies require CMAQ-based distributional estimates of ozone, acidic deposition, $PM_{2.5}$, and visibility on seasonal and annual time frames. Because it is not financially feasible to execute CMAQ over such extended time periods, CMAQ must be executed for a finite number of episodes under a variety of meteorological classes. A statistical procedure called aggregation, must then be applied to the CMAQ outputs to derive seasonal and annual estimates.

The objective of this research is to develop an aggregation approach and set of episodes that would support model-based distributional estimates (over the continental domain) of air quality parameters. The approach utilized cluster analysis and the 700 mb *u* and *v* wind field components over the time period 1984-1992 to define homogeneous meteorological clusters. A total of 20 clusters (five per season) were identified by the technique. A stratified sample of 40 events was selected from the clusters, using a systematic sampling technique.

This stratified sample is then evaluated through a comparison of aggregated estimates of the mean extinction coefficients (b_{ext}) to the actual mean b_{ext} observed at 201 stations nationwide for a nine year period (1984-1992). The b_{ext}, a measure of visibility, was selected for use in the evaluation for two reasons. First, of all of the air quality parameters simulated by CMAQ, this visibility parameter provides one of the most spatially and temporally comprehensive data sets available, and second, the b_{ext} can serve as a surrogate for $PM_{2.5}$ for which little data exists. Results from the evaluation revealed a high level of agreement ($r^2 = 0.988$) indicating that the aggregation and episode selection scheme was indeed representative.

---

*On assignment from the National Oceanic and Atmospheric Administration, U.S. Department of Commerce. Corresponding author address: Brian Eder, MD-80, Research Triangle Park, NC 27711. E-mail: eder@hpcc.epa.gov

**On assignment from the National Oceanic and Atmospheric Administration, U.S. Department of Commerce.

17.0 AN AGGREGATION AND EPISODE SELECTION SCHEME DESIGNED TO SUPPORT MODELS-3 CMAQ

17.1 Introduction

This chapter describes the development of an aggregation and episode selection scheme to support the derivation of annual and seasonal estimates of air quality parameters in Models-3 CMAQ. Relevant background information regarding this activity, as well as a precise statement of the present objectives, is provided in this section. Section 17.2 summarizes the important elements of the approach and the overall strategy, including the rationale behind the methods and the limitations associated with them. Details of the development of an aggregation and episode selection are provided in sections 17.3, 17.4, and 17.5. Section 17.6 contains an example application and evaluation of the methodology using one particular air quality parameter (b_{ext}), and section 17.7 provides a summary and discussion.

17.1.1 Background

In support of studies mandated by the 1990 Clean Air Act Amendments, the Models-3 Community Multiscale Air Quality (CMAQ) model is used by EPA Program Offices to estimate deposition and air concentrations associated with specified levels of emissions. Assessment studies and effects models require CMAQ-based distributional estimates (such as annual and seasonal averages) of ozone, acidic deposition, and measures related to visibility. Such estimates would ideally be obtained by using CMAQ to simulate atmospheric chemical processes associated with meteorological conditions occurring on a daily basis over several years. However, for logistical and cost reasons it is not currently feasible to execute CMAQ over an extended time period such as a full year. Therefore, in practice CMAQ must be executed for a finite number of episodes or "events," which are selected to represent a variety of meteorological classes. A statistical procedure called aggregation, must then be applied to the outputs from CMAQ to derive the required annual- and seasonal-average estimates from this finite number of events. The objective of the research described in this chapter is to develop such an aggregation approach and evaluate its effectiveness using the b_{ext}.

The basic problem of developing representative meteorological categories has been explored by other researchers for a variety of purposes, including Fernau and Samson (1990a,b); Davis and Kalkstein (1990); Eder et al. (1994). The approach used here is based on a variation of the methods previously used by Brook et al. (1995a,b) in selecting a 30-event aggregation set for the Regional Acid Deposition Model (RADM). The approach of Brook et al. involved four major components. Cluster analysis of wind fields was used to determine meteorologically representative categories. The determination of the number of clusters to retain was based upon within-group variance patterns and prior work by Fernau and Samson (1990a,b). A procedure for aggregating the episodic results into annual totals and averages involved frequency-weighted sums and estimated deposition-precipitation relationships. Event selection procedures were designed to emphasize categories that accounted for most of the annual wet sulfate deposition,

while also representing some winter and dry events. A summary of some specific elements of their approach is provided in Table 17-1.

Table 17-1 Summary of Methodology Used by Brook et al. (1995a; 1995b) for RADM

1. Determination of categories

- Used Ward's (1963) method of cluster analysis, which minimizes within-cluster sums of squares, in an agglomerative, hierarchical mode for wind flow parameters. Used eastern North American zonal *u* and meridional *v* 85-kPa wind components for 0000 UTC with 5° spatial resolution (two variables at 48 grid nodes over three days).
- Clustered "consecutive" 3-day periods from 1979, 1981, and 1983, with subsequent classification of remaining "running" 3-day periods from 1979-1985 into one of these clusters.

2. Determination of number of clusters to retain

- Examined stepwise increases in within-group variance with decreasing number of clusters, expressed through F-statistic.
- Retained 19 clusters based on results for wind flow, sulfate deposition, and prior work by Fernau and Samson (1990a,b). Used quantitative information but somewhat subjective criteria.

3. Development of aggregation procedure

- Estimated total deposition for the group of sampled categories, from the sampled events (weighted sum, accounting for the number of events sampled from each cluster and frequency of occurrence of the clusters).
- Scaled up by ratio of total annual deposition to an estimate of annual deposition that is based on aggregating the sampled categories. Estimates used either mean deposition from a sampled category or deposition estimated from the deposition-precipitation relationship in the category.

4. Selection of "optimum" set of events

- Subdivided the 19 categories into wet and dry subsets, resulting in 38 new categories.
- Primarily represented categories that accounted for most of the annual wet sulfate deposition (at least 75% when combined). Selected 19 events from these categories. Also selected 11 events from winter (5) and dry (6) events to represent seasonal deposition differences, dry periods, and possible nonlinear effects.
- Number of events selected from each category was based on proportionality to the frequency of occurrence of the category and the percent of total sulfate accounted for by the category.
- Examined 20 potential sets (each randomly generated) meeting all criteria, selected the one that minimized RMSE for annual sulfate deposition (primarily) and precipitation (secondarily) at 13 sites. Selected sets in stages, first choosing a set of 19 events from the wet categories and then a set of 11 events from winter and dry periods.

17.1.2 Objectives

The present objectives differ somewhat from those which motivated the earlier research. RADM was primarily designed to address issues involving acidic deposition. CMAQ addresses a more

diverse collection of air quality parameters with equal importance. In addition, CMAQ will be applied to a continental domain that is significantly larger than geographic area for which estimates are supplied by RADM. The extension from the RADM domain to a continental domain is extremely ambitious as it relates to episode selection and aggregation. Therefore, the development of an approach that accommodates this larger continental domain is particularly challenging.

The objective of the activity described in this chapter is the development of an aggregation and episode selection approach that supports model-based annual and seasonal air quality estimates that are at least as accurate (with respect to sampling uncertainty) as those achieved by RADM, in consideration of the more general applicability envisioned for CMAQ both with respect to air quality parameters and geographic representation. This accuracy must be preserved while minimizing any additional cost. In essence, "cost" refers to the number of events for which the model provides estimates, each of which adds cost in the form of both computational processing time and human labor.

17.2 Summary of the Approach

The analysis was carried out in phases, with information gathered in each phase contributing to the design of the next. For this reason, this chapter is structured to present complete descriptions of the methodology and results achieved in each phase, in sequence, in sections 17.3, 17.4, and 17.5. This section is intended as an overview of the process prior to those detailed descriptions. This overview consists of descriptions of some key elements of the methodology, the rationale, scope, and limitations associated with the methodology, and the strategy used to move in phases toward the final result.

17.2.1 Basic Elements of the Methodology

Simply stated, the methods that we have employed involve the determination of meteorologically representative categories, the selection of events from those categories, and the use of evaluative tools to ensure that the detailed aspects of those activities are defined in such a way as to achieve optimal results, to the extent that we can measure optimality.

A specific goal is the definition of meteorological categories that account for a significant proportion of the variability exhibited by the air quality characterizations of interest. The basic approach used in the current analysis for the determination of categories and event selection components is related to that of Brook et al. (1995a,b), but certain fundamental considerations have been modified to reflect the differences inherent in the present objectives as described in section 17.1. The common element is the cluster analysis of zonal u and meridional v wind components to define meteorological categories.

The definition of meteorological categories is designed to support the selection of events from those categories in a process known as stratified sampling (Cochran, 1977). Stratified sampling

exploits the internal homogeneity of the meteorological categories, or "strata," to achieve more precise estimates than would be possible using simple random sampling (i.e., randomly selecting events without regard to meteorological category). Certain variations of stratified sampling are relevant to this analysis. One relatively inefficient option for invoking stratified sampling would involve selecting the same number of events from each category/stratum. This is known as "equal allocation." An alternative is "proportional allocation," which involves selecting numbers of events in direct proportion to the size of the stratum. Thus, more events are selected from strata that contain large numbers of events than from smaller strata. This is potentially much more efficient than equal allocation, in the sense that it leads to much more precise (i.e., lower variance) estimates. Estimates exhibiting absolute maximum efficiency (i.e., minimum variance) are obtained by modifying this method slightly so that the number of events selected from each stratum is in direct proportion to the product of the size of the stratum times the internal variability (as characterized by the standard deviation of the measurement of interest) within the stratum. Thus, strata exhibiting significant variability among events are sampled more heavily than strata in which events are more uniform. This is known as "optimum allocation," which is identical to proportional allocation when within-stratum variances are equal.

While wind flow parameters were used to define the meteorological categories, other meteorological parameters were used in subsequent phases of the analysis to refine aspects of the episode selection methodology, and as evaluative tools to assess the effectiveness of the approach. These parameters include visibility (as represented by the b_{ext}), temperature, and relative humidity. Their specific roles are discussed in more detail in the following sections.

17.2.2 Rationale, Scope, and Limitations

As stated previously, the approach to selecting an aggregation and episode scheme is based upon the definition of meteorological categories that account for a significant proportion of the variability exhibited by the air quality characterizations of interest. Strictly speaking these characterizations include parameters such as acidic deposition, air concentrations, and measures of visibility. Therefore, it might be argued that the definition of categories should be formulated directly using these parameters that are ultimately of interest. However, it is equally important that the model simulate the particular transport mechanisms involved in the associated atmospheric processes, and in particular that source-attribution analyses be facilitated. This requires that categories be defined with an emphasis on wind flow parameters. Indeed, characterizations of basic wind field patterns in essence describe frontal passages, along with all of the meteorological properties typically associated with them.

In view of the importance placed on the accurate simulation of transport mechanisms, a complete evaluation of the episode selection and aggregation methodology would require an assessment of the accuracy with which transport is represented. However, this accuracy cannot be measured, as there is no technique available to support a direct, quantifiable assessment of the representation of atmospheric transport. In addition, with the exception of b_{ext}, there are little air quality data available with the required spatial and temporal resolution and range to support a direct

evaluation of the methods described in this chapter with regard to the outcome parameters that will be of primary interest in CMAQ.

For these reasons two meteorological parameters (in addition to b_{ext}), which are known to be related to many of the air quality parameters of interest, and for which appropriately resolved data are available, were used as evaluative measures in this analysis. Specifically, temperature and relative humidity were used; however, primary emphasis will be placed upon the b_{ext}, which provides a surrogate measure for fine particles. It must be recognized that this constitutes a secondary evaluative tool, in the sense that the effectiveness of the approach cannot be directly measured as it relates to atmospheric transport or to specific air quality parameters, both of which are primary outcomes. For this reason, the methods were not developed and refined solely toward the goal of optimizing performance associated with the estimation of visibility. Instead, this performance was evaluated in combination with other considerations that were believed to be important but for which performance may not be readily quantifiable.

17.2.3 Strategy

The basic strategy used for the selection of events to support aggregation-based estimation is described in the steps outlined below. The term "cluster" describes a collection of events that are defined to be meteorologically similar based upon cluster analysis results. The term "stratum" describes a collection of meteorologically similar events to be used in stratified sampling. In this chapter, "stratum" and "cluster" are essentially interchangeable since the clusters defined in the analysis are ultimately used as the strata for sampling purposes.

1. We explored different approaches to the cluster analysis of wind components, each of which resulted in the definition of a set of clusters (strata) of meteorologically similar events, for possible use in alternative stratification schemes. Some alternatives that were explored include annually defined clusters (i.e., strata defined using cluster analysis of daily wind field data from several years, without regard to season), seasonally defined clusters (i.e., strata defined using distinct cluster analyses of wind field data pertaining to different seasons), and regionally defined clusters (i.e., strata defined using distinct cluster analyses of wind field data for different geographic regions).

2. The alternative stratification schemes explored in step 1 were compared using relative efficiencies and meteorological considerations. The concept of relative efficiency relates to the variance associated with an estimate derived using different sampling schemes. We explored the variances associated with estimates of the annual means of the evaluative meteorological parameters described above (visibility, temperature, relative humidity). The relative efficiency of each stratification scheme is defined as the ratio of the variance associated with simple random sampling to the variance associated with stratified sampling using that scheme. A large relative efficiency is indicative of a high degree of precision (lower variance) associated with the estimate of interest. As discussed previously, since these evaluative meteorological parameters do not afford a complete, direct assessment of

the validity of process with regard to the parameters to which it is ultimately to be applied, meteorological considerations were taken into account in combination with the relative efficiencies in order to select a general stratification scheme. The selected scheme (seasonal stratification) was considered for more detailed refinement in step 3.

3. We determined an appropriate number of clusters to retain in combination with an acceptable number of events that would be necessary to achieve the objectives. The determination was based on estimated standard deviations associated with several alternative formulations, as well as other considerations. The standard deviations relate specifically to estimates of the annual means and 90th percentiles of the evaluative meteorological parameters. The "other considerations" included the objective of matching or exceeding the performance of the current aggregation methodology used for RADM, as well as a goal of avoiding unsampled clusters. Unsampled clusters (the inclusion of clusters for which no events would be selected) were considered to be undesirable because there would be no information available in the aggregation process to account for events contained in such a cluster. In concept, our view was that any unsampled cluster should be combined with another cluster to which it is most similar. In practice, we achieved this by constraining ourselves to collections of clusters that were adequate to support the sampling of at least one event from each cluster. Twenty clusters were ultimately retained, consisting of five clusters defined in each of the four seasons, and the number of events necessary to achieve the objectives was determined to be 40.

4. A stratified sample of 40 events was randomly selected from the 20 clusters defined in step 3. Proportional allocation was used in determining the number of events to be selected from each cluster (stratum). Optimum allocation was considered but was not used for several reasons, including: (1) it requires the quantification of the variance of a primary outcome parameter, whereas only secondary evaluative outcomes (visibility, temperature, relative humidity) were available as discussed previously, and (2) the variance of any outcome parameter varies geographically, so that optimum allocation would likely result in differing numbers of events depending upon the geographic location, whereas proportional allocation would not. It was verified that, at least based upon the evaluative outcome parameters that are available, in most geographic locations the distribution of events that arises from proportional allocation does not differ substantially from that arising from optimum allocation.

Details concerning the implementation of this approach are discussed in the following sections. Sections 17.3 and 17.4 correspond to steps 1 and 2 in the strategy outlined above, and section 17.5 includes a discussion of steps 3 and 4.

17.3 Cluster Analysis of Wind Fields

The cluster analysis of wind components is described in this section. This includes a description of the wind field data, the basic analysis technique, variations of the basic technique, and methods of presentation. Some graphical results of exploratory analyses are also included.

17.3.1 Description of Wind Data

To accommodate the continental domain and to achieve adequate spatial resolution, the cluster analysis involves data at 336 grid nodes with 2.5° spatial resolution, as obtained from the NCEP/NCAR 40-year reanalysis project (Kalnay et al., 1996). In this analysis, 700 mb wind components for 1800 UTC have been used, in consideration of the mountainous western regions in the domain. Corners of the grid were cut back to guard against excessive influence from ocean-based meteorology. Graphical illustrations of this domain are referenced later in this section.

17.3.2 Basic Cluster Analysis Technique

Cluster analysis, in the present formulation, involves the classification of a set of observations into categories that are internally homogeneous with respect to defined multivariate relationships in the data. In this case "multivariate" refers to the multiple variables used to characterize wind fields, consisting of the u and v components applicable to each location within the previously described domain and extending over an event that includes multiple days.

A 12-year period (1984-1995) was considered in the exploratory cluster analyses, later refined to a 9-year period (1984-1992) for the final clustering upon which episode selection was based. Since CMAQ is actually run for a 5-day period for each event (the first two days establish initial conditions, and model predictions from days 3-5 are saved as a "3-day event"), 5-day periods were clustered rather than 3-day periods. To make the analysis computationally feasible, the first, third, and fifth days of each 5-day event were considered. Based upon the performance noted by Fernau and Samson (1990a,b), Ward's method of cluster analysis was used (Ward, 1963), minimizing within-cluster sums of squares, in an agglomerative (i.e., moving from many clusters toward fewer clusters), hierarchical (i.e., once clusters are joined they cannot be separated) process. Thus, if a single observation (event) is considered to consist of 2,016 elements (the 2 u and v components × 336 grid nodes × 3 days considered per event), then the objective of the cluster analysis is to divide these observations into clusters (categories) for which the within-cluster sum of squares (sum of squared differences between the elements of individual observations or means) is minimized.

In the exploratory analyses, clusters were initially defined based upon "consecutive" rather than "running," or overlapping 5-day periods from 1987-1992. Then, each remaining event ("running" 5-day periods from 1984 through 1995) was classified into the cluster that minimizes the sum (over the 336 grid nodes and three days) of the squared deviations of each u and v component from the cluster mean u and v. In the final cluster analysis, using 1984-1992 data, consecutive 5-day periods from 1984 through 1992 were clustered, and remaining events were classified into

those clusters according to the same criteria described above. Cluster analyses were carried out using SAS (SAS Institute Inc., 1989); however, due to the extreme computational burden of these analyses it was necessary to calculate the distance matrix externally from the clustering procedure itself.

17.3.3 Illustration of Cluster Analysis Results

Representative results from the selected exploratory analyses, as well as all results from the final cluster formulation, are illustrated graphically. Specifically, cluster definitions are illustrated using maps of cluster average wind fields. In some cases, these are supplemented with specialized maps illustrating the intracluster variability in the wind fields. Star chart histograms are also used to illustrate the frequency of occurrence of events from each cluster, for each month of the year.

To provide proper perspective for a review of this analysis, it is useful to consider preliminary results for a set of 30 clusters initially defined using annual data from 1984-1995. The most prevalent cluster (labeled Cluster 1) accounted for 12.19% of all 5-day events during this time period, with nearly all of those events occurring during the summer months. Map-based graphs of mean wind vectors for this cluster are contained in Figure 17-1 (a-c). Three maps are included, representing mean vectors for days 1, 3, and 5 of the 5-day event. These maps illustrate largely stagnant conditions associated with an anticyclonic pattern centered over the southeastern U.S.; a zonal flow over southern Canada and a trough over the west coast of the U.S.

As a second example, Figure 17-2(a-c) illustrates mean wind vectors for a somewhat less prevalent cluster that accounted for 3.65% of all 5-day events during this time period (ranking ninth in overall prevalence and labeled as Cluster 9). Most of these events occurred between the months of October and April, characterized by northwesterly winds associated with a large-scale trough moving through the central and eastern portion of the domain.

While these maps are effective in illustrating average behavior associated with each cluster, they do not give any indication of the variability inherent in the clusters. Figures 17-4 (a-c) and 17-5 (a-c) contain additional maps that address this issue. The first map (Figure 17-3a) illustrates the wind field for the third day of an individual event (January 23-27, 1989) that was assigned to Cluster 9. Comparison of this map to the mean wind field for day 3 of Cluster 9 (Figure 17-2b) reveals fairly close resemblance between the two. By contrast, the maps in Figures 17-3b and 17-4c depict the third day from two other events belonging to Cluster 9. These patterns do not resemble the mean wind field as closely, and are indicative of the variability among individual events that were assigned to this cluster.

Clearly it would be useful to simultaneously visualize the variability exhibited by all of the wind fields assigned to each day of Cluster 9, and Figure 17-4 (a-c) represents an attempt to do this. These maps contain the mean wind vectors for each day of Cluster 9 on a thinned-out grid that only includes alternating grid nodes. In addition, the maps contain groups of small dots, each of which depicts the location of the wind vector arrowhead for an individual event assigned to this

cluster. The groups of dots collectively illustrate the distribution of arrowheads for all events belonging to Cluster 9.

The dots surrounding each mean wind vector arrowhead appear in a somewhat circular pattern, and the extent of spread exhibited by the dots illustrates the degree of variability among wind vectors assigned to the cluster. Similar patterns characterize the variability associated with other clusters (not shown). Clearly there is substantial variability associated with the wind vectors assigned to individual clusters. This variability emphasizes the ambitious nature of the endeavor. In essence, the goal is to categorize many years worth of meteorological patterns into a finite number of classes. Furthermore, each meteorological pattern does not simply describe a single location at a given point in time; it is required to simultaneously represent a broad spatial domain over a significant temporal period. Indeed, it should not be surprising that a substantial amount of variability is associated with the result.

Figure 17-5 (a-e) contains star chart histograms of the 30 clusters defined using annual data. Each chart illustrates the frequency of 5-day events belonging to a given cluster, and the clusters themselves are ordered according to overall frequency of occurrence. As shown on the charts, events from Cluster 1 accounted for 12.19% of all 5-day events between 1984 and 1995, those from Cluster 2 accounted for 12.10% of all events, etc. The numbers arranged radially on each chart depict the number of events belonging to the cluster from each month of the year. The length of the line pointing to each month is proportional to this frequency of occurrence, and the ends of the lines are connected to facilitate the visualization of patterns.

Several observations may be made based upon these charts:

- Although defined using annual data, the cluster frequencies reveal definite seasonal tendencies. That is, clusters do not occur randomly throughout the year, but rather exhibit a tendency to occur more frequently within specific seasons. Thus, the annual clustering procedure successfully identifies and discriminates wind field patterns that are associated with seasonally distinct meteorological classes.
- While clusters containing summer events tend to be quite distinct from those containing winter events (and vice versa), many clusters contain events from a combined "transitional" season that includes both spring and fall months.
- The two most prevalent clusters heavily emphasize the summer months; each of these clusters includes more than twice as many events as any other cluster, with the vast majority of summer events contained in them.

The disproportionate representation of summer events by two of the 30 clusters is not surprising, since the wind fields are expected to be less variable in the summer. However, seasonal differences in meteorology and atmospheric chemistry are important in explaining the variability exhibited by the air quality parameters of interest. The addition of more warm season clusters

could provide improved resolution in this regard. This is the primary motivation for conducting analyses using seasonally distinct clustering.

17.4 Evaluation of Alternative Aggregation Approaches

The previous illustration clarifies the motivation for investigating seasonally distinct clustering. Similarly, regionally distinct clustering offers an alternative that might provide improved resolution of wind field groupings on smaller spatial scales. An added dimension to the problem is that the number of clusters to be retained clearly affects the degree of resolution. To gain an understanding of the importance of these considerations as they relate to estimation of the meteorological parameters used as evaluative tools in this analysis, these and other alternatives were explored in several combinations. These explorations, designed to expose patterns and trends from which to make an informed selection of a general approach, are described in this section.

17.4.1 Description of Alternative Approaches

Several variations of the *u* and *v* wind vector clustering were investigated. As discussed previously, these were selected to investigate patterns and properties, and not necessarily to be considered as final candidates for cluster definitions. They are as follows:

- Annually defined strata with variations in the number of strata: 5, 10, 20, 30, 60, and 90 clusters;

- Seasonally defined strata using warm and cold seasons: totals of 10, 20, 30, and 60 clusters equally divided between the warm season April-September period and the cold season October-March period;

- Seasonally defined strata approximately equally divided among summer (June, July, August), winter (December, January, February), and transitional (spring and autumn combined) seasons: totals of 20, 30, and 60 clusters;

- Seasonally defined strata equally divided between summer and winter seasons, and with approximately twice as many strata defined for the transitional season: totals of 20 and 30 clusters;

- Seasonally defined strata approximately equally divided among summer, winter, spring (March, April, May), and autumn (September, October, November) seasons: totals of 20 and 30 clusters; and

- Regionally defined strata: 30 clusters identified in each of four separate cluster analyses for the northeast, southeast, northwest, and southwest subsets of the domain

We also investigated the alternatives of strata defined to simply mirror the four seasons (disregarding all clusters), strata defined by clustering of 3-day events rather than 5-day events, and strata defined by clustering the meteorological parameters used to evaluate the approach.

17.4.2 Description of Meteorological Data

For the alternative stratification schemes, preliminary testing was performed by examining the uncertainty associated with the use of cluster-based stratified sampling to estimate the annual mean of daily noontime levels of visibility, temperature, and relative humidity, with primary emphasis placed upon visibility as discussed previously. Visibility (units of km^{-1}) was specifically expressed as the light extinction (b_{ext}), less observations with precipitation, and less observations with relative humidity greater than 90%. The light-extinction coefficient is often used to characterize visibility, although in general, it has limited ability to predict human visibility. The visual range v_r (km) can be estimated from the b_{ext} by using the Koschmieder equation:

$$v_r = \frac{3.91}{b_{ext}} \tag{17-1}$$

Temperature is in units of degrees Celsius, and relative humidity in percent. These parameters were taken from 201 locations in the continental U.S. for which coverage was at least 99%, as illustrated in Figure 17-6. This was specifically defined as sites exhibiting at least 99% completeness for light extinction coefficient; allowances were made for missing observations that were associated with precipitation so as not to bias the inclusion of sites toward drier climates.

17.4.3 Analysis Methods

The average relative efficiency associated with the estimation of mean annual visibility, temperature, and relative humidity, using each alternative stratification scheme, was used for comparison of the schemes. Specifically, at each location and for each scheme, the variance of an aggregation-based estimate (Cochran, 1977) of the annual mean was determined in three ways, assuming that the estimated mean was calculated using (1) a stratified sample with equal allocation across strata, (2) a stratified sample with proportional allocation across strata, and (3) simple random sampling, with a total sample size consisting of the same numbers of events in each case. Also at each location, the ratio of the simple random sampling variance to the variance associated with each of the two stratified sampling designs was calculated and expressed as the relative efficiency of each of those designs. Finally, those relative efficiencies were averaged across sites to provide an indication of the overall efficiency of each scheme.

This is best explained using a specific example. First, suppose that the mean annual temperature at a given location is estimated as the average of the daily temperatures from 30 randomly sampled 3-day events from the period 1984-1992, completely disregarding any information related to clusters. Suppose that the standard deviation associated with that estimate is 1.5°C, so

that a 95% confidence interval would yield the estimated mean ±2.94°C (=1.96×1.5). Second, suppose that the mean is instead estimated as a weighted average from 30 3-day events, using two events per cluster (i.e., stratified sampling with equal allocation), and using the frequency of occurrence of each cluster as the weight applied to the temperature from the corresponding event. Suppose that the standard deviation associated with that estimate is 1.0°C, compared to 1.5°C from simple random sampling. Last, suppose that 30 events are selected using proportional allocation (i.e., the number of events selected from a cluster is proportional to the number of events belonging to the cluster), and that the standard deviation of the resulting estimated annual mean temperature is 0.8°C. These standard deviations (1.5, 1.0, and 0.8) translate to variances of 2.25, 1.0, and 0.64 for simple random sampling, stratified sampling with equal allocation, and stratified sampling with proportional allocation, respectively. Thus, for this hypothetical location, the relative efficiency of stratified sampling with equal allocation is 2.25/1.0=2.25, and the relative efficiency of stratified sampling with proportional allocation is 2.25/0.64=3.52. Proportional allocation is more efficient than equal allocation in the sense that it leads to lower variances and therefore tighter confidence intervals bounding the estimated mean.

17.4.4 Results

Tables 17-2 (a-b) and 17-3 present mean relative efficiencies associated with annual means of the daily noontime temperature, relative humidity, and extinction coefficient, as estimated using aggregation approaches based upon the various schemes described above. In each table, results are presented to illustrate the relative efficiency of estimation methods using equal allocation (equal numbers of events selected to represent each cluster) and proportional allocation (numbers of events selected in direct proportion to the total number of events categorized into the given cluster). Relative efficiencies reported in this section are valid for any number of events that might be selected, as relative efficiency is invariant to sample size under equal or proportional allocation

In the case of proportional allocation, the relative efficiency actually refers to the minimum variance that might theoretically be achieved if proportional allocation were carried out precisely. In practice this might only be possible if a very large number of events were to be sampled, since the appropriate proportions might otherwise dictate sampling of fractional numbers of events from some clusters. Therefore, the relative efficiency reported for proportional allocation may be thought of as an upper limit to the relative efficiency that might actually be achieved in practice. In all likelihood, this upper limit cannot be attained, but it should be possible to achieve a relative efficiency occurring somewhere within the range defined by this upper limit and the relative efficiency associated with equal allocation of events among clusters.

The first six rows in Table 17-2a illustrate relative efficiencies associated with various numbers of annually defined strata (i.e., clusters emerging from cluster analyses of daily wind field data from 1984-1995 without regard to season). Several observations may be made by inspecting the first six rows in Table 17-2a:

- The relative efficiency associated with the estimation of mean temperature is consistently highest, followed by that of relative humidity. This implies that the meteorological clusters are most useful in distinguishing between events with regard to temperature, and least useful in distinguishing extinction coefficient.

- In the case of temperature, the variability associated with stratified sampling using wind field-based clusters is consistently less than the variability associated with simple random sampling (i.e., relative efficiencies are uniformly greater than 1.0). Thus, in each scheme the clusters contribute important information that explains variation in temperature.

- For the estimation of mean relative humidity and mean extinction coefficient, the use of stratified sampling based upon wind field clusters is consistently more efficient than simple random sampling if proportional allocation is approximately satisfied. In most cases, the use of equal allocation actually results in less efficient estimation than simple random sampling; this reflects a wide range of stratum sizes that would be inappropriately represented using equal allocation.

- As would be expected, the efficiency associated with proportional allocation increases as the number of strata increases, incorporating more refined representations of the meteorological classes within the strata.

- The efficiency associated with equal allocation decreases as the number of strata increases. The stratum sizes become more divergent when more strata are defined, so that the inefficiency of equal allocation is magnified.

Based upon the well-known properties of stratified sampling discussed above, our objective was to design and implement a scheme based upon approximate proportional allocation. The numbers for equal allocation in these tables merely served to provide a lower bound on the efficiency that could be realized, since it was known that the precise degree of efficiency reported for proportional allocation might not be achievable in practice due to the requirement of sampling integer-valued numbers of events.

As discussed in section 17.3.3 above in regard to the analysis illustrated in the "30 Strata" row of the table, summer events are disproportionately represented by two of the 30 clusters. To evaluate the effect of improving the resolution of summer meteorological patterns, as well as the effects of imposing constraints that would alter the resolution of families of clusters under a variety of scenarios, various implementations of seasonally distinct clustering were investigated. The last four rows of Table 17-2a illustrate results associated with stratum definitions based upon a simple warm/cold seasonal dichotomy, in which separate cluster analyses were conducted to force equal numbers of strata for each season. The following observations may be made based upon this portion of the table:

- With the exception of extinction coefficient estimation under proportional allocation, stratification using seasonally defined clusters consistently yields improved efficiency over stratification using the same number of annually defined clusters. Thus, although the annually defined clusters do adhere to a seasonal pattern, the improved resolution afforded by the forced inclusion of more warm weather clusters (and reduction of cold weather clusters) is particularly effective in explaining variation in temperature.

- For seasonally defined clusters, the relative gains in efficiency associated with using equal allocation are large as compared to the potential gains associated with using proportional allocation. Thus, in departing from proportional allocation (which is not precisely achievable in practice as discussed above), seasonally defined clusters are likely to afford improved efficiency over annually defined clusters.

Results associated with further seasonal stratification schemes are illustrated in Table 17-2b. The first two rows correspond to approximately equal numbers of clusters divided among summer, winter, and transitional (spring and autumn combined) seasons, the next two rows correspond to equal numbers of clusters divided between summer and winter with approximately twice as many transitional season clusters, and the fifth and sixth rows correspond to approximately equal numbers of clusters divided among four seasons. In each case, the exact distributions are constrained to result in total numbers of strata that are directly comparable to the numbers of strata investigated in other seasonal and annual analyses.

Under proportional allocation, stratification schemes based on three or four seasons offer significantly improved efficiency in the estimation of mean temperature compared to two-season and annual stratification schemes with comparable total numbers of strata. They also demonstrate slight but uniform improvement in the estimation of extinction coefficient, and mixed results in the estimation of relative humidity.

Table 17-2a. Mean relative efficiency[1] associated with estimation of the annual (1984-1995) mean of the indicated parameter, using various stratified[2] sampling[3] approaches relative to simple random sampling. *Continental analysis.*

Method	Temperature		Relative Humidity		RH-Adjusted Extinction Coefficient	
	Equal Allocation Across Strata	Proportional Allocation	Equal Allocation Across Strata	Proportional Allocation	Equal Allocation Across Strata	Proportional Allocation
5 Strata	2.34	2.41	1.14	1.18	1.01	1.12
10 Strata	2.29	2.50	1.09	1.22	0.90	1.14
20 Strata	2.11	2.83	0.88	1.26	0.69	1.16
30 Strata	2.08	2.86	0.86	1.28	0.67	1.17
60 Strata	1.81	3.05	0.76	1.32	0.59	1.19
90 Strata	1.43	3.10	0.62	1.33	0.53	1.20
10 Strata Defined Seasonally (5 Warm, 5 Cold)	2.62	2.94	1.11	1.26	0.93	1.13
20 Strata Defined Seasonally (10 Warm, 10 Cold)	2.91	3.54	1.11	1.35	0.89	1.16
30 Strata Defined Seasonally (15 Warm, 15 Cold)	3.14	3.60	1.17	1.37	0.91	1.17
60 Strata Defined Seasonally (30 Warm, 30 Cold)	2.74	3.89	0.98	1.39	0.77	1.20

[1] Relative efficiency is defined as the ratio of the variance associated with simple random sampling to the variance associated with stratified sampling. The table entries are means of station-specific efficiency ratios, averaged across stations within the continental domain.

[2] Unless otherwise noted, stratum definitions are based on annual clustering of 5-day events from a temporal subsample of the wind field data; the remainder of the sample is then classified into those strata.

[3] Reflects sampling of 3-day events from 1984-1995.

Table 17-2b. Mean relative efficiency[1] associated with estimation of the annual (1984-1995) mean of the indicated parameter, using various stratified sampling[2] approaches relative to simple random sampling. *Continental analysis.*

Method	Temperature		Relative Humidity		RH-Adjusted Extinction Coefficient	
	Equal Allocation Across Strata	Proportional Allocation	Equal Allocation Across Strata	Proportional Allocation	Equal Allocation Across Strata	Proportional Allocation
20 Strata Defined Seasonally (6 Summer, 6 Winter, 7 Transitional)	2.66	3.91	0.95	1.31	0.90	1.18
30 Strata Defined Seasonally (10 Summer, 10 Winter, 10 Transitional)	2.60	4.12	0.87	1.35	0.78	1.20
20 Strata Defined Seasonally (5 Summer, 5 Winter, 10 Transitional)	3.31	4.06	1.06	1.33	0.89	1.19
30 Strata Defined Seasonally (8 Summer, 8 Winter, 14 Transitional)	2.91	4.17	0.96	1.36	0.80	1.20
20 Strata Defined Seasonally (5 Summer, 5 Winter, 5 Spring, 5 Fall)	3.23	3.86	1.11	1.36	0.92	1.18
30 Strata Defined Seasonally (8 Summer, 8 Winter, 7 Spring, 7 Fall)	2.82	3.88	1.03	1.38	0.84	1.19
4 Strata Defined as Seasons (Dec-Feb, etc.)	2.93	2.93	1.21	1.21	1.12	1.12
30 Strata Defined by Clustering 3-Day Events	2.24	2.78	0.97	1.29	0.76	1.16
30 Strata; Seasonality Removed from Met. Parameters	0.92	1.28	0.74	1.15	0.63	1.09
30 Strata Defined by Clustering Lt. Ext. Coeff.	0.51	1.89	0.30	1.11	0.57	1.45

[1] Relative efficiency is defined as the ratio of the variance associated with simple random sampling to the variance associated with stratified sampling. The table entries are means of station-specific efficiency ratios, averaged across stations within the continental domain.

[2] Reflects sampling of 3-day events from 1984-1995.

The final four rows of Table 17-2b address issues that are useful in that they provide additional perspective for this analysis. They are discussed in sequence below:

- In view of the improvement associated with seasonal stratification schemes relative to annual stratification, a natural question to ask is whether a seasonal scheme with one stratum per season (i.e., no cluster analysis) is sufficient to support comparable efficiency. Based upon the results in Table 17-2b, this method offers overall improvement relative to an annual scheme with an approximately equal number of strata (i.e., five strata as shown in the first row of Table 17-2a). As might be expected, it is significantly less efficient than the use of 20 strata equally divided among four seasons, but not dramatically so.

- Another natural question is whether the clustering of five-day events (using wind data from the first, third, and fifth days) has a noticeable impact on this analysis relative to the clustering of three-day events that previous investigators have pursued. Based upon results in Table 17-2b, the definition of 30 strata using annual clustering of three-day events produces similar results to those associated with 30 strata using five-day event clustering (fourth row of 17-2a) with respect to the evaluative parameters. Note that this does not necessarily address differences with respect to the characterization of transport.

- A consistent result in these analyses is that the relative efficiency associated with the estimation of mean temperature is much greater than that associated with the estimation of mean relative humidity, which in turn is slightly greater than the relative efficiency associated with extinction coefficient. Since the preliminary results demonstrate associations between the clusters and the seasons (even for annually defined clusters), one might hypothesize that this characteristic is related to the more pronounced seasonal trends associated with temperature and the less pronounced trends associated with extinction coefficient. Table 17-2b illustrates relative efficiencies associated with the three meteorological parameters following the removal of seasonal trends from each. (Trends were removed by analyzing deviations of each parameter from a sinusoidal curve fitted to the raw data at each location.) Indeed, the relative efficiencies for the three parameters are much more comparable in this context, and much more similar to the results for extinction coefficient in other analyses. This analysis lends support to the use of extinction coefficient as the primary evaluative outcome, because it reflects the ability of each scheme to characterize short-term meteorological patterns apart from long-term seasonal trends.

- A final investigation in Table 17-2b also relates to the utility of extinction coefficient as the primary evaluative outcome. Under proportional allocation, the relative efficiencies associated with it are not dramatically greater than 1.0, indicating that stratified sampling based upon wind field clustering produces consistent but not dramatic gains in efficiency (relative to simple random sampling) in the estimation of mean extinction coefficient. To put this observation in its proper perspective, it is useful to consider the maximum relative efficiency that might be achieved from any stratified analysis. In particular, a stratification

of events was performed based upon extinction coefficient itself (rather than wind fields). Under these optimal conditions, the relative efficiency associated with a 30-stratum scheme was still only 1.45, compared to a range of 1.17–1.20 for other 30-stratum schemes based upon wind field clusters. Considered in this context, relative efficiencies encountered in these tables are encouraging. (This clustering of extinction coefficient provides some useful perspective regarding this evaluative outcome parameter, but is not pursued as a recommended methodology for estimation based upon the rationale outlined in section 2.2.)

To evaluate the utility of regionally distinct stratification schemes, the continental domain was divided into four quadrants and cluster analyses were performed on wind fields within each region, resulting in four sets of 30 annually defined strata. For each region, relative efficiencies were summarized as in the previously described analyses. Since the mean relative efficiencies are constrained to sites within each region, results in Table 17-2a are inappropriate for comparison to these regional mean relative efficiencies. Therefore, Table 17-3 also includes mean relative efficiencies only for the sites within each region, from comparable clustering of continental data. These are displayed in combination with the results for strata defined using regional data.

For example, using 30 strata under proportional allocation, clustering of wind fields in the northeast quadrant of the domain results in a mean relative efficiency (averaged over sites in that quadrant) of 1.65 associated with the estimation of mean temperature. For 30 strata, from clusters defined over the entire continental domain, the mean relative efficiency, over those same northeast sites is 3.14. The results in Table 17-3 collectively demonstrate that, under proportional allocation, regional stratification produces either no gains or only slight gains in efficiency in both the southeast and southwest regions for any of the evaluative parameters. In the northeast and northwest regions, this technique is markedly less efficient than continental clustering with regard to temperature, and somewhat less efficient with regard to relative humidity. There is only a negligible effect on extinction coefficient.

This result has significant importance, because it demonstrates that in the northern half of the domain, clustering of continental wind field data is actually more effective than clustering regional data in explaining variation in some meteorological parameters on a regional scale. Thus, the wind field patterns associated with different levels of temperature (and, less markedly, relative humidity) in a northern region are more distinctly identified on a continental scale than on a regional scale. Furthermore, wind field patterns associated with different levels of extinction coefficient (a primary evaluative parameter due to its close association with fine particles) in a given region are no more distinctly identified on a regional scale than on a continental scale.

Table 17-3. Mean relative efficiency[1] associated with estimation of the annual (1984-1995) mean of the indicated parameter, using various stratified sampling[2] approaches relative to simple random sampling. *Regional analysis.*

Region/Method	Temperature		Relative Humidity		RH-Adjusted Extinction Coefficient	
	Equal Allocation Across Strata	Proportional Allocation	Equal Allocation Across Strata	Proportional Allocation	Equal Allocation Across Strata	Proportional Allocation
Northeast; 30 Strata Def. Using Regional Data	1.41	1.65	0.98	1.15	0.95	1.27
Northeast; 30 Strata Def. Using Continental Data	2.27	3.14	0.77	1.20	0.61	1.28
Southeast; 30 Strata Def. Using Regional Data	2.35	2.72	1.04	1.32	0.77	1.22
Southeast; 30 Strata Def. Using Continental Data	2.02	2.62	0.83	1.24	0.61	1.20
Southwest; 30 Strata Def. Using Regional Data	1.95	2.42	0.94	1.26	0.81	1.01
Southwest; 30 Strata Def. Using Continental Data	1.88	2.43	0.89	1.22	0.84	1.04
Northwest; 30 Strata Def. Using Regional Data	1.17	1.66	0.92	1.27	0.82	1.08
Northwest; 30 Strata Def. Using Continental Data	1.96	2.82	1.01	1.47	0.71	1.03

[1] Relative efficiency is defined as the ratio of the variance associated with simple random sampling to the variance associated with stratified sampling. The table entries are means of station-specific efficiency ratios, averaged across stations within the continental domain.
[2] Reflects sampling of 3-day events from 1984-1995.

In view of the current objective of matching or exceeding the performance of the current RADM stratification scheme over the continental domain, it is appropriate to compare the relative efficiency of the stratification scheme used in the aggregation of RADM output compared to the relative efficiency of the schemes defined above. Table 17-4 addresses this specific issue. In addition to the results associated with equal and proportional allocation, this table illustrates the mean relative efficiencies associated with the actual allocation of the 30 RADM events, which lies somewhere between those extremes. (Proportional allocation was not a specific goal of the methods developed for RADM, although it is not inconsistent with the less formally stated goal of selecting more events from the clusters that accounted for most of the acidic deposition.)

Table 17-4. Mean relative efficiency[1] associated with estimation of the annual (1982-1985) mean of the indicated parameter, using various stratified sampling[2] approaches relative to simple random sampling. *RADM comparative analysis.*

Method	Temperature			Relative Humidity			RH-Adjusted Extinction Coefficient		
	Equal Alloc.	Propor-tional Alloc.	Actual Alloc. of RADM Events	Equal Alloc.	Propor-tional Alloc.	Actual Alloc. of RADM Events	Equal Alloc.	Propor-tional Alloc.	Actual Alloc. of RADM Events
19 Existing RADM Strata Defined from Clustering 1979-83 3-Day Events	0.98	1.58	1.45	0.76	1.18	1.07	0.67	1.18	1.11
38 Existing RADM Strata Defined After Separating Wet & Dry Categories	0.83	1.76	1.12	0.59	1.19	0.88	0.49	1.17	0.92
4 Strata Defined as Seasons (Dec-Feb, etc.)	3.06	3.05	2.77	1.13	1.13	1.02	1.17	1.18	1.11

[1] The table entries are means of station-specific efficiency ratios, averaged across stations within the RADM geographic domain.
[2] Reflects sampling of 3-day events from 1982-1985.

In the RADM development, 19 strata were defined based upon clustering of 3-day events occurring between 1979 and 1983. These were then subdivided into wet and dry categories, ultimately resulting in twice as many (38) strata that are actually employed in aggregation-based estimation. (Events from the 1982-1985 time period were classified into these strata, with 30 events selected for use in RADM.) The temporal and spatial domains applicable to the RADM development differ from those of the current analysis; therefore, any comparisons should be considered in this context.

The RADM domain approximately corresponds to the combined northeast and southeast regions displayed in Table 17-3. A comparison of Table 17-4 to Table 17-3 results under proportional allocation suggests superior performance associated with the strata identified using clustering of continental wind field data, with respect to the outcome measures used here. When the actual allocation of RADM events is considered, the superiority of proportional allocation associated with the continental analysis is further elevated.

17.5 Refinement of the Sampling Approach

Based, in part, on the results discussed in section 17.4, a stratified sampling scheme involving seasonal clustering based upon four distinct seasons was selected for further consideration and refinement. The general superiority of three- and four-season stratification schemes was discussed previously in relation to results depicted in Table 17-2 (a-b), and a four-season scheme was selected following additional considerations regarding differences in emission patterns between spring and autumn that would not be apparent using our evaluative parameters alone.

Another benefit of using this type of scheme is that it naturally lends itself to the development of seasonal estimates based upon four-season partitions. The derivation of such estimates from a two- or three-season scheme would not be as well defined, and the estimates themselves would likely be less precise.

Having selected this general approach, refinements were needed to determine an appropriate number of strata, and to arrive at an adequate number of events for sampling. These refinements, and a description of the sample of events that ultimately was selected, are discussed in this section. This aspect of the analysis was limited to a refined time frame consisting of the nine-year period from 1984-1992, which was targeted to ultimately represent baseline meteorology for use in modeling.

17.5.1 Determination of Appropriate Numbers of Strata and Events

The analysis proceeded under the assumption that, in order to satisfy the goal of matching or exceeding the performance of the RADM 30-event stratification scheme, a minimum of 30 events would be required in the framework of the continental domain. The precision associated with the estimation of annual means of the evaluative parameters was investigated for a range of 30 to 60 events, and for 16, 20, 24, and 28 seasonally defined strata (4, 5, 6, and 7 strata per season, respectively).

These numbers of strata were chosen as candidates because 19 wind field-based clusters were defined in the RADM scheme, which offers a certain degree of resolution with regard to the characterization of transport (which is not specifically addressed by the evaluative parameters investigated here). The range of 16 to 28 strata was selected to provide comparable resolution of wind fields and associated transport, noting that higher numbers of strata result in greater variation in the sizes of those strata, and this would force a more pronounced deviation from the goal of proportional allocation. As discussed previously, a primary goal was to ensure that every stratum is sampled, i.e., that there are no clusters which go unrepresented in the final set of events.

Note that we did not adhere to traditional rules of thumb regarding the determination of appropriate numbers of clusters to retain. These rules are based upon an assumption that some finite number of clusters is appropriate to represent the variability inherent in these patterns, and that additional clusters beyond that point add relatively little information. In reality, clusters defined during this process represent a continuum, and traditional F-test statistics illustrate this continuum quite smoothly. There is no magic number of clusters after which the relative importance of additional clusters drops noticeably. Indeed, as cluster analysis is used here merely for the definition of strata and not as an end in itself, there is no compelling reason to be restricted by existing conventions regarding determinations of an optimal number of clusters.

Standard deviations associated with estimation under all of the combinations described above are illustrated in Table 17-5. Furthermore, the process was repeated after seasonal adjustment of

each outcome parameter (seasonality was removed by analyzing deviations from a fitted sinusoidal curve), to ensure that long-term seasonal trends do not unduly influence any pattern. The standard deviations in Table 17-5 provide an indication of the degree of precision associated with estimation, and are influenced by the observed within-stratum variability of the parameter. One would expect the inclusion of more strata to facilitate greater precision, unless this increased precision is offset by incurred deviations from proportional allocation.

Table 17-5. Standard deviation[1] associated with estimation of the annual mean of the indicated parameter, using stratified sampling[2] with 16, 20, 24, or 28 strata and 30, 35, 40, 45, 50, 55, or 60 events. *Continental analysis.*

No. of Events	Temperature, deg. C				Relative Humidity, %				RH-Adjusted Extinction Coefficient, km^{-1} ($\times 10^3$)			
	16 Strata	20 Strata	24 Strata	28 Strata	16 Strata	20 Strata	24 Strata	28 Strata	16 Strata	20 Strata	24 Strata	28 Strata
	NOT SEASONALLY ADJUSTED											
30	0.97	0.98	0.95	0.95	2.38	2.40	2.38	2.40	6.69	6.73	6.73	6.77
35	0.89	0.89	0.87	0.87	2.19	2.20	2.20	2.21	6.03	6.08	6.10	6.23
40	0.83	0.83	0.81	0.81	2.04	2.05	2.06	2.05	5.71	5.63	5.70	5.71
45	0.79	0.77	0.76	0.75	1.93	1.92	1.93	1.93	5.38	5.34	5.33	5.36
50	0.74	0.74	0.72	0.72	1.82	1.83	1.82	1.82	5.09	5.06	5.07	5.08
55	0.71	0.70	0.69	0.68	1.74	1.74	1.73	1.73	4.78	4.79	4.83	4.83
60	0.67	0.67	0.66	0.65	1.66	1.66	1.65	1.65	4.62	4.62	4.60	4.60
	SEASONALLY ADJUSTED											
30	0.75	0.76	0.75	0.75	2.32	2.34	2.33	2.35	6.67	6.70	6.70	6.75
35	0.69	0.69	0.69	0.69	2.14	2.15	2.16	2.16	6.01	6.05	6.08	6.21
40	0.64	0.64	0.64	0.64	1.99	2.01	2.02	2.01	5.69	5.61	5.68	5.69
45	0.61	0.60	0.60	0.60	1.89	1.88	1.89	1.88	5.36	5.32	5.31	5.34
50	0.57	0.57	0.57	0.57	1.78	1.79	1.78	1.78	5.07	5.04	5.05	5.06
55	0.54	0.54	0.54	0.54	1.70	1.70	1.70	1.69	4.77	4.78	4.81	4.81
60	0.52	0.52	0.51	0.51	1.62	1.62	1.62	1.62	4.60	4.60	4.59	4.59

[1] The table entries reflect the standard deviation associated with the average station-specific variances (averaged across stations within the continental domain).
[2] Results reflect sampling of 3-day events from 1984-1992.

For temperature and relative humidity, the table suggests that for any given number of events, any effect associated with different numbers of strata is negligible. For extinction coefficient, standard

deviations for 30 and 35 event schemes increase slightly with increasing numbers of strata. There is a minimum standard deviation associated with 20 strata for the 40-event scheme, and only negligible effects across strata for greater numbers of events.

The objective of this determination was to develop a sufficiently large set of strata to provide some resolution with regard to the characterization of transport, yet be sufficiently concise to avoid any reduction in precision that would result from unsampled strata or from the inability to approximately satisfy proportional allocation. In consideration of these criteria and the above results, 20 strata were determined to constitute an appropriately sized set.

Figure 17-7 (a-c) provides perspective regarding the relative precision provided by sample sizes of 25 or more events associated with estimation of annual means of the evaluative parameters, based upon the use of 20 seasonally defined clusters as strata. The standard deviation displayed in each graph is actually associated with the average of the variances across sites. These graphs illustrate the advantage of stratified sampling with proportional allocation relative to simple random sampling. They also illustrate the relative gains in precision (expressed as reduction in standard deviation) that are realized as the number of events is increased. The star symbols plotted on the graphs indicate the actual standard deviation that would be realized for selected sample sizes under a 20-stratum scheme, with events distributed in accordance with proportional allocation to the extent possible. The selected sample sizes were chosen based upon practical limitations involving the number of events that might realistically be implemented. The stars do not fall strictly on the proportional allocation curve because of limitations associated with the sampling of integer-valued numbers of events.

These graphs indicate that, for temperature, it might be practical to achieve a standard deviation in the range of 0.6–1.0°C, and that a much larger sample size would be needed to reduce the standard deviation below 0.5°C. Similarly, standard deviations associated with estimates of mean relative humidity can possibly be achieved in the range of 1.5–2.5%, and realistic standard deviations associated with extinction coefficient might be in the range of 0.0045–0.0070 km^{-1}. Geographic variability with respect to many of these results is described later in this section.

Although the estimation of mean levels of parameters is likely to be a primary point of emphasis for many model-based results, the accurate estimation of extremes is also of significant importance. This issue was specifically addressed by investigating the precision associated with the estimation of the 90th percentiles of the evaluative parameters.

In contrast to the standard deviations associated with estimation of the mean, there is no closed-form solution to determine the variability associated with the estimation of 90th percentiles. Therefore, a Monte Carlo-type resampling approach was utilized to estimate these standard deviations. This specifically involved randomly selecting 200 artificial samples of actual data, each consisting of the required number of events, from the 20 seasonally defined strata. From each sample and at each site location, the 90th percentile of the parameter was estimated. The variance of the resulting collection of 200 estimates was averaged across sites, and the associated

standard deviation served as an estimate of the precision associated with the particular sample size. This exercise was repeated for sets of 30, 40, 50, and 60 events.

The graphs in Figure 17-8(a-c) illustrate the resulting standard deviations, along with the standard deviations associated with estimation of the mean using the indicated number of events. As would be expected, the standard deviations associated with estimation of the 90th percentile are higher than those associated with estimation of the mean of each parameter. This difference is most pronounced for extinction coefficient, with standard deviations for 90th percentile estimation being approximately three times those for mean estimation. For relative humidity, they are approximately twice as large. The difference is least pronounced for temperature, where the increase is less then 20%. In each case, there is only slight, gradual improvement in the precision of 90th percentile estimation for sample sizes of greater than 40 events.

The next step is to arrive at an appropriate number of events to be distributed among these 20 strata. Table 17-6 displays the standard deviation associated with the estimation of the annual mean of each evaluative parameter (both raw and seasonally adjusted) that would result from samples consisting of 30, 40, 50, and 60 events. For comparison purposes, these standard deviations represent average variances restricted to the RADM geographic domain. The table also displays the standard deviation associated with the aggregation of 30 3-day events in a sample stratified using the original RADM clusters. From this, it is clear that any number of events would be sufficient to provide improved resolution relative to the RADM scheme, in the context of the evaluative parameters reviewed here.

Although these results suggest that a 30-event sample would be sufficient to meet the objective of matching or exceeding the performance of the RADM approach with regard to estimation precision for these outcome parameters, other results displayed in this section demonstrate clear improvement in the precision associated with estimation of both means and extremes by moving from a 30-event sample to a 40-event sample. In addition, a 40-event set is needed to ensure equal precision to the RADM approach with regard to the estimation of wet deposition amounts. The RADM set of 30 events included 20 events from categories that were identified as "wet", i.e., for which average wet SO_4^{2-} deposition exceeded the median for each cluster. In other words, 20 events were selected from the "wettest" 50% of all events.

This oversampling of wet events was originally pursued to ensure the adequate representation of those events that contributed most significantly to wet deposition, because the accurate characterization of wet deposition was the primary purpose of RADM at that time. However, concerns have since arisen that the disproportionate representation of these events may have introduced an overall bias with regard to the ambient concentrations of pollutants that are influenced by cloud cover and precipitation. In view of these concerns, and since wet deposition is not the primary focus for CMAQ, the oversampling of wet events was deemed inappropriate for present purposes. In the absence of this oversampling, it is still necessary to include a sufficient number of events to ensure that wet deposition is characterized as accurately here as in the RADM approach. This would require approximately 20 wet events, and the same median-based

definition of wet versus dry events implies that approximately 20 dry events should also be included. Therefore, a total of 40 events was deemed necessary to satisfy all of the objectives.

Table 17-6. Standard deviation[1] associated with estimation of the annual mean of the indicated parameter, using stratified sampling[2] with 20 strata and 30, 40, 50, or 60 events. *RADM comparative analysis.*

No. of Events	Temperature, deg. C		Relative Humidity, %		RH-Adjusted Extinction Coefficient, km^{-1} ($\times 10^3$)	
	20 Strata	Existing RADM Sample (30 Events)	20 Strata	Existing RADM Sample (30 Events)	20 Strata	Existing RADM Sample (30 Events)
	NOT SEASONALLY ADJUSTED					
30	0.96	1.78	2.34	2.58	6.65	8.28
40	0.82		2.01		5.60	
50	0.73		1.79		5.01	
60	0.66		1.63		4.59	
	SEASONALLY ADJUSTED					
30	0.74	0.82	2.32	2.41	6.64	8.23
40	0.63		1.99		5.60	
50	0.56		1.77		5.00	
60	0.51		1.61		4.58	

[1] The table entries reflect the standard deviation associated with the average station-specific variances (averaged across stations within the RADM geographic domain).
[2] "Existing RADM Sample" results reflect sampling of 3-day events from 1982-1985. Other results reflect sampling of 3-day events from 1984-1992.

Recalling that for 40 events the precision associated with the estimation of mean annual extinction coefficient (the primary evaluative parameter) was optimized using 20 seasonally defined strata (Table 17-5), a final plan was adopted for sampling 40 events from 20 strata (5 strata per season) using approximately proportional allocation.

Figure 17-9(a-d) displays star chart histograms of the 20 clusters defined as strata in this arrangement. Each chart illustrates the frequency of occurrence of 5-day events belonging to a given cluster, and the clusters themselves are ordered according to overall frequency of occurrence. The numbers arranged radially on each chart depict the number of events belonging to the cluster from each month of the year. Map-based graphs of mean wind vectors for day 3 of each cluster are contained in Figures 17-10 through 17-29.

In order to examine the impact of this scheme geographically (in the context of the precision associated with the estimation of mean levels of the evaluative parameters), we examined graphically (not shown), the standard deviation at each site location alongside the actual mean with which that standard deviation is associated. Similarly, analogous information associated with the estimation of 90th percentiles were examined. This examination confirmed the relative geographic uniformity with respect to the standard deviations, which serves as support for the use of "average" standard deviations in drawing conclusions throughout this section.

17.5.2 Selection of Stratified Sample of Events

A stratified sample of events was randomly selected from the 20 seasonally defined strata for the period 1984-1992. The sample was selected without replacement to ensure that no single day was selected into more than one five-day event, i.e., that there was no overlap between selected events. Systematic sampling (Cochran, 1977) was used within each stratum for which more than one event was to be selected. Specifically, all events assigned to the stratum were ordered chronologically, an event was selected near the beginning of that ordering, and subsequent events were selected to be evenly spaced throughout the remainder of the ordering. If k events were to be sampled from a cluster containing n events, to illustrate the simple case in which n/k is integer valued, the first event would be randomly selected from any of the chronologically first n/k events, and every (n/k)th subsequent event would be selected. The purpose of this approach was to ensure appropriate representation over the entire nine-year period.

Table 17-7 displays the total number of events belonging to each stratum, the number of events sampled, and the dates of the sampled events. These dates are the middle dates of the three-day events for which the model ultimately is to be run (i.e., the last three days of the sampled five-day event). This sample of 40 events includes representation from every month of the year, and from every year during the period 1984-1992. Table 17-8 illustrates this representation by displaying the number of events selected from each month and from each year.

Table 17-7. Stratum sizes, number of sampled events per stratum, and dates of events in sample. *Dates shown are for middle day of 3-day event.*

Stratum	Season	Total # of Days in Stratum, 1984-1992	Number of Sampled Events	Event Dates
1	Spring	292	3	12 March 1985, 08 May 1987, 27 March 1990
2	Summer	267	3	17 July 1985, 20 August 1987, 10 August 1990
3	Autumn	238	3	08 September 1986, 12 October 1988, 08 October 1991
4	Winter	210	3	04 January 1986, 15 December 1988, 02 December 1992
5	Spring	200	2	07 May 1984, 06 March 1990
6	Winter	188	2	03 January 1987, 07 January 1992
7	Spring	185	2	01 April 1986, 26 March 1991
8	Summer	171	2	05 August 1986, 29 June 1992
9	Summer	171	2	07 August 1984, 12 July 1989
10	Winter	170	2	18 January 1984, 25 January 1989
11	Autumn	168	2	18 October 1985, 12 September 1991
12	Autumn	150	2	17 November 1987, 14 September 1992
13	Winter	139	2	19 February 1985, 27 January 1990
14	Autumn	135	2	17 October 1988, 24 November 1991
15	Summer	129	2	03 July 1987, 09 July 1992
16	Autumn	128	2	25 November 1985, 07 November 1990
17	Winter	102	1	18 December 1989
18	Summer	90	1	22 July 1989
19	Spring	89	1	09 May 1990
20	Spring	62	1	30 April 1991

Table 17-8. Number of sampled events representing each month of the year and each year from the period 1984-1992.

Month	Number of Events in Sample	Year	Number of Events in Sample
January	6	1984	3
February	1	1985	5
March	4	1986	4
April	2	1987	5
May	3	1988	3
June	1	1989	4
July	5	1990	6
August	4	1991	5
September	3	1992	5
October	4		
November	4		
December	3		

17.6 Application and Evaluation

In this section, examples of the aggregation calculation for annual mean concentrations and total wet depositions, applicable to this sample of events, are provided. Following this example is a description of an evaluation exercise in which the aggregation calculation was carried out for light extinction coefficient, and the aggregated estimates were compared to the actual values based on data from all of the days in the period.

17.6.1 Application of the Aggregation Procedure

Aggregation calculations will be applied to model-based depositions and concentrations obtained for each sampled event, to achieve unbiased estimates for annual and seasonal means and other summary statistics within each grid cell. Since the goal of sampling from every defined stratum is achieved in this approach, these calculations are simplified in comparison to earlier aggregation methods (NAPAP, 1991). In essence, these aggregation calculations merely produce weighted means, totals, or other summary measures, from the sample of events.

To illustrate the aggregation approach, consider the estimation of a mean annual air concentration using model output for the 40 events selected above. These events represent 20 strata; denote these using the subscript i, i=1,2, . . . , 20. Let f_i denote the frequency of occurrence associated

with stratum i, i.e., the total number of 3-day events belonging to the stratum during the period 1984-1992. For an individual grid cell, also let

$$\bar{C}_{MODEL_i}$$

represent the mean model-based concentration associated with all sampled events from stratum i. Thus, for strata with a single sampled event, it is just the event mean concentration in the grid cell. For strata with two or three sampled events, it is the mean concentration for all of those events. Then the estimated annual mean air concentration is given by

$$Mean\ Air\ Concentration = \frac{\sum_{i=1}^{20} f_i \bar{C}_{MODEL_i}}{\sum_{i=1}^{20} f_i} \tag{17-2}$$

Estimates for most other parameters (e.g., dry depositions) and other summary statistics are calculated using similar methods. The calculation for wet deposition is different, primarily because the weighting is partially dictated by precipitation. Let

$$\bar{D}_{MODEL_i},\ \bar{P}_{MODEL_i},\ P_{MEAS_i}$$

represent the mean 3-day modeled deposition for sampled events in stratum i, the mean 3-day modeled precipitation for sampled events in stratum i, and the total measured precipitation accounted for by all events belonging to stratum i, respectively. Then the estimated total annual wet deposition is given by

$$Total\ Wet\ Deposition = \sum_{i=1}^{20} \left(\frac{\bar{D}_{MODEL_i}}{\bar{P}_{MODEL_i}} \right) \times P_{MEAS_i} \times \frac{1}{3 \times 9} \tag{17-3}$$

This expression can be thought of as a weighted sum in which the model-estimated wet concentration for a stratum is weighted by the total measured precipitation associated with the stratum. The final component of this expression is included to reflect the fact that each day is counted three times in the calculated sum (due to the use of 3-day events) and that the strata are defined over a nine-year period.

17.6.2 Evaluation

In order to determine the effectiveness of the aggregation technique and subsequent episode selection, comparisons were made between the observed mean b_{ext}s for the period 1984-1992 and the aggregated estimates of that mean using the stratified sample of events described in 17.5.2 and listed in Table 17-7. This preliminary evaluation, which includes simple regression analysis, is similar to that performed on RADM (Eder and LeDuc, 1996; Eder et al.,1996).

Results comparing the observed and aggregated mean b_{ext}s (based on Equation 17-2) are promising as seen in the scatterplot provide in Figure 17-30. The correlation between the 201 observed and aggregated mean b_{ext} was very high correlation ($r^2 = 0.988$). Estimates of the regression coefficients between the observed and aggregated mean b_{ext}s reveal an intercept value of -0.0012 that is not significantly different from zero ($\alpha = 0.05$). The slope (1.018), however; is significantly different from 1.0, ($\alpha = 0.05$) indicating a slight tendency for these particular episodes to provide an over-estimate of the expected mean b_{ext}. This slight, "apparent" bias is, however, well within the expected variability associated with the particular set of episodes in this stratified sample. To wit, selection of a different random set of episodes would just as likely result in a slight under-estimate of the expected mean b_{ext}.

Perhaps a better way to illustrate the effectiveness of this technique can be shown through an examination of the percent deviation in aggregate estimates of the mean b_{ext} (where the deviations are relative to the observed mean (aggregated b_{ext} - observed b_{ext} / b_{ext} observed). These percent deviations, which were calculated over the period 1984 -1992, are presented in Figure 17-31. For the most part, the deviations are within ± 10%, indicating excellent agreement between the actual mean b_{ext} and the aggregated estimates of the mean b_{ext}.

The slight over prediction tendency mentioned above appears to be somewhat spatially biased as also seen in Figure 17-31. As seen in the top of the figure, areas of generally positive deviations (aggregation approach yields a higher b_{ext}, hence lower visibilities than observed) appear to concentrate from east Texas into the southeastern states and again in the upper midwest between Minnesota and the Dakotas. The states of California and Idaho also exhibit positive deviations. Negative deviations, presented in the bottom of the Figure 17-31, tend to predominate from the northeast states into the Great Lake States and southwestward toward the states of Kansas, New Mexico and Arizona. This spatial dependence of the estimates is, once again, well within the expected variability. Selection of a different random set of episodes would likely result in a different pattern of positive and negative deviations, as there is a natural tendency for sites at close proximity to behave in a similar fashion.

The scatter plot in Figure 17-30 also reveals an increase in variance about the regression line starting at an observed mean b_{ext} of 0.085. Unlike the positive bias, discussed above, this increase in variance does not appear to be spatially biased, but rather exhibits a random distribution across the domain. This is represented in Figure 17-31 by the scattering of the larger biases (i.e. biases > 5.0%) evenly across the domain.

17.7 Summary and Discussion

The objective of this research was to develop a new aggregation approach and set of events to support model-based distributional estimates of air quality parameters (acidic deposition, air concentrations, and measures related to visibility) over the continental domain. The basic approach is to define meteorological categories that account for a significant proportion of the variability exhibited by these air quality parameters, as well as the particular transport mechanisms involved, so that source-attribution analyses are facilitated. This requires that categories be defined with an emphasis on wind flow parameters. To this end, the cluster analysis of zonal u and meridional v wind field components has been used to determine meteorologically representative categories.

The research described in this chapter was carried out in three phases:

- Phase 1: Various stratification schemes were evaluated and compared on different temporal and geographic scales to support the selection of a preferred general methodology. The selected methodology involved clustering of wind field data over the continental domain within each of the four seasons, and defining strata to be equivalent to the resulting clusters. This methodology demonstrated superior relative efficiency compared to methods defined on an annual time frame or on a regional scale for estimates involving the evaluative meteorological parameters, and is designed to support seasonal estimation with both simplicity and precision.
- Phase 2: Determinations were made regarding appropriate numbers of clusters and events to support sampling using the general methodology selected in Phase 1. The resulting scheme involved a total of 20 clusters (5 per season), and 40 events, defined over the time period 1984-1992. This scheme affords superior precision to previous approaches for estimates involving the evaluative meteorological parameters, supports approximately equivalent representation of wet events to those approaches without oversampling, and provides adequate resolution of wind field patterns that characterize transport.
- Phase 3: A stratified sample of events was selected under approximate proportional allocation, using systematic sampling within strata, in accordance with the scheme determined in Phase 2. This sample was successfully evaluated through a comparison of aggregated estimates of the mean b_{ext} to the actual mean b_{ext}, revealing a high level of agreement, although there was a slight tendency of the aggregation and episode selection technique to over-estimate the expected mean b_{ext}.

The goal of this research was to categorize many years worth of meteorological patterns into a few classes. This represents a very ambitious goal, and it should not be surprising that there is substantial variability associated with the wind vectors assigned to individual clusters. Nevertheless, the results described above suggest that the approach achieves a reasonable characterization of frontal passage scenarios and leads to clusters that explain variation in the

evaluative meteorological parameters used in this analysis (temperature, relative humidity, and visibility), and therefore can be used to achieve improved estimates of these parameters relative to estimates obtained from simple random sampling. Moreover, the constrained definition of distinct seasonally-based clusters brings further improvement to the ability of the clusters to explain the variation in these parameters, and therefore leads to more precise estimates associated with them. The evaluative parameters were selected for their known associations with many air quality parameters of interest, thus suggesting that the clusters should also be effective in defining strata from which events can be selected to estimate those air quality parameters.

17.8 References

Brook, J.R., P.J. Samson, and S. Sillman, 1995a. Aggregation of selected three-day periods to estimate annual and seasonal wet deposition totals for sulfate, nitrate, and acidity. Part I: A synoptic and chemical climatology for eastern North America. *Journal of Applied Meteorology*, **34**, 297-325.

Brook, J.R., P.J. Samson, and S. Sillman, 1995b. Aggregation of selected three-day periods to estimate annual and seasonal wet deposition totals for sulfate, nitrate, and acidity. Part II: Selection of events, deposition totals, and source-receptor relationships. *Journal of Applied Meteorology*, **34**, 326-339.

Cochran, W.G., 1977. *Sampling Techniques*. Wiley & Sons, New York.

Davis, R.E. and L.S. Kalkstein, 1990. Development of an automated spatial synoptic climatological classification. *International Journal of Climatology*, **10**, 769-794.

Eder, B. K., J. M. Davis and P. Bloomfield, 1994. An automated classification scheme designed to better elucidate the dependence of ozone on meteorology. *Journal of Applied Meteorology*, **33**, 1182-1199.

Eder, B. K., S.K. LeDuc and F. Vestal, 1996. Aggregation of selected RADM simulations to estimate annual ambient air concentrations of fine particulate matter. Ninth Joint Conference on Applications of Air pollution Meteorology with the A&WMA, Jan.28-Feb. 2, Atlanta, GA.

Eder, B. K. and S.K. LeDuc, 1996. Can selected RADM simulations be aggregated to estimate annual concentrations of fine particulate matter? Proceedings of the International Specialty Conference on the Measurement of Toxic and Related Air Pollutants, May 7 - 9, Research Triangle Park, NC.

Fernau, M.E. and P.J. Samson, 1990a. Use of cluster analysis to define periods of similar meteorology and precipitation chemistry in eastern North America. Part I: Transport patterns. *Journal of Applied Meteorology*, **29**, 735-750.

Fernau, M.E. and P.J. Samson, 1990b. Use of cluster analysis to define periods of similar meteorology and precipitation chemistry in eastern North America. Part II: Precipitation patterns and pollutant deposition. *Journal of Applied Meteorology*, **29**, 751-761.

Kalnay, E., M. Kanamitsu, R. Kistler, W. Collins, D. Deaven, L. Gandin, M. Iredell, S. Saha, G. White, J. Woollen, Y. Zhu, M. Chelliah, W. Ebisuzaki, W. Higgins, J. Janowiak, K. Mo, C. Ropelewski, J. Wang, A. Leetmaa, R. Reynolds, R. Jenne and D. Joseph, 1996. The NCEP/NCAR 40-year reanalysis project. *Bull. Amer. Meteor. Soc.*, **77**, 437-471.

NAPAP, 1991. *National Acid Precipitation Assessment Program 1990 Integrated Assessment Report*, National Acid Precipitation Assessment Program, 722 Jackson Place NW, Washington, D.C.

SAS Institute Inc., 1989. *SAS/STAT® User's Guide, Version 6, Fourth Edition, Volume 1.* SAS Institute Inc., Cary, NC.

Ward, J.H., 1963. Hierarchical grouping to optimize an objective function. *Journal of the American Statistical Association* **58**, 236-244.

This chapter is taken from *Science Algorithms of the EPA Models-3 Community Multiscale Air Quality (CMAQ) Modeling System*, edited by D. W. Byun and J. K. S. Ching, 1999.

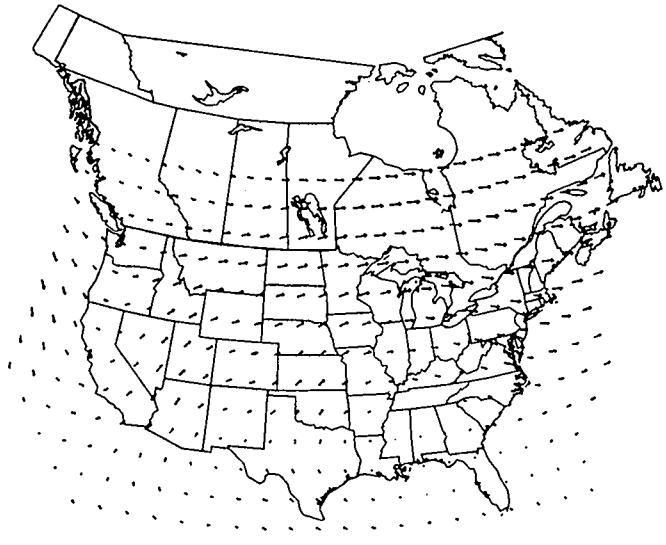

Fig. 17.1 (a) Mean wind vectors for day 1 of annually defined cluster 1 (of 30).

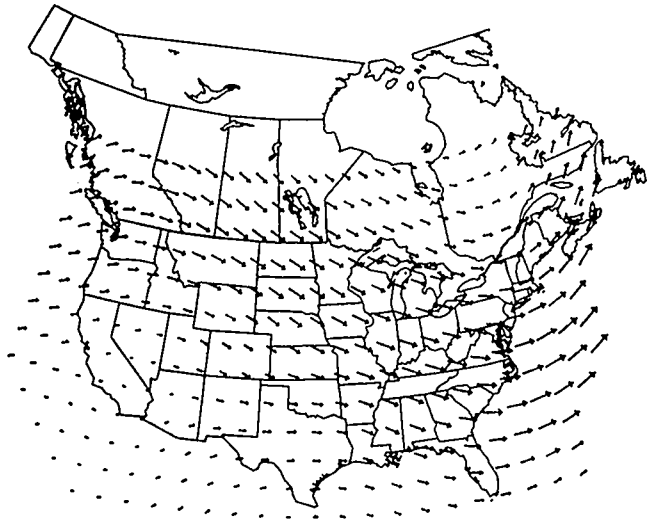

Fig.17.2 (c) Mean wind vectors for day 5 of annually defined cluster 9 (of 30).

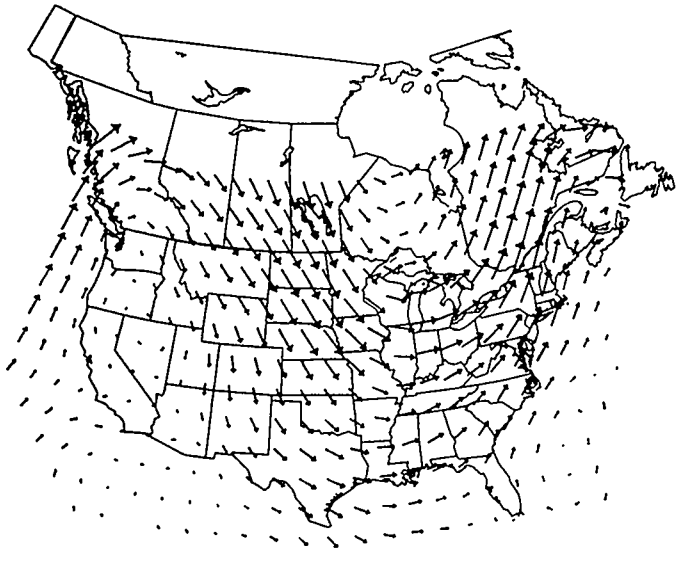

Fig. 17.3 (a) Actual wind vectors for 25 January 1986, day 3 of cluster 9 (of 30).

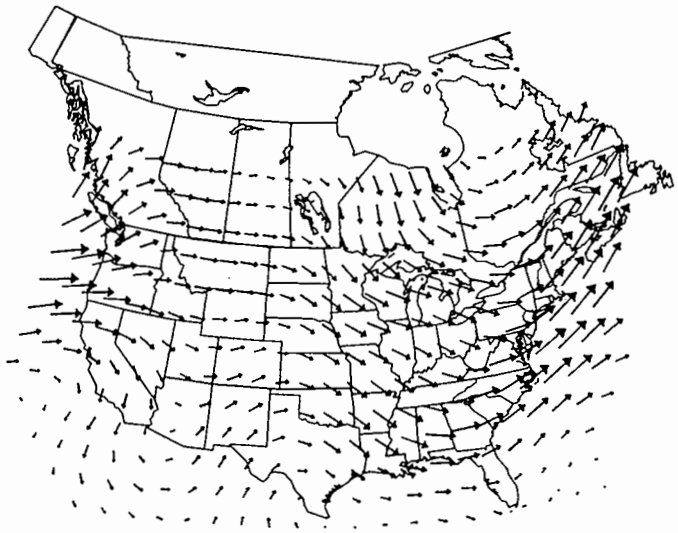

Fig. 17.3 (b) Actual wind vectors for 13 January 1988, day 3 of cluster 9 (of 30).

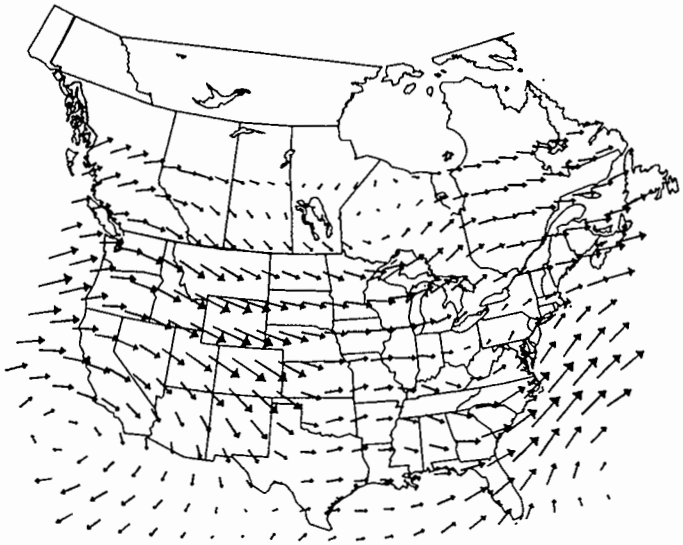

Fig. 17.3 (c) Actual wind vectors for 8 January 1990, day 3 of cluster 9 (of 30).

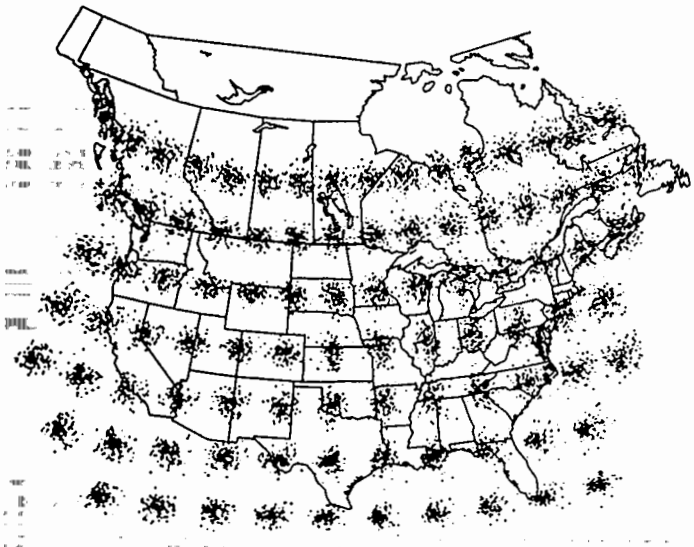

Fig. 17.4 (a) Mean and distribution of wind vectors for day 1 of cluster 9 (of 30).

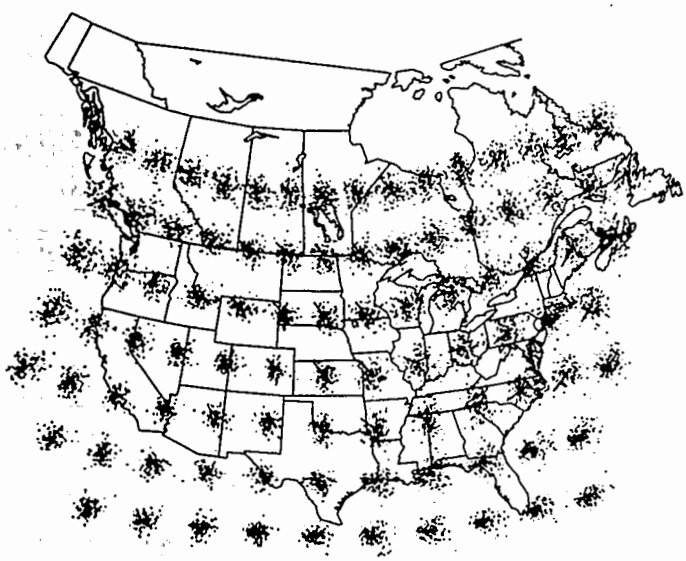

Fig. 17.4 (b) Mean and distribution of wind vectors for day 3 of cluster 9 (of 30).

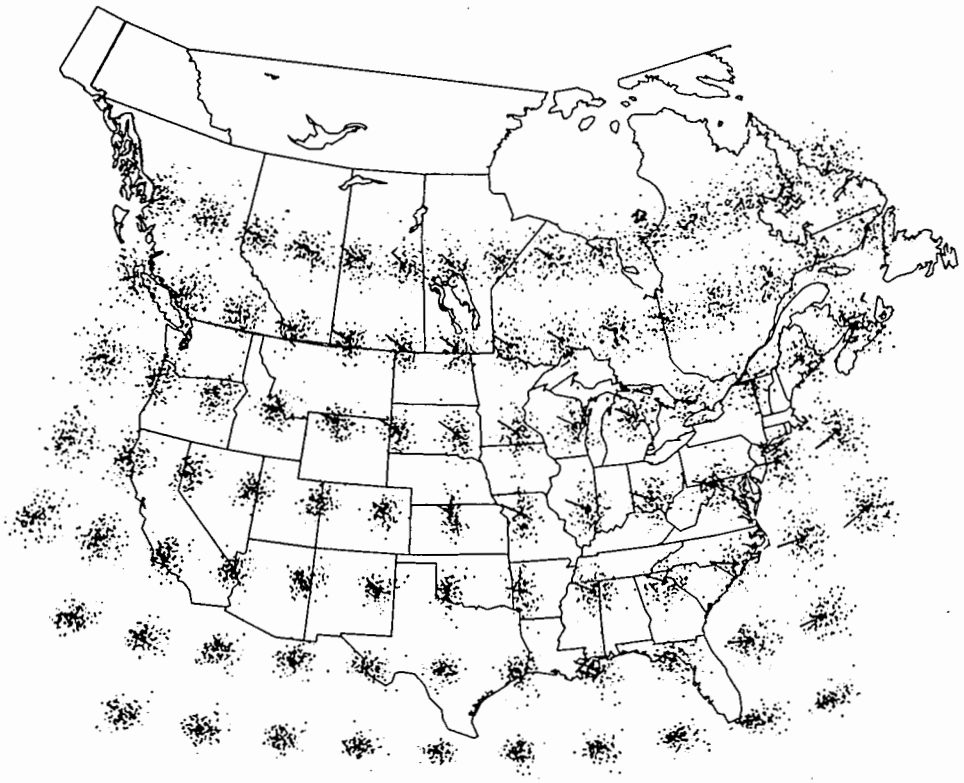

Fig. 17.4 (c) Mean and distribution of wind vectors for day 5 of cluster 9 (of 30).

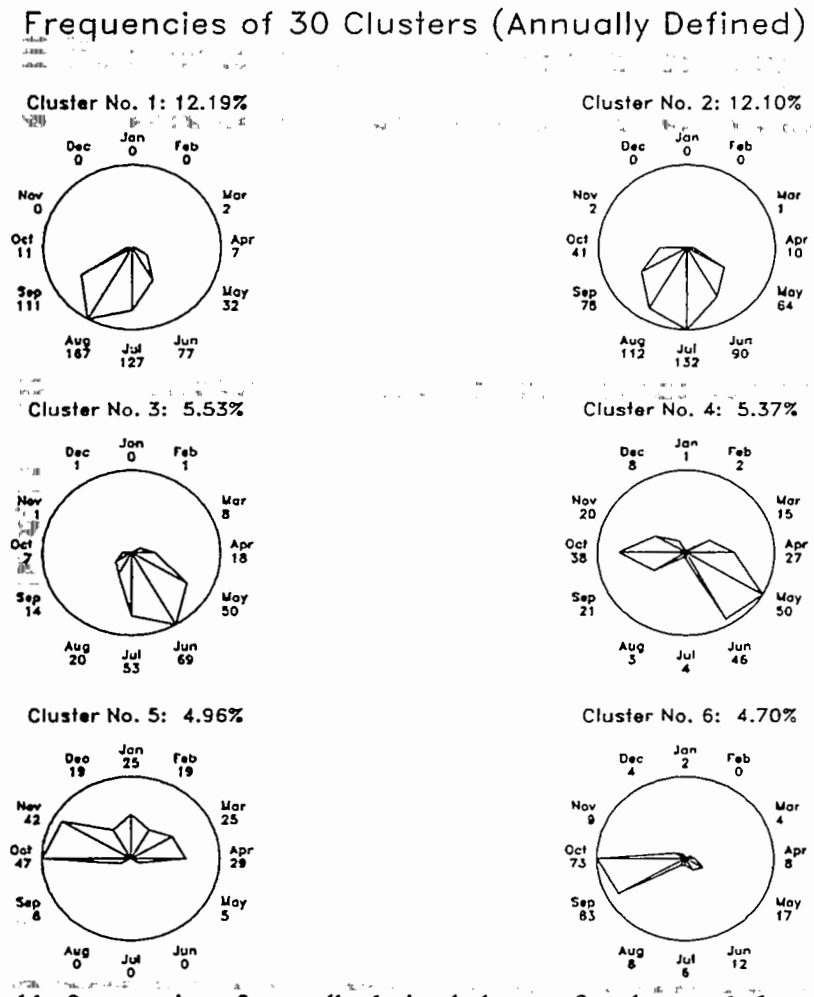

Fig. 17.5 (a) Monthly frequencies of annually derived clusters for clusters 1-6.

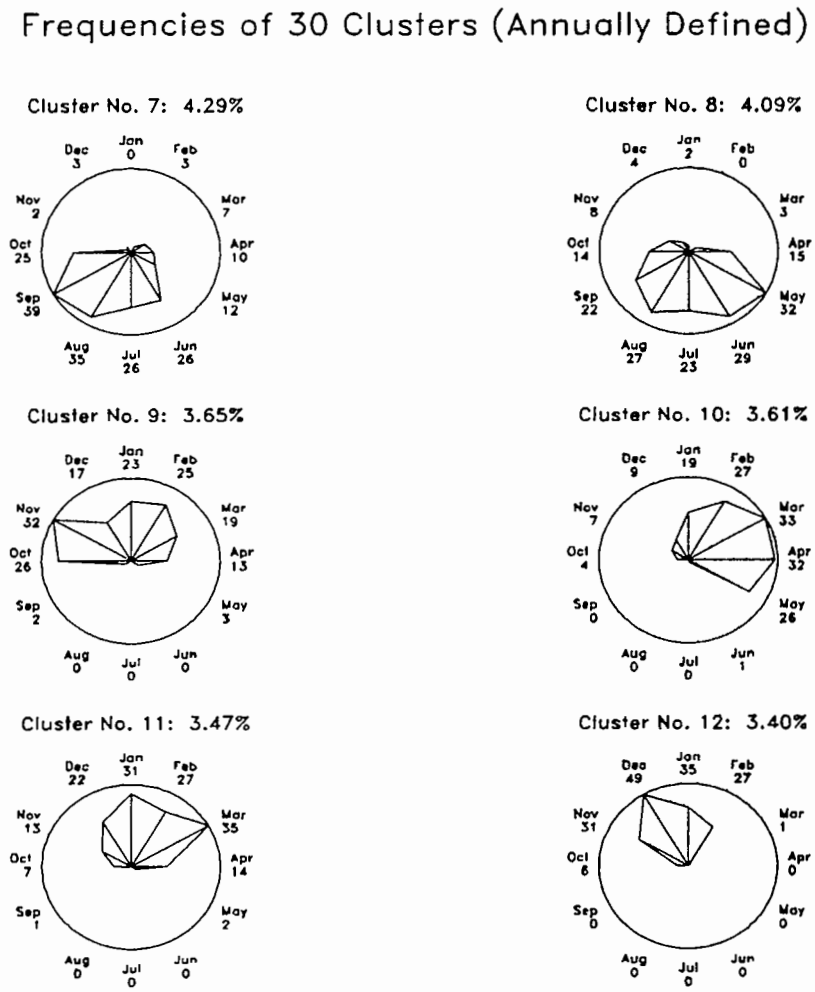

Fig. 17.5 (b) Monthly frequencies of annually derived clusters for clusters 7-12.

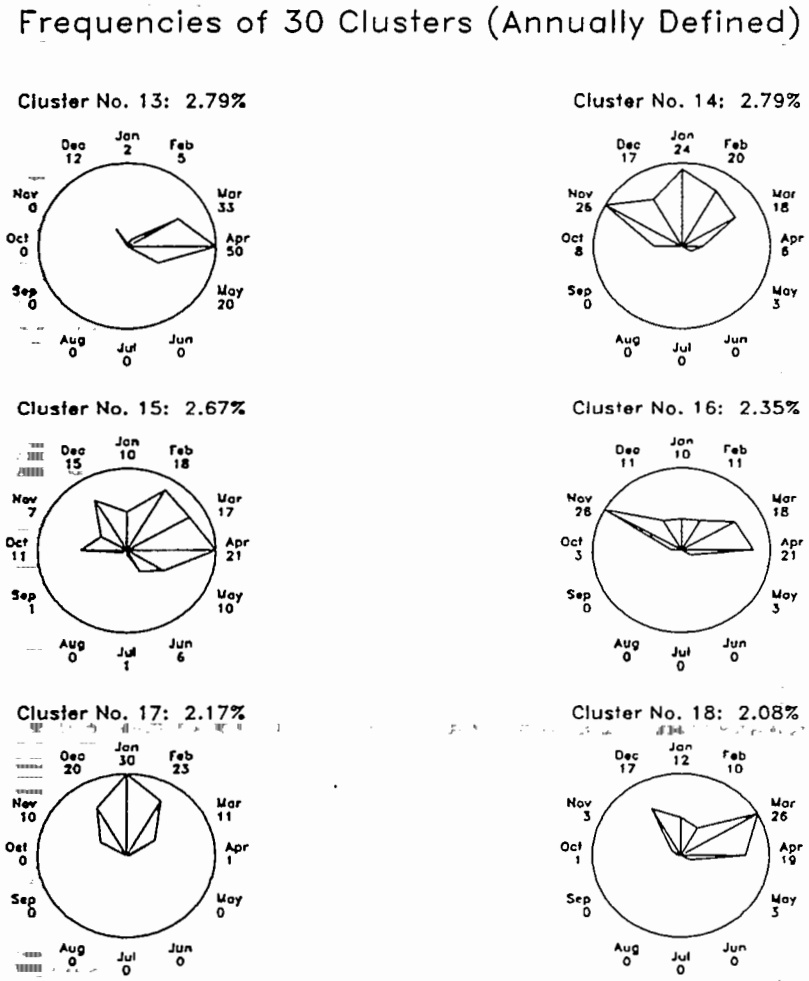

Fig. 17.5 (c) Monthly frequencies of annually derived clusters for clusters 13-18.

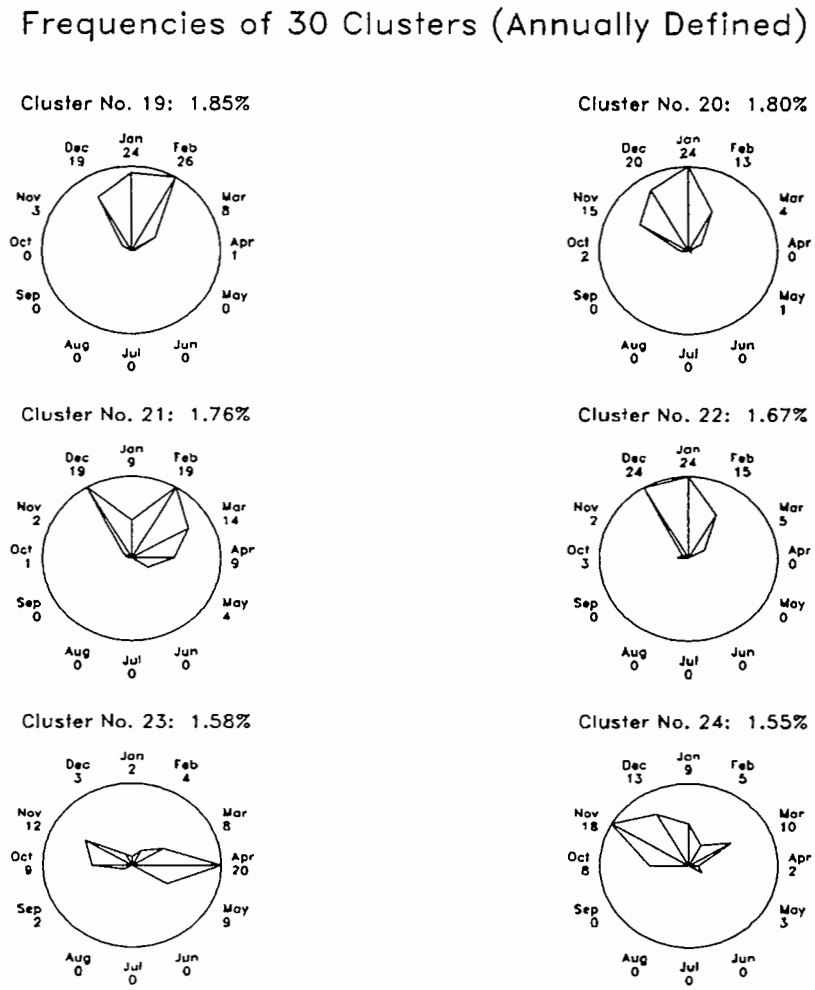

Fig. 17.5 (d) Monthly frequencies of annually derived clusters for clusters 19-24.

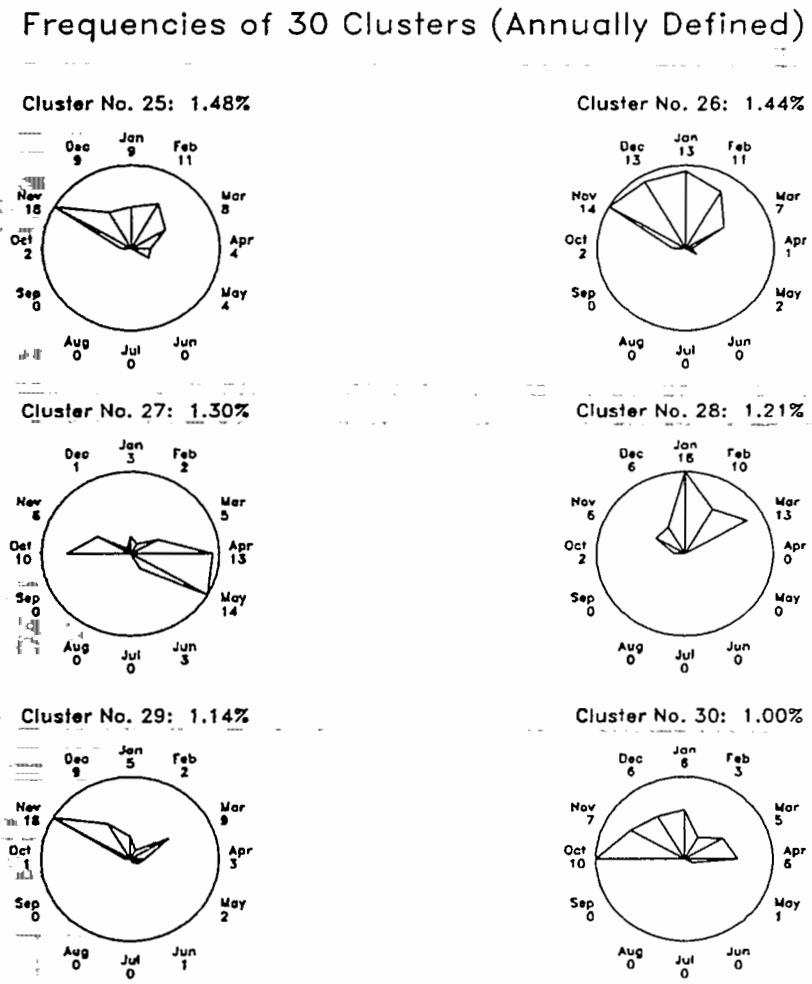

Fig. 17.5 (e) Monthly frequencies of annually derived clusters for clusters 25-30.

Fig. 17.6 Site locations for 201 meteorological parameters used in the evaluation.

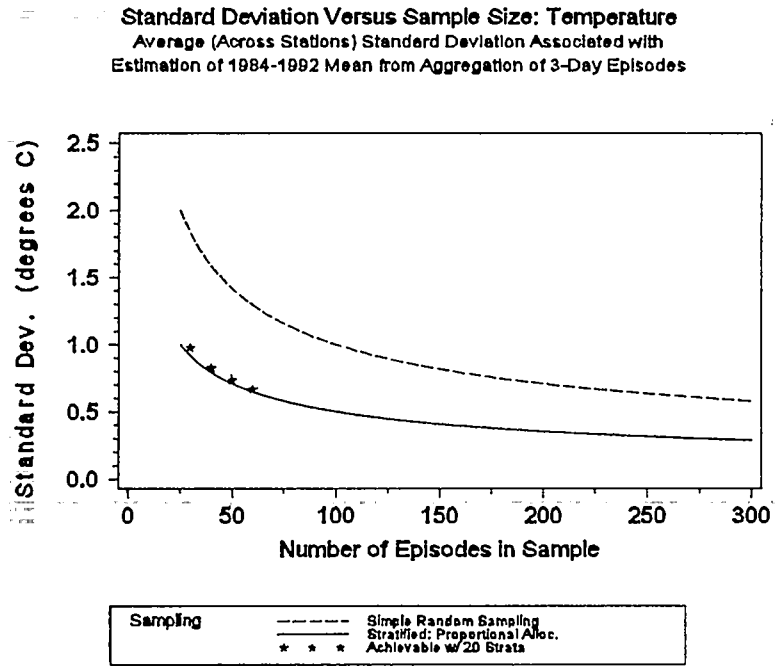

Fig. 17.7 (a) Standard deviation of estimated mean temperature versus sample size.

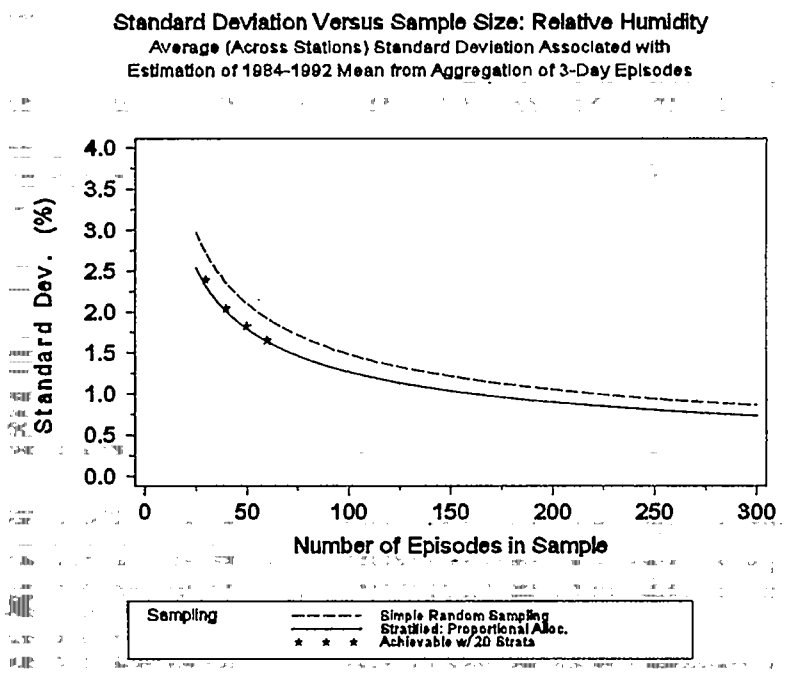

Fig. 17.7 (b) Standard deviation of estimated mean relative humidity versus sample size.

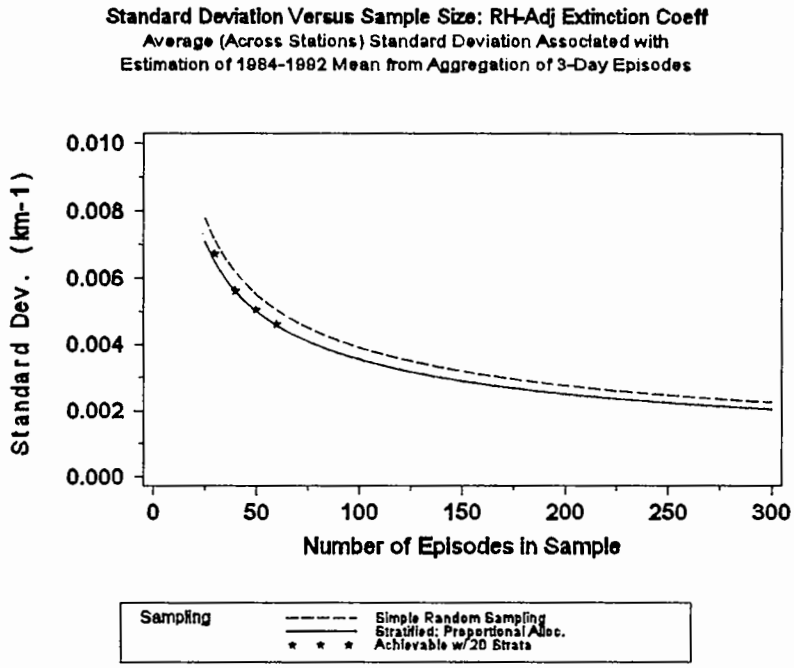

Fig. 17.7 (c) Standard deviation of estimated mean extinction coefficient (adjusted for relative humidity) versus sample size.

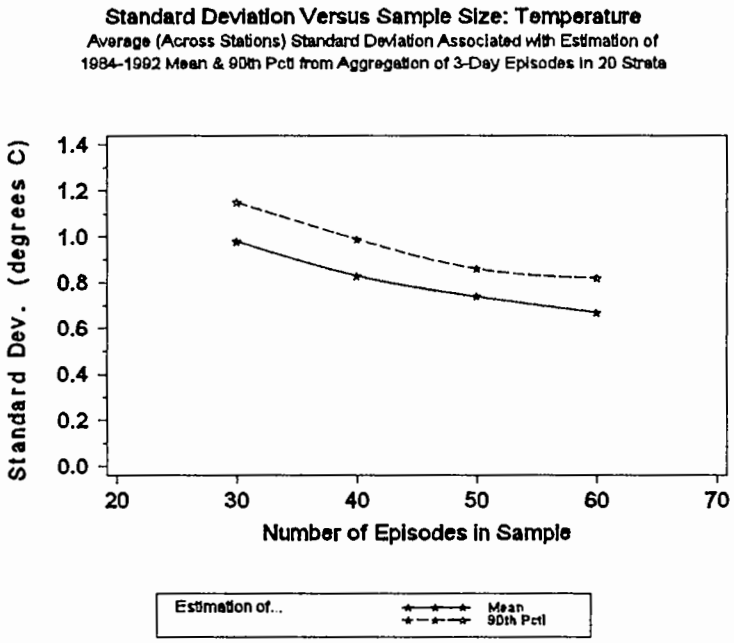

Fig. 17.8 (a) Standard deviation of estimated mean and 90th percentile temperature versus sample size.

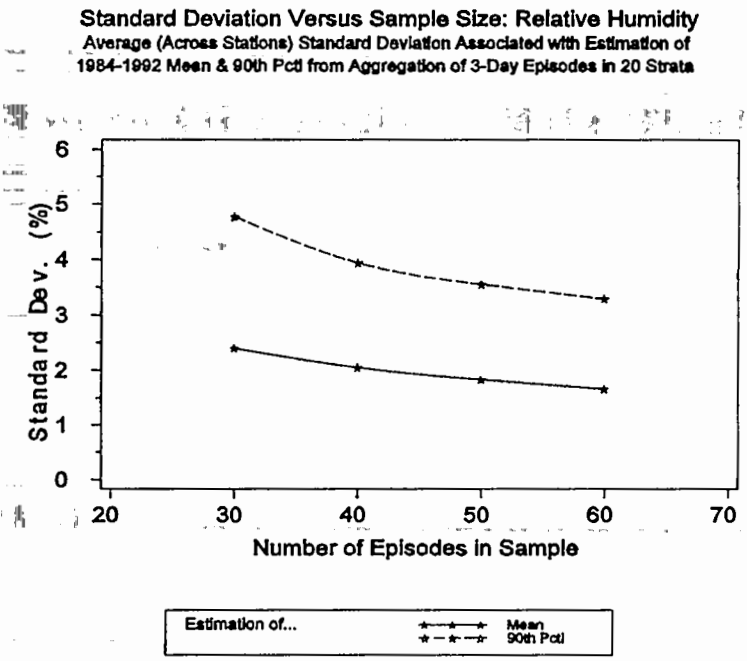

Fig. 17.8 (b) Standard deviation of estimated mean and 90th percentile relative humidity versus sample size.

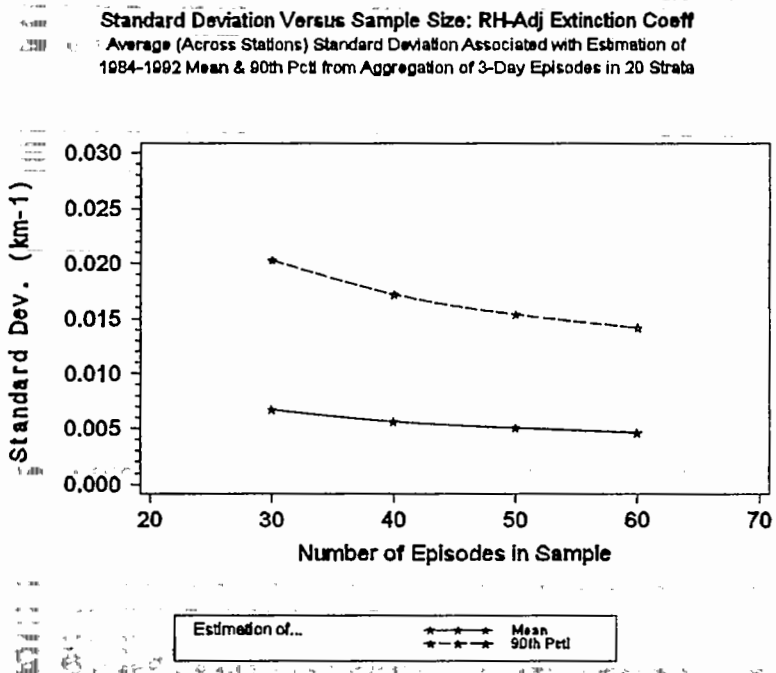

Fig. 17.8 (c) Standard deviation of estimated mean and 90th percentile extinction coefficient (adjusted for relative humidity) versus sample size.

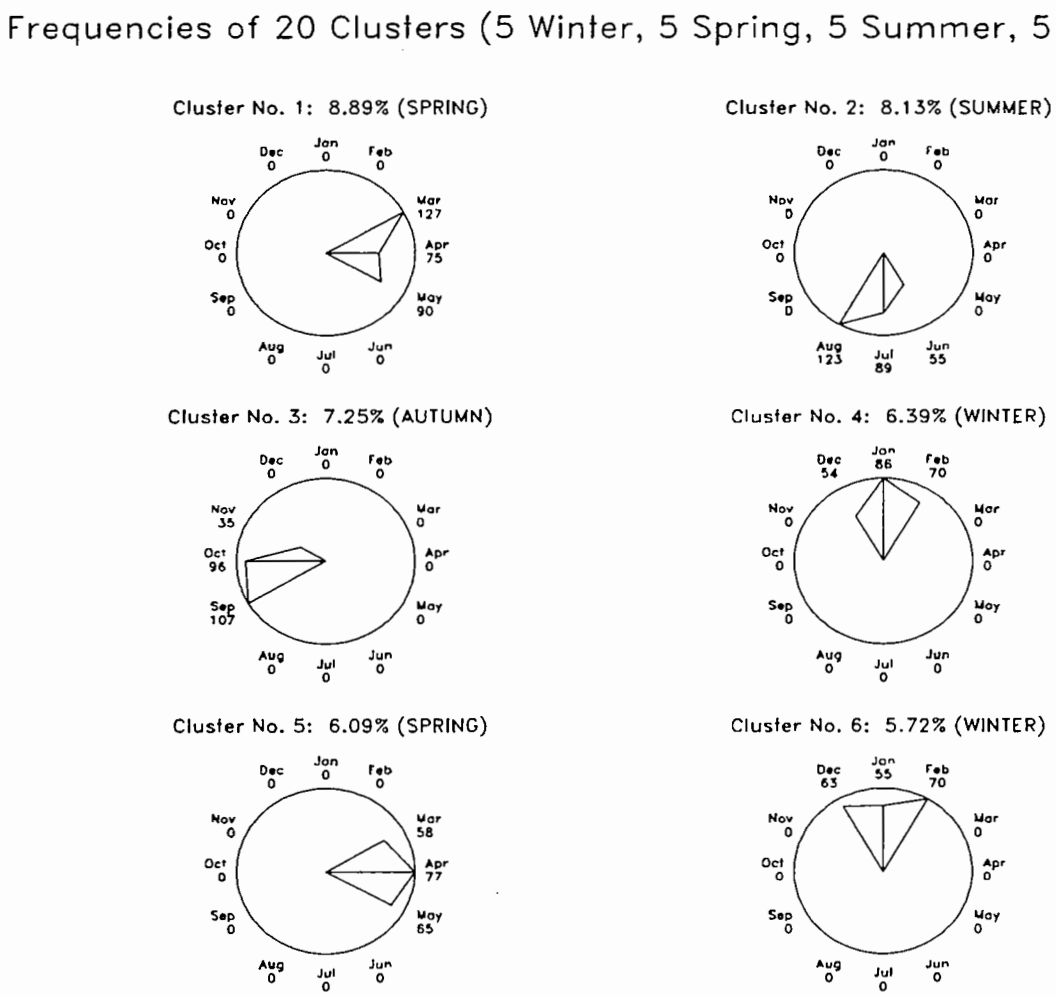

Fig. 17.9 (a) Monthly frequencies of seasonally derived clusters for clusters 1-6.

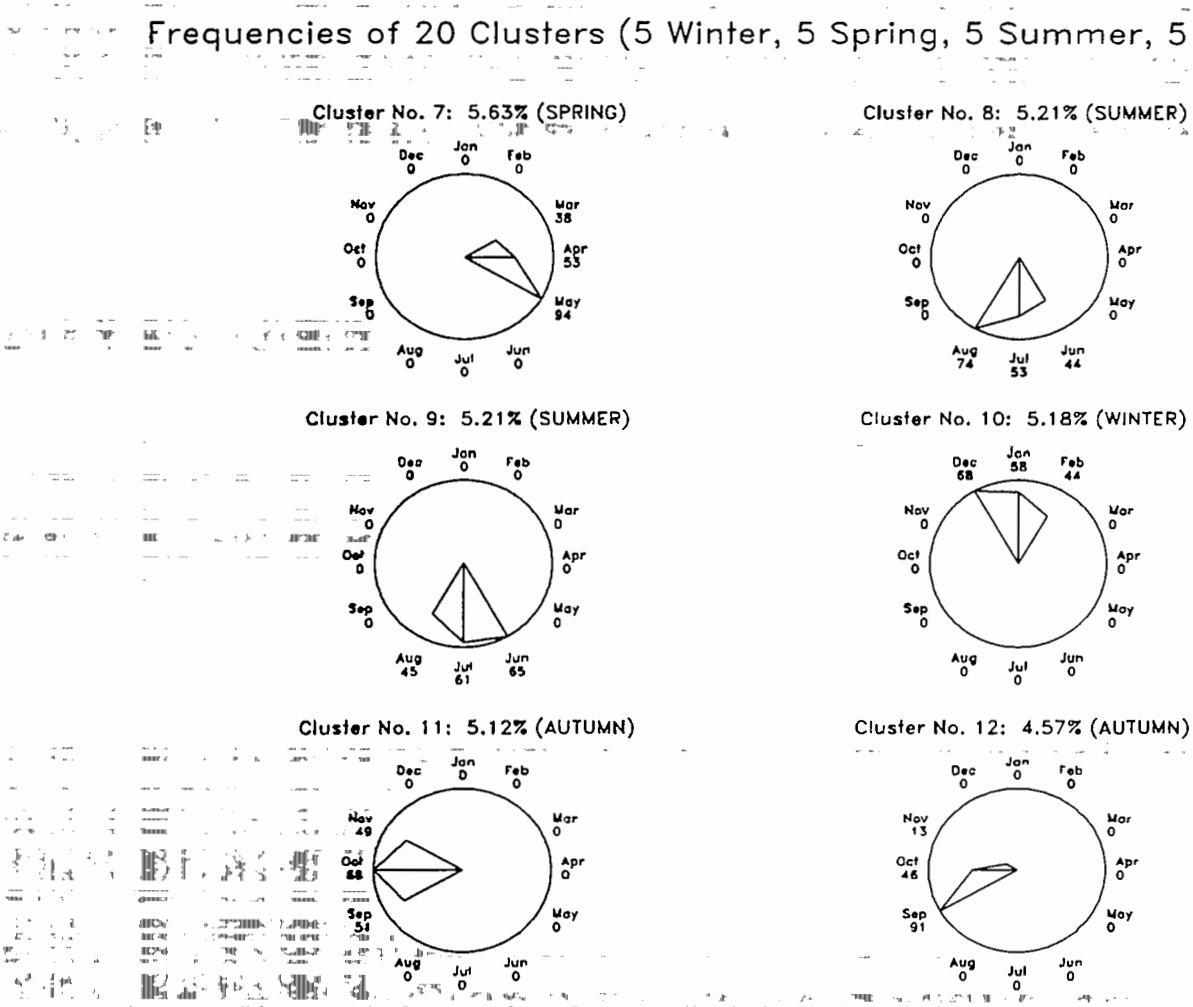

Fig. 17.9 (b) Monthly frequencies of seasonally derived clusters for clusters 7-12.

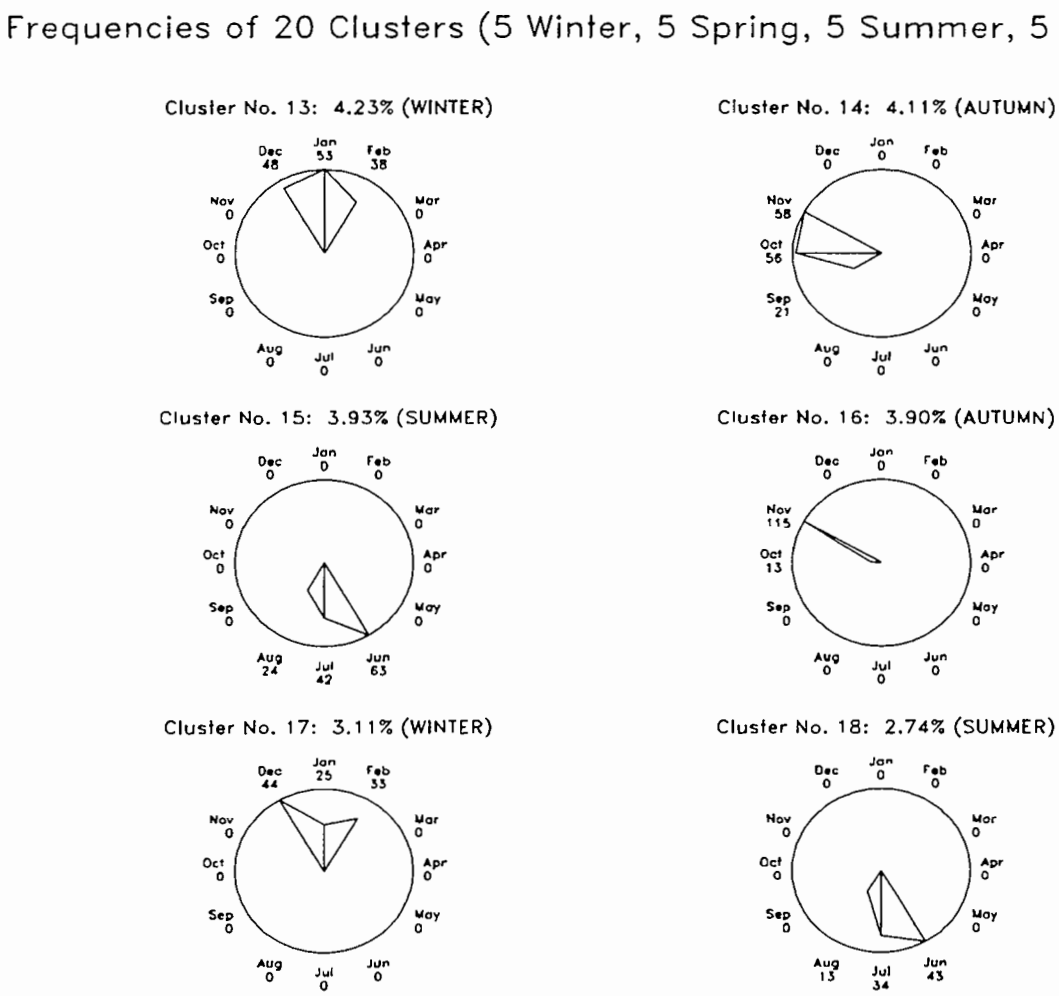

Fig. 17.9 (c) Monthly frequencies of seasonally derived clusters for clusters 13-18.

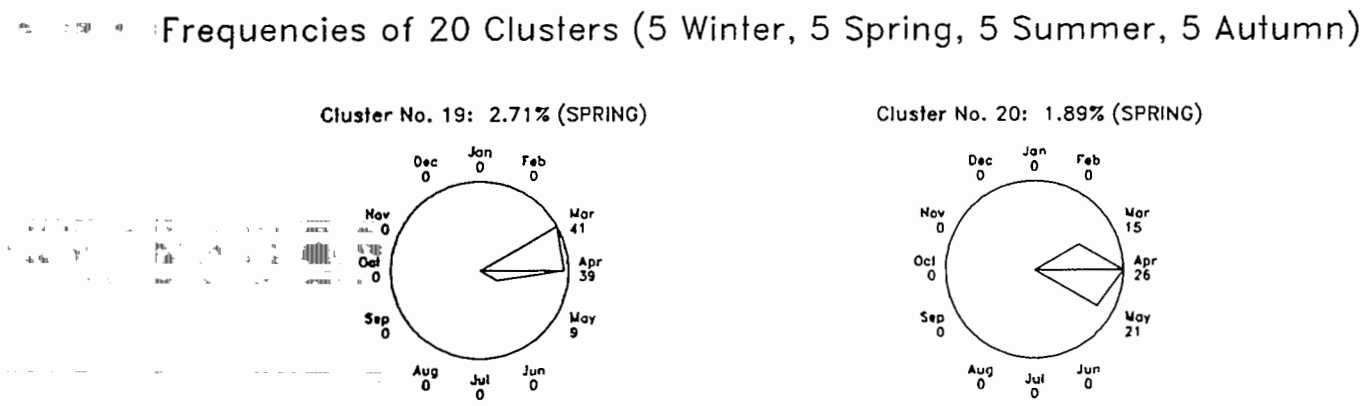

Fig. 17.9 (d) Monthly frequencies of seasonally derived clusters for clusters 19-20.

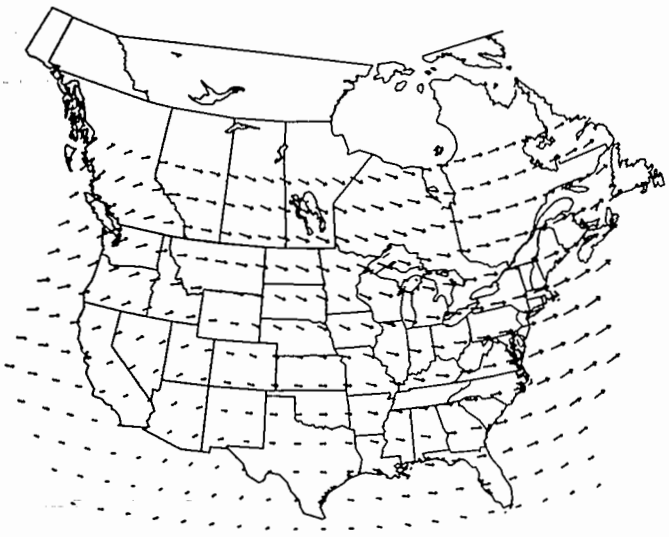

Fig. 17.10 Mean wind vectors for day 3 of seasonally (Spring) defined cluster 1 (of 20).

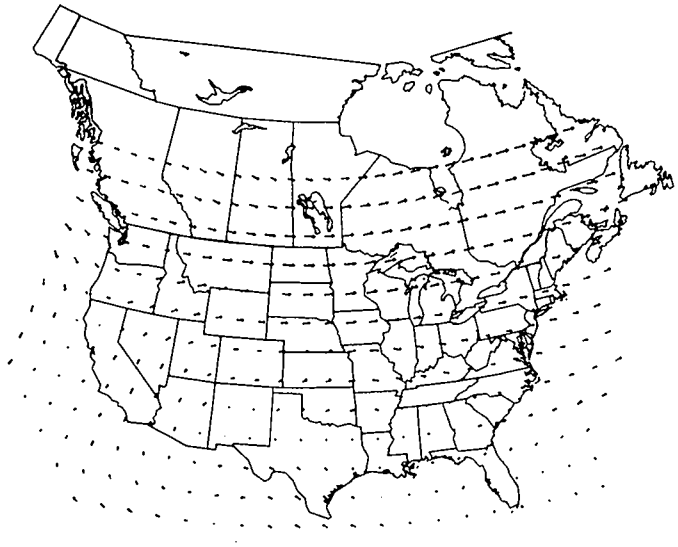

Fig. 17.11 Mean wind vectors for day 3 of seasonally (Summer) defined cluster 2 (of 20).

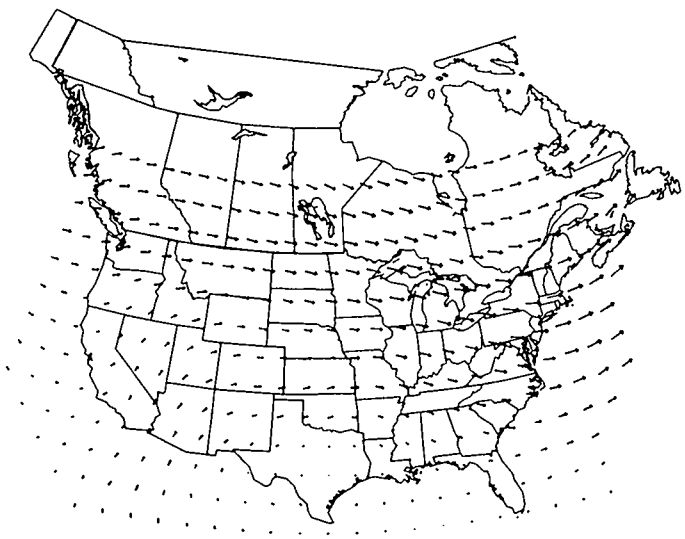

Fig. 17.12 Mean wind vectors for day 3 of seasonally (Autumn) defined cluster 3 (of 20).

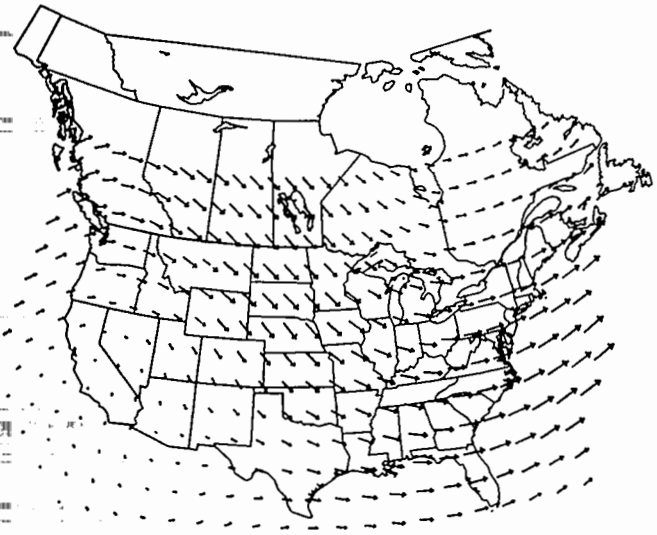

Fig. 17.13 Mean wind vectors for day 3 of seasonally (Winter) defined cluster 4 (of 20).

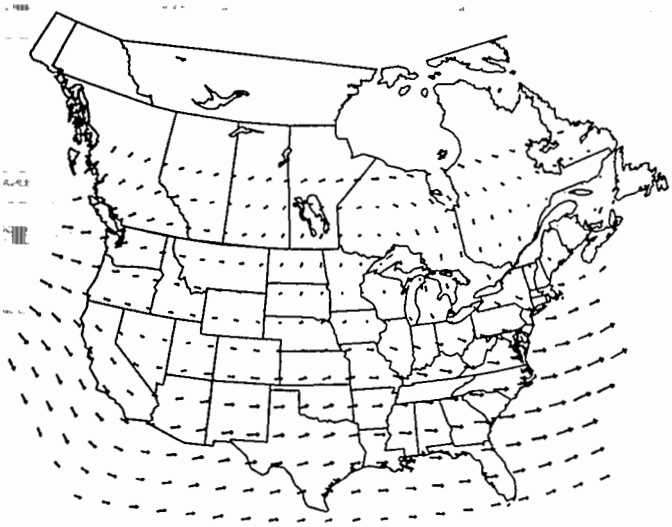

Fig. 17.14 Mean wind vectors for day 3 of seasonally (Spring) defined cluster 5 (of 20).

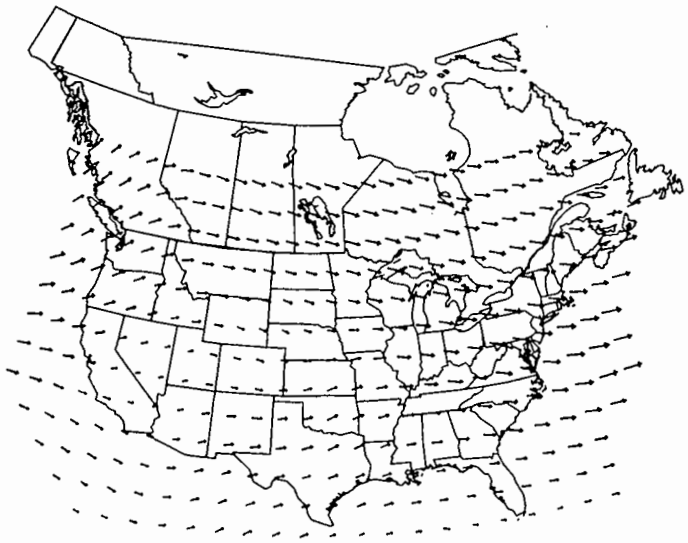

Fig. 17.15 Mean wind vectors for day 3 of seasonally (Winter) defined cluster 6 (of 20).

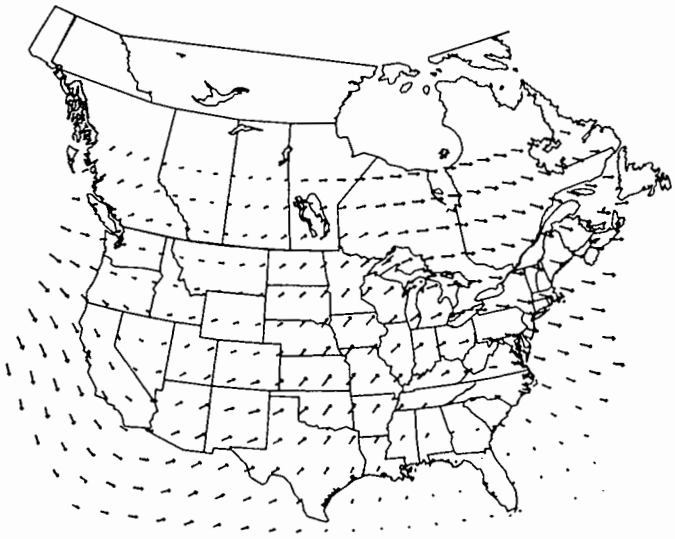

Fig. 17.16 Mean wind vectors for day 3 of seasonally (Spring) defined cluster 7 (of 20).

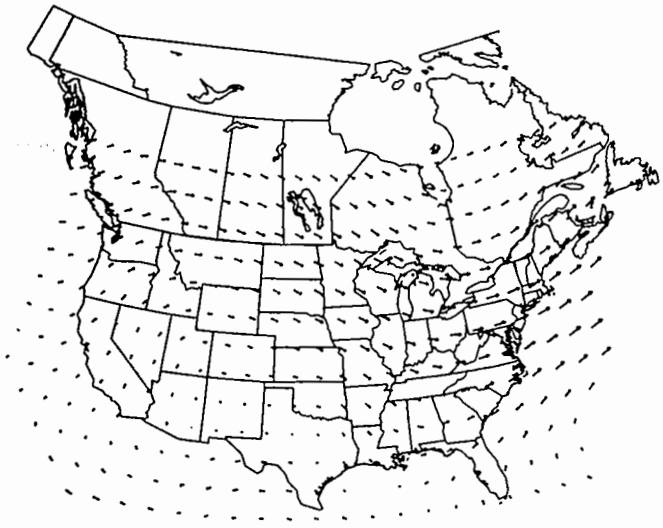

Fig. 17.17 Mean wind vectors for day 3 of seasonally (Summer) defined cluster 8 (of 20).

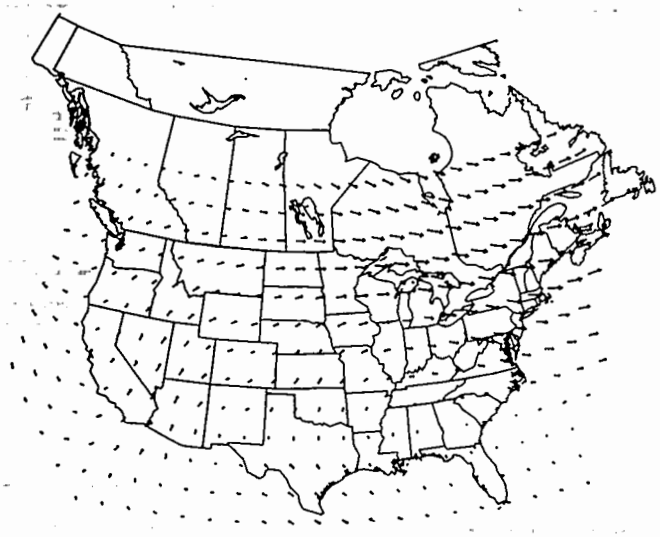

Fig. 17.18 Mean wind vectors for day 3 of seasonally (Summer) defined cluster 9 (of 20).

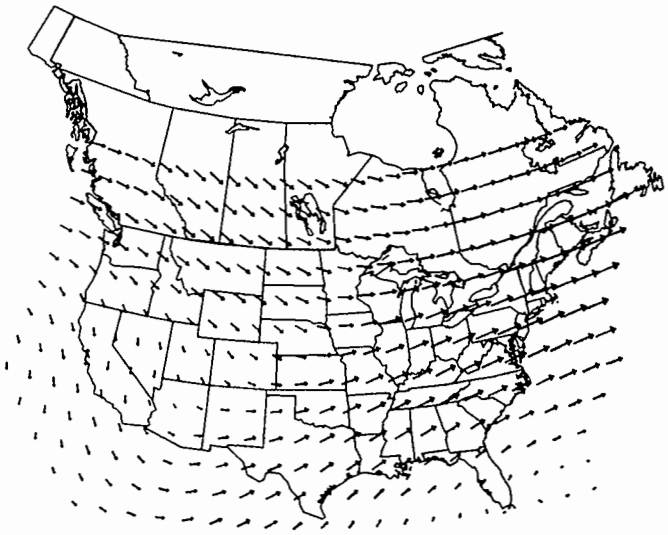

Fig. 17.19 Mean wind vectors for day 3 of seasonally (Winter) defined cluster 10 (of 20).

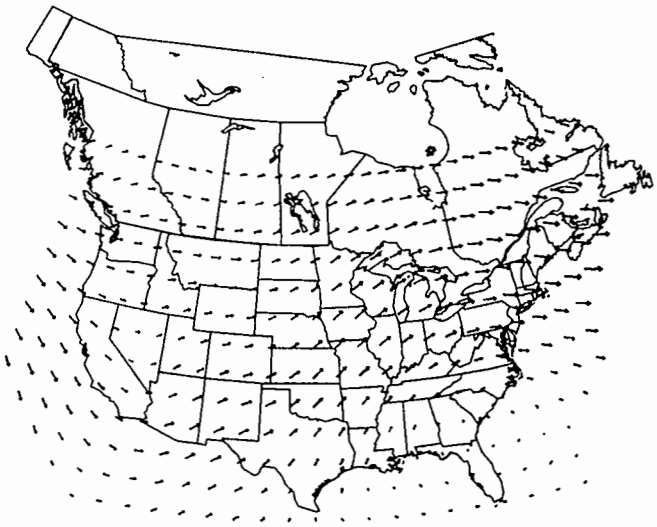

Fig. 17.20 Mean wind vectors for day 3 of seasonally (Autumn) defined cluster 11 (of 20).

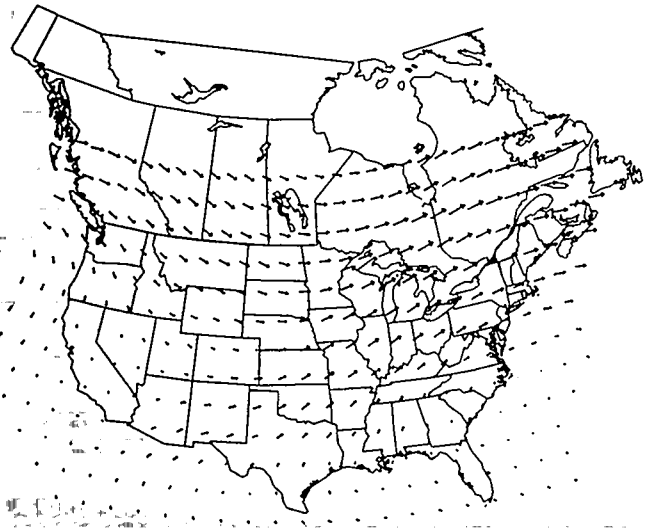

Fig. 17.21 Mean wind vectors for day 3 of seasonally (Autumn) defined cluster 12 (of 20).

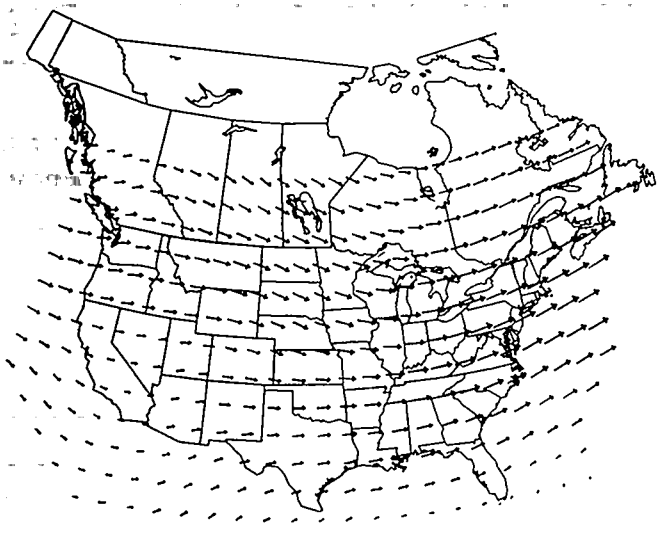

Fig. 17.22 Mean wind vectors for day 3 of seasonally (Winter) defined cluster 13 (of 20).

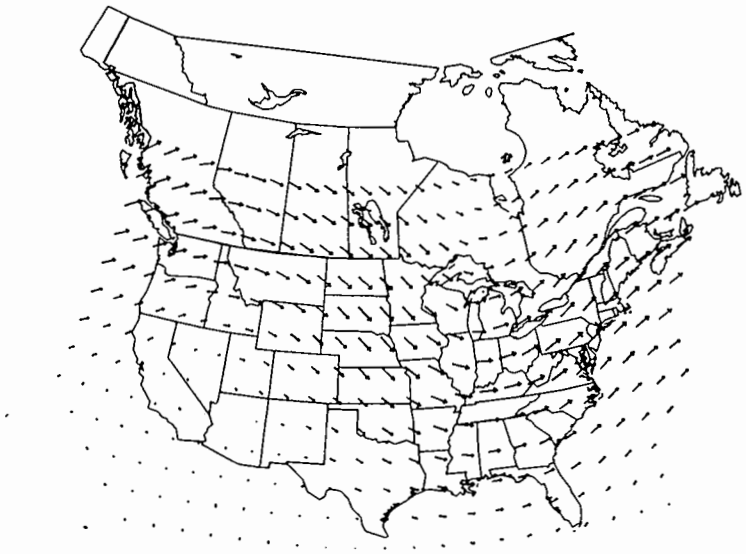

Fig. 17.23 Mean wind vectors for day 3 of seasonally (Autumn) defined cluster 14 (of 20).

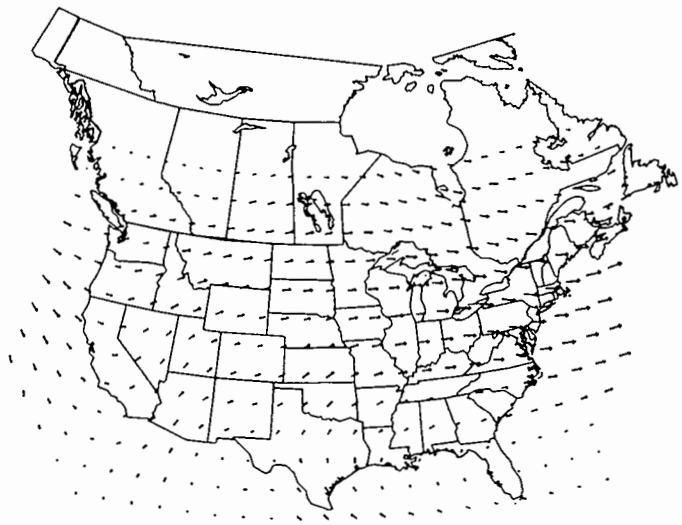

Fig. 17.24 Mean wind vectors for day 3 of seasonally (Summer) defined cluster 15 (of 20).

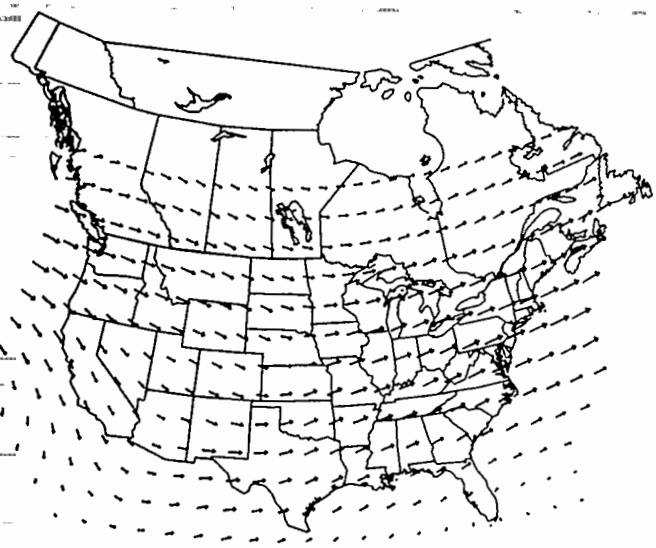

Fig. 17.25 Mean wind vectors for day 3 of seasonally (Autumn) defined cluster 16 (of 20).

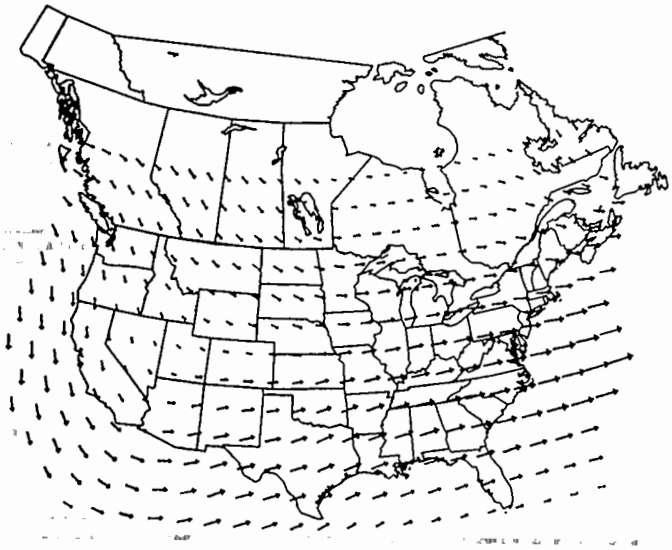

Fig. 17.26 Mean wind vectors for day 3 of seasonally (Winter) defined cluster 17 (of 20).

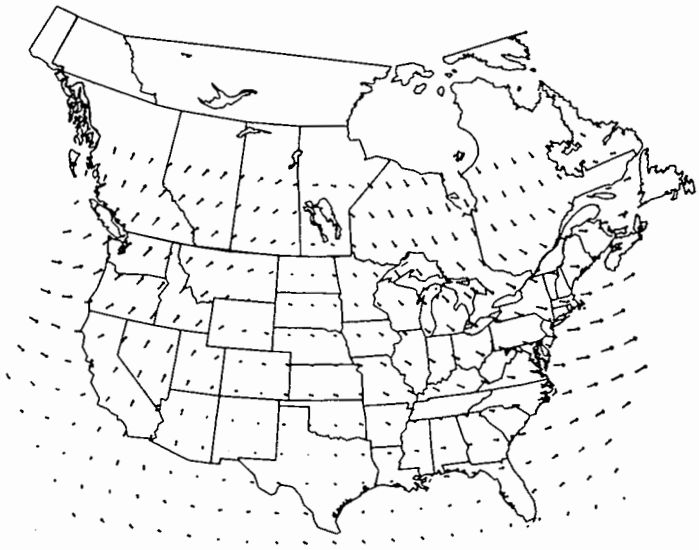

Fig. 17.27 Mean wind vectors for day 3 of seasonally (Summer) defined cluster 18 (of 20).

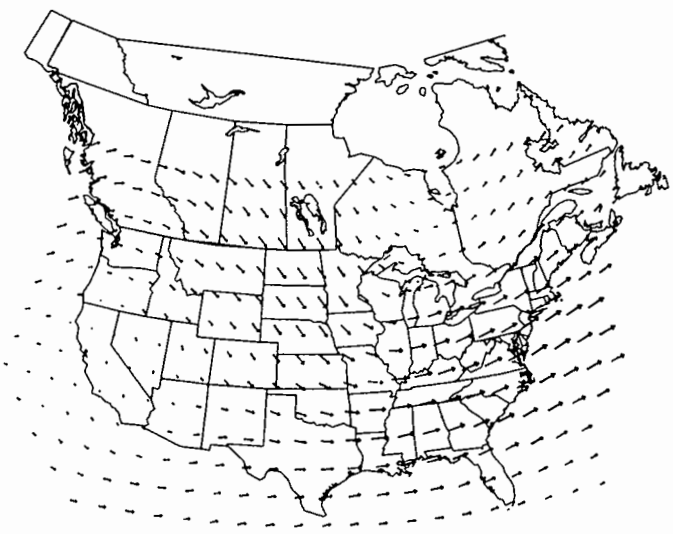

Fig. 17.28 Mean wind vectors for day 3 of seasonally (Spring) defined cluster 19 (of 20).

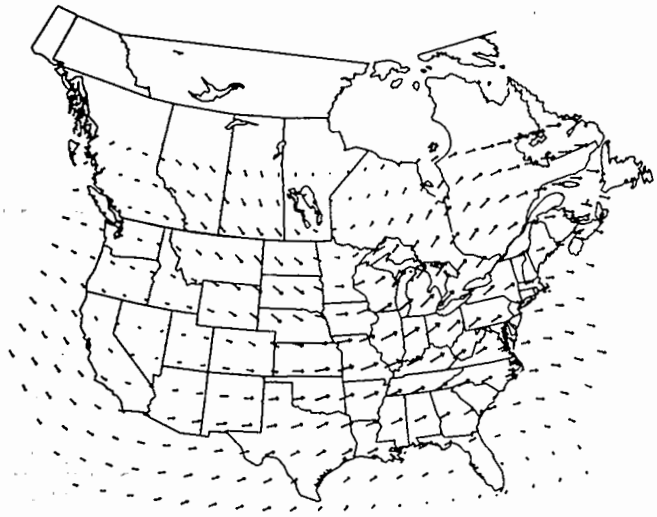

Fig. 17.29 Mean wind vectors for day 3 of seasonally (Spring) defined cluster 20 (of 20).

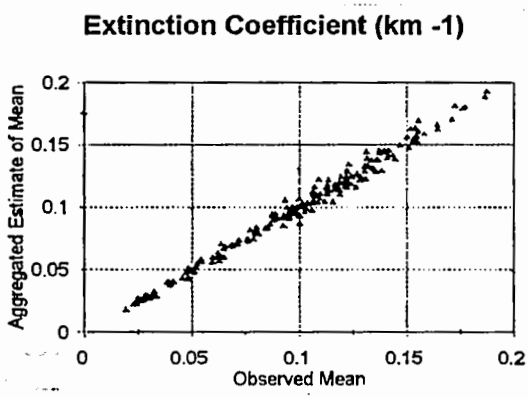

Fig. 17.30 Scatterplot of the observed mean b_{ext} (km^{-1}) versus the aggregated estimate of the mean b_{ext} (km^{-1}) for the period 1984-1992.

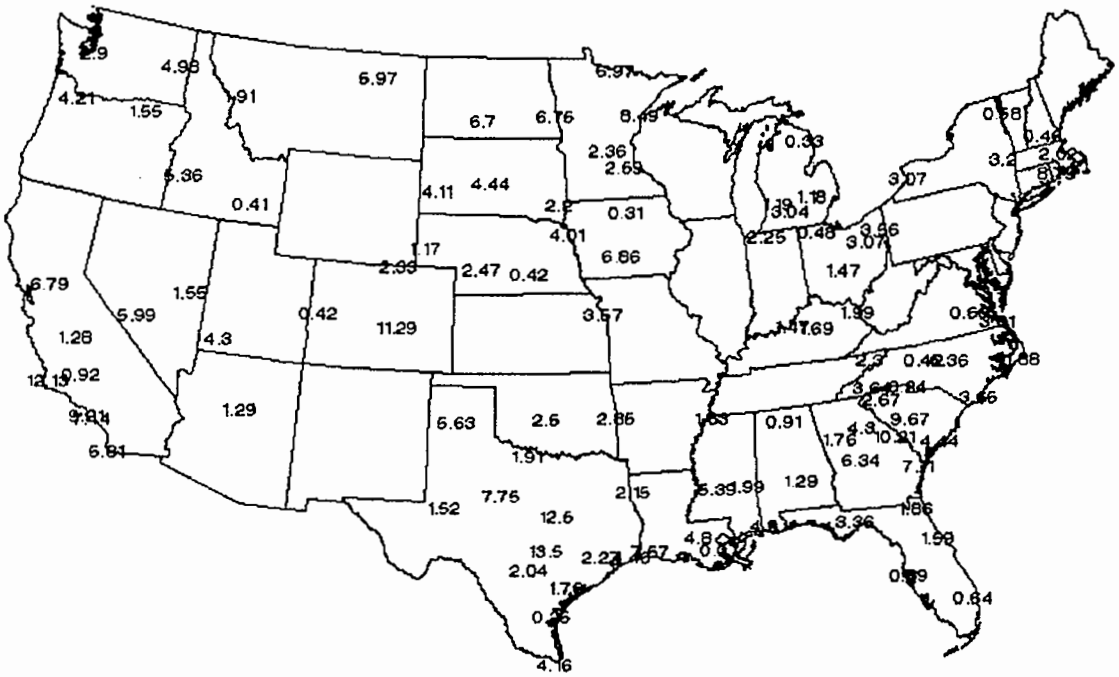

Fig. 17.31 Spatial variation of the bias of the aggregated estimates of the mean bext (km-1) for the period 1984-1992. (Deviations (%) are relative to the observed mean: aggregate-observed/observed). Top figure indicates sites with positive bias, bottom figure sites with negative bias.

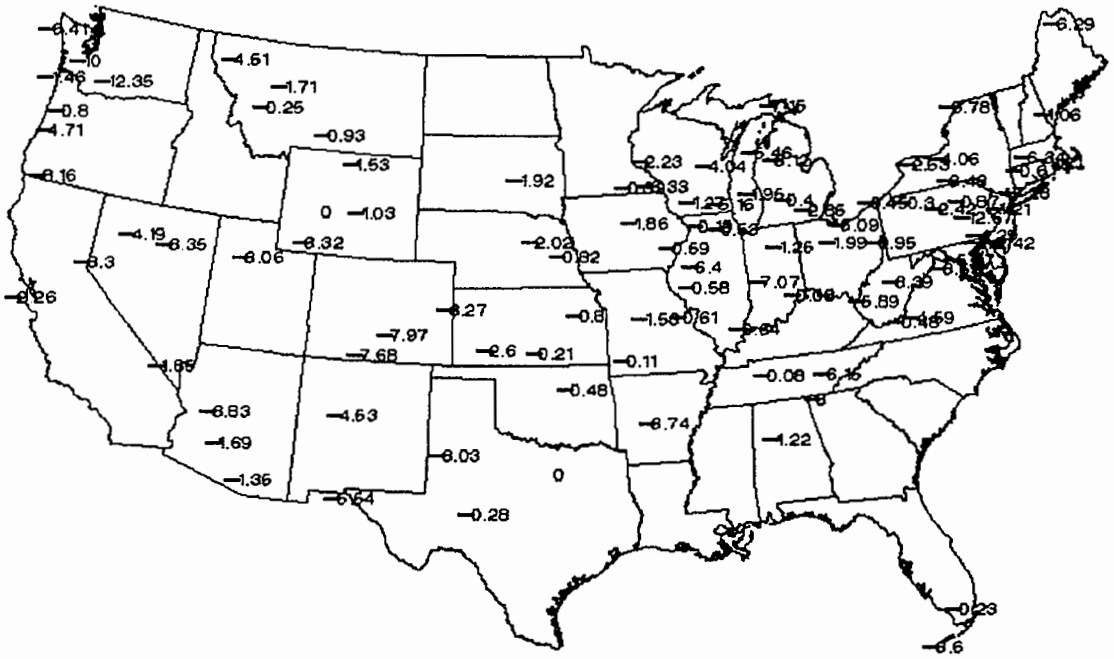

Chapter 18

INTEGRATION OF SCIENCE CODES INTO MODELS-3

Jeffrey Young*
Atmospheric Modeling Division
National Exposure Research Laboratory
U.S. Environmental Protection Agency
Research Triangle Park, NC 27711

ABSTRACT

A complete group of CMAQ science codes has been integrated into the Models-3 system following a set of rules to ensure compatibility and compliance with design principles that enable modularity and flexibility and that allow easy modification and replacement of science process components. This chapter describes the concept of classes and modules, the Models-3 input/output application programming interface, science code configuration management, and model building and execution concepts

*On assignment from the National Oceanic and Atmospheric Administration, U.S. Department of Commerce. Corresponding author address: Jeffrey Young, MD-80, Research Triangle Park, NC 27711. E-mail: yoj@hpcc.epa.gov

18.0 INTEGRATION OF SCIENCE CODES INTO MODELS-3

18.1 Introduction

Integration of the Community Multiscale Air Quality (CMAQ) science into the Models-3 design paradigm takes place at the level of transforming the science, described by systems of partial differential equations, into a discretized and parameterized numerical model. The integral parts that are involved in the process are the coding language (Fortran 77, currently), an operational design, a set of coding rules, computer platforms, model data access methods and storage management, and a public code repository. Models-3 is a user interface system designed to facilitate the development and use of simulation models by scientists, model developers and regulatory users. The Models-3 framework provides a high-performance computational structure for a community modeling system that currently contains distinct emissions, meteorological, and chemical transport air quality models. In this chapter we define a model as a single, complete executable built from a set of compiled subroutines that define either a core environmental simulation model or a processing system that provides data to a simulation model. The framework also links the models to data management tools and analysis/visualization software.

A complete set of CMAQ science codes has been integrated into the Models-3 system. The development and integration of these codes has followed a set of principles relating to design and implementation concepts that are discussed in this chapter.

We have promulgated a small set of software requirements and integration rules related to these concepts so that science codes can be developed that conform to Models-3 requirements. With this approach, the general user community may readily develop and execute models that use the rich and growing base of science codes and data that reside in Models-3. A user may contribute to that base and allow others to integrate his developments by applying these integration rules.

With access to all the released, or publicly available source files, a developer can supplement his own codes and readily develop and test model versions within a highly modularized building environment. On the other hand, people whose primary interest is studying the effects of control strategies or regulatory applications can easily build and execute standard model versions for different emissions scenarios and modeling domains.

The Models-3 and CMAQ systems have been developed to foster community access, and to facilitate the improvement of the CMAQ system over time by the easy inclusion of new scientific models and modules developed by researchers in the larger scientific community.

The CMAQ system contains a number of models needed to carry out an air quality model application. Defining a "model" to be an executable built for a specific application, the codes that make up the model are relatively general. To build a specific model, the user selects a set of fundamental criteria that determine the application, such as the modeling domain, the chemical mechanism, and physical process solvers. The reader is referred to Chapter 15 for details. Defining a generic model as the set of codes from which a particular application can be built, the following generic CMAQ models are currently available in the system:

- **ICON** provides the required initial conditions for a model simulation as concentrations of specified individual chemical species for the complete modeling domain.

- **BCON** provides the needed simulation boundary conditions as concentrations of individual chemical species for the grid cells surrounding the modeling domain.

- **Emissions-Chemistry Interface Processor (ECIP)** transforms emission files produced by the Models-3 Emissions Processing and Projection System (MEPPS) into an hourly, 3-D emissions data file for the CMAQ Chemical Transport Model (CCTM). For a detailed discussion of the MEPPS operations, refer to Chapter 6 of the Models-3 User Manual [6].

- **The Meteorology-Chemistry Interface Processor (MCIP)** interprets the output from a meteorological model, such as the Penn State/NCAR fifth-generation Mesoscale Model (MM5) [8], and prepares the data for use in the CCTM.

- **The Landuse Processor (LUPROC)** provides a high-resolution landuse database for the CMAQ system. For example, MCIP uses the output from LUPROC to obtain surface characteristics for computing dry deposition and other planetary boundary layer parameters.

- **The photolysis model (JPROC)** computes photolytic rate constants (j-values) for the gas-phase chemistry used in the CCTM.

- **The Plume Dynamics Model (PDM)** generates plume dimensions and positions along with other related data for use in applying the plume-in-grid module in a CCTM simulation.

- **The CMAQ Chemical Transport Model (CCTM)** simulates the chemical and physical processes affecting tropospheric pollutants and estimates pollutant concentrations (e.g., ozone, particulate matter ($PM_{2.5}$ and PM_{10}), and carbon monoxide) and acid deposition.

The reader is referred to the Models-3 User Manual [6] for more details and descriptions of the usage of these models.

Each generic model consists of a complete set of codes that can be compiled and linked into different model executables by means of specific user-selected options with regard to groups of code called modules, the horizontal grid and vertical layer domain, the chemical mechanism, the computer platform, and compiling options.

One of the key issues in modeling is the manner in which developers and users must deal with reading, writing and using model data. Models-3 provides a user-friendly Input/Output Applications Programming Interface (I/O API) library [4] that enables a universal approach to managing data across subroutines, models, platforms, and networks.

The organization of the remainder of this chapter is as follows: We discuss the concepts that lead to and the implementation of classes and modules in the next section (18.2). We describe I/O API usage and function in Section 18.3. Code management, an important consideration for complex models, is discussed in Section 18.4. In Section 18.5 we discuss how a model is organized and constructed through Models-3. Issues in regards to executing a particular model are discussed in Section 18.6. Using the Models-3 framework to construct and execute a model

is summarized in Section 18.7. Finally in Section 18.8, we discuss concepts and issues that address Models-3 compliant coding practice and how to ensure code development that is conformant to the Models-3 system.

18.2 Classes and Modules

18.2.1 Operational Design

The design concept of code classes is used to facilitate the plug&play capability in the Models-3/CMAQ system. Science process modules are grouped into classes that are primarily based on the time-splitting paradigm used in a CMAQ Chemical Transport Model (CCTM). Generally each class is associated with a particular science process. A module consists of a complete set of subroutines capable of modifying the concentration field related to the science process associated with the module's class. The CCTM is designed so that each module computes the changes in the concentration field (CGRID) specific to that particular science process. A science module operates on the entire three-dimensional gridded concentration field for a period of time called the synchronization time step interval. The module performs whatever looping over that grid and over whatever internal time steps that are necessary to complete its function.

Table 18-1 lists the classes and associated processes and modules currently available for the CCTM. In building a particular CCTM, one module is selected from each class.

The other CMAQ models (i.e., those other than the CCTM) do not generally follow the time-splitting science process paradigm. However, for convenience and consistency in model building, and for code organization, we have extended the concept of classes and modules to apply to the other CMAQ models. Class and module organizations similar to those in Table 18-1 exist for the other models but are less extensive.

Table 18-1. The Classes, Processes, and Modules Available in CCTM

CLASS	(PROCESS)	MODULES
driver	(Control Model Execution)	ctm
init	(Initialize Model)	init
hadv	(Horizontal Advection)	hbot (Bott's scheme)
		hppm (Piecewise Parabolic Method)
		hadv_noop (no operation)
vadv	(Vertical Advection)	vbot (Bott's scheme)
		vppm (Piecewise Parabolic Method)
		vadv_noop (no operation)
hdiff	(Horizontal Diffusion)	unif (Uniform eddy diffusion)
		hdiff_noop (no operation)
vdiff	(Vertical Diffusion)	eddy (eddy diffusion)
		vdiff_noop (no operation)
adjcon	(Advected Mass Adjustment)	denrate
		adjcon_noop (no operation)
phot	(Photolytic Rate Constants)	phot
		phot_noop (no operation)
chem	(Gas Chemistry Solver)	smvgear (SMVGEAR solver)
		qssa (Vectorized QSSA solver)
		chem_noop (no operation)
aero	(Aerosol Solver)	aero
		aero_noop (no operation)
aero_depv	(Aerosol Dry Deposition)	aero_depv
		aero_depv_noop (no operation)
cloud	(Cloud and Aqueous Chemistry)	cloud_radm (RADM cloud scheme)
		cloud_noop (no operation)
ping	(Plume-in-Grid)	ping_smvgear (uses SMVGEAR solver)
		ping_qssa (uses QSSA solver)
		ping_noop (no operation)
procan	(Process Analysis)	pa
couple	(Couple for Transport)	gencoor
util	(Utility Processing)	util

18.2.2 CGRID

To facilitate the science processing for the different chemistries involved in CMAQ, the concentration field array CGRID, is partitioned into four species classes: gas chemistry, aerosols, non-reactive, and tracer species. This order is mandatory and maintained throughout the processing. A subroutine, CGRID_MAP provides the means to correctly index into the CGRID array for each science process that deals with individual classes of species. The tracer species group is user-determined and may be empty in CGRID. Aqueous chemistry is dealt with solely in the cloud processing, and currently aqueous species are not transported outside of the cloud processing, therefore do not appear explicitly in CGRID. A subroutine call to CGRID_MAP provides pointers to the locations of the species classes within CGRID. A process that deals only with one of the classes (e.g. aerosols) can thus determine which part of CGRID it needs to access.

18.2.3 Class Driver

Generally, each module within a class requires a "class-driver," which is the top level subroutine within the module - it is at the top of the call chain for that module. Exceptions for this paradigm exist for the util, procan, phot, and aero_depv classes. The class-driver presents a fixed name and calling interface to the driver class subroutine SCIPROC that calls all the science process modules. The calling interface consists of a subroutine argument list containing CGRID, the current scenario data and time, and a time step vector. Each class also contains a "no-operation" module, if appropriate. The no-op module has the fixed name and call interface for that class, but performs no calculations. When called, it merely returns control to SCIPROC.

The following algorithm illustrates the processing and call sequence used in a CMAQ model for fractional time steps processed non-symmetrically with respect to the chemistry processes:

```
Load CGRID from initial data; set initial Date/Time
Get the TimeStep vector:   TimeStep[1] = output time interval
                           TimeStep[2] = synchronization time interval
                           TimeStep[3] = horizontal advection time interval
Foreach output_time_step

      Call Couple ( CGRID, Date, Time, TimeStep )*

      Foreach sync_step  [in output time interval]
            Call Horizontal_Advection ( CGRID, Date, Time, TimeStep )
            Call Vertical_Advection   ( CGRID, Date, Time, TimeStep )
            Call Mass_Adjustment      ( CGRID, Date, Time, TimeStep )
            Call Horizontal_diffusion ( CGRID, Date, Time, TimeStep )
            Call De-Couple            ( CGRID, Date, Time, TimeStep )*
            Call Vertical_diffusion   ( CGRID, Date, Time, TimeStep )
            Call Plume_in_Grid        ( CGRID, Date, Time, TimeStep )
            Call Gas_Chemistry        ( CGRID, Date, Time, TimeStep )
            Call Aerosol              ( CGRID, Date, Time, TimeStep )
            Call Cloud                ( CGRID, Date, Time, TimeStep )
            Advance Date/Time by synchronization time interval
            Call Couple               ( CGRID, Date, Time, TimeStep )*
      End Foreach sync_step

      Call De-Couple ( CGRID, Date, Time, TimeStep )*
      Write Concentration File

End Foreach output_time_step
```

* Couple CGRID concentrations with, or de-couple CGRID from the air density x the Jacobian of the computational grid. See Chapter 6 for a complete discussion on the concept.

Not shown in the algorithm are processes that deal with source emissions (in either Vertical_diffusion or Gas_chemistry), dry deposition (in Vertical_diffusion), and wet deposition (in Cloud). Also not shown are calls to process analysis routines after each science process, which compute the integrated process rates for that particular process. Such calls are also embedded in science process modules that affect CGRID, such as emissions injection in either the vertical diffusion process or gas chemistry. The Science Process Code Template in Section 18.8.3 below illustrates how these calls can be integrated within a module.

In order to maintain the Models-3/CMAQ modularity and data-independence, the science process class-drivers must adhere to coding standards with regard to the calling interface, file data I/O, and standardized, uniform domain and mechanism data within global include files. See Section 18.5, below, and Chapter 15 for a more complete discussion on the use of global include files. These coding standards have not been propagated to the level below the class-driver. At the sub-module level there are no strict I/O or coding standards, however we offer suggestions to facilitate the potential incorporation of a module into the Models-3 system in Section 18.8 below.

18.2.4 Synchronization Time Step

There are many different time scales that are important in modeling. The CCTM deals with four levels of time stepping:

1. **Output time step** - the time interval for which output data is written to disk.

2. **Synchronization time step** - the time interval for which the science processes, represented by science modules, are considered to run independently of the other processes. This is the time interval during which no interaction with the other time-split science processes needs to take place.

3. **Advection time step** - the time interval over which horizontal advection occurs. It may be less than or the same as the synchronization time interval.

4. **Local or internal time looping** - a possibly variable time interval that subdivides the synchronization time step and is dependent on the user's implementation of a particular algorithm.

There may also be some science processes that don't fit into this type of time scale hierarchy. The sub-grid cloud time step in CCTM for example, has a fixed lifetime that may span the synchronization time interval.

In the CCTM the synchronization time step is essentially the time interval over which the chemistry processes are considered to be time-split and independent of the other processes.

The proper relationship between the first three time steps listed above is determined by the "ADVSTEP" algorithm. Based on a user-supplied output time step interval, and optionally an upper and lower limit for the synchronization time step interval,[1] the algorithm:

- Ensures the synchronization time interval evenly divides the output time interval.

- Ensures the synchronization interval to not be greater than the upper limit.

- Determines a horizontal advection time interval that ensures all horizontal advection calculations satisfy a Courant condition with respect to the horizontal winds for each output time step. See Chapter 7 for details about the Courant condition requirement.

[1]If these limits are not specified, the algorithm uses defaults of 900 and 300 seconds, respectively.

- Attempts to establish a horizontal advection time interval as close to the synchronization interval as possible, but evenly divides the synchronization interval.

- In case the Courant condition restriction forces an advection time interval to be less than the lower synchronization interval limit, sets advection time intervals to be as close to the lower limit as possible but still evenly divide[2] the lower limit.

- If none of these criteria can be satisfied, reports the issue and aborts the execution.

18.3 Input/Output Applications Programming Interface

A model needs access to external data. Data access, including output to external files, is done at the module level. The Models-3 I/O API [4] provides a standardized interface to external data that enables a user to follow the object oriented design concept of *encapsulation*. For example, all basic and some derived meteorological data are calculated outside the CCTM (see MCIP documentation in Chapter 12, e.g.) and available to a module through calls to the Models-3 I/O API library [4]. Thus the user can avoid the re-calculation of various meteorological variables within subroutines using different algorithms and parameterizations to re-compute essentially the same quantities, which may give rise to errors and modeling inconsistencies. It is expected that the modules treat these I/O API data completely independently, not knowing or caring if files have been opened or read by any other module. In particular, any subroutine within a module can open an I/O API file. It is recommended that at least one routine within a module, preferably the class-driver, should open any I/O API files that are required in the module.

In general, the I/O API provides the Models-3 user with a library containing both Fortran and C routines, which manage all the necessary file manipulations for data storage and access. The main requirement is that the user follows the I/O API conventions for data structures, naming conventions, and representations of scenario date and time. The I/O API routines manage access to the files in such a manner that data can be read or written flexibly, virtually in any order, and freeing the user from being concerned with low level file manipulation details, such as the order or format of file variables.

In addition, the I/O API routines can be used for both file storage and cross-media model coupling using Parallel Virtual Machine (PVM) mailboxes.

For file storage and access, the I/O API, which is the standard data access library for Models-3, is built on top of NCAR's netCDF files [5]. NetCDF (network Common Data Form) is a library that provides an interface for array-oriented data access. The netCDF library also defines a machine-independent format for representing scientific data. Together, the interface, library, and format support the creation, access, and sharing of scientific data. The netCDF software was developed at the Unidata Program Center in Boulder, Colorado. The freely available source can be obtained by anonymous FTP [5].

The I/O API provides a variety of data structure types for organizing the data, and a set of access routines that offer selective direct access to the data in terms meaningful to the user.

[2]Strictly speaking, this means divides without remainder, not by a factor of two.

Since they are netCDF files, I/O API files share the following characteristics:

1. They are machine-independent and network-transparent. Files created on a Cray Supercomputer can be read on a desktop workstation (or vice versa) either via NFS mounting or FTP, with no data format translation necessary;

2. They are self-describing. That is, they contain headers that provide a complete set of information necessary to use and interpret the data they contain;

3. They are direct access. A small subset of a large dataset may be accessed efficiently without first reading through all the preceding data. This feature is mandatory in visualization requiring rapid access of large datasets;

4. They are appendable. Data can be appended to a netCDF dataset along one dimension without copying the dataset or redefining its structure. For example, the I/O API can add more time step data to a previously created file; and

5. They are sharable. One writer and multiple readers may simultaneously access the same netCDF file. This means, for example, that visualization tools can access the file and display data while the file is being created by the model.

The I/O API has been designed to support a variety of data types used in the environmental sciences, among them:

- Gridded data (e.g., concentration or meteorological fields);
- Grid-boundary data (for model boundary conditions);
- Scattered data (e.g., meteorology observations or source level emissions); and
- Sparse matrix data (a specialized data type used in an emissions model).

I/O API files support three different time step structures:

1. Time-stepped with regular time steps (e.g. hourly model output concentration fields or twice-daily upper air meteorology observation profiles);

2. Time-independent (e.g. terrain height); and

3. Restart, which always maintains the last two time step records of output from a running process as "even" and "odd." The "odd" is available for restart in case of a crash while the "even" step is being written, and vice versa. Restart data does not consume an inordinate amount of disk space with only two time steps worth of data at all times.

The I/O API provides automated built-in mechanisms to support production and application requirements for dataset histories and audit trails:

- Identifiers of the program execution that produced the file.

- Description of the study scenario in which the file was generated.

The I/O API also contains an extensive set of utility routines for manipulating dates and times, performing coordinate conversions, storing and recalling grid definitions, sparse matrix arithmetic, etc. There are a variety of related programs that perform various analysis or data-manipulation tasks, including statistical analysis, file comparison, and data extraction. Section 18.8.3 below illustrates the use of some of these utilities in coding practice, and the web site [5] provides background materials, a user manual, and a tutorial.

18.4 Code Configuration Management

18.4.1 The Need

Faced with a large and growing community that uses and develops a wide variety of programs, modules and codes, it is imperative to systematically manage the cross-community access to this software. Typically, successful management of software involves:

- A repository - a place where all of the public code resides;
- The concept of archived code - codes that have been deposited into the repository in such a manner that anyone can extract the exact code at a later time. This involves some kind of transformation program to maintain master copies of the codes with embedded change tables;
- The concept of revision control - archiving codes results in modifying the tags or unique revision identifiers in the change tables in the master copies in order to recover the exact code at a later date; and
- The concept of released code - codes that have reached some state of maturity and have been designated with some kind of "released" status. They can be used with reasonable expectation of reliability.

The paradigm used employs the following scenario.

1. A user modifies or develops code. The code may be one subroutine or many, possibly comprising whole science models. The code may originate from "scratch," or be extracted from the repository and modified.

2. After testing or reaching a point of being satisfied with his/her results, he/she decides to save it in the repository so that others can have access to it.

3. Some archived codes may still be in an experimental, or development, state while others may be reasonably stable and more completely tested. The latter may be designated as "released." There is no enforceable means to control access based on an experimental or released state. The community will have and should have access indiscriminately, well aware that using development state code is risky.

4. As the user continues to work with the codes, he/she may make enhancements or discover and fix errors. The upgrades are then installed in the repository, which automatically assigns unique revision identifiers.

5. The repository is located where it is conveniently accessible to all pertinent users, and it is maintained by an administrator who sets and enforces general access rules.

18.4.2 The Tool

There are many configuration management tools both free and commercially available. We chose The Concurrent Versions System (CVS) [1] mainly because of its versatility. CVS controls the concurrent editing of sources by several users working on releases built from a hierarchical set of directories. CVS uses the Revision Control System (RCS) [2] as the base system. Other reasons that CVS was an attractive choice include:

- It works on virtually all UNIX platforms and many PCs;
- It is publicly available and free;
- CVS is a state-of-the-art system, constantly being improved; and
- MM5 codes are managed by CVS, and MM5 is a primary meteorology model for the CMAQ system.

From the UNIX man pages (online manual):

> CVS is a front end to the Revision Control System (RCS) that extends the notion of revision control from a collection of files in a single directory to a hierarchical collection of directories consisting of revision controlled files. These directories and files can be combined together to form a software release. CVS provides the functions necessary to manage these software releases and to control the *concurrent* editing of source files among multiple software developers [emphasis added].
>
> The Revision Control System (RCS) manages multiple revisions of files. RCS automates the storing, retrieval, logging, identification, and merging of revisions.

Another widely used source code management system is the Source Code Control System (SCCS), which is usually distributed with UNIX systems. The main note is that RCS and SCCS act on files only, while CVS operates on projects. Working with entire projects works better and easier with CVS. Multi-developer project development works better with CVS as well. CVS supports a client/server mode of operation that can be very useful. CVS also allows customization by adding hooks so that local scripts or programs can be called when executing various CVS commands. This can be useful to force naming conventions of tags, or reference to bug-tracking software, etc. Thus CVS adds power and features that are attractive for the ModelsS-3/CMAQ system.

18.4.3 The Repository

The repository structure, that is, the UNIX directory hierarchy, follows the class/module organization discussed above in Section 18.2. The repository is actually divided into many repositories, one for each generic model. This division makes it easier to maintain the class/module organization that is important for the model building operation described below in Section 18.5.

CVS allows for the use of a "modules" file[3], which enables a user to easily check out or extract a complete CMAQ module. For example, a module might be checked out by a user to make code modifications, and complete modules are checked out during the model building operation.

The following shows a symbolic CVS UNIX directory tree that represents the current structure for the CCTM:

[3]The terminology is unfortunate. The CVS *modules* file has no intrinsic relationship with the CMAQ classes/module design implementation.

```
...CCTM -+-> CVSROOT ---+-> CVS administrative files
         |              |
         \-> src -------+-> driver --+-------> ctm ------+-> RCS files
                        |
                        +-> hadv ---+---> hadv_noop ---+-> RCS files
                        |           +---> hbot --------+-> RCS files
                        |           +---> hppm --------+-> RCS files
                        |
                        +-> vadv ---+---> vadv_noop ---+-> RCS files
                        |           +---> vbot --------+-> RCS files
                        |           +---> vppm --------+-> RCS files
                        |
                        +-> vdiff --+---> vdiff_noop --+-> RCS files
                        |           +---> eddy --------+-> RCS files
                        |
                        +-> chem ---+---> chem_noop ---+-> RCS files
                        |           +---> smvgear -----+-> RCS files
                        |           +---> qssa --------+-> RCS files
                        |
                        +-> phot ---+---> phot_noop ---+-> RCS files
                        |           +---> phot --------+-> RCS files
                        |
                        +-> aero ---+---> aero_noop ---+-> RCS files
                        |           +---> aero --------+-> RCS files
                        |
                        +-> couple -+---> gencoor -----+-> RCS files
                        |
                        +-> cloud --+---> cloud_noop --+-> RCS files
                        |           +---> cloud_radm --+-> RCS files
                        |
                        +-> procan -+---> pa ----------+-> RCS files
                        |
                        +-> hdiff --+---> hdiff_noop --+-> RCS files
                        |           +---> unif --------+-> RCS files
                        |
                        +-> init ---+---> init --------+-> RCS files
                        |
                        +-> util ---+---> util --------+-> RCS files
                        |
                        +-> aero_depv +-> aero_depv_noop +-> RCS files
                        |             +-> aero_depv -+-> RCS files
                        |
                        +-> adjcon -+---> adjcon_noop -+-> RCS files
                        |           \---> denrate -----+-> RCS files
                        |
                        \-> ping ---+---> ping_noop ---+-> RCS files
                                    +---> ping_qssa ---+-> RCS files
                                    \---> ping_smvgear +-> RCS files
```

The symbolic tree is shown relative to the subdirectory in the repository named for the CCTM model. Similar trees exist for each of the generic models. The RCS files are the revision control history files that contain the change tables to reconstruct the actual source code according to a specific revision identifier. Also note that the tree closely follows the organization of classes and modules for the CCTM described in Table 18-1, and contains alternate modules within the classes. In particular, most classes contain a "no-operation" (_noop) module that allows a user to essentially turn off that particular science process modeling. This is useful, for example in debugging, where rapid turn-around is important, and a computationally demanding module that is not needed can be bypassed.

18.5 How a Model is Constructed

18.5.1 Object Oriented Concepts

To make the Models-3/CMAQ system robust and flexible, object oriented concepts were incorporated into the design of the CMAQ system. Incorporating these ideas into the design helps avoid introducing errors when code modifications are necessary. Additionally, the system is capable of easy and efficient modification, allowing the user to quickly make models for different applications.

The implementation language for CMAQ is Fortran 77, which imposes limits on how far one can go in terms of object oriented design. In particular, since Fortran is a static language, objects cannot be instantiated dynamically; they must be declared explicitly in the source code to be created at compile time. However, to encourage a user community that will be contributing code for future enhancements, every attempt has been made to adhere to the Fortran 77 standard. In the future, the use of other implementation languages such as Fortran 90 will be considered.

18.5.2 Global Name Table Data

In order to implement modularity and data-independence, we have employed design ideas that draw heavily from the object-oriented concept of *inheritance* and code re-use. The data structures in the codes that deal with the domain sizes, chemical mechanism, I/O API, logical file names, general constants, and CGRID pointers are determined by Fortran declarations in data and parameter statements that are created through the Models-3 system. These data structures pertain to a particular application (domain, mechanism, etc.) and are meant to apply globally, not only to one particular CCTM through all its subroutines, but also to all the models that supply data to the CCTM for that application. These data structures are contained in Fortran INCLUDE files, which are essentially header files, included in the declaration sections near the top of the Fortran code source files. The inclusion of these source files is made automatic by using a generic string that represents the include file and which is parsed and expanded to the actual include file during a pre-processing stage in the compilation. The Fortran global include files contain name tables that define:

1. The computational grid domain;
2. The chemical mechanism;
3. The I/O API interface, including logical file names;
4. The global modeling constants; and
5. Other constants or parameters that apply across the model.

In order to effect the implementation of the include files into the code, a special compiling system, m3bld, has been developed [3], which reads a configuration file that, based on the application, completely determines the model executable to be built. The ASCII configuration file can be generated either by the Models-3 system or by the user following a few, simple syntactical rules illustrated below. For additional details, the reader is referred to Chapter 15.

In addition to the global include files, the configuration file contains module commands that tell m3bld to extract the codes for that module from the model code repository for compilation.

18.5.3 Build Template

The following exhibit is an example of a configuration file that m3bld would use to build a model executable: (The numerals at the left-hand margin are labels for the legend and are not part of the configuration file. The "//" represents a non-parsed, comment line.)

Example Configuration File

```
(1)  model TUTO_r4y;

(2)  cpp_flags     " -Demis_vdif  " ;
(2)  f77_flags     " -e -fast -O4 -xtarget=ultra2 -xcache=16/32/1:1024/64/1" ;
(2)  link_flags    " -e -fast -O4 -xtarget=ultra2" ;

(3)  libraries     " -L/home/models3/tools/IOAPI/release/m3io/lib/SunOS5 -lm3io
                   -L/home/models3/tools/netCDF/SunOS5 -lnetcdf" ;

(4)  global verbose;

(5)  include   SUBST_BLKPRM      /work/rep/include/release/BLKPRM_500.EXT;
(5)  include   SUBST_CONST       /work/rep/include/release/CONST3_RADM.EXT;
(5)  include   SUBST_FILES_ID    /work/rep/include/release/FILES_CTM.EXT;
(5)  include   SUBST_EMPR_VD     /work/rep/include/release/EMISPRM.vdif.EXT;
(5)  include   SUBST_EMPR_CH     /work/rep/include/release/EMISPRM.chem.EXT;
(5)  include   SUBST_IOPARMS     /work/rep/include/release/PARMS3.EXT;
(5)  include   SUBST_IOFDESC     /work/rep/include/release/FDESC3.EXT;
(5)  include   SUBST_IODECL      /work/rep/include/release/IODECL3.EXT;
(5)  include   SUBST_XSTAT       /work/rep/include/release/XSTAT3.EXT;
(6)  include   SUBST_COORD_ID    /work/yoj/tgt/BLD/COORD.EXT;
(6)  include   SUBST_HGRD_ID     /work/yoj/tgt/BLD/HGRD.EXT;
(6)  include   SUBST_VGRD_ID     /work/yoj/tgt/BLD/VGRD.EXT;
(6)  include   SUBST_RXCMMN      /work/yoj/tgt/BLD/RXCM.EXT;
(6)  include   SUBST_RXDATA      /work/yoj/tgt/BLD/RXDT.EXT;
(6)  include   SUBST_GC_SPC      /work/yoj/tgt/BLD/GC_SPC.EXT;
(6)  include   SUBST_GC_EMIS     /work/yoj/tgt/BLD/GC_EMIS.EXT;
(6)  include   SUBST_GC_ICBC     /work/yoj/tgt/BLD/GC_ICBC.EXT;
(6)  include   SUBST_GC_DIFF     /work/yoj/tgt/BLD/GC_DIFF.EXT;
(6)  include   SUBST_GC_DDEP     /work/yoj/tgt/BLD/GC_DDEP.EXT;
(6)  include   SUBST_GC_DEPV     /work/yoj/tgt/BLD/GC_DEPV.EXT;
(6)  include   SUBST_GC_ADV      /work/yoj/tgt/BLD/GC_ADV.EXT;
(6)  include   SUBST_GC_CONC     /work/yoj/tgt/BLD/GC_CONC.EXT;
(6)  include   SUBST_GC_G2AE     /work/yoj/tgt/BLD/GC_G2AE.EXT;
(6)  include   SUBST_GC_G2AQ     /work/yoj/tgt/BLD/GC_G2AQ.EXT;
(6)  include   SUBST_GC_SCAV     /work/yoj/tgt/BLD/GC_SCAV.EXT;
(6)  include   SUBST_GC_WDEP     /work/yoj/tgt/BLD/GC_WDEP.EXT;
(6)  include   SUBST_AE_SPC      /work/yoj/tgt/BLD/AE_SPC.EXT;
(6)  include   SUBST_AE_EMIS     /work/yoj/tgt/BLD/AE_EMIS.EXT;
(6)  include   SUBST_AE_ICBC     /work/yoj/tgt/BLD/AE_ICBC.EXT;
(6)  include   SUBST_AE_DIFF     /work/yoj/tgt/BLD/AE_DIFF.EXT;
(6)  include   SUBST_AE_DDEP     /work/yoj/tgt/BLD/AE_DDEP.EXT;
```

Example Configuration File

```
(6)  include   SUBST_AE_DEPV     /work/yoj/tgt/BLD/AE_DEPV.EXT;
(6)  include   SUBST_AE_ADV      /work/yoj/tgt/BLD/AE_ADV.EXT;
(6)  include   SUBST_AE_CONC     /work/yoj/tgt/BLD/AE_CONC.EXT;
(6)  include   SUBST_AE_A2AQ     /work/yoj/tgt/BLD/AE_A2AQ.EXT;
(6)  include   SUBST_AE_SCAV     /work/yoj/tgt/BLD/AE_SCAV.EXT;
(6)  include   SUBST_AE_WDEP     /work/yoj/tgt/BLD/AE_WDEP.EXT;
(6)  include   SUBST_NR_SPC      /work/yoj/tgt/BLD/NR_SPC.EXT;
(6)  include   SUBST_NR_EMIS     /work/yoj/tgt/BLD/NR_EMIS.EXT;
(6)  include   SUBST_NR_ICBC     /work/yoj/tgt/BLD/NR_ICBC.EXT;
(6)  include   SUBST_NR_DIFF     /work/yoj/tgt/BLD/NR_DIFF.EXT;
(6)  include   SUBST_NR_DDEP     /work/yoj/tgt/BLD/NR_DDEP.EXT;
(6)  include   SUBST_NR_DEPV     /work/yoj/tgt/BLD/NR_DEPV.EXT;
(6)  include   SUBST_NR_ADV      /work/yoj/tgt/BLD/NR_ADV.EXT;
(6)  include   SUBST_NR_N2AE     /work/yoj/tgt/BLD/NR_N2AE.EXT;
(6)  include   SUBST_NR_N2AQ     /work/yoj/tgt/BLD/NR_N2AQ.EXT;
(6)  include   SUBST_NR_SCAV     /work/yoj/tgt/BLD/NR_SCAV.EXT;
(6)  include   SUBST_NR_WDEP     /work/yoj/tgt/BLD/NR_WDEP.EXT;
(6)  include   SUBST_TR_SPC      /work/yoj/tgt/BLD/TR_SPC.EXT;
(6)  include   SUBST_TR_EMIS     /work/yoj/tgt/BLD/TR_EMIS.EXT;
(6)  include   SUBST_TR_ICBC     /work/yoj/tgt/BLD/TR_ICBC.EXT;
(6)  include   SUBST_TR_DIFF     /work/yoj/tgt/BLD/TR_DIFF.EXT;
(6)  include   SUBST_TR_DDEP     /work/yoj/tgt/BLD/TR_DDEP.EXT;
(6)  include   SUBST_TR_DEPV     /work/yoj/tgt/BLD/TR_DEPV.EXT;
(6)  include   SUBST_TR_ADV      /work/yoj/tgt/BLD/TR_ADV.EXT;
(6)  include   SUBST_TR_T2AQ     /work/yoj/tgt/BLD/TR_T2AQ.EXT;
(6)  include   SUBST_TR_SCAV     /work/yoj/tgt/BLD/TR_SCAV.EXT;
(6)  include   SUBST_TR_WDEP     /work/yoj/tgt/BLD/TR_WDEP.EXT;

     // Process Analysis / Integrated Reaction Rates processing
(6)  include   SUBST_PACTL_ID    /work/yoj/tgt/BLD/PA_CTL.EXT;
(6)  include   SUBST_PACMN_ID    /work/yoj/tgt/BLD/PA_CMN.EXT;
(6)  include   SUBST_PADAT_ID    /work/yoj/tgt/BLD/PA_DAT.EXT;

(7)  module ctm release ;

(7)  module init release ;

     // options are denrate and adjcon_noop
(7)  module denrate release ;

(7)  module gencoor release ;
     // options are hbot and hadv_noop
(7)   module hppm release ;

    // options are vbot and vadv_noop
(7)   module vppm release ;

    // options are phot and phot_noop

(7)   module phot release ;

    // options are ping_qssa, ping_smvgear and ping_noop
```

Example Configuration File

```
 (7)  module ping_qssa release ;

    // options are qssa, smvgear and chem_noop
(7)  module qssa release ;

    // aerosols
(7)  module aero release ;
     // aerosol dep vel
(7)  module aero_depv release ;

    // options are eddy and vdiff_noop
(7)  module eddy release ;

    // options are const and hdiff_noop
(7)  module unif release ;

    // options are cloud_radm and cloud_noop
(7)  module cloud_radm release ;

    // options are pa and pa_noop, which requires the replacment of the three
    // global include files with their pa_noop counterparts
(7)  module pa release ;

(7)  module util release ;
```

Legend:

(1) - Model name definition. This string is what the model executable will be named.

(2) - The C pre-processor, Fortran compiler and link flags. The flags specified indicate that the model is to be compiled with the option to input emissions in the vertical diffusion processing, and to compile and link on a Sun Sparc, Ultra-30 workstation.

(3) - I/O API and netCDF object libraries to be linked. The format is virtually identical to that of a UNIX make command.

(4) - m3bld flag: one of many options. verbose indicates report all actions. Other options are:

- compile_all - force compile, even if object files are current
- clean_up - remove all source files upon successful completion
- no_compile - do everything except compile
- no_link - do everything except link
- one_step - compile and link in one step
- parse_only - checks config file syntax
- show_only - show requested commands but doesn't execute them

(5), (6) - global include files. The syntax is:

include **internal-string** **full-path-name.**

Every routine that requires a specific include file must contain a Fortran include statement using the **internal-string** (see Section 18.3 for examples).

(5) - " fixed" global include files. The fixed include files have been constructed outside of the Models-3 framework and contain global data not directly related to the domain or chemical mechanism such as modeling

Example Configuration File

```
constants and file logical names.
(6) - The Models-3 framework automatically generates all the include files
labeled (6). The user supplies information through the Models-3 Science
Manager that determines the data in these include files. These data define
the complete problem domain for a particular CMAQ application. See Chapter
15 for a complete discussion.
(7) - The module name to extract from the model code repository and an
optional revision flag to select a particular module version. The syntax is:
 module module name revision flag.
```

For additional information on this implementation, the reader is referred to the Model Building Tool described in Fine et al. [3].

18.6 How a Model is Executed

In order to run a model executable, various UNIX environment variables must be set in the shell that invokes the execute command. Generally, these involve the modeling scenario start date and time, the run duration, the output time step interval, various internal code flags that differ among the models, and all the input and output logical, or symbolic file names (see Section 15.4.3 in Chapter 15). There are various ways by which external file names can be referenced in the code, but the most general across all UNIX platforms is to link them by means of environment variables. There are I/O API utility functions that allow a user easy access to these variables within the code, making such accesses generic and portable.

An additional feature that is provided through the I/O API is to declare a file "volatile" by appending a -v flag in the shell's declaration for the environment variable. By doing this, the I/O API will cause the netCDF file to update (sync) its disk copy after every write and thereby update the netCDF header. Otherwise, netCDF file headers are not updated until the files are closed. This is useful, for example, to allow a user to analyze an open netCDF file using visualization tools while the model is executing. It is also useful in case of a system crash. A CCTM model can be restarted at the scenario time step after the last successful write using the aborted output file as the input initial data.

18.7 Using the Models-3 Framework

The Models-3 framework simplifies the model building and model execution tasks, especially if key objects have been pre-defined. Thus if a user is conducting a study that uses the same domain or chemical mechanism, but uses different code options, e.g., then rebuilding and re-executing using the framework makes conducting the study very straightforward. Other examples where the framework greatly simplifies operational tasks would be where a model is to be applied on different domains, or for control strategies in which the only thing that changes are the emissions input files. A knowledgeable user is still able to build and execute model applications outside the framework. In fact, one can easily run model applications using executables and UNIX scripts generated by the framework.

In general, in order to build a model within the framework, the coordinate system, horizontal grid and vertical layer definitions, and chemical mechanism must be specified. This is done within the Models-3 Science Manager component. If objects required for a particular application, such as a coordinate system specification, are already defined, then the user needs only to select those objects. The Configuration File Manager, an additional subcomponent within the Science Manager, allows a user to control the module definitions and fixed [4] include files that go into the configuration file used to build the model. Also the user can specify compiling and linking flags related to a specific platform on which the model is to be executed.

With all required Models-3 objects defined, the task of building a model is made simple using the Models-3 component, Model Builder. It's important to note that as users develop models, the set of objects will grow to become a rich pool from which to select for a particular application. The Models-3 framework was designed to allow extensive re-use of objects. Model Builder generates all the "non-fixed" include files, then builds a model, linking in the include files including the user-specified fixed ones. See the section above for the include file definitions. Perhaps one of the most useful features of the Models-3 framework is the ability to graphically set up and execute single or multiple model executions with automatic data registration. This allows a user to carefully control the order of model executions and the management of all the input and output data. The Models-3 component that performs this function is the Study Planner. Study Planner allows a user to specify input data sets, executables, and UNIX environment variables, and to initiate (possibly multiple) model runs.

18.8 Conformant Code

18.8.1 Thin Interface

As mentioned above in section 18.5.1 , the Models-3/CMAQ system was designed to be robust and flexible with respect to the interchange of modules and the elimination of cross-module data dependencies. Consequently, the concept of a "thin interface" has been employed in the design, which applies principally to the class-drivers. At the least, the thin interface implementation implies the following requirements:

- Eliminate global memory references (across modules). This implies no common blocks across modules, no hidden data paths, no "back doors";
- Each module reads and interpolates its required data independently. The I/O API helps to ensure this kind of data independence; and
- Standardized argument list (CGRID, Date, Time, TimeStep) for the class-driver, as described in the section above.

These requirements attempt to incorporate the object-oriented idea of encapsulation in the Models-3/CMAQ design. The following quotation is from Rumbaugh et al. [7]:

> Encapsulation (also information hiding) consists of separating the external aspects of an object, which are accessible to other objects, from the internal

[4] not generated by the framework

> implementation details of the object, which are hidden from other objects. Encapsulation prevents a program from becoming so interdependent that a small change has massive ripple effects. The *implementation* of an object can be changed without affecting the applications that use it [emphasis added].

The encapsulation design makes the CMAQ system safer and enables the transaction processing, plug&play capability. This design also makes it easier for a user to trace data and usage within a module, particularly at the class-driver level.

18.8.2 Coding Rules

In order to maintain the object oriented concepts implemented in the CMAQ system design, we have established a small set of coding rules that apply for those that develop CMAQ science and affect the low-level design of the models. We have developed standards to control data dependencies at the class-driver level, but we have not propagated these coding standards to the sub-module level.

1. The models are generally coded in Fortran (Fortran-77 conventions are used). It is possible to link in subroutines written in the C language, although this has not been done within the current CMAQ implementation.

2. The modules must be controlled by a top-level class-driver routine, whose calling arguments must be the computational concentration grid array, CGRID, the current scenario data and time, and the controlling time step vector. See the section above.

3. The class-driver is also responsible for any temporal integration required within the module. (The time steps for process integration at the module level are usually shorter than those of the CCTM synchronization time step.)

4. Any reads and writes for the module should be done at the level of the class-driver routine. Although not absolutely necessary, this is strongly suggested because it is usually much easier to control the timing of the data accesses at the highest level of the module where the current scenario date and time are known.

5. Use the IMPLICIT NONE Fortran declaration to maintain some control on typographic errors and undefined variables. Although not standard Fortran-77, the use of IMPLICIT NONE forces the developer to declare all internal variables.

6. Use the global include files for domain definitions, chemical mechanism data, and other data where available.

7. Use the I/O API for external data references where appropriate. For an illustration of these rules, the reader is referred to the code template below.

At the sub-module level there are no strict I/O or coding standards. Here it is envisioned that individual researchers/programmers use their own coding styles for their algorithms. However the following suggestions are offered to facilitate the potential incorporation of a module into the CMAQ system:

- It is expected that MKS units are used for input and output variables, as these units have been standardized throughout the CMAQ system. Within a sub-module subroutine whatever units are most convenient can be used. However, the developer must be responsible for any unit conversions to MKS for input and output, and thus avoid any potential errors.

- For efficiency and performance considerations, operations may need to be done on groups of grid cells (a block of cells) at a time. If there are N cells in the block and the entire domain contains M cells, then the entire domain can be decomposed into M/N blocks. We have used N=500. For operations in the horizontal (x,y), the cell constraint becomes $X \times Y \leq$ N, where X= number of cells in the x-direction, and Y= number of cells in the y-direction. For operations in both the horizontal and vertical, the constraint becomes $X \times Y \times Z \leq$ N, where Z= number of cells in the z-direction. There may be some operations, such as for some horizontal advection schemes, where this decomposition into blocks becomes more difficult or impossible.

18.8.3 Science Process Code Template

The following demonstrates what a science process class-driver Fortran 77 subroutine might look like. We recommend that a code developer follows this template, where appropriate, to get maximum benefit from the design concepts implemented in the Models-3/CMAQ system. This template is generic and attempts to show most, if not all the features available. Some class-drivers and most other sub-programs within a module may not have, nor require, most or any of these features. (The numerals at the left-hand margin are for the legend and are not part of the text, and the text within "< >" indicates code not included.)

Example of Science Process Class-driver

```
( 1)        SUBROUTINE VDIFF SUBST_GRID_ID ( CGRID, JDATE, JTIME, TSTEP )
( 2) C-----------------------------------
( 2) C Function:
( 2)
( 2) C Preconditions:
( 2)
( 2) C Subroutines and Functions Called:
( 2)
( 2) C Revision History:
( 2) C-----------------------------------
( 3)        IMPLICIT NONE

( 4)        INCLUDE SUBST_HGRD_ID    ! horizontal dimensioning parameters
( 4)        INCLUDE SUBST_VGRD_ID    ! vertical dimensioning parameters

( 5)        INCLUDE SUBST_GC_SPC     ! gas chemistry species table
( 5)        INCLUDE SUBST_GC_EMIS    ! gas chem emis surrogate names and map table
( 5)        INCLUDE SUBST_GC_DEPV    ! gas chem dep vel surrogate names and map table
( 5)        INCLUDE SUBST_GC_DDEP    ! gas chem dry dep species and map table
( 5)        INCLUDE SUBST_GC_DIFF    ! gas chem diffusion species and map table

( 5)        INCLUDE SUBST_AE_SPC     ! aerosol species table
( 5)        INCLUDE SUBST_AE_DEPV    ! aerosol dep vel surrogate names and map table
( 5)        INCLUDE SUBST_AE_DDEP    ! aerosol dry dep species and map table
( 5)        INCLUDE SUBST_AE_DIFF    ! aerosol diffusion species and map table

( 5)        INCLUDE SUBST_NR_SPC     ! non-reactive species table
( 5)        INCLUDE SUBST_NR_EMIS    ! non-react emis surrogate names and map table
( 5)        INCLUDE SUBST_NR_DEPV    ! non-react dep vel surrogate names and map table
```

Example of Science Process Class-driver

```
( 5)        INCLUDE SUBST_NR_DDEP    ! non-react dry dep species and map table
( 5)        INCLUDE SUBST_NR_DIFF    ! non-react diffusion species and map table

( 5)        INCLUDE SUBST_TR_SPC     ! tracer species table
( 5)        INCLUDE SUBST_TR_EMIS    ! tracer emis surrogate names and map table
( 5)        INCLUDE SUBST_TR_DEPV    ! tracer dep vel surrogate names and map table
( 5)        INCLUDE SUBST_TR_DDEP    ! tracer dry dep species and map table
( 5)        INCLUDE SUBST_TR_DIFF    ! tracer diffusion species and map table

( 6) #ifdef emis_vdif
( 6)        INCLUDE SUBST_EMPR_VD    ! emissions processing in vdif
( 6) #else
( 6)        INCLUDE SUBST_EMPR_CH    ! emissions processing in chem
( 6) #endif
( 7)        INCLUDE SUBST_PACTL_ID   ! PA control parameters
( 7)        INCLUDE SUBST_CONST      ! constants
( 7)        INCLUDE SUBST_FILES_ID   ! file name parameters
( 7)        INCLUDE SUBST_IOPARMS    ! I/O parameters definitions
( 7)        INCLUDE SUBST_IOFDESC    ! file header data structure
( 7)        INCLUDE SUBST_IODECL     ! I/O definitions and declarations
( 7)        INCLUDE SUBST_XSTAT      ! M3EXIT status codes
( 4)        INCLUDE SUBST_COORD_ID   ! coordinate and domain definitions (req IOPARMS)

( 8) C Arguments:
( 8)
( 8)        REAL         CGRID( NCOLS,NROWS,NLAYS,* )   !  concentrations
( 8)        INTEGER      JDATE         ! current model date, coded YYYYDDD
( 8)        INTEGER      JTIME         ! current model time, coded HHMMSS
( 8)        INTEGER      TSTEP( 3 )    ! time step vector (HHMMSS)
( 8)                                   ! TSTEP(1) = local output step
( 8)                                   ! TSTEP(2) = sciproc sync.  step (chem)
( 8)                                   ! TSTEP(3) = advection time step

( 9) C Parameters:
( 9)        <   >
(10) C External Functions not previously declared in IODECL3.EXT:
(10)
(10)        INTEGER      SECSDIFF, SEC2TIME, TIME2SEC
(10)        EXTERNAL     SECSDIFF, SEC2TIME, TIME2SEC

(11) C File variables:
(11)        <   >
(12) C Local variables:
(12)        <   >
(13)        IF ( FIRSTIME ) THEN
(13)
(13)           FIRSTIME = .FALSE.
(13)
(13)           LOGDEV = INIT3()
(13)
(13) C Open the met files:
(13)
(13)           IF ( .NOT.  OPEN3( MET_CRO_3D, FSREAD3, PNAME ) ) THEN
(13)              XMSG = 'Could not open '// MET_CRO_3D // ' file'
(13)              CALL M3EXIT( PNAME, JDATE, JTIME, XMSG, XSTAT1 )
(13)              END IF
(13)
(13)           < open other met files >
(13)
(13) C Open Emissions files:
(13)
(13)           < do other intialization or operations that need be done only once >
(13)
(13)           END IF           !  if firstime

(14) C set file interpolation to middle of time step
```

Example of Science Process Class-driver

```
(14)
(14)        MDATE = JDATE
(14)        MTIME = JTIME
(14)        MSTEP = TIME2SEC( TSTEP( 2 ) )
(14)        CALL NEXTIME ( MDATE, MTIME, SEC2TIME( MSTEP / 2 ) )

(15) C read&interpolate met data
(15)
(15)       VNAME = 'DENSA_J'
(15)       IF ( .NOT.  INTERP3( MET_CRO_3D, VNAME, PNAME,
(15)      &                     MDATE, MTIME, NCOLS*NROWS*NLAYS,
(15)      &                     RRHOJ ) ) THEN
(15)          XMSG = 'Could not interpolate DENSA_J from ' // MET_CRO_3D
(15)          CALL M3EXIT( PNAME, MDATE, MTIME, XMSG, XSTAT1 )
(15)          END IF
(15)
(15)        < do other reads >
(15)
(15) C read&interpolate deposition velocities
(15)
(15)        < do operations >
(15)
(15) C read&interpolate emissions
(15)
(15)        CALL RDEMIS ( MDATE, MTIME, NCOLS, NROWS, EMISLYRS, NEMIS, EM_TRAC,
(15)      &               VDEMIS )
(15)
(16)        IF (LIPR) CALL PA_UPDATE_EMIS ( 'VDIF', VDEMIS, JDATE, JTIME, TSTEP )

            < do other operations >

(17)        CALL EDYINTB SUBST_GRID_ID ( EDDYV, DT, JDATE, JTIME, TSTEP( 2 ) )

(18)        DO 345 R = 1, NROWS
(18)           DO 344 C = 1, NCOLS

                < do operations >

(19)            DO 301 N = 1, NSTEPS( C,R )

                   < do operations >

(19) 301        CONTINUE        !  end time steps loop
(18) 344     CONTINUE           !  end loop on col C
(18) 345   CONTINUE             !  end loop on row R

(20) C If last call this hour:  write accumulated depositions:
(20)
(20)        WSTEP = WSTEP + TIME2SEC( TSTEP( 2 ) )
(20)        IF ( WSTEP .GE.  TIME2SEC( TSTEP( 1 ) ) ) THEN
(20)           MDATE = JDATE
(20)           MTIME = JTIME
(20)           CALL NEXTIME( MDATE, MTIME, TSTEP( 2 ) )
(20)           WSTEP = 0
(20)
(20)           IF ( .NOT.  WRITE3( CTM_DRY_DEP_1,
(20)      &                        ALLVAR3, MDATE, MTIME, DDEP ) ) THEN
(20)           XMSG = 'Could not write ' // CTM_DRY_DEP_1 // ' file'
(20)      ,    CALL M3EXIT( PNAME, MDATE, MTIME, XMSG, XSTAT1 )
(20)           END IF
(20)
(20)           WRITE( LOGDEV, '( /5X, 3( A, :, 1X ), I8, " :" , I6.6 )' )
(20)      &          'Timestep written to', CTM_DRY_DEP_1,
(20)      &          'for date and time', MDATE, MTIME
(20)
(16)           IF (LIPR) CALL PA_UPDATE_DDEP ( 'VDIF', DDEP, JDATE, JTIME, TSTEP )
```

Example of Science Process Class-driver

```
(20)
(20)        < do other operations >
(20)
(20)        END IF

(21)        RETURN
(21)        END
```

Legend:

```
( 1) - Class-driver subroutine internal name.  Note the calling argument list.  It is fixed for
class-drivers.  The string " SUBST_GRID_ID"  is used for developing run-time nesting applications,
which has not been fully implemented in the  current version.  By specifying subroutine names
associated with a particular nest and using corresponding domain include files for that
subroutine, it is possible to set up a multi-nest application.  The details have not been
discussed because this kind of nesting has not been implemented in the current release of the
Models-3/CMAQ system.
( 2) - Header comments.  Highly recommended for internal documentation.
( 3) - Highly recommended for Fortran.  IMPLICIT NONE will catch typo's and other undeclared
variable errors at compile time.
( 4) - Domain array dimensioning and looping global variables, e.g.  NCOLS, NROWS, NLAYS.
( 5) - Chemical mechanism array dimensioning and looping global variables.
( 6) - C Preprocessor flags that determine which emissions control dimensioning and looping
variables are compiled.
( 7) - Other global array dimensioning and looping global variables including those for the I/O
API.  The logical variable LIPR is defined in the SUBST_PACTL_ID include file for use at lines
labeled (16).
( 8) - Declarations for the argument list (standardized).
( 9) - Declarations and PARAMETER statements for local Fortran parameters.
(10) - Declarations for external functions not previously declared.
(11) - Declarations for arrays to hold external file data.
(12) - Declarations for local variables.
(13) - Code section for subroutine initialization and for any local data that need not be set at
every entry into the subroutine.  Such data would require a SAVE statement in the declarations.
For example FIRSTIME is initialized to .TRUE. in the local variables section (12).
(14) - Illustrates using an I/O API function to set file interpolation time.
(15) - Read accesses from I/O API files using the I/O API time-interpolation function.
(16) - Call to process analysis routine to obtain data for the optional integrated process rates
function.
(17) - Illustrates call to another science process within the module.
(18) - Main computational loop over the horizontal grid.
(19) - Time step loop over sub-synchronization time step intervals.
(20) - Illustrates writing to an I/O API file within a module.
(21) - Subroutine end
```

18.8.4 Robustness and Computational Efficiency

Scientists, while working in their discipline, are generally not interested in the physical situations that don't significantly affect the phenomena they are studying and modeling. Typically, the scientist works with box models, and uses specialized data to test hypotheses, parameterizations and numerical schemes. The focus is to generate new results based on output from these relatively simple models. In trying to integrate these codes into a more general grid model, problems may arise when modeling simulations carry their formulations into regimes not explored in initial studies, therefore not properly accounted for in the grid model. The scientist who is developing codes that may go into a grid model should be cognizant of these issues and should make every effort to make the codes robust.

Another issue is code efficiency. In order to handle the pathological situations, codes like these may become inefficient, spending many cycles dealing with the "off-problem" cases. A good example is solving for the roots of a cubic polynomial whose coefficients, depending closely on the locally modeled physics, may range over broad values. So, in addition to robustness, attention should be paid to code performance. As the science improves in environmental modeling, this usually translates into increased computational complexity. Although hardware performance is continually improving, it cannot keep pace with the computational demands of new science developments. Not typically the main interest of the science developer, software performance is nevertheless a critical issue and must be addressed. Otherwise scientifically sound models will not be of much general use if they take an inordinate amount of time to execute.

18.9 Conclusion

The CMAQ system has been designed and implemented in such a way that its integration into Models-3 allows access to the extensive functionality of the Models-3 framework. Users can easily select important model options and can readily develop and execute models that apply to their requirements.

We have integrated the CMAQ codes into the Models-3 system by following the basic set of guidelines and rules presented in this chapter.

18.10 References

[1] http://interactivate.com/public/cvswebsites/cvs_toc.html, http://www.cyclic.com/cvs/, and the UNIX man pages

[2] http://www.cs.cmu.edu/People/vaschelp/Archiving/Rcs/, and the UNIX man pages

[3] Fine, S. S., W. T. Smith, D. Hwang, T. L. Turner, 1998: Improving model development with configuration management, IEEE Computational Science and Engineering, 5(1, Ja-Mr), 56-65. and http://envpro.ncsc.org/pub_files/fine1998b.html

[4] http://sage.mcnc.org/products/ioapi/

[5] ftp://ftp.unidata.ucar.edu/pub/netcdf/

[6] EPA Third-Generation Air Quality Modeling System, Models-3 Volume 9b, User Manual, Appendices, June 1998, EPA-600/R-98/069(b)

[7] J. Rumbaugh, M. Blaha, W. Premerlani, F. Eddy, and W. Lorensen, 1991: Object-Oriented Modeling and Design, Prentice Hall

[8] Grell, G. A., J. Dudhia and D. R. Stauffer, 1994: A description of the fifth-generation Penn State/NCAR mesoscale model (MM5). NCAR Technical Note, NCAR/TN-398+STR, 122 pp.

EPA/600/R-99/030

This chapter is taken from *Science Algorithms of the EPA Models-3 Community Multiscale Air Quality (CMAQ) Modeling System*, edited by D. W. Byun and J. K. S. Ching, 1999.

☆ U.S. GOVERNMENT PRINTING OFFICE: 1999 – 750 - 101 / 00062

United States
Environmental Protection Agency
Center for Environmental Research Information
Cincinnati, OH 45268

Please make all necessary changes on the below label, detach or copy, and return to the address in the upper left-hand corner.

If you do not wish to receive these reports CHECK HERE ☐; detach, or copy this cover, and return to the address in the upper left-hand corner.

Official Business
Penalty for Private Use
$300

EPA/600/R-99/030